

Молба

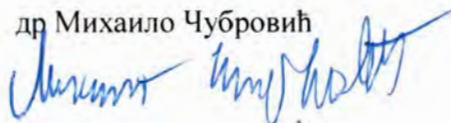
Научном већу Института за физику у Београду

С обзиром да испуњавам критеријуме прописане од стране Министарства просвете, науке и технолошког развоја за стицање звања научног сарадника, молим Научно веће Института за физику у Београду да покрене поступак за мој избор у то звање. У прилогу се налазе:

Мишљење руководиоца пројекта с предлогом чланова комисије
Стручна биографија
Преглед научних активности
Елементи за квалитативну анализу рада
Елементи за квантитативну анализу рада
Списак објављених радова
Подаци о цитираности радова
Докторска диплома и уверење о нострификацији
Докторска дисертација
Копије објављених радова
Пратећа документација

Београд, 25. 01. 2017.

др Михаило Чубровић



Научном већу Института за физику у Београду

Београд, 31. јануар 2017. године

Предмет: Мишљење руководица пројекта о избору др Михаила Чубровића у звање научни сарадник

Др Михаило Чубровић је заинтересован за сарадњу са Лабораторијом за примену рачунара у науци, у оквиру Националног центра изузетних вредности за изучавање комплексних система Института за физику у Београду, као и за ангажман на пројекту основних истраживања Министарства просвете, науке и технолошког развоја Републике Србије ОН171017, под називом "Моделирање и нумеричке симулације сложених вишечестичних физичких система". На поменутом пројекту радио би на темама везаним за проучавање јако корелисаних квантних система. С обзиром да испуњава све предвиђене услове у складу са Правилником о поступку, начину вредновања и квантитативном исказивању научноистраживачких резултата истраживача МПНТР, сагласан сам са покретањем поступка за избор др Михаила Чубровића у звање научни сарадник.

За састав комисије за избор др Михаила Чубровића у звање научни сарадник предлагем:

- (1) др Антун Балаж, научни саветник, Институт за физику у Београду
- (2) др Милица Миловановић, научни саветник, Институт за физику у Београду
- (3) др Ивана Васић, научни сарадник, Институт за физику у Београду
- (4) др Михајло Ваневић, доцент Физичког факултета Универзитета у Београду

Руководилац пројекта ОН171017

др Антун Балаж
научни саветник

Стручна биографија

Михаило Чубровић је рођен 04. 05. 1985. године у Београду. Математичку гимназију је завршио 2004. године, и уписао Физички факултет Универзитета у Београду, смер Теоријска и експериментална физика. Дипломски рад под називом “On topological defects in quantum and classical glass systems” урадио је на Институту за физику у Београду, под руководством др Милана Петровића. Дипломирао је, на теоријском смеру, децембра 2008. године, са просечном оценом 9.85. Од 2003. године до завршетка студија је био стипендиста Министарства за науку.

Докторске студије је започео фебруара 2009. године на Лоренцовом институту Универзитета у Лајдену, Холандија (Lorentz Institute, Leiden University), под вођством проф. Јана Занена (Jan Zaanen) и др Кунрада Схалма (Koenraad Schalm). Фебруара 2013. године одбранио је докторску тезу под насловом “Holography, Fermi surfaces and Criticality”. Дисертација је нострификована јануара 2017. године, решењем Министарства за просвету, науку и технолошки развој бр. 612-01-02635/2016-06. У току докторских студија био је запослен као млађи истраживач на Лоренцовом институту, и као асистент у настави на Универзитету у Лајдену.

Постдокторско усавршавање је започео септембра 2013. године на Институту за теоријску физику Универзитета у Келну, Немачка (Institute of Theoretical Physics, University of Cologne), у групи проф. Ахима Роша (Achim Rosch). У току постдокторског усавршавања био је такође запослен као асистент у настави.

У току докторских студија и након тога учествовао је на неколико школа и презентовао своје резултате на више конференција и радионица. Објавио је укупно 10 публикација, од тога 1 рад у часопису категорије M21a (класификован као “Highly cited paper” у бази података Web of Science), 8 радова у часописима категорије M21, 1 рад у часопису категорије M23 и једно поглавље у зборнику водећег међународног значаја M13. Његови радови су, по бази података Web of Science, цитирани укупно 323 пута без аутоцитата. Његов Хиршов индекс износи 5.

Преглед научних активности

Научно-истраживачки рад др Михаила Чубровића је фокусиран на везе између јако корелисаних електронских система и физике високих енергија, посебно на не-Фермијеве течности и њихову везу са квантном критичношћу, а онедавно и на неравнотежне особине јако корелисаних система. Друга, споредна област интересовања су нелинеарна динамика и комплексни системи. Радови кандидата комбинују аналитичке (теоријске) и нумеричке методе.

Фермионска квантна критичност и AdS/CFT кореспонденција. Основно питање радова [A1, B4-B6] је: можемо ли разумети не-Фермијеве течности и чудне метале (strange metals) на нивоу теорије средњег поља аналогне Ландауовој теорији Фермијевих течности, те постоји ли генеричко (РГ стабилно) стање интерагујућих електрона, које не нарушава никакву симетрију а које се разликује од Фермијеве течности. Идеја је да се проблем формулише преко AdS/CFT кореспонденције (холографског принципа), дуалности између отворених и затворених струна откривене крајем деведесетих година прошлог века. Дуалност повезује теорију поља (строго узев, гејц теорију) са интеракцијама реда величине g са гравитацијом у анти-де Ситеровом простору са гравитационом константом реда $1/g$. Тако јако корелисани системи одговарају слабо интерагујућој, квазикласичној гравитацији. Први покушај [A1] је показао да већ јако упрошћен модел, који одговара електронима ниске густине у интеракцији са (неидентификованом) јако интерагујућом гејц теоријом, показује Фермијеве површи са стабилним квазичестицама, сличним Фермијевој течности. Рад [B6] доноси целовитију теорију, у којој се показује да систем има две фазе, од којих једна одговара Фермијевој течности, а друга не-Фермијевој течности са неким квантно-критичним особинама (аномално скалирање по енергији, не и по импулсу). Овде је изведен нови елемент “холографског речника”, тј. нови елемент AdS/CFT дуалности: скок дистрибуције импулса на Фермијевој површи Z одговара одређеној одржаној струји (билинеарном оператору) у AdS простору; разрађен је и општи формализам за рачун са билинеарним операторима који се може употребити и за друге параметре уређења. У [B4, B5] се разматрају пре свега формална питања значајна за разумевање саме кореспонденције: испоставља се да је нестабилност критичне Фермијеве површи дуална суперрадиационој нестабилности наелектрисане црне рупе, док Фермијева течност одговара Лифшицовој геометрији. На основу тога, у [B4] је конструисан цео фазни дијаграм система, и формулисан је метод који омогућава да се на гравитационој страни кореспонденције оде и даље од квазикласичног третмана, тј. да се узму у обзир и квантне корекције. Методолошки, ови радови комбинују аналитичка извођења на основу “холографског речника”, тј. асимптотских решења Ајнштајнових једначина која се могу добити аналитички, и самоусаглашено нумеричко решавање целог система једначина (за метрику, гејц поља и поља материје) у AdS простору.

У радовима [B2, B7] такође су у холографским моделима проучавани јако интерагујући електрони, али сада у спољашњем магнетном пољу. У [B7] се, поред општих тестова важних за разумевање самог метода и за додатну потврду да теорија показује присуство Фермијеве површи (Ландауови нивои, рачунање густине у зависности од магнетног поља, итд), даје крајње поједностављен модел квантног Холовог ефекта и изводе фактори попуњености у фази Фермијеве и не-Фермијеве течности. Показује се да у овом моделу не-Фермијева фаза доводи до фракционе попуњености, док нормални метал даје целобројни ефекат. У [B2] је дат физички боље мотивисан модел екситона (парова електрон-шупљина) у билинеарном формализму претходно развијеном у [B6]. Показано је како долази до магнетне катализе и кондензације екситона под дејством магнетног поља, и конструисан је фазни дијаграм који је упоређен са резултатима из литературе за екситоне у двослојном графену.

Конфајнмент у ефективним гејџ теоријама и тешки фермиони. У раду [B1] разматра се концепт фракционализације електрона који је, у радовима Сачдева, Војте и других, постао важан кандидат за разумевање чудних метала, и њему сродан проблем конфајнмент/деконфајнмент прелаза у ефективним гејџ пољима каква се јављају у опису високо корелисаних система. Главна физичка мотивација су тешки фермиони.

Нелинеарни и неравнотежни системи [B3,B8,C1]. Овде се за сад не може говорити о кохерентном истраживачком програму, већ је размотрен низ ситнијих, независних питања. У [B8] разматрају се ненинтеграбилни Хамилтонови системи, и изводи се кинетичка једначина која описује еволуцију нестабилних орбита у фазном простору. У [C1] се сличан формализам нелокалних кинетичких једначина примењује на геометрију појединих полимера у конфинираној геометрији, предвиђа се звонасти облик криве NMR одзива и пореди са експерименталним резултатима из литературе.

Рад [B3] проучава термализацију једнодимензионог ланца неинтерагујућих фермиона у контакту са термостатом путем Линдбладове једначине. У одсуству меморије у термостату, термализација је нагла и понаша се као фазни прелаз првог реда. Меморијски ефекти непертурбативно мењају слику, и доводе до веома споре термализације. Велика мана је потпуно занемаривање интеракција и право питање је шта ће се десити у њиховом присуству – очекивање је да интеграбилност система има кључну улогу за дистинкцију између брзе и споре термализације. У току је рад на овом проблему у TFD (thermofield dynamics) формализму, што ће убудуће бити један од главних праваца рада кандидата, но на жалост публикабилних резултата још нема.

Елементи за квалитативну анализу рада

1. Квалитет научних резултата

Научни ниво и значај резултата. Кандидат је до сада објавио 10 радова, од тога 1 у часопису M21a (међународни часопис изузетне вредности), 8 у часописима категорије M21 (врхунски међународни часопис) и 1 у часопису категорије M23 (међународни часопис).

Утицајност. Радови у области јако корелисаних Фермијевих и не-Фермијевих течности испитиваних методом AdS/CFT били су међу првим радовима овог правца и иницирали су даљи рад многих истраживача, што се види по одзиву на рад [A1] објављен у часопису Science, који је, иако полази од крајње поједностављеног модела, имао срећу да буди први рад у коме је показано постојање Фермијевих површи у AdS/CFT формализму па је цитиран 263 пута без аутоцитата ("Highly cited paper" по бази података Web of Science) и чија је методологија у основи холографских проучавања јако корелисаних електрона.

Награде. Кандидат је био стипендиста Министарства за науку Републике Србије у периоду 2003-2008. године. Добитник је годишње награде Одсека за физику Универзитета у Лајдену за научни рад "Trots op..." 2009. године и годишње награде истог одсека за најбољу тезу 2013 године.

Цитираност. Према бази Web of Science, радови кандидата су цитирани укупно 323 пута, без самоцитата, уз Хиршов индекс 5.

Параметри квалитета часописа. Кандидат је објавио радове у следећим часописима:

- 3 рада у Journal of High Energy Physics (ИФ=6.023)
- 3 рада у Physical Review D (ИФ=4.506)
- 1 рад у Physical Review B (ИФ=3.718)
- 1 рад у Physical Review E (ИФ=2.252)
- 1 рад у Science (ИФ=34.661)
- 1 рад у European Physical Journal D (ИФ=1.208)

Укупан импакт фактор радова кандидата је 73.25.

Међународна сарадња. Кандидат је завршио докторске студије и докторирао на универзитету у Лајдену, са којим и данас има активну сарадњу. Након тога, био је на постдокторском усавршавању на Универзитету у Келну. Кандидат је сарађивао и са Универзитетом у Франкфурту (Institute for Theoretical Physics, J.-W. Goethe-University), Институтом за напредне студије у Франкфурту (Frankfurt Institute for Advanced Studies) и Универзитетом у Гетингену (Institute for Theoretical Physics, Georg August University, Goettingen), што се види из радова са коауторима. Током лета 2007. године био је у тромесечној посети Институту за напредне студије у Франкфурту. Остварио је краће посете бројним универзитетима и институтима где је на семинарима представио своје радове.

2. Ангажованост у формирању научних кадрова

Кандидат је у летњем семестру 2010. и 2011. године био асистен на предмету Theory of Condensed Matter на Универзитету у Лајдену. На Универзитету у Келну био је асистент на

предметима Advanced Quantum Mechanics (зима 2013), Quantum Mechanics (лето 2014) и Quantum Field Theory (лето 2015). На универзитету у Лајдену кандидат је радио са мастер студентима (Piet Schijven & Jelle Brill), који су се укључили у рад на публикацији [B7].

3. Нормирање броја коауторских радова

Сви радови кандидата укључују нумеричке симулације. По Правилнику, рад [B7] и рад у зборнику [D1] рачунају се са коефицијентом 0.83, јер имају укупно шест коаутора. Остали радови имају мање од пет аутора, и рачунају се са пуним бројем бодова.

4. Активност у научним у научно-стручним друштвима

Кандидат је рецензент часописа Journal of High Energy Physics (ИФ=6.023).

5. Конкретни научни допринос кандидата у реализацији резултата у научним центрима и земљи и иностранству

Кандидат има два рада у којима је једини аутор, [B1] и [B8]. Кандидат има четири рада у којима је први аутор: [A1], [B5], [B6] и [C1]. У радовима [A1, B6, C1] кандидат је радио све нумеричке прорачуне и већину аналитичких, а у [B5] је радио пре свега део који се односи на модел “black hole with Dirac hair” и спектралне функције, док су прорачуне са моделом електронске звезде радили други коаутори. У раду [B2] кандидат је радио све аналитичке прорачуне и део нумеричких, а у [B7] је радио део који се односи на рачунање скалирања и фазног дијаграма, и надзирао студенте у нумеричком раду. У раду [B4] кандидат је радио углавном аналитички део, а у раду [B3] део везан за Линдбладову једначину (без транспорта).

Радови [B8] и [C1] су урађени у току основних студија на Физичком факултету у Београду: [B8] у сарадњи са Институтом за физику у Београду, а [C1] у сарадњи са Институтом за напредне студије у Франкфурту. Радови [A1], [B4-7] су настали у току докторских студија на универзитету у Лајдену, а [B7] је укључивао и сарадњу са Универзитетом у Франкфурту. Радови [B1-B3] су настали у току постдока на Универзитету у Келну, а у сарадњи са Универзитетима у Лајдену и Франкфурту [B3] и у сарадњи са Универзитетом у Гетингену [B2].

Елементи за квантитативну анализу рада

Кандидат је објавио укупно 10 публикација, од тога 1 рад у часопису категорије M21a (класификован као “Highly cited paper” у бази података Web of Science), 8 радова у часописима категорије M21, 1 рад у часопису категорије M23 и једно поглавље у зборнику водећег међународног значаја M13. Његови радови су, по бази података Web of Science, цитирани укупно 323 пута без ауоцитата. Његов Хиршов индекс износи 5.

Следе остварени резултати по категоријама.

| Категорија | М бодова по раду | Број радова | Укупно М бодова | Нормирани број М бодова |
|------------|------------------|-------------|-----------------|-------------------------|
| M13 | 7 | 1 | 7 | 5.83 |
| M21a | 10 | 1 | 10 | 10 |
| M21 | 8 | 8 | 64 | 62.67 |
| M23 | 3 | 1 | 3 | 3 |
| M33 | 1 | 2 | 2 | 2 |
| M34 | 0.5 | 7 | 3.5 | 3.5 |
| M71 | 6 | 1 | 6 | 6 |

Поређење са минималним квантитативним резултатима за избор у звање научни сарадник.

| Минималан број М бодова | Укупно | Нормирани резултат кандидата |
|-----------------------------|--------|------------------------------|
| Укупно | 16 | 91 |
| M10+M20+M31+M32+M33+M41+M42 | 10 | 81.5 |
| M11+M12+M21+M22+M23 | 6 | 75.67 |

Списак радова

Радови у међународним часописима изузетних вредности (M21a)

[A1]

М. Čubrović, J. Zaanen, K. Schalm

String theory, quantum phase transitions and the emergent Fermi liquid, *Science* **325**, 439, 2009.

[arXiv:0904.1993[hep-th]]

7 страна, 263 цитата без аутоцитата, ИФ за 2009. годину 29.747, ИФ за 2015. годину 34.661

Радови у врхунским међународним часописима (M21)

[B1]

М. Čubrović

Confinement/deconfinement transition from symmetry breaking in gauge/gravity duality, *JHEP* **2016**, 102, 2016. [arXiv:1605.07849[hep-th]]

38 страна, ИФ за 2015. годину 6.023, ИФ за 2014. годину 6.220

[B2]

Е. Gubankova, М. Čubrović, J. Zaanen

Exciton-driven quantum phase transitions in holography, *Phys. Rev. D* **92** 086004, 2015.

[arXiv:1412.2373[hep-th]]

35 страна, 1 цитат без аутоцитата, ИФ за 2015. годину 4.506, ИФ за 2013. годину 4.864

[B3]

М. V. Medvedyeva, М. T. Čubrović, S. Kehrein

Dissipation-induced first-order decoherence phase transition in a noninteracting fermionic system, *Phys. Rev. B* **91** 205416, 2015. [arXiv:1409.1625[cond-mat]]

11 страна, 3 цитата без аутоцитата, ИФ за 2015. годину 3.718, ИФ за 2014. годину 3.736

[B4]

М. V. Medvedyeva, Е. Gubankova, М. Čubrović, K. Schalm, J. Zaanen

Quantum corrected phase diagram of holographic fermions, *JHEP* **2013**, 25, 2013.

[arXiv:1302.5149[hep-th]]

26 страна, 3 цитата без аутоцитата, ИФ за 2016. годину 6.023, ИФ за 2013. годину 5.618

[B5]

М. Čubrović, Y. Liu, K. Schalm, Y.-W. Sun, J. Zaanen

Spectral probes of the holographic Fermi liquid ground state: Dialing between the electron star and the AdS Dirac hair, *Phys. Rev. D* **84** 086002, 2013. [arXiv:1106.1798[hep-th]]

16 страна, 18 цитата без аутоцитата, ИФ за 2015. годину 4.506, ИФ за 2013. годину 4.864

[B6]

М. Čubrović, J. Zaanen, K. Schalm

Constructing the AdS dual of a Fermi liquid: black holes with Dirac hair, *JHEP* **2011**, 17, 2011.

[arXiv:1012.5681[hep-th]]

29 страна, 13 цитата без аутоцитата, ИФ за 2015. годину 6.023, ИФ за 2011. годину 5.831

[B7]

E. Gubankova, J. Brill, M. Čubrović, K. Schalm, P. Schijven, J. Zaanen
Holographic fermions in external magnetic fields, Phys. Rev. D **84** 106003, 2011.
[arXiv:1011.4051[hep-th]]

27 страна, 15 цитата без аутоцитата, ИФ за 2015. годину 4.506, ИФ за 2011. годину 4.558

[B8]

M. Čubrović

Fractional kinetic model for chaotic transport in nonintegrable Hamiltonian systems, Phys. Rev. E
72, 025204(R), 2005.

4 стране, ИФ за 2015. годину 2.252, ИФ за 2005. годину 2.418

Радови у међународним часописима (M23)

[C1]

M. Čubrović, O. Obolensky, A. Solov'ov

Semistiff polymer model of unfolded proteins and its application to NMR residual dipolar couplings, Eur. J. Phys. D **51**, 41, 2009.

9 страна, 4 цитата без аутоцитата, ИФ за 2015. годину 1.208, ИФ за 2009. годину 1.420

Рад у тематском зборнику водећег међународног значаја (M13)

[D1]

E. Gubankova, J. Brill, M. Čubrović, K. Scalm, P. Schijven, J. Zaanen

Holographic description of strongly correlated electrons in external magnetic fields
D. Kharzeev et al (eds.), Strongly interacting matter in magnetic fields, Lecture Notes in Physics
871, Springer-Verlag Berlin Heidelberg, 2013. (ISBN 978-3-642-37304-6), p. 555.

35 страна

Саопштења са међународних скупова штампана у целини (M33)

[E1]

M. Čubrović

Regimes of stability and scaling relations for the removal time in the asteroid belt: a simple kinetic model and numerical tests

(Z. Knežević, A. Milani, eds.), IAUC197 **2004**, 209, 2004.

IAU Colloquium No. 197: „Dynamics of Populations of Planetary Systems”, Belgrade, Serbia,
September 1-5. 2004

8 страна

[E2]

M. Čubrović

Fully analytic kinetic model of resonance dynamics in the Solar system, Publ. Astron. Obs.
Belgrade **80**, 173, 2006.

Proceedings of the XIV National conference of astronomers of Serbia and Montenegro

5 страна

Саопштења са међународних скупова штампана у изводима (M34)

[F1]

M. Čubrović

DPG spring meeting, Berlin, Germany, March 15-20 2015: Dissipation-induced first order decoherence phase transition in a non-interacting fermionic system

[F2]

M. Čubrović

DPG spring meeting, Dresden, Germany, March 30-April 4 2014: Heavy fermion quantum critical point from AdS/CFT correspondence

[F3]

M. Čubrović, J. Zaanen, K. Schalm

Physics@FOM 2013, Veldhoven, Netherlands, January 22-24. 2013: The strange metals and Fermi liquids of holography

[F4]

M. Čubrović, K. Schalm, J. Zaanen

Physics@FOM 2012, Veldhoven, Netherlands, January 17-19. 2012: Novel stable phases of matter from AdS/CFT correspondence

[F5]

M. Čubrović, K. Schalm, J. Zaanen

SFKM2011 – Symposium on Physics of Condensed Matter, Belgrade, Serbia, April 2011: Fermionic quantum criticality from AdS/CFT correspondence

[F6]

M. Čubrović, J. Zaanen, K. Schalm

Physics@FOM 2011, Veldhoven, Netherlands, January 18-20. 2011: Geometry encoding for statistics: from Fermi liquids to Cooper pairing

[F7]

M. Čubrović

Let's Face Chaos Through Nonlinear Dynamics, Maribor, Slovenia, June 26. – July 10. 2005: Universality and scaling in nonlinear Hamiltonian systems – escape times, Lyapunov exponents and inverse chaotic scattering

Објављена докторска дисертација (M71)

Дана 27. фебруара 2013. године на Универзитету у Лајдену кандидат је одбранио докторску дисертацију “Holography, Fermi surfaces and Criticality” (Холографија, Фермијеве површи и критично понашање). Комисију за преглед и оцену тезе су чинили проф. Ј. Занен (супервизор), др. К. Схалм (косупервизор), проф. Х. Лу (Hong Liu), проф. Е. Елиел (E. Eliel), проф. Е. Верлинде (E. Verlinde), проф. Ц. В. Ј. Бенакер (C. W. J. Beenakker) и проф. Ј. М. Ван Рајтенбек (J. M. Van Ruitenbeek). Дисертација је објављена као: Holography, Fermi surfaces and Criticality, Casimir PhD Series, Delft-Leiden, 2013 (ISBN 978-90-8593-099-0).



Република Србија
МИНИСТАРСТВО ПРОСВЕТЕ,
НАУКЕ И ТЕХНОЛОШКОГ РАЗВОЈА

Број: 612-01-02635/2016-06

Датум: 09.01.2017. године

Немањина 22-26

Београд

ЈК

На основу члана 105б. став 4. Закона о високом образовању („Службени гласник РС”, бр. 76/05, аутентично тумачење – 100/07, 97/08, 44/10, 93/12, 89/13, 99/14, 45/15 – аутентично тумачење и 68/15), члана 192. став 1. Закона о општем управном поступку („Службени гласник СРЈ”, бр. 33/97 и 31/01. „Службени гласник РС”, број 30/10) и члана 23. став 2. Закона о државној управи („Службени гласник РС”, бр. 79/05, 101/07, 95/10 и 99/14), решавајући по захтеву Михаила Чубровића из Београда, Република Србија, за признавање високошколске исправе издате у Краљевини Холандији, ради запошљавања,

министар просвете, науке и технолошког развоја доноси

РЕШЕЊЕ

Диплома коју је 27.02.2013. године на име Михаило Чубровић издао Универзитет у Лајдену (Universiteit Leiden), Лајден, Краљевина Холандија, о завршеним докторским академским студијама, студијски програм: Физика, звање/квалификација: Doctor, **признаје се** као диплома докторских академских студија трећег степена високог образовања (180 ЕСПБ), у оквиру образовно-научног поља Природно-математичких наука, научна, односно стручне области Физичке науке, ради запошљавања.

Ово решење омогућава имаоцу општи приступ тржишту рада у Републици Србији, али га не ослобађа од испуњавања посебних услова за бављење професијама које су регулисане законом или другим прописом.

Образложење

Овом министарству обратило се Михаило Чубровић из Београда, Република Србија захтевом за признавање дипломе Универзитета у Лајдену (Universiteit Leiden), Лајден, Краљевина Холандија, о завршеним докторским академским студијама, студијски програм: Физика, звање/квалификација: Doctor, ради запошљавања.

Уз захтев, подносилац захтева доставио је:

- 1) оверену копију дипломе издате 27.02.2013. године, коју је издао Универзитет у Лајдену (Universiteit Leiden), Лајден, Краљевина Холандија, студије трећег степена високог образовања (180 ЕСПБ), студијски програм : Физика, звање/квалификација: Doctor,
- 2) оверени превод дипломе са латинског на енглески и са енглеског на српски језик,
- 3) апстракт рада на енглеском језику,
- 4) примерак докторске дисертације на изворном језику,
- 5) радну биографију и листу радова на енглеском језику,
- 6) пријавни формулар и
- 7) доказ о уплати таксе за професионално признавање.

Чланом 105 б. став 4. прописано је да Министар доноси решење о професионалном признавању у року од 90 дана од дана пријема уредног захтева.

Одредбама члана 192. Закона о општем управном поступку прописано је да на основу одлучних чињеница утврђених у поступку орган надлежан за решавање доноси решење у управној ствари која је предмет поступка.

Одредбама члана 23. став 2. Закона о државној управи прописано је да Министар представља Министарство, доноси прописе и решења у управним и другим појединачним стварима и одлучује о другим питањима из делокруга Министарства.

Чланом 104. став 1. Закона о високом образовању, прописано је да признавање стране високошколске исправе јесте поступак којим се имаоцу те исправе утврђује право на наставак образовања, односно на запошљавање. Поступак признавања стране високошколске исправе спроводи се у складу са одредбама овог закона, ако међународним уговором није предвиђено другачије.

Сходно одредбама члана 105. став 1. и 6. Закона о високом образовању и васпитању, ENIC/NARIC центар при Министарству просвете, науке и технолошког развоја, прибавио је релевантне информације о студијском програму на ком је стечена диплома из става 2. тачка 1) образложења овог решења.

У складу са чланом 105. став 4. Закона о високом образовању, комисија коју је именовао министар извршила је прво вредновање студијског програма на коме је стечена диплома из става 2. тачка 1) образложења овог решења, и дала предлог за признавање дипломе ради запошљавања.

Подносилац захтева је доставио доказ о уплати таксе у складу са чланом 2. став 1. Правилника о висини таксе за професионално признавање страних високошколских исправа („Службени гласник РС”, број 83/2015).

Имајући у виду наведено, решено је као у диспозитиву овог решења.

Упутство о правном средству: Ово решење је коначно у управном поступку и против истог може се покренути управни спор. Тужба се подноси Управном суду у року од 30 дана од дана пријема овог решења.

Решење доставити:

– Михаило Чубровић, ул. Мирослава Јовановића бр. 7/2, 11160 Београд и *

– Архива.

МИНИСТАР

Младен Шарчевић



RECTOR ET COLLEGIVM DECANORVM VNIVERSITATIS LVGDVNO-BATAVAE LECTORIBVS SALVTEM

SAPIENTI CONSILIO A MAIORIBVS NOSTRIS INSTITVTVM EST, VT BONARVM ARTIVM STVDIOSI, ANTEA QVAM DOCTRINAM SVAM AD COMMVNEM VITAE VSVM CONFERRENT, LAVDABILITER PERACTIS STVDIIS ACADEMICIS PVBLICVM PETERENT INDVSTRIAE ET ERVDITIONIS TESTIMONIVM ET DOCVMENTVM.

QVAMOBREM CVM ORNATISSIMVS *Mihailo Čubrović*

LEGIBVS ACADEMICIS SATISFECISSET ATQVE AD SVMMOS HONORES IAM CONTENDERET IPSIVS ERVDITIONI DEBITOS, NOS, QVO CAVSAM HONESTISSIMAM ADIVVAREMVS, CVM DE PROGRESSIBVS EIVS IN DISCIPLINIS AD FACVLTATEM

Mathematicae et disciplinarum naturalium

PERTINENTIBVS DISQVISATIONEM INSTITVIMVS TVM AVDIVIMVS EVM DEFENDENTEM SPECIMEN, QVOD INSCRIBITVR

Holography, Fermi surfaces and criticality

IN QVIBVS OMNIBVS CVM SESE TALEM PRAESTITERIT, VT NOBIS DOCTRINAM ET DILIGENTIAM PROBARET, HONORIFICVM QVOD EI DEBETVR VIRTVTIS TESTIMONIVM TRIBVIMVS. QVAPROPTER NOS PRO POTESTATE NOBIS CONCESSA EVNDEM

Mihailo Čubrović

DOCTOREM SOLLEMNI MORE CREAVIMVS ET RENVNTIAVIMVS ET EI CONCESSIMVS QVIDQVID IVRIS ET HONORIS DOCTORI LEGITIME CREATO AVT LEGE AVT LONGA CONSVETVDINE TRIBVI HABERIQVE SOLET. CVIVS REI QVO SIT CERTIOR ET TESTATOR FIDES, DIPLOMA HOC PVBLICVM MANV RECTORIS, PROMOTORIS NECNON ACTVARI SVBSCRIPTVM ET MAIORE VNIVERSITATIS SIGILLO CONFIRMATVM EI TRADENDVM CVRAVIMVS.

DATVM LVGDVNI BATAVORVM DIE *XXVII* MENSIS *Februarii* ANNI *MMXIII*



[Signature]

RECTOR MAGNIFICVS

[Signature]
PROMOTOR(ES)

[Signature]
ACTVARIVS

[Signature]

Web of Science™ InCites™ Journal Citation Reports® Essential Science Indicators™ EndNote™
Sign In Help English

WEB OF SCIENCE™

Search
My Tools Search History Marked List

Results: 12
(from Web of Science Core Collection)

Select articles grouped for author name **cubrovic m***

You searched for: AUTHOR:
(cubrovic m*) [...More](#)

Create Alert

Refine Results

Web of Science Categories

- PHYSICS PARTICLES FIELDS (6)
- ASTRONOMY ASTROPHYSICS (5)
- PHYSICS FLUIDS PLASMAS (1)
- PHYSICS CONDENSED MATTER (1)
- PHYSICS ATOMIC MOLECULAR CHEMICAL (1)

[more options / values...](#)

Refine

Document Types

- ARTICLE (10)
- PROCEEDINGS PAPER (2)

[more options / values...](#)

Refine

Research Areas

Authors

Group Authors

Editors

Source Titles

Book Series Titles

Conference Titles

Publication Years

Organizations-Enhanced

Sort by: **Times Cited -- highest to lowest**
Page 1 of 1

Select Page

Save to EndNote online
Add to Marked List

- 1. String Theory, Quantum Phase Transitions, and the Emergent Fermi Liquid**

By: **Cubrovic, Mihailo**; Zaanen, Jan; Schalm, Koenraad
 SCIENCE Volume: 325 Issue: 5939 Pages: 439-444
 Published: JUL 24 2009

View Abstract
- 2. Spectral probes of the holographic Fermi ground state: Dialing between the electron star and AdS Dirac hair**

By: **Cubrovic, Mihailo**; Liu, Yan; Schalm, Koenraad; et al.
 PHYSICAL REVIEW D Volume: 84 Issue: 8 Article Number: 086002
 Published: OCT 6 2011

View Abstract
- 3. Holographic fermions in external magnetic fields**

By: Gubankova, E.; Brill, J.; **Cubrovic, M.**; et al.
 PHYSICAL REVIEW D Volume: 84 Issue: 10 Article Number: 106003
 Published: NOV 2 2011

View Abstract
- 4. Constructing the AdS dual of a Fermi liquid: AdS black holes with Dirac hair**

By: **Cubrovic, Mihailo**; Zaanen, Jan; Schalm, Koenraad
 JOURNAL OF HIGH ENERGY PHYSICS Issue: 10 Article Number: 017
 Published: OCT 2011

View Abstract
- 5. Semistiff polymer model of unfolded proteins and its application to NMR residual dipolar couplings**

By: **Cubrovic, M.**; Obolensky, O. I.; Solov'yov, A. V.
 EUROPEAN PHYSICAL JOURNAL D Volume: 51 Issue: 1
 Pages: 41-49 Published: JAN 2009

View Abstract
- 6. Dissipation-induced first-order decoherence phase transition in a noninteracting fermionic system**

By: Medvedyeva, M. V.; **Cubrovic, M. T.**; Kehrein, S.
 PHYSICAL REVIEW B Volume: 91 Issue: 20 Article Number: 205416
 Published: MAY 13 2015

View Abstract
- 7. Quantum corrected phase diagram of holographic fermions**

By: Medvedyeva, Mariya V.; Gubankova, Elena; **Cubrovic, Mihailo**; et al.
 JOURNAL OF HIGH ENERGY PHYSICS Issue: 12 Article Number: 025
 Published: DEC 3 2013

View Abstract
- 8. Confinement/deconfinement transition from symmetry breaking in gauge/gravity duality**

Analyze Results

Create Citation Report

Times Cited: 270
(from Web of Science Core Collection)

Highly Cited Paper

Usage Count

Times Cited: 20
(from Web of Science Core Collection)

Usage Count

Times Cited: 17
(from Web of Science Core Collection)

Usage Count

Times Cited: 14
(from Web of Science Core Collection)

Usage Count

Times Cited: 5
(from Web of Science Core Collection)

Usage Count

Times Cited: 3
(from Web of Science Core Collection)

Usage Count

Times Cited: 3
(from Web of Science Core Collection)

Usage Count

Times Cited: 1
(from Web of Science Core Collection)

- Funding Agencies
- Languages
- Countries/Territories
- ESI Top Papers
- Open Access

For advanced refine options, use

Analyze Results

| | | |
|-------------------------------|--|--|
| | By: Cubrovic, Mihailo JOURNAL OF HIGH ENERGY PHYSICS Issue: 10 Article Number: 102 Published: OCT 19 2016 | Collection) Usage Count |
| View Abstract | | |
| 9. | Fractional kinetic model for chaotic transport in nonintegrable Hamiltonian systems By: Cubrovic, M PHYSICAL REVIEW E Volume: 72 Issue: 2 Article Number: 025204 Part: 2 Published: AUG 2005 | Times Cited: 1 (from Web of Science Core Collection) Usage Count |
| | View Abstract | |
| 10. | Exciton-driven quantum phase transitions in holography By: Gubankova, E.; Cubrovic, M. ; Zaanen, J. PHYSICAL REVIEW D Volume: 92 Issue: 8 Article Number: 086004 Published: OCT 28 2015 | Times Cited: 0 (from Web of Science Core Collection) Usage Count |
| | View Abstract | |
| 11. | Fully analytical kinetic model of resonance dynamics in the solar system By: Cubrovic, Mihailo Edited by: Knezevic, Z; Cvetkovic, Z; Cirkovic, MM Conference: 14th National Conference of Astronomers of Serbia and Montenegro Location: Belgrade, SERBIA Date: OCT 12-15, 2005 Proceedings of the 14th National Conference of Astronomers of Serbia and Montenegro Book Series: PUBLICATIONS OF THE ASTRONOMICAL OBSERVATORY OF BELGRADE--SERIES Issue: 80 Pages: 173-177 Published: 2006 | Times Cited: 0 (from Web of Science Core Collection) Usage Count |
| | View Abstract | |
| 12. | Regimes of stability and scaling relations for the removal time in the asteroid belt: a simple kinetic model and numerical tests By: Cubrovic, Mihailo Edited by: Knezevic, Z; Milani, A Conference: 197th Colloquium of the International-Astronomical-Union Location: Belgrade, SERBIA MONTENEG Date: AUG 31-SEP 04, 2004 Sponsor(s): Int Astron Union; IAU Div 1 & Div 3; IAU No 7, No 20 & No 22 Dynamics of Populations of Planetary Systems Book Series: IAU COLLOQUIUM Volume: 197 Pages: 209-216 Published: 2005 | Times Cited: 0 (from Web of Science Core Collection) Usage Count |
| | View Abstract | |

Select Page [Save to EndNote online](#) [Add to Marked List](#)

Sort by: [Times Cited -- highest to lowest](#)
 Show: [50 per page](#)

12 records matched your query of the 36,466,594 in the data limits you selected.

Citation Report: 12

(from Web of Science Core Collection)

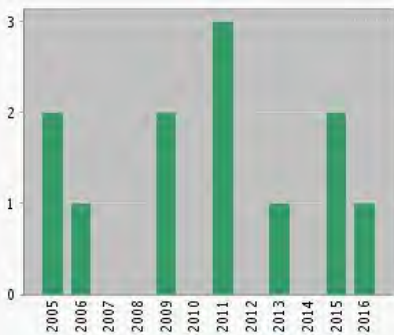
You searched for: **AUTHOR:** (cubrovic m*)

Timespan: All years. Indexes: SCI-EXPANDED, SSCI, A&HCI, CPCI-S, CPCI-SSH, ESCI.

[...Less](#)

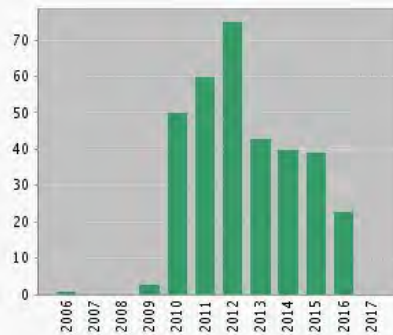
This report reflects citations to source items indexed within Web of Science Core Collection. Perform a Cited Reference Search to include citations to items not indexed within Web of Science Core Collection.

Published Items in Each Year



The latest 20 years are displayed.

Citations in Each Year



The latest 20 years are displayed.

| | |
|---|-------|
| Results found: | 12 |
| Sum of the Times Cited [?] | 334 |
| Sum of Times Cited without self-citations [?] | 323 |
| Citing Articles [?] | 292 |
| Citing Articles without self-citations [?] | 286 |
| Average Citations per Item [?] | 27.83 |
| h-index [?] | 5 |

Sort by: Times Cited -- highest to lowest

Page 1 of 2

| | 2013 | 2014 | 2015 | 2016 | 2017 | Total | Average Citations per Year |
|--|------|------|------|------|------|-------|----------------------------|
| Use the checkboxes to remove individual items from this Citation Report or restrict to items published between 1996 and 2017 | 43 | 40 | 39 | 23 | 0 | 334 | 27.83 |
| 1. String Theory, Quantum Phase Transitions, and the Emergent Fermi Liquid By: Cubrovic, Mihailo; Zaanen, Jan; Schalm, Koenraad SCIENCE Volume: 325 Issue: 5939 Pages: 439-444 Published: JUL 24 2009 | 33 | 30 | 30 | 16 | 0 | 270 | 30.00 |
| 2. Spectral probes of the holographic Fermi ground state: Dialing between the electron star and AdS Dirac hair By: Cubrovic, Mihailo; Liu, Yan; Schalm, Koenraad; et al. PHYSICAL REVIEW D Volume: 84 Issue: 8 Article Number: 086002 Published: OCT 6 2011 | 4 | 4 | 1 | 1 | 0 | 20 | 2.86 |
| 3. Holographic fermions in external magnetic fields By: Gubankova, E.; Brill, J.; Cubrovic, M.; et al. PHYSICAL REVIEW D Volume: 84 Issue: 10 Article Number: 106003 Published: NOV 2 2011 | 3 | 2 | 4 | 1 | 0 | 17 | 2.43 |
| 4. Constructing the AdS dual of a Fermi liquid: AdS black holes with Dirac hair By: Cubrovic, Mihailo; Zaanen, Jan; Schalm, Koenraad JOURNAL OF HIGH ENERGY PHYSICS Issue: 10 Article Number: 017 Published: OCT 2011 | 3 | 2 | 1 | 1 | 0 | 14 | 2.00 |
| 5. Semistiff polymer model of unfolded proteins and its application to NMR residual dipolar couplings By: Cubrovic, M.; Obolensky, O. I.; Solov'yov, A. V. EUROPEAN PHYSICAL JOURNAL D Volume: 51 Issue: 1 Pages: 41-49 | 0 | 2 | 0 | 0 | 0 | 5 | 0.56 |

Published: JAN 2009

6. **Dissipation-induced first-order decoherence phase transition in a noninteracting fermionic system**

By: Medvedyeva, M. V.; Cubrovic, M. T.; Kehrein, S.
 PHYSICAL REVIEW B Volume: 91 Issue: 20 Article Number: 205416
 Published: MAY 13 2015

7. **Quantum corrected phase diagram of holographic fermions**

By: Medvedyeva, Mariya V.; Gubankova, Elena; Cubrovic, Mihailo; et al.
 JOURNAL OF HIGH ENERGY PHYSICS Issue: 12 Article Number: 025
 Published: DEC 3 2013

8. **Confinement/deconfinement transition from symmetry breaking in gauge/gravity duality**

By: Cubrovic, Mihailo
 JOURNAL OF HIGH ENERGY PHYSICS Issue: 10 Article Number: 102
 Published: OCT 19 2016

9. **Fractional kinetic model for chaotic transport in nonintegrable Hamiltonian systems**

By: Cubrovic, M
 PHYSICAL REVIEW E Volume: 72 Issue: 2 Article Number: 025204 Part: 2
 Published: AUG 2005

10. **Exciton-driven quantum phase transitions in holography**

By: Gubankova, E.; Cubrovic, M.; Zaanen, J.
 PHYSICAL REVIEW D Volume: 92 Issue: 8 Article Number: 086004
 Published: OCT 28 2015

| | | | | | | |
|---|---|---|---|---|---|------|
| 0 | 0 | 0 | 3 | 0 | 3 | 1.00 |
| 0 | 0 | 3 | 0 | 0 | 3 | 0.60 |
| 0 | 0 | 0 | 1 | 0 | 1 | 0.50 |
| 0 | 0 | 0 | 0 | 0 | 1 | 0.08 |
| 0 | 0 | 0 | 0 | 0 | 0 | 0.00 |

Select Page



Save to Text File



Sort by: Times Cited -- highest to lowest

Page 1 of 2

12 records matched your query of the 36,466,594 in the data limits you selected.

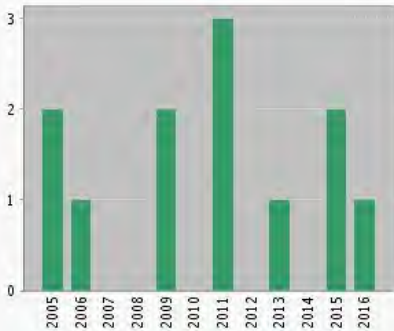
Citation Report: 12

(from Web of Science Core Collection)

You searched for: **AUTHOR:** (cubrovic m*) ...More

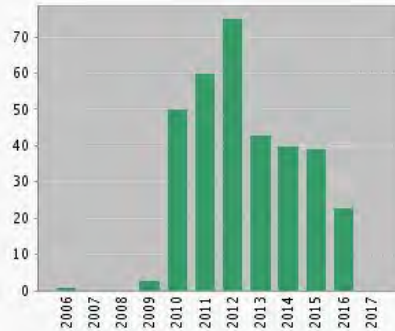
This report reflects citations to source items indexed within Web of Science Core Collection. Perform a Cited Reference Search to include citations to items not indexed within Web of Science Core Collection.

Published Items in Each Year



The latest 20 years are displayed.

Citations in Each Year



The latest 20 years are displayed.

| | |
|--|-------|
| Results found: | 12 |
| Sum of the Times Cited [?]: | 334 |
| Sum of Times Cited without self-citations [?]: | 323 |
| Citing Articles [?]: | 292 |
| Citing Articles without self-citations [?]: | 286 |
| Average Citations per Item [?]: | 27.83 |
| h-index [?]: | 5 |

Sort by: Times Cited -- highest to lowest

Page 2 of 2

Use the checkboxes to remove individual items from this Citation Report

or restrict to items published between 1996 and 2017 Go

11. **Fully analytical kinetic model of resonance dynamics in the solar system**

By: Cubrovic, Mihailo
 Edited by: Knezevic, Z; Cvetkovic, Z; Cirkovic, MM
 Conference: 14th National Conference of Astronomers of Serbia and Montenegro
 Location: Belgrade, SERBIA Date: OCT 12-15, 2005
 Proceedings of the 14th National Conference of Astronomers of Serbia and Montenegro Book Series: PUBLICATIONS OF THE ASTRONOMICAL OBSERVATORY OF BELGRADE--SERIES Issue: 80 Pages: 173-177
 Published: 2006

12. **Regimes of stability and scaling relations for the removal time in the asteroid belt: a simple kinetic model and numerical tests**

By: Cubrovic, Mihailo
 Edited by: Knezevic, Z; Milani, A
 Conference: 197th Colloquium of the International-Astronomical-Union Location: Belgrade, SERBIA MONTENEG Date: AUG 31-SEP 04, 2004
 Sponsor(s): Int Astron Union; IAU Div 1 & Div 3; IAU No 7, No 20 & No 22
 Dynamics of Populations of Planetary Systems Book Series: IAU COLLOQUIUM Volume: 197 Pages: 209-216 Published: 2005

| | 2013 | 2014 | 2015 | 2016 | 2017 | Total | Average Citations per Year |
|--|------|------|------|------|------|-------|----------------------------|
| | 43 | 40 | 39 | 23 | 0 | 334 | 27.83 |
| 11. Fully analytical kinetic model of resonance dynamics in the solar system | 0 | 0 | 0 | 0 | 0 | 0 | 0.00 |
| 12. Regimes of stability and scaling relations for the removal time in the asteroid belt: a simple kinetic model and numerical tests | 0 | 0 | 0 | 0 | 0 | 0 | 0.00 |

Select Page Save to Text File

Sort by: Times Cited -- highest to lowest

Page 2 of 2

12 records matched your query of the 36,466,594 in the data limits you selected.



© 2017 [THOMSON REUTERS](#)

[TERMS OF USE](#)

[PRIVACY POLICY](#)

[FEEDBACK](#)

| | | | | | | | |
|-----------------|----------|---------------------------|-------------------------------|----------|-----------|------|-----------|
| Web of Science™ | InCites™ | Journal Citation Reports® | Essential Science Indicators™ | EndNote™ | Sign In ▾ | Help | English ▾ |
|-----------------|----------|---------------------------|-------------------------------|----------|-----------|------|-----------|

Search
Return to Search Results
My Tools ▾
Search History
Marked List

Citing Articles: 263
(from Web of Science Core Collection)

For: String Theory, Quantum Phase Transitions, and the Emergent Fermi Liquid ...[More](#)

Times Cited Counts
270 in All Databases

270 in Web of Science Core Collection

2 in BIOSIS Citation Index

4 in Chinese Science Citation Database

0 data sets in Data Citation Index

0 publication in Data Citation Index

1 in Russian Science Citation Index

0 in SciELO Citation Index

[View Additional Times Cited Counts](#)

Refine Results

Web of Science Categories ▾

- PHYSICS PARTICLES FIELDS (198)
- ASTRONOMY ASTROPHYSICS (81)
- PHYSICS MULTIDISCIPLINARY (38)
- PHYSICS CONDENSED MATTER (23)
- PHYSICS NUCLEAR (14)

[more options / values...](#)

Refine

Document Types ▾

- ARTICLE (254)
- REVIEW (9)
- PROCEEDINGS PAPER (4)
- BOOK CHAPTER (1)

[more options / values...](#)

Refine

Research Areas ▾

Authors ▾



Group Authors ▾

Editors ▾

Source Titles ▾

Sort by: **Publication Date -- newest to oldest** ▾

◀ Page 1 of 6 ▶

Select Page
 
Save to EndNote online ▾
Add to Marked List

[Analyze Results](#)

[Create Citation Report](#)

1. **Realizing infrared power-law liquids in the cuprates from unparticle interactions**

By: Limtragool, Kridsanaphong; Setty, Chandan; Leong, Zhidong; et al.

PHYSICAL REVIEW B Volume: 94 Issue: 23 Article Number: 235121 Published: DEC 8 2016

[View Abstract](#)
2. **Holographic fermions at strong translational symmetry breaking: a Bianchi-VII case study**

By: Bagrov, A.; Kaplis, N.; Krikun, A.; et al.

JOURNAL OF HIGH ENERGY PHYSICS Issue: 11 Article Number: 057 Published: NOV 9 2016

[View Abstract](#)
3. **Understanding strongly coupling magnetism from holographic duality**

By: Cai, Rong-Gen; Yang, Run-Qiu

Conference: 2nd LeCosPA International Symposium on Everything about Gravity Location: Taipei, TAIWAN Date: DEC 14-18, 2015

Sponsor(s): LeCosPA; Assoc Asia Pacific Phys Soc, Div Astrophys Cosmol Grav

INTERNATIONAL JOURNAL OF MODERN PHYSICS D Volume: 25 Issue: 13 Special Issue: SI Article Number: 1645011 Published: NOV 2016

[Full Text from Publisher](#)
[View Abstract](#)
4. **Engineering holographic phase diagrams**

By: Chen, Jiunn-Wei; Dai, Shou-Huang; Maity, Debaprasad; et al.

PHYSICAL REVIEW D Volume: 94 Issue: 8 Article Number: 086004 Published: OCT 10 2016

[View Abstract](#)
5. **Magnetocaloric and magnetic properties of La₂NiMnO₆ double perovskite**

By: Masrour, R.; Jabbar, A.

CHINESE PHYSICS B Volume: 25 Issue: 8 Article Number: 087502 Published: AUG 2016

[View Abstract](#)
6. **Large N thirring matter in three dimensions**

By: Goykhman, Mikhail

JOURNAL OF HIGH ENERGY PHYSICS Issue: 7 Article Number: 034 Published: JUL 7 2016

[View Abstract](#)
7. **Quick introduction into AdS/CFT correspondence in physics of strongly correlated systems**

By: Belonenko, M. B.; Konobeeva, N. N.; Galkina, E. N.

NANOSYSTEMS-PHYSICS CHEMISTRY MATHEMATICS Volume: 7 Issue: 3 Pages: 410-421 Published: JUN 2016

Times Cited: 0
(from Web of Science Core Collection)

Usage Count ▾

Times Cited: 0
(from Web of Science Core Collection)

Usage Count ▾

| | |
|------------------------|---|
| Book Series Titles | ◀ |
| Conference Titles | ◀ |
| Publication Years | ◀ |
| Organizations-Enhanced | ◀ |
| Funding Agencies | ◀ |
| Languages | ◀ |
| Countries/Territories | ◀ |
| ESI Top Papers | ◀ |
| Open Access | ◀ |

For advanced refine options, use

Analyze Results

- [View Abstract](#)
8. **Dense Chern-Simons matter with fermions at large N**
 By: Geracie, Michael; Goykhman, Mikhail; Son, Dam T.
JOURNAL OF HIGH ENERGY PHYSICS Issue: 4 Article Number: 103 Published: APR 18 2016

[View Abstract](#)

Times Cited: 3
(from Web of Science Core Collection)
Usage Count ▾
 9. **Pseudo-gap phase and duality in a holographic fermionic system with dipole coupling on Q-lattice**
 By: Ling, Yi; Liu, Peng; Niu, Chao; et al.
CHINESE PHYSICS C Volume: 40 Issue: 4 Article Number: 043102 Published: APR 2016

[View Abstract](#)

Times Cited: 0
(from Web of Science Core Collection)
Usage Count ▾
 10. **Few cycle pulses in semi-holographic Fermi liquid with impurities**
 By: Belonenko, Mikhail B.; Konobeeva, Natalia N.; Galkina, Elena N.
MODERN PHYSICS LETTERS B Volume: 30 Issue: 8 Article Number: 1650092 Published: MAR 30 2016

[Full Text from Publisher](#) [View Abstract](#)

Times Cited: 0
(from Web of Science Core Collection)
Usage Count ▾
 11. **Quantum Phase Transition between a Topological and a Trivial Semimetal from Holography**
 By: Landsteiner, Karl; Liu, Yan; Sun, Ya-Wen
PHYSICAL REVIEW LETTERS Volume: 116 Issue: 8 Article Number: 081602 Published: FEB 25 2016

[View Abstract](#)

Times Cited: 2
(from Web of Science Core Collection)
Usage Count ▾
 12. **Crowd behavior analysis: A review where physics meets biology**
 By: Kok, Ven Jyn; Lim, Mei Kuan; Chan, Chee Seng
NEUROCOMPUTING Volume: 177 Pages: 342-362 Published: FEB 12 2016

[Full Text from Publisher](#) [View Abstract](#)

Times Cited: 0
(from Web of Science Core Collection)
Usage Count ▾
 13. **Holographic competition of phases and superconductivity**
 By: Kiritsis, Elias; Li, Li
JOURNAL OF HIGH ENERGY PHYSICS Issue: 1 Article Number: 147 Published: JAN 25 2016

[View Abstract](#)

Times Cited: 3
(from Web of Science Core Collection)
Usage Count ▾
 14. **Fermionic response in finite-density ABJM theory with broken symmetry**
 By: DeWolfe, Oliver; Gubser, Steven S.; Henriksson, Oscar; et al.
PHYSICAL REVIEW D Volume: 93 Issue: 2 Article Number: 026001 Published: JAN 12 2016

[View Abstract](#)

Times Cited: 0
(from Web of Science Core Collection)
Usage Count ▾
 15. **Semiholographic Approach in Calculation of Tunneling Current in Graphene with Deep Impurities**
 By: Belonenko, M. B.; Konobeeva, N. N.
JOURNAL OF NANO- AND ELECTRONIC PHYSICS Volume: 8 Issue: 4 Article Number: 04029 Published: 2016

[Full Text from Publisher](#) [View Abstract](#)

Times Cited: 0
(from Web of Science Core Collection)
Usage Count ▾
 16. **DEMISTIFYING THE HOLOGRAPHIC MYSTIQUE: A CRITICAL REVIEW**
 By: Khveshchenko, D. V.
LITHUANIAN JOURNAL OF PHYSICS Volume: 56 Issue: 3 Pages: 125-148 Published: 2016

[View Abstract](#)

Times Cited: 0
(from Web of Science Core Collection)
Usage Count ▾
 17. **Propagation of few cycle optical pulses in marginal Fermi liquid and ADS/CFT correspondence**

Times Cited: 1
(from Web of Science Core Collection)

- By: Konobeeva, N. N.; Belonenko, M. B.
PHYSICA B-CONDENSED MATTER Volume: 478 Pages: 43-46 Published: DEC 1 2015
[Full Text from Publisher](#) [View Abstract](#)
 Collection) **Usage Count**
18. **Scaling of the holo graphic AC conductivity for non-Fermi liquids at criticality**
 By: Kiritzis, Elias; Pena-Benitez, Francisco
JOURNAL OF HIGH ENERGY PHYSICS Issue: 11 Article Number: 177 Published: NOV 25 2015
[View Abstract](#)
Times Cited: 1
(from Web of Science Core Collection)
Usage Count
19. **Fermionic phase transition induced by the effective impurity in holography**
 By: Fang, Li -Qing; Kuang, Xiao-Mei; Wang, Bin; et al.
JOURNAL OF HIGH ENERGY PHYSICS Issue: 11 Article Number: 134 Published: NOV 20 2015
[View Abstract](#)
Times Cited: 0
(from Web of Science Core Collection)
Usage Count
20. **Bekenstein-Hawking Entropy and Strange Metals**
 By: Sachdev, Subir
PHYSICAL REVIEW X Volume: 5 Issue: 4 Published: NOV 13 2015
[Full Text from Publisher](#) [View Abstract](#)
Times Cited: 18
(from Web of Science Core Collection)
Usage Count
21. **Massive 2-form field and holographic ferromagnetic phase transition**
 By: Cai, Rong-Gen; Yang, Run-Qiu; Wu, Ya-Bo; et al.
JOURNAL OF HIGH ENERGY PHYSICS Issue: 11 Article Number: 021 Published: NOV 5 2015
[View Abstract](#)
Times Cited: 2
(from Web of Science Core Collection)
Usage Count
22. **Insulator/metal phase transition and colossal magnetoresistance in holographic model**
 By: Cai, Rong-Gen; Yang, Run-Qiu
PHYSICAL REVIEW D Volume: 92 Issue: 10 Article Number: 106002 Published: NOV 5 2015
[View Abstract](#)
Times Cited: 4
(from Web of Science Core Collection)
Usage Count
23. **Emergence in holographic scenarios for gravity**
 By: Dieks, Dennis; van Dongen, Jeroen; de Haro, Sebastian
STUDIES IN HISTORY AND PHILOSOPHY OF MODERN PHYSICS Volume: 52 Pages: 203-216 Part: B Published: NOV 2015
[Full Text from Publisher](#) [View Abstract](#)
Times Cited: 2
(from Web of Science Core Collection)
Usage Count
24. **Holographic model for antiferromagnetic quantum phase transition induced by magnetic field**
 By: Cai, Rong-Gen; Yang, Run-Qiu; Kusmartsev, F. V.
PHYSICAL REVIEW D Volume: 92 Issue: 8 Article Number: 086001 Published: OCT 7 2015
[View Abstract](#)
Times Cited: 2
(from Web of Science Core Collection)
Usage Count
25. **Entanglement entropy of magnetic electron stars**
 By: Albash, Tameem; Johnson, Clifford V.; MacDonald, Scott
JOURNAL OF HIGH ENERGY PHYSICS Issue: 9 Article Number: 173 Published: SEP 24 2015
[View Abstract](#)
Times Cited: 0
(from Web of Science Core Collection)
Usage Count
26. **Holographic antiferromagnetic quantum criticality and AdS(2) scaling limit**
 By: Cai, Rong-Gen; Yang, Run-Qiu; Kusmartsev, F. V.
PHYSICAL REVIEW D Volume: 92 Issue: 4 Article Number: 046005 Published: AUG 27 2015
[View Abstract](#)
Times Cited: 3
(from Web of Science Core Collection)
Usage Count
27. **Ab initio holography**
Times Cited: 3

By: Lunts, Peter; Bhattacharjee, Subhro; Miller, Jonah; et al.
JOURNAL OF HIGH ENERGY PHYSICS Issue: 8 Article
 Number: 107 Published: AUG 21 2015

[View Abstract](#)

(from Web of Science Core
 Collection)

Usage Count 

28. **Antisymmetric tensor field and spontaneous magnetization in holographic duality**

By: Cai, Rong-Gen; Yang, Run-Qiu
PHYSICAL REVIEW D Volume: 92 Issue: 4 Article Number:
 046001 Published: AUG 10 2015

[View Abstract](#)

Times Cited: 6
 (from Web of Science Core
 Collection)

Usage Count 

29. **Strange metal without magnetic criticality**

By: Tomita, Takahiro; Kuga, Kentaro; Uwatoko, Yoshiya; et al.
SCIENCE Volume: 349 Issue: 6247 Pages: 506-509
 Published: JUL 31 2015

[View Abstract](#)

Times Cited: 15
 (from Web of Science Core
 Collection)

Usage Count 

30. **Anomalous magnetoconductivity and relaxation times in holography**

By: Jimenez-Alba, Amadeo; Landsteiner, Karl; Liu, Yan; et al.
JOURNAL OF HIGH ENERGY PHYSICS Issue: 7 Article
 Number: 117 Published: JUL 22 2015

[View Abstract](#)

Times Cited: 8
 (from Web of Science Core
 Collection)

Usage Count 

31. **Dynamics of few cycle optical pulses in a non-Fermi liquid and AdS/CFT correspondence**

By: Belonenko, Mikhail B.; Konobeeva, Natalia N.; Galkina, Elena
 N.
MODERN PHYSICS LETTERS B Volume: 29 Issue: 19
 Article Number: 1550096 Published: JUL 20 2015

[Full Text from Publisher](#)

[View Abstract](#)

Times Cited: 1
 (from Web of Science Core
 Collection)

Usage Count 

32. **Fermi surface behavior in the ABJM M2-brane theory**

By: DeWolfe, Oliver; Henriksson, Oscar; Rosen, Christopher
PHYSICAL REVIEW D Volume: 91 Issue: 12 Article
 Number: 126017 Published: JUN 29 2015

[View Abstract](#)

Times Cited: 1
 (from Web of Science Core
 Collection)

Usage Count 

33. **Anisotropic Fermi surface from holography**

By: Fang, Li Qing; Ge, Xian-hui; Wu, Jian-Pin; et al.
PHYSICAL REVIEW D Volume: 91 Issue: 12 Article
 Number: 126009 Published: JUN 17 2015

[View Abstract](#)

Times Cited: 4
 (from Web of Science Core
 Collection)

Usage Count 

34. **Introduction to holographic superconductor models**

By: Cai RongGen; Li Li; Li LiFang; et al.
SCIENCE CHINA-PHYSICS MECHANICS & ASTRONOMY
 Volume: 58 Issue: 6 Article Number: UNSP 060401
 Published: JUN 2015

[View Abstract](#)

Times Cited: 54
 (from Web of Science Core
 Collection)

 **Highly Cited Paper**

Usage Count 

35. **Dynamically generated gap from holography in the charged black brane with hyperscaling violation**

By: Kuang, Xiao-Mei; Papantonopoulos, Eleftherios; Wang, Bin;
 et al.
JOURNAL OF HIGH ENERGY PHYSICS Issue: 4 Article
 Number: 137 Published: APR 24 2015

[View Abstract](#)

Times Cited: 5
 (from Web of Science Core
 Collection)

Usage Count 











36. **Towards a field-theory interpretation of bottom-up holography**

By: Jacobs, V. P. J.; Grubinskas, S.; Stoof, H. T. C.
JOURNAL OF HIGH ENERGY PHYSICS Issue: 4 Article
 Number: 033 Published: APR 8 2015

[View Abstract](#)

Times Cited: 2
 (from Web of Science Core
 Collection)

Usage Count 

37. **Magnetic oscillations in a holographic liquid**
By: Puletti, V. Giangreco M.; Nowling, S.; Thorlacius, L.; et al.
PHYSICAL REVIEW D Volume: 91 Issue: 8 Article Number: 086008 Published: APR 8 2015
[View Abstract](#)
Times Cited: 0
(from Web of Science Core Collection)
Usage Count 
38. **Holographic superconducting quantum interference device**
By: Takeuchi, Shingo
INTERNATIONAL JOURNAL OF MODERN PHYSICS A
Volume: 30 Issue: 9 Article Number: 1550040 Published: MAR 30 2015
[Full Text from Publisher](#) [View Abstract](#)
Times Cited: 4
(from Web of Science Core Collection)
Usage Count 
39. **Quasilocal strange metal**
By: Sur, Shouvik; Lee, Sung-Sik
PHYSICAL REVIEW B Volume: 91 Issue: 12 Article Number: 125136 Published: MAR 23 2015
[View Abstract](#)
Times Cited: 15
(from Web of Science Core Collection)
Usage Count 
40. **Holographic Fermi surfaces at finite temperature in top-down constructions**
By: Cosnier-Horeau, Charles; Gubser, Steven S.
PHYSICAL REVIEW D Volume: 91 Issue: 6 Article Number: 066002 Published: MAR 6 2015
[View Abstract](#)
Times Cited: 1
(from Web of Science Core Collection)
Usage Count 
41. **Analogue holographic correspondence in optical metamaterials**
By: Khveshchenko, D. V.
EPL Volume: 109 Issue: 6 Article Number: 61001 Published: MAR 2015
[View Abstract](#)
Times Cited: 1
(from Web of Science Core Collection)
Usage Count 
42. **Fermionic response in a zero entropy state of N=4 super-Yang-Mills**
By: DeWolfe, Oliver; Gubser, Steven S.; Rosen, Christopher
PHYSICAL REVIEW D Volume: 91 Issue: 4 Article Number: 046011 Published: FEB 26 2015
[View Abstract](#)
Times Cited: 3
(from Web of Science Core Collection)
Usage Count 
43. **Coexistence and competition of ferromagnetism and p-wave superconductivity in holographic model**
By: Cai, Rong-Gen; Yang, Run-Qiu
PHYSICAL REVIEW D Volume: 91 Issue: 2 Article Number: 026001 Published: JAN 6 2015
[View Abstract](#)
Times Cited: 13
(from Web of Science Core Collection)
Usage Count 
44. **TAKING A CRITICAL LOOK AT HOLOGRAPHIC CRITICAL MATTER**
By: Khveshchenko, D. V.
LITHUANIAN JOURNAL OF PHYSICS Volume: 55 Issue: 3 Pages: 208-226 Published: 2015
[View Abstract](#)
Times Cited: 1
(from Web of Science Core Collection)
Usage Count 
45. **Holographic Fermions in Anisotropic Einstein-Maxwell-Dilaton-Axion Theory**
By: Fang, Li-Qing; Kuang, Xiao-Mei
ADVANCES IN HIGH ENERGY PHYSICS Article Number: 658607 Published: 2015
[Full Text from Publisher](#) [View Abstract](#)
Times Cited: 0
(from Web of Science Core Collection)
Usage Count 
46. **Duality between zeroes and poles in holographic systems with massless fermions and a dipole coupling**
By: Alsup, James; Papantonopoulos, Eleftherios; Siopsis, George; et al.
PHYSICAL REVIEW D Volume: 90 Issue: 12 Article Number: 126013 Published: DEC 30 2014
Times Cited: 6
(from Web of Science Core Collection)
Usage Count 

[View Abstract](#)47. **Holographic phase transition and quasinormal modes in Lovelock gravity**

By: Lin, Kai; de Oliveira, Jeferson; Abdalla, Elcio
 PHYSICAL REVIEW D Volume: 90 Issue: 12 Article
 Number: 124071 Published: DEC 24 2014

Times Cited: 4
 (from Web of Science Core Collection)

Usage Count [View Abstract](#)48. **Holographic fermionic system with dipole coupling on Q-lattice**

By: Ling, Yi; Liu, Peng; Niu, Chao; et al.
 JOURNAL OF HIGH ENERGY PHYSICS Issue: 12 Article
 Number: 149 Published: DEC 22 2014

Times Cited: 9
 (from Web of Science Core Collection)

Usage Count [View Abstract](#)49. **Formation of Fermi surfaces and the appearance of liquid phases in holographic theories with hyperscaling violation**

By: Kuang, Xiao-Mei; Papantonopoulos, Eleftherios; Wang, Bin; et al.
 JOURNAL OF HIGH ENERGY PHYSICS Issue: 11 Article
 Number: 086 Published: NOV 18 2014

Times Cited: 8
 (from Web of Science Core Collection)

Usage Count [View Abstract](#)50. **Holographic quenches and fermionic spectral functions**

By: Callebaut, N.; Craps, B.; Galli, F.; et al.
 JOURNAL OF HIGH ENERGY PHYSICS Issue: 10 Article
 Number: 172 Published: OCT 30 2014

Times Cited: 3
 (from Web of Science Core Collection)

Usage Count [View Abstract](#)

Select Page

[Save to EndNote online](#) [Add to Marked List](#)Sort by: **Publication Date -- newest to oldest**

◀ Page 1 of 6 ▶

Show: **50 per page**

263 records matched your query of the 36,466,594 in the data limits you selected.

| | | | | | | | |
|-----------------|----------|---------------------------|-------------------------------|----------|-----------|------|-----------|
| Web of Science™ | InCites™ | Journal Citation Reports® | Essential Science Indicators™ | EndNote™ | Sign In ▾ | Help | English ▾ |
|-----------------|----------|---------------------------|-------------------------------|----------|-----------|------|-----------|

WEB OF SCIENCE™

Search
Return to Search Results
My Tools ▾
Search History
Marked List

Citing Articles: 263
(from Web of Science Core Collection)

For: String Theory, Quantum Phase Transitions, and the Emergent Fermi Liquid ...[More](#)

Times Cited Counts
270 in All Databases

270 in Web of Science Core Collection

2 in BIOSIS Citation Index

4 in Chinese Science Citation Database

0 data sets in Data Citation Index

0 publication in Data Citation Index

1 in Russian Science Citation Index

0 in SciELO Citation Index

[View Additional Times Cited Counts](#)

Refine Results

Web of Science Categories ▾

- PHYSICS PARTICLES FIELDS (198)
- ASTRONOMY ASTROPHYSICS (81)
- PHYSICS MULTIDISCIPLINARY (38)
- PHYSICS CONDENSED MATTER (23)
- PHYSICS NUCLEAR (14)

[more options / values...](#)

Refine

Document Types ▾

- ARTICLE (254)
- REVIEW (9)
- PROCEEDINGS PAPER (4)
- BOOK CHAPTER (1)

[more options / values...](#)

Refine

Research Areas ▾

Authors ▾

Group Authors ▾

Editors ▾

Source Titles ▾

Sort by: Publication Date -- newest to oldest ▾
 Page of 6

Select Page

Save to EndNote online ▾
 Add to Marked List

51. **QCD and strongly coupled gauge theories: challenges and perspectives**
By: Brambilla, N.; Eidelman, S.; Foka, P.; et al.
EUROPEAN PHYSICAL JOURNAL C Volume: 74 Issue: 10
Article Number: 2981 Published: OCT 21 2014

View Abstract

Analyze Results

Create Citation Report

Times Cited: 123
(from Web of Science Core Collection)

Highly Cited Paper

Usage Count ▾

52. **Paramagnetism-ferromagnetism phase transition in a dyonic black hole**
By: Cai, Rong-Gen; Yang, Run-Qiu
PHYSICAL REVIEW D Volume: 90 Issue: 8 Article Number: 081901 Published: OCT 14 2014

View Abstract

Times Cited: 16
(from Web of Science Core Collection)

Usage Count ▾

53. **Pseudogap phenomena in ultracold atomic Fermi gases**
By: Chen, Qijin; Wang, Jibiao
FRONTIERS OF PHYSICS Volume: 9 Issue: 5 Pages: 539-570 Published: OCT 2014

View Abstract

Times Cited: 9
(from Web of Science Core Collection)

Usage Count ▾

54. **Pairing induced superconductivity in holography**
By: Bagrov, Andrey; Meszner, Balazs; Schalm, Koenraad
JOURNAL OF HIGH ENERGY PHYSICS Issue: 9 Article Number: 106 Published: SEP 18 2014

View Abstract

Times Cited: 0
(from Web of Science Core Collection)

Usage Count ▾

55. **Optical Response of Sr2RuO4 Reveals Universal Fermi-Liquid Scaling and Quasiparticles Beyond Landau Theory**
By: Stricker, D.; Mravlje, J.; Berthod, C.; et al.
PHYSICAL REVIEW LETTERS Volume: 113 Issue: 8 Article Number: 087404 Published: AUG 22 2014

View Abstract

Times Cited: 12
(from Web of Science Core Collection)

Usage Count ▾

56. **AdS/CFT and Landau Fermi liquids**
By: Davison, Richard A.; Goykhman, Mikhail; Parnachev, Andrei
JOURNAL OF HIGH ENERGY PHYSICS Issue: 7 Article Number: 109 Published: JUL 23 2014

View Abstract

Times Cited: 6
(from Web of Science Core Collection)

Usage Count ▾

57. **Holographic interaction effects on transport in Dirac semimetals**
By: Jacobs, V. P. J.; Vandoren, S. J. G.; Stoof, H. T. C.
PHYSICAL REVIEW B Volume: 90 Issue: 4 Article Number: 045108 Published: JUL 9 2014


View Abstract

Times Cited: 6
(from Web of Science Core Collection)

Usage Count ▾

58. **Entanglement entropy of compressible holographic matter: Loop corrections from bulk fermions**
By: Swingle, Brian; Huijse, Liza; Sachdev, Subir











Times Cited: 2
(from Web of Science Core Collection)

| | | | |
|------------------------|--|---|---|
| Book Series Titles | | PHYSICAL REVIEW B Volume: 90 Issue: 4 Article Number: 045107 Published: JUL 9 2014 | Usage Count |
| Conference Titles | | View Abstract | |
| Publication Years | | 59. Anisotropic plasma with a chemical potential and scheme-independent instabilities | Times Cited: 20 <i>(from Web of Science Core Collection)</i> |
| Organizations-Enhanced | | By: Cheng, Long; Ge, Xian-Hui; Sin, Sang-Jin PHYSICS LETTERS B Volume: 734 Pages: 116-121 Published: JUN 27 2014 | Usage Count |
| Funding Agencies | | Full Text from Publisher View Abstract | |
| Languages | | 60. An analytic analysis of d-dimensional Gauss-Bonnet holographic superconductor in Born-Infeld electrodynamics | Times Cited: 1 <i>(from Web of Science Core Collection)</i> |
| Countries/Territories | | By: Guo, Xiong-Ying; Zhang, Li-Chun; Zhao, Ren MODERN PHYSICS LETTERS A Volume: 29 Issue: 19 Article Number: 1450083 Published: JUN 21 2014 | Usage Count |
| ESI Top Papers | | Full Text from Publisher View Abstract | |
| Open Access | | 61. Holographic duality and the resistivity of strange metals | Times Cited: 63 <i>(from Web of Science Core Collection)</i> |
| | | By: Davison, Richard A.; Schalm, Koenraad; Zaanen, Jan PHYSICAL REVIEW B Volume: 89 Issue: 24 Article Number: 245116 Published: JUN 12 2014 |  Highly Cited Paper |
| | | View Abstract | Usage Count |
| | | 62. Cold planar horizons are floppy | Times Cited: 7 <i>(from Web of Science Core Collection)</i> |
| | | By: Hartnoll, Sean A.; Santos, Jorge E. PHYSICAL REVIEW D Volume: 89 Issue: 12 Article Number: 126002 Published: JUN 3 2014 | Usage Count |
| | | View Abstract | |
| | | 63. Entanglement entropy as a probe of the proximity effect in holographic superconductors | Times Cited: 0 <i>(from Web of Science Core Collection)</i> |
| | | By: Kuang, Xiao-Mei; Papantonopoulos, Eleftherios; Wang, Bin JOURNAL OF HIGH ENERGY PHYSICS Issue: 5 Published: MAY 28 2014 | Usage Count |
| | | View Abstract | |
| | | 64. BCS instabilities of electron stars to holographic superconductors | Times Cited: 2 <i>(from Web of Science Core Collection)</i> |
| | | By: Liu, Yan; Schalm, Koenraad; Sun, Ya-Wen; et al. JOURNAL OF HIGH ENERGY PHYSICS Issue: 5 Article Number: 122 Published: MAY 27 2014 | Usage Count |
| | | View Abstract | |
| | | 65. Fermi liquids from D-branes | Times Cited: 0 <i>(from Web of Science Core Collection)</i> |
| | | By: Rozali, Moshe; Smyth, Darren JOURNAL OF HIGH ENERGY PHYSICS Issue: 5 Article Number: 129 Published: MAY 27 2014 | Usage Count |
| | | View Abstract | |
| | | 66. Entanglement and correlations near extremality: CFTs dual to Reissner-Nordstrom AdS(5) | Times Cited: 8 <i>(from Web of Science Core Collection)</i> |
| | | By: Andrade, Tomas; Fischetti, Sebastian; Marolf, Donald; et al. JOURNAL OF HIGH ENERGY PHYSICS Issue: 4 Article Number: 023 Published: APR 3 2014 | Usage Count |
| | | View Abstract | |
| | | 67. Schrodinger Fermi liquids | Times Cited: 5 <i>(from Web of Science Core Collection)</i> |
| | | By: Wang, Juven PHYSICAL REVIEW D Volume: 89 Issue: 4 Article Number: 046008 Published: FEB 27 2014 | Usage Count |
| | | View Abstract | |

For advanced refine options, use

[Analyze Results](#)

68. **Small treatise on spin-3/2 fields and their dual spectral functions**
 By: Liu, James T.; Zayas, Leopoldo A. Pando; Yang, Zhenbin
 JOURNAL OF HIGH ENERGY PHYSICS Issue: 2 Article
 Number: 095 Published: FEB 24 2014
[View Abstract](#)
 Times Cited: 1
(from Web of Science Core Collection)
 Usage Count
69. **Mimic the optical conductivity in disordered solids via gauge/gravity duality**
 By: Sun, Jia-Rui; Wu, Shang-Yu; Zhang, Hai-Qing
 PHYSICS LETTERS B Volume: 729 Pages: 177-184
 Published: FEB 5 2014
[Full Text from Publisher](#) [View Abstract](#)
 Times Cited: 8
(from Web of Science Core Collection)
 Usage Count
70. **N=1 SUSY AdS(4) vacua in IIB SUGRA on group manifolds**
 By: Solard, G.
 JOURNAL OF HIGH ENERGY PHYSICS Issue: 2 Article
 Number: 017 Published: FEB 5 2014
[View Abstract](#)
 Times Cited: 2
(from Web of Science Core Collection)
 Usage Count
71. **Holographic entanglement entropy of semi-local quantum liquids**
 By: Erdmenger, Johanna; Pang, Da Wei; Zeller, Hansjoerg
 JOURNAL OF HIGH ENERGY PHYSICS Issue: 2 Article
 Number: 016 Published: FEB 5 2014
[View Abstract](#)
 Times Cited: 2
(from Web of Science Core Collection)
 Usage Count
72. **Conformal field theories in a periodic potential: Results from holography and field theory**
 By: Chesler, Paul; Lucas, Andrew; Sachdev, Subir
 PHYSICAL REVIEW D Volume: 89 Issue: 2 Article Number:
 026005 Published: JAN 21 2014
[View Abstract](#)
 Times Cited: 34
(from Web of Science Core Collection)
 Usage Count
73. **The charged Lifshitz black brane geometry and the bulk dipole coupling**
 By: Wu, Jian-Pin
 PHYSICS LETTERS B Volume: 728 Pages: 450-456
 Published: JAN 20 2014
[Full Text from Publisher](#) [View Abstract](#)
 Times Cited: 9
(from Web of Science Core Collection)
 Usage Count
74. **A holographic model of SQUID**
 By: Cai, Rong-Gen; Wang, Yong-Qiang; Zhang, Hai-Qing
 JOURNAL OF HIGH ENERGY PHYSICS Issue: 1 Article
 Number: 039 Published: JAN 9 2014
[View Abstract](#)
 Times Cited: 8
(from Web of Science Core Collection)
 Usage Count
75. **Intermediate coupling model of the cuprates**
 By: Das, Tanmoy; Markiewicz, R. S.; Bansil, A.
 ADVANCES IN PHYSICS Volume: 63 Issue: 3 Pages:
 151-266 Published: 2014
[View Abstract](#)
 Times Cited: 17
(from Web of Science Core Collection)
 Usage Count
76. **Holographic fermions with running chemical potential and dipole coupling**
 By: Fang, Li Qing; Ge, Xian-Hui; Kuang, Xiao-Mei
 NUCLEAR PHYSICS B Volume: 877 Issue: 3 Pages: 807-824
 Published: DEC 21 2013
[Full Text from Publisher](#) [View Abstract](#)
 Times Cited: 11
(from Web of Science Core Collection)
 Usage Count
77. **Simulating analogue holography in flexible Dirac metals**
 By: Khveshchenko, D. V.
 EPL Volume: 104 Issue: 4 Article Number: 47002
 Published: NOV 2013
[View Abstract](#)
 Times Cited: 7
(from Web of Science Core Collection)
 Usage Count

78. **Observation of Majorana quantum critical behaviour in a resonant level coupled to a dissipative environment**
By: Mebrahtu, H. T.; Borzenets, I. V.; Zheng, H.; et al.
NATURE PHYSICS Volume: 9 Issue: 11 Pages: 732-737
Published: NOV 2013
[View Abstract](#)
Times Cited: **16**
(from Web of Science Core Collection)
Usage Count 
79. **Black branes in flux compactifications**
By: Torroba, Gonzalo; Wang, Huajia
JOURNAL OF HIGH ENERGY PHYSICS Issue: 10 Article Number: 126
Published: OCT 21 2013
[View Abstract](#)
Times Cited: **2**
(from Web of Science Core Collection)
Usage Count 
80. **Aspects of current correlators in holographic theories with hyperscaling violation**
By: Edalati, Mohammad; Pedraza, Juan F.
PHYSICAL REVIEW D Volume: 88 Issue: 8 Article Number: 086004
Published: OCT 18 2013
[View Abstract](#)
Times Cited: **19**
(from Web of Science Core Collection)
Usage Count 
81. **Bose-Fermi competition in holographic metals**
By: Liu, Yan; Schalm, Koenraad; Sun, Ya-Wen; et al.
JOURNAL OF HIGH ENERGY PHYSICS Issue: 10 Article Number: 064
Published: OCT 10 2013
[View Abstract](#)
Times Cited: **6**
(from Web of Science Core Collection)
Usage Count 
82. **How to construct a gravitating quantum electron star**
By: Allais, Andrea; McGreevy, John
PHYSICAL REVIEW D Volume: 88 Issue: 6 Article Number: 066006
Published: SEP 17 2013
[View Abstract](#)
Times Cited: **11**
(from Web of Science Core Collection)
Usage Count 
83. **Charge transport by holographic Fermi surfaces**
By: Faulkner, Thomas; Iqbal, Nabil; Liu, Hong; et al.
PHYSICAL REVIEW D Volume: 88 Issue: 4 Article Number: 045016
Published: AUG 21 2013
[View Abstract](#)
Times Cited: **14**
(from Web of Science Core Collection)
Usage Count 
84. **Probing holographic semilocal quantum liquids with D-branes**
By: Pang, Da-Wei
PHYSICAL REVIEW D Volume: 88 Issue: 4 Article Number: 046002
Published: AUG 15 2013
[View Abstract](#)
Times Cited: **7**
(from Web of Science Core Collection)
Usage Count 
85. **Inflammatory factors gene polymorphism in recurrent oral ulceration**
By: Sun, Mao; Fu, Shan-Min; Dong, Guang-Ying; et al.
JOURNAL OF ORAL PATHOLOGY & MEDICINE Volume: 42 Issue: 7 Pages: 528-534
Published: AUG 2013
[View Abstract](#)
Times Cited: **1**
(from Web of Science Core Collection)
Usage Count 
86. **Dynamical gap from holography in the charged dilaton black hole**
By: Kuang, Xiao-Mei; Wang, Bin; Wu, Jian-Pin
CLASSICAL AND QUANTUM GRAVITY Volume: 30 Issue: 14 Article Number: 145011
Published: JUL 21 2013
[View Abstract](#)
Times Cited: **11**
(from Web of Science Core Collection)
Usage Count 
87. **Vortex lattices and crystalline geometries**
By: Bao, Ning; Harrison, Sarah; Kachru, Shamit; et al.
PHYSICAL REVIEW D Volume: 88 Issue: 2 Article Number: 026002
Published: JUL 8 2013
[View Abstract](#)
Times Cited: **22**
(from Web of Science Core Collection)
Usage Count 
88. **A universal fermionic analogue of the shear viscosity**
Times Cited: **4**
(from Web of Science Core Collection)

By: Erdmenger, Johanna; Steinfurt, Stephan
JOURNAL OF HIGH ENERGY PHYSICS Issue: 7 Article
Number: 018 Published: JUL 2013

[View Abstract](#)

Collection)

Usage Count 

89. **Friedel oscillations and horizon charge in 1D holographic liquids**

By: Faulkner, Thomas; Iqbal, Nabil
JOURNAL OF HIGH ENERGY PHYSICS Issue: 7 Article
Number: 060 Published: JUL 2013

[View Abstract](#)

Times Cited: **12**
(from Web of Science Core Collection)

Usage Count 

90. **Further studies on holographic insulator/superconductor phase transitions from Sturm-Liouville eigenvalue problems**

By: Li, Huai-Fan
JOURNAL OF HIGH ENERGY PHYSICS Issue: 7 Article
Number: 135 Published: JUL 2013

[View Abstract](#)

Times Cited: **0**
(from Web of Science Core Collection)

Usage Count 

91. **The analytical treatments on the low energy behaviors of the holographic non-relativistic fermions**

By: Wu, Jian-Pin
PHYSICS LETTERS B Volume: 723 Issue: 4-5 Pages:
448-454 Published: JUN 25 2013

[Full Text from Publisher](#)

[View Abstract](#)

Times Cited: **3**
(from Web of Science Core Collection)

Usage Count 

92. **Stripe instabilities of geometries with hyperscaling violation**

By: Iizuka, Norihiro; Maeda, Kengo
PHYSICAL REVIEW D Volume: 87 Issue: 12 Article
Number: 126006 Published: JUN 10 2013

[View Abstract](#)

Times Cited: **13**
(from Web of Science Core Collection)

Usage Count 

93. **Self-energy of strongly interacting fermions in medium: A holographic approach**

By: Seo, Yunseok; Sin, Sang-Jin; Zhou, Yang
PHYSICS LETTERS B Volume: 723 Issue: 1-3 Pages:
207-212 Published: JUN 10 2013

[Full Text from Publisher](#)

[View Abstract](#)

Times Cited: **1**
(from Web of Science Core Collection)

Usage Count 

94. **Thermal mass and plasmino for strongly interacting fermions via holography**

By: Seo, Yunseok; Sin, Sang-Jin; Zhou, Yang
JOURNAL OF HIGH ENERGY PHYSICS Issue: 6 Article
Number: 076 Published: JUN 2013

[View Abstract](#)

Times Cited: **1**
(from Web of Science Core Collection)

Usage Count 

95. **Fermi-like liquid from Einstein-DBI-dilaton system**

By: Pal, Shesansu Sekhar
JOURNAL OF HIGH ENERGY PHYSICS Issue: 4 Article
Number: 007 Published: APR 2013

[View Abstract](#)

Times Cited: **5**
(from Web of Science Core Collection)

Usage Count 

96. **Emergence of gap from holographic fermions on charged Lifshitz background**

By: Wu, Jian-Pin
JOURNAL OF HIGH ENERGY PHYSICS Issue: 4 Article
Number: 073 Published: APR 2013

[View Abstract](#)

Times Cited: **6**
(from Web of Science Core Collection)

Usage Count 

97. **Holographic models for undoped Weyl semimetals**

By: Guerso, Umut; Jacobs, Vivian; Plauschinn, Erik; et al.
JOURNAL OF HIGH ENERGY PHYSICS Issue: 4 Article
Number: 127 Published: APR 2013

[View Abstract](#)

Times Cited: **6**
(from Web of Science Core Collection)

Usage Count 

- 98. **A novel mechanism to generate FFLO states in holographic superconductors**

By: Alsup, James; Papantonopoulos, Eleftherios; Siopsis, George
PHYSICS LETTERS B Volume: 720 Issue: 4-5 Pages: 379-384 Published: MAR 26 2013

[Full Text from Publisher](#)
[View Abstract](#)

Times Cited: 12
(from Web of Science Core Collection)

Usage Count
- 99. **Semi-local quantum criticality in string/M-theory**

By: Donos, Aristomenis; Gauntlett, Jerome P.; Pantelidou, Christiana
JOURNAL OF HIGH ENERGY PHYSICS Issue: 3 Article Number: 103 Published: MAR 2013

[View Abstract](#)

Times Cited: 16
(from Web of Science Core Collection)

Usage Count
- 100. **Entangled dilaton dyons**

By: Kundu, Nilay; Narayan, Prithvi; Sircar, Nilanjan; et al.
JOURNAL OF HIGH ENERGY PHYSICS Issue: 3 Article Number: 155 Published: MAR 2013

[View Abstract](#)

Times Cited: 15
(from Web of Science Core Collection)

Usage Count

Select Page

[Save to EndNote online](#)
[Add to Marked List](#)



Sort by: Publication Date -- newest to oldest

Show: 50 per page

◀ Page 2 of 6 ▶

263 records matched your query of the 36,466,594 in the data limits you selected.

| | | | | | | | |
|-----------------|----------|---------------------------|-------------------------------|----------|-----------|------|-----------|
| Web of Science™ | InCites™ | Journal Citation Reports® | Essential Science Indicators™ | EndNote™ | Sign In ▾ | Help | English ▾ |
|-----------------|----------|---------------------------|-------------------------------|----------|-----------|------|-----------|

Search
Return to Search Results
My Tools ▾
Search History
Marked List

Citing Articles: 263
(from Web of Science Core Collection)

For: String Theory, Quantum Phase Transitions, and the Emergent Fermi Liquid ...[More](#)

Times Cited Counts
270 in All Databases

270 in Web of Science Core Collection

2 in BIOSIS Citation Index

4 in Chinese Science Citation Database

0 data sets in Data Citation Index

0 publication in Data Citation Index

1 in Russian Science Citation Index

0 in SciELO Citation Index

[View Additional Times Cited Counts](#)

Refine Results

Web of Science Categories ▾

- PHYSICS PARTICLES FIELDS (198)
- ASTRONOMY ASTROPHYSICS (81)
- PHYSICS MULTIDISCIPLINARY (38)
- PHYSICS CONDENSED MATTER (23)
- PHYSICS NUCLEAR (14)

[more options / values...](#)

Refine

Document Types ▾

- ARTICLE (254)
- REVIEW (9)
- PROCEEDINGS PAPER (4)
- BOOK CHAPTER (1)

[more options / values...](#)

Refine

Research Areas ▾

Authors ▾



Group Authors ▾

Editors ▾

Source Titles ▾

Sort by: **Publication Date -- newest to oldest** ▾

Page 3 of 6

Select Page
 
Save to EndNote online ▾
Add to Marked List

[Analyze Results](#)

[Create Citation Report](#)

101. **Holographic fermions on a charged Lifshitz background from Einstein-Dilaton-Maxwell model**

By: Wu, Jian-Pin
JOURNAL OF HIGH ENERGY PHYSICS Issue: 3 Article Number: 083 Published: MAR 2013

[View Abstract](#)
102. **Holographic fermions in charged dilaton black branes**

By: Li, Wei-Jia; Wu, Jian-Pin
NUCLEAR PHYSICS B Volume: 867 Issue: 3 Pages: 810-826 Published: FEB 21 2013

[Full Text from Publisher](#) [View Abstract](#)
103. **STRANGE METALS AND HOLOGRAPHIC ENTANGLEMENT ENTROPY**

By: Takayanagi, Tadashi
INTERNATIONAL JOURNAL OF MODERN PHYSICS A Volume: 28 Issue: 3-4 Special Issue: SI Article Number: 1340004 Published: FEB 10 2013

[Full Text from Publisher](#) [View Abstract](#)
104. **An introduction to gauge-gravity duality and its application in condensed matter**

By: Green, A. G.
CONTEMPORARY PHYSICS Volume: 54 Issue: 1 Pages: 33-48 Published: FEB 1 2013

[View Abstract](#)
105. **Anomalous zero sound**

By: Gorsky, A.; Zayakin, A. V.
JOURNAL OF HIGH ENERGY PHYSICS Issue: 2 Article Number: 124 Published: FEB 2013

[View Abstract](#)
106. **Fermi surfaces and analytic Green's functions from conformal gravity**

By: Li, Jun; Liu, Hai-Shan; Lu, H.; et al.
JOURNAL OF HIGH ENERGY PHYSICS Issue: 2 Article Number: 109 Published: FEB 2013

[View Abstract](#)
107. **Wilson line response of holographic superconductors in Gauss-Bonnet gravity**

By: Cai, Rong-Gen; Li, Li; Li, Li-Fang; et al.
PHYSICAL REVIEW D Volume: 87 Issue: 2 Article Number: 026002 Published: JAN 14 2013

[View Abstract](#)
108. **Holographic dual of the lowest Landau level**

By: Blake, Mike; Bolognesi, Stefano; Tong, David; et al.
JOURNAL OF HIGH ENERGY PHYSICS Issue: 12 Article

Times Cited: 4
(from Web of Science Core Collection)

Usage Count ▾

Times Cited: 12
(from Web of Science Core Collection)

Usage Count ▾

Times Cited: 1
(from Web of Science Core Collection)

Usage Count ▾

Times Cited: 8
(from Web of Science Core Collection)

Usage Count ▾

Times Cited: 7
(from Web of Science Core Collection)

Usage Count ▾

Times Cited: 5
(from Web of Science Core Collection)

Usage Count ▾

Times Cited: 1
(from Web of Science Core Collection)

Usage Count ▾

Times Cited: 7
(from Web of Science Core Collection)

Usage Count ▾

| | |
|------------------------|---|
| Book Series Titles | ◀ |
| Conference Titles | ◀ |
| Publication Years | ◀ |
| Organizations-Enhanced | ◀ |
| Funding Agencies | ◀ |
| Languages | ◀ |
| Countries/Territories | ◀ |
| ESI Top Papers | ◀ |
| Open Access | ◀ |

For advanced refine options, use

[Analyze Results](#)

Number: 039 Published: DEC 2012

[View Abstract](#)Usage Count 109. **Holographic fermions in charged Lifshitz theory**By: Fang, Li Qing; Ge, Xian-Hui; Kuang, Xiao-Mei
PHYSICAL REVIEW D Volume: 86 Issue: 10 Article
Number: 105037 Published: NOV 20 2012[View Abstract](#)Times Cited: **19**
(from Web of Science Core
Collection)Usage Count 110. **Strongly correlated quantum fluids: ultracold quantum gases, quantum chromodynamic plasmas and holographic duality**By: Adams, Allan; Carr, Lincoln D.; Schaefer, Thomas; et al.
NEW JOURNAL OF PHYSICS Volume: 14 Article Number:
115009 Published: NOV 19 2012[Full Text from Publisher](#)[View Abstract](#)Times Cited: **67**
(from Web of Science Core
Collection)Usage Count 111. **Fermi surfaces in N=4 super-Yang-Mills theory**By: DeWolfe, Oliver; Gubser, Steven S.; Rosen, Christopher
PHYSICAL REVIEW D Volume: 86 Issue: 10 Article
Number: 106002 Published: NOV 6 2012[View Abstract](#)Times Cited: **14**
(from Web of Science Core
Collection)Usage Count 112. **Charged black branes with hyperscaling violating factor**By: Alishahiha, Mohsen; Colgain, Eoin O.; Yavartanoo, Hossein
JOURNAL OF HIGH ENERGY PHYSICS Issue: 11 Article
Number: 137 Published: NOV 2012[View Abstract](#)Times Cited: **45**
(from Web of Science Core
Collection)Usage Count 113. **Hyperscaling violation: a unified frame for effective holographic theories**By: Kim, Bom Soo
JOURNAL OF HIGH ENERGY PHYSICS Issue: 11 Article
Number: 061 Published: NOV 2012[View Abstract](#)Times Cited: **7**
(from Web of Science Core
Collection)Usage Count 114. **Pomeranchuk instability in a non-Fermi liquid from holography**By: Edalati, Mohammad; Lo, Ka Wai; Phillips, Philip W.
PHYSICAL REVIEW D Volume: 86 Issue: 8 Article Number:
086003 Published: OCT 8 2012[View Abstract](#)Times Cited: **6**
(from Web of Science Core
Collection)Usage Count 115. **Magnetic and electric AdS solutions in string- and M-theory**By: Donos, Aristomenis; Gauntlett, Jerome P.; Pantelidou, Christiana
CLASSICAL AND QUANTUM GRAVITY Volume: 29 Issue: 19
Article Number: 194006 Published: OCT 7 2012[View Abstract](#)Times Cited: **29**
(from Web of Science Core
Collection)Usage Count 116. **A maximally supersymmetric Kondo model**By: Harrison, Sarah; Kachru, Shamit; Torroba, Gonzalo
CLASSICAL AND QUANTUM GRAVITY Volume: 29 Issue: 19
Article Number: 194005 Published: OCT 7 2012[View Abstract](#)Times Cited: **11**
(from Web of Science Core
Collection)Usage Count 117. **Fractionalization of holographic Fermi surfaces**By: Hartnoll, Sean A.; Huijse, Liza
CLASSICAL AND QUANTUM GRAVITY Volume: 29 Issue: 19
Article Number: 194001 Published: OCT 7 2012[View Abstract](#)Times Cited: **23**
(from Web of Science Core
Collection)Usage Count 118. **Luttinger's theorem, superfluid vortices and holography**Times Cited: **14**
(from Web of Science Core
Collection)

By: Iqbal, Nabil; Liu, Hong

[CLASSICAL AND QUANTUM GRAVITY](#) Volume: 29 Issue: 19
Article Number: 194004 Published: OCT 7 2012

[View Abstract](#)

Usage Count 

119. **Thermal correlators in holographic models with Lifshitz scaling**

By: Keranen, Ville; Thorlacius, Larus

[CLASSICAL AND QUANTUM GRAVITY](#) Volume: 29 Issue: 19
Article Number: 194009 Published: OCT 7 2012

[View Abstract](#)

Times Cited: **14**

(from Web of Science Core Collection)

Usage Count 

120. **Large-density field theory, viscosity and '2k(F)' singularities from string duals**

By: Polchinski, Joseph; Silverstein, Eva

[CLASSICAL AND QUANTUM GRAVITY](#) Volume: 29 Issue: 19
Article Number: 194008 Published: OCT 7 2012

[View Abstract](#)

Times Cited: **15**

(from Web of Science Core Collection)

Usage Count 

121. **Holographic aspects of two-charged dilatonic black hole in AdS(5)**

By: Alishahiha, Mohsen; Mozaffar, M. Reza Mohammadi; Mollabashi, Ali

[JOURNAL OF HIGH ENERGY PHYSICS](#) Issue: 10 Article Number: 003 Published: OCT 2012

[View Abstract](#)

Times Cited: **7**

(from Web of Science Core Collection)

Usage Count 

122. **Towards a holographic realization of Homes' law**

By: Erdmenger, Johanna; Kerner, Patrick; Mueller, Steffen

[JOURNAL OF HIGH ENERGY PHYSICS](#) Issue: 10 Article Number: 021 Published: OCT 2012

[View Abstract](#)

Times Cited: **11**

(from Web of Science Core Collection)

Usage Count 

123. **Fluctuations in finite density holographic quantum liquids**

By: Goykhman, Mikhail; Parnachev, Andrei; Zaanen, Jan

[JOURNAL OF HIGH ENERGY PHYSICS](#) Issue: 10 Article Number: 045 Published: OCT 2012

[View Abstract](#)

Times Cited: **12**

(from Web of Science Core Collection)

Usage Count 

124. **Lattice potentials and fermions in holographic non Fermi-liquids: hybridizing local quantum criticality**

By: Liu, Yan; Schalm, Koenraad; Sun, Ya-Wen; et al.

[JOURNAL OF HIGH ENERGY PHYSICS](#) Issue: 10 Article Number: 036 Published: OCT 2012

[View Abstract](#)

Times Cited: **15**

(from Web of Science Core Collection)

Usage Count 

125. **Supersymmetric quantum criticality supported by baryonic charges**

By: Donos, Aristomenis; Gauntlett, Jerome P.

[JOURNAL OF HIGH ENERGY PHYSICS](#) Issue: 10 Article Number: 120 Published: OCT 2012

[View Abstract](#)

Times Cited: **11**

(from Web of Science Core Collection)

Usage Count 

126. **On holographic entanglement entropy of charged matter**

By: Kulaxizi, Manuela; Parnachev, Andrei; Schalm, Koenraad

[JOURNAL OF HIGH ENERGY PHYSICS](#) Issue: 10 Article Number: 098 Published: OCT 2012

[View Abstract](#)

Times Cited: **15**

(from Web of Science Core Collection)

Usage Count 

127. **Spin and holographic metals**

By: Alexandrov, Victor; Coleman, Piers











[PHYSICAL REVIEW B](#) Volume: 86 Issue: 12 Article Number: 125145 Published: SEP 28 2012











[View Abstract](#)

Times Cited: **2**

(from Web of Science Core Collection)

Usage Count 

128. **Searching for non-Fermi liquids under holographic light**
By: Khveshchenko, D. V.
PHYSICAL REVIEW B Volume: 86 Issue: 11 Article Number: 115115 Published: SEP 12 2012
[View Abstract](#)
Times Cited: 5
(from Web of Science Core Collection)
Usage Count 
129. **Strange metals in one spatial dimension**
By: Gopakumar, Rajesh; Hashimoto, Akikazu; Klebanov, Igor R.; et al.
PHYSICAL REVIEW D Volume: 86 Issue: 6 Article Number: 066003 Published: SEP 6 2012
[View Abstract](#)
Times Cited: 20
(from Web of Science Core Collection)
Usage Count 
130. **Hawking Radiation and Nonequilibrium Quantum Critical Current Noise**
By: Sonner, Julian; Green, A. G.
PHYSICAL REVIEW LETTERS Volume: 109 Issue: 9 Article Number: 091601 Published: AUG 27 2012
[View Abstract](#)
Times Cited: 27
(from Web of Science Core Collection)
Usage Count 
131. **Analytic fermionic Green's functions from holography**
By: Gubser, Steven S.; Ren, Jie
PHYSICAL REVIEW D Volume: 86 Issue: 4 Article Number: 046004 Published: AUG 14 2012
[View Abstract](#)
Times Cited: 21
(from Web of Science Core Collection)
Usage Count 
132. **Degenerate rotating black holes, chiral CFTs and Fermi surfaces I - Analytic results for quasinormal modes**
By: Berkooz, Micha; Frishman, Anna; Zait, Amir
JOURNAL OF HIGH ENERGY PHYSICS Issue: 8 Article Number: 109 Published: AUG 2012
[View Abstract](#)
Times Cited: 5
(from Web of Science Core Collection)
Usage Count 
133. **Fermions on a Lifshitz background**
By: Alishahiha, Mohsen; Mozaffar, M. Reza Mohammadi; Mollabashi, Ali
PHYSICAL REVIEW D Volume: 86 Issue: 2 Article Number: 026002 Published: JUL 3 2012
[View Abstract](#)
Times Cited: 27
(from Web of Science Core Collection)
Usage Count 
134. **Spectral weight in holographic scaling geometries**
By: Hartnoll, Sean A.; Pourhasan, Razieh
JOURNAL OF HIGH ENERGY PHYSICS Issue: 7 Article Number: 078 Published: JUL 2012
[View Abstract](#)
Times Cited: 39
(from Web of Science Core Collection)
Usage Count 
135. **Study of anisotropic black branes in asymptotically anti-de Sitter**
By: Iizuka, Norihiro; Maeda, Kengo
JOURNAL OF HIGH ENERGY PHYSICS Issue: 7 Article Number: 129 Published: JUL 2012
[View Abstract](#)
Times Cited: 17
(from Web of Science Core Collection)
Usage Count 
136. **Dipole coupling effect of holographic fermion in the background of charged Gauss-Bonnet AdS black hole**
By: Kuang, Xiao-Mei; Wang, Bin; Wu, Jian-Pin
JOURNAL OF HIGH ENERGY PHYSICS Issue: 7 Article Number: 125 Published: JUL 2012
[View Abstract](#)
Times Cited: 15
(from Web of Science Core Collection)
Usage Count 
137. **Holography and condensed matter**
By: Benini, Francesco
FORTSCHRITTE DER PHYSIK-PROGRESS OF PHYSICS Volume: 60 Issue: 7-8 Special Issue: SI Pages: 810-821 Published: JUL 2012
[View Abstract](#)
Times Cited: 5
(from Web of Science Core Collection)
Usage Count 

138. **Fermi Surfaces in Maximal Gauged Supergravity**
 By: DeWolfe, Oliver; Gubser, Steven S.; Rosen, Christopher
PHYSICAL REVIEW LETTERS Volume: 108 Issue: 25
 Article Number: 251601 Published: JUN 19 2012
[View Abstract](#)
Times Cited: 18
(from Web of Science Core Collection)
Usage Count 
139. **Quantum critical phase and Lifshitz transition in an extended periodic Anderson model**
 By: Laad, M. S.; Koley, S.; Taraphder, A.
JOURNAL OF PHYSICS-CONDENSED MATTER Volume: 24
 Issue: 23 Article Number: 232201 Published: JUN 13 2012
[View Abstract](#)
Times Cited: 2
(from Web of Science Core Collection)
Usage Count 
140. **Quantum Electron Star**
 By: Allais, Andrea; McGreevy, John; Suh, S. Josephine
PHYSICAL REVIEW LETTERS Volume: 108 Issue: 23
 Article Number: 231602 Published: JUN 8 2012
[View Abstract](#)
Times Cited: 22
(from Web of Science Core Collection)
Usage Count 
141. **Schrodinger holography with and without hyperscaling violation**
 By: Kim, Bom Soo
JOURNAL OF HIGH ENERGY PHYSICS Issue: 6 Article
 Number: 116 Published: JUN 2012
[View Abstract](#)
Times Cited: 24
(from Web of Science Core Collection)
Usage Count 
142. **The spin of holographic electrons at nonzero density and temperature**
 By: Herzog, Christopher P.; Ren, Jie
JOURNAL OF HIGH ENERGY PHYSICS Issue: 6 Article
 Number: 078 Published: JUN 2012
[View Abstract](#)
Times Cited: 11
(from Web of Science Core Collection)
Usage Count 
143. **Holographic spectral function in nonequilibrium states**
 By: Banerjee, Souvik; Iyer, Ramakrishnan; Mukhopadhyay, Ayan
PHYSICAL REVIEW D Volume: 85 Issue: 10 Article
 Number: 106009 Published: MAY 22 2012
[View Abstract](#)
Times Cited: 11
(from Web of Science Core Collection)
Usage Count 
144. **Banishing AdS ghosts with a UV cutoff**
 By: Andrade, Tomas; Faulkner, Thomas; Marolf, Donald
JOURNAL OF HIGH ENERGY PHYSICS Issue: 5 Article
 Number: 011 Published: MAY 2012
[View Abstract](#)
Times Cited: 6
(from Web of Science Core Collection)
Usage Count 
145. **Holography and ARPES sum-rules**
 By: Guerso, Umut; Plauschinn, Erik; Stoof, Henk; et al.
JOURNAL OF HIGH ENERGY PHYSICS Issue: 5 Article
 Number: 018 Published: MAY 2012
[View Abstract](#)
Times Cited: 13
(from Web of Science Core Collection)
Usage Count 
146. **Holographic entanglement entropy and Fermi surfaces**
 By: Shaghoulian, Edgar
JOURNAL OF HIGH ENERGY PHYSICS Issue: 5 Article
 Number: 065 Published: MAY 2012
[View Abstract](#)
Times Cited: 43
(from Web of Science Core Collection)
Usage Count 
147. **Holographic quantum criticality and strange metal transport**
 By: Kim, Bom Soo; Kiritsis, Elias; Panagopoulos, Christos
NEW JOURNAL OF PHYSICS Volume: 14 Article Number:
 043045 Published: APR 30 2012
[Full Text from Publisher](#) [View Abstract](#)
Times Cited: 18
(from Web of Science Core Collection)
Usage Count 
148. **Holographic p-wave superconductors in quasi-topological gravity**
Times Cited: 12
(from Web of Science Core Collection)

| | |
|---|--|
| <p>By: Kuang, Xiao-Mei; Li, Wei-Jia; Ling, Yi CLASSICAL AND QUANTUM GRAVITY Volume: 29 Issue: 8 Article Number: 085015 Published: APR 21 2012</p> <p>View Abstract</p> | <p>Usage Count ▾</p> |
| <p>149. Semi-local quantum liquids By: Iqbal, Nabil; Liu, Hong; Mezei, Mark JOURNAL OF HIGH ENERGY PHYSICS Issue: 4 Article Number: 086 Published: APR 2012</p> <p>View Abstract</p> | <p>Times Cited: 36 <i>(from Web of Science Core Collection)</i></p> <p>Usage Count ▾</p> |
| <p>150. Dynamic gap from holographic fermions in charged dilaton black branes By: Wu, Jian-Pin; Zeng, Hua-Bi JOURNAL OF HIGH ENERGY PHYSICS Issue: 4 Article Number: 068 Published: APR 2012</p> <p>View Abstract</p> | <p>Times Cited: 10 <i>(from Web of Science Core Collection)</i></p> <p>Usage Count ▾</p> |

Select Page |   | [Save to EndNote online](#) ▾ | [Add to Marked List](#)

Sort by: [Publication Date -- newest to oldest](#) ▾

Show: [50 per page](#) ▾

◀ Page 3 of 6 ▶

263 records matched your query of the 36,466,594 in the data limits you selected.

Web of Science™ InCites™ Journal Citation Reports® Essential Science Indicators™ EndNote™
Sign In Help English

WEB OF SCIENCE™

Search
Return to Search Results
My Tools Search History Marked List

Citing Articles: 263
(from Web of Science Core Collection)

For: String Theory, Quantum Phase Transitions, and the Emergent Fermi Liquid ...[More](#)

Times Cited Counts
270 in All Databases

270 in Web of Science Core Collection
2 in BIOSIS Citation Index
4 in Chinese Science Citation Database
0 data sets in Data Citation Index
0 publication in Data Citation Index
1 in Russian Science Citation Index
0 in SciELO Citation Index

[View Additional Times Cited Counts](#)

Refine Results

Web of Science Categories

- PHYSICS PARTICLES FIELDS (198)
- ASTRONOMY ASTROPHYSICS (81)
- PHYSICS MULTIDISCIPLINARY (38)
- PHYSICS CONDENSED MATTER (23)
- PHYSICS NUCLEAR (14)

[more options / values...](#)

Refine

Document Types

- ARTICLE (254)
- REVIEW (9)
- PROCEEDINGS PAPER (4)
- BOOK CHAPTER (1)

[more options / values...](#)

Refine

Research Areas

Authors

Group Authors

Editors

Source Titles

Sort by: Publication Date -- newest to oldest
Page 4 of 6

Select Page
Save to EndNote online
Add to Marked List

Analyze Results
Create Citation Report

151. **Interplay between interaction and chiral anomaly in the holographic approach**
 By: Kim, Ki-Seok; Tsukioka, Takuya
 PHYSICAL REVIEW D Volume: 85 Issue: 4 Article Number: 045011 Published: FEB 8 2012

View Abstract

152. **Soliton stars as holographic confined Fermi liquids**
 By: Bhattacharya, Jyotirmoy; Ogawa, Noriaki; Takayanagi, Tadashi; et al.
 JOURNAL OF HIGH ENERGY PHYSICS Issue: 2 Article Number: 137 Published: FEB 2012

View Abstract

153. **On field theory thermalization from gravitational collapse**
 By: Garfinkle, David; Zayas, Leopoldo A. Pando; Reichmann, Dori
 JOURNAL OF HIGH ENERGY PHYSICS Issue: 2 Article Number: 119 Published: FEB 2012

View Abstract

154. **Hidden Fermi surfaces in compressible states of gauge-gravity duality**
 By: Huijse, Liza; Sachdev, Subir; Swingle, Brian
 PHYSICAL REVIEW B Volume: 85 Issue: 3 Article Number: 035121 Published: JAN 25 2012

View Abstract

155. **Friedel oscillations in holographic metals**
 By: Puletti, V. Giangreco M.; Nowling, S.; Thorlacius, L.; et al.
 JOURNAL OF HIGH ENERGY PHYSICS Issue: 1 Article Number: 073 Published: JAN 2012

View Abstract

156. **What Can Gauge-Gravity Duality Teach Us About Condensed Matter Physics?**
 By: Sachdev, Subir
 Edited by: Langer, JS
 ANNUAL REVIEW OF CONDENSED MATTER PHYSICS, VOL 3
 Book Series: Annual Review of Condensed Matter Physics
 Volume: 3 Pages: 9-33 Published: 2012

View Abstract

157. **Holographic Fermi and non-Fermi liquids with transitions in dilaton gravity**
 By: Iizuka, Norihiro; Kundu, Nilay; Narayan, Prithvi; et al.
 JOURNAL OF HIGH ENERGY PHYSICS Issue: 1 Article Number: 094 Published: JAN 2012

View Abstract

Times Cited: 2
(from Web of Science Core Collection)

Usage Count

Times Cited: 1
(from Web of Science Core Collection)

Usage Count

Times Cited: 45
(from Web of Science Core Collection)

Usage Count

Times Cited: 208
(from Web of Science Core Collection)

Highly Cited Paper

Usage Count

Times Cited: 6
(from Web of Science Core Collection)

Usage Count

Times Cited: 109
(from Web of Science Core Collection)

Highly Cited Paper

Usage Count

Times Cited: 92
(from Web of Science Core Collection)

Highly Cited Paper

Usage Count

| | |
|------------------------|---|
| Book Series Titles | ◀ |
| Conference Titles | ◀ |
| Publication Years | ◀ |
| Organizations-Enhanced | ◀ |
| Funding Agencies | ◀ |
| Languages | ◀ |
| Countries/Territories | ◀ |
| ESI Top Papers | ◀ |
| Open Access | ◀ |

For advanced refine options, use

Analyze Results

158. **Holographic non-relativistic fermionic fixed point by the charged dilatonic black hole**

By: Li, Wei-Jia; Meyer, Rene; Zhang, Hongbao
 JOURNAL OF HIGH ENERGY PHYSICS Issue: 1 Article
 Number: 153 Published: JAN 2012

View Abstract

Times Cited: 15
 (from Web of Science Core Collection)

Usage Count ▼

159. **Holographic Fermi surfaces and entanglement entropy**

By: Ogawa, Noriaki; Takayanagi, Tadashi; Ugajin, Tomonori
 JOURNAL OF HIGH ENERGY PHYSICS Issue: 1 Article
 Number: 125 Published: JAN 2012

View Abstract

Times Cited: 131
 (from Web of Science Core Collection)

 **Highly Cited Paper**

Usage Count ▼

160. **Helical Luttinger liquids and three-dimensional black holes**

By: Balasubramanian, Vijay; Garcia-Etxebarria, Inaki; Larsen, Finn; et al.
 PHYSICAL REVIEW D Volume: 84 Issue: 12 Article
 Number: 126012 Published: DEC 20 2011

View Abstract

Times Cited: 9
 (from Web of Science Core Collection)

Usage Count ▼

161. **Universal Fermionic Spectral Functions from String Theory**

By: Gauntlett, Jerome P.; Sonner, Julian; Waldram, Daniel
 PHYSICAL REVIEW LETTERS Volume: 107 Issue: 24
 Article Number: 241601 Published: DEC 6 2011

View Abstract

Times Cited: 23
 (from Web of Science Core Collection)

Usage Count ▼

162. **Towards a holographic marginal Fermi liquid**

By: Jensen, Kristan; Kachru, Shamit; Karch, Andreas; et al.
 PHYSICAL REVIEW D Volume: 84 Issue: 12 Article
 Number: 126002 Published: DEC 2 2011

View Abstract

Times Cited: 35
 (from Web of Science Core Collection)

Usage Count ▼

163. **Bosonic excitations of the AdS₄ Reissner-Nordstrom black hole**

By: Davison, Richard A.; Kaplis, Nikolaos K.
 JOURNAL OF HIGH ENERGY PHYSICS Issue: 12 Article
 Number: 037 Published: DEC 2011

View Abstract

Times Cited: 12
 (from Web of Science Core Collection)

Usage Count ▼

164. **Holographic non-relativistic fermionic fixed point and bulk dipole coupling**

By: Li, Wei-Jia; Zhang, Hongbao
 JOURNAL OF HIGH ENERGY PHYSICS Issue: 11 Article
 Number: 018 Published: NOV 2011

View Abstract

Times Cited: 14
 (from Web of Science Core Collection)

Usage Count ▼

165. **Spectral function of the supersymmetry current**

By: Gauntlett, Jerome P.; Sonner, Julian; Waldram, Daniel
 JOURNAL OF HIGH ENERGY PHYSICS Issue: 11 Article
 Number: 153 Published: NOV 2011

View Abstract

Times Cited: 20
 (from Web of Science Core Collection)

Usage Count ▼

166. **A holographic flat band**

By: Laia, Joao N.; Tong, David
 JOURNAL OF HIGH ENERGY PHYSICS Issue: 11 Article
 Number: 125 Published: NOV 2011

View Abstract

Times Cited: 17
 (from Web of Science Core Collection)

Usage Count ▼











167. **Fermionic probes of local quantum criticality in one dimension**

By: Rangamani, Mukund; Withers, Benjamin
 PHYSICAL REVIEW D Volume: 84 Issue: 8 Article Number:
 086003 Published: OCT 11 2011

View Abstract

Times Cited: 2
 (from Web of Science Core Collection)

Usage Count ▼

168. **Absence of a Fermi surface in classical minimal four-dimensional gauged supergravity**
By: Belliard, Raphael; Gubser, Steven S.; Yarom, Amos
JOURNAL OF HIGH ENERGY PHYSICS Issue: 10 Article Number: 055 Published: OCT 2011
[View Abstract](#)
Times Cited: 13
(from Web of Science Core Collection)
Usage Count 
169. **Striped instability of a holographic Fermi-like liquid**
By: Bergman, Oren; Jokela, Niko; Lifschytz, Gilad; et al.
JOURNAL OF HIGH ENERGY PHYSICS Issue: 10 Article Number: 034 Published: OCT 2011
[View Abstract](#)
Times Cited: 40
(from Web of Science Core Collection)
Usage Count 
170. **A chiral magnetic effect from AdS/CFT with flavor**
By: Hoyos, Carlos; Nishioka, Tatzuma; O'Bannon, Andy
JOURNAL OF HIGH ENERGY PHYSICS Issue: 10 Article Number: 084 Published: OCT 2011
[View Abstract](#)
Times Cited: 30
(from Web of Science Core Collection)
Usage Count 
171. **Model of a Fermi liquid using gauge-gravity duality**
By: Sachdev, Subir
PHYSICAL REVIEW D Volume: 84 Issue: 6 Article Number: 066009 Published: SEP 21 2011
[View Abstract](#)
Times Cited: 55
(from Web of Science Core Collection)
Usage Count 
172. **Neutral order parameters in metallic criticality in $d=2+1$ from a hairy electron star**
By: Edalati, Mohammad; Lo, Ka Wai; Phillips, Philip W.
PHYSICAL REVIEW D Volume: 84 Issue: 6 Article Number: 066007 Published: SEP 12 2011
[View Abstract](#)
Times Cited: 15
(from Web of Science Core Collection)
Usage Count 
173. **Rapid thermalization in field theory from gravitational collapse**
By: Garfinkle, David; Zayas, Leopoldo A. Pando
PHYSICAL REVIEW D Volume: 84 Issue: 6 Article Number: 066006 Published: SEP 8 2011
[View Abstract](#)
Times Cited: 68
(from Web of Science Core Collection)
Usage Count 
174. **Charged magnetic brane correlators and twisted Virasoro algebras**
By: D'Hoker, Eric; Kraus, Per
PHYSICAL REVIEW D Volume: 84 Issue: 6 Article Number: 065010 Published: SEP 7 2011
[View Abstract](#)
Times Cited: 4
(from Web of Science Core Collection)
Usage Count 
175. **Some properties of the holographic fermions in an extremal charged dilatonic black hole**
By: Wu, Jian-Pin
PHYSICAL REVIEW D Volume: 84 Issue: 6 Article Number: 064008 Published: SEP 6 2011
[View Abstract](#)
Times Cited: 23
(from Web of Science Core Collection)
Usage Count 
176. **Holography of charged black holes with RF_2 corrections**
By: Cai, Rong-Gen; Pang, Da-Wei
PHYSICAL REVIEW D Volume: 84 Issue: 6 Article Number: 066004 Published: SEP 2 2011
[View Abstract](#)
Times Cited: 10
(from Web of Science Core Collection)
Usage Count 
177. **Holographic charge density waves**
By: Aperis, Alexandros; Kotetes, Panagiotis; Papantonopoulos, Eleftherios; et al.
PHYSICS LETTERS B Volume: 702 Issue: 2-3 Pages: 181-185 Published: AUG 11 2011
[Full Text from Publisher](#) [View Abstract](#)
Times Cited: 14
(from Web of Science Core Collection)
Usage Count 

178. **Stellar spectroscopy: Fermions and holographic Lifshitz criticality**
 By: Hartnoll, Sean A.; Hofman, Diego M.; Vegh, David
 JOURNAL OF HIGH ENERGY PHYSICS Issue: 8 Article Number: 096 Published: AUG 2011
[View Abstract](#)
Times Cited: 38
(from Web of Science Core Collection)
Usage Count
179. **Holographically smeared Fermi surface: Quantum oscillations and Luttinger count in electron stars**
 By: Hartnoll, S. A.; Hofman, D. M.; Tavanfar, A.
 EPL Volume: 95 Issue: 3 Article Number: 31002 Published: AUG 2011
[View Abstract](#)
Times Cited: 26
(from Web of Science Core Collection)
Usage Count
180. **Integrating out geometry: holographic Wilsonian RG and the membrane paradigm**
 By: Faulkner, Thomas; Liu, Hong; Rangamani, Mukund
 JOURNAL OF HIGH ENERGY PHYSICS Issue: 8 Article Number: 051 Published: AUG 2011
[View Abstract](#)
Times Cited: 81
(from Web of Science Core Collection)
Usage Count
181. **Holographic Fermi arcs and a d-wave gap**
 By: Benini, Francesco; Herzog, Christopher P.; Yarom, Amos
 PHYSICS LETTERS B Volume: 701 Issue: 5 Pages: 626-629 Published: JUL 27 2011
[Full Text from Publisher](#) [View Abstract](#)
Times Cited: 40
(from Web of Science Core Collection)
Usage Count
182. **Deconstructing holographic liquids**
 By: Nickel, Dominik; Son, Dam T.
 NEW JOURNAL OF PHYSICS Volume: 13 Article Number: 075010 Published: JUL 22 2011
[Full Text from Publisher](#) [View Abstract](#)
Times Cited: 46
(from Web of Science Core Collection)
Usage Count
183. **Fermi surfaces and gauge-gravity duality**
 By: Huijse, Liza; Sachdev, Subir
 PHYSICAL REVIEW D Volume: 84 Issue: 2 Article Number: 026001 Published: JUL 5 2011
[View Abstract](#)
Times Cited: 66
(from Web of Science Core Collection)
Usage Count
184. **The spacetime of a Dirac fermion**
 By: Mei, Jianwei
 PHYSICS LETTERS B Volume: 701 Issue: 2 Pages: 279-284 Published: JUL 4 2011
[Full Text from Publisher](#) [View Abstract](#)
Times Cited: 0
(from Web of Science Core Collection)
Usage Count
185. **Holographic fermions in charged Gauss-Bonnet black hole**
 By: Wu, Jian-Pin
 JOURNAL OF HIGH ENERGY PHYSICS Issue: 7 Article Number: 106 Published: JUL 2011
[View Abstract](#)
Times Cited: 18
(from Web of Science Core Collection)
Usage Count
186. **Charged dilatonic black holes and their transport properties**
 By: Gouteraux, Blaise; Kim, Bom Soo; Meyer, Rene
 Conference: 16th European Workshop on String Theory
 Location: Madrid, SPAIN Date: JUN 14-18, 2010
 Sponsor(s): European Marie Curie Res Train Network
 FORTSCHRITTE DER PHYSIK-PROGRESS OF PHYSICS
 Volume: 59 Issue: 7-8 Special Issue: SI Pages: 723-729
 Published: JUL 2011
[View Abstract](#)
Times Cited: 16
(from Web of Science Core Collection)
Usage Count
187. **Strange metallic behaviour and the thermodynamics of charged dilatonic black holes**
 By: Meyer, Rene; Gouteraux, Blaise; Kim, Bom Soo
 Conference: 16th European Workshop on String Theory
 Location: Madrid, SPAIN Date: JUN 14-18, 2010
Times Cited: 10
(from Web of Science Core Collection)
Usage Count

Sponsor(s): European Marie Curie Res Train Network
FORTSCHRITTE DER PHYSIK-PROGRESS OF PHYSICS
 Volume: 59 Issue: 7-8 Special Issue: SI Pages: 741-748
 Published: JUL 2011

[View Abstract](#)

188. **A HOLOGRAPHIC MODEL OF STRANGE METALS**

By: Lee, Bum-Hoon; Pang, Da-Wei; Park, Chanyong
INTERNATIONAL JOURNAL OF MODERN PHYSICS A
 Volume: 26 Issue: 14 Pages: 2279-2305 Published: JUN 10 2011

[Full Text from Publisher](#)

[View Abstract](#)

Times Cited: 10
(from Web of Science Core Collection)

Usage Count 

189. **Electrodynamics of correlated electron materials**

By: Basov, D. N.; Averitt, Richard D.; van der Marel, Dirk; et al.
REVIEWS OF MODERN PHYSICS Volume: 83 Issue: 2
 Pages: 471-541 Published: JUN 2 2011

[View Abstract](#)

Times Cited: 243
(from Web of Science Core Collection)

 **Highly Cited Paper**

Usage Count 

190. **Semi-holographic Fermi liquids**

By: Faulkner, Thomas; Polchinski, Joseph
JOURNAL OF HIGH ENERGY PHYSICS Issue: 6 Article
 Number: 012 Published: JUN 2011

[View Abstract](#)

Times Cited: 66
(from Web of Science Core Collection)

Usage Count 

191. **Emergent quantum criticality, Fermi surfaces, and AdS(2)**

By: Faulkner, Thomas; Liu, Hong; McGreevy, John; et al.
PHYSICAL REVIEW D Volume: 83 Issue: 12 Article
 Number: 125002 Published: JUN 1 2011

[View Abstract](#)

Times Cited: 202
(from Web of Science Core Collection)

 **Highly Cited Paper**

Usage Count 

192. **Current issues of iron-based superconductors**

By: Park, K. -S.; Kim, D.; Han, H.; et al.
 Conference: Joint International Conference of 7th Asian Meeting on Ferroelectricity (AMF)/7th Asian Meeting on Electroceramics (AMEC) Location: Jeju, SOUTH KOREA Date: JUN 28-JUL 01, 2010
 Sponsor(s): Korean Ceram Soc; Korean Phys Soc; Korean Federat Sci & Technol Soc; Natl Res Fdn; IEEE-UFFC; Lotte Scholarship Fdn; Hynix Semicond Inc; Park Syst; Seoul Natl Univ; Kyonggi Univ; Univ Ulsan; Changwon Natl Univ; Jeju Special Self-Governing Prov; Korea Tourism Org
CURRENT APPLIED PHYSICS Volume: 11 Issue: 3
 Supplement: S Pages: S33-S41 Published: MAY 2011

[Full Text from Publisher](#)

[View Abstract](#)

Times Cited: 1
(from Web of Science Core Collection)

Usage Count 

193. **d plus id holographic superconductors**

By: Chen, Jiunn-Wei; Liu, Yu-Sheng; Maity, Debaprasad
JOURNAL OF HIGH ENERGY PHYSICS Issue: 5 Article
 Number: 032 Published: MAY 2011

[View Abstract](#)

Times Cited: 8
(from Web of Science Core Collection)

Usage Count 

194. **Mottness collapse and statistical quantum criticality**

By: Zaanen, J.; Overbosch, B. J.
PHILOSOPHICAL TRANSACTIONS OF THE ROYAL SOCIETY A-MATHEMATICAL PHYSICAL AND ENGINEERING SCIENCES
 Volume: 369 Issue: 1941 Pages: 1599-1625 Published: APR 28 2011

[View Abstract](#)

Times Cited: 16
(from Web of Science Core Collection)

Usage Count 

195. **Holographic non-Fermi-liquid fixed points**

By: Faulkner, Tom; Iqbal, Nabil; Liu, Hong; et al.
PHILOSOPHICAL TRANSACTIONS OF THE ROYAL SOCIETY A-MATHEMATICAL PHYSICAL AND ENGINEERING SCIENCES
 Volume: 369 Issue: 1941 Pages: 1640-1669 Published: APR 28 2011

[View Abstract](#)

Times Cited: 23
(from Web of Science Core Collection)

Usage Count 

196. **Holographic optics and negative refractive index**
 By: Amariti, Antonio; Forcella, Davide; Mariotti, Alberto; et al.
JOURNAL OF HIGH ENERGY PHYSICS Issue: 4 Article
 Number: 036 Published: APR 2011
[View Abstract](#)
Times Cited: 15
(from Web of Science Core Collection)
Usage Count
197. **Holography of charged dilatonic black branes at finite temperature**
 By: Cadoni, Mariano; Pani, Paolo
JOURNAL OF HIGH ENERGY PHYSICS Issue: 4 Article
 Number: 049 Published: APR 2011
[View Abstract](#)
Times Cited: 32
(from Web of Science Core Collection)
Usage Count
198. **Shear channel correlators from hot charged black holes**
 By: Brattan, Daniel K.; Gentle, Simon A.
JOURNAL OF HIGH ENERGY PHYSICS Issue: 4 Article
 Number: 082 Published: APR 2011
[View Abstract](#)
Times Cited: 4
(from Web of Science Core Collection)
Usage Count
199. **A study on charged neutron star in AdS(5)**
 By: Parente, Vincenzo; Roychowdhury, Raju
JOURNAL OF HIGH ENERGY PHYSICS Issue: 4 Article
 Number: 111 Published: APR 2011
[View Abstract](#)
Times Cited: 2
(from Web of Science Core Collection)
Usage Count
200. **Fractal Structure Favoring Superconductivity at High Temperatures in a Stack of Membranes Near a Strain Quantum Critical Point**
 By: Poccia, Nicola; Ricci, Alessandro; Bianconi, Antonio
JOURNAL OF SUPERCONDUCTIVITY AND NOVEL MAGNETISM Volume: 24 Issue: 3 Pages: 1195-1200
 Published: APR 2011
[View Abstract](#)
Times Cited: 15
(from Web of Science Core Collection)
Usage Count

Select Page



Save to EndNote online

Add to Marked List

Sort by: **Publication Date -- newest to oldest**

◀ Page 4 of 6 ▶

Show: **50 per page**

263 records matched your query of the 36,466,594 in the data limits you selected.

| | | | | | | | |
|-----------------|----------|---------------------------|-------------------------------|----------|-----------|------|-----------|
| Web of Science™ | InCites™ | Journal Citation Reports® | Essential Science Indicators™ | EndNote™ | Sign In ▾ | Help | English ▾ |
|-----------------|----------|---------------------------|-------------------------------|----------|-----------|------|-----------|

WEB OF SCIENCE™

Search
Return to Search Results
My Tools ▾
Search History
Marked List

Citing Articles: 263
(from Web of Science Core Collection)

For: String Theory, Quantum Phase Transitions, and the Emergent Fermi Liquid ...[More](#)

Times Cited Counts
270 in All Databases

270 in Web of Science Core Collection

2 in BIOSIS Citation Index

4 in Chinese Science Citation Database

0 data sets in Data Citation Index

0 publication in Data Citation Index

1 in Russian Science Citation Index

0 in SciELO Citation Index

[View Additional Times Cited Counts](#)

Refine Results

Web of Science Categories ▾

- PHYSICS PARTICLES FIELDS (198)
- ASTRONOMY ASTROPHYSICS (81)
- PHYSICS MULTIDISCIPLINARY (38)
- PHYSICS CONDENSED MATTER (23)
- PHYSICS NUCLEAR (14)

[more options / values...](#)

Refine

Document Types ▾

- ARTICLE (254)
- REVIEW (9)
- PROCEEDINGS PAPER (4)
- BOOK CHAPTER (1)

[more options / values...](#)

Refine

Research Areas ▾

Authors ▾

Group Authors ▾

Editors ▾

Source Titles ▾

Sort by: **Publication Date -- newest to oldest** ▾

Page 5 of 6

Select Page

Save to EndNote online ▾
Add to Marked List

[Analyze Results](#)

[Create Citation Report](#)

201. **Holographic quantum criticality from multi-trace deformations**

By: Faulkner, Thomas; Horowitz, Gary T.; Roberts, Matthew M.
JOURNAL OF HIGH ENERGY PHYSICS Issue: 4 Article Number: 051 Published: APR 2011

[View Abstract](#)
202. **Holographic phase transitions of p-wave superconductors in Gauss-Bonnet gravity with backreaction**

By: Cai, Rong-Gen; Nie, Zhang-Yu; Zhang, Hai-Qing
PHYSICAL REVIEW D Volume: 83 Issue: 6 Article Number: 066013 Published: MAR 22 2011

[View Abstract](#)
203. **Adventures in holographic dimer models**

By: Kachru, Shamit; Karch, Andreas; Yaida, Sho
NEW JOURNAL OF PHYSICS Volume: 13 Article Number: 035004 Published: MAR 16 2011

[Full Text from Publisher](#) [View Abstract](#)
204. **Polyakov loop of antisymmetric representations as a quantum impurity model**

By: Mueck, Wolfgang
PHYSICAL REVIEW D Volume: 83 Issue: 6 Article Number: 066006 Published: MAR 8 2011

[View Abstract](#)
205. **Conductivity in an anisotropic background**

By: Lee, Bum-Hoon; Nam, Siyoung; Pang, Da-Wej; et al.
PHYSICAL REVIEW D Volume: 83 Issue: 6 Article Number: 066005 Published: MAR 3 2011

[View Abstract](#)
206. **Dynamically Generated Mott Gap from Holography**

By: Edalati, Mohammad; Leigh, Robert G.; Phillips, Philip W.
PHYSICAL REVIEW LETTERS Volume: 106 Issue: 9 Article Number: 091602 Published: MAR 1 2011

[View Abstract](#)
207. **Dynamical gap and cupratelike physics from holography**

By: Edalati, Mohammad; Leigh, Robert G.; Lo, Ka Wai; et al.
PHYSICAL REVIEW D Volume: 83 Issue: 4 Article Number: 046012 Published: FEB 25 2011

[View Abstract](#)
208. **Electron stars for holographic metallic criticality**

By: Hartnoll, Sean A.; Tavanfar, Alireza
PHYSICAL REVIEW D Volume: 83 Issue: 4 Article Number: 046003 Published: FEB 2 2011

Times Cited: 33
(from Web of Science Core Collection)

Usage Count ▾

Times Cited: 39
(from Web of Science Core Collection)

Usage Count ▾

Times Cited: 26
(from Web of Science Core Collection)

Usage Count ▾

Times Cited: 8
(from Web of Science Core Collection)

Usage Count ▾

Times Cited: 15
(from Web of Science Core Collection)

Usage Count ▾

Times Cited: 38
(from Web of Science Core Collection)

Usage Count ▾

Times Cited: 38
(from Web of Science Core Collection)

Usage Count ▾

Times Cited: 101
(from Web of Science Core Collection)

| | | |
|----------------------------------|---|---|
| Book Series Titles | View Abstract | Usage Count |
| Conference Titles | 209. Fermion bag approach to the sign problem in strongly coupled lattice QED with Wilson fermions | Times Cited: 3 <i>(from Web of Science Core Collection)</i> |
| Publication Years | By: Chandrasekharan, Shailesh; Li, Anyi JOURNAL OF HIGH ENERGY PHYSICS Issue: 1 Article Number: 018 Published: JAN 2011 | Usage Count |
| Organizations-Enhanced | View Abstract | |
| Funding Agencies | 210. Degenerate stars and gravitational collapse in AdS/CFT | Times Cited: 30 <i>(from Web of Science Core Collection)</i> |
| Languages | By: Arsiwalla, Xerxes; de Boer, Jan; Papadodimas, Kyriakos; et al. JOURNAL OF HIGH ENERGY PHYSICS Issue: 1 Article Number: 144 Published: JAN 2011 | Usage Count |
| Countries/Territories | View Abstract | |
| ESI Top Papers | 211. Sum rules from an extra dimension | Times Cited: 28 <i>(from Web of Science Core Collection)</i> |
| Open Access | By: Gulotta, Daniel R.; Herzog, Christopher P.; Kaminski, Matthias JOURNAL OF HIGH ENERGY PHYSICS Issue: 1 Article Number: 148 Published: JAN 2011 | Usage Count |
| For advanced refine options, use | | |
| Analyze Results | View Abstract | |
| | 212. Chiral anomalies and AdS/CMT in two dimensions | Times Cited: 38 <i>(from Web of Science Core Collection)</i> |
| | By: Jensen, Kristan JOURNAL OF HIGH ENERGY PHYSICS Issue: 1 Article Number: 109 Published: JAN 2011 | Usage Count |
| | View Abstract | |
| | 213. Characteristic length of a holographic superconductor with d-wave gap | Times Cited: 9 <i>(from Web of Science Core Collection)</i> |
| | By: Zeng, Hua-Bi; Jiang, Yu; Fan, Zhe-Yong; et al. PHYSICAL REVIEW D Volume: 82 Issue: 12 Article Number: 126014 Published: DEC 28 2010 | Usage Count |
| | View Abstract | |
| | 214. Magnetic field-induced quantum criticality via new asymptotically AdS(5) solutions | Times Cited: 20 <i>(from Web of Science Core Collection)</i> |
| | By: D'Hoker, Eric; Kraus, Per CLASSICAL AND QUANTUM GRAVITY Volume: 27 Issue: 21 Article Number: 215022 Published: NOV 21 2010 | Usage Count |
| | View Abstract | |
| | 215. Non-mean-field quantum critical points from holography | Times Cited: 19 <i>(from Web of Science Core Collection)</i> |
| | By: Evans, Nick; Jensen, Kristan; Kim, Keun-Young PHYSICAL REVIEW D Volume: 82 Issue: 10 Article Number: 105012 Published: NOV 15 2010 | Usage Count |
| | View Abstract | |
| | 216. Notes on properties of holographic strange metals | Times Cited: 10 <i>(from Web of Science Core Collection)</i> |
| | By: Lee, Bum-Hoon; Pang, Da-Wei PHYSICAL REVIEW D Volume: 82 Issue: 10 Article Number: 104011 Published: NOV 3 2010 | Usage Count |
| | View Abstract | |
| | 217. Gauge gravity duality for d-wave superconductors: prospects and challenges | Times Cited: 60 <i>(from Web of Science Core Collection)</i> |
| | By: Benini, Francesco; Herzog, Christopher P.; Rahman, Rakibur; et al. JOURNAL OF HIGH ENERGY PHYSICS Issue: 11 Article Number: 137 Published: NOV 2010 | Usage Count |
| | View Abstract | |
| | 218. Effective holographic theories for low-temperature condensed matter systems | Times Cited: 219 <i>(from Web of Science Core Collection)</i> |
| | By: Charmousis, Christos; Gouteraux, Blaise; Kim, Bom Soo; et | |

- al.
JOURNAL OF HIGH ENERGY PHYSICS Issue: 11 Article
 Number: 151 Published: NOV 2010
[View Abstract](#)
Highly Cited Paper
Usage Count ▾
219. **Fermion correlators in non-abelian holographic superconductors**
 By: Gubser, Steven S.; Rocha, Fabio D.; Yarom, Amos
JOURNAL OF HIGH ENERGY PHYSICS Issue: 11 Article
 Number: 085 Published: NOV 2010
[View Abstract](#)
Times Cited: 20
(from Web of Science Core Collection)
Usage Count ▾
220. **Zero sound in effective holographic theories**
 By: Lee, Bum-Hoon; Pang, Da-Wei; Park, Chanyong
JOURNAL OF HIGH ENERGY PHYSICS Issue: 11 Article
 Number: 120 Published: NOV 2010
[View Abstract](#)
Times Cited: 13
(from Web of Science Core Collection)
Usage Count ▾
221. **Strange metals and the AdS/CFT correspondence**
 By: Sachdev, Subir
JOURNAL OF STATISTICAL MECHANICS-THEORY AND EXPERIMENT Article Number: P11022 Published: NOV 2010
[View Abstract](#)
Times Cited: 7
(from Web of Science Core Collection)
Usage Count ▾
222. **Density-matrix renormalization-group study of coupled Luttinger liquids**
 By: Moukouri, S.; Eidelstein, E.
PHYSICAL REVIEW B Volume: 82 Issue: 16 Article
 Number: 165132 Published: OCT 29 2010
[View Abstract](#)
Times Cited: 1
(from Web of Science Core Collection)
Usage Count ▾
223. **Holographic Metals and the Fractionalized Fermi Liquid**
 By: Sachdev, Subir
PHYSICAL REVIEW LETTERS Volume: 105 Issue: 15
 Article Number: 151602 Published: OCT 4 2010
[View Abstract](#)
Times Cited: 91
(from Web of Science Core Collection)
Usage Count ▾
224. **Normalizable fermion modes in a holographic superconductor**
 By: Gubser, Steven S.; Rocha, Fabio D.; Talavera, Pedro
JOURNAL OF HIGH ENERGY PHYSICS Issue: 10 Article
 Number: 087 Published: OCT 2010
[View Abstract](#)
Times Cited: 20
(from Web of Science Core Collection)
Usage Count ▾
225. **Global Phase Diagram of the Kondo Lattice: From Heavy Fermion Metals to Kondo Insulators**
 By: Yamamoto, Seiji J.; Si, Qimiao
JOURNAL OF LOW TEMPERATURE PHYSICS Volume: 161
 Issue: 1-2 Pages: 233-262 Published: OCT 2010
[View Abstract](#)
Times Cited: 14
(from Web of Science Core Collection)
Usage Count ▾
226. **Thermodynamics of quasiconformal theories from gauge/gravity duality**
 By: Alanen, Janne; Kajantie, Keijo; Tuominen, Kimmo
PHYSICAL REVIEW D Volume: 82 Issue: 5 Article Number:
 055024 Published: SEP 29 2010
[View Abstract](#)
Times Cited: 22
(from Web of Science Core Collection)
Usage Count ▾
227. **Zero sound in strange metallic holography**
 By: Hoyos, Carlos; O'Bannon, Andy; Wu, Jackson M. S.
JOURNAL OF HIGH ENERGY PHYSICS Issue: 9 Article
 Number: 086 Published: SEP 2010
[View Abstract](#)
Times Cited: 19
(from Web of Science Core Collection)
Usage Count ▾
228. **Strange Metal Transport Realized by Gauge/Gravity Duality**
 By: Faulkner, Thomas; Iqbal, Nabil; Liu, Hong; et al.
Usage Count ▾
Times Cited: 68
(from Web of Science Core Collection)

SCIENCE Volume: 329 Issue: 5995 Pages: 1043-1047
Published: AUG 27 2010

[View Abstract](#)

Usage Count 

229. **Holographic non-Fermi liquid in a background magnetic field**

By: Basu, Pallab; He, JianYang; Mukherjee, Anindya; et al.
PHYSICAL REVIEW D Volume: 82 Issue: 4 Article Number: 044036
Published: AUG 20 2010

[View Abstract](#)

Times Cited: **19**
(from Web of Science Core Collection)

Usage Count 

230. **More holographic Berezinskii-Kosterlitz-Thouless transitions**

By: Jensen, Kristan
PHYSICAL REVIEW D Volume: 82 Issue: 4 Article Number: 046005
Published: AUG 19 2010

[View Abstract](#)

Times Cited: **29**
(from Web of Science Core Collection)

Usage Count 

231. **Quantum phase transitions of metals in two spatial dimensions. I. Ising-nematic order**

By: Metlitski, Max A.; Sachdev, Subir
PHYSICAL REVIEW B Volume: 82 Issue: 7 Article Number: 075127
Published: AUG 16 2010

[View Abstract](#)

Times Cited: **142**
(from Web of Science Core Collection)

 **Highly Cited Paper**

Usage Count 

232. **Scale-free structural organization of oxygen interstitials in La₂CuO_{4+y}**

By: Fratini, Michela; Poccia, Nicola; Ricci, Alessandro; et al.
NATURE Volume: 466 Issue: 7308 Pages: 841-844
Published: AUG 12 2010

[View Abstract](#)

Times Cited: **124**
(from Web of Science Core Collection)

Usage Count 

233. **Quantum phase transitions in holographic models of magnetism and superconductors**

By: Iqbal, Nabil; Liu, Hong; Mezei, Mark; et al.
PHYSICAL REVIEW D Volume: 82 Issue: 4 Article Number: 045002
Published: AUG 3 2010

[View Abstract](#)

Times Cited: **73**
(from Web of Science Core Collection)

Usage Count 

234. **Black hole thermodynamics and heavy fermion metals**

By: Brynjolfsson, E. J.; Danielsson, U. H.; Thorlacius, L.; et al.
JOURNAL OF HIGH ENERGY PHYSICS Issue: 8 Article Number: 027
Published: AUG 2010

[View Abstract](#)

Times Cited: **12**
(from Web of Science Core Collection)

Usage Count 

235. **Holography of charged dilaton black holes**

By: Goldstein, Kevin; Kachru, Shamit; Prakash, Shiroman; et al.
JOURNAL OF HIGH ENERGY PHYSICS Issue: 8 Article Number: 078
Published: AUG 2010

[View Abstract](#)

Times Cited: **139**
(from Web of Science Core Collection)

 **Highly Cited Paper**

Usage Count 

236. **Peak-dip-hump lineshape from holographic superconductivity**

By: Chen, Jiunn-Wei; Kao, Ying-Jer; Wen, Wen-Yu
PHYSICAL REVIEW D Volume: 82 Issue: 2 Article Number: 026007
Published: JUL 28 2010

[View Abstract](#)

Times Cited: **19**
(from Web of Science Core Collection)

Usage Count 

237. **Controlled expansion for certain non-Fermi-liquid metals**

By: Mross, David F.; McGreevy, John; Liu, Hong; et al.
PHYSICAL REVIEW B Volume: 82 Issue: 4 Article Number: 045121
Published: JUL 26 2010

[View Abstract](#)

Times Cited: **115**
(from Web of Science Core Collection)

Usage Count 

238. **Holographic Berezinskii-Kosterlitz-Thouless**

Times Cited: **62**

Transitions

By: Jensen, Kristan; Karch, Andreas; Son, Dam T.; et al.
PHYSICAL REVIEW LETTERS Volume: 105 Issue: 4 Article
 Number: 041601 Published: JUL 20 2010

[View Abstract](#)

(from Web of Science Core Collection)

Usage Count 

239. **Strange metallic behavior in anisotropic background**

By: Lee, Bum-Hoon; Pang, Da-Wei; Park, Chanyong
JOURNAL OF HIGH ENERGY PHYSICS Issue: 7 Article
 Number: 057 Published: JUL 2010

[View Abstract](#)

Times Cited: 15

(from Web of Science Core Collection)

Usage Count 

240. **Holographic superconductors from Einstein-Maxwell-Dilaton gravity**

By: Liu, Yan; Sun, Ya-Wen
JOURNAL OF HIGH ENERGY PHYSICS Issue: 7 Article
 Number: 099 Published: JUL 2010

[View Abstract](#)

Times Cited: 17

(from Web of Science Core Collection)

Usage Count 

241. **Inhomogeneous structures in holographic superfluids. I. Dark solitons**

By: Keranen, Ville; Keski-Vakkuri, Esko; Nowling, Sean; et al.
PHYSICAL REVIEW D Volume: 81 Issue: 12 Article
 Number: 126011 Published: JUN 24 2010

[View Abstract](#)

Times Cited: 19

(from Web of Science Core Collection)

Usage Count 

242. **Membranes with topological charge and AdS(4)/CFT3 correspondence**

By: Klebanov, Igor R.; Pufu, Silviu S.; Tesileanu, Tiberiu
PHYSICAL REVIEW D Volume: 81 Issue: 12 Article
 Number: 125011 Published: JUN 14 2010

[View Abstract](#)

Times Cited: 24

(from Web of Science Core Collection)

Usage Count 

243. **Holography of charged dilaton black holes in general dimensions**

By: Chen, Chiang-Mei; Pang, Da-Wei
JOURNAL OF HIGH ENERGY PHYSICS Issue: 6 Article
 Number: 093 Published: JUN 2010

[View Abstract](#)

Times Cited: 27

(from Web of Science Core Collection)

Usage Count 

244. **Cooper pairing near charged black holes**

By: Hartman, Thomas; Hartnoll, Sean A.
JOURNAL OF HIGH ENERGY PHYSICS Issue: 6 Article
 Number: 005 Published: JUN 2010

[View Abstract](#)

Times Cited: 21

(from Web of Science Core Collection)

Usage Count 

245. **Fermionic operator mixing in holographic p-wave superfluids**

By: Ammon, Martin; Erdmenger, Johanna; Kaminski, Matthias; et al.
JOURNAL OF HIGH ENERGY PHYSICS Issue: 5 Article
 Number: 053 Published: MAY 2010

[View Abstract](#)

Times Cited: 39

(from Web of Science Core Collection)

Usage Count 

246. **Holographic metamagnetism, quantum criticality, and crossover behavior**

By: D'Hoker, Eric; Kraus, Per
JOURNAL OF HIGH ENERGY PHYSICS Issue: 5 Article
 Number: 083 Published: MAY 2010

[View Abstract](#)

Times Cited: 26

(from Web of Science Core Collection)

Usage Count 

247. **Holographic aspects of three dimensional QCD from string theory**

By: Hong, Deog Ki; Yee, Ho-Ung
JOURNAL OF HIGH ENERGY PHYSICS Issue: 5 Article
 Number: 036 Published: MAY 2010

[View Abstract](#)

Times Cited: 7

(from Web of Science Core Collection)

Usage Count 

248. **A holographic quantum critical point at finite magnetic field and finite density**

By: Jensen, Kristan; Karch, Andreas; Thompson, Ethan G.
JOURNAL OF HIGH ENERGY PHYSICS Issue: 5 Article
Number: 015 Published: MAY 2010

[View Abstract](#)

Times Cited: 32
(from Web of Science Core Collection)

Usage Count ▾

249. **Emergence of non-Fermi-liquid behavior due to Fermi surface reconstruction in the underdoped cuprate superconductors**

By: Das, Tanmoy; Markiewicz, R. S.; Bansil, A.
PHYSICAL REVIEW B Volume: 81 Issue: 18 Article
Number: 184515 Published: MAY 1 2010

[View Abstract](#)

Times Cited: 22
(from Web of Science Core Collection)

Usage Count ▾

250. **Generalized Lifshitz-Kosevich scaling at quantum criticality from the holographic correspondence**

By: Hartnoll, Sean A.; Hofman, Diego M.
PHYSICAL REVIEW B Volume: 81 Issue: 15 Article
Number: 155125 Published: APR 15 2010

[View Abstract](#)

Times Cited: 16
(from Web of Science Core Collection)

Usage Count ▾

Select Page



Save to EndNote online ▾

Add to Marked List

Sort by: **Publication Date -- newest to oldest** ▾

◀ Page 5 of 6 ▶

Show: **50 per page** ▾

263 records matched your query of the 36,466,594 in the data limits you selected.

| | | | | | | | |
|-----------------|----------|---------------------------|-------------------------------|----------|-----------|------|-----------|
| Web of Science™ | InCites™ | Journal Citation Reports® | Essential Science Indicators™ | EndNote™ | Sign In ▾ | Help | English ▾ |
|-----------------|----------|---------------------------|-------------------------------|----------|-----------|------|-----------|

WEB OF SCIENCE™

Search
Return to Search Results
My Tools ▾
Search History
Marked List

Citing Articles: 263
(from Web of Science Core Collection)

For: String Theory, Quantum Phase Transitions, and the Emergent Fermi Liquid ...[More](#)

Times Cited Counts
270 in All Databases

270 in Web of Science Core Collection

2 in BIOSIS Citation Index

4 in Chinese Science Citation Database

0 data sets in Data Citation Index

0 publication in Data Citation Index

1 in Russian Science Citation Index

0 in SciELO Citation Index

[View Additional Times Cited Counts](#)

Refine Results

Web of Science Categories ▾

- PHYSICS PARTICLES FIELDS (198)
- ASTRONOMY ASTROPHYSICS (81)
- PHYSICS MULTIDISCIPLINARY (38)
- PHYSICS CONDENSED MATTER (23)
- PHYSICS NUCLEAR (14)

[more options / values...](#)

Refine

Document Types ▾

- ARTICLE (254)
- REVIEW (9)
- PROCEEDINGS PAPER (4)
- BOOK CHAPTER (1)

[more options / values...](#)

Refine

Research Areas ▾

Authors ▾

Group Authors ▾

Editors ▾

Source Titles ▾

Sort by: **Publication Date -- newest to oldest** ▾

Page 6 of 6

Select Page

Save to EndNote online ▾
Add to Marked List

[Analyze Results](#)

[Create Citation Report](#)

- 251. **Transport coefficients from extremal Gauss-Bonnet black holes**

By: Cai, Rong-Gen; Liu, Yan; Sun, Ya-Wen
JOURNAL OF HIGH ENERGY PHYSICS Issue: 4 Article
 Number: 090 Published: APR 2010

[View Abstract](#)
- 252. **Towards strange metallic holography**

By: Hartnoll, Sean A.; Polchinski, Joseph; Silverstein, Eva; et al.
JOURNAL OF HIGH ENERGY PHYSICS Issue: 4 Article
 Number: 120 Published: APR 2010

[View Abstract](#)
- 253. **Phase transitions between Reissner-Nordstrom and dilatonic black holes in 4D AdS spacetime**

By: Cadoni, Mariano; D'Appollonio, Giuseppe; Pani, Paolo
JOURNAL OF HIGH ENERGY PHYSICS Issue: 3 Article
 Number: 100 Published: MAR 2010

[View Abstract](#)
- 254. **Charged magnetic brane solutions in AdS(5) and the fate of the third law of thermodynamics**

By: D'Hoker, Eric; Kraus, Per
JOURNAL OF HIGH ENERGY PHYSICS Issue: 3 Article
 Number: 095 Published: MAR 2010

[View Abstract](#)
- 255. **Emergent quantum near-criticality from baryonic black branes**

By: Herzog, Christopher P.; Klebanov, Igor R.; Pufu, Silviu S.; et al.
JOURNAL OF HIGH ENERGY PHYSICS Issue: 3 Article
 Number: 093 Published: MAR 2010

[View Abstract](#)
- 256. **Holographic superconductor/insulator transition at zero temperature**

By: Nishioka, Tatzuma; Ryu, Shinsei; Takayanagi, Tadashi
JOURNAL OF HIGH ENERGY PHYSICS Issue: 3 Article
 Number: 131 Published: MAR 2010

[View Abstract](#)
- 257. **Supergravity as a constrained BF theory**

By: Durka, R.; Kowalski-Glikman, J.; Szczachor, M.
PHYSICAL REVIEW D Volume: 81 Issue: 4 Article Number: 045022
 Published: FEB 15 2010

[View Abstract](#)
- 258. **Peculiar properties of a charged dilatonic black hole in AdS(5)**

Times Cited: 12
(from Web of Science Core Collection)

Usage Count ▾

Times Cited: 210
(from Web of Science Core Collection)

Highly Cited Paper

Usage Count ▾

Times Cited: 64
(from Web of Science Core Collection)

Usage Count ▾

Times Cited: 39
(from Web of Science Core Collection)

Usage Count ▾

Times Cited: 16
(from Web of Science Core Collection)

Usage Count ▾

Times Cited: 91
(from Web of Science Core Collection)

Usage Count ▾

Times Cited: 3
(from Web of Science Core Collection)

Usage Count ▾

Times Cited: 124
(from Web of Science Core Collection)

| | | |
|--|---|--|
| <p>Book Series Titles ◀</p> <p>Conference Titles ◀</p> <p>Publication Years ◀</p> <p>Organizations-Enhanced ◀</p> <p>Funding Agencies ◀</p> <p>Languages ◀</p> <p>Countries/Territories ◀</p> <p>ESI Top Papers ◀</p> <p>Open Access ◀</p> <p><i>For advanced refine options, use</i></p> <p>Analyze Results</p> | <p>By: Gubser, Steven S.; Rocha, Fabio D. PHYSICAL REVIEW D Volume: 81 Issue: 4 Article Number: 046001 Published: FEB 15 2010</p> <p style="text-align: center;">View Abstract</p> <p>259. Holographic lattices, dimers, and glasses</p> <p>By: Kachru, Shmit; Karch, Andreas; Yaida, Sho PHYSICAL REVIEW D Volume: 81 Issue: 2 Article Number: 026007 Published: JAN 15 2010</p> <p style="text-align: center;">View Abstract</p> <p>260. Holographic Duality with a View Toward Many-Body Physics</p> <p>By: McGreevy, John ADVANCES IN HIGH ENERGY PHYSICS Article Number: 723105 Published: 2010</p> <p style="text-align: center;">Full Text from Publisher View Abstract</p> <p>261. Global Existence, Uniqueness, and Asymptotic Behavior of Solution for p-Laplacian Type Wave Equation</p> <p>By: Chen, Caisheng; Yao, Huaping; Shao, Ling JOURNAL OF INEQUALITIES AND APPLICATIONS Article Number: 216760 Published: 2010</p> <p style="text-align: center;">Full Text from Publisher View Abstract</p> <p>262. BCS superconductivity in quantum critical metals</p> <p>By: She, Jian-Huang; Zaanen, Jan PHYSICAL REVIEW B Volume: 80 Issue: 18 Article Number: 184518 Published: NOV 2009</p> <p style="text-align: center;">View Abstract</p> <p>263. Low-energy effective theory of Fermi surface coupled with U(1) gauge field in 2+1 dimensions</p> <p>By: Lee, Sung-Sik PHYSICAL REVIEW B Volume: 80 Issue: 16 Article Number: 165102 Published: OCT 2009</p> <p style="text-align: center;">View Abstract</p> | <p>Usage Count ▼</p> <p>Times Cited: 58 <i>(from Web of Science Core Collection)</i></p> <p>Usage Count ▼</p> <p>Times Cited: 236 <i>(from Web of Science Core Collection)</i></p> <p> Highly Cited Paper</p> <p>Usage Count ▼</p> <p>Times Cited: 3 <i>(from Web of Science Core Collection)</i></p> <p>Usage Count ▼</p> <p>Times Cited: 25 <i>(from Web of Science Core Collection)</i></p> <p>Usage Count ▼</p> <p>Times Cited: 135 <i>(from Web of Science Core Collection)</i></p> <p>Usage Count ▼</p> |
|--|---|--|

Select Page | | **Save to EndNote online** ▼ | **Add to Marked List**

Sort by: **Publication Date -- newest to oldest** ▼

Show: **50 per page** ▼

◀ Page 6 of 6 ▶

263 records matched your query of the 36,466,594 in the data limits you selected.

Web of Science™ InCites™ Journal Citation Reports® Essential Science Indicators™ EndNote™
Sign In Help English ▾

WEB OF SCIENCE™

Search
Return to Search Results
My Tools ▾ Search History Marked List

Citing Articles: 18

(from Web of Science Core Collection)

For: Spectral probes of the holographic Fermi ground state: Dialing between the electron star and AdS Dir ...[More](#)

Times Cited Counts

[20 in All Databases](#)

20 in Web of Science Core Collection

0 in BIOSIS Citation Index

0 in Chinese Science Citation Database

0 data sets in Data Citation Index

0 publication in Data Citation Index

0 in Russian Science Citation Index

0 in SciELO Citation Index

[View Additional Times Cited Counts](#)

Refine Results

Web of Science Categories ▾

- PHYSICS PARTICLES FIELDS (15)
- ASTRONOMY ASTROPHYSICS (3)
- PHYSICS MULTIDISCIPLINARY (2)
- PHYSICS CONDENSED MATTER (1)

[more options / values...](#)

Refine

Document Types ▾

- ARTICLE (17)
- REVIEW (1)

[more options / values...](#)

Refine

Research Areas ▾

Authors ▾

Group Authors ▾

Editors ▾

Source Titles ▾

Book Series Titles ▾

Sort by: Publication Date -- newest to oldest ▾
Page 1 of 1

Select Page

Save to EndNote online ▾

Add to Marked List


[Analyze Results](#)
[Create Citation Report](#)

| | | |
|----|---|--|
| 1. | <p>Holographic fermions at strong translational symmetry breaking: a Bianchi-VII case study</p> <p>By: Bagrov, A.; Kaplis, N.; Krikun, A.; et al. JOURNAL OF HIGH ENERGY PHYSICS Issue: 11 Article Number: 057 Published: NOV 9 2016</p> <p style="text-align: center; border: 1px solid #ccc; padding: 2px 5px;">View Abstract</p> | <p>Times Cited: 0 <i>(from Web of Science Core Collection)</i></p> <p>Usage Count ▾</p> |
| 2. | <p>Polarized solutions and Fermi surfaces in holographic Bose-Fermi systems</p> <p>By: Nitti, Francesco; Policastro, Giuseppe; Vanel, Thomas JOURNAL OF HIGH ENERGY PHYSICS Issue: 12 Article Number: 027 Published: DEC 3 2014</p> <p style="text-align: center; border: 1px solid #ccc; padding: 2px 5px;">View Abstract</p> | <p>Times Cited: 3 <i>(from Web of Science Core Collection)</i></p> <p>Usage Count ▾</p> |
| 3. | <p>Holographic quenches and fermionic spectral functions</p> <p>By: Callebaut, N.; Craps, B.; Galli, F.; et al. JOURNAL OF HIGH ENERGY PHYSICS Issue: 10 Article Number: 172 Published: OCT 30 2014</p> <p style="text-align: center; border: 1px solid #ccc; padding: 2px 5px;">View Abstract</p> | <p>Times Cited: 3 <i>(from Web of Science Core Collection)</i></p> <p>Usage Count ▾</p> |
| 4. | <p>BCS instabilities of electron stars to holographic superconductors</p> <p>By: Liu, Yan; Schalm, Koenraad; Sun, Ya-Wen; et al. JOURNAL OF HIGH ENERGY PHYSICS Issue: 5 Article Number: 122 Published: MAY 27 2014</p> <p style="text-align: center; border: 1px solid #ccc; padding: 2px 5px;">View Abstract</p> | <p>Times Cited: 2 <i>(from Web of Science Core Collection)</i></p> <p>Usage Count ▾</p> |
| 5. | <p>Schrodinger Fermi liquids</p> <p>By: Wang, Juven PHYSICAL REVIEW D Volume: 89 Issue: 4 Article Number: 046008 Published: FEB 27 2014</p> <p style="text-align: center; border: 1px solid #ccc; padding: 2px 5px;">View Abstract</p> | <p>Times Cited: 5 <i>(from Web of Science Core Collection)</i></p> <p>Usage Count ▾</p> |
| 6. | <p>Bose-Fermi competition in holographic metals</p> <p>By: Liu, Yan; Schalm, Koenraad; Sun, Ya-Wen; et al. JOURNAL OF HIGH ENERGY PHYSICS Issue: 10 Article Number: 064 Published: OCT 10 2013</p> <p style="text-align: center; border: 1px solid #ccc; padding: 2px 5px;">View Abstract</p> | <p>Times Cited: 6 <i>(from Web of Science Core Collection)</i></p> <p>Usage Count ▾</p> |
| 7. | <p>Charge transport by holographic Fermi surfaces</p> <p>By: Faulkner, Thomas; Iqbal, Nabil; Liu, Hong; et al. PHYSICAL REVIEW D Volume: 88 Issue: 4 Article Number: 045016 Published: AUG 21 2013</p> <p style="text-align: center; border: 1px solid #ccc; padding: 2px 5px;">View Abstract</p> | <p>Times Cited: 14 <i>(from Web of Science Core Collection)</i></p> <p>Usage Count ▾</p> |
| 8. | <p>An introduction to gauge-gravity duality and its application in condensed matter</p> <p>By: Green, A. G. CONTEMPORARY PHYSICS Volume: 54 Issue: 1 Pages: 33-48 Published: FEB 1 2013</p> | <p>Times Cited: 8 <i>(from Web of Science Core Collection)</i></p> <p>Usage Count ▾</p> |




| | |
|------------------------|---|
| Conference Titles | ◀ |
| Publication Years | ◀ |
| Organizations-Enhanced | ◀ |
| Funding Agencies | ◀ |
| Languages | ◀ |
| Countries/Territories | ◀ |
| ESI Top Papers | ◀ |
| Open Access | ◀ |


For advanced refine options, use


[Analyze Results](#)

- [View Abstract](#)
9. **Charged black branes with hyperscaling violating factor**
 By: Alishahiha, Mohsen; Colgain, Eoin O.; Yavartanoo, Hossein
 JOURNAL OF HIGH ENERGY PHYSICS Issue: 11 Article Number: 137 Published: NOV 2012
[View Abstract](#)
Times Cited: 45
(from Web of Science Core Collection)
Usage Count ▼
10. **Lattice potentials and fermions in holographic non Fermi-liquids: hybridizing local quantum criticality**
 By: Liu, Yan; Schalm, Koenraad; Sun, Ya-Wen; et al.
 JOURNAL OF HIGH ENERGY PHYSICS Issue: 10 Article Number: 036 Published: OCT 2012
[View Abstract](#)
Times Cited: 15
(from Web of Science Core Collection)
Usage Count ▼
11. **Fermions on a Lifshitz background**
 By: Alishahiha, Mohsen; Mozaffar, M. Reza Mohammadi; Mollabashi, Ali
 PHYSICAL REVIEW D Volume: 86 Issue: 2 Article Number: 026002 Published: JUL 3 2012
[View Abstract](#)
Times Cited: 27
(from Web of Science Core Collection)
Usage Count ▼
12. **Quantum Electron Star**
 By: Allais, Andrea; McGreevy, John; Suh, S. Josephine
 PHYSICAL REVIEW LETTERS Volume: 108 Issue: 23 Article Number: 231602 Published: JUN 8 2012
[View Abstract](#)
Times Cited: 22
(from Web of Science Core Collection)
Usage Count ▼
13. **Spatially homogeneous Lifshitz black holes in five dimensional higher derivative gravity**
 By: Liu, Yan
 JOURNAL OF HIGH ENERGY PHYSICS Issue: 6 Article Number: 024 Published: JUN 2012
[View Abstract](#)
Times Cited: 3
(from Web of Science Core Collection)
Usage Count ▼
14. **Semi-local quantum liquids**
 By: Iqbal, Nabil; Liu, Hong; Mezei, Mark
 JOURNAL OF HIGH ENERGY PHYSICS Issue: 4 Article Number: 086 Published: APR 2012
[View Abstract](#)
Times Cited: 36
(from Web of Science Core Collection)
Usage Count ▼
15. **Soliton stars as holographic confined Fermi liquids**
 By: Bhattacharya, Jyotirmoy; Ogawa, Noriaki; Takayanagi, Tadashi; et al.
 JOURNAL OF HIGH ENERGY PHYSICS Issue: 2 Article Number: 137 Published: FEB 2012
[View Abstract](#)
Times Cited: 1
(from Web of Science Core Collection)
Usage Count ▼
16. **Hidden Fermi surfaces in compressible states of gauge-gravity duality**
 By: Huijse, Liza; Sachdev, Subir; Swingle, Brian
 PHYSICAL REVIEW B Volume: 85 Issue: 3 Article Number: 035121 Published: JAN 25 2012
[View Abstract](#)
Times Cited: 208
(from Web of Science Core Collection)
 **Highly Cited Paper**
Usage Count ▼
17. **Friedel oscillations in holographic metals**
 By: Puletti, V. Giangreco M.; Nowling, S.; Thorlacius, L.; et al.
 JOURNAL OF HIGH ENERGY PHYSICS Issue: 1 Article Number: 073 Published: JAN 2012
[View Abstract](#)
Times Cited: 6
(from Web of Science Core Collection)
Usage Count ▼
18. **Spectral function of the supersymmetry current**
 By: Gauntlett, Jerome P.; Sonner, Julian; Waldram, Daniel
 JOURNAL OF HIGH ENERGY PHYSICS Issue: 11 Article Number: 153 Published: NOV 2011
Times Cited: 20
(from Web of Science Core Collection)
Usage Count ▼

[View Abstract](#)

Select Page |   | [Save to EndNote online](#)  | [Add to Marked List](#)

Sort by: [Publication Date -- newest to oldest](#) 

Show: [50 per page](#) 

◀ Page of 1 ▶

18 records matched your query of the 36,466,594 in the data limits you selected.

| |
|--|
| |
|--|

Web of Science™ InCites™ Journal Citation Reports® Essential Science Indicators™ EndNote™
Sign In Help English

WEB OF SCIENCE™

Search
Return to Search Results
My Tools Search History Marked List

Citing Articles: 15
(from Web of Science Core Collection)

For: Holographic fermions in external magnetic fields [...More](#)

Times Cited Counts
[17 in All Databases](#)

17 in Web of Science Core Collection

0 in BIOSIS Citation Index

0 in Chinese Science Citation Database

0 data sets in Data Citation Index

0 publication in Data Citation Index

0 in Russian Science Citation Index

0 in SciELO Citation Index

[View Additional Times Cited Counts](#)

Refine Results

Web of Science Categories

- PHYSICS PARTICLES FIELDS (15)
- ASTRONOMY ASTROPHYSICS (2)

[more options / values...](#)

[Refine](#)

Document Types

- ARTICLE (15)

[Refine](#)

Research Areas

Authors

Group Authors

Editors

Source Titles

Book Series Titles

Conference Titles

Publication Years

Organizations-Enhanced

Sort by: Publication Date -- newest to oldest
Page 1 of 1

Select Page
[Save to EndNote online](#)
[Add to Marked List](#)

[Analyze Results](#)
[Create Citation Report](#)

1. **Ward identities and relations between conductivities and viscosities in holography**

By: Hoyos, Carlos; Rodriguez Fernandez, David
JOURNAL OF HIGH ENERGY PHYSICS Issue: 1 Article Number: 013 Published: JAN 4 2016

[View Abstract](#)
2. **Magnetic oscillations in a holographic liquid**

By: Puletti, V. Giangreco M.; Nowling, S.; Thorlacius, L.; et al.
PHYSICAL REVIEW D Volume: 91 Issue: 8 Article Number: 086008 Published: APR 8 2015

[View Abstract](#)
3. **Flux and Hall states in ABJM with dynamical flavors**

By: Bea, Yago; Jokela, Niko; Lippert, Matthew; et al.
JOURNAL OF HIGH ENERGY PHYSICS Issue: 3 Article Number: 009 Published: MAR 2 2015

[View Abstract](#)
4. **Horava-Lifshitz gravity and effective theory of the fractional quantum Hall effect**

By: Wu, Chaolun; Wu, Shao-Feng
JOURNAL OF HIGH ENERGY PHYSICS Issue: 1 Article Number: 120 Published: JAN 22 2015

[View Abstract](#)
5. **Holographic spontaneous parity breaking and emergent hall viscosity and angular momentum**

By: Son, Dam Thanh; Wu, Chaolun
JOURNAL OF HIGH ENERGY PHYSICS Issue: 7 Article Number: 076 Published: JUL 17 2014

[View Abstract](#)
6. **Crystalline geometries from a fermionic vortex lattice**

By: Mozaffar, M. Reza Mohammadi; Mollabashi, Ali
PHYSICAL REVIEW D Volume: 89 Issue: 4 Article Number: 046007 Published: FEB 20 2014

[View Abstract](#)
7. **Emergence of gap from holographic fermions on charged Lifshitz background**

By: Wu, Jian-Pin
JOURNAL OF HIGH ENERGY PHYSICS Issue: 4 Article Number: 073 Published: APR 2013

[View Abstract](#)
8. **Holographic fermions in charged dilaton black branes**

By: Li, Wei-Jia; Wu, Jian-Pin
NUCLEAR PHYSICS B Volume: 867 Issue: 3 Pages: 810-826 Published: FEB 21 2013

Times Cited: 0
(from Web of Science Core Collection)

[Usage Count](#)

Times Cited: 0
(from Web of Science Core Collection)

[Usage Count](#)

Times Cited: 3
(from Web of Science Core Collection)

[Usage Count](#)

Times Cited: 6
(from Web of Science Core Collection)

[Usage Count](#)

Times Cited: 13
(from Web of Science Core Collection)

[Usage Count](#)

Times Cited: 9
(from Web of Science Core Collection)

[Usage Count](#)

Times Cited: 6
(from Web of Science Core Collection)

[Usage Count](#)

Times Cited: 12
(from Web of Science Core Collection)

[Usage Count](#)

- Funding Agencies
- Languages
- Countries/Territories
- ESI Top Papers
- Open Access

For advanced refine options, use

[Analyze Results](#)

[Full Text from Publisher](#) [View Abstract](#)

9. **Holographic dual of the lowest Landau level**
 By: Blake, Mike; Bolognesi, Stefano; Tong, David; et al.
 JOURNAL OF HIGH ENERGY PHYSICS Issue: 12 Article
 Number: 039 Published: DEC 2012

[View Abstract](#)

Times Cited: 7
 (from Web of Science Core Collection)

Usage Count

10. **Fluctuations in finite density holographic quantum liquids**
 By: Goykhman, Mikhail; Parnachev, Andrei; Zaanen, Jan
 JOURNAL OF HIGH ENERGY PHYSICS Issue: 10 Article
 Number: 045 Published: OCT 2012

[View Abstract](#)

Times Cited: 12
 (from Web of Science Core Collection)

Usage Count

11. **d-wave holographic superconductors with backreaction in external magnetic fields**
 By: Ge, Xian-Hui; Tu, Shao Fei; Wang, Bin
 JOURNAL OF HIGH ENERGY PHYSICS Issue: 9 Article
 Number: 088 Published: SEP 2012

[View Abstract](#)

Times Cited: 9
 (from Web of Science Core Collection)

Usage Count

12. **A gapless hard wall: magnetic catalysis in bulk and boundary**
 By: Bolognesi, Stefano; Laia, Joao N.; Tong, David; et al.
 JOURNAL OF HIGH ENERGY PHYSICS Issue: 7 Article
 Number: 162 Published: JUL 2012

[View Abstract](#)

Times Cited: 11
 (from Web of Science Core Collection)

Usage Count

13. **Dynamic gap from holographic fermions in charged dilaton black branes**
 By: Wu, Jian-Pin; Zeng, Hua-Bi
 JOURNAL OF HIGH ENERGY PHYSICS Issue: 4 Article
 Number: 068 Published: APR 2012

[View Abstract](#)

Times Cited: 10
 (from Web of Science Core Collection)

Usage Count

14. **Fluctuations of a holographic quantum Hall fluid**
 By: Jokela, Niko; Jaervinen, Matti; Lippert, Matthew
 JOURNAL OF HIGH ENERGY PHYSICS Issue: 1 Article
 Number: 072 Published: JAN 2012

[View Abstract](#)

Times Cited: 9
 (from Web of Science Core Collection)

Usage Count

15. **Spectral function of the supersymmetry current**
 By: Gauntlett, Jerome P.; Sonner, Julian; Waldram, Daniel
 JOURNAL OF HIGH ENERGY PHYSICS Issue: 11 Article
 Number: 153 Published: NOV 2011

[View Abstract](#)

Times Cited: 20
 (from Web of Science Core Collection)

Usage Count

Select Page [Save to EndNote online](#) [Add to Marked List](#)

Sort by: [Publication Date -- newest to oldest](#) Page 1 of 1

Show: [50 per page](#)

15 records matched your query of the 36,466,594 in the data limits you selected.

Web of Science™ InCites™ Journal Citation Reports® Essential Science Indicators™ EndNote™
Sign In Help English

WEB OF SCIENCE™

Search
Return to Search Results My Tools Search History Marked List

Citing Articles: 13
(from Web of Science Core Collection)

For: Constructing the AdS dual of a Fermi liquid: AdS black holes with Dirac hair ...[More](#)

Times Cited Counts
[14 in All Databases](#)

14 in Web of Science Core Collection
0 in BIOSIS Citation Index
0 in Chinese Science Citation Database
0 data sets in Data Citation Index
0 publication in Data Citation Index
0 in Russian Science Citation Index
0 in SciELO Citation Index
[View Additional Times Cited Counts](#)

Refine Results

Web of Science Categories

- PHYSICS PARTICLES FIELDS (11)
- ASTRONOMY ASTROPHYSICS (4)
- PHYSICS MULTIDISCIPLINARY (2)

[more options / values...](#) Refine

Document Types

ARTICLE (13) Refine

Research Areas

Authors

Group Authors

Editors

Source Titles

Book Series Titles

Conference Titles

Publication Years

Sort by: Publication Date -- newest to oldest Page 1 of 1

Select Page

Save to EndNote online
Add to Marked List

1. **Holographic Fermi liquids in a spontaneously generated lattice**
By: Alsup, James; Papantonopoulos, Eleftherios; Siopsis, George; et al.
[PHYSICAL REVIEW D](#) Volume: 93 Issue: 10 Article Number: 105045 Published: MAY 27 2016
View Abstract
2. **Duality between zeroes and poles in holographic systems with massless fermions and a dipole coupling**
By: Alsup, James; Papantonopoulos, Eleftherios; Siopsis, George; et al.
[PHYSICAL REVIEW D](#) Volume: 90 Issue: 12 Article Number: 126013 Published: DEC 30 2014
View Abstract
3. **Holographic quenches and fermionic spectral functions**
By: Callebaut, N.; Craps, B.; Galli, F.; et al.
[JOURNAL OF HIGH ENERGY PHYSICS](#) Issue: 10 Article Number: 172 Published: OCT 30 2014
View Abstract
4. **Phenomenological Characterization of Semiholographic Non-Fermi Liquids**
By: Mukhopadhyay, Ayan; Policastro, Giuseppe
[PHYSICAL REVIEW LETTERS](#) Volume: 111 Issue: 22 Article Number: 221602 Published: NOV 27 2013
View Abstract
5. **Charge transport by holographic Fermi surfaces**
By: Faulkner, Thomas; Iqbal, Nabil; Liu, Hong; et al.
[PHYSICAL REVIEW D](#) Volume: 88 Issue: 4 Article Number: 045016 Published: AUG 21 2013
View Abstract
6. **Holographic models for undoped Weyl semimetals**
By: Guerso, Umut; Jacobs, Vivian; Plauschinn, Erik; et al.
[JOURNAL OF HIGH ENERGY PHYSICS](#) Issue: 4 Article Number: 127 Published: APR 2013
View Abstract
7. **Fluctuations in finite density holographic quantum liquids**
By: Goykhman, Mikhail; Parnachev, Andrei; Zaanen, Jan
[JOURNAL OF HIGH ENERGY PHYSICS](#) Issue: 10 Article Number: 045 Published: OCT 2012
View Abstract
8. **Lattice potentials and fermions in holographic non Fermi-liquids: hybridizing local quantum criticality**

- Organizations-Enhanced
- Funding Agencies
- Languages
- Countries/Territories
- ESI Top Papers
- Open Access

For advanced refine options, use

Analyze Results

By: Liu, Yan; Schalm, Koenraad; Sun, Ya-Wen; et al.
JOURNAL OF HIGH ENERGY PHYSICS Issue: 10 Article
 Number: 036 Published: OCT 2012

View Abstract

9. **Quantum Electron Star**
 By: Allais, Andrea; McGreevy, John; Suh, S. Josephine
PHYSICAL REVIEW LETTERS Volume: 108 Issue: 23
 Article Number: 231602 Published: JUN 8 2012

View Abstract

10. **Holographic spectral function in nonequilibrium states**
 By: Banerjee, Souvik; Iyer, Ramakrishnan; Mukhopadhyay, Ayan
PHYSICAL REVIEW D Volume: 85 Issue: 10 Article
 Number: 106009 Published: MAY 22 2012

View Abstract

11. **Semi-local quantum liquids**
 By: Iqbal, Nabil; Liu, Hong; Mezei, Mark
JOURNAL OF HIGH ENERGY PHYSICS Issue: 4 Article
 Number: 086 Published: APR 2012

View Abstract

12. **Friedel oscillations in holographic metals**
 By: Puletti, V. Giangreco M.; Nowling, S.; Thorlacius, L.; et al.
JOURNAL OF HIGH ENERGY PHYSICS Issue: 1 Article
 Number: 073 Published: JAN 2012

View Abstract

13. **Spectral function of the supersymmetry current**
 By: Gauntlett, Jerome P.; Sonner, Julian; Waldram, Daniel
JOURNAL OF HIGH ENERGY PHYSICS Issue: 11 Article
 Number: 153 Published: NOV 2011

View Abstract

Usage Count

Times Cited: **22**
(from Web of Science Core Collection)

Usage Count

Times Cited: **11**
(from Web of Science Core Collection)

Usage Count

Times Cited: **36**
(from Web of Science Core Collection)

Usage Count

Times Cited: **6**
(from Web of Science Core Collection)

Usage Count

Times Cited: **20**
(from Web of Science Core Collection)

Usage Count

Select Page

Save to EndNote online

Add to Marked List

Sort by: **Publication Date -- newest to oldest**
Page 1 of 1

Show: **50 per page**

13 records matched your query of the 36,466,594 in the data limits you selected.

Web of Science™ InCites™ Journal Citation Reports® Essential Science Indicators™ EndNote™
Sign In Help English ▾

WEB OF SCIENCE™

Search
Return to Search Results
My Tools ▾ Search History Marked List

Citing Articles: 4
(from Web of Science Core Collection)

For: Semistiff polymer model of unfolded proteins and its application to NMR residual dipolar couplings
[...More](#)

Times Cited Counts
[5 in All Databases](#)

- 5 in Web of Science Core Collection
- 0 in BIOSIS Citation Index
- 0 in Chinese Science Citation Database
- 0 data sets in Data Citation Index
- 0 publication in Data Citation Index
- 0 in Russian Science Citation Index
- 0 in SciELO Citation Index

[View Additional Times Cited Counts](#)

Refine Results

Web of Science Categories ▾

- PHYSICS ATOMIC MOLECULAR CHEMICAL (2)
- PHYSICS APPLIED (1)
- OPTICS (1)
- CHEMISTRY PHYSICAL (1)
- CHEMISTRY MULTIDISCIPLINARY (1)

[more options / values...](#)

Refine

Document Types ▾

- ARTICLE (2)
- REVIEW (1)
- PROCEEDINGS PAPER (1)

[more options / values...](#)

Refine

Research Areas ▾

Authors ▾

Group Authors ▾

Editors ▾

Source Titles ▾

Book Series Titles ▾

Sort by: Publication Date -- newest to oldest ▾
 Page of 1

Select Page

Save to EndNote online ▾
 Add to Marked List

Analyze Results
 Create Citation Report

1. **Exploring Free-Energy Landscapes of Intrinsically Disordered Proteins at Atomic Resolution Using NMR Spectroscopy**

Times Cited: 47
(from Web of Science Core Collection)
Usage Count ▾

By: Jensen, Malene Ringkjober; Zweckstetter, Markus; Huang, Jie-rong; et al.
CHEMICAL REVIEWS Volume: 114 Issue: 13 Pages: 6632-6660 Published: JUL 9 2014
2. **Quantitative thermodynamic model for globular protein folding**

Times Cited: 1
(from Web of Science Core Collection)
Usage Count ▾

By: Yakubovich, Alexander V.; Solov'yov, Andrey V.
EUROPEAN PHYSICAL JOURNAL D Volume: 68 Issue: 6 Article Number: 145 Published: JUN 23 2014

View Abstract
3. **Investigation of the Polymeric Properties of alpha-Synuclein and Comparison with NMR Experiments: A Replica Exchange Molecular Dynamics Study**

Times Cited: 16
(from Web of Science Core Collection)
Usage Count ▾

By: Narayanan, Chitra; Weinstock, Daniel S.; Wu, Kuen-Phon; et al.
JOURNAL OF CHEMICAL THEORY AND COMPUTATION Volume: 8 Issue: 10 Pages: 3929-3942 Published: OCT 2012

View Abstract
4. **Statistical Mechanics Model for Protein Folding**

Times Cited: 1
(from Web of Science Core Collection)
Usage Count ▾

By: Yakubovich, Alexander; Solov'yov, Andrey V.; Greiner, Walter
 Edited by: Solov'yov, AV; Surdutovich, E
 Conference: 4th International Symposium on Atomic Cluster Collisions (ISACC 2009) Location: Ann Arbor, MI Date: JUL 14-18, 2009
 Sponsor(s): Frankfurt Inst Adv Studies; Oakland Univ
ISACC 2009: FOURTH INTERNATIONAL SYMPOSIUM ON ATOMIC CLUSTER COLLISIONS: STRUCTURE AND DYNAMICS FROM THE NUCLEAR TO THE BIOLOGICAL SCALE Book Series: AIP Conference Proceedings Volume: 1197 Pages: 186-200 Published: 2009

View Abstract

Select Page

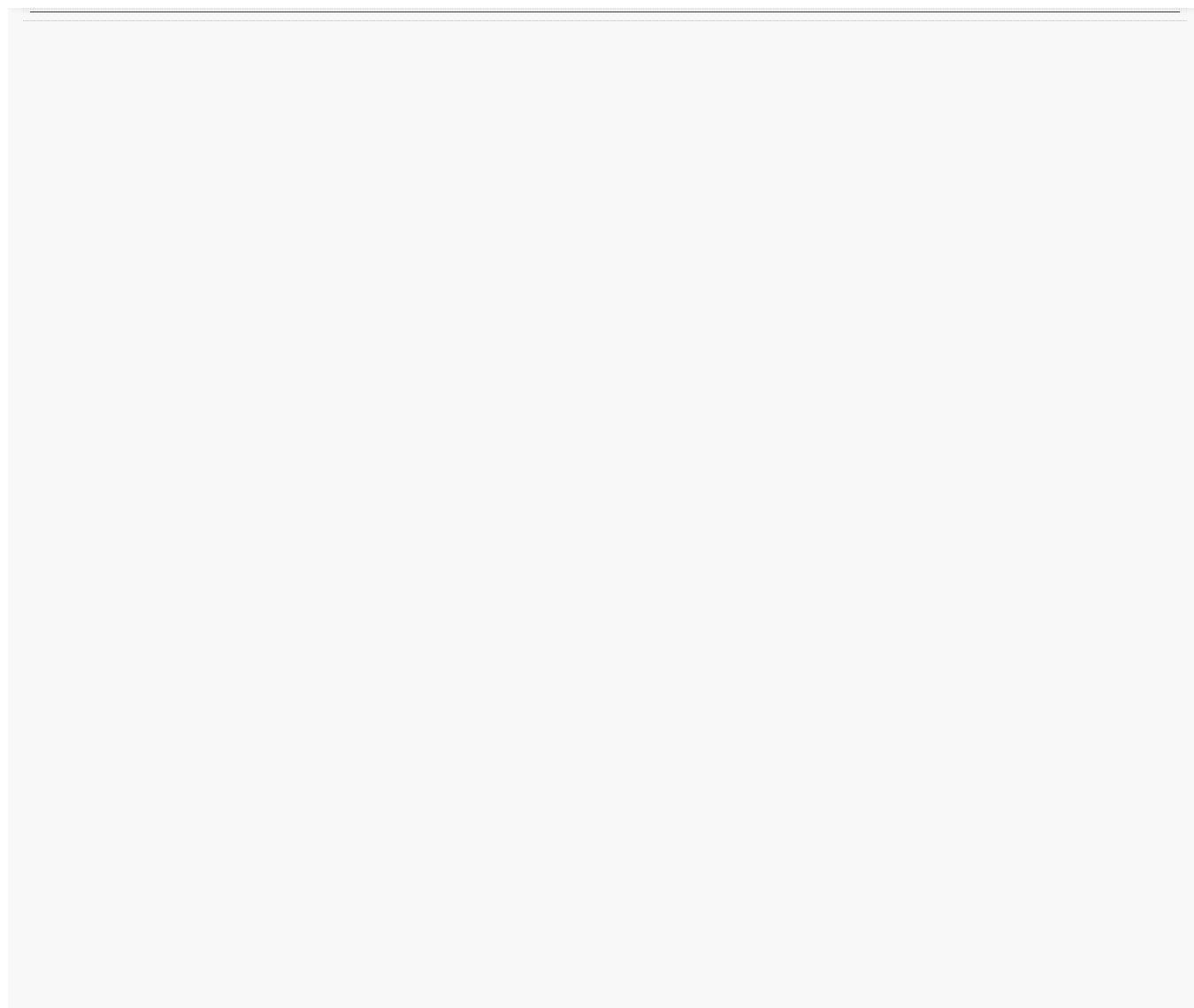
Save to EndNote online ▾
 Add to Marked List

Sort by: Publication Date -- newest to oldest ▾
 Page of 1

Show: 50 per page ▾

4 records matched your query of the 36,466,594 in the data limits you selected.

| | |
|---|---|
| Conference Titles | ◀ |
| Publication Years | ◀ |
| Organizations-Enhanced | ◀ |
| Funding Agencies | ◀ |
| Languages | ◀ |
| Countries/Territories | ◀ |
| ESI Top Papers | ◀ |
| Open Access | ◀ |
| <i>For advanced refine options, use</i> | |
| Analyze Results | |



Web of Science™ InCites™ Journal Citation Reports® Essential Science Indicators™ EndNote™
Sign In Help English

WEB OF SCIENCE™

Search
Return to Search Results
My Tools Search History Marked List

Citing Articles: 3

(from Web of Science Core Collection)

For: Dissipation-induced first-order decoherence phase transition in a noninteracting fermionic system
[...More](#)

Times Cited Counts

3 in All Databases

3 in Web of Science Core Collection

0 in BIOSIS Citation Index

0 in Chinese Science Citation Database

0 data sets in Data Citation Index

0 publication in Data Citation Index

0 in Russian Science Citation Index

0 in SciELO Citation Index

[View Additional Times Cited Counts](#)

Refine Results

Web of Science Categories

- PHYSICS MULTIDISCIPLINARY (1)
- PHYSICS MATHEMATICAL (1)
- PHYSICS ATOMIC MOLECULAR CHEMICAL (1)
- OPTICS (1)
- MECHANICS (1)

[more options / values...](#)

Refine

Document Types

- ARTICLE (3)

Refine

Research Areas

Authors

Group Authors

Editors

Source Titles

Book Series Titles

Conference Titles

Sort by: Publication Date -- newest to oldest

Page 1 of 1

Select Page Save to EndNote online Add to Marked List

[Analyze Results](#)
[Create Citation Report](#)

1. **Critical relaxation with overdamped quasiparticles in open quantum systems**

By: Lang, Johannes; Piazza, Francesco
 PHYSICAL REVIEW A Volume: 94 Issue: 3 Article Number: 033628 Published: SEP 23 2016

View Abstract
2. **Resummation for Nonequilibrium Perturbation Theory and Application to Open Quantum Lattices**

By: Li, Andy C. Y.; Petruccione, F.; Koch, Jens
 PHYSICAL REVIEW X Volume: 6 Issue: 2 Article Number: 021037 Published: JUN 16 2016

Full Text from Publisher

View Abstract
3. **Connected correlations, fluctuations and current of magnetization in the steady state of boundary driven XXZ spin chains**

By: Buca, B.; Prosen, T.
 JOURNAL OF STATISTICAL MECHANICS-THEORY AND EXPERIMENT Article Number: 023102 Published: FEB 2016

View Abstract

Select Page Save to EndNote online Add to Marked List

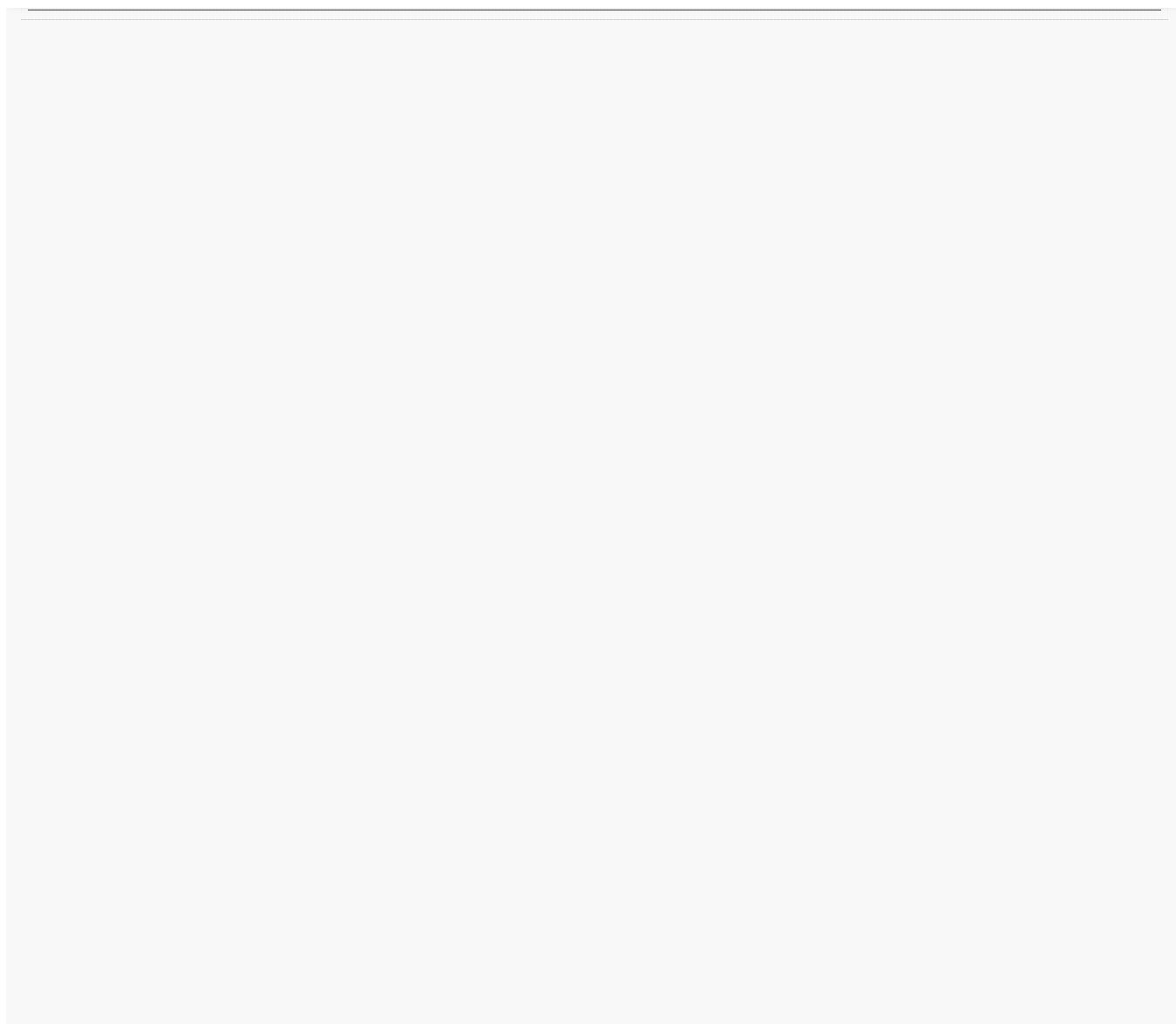
Sort by: Publication Date -- newest to oldest

Show: 50 per page

Page 1 of 1

3 records matched your query of the 36,466,594 in the data limits you selected.

| |
|--|
| Publication Years ◀ |
| Organizations-Enhanced ◀ |
| Funding Agencies ◀ |
| Languages ◀ |
| Countries/Territories ◀ |
| ESI Top Papers ◀ |
| Open Access ◀ |
| <i>For advanced refine options, use</i> Analyze Results |



Web of Science™ InCites™ Journal Citation Reports® Essential Science Indicators™ EndNote™
Sign In Help English

WEB OF SCIENCE™

Search
Return to Search Results
My Tools Search History Marked List

Citing Articles: 3
(from Web of Science Core Collection)

For: Quantum corrected phase diagram of holographic fermions
[...More](#)

Times Cited Counts
[3 in All Databases](#)

- 3 in Web of Science Core Collection
- 0 in BIOSIS Citation Index
- 0 in Chinese Science Citation Database
- 0 data sets in Data Citation Index
- 0 publication in Data Citation Index
- 0 in Russian Science Citation Index
- 0 in SciELO Citation Index

[View Additional Times Cited Counts](#)

Refine Results

Web of Science Categories ▼

- PHYSICS PARTICLES FIELDS (3)
- ASTRONOMY ASTROPHYSICS (3)

[more options / values...](#)

[Refine](#)

Document Types ▼

- ARTICLE (3)

[Refine](#)

Research Areas ▼

Authors ▼

Group Authors ▼

Editors ▼

Source Titles ▼

Book Series Titles ▼

Conference Titles ▼

Publication Years ▼

Organizations-Enhanced ▼

Sort by: Publication Date -- newest to oldest
◀ Page 1 of 1 ▶

Select Page

Save to EndNote online ▼
Add to Marked List

- 1. Fermi surface behavior in the ABJM M2-brane theory**

By: DeWolfe, Oliver; Henriksson, Oscar; Rosen, Christopher
PHYSICAL REVIEW D Volume: 91 Issue: 12 Article Number: 126017 Published: JUN 29 2015

View Abstract
- 2. Magnetic oscillations in a holographic liquid**

By: Puletti, V. Giangreco M.; Nowling, S.; Thorlacius, L.; et al.
PHYSICAL REVIEW D Volume: 91 Issue: 8 Article Number: 086008 Published: APR 8 2015

View Abstract
- 3. Fermionic response in a zero entropy state of N=4 super-Yang-Mills**

By: DeWolfe, Oliver; Gubser, Steven S.; Rosen, Christopher
PHYSICAL REVIEW D Volume: 91 Issue: 4 Article Number: 046011 Published: FEB 26 2015

View Abstract

Sort by: Publication Date -- newest to oldest
◀ Page 1 of 1 ▶

Select Page

Save to EndNote online ▼
Add to Marked List

Show: 50 per page

3 records matched your query of the 36,466,594 in the data limits you selected.

| |
|--|
| Funding Agencies ◀ |
| Languages ◀ |
| Countries/Territories ◀ |
| ESI Top Papers ◀ |
| Open Access ◀ |
| <i>For advanced refine options, use</i> Analyze Results |

Web of Science™ InCites™ Journal Citation Reports® Essential Science Indicators™ EndNote™ Sign In Help English

WEB OF SCIENCE™ THOMSON REUTERS™

Search Return to Search Results My Tools Search History Marked List

Citing Articles: 1
(from Web of Science Core Collection)

For: Confinement/deconfinement transition from symmetry breaking in gauge/gravity duality ...[More](#)

Times Cited Counts
1 in All Databases

- 1 in Web of Science Core Collection
- 0 in BIOSIS Citation Index
- 0 in Chinese Science Citation Database
- 0 data sets in Data Citation Index
- 0 publication in Data Citation Index
- 0 in Russian Science Citation Index
- 0 in SciELO Citation Index

[View Additional Times Cited Counts](#)

Sort by: **Publication Date -- newest to oldest** Page 1 of 1

Select Page **Save to EndNote online** **Add to Marked List**

Analyze Results
Create Citation Report

1. **Criteria for superfluid instabilities of geometries with hyperscaling violation**
By: Cremonini, Sera; Li, Li
JOURNAL OF HIGH ENERGY PHYSICS Issue: 11 Article
Number: 137 Published: NOV 22 2016

Times Cited: 0
(from Web of Science Core Collection)

Usage Count

[View Abstract](#)

Select Page **Save to EndNote online** **Add to Marked List**

Sort by: **Publication Date -- newest to oldest** Page 1 of 1
Show: **50 per page**

1 records matched your query of the 36,466,594 in the data limits you selected.

Web of Science Categories
PHYSICS PARTICLES FIELDS (1) [Refine](#)

Document Types
ARTICLE (1) [Refine](#)

Research Areas

Authors

Group Authors

Editors

Source Titles

Book Series Titles

Conference Titles

Publication Years

Organizations-Enhanced

Funding Agencies

| | |
|---|---|
| Languages | ◀ |
| Countries/Territories | ◀ |
| ESI Top Papers | ◀ |
| Open Access | ◀ |
| <i>For advanced refine options, use</i> | |
| Analyze Results | |



Mihailo Cubrovic <mcubrovic@gmail.com>

Your editor/referee payment

1

JHEP Editorial Office <jhep-eo@jhep.sissa.it> 28. 2016. 14:29
: JHEP Editorial Office <jhep-eo@jhep.sissa.it>
: cubrovic@lorentz.leidenuniv.nl

Dear Prof. Mihailo Cubrovic,

We are ready to process your editor/referee payment for the articles handled last year(s).

Before proceeding, we need you to connect to:

<https://jhep.sissa.it/jp/intro/b090409688550f3cc93f4ed88ec6cafb>

Please *fill in* the form thoroughly, *print* it, *sign* it and send it in original by *ordinary mail* (no e-mail) to:

SISSA Medialab Srl
Via Bonomea, 265
34136 - Trieste
Italy

The form will stay online until 30 November 2016.

Please ignore any duplicate e-mails that you may have received. This same message may have been sent to different addresses of yours to increase the chances of getting in touch with you.

Do not hesitate to contact jhep-administration@jhep.sissa.it if you should have any queries.

Thank you and best regards,
JHEP Editorial Office



Universiteit Leiden

Dear Sir, Madam,

Herewith we confirm that dr. Mikhail Cubrovic was the teaching assistant for the course Theory of Condensed matter in summer semester 2010 and 2011.

With kind regards,

A handwritten signature in black ink, consisting of a large, stylized 'M' and 'Z' intertwined, with a horizontal line extending to the right.

Prof. Dr. J. Zaanen

P.O . Box 9504

2300 RA Leiden

The Netherlands



To whom it may concern

Cologne, 06/02/2017

**Confirmation teaching assistance at the Institute for Theoretical
Physics, University of Cologne**

Dear Madam/Sir,

We confirm that Mr. Mihailo Cubrovic was the teaching assistant for the courses Advanced Quantum Mechanics (fall 2013), Quantum Mechanics (spring 2014) and Quantum Field Theory (spring 2015) at the Institute for Theoretical Physics, University of Cologne. If you have any further questions, please, do not hesitate to contact me.

Sincerely,

A handwritten signature in blue ink, appearing to read 'S. Diehl'.

GESCHÄFTSFÜHRENDER DIREKTOR
INSTITUT FÜR THEORETISCHE PHYSIK

Prof. Dr. Sebastian Diehl

“ALS JE HET EENMAAL BEGRIJPT IS HET SIMPEL”

Mihailo Cubrovic liet onlangs zien dat de snaartheorie helemaal niet zo exotisch is als wordt gedacht. Je kunt er bijvoorbeeld eenvoudig mee verklaren hoe hoge temperatuur supergeleiding werkt. Nou ja, eenvoudig.

Er zat twee jaar tussen naar Leiden willen en in Leiden aan een promotieonderzoek werken, twee maanden tussen de snaartheorie leren kennen en toepassen en twee weken tussen de acceptatie van een artikel en de publicatie ervan in *Science*. Mihailo Cubrovic is een man van records, zou je kunnen zeggen. Hij verklaart graag dat het toch allemaal minder spectaculair is verlopen als de opsomming het doet lijken.

“Ik kwam naar Leiden na mijn halve leven in Belgrado om te werken aan supergeleidingsexperimenten”, vertelt Cubrovic. “Dat ik in *no time* tot over mijn oren in de snaartheorie zou zitten was voor mij ook een verrassing”, maar een aangename, mogen we van hem aannemen.

“Ik wist dat de snaartheorie wat aan glans aan het verliezen was, maar toch besloten mijn begeleider Jan Zaanen en ik ermee te gaan rekenen. Met een vaag vermoeden, maar ook uit pure nieuwsgierigheid”, geeft de Servische onderzoeker toe. “Om met de snaartheorie te willen verklaren dat bij relatief hoge temperaturen ook supergeleiding mogelijk is, was een gok. Maar een gok die goed bleek.”

Big Bang

Om te begrijpen wat Cubrovic en zijn begeleiders Jan Zaanen en Koenraad Schalm precies hebben gedaan, is het van belang twee zaken in ogenschouw te nemen. Allereerst dat de snaartheorie zich grotendeels richt op een verklaring voor de oorsprong van de Big Bang. Namelijk het moment waarop grote hoeveelheden deeltjes samenkomen in een klein punt.

“En dat is ook het geval in een situatie waarin je bijvoorbeeld kristallen met afkoeling stilzet tot op het punt dat ze overgaan in supergeleiding”, vertelt Cubrovic. Al was de Big Bang geen quantum condensaat, zoals dat heet, de situatie van supergeleiding en de Big Bang singulariteit zijn wel beide ‘quantumkritische’ toestanden te noemen.

Dan zijn we voor sommige stoffen nog niet op het absolute nulpunt. Uit experimenten blijkt dat elektronen in deze situatie, een microscopische schaal, zich op dezelfde manier gedragen als elektronen op macroscopische schaal. Tijdens de Big Bang dus, en dat is het tweede punt dat op het werk van Cubrovic betrekking heeft.

Het maakte dat we dachten aan de snaartheorie voor een oplossende beschrijving.

Althans een specifiek onderdeel van de snaartheorie, de zogenaamde de AdS/CFT correspondentie, of *Anti-de Sitter/conformal field theory*. Die beschrijft de kwantummechanische elektronenwereld

MIHAILO CUBROVIC

als een wereld die veel meer lijkt op de onze: het is een klassieke wereld die in de greep is van zwaartekracht en lichtstralen, met een vreemde ‘anti de Sitter’ kromming (genoemd naar de Leidse fysicus de Sitter), terwijl het nodig blijkt dat zich in het middelpunt van deze wereld een elektrisch geladen zwart gat bevindt. Met die machinerie berekenden de Leidse onderzoekers dat de vibraties van zo’n zwart gat tot een collectieve ordening van elektronen leiden: precies het gedrag in de kwantumkritische toestand.

Geen benul

De laatste jaren ligt de snaartheorie onder vuur omdat concrete voorspellingen voor experimenten uitblijven en de theorie daardoor ontstaat het gevoel dat de theorie dus wel niet van direct belang kan zijn voor het begrip van de wereld om ons heen. De kritiek op het werk van Cubrovic valt daarom ook wel te raden: ook nu blijft het vooral een wiskundige verklaring. Overeind blijft dat het behalve Cubrovic, Zaanen en Schalm tot nu toe niemand nog gelukt is hogetemperatuursupergeleiding theoretisch te verklaren. Het is dan ook de eerste keer dat een berekening op basis van de snaartheorie in Science staat, en zo snel is gepubliceerd, ondanks de grote bekendheid die de theorie heeft.

De begeleider van Cubrovic, de Leidse hoogleraar theoretische natuurkunde Zaanen, verwoordt zijn enthousiasme als volgt: “Men dacht altijd dat als je die kwantum-kritische toestand begrijpt, je ook hogetemperatuursupergeleiding kunt begrijpen. Maar ondanks dat de experimenten boekdelen spraken, hadden we geen flauw benul hoe je dit fenomeen kon beschrijven.”

Volgens Cubrovic kan de snaartheorie zich in de toekomst vaker bewijzen. Hij zal er in zijn onderzoek op doorgaan, ook al is het onderwerp relatief nieuw en zal hij zich nog verder in de snaartheorie moeten verdiepen. Dat betekent niet dat hij er dag en nacht mee bezig is, zegt hij desgevraagd.

“Ik heb me de theorie eigen gemaakt, en dat was niet eenvoudig. Het ging met horten en stoten.” Een Eureka-moment kan hij zich niet meer herinneren. “Er was geen duidelijke doorbraak. We zijn bij de basis begonnen te rekenen en daarna steeds een stap verder gegaan.” Dat ze zo snel tot een passende theorie kwamen, was voor Cubrovic ook een verrassing. Alhoewel, aarzelend en terugkijkend op zijn ontdekkig van de kracht van de snaartheorie, zegt hij nu: “als je het eenmaal begrijpt is het simpel.”

Marco van Kerkhoven



String Theory, Quantum Phase Transitions, and the Emergent Fermi Liquid

Mihailo Cubrovic *et al.*
Science **325**, 439 (2009);
DOI: 10.1126/science.1174962

This copy is for your personal, non-commercial use only.

If you wish to distribute this article to others, you can order high-quality copies for your colleagues, clients, or customers by [clicking here](#).

Permission to republish or repurpose articles or portions of articles can be obtained by following the guidelines [here](#).

The following resources related to this article are available online at www.sciencemag.org (this information is current as of April 4, 2014):

Updated information and services, including high-resolution figures, can be found in the online version of this article at:

<http://www.sciencemag.org/content/325/5939/439.full.html>

Supporting Online Material can be found at:

<http://www.sciencemag.org/content/suppl/2009/06/25/1174962.DC1.html>

This article **cites 22 articles**, 1 of which can be accessed free:

<http://www.sciencemag.org/content/325/5939/439.full.html#ref-list-1>

This article has been **cited by** 38 article(s) on the ISI Web of Science

This article has been **cited by** 3 articles hosted by HighWire Press; see:

<http://www.sciencemag.org/content/325/5939/439.full.html#related-urls>

This article appears in the following **subject collections**:

Physics

<http://www.sciencemag.org/cgi/collection/physics>

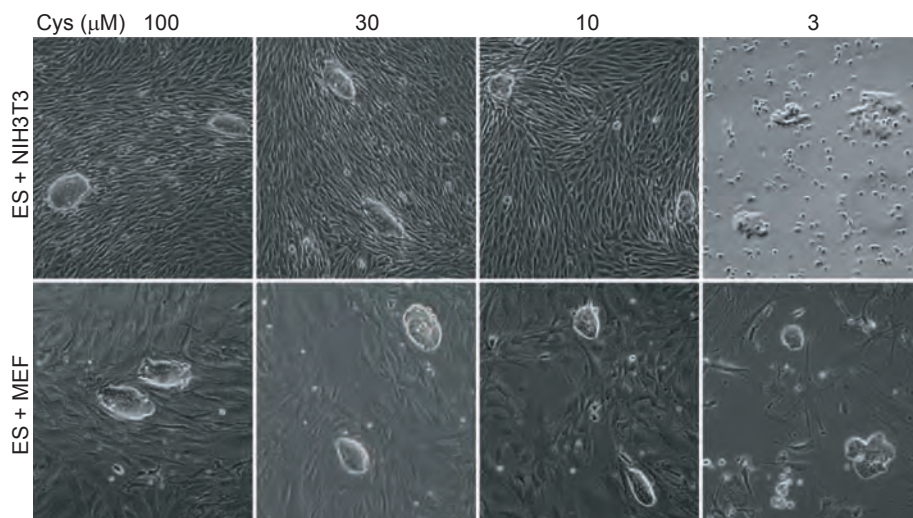


Fig. 6. Effects of cysteine deprivation on the growth of ES, MEF, and 3T3 cells. Cocultures of ES/MEF or ES/3T3 cells were subjected for 2 days to media containing varying amounts of supplemented cysteine. Cysteine deprivation severely impeded MEF cell growth at 10 and 3 μM and 3T3 growth at 3 μM (see also fig. S5). Although colony morphology was altered under the most severe conditions of cysteine deprivation, ES cell colonies were observed under all culture conditions tested.

of three inactivating mutations (13). Although highly conserved in gene organization, as well as primary amino acid sequence of the predicted TDH open reading frame, the human TDH gene carries AG-to-GG splice acceptor mutations in exons 4 and 6, as well as a nonsense mutation within exon 6 wherein arginine codon 214 is replaced by a translational stop codon. Whereas polymorphic variation within the human population has been observed for the exon 4 splice acceptor mutation, with some individuals carrying the normal AG splice acceptor dinucleotide and others carrying the GG variant, all individuals genotyped to date carry both the splice acceptor and nonsense mutations in exon 6. Reverse transcriptase-PCR analysis of TDH transcripts expressed in human fetal liver tissue showed complete skipping of exon 4 and either complete skipping or aberrant splicing of exon 6 (fig. S8). Given that exons 4 and 6 encode segments of the enzyme critical to its function and that truncation via the nonsense codon at amino acid 214 would also be predicted to yield an inactive variant, it appears that the human gene is incapable of producing an active TDH enzyme. Remarkably, all metazoans whose genomes have been sequenced to date, including chimpanzees, appear to contain an intact TDH gene (14). Unless humans evolved adaptive capabilities sufficient to overcome three mutational lesions, it would appear they are TDH deficient.

Human ES cells grow at a far slower rate than mouse ES cells, with a doubling time of 35 hours (15). Whether the slower growth rate of human ES cells reflects the absence of a functional TDH enzyme can perhaps be tested by introducing, into human ES cells, either a repaired human TDH gene or the intact TDH gene of a closely related mammal. That this strategy might work is supported by the expression in human cells of a functional form of the 2-amino-3-ketobutyrate-

CoA ligase enzyme that converts the short-lived product of TDH-mediated catabolism of threonine into acetyl-CoA and glycine (Fig. 1B). It is possible that the culture conditions used to grow human ES cells do not match the ICM environment of the human embryo, in which the cell division cycle is more rapid than the 35-hour doubling time of cultured human ES cells (16). If human ES cells do not use the TDH enzyme to acquire an advantageous metabolic state for rapid growth, and if conditions can be adapted to facilitate the rapid proliferation of human ES cells in culture, the tools and approaches that we describe here may prove useful. As often happens in science, findings made in one experimental system

can open avenues of investigation useful for other matters of inquiry. Finally, it is important to consider whether humans benefit from some form of selective advantage as a consequence of mutational inactivation of the TDH gene.

References and Notes

1. B. Alberts *et al.*, in *Molecular Biology of the Cell* (Garland, New York, ed. 5, 2007), p. 1.
2. M. H. L. Snow, *J. Embryol. Exp. Morphol.* **42**, 293 (1977).
3. A. G. Smith, *Annu. Rev. Cell Dev. Biol.* **17**, 435 (2001).
4. B. P. Tu *et al.*, *Proc. Natl. Acad. Sci. U.S.A.* **104**, 16886 (2007).
5. L. Warren, J. M. Buchanan, *J. Biol. Chem.* **229**, 613 (1957).
6. H. Weissbach, A. Peterkofsky, B. G. Redfield, H. Dickerman, *J. Biol. Chem.* **238**, 3318 (1963).
7. E. A. Phear, D. M. Greenberg, *J. Am. Chem. Soc.* **79**, 3737 (1957).
8. R. A. Dale, *Biochim. Biophys. Acta* **544**, 496 (1978).
9. E. Almaas, B. Kovacs, T. Vicsek, Z. N. Oltvai, A. L. Barabasi, *Nature* **427**, 839 (2004).
10. J. L. Hartman, *Proc. Natl. Acad. Sci. U.S.A.* **104**, 11,700 (2007).
11. T. Kuzuoka *et al.*, *J. Bacteriol.* **185**, 4483 (2003).
12. F. A. Brook, R. L. Gardner, *Proc. Natl. Acad. Sci. U.S.A.* **94**, 5709 (1997).
13. A. J. Edgar, *BMC Genet.* **3**, 18 (2002).
14. K. D. Pruitt, T. Tatusova, D. R. Maglott, *Nucleic Acids Res.* **35**, D61 (2007).
15. M. Amit *et al.*, *Dev. Biol.* **227**, 271 (2000).
16. K. Hardy, A. H. Handside, R. M. T. Winston, *Development* **107**, 597 (1989).
17. We thank B. Tu for the help with LC-MS/MS analysis; J. De Brabander and J. Ready for guidance on the chemical properties of threonine analogs; E. Olson for providing the AOK-5P line of iPSC cells; D. Chong for technical assistance with in situ hybridization assays; and J. Goldstein, M. Rosen, and W. Neaves for helpful scientific input. This work was funded by an NIH Directors Pioneer Award, and unrestricted funds provided to S.L.M. by an anonymous donor.

Supporting Online Material

www.sciencemag.org/cgi/content/full/1173288/DC1
Materials and Methods
Figs. S1 to S8

9 March 2009; accepted 17 June 2009
Published online 9 July 2009;
10.1126/science.1173288

Include this information when citing this paper.

String Theory, Quantum Phase Transitions, and the Emergent Fermi Liquid

Mihailo Čubrović, Jan Zaanen, Koenraad Schalm*

A central problem in quantum condensed matter physics is the critical theory governing the zero-temperature quantum phase transition between strongly renormalized Fermi liquids as found in heavy fermion intermetallics and possibly in high-critical temperature superconductors. We found that the mathematics of string theory is capable of describing such fermionic quantum critical states. Using the anti-de Sitter/conformal field theory correspondence to relate fermionic quantum critical fields to a gravitational problem, we computed the spectral functions of fermions in the field theory. By increasing the fermion density away from the relativistic quantum critical point, a state emerges with all the features of the Fermi liquid.

Quantum many-particle physics lacks a general mathematical theory to deal with fermions at finite density. This is known as the “fermion sign problem”:

There is no recourse to brute-force lattice models because the statistical path-integral methods that work for any bosonic quantum field theory do not work for finite-density Fermi systems.

The nonprobabilistic fermion problem is known to be of exponential complexity (1), and in the absence of a general mathematical framework, all that remains is phenomenological guesswork in the form of the Fermi-liquid theory describing the state of electrons in normal metals and the mean-field theories describing superconductivity and other manifestations of spontaneous symmetry breaking. This problem has become particularly manifest in quantum condensed matter physics with the discovery of electron systems undergoing quantum phase transitions that are reminiscent of the bosonic quantum critical systems (2) but are governed by fermion statistics. Empirically well-documented examples are found in the “heavy fermion” intermetallics, where the zero-temperature transition occurs between different Fermi liquids with quasi-particle masses that diverge at the quantum critical point [(3) and references therein]. Such fermionic quantum critical states are believed to have a direct bearing on the problem of high-critical temperature (high- T_c) superconductivity because of the observation of quantum critical features in the normal state of optimally doped cuprate high- T_c superconductors [(4); (5) and references therein].

A large part of the fermion sign problem is to understand this strongly coupled fermionic quantum critical state. The emergent scale invariance and conformal symmetry at critical points is a benefit in isolating deep questions of principle. The fundamental problem is: How does the system get rid of the scales of Fermi energy and Fermi momentum that are intrinsically rooted in the workings of Fermi-Dirac statistics (6, 7)? From another perspective, how can one construct a renormalization group with a relevant “operator” that describes the emergence of a statistics-controlled (heavy) Fermi liquid from the critical state (3), or perhaps the emergence of a high- T_c superconductor? Here, we show that a mathematical method developed in string theory has the capacity to answer at least some of these questions.

String theory for condensed matter. Our analysis makes use of the AdS/CFT correspondence: a duality relation between classical gravitational physics in a $d + 1$ -dimensional “bulk” space-time with an anti-de Sitter (AdS) geometry and a strongly coupled conformal (quantum critical) field theory (CFT), with a large number of degrees of freedom, that occupies a flat or spherical d -dimensional “boundary” space-time. Applications of AdS/CFT to quantum critical systems have already been studied in the context of the quark-gluon plasma (8, 9), superconductor-insulator transitions (10–14), and cold atom systems at the Feshbach resonance (15–17), but so far the focus has been on bosonic currents [see (18, 19) and references therein]. Although

AdS/CFT is convenient, in principle the ground state or any response of a bosonic statistical field theory can also be computed directly by averaging on a lattice. For fermions, statistical averaging is not possible because of the sign problem. There are, however, indications that AdS/CFT should be able to capture finite-density Fermi systems as well. Ensembles described through AdS/CFT can exhibit a specific heat that scales linearly with the temperature characteristic of Fermi systems (20), zero sound (20–22), and a minimum energy for fermionic excitations (23, 24).

To address the question of whether AdS/CFT can describe finite-density Fermi systems and the Fermi liquid in particular, we compute the single charged fermion propagators and the associated spectral functions that are measured experimentally by angle-resolved photoemission spectroscopy (“AdS-to-ARPES”) and indirectly by scanning tunneling microscopy. The spectral functions contain the crucial information regarding the nature of the fermion states. These are computed on the AdS side by solving for the on-shell (classical) Dirac equation in the curved AdS space-time background with sources at the boundary. A temperature T and finite $U(1)$ chemical potential μ_0 for electric charge is imposed in the field theory by studying the Dirac equation in the background of an AdS Reissner-Nordstrom black hole. We do so with the expectation that the $U(1)$ chemical potential induces a finite density of the charged fermions. The procedure to compute the retarded CFT propagator from the dual AdS description is then well established (8, 19). Relative to the algorithm for computing bosonic responses, the treatment of Dirac waves in AdS is more delicate but straightforward; details are provided in (25). The equations obtained this way are solved numerically and the output is the retarded single fermion propagator $G_R(\omega, k)$ at finite T . Its imaginary part is the single fermion spectral function $A(\omega, k) = -(\pi)^{-1} \text{Im} \text{Tr}[i\gamma^0 G_R(\omega, k)]$ that can be directly compared with ARPES experiments (26).

The reference point for this comparison is the quantum critical point described by a zero chemical potential ($\mu_0 = 0$), zero temperature ($T = 0$), and conformal and Lorentz invariant field theory. (Below, we use relativistic notation where $c = 1$.) Here the fermion propagators $\langle \bar{\Psi}\Psi \rangle \equiv G(\omega, k)$ are completely fixed by symmetry to be of the form

$$G_{\Delta_\Psi}^{\text{CFT}}(\omega, k) \sim \frac{1}{(\sqrt{-\omega^2 + k^2})^{d-2\Delta_\Psi}} \quad (1)$$

where Δ_Ψ is the scaling dimension of the fermion field. Through the $\text{AdS}_{d+1}/\text{CFT}_d$ dictionary, Δ_Ψ is related to the mass parameter in the $d + 1$ -dimensional AdS Dirac equation. Unitarity bounds this mass from below in units of the AdS radius $mL = \Delta_\Psi - d/2 > -1/2$ (we set $L = 1$ in the remainder). The choice of which value to use for m will prove essential to show the emergence of the Fermi liquid. The lower end of the unitarity-bound $m = -1/2 + \delta$, $\delta \ll 1$, corresponds to introducing a fermionic conformal operator with weight $\Delta_\Psi = [(d - 1)/2] + \delta$. This equals the scaling dimension of a nearly free fermion. Even though the underlying CFT is strongly coupled, the absence of a large anomalous dimension for a fermion with mass $m = -1/2 + \delta$ argues that such an operator fulfills a spectator role and is only weakly coupled to this CFT. We therefore use such values in our calculations. Our expectation is that the Fermi liquid, as a system with well-defined quasi-particle excitations, can be described in terms of weakly interacting long-range fields. As we increase m from $m = -1/2 + \delta$, the interactions increase and we can expect the quasi-particle description to cease to be valid beyond $m = 0$. For that value $m = 0$, and beyond $m > 0$, the naïve scaling dimension Δ_O of the fermion-bilinear $O_{\Delta_O} = \bar{\Psi}\Psi$ is marginal or irrelevant, and it is hard to see how the ultraviolet conformal theory can flow to a Fermi-liquid state, assuming that all vacuum state changes are caused by the condensation of bosonic oper-

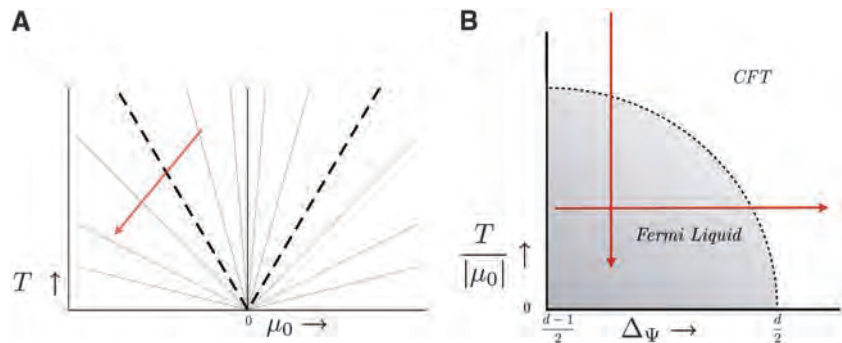


Fig. 1. (A) The phase diagram near a quantum critical point. Gray lines depict lines of constant μ_0/T ; the spectral function of fermions is unchanged along each line if the momenta are appropriately rescaled. As we increase μ_0/T we cross over from the quantum critical regime to the Fermi liquid. (B) The trajectories in parameter space (μ_0/T , Δ_Ψ) studied here. We show the crossover from the quantum critical regime to the Fermi liquid by varying μ_0/T while keeping Δ_Ψ fixed; we cross back to the critical regime varying $\Delta_\Psi \rightarrow d/2$ for μ_0/T fixed. The boundary region is not an exact curve but only a qualitative indication.

Institute-Lorentz for Theoretical Physics, Leiden University, P.O. Box 9506, Leiden, Netherlands.

*To whom correspondence should be addressed. E-mail: kschalm@lorentz.leidenuniv.nl

ators. This intuition is borne out by our results: When $m \geq 0$, the standard Fermi liquid disappears. A similar approach to describing fermionic quantum criticality (27) discusses the special case $m = 0$ or $\Delta_\Psi = d/2$ in detail; an early attempt to describe the $m = 0$ system is (28).

The emergent Fermi liquid. With an eye toward experiment, we consider the AdS₄ dual to a relativistic CFT₃ in $d = 2 + 1$ dimensions (25). We do not know the detailed microscopic CFT, nor do we know whether a dual AdS with fermions as the sole $U(1)$ charged field exists as a fully quantum-consistent theory for all values of $m = \Delta_\Psi - d/2$, but the behavior of fermion spectral functions at a strongly coupled quantum critical point can be deduced nonetheless. Aside

from Δ_Ψ , the spectral function will depend on the dimensionless ratio μ_0/T as well as the $U(1)$ charge g of the fermion; we set $g = 1$ from here on, as we expect that only large changes away from $g = 1$ will change our results qualitatively. We therefore study the system as a function of μ_0/T and Δ_Ψ . Our approach is sketched in Fig. 1B. We first study the spectral behavior as a function of μ_0/T for fixed $\Delta_\Psi < 3/2$; then we study the spectral behavior as we vary the scaling dimension Δ_Ψ from 1 to $3/2$ for fixed μ_0/T coding for an increasingly interacting fermion. Note that our setup and numerical calculations necessitate a finite value of μ_0/T ; all our results are at nonzero T .

Our analysis starts near the reference point $\mu_0/T \rightarrow 0$, where the long-range behavior of

the system is controlled by the quantum critical point (Fig. 1A). Here we expect to recover conformal invariance, as the system forgets about any well-defined scales, and the spectral function should be controlled by the branchcut at $\omega = k$ in the Green's function (Eq. 1): (i) For $\omega < k$ it should vanish. (ii) At $\omega = k$ we expect a sharp peak, which for $\omega \gg k$ scales as $\omega^{2\Delta_\Psi-d}$. Figure 2A shows this expected behavior of spectral function for three different values of the momentum for a fermionic operator with weight $\Delta_\Psi = 5/4$ computed from AdS₄ following the setup in (25).

Turning on μ_0/T while holding $\Delta_\Psi = 5/4$ fixed shifts the center location of the two branchcuts to an effective chemical potential $\omega = \mu_{\text{eff}}$; this bears out our expectation that the $U(1)$ chemical potential induces a finite fermion density. Although the peak at the location of the negative branchcut $\omega \sim \mu_{\text{eff}} - k$ stays broad, the peak at the other branchcut $\omega \sim \mu_{\text{eff}} + k$ sharpens distinctly as the size of μ_0/T is increased (Fig. 2B). We identify this peak with the quasi-particle of the Fermi liquid and its appearance as the crossover between the quantum critical regime and the Fermi-liquid regime. The spectral properties of the Fermi liquid are very well known and display a number of uniquely identifying characteristics (29, 30). If this identification is correct, all these characteristics must be present in our spectra as well.

1) The quasi-particle should approach a delta function at the Fermi momentum $k = k_F$. In Fig. 2B we see the peak narrow as we increase k , then peak and broaden back out as we pass $k \sim k_F$ (recall that $T = 0$ is outside our numerical control and the peak always has some broadening). In addition, the spectrum should vanish identically at the Fermi energy $A(\omega = E_F, k) = 0$, independent of k (Fig. 2C).

2) The quasi-particle should have linear dispersion relation near the Fermi energy with a renormalized Fermi velocity v_F different from the underlying relativistic speed $c = 1$. In Fig. 3 we plot the maximum of the peak ω_{max} as a function of k . At high k we recover the linear dispersion relation $\omega = |k|$ underlying the Lorentz invariant branchcut in Eq. 1. Near the Fermi energy and Fermi momentum, however, this dispersion relation changes to a slope $v_F \equiv \lim_{\omega \rightarrow E_F, k \rightarrow k_F} (\omega - E_F)/(k - k_F)$ clearly less than unity.

Note that the Fermi energy E_F is not located at zero frequency. Recall, however, that the AdS chemical potential μ_0 is the bare $U(1)$ chemical potential in the CFT. This is confirmed in Fig. 3 from the high- k behavior: Its Dirac point is μ_0 . On the other hand, the chemical potential felt by the IR fermionic degrees of freedom is renormalized to the value $\mu_F = \mu_0 - E_F$. As is standard, the effective energy $\tilde{\omega} = \omega - E_F$ of the quasi-particle is measured with respect to E_F .

3) At low temperatures, Fermi-liquid theory predicts the width of the quasi-particle peak to

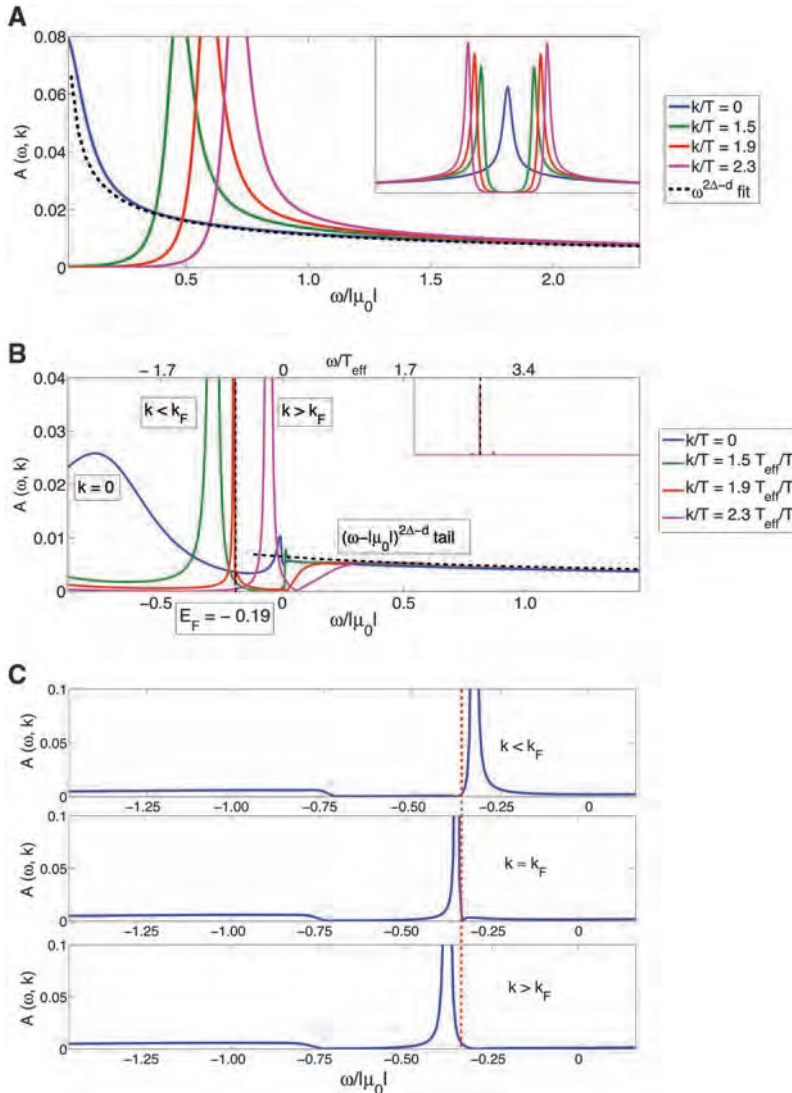


Fig. 2. (A) The spectral function $A(\omega, k)$ for $\mu_0/T = 0.01$ and $m = -1/4$. The spectral function has the asymptotic branchcut behavior of a conformal field of dimension $\Delta_\Psi = d/2 + m = 5/4$: It vanishes for $\omega < k$, save for a finite T tail, and for large ω it scales as $\omega^{2\Delta_\Psi-d}$. (B) The emergence of the quasi-particle peak as we change the chemical potential to $\mu_0/T = -30.9$ for the same value $\Delta_\Psi = 5/4$. The three displayed momenta k/T are rescaled by a factor T_{eff}/T for the most meaningful comparison with those in (A) (25). The insets show the full scales of the peak heights and the dominance of the quasi-particle peak for $k \sim k_F$. (C) Vanishing of the spectral function at E_F for $\Delta_\Psi = 1.05$ and $\mu_0/T = -30.9$. The deviation of the dip location from E_F is a finite temperature effect; it decreases with increasing μ_0/T .

grow quadratically with temperature. Figure 4, A and B, shows this distinctive behavior up to a critical temperature, $T_c/\mu_0 \sim 0.16$. This temper-

ature behavior directly follows from the fact that the imaginary part of the self-energy $\Sigma(\omega, k) = \omega - k - [\text{Tr } i\gamma^0 G(\omega, k)]^{-1}$ should have no linear

term when expanded around E_F : $\text{Im } \Sigma(\omega, k) \sim (\omega - E_F)^2 + \dots$. This is shown in Fig. 4, C and D.

These results give us confidence that we have identified the characteristic quasi-particles at the Fermi surface of the Fermi liquid emerging from the quantum critical point.

We now discuss how this Fermi liquid evolves when we increase the bare μ_0 (Fig. 5). Similar to the fermion chemical potential μ_F , the fundamental control parameter of the Fermi liquid, the fermion density ρ_F , is not directly related to the AdS μ_0 . We can, however, infer it from the Fermi momentum k_F that is set by the quasi-particle pole via Luttinger's theorem $\rho_F \sim k_F^d$. The more illustrative figure is therefore Fig. 5B, which shows the quasi-particle characteristics as a function of k_F/T . We find that the quasi-particle velocities decrease slightly with increasing k_F , rapidly leveling off to a finite constant less than the relativistic speed. Thus, the quasi-particles become increasingly heavy as their mass $m_F \equiv k_F/v_F$ approaches linear growth with k_F . The Fermi energy E_F also shows linear growth. Suppose the heavy Fermi-quasi-particle system has the underlying canonical nonrelativistic dispersion relation $E = k^2/(2m_F) = k_F^2/(2m_F) + v_F(k - k_F) + \dots$; in that case, the observed Fermi energy E_F should equal the renormalized Fermi energy $E_F^{(\text{ren})} \equiv k_F^2/(2m_F)$. Figure 5B shows that these energies E_F and $E_F^{(\text{ren})}$

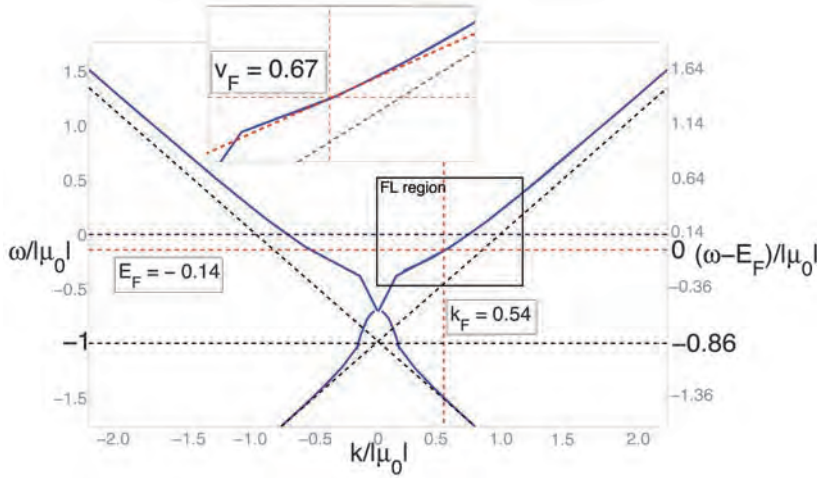
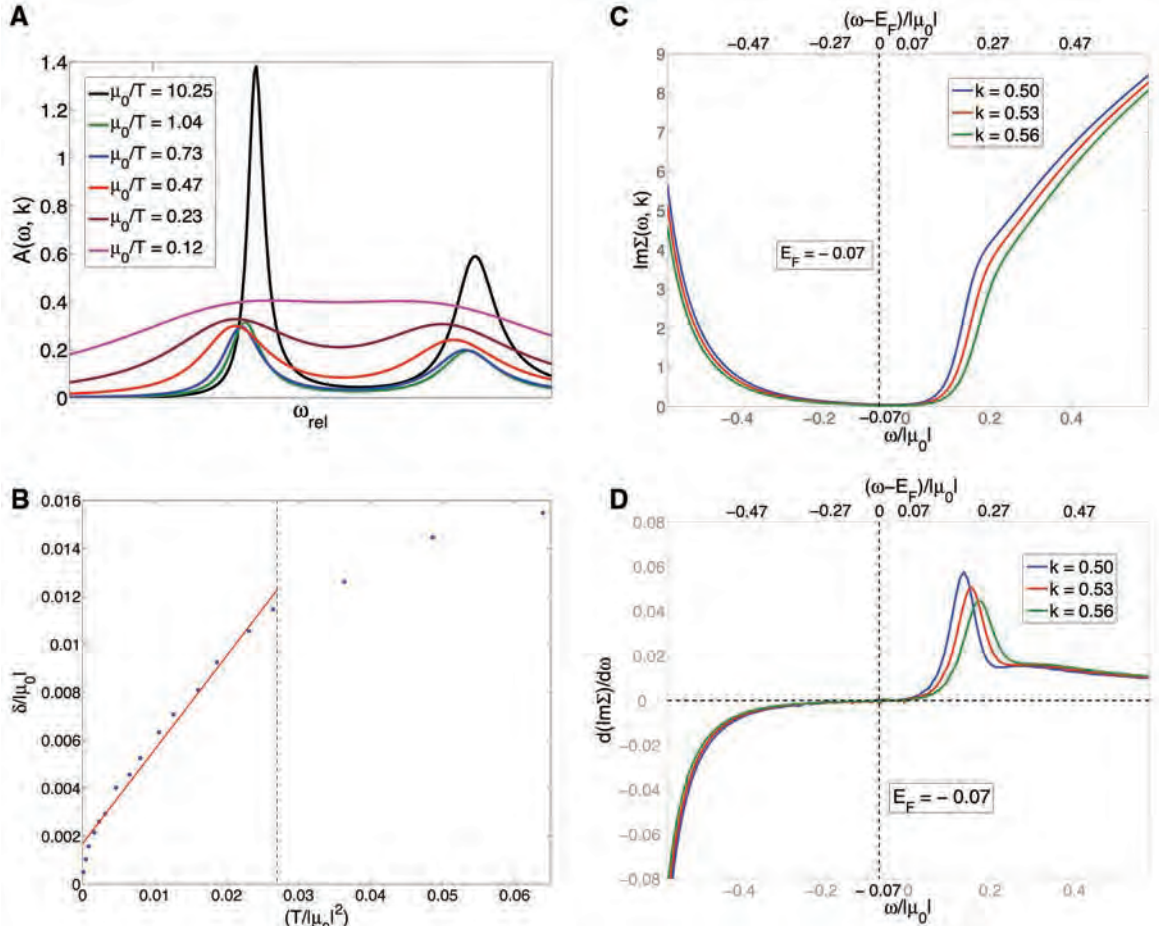


Fig. 3. Maxima in the spectral function as a function of k/μ_0 for $\Delta_\psi = 1.35$ and $\mu_0/T = -30.9$. Asymptotically for large k the negative- k branchcut recovers the Lorentz-invariant linear dispersion with unit velocity, but with the zero shifted to $-\mu_0$. The peak location of the positive- k branchcut that changes into the quasi-particle peak changes noticeably. It gives the dispersion relation of the quasi-particle near (E_F, k_F) . The change of the slope from unity shows renormalization of the Fermi velocity. This is highlighted in the inset. Note that the Fermi energy E_F is not located at $\omega_{\text{AdS}} = 0$. The AdS calculation visualizes the renormalization of the bare chemical potential $\mu_0 = \mu_{\text{AdS}}$ to the effective chemical potential $\mu_F = \mu_0 - E_F$ felt by the low-frequency fermions.

Fig. 4. (A) Temperature dependence of the quasi-particle peak for $\Delta_\psi = 5/4$ and $k/k_F \approx 0.5$; all curves have been shifted to a common peak center. (B) The quasi-particle peak width $\delta \sim \text{Re } \Sigma(\omega, k = k_F)$ for $\Delta_\psi = 5/4$ as a function of T^2 ; it reflects the expected behavior $\delta \sim T^2$ up to a critical temperature T_c/μ_0 , beyond which the notion of a quasi-particle becomes untenable. (C and D) The imaginary part of the self-energy $\Sigma(\omega, k)$ near E_F, k_F for $\Delta_\psi = 1.4$, $\mu_0/T = -30.9$. The defining $\text{Im } \Sigma(\omega, k) \sim (\omega - E_F)^2 + \dots$ dependence for Fermi-liquid quasi-particles is faint in (C) but obvious in (D). It shows that the intercept of $\partial_\omega \text{Im } \Sigma(\omega, k)$ vanishes at E_F, k_F .



track each other remarkably well. We therefore infer that the true zero of energy of the Fermi quasi-particle is set by the renormalized Fermi energy as deduced from the Fermi velocity and Fermi momentum.

Although the true quasi-particle behavior disappears at $T > T_c$, Fig. 5A indicates that in the limit $k_F/T \rightarrow 0$ the quasi-particle pole strength vanishes, $Z_k \rightarrow 0$, while the Fermi velocity v_F remains finite; v_F approaches the bare

velocity $v_F = 1$. This is seemingly at odds with the heavy Fermi liquid relation $Z_k \sim m_{\text{micro}}/m_F = m_{\text{micro}}v_F/k_F$. The resolution is the restoration of Lorentz invariance at zero density. From general Fermi liquid considerations it follows that $v_F = Z_k(1 + \partial_k \text{Re} \Sigma|_{E_F, k_F})$ and $Z_k = 1/(1 - \partial_\omega \text{Re} \Sigma|_{E_F, k_F})$, where $\partial_{k,\omega} \text{Re} \Sigma$ refers to the momentum and energy derivatives of the real part of the fermion self-energy $\Sigma(\omega, k)$ at k_F, E_F . Lorentz invariance imposes $\partial_\omega \Sigma' = -\partial_k \Sigma'$, which allows

Fig. 5. The quasi-particle characteristics as a function of μ_0/T for $\Delta_\Psi = 5/4$. **(A)** The change of k_F, v_F, m_F, E_F , and the pole strength Z (the total weight between half-maxima) as we change μ_0/T . Beyond a critical value $(\mu_0/T)_c$ we lose the characteristic T^2 broadening of the peak and there is no longer a real quasi-particle, although the peak is still present. For the Fermi liquid, k_F/T rather than μ_0/T is the defining parameter. **(B)** We can invert this relation, and **(B)** shows the quasi-particle characteristics as a function of k_F/T . Note the linear relationships of m_F and E_F to k_F and that the renormalized Fermi energy $E^{(\text{ren})} \equiv k_F^2/(2m_F)$ matches the empirical value E_F remarkably well.

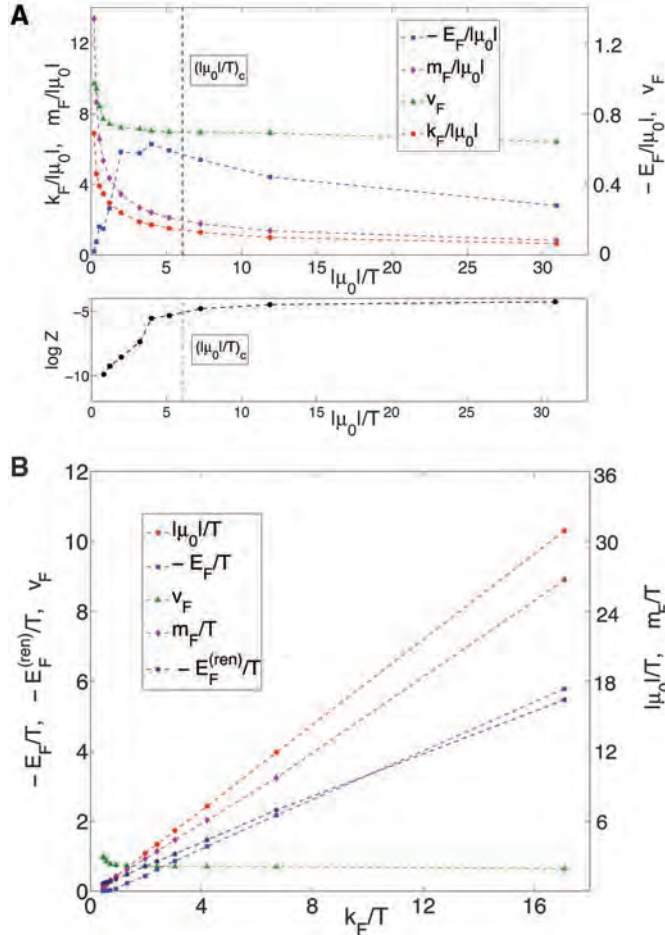
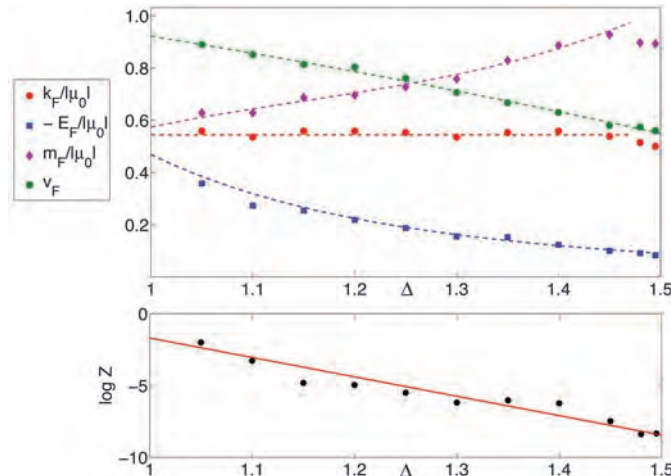


Fig. 6. The quasi-particle characteristics as a function of the Dirac fermion mass $-1/2 < m < 0$ corresponding to $1 < \Delta_\Psi < 3/2$ for $\mu_0/T = -30.9$. The upper panel shows the independence of k_F of the mass. This indicates Luttinger's theorem if the anomalous dimension Δ_Ψ is taken as an indicator of the interaction strength. Note that v_F and E_F both approach finite values as $\Delta_\Psi \rightarrow 3/2$. The lower panel shows the exponential vanishing pole strength Z (the integral between the half-maxima) as $m \rightarrow 0$.



for vanishing Z_k with $v_F \rightarrow 1$. Interestingly, the case has been made that such a relativistic fermionic behavior might be underlying the physics of cuprate high- T_c superconductors (31).

Finally, we address the important question of what happens when we vary the conformal dimension Δ_Ψ of the fermionic operator. Figure 6 shows that the Fermi momentum k_F stays constant as we increase Δ_Ψ . This completes our identification of the new phase as the Fermi liquid: It indicates that the AdS dual obeys Luttinger's theorem, if we can interpret the conformal dimension of the fermionic operator as a proxy for the interaction strength. We find furthermore that the quasi-particle pole strength vanishes as we approach $\Delta_\Psi = 3/2$. This confirms our earlier assumption that it is essential to study the system for $\Delta_\Psi < d/2$ and that the point $\Delta_\Psi = d/2$, where the naive fermion bilinear becomes marginal, signals the onset of a new regime. Because the fermion bilinear is marginal at that point, this ought to be an interesting regime in its own right, and we refer to (27) for a discussion thereof (32). Highly remarkable is that the pole strength vanishes in an exponential fashion rather than the anticipated algebraic behavior (6, 7). This could indicate that an essential singularity governs the critical point at $\Delta_\Psi = d/2$, and we note that such a type of behavior was identified by Lawler *et al.* in their analysis of the Pomeranchuk instability in $d = 2 + 1$ dimensions using the Haldane patching bosonization procedure (33). Note that this finite μ_0/T transition as we vary Δ_Ψ has no clear symmetry change, similar to (7). However, this may be an artifact of the fact that our theory is not quantum mechanically complete (25). Note also that the quasi-particle velocity and the renormalized Fermi energy $E_F = v_F(k - k_F) - E$ stay finite at the $\Delta_\Psi = 3/2$ transition with $Z \rightarrow 0$, which could indicate an emergent Lorentz invariance for the reasons discussed above.

Concluding remarks. We have presented evidence that the AdS dual description of strongly coupled field theories can describe the emergence of the Fermi liquid from a quantum critical state, as a function of both density and interaction strength, as encoded in the conformal dimension of the fermionic operators. From the AdS gravity perspective, it was unclear whether this would happen. Sharp peaks in the CFT spectral function correspond to so-called quasi-normal modes of black holes (34), but Dirac quasi-normal modes have received little study [see, e.g., (35)]. It is remarkable that the AdS calculation processes the Fermi-Dirac statistics essential to the Fermi liquid correctly. This is manifested by the emergent renormalized Fermi energy and the validity of Luttinger's theorem. The AdS gravity computation, however, is completely classical without explicit quantum statistics, although we do probe the system with a fermion. It would therefore be interesting to fully understand the AdS description of what is happening, in particular how the emergent scales

E_F and k_F feature in the geometry. An early indication of such scales was seen in (24, 36) in a variant of the story that geometry is not universal in string theory: The geometry depends on the probe used, and different probes experience different geometric backgrounds. The absence of these scales in the general relativistic description of the AdS black hole could thus be an artifact of the Riemannian metric description of space-time.

Regardless of these questions, AdS/CFT has shown itself to be a powerful tool to describe finite-density Fermi systems. The description of the emergent Fermi liquid presented here argues that AdS/CFT is uniquely suited as a computational device for field theory problems suffering from fermion sign problems. AdS/CFT represents a rich mathematical environment and a new approach to qualitatively and quantitatively investigate important questions in quantum many-body theory at finite fermion density.

References and Notes

1. M. Troyer, U. J. Wiese, *Phys. Rev. Lett.* **94**, 170201 (2005).
2. S. Sachdev, *Quantum Phase Transitions* (Cambridge Univ. Press, Cambridge, 1999).
3. J. Zaanen, *Science* **319**, 1295 (2008).
4. D. van der Marel *et al.*, *Nature* **425**, 271 (2003).
5. J. Zaanen, *Nature* **430**, 512 (2004).
6. T. Senthil, *Phys. Rev. B* **78**, 035103 (2008).
7. F. Krüger, J. Zaanen, *Phys. Rev. B* **78**, 035104 (2008).

8. D. T. Son, A. O. Starinets, *Annu. Rev. Nucl. Part. Sci.* **57**, 95 (2007).
9. S. S. Gubser, A. Karch, <http://arxiv.org/abs/0901.0935> (2009).
10. C. P. Herzog, P. Kovtun, S. Sachdev, D. T. Son, *Phys. Rev. D* **75**, 085020 (2007).
11. S. A. Hartnoll, P. K. Kovtun, M. Muller, S. Sachdev, *Phys. Rev. B* **76**, 144502 (2007).
12. S. S. Gubser, *Phys. Rev. D* **78**, 065034 (2008).
13. S. A. Hartnoll, C. P. Herzog, G. T. Horowitz, *Phys. Rev. Lett.* **101**, 031601 (2008).
14. S. A. Hartnoll, C. P. Herzog, G. T. Horowitz, *J. High Energy Phys.* **0812**, 015 (2008).
15. D. T. Son, *Phys. Rev. D* **78**, 046003 (2008).
16. K. Balasubramanian, J. McGreevy, *Phys. Rev. Lett.* **101**, 061601 (2008).
17. A. Adams, K. Balasubramanian, J. McGreevy, *J. High Energy Phys.* **0811**, 059 (2008).
18. S. A. Hartnoll, *Science* **322**, 1639 (2008).
19. S. A. Hartnoll, <http://arxiv.org/abs/0903.3246> (2009).
20. M. Kulaxizi, A. Parnachev, *Nucl. Phys. B* **815**, 125 (2009).
21. A. Karch, D. T. Son, A. O. Starinets, *Phys. Rev. Lett.* **102**, 051602 (2009).
22. M. Kulaxizi, A. Parnachev, *Phys. Rev. D* **78**, 086004 (2008).
23. L. Brits, M. Rozali, <http://arxiv.org/abs/0810.5321> (2008).
24. H. H. Shieh, G. van Anders, *J. High Energy Phys.* **0903**, 019 (2009).
25. See supporting material on Science Online.
26. ARPES Fermi-surface measurements assume that electrons are the only relevant charged objects. If this is so, then it measures the electron (i.e., fermion) spectral function. This spectral function is what we compute here, even though in our AdS setup the fermions are almost certainly not the only charged objects.
27. H. Liu, J. McGreevy, D. Vegh, <http://arxiv.org/abs/0903.2477> (2009).

28. S. S. Lee, *Phys. Rev. D* **79**, 086006 (2009).
29. E. M. Lifshitz, L. P. Pitaevskii, *Statistical Physics, Part 2* (Pergamon, Oxford, 1980).
30. H. J. Schulz, G. Cuniberti, P. Pieri, in *Field Theories for Low-Dimensional Condensed Matter Systems*, G. Morandi, P. Sodano, A. Tagliacozzo, V. Tognetti, Eds. (Springer, Berlin, 2000), chap. 2.
31. M. Randeria, A. Paramakanti, N. Trivedi, *Phys. Rev. B* **69**, 144509 (2004).
32. Note that the $m = 0$ spectral peak discussed in (27) is therefore not the peak we identified with the quasi-particle state. See (25).
33. M. J. Lawler, V. Fernandez, D. G. Barci, E. Fradkin, L. Oxman, *Phys. Rev. B* **73**, 085101 (2006).
34. P. K. Kovtun, A. O. Starinets, *Phys. Rev. D* **72**, 086009 (2005).
35. H. T. Cho, A. S. Cornell, J. Doukas, W. Naylor, *Phys. Rev. D* **77**, 016004 (2008).
36. M. Rozali, H. H. Shieh, M. Van Raamsdonk, J. Wu, *J. High Energy Phys.* **0801**, 053 (2008).
37. We thank F. Denef, S. Hartnoll, H. Liu, J. McGreevy, S. Sachdev, D. Sadri, and D. Vegh for discussions. Supported by a VIDI Innovative Research Incentive Grant (K.S.) from the Netherlands Organization for Scientific Research (NWO) and by a Spinoza Award (J.Z.) from NWO and the Dutch Foundation for Fundamental Research on Matter (FOM).

Supporting Online Material

www.sciencemag.org/cgi/content/full/1174962/DC1

SOM Text

Fig. S1

References

14 April 2009; accepted 16 June 2009

Published online 25 June 2009;

10.1126/science.1174962

Include this information when citing this paper.

REPORTS

Radio Imaging of the Very-High-Energy γ -Ray Emission Region in the Central Engine of a Radio Galaxy

The VERITAS Collaboration, the VLBA 43 GHz M87 Monitoring Team, the H.E.S.S. Collaboration, the MAGIC Collaboration*

The accretion of matter onto a massive black hole is believed to feed the relativistic plasma jets found in many active galactic nuclei (AGN). Although some AGN accelerate particles to energies exceeding 10^{12} electron volts and are bright sources of very-high-energy (VHE) γ -ray emission, it is not yet known where the VHE emission originates. Here we report on radio and VHE observations of the radio galaxy Messier 87, revealing a period of extremely strong VHE γ -ray flares accompanied by a strong increase of the radio flux from its nucleus. These results imply that charged particles are accelerated to very high energies in the immediate vicinity of the black hole.

Active galactic nuclei (AGN) are extragalactic objects thought to be powered by massive black holes in their centers. They can show strong emission from the core, which is often dominated by broadband continuum radiation ranging from radio to x-rays and by substantial flux variability on different time scales. More than 20 AGN have been es-

tablished as very-high-energy (VHE) γ -ray emitters with measured energies above 0.1 TeV; the jets of most of these sources are believed to be aligned with the line of sight to within a few degrees. The size of the VHE γ -ray emission region can generally be constrained by the time scale of the observed flux variability (1, 2), but its location remains unknown.

We studied the inner structure of the jet of the giant radio galaxy Messier 87 (M87), a known VHE γ -ray-emitting AGN (2–5) with a $(6.0 \pm$

$0.5) \times 10^9$ solar mass black hole (6) (scaled by distance), located 16.7 Mpc (54 million light years) away in the Virgo cluster of galaxies. The angle between its plasma jet and the line of sight is estimated to lie between 15° and 25° [see supporting online material (SOM) text]. The substructures of the jet, which are expected to scale with the Schwarzschild radius R_s of the black hole (7), are resolved in the x-ray, optical, and radio wave bands (8) (Fig. 1). High-frequency radio very-long-baseline interferometry (VLBI) observations with resolution under a milli-arc second (milli-arc sec) are starting to probe the collimation region of the jet (9). With its proximity, bright and well-resolved jet, and very massive black hole, M87 provides a unique laboratory in which to study relativistic jet physics in connection with the mechanisms of VHE γ -ray emission in AGN.

VLBI observations of the M87 inner jet show a well-resolved, edge-brightened structure extending to within 0.5 milli-arc sec (0.04 pc or $70 R_s$) of the core. Closer to the core, the jet has a wide opening angle, suggesting that this is the collimation region (9). Generally, the core can be offset from the actual location of the black hole by an unknown amount (10), in which case it could mark the location of a shock structure or the region where the jet becomes optically thin. However, in the case of M87, a weak structure

*The full list of authors and affiliations is presented at the end of this paper.

Confinement/deconfinement transition from symmetry breaking in gauge/gravity duality

Mihailo Čubrović

*Institute for Theoretical Physics, University of Cologne,
Zùlpicher Strasse 77, D-50937, Cologne, Germany*

E-mail: mcubrovic@gmail.com

ABSTRACT: We study the confinement/deconfinement transition in a strongly coupled system triggered by an independent symmetry-breaking quantum phase transition in gauge/gravity duality. The gravity dual is an Einstein-scalar-dilaton system with AdS near-boundary behavior and soft wall interior at zero scalar condensate. We study the cases of neutral and charged condensate separately. In the former case the condensation breaks the discrete \mathbb{Z}_2 symmetry while a charged condensate breaks the continuous $U(1)$ symmetry. After the condensation of the order parameter, the non-zero vacuum expectation value of the scalar couples to the dilaton, changing the soft wall geometry into a non-confining and anisotropically scale-invariant infrared metric. In other words, the formation of long-range order is immediately followed by the deconfinement transition and the two critical points coincide. The confined phase has a scale — the confinement scale (energy gap) which vanishes in the deconfined case. Therefore, the breaking of the symmetry of the scalar (\mathbb{Z}_2 or $U(1)$) in turn restores the scaling symmetry in the system and neither phase has a higher overall symmetry than the other. When the scalar is charged the phase transition is continuous which goes against the Ginzburg-Landau theory where such transitions generically only occur discontinuously. This phenomenon has some commonalities with the scenario of deconfined criticality. The mechanism we have found has applications mainly in effective field theories such as quantum magnetic systems. We briefly discuss these applications and the relation to real-world systems.

KEYWORDS: AdS-CFT Correspondence, Gauge-gravity correspondence, Holography and condensed matter physics (AdS/CMT), Holography and quark-gluon plasmas

ARXIV EPRINT: [1605.07849](https://arxiv.org/abs/1605.07849)

Contents

| | | |
|----------|---|-----------|
| 1 | Introduction | 1 |
| 2 | Gravity setup | 4 |
| 3 | Solutions in the infrared: soft-wall and AdS-like | 8 |
| 3.1 | Neutral solutions | 8 |
| 3.1.1 | No symmetry breaking | 8 |
| 3.1.2 | Symmetry-breaking order parameter | 9 |
| 3.2 | Charged solutions | 11 |
| 3.2.1 | No symmetry breaking | 11 |
| 3.2.2 | Symmetry-breaking order parameter | 12 |
| 3.3 | Resume of the geometries | 13 |
| 4 | Phase diagram and thermodynamics | 13 |
| 4.1 | The condensation of the boson at $T = 0$ | 14 |
| 4.1.1 | The neutral case | 15 |
| 4.1.2 | The charged case | 17 |
| 4.2 | Free energies and phases at zero temperature | 18 |
| 4.3 | Finite temperature thermodynamics | 20 |
| 4.4 | Structure of the phase diagram | 23 |
| 5 | Response functions and bound states | 24 |
| 5.1 | Definition and equations of motion | 24 |
| 5.2 | Effective Schrödinger equation for the response functions | 26 |
| 5.3 | Numerics | 27 |
| 5.3.1 | AC conductivity | 27 |
| 5.3.2 | Retarded propagator | 29 |
| 5.3.3 | Charge susceptibility | 30 |
| 6 | Conclusions and discussion | 30 |
| A | A short summary of numerical calculations | 34 |

1 Introduction

The gauge/gravity duality, AdS/CFT correspondence or holography [1, 2] is by now a well-established area, providing insights into fundamental issues of string theory and quantum gravity but also into strongly-coupled physics in various areas such as quantum chromodynamics (QCD) and condensed matter systems [4]. In such studies, the spacetime has

anti de Sitter (AdS) geometry at large distances, near the boundary of the space, while the interior is deformed away from AdS by various matter and gauge fields. This means that the high-energy behavior (ultraviolet, UV) of the field theory, determined by the near-boundary geometry, is conformally invariant but the interesting low-energy (infrared, IR) physics is determined by the geometry of the interior which can look differently for various configurations of fields and matter. The basic idea is that the radial coordinate on the gravity side corresponds to the energy scale in field theory: as we travel from the boundary toward the interior, we probe lower and lower energy scales.

One outstanding problem where AdS/CFT has provided some insights is the confinement/deconfinement transition in strongly coupled gauge theories. In the confined phase, only gauge-neutral bound states (mesons or baryons) can be observed. In the deconfined phase, individual gauge-charged particles are also observable. The fact that the gauge-charged excitations confine to form gauge-neutral bound states means that a gap opens, as we only see the gauge-neutral bound states at finite energies; the number of the degrees of freedom is effectively reduced at low energies. In AdS/CFT, this in turn means that the scale of the spacetime in the dual gravity model shrinks to zero in the interior. Such geometries are called soft-wall geometries, if the scale shrinks continuously, or hard-wall geometries if the spacetime is sharply cut off at some finite radius. Soft-wall geometries (which are more realistic than the hard-wall idealization) are obtained by coupling a neutral scalar — dilaton — to the metric in a non-minimal way. They were first used in so-called AdS/QCD studies in [3, 21, 32–34].

Typically, as the temperature rises, the system undergoes a confinement/deconfinement phase transition: when the system deconfines, the free energy of individual gauge-charged particles becomes finite, and they can be observed. This is the dominant mechanism in quark-gluon plasmas in QCD. But confinement/deconfinement is also present in condensed matter systems. Here the gauge field is not microscopic but emergent in the low-energy description. In the confined phase the degrees of freedom are bound into gauge-neutral excitations which are seen as normal electrons, i.e. quasiparticles. In the deconfined regime, the excitations are gauge-charged and not observable by ordinary probes in experiment. This might explain some non-Fermi liquid materials [10–15]. This topic was addressed e.g in [29] as well as in a series of very general and systematic studies by Kiritsis and coworkers [24–26]. In such systems, it is realistic to assume that deconfinement can also happen as a quantum phase transition, at zero temperature, when some parameter is varied. Deconfined gauge theories in AdS/CFT often have full conformal symmetry (dual to AdS geometry) or at least some form of anisotropic scale covariance (with different scaling exponents along different coordinates) which arguably can be expected to hold at high energies for many realistic gauge theories [3] while a confined theory has an explicit scale because the energy of gauge-neutral bound states or, equivalently, the position of the wall z_w along the radial direction sets a scale. The confinement/deconfinement transition can thus be treated also as a symmetry-breaking transition, where scale covariance is lost. The scaling properties of dilaton spacetimes have recently become known as hyperscaling geometries [27, 30, 31] and have attracted attention also independently of the confinement/deconfinement problems.

Another class of problems where strongly-coupled models are provided by AdS/CFT are the order/disorder quantum phase transitions where some field O acquires a vacuum expectation value (VEV). A textbook example is the famous holographic superconductor [5–7] where a charged field condenses, breaking the $U(1)$ symmetry, similarly to the superconducting transition in metals. While many such systems are described by the Landau-Ginzburg paradigm, this paradigm fails in some strongly-coupled systems. Many variations of such models have been proposed [36–40] where a dilaton is also present, or it is precisely the dilaton that condenses. The work [36] in particular addresses the setup similar as in our study: a scalar which condenses in the presence of a separate dilaton (however, explicit calculation with backreaction on dilaton and geometry was not done to check if the confinement/deconfinement transition exists). This opens an alley to study the interplay of the two transitions, the confinement/deconfinement transition and the order/disorder transition.

Our idea is to explore the interplay of the two above phenomena: the confinement/deconfinement transition and the condensation of an order parameter. They might in principle be independent, or one might foster or hinder the other. Well-studied examples of holographic superconductors [5] or superconductor-dilaton systems [37, 38] suggest that order parameter condensation often makes the length scale in the interior decrease faster: a charged black AdS-Reissner-Nordström black hole, which in deep interior has the AdS_2 geometry of finite radius, upon condensation turns into a Lifshitz spacetime whose length scale vanishes in the interior [4, 7]; in [29] this was interpreted as turning a fractionalized non-Fermi liquid into a system closer to a Fermi liquid. On general grounds one also expects that an ordered system can be expressed in terms of fewer degrees of freedom (in terms of the fluctuations of the order parameter rather than all microscopic degrees of freedom).

We will however present an example where the opposite occurs, i.e. the formation of a condensate destroys the soft-wall geometry and deconfinement takes place. Thus the phase transition is not a straightforward symmetry-breaking transition: on one hand, the condensate breaks a symmetry, on the other hand, another symmetry is restored as the deconfinement happens. This happens because the confinement scale (the energy gap) vanishes so scale invariance is restored. Our main interest is how this transition looks and what is its nature. We find that the phase transition can be continuous, contrary to the prediction of the Ginzburg-Landau theory where such transitions (where the two phases have different symmetries neither of which is a subgroup of the other) can only occur through phase coexistence or a first-order transition.

This has some common logic with the deconfined criticality concept of [10, 11]. Denote the full symmetry group of the non-soft-wall geometry by \mathbb{G}_1 and its subgroup which remains after confinement by \mathbb{G}_2 . We do not know what exactly $\mathbb{G}_{1,2}$ are but generically \mathbb{G}_1 will contain some scale invariance which stems from the scaling behavior of the IR geometry, while the confined system has a scale (the confinement gap) and thus \mathbb{G}_2 does not contain any scaling symmetry. Denote further the symmetry group broken by the condensate formation by \mathbb{H}_1 and its residual subgroup by \mathbb{H}_2 (in our case, we have $(\mathbb{H}_1, \mathbb{H}_2) = (\mathbb{Z}_2, \mathbb{I})$ for the neutral scalar and $(\mathbb{H}_1, \mathbb{H}_2) = (U(1), \mathbb{I})$ for the charged scalar. Now in our paper we have a transition from the confined-disordered phase (symmetry group $\mathbb{G}_2 \otimes \mathbb{H}_1$) to the

deconfined-ordered phase with the symmetry $\mathbb{G}_1 \otimes \mathbb{H}_2$. We have $\mathbb{G}_2 < \mathbb{G}_1$ and $\mathbb{H}_2 < \mathbb{H}_1$ so the critical point partly breaks, and partly restores symmetry. The same situation occurs in deconfined criticality scenario but the detailed physics is different: at a deconfined critical point (*only* at the critical point) there is an additional topological conserved quantity which governs the transition. We will comment on this in the paper in more detail, however no direct relation or equivalence can be established at this level. We cite the deconfined criticality as an inspiration and possible direction of future work, not something that our present results are directly relevant for.

Although the specific problem of how condensation of a scalar may influence the confinement/deconfinement transition was not studied so far to the best of our knowledge, a lot of work was done on Einstein-Maxwell-dilaton systems in other contexts. After the pioneering work in [3] which first drew attention to the AdS/QCD alley of research, confinement was studied in [32–34] and more systematically in [22, 23] with finite temperature behavior further explored in [21]. These authors have studied a neutral Einstein-dilaton system and have classified geometries which lead to confinement as well as the nature of the phase transition (first-order or continuous). Charged systems have been studied in [24–27]. The non-condensed phases of our system (without the order parameter) are just a small subset of the systems studied in [25] and we will frequently compare our case to their general results throughout the paper. Charged EMD systems are particularly well studied as top-down constructions regularly include charged fields. The charged case we consider is also closely related to the dilatonic charged black holes considered in [18–20] as possible candidates for gravity duals of Fermi liquids. The issue of a scalar condensation in the presence of dilaton is also rather extensively studied, e.g. in [39, 40] but in these cases the dilaton does not lead to a soft wall geometry so there is no confinement which can be destroyed upon condensation. In [35, 37, 38] the dilaton itself is charged (i.e., a charged scalar is coupled to the curvature) and the phenomenology was found to be similar to the basic holographic superconductor [5].

In section 2 we give the gravity setup and explain our model. Section 3 sums up different solutions for the geometry, depending on the bulk mass (conformal dimensions) of the scalar field and classifies the solutions into confined and deconfined ones. In section 4 we explain how the condensation of the order parameter proceeds and how it leads to deconfinement, and finally construct the phase diagram of the system. In the fifth section we study the response functions (conductivity, charge susceptibility and the retarded propagator of the scalar field) and show how various phases and their symmetries can be inspected from the response functions which are in principle measurable quantities. The last section sums up the conclusions and discusses possible directions of further work. The appendix contains a detailed description of the numerical calculations.

2 Gravity setup

We have the Einstein-(Maxwell)-scalar-dilaton system in asymptotically AdS_{D+1} space-time, with or without the Maxwell sector: the metric $g_{\mu\nu}$, the dilaton scalar Φ and the (neutral or charged) scalar χ . If the system is charged, there is also the electric field A_μ

where only the electric component A_0 is nonzero (we do not consider magnetic systems). The dilaton Φ couples to the curvature R in the string frame and is always neutral; thus unlike the models where the dilaton (actually, a non-minimally coupled scalar) is itself the charged field that condenses, we want the dilaton to perform its usual work, i.e. to control the scale (and confinement). This will be crucial to study the influence of the order parameter on the confining properties. We find it more convenient to work in the Einstein frame where the dilaton does not couple non-minimally to the metric but to the matter fields only. The scalar χ is minimally coupled to gravity and to the Maxwell field with charge q (including the possibility $q = 0$). We now have the action:

$$S = \int dt \int d^D x \sqrt{-g} (R - \Lambda + L_\Phi + L_\psi + L_{EM}) \tag{2.1}$$

$$L_\Phi = -\xi (\partial\Phi)^2 - V(\Phi) \tag{2.2}$$

$$L_\chi = -\frac{1}{2} Z(\Phi) (D\chi)^2 - \frac{m_\chi^2}{2} \chi^2 = -\frac{1}{2} Z(\Phi) (\partial\chi)^2 - \frac{q^2}{2f(z)^2} Z(\Phi) A_0^2 \chi^2 - \frac{e^{-2A}}{2\xi f} m_\chi^2 \chi^2 \tag{2.3}$$

$$L_{EM} = -\frac{1}{4} \mathcal{T}(\Phi) F^2 = -\frac{1}{2} \mathcal{T}(\Phi) (\partial A_0)^2. \tag{2.4}$$

This is just the minimal symmetry-allowed action for these fields apart from the exponential couplings of the dilaton. In string theory we would have $\xi = 4/(D-1)$ but since our model is purely phenomenological we can leave it as an arbitrary positive constant. We have subtracted the constant piece, i.e. the cosmological constant $\Lambda = -D(D-1)/2$ from the dilaton potential, so the AdS solution corresponds to $\Phi = 0$ (and $\chi = 0$). The geometry is AdS_{D+1} in the far field (UV, near-boundary) region while, with a suitable choice of $V(\Phi), Z(\Phi), \mathcal{T}(\Phi)$ it narrows into a soft wall in the interior (IR). The AdS radius is rescaled to $L = 1$. The potential of the scalar is fixed to just the mass term, like in [5, 6], as it suffices to achieve condensation (and is a consistent truncation of more elaborate, top-down potentials). As explained in [5], the field χ , even when charged, can be made real, i.e. its phase can be put to zero.

Now we come to the question of choosing the model, i.e. the dilaton potentials $V(\Phi), Z(\Phi), \mathcal{T}(\Phi)$. The basic picture of confinement in AdS/CFT means the dilaton potential should produce a soft-wall geometry but we also want to study its interplay with the establishment of (bosonic) long-range order and condensation. We want to engineer the dilaton potentials so that the scalar is unstable to condensation into a hairy black hole with $\chi(z) \neq 0$ for some m_χ^2 in the soft wall background *and* that the soft wall dilaton is in turn unstable to transition into a non-confining (non-soft-wall) solution upon the formation of scalar hair. This means that, upon dialing m_χ^2 , we should have two possible solutions for the scalar, $\chi(z) = 0$ and $\chi(z) \neq 0$, each with a different nonzero solution for the dilaton $\Phi(z)$. The following potentials will serve us well:

$$V(\Phi) = V_0 \Phi^{\frac{2\nu-2}{\nu}} e^{2\Phi} \tag{2.5}$$

$$Z(\Phi) = Z_0 e^{\gamma\Phi}, \quad D-1 < \gamma < 2D \tag{2.6}$$

$$\mathcal{T}(\Phi) = T_0 e^{\tau\Phi}, \quad \tau > 2D-4, \quad \tau^2 > \left(\gamma + \frac{D-2}{8}\right)^2 + \frac{1}{D}. \tag{2.7}$$

The limitations for γ and τ follow from the requirement that the stress-energy tensor of the EM field and also of the charged scalar field χ should stay finite and not dominate over the components of the Einstein tensor. In top-down constructions from supergravity the functions $Z(\Phi), V(\Phi), \mathcal{T}(\Phi)$ are typically all purely exponential in Φ (or linear combinations of such exponentials), with fixed exponent values. In our bottom-up approach these exponents are free parameters and by tuning these we can study the behavior we are looking for. We have added a power-law prefactor to (2.5) for reasons of better analytical tractability: the soft wall solution for the scale factor $A(z)$ is simplified with this choice for $V(\Phi)$ and at the leading order reads just $A(z) = z^\nu$ with subleading corrections for $z \rightarrow \infty$ whereas with a purely exponential $V(\Phi)$ it would have been more complicated also at leading order. We conjecture that the phase diagram and overall behavior of the system would be similar for $V \propto e^{\kappa\Phi}$. In a companion publication we derive our model from a superpotential which demonstrates the stability of the system, giving legitimacy to (2.5). The prefactors Z_0, \mathcal{T}_0 merely rescale the amplitudes of χ, A_0 and can be put to unity (they have no physical meaning). Notice the case $\nu = 1$ is special: then we get the linear dilaton theory, the potentials V, Z, \mathcal{T} become purely exponential and can be embedded in a supergravity action. Finally, the potentials (2.5)–(2.7) are the expressions in IR: near the AdS boundary they are corrected to ensure the AdS asymptotics.

For analytical considerations it is convenient to parametrize the metric as:¹

$$ds^2 = e^{-2A(z)} \left(-f(z)dt^2 + \frac{dz^2}{f(z)} + d\mathbf{x}^2 \right), \quad (2.8)$$

with the coordinates $(t, z, x_1, \dots, x_{D-1})$, where x_i are the transverse spatial coordinates, i.e. the spatial coordinates in field theory and z is the radial distance in AdS space: the AdS boundary (UV of the field theory) sits at $z = 0$ and the interior (IR in field theory) is at $z \rightarrow \infty$. At equilibrium, the fields are static, homogenous and isotropic, so they depend only on z . The equations of motion read:

$$A'' + (A')^2 = \frac{1}{D-1} \frac{1}{f^2} T_{00} + T_{zz} = \frac{1}{2(D-1)} Z(\chi')^2 + \frac{1}{D-1} \xi(\Phi')^2 \quad (2.9)$$

$$f'' - (D-1)f'A' = 2 \left(\frac{1}{f} T_{00} + T_{ii} \right) = 2e^{2A} \mathcal{T}(A'_0)^2 \quad (2.10)$$

$$\Phi'' + \left(\frac{f'}{f} - (D-1)A' \right) \Phi' - \frac{e^{-2A} \partial_\Phi V}{\xi f} - \frac{e^{2A} f}{2\xi} (\chi')^2 \partial_\Phi Z - \frac{e^{-3A}}{f} (A'_0)^2 \partial_\Phi \mathcal{T} = 0 \quad (2.11)$$

$$\chi'' + \left(\frac{f'}{f} - (D-1)A' + \Phi' \frac{\partial_\Phi Z}{Z} \right) \chi' - \frac{2e^{-2A}}{2f} m_\chi^2 \chi + \frac{q^2}{f^2} Z A_0^2 \chi = 0 \quad (2.12)$$

$$A_0'' - \left((D-3)A' - \frac{\partial_\Phi \mathcal{T}}{\mathcal{T}} \right) A_0' - \frac{2Z}{f\mathcal{T}} e^{-3A} \chi^2 A_0 = 0. \quad (2.13)$$

The prime denotes the radial derivative. As we have only two independent functions in the metric, it suffices to take two combinations of the Einstein equations. Due to homogeneity

¹In numerical calculations we find it convenient to use a different parametrization of the metric. Equations of motion and the description of the numerical algorithm can be found in appendix A.

we have $T_{x_1x_1} = T_{x_2x_2} = \dots = T_{x_{D-1}x_{D-1}} \equiv T_{ii}$ and the off-diagonal components are zero. The energy-momentum tensor $T^{\mu\nu} = T_{\Phi}^{\mu\nu} + T_{\chi}^{\mu\nu} + T_{EM}^{\mu\nu}$ reads

$$T_{\Phi}^{00} = \xi g^{zz} (\Phi')^2 - V, \quad T_{\Phi}^{zz} = T_{\Phi}^{ii} = -\xi g^{zz} (\Phi')^2 - V \quad (2.14)$$

$$T_{\chi}^{00} = \frac{Zg^{zz}(\chi')^2}{2} + \frac{Zg^{zz}A_0^2\chi^2}{2} - m_{\chi}^2\chi^2, \quad T_{\chi}^{zz} = T_{\chi}^{ii} = -\frac{Zg^{zz}(\chi')^2}{2} - \frac{Zg^{zz}A_0^2\chi^2}{2} - m_{\chi}^2\chi^2 \quad (2.15)$$

$$T_{EM}^{00} = T_{EM}^{zz} = -\mathcal{T}g^{00}g^{zz}(A_0')^2, \quad T_{EM}^{ii} = -2\mathcal{T}g^{00}g^{zz}(A_0')^2 \quad (2.16)$$

In order to have AdS asymptotics, the metric functions must satisfy $A(z \rightarrow 0) = \log z$ and $f(z \rightarrow 0) = 1$. The near-boundary expansion of the gauge field is of the form

$$A_0(z \rightarrow 0) = \mu - \rho z^{D-2} + \dots \quad (2.17)$$

which determines the chemical potential μ and the charge density ρ . One can work either in the canonical ensemble (fixing ρ) or in the grand canonical ensemble (fixing μ). For our purposes it doesn't matter much which variant we choose; in the concrete numerical examples we always fix the chemical potential. The scalar has the near-boundary behavior:

$$\chi = \chi_- z^{\Delta_-} (1 + c_{-1}z + c_{-2}z^2 + \dots) + \chi_+ z^{\Delta_+} (1 + c_{+1}z + c_{+2}z^2 + \dots) \quad (2.18)$$

where the leading and subleading branches χ_{\mp} have the conformal dimension $\Delta_{\pm} = D/2 \pm \sqrt{D^2/4 + m_{\chi}^2}$. In field theory, one of these is the source of the order parameter O_{χ} dual to χ and the other is its the vacuum expectation value (VEV). We pick χ_+ as the VEV, so the formation of the condensate means $\chi_+ \neq 0$ for $\chi_- = 0$ — nonzero subleading component (VEV) for zero leading (source) term. It usually turns out that the scalar can condense for negative enough mass squared, i.e. for $m_{\chi}^2 < m_{BF}^2$ for some bound m_{BF} (Breitenlohner-Friedmann bound [17]) that depends on the spacetime, i.e. on geometry; in AdS_{D+1} of unit radius it is $m_{BF}^2 = -D^2/4$. Similar asymptotics as in (2.18) hold for the dilaton Φ when the near-boundary form of the potential starts from a quadratic term: $V(\Phi(z \rightarrow 0)) \sim m_{\Phi}^2 \Phi^2 + \dots$. We tune m_{Φ}^2 above the bound for condensation because we never consider the condensed state of the dilaton. This leaves Φ_- as the sole free parameter. Obviously, Φ_- sources some field theory operator O_{Φ} of dimension $D/2 - \sqrt{D^2/4 + m_{\Phi}^2}$ which does not condense and thus does not break a symmetry. Still, the value of Φ_- influences the bulk solution and consequently may influence the condensation of χ or the confinement/deconfinement transition. In accordance with the main idea of the paper, we mainly focus on the condensation of O_{χ} at fixed Φ and only briefly discuss the meaning of O_{Φ} .

In absence of the scalar χ and apart from the subleading correction in the dilaton potential V , our system is one of the many cases of Einstein-dilaton and Einstein-Maxwell-dilaton systems considered systematically in [25]. Our parameter values are similar to a solution that the authors of [25] call “near-extremal case”. For each solution, we check that the value of the parameters we use for γ, δ, ν are consistent with the Gubser criterion for “good” curvature singularities in IR [16]. A good singularity means that, even though

the curvature becomes infinite at $z \rightarrow \infty$, it can be trapped by a horizon. A systematic discussion of allowed parameter values (for purely exponential potentials) can be found in the cited reference [25]. The exponent ν is also a free parameter with the limitation $\nu \geq 1$. In numerical calculations, unless specified differently, we take $\nu = 2$ and $D = 4$ for calculations, though any $D > 2$ again leads to similar results. An account of numerical calculations can be found in the appendix; the procedure is essentially iterative, repeatedly computing the profile of the scalar $\chi(z)$ and then updating the metric and the dilaton in the presence of $\chi(z)$.

3 Solutions in the infrared: soft-wall and AdS-like

3.1 Neutral solutions

3.1.1 No symmetry breaking

At zero temperature (which is central for studying the ground state) the space extends to $z \rightarrow \infty$. The authors of [23] have performed a classification of asymptotically AdS Einstein-dilaton systems (without other fields), motivated by AdS/QCD studies. Their results can be summed up as follows. The scale factor $A(z)$ either has a singularity at finite z , or at $z = \infty$. In the former case, the metric can be conformally equivalent to AdS with $A(z) \sim \alpha \log z$ (type Ib geometry), which is never confining whereas the soft-wall solutions with $A(z) \sim z^\nu$ (type Ia geometry) are confining for $\nu \geq 1$. If the singularity is to be found at finite $z = z_W$, then the logarithmic approach $A(z) \sim \log(z_W - z)$ (type IIb geometry) does not give confinement whereas a power-law $A(z) \sim 1/(z_W - z)^\nu$ (type IIa solution) does, for any ν .² We have nothing to add here: our system is a special case of the systems considered in [23], with slightly different $V(\Phi)$.

To solve our equations of motion (2.9)–(2.12), notice first that the equation (2.10) is decoupled from all matter fields and yields the solution

$$f(z) = C_0 + C_1 \int dz e^{(D-1)A(z)}. \tag{3.1}$$

A growing scale $A(z)$ in the interior would lead to a bad singularity according to the criterion of Gubser [16].³ Therefore, we need to suppose that $A(z)$ is a monotonically growing function of z , as also discussed in [23]. This in turn means that the non-constant term in (3.1) is likewise growing, so $C_1 < 0$ (in order to have a solution for the position of the horizon, defined by $f(z_{hor}) = 0$) and for correct AdS asymptotics $C_0 = 1$. Now C_1 is determined by the boundary condition in the interior: at zero temperature, the space is

²Let us quickly remind the reader where this comes from. The defining criterion for confinement is that the Wilson loop operator follows the area law. The Wilson loop, defined as the potential energy of a quark-antiquark pair separated by distance L , is holographically expressed as the action of a classical string embedded in spacetime, with a rectangular loop at the AdS boundary with sides equal to L and the time T . If the metric is of the form (2.8), one can plug it in into the expression for the string action and find the action scales as $e^{-2A(z_s)}$, where z_s is a stationary point: $A'(z_s) = 0$. From this the above conclusions follow, bearing in mind that one may have $z_s \rightarrow \infty$.

³To remind the reader, the paper [16] shows that a curvature singularity is physically meaningful if it can be obtained as the limit of a geometry with horizon, so that the horizon hides the singularity.

infinite so $C_1 = 0$, $f(z) = 1$ as expected for a neutral system. At nonzero temperature T , the position of the horizon is determined by the condition $f(z_h) = 0$.

We are left with one Einstein equation for $A(z)$ and two Klein-Gordon-like equations for the two scalars. It is easiest to start from an ansatz $A(z) \sim z^\nu$ to get a soft wall (type Ia) solution

$$\begin{aligned}
 A(z) &= z^\nu \left(1 + \frac{a_1}{z} + \frac{a_2}{z^2} + \dots \right) \\
 f(z) &= 1 - \frac{(D-1)^{1/\nu} \mathcal{M}}{\nu z^{\nu-1}} e^{(D-1)z^\nu}, \quad \chi(z) = 0 \\
 \Phi(z) &= \sqrt{\frac{D-1}{\nu\xi}} \sqrt{\nu z^{2\nu} + (\nu-1)z^\nu} \left(1 + \frac{\phi_{11}}{z} + \frac{\phi_{12}}{z^2} + \dots \right) + \\
 &\quad + \frac{\nu-1}{\nu\sqrt{\xi}} \log \left(\nu z^{\frac{\nu}{2}} + \sqrt{\nu^2 z^\nu + \nu^2 - \nu} \right) \left(1 + \frac{\phi_{21}}{z} + \frac{\phi_{22}}{z^2} + \dots \right). \quad (3.2)
 \end{aligned}$$

These forms are exact as $z \rightarrow \infty$ and the coefficients a_i, ϕ_{ij} can be found analytically at arbitrary order in principle. We are not interested in the details of the small z (UV) geometry, as long as enough free parameters remain that the solution can be continued to the AdS_{D+1} boundary conditions. The red shift function includes the rescaled black hole mass \mathcal{M} , which is related to the position of the horizon as $\mathcal{M} = z_h^{\nu-1}$, the horizon being determined through the transcendental equation $f(4\pi D/T) = 0$ which we will not explore here in detail. Importantly, the thermal solution smoothly crosses into the zero temperature solution and all temperatures down to $T = 0$ are defined, which is not always the case with Einstein-(Maxwell)-dilaton systems, see e.g. [25]. There is another solution, however: starting from the ansatz $A(z) \sim \alpha \log z$ we get a type Ib solution

$$\begin{aligned}
 A(z) &= \alpha \log z \left(1 + \frac{a_1}{z} + \frac{a_2}{z^2} + \dots \right), & \alpha &= \frac{\xi}{D-1+\xi} \\
 f(z) &= 1 - \frac{\mathcal{M}}{\alpha(D-1)} z^{(D-1)\alpha}, & \chi(z) &= 0 \\
 \Phi(z) &= \phi_0 \log z \left(1 + \frac{\phi_1}{z} + \frac{\phi_2}{z \log z} + \frac{\phi_3}{z^2} + \frac{\phi_4}{z^2 \log z} + \dots \right), & \phi_0 &= \frac{D-1}{D-1+\xi}. \quad (3.3)
 \end{aligned}$$

Which of these is the ground state is to be determined by comparing the free energies, our task in the next section (it turns out the confining solution Ia is the correct choice). These solutions have a curvature singularity at $z \rightarrow \infty$: the Ricci scalar for (3.2) is

$$R = -D(D-1)\nu^2 e^{2z^\nu} z^{2\nu-2} + \dots \quad (3.4)$$

which diverges for z large but can be trapped by a thermal horizon for any finite z_h so that R is finite as $z_h \rightarrow 0$. This follows from the form of $f(z)$ in (3.2) and makes the solution physically meaningful.

3.1.2 Symmetry-breaking order parameter

Now consider the symmetry-broken solution with $\chi(z) \neq 0$. If we require the physically logical (and simplest) choice of purely exponential $Z(\Phi)$ as in (2.6), then the only way

to satisfy (2.9) while keeping the scaling function $A(z) \sim z^\nu$ is to “reduce” the dilaton, i.e. make its growth slower than z^ν : otherwise, an additional source on the r.h.s. of equation (2.9) can only make $A(z)$ grow even faster, never slower (remember the r.h.s. is the kinetic energy of the scalar field which cannot be negative; adding a new nonzero field cannot reduce the sum). Thus we seek for a scalar $\chi(z)$ which, when coupled to $\Phi(z)$, gives it a logarithmic behavior $\Phi(z) \sim \phi_0 \log z$. Such a solution indeed exists. We deliberately postpone the discussion of the mechanism of the scalar instability to condensation, i.e. of the scalar fluctuations in background (3.2) which lead to the new solution discussed in this subsection. This mechanism (and the value of m_χ^2 at which it happens) will be discussed in the next section, before constructing the phase diagram. For now we are content to show that the solution exists. To the best of our knowledge, this kind of solution was not analytically constructed in earlier work.

The solution is now of type IbC (Ib with condensate):

$$\begin{aligned}
 A(z) &= \alpha \log z \left(1 + \frac{a_1}{z} + \frac{a_2}{z^2} + \dots \right), \quad \alpha = \frac{\gamma + 2}{2\gamma - 2(D - 1)} \\
 f(z) &= 1 - \frac{\mathcal{M}}{\alpha(D - 1)} z^{(D-1)\alpha} \\
 \Phi(z) &= \phi_0 \log z \left(1 + \frac{b_1}{z} + \frac{b_2}{z \log z} + \frac{b_3}{z^2} + \frac{b_4}{z^2 \log z} + \dots \right), \quad \phi_0 = \frac{D + 1}{\gamma + 1 - D} \\
 \chi(z) &= \chi_0 z^{-\frac{\gamma \phi_0}{2}}, \quad \phi_0 = \frac{D + 1}{2(\gamma + 2)} \alpha = \frac{D + 1}{\gamma - (D - 1)} \\
 \chi_0 &= \frac{\sqrt{2(\gamma^2 + 2\gamma + 2D^2(\gamma + 2 - 2\xi) - 4\xi - D((\gamma + 2)^2 + 8\xi))}}{(D + 1)\gamma}. \tag{3.5}
 \end{aligned}$$

Interestingly, the value of ν does not appear in the solution at leading order (of course, it does appear in the subleading corrections a_i, b_i). The solutions for ϕ_0, χ_0 show that we need the condition $\gamma > D - 1$ to avoid the growing metric scale in the interior. The crucial observation in the above discussion was that adding bosonic fields (for which $T_{00}/f^2 + T_{zz}$ is always positive) cannot destroy the soft wall solution. We find there is no solution with two scalars, Φ and χ , and with the couplings (2.5)–(2.6), which has a soft-wall metric scale behavior $A(z) \sim z^\nu$. This can be seen more rigorously from the superpotential approach. There is thus an interesting bifurcation-like behavior as the amplitude of the order parameter field is varied: there are two competing solutions for $\langle O_\chi \rangle = \chi(z = 0)$ but only one of them survives as $\langle O \rangle$ grows away from zero. Is this solution acceptable? The curvature behaves as

$$R = -4\alpha(3\alpha + 2)z^{2\alpha-2} + \dots \propto z^{\frac{\gamma-2D}{\gamma-D+1}}, \tag{3.6}$$

the exponent being positive precisely in the allowed interval of γ values, $D - 1 < \gamma < 2D$. Thus we again have a singularity, and it is again a “good” singularity according to [16]. This is in line with the results of [25] for “near-extremal” solutions: acceptable solutions are only those with a singularity; those without a curvature singularity are cosmological solutions with an unacceptable singularity at small z .

3.2 Charged solutions

3.2.1 No symmetry breaking

Instead of a neutral scalar we now take a charged scalar, i.e. the typical holographic superconductor setting, coupled to a dilaton. The results should not depend crucially on the spin of the charged field as long as it is integer; half-integers fields, i.e. fermions may well behave differently as they have different pressure (spatial components of the stress tensor). We will not analyze the fermionic case here.

For further convenience we adopt the terminology of [28, 29], used also in [27], to roughly classify the charged solutions in terms of the charge distribution in the bulk and how it influences the geometry. On one hand, we have (1) IR-neutral solutions where the *Maxwell contribution* to $T_{\mu\nu}$ is subleading so that the IR geometry is not influenced by $A_0(z)$ in the first approximation, as opposed to (2) IR-charged solutions where $A_0(z)$ contributes at leading order. The second criterion is whether the solution is fractionalized or coherent: (a) fractionalized solutions are those where *the charged fields* do not contribute to $T_{\mu\nu}$ and thus to geometry in the IR at leading order whereas in (b) cohesive solutions they contribute. In the fractionalized case the electric flux in the IR $\int \star [\mathcal{T}(\Phi)F]$ is non-zero while it is zero for cohesive solutions. The physical interpretation of the fractionalized/coherent dichotomy is still unclear. The logical explanation would be that in the fractionalized case the charge-carrying degrees of freedom are not those which are seen in the spectrum as they are charged under the gauge group and are not seen by the gauge-neutral probe ("gauginos"), as opposed to the gauge-neutral composite excitations of the coherent case ("mesinos"). This interpretation suggests a close relation between the confinement/deconfinement and coherence/fractionalization. The trouble is that many examples exist both of fractionalized but confined systems (the dilatonic black holes of [18–20]) and coherent but deconfined systems (the electron star and the dilatonic electron star of [29]). While confinement is about the behavior of the Wilson operator and the gauge field excitations, coherence is about the emergence of stable composite gauge-neutral excitations. Examples where the quarks emerge only after the gauge field compactifies are known in AdS/CFT [41] but the understanding of the phenomenon is lacking. We plan to address this issue in more detail in future work; here we will just state the fractionalization/coherence nature of our geometries and comment briefly on the interpretation in the conclusions. For more information on the general problems of fractionalization in this context see [19, 20, 27].

Let us now study the charged solutions. Notice first that a charged solution without condensate can only exist in the presence of a charged horizon. Such a solution must be fractionalized as none of the charge carriers have a dual VEV at the boundary. It reads

$$\begin{aligned}
 A(z) &= z^\nu \left(1 + \frac{a_1}{z} + \frac{a_2}{z^2} + \dots \right) \\
 f(z) &= 1 - \mathcal{M}(T)e^{(D-1)z^\nu} + \frac{2Q^2}{2\nu-3}e^{(\tau+4-2D)z^\nu}z^{3-2\nu} \left(1 + \frac{f_1}{z} + \frac{f_2}{z^2} + \dots \right) \\
 \Phi(z) &= z^\nu \left(1 + \frac{\phi_1 \log z}{z} + \frac{\phi_2}{z} + \dots \right), \quad \chi(z) = 0 \\
 A_0(z) &= a_0 - Qe^{-(\tau-(D-3))z^\nu}z^{1-\nu} \left(1 + \frac{a_1}{z} + \frac{a_2}{z^2} + \dots \right). \tag{3.7}
 \end{aligned}$$

Now the horizon carries the charge Q and at zero temperature $\mathcal{M}(T = 0) = 0$, so

the extremal horizon is degenerate and located at $z = \infty$. Again, we are not interested in the (complicated) analytical form of $\mathcal{M}(T)$. The electric flux at the horizon is $\sqrt{-g}g_0g_zz\mathcal{T}(\Phi)A'_0 = \mathcal{T}(\Phi)A'_0 \sim e^{-(D-3)z^\nu} \times e^{\tau z^\nu} a_1 e^{(D-3-\tau)z^\nu} \sim a_1$ which is a generically nonzero constant for $z \rightarrow \infty$, meaning that the solution is fractionalized. On the other hand, it is confining, as it is of type Ia (we call it IaQ, as it has charge) and the metric scale diminishes exponentially in the IR (we call it IaQ to emphasize it is charged). In fact, this solution is quite similar to the top-down dilatonic black hole with two-exponent potential discussed in [18–20]. Although fractionalized, it still confining so it fits into our main story: deconfinement from independent symmetry breaking.

3.2.2 Symmetry-breaking order parameter

Postulating a nonzero profile for the scalar field and requiring that the scalar contributes at leading order in the equation (2.9), we find the solution IbQC, the non-confining charged solution:

$$\begin{aligned}
 A(z) &= \alpha \log z \left(1 + \frac{a_1}{z} + \frac{a_2}{z^2} + \dots \right) \\
 f(z) &= 1 - \mathcal{M}(T) \frac{z^{(D-1)\alpha+1}}{(D-1)\alpha+1} + \frac{2Q^2}{z^\beta} \left(1 + \frac{f_1}{z} + \frac{f_2}{z^2} + \dots \right) \\
 \Phi(z) &= \phi_0 \log z \left(1 + \frac{\phi_1 \log z}{z} + \frac{\phi_2}{z} + \dots \right) \\
 \chi(z) &= \chi_0 z^{-\frac{\gamma\phi_0}{2}} \left(1 + \frac{\chi_1}{z} + \frac{\chi_2}{z^2} + \dots \right) \\
 A_0(z) &= a_0 - Qz^{-\frac{10+11\gamma+9\tau}{10+10\gamma+8\tau}} \left(1 + \frac{a_1 \log z}{z} + \frac{a_2}{z} + \dots \right), \tag{3.8}
 \end{aligned}$$

and the exponents read

$$\alpha = \frac{4 + 4\gamma + 3\tau}{5 + 5\gamma + 4\tau}, \quad \beta = \frac{2\tau + 3\gamma + 2}{4\tau + 5\gamma + 5}, \quad \phi_0 = \frac{1}{4\tau + 5\gamma + 5}. \tag{3.9}$$

The charged horizon is still degenerate at zero temperature. Comparing the stress tensors by plugging in the solution (3.8) into (2.14)–(2.16), we easily find that $T_{EM} \ll T_\Phi, T_\chi$ for $z \rightarrow \infty$, so according to the criterion of [25] the solution is IR neutral. Being of type Ib (we denote it IbQC, as it is charged and has the condensate), it is not confining, and the IR flux is $z^{-2-\frac{9\gamma+5\tau+8}{10+10\gamma+8\tau}}$ which goes to zero for $z \rightarrow \infty$ since γ and τ are positive and all the coefficients in both numerator and denominator of the exponent are positive. The solution IbQC is thus coherent and deconfined. On one hand, the fact that the non-condensed solution IaQ is fractionalized while the condensed solution IbQC is coherent is perfectly logical, since in the non-condensed case all the charge is on the horizon, whereas in the presence of the condensate it carries all the charge. The fact that the fractionalized solution is confined and the coherent one is deconfined may sound strange; e.g. in [27] the intuition is expressed that confined solutions should be coherent. But as we have already commented the zoo of field theories in gauge/gravity duality offers many counterexamples. At least, one expects that the coherent nature of the systems shows up as poles, i.e. bound states in the bottom half-plane of complex-frequency response functions of matter fields

(the scalar χ), independently of the presence or absence of confinement. We will check this in section 5.

Can we get a soft wall with charged condensate? We were unable to find such a solution either analytically or numerically. The conclusion is again that the competition of two scalars (dilaton and order parameter) destroys the confining solution. Of course, by adjusting the potentials V, Z, \mathcal{T} we could get many different phase diagrams but in the present model there is a strict competition between the soft wall and the condensate. Finally, the singularity properties of both charged solutions are analogous to the charge-neutral case: the singularities exist but are physically allowed.

3.3 Resume of the geometries

We have found five solutions: Ia, Ib, IaQ, IbC, IbQC. Only two of them compete in the same regime, Ia and Ib, and the preferred solution has to be found by computing the energy. Geometries Ia, IaQ are confined whereas Ib, IbC, IbQC are deconfined. Among the charged geometries, IaQ is fractionalized whereas IbQC is coherent, and both are IR neutral. In figure 1 we plot the metric functions $A(z), f(z)$ and the bulk profile of the dilaton and the scalar field $\Phi(z), \chi(z)$ at zero temperature, at zero chemical potential in the panel (A) and at finite chemical potential in the panel (B). The most obvious feature of the solutions is the sharp exponential fall-off of the scale factor e^{-2A} for soft-wall geometries versus much slower fall-off for deconfined solutions where the blue curve $e^{-2A}z^2$ is almost flat, i.e. the solution behaves almost as AdS in the IR. This is logical, as the volume in the IR counts the degrees of freedom of the low-energy excitations; at low enough energies, such excitations are completely absent in the confined phase. In fact, as can be seen from the analytical form of the solutions (3.5), (3.8), the factor e^{-2A} in the deconfined phase behaves as a power law just like in AdS, only with a different power. In [25, 27, 30, 31] such geometries are classified in terms of hyperscaling exponents, where the time, space and energy (i.e., radial distance in AdS) are each scale-covariant but with different exponents. It turns out these three exponents can be described by combinations of two parameters, the Lifshitz exponent ζ and the hyperscaling violation exponent θ ; if $\theta = 0$ the geometry obeys the hyperscaling whereas for $\theta \neq 0$ it is hyperscaling-violating. For a Lorentz-invariant system we have $\zeta = 1$; values different from unity mean that the dispersion relation is nonlinear and the Lorentz invariance broken. The neutral deconfined geometries (3.3) and (3.5) have $\zeta = 1$ but the hyperscaling exponent is nontrivial and reads $\theta = D(1 + \alpha)$. The charged version (3.8) has both exponents nontrivial ($\zeta > 0 \neq 1$ and $\theta \neq 0$). Note that the $\zeta < 0$ case is hard to interpret physically and thus we have checked that all of our geometries have $\zeta > 0$.

4 Phase diagram and thermodynamics

We will consider the ground state of our system as a function of the parameters and external sources of the theory. Parameters of the theory are the exponents ν, τ, γ and the conformal dimension (bulk mass) Δ_χ . The ranges of the allowed values of ν, τ, γ are chosen in such a way that the dependence on their values is smooth and unlikely to lead to

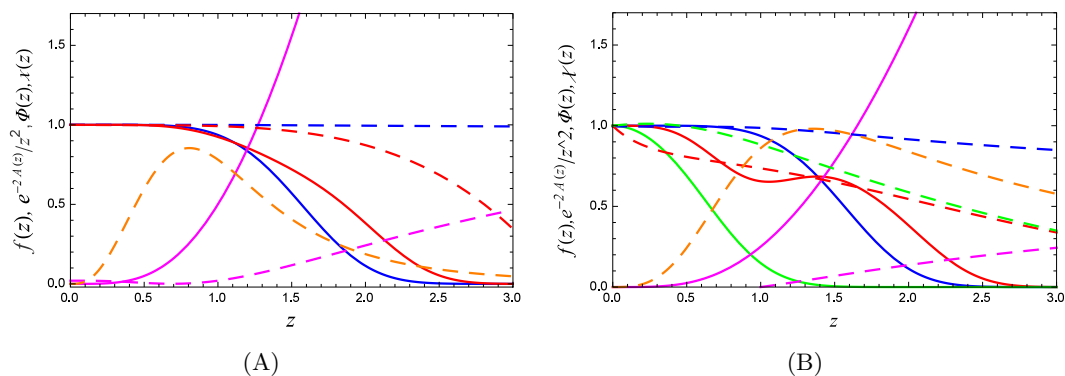


Figure 1. (A) The metric functions $e^{-2A(z)}z^2, f(z)$ (blue, red) and the bulk fields $\Phi(z), \chi(z)$ (magenta, orange) in the confined regime (geometry Ia, full lines) and in the deconfined regime (geometry IbC, dashed lines). The blue line corresponds to the ratio of the scale factor in our system and the AdS scale factor $1/z^2$. The confining regime has a soft wall in the IR and its IR scale falls practically to zero already at $z \sim 3$. (B) Same as the previous figure but for the charged field at the chemical potential $\mu = 1$; now we plot also the gauge field $A_0(z)$ (green). The basic phenomenology is the same as in (A): the soft wall broadens and the scale factor e^{-2A} has no characteristic scale z_W at which it falls off rapidly. The plots are in $D = 4$ and the parameter values are $\nu = 2, \gamma = 4$ (both A and B), and $\tau = 5$ for the charged case (B). For the neutral case we pick $m_\chi^2 = 1/4$ and $m_\chi^2 = -1/4$ whereas for the charged case we have $m_\chi^2 = 8$ and $m_\chi^2 = 4$.

phase transitions; furthermore, these exponents characterize the running couplings in field theory, which include also the information at different energy scales and probably cannot be realistically tuned. Therefore, the dependence of the thermodynamic quantities on ν, τ, γ will not be explored. The typical procedure in holographic superconductor literature would be to tune $\Delta_\chi = D/2 + \sqrt{D^2/4 + m_\chi^2}$ as a proxy for coupling strength in field theory, and this is what we shall do. The requirement for condensation fully fixes the solution $\chi(z)$, as we remind below, and we have no sources for O_χ . However, there is one free parameter in the theory at fixed parameter values: the operator O_Φ dual to the dilaton in the UV. Therefore, the phase transitions are driven by dialing the scaling dimension Δ_χ and the expectation value of the operator O_Φ dual to the dilaton. When not explicitly stated, we will assume a fixed O_Φ and study the phase transitions as a function of Δ_χ .

4.1 The condensation of the boson at $T = 0$

We expect that at some $\Delta_\chi = \Delta_c$ the neutral bosonic operator O_χ acquires a nonzero expectation value. As we know [5], the expectation value in field theory is given by the subleading term in the UV expansion (2.18) at zero source term

$$\langle O_\chi \rangle = \chi_+ |_{\chi_- = 0}. \quad (4.1)$$

One can also consider an alternative quantization where the VEV is given by χ_- , provided both terms are normalizable, but we will stick with the standard quantization. At this place one should differentiate between the neutral and the charged case. In the neutral case, no continuous symmetry is broken and the phase transition is more akin to nucleation, where

the oscillating modes of the scalar add up to a significant perturbation which eventually changes the metric. Whether the oscillations are strong enough or not to lead to a new ground state in principle depends on the parameters of the system. The charged case is expected to be simpler: here, the instability is supposed to be rooted in the Higgs mechanism which breaks the U(1) symmetry, and one expects this to happen for any charged scalar (independently of the m_χ^2 value). The charged scalar is thus expected to always condense at $T = 0$, at least in absence of the dilaton. In the presence of the dilaton, things can become more complicated, as we shall see.

4.1.1 The neutral case

The critical value of the conformal dimension⁴ Δ_c can be related to the violation of the Breitenlohner-Freedman (BF) stability bound in the interior. To remind, the idea is to rewrite the Klein-Gordon equation for the scalar with energy ω as an effective Schrödinger equation for the rescaled scalar $\tilde{\chi}(z) = \chi(z)/B(z)$ with energy ω^2 :

$$\tilde{\chi}'' - V_{\text{eff}}(z)\tilde{\chi} = -\frac{\omega^2}{f^2}\tilde{\chi}(z) \tag{4.2}$$

and the effective potential

$$V_{\text{eff}} = \frac{e^{-2A}}{f} m_\chi^2 - \frac{B'}{B} \left(\frac{f'}{f} + \frac{\partial_\Phi Z}{Z} \Phi' - (D-1)A' \right) - \frac{B''}{B}, \tag{4.3}$$

where the rescaling factor is

$$B(z) = \frac{e^{-\frac{D-1}{2}A} - \frac{\partial_\Phi Z}{2Z} \Phi}{\sqrt{f}}. \tag{4.4}$$

If the energy of χ becomes imaginary, i.e. the Schrödinger energy ω^2 becomes negative, it means there is an exponentially growing mode which likely signifies an instability, and the scaling dimension becomes complex [17]. In the Schrödinger formalism, it means that $\tilde{\chi}$ forms a bound state. We are not allowed to violate the bound in the UV, to prevent violating the AdS asymptotics assumed in the gauge/gravity duality, but an instability in the interior is perfectly allowed and signifies the change of IR physics, i.e. of the field theory ground state. In AdS-RN background, the instability of the neutral scalar is given simply by the BF bound of the near-horizon AdS₂, which equals $-1/4$ [5, 8]. We do not have a near-horizon AdS region and there is no simple formula for the critical mass (dimension) m_c^2 (Δ_c) but the logic is the same: we are looking for complex energies, i.e. bound states in the Schrödinger formalism.

In geometry Ia the effective potential reads

$$V_{\text{eff}} = m_\chi^2 e^{-2z\nu} - \frac{(D-\gamma-1)\nu(\nu-1)}{2} z^{\nu-2} + \frac{(D-\gamma-1)^2 \nu^2}{4} z^{2\nu-2} \tag{4.5}$$

which is positive and growing to infinity at large z . For any bound states to exist, we need to have a sufficiently deep and broad potential well below zero energy, i.e. the potential

⁴We will use the conformal dimension Δ_χ and the bulk mass squared m_χ^2 interchangeably as they are uniquely related to each other through $\Delta_\chi = D/2 + \sqrt{D^2/4 + m_\chi^2}$.

needs to grow to infinity also on the “left-hand side”, for small z , and fall sufficiently low in-between. Now we remember that for $z \rightarrow 0$ the potential certainly goes to positive infinity because $m_\chi^2 > -D^2/4$ (i.e., we do not want bound states in the far UV region, sitting at $z \rightarrow 0$). Now the question is what the potential looks like for some intermediate z_1 which is still large enough that the IR solution (geometry Ia) is valid. Assuming that $z_1 \sim 1$, this depends on the combination $m_\chi^2 - (D - \gamma - 1)\nu(\nu - 1)/2 + (D - \gamma - 1)^2\nu^2/4$ — the second and third term are both positive, and the question is whether there is a value of $m_\chi^2 > -D^2/4$ which is nevertheless sufficiently negative to make V_{eff} negative. This is obviously a question of numerical calculation but we can see that for $\gamma = D - 1 + \epsilon$ for ϵ small the second and the third term in (4.5) have practically zero coefficients and not too large $|m_\chi^2|$ suffices to push V_{eff} below zero in some interval. We conclude that we can expect a BF-type instability at some critical m_c^2 . We have seen this means the geometry Ia is modified, presumably into IbC, and at finite m_c^2 , analogously to the neutral holographic superconductor in AdS-RN [5, 8].

Having shown that there is indeed a mechanism for the condensation of the order parameter in the soft-wall regime, we should also check if the geometry IbC is stable in the presence of the condensate. In geometry IbC the effective potential is:

$$V_{\text{eff}} = V_\infty + \frac{m_\chi^2}{z^{2\alpha}} + \frac{\kappa(\kappa + 1)}{z^2} \tag{4.6}$$

where $\kappa = \frac{(D-1)\alpha + \gamma\phi_0}{2}$ and V_∞ is a z -independent constant. The inverse square term is always positive and the power of the mass term varies between $-\infty$ for $\gamma \rightarrow D - 1$ and -2 for $\gamma = 2D$ (we see this from the expressions for α, ϕ_0 in (3.5)). Thus the $1/z^2$ term dominates at large z for the allowed values of γ (from (2.6)) and approaches zero from above as $z \rightarrow \infty$; this means the potential approaches the constant V_∞ from above. This in turn means there is no room for bound states — the potential in the UV is positive and decaying and never falls below zero.⁵ Therefore, the geometry IbC is stable in the presence of the scalar. Numerical plot of the potential in figure 2 confirms the above discussion. In the panel (A) there is a potential well with bound states for all masses below some $m_c^2 \sim 6$ which is thus the critical value for the condensation. In panel (B) the well turns out too shallow to allow the formation of bound states: the geometry is stable. All curves are for $m_\chi^2 \geq -D^2/4$ as for this value there is a potential well near $z = 0$ and the outer AdS region becomes unstable.

In the numerical calculation, we shoot for the solution of a two-point boundary value problem which satisfies the boundary condition (2.18) for χ at the AdS boundary and the expected asymptotics for $\chi(z)$ from (3.5) in the interior. We do this as a part of the complete calculation (with backreaction on geometry, see the appendix). In this way we can find the dependence of the VEV $\langle O_\chi \rangle$ on the conformal dimension Δ_χ . In figure 3(A), the blue curve jumps at the transition, signifying that the transition is of first order. This is different from the infinite-order BKT-type (stretched-exponential) scaling laws found in [5, 8] for

⁵This picture changes for $\gamma > 2D$ — then the mass term dominates for $z \rightarrow \infty$ and for negative mass squared it forms a potential well. But in our model one always has $\gamma < 2D$ so we do not explore this case in detail.

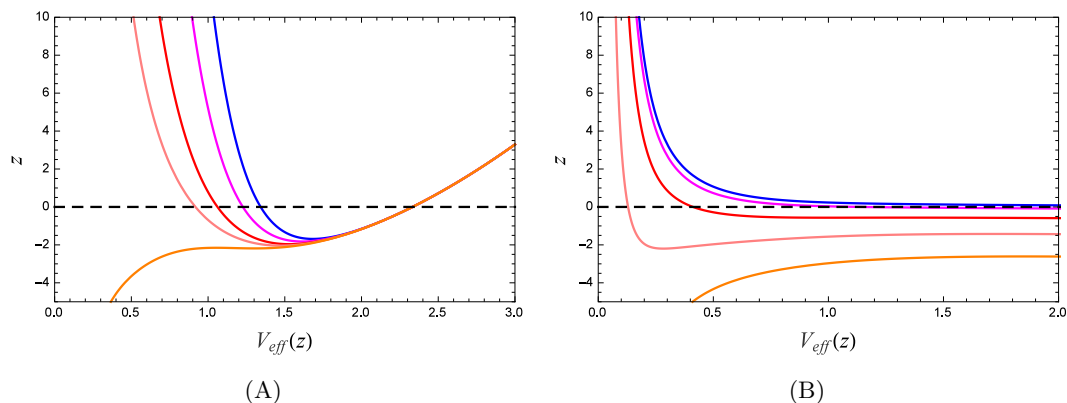


Figure 2. The effective Schrödinger potential $V_{\text{eff}}(z)$ defined by (4.3) for a range bulk masses (conformal dimensions) $m_\chi^2 = 6, 2, 0, -2, -4$ (blue, magenta, red, pink, orange) and $D = 4, \nu = 2, \gamma = 4$. The instability corresponds to bound states, i.e. existence of a sufficiently deep and broad potential well. In (A), we can fit a bound state for all masses shown, for the last one just a single bound state, thus $m_c^2 \sim 6$ corresponds to the BF bound. For such masses, the geometry will remorph and we will enter the condensed phase. This phase is stable, as in (B) the potential well is too shallow to accommodate a bound state. Notice that for $m_\chi^2 = -4$ the potential develops a well in the outer region, i.e. this is the BF bound for AdS_5 .

a neutral scalar in AdS-RN background because the BKT scaling originates in so-called Efimov states in the IR which depend on the details of the potential for the scalar [8] and would require a fine tuning of the dilaton potentials too. First-order transition is not unknown even for a charged scalar if it is non-minimally coupled to the metric [37, 38]. We also expect the condensate to vanish at higher temperatures, a case which we find too difficult for analytical work so we limit ourselves to numerics. The result is shown in figure 3: there is again a jump at the critical temperature.

4.1.2 The charged case

The charged problem can usually be understood as the textbook Abelian-Higgs instability where the gauge field develops an effective mass term $|\chi|^2 A_0$ and the mass of the scalar is effectively negative as it acquires a correction $-g^{00} A_0^2$, leading to instability and condensation. Without dilaton, in AdS-Reissner-Nordstrom background, this correction to the scalar mass grows fast enough near the horizon to produce an instability even at positive m_χ^2 [9]. For our system the equation for the charged scalar in IR geometry IaQ (eq. (3.7)) reads

$$\chi'' - \nu(\tau + 3 - \gamma - D)z^{\nu-1}\chi' - \frac{e^{(\tau-2D+2)z^\nu}}{\xi} \left(m_\chi^2 - \xi a_1^2 q^2 z^{2\nu-2} e^{(\gamma-\tau)z^\nu} \right) \chi = 0 \quad (4.7)$$

Now the negative correction to the effective mass of the scalar may grow or diminish as $z \rightarrow \infty$, depending essentially on the sign of $\gamma - \tau$. If $\gamma > \tau$ the correction dominates the bare mass term and we always have a mode growing at $z \rightarrow \infty$ but if $\gamma < \tau$ it is subleading and does not influence the behavior of $\chi(z \rightarrow \infty)$ at leading order. Looking

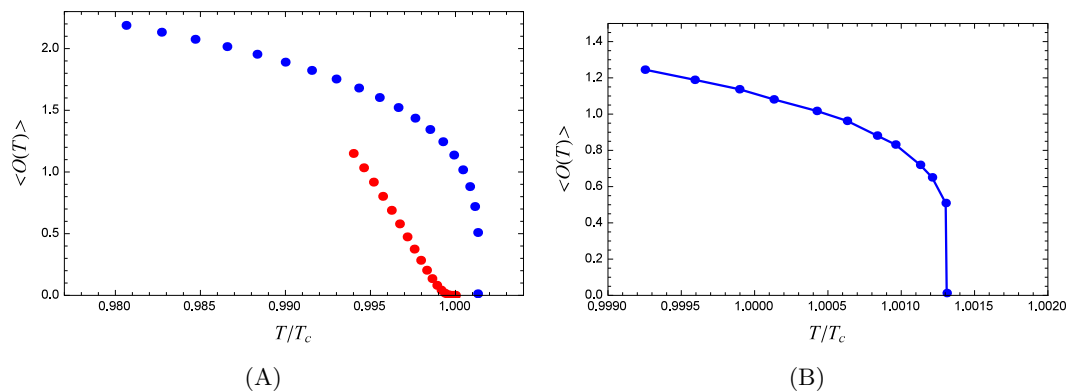


Figure 3. (A) Expectation value of the scalar $\langle O_\chi \rangle$ as a function of temperature for $m_\chi^2 = -2$, for the neutral scalar (blue) and the charged scalar with $q = 1$ (red), in $D = 4$ and for $\nu = 2, \gamma = 4$; for the charged scalar $\tau = 5$. The neutral scalar has a first-order quantum phase transition and its value jumps from zero, whereas in the charged case the quantum phase transition shows a continuous BKT-like exponential form $\exp\left(- (T_c - T)^{-1/2}\right)$. The unit of temperature is T_c — the critical temperature for the *charged* case. In (B) we zoom-in near the critical temperature for the neutral case to make it obvious that there is a jump.

at our conditions (2.5)–(2.6), we see this is always the case. Naively, one may guess that the critical value is $m_c^2 = 0$ but since our analysis ignores all subleading terms one should check numerically (numerics confirms that this is indeed the critical value, see the phase diagram in figure 7). Amusingly, the scaling with temperature and conformal dimension is now consistent with the BKT-like form:

$$\langle O_\chi \rangle = \text{const.} \times e^{-\frac{1}{\sqrt{-m_\chi^2}}}. \quad (4.8)$$

Although the numerical fit to the $e^{-1/(-m_\chi^2)^n}$ law with $n = 1/2$ is good, we cannot exclude the possibility that the exponent n weakly depends on ν and that it is not exactly $1/2$; we have no analytical estimate for n . The condensate formation is now, strictly speaking, not a consequence of the coupling with the gauge field at all (remember the term $q^2 g^{00} A_0^2$ is now exponentially suppressed) but merely the consequence of growing modes for negative scalar mass. Thus the mechanism is essentially the same as for the neutral scalar and the fact that the neutral scalar undergoes a discontinuous transition reminds us that the details of this process depend sensitively on the IR geometry. The temperature scaling is of the same form as the scaling with m_χ^2 (4.8) and is shown as red points in figure 3.

4.2 Free energies and phases at zero temperature

Now that we have explained the instability that seeds the condensation, we will compute the free energy (on-shell action) of the system as a function of Δ_χ and T , to study the order of the transition and the full phase diagram. We thus need to evaluate (2.1) on-shell for solutions Ia and IbC: $\mathcal{F} = \int d^D x L|_{Ia, IbC} + \mathcal{F}_{bnd}$. The boundary terms are given by

$$\mathcal{F}_{bnd} = \oint_{bnd} \sqrt{g_{\text{ind}}} \left(-2K - \lambda - \frac{1}{2} A_0 A_0' - \chi^2 - 2\Phi\Phi' \right), \quad (4.9)$$

Here, g_{ind} is the induced metric at the boundary, K is the trace of the extrinsic curvature, λ is the boundary cosmological constant, and the remaining terms come from the gauge field, the scalar and the dilaton. The counterterm for the scalar is in accordance with our choice that χ_+ is the VEV; had we chosen χ_- for the VEV the counterterm would be $-2\chi'\chi$, analogous to the situation for the dilaton. The comparison of free energies is best done numerically but even analytically we can draw some conclusions. Let us first consider the quantum phase transitions as a function of Δ_χ at fixed Φ_- and discuss the free energies at zero temperature.⁶ Our analytical solutions are only valid in the large z region, whereas for smaller z they cross over into the AdS_{D+1} forms, so the radial integral in (4.9) goes from some $z_1 \sim 1$. The difference between the energy of the solution Ia (we will show numerically it is indeed preferred to Ib) and IbC is

$$\mathcal{F}_{Ia} - \mathcal{F}_{IbC} \sim \chi_+^2 z^{2\Delta_\chi} + \int_{z_1}^{\infty} dz \left[(D^2 - D)z^{-(D-1)\alpha} + \chi_0^2 m_\chi^2 z^{-\gamma\phi_0} + \dots \right]. \quad (4.10)$$

The difference in free energies at leading order has terms proportional to the squared amplitude of the order parameter (in the UV — χ_- , i.e. $\langle O_\chi \rangle$ and in the IR — χ_0) but also a χ -independent term (coming from the Ricci scalar and cosmological constant terms in geometry IbC) so we expect that the transition, determined by $\mathcal{F}_{Ia} - \mathcal{F}_{IbC} = 0$ generically happens at nonzero amplitudes $\langle O_\chi \rangle, \chi_0$ and we can exclude a continuous transition. This is again in line with the discreteness of the symmetry broken and the discontinuous nature of the transition. On the other hand, for the charged geometries IaQ and IbQC there is also the boundary contribution $A_0(z \rightarrow 0)A'_0(z \rightarrow 0)$ so

$$\mathcal{F}_{IaQ} - \mathcal{F}_{IbQC} = \frac{\mu(\rho_{IaQ} - \rho_{IbQC})}{2} + \chi_+^2 z^{2\Delta_\chi} - \int_{z_1}^{\infty} dz z^{-(D-1)\alpha} \chi_0^2 (4 + 7\gamma)^2 + \dots \quad (4.11)$$

Now there is no χ -independent term and the dominant terms in the energy difference are proportional to the squared amplitude of the condensate, or to the difference in charge densities $\rho_{IaQ} - \rho_{IbQC}$ which, according to the Gauss-Ostrogradsky theorem, also has to be proportional to the bulk density of the charged field, $q^2 \chi(z)^2$. Therefore, one can expect that the energy difference grows from zero at $\langle O_\chi \rangle = 0$, as in a continuous phase transition. We have assumed that the chemical potential is kept constant across the transition (grand canonical ensemble). Now we will check our conclusions numerically.

First of all let us show that the confined solution is indeed the ground state in absence of the condensate. In figure 4(A) we plot the on-shell action of the solutions Ia (3.2) and Ib (3.3) and we see that Ia indeed always has lower energy — the system is confining. Now consider the free energies as functions of m_χ^2 and the temperature. In figure 4(B) we compare the free energies as functions of the conformal dimension for the neutral system and confirm the discontinuous nature of the transition: the curves have different derivatives at the transition point. Here we also scan for different values of the source Φ_- , which change the value of the transition point Δ_χ but, importantly, do not introduce new phases. This is easily understood from the discussion in section IV.A.1 and also from eq. (4.10). Dialing Φ_- influences the matching between the solutions in the UV and the solutions in IR without introducing new IR solutions, so we are still left with the choice between Ia

⁶At $T = 0$ the free energy is just the total energy \mathcal{E} of the system, since $\mathcal{F} = \mathcal{E} - TS$. For simplicity of notation, we will still call it \mathcal{F} just like the finite temperature case.

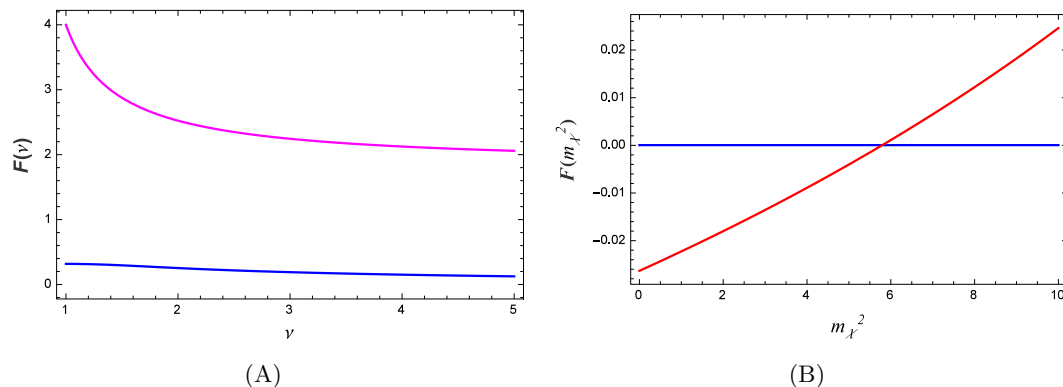


Figure 4. (A) Free energy at zero temperature as a function of the scaling exponent ν in the absence of condensate, for geometry Ia (confining, blue) and Ib (nonconfining, magenta). Obviously the soft-wall geometry always has lower free energy, thus it is always preferred: in absence of condensate we have a confining soft wall. The units on the vertical axis are arbitrary. (B) Free energy at zero temperature as a function of the bulk mass m_χ^2 for geometry Ia (confining, no condensate, blue) and for geometry IbC (nonconfining, with condensate, red). Both solutions exist before and after the critical point, where their energies $F(m_\chi^2)$ intersect at finite angle, thus the phase transition is of first order. The solid, dashed and dotted lines are from three different values of the source $\Phi_- = 0.1, 0.2, 0.5$ — the source shifts the location of the transition but does not change the behavior qualitatively. The free energy is in computational units and the parameters are $\nu = 3/2, \gamma = D = 4$.

and IbC. Concerning the scalar condensation, different values of Φ_- reshape the effective potential, influencing the point z_1 where the geometry crosses over to the IR asymptotics and thus the width of the potential well, so it starts supporting bound states for different values of m_χ^2 . Finally, the free energy difference depends on the IR quantities ϕ_0, χ_0 which are determined by the matching to the UV solution. Their values influence the location of the transition point but not the nature of the transition.

For the charged case the free energy is given in figure 5. The transition is now continuous and the zoom-in near the origin clarifies that the critical point lies at $m_\chi^2 = 0$. Interestingly, the three values of the O_Φ source now all give the same critical point, at zero mass squared. The curves for different values of O_Φ only differ in the deconfined phase, with nonzero $\langle O_\chi \rangle$, and coincide as long as no condensate forms. At first, this may sound strange. However, a look at the effective potential (4.7) shows that the negative term is now exponentially growing at large z and thus the potential well is always in the deep IR region, rather than in the middle as in the neutral case (figure 2). It is thus understandable that it is not affected by the matching to the UV solution with given Φ_- .

We have already established that our confinement/deconfinement transition may be of continuous or discontinuous nature. Both cases are in principle known even in field theory, and all the more so among the many condensed matter systems where some kind of fractionalization picture is appropriate.

4.3 Finite temperature thermodynamics

At finite temperature, the free energy is still the value of the on-shell action but the radial integration now terminates at finite z_h . In the leading term of the action in geometry Ia,

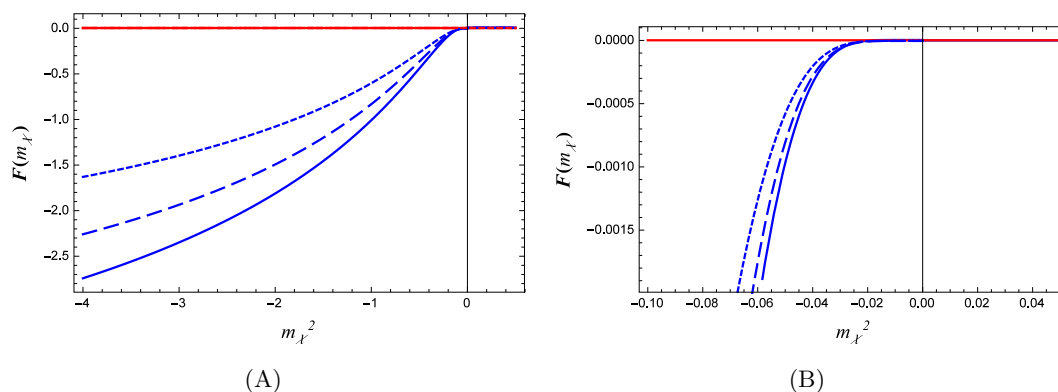


Figure 5. Same as in figure 4(B) but for the charged order parameter with $q = 1$ (A), with a zoom-in near $m_c^2 = 0$ (B). The new solution with condensate branches off smoothly and with continuous first derivative, thus the phase transition is continuous. It is consistent with BKT-like scaling $e^{-1/\sqrt{\Delta_c^2 - \Delta^2}}$. The three values of source (solid, dashed, dotted lines, same as in the previous figure) leave the critical point $m_c^2 = 0$ invariant and only influence the deconfined, condensed phase. The free energy is in arbitrary units and $\tau = 6$.

which stems from the dilaton potential:

$$\mathcal{F}_{Ia} \sim -V_0 \int_{z_1}^{z_h} dz \frac{e^{-(D-3)z^\nu}}{z^2} + \dots \quad (4.12)$$

we need to perform the radial integration from the crossover-to-AdS-scale z_1 to the horizon z_h and expand the result about z_h . Therefore, we integrate from “deep IR” at z_h to “the UV of the IR”, i.e. the location where the geometry crosses over to the asymptotic AdS_{D+1} . Clearly, the integral is dominated by the exponential term and our free energy scales as

$$\mathcal{F}(T \rightarrow 0) \propto \frac{1}{z_h^2} \Gamma_{2-1/\nu}((D-3)z_h^\nu) \sim \text{const.} \times e^{-\frac{D-2}{T^\nu} T^{3-\nu}} \quad (4.13)$$

where the power-law correction $T^{3-\nu}$ is in fact unimportant (we don’t consider $D < 3$ so the exponent $-(D-2)/T^\nu$ is always negative) and the free energy has an extremely slow growth at low T . Clearly, the entropy $S = \partial\mathcal{F}/\partial T$ is zero at zero temperature, and is extremely low at low T (much smaller than for any system with the scaling $\mathcal{F} \sim T^x$ for any power x). Thus the effective number of the degrees of freedom is much reduced because of the confinement. The same scaling is obtained for the charged case.⁷ At high temperatures (compared to the confinement gap) we can expand the action in $1/T$ and get

$$\mathcal{F}(1/T \rightarrow 0) \propto \frac{\Gamma(1-1/\nu)}{z_h^2} \sim \text{const.} \times T^2, \quad (4.14)$$

the quadratic behavior of the free energy and the linear behavior of entropy characteristic of Fermi liquids.⁸ This result was found for a dilatonic black hole in [18] and our system

⁷One may wonder whether this slow growth of entropy can actually be observed. It is possible that any amount of disorder in the system would make the entropy significantly larger. At least theoretically, however, an exponentially slow growth is not unusual in dilatonic setups, see e.g. [21].

⁸For high temperature we get $T \sim 4\pi D/z_h$ but this is not an exact relation and is not even close at low T (unlike the textbook Schwarzschild or RN black hole without the dilaton).

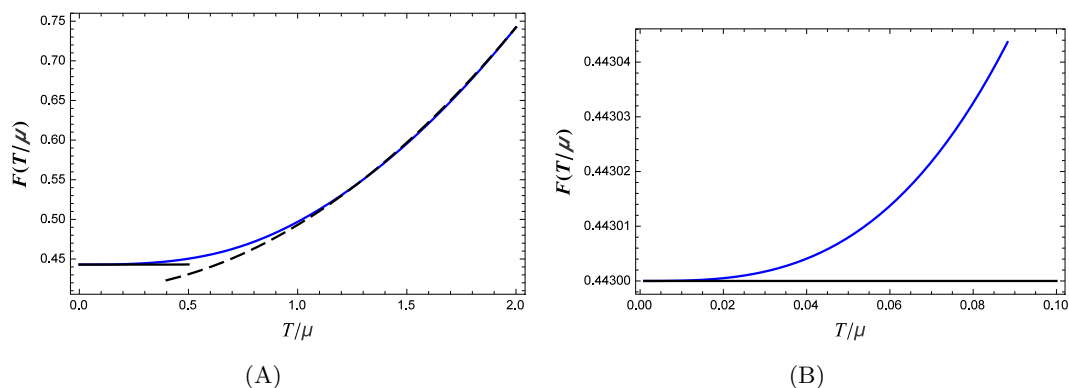


Figure 6. Temperature dependence of the free energy $\mathcal{F}(T)$ for the charged system in the confined phase ($m_\chi^2 = 4$), for $\mu = 1, \nu = 2, \gamma = 4, \tau = 6$. The dashed and the dotted black lines are the analytical estimates (4.13), (4.14) for the confined phase. In (A) we cover a broad range of temperatures, showing both the low-temperature regime with the scaling (4.13) and the high-temperature regime (4.14). In (B), we zoom in at low temperatures, showing the very slow growth of free energy and entropy. The analytical estimates for the low-temperature scalings are determined only up to the UV contribution, which was assumed approximately constant and was fit to the numerics.

behaves similarly at high temperatures (in fact, our confined charged system only differs from it by the choice of the dilaton potential, which likely influences the low-temperature behavior but not the high- T asymptotics). Even though we have no fermions in the system, the quadratic scaling is perhaps not so surprising: one may expect it in any confined system, where only the gauge-neutral bound states are observable. Notice, however, that at high temperatures we expect a dimensional scaling to take place

In the deconfined phase, the exponential scaling is gone and we have a simple scaling law for both low and high temperatures:

$$\mathcal{F}(T) \propto z_h^{-(D-1)\alpha} \sim \text{const.} \times T^x. \tag{4.15}$$

For high temperatures the exponent is $x = (D - 1)\alpha$; for low T the relation $T(z_h)$ is complicated but behaves as a power-law, so \mathcal{F} still scales as a power law of the temperature. This anomalous power law for all temperatures is precisely in line with the hyperscaling-violating nature of the system: the metric has power-law scaling and has no sharp scale where low- T regime cross over to high- T regime. These findings are illustrated in figure 6, where we plot the numerical calculation of $\mathcal{F}(T)$ together with analytical scaling laws for the confined system. We have chosen a large and positive scalar mass $m_\chi^2 = 4$ to avoid the phase transition to the condensed deconfined system, since the purpose of the figure is to study the different scaling regimes in the same phase, not the phase transition (which is discontinuous in T for the neutral system and of infinite order in T in the charged system, same as the scaling with m_χ^2). Notice that the analytical estimates (4.13)–(4.15) are only the IR contribution, and the true free energy is obtained by adding the UV contribution, which is fit as a constant in figure 6 (assuming that the T -dependence in the UV is weak, though in reality it is certainly not strictly constant).

4.4 Structure of the phase diagram

We are now in position to construct the whole phase diagram. The phases are the same both for the neutral and for the charged case, except that the critical line is of different nature (first-order and smooth, respectively). The phase diagram is sketched in figure 7. For small enough conformal dimension Δ_χ and temperature T , the scalar condenses and the system deconfines, restoring the scale invariance at low energies. As the temperature rises, the long-range order of the scalar is lost and we are back to the confined regime. This shows our main point — the confinement/deconfinement transition is triggered by the long-range order of O . What does this mean symmetry-wise? On one hand, the condensation of O certainly breaks a symmetry — \mathbb{Z}_2 (neutral) or $U(1)$ (charged). But on the other hand the deconfinement restores a symmetry: as we have explained, the deconfined geometries are anisotropically scale-covariant (hyperscaling), of the form $ds^2 = z^{-2\kappa}(-f_0 z^{-\eta} dt^2 + d\mathbf{x}^2 + f_0^{-1} z^\eta dz^2)$. In absence of charge ($f_0 = 1, \eta = 0$), all coordinates in field theory can be rescaled as $x^\mu \mapsto \lambda x^\mu$ though the energy (dual to z) scales differently (this is sometimes called generalized conformal symmetry, [25]). With nontrivial f the scaling exponent is different along different axes but there is still some invariance to dilatations (rescaling of coordinates). At the same time, in the soft-wall case with $ds^2 \propto e^{-2z^\nu}$ there is no scale invariance at all. Overall, neither phase is more symmetric than the other: denoting the symmetry group of the scaling system in field theory by \mathbb{G}_1 , we expect it to be broken in the confined phase down to some subgroup $\mathbb{G}_2 < \mathbb{G}_1$, while the symmetry of the scalar (\mathbb{Z}_2 or $U(1)$) is fully broken in the deconfined phase. Since we have a bottom-up model we don't have the explicit form of the field theory Lagrangian and so we cannot fully determine $\mathbb{G}_{1,2}$. Both certainly include the spacetime translations and rotations and \mathbb{G}_1 , as discussed, contains also dilatations. In special cases, e.g. when the field theory is $\mathcal{N} = 4$ super-Yang-Mills, it will be the full conformal group and the deconfinement will be the restoration of the full conformal symmetry. In any case, the symmetry at the critical point changes like

$$\mathbb{G}_2 \otimes \mathbb{Z}_2 \mapsto \mathbb{G}_1 \otimes \mathbb{I}, \quad \mathbb{G}_2 \otimes U(1) \mapsto \mathbb{G}_1 \otimes \mathbb{I}. \quad (4.16)$$

The neutral case where the phase transition is discontinuous could be related to the Landau-Ginzburg theory which generically predicts that in such situations, when no overall symmetry reduction occurs, the two phases can be separated by a first-order transition or by a finite area of phase coexistence. But the charged case where the transition is continuous is of non-Landau-Ginzburg type. This case in particular resembles the concept of deconfined criticality proposed as an explanation for the physics of some strongly coupled quantum critical points in $D = 3$ [10, 11]. We would like to understand how one could probe such phase diagrams in nature, having in mind the handicap that in a bottom-up gauge/gravity model we do not know the explicit form of the action to directly inspect the symmetries of different phases. We would also like to gain a better knowledge of the confinement/deconfinement transition itself: we cannot directly identify the gauge-charged and gauge-neutral degrees of freedom but we can detect the existence of bound states in the confined phase and explore their dispersion relation, a technique particularly used in AdS/QCD, where the quark confinement is recognized from the linear scaling of bound

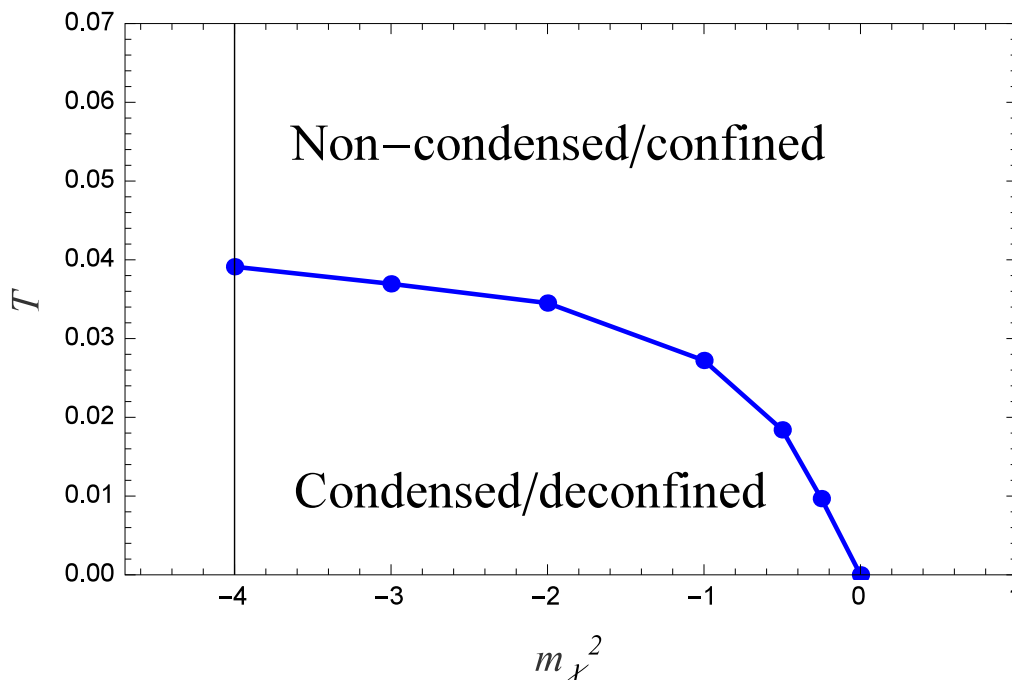


Figure 7. Phase diagram in the Δ_χ - T plane for the charged scalar. Blue dots denote the numerical results for the onset of the condensation of the scalar; the line is just to guide the eye. The condensed/deconfined phase (geometry IaQ) is located to the left and below the boundary line; the rest is the non-condensed/deconfined phase (geometry IbQC). For the neutral case the phase diagram is similar. The key finding is that the deconfinement transition coincides with the onset of the long-range order. The vertical black line denotes the BF bound for AdS_5 .

state masses, $m_n \propto n$ [22, 32–34]. We can also look for the signs of symmetry breaking in the response functions. Bound states can be detected in this way too, since they manifest as poles of correlation functions in the imaginary half-plane, separated from the possible quasiparticle peak by a gap (the binding energy).

Finally, one should have in mind that at very high temperatures it is possible that both confined and deconfined solutions (i.e., all the solutions we have considered) give way to the solution with zero dilaton profile, i.e. the system becomes just a (neutral, Schwarzschild or charged, Reissner-Nordstrom) black hole, as pointed out in [39, 40]. This depends on the parameters of the dilaton potentials; for some values such solutions exist and for some not. We have not checked the existence of this regime explicitly and will not consider it; it is not relevant for the low-temperature and zero-temperature phase transitions we consider here.

5 Response functions and bound states

5.1 Definition and equations of motion

In this section we will try to understand better the nature of different phases by computing the electric AC conductivity $\sigma(\omega, k = 0)$ and charge susceptibility $\xi(\omega, k)$ of our system as well as the retarded propagator $G_R(\omega, k)$ of the order parameter O_χ , in particular by

looking at the bottom half of the complex frequency plane where one can find the poles corresponding to the bound states typical of confined systems. In this section we consider the $T = 0$ case as we are interesting in the properties of the ground state (and its excitations encoded in the pole structure), not the finite-temperature fluctuations. According to the basic dictionary (e.g. [4]) the conductivity, as the response of the current to the imposed (transverse) electric field, is proportional to the ratio of the source and VEV terms of the fluctuation of the spatial component of the bulk electromagnetic field:

$$\delta A_x(z; \omega, k) = \delta A_x^{(0)} + \delta A_x^{(1)} z + \dots, \quad \sigma(\omega, k) = \frac{1}{i\omega} \frac{\delta A_x^{(1)}}{\delta A_x^{(0)}} + \frac{1}{i\omega} R(\omega, k), \quad (5.1)$$

where $R(\omega, k)$ is the regulator connected to the boundary counterterms in the action. Without entering into detailed discussion, we can quote that in $D = 3$ no regulator is needed ($R = 1$) whereas in $D = 4$ we have $R = k^2 - \omega^2$ [9]. Charge susceptibility is the response of the charge density to the applied electric field, and therefore can be computed analogously from the fluctuation of A_0 :

$$\delta A_0(z; \omega, k) = \delta A_0^{(0)} + \delta A_0^{(1)} z + \dots, \quad \xi(\omega, k) = \frac{\delta A_0^{(1)}}{\delta A_0^{(0)}} = \frac{\delta \rho}{\delta \mu}, \quad (5.2)$$

so the susceptibility can be interpreted as the ratio of the charge density fluctuation and the fluctuation in chemical potential. The conductivity mainly makes sense at zero momentum (in the absence of a lattice) whereas susceptibility can also be considered as a function of momentum, to study the spatial modulation of the charge density, as in [42]. The equations of motion are really the variational equations from the action (2.1)–(2.4) about the equilibrium solutions $A_0(z; \omega, k)$ and $A_x(z; \omega, k) = 0$:

$$\delta A_x'' - \left((D-3)A' - \frac{\partial_\Phi \mathcal{T}}{\mathcal{T}} \Phi' \right) \delta A_x' - \left(\frac{\omega^2}{f^2} - \frac{k^2}{f} - \frac{2q^2 e^{-3A}}{f\mathcal{T}} \chi^2 \right) \delta A_x = 0 \quad (5.3)$$

$$\delta A_0'' - \left((D-3)A' - \frac{\partial_\Phi \mathcal{T}}{\mathcal{T}} \Phi' \right) \delta A_0' - \left(\frac{\omega^2}{f^2} - \frac{k^2}{f} - \frac{4q^2 e^{-3A}}{f\mathcal{T}} A_0 \chi^2 \right) \delta A_0 = 0. \quad (5.4)$$

Even though the fluctuations $\delta A_0, \delta A_x$ are coupled to the fluctuations of the metric, we do not consider the full system of fluctuation equations here. For a charged system, this amounts to working in the limit of large charge, where the probe barely has any influence on the system.

Finally, to study the symmetry breaking we explore also the fluctuation of the scalar field $\delta\chi$ which determines the retarded propagator $G_R(\omega, k)$ of the field O in field theory. According to the dictionary, the retarded propagator is again the ratio of the leading boundary components, χ_-/χ_+ , of the fluctuation $\Delta\chi(z; \omega, k)$ which satisfies exactly the same Klein-Gordon equation (2.12) as the equilibrium solution, only at finite energy and momentum:

$$\delta\chi'' + \left(\frac{f'}{f} - (D-1)A' - \frac{\partial_\Phi Z}{Z} \Phi' \right) \delta\chi' - \left(\frac{\omega^2}{f^2} - \frac{k^2}{f} + \frac{e^{-2A}}{f} m_\chi^2 - \frac{q^2}{f^2} e^{\tau\Phi} A_0^2 \right) \delta\chi = 0. \quad (5.5)$$

Unlike the BF bound calculation, we are not exclusively interested in the case when the energy ω is pure imaginary but will consider general values of energy (with non-positive imaginary part, since the poles in the upper half-plane are forbidden).

5.2 Effective Schrödinger equation for the response functions

It is well-known (e.g. [43, 44]) that the IR behavior of the effective Schrödinger problem for various quantities like (5.3), (5.4)(5.5) is related to the energy scaling of the corresponding response functions in field theory, defined as the ratio of the leading and subleading component of the bulk field in the boundary. The aforementioned references study the case when the equation can be written in the form $A_x'' - V(z)A_x = -\omega^2 A_x$ (and similarly for any other field instead of A_x) with $V(z) \sim 1/z^2$ in the IR. The inverse-square potential is famous for allowing a conformal-invariant solution, and simple scaling arguments together with flux conservation lead to the conclusion that the z -scaling of the solutions to the Schrödinger equation in IR determines the ω -scaling of the response function (essentially, the solution is a function of ωz only, and since the flux must be conserved (z -independent) it is also ω -independent, which relates the scaling with z to the scaling with ω). In our problem, even in the deconfined case with no soft wall, the behavior of the potential is in general different from $1/z^2$, and no quantitative results on the frequency scaling can be drawn. We can, however, decide if the spectrum is gapped or continuous, and if the gaps are “hard” (zero spectral weight of the response function) or “soft” (exponentially suppressed nonzero weight).

As the charge susceptibility in dilaton systems was never studied so far, we give a more detailed analysis of the effective potential. The equation (5.4) can be recast as a Schrödinger problem with an effective potential

$$V_{\text{eff}}(z; \omega, k) = -\frac{\omega^2}{f^2} + \frac{k^2}{f} + \frac{e^{-2A}}{f} m_\chi^2 + \frac{X''}{X} + B \frac{X'}{X} \quad (5.6)$$

with $B = (D-3)A' - \tau\Phi'$ and $X = e^{-\int B/2} = e^{(D-1)/2A - \gamma\Phi/\sqrt{f}}$. Starting from the confined phase (in the charge-neutral case), we see that the potential for the confining geometry behaves in the IR as

$$V_{\text{eff}}(z \rightarrow \infty; \omega, k) = -\omega^2 + k^2 - \frac{\nu(\nu-1)(\tau-D+3)}{2} z^{\nu-2} + \frac{3}{4} \nu^2 (\tau-D+3)^2 z^{2\nu-2} + \dots, \quad (5.7)$$

thus it grows to infinity in the IR (the subleading terms were left out). For finite z (still far enough from the AdS boundary), it is positive if $\omega^2 < \omega_0^2 + k^2$ for some constant ω_0 , i.e. the spectrum is discrete and gapped for small energies. In the bulk, a gap in the spectrum simply means that there is no tunneling of the infalling solution toward the far IR at $z \rightarrow \infty$ (in the terminology of [43], the reflection coefficient is zero). This means that the integral $\int dz \sqrt{2V_{\text{eff}}(z)}/z^2$ has to diverge at large z . For (5.7) the integral behaves as $\int dz z^{\nu-3}$ and thus diverges for $\nu \geq 2$. Therefore, the gaps might be hard or soft depending on the parameters.

For $\omega > \sqrt{\omega_0^2 + k^2}$ we expect a continuum, as the effective potential does not have a well anymore. In the deconfined neutral background, the potential looks like

$$V_{\text{eff}}(z \rightarrow \infty; \omega, k) = -\frac{(D-3)\alpha - \phi_0\tau}{2z} - \omega^2 + k^2 + \frac{3}{4z} ((D-3)\alpha - \phi_0\tau)^2 (\log z)^2 + \dots, \quad (5.8)$$

which grows to infinity in the IR but logarithmically slowly, whereas on the other side it again depends on $\omega - \sqrt{\omega_0^2 + k^2}$. The spectrum is thus still gapped and discrete but (since

the well is now shallow, because of the logarithmic growth) the bound states are expected to come closer to each other. Also, the tunneling probability behaves as $\int dz \log z/z^2$ which is finite for $z \rightarrow \infty$, and the gaps is always soft. In the charged case, the effective potential is augmented by a positive term proportional to $q^2 A_0 \chi^2$ which is independent of ω, k . Therefore, the threshold ω_0 is increased but the qualitative behavior remains the same. Similar conclusions hold for the other response functions: the gaps are always soft for the deconfined phase, and may be hard or soft for the confined phase.

5.3 Numerics

5.3.1 AC conductivity

The AC conductivity best encapsulates the breaking of a continuous symmetry (4.16) through the existence of the zero mode. The AC conductivity on the real frequency axis, as well as in the bottom half-plane of complex ω , is given in figure 8. In this plot we show the conductivity $\Re\sigma(\omega, k = 0)$ as a function of the real frequency $\Re\omega$ for a range of $\Im\omega$ values (at zero momentum). We first show the set of curves $\Re\sigma(\Re\omega)$ computed at different $\Im\omega$ values, where the curves at different $\Im\omega$ values are vertically shifted in the figure to be visible together (panels A, B); the x -axis is the real frequency axis and the y -axis is the magnitude of the conductivity minus the vertical shift. In parallel we show the same data as two-dimensional color maps $\Re\sigma(\Re\omega, \Im\omega)$ (panels C, D); now the y -axis is the imaginary part of the frequency, and the lighter areas denote higher values. We use the same recipe to show the curves $\Im G_R(\omega, k)$ and $\xi(\omega, k)$ in later figures.

In the charged confined non-condensed system (panels A, C), there is no gap at small frequencies as the continuous U(1) symmetry is preserved. On the other hand, confinement means the existence of stable bound states ("glueballs"), i.e. poles on the real axis. These are seen as sharp peaks in $\Re\sigma(\omega)$ for real ω . For nonzero $\Im\omega$ the poles apparently turn into branch cuts (the vertical lines); the resolution of our numerics is limited so we are not sure if these are branch cuts or strings of poles along the vertical ($\Im\omega$) axis. Such poles on the real axis have been seen also in [9] in the simple holographic superconductor (without dilaton) when the scalar mass is exactly at the BF bound for AdS_{D+1} ; the relation to our result is not clear but this fact is certainly interesting and we plan to look more carefully into it. Naively, it looks like a bad metal: the AC conductivity is continuous and gapless but small except on a discrete set of real frequencies where the bound states lie.

After deconfinement and the onset of superconductivity (figure 8B, D), the Dirac delta peak at $\omega = 0$ is followed by a gap, which shows the breaking of the U(1) symmetry (this is particularly obvious in the panel B). The bound states do not sit at the real axis anymore. It is again not clear from the numerics if they turn into branch cuts or strings of poles in the complex plane but in any case they do not reach the real axis anymore. In this and further spectral plots, we use the critical temperature as a suitable unit of energy to express the frequencies and momenta; a more usual choice would be the chemical potential, but it is absent in the neutral case, so we have opted for T_c as a natural and physical scale.

Therefore, we witness both the breaking of the U(1) symmetry (Dirac delta peak followed by the gap) and the deconfinement (absence of stable bound states), but not the restoration of scale invariance since our probe is charged and sees the nonzero chemical

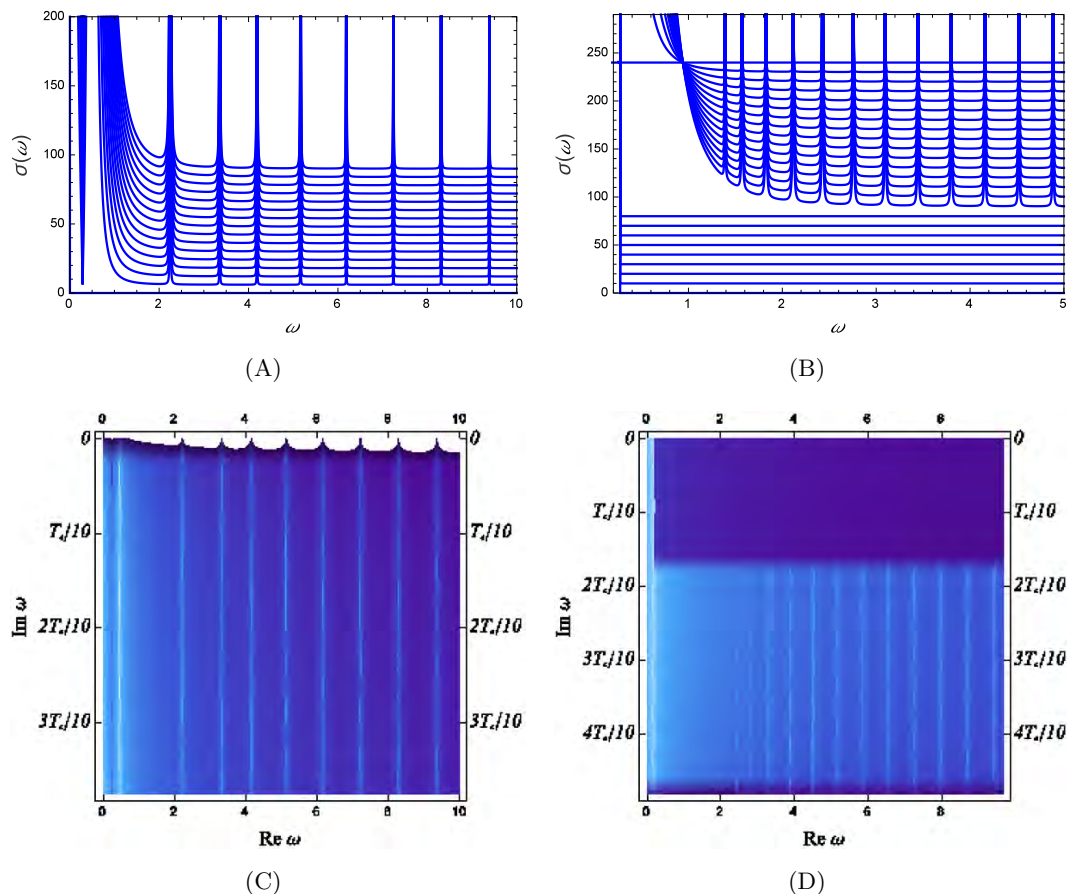


Figure 8. Conductivity $\Re\sigma(\omega)$ in the confined/non-condensed phase ($m_\chi^2 = 2$, A,C) and in the deconfined/condensed phase ($m_\chi^2 = -2$, B,D) in a U(1)-charged system at $\mu = 1$, for a range of $\Im\omega$ values starting from zero (the real axis). In the deconfined/superconducting phase there is only the $\omega = 0$ pole at the real axis (visible for the first curve in the panel B; in the color map panel D it is hard to recognize since it is very narrow), followed by a gap. The gap is expectedly absent in the confined/non-superconducting phase, as the continuous U(1) symmetry is preserved. On the other hand, the confinement/deconfinement transition is visible through the stability of bound states: in the confined regime these states have an infinite lifetime at $T = 0$ and thus manifest as sharp peaks (poles) on the real axis (the bright white spots on the real axis in the density plot). In the deconfined regime these states are pushed to a finite distance below the real axis and look more like branch cuts. For all calculations in a charged system in this section we use $D = 4, \nu = 3/2, \gamma = 4, \tau = 6, \mu = 1$ and $m_\chi^2 = 1/4$ for the confined case and $m_\chi^2 = -1/4$ for the deconfined case.

potential which sets a scale. It is instructive to compare this situation to the charge-neutral case in figure 9. The superconducting gap now has to vanish from the spectrum. Only the presence or absence of confinement is now seen — bound states as poles on the real axis (again apparently continuing as branch cuts below the real axis) in the confined regime and their absence in the deconfined regime. Notice that our confined phase is fractionalized and the deconfined phase is coherent — therefore, our poles are *not* “mesinos”, they are closer to “glueballs”, i.e. complex bound states which contain charged gauge bosons.

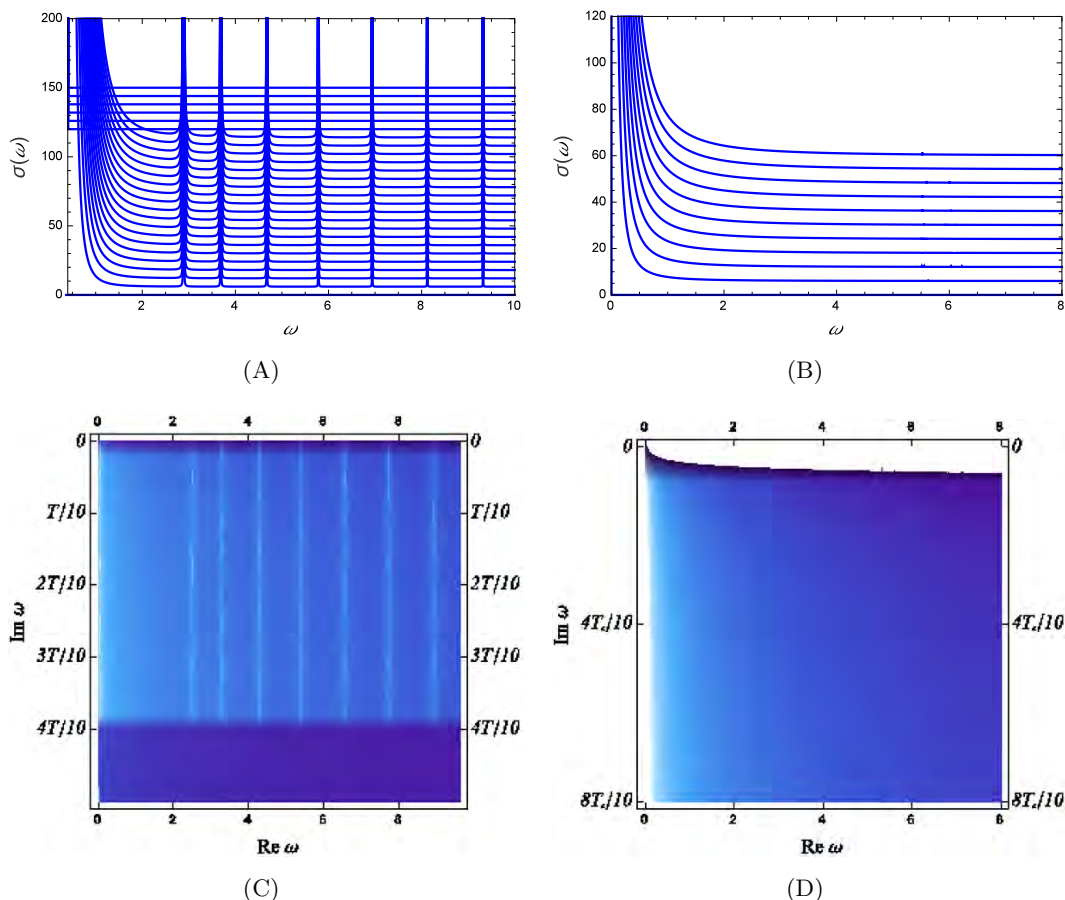


Figure 9. Conductivity $\Re\sigma(\omega)$ in the confined/non-condensed phase ($m_\chi^2 = 8$, A,C) and in the deconfined/condensed phase ($m_\chi^2 = 4$, B,D) in a neutral system, for a range of $\Im\omega$ values starting from zero (the real axis). Neither phase is superconducting thus neither phase has a gap but rather a continuous background behaving as $1/\omega^n$. But the confined case again has long-living bound states corresponding to poles on the real axis, while upon deconfinement these poles vanish completely. The parameters are $D = 4, \nu = 3/2, \gamma = 4$ and $m_\chi^2 = 4$ for the deconfined case and $m_\chi^2 = 8$ for the confined case (also in the remaining plots for the neutral system in this section).

5.3.2 Retarded propagator

A probe which specifically shows the restoration of scale invariance is the retarded propagator $G_R(\omega, k)$, given in figure 10. In the confined regime we see well-defined quasiparticles, due to nonzero chemical potential. But since quasiparticles exist at finite binding energies, the spectrum is gapped and starts from nonzero energy (A, C). Once the system is deconfined, scale invariance is restored and $G_R(\omega) \sim 1/\omega^n$ (B, D). Unlike conductivity, which is not sensitive confinement/deconfinement, the scalar probe differentiates between them: in their absence, it shows no quasiparticles. Another way to understand it is that at low energies (in deep interior) the local chemical potential behaves as $e^{-A}A_0/\sqrt{f} \sim z^{-2\alpha+\phi_0\tau/2}$ while the scale of the metric (the confinement scale) drops faster as $z^{-2\alpha}$, so the confinement scale is above the chemical potential and the probe sees no chemical potential at all.

When the system is neutral and the symmetry to be broken is discrete, we expect to see the presence/absence of scale invariance in much the same way as before but we expect no quasiparticle in either phase, since the chemical potential is zero. The plot for the neutral case is shown in figure 11: now there is indeed no quasiparticle in either phase as the chemical potential and density are zero. But we still detect a scaleful, though continuous spectrum in the confined case, whereas the deconfined case looks pretty much the same as with a charged boson — just a power-law decay. Again, this is *not* about fractionalization — the confined phase, with quasiparticles in figure 10(A,C), has “gauginos” which the gauge-neutral probe cannot see, and the deconfined phase, with no quasiparticles in figure 10(B,D), has “mesinos” which the gauge probe can see. The bottom line is that the probe apparently couples mainly to the gauge field bound states, and in general that the presence/absence of quasiparticles may not be directly related to fractionalization.

5.3.3 Charge susceptibility

Charge susceptibility is interesting as it shows the absence of metallic behavior in both the confined and deconfined phase. Both phases show a gap followed by a series of dispersing poles. This is in line with our analytical finding that both backgrounds give a potential well for δA_0 , inhabited with bound states. But since the well is rising towards infinity very slowly in the deconfined phase, the spacing between the bound states is small in this case. In [42] the authors have explored mainly the momentum dependence of the susceptibility at zero frequency, finding the Friedel oscillations and the singularity at $k = 2k_F$, as expected for a system with zero modes at *finite* momentum, resembling a Fermi surface. In figure 12, in particular in the $\omega - k$ maps (panels B,D) we see that no oscillatory behavior exists for $\chi(\omega = 0, k)$ (the bottom edge of figure 12 C,D) and in particular no pole at $\omega = 0$ exists for any finite k . This tells that our system is different from a normal metal even in the confined phase, and this is not because it is fractionalized (since the RN black hole studied in [42] is also fractionalized).

6 Conclusions and discussion

We have considered an Einstein-(Maxwell)-dilaton-scalar system where the scalar can condense (acquire a VEV) and thus break a symmetry, discrete if neutral or continuous if charged. This in turn remorphs the geometry from a soft-wall, confining form to a deconfined, power-law-scaling form. This goes against the common intuition that a condensate always “narrows” the geometry, which indeed happens in absence of a dilaton with a suitably chosen coupling, e.g. in the textbook holographic superconductor where an AdS-RN background with a near-horizon AdS₂ throat with finite AdS radius typically turns into a Lifshitz-type geometry whose scale shrinks to zero in the interior. From a general viewpoint, it is not so surprising that the huge “zoo” of dilatonic theories contains counterexamples to this behavior, as we have great freedom in choosing the dilaton potentials. But from the viewpoint of field theory and applied gauge/gravity duality, this is interesting as it tells us that we can consider situations in which breaking a symmetry with an order parameter

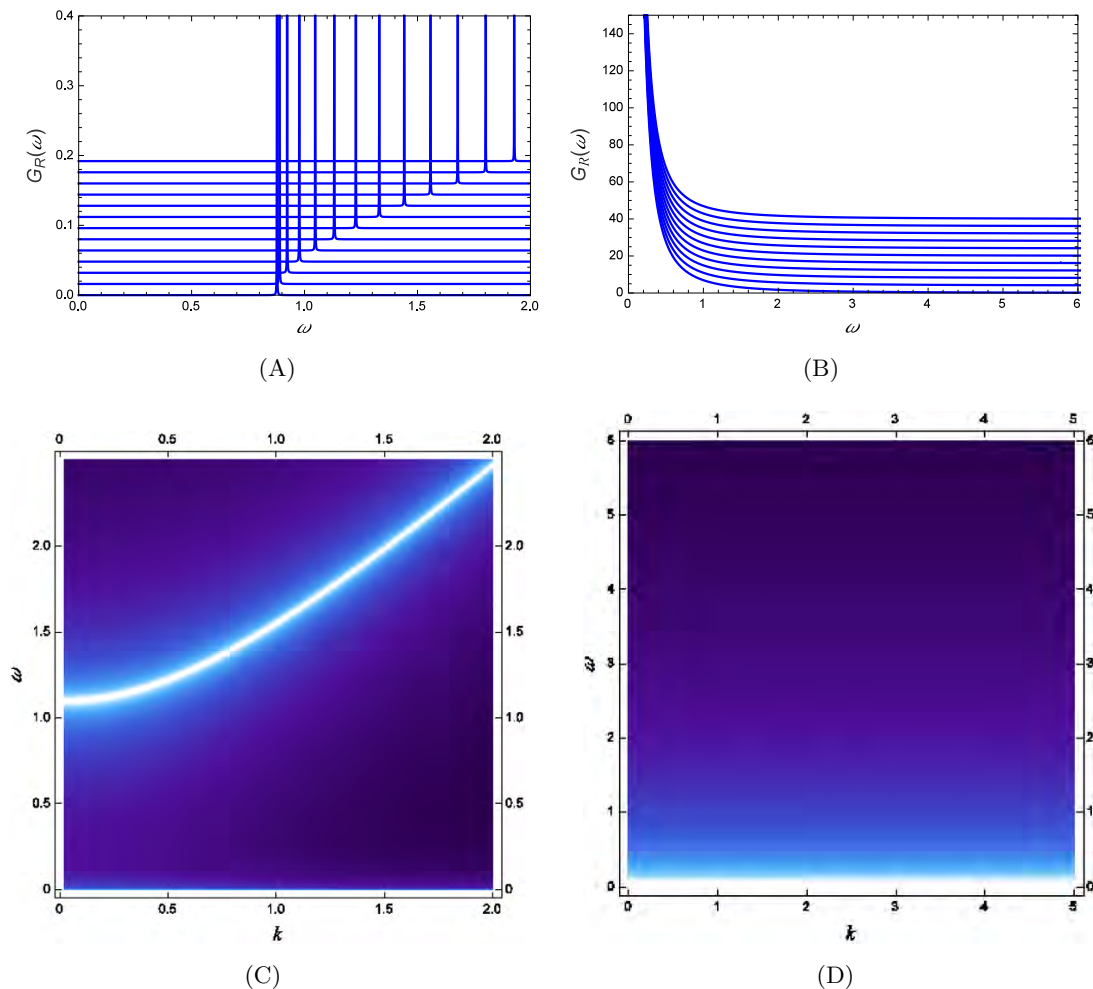


Figure 10. The retarded propagator $\Im G_R(\omega)$ for a range of momentum values ($0 < k < 1.5$) in a charged system ($\mu = 1$), in the confined regime ($m_\chi^2 = -2$, A,C) and in the deconfined regime ($m_\chi^2 = 2$, B,D). In the confined case we see gapped quasiparticle excitations, starting at $\omega \approx 1 > 0$ since we see the bound states in the soft wall which have a discrete and gapped spectrum. In field theory, it means we see gauge-neutral particles. In the deconfined regime, no quasiparticle is present and we have a featureless power-law spectrum $\Im G_R(\omega) \propto 1/\omega^n$. From the gravity viewpoint, it is because the potential has no bound states. From the field theory viewpoint, it means we have gauge-colored excitations which are not visible through a gauge-neutral probe. We thus see the deconfinement transition.

can actually restore another symmetry, since confined systems have a scale (the confinement gap) which vanishes upon condensation. In the simplest case, we can thus expect that conformal symmetry is restored. In practice, it is not the full conformal symmetry but some subset of it, i.e. some scale invariance. We therefore see a non-Ginzburg-Landau phase transition, where neither phase has a higher overall symmetry than the other and the transition can be continuous (in the charged case). This may be related to the picture of deconfined criticality proposed in [10, 11]. But one should be careful, since the transition mechanism in [10, 11] is related to the existence of a new, topological conserved quantity

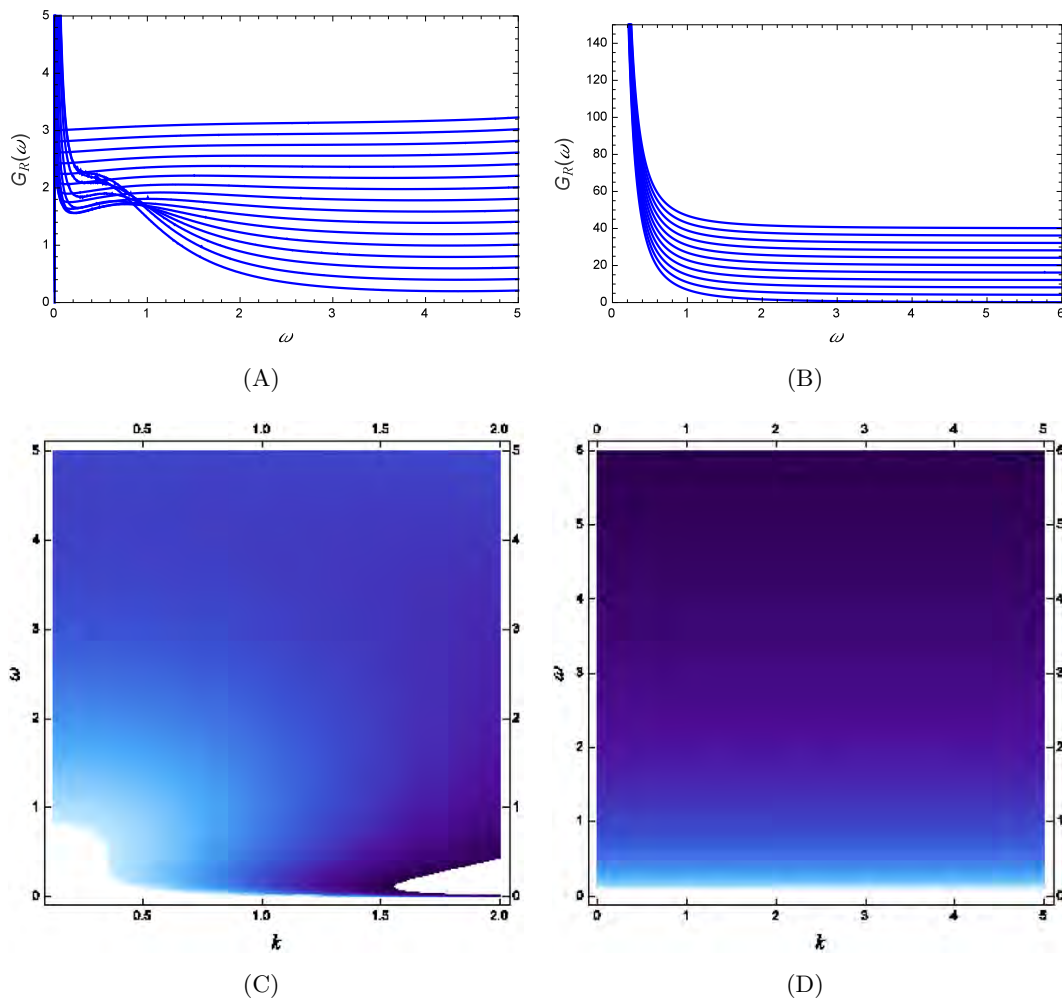


Figure 11. The retarded propagator $\Im G_R(\omega)$ in the confined/non-condensed phase (A,C) and in the deconfined/condensed phase (B,D) in a neutral system. While the deconfined case is again an almost exact power law, the confined case has a scale but no quasiparticle. The discrete Z_2 symmetry has no zero modes upon breaking. The retarded propagator is thus not so useful when the system is neutral.

which only exists at the critical point. In our setup we cannot study geometry or lattice effects and definitely cannot argue anything about topology. The connection is thus very loose and we only see it as inspiration for further work. It would be interesting to consider a setup where the topologically protected gauge flux analogous to that at a deconfined critical point can be detected.

It would also be nice to understand our system better from the gravity side, by deriving our solutions from a superpotential and inspecting how generic this behavior is, which we address in a subsequent publication. It is also interesting to apply our findings to real-world systems. While in QCD there is no obvious additional order parameter that may condense, such situations are abundant in condensed matter systems, mainly in the context of the fractionalization paradigm, where certain non-Fermi-liquid phases are argued to consist

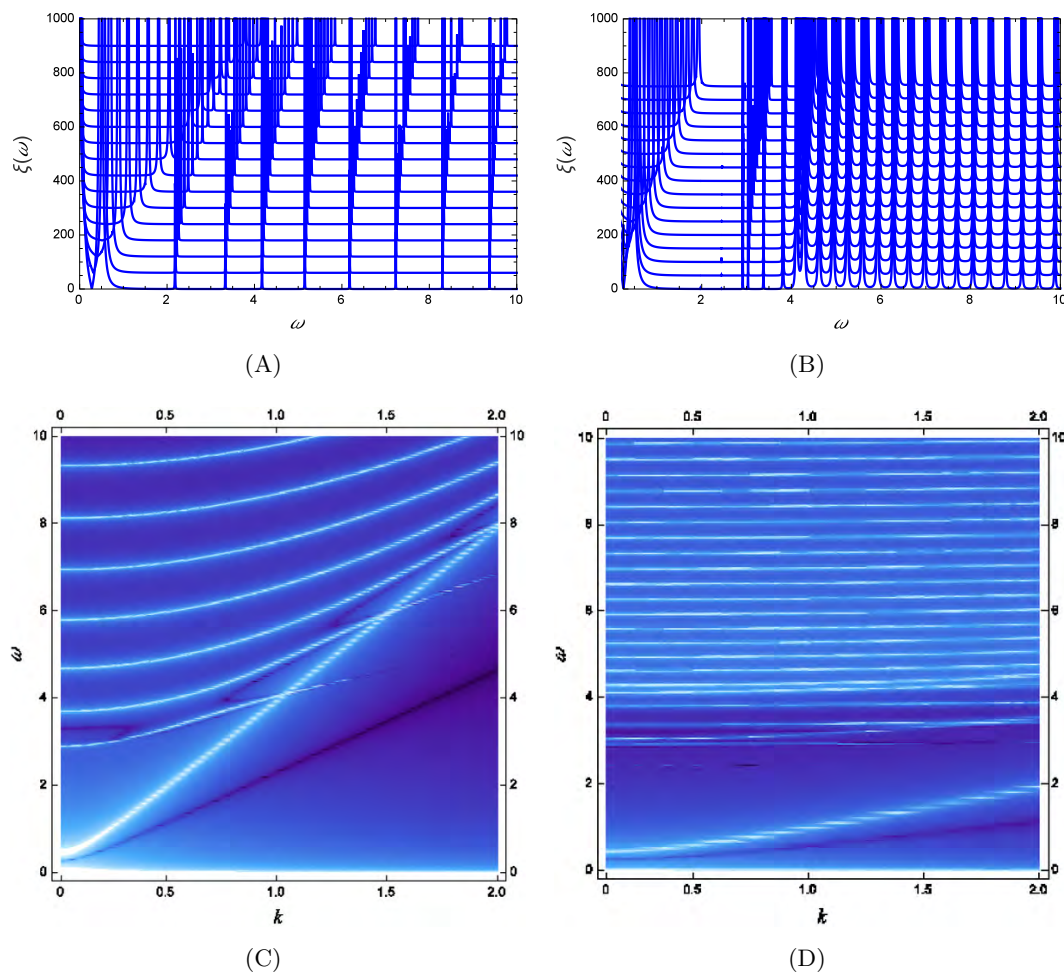


Figure 12. Charge susceptibility $\xi(\omega)$ in the confined/non-condensed phase (A,C) and in the deconfined/condensed phase (B,D) in a charged system. Both cases show bound states; this might look surprising for the deconfined case but is in accordance with the effective potentials in eqs. (5.7)–(5.8). This probe is thus not very useful for detecting the transition but shows the absence of peaks at $\omega = 0$ and $k = 2k_F > 0$, indicating that even the confined phase is different from a normal Fermi liquid.

of gauge-charged excitations which are therefore not observable as quasiparticles. This is also relevant for the heavy fermion systems, where a long-range order is present (the antiferromagnetic ordering, the SO(3) equivalent of our scalar neutral order parameter) and is connected to the disappearance of a normal Fermi liquid, which can be related to the deconfinement of the gauge-charged spinons and holons (in this case, of course, the gauge field is emergent and not microscopic) [12–15]. However, great care must be taken to interpret the fractionalization concept properly, as it is distinct from confinement — in our case, the confined phase is fractionalized and the deconfined phase is coherent. This will also be addressed in our future work.

Acknowledgments

We are grateful to A. Rosch for helpful discussions and careful reading of the manuscript as well as to M. V. Medvedyeva, K. E. Schalm and J. Zaanen for helpful discussions and support.

A A short summary of numerical calculations

For numerical work we find it more convenient to introduce a different coordinate choice where the metric reads

$$ds^2 = -\frac{f(z)h(z)dt^2}{z^2} + \frac{dx^2}{z^2} + \frac{dz^2}{f(z)z^2}. \quad (\text{A.1})$$

The boundary is again at $z = 0$ and the space extends to $z \rightarrow \infty$. It is easy to derive the relations between this parametrization and the one used in the main text. Now the boundary conditions for small z are $f(z \rightarrow 0), h(z \rightarrow 0) \rightarrow 1$. The Einstein equations read

$$zf' - Df + D + \frac{2}{D-1}T^{00} = 0 \quad (\text{A.2})$$

$$\frac{h'}{h}zf = \frac{2}{D-2}(T^{00} - T^{zz}). \quad (\text{A.3})$$

Therefore, both metric functions have first-order equations and we can only impose two boundary conditions for the metric. However, we have more than two physical requirements. The physical requirement for h (which is proportional to the scale factor e^{-2A} in the metric (2.8)) is $h(z \rightarrow \infty) \rightarrow 0$ and for f the first derivative should vanish: $f'(z \rightarrow \infty) \rightarrow 0$. In addition, in order to have an asymptotically AdS geometry we need $f(z \rightarrow 0) = 1$ and $h(z \rightarrow 0) = 1$. We implement this by introducing some cutoff z_Λ and imposing the analytical solutions we have found for the metric in section III for all $z < z_\Lambda$ (the analytical solutions of course automatically satisfy the necessary requirements in the interior). Then we start the integrator at z_Λ , using the condition $f(z = 0) = h(z = 0) = 1$ as the sole boundary condition for the numerics. At finite temperature, the space terminates at the horizon z_h whose value is determined by the temperature, and in this case f itself vanishes at the horizon: $f(z_h) = 0$. In practice, it means we use the analytical ansatz for f, h in the interval $z_h > z > z_h - \epsilon$ and start the integration at $z = z_h - \epsilon$, again with the boundary condition $h(z) = 1$.

The equations of motion for the gauge and matter fields are

$$\Phi'' - \left(\frac{h'}{2h} - (D-1)z\right)\Phi' + \frac{g_{zz}}{\xi}\partial_\Phi V - \frac{4}{\xi(D-1)}g^{00}\mathcal{T}A_0^2 = 0 \quad (\text{A.4})$$

$$A_0'' - \left(\frac{h'}{2h} - (D-3)z - \frac{\partial_\Phi \mathcal{T}}{\mathcal{T}}\Phi'\right)A_0' - 2q^2\frac{Z}{\mathcal{T}}\sqrt{g_{00}g_{zz}}|\chi|^2 = 0 \quad (\text{A.5})$$

$$\chi'' - \left(\frac{h'}{2h} - (D-1)z\right)\chi' - \frac{m_\chi^2}{\xi z^2 f} + \frac{q^2 Z}{f^2}A_0^2\chi = 0. \quad (\text{A.6})$$

Here we have three second-order equations and two boundary conditions per field. For A_0 , one condition is that the electric field should vanish in the interior: $-A_0'(z \rightarrow \infty) \rightarrow 0$

and the other is to impose the chemical potential or the charge density at the boundary ($A_0(z \rightarrow 0) = \mu$ or $A_0(z)/z^{D-2}|_{z \rightarrow 0} = -\rho$). For Φ and χ the only physically obvious boundary condition is to set the leading branch in the small- z expansion (2.18) to zero (remember we pick the dilaton potential V in the UV in such a way that the subleading branch of the dilaton also falls off quickly enough that no condensation occurs). The other boundary condition for Φ, χ is again set by the analytical expansion for z large, similar as for the metric.

It is well known that the integration is unstable if started from the boundary. We therefore start from the interior and impose all boundary conditions in the interior. Physical requirements for $z \rightarrow 0$ are then obtained by shooting. We start from $z_1 \equiv z_\Lambda$ at $T = 0$ or from $z_1 \equiv z_h - \epsilon$ at finite T and iterate the procedure in two stages. The first iteration assumes some essentially arbitrary metric in the whole space (AdS $_{D+1}$ works well) and solves first the coupled system for f, h, A_0, Φ . For f , the boundary condition is the analytical estimate $f_{\text{anal}}(z_1)$. We similarly impose the analytical estimate for Φ while for Φ' we try an arbitrary value C_1 . For h we also start from an arbitrary value C_2 . For the gauge field we impose the physical boundary condition for the derivative ($A'_0(z_1) = 0$) whereas the other condition is arbitrary ($A_0(z_1) = C_3$). We thus have three free parameters C_1, C_2, C_3 so we can shoot for the correct UV behavior of A_0, Φ, h . This procedure does *not* guarantee the correct behavior for $f(0)$ and $h(z_1)$ as we do not shoot for them but when one lands at the correct solution, these turn out to be automatically satisfied (if not, one should play around a bit with the starting values of the shooting parameter $h(z_1)$). In the next stage, we solve the equation for χ with the conditions $\chi(z_1) = C_4 \chi_{\text{anal}}(z_1)$ and $\chi'(z_1) = C_4 \chi'_{\text{anal}}(z_1)$, leaving the overall normalization C_4 as a free parameter. Then we shoot for the required behavior in the UV (this will yield the solution with nonzero VEV, if it exists; if not, it will give the solution $\chi(z) = 0$). After that, we update the metric and the stress tensor and repeat the whole procedure, again in two steps, first for f, h, Φ, A_0 and then for χ . After 5 – 10 steps (a few minutes of computation time) the procedure converges. One should check that the solution is independent of the cutoff z_1 . At zero temperature, for confining backgrounds the overall scale falls off very sharply and typically $z_1 \approx 3 - 4$ is enough while for nonconfining geometries one needs $z_\Lambda \approx 6 - 10$. At finite temperature, the size of the “analytical” region in the interior ϵ can be made quite small, of the order 10^{-3} . A cutoff in the UV is also necessary and is roughly of the size 10^{-6} .

Open Access. This article is distributed under the terms of the Creative Commons Attribution License ([CC-BY 4.0](https://creativecommons.org/licenses/by/4.0/)), which permits any use, distribution and reproduction in any medium, provided the original author(s) and source are credited.

References

- [1] E. Witten, *Anti-de Sitter space and holography*, *Adv. Theor. Math. Phys.* **2** (1998) 253 [[hep-th/9802150](https://arxiv.org/abs/hep-th/9802150)] [[INSPIRE](https://inspirehep.net/literature/48176)].
- [2] S.S. Gubser, I.R. Klebanov and A.M. Polyakov, *Gauge theory correlators from noncritical string theory*, *Phys. Lett. B* **428** (1998) 105 [[hep-th/9802109](https://arxiv.org/abs/hep-th/9802109)] [[INSPIRE](https://inspirehep.net/literature/48176)].

- [3] E. Witten, *Anti-de Sitter space, thermal phase transition and confinement in gauge theories*, *Adv. Theor. Math. Phys.* **2** (1998) 505 [[hep-th/9803131](#)] [[INSPIRE](#)].
- [4] J. Zaanen, Y. Liu, Y.-W. Sun and K. Schalm, *Holographic duality in condensed matter systems*, Cambridge University Press, (2015).
- [5] S.A. Hartnoll, C.P. Herzog and G.T. Horowitz, *Holographic superconductors*, *JHEP* **12** (2008) 015 [[arXiv:0810.1563](#)] [[INSPIRE](#)].
- [6] S.A. Hartnoll, C.P. Herzog and G.T. Horowitz, *Building a holographic superconductor*, *Phys. Rev. Lett.* **101** (2008) 031601 [[arXiv:0803.3295](#)] [[INSPIRE](#)].
- [7] G.T. Horowitz, *Introduction to holographic superconductors*, *Lect. Notes Phys.* **828** (2011) 313 [[arXiv:1002.1722](#)] [[INSPIRE](#)].
- [8] N. Iqbal, H. Liu, M. Mezei and Q. Si, *Quantum phase transitions in holographic models of magnetism and superconductors*, *Phys. Rev. D* **82** (2010) 045002 [[arXiv:1003.0010](#)] [[INSPIRE](#)].
- [9] G.T. Horowitz and M.M. Roberts, *Holographic superconductors with various condensates*, *Phys. Rev. D* **78** (2008) 126008 [[arXiv:0810.1077](#)] [[INSPIRE](#)].
- [10] T. Senthil, A. Vishwanath, L. Balents, S. Sachdev and M.P.A. Fisher, *‘Deconfined’ quantum critical points*, *Science* **303** (2004) 1490 [[cond-mat/0311326](#)].
- [11] T. Senthil, L. Balents, S. Sachdev, A. Vishwanath and M.P.A. Fisher, *Quantum criticality beyond the Ginzburg-Landau-Wilson paradigm*, *Phys. Rev. B* **70** (2004) 144407 [[cond-mat/0312617](#)].
- [12] H.v. Löhneysen, A. Rosch, M. Vojta and P. Wölfle, *Fermi-liquid instabilities at magnetic quantum phase transitions*, *Rev. Mod. Phys.* **79** (2007) 1015 [[INSPIRE](#)].
- [13] T. Senthil, S. Sachdev and M. Vojta, *Fractionalized Fermi liquids*, *Phys. Rev. Lett.* **90** (2003) 216403 [[cond-mat/0209144](#)] [[INSPIRE](#)].
- [14] T. Senthil, S. Sachdev and M. Vojta, *Quantum phase transitions out of a heavy Fermi liquid*, *Physica B* **359** (2005) 9 [[cond-mat/0409033](#)].
- [15] T. Senthil, M. Vojta and S. Sachdev, *Weak magnetism and non-Fermi liquids near heavy-fermion critical points*, *Phys. Rev. B* **69** (2004) 035111 [[cond-mat/0305193](#)] [[INSPIRE](#)].
- [16] S.S. Gubser, *Curvature singularities: the good, the bad and the naked*, *Adv. Theor. Math. Phys.* **4** (2000) 679 [[hep-th/0002160](#)] [[INSPIRE](#)].
- [17] I.R. Klebanov and E. Witten, *AdS/CFT correspondence and symmetry breaking*, *Nucl. Phys. B* **556** (1999) 89 [[hep-th/9905104](#)] [[INSPIRE](#)].
- [18] S.S. Gubser and F.D. Rocha, *Peculiar properties of a charged dilatonic black hole in AdS₅*, *Phys. Rev. D* **81** (2010) 046001 [[arXiv:0911.2898](#)] [[INSPIRE](#)].
- [19] O. DeWolfe, S.S. Gubser and C. Rosen, *Fermi surfaces in N = 4 super-Yang-Mills theory*, *Phys. Rev. D* **86** (2012) 106002 [[arXiv:1207.3352](#)] [[INSPIRE](#)].
- [20] O. DeWolfe, S.S. Gubser and C. Rosen, *Fermionic response in a zero entropy state of N = 4 super-Yang-Mills*, *Phys. Rev. D* **91** (2015) 046011 [[arXiv:1312.7347](#)] [[INSPIRE](#)].
- [21] U. Gürsoy, *Continuous Hawking-Page transitions in Einstein-scalar gravity*, *JHEP* **01** (2011) 086 [[arXiv:1007.0500](#)] [[INSPIRE](#)].

- [22] U. Gürsoy and E. Kiritsis, *Exploring improved holographic theories for QCD: Part I*, *JHEP* **02** (2008) 032 [[arXiv:0707.1324](#)] [[INSPIRE](#)].
- [23] U. Gürsoy, E. Kiritsis and F. Nitti, *Exploring improved holographic theories for QCD: Part II*, *JHEP* **02** (2008) 019 [[arXiv:0707.1349](#)] [[INSPIRE](#)].
- [24] C. Charmousis, *Dilaton space-times with a Liouville potential*, *Class. Quant. Grav.* **19** (2002) 83 [[hep-th/0107126](#)] [[INSPIRE](#)].
- [25] C. Charmousis, B. Gouteraux, B.S. Kim, E. Kiritsis and R. Meyer, *Effective holographic theories for low-temperature condensed matter systems*, *JHEP* **11** (2010) 151 [[arXiv:1005.4690](#)] [[INSPIRE](#)].
- [26] B. Gouteraux and E. Kiritsis, *Generalized holographic quantum criticality at finite density*, *JHEP* **12** (2011) 036 [[arXiv:1107.2116](#)] [[INSPIRE](#)].
- [27] B. Gouteraux and E. Kiritsis, *Quantum critical lines in holographic phases with (un)broken symmetry*, *JHEP* **04** (2013) 053 [[arXiv:1212.2625](#)] [[INSPIRE](#)].
- [28] S.A. Hartnoll, *Horizons, holography and condensed matter*, [arXiv:1106.4324](#) [[INSPIRE](#)].
- [29] S.A. Hartnoll and L. Huijse, *Fractionalization of holographic Fermi surfaces*, *Class. Quant. Grav.* **29** (2012) 194001 [[arXiv:1111.2606](#)] [[INSPIRE](#)].
- [30] K. Goldstein, S. Kachru, S. Prakash and S.P. Trivedi, *Holography of charged dilaton black holes*, *JHEP* **08** (2010) 078 [[arXiv:0911.3586](#)] [[INSPIRE](#)].
- [31] K. Goldstein, N. Iizuka, S. Kachru, S. Prakash, S.P. Trivedi and A. Westphal, *Holography of dyonic dilaton black branes*, *JHEP* **10** (2010) 027 [[arXiv:1007.2490](#)] [[INSPIRE](#)].
- [32] A. Karch, E. Katz, D.T. Son and M.A. Stephanov, *Linear confinement and AdS/QCD*, *Phys. Rev. D* **74** (2006) 015005 [[hep-ph/0602229](#)] [[INSPIRE](#)].
- [33] B. Batell and T. Gherghetta, *Dynamical Soft-Wall AdS/QCD*, *Phys. Rev. D* **78** (2008) 026002 [[arXiv:0801.4383](#)] [[INSPIRE](#)].
- [34] J.I. Kapusta and T. Springer, *Potentials for soft wall AdS/QCD*, *Phys. Rev. D* **81** (2010) 086009 [[arXiv:1001.4799](#)] [[INSPIRE](#)].
- [35] M. Cadoni, G. D'Appollonio and P. Pani, *Phase transitions between Reissner-Nordstrom and dilatonic black holes in 4D AdS spacetime*, *JHEP* **03** (2010) 100 [[arXiv:0912.3520](#)] [[INSPIRE](#)].
- [36] A. Salvio, *Transitions in dilaton holography with global or local symmetries*, *JHEP* **03** (2013) 136 [[arXiv:1302.4898](#)] [[INSPIRE](#)].
- [37] Y. Liu and Y.-W. Sun, *Holographic superconductors from Einstein-Maxwell-dilaton gravity*, *JHEP* **07** (2010) 099 [[arXiv:1006.2726](#)] [[INSPIRE](#)].
- [38] M. Cadoni, P. Pani and M. Serra, *Infrared behavior of scalar condensates in effective holographic theories*, *JHEP* **06** (2013) 029 [[arXiv:1304.3279](#)] [[INSPIRE](#)].
- [39] A. Salvio, *Holographic superfluids and superconductors in dilaton-gravity*, *JHEP* **09** (2012) 134 [[arXiv:1207.3800](#)] [[INSPIRE](#)].
- [40] Z. Fan, *Holographic superconductors with hidden Fermi surfaces*, [arXiv:1311.4110](#) [[INSPIRE](#)].
- [41] D. Mateos, R.C. Myers and R.M. Thomson, *Holographic phase transitions with fundamental matter*, *Phys. Rev. Lett.* **97** (2006) 091601 [[hep-th/0605046](#)] [[INSPIRE](#)].

- [42] M. Blake, A. Donos and D. Tong, *Holographic charge oscillations*, *JHEP* **04** (2015) 019 [[arXiv:1412.2003](#)] [[INSPIRE](#)].
- [43] G.T. Horowitz and M.M. Roberts, *Zero temperature limit of holographic superconductors*, *JHEP* **11** (2009) 015 [[arXiv:0908.3677](#)] [[INSPIRE](#)].
- [44] T. Faulkner, H. Liu, J. McGreevy and D. Vegh, *Emergent quantum criticality, Fermi surfaces and AdS₂*, *Phys. Rev. D* **83** (2011) 125002 [[arXiv:0907.2694](#)] [[INSPIRE](#)].

Exciton-driven quantum phase transitions in holographyE. Gubankova,^{1,*} M. Čubrović,^{2,†} and J. Zaanen^{2,‡}¹*Instituut Lorentz, Leiden University, Niels Bohrweg 2, 2300 RA Leiden, Netherlands*²*Institute for Theoretical Physics, J. W. Goethe-University, D-60438 Frankfurt am Main, Germany*

(Received 11 April 2015; published 28 October 2015)

We study phase transitions driven by fermionic double-trace deformations in gauge-gravity duality. Both the strength of the double-trace deformation and the infrared conformal dimension/self-energy scaling of the quasiparticle can be used to decrease the critical temperature to zero, leading to a line of quantum critical points. The self-energy scaling is controlled indirectly through an applied magnetic field and the quantum phase transition naturally involves the condensation of a fermion bilinear which models the spin density wave in an antiferromagnetic state. The nature of the quantum critical points depends on the parameters and we find either a Berezinsky-Kosterlitz-Touless-type transition or one of two distinct second-order transitions with non-mean-field exponents. One of these is an anomalous branch where the order parameter of constituent non-Fermi liquid quasiparticles is enhanced by the magnetic field. Stabilization of ordered non-Fermi liquids by a strong magnetic field is observed in experiments with highly oriented pyrolytic graphite.

DOI: 10.1103/PhysRevD.92.086004

PACS numbers: 11.25.Tq, 71.27.+a

I. INTRODUCTION

The anti-de Sitter/conformal field theory correspondence (AdS/CFT) or gauge/gravity duality is a new proving ground to describe strongly correlated systems, and its application to unresolved questions in condensed matter is an exciting new direction. It is especially compelling, as conventional methods, such as large- N [1] and $(4 - \epsilon)$ -type [2] expansions fail to describe quantum critical behavior in $2 + 1$ -dimensional systems. The primary examples of such are the strange metal states in the high- T_c cuprates and heavy fermion systems. Both systems are characterized by anomalous behavior of transport and thermodynamic quantities. In heavy fermions, the Sommerfeld coefficient grows as the temperature is lowered, meaning that the effective mass of the electrons on the Fermi surface diverges or the Fermi energy of the electrons vanishes [3]. In the strange metal phase of the high- T_c superconductors as well as in heavy fermions near a quantum phase transition, the resistivity is linear with temperature $\rho \sim T$. These anomalous behaviors are partly explained by the phenomenological marginal Fermi liquid model [4], and it is an early success of AdS/CFT that the marginal Fermi liquid can be seen to emerge as the low-energy dynamics of a consistent theory.

A particularly simple gravity description for strongly interacting finite-density matter is the planar AdS-Reissner-Nordström (AdS-RN) black hole (BH), which is dual to a system at finite chemical potential. While the AdS-RN black hole is a natural starting point to study the universal

aspects of finite charge density systems, the universality of a black hole makes it difficult to explain experiments that are keen on the nature of the charge carriers, such as transport properties (e.g. conductivity). In particular the dominance of Pauli blocking for observed physics, requires that at the minimum one needs to add free Dirac fermions to the AdS-RN background. A self-consistent treatment shows that this system is unstable to a quasi-Lifshitz geometry in the bulk [5–7], that encodes for a deconfined Fermi liquid system [8–11]. Here we shall initiate the study of instabilities in the unstable metallic AdS-RN phase that are driven by Fermi bilinears.

The essential low-energy property of the metallic system dual to the AdS-RN black hole background is the emergence of Fermi surfaces [12,13] where the notion of a quasiparticle need not be well defined, i.e. stable [14]. In Ref. [15], we used the magnetic field as an external probe to change the characteristics of the Fermi surface excitations and as a consequence the transport properties of the system. It strongly suggested that a quantum phase transition should occur when the underlying quasiparticle becomes (un)stable as a function of the magnetic field. The study in this article of the influence on stability of Fermi bilinears allows us to show that there is a phase transition between the two regimes and that for a specific set of parameters the critical temperature vanishes. Our work is therefore also a fermionic companion to Ref. [16].

Continuing the connection of AdS models to actual observations, the results we find resemble other experimental findings in quantum critical systems. At low temperatures and in high magnetic fields, the resistance of single-layer graphene at the Dirac point undergoes a thousandfold increase within a narrow interval of field strengths [17]. The abruptness of the increase suggests that

* Also at ITEP, Moscow, Russia.
elena1@mit.edu

† cubrovic@lorentz.leidenuniv.nl

‡ jan@lorentz.leidenuniv.nl

a transition to a field-induced insulating, ordered state occurs at the critical field h_c [18]. In bilayer graphene, measurements taken at the filling factor $\nu = 0$ point show that, similar to single-layer graphene, the bilayer becomes insulating at strong magnetic field [19]. In these systems, the divergent resistivity in strong magnetic fields was analyzed in terms of Kosterlitz-Thouless localization [18] and the gap opening in the zeroth Landau level [20]. However, it remains a theoretical challenge to explain a highly unusual approach to the insulating state. Despite the steep divergence of resistivity, the profile of ρ vs T at fixed h saturates to a T -independent value at low temperatures, which is consistent with gapless charge-carrying excitations [18]. Moreover, in highly oriented pyrolytic graphite in the magnetic field, the temperature of the metal-insulator phase transition $T_c(h)$ increases with increasing field strength, contrary to the $T_c(h)$ dependence in the classical low-field limit [21]. The anomalous $T_c(h)$ behavior has been successfully modeled within a dynamical gap picture [22]. The available data suggest that by tuning the magnetic field graphene approaches a quantum critical point, beyond which a new insulating phase develops with anomalous behavior $T_c(h)$. This picture is in agreement with expectations of quantum critical behavior, where e.g. in heavy fermion metal a new magnetically ordered state (antiferromagnet) emerges when tuned through the quantum critical point [3].

We shall see that the same qualitative physics emerges with our use of the the magnetic field as a knob to tune to the IR fixed point to gain some insight into the quantum critical behavior driven by fermion bilinears. In our gauge/gravity dual prescription, the unusual properties characteristic for quantum criticality can be understood as being controlled by the scaling dimension of the fermion operator in the emergent IR fixed point. The novel insight of AdS/CFT is that the low-energy behavior of a strongly coupled quantum critical system is governed by a nontrivial unstable fixed point which exhibits nonanalytic scaling behavior in the temporal direction only (the retarded Green's function of the IR CFT is $G_{\text{IR}}^R \sim \omega^{2\nu}$) [14]. This fixed point manifests itself as a near-horizon region of the black hole with AdS₂ geometry which is (presumably) dual to a one-dimensional IR CFT. Building on the semilocal description of the quasiparticle characteristics by simple Dyson summation in a Fermi gas coupled to this 1 + 1-dimensional IR CFT [23] an appealing picture arises that quantum critical fermionic fluctuations in the IR CFT generate relevant order parameter perturbations of the Fermi liquid theory. Whether this is truly what is driving the physics is an open question. Regardless, quantum critical matter is universal in the sense that no information about the microscopic nature of the material enters. Qualitatively our study should apply to any bilinear instability in the strange metal phase of unconventional superconductors, heavy fermions as well as for a critical

point in graphene. Universality makes applications of AdS/CFT to quantum critical phenomena justifiable and appealing.

The paper is organized as follows. In Sec. II, we review the AdS-RN black hole solution in AdS-Einstein-Maxwell gravity coupled to charged fermions and the dual interpretation as a quantum critical fermion system at finite density. In Sec. III we use the bilinear formalism put forward in Ref. [6] to explore an instability of a quantum system towards a quantum phase transition using the AdS dual description. We study a quantum phase transition to an insulating phase as a function of the magnetic field. For completeness we test the various phases by a spectral analysis in Sec. IV. We conclude by discussing a phase space in (h, T) variables for a quantum critical matter at nonzero temperatures.

II. HOLOGRAPHIC FERMIONS IN THE BACKGROUND OF A DYONIC BLACK HOLE

The gravity dual to a 2 + 1-dimensional CFT at finite density in the presence of a magnetic field starts with the Einstein-Maxwell action describing an asymptotically AdS₄ geometry:

$$S_g = \frac{1}{2\kappa^2} \int d^4x \sqrt{-g} \left(\mathcal{R} + 6 - \frac{1}{g_F^2} F_{MN} F^{MN} \right). \quad (1)$$

Here A_M is the gauge field, g_F^2 is an effective dimensionless gauge coupling and the curvature radius of AdS₄ is set to unity. The equations of motion following from Eq. (1) are solved by a dyonic AdS black hole, having both electric and magnetic charge

$$ds^2 = \frac{1}{(1-z)^2} \left(-f dt^2 + dx^2 + dy^2 + \frac{dz^2}{f} \right) \quad (2)$$

where the redshift factor f and the vector field A_M are given by

$$f = z(3 - 3z + z^2 - (Q^2 + H^2)(1-z)^3), \\ A_t = \mu z, \quad A_y = hx, \quad \text{with } \mu = g_F Q, \quad h = g_F H. \quad (3)$$

The AdS boundary is reached for $z \rightarrow 1$, the black hole horizon is at $z \rightarrow 0$ and the electric and magnetic charge of the black hole Q and H , encoding the chemical potential μ and magnetic field h of the dual CFT, are scaled such that the black hole temperature equals¹

$$T = \frac{1}{4\pi} (3 - (Q^2 + H^2)). \quad (4)$$

¹The independent black hole mass parameter is restored after rescaling $t \rightarrow Mt$, $x \rightarrow Mx$, $y \rightarrow My$ and $h \rightarrow M^{-2}h$.

In these units, the extremal $T = 0$ black hole corresponds to $Q^2 + H^2 = 3$ and in this case the red shift factor develops a double zero at the horizon

$$f = 3z^2(z - z_*)(z - \bar{z}_*), \quad z_* = (4 + i\sqrt{2})/3. \quad (5)$$

To include the bulk fermions, we consider a spinor field ψ in the AdS_4 of charge q and mass m , which is dual to a fermionic operator \mathcal{O} in the boundary CFT_3 of charge q and dimension

$$\Delta_\psi = \frac{3}{2} + m, \quad (6)$$

with $m \geq -\frac{1}{2}$ (in units of the AdS radius). The quadratic action for ψ reads

$$S_\psi = \int d^4x \sqrt{-g} (\bar{\psi} \Gamma^M \mathcal{D}_M \psi - m \bar{\psi} \psi), \quad (7)$$

where $\bar{\psi} = \psi^\dagger i\Gamma^{\hat{t}}$, and

$$\mathcal{D}_M = \partial_M + \frac{1}{4} \omega_{Mab} \Gamma^{ab} - iqA_M, \quad (8)$$

where ω_{Mab} is the spin connection, and $\Gamma^{ab} = \frac{1}{2} [\Gamma^a, \Gamma^b]$. Here, M and a, b denote the bulk space-time and tangent-space indices respectively, while μ, ν are indices along the boundary directions, i.e. $M = (z, \mu)$. The Dirac equation in the dyonic AdS-black hole background becomes

$$\left(\Gamma^{\hat{z}} \sqrt{f} \partial_z + \Gamma^{\hat{z}} \frac{\sqrt{f}}{2(1-z)} \left(3 + \frac{(1-z)f'}{2f} \right) - \Gamma^{\hat{t}} \frac{i(\omega + q\mu z)}{\sqrt{f}} - \frac{1}{(1-z)} m + \Gamma^{\hat{x}} \partial_x + \Gamma^{\hat{y}} i(k_y - qhx) \right) \psi = 0 \quad (9)$$

where ψ is the Fourier transform in the y directions and time. The z and x dependences can be separated as in Refs. [15,24,25]. Define

$$\begin{aligned} P &= \Gamma^{\hat{z}} \sqrt{f} \left(\partial_z + \frac{1}{2(1-z)} \left(3 + \frac{(1-z)f'}{2f} \right) \right) \\ &\quad - \Gamma^{\hat{t}} \frac{i(\omega + q\mu z)}{\sqrt{f}} - \frac{1}{(1-z)} m, \\ Q &= \Gamma^{\hat{x}} \partial_x + \Gamma^{\hat{y}} (ik_y - iqx), \end{aligned} \quad (10)$$

in terms of which the Dirac equation is $(P + Q)\psi = 0$. In order to separate the variables, we can proceed by finding the matrix U such that $UP\psi = -UQ\psi = \lambda\psi$. The idea is that, although P and Q do not commute, we can find U so that $[UP, UQ]$ commute and can be diagonalized simultaneously [15].² To this end, U must satisfy the relations

²Rather the part in P not proportional to the identity *anti-commutes* with Q . This realization shows why the relations in the next sentence are the solution.

$\{U, \Gamma^z\} = 0$, $\{U, \Gamma^t\} = 0$, $[U, \Gamma^x] = 0$, $[U, \Gamma^y] = 0$. A clear solution is $U = [\Gamma^z, \Gamma^t]$.

In a convenient gamma matrix basis (Minkowski signature) [14]

$$\begin{aligned} \Gamma^{\hat{z}} &= \begin{pmatrix} -\sigma^3 & 0 \\ 0 & -\sigma^3 \end{pmatrix}, & \Gamma^{\hat{t}} &= \begin{pmatrix} i\sigma^1 & 0 \\ 0 & i\sigma^1 \end{pmatrix}, \\ \Gamma^{\hat{x}} &= \begin{pmatrix} -\sigma^2 & 0 \\ 0 & \sigma^2 \end{pmatrix}, \\ \Gamma^{\hat{y}} &= \begin{pmatrix} 0 & \sigma^2 \\ \sigma^2 & 0 \end{pmatrix}, & \Gamma^{\hat{s}} &= \begin{pmatrix} 0 & i\sigma^2 \\ -i\sigma^2 & 0 \end{pmatrix} \equiv i\Gamma^{\hat{t}}\Gamma^{\hat{x}}\Gamma^{\hat{y}}\Gamma^{\hat{z}} \end{aligned} \quad (11)$$

the matrix U equals

$$U = \begin{pmatrix} -i\sigma^2 & 0 \\ 0 & -i\sigma^2 \end{pmatrix}. \quad (12)$$

This choice of the basis allows one to obtain $k_y = 0$ spectral functions in a simple way. In the absence of a magnetic field one can use rotational invariance to rotate to a frame where this is so. The gauge choice for the magnetic field obviously breaks the isotropy, but the physical isotropy still ensures that the spectral functions simplify in this basis [15]. The x -dependent part of the Dirac equation can be solved analytically in terms of Gaussian-damped Hermite polynomials $H_n(\sqrt{qh}(x + \frac{k_y}{qh}))$ with eigenvalues $\lambda_n = \sqrt{|qh|}n$ quantized in terms of the Landau index $n = 0, 1, \dots$ [15,24,25]. The Dirac equation $(P - U^{-1}\lambda)\psi = 0$, where λ is a diagonal matrix in terms of λ_n and whose square is proportional to the identity, then reduces to

$$\left(\left(\partial_z + \frac{1}{2(1-z)} \left(3 + \frac{(1-z)f'}{2f} \right) \right) \Gamma^{\hat{z}} - \frac{i(\omega + q\mu z)}{f} \Gamma^{\hat{t}} - \frac{m}{\sqrt{f}(1-z)} - U^{-1} \frac{\lambda_n}{\sqrt{f}} \right) \psi = 0. \quad (13)$$

We introduce now the projectors Π_α that split the four-component bispinors into two two-component spinors $\Psi = (\psi_1, \psi_2)^T$ where the index $\alpha = 1, 2$ is the Dirac index of the boundary theory

$$\Pi_\alpha = \frac{1}{2} \left(1 - (-1)^\alpha \Gamma^{\hat{z}} \Gamma^{\hat{t}} \frac{1}{|\lambda|} Q \right), \quad \alpha = 1, 2,$$

$$\Pi_1 + \Pi_2 = 1. \quad (14)$$

The projectors commute with both P and Q (recall that $Q^2 = \lambda^2 \mathbb{1}$). At zero magnetic field projectors are given by $\Pi_\alpha = \frac{1}{2} (1 - (-1)^\alpha \Gamma^{\hat{z}} \Gamma^{\hat{t}} \hat{k}_i \Gamma^i)$ with unit vector $\hat{k}_i = \vec{k}/|\vec{k}|$. The projections $\psi_\alpha = \Pi_\alpha \psi$ with $\alpha = 1, 2$ therefore decouple from each other and one finds two independent copies of the two-component Dirac equation:

$$\left(\partial_z + \frac{1}{2} \left(\frac{3}{1-z} + \frac{f'}{2f} \right) - \frac{i(\omega + \mu_q z)}{f} \sigma^2 + \frac{m}{\sqrt{f}(1-z)} \sigma^3 + \frac{\lambda_n}{\sqrt{f}} \sigma^1 \right) \psi_{1;2} = 0, \quad (15)$$

where the magnetic momentum $\lambda_n = \sqrt{2|qh|n}$ is Landau quantized with integer values $n = 0, 1, \dots$ and $\mu_q \equiv \mu q$. It is identical to the AdS-Dirac equation for an AdS-RN black hole with zero magnetic charge when the discrete eigenvalue λ is identified with the (size of the) momentum k .

As we have shown in Ref. [15], solving Eq. (15) is equivalent to solving the Dirac equation at zero magnetic field but with a rescaled chemical potential and fermion charge. At $T = 0$ the mapping is given by [15]

$$\begin{aligned} (\mu_q, h, q) &\mapsto (\mu_{q,\text{eff}}, h_{\text{eff}}, q_{\text{eff}}) \\ &= \left(\sqrt{3}q \sqrt{1 - \frac{h^2}{3}}, 0, q \sqrt{1 - \frac{h^2}{3}} \right), \end{aligned} \quad (16)$$

which we will use further.

III. BILINEAR APPROACH TO PARTICLE-HOLE PAIRING

The objective of this paper is to use the magnetic field as a tool to probe our unstable quantum critical system dual to the dyonic AdS-RN geometry. We show that the instability is manifest in the appearance of ordering in the system: the magnetic field acts as a catalyzer for the particle-hole pairing. In particular, we will find an unusual behavior for the critical temperature of the normal to paired phase transition as the dialing of the magnetic field drives the system to a quantum critical point: for a critical magnetic field the critical temperature vanishes indicating a new emergent quantum critical point.

We will identify the bulk quantities in the bilinear approach which are dual to the sought-for quantities on the CFT side. We have given the setup of the bilinear formalism in Ref. [6]. Here, we will first give a concise review with the focus on the transport properties and the influence of magnetic fields, and then derive the bilinear equations relevant for computing the pairing gap.

A. Bulk propagators and currents

A controlled method for calculating the expectation value of some composite operator J with the structure of a fermion bilinear ($J \sim \psi^\dagger \psi$) has been put forward in Ref. [6] and it is based on a relation between the bulk and the boundary propagator in the isotropic single-particle approximation. This allows us to identify the familiar quantities at the boundary by matching the resulting expression to known thermodynamic relations. The crucial object was identified in Ref. [6]

$$J^\mu(E, p, z) = \int d\omega \int d^2k \bar{\psi}(\omega, k, z) \Gamma^\mu \psi(E - \omega, p - k, z) \quad (17)$$

and it is the spatial average of the $U(1)$ current four-vector in the bulk.³ The metric then assumes the form given in the first section by Eq. (2) (so that the horizon is located at $z_H = 0$ and the boundary is at $z_0 \rightarrow 1$). Having defined the radial projection of the bulk Dirac equation in Eq. (14) we can also define the radial projections of the current as

$$J_\alpha^\mu(E, p, z) = \int d\omega \int d^2k \bar{\psi}_\alpha(\omega, k, z) \gamma^\mu \psi_\alpha(E - \omega, p - k, z), \quad (18)$$

where $\alpha = 1, 2$ and γ^μ is a Pauli matrix acting in the boundary frame.

The boundary interpretation of this current is, however, subtler than the simple $U(1)$ conserved current which it is in the bulk [6]: it expresses the Migdal theorem, i.e. the density of quasiparticles in the vicinity of the Fermi surface. To see this, express the bulk spinors $\psi_\alpha(z)$ at an arbitrary value of z through the bulk-to-boundary propagators $\mathcal{G}_\alpha(z, z')$ and the boundary spinors $\psi_\alpha(z_0)$ as

$$\psi_\alpha(z) = \mathcal{G}_\alpha(z_H, z) \mathcal{G}_\alpha^{-1}(z_H, z_0) \psi_\alpha(z_0). \quad (19)$$

The meaning of the above expressions is clear: the spinors evolve from their horizon values toward the values in the bulk at some z , under the action of the bulk-to-boundary propagator $\mathcal{G}_\alpha(z, z')$ acting upon them (normalized by its value at the boundary). To find the relation with the boundary Green's function we need to know the asymptotics of the solutions of the Dirac equation (15) at the boundary; see Eq. (A6) in Appendix A:

$$\begin{aligned} \psi_1 &\sim a_1 (1-z)^{3/2-m} \psi_{0,+}^{\text{in}} + b_1 (1-z)^{3/2+m} \psi_{0,-}^{\text{in}}, \\ \psi_2 &\sim a_2 (1-z)^{5/2-m} \psi_{0,+}^{\text{in}} + b_2 (1-z)^{5/2+m} \psi_{0,-}^{\text{in}}. \end{aligned} \quad (20)$$

On the other hand, the boundary retarded propagator is given by the dictionary entry [26], Eq. (A9), where $\gamma^0 = i\sigma^1$.

The bulk-to-boundary Green's function (in dimensionless units) can be constructed from the solutions to the Dirac equation [27] as in Eq. (A4). Using Eq. (A6) and the expression for the Wronskian, we arrive at the following relation between the boundary asymptotics of the solutions ψ^{in} and ψ^{bdy} :

$$\psi_\alpha^{\text{in}}(z_0) = \left(\frac{(1-z)^{-2m}}{G_\alpha} (-i\gamma^0) + 1 \right) \psi_\alpha^{\text{bdy}}(z_0). \quad (21)$$

³As shown in Ref. [6], even though the current is defined as a spatial average, the only mode that contributes at the leading order (tree level) is the quasinormal mode at $k = k_F$.

Taking into account the dictionary entry for the boundary propagator from Eq. (A9) and the representation (19) for ψ^{in} and ψ^{bdy} , the retarded propagator at the boundary is

$$\begin{aligned} G_\alpha &= \lim_{z_0 \rightarrow 1} (1 - z_0)^{-2m} \psi_\alpha^{\text{bdy}}(z_0) (\psi_\alpha^{\text{in}}(z_0))^{-1} \\ &= \lim_{z_0 \rightarrow 1} \mathcal{G}_\alpha(z_H, z_0) \gamma^0 \mathcal{G}_\alpha(z_H, z_0) \end{aligned} \quad (22)$$

with $z_H = 0$. Using Eq. (22) and the definition for the current in Eq. (18) it can now be shown that the current $J_1^\mu \sim \int \tilde{G}_1 \gamma^\mu G_1$ for an on-shell solution becomes at the boundary [6]

$$J_1^\mu(\omega = 0, k = k_F, z_0 \rightarrow 1) = \frac{1 + 2m}{\mu} \int d\omega \gamma^\mu G_1(\omega, k_F). \quad (23)$$

It is well known [28] that the integral of the propagator is related to the charge density. In particular, for $\gamma^\mu = \gamma^0$ and for the horizon boundary conditions chosen so that $G = G_F$ (Feynman propagator), we obtain

$$J_1^0 \equiv \int d\omega \psi_1^\dagger \psi_1 = \frac{1 + 2m}{\mu} n_F, \quad (24)$$

i.e. the bilinear J^0 directly expresses the charge density $n_F = \text{tr}(i\gamma^0 G)|_{\text{on-shell}} \sim |b_1(k_F)|^2$. Notice that to achieve this we need to set $\omega = k - k_F = 0$, i.e. look at the location of the Fermi surface. By analogy, we can now see that the components $J^{1,2}$ correspond to current densities. In particular, the ratio of the spatial components J_1^i/E^j in the external electric field \mathbf{E} readily gives the expression for the conductivity tensor σ_{ij} . Finally, the formalism outlined above allows us to define an arbitrary bilinear $J^A = \int \tilde{\psi} \hat{A} \psi$ and to compute its expectation value. By choosing the matrix \hat{A} appropriately we are able to model particle-hole, particle-particle or any other current. Notice however that all bilinears J^A are proportional on shell, as can be seen from Eqs. (22)–(23), which hold also for any other matrix \hat{A} sandwiched between the two bulk propagators. The proportionality is at fixed parameters (μ , T , etc.) so the dependences of the form $J^A(\mu)$ and $J^A(T)$ will be different for different choices of \hat{A} .

To introduce another crucial current, we will study the form of the action. (We will define our action to model the quantum phase transition and to define the pairing excitonic gap in Sec. III B.) We pick a gauge, Eq. (3), so that the Maxwell field is $A_\mu = (\Phi(z), 0, h(z)x, 0, 0)$, meaning that the nonzero components of $F^{\mu\nu}$ are $F^{z0} = \partial_z \Phi$, $F^{z2} = x \partial_z h$, $F^{12} = h$ and their antisymmetric pairs. The total action [Eqs. (1) and (7)] is now

$$\begin{aligned} S &= \int dz d^3x \sqrt{-g} \left(\frac{1}{2\kappa^2} \left(\mathcal{R} + 6 - \frac{1}{4g_F^2} F_{MN} F^{MN} \right) \right. \\ &\quad \left. + \bar{\psi} \Gamma^M \mathcal{D}_M \psi - m \bar{\psi} \psi \right) \\ &\quad + \int d^3x \sqrt{-h} \left(\mathcal{R}_{\text{bnd}} A_\mu n_\nu F^{\mu\nu} + \sum_\alpha \bar{\psi}_\alpha (-i\sigma^3) \psi_\alpha \right), \end{aligned} \quad (25)$$

where $\bar{\psi}_\alpha = i\psi_\alpha^\dagger \sigma^1$. The second integral is the boundary term added to regularize the bulk action, for which the fermion part vanishes on shell. Knowing the metric (2) and the form of A^μ , we find that the total action (free energy, from the dictionary) can be expressed as [6]

$$\mathcal{F} = \mathcal{F}_{\text{hor}} - \frac{1}{2}(\mu\rho + h\mathcal{M}) + \frac{3}{2}K \quad (26)$$

where \mathcal{F}_{hor} is the free energy at the horizon, which does not depend on the physical quantities on the boundary as long as the metric is fixed [6] so we can disregard it here. In Eq. (26), μ , ρ and h , \mathcal{M} are the leading and subleading terms in the electric and magnetic field

$$\begin{aligned} \Phi(z \rightarrow z_0) &= \mu, & \partial_z \Phi(z \rightarrow z_0) &= \rho, \\ h(z \rightarrow z_0) &= h, & \partial_z h(z \rightarrow z_0) &= \mathcal{M}, \end{aligned} \quad (27)$$

and the fermionic contribution is proportional to

$$K = \int d\omega \int d^2k \sum_\alpha \bar{\psi}_\alpha(\omega, k, z) \psi_\alpha(E - \omega, p - k, z) \quad (28)$$

which brings us to the second crucial bilinear. Along the lines of the derivation (18)–(23), we see that the fermionic contribution to the boundary action (25) is proportional to

$$K = 2 \sum_\alpha \text{Re} G_\alpha, \quad (29)$$

i.e. it is the real part of the boundary propagator.⁴ The bulk fermionic term does not contribute, being proportional to the equation of motion, while the boundary terms include the holographic factors of the form $(1 - z_0)^n$. In accordance with our earlier conclusion that the on-shell bilinears are all proportional, we can reexpress the free energy in Eq. (26) as

$$\mathcal{F} = \mathcal{F}_{\text{hor}} - \frac{1}{2}(\mu\rho + h\mathcal{M}) + \frac{3}{4m + 2} \mu J_1^0 \quad (30)$$

where the chemical potential reappears in the prefactor and the fermionic term becomes of the form μJ_1^0 , confirming again that J_1^0 can be associated with the number density.

⁴In Ref. [6] this bilinear was denoted by I . In the present paper a different bilinear is called I_\pm .

B. Pairing currents

Now we will put to work our bilinear approach in order to explicitly compute the particle-hole (excitonic) pairing operator. We add a scalar field which interacts with fermions by the Yukawa coupling as done in Ref. [29]. Both scalar and fermion fields are dynamical. The matter action is given by

$$\begin{aligned} S_\psi &= i \int dz d^3x \sqrt{-g} (\bar{\psi} \Gamma^M D_M^\psi \psi - m_\psi \bar{\psi} \psi - \lambda |\phi|^2 \bar{\psi} \psi), \\ S_G &= \int dz d^3x \sqrt{-g} \frac{1}{2} G_{\text{int}} (\phi \bar{\psi} \Gamma \psi + \phi^* \bar{\psi} \bar{\Gamma} \psi), \\ S_\phi &= - \int dz d^3x \sqrt{-g} (|D_M^\phi \phi|^2 + V(|\phi|)) \end{aligned} \quad (31)$$

where the covariant derivatives are $D_M^\psi = \nabla_M + \frac{1}{4} \omega_{Mab} \Gamma^{ab} - i q_\psi A_M$, $D_M^\phi = \nabla_M - i q_\phi A_M$, and $\bar{\psi} = \psi^\dagger i \Gamma^t$. The gamma-matrix structure of the Yukawa interaction is specified further. Matter action is supplemented by the gauge-gravity action

$$S_A = \frac{1}{2\kappa^2} \int dz d^3x \sqrt{-g} \left(R + \frac{6}{L^2} - \frac{1}{4g_F^2} F_{MN} F^{MN} \right). \quad (32)$$

We take the AdS radius $L = 1$ and $g_F = 1$. The gauge field components A_0 and A_2 are responsible for the chemical potential and magnetic field, respectively, in the boundary theory. As in Ref. [29], we assume $\lambda = 0$ and $V(|\phi|) = m_\phi^2 |\phi|^2$ and the scalar is real $\phi^* = \phi$. For the particle-hole sector, the scalar field is neutral $q_\phi = 0$.

The Yukawa coupling G_{int} is allowed to be positive and negative. When the coupling is positive $G_{\text{int}} > 0$, a repulsive interaction makes it harder to form the particle-hole condensate. Therefore it lowers the critical temperature and can be used as a knob to tune to a vanishing critical temperature $T_c = 0$ at a critical value G_{int}^c which defines a quantum critical point. When the coupling is negative $G_{\text{int}} < 0$, an attractive interaction facilitates pairing and helps to form the condensate.

Both situations can be described when the interaction term is viewed as a dynamical mass of either sign due to the fact that it is in the $\bar{\psi} \psi$ channel. For $G_{\text{int}} > 0$, the interaction $G_{\text{int}} \phi$ introduces a new massive pole: the massless free fermion field acquires a mass which makes it harder to condense. For $G_{\text{int}} < 0$, there is a tachyonic instability. The exponentially growing tachyonic mode is resolved by a condensate formation, a new stable ground state. It can be shown that we do not need a nonzero chemical potential to form a condensate in this case. A similar situation was considered in Ref. [16] for the superconducting instability

where the spontaneous symmetry breaking of $U(1)$ was achieved by the boundary double-trace deformation. In our case for the electron-hole pairing, Z_2 symmetry is spontaneously broken by a neutral order parameter. Next we discuss the choice for the gamma-matrix structure Γ of the Yukawa interaction (31) and the corresponding pairing parameter Δ

$$\Delta = G_{\text{int}} \langle \bar{\psi} \Gamma \psi \rangle. \quad (33)$$

Now we explain our choice of the pairing operator and give a rigorous justification for this choice.

In principle, any operator that creates a particle and a hole with the same quantum numbers could be taken to define Δ . This translates into the requirements

$$[\Gamma, \Gamma^t] = 0, \quad \{\Gamma, \Gamma^0\} = 0, \quad [\Gamma, \hat{C}] = 0. \quad (34)$$

(Anti)commutation with (time) space gamma matrices is required for the preservation of homogeneity and isotropy, and the last one is there to preserve the particle-hole symmetry. In the basis we have adopted, Eq. (11), $(\Gamma^t)^* = -\Gamma^t$ and $\Gamma^{z*} = \Gamma^z$, and therefore the charge conjugation is represented as

$$\hat{C}: \psi \rightarrow \Gamma^0 \Gamma^3 \psi^*. \quad (35)$$

We will also consider the parity of the order parameter. As defined in Ref. [30], parity in the presence of the AdS boundary acts as $x^1 \rightarrow -x^1$ with x^2, z unchanged, while the transformation of the spinor is given by

$$\hat{P}: \psi \rightarrow \Gamma^1 \Gamma^5 \psi. \quad (36)$$

We can now expand Γ in the usual basis:

$$\mathbb{B} = \{I, \Gamma^\mu, \Gamma^5, \Gamma^5 \Gamma^\mu, [\Gamma^\mu, \Gamma^\nu]\} \quad (37)$$

where the indices in the commutators $[\Gamma^\mu, \Gamma^\nu]$ run along the six different combinations, and check directly that the conditions (34) can only be satisfied by the matrices $I, \Gamma^5 \Gamma^i$ and $[\Gamma^0, \Gamma^z]$. This gives three candidate bilinears:

- (i) For $\Gamma = I$ we get the bulk current $\bar{\psi} \psi = -(\psi_1^\dagger \sigma^1 \psi_1 + \psi_2^\dagger \sigma^1 \psi_2)$, i.e. the mass operator in the bulk. As noted in this section and in more detail in Ref. [6], it can be identified as proportional to the bulk mass term. As such, it describes the free energy per particle, as can be seen from the expression for the free energy (26). The equation of motion for $K = \langle \bar{\psi} \psi \rangle$ [Eq. (28)] exclusively depends on the $U(1)$ current and thus

cannot encapsulate the density of the neutral particle-hole pairs: indeed, we directly see that the right-hand side equals zero if the total charge current vanishes.

- (ii) For $\Gamma = i\Gamma^y\Gamma^5$, the bulk current is $\bar{\psi}i\Gamma^y\Gamma^5\psi = -(\psi_1^\dagger\sigma^1\psi_1 - \psi_2^\dagger\sigma^1\psi_2)$. The crucial difference with respect to the first case is the relative minus sign. It is due to this sign that the current *couples to itself*, i.e. it is a response to a nonzero parameter G_{int} , as we will see soon.
- (iii) For $\Gamma = \Gamma^z$, the resulting bulk current is $\bar{\psi}\Gamma^z\psi = -i(\psi_1^\dagger\sigma^2\psi_1 + \psi_2^\dagger\sigma^2\psi_2)$. It sources the radial gauge field A_z which is believed to be equal to zero in all meaningful holographic setups, as the radial direction corresponds to the renormalization group (RG) scale. Thus, this operator is again not the response to the attractive pairing interaction.

We are therefore left with one possibility only: $\Gamma = i\Gamma^2\Gamma^5$ which is also consistent with the choice of our gauge at nonzero magnetic field. We will therefore work with the channel

$$\Gamma \equiv i\Gamma^y\Gamma^5 = \begin{pmatrix} 1 & 0 \\ 0 & -1 \end{pmatrix}. \quad (38)$$

As we have discussed earlier, the isotropy in the x - y plane remains unbroken by the radial magnetic field, and hence the expectation value should in fact be ascribed to the current $I^\mu = i\bar{\psi}\Gamma^\mu\Gamma^5\psi$ with $\mu = 1, 2$. We show the equivalence of the $i\Gamma^x\Gamma^5$ and $i\Gamma^y\Gamma^5$ order parameters below. The choice of the y channel is motivated by technical simplicity due to the form of the projection operator and the fermion basis we use, Eq. (14): $\Pi_\alpha = \frac{1}{2}(1 - (-1)^\alpha\Gamma^3\Gamma^0\Gamma^1)$ with $\alpha = 1, 2$, since $\Gamma^3\Gamma^0\Gamma^1 = -i\Gamma^2\Gamma^5$ with $\Gamma^5 = i\Gamma^0\Gamma^1\Gamma^2\Gamma^3$. Finally, we note that the structure of the currents defined in Eqs. (17) and (18) depends on the basis choice and that the currents as such have no physical interpretation in the boundary theory: physical meaning can only be ascribed to the expectation values [6]. It is exactly the expectation values that encode for the condensation (order) on the field theory side [6,30].

The AdS/CFT correspondence does not provide a straightforward way to match a double-trace condensate to a boundary operator, though only single-trace fields are easy to identify with the operators at the boundary. Indeed, in holographic superconductors a superconducting condensate is modeled by a charged scalar field $\langle\Phi\rangle$ (see e.g. Ref. [31]). As in Ref. [30], we argue by matching discrete symmetries on the gravity and field theory sides, that the expectation of the bulk current $\langle\bar{\psi}i\Gamma^2\Gamma^5\psi\rangle$ is the gravity dual of the pairing particle-hole gap. Let us consider properties of the corresponding

condensates with respect to discrete symmetries, parity and charge conjugation, in the AdS four-dimensional space. According to Eq. (36), $\langle\bar{\psi}\psi\rangle$ and $\langle\bar{\psi}\Gamma^3\psi\rangle$ are scalars and parity even, while $\langle\bar{\psi}i\Gamma^2\Gamma^5\psi\rangle$ is a pseudoscalar and parity odd. As for the charge conjugation, we easily find that $\langle\bar{\psi}\psi\rangle$ and $\langle\bar{\psi}i\Gamma^2\Gamma^5\psi\rangle$ commute with \hat{C} , while $\langle\bar{\psi}\Gamma^3\psi\rangle$ anticommutes. Since the latter is the component of a vector current while the former two are (pseudo)scalars, we find that all operators preserve the particle number, as promised. The magnetic field H is odd under both parity and charge conjugation, and therefore it is unaffected by $\hat{C}\hat{P}$. The condensate $\langle\bar{\psi}\psi\rangle$ is also unaffected by $\hat{C}\hat{P}$; however $\langle\bar{\psi}i\Gamma^2\Gamma^5\psi\rangle$ and $\langle\bar{\psi}\Gamma^3\psi\rangle$ spontaneously break the $\hat{C}\hat{P}$ symmetry.

In the three-dimensional boundary theory, gamma matrices can be deduced from the four-dimensional bulk gamma matrices; and the four component Dirac spinor ψ is dual to a two-component spinor operator Ψ . As has been also found in Ref. [30], the three-dimensional condensate $\bar{\Psi}\Psi$ is odd under parity and even under charge conjugation, and therefore it is odd under $\hat{C}\hat{P}$. We summarize the transformation properties of the four- and three-dimensional condensates together with the magnetic field

| | $\langle\bar{\psi}\psi\rangle_{4d}$ | $\langle\bar{\psi}\Gamma^3\psi\rangle_{4d}$ | $\langle\bar{\psi}i\Gamma^2\Gamma^5\psi\rangle_{4d}$ | $\langle\bar{\Psi}\Psi\rangle_{3d}$ | H |
|------------------|-------------------------------------|---|--|-------------------------------------|-----|
| \hat{P} | + | + | - | - | - |
| \hat{C} | + | - | + | + | - |
| $\hat{C}\hat{P}$ | + | - | - | - | + |

(39)

which shows that the symmetry properties are matched between $\langle\bar{\psi}i\Gamma^2\Gamma^5\psi\rangle_{4d}$ and $\langle\bar{\Psi}\Psi\rangle_{3d}$ condensates: they spontaneously break the CP symmetry while the magnetic field leaves it intact. Therefore our AdS/CFT dictionary between the bulk and boundary quantities is $\psi \leftrightarrow \Psi$ and $\langle\bar{\psi}i\Gamma^2\Gamma^5\psi\rangle \leftrightarrow \langle\bar{\Psi}\Psi\rangle$, with the corresponding conformal dimensions of boundary operators given by Eq. (84) and Eq. (83).

The natural bulk extension is now the current

$$I = (-i) \int d\omega \int d^2k \bar{\psi}(\omega, k, z) \Gamma \psi(E - \omega, p - k, z) \quad (40)$$

and it is understood that in nonzero magnetic field the integration over k degenerates into the sum over Landau levels (this holds for all currents in this section). We will soon show that a complete set of bulk equations of motion for the operator (40) requires a set of currents that we label J_\pm , I_\pm and K_\pm . In the representation (11) we introduce the following bilinears of the fermion field:

$$\begin{aligned}
J_{\pm}(E, p, z) &= (-i) \int d\omega \int d^2k (\bar{\psi}_1(\omega, k, z) \sigma^1 \psi_1(E - \omega, p - k, z) \pm \bar{\psi}_2(\omega, k, z) \sigma^1 \psi_2(E - \omega, p - k, z)) \\
&\equiv J_1(E, p, z) \pm J_2(E, p, z), \\
I_{\pm}(E, p, z) &= (-i) \int d\omega \int d^2k (\bar{\psi}_1(\omega, k, z) \psi_1(E - \omega, p - k, z) \pm \bar{\psi}_2(\omega, k, z) \psi_2(E - \omega, p - k, z)) \\
&\equiv I_1(E, p, z) \pm I_2(E, p, z), \\
K_{\pm}(E, p, z) &= - \int d\omega \int d^2k (\bar{\psi}_1(\omega, k, z) \sigma^2 \psi_1(E - \omega, p - k, z) \pm \bar{\psi}_2(\omega, k, z) \sigma^2 \psi_2(E - \omega, p - k, z)) \\
&\equiv K_1(E, p, z) \pm K_2(E, p, z),
\end{aligned} \tag{41}$$

where the pairing parameter $\langle \bar{\psi} \Gamma \psi \rangle$ in Eq. (40) is $I \equiv I_-$, the index 0 for the zeroth component is omitted in J_{\pm} , and $\bar{\psi}_{\alpha} = i\psi_{\alpha}^{\dagger} \sigma^1$.

Let us now study the dynamics of the system. We need to know the evolution equations for the currents and the scalar field and to complement them with the Maxwell equations. We will show that the equations of motion for all currents generically have nonzero solutions. This suggests that, due to the coupling with the UV CFT, the pairing can occur spontaneously, without explicitly adding new terms to the action (there is no need to add an interaction for fermions in the bulk). Nevertheless, we will also analyze the situation with nonzero G_{int} and show what new phenomena it brings as compared to UV CFT-only coupling (i.e. no bulk coupling).

Let us start from the equations of motion. The Dirac and Klein-Gordon equations are to be complemented with the Maxwell equation

$$\begin{aligned}
\nabla^M F_{MN} &= iq_{\phi} (\phi^* (\nabla_N - iq_{\phi} A_N) \phi - \phi (\nabla_N + iq_{\phi} A_N) \phi^*) \\
&\quad - iq_{\psi} \bar{\psi} \Gamma_N \psi
\end{aligned} \tag{42}$$

which is reduced when the scalar is real, $\phi^* = \phi$, to

$$\nabla^M F_{MN} = 2q_{\phi}^2 \phi^2 A_N - iq_{\psi} \bar{\psi} \Gamma_N \psi. \tag{43}$$

In the background of a dyonic black hole with the metric

$$ds^2 = \frac{1}{(1-z)^2} \left(-f dt^2 + \frac{dz^2}{f} + dx^2 + dy^2 \right) \tag{44}$$

the Maxwell equation for the component A_0 is

$$\partial_z^2 A_0 - \frac{2q_{\phi}^2 \phi^2}{(1-z)^2 f} A_0 - \frac{iq_{\psi} J_+}{(1-z)^2 f} = 0 \tag{45}$$

where we have used $\bar{\psi} \Gamma_0 \psi \rightarrow -J_+$.

In our setup we ignore the backreaction to $A_2 = Hx$, treating it as a fixed external field. The justification comes from the physics on the field theory side: we consider a stationary nonmagnetic system with zero

current and magnetization density. In the bulk, this means that the currents sourced by—and backreacting to—the magnetic field arise as corrections of higher order that can be neglected to a good approximation.⁵ Inclusion of the second Maxwell equation for A_2 would likely only lead to a renormalization of the magnetic field $H \mapsto H + \delta H$ without quantitative changes of the physics.

The equations of motion for the matter fields read

$$\begin{aligned}
e_A^M \Gamma^M (\tilde{D}_M^{\psi} - iq_{\psi} A_M) \psi - m_{\psi} \psi - iG_{\text{int}} \phi \Gamma \psi &= 0, \\
-(\partial_M - iq_{\phi} A_M) (\partial^M - iq_{\phi} A^M) \phi + \frac{1}{2} \frac{\phi}{|\phi|} V'(|\phi|) \\
- \frac{1}{2} G_{\text{int}} \bar{\psi} \Gamma \psi &= 0
\end{aligned} \tag{47}$$

where we included the connection to the definition $\tilde{D}_M = \nabla_M + \frac{1}{4} \omega_{Mab} \Gamma^{ab}$. In the dyonic black hole background, the Dirac equation is

$$\begin{aligned}
\left[(\partial_z + \mathcal{A}) \Gamma^z - \frac{i(\omega + qA_0)}{f} \Gamma^t - \frac{m}{\sqrt{f}(1-z)} \right. \\
\left. \mp \frac{iG_{\text{int}} \phi}{\sqrt{f}(1-z)} - U^{-1} \frac{\lambda_n}{\sqrt{f}} \right] \psi = 0
\end{aligned} \tag{48}$$

⁵To see this, consider the corresponding Maxwell equation

$$\partial_z^2 A_2 + \frac{\partial_z f}{f} \partial_z A_2 = \frac{2q_{\phi}^2 \phi^2}{\sqrt{f}(1-z)^3} A_2 + \frac{iq_{\psi}}{\sqrt{f}(1-z)^3} K_+, \tag{46}$$

and insert the ansatz $A_2 = Hx + \delta(z, x)$. The resulting relation for the neutral scalar $q_{\phi} = 0$ $\partial_z (f \partial_z \delta) = -q/(\sqrt{f}(1-z)^3)$ predicts $K \sim \bar{\psi}_{\alpha} \sigma^3 \psi_{\alpha} \sim \delta$, compared to the analogous estimate for the electrostatic backreaction $J \sim \bar{\psi}_{\alpha} \sigma^1 \psi_{\alpha} \sim \mu$. Thus the spatial current is of order of the small correction to the field, δ . The reason obviously lies in the fact that the magnetic monopole sources a z -independent field.

where $q_\psi \equiv q$, the scalar is neutral $q_\phi = 0$, $m_\psi \equiv m$ and

$$\begin{aligned} \mathcal{A} &= \frac{1}{2} \left(\frac{3}{(1-z)} + \frac{f'}{2f} \right), & A_0 &= \mu z, \\ \lambda_n &= \sqrt{2qhn}, & U^{-1} &= \begin{pmatrix} i\sigma^2 & 0 \\ 0 & i\sigma^2 \end{pmatrix} \end{aligned} \quad (49)$$

with $f' \equiv \partial_z f$. In the limit $\omega = 0$ it is written as follows:

$$\begin{aligned} \left(\partial_z + \mathcal{A} - \frac{iqA_0}{f} \sigma^2 + \frac{m}{\sqrt{f}(1-z)} \sigma^3 \right. \\ \left. \pm \frac{iG_{\text{int}}\phi}{\sqrt{f}(1-z)} \sigma^3 + \frac{\lambda_n}{\sqrt{f}} \sigma^1 \right) \psi_{1;2} = 0. \end{aligned} \quad (50)$$

We write the bilinears in short as

$$\begin{aligned} I_\pm &= \psi_1^\dagger \sigma^1 \psi_1 \pm \psi_2^\dagger \sigma^1 \psi_2, \\ J_\pm &= \psi_1^\dagger \psi_1 \pm \psi_2^\dagger \psi_2, \\ K_\pm &= \psi_1^\dagger \sigma^3 \psi_1 \pm \psi_2^\dagger \sigma^3 \psi_2, \end{aligned} \quad (51)$$

with $\bar{\psi}_1 \equiv \psi_1^\dagger i\sigma^1$. Therefore $I_- = (-i)\bar{\psi}\Gamma\psi$ because $\bar{\psi} = \psi^\dagger \Gamma^t$. We rewrite the Dirac equation for the bilinears

$$\begin{aligned} (\partial_z + 2\mathcal{A})J_\pm + \frac{2m}{\sqrt{f}(1-z)}K_\pm + \frac{2\lambda_n}{\sqrt{f}}I_\pm \\ + \frac{2iG_{\text{int}}}{\sqrt{f}(1-z)}\phi K_\mp = 0, \\ (\partial_z + 2\mathcal{A})I_\pm + \frac{2qA_0}{f}K_\pm + \frac{2\lambda_n}{\sqrt{f}}J_\pm = 0, \\ (\partial_z + 2\mathcal{A})K_\pm - \frac{2qA_0}{f}I_\pm + \frac{2m}{\sqrt{f}(1-z)}J_\pm \\ + \frac{2iG_{\text{int}}}{\sqrt{f}(1-z)}\phi J_\mp = 0. \end{aligned} \quad (52)$$

The pairing parameter is obtained by averaging the current I_-

$$\Delta = iG_{\text{int}}\langle I_- \rangle. \quad (53)$$

This system should be accompanied by the equation of motion for the neutral scalar field. In the limit of $\omega = 0$ and $k_i = 0$ it is given by

$$-\frac{1}{\sqrt{-g}}\partial_z \left(\sqrt{-g} \frac{1}{g_{zz}} \partial_z \phi \right) + \frac{1}{2}V'(|\phi|) - \frac{1}{2}G_{\text{int}}\bar{\psi}\Gamma\psi = 0 \quad (54)$$

where $g \equiv \det g_{MN}$. In the dyonic black hole background, the equation of motion for the scalar is

$$\partial_z^2 \phi + \mathcal{B}\partial_z \phi - \frac{m_\phi^2}{f(1-z)^2} \phi + \frac{iG_{\text{int}}}{2f(1-z)^2} I_- = 0 \quad (55)$$

where

$$\mathcal{B} = \frac{2}{(1-z)} + \frac{f'}{f}. \quad (56)$$

The system of equations (52) and (55) is solved, at the lowest Landau level, for the unknown I_\pm, J_\pm, K_\pm and ϕ . We do not consider the backreaction of the spinor and scalar fields to the gauge field, and therefore we omit the Maxwell equation (45).

Since the magnetic field is encapsulated in the parameter mapping (16), we may put $\lambda_n = 0$ and use the rescaled fermion charge; furthermore, the terms proportional to off-shell (discrete) momentum cancel out due to symmetry reasons, as explained in Ref. [6]. Another key property of the magnetic systems is that, at high magnetic fields, the ratio μ_{eff}/T can approach zero at arbitrarily small temperatures (including $T \rightarrow 0$).

Next we set up boundary conditions at the IR and UV for the system of equations (52). It is enough to establish the boundary conditions for the fermion components. At the horizon we choose the incoming wave into the black hole. However, as we consider static solutions $\omega = 0$, it is enough to take a regular solution, not growing to infinity as we approach horizon. We write the Dirac equation at the horizon $z \sim 0$ for the upper component $\psi_1 = (y_1, y_2)$,

$$\begin{aligned} \left(\partial_z + \mathcal{A} - \frac{i\mu q z}{f} \sigma^2 + \frac{m + G_{\text{int}}\phi}{\sqrt{f}(1-z)} \sigma^3 + \frac{\lambda_n}{\sqrt{f}} \sigma^1 \right) \begin{pmatrix} y_1 \\ y_2 \end{pmatrix} = 0, \\ \mathcal{A} = \frac{1}{2} \left(\frac{3}{1-z} + \frac{f'}{2f} \right) \end{aligned} \quad (57)$$

where at $T = 0$ the metric factor is $f = z(3 - 3z + z^2 - 3(1-z)^3)$. Near the horizon it becomes

$$\left(\partial_z + \frac{1}{2z} - \frac{i\mu_q}{6z} \sigma^2 + \frac{m + G\phi}{z\sqrt{6}} \sigma^3 + \frac{\lambda_n}{z\sqrt{6}} \sigma^1 \right) \begin{pmatrix} y_1 \\ y_2 \end{pmatrix} = 0. \quad (58)$$

Explicitly, the system is written as

$$\begin{aligned} \partial_z y_1 + \frac{1}{z} \left(\frac{1}{2} + \frac{m + G_{\text{int}}\phi}{\sqrt{6}} \right) y_1 + \frac{1}{z} \left(\frac{\lambda_n}{\sqrt{6}} - \frac{\mu_q}{6} \right) y_2 = 0, \\ \partial_z y_2 + \frac{1}{z} \left(\frac{1}{2} - \frac{m + G_{\text{int}}\phi}{\sqrt{6}} \right) y_2 + \frac{1}{z} \left(\frac{\lambda_n}{\sqrt{6}} + \frac{\mu_q}{6} \right) y_1 = 0. \end{aligned} \quad (59)$$

The solution reads

$$\begin{aligned} y_1 &= C_1 z^{-\frac{1}{2}-\nu} + C_2 z^{-\frac{1}{2}+\nu}, \\ y_2 &= \frac{1}{\frac{\mu_q}{6} - \frac{\lambda_n}{\sqrt{6}}} \left(C_1 \left(\frac{m + G_{\text{int}}\phi}{\sqrt{6}} - \nu \right) z^{-\frac{1}{2}-\nu} \right. \\ &\quad \left. + C_2 \left(\frac{m + G_{\text{int}}\phi}{\sqrt{6}} + \nu \right) z^{-\frac{1}{2}+\nu} \right) \end{aligned} \quad (60)$$

where C_1, C_2 are constants and

$$\nu = \frac{1}{6} \sqrt{6(m + G_{\text{int}}\phi)^2 + 6\lambda_n^2 - \mu_q^2}. \quad (61)$$

We choose the solution with the regular behavior $y \sim z^{-\frac{1}{2}+\nu}$. The solution for z_i in the lower component $\psi_2 = (z_1, z_2)$ where $\psi = (\psi_1, \psi_2)$ is obtained from y_i by a substitute $G_{\text{int}} \rightarrow -G_{\text{int}}$. We have for the bilinear combinations

$$\begin{aligned} I_{\pm} &= y_1^{\dagger} y_2 + y_2^{\dagger} y_1 \pm (y \rightarrow z), \\ J_{\pm} &= y_1^{\dagger} y_1 + y_2^{\dagger} y_2 \pm (y \rightarrow z), \\ K_{\pm} &= y_1^{\dagger} y_1 - y_2^{\dagger} y_2 \pm (y \rightarrow z), \end{aligned} \quad (62)$$

where $\psi_1 = (y_1, y_2)$ and $\psi_2 = (z_1, z_2)$.

We impose two boundary conditions for Eq. (55): at the horizon $\phi'(z=0) = 0$ and at the AdS boundary $\phi(z=1) = 0$.

At the AdS boundary, the boundary conditions for the currents are known from Ref. [6]: one should extract the normalizable components of J, I, K in order to read off the expectation values. However, a normalizable solution is defined in terms of an absence of a source for the fundamental Dirac field ψ_{α} rather than the composite fields such as J_{\pm} . The solution is to put the source of the Dirac field to zero and then to read off the desired normalizable solution for J_{\pm} directly. Under the assumption that the electrostatic potential A_0 is regular, from Eq. (20) the composite field densities behave near the AdS boundary $z_0 = 1$ as

$$\begin{aligned} \mathcal{J}_1 &= \psi_1^{\dagger} \psi_1 \rightarrow a_1^2 (1-z)^{3-2m} + b_1^2 (1-z)^{3+2m}, \\ \mathcal{I}_1 &= \psi_1^{\dagger} \sigma^1 \psi_1 \rightarrow a_1 b_1 (1-z)^3, \\ \mathcal{K}_1 &= \psi_1^{\dagger} \sigma^3 \psi_1 \rightarrow a_1^2 (1-z)^{3-2m} - b_1^2 (1-z)^{3+2m}, \end{aligned} \quad (63)$$

and

$$\begin{aligned} \mathcal{J}_2 &= \psi_2^{\dagger} \psi_2 \rightarrow a_2^2 (1-z)^{5-2m} + b_2^2 (1-z)^{5+2m}, \\ \mathcal{I}_2 &= \psi_2^{\dagger} \sigma^1 \psi_2 \rightarrow a_2 b_2 (1-z)^5, \\ \mathcal{K}_2 &= \psi_2^{\dagger} \sigma^3 \psi_2 \rightarrow a_2^2 (1-z)^{5-2m} - b_2^2 (1-z)^{5+2m}. \end{aligned} \quad (64)$$

The currents we have defined in Eq. (41) are the averaged densities, e.g. $J_1 = \int d\omega d^2k \mathcal{J}_1$. A normalizable solution in $\mathcal{J}_{\pm} = \mathcal{J}_1 \pm \mathcal{J}_2$ is thus defined by the vanishing of both the leading and the subleading term.

In what follows the AdS evolution equations (52) and (55) with appropriate boundary conditions are solved numerically with a shooting method from the horizon. Unlike the recent study in Ref. [30] where only in the presence of the four-Fermi bulk coupling G_{int} one finds a nontrivial solution for the averaged current $\langle I_{-} \rangle$ with the IR boundary taken at $z=0$, we will generically have a nonzero expectation value even for $G_{\text{int}} = 0$. In Ref. [30], one needed to introduce an IR cutoff, such as the hard wall, positioned at a radial slice $z = z_{*}$. In our setup, the choice of the boundary conditions in the UV guarantees that the condensate will form irrespectively of the IR geometry, as it specifically picks the quasinormal mode of the fermion.

We repeat the same calculations for the x -component order parameter

$$\tilde{\Gamma} \equiv i\Gamma^x \Gamma^5 = \begin{pmatrix} 0 & 1 \\ 1 & 0 \end{pmatrix}. \quad (65)$$

The pairing current defined as

$$\tilde{I} = (-i) \int d\omega \int d^2k \bar{\psi}(\omega, k, z) \tilde{\Gamma} \psi(E - \omega, p - k, z) \quad (66)$$

requires us to introduce the following currents:

$$\begin{aligned} \tilde{J}_{\pm}(E, p, z) &= (-i) \int d\omega \int d^2k (\bar{\psi}_1(\omega, k, z) \sigma^1 \psi_2(E - \omega, p - k, z) \pm \bar{\psi}_2(\omega, k, z) \sigma^1 \psi_1(E - \omega, p - k, z)) \\ &\equiv \tilde{J}_1(E, p, z) \pm \tilde{J}_2(E, p, z), \\ \tilde{I}_{\pm}(E, p, z) &= (-i) \int d\omega \int d^2k (\bar{\psi}_1(\omega, k, z) \psi_2(E - \omega, p - k, z) \pm \bar{\psi}_2(\omega, k, z) \psi_1(E - \omega, p - k, z)) \\ &\equiv \tilde{I}_1(E, p, z) \pm \tilde{I}_2(E, p, z), \\ \tilde{K}_{\pm}(E, p, z) &= - \int d\omega \int d^2k (\bar{\psi}_1(\omega, k, z) \sigma^2 \psi_2(E - \omega, p - k, z) \pm \bar{\psi}_2(\omega, k, z) \sigma^2 \psi_1(E - \omega, p - k, z)) \\ &\equiv \tilde{K}_1(E, p, z) \pm \tilde{K}_2(E, p, z). \end{aligned} \quad (67)$$

A tilde is used to distinguish the two cases of pairings involving x and y components. Using the Dirac equation at $\omega = 0$

$$\left(\partial_z + \mathcal{A} - \frac{iqA_0}{f} \sigma^2 + \frac{m}{\sqrt{f}(1-z)} \sigma^3 + \frac{\lambda_n}{\sqrt{f}} \sigma^1 \right) \psi_{1;2} + \frac{iG_{\text{int}}\phi}{\sqrt{f}(1-z)} \sigma^3 \psi_{2;1} = 0 \quad (68)$$

where the pairing parameter is obtained by averaging the current \tilde{I}_+

$$\tilde{\Delta} = iG_{\text{int}}\langle\tilde{I}_+\rangle \quad (69)$$

we get the following set of coupled equations for the bilinears defined in Eq. (67):

$$\begin{aligned} (\partial_z + 2\mathcal{A})\tilde{J}_\pm + \frac{2m}{\sqrt{f}(1-z)}\tilde{K}_\pm + \frac{2\lambda_n}{\sqrt{f}}\tilde{I}_\pm \\ + \frac{2iG_{\text{int}}}{\sqrt{f}(1-z)}\phi K_+ = 0, \\ (\partial_z + 2\mathcal{A})\tilde{I}_\pm + \frac{2q\Phi}{f}\tilde{K}_\pm + \frac{2\lambda_n}{\sqrt{f}}\tilde{J}_\pm = 0, \\ (\partial_z + 2\mathcal{A})\tilde{K}_\pm - \frac{2q\Phi}{f}\tilde{I}_\pm + \frac{2m}{\sqrt{f}(1-z)}\tilde{J}_\pm \\ + \frac{2iG_{\text{int}}}{\sqrt{f}(1-z)}\phi J_+ = 0. \end{aligned} \quad (70)$$

There are no minus components for the $G_{\text{int}}\phi$ term in the first and third equations of Eq. (70), and these terms contain currents without tildes defined in Eq. (41). The equation of motion for the scalar is

$$\partial_z^2\phi + \mathcal{B}\partial_z\phi - \frac{m_\phi^2}{f(1-z)^2}\phi + \frac{iG_{\text{int}}}{2f(1-z)^2}\tilde{I}_+ = 0. \quad (71)$$

The system of equations (52), (55) and (70), (71) differ only in the G_{int} term: they are identical without it, though currents are defined differently. Therefore, provided there is no ‘‘source’’ in the equations of motion, i.e. there is no Yukawa interaction $G_{\text{int}} = 0$, the x and y components of gamma matrices produce the vacuum expectation values (VEVs)

$$\langle I_\pm \rangle = \langle \tilde{I}_\pm \rangle \quad (72)$$

and according to the definitions of the pairing parameters

$$\Delta \rightarrow \langle I_- \rangle, \quad \tilde{\Delta} \rightarrow \langle I_+ \rangle \quad (73)$$

where I_\pm is found from Eq. (52). However, the equations for the plus and minus components in Eq. (52) are identical. In particular,

$$\langle I_+ \rangle = \langle I_- \rangle \quad (74)$$

which proves that x - y rotational symmetry is intact and

$$\Delta = \tilde{\Delta}. \quad (75)$$

Further we consider only the y component for simplicity.

C. Quantum criticality in the electron-hole channel

1. Thermodynamic behavior

We will first use the bilinear formalism to inspect the thermodynamics, in particular the phase transition that happens at high magnetic fields and the behavior of the pair density after the phase transition has occurred. To detect the transition, we can simply plot the free energy (26) at a fixed temperature as a function of the magnetic field. The action can be rewritten in terms of the gauge field and currents as

$$S = \int dz d^3x \left(\frac{1}{2} \Phi \partial_{zz} \Phi + \frac{1}{2} H^2 - I_- \Delta \right) \quad (76)$$

and we need to include also the boundary term that fixes the boundary values of the gauge field:

$$S_{\text{bnd}} = \int d^3x \sqrt{-h} A_\mu n_\nu F^{\mu\nu} = \int d^3x \Phi \partial_z \Phi \quad (77)$$

where $n_\mu = (0, 0, 0, 1)$ is the unit normal to the AdS_4 boundary, and h is the induced metric for which $\sqrt{-h} = z_0^{-3}$. Identifying $\Phi(z_0) = \mu$ and $\partial_z \Phi(z_0) = \rho$ and using the Maxwell equation (45), we arrive at the final expression

$$\begin{aligned} \mathcal{F} &= \mathcal{F}_{\text{bulk}} + \mathcal{F}_{\text{bnd}} \\ &= \int d^3x \left(\frac{(1-z_0)^{1+2m}}{2\sqrt{f}} J_+ \Phi + \frac{1}{2} h^2 - I_- \Delta \right) \\ &\quad + \int d^3x \left(\frac{\mu}{2m+1} J_1^0 (1-z_0)^{1+2m} + \frac{1}{2} \mu \rho \right). \end{aligned} \quad (78)$$

In particular, we see that I_- is indeed the response to the bulk order parameter Δ . When the coupling G_{int} is set to zero, the I_- term in the bulk part of Eq. (78) will be absent. Let us first see what happens in that case. The free energy is then unaffected by the pairing, and we can only follow the dependence on the magnetic field (Fig. 1). We see the nonanalyticity in the free energy at the point $h = h_c$. The underlying mechanism can be understood from the mapping (16): it is the disappearance of the coherent quasiparticle due to the lowering of the effective chemical potential μ_{eff} . The pairing arises as a byproduct of the interaction with the boundary CFT and does not influence the transition.

With the contact interaction, corresponding to electron-hole attraction in the infrared, we can further rewrite Eq. (78) observing that generically

$$J_1(z, \omega) = \frac{1}{2} G_R(z, \omega) I_-(z, \omega), \quad (79)$$

which gives the following result for the fermionic free energy:

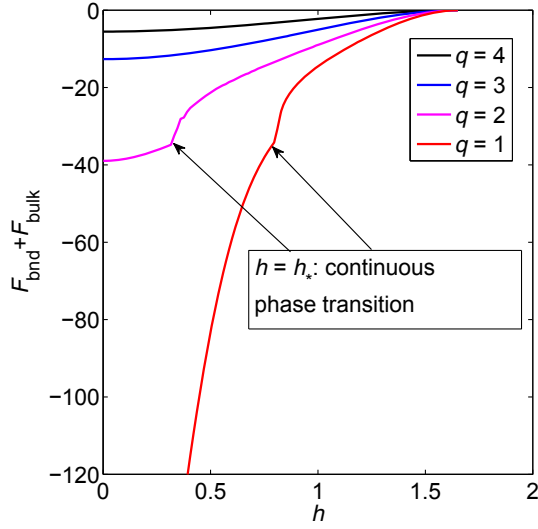


FIG. 1 (color online). Total (bulk plus boundary) free energy of the system $\mathcal{F}(h)$ for increasing values of the charge q . An explicit pairing term $G_{\text{int}} = 2$ has been chosen in order to suppress the stable Fermi surfaces and emphasize the phase transition at $h = h_*$. Still, for higher q values, the $\nu < 1/2$ quasiparticles become subdominant compared to $\nu > 1/2$ ones and the transition is lost. The bulk mass is $m = 0.10$.

$$\mathcal{F}_f = (1 - z_0)^{1+2m} J_1(z_0, \omega = 0) \left(\frac{3\mu}{4m+2} - 2\Delta G_R^{-1}(\omega = 0) \right). \quad (80)$$

The minus sign already makes it obvious that the derivative of the free energy can change sign, signifying a new critical point. To probe the transition point itself, however, we need to rewrite the relation (79) for on-shell values. Then the denominator of G_R vanishes, the current J_1 exactly captures the jump of the particle number on the Fermi surface [6] and Eq. (24) becomes $J_1 = 3\mu/(2m+1) \times Z$, so we need to replace $G_R \mapsto Z$, which gives the equation for the critical point:

$$\mathcal{F}_f = (1 - z_0)^{-2m} J_1(h) \left[\frac{3^{3/2} q}{4(\Delta_\Psi - 1)} \sqrt{1 - \frac{h^2}{3}} - \frac{2G_{\text{int}} I_-(h)}{Z(h)} \right]. \quad (81)$$

We have also used $\Delta_\Psi = 3/2 + m$ in order to write the equation purely in terms of the boundary quantities, and emphasized that Z and J_1 are also complicated functions of h , since h determines the effective chemical potential. Notice that only \mathcal{F}_{bnd} contributes to the fermionic term, while both $\mathcal{F}_{\text{bulk}}$ and \mathcal{F}_{bnd} contribute to the gauge field term. For $G_{\text{int}} = 0$, the second term vanishes and the free energy can only have a nonanalyticity when $J_1(h_c)$ has it. It is a first-order transition already identified in the magnetic case in Ref. [15] and studied from a more general viewpoint in Ref. [6]: the magnetic field depletes the Landau levels of

their quasiparticles and the Fermi surface vanishes. This first-order jump happens at some critical μ_{eff} and we will denote the corresponding value of the magnetic field by h_c . If, however, G_{int} becomes finite, we can see that the first term decreases with h while the second increases, since $Z(h)$ decreases. Thus, the overall free energy $\mathcal{F} = \mathcal{F}_f + \mathcal{F}_{\text{gauge}}$ will have a saddle point ($\mathcal{F}_{\text{gauge}}$ always decreases with h). We can now conclude that the following behavior with respect to G_{int} can take place:

- (i) For $0 \leq G_{\text{int}} < G_{\text{int}}^0$, the second term in Eq. (81) is always negligible and the system only has the first-order transition at $h = h_c$.
- (ii) For $G_{\text{int}}^0 < G_{\text{int}} < G_{\text{int}}^1$, the interplay of the first and the second term in Eq. (81) gives rise to a local stationary point (but not an extremum) at some $h = h_*$. This can potentially be a new critical point. In order to understand it better we will later perform a detailed analysis of the infrared behavior of the currents. It will turn out that it can be either a second-order transition or an infinite-order, Berezinsky-Kosterlitz-Touless (BKT)-type transition.
- (iii) For $G_{\text{int}} > G_{\text{int}}^1$, the Dirac hair cannot be formed and we have $J_1 = 0$ for any magnetic field, including zero. Since in this regime the pairing cannot occur even though G_{int} is large, this means we are in fact outside the applicability of the mean-field approach.

In Fig. 1 we show the second, arguably most interesting case. A second-order nonanalyticity in the free energy is obvious, as long as the stable quasiparticles with $\nu > 1/2$ do not overpower the unstable quasiparticles that govern the transition at $h = h_*$.

The conclusion we wish to emphasize is that order parameter physics is able to stabilize the non-Fermi liquids, while it is known [6,7] that in the absence of additional degrees of freedom a consistent backreaction treatment tends to leave only the stable, Fermi liquid surfaces. The physical nature of the point h_* will be the object of further analysis. The next section will reveal more on the actual pairing phenomenology, showing the new phase to be characterized by an anomalous, growing dependence $\Delta(h)$.

2. Analysis of critical points

Having analyzed the thermodynamics and found the existence of critical points, we will now study the behavior of the order parameter Δ in the most interesting regime, for $G_{\text{int}}^0 < G_{\text{int}} < G_{\text{int}}^1$, where the critical points are expected to appear.

In a nutshell, we will find that the region between G_{int}^0 and G_{int}^1 can be further subdivided into three regions, delimited by the values G_c^* , G_c^{**} and G_c , characterized by one or two second-order transitions or a BKT transition. We will also show that the pairing is favored for high effective chemical potentials when the density is high enough for the gravitational interaction to produce bound states. Finally, at small h values the pairs vanish as $\Delta \propto$

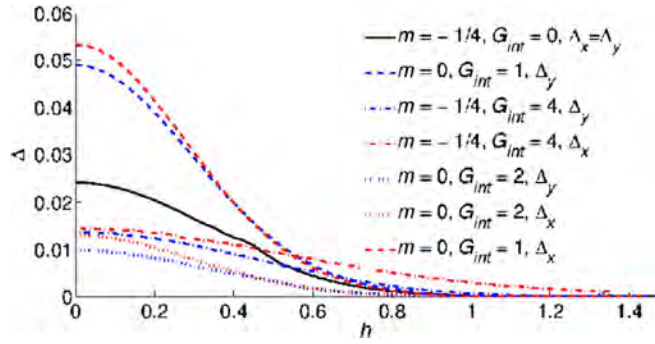


FIG. 2 (color online). Dependence for the x and y components of the pairing order $\Delta_x(h)$ and $\Delta_y(h)$ for $G_{\text{int}} = 0$ (coinciding solid line) and for $G_{\text{int}} = 1, 2, 4$ (dashed, dotted and dash-dotted lines). The coinciding solid line $\Delta_x = \Delta_y$ demonstrates the x - y rotational invariance. For $G_{\text{int}} > 0$, increasing the bare coupling decreases Δ (and lowers T_c) which provides a way to tune to the quantum critical point. Lowering the mass of the bulk fermion enhances pairing and increases Δ as seen for $m = 0$ and $m = -1/4$.

$\exp((T_c - T)^\beta)$ with $0 < \beta < 1$ (presumably $\beta = 1/2$) and finally reach zero density $\Delta = 0$ for $T \leq T_c$, while for higher magnetic fields the trend is reversed and the order parameter starts growing with h .

In order to construct the phase diagram, we will first study $\Delta(h)$ at fixed temperature [Fig. 3(a)]. We see that for $m = -1/4$ (smooth curves) the gap vanishes following a function which is smoother than a power law. Indeed, it turns out that for $h < h_c$ we have the infinite-order BKT scaling behavior

$$\Delta \sim \mu \exp\left(-\frac{C}{2\sqrt{q}(h_c - h)}\right). \quad (82)$$

The scaling (82) will be proven in Sec. IV. Similar behavior has been obtained in Ref. [32] where the scalar mass has been tuned to the quantum phase transition: $\Delta \sim \mu \exp\left(-\frac{C}{2\sqrt{m_c^2 - m^2}}\right)$. Notice also that the value h_c is very high, corresponding to the magnetic length of the order $\sqrt{h\mu_{\text{eff}}^2} \sim 10^2$ (we use $1/\mu_{\text{eff}}$ as the natural unit of length).

The above behavior is characteristic of the normal metal parent materials, i.e. $\nu_{k_F} > 1/2$. At small values of ν_{k_F} (i.e. Δ_Ψ close to $3/2$ or small μ_q), the anomalous growing dependence $\Delta(h)$ appears (found also in the previous section at strong enough magnetic fields) as shown by the dashed curves in Fig. 3(a). The nature of the dependence $\Delta(h)$ is rooted in the unstable Fermi surfaces with $\nu_{k_F} \rightarrow 0$ and can be understood from the analysis of the bilinear equations in the AdS_2 region, which we postpone until the next section.

We study the relation $\Delta(h)$ at different values of the pairing coupling G_{int} . For $G_{\text{int}} > 0$, Δ decreases as we increase G_{int} : repulsive interaction destructs the pairing, as given in Fig. 2. For $G_{\text{int}} < 0$, Δ increases as the absolute value of G_{int} is increased: attractive interaction triggers and enhances the pairing, as given in Fig. 3(b). Combining the two cases, when the sign of G_{int} is taken into account, the dependence Δ versus G_{int} is decaying. Lowering the mass of the bulk fermion enhances pairing as can be seen by comparing cases $m = 0$ and $m = -1/4$ in Fig. 2. As shown in Fig. 2, pairing parameters with the x and y components

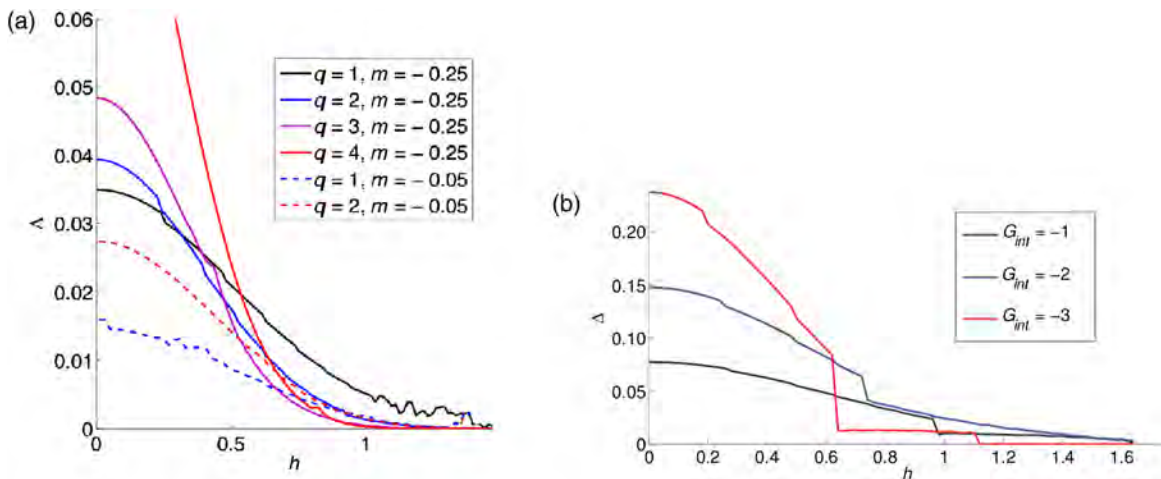


FIG. 3 (color online). (a) Dependence $\Delta(h)$ (in dimensionless units) for $m = -1/4$ (smooth lines) and $m = -1/20$ and for increasing values of the fermion charge. At fixed fermion charge in the Fermi liquid regime ($\nu_{k_F} < 1/2$), the magnetic field reduces the pair density, while small charges reduce the number of pairing particles, thus also reducing $\langle \Delta \rangle$. In the non-Fermi liquid regime ($\nu_{k_F} > 1/2$) for $h > h_c$ we observe an anomalous, power-law growing behavior of the gap. (b) Dependence $\Delta(h)$ for $m = -1/4$ and the negative bulk coupling G_{int} . For increasing absolute values of the bulk coupling G_{int} the pairing order Δ is enhanced. A new value h_* arises where the order parameter drops to zero due to competition between the channel K_1 and the quasiparticle density channel I_1 . For a large absolute value of G_{int} eventually $h_* = 0$ and we are out of the mean-field regime. The temperature is $T = 5.6 \times 10^{-4}$.

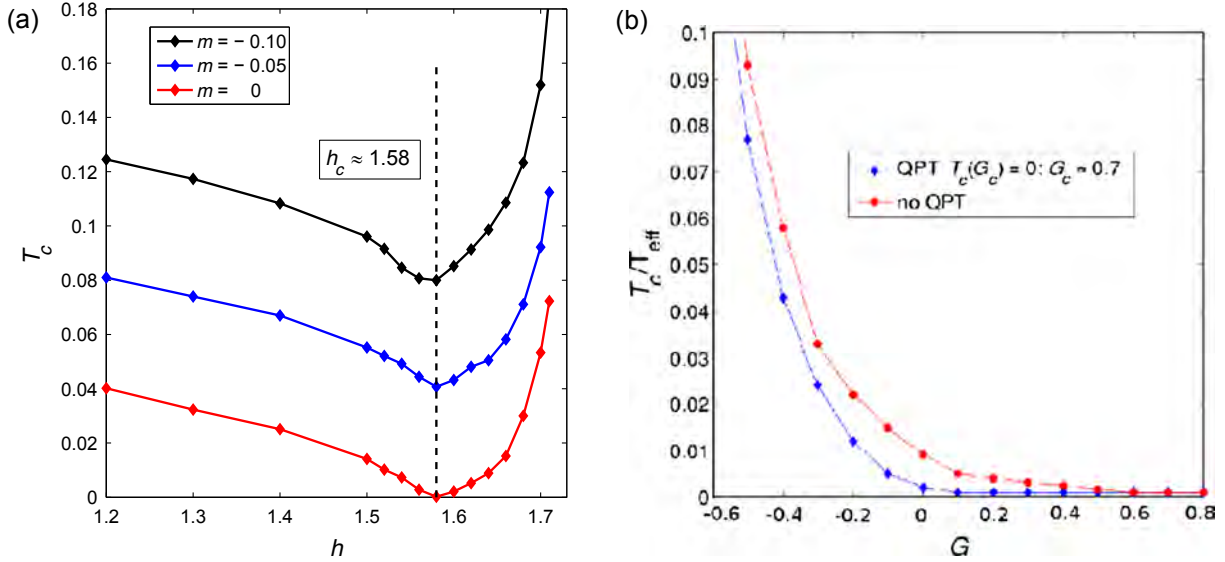


FIG. 4 (color online). Critical temperature T_c vs the magnetic field (a) and the coupling G_{int} (b), for $q = 1$. In (a), we again see the anomalous branch starting at $h_c \approx 1.58$, that signifies the exit from the Landau-Ginzburg regime and the mean field scaling into a new phase. Higher curves do not possess the QCP and arise when the system is always in the condensed phase. The coupling is $G = 0.7$. In (b), we see T_c vanish at the QCP $G_c \approx 1.1$, corresponding to the QPT with a non-mean field exponent $T_c \sim |G_c - G|^\beta$, $\beta > 1$. In the higher curve, T_c remains nonzero for all G_{int} , with no QPT for this set of parameters. The bulk mass is $m = -0.10$.

are identical for $G_{\text{int}} = 0$, which proves that the x - y plane rotational symmetry is intact. As G_{int} is switched on, it disrupts pairing in both channels in a slightly different way causing Δ_x and Δ_y to deviate from each other. An important novel feature distinguishing $G_{\text{int}} > 0$ and $G_{\text{int}} < 0$ is the appearance of the second anomalous branch for $G_{\text{int}} < 0$ as seen in Fig. 3 where the magnetic field enhances pairing: the rising $\Delta(h)$ manifests magnetic catalysis (MC).

The motivation to consider $G_{\text{int}} > 0$ was the ability to reduce the critical temperature to zero and to tune to the quantum critical point. On the other hand, adding $G_{\text{int}} < 0$ increases the critical temperature; however we can tune to vanishing T_c by adjusting other parameters such as the magnetic field. Figures 2 and 3(b) can be used to extract the quantum critical point (QCP) $h = h_c$ when $\Delta = 0$ (or $T_c = 0$) at fixed G_{int} . Upon varying the coupling G_{int} , the QCP becomes the quantum critical line (QCL) $h_c(G_c)$ or $G_c(h_c)$. In Fig. 3(b), for growing G_c , h_c decreases in the normal branch and h_c increases in the anomalous branch. In the normal branch, h depletes the particles from the Fermi surface decreasing the pairing density. Therefore h destroys the condensate. In the anomalous branch though, h enhances the condensation (magnetic catalysis).

The next step toward the phase diagram is the dependence of the critical temperature on the external magnetic field $T_c(h)$. A typical situation is given in Fig. 4(a). We have captured both branches so we see the expected twofold behavior, with the decrease of T_c up to $h = h_c$ and a subsequent increase. A precise tuning of the mass toward zero is necessary to enter the quantum critical regime where $T_c(h_c) = 0$. For reference, we have also

shown the cases $m = -0.10$ and $m = -0.05$, where the approach of the critical point is seen but $T_c(h_c)$ is still a finite minimum.

Figure 4(b) shows the decreasing dependence of the critical temperature T_c vs the coupling strength G_{int} . For the blue curve T_c vanishes at the QCP $G_c \approx 1.1$. It corresponds to the quantum phase transition (QPT) of the second order with a non-mean field exponent $T_c \sim |G_c - G|^\beta$, $\beta > 1$. For the red curve, T_c remains nonzero for all couplings G_{int} . It happens when the system is always in the condensed phase (an extreme RN-AdS black hole is unstable) [33]. As seen from Fig. 4(b), G_{int} is a sensitive “knob” to adjust the critical temperature T_c .

Finally, after studying the influence of the fermion charge q and the bulk mass m on the relation $T_c(h)$, we conclude with Fig. 5, showing the critical temperature vs the magnetic field for different couplings G_{int} . We find *four distinct regimes* located in the interval $G^0 < G < G^1$ (we omit the “int” subscript in G_{int} for now). The delimiting points are denoted by G_c^* , G_c^{**} and G_c , with $G^0 < G_c^* < G_c^{**} < G_c < G^1$.

- (i) For $G < G_c^*$ the critical temperature is nonzero, as demonstrated in Fig. 4(b) and also by the red curve in Fig. 5. There is thus no QCP and the normal and anomalous regimes are separated by a crossover.
- (ii) For $G_c^* < G < G_c^{**}$, there are two second-order phase transitions, one for the normal and one for the anomalous branch. This case is represented by the blue curve in Fig. 5, and can also be seen in Fig. 3(a). The quantum phase transition corresponding to the anomalous branch scales with a non-mean

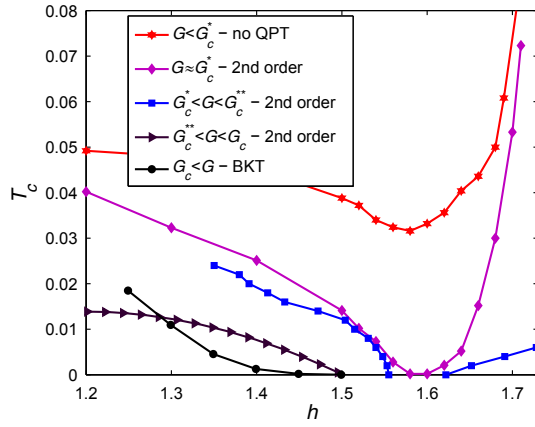


FIG. 5 (color online). Critical temperature T_c vs the magnetic field h for different couplings G_{int} . Depending on the coupling G_{int} , there are the BKT and second-order phase transitions. At $T_c = 0$, the QCP becomes QCL (h_c, G_c) with a decreasing/increasing dependence on h_c as G_c is increased which corresponds to the normal/anomalous branch.

field exponent $T_c \sim |h_c - h|^{\delta'}$, $\delta' > 1$. The limiting case of $G = G_c^*$ is given by the magenta curve, where the two critical points coincide.

- (iii) For $G_c^{**} < G < G_c$, there is the second-order phase transition with the non-mean field exponent $T_c \sim (h_c - h)^\delta$, $\delta < 1$, which describes the normal branch. This is the dark violet curve in Fig. 5, similar to the regime in Fig. 3(b).
- (iv) For $G > G_c$, there is an infinite-order phase transition of the BKT type with the characteristic exponential scaling $T_c \sim \exp(-\frac{C}{\sqrt{h_c - h}})$. This is the black curve in the figure.

Finally, based on the data from Fig. 5 and some additional calculations, we can draw the phase diagram in terms of the magnetic field h and the coupling G_{int} , given in Fig. 6. The QCL (solid line) separates the condensed (ordered) from uncondensed (disordered) phases. The position of the QCL is extracted from the phase transition curve of the critical temperature vs the magnetic field: the QCL where the critical temperature vanishes is given by the relation $G_c(h_c)$. From the dependence $G_c(h)$, one can translate the scaling exponents T_c vs G into T_c vs h : $T_c \sim |G_c - G|^\beta \rightarrow |G_c(h_c) - G|^\beta \rightarrow |h_c - h|^\delta$.

In Fig. 6, increasing the coupling G and the magnetic field h destroy the pairing condensate except in the non-Fermi liquid regime. This twofold behavior manifests itself through a double-valued function $h_c(G_c)$ in some parameter range. Indeed, the region with a condensed non-Fermi liquid is enhanced by the magnetic field, which is a consequence of the magnetic catalysis and the Callan-Rubakov effect discussed in the next section.

A deeper understanding of the phase diagram can be reached by considering the scaling dimensions of the condensate and the fermion field. With some foresight

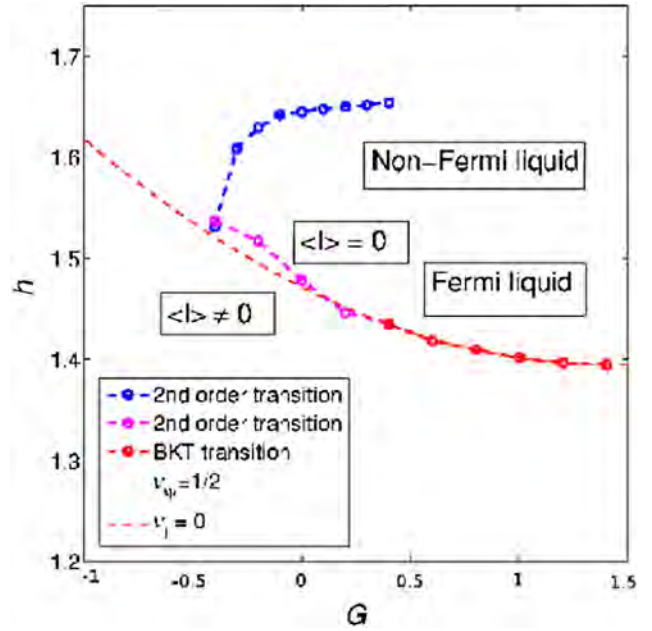


FIG. 6 (color online). Phase diagram h vs G for the condensed/normal (non-)Fermi liquids. G and h destroy the condensate except for the non-Fermi liquid. The ordered non-Fermi liquid is enhanced and stabilized by the strong magnetic field, which is also seen experimentally in pyrolytic graphite.

from the next subsection, we note that the IR conformal dimension of the operator which condenses $\delta_l = 1/2 + \nu_l$, where the bulk pairing current $\tilde{I} = \sqrt{c}I$ is the gravity dual of the excitonic condensate, is given by Eq. (95)

$$\nu_l = \sqrt{\frac{2}{3}} \sqrt{(m + \Delta)^2 + 2qh - \frac{\mu_q^2}{6}}. \quad (83)$$

On the other hand, the IR conformal dimension of the fermion operator $\delta_\psi = 1/2 + \nu_\psi$, where the bulk fermion field ψ is dual to the boundary fermion Ψ , is given by

$$\nu_\psi = \frac{1}{6} \sqrt{m^2 + k_F^2(h) - \frac{\mu_{q,\text{eff}}^2}{6}}, \quad \mu_{q,\text{eff}} = \sqrt{3q} \sqrt{1 - h^2/3}. \quad (84)$$

Importantly, the ratio ν_l/ν_ψ is first a decreasing and then an increasing function of the magnetic field h (see left panel of Fig. 8 in Ref. [15] for ν_ψ). At the dashed line the IR dimension ν_l of the operator with the gravity dual pairing current becomes imaginary, signaling the pairing instability. This is analogous to the instability of a scalar operator, when the Breitenlohner-Freedman (BF) bound in the AdS_2 is violated but the BF bound in the AdS_4 remains unbroken. The dash-dotted line corresponds to the locus of points in the phase diagram where $\nu_\psi = 1/2$, separating the Fermi liquid from the non-Fermi liquid behavior as

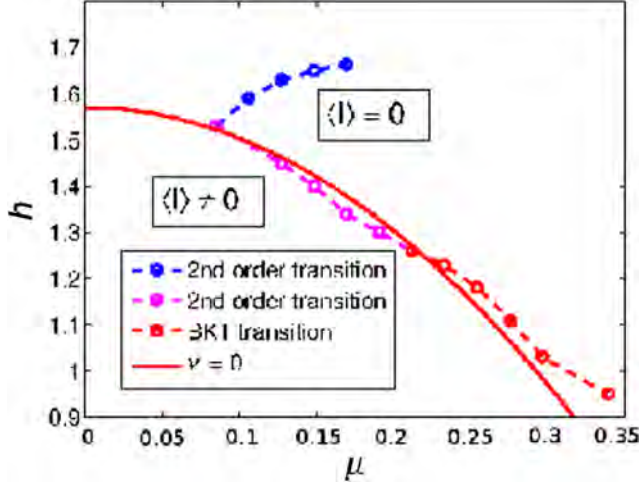


FIG. 7 (color online). Phase diagram h vs q for the condensed/normal (non-)Fermi liquids. Increasing the fermion charge at zero temperature is equivalent to increasing the chemical potential. It stabilizes the condensate in the anomalous regime and then destabilizes it in the normal branch. We can thus qualitatively relate q to G , the coupling constant from the previous figure.

discussed in Ref. [14]. Since $\nu_\psi(h)$ is a monotonically decreasing function, coherent quasiparticles disappear at large magnetic field resulting in the non-Fermi liquid regime at $\nu_\psi \leq \frac{1}{2}$ (upper part of the phase diagram). Notably, there is a similarity between our phase diagram (Fig. 6) and the phase diagram obtained for a scalar field (Fig. 14 in Ref. [16]), which uses the double-trace deformation as the control parameter. This may provide an insight into the mechanism of suppression/enhancement of the ordered phase at small/large magnetic fields.

We can redraw our phase diagram in terms of the magnetic field h vs the chemical potential μ (Fig. 7) to be able to compare our result with the literature [34].

It is worth noting that our phase diagram exhibits the same main features as the analogous phase diagram obtained using the Sakai-Sugimoto model (Fig. 8 in Ref. [34]). Primarily, it also has two regions of weak magnetic field where the condensate is destroyed by the magnetic field (“inverse” magnetic catalysis) and a regime of strong magnetic field which enhances the condensate (magnetic catalysis). Likewise, Fig. 5 shows the same structure as the analogous Fig. 9(b) in Ref. [34]. Thus there are two regimes with opposite dependence $\Delta(h)$ is a robust finding. We will discuss the reasons for it in the next section.

3. Pairing, double-trace deformations and conformal field theory

We will conclude our study of the phase diagram by offering an alternative viewpoint of the observed critical phenomena. Dialing the pairing coupling to drive the system toward QPT can also be understood as dialing the double-trace deformation in the boundary theory [16].

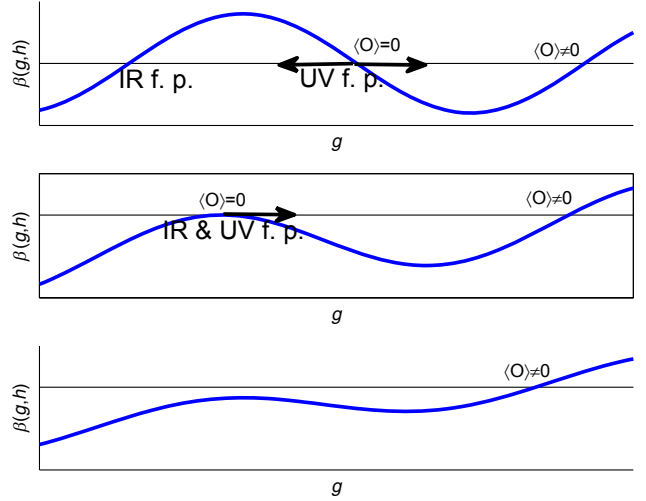


FIG. 8 (color online). Two-loop beta function for the double-trace coupling for decreasing magnetic field values. The disappearance of the original UV and IR fixed points at the critical magnetic field $h = h_c$ leads to conformality loss and the BKT scaling behavior, the middle panel. At $h < h_c$, the bottom panel, the system flows to a new IR fixed point with spontaneous symmetry breaking and nonzero condensate of a scalar field $\langle O \rangle \neq 0$.

For example, in the Gross-Neveu model with vector $SU(N_f)$ symmetry, the four-fermion coupling operator is relevant at the UV fixed point. Hence, as a relevant deformation in UV, it can drive the RG flow of the system to a new IR fixed point with spontaneous symmetry breaking. In holography, the multitrace deformations which are introduced on the boundary and correspond to the multiparticle states in gravity are a powerful knob that can drive the theory either to a free CFT at the IR fixed point or to a CFT with the spontaneously broken symmetry. An RG flow of this kind has been considered in Ref. [35], where the relevant double-trace deformation at the UV fixed point drives the theory toward the asymptotically free IR fixed point. In the gravity dual theory, it corresponds to different boundary conditions imposed at the AdS_4 boundary (alternative/standard quantization), and the UV and IR CFTs are related by a Legendre transform [35].

As an illustration, consider a scalar theory in the bulk as in Ref. [32]. One can hope that this case at least qualitatively captures the behavior of our system as a bilinear fermion combination bosonizes into a scalar field. Figure 8 shows schematically the two-loop beta function for the double-trace coupling for decreasing magnetic field value. At strong magnetic fields, Fig. 8 (top), the theory exhibits the usual RG flow from the strongly coupled UV fixed point (with a Landau pole at the QCP: $g_c \rightarrow \infty$) to a free fermion (a noninteracting theory at $g \rightarrow 0$) at the IR fixed point, with no expectation value for the scalar operator O . At the QCP i.e. $h = h_c$, Fig. 8 (middle), the UV and IR fixed points merge and annihilate, leading to the BKT scaling [36]

$$\Lambda_{\text{IR}} \sim \mu \exp\left(-\frac{C}{\sqrt{h_c - h}}\right) \sim \mu \exp\left(-\frac{C'}{\sqrt{g - g_c}}\right), \quad (85)$$

which can be interpreted as a distance along the RG trajectory to get to the nontrivial IR fixed point with broken symmetry. In this case, the QPT is of infinite order and where the critical temperature T_c and the order parameter $\langle O \rangle$ are governed by the exponential BKT scaling of Eq. (85) as $T_c \sim \langle O \rangle \sim \Lambda_{\text{IR}}$. When the magnetic field h is further decreased, Fig. 8 (bottom), the theory becomes gapped leading to an apparent conformality loss [36] and the QPT is now of second order.

In this paper we use the Yukawa coupling (or four-fermion coupling) in the bulk. However, the results we obtain are in line with the theory having a double-trace deformation on the boundary as described by Fig. 8: we have observed the rise of a new critical point. Figure 3(b) in particular conveys the message: at some $h_* < h_c$ we observe a transition from the quasiparticle regime to an electron-hole condensate. Formally, it comes from the competition between the pairing channel and the particle-photon interaction, encoded by the bilinears K_1 and I_1 . Physically, it corresponds to the competition between the Fermi surface “order” and the pairing order. At $h = h_c$, it is the entrance into the non-Fermi liquid region ($\nu < 1/2$) that drives the transition. At very high G_{int} values, the pairing is again suppressed which we interpret as the consequence of the Fermi surface depletion. The number density near the Fermi momentum is given by the current J_0 . In Eq. (52), it is clear that the gauge field term, encoding for the chemical potential (and implicitly density), is competing with the term containing $\Delta(r)$, i.e. the term proportional to the coupling G_{int} . When the latter is dominant, the pairing is highly enhanced but only up to the point that all electrons are “used up,” and their total number density is small. Notice also how Δ drastically increases at nonzero G_{int} , growing by about an order of magnitude.

D. AdS₂ analysis of the critical exponents

Most of our conclusions so far were driven by numerical results, with some qualitative analytical insight. A somewhat more detailed analytical understanding of the model can be gained by considering the far IR region, corresponding to the AdS₂ throat of the RN black hole.

We will follow the arguments of Ref. [32], where it was shown by analyzing the AdS₂ region that a new IR scale Λ_{IR} is generated which leads to the scaling behavior for the critical temperature T_c and the condensate Δ vs a tuning parameter (the magnetic field in our case). The key point of this analysis is to show that an instability for a scalar field develops in a certain parameter range. In particular, for a neutral scalar field the mass should be lower than the AdS₂ BF bound, $m^2 R^2 < -\frac{3}{2}$ (where R is the AdS₄ radius), which corresponds to a point where the IR conformal dimension

becomes imaginary. For a charged scalar, the mass value can be slightly higher if the product of the charge and the chemical potential, μ_q is sufficiently large. We therefore consider a composite bosonic field, which can be constructed as a bilinear combination of ψ 's and in our case it is given by a bulk current.

Let us start by recalling that at $T = 0$, the redshift factor develops a double zero near the horizon: $f \approx 6z^2$. Adopting the rescaled coordinates ζ, τ instead of the dimensionless coordinates z, t

$$\frac{1}{z} - 1 = \frac{\omega}{6\zeta}, \quad t = \frac{\tau}{\omega}, \quad (86)$$

with $\omega \rightarrow 0$ and ζ, τ finite, the metric (2) becomes near the horizon

$$ds^2 = \frac{1}{6\zeta^2}(-d\tau^2 + d\zeta^2) + dx^2 + dy^2, \quad (87)$$

where the gauge field is

$$A_\tau = \frac{\mu}{6\zeta}. \quad (88)$$

In this metric, the currents defined in Eq. (41) become

$$\begin{aligned} J(E, p, z) &= (-i) \int d\omega \int d^2 k \bar{\psi}(\omega, k, z) \sigma^1 \psi(E - \omega, p - k, z), \\ I(E, p, z) &= (-i) \int d\omega \int d^2 k \bar{\psi}(\omega, k, z) \psi(E - \omega, p - k, z), \\ K(E, p, z) &= - \int d\omega \int d^2 k \bar{\psi}(\omega, k, z) \sigma^2 \psi(E - \omega, p - k, z), \end{aligned} \quad (89)$$

with $\bar{\psi} = i\psi^\dagger \sigma^1$. The Dirac equation at $\omega = k = 0$ assumes the form

$$\left(\partial_\zeta - i \frac{\mu_q}{\sqrt{6}e_\zeta} \sigma^2 + \frac{(m + \Delta)}{e_\zeta} \sigma^3 + \frac{\lambda}{e_\zeta} \sigma^1, \right) \psi = 0, \quad (90)$$

giving the following equations of motion for the currents:

$$\partial_\zeta J + \frac{2(m + \Delta)}{e_\zeta} K + \frac{2\lambda}{e_\zeta} I = 0, \quad (91)$$

$$\partial_\zeta I + 2 \frac{\mu_q}{\sqrt{6}e_\zeta} K + \frac{2\lambda}{e_\zeta} J = 0, \quad (92)$$

$$\partial_\zeta K - 2 \frac{\mu_q}{\sqrt{6}e_\zeta} I + \frac{2(m + \Delta)}{e_\zeta} J = 0 \quad (93)$$

where $e_\zeta = \sqrt{6}\zeta$, $\mu_q = \mu q$, $h_q = h q$, $\lambda = 2|h_q|l$, $l = 1, 2, \dots$ and $\Delta = -(I)$. Differentiating the second equation for I with respect to ζ and eliminating the derivatives of J

and K currents from the other two equations, we obtain the zero-energy Schrödinger equation:

$$\partial_{\tilde{\zeta}}^2 \tilde{I} - \frac{\nu_{\tilde{l}}^2 - 1/4}{\tilde{\zeta}^2} \tilde{I} = 0, \quad (94)$$

$$\nu_{\tilde{l}} = \sqrt{\frac{2\lambda^2}{3} - \frac{\mu_q^2}{9}}, \quad (95)$$

where $\tilde{I} = I\sqrt{\tilde{\zeta}}$. We assume that condensation occurs for the lowest (first) Landau level ($l = 1$) and it is caused by an instability when $\nu_{\tilde{l}}$ becomes imaginary. Therefore we can represent the conformal dimension as

$$\tilde{\nu}_{\tilde{l}} = \sqrt{\frac{4}{3}(h_q^c - h_q)}, \quad h_q^c = \frac{\mu_q^2}{12} \quad (96)$$

where $\nu_{\tilde{l}} \equiv i\tilde{\nu}_{\tilde{l}}$, and h_q^c is found from the condition $\nu_{\tilde{l}} = 0$. Generalizing for $m \neq 0$ we get

$$\nu_{\tilde{l}} = \sqrt{\frac{2}{3}(\lambda^2 + m^2) - \frac{\mu_q^2}{9}}, \quad (97)$$

$$h_q^c = -\frac{m^2}{2} + \frac{\mu_q^2}{12}, \quad (98)$$

in dimensionless units.

Now consider the scaling behavior near the quantum critical point, $h \approx h_c$ or $G \approx G_c$ (solid red line in the phase diagram Fig. 6). As in Ref. [32], imposing the Dirichlet boundary condition $\tilde{I}(\zeta = \zeta_{\text{IR}}) = 0$ gives an oscillatory solution of Eq. (94):

$$I(\zeta) = \sin\left(\tilde{\nu} \log \frac{\zeta}{\zeta_{\text{UV}}}\right), \quad (99)$$

where ζ_{UV} is the location of the boundary of the AdS₂ throat. In order to satisfy the boundary condition we should have

$$\tilde{\nu} \log \frac{\zeta_{\text{IR}}}{\zeta_{\text{UV}}} = \pi. \quad (100)$$

According to the discussion in Sec. IV of Ref. [32], this means that a new IR scale is generated

$$\Lambda_{\text{IR}} \sim \frac{1}{\zeta_h} \sim \mu \exp\left(-\frac{\pi}{\tilde{\nu}}\right), \quad (101)$$

where μ is the UV scale, that leads to the infinite-order BKT scaling behavior:

$$\begin{aligned} T_c &\sim \mu \exp\left(-\frac{C}{\sqrt{h_q^c - h_q}}\right), \\ \Delta &\sim \mu \exp\left(-\frac{C}{2\sqrt{h_q^c - h_q}}\right), \end{aligned} \quad (102)$$

with $C = \frac{\pi}{\sqrt{4/3}}$ and h_q^c given by Eq. (98). The factor of 2 in the exponent comes from the difference in operator dimensions in the intermediate conformal regime: the current I scales as a dimension-1/2 operator and the temperature scales with dimension 1. Equation (102) describes the behavior below the critical magnetic field $h < h_c$, which can be seen in Fig. 5. Since $h_q = hq$, increasing the charge q would produce higher curves.

Choosing the mass m as a tuning parameter, we obtain the infinite-order BKT scaling behavior from the condition $\nu_{\tilde{l}} = 0$ in Eq. (98):

$$\begin{aligned} T_c &\sim \mu \exp\left(-\frac{C'}{\sqrt{m_c^2 - m^2}}\right), \\ \Delta &\sim \mu \exp\left(-\frac{C'}{2\sqrt{m_c^2 - m^2}}\right), \end{aligned} \quad (103)$$

with $C' = \frac{\pi}{\sqrt{2/3}}$ and $m_c^2 = -2h_q + \mu_q^2/6$. The scaling behavior from Eqs. (102) and (103) describes the BKT regime found also for the condensation of a scalar field in Ref. [32], with the condensed phase for $h < h_c$ (or at $m^2 < m_c^2$) and the normal state with zero condensate at $h > h_c$ (or at $m^2 > m_c^2$).

While the above analysis fits well into the results we have found for the normal branch, the anomalous branch, where at high $h > h_c$ the magnetic field catalyzes and enhances the condensate is still to be explained. The scaling behavior in this region is given by

$$T_c \sim \Delta \sim |h - h_c|^\delta, \quad (104)$$

where $\delta > 1$. In Figs. 3(a) and 4(a), a sharp increase with h is found, which is in agreement with field theory calculations of magnetic catalysis [22] and experiments on graphite in strong magnetic fields [18]. We leave the explanation of this regime within the AdS₂ analysis for further work.

For $m = 0$, the equation of motion for I can be reduced to a Schrödinger-like equation also in the general AdS₄ case. This is what we will do in the next subsection.

E. The $m = 0$ formalism

As elucidated before in a slightly different context [14], nonzero contributions to the current (corresponding to the quasiparticles at the boundary) are quantified by counting the bound states at zero energy for the formal wave function I_- of the above equation. An important novel feature in our

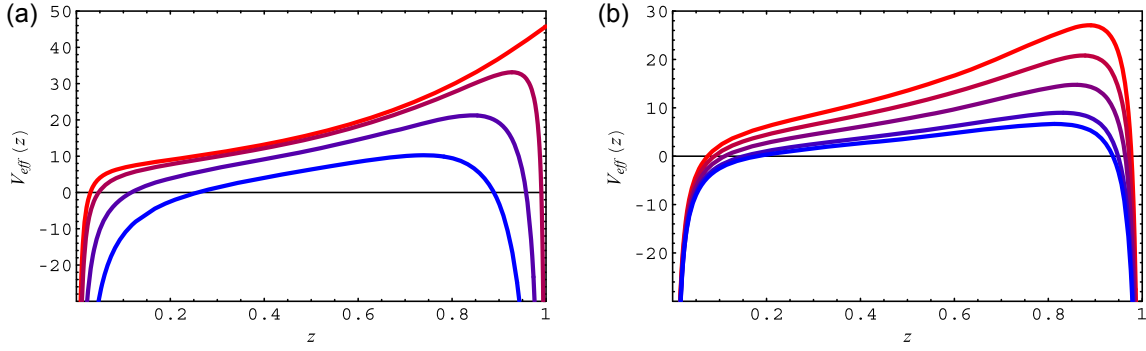


FIG. 9 (color online). Effective potential for the current \tilde{I}_- for $m = 0$, $q = 2$, $T = 0.001 \times 10^{-3}$ and $h = 0$, $G_{\text{int}} = 0, 1/3, 2/3, 1$ [red to blue, (a)] and $G_{\text{int}} = 0.2$, $h = 0, 0.50, 1.00, 1.50, 1.71$ [red to blue, (b)]. The pairing interaction opens the near-boundary gap (a), which gets wider but shallower as the magnetic field increases (b). The competition between the broadening and the shallowing effect gives rise to the transition between the normal and anomalous regime at $h = h_c$.

setup is that the momentum is quantized due to the magnetic field, and thus we cannot use the usual quasi-classical (WKB) formalism. Still, in the massless limit we will be able to gain some more insight by constructing an effective Schrödinger equation with a formal WKB momentum, that can be studied analytically.

Notice first that the RN geometry allows the spin connection term from Eq. (8) to be absorbed into the definition of the currents as it is a total derivative [14]:

$$\mathcal{A} = \partial_z(-gg^{zz})^{1/4}. \quad (105)$$

Upon implementing Eq. (105), the system (52) for $m = 0$ and in the static limit $\omega \rightarrow 0$ is simplified to

$$e_z \partial_z J_{\pm} + 2\Delta K_{\mp} + 2e_i \lambda I_{\pm} = 0, \quad (106a)$$

$$e_z \partial_z I_{\pm} + 2e_i \Phi K_{\pm} + 2\lambda e_i J_{\pm} = 0, \quad (106b)$$

$$e_z \partial_z K_{\pm} - 2e_i \Phi I_{\pm} + 2\Delta J_{\mp} = 0, \quad (106c)$$

where the vierbeine of the metric (2) are $e_z = (1-z)\sqrt{f}$, $e_i = (1-z)/\sqrt{f}$, $e_{\bar{i}} = (1-z)$, and the scalar potential is rescaled as $q\Phi \rightarrow \Phi$ to absorb q . As before, the magnetic field is implemented by rescaling the chemical potential and the fermion charge as given by Eq. (16), meaning that we can put $\lambda = 0$. The expectation values are given by the minus component, with only three coupled equations for J_- , K_- , I_- remaining to be solved. In order to understand the phenomenology of the bulk pair current, it is useful to eliminate J_- from Eq. (106). Rescaling I_- as

$$I_- \mapsto \tilde{I}_- \equiv I_- \frac{e_i \Phi}{e_z} \equiv I_- \tilde{\Phi} \quad (107)$$

we first easily eliminate J_- and differentiate Eq. (106b) with respect to z . The derivative $\partial_z K_-$ can be expressed from Eq. (106c) and K_- from Eq. (106b). In this way we arrive at the second-order equation involving I_- only and having the form of the Schrödinger equation for \tilde{I}_- :

$$\partial_{zz} \tilde{I}_- - \left[\frac{2\partial_z \tilde{\Phi}}{\tilde{\Phi}} + 4\tilde{\Phi}^2 - \Delta \partial_{zz} \log \tilde{\Phi} \right] \tilde{I}_- = 0. \quad (108)$$

Notice that the term containing the first derivative vanishes automatically due to the transform (107).

We are interested in the behavior of the current in the limit $z \rightarrow z_0 = 1$. While the Schrödinger formulation might in some cases be more convenient also for computational reasons, the real benefit is that we can use a formal WKB scheme to arrive at surprisingly accurate solutions without solving the differential equation. Equation (108) has the form $(\partial_{zz} - V_{\text{eff}}(z))\tilde{I}_- = 0$, where the effective potential obeys the inverse square law near the boundary [we also use the relation (69)]:

$$V_{\text{eff}}(z \rightarrow 1) = \delta^2(1-z) - \frac{8\Delta}{(1-z)^2} + \mu^2(1-z)^2 + O(1) \quad (109)$$

where $\Delta \equiv \Delta(z \rightarrow z_0) \approx \text{const}$; although, strictly speaking, one needs to compute Δ self-consistently given the value of G_{int} , for qualitative considerations we may assume a constant Δ proportional to G_{int} . The formal squared Dirac delta function is there to enforce the condition $J_{\pm}(z_0) = I_{\pm}(z_0) = K_{\pm}(z_0) = 0$. The typical appearance of the potential is given in Fig. 9. The development of the electron-hole condensate can be seen as the accumulation of bound states inside the potential well, analogously to the similar logic for electron states in Fermi and non-Fermi liquids, elucidated in Ref. [14] and applied in Ref. [37]. We can easily visualize our findings on the transition points $h = h_*$ and $h = h_c$ by looking at the potential (Fig. 9). In the figures, we have left out the Dirac-delta squared spike at the boundary, as it is completely localized and only ensures that the currents reach zero at $z = 1$, exerting no influence on the behavior at small but finite $1-z$ values. Importantly, the near-boundary gap opens with $\Delta > 0$, supporting the electron-hole pair

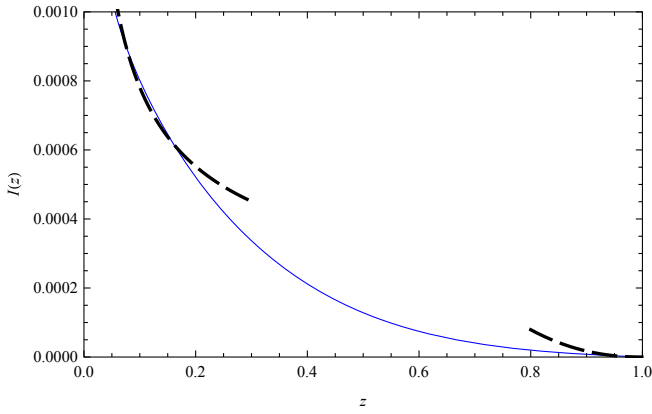


FIG. 10 (color online). Radial profile of the excitonic condensate (solid line) from the numerical solution of the effective Schrödinger equation. The transformation law between radial coordinates is $r = \frac{1}{1-z}$. The fits (dashed lines) are the asymptotic behaviors $(1-z)^3 \rightarrow \frac{1}{r^3}$ at $z \sim 1$ in the UV and $\frac{1}{z} \rightarrow \frac{1}{r-1}$ at $z \sim 0$ in the IR.

condensate near the boundary. The influence of the magnetic field through the relation $q \mapsto q\sqrt{1-H^2/(Q^2+H^2)}$ is subtler: it makes the potential well both broader and shallower. The former generally facilitates the formation of bound states, while the latter acts against it. It is this competition that gives rise to the transition from the normal toward the anomalous region at $h = h_c$.

Within the WKB approximation, the solution to Eq. (108) can be written as

$$\tilde{I}_-(z) = \frac{(1-z)^2}{\sqrt{V_{\text{eff}}(z)}} \left(\exp(-\sqrt{-V_{\text{eff}}(z)}) + \exp\left(\frac{3\pi}{4}i - \sqrt{V_{\text{eff}}(z)}\right) \right). \quad (110)$$

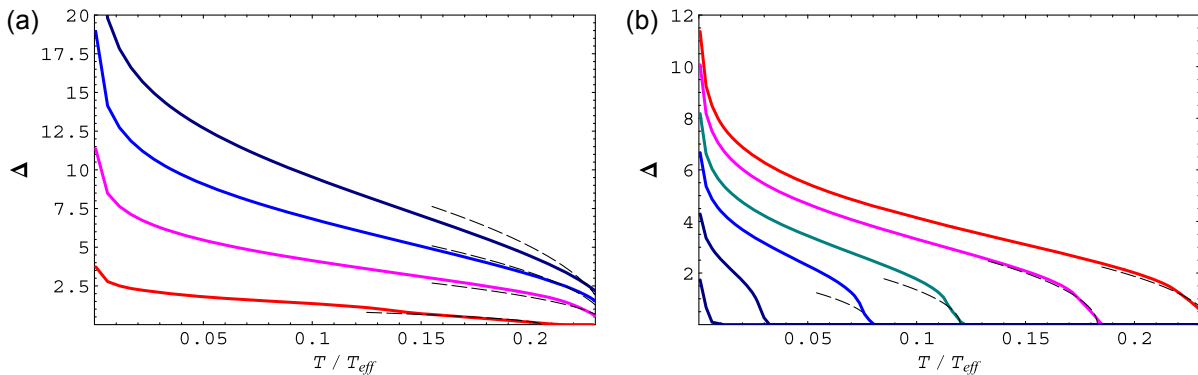


FIG. 11 (color online). Order parameter of the pair density Δ vs the temperature (all in dimensionless units) (a) for $h = 1$ and different values of the coupling strength $q = 1, 3, 5, 7$ (red, magenta, blue, black) and (b) for $q = 3$ and different values of the magnetic field $h = 0, 0.8, 1.2, 1.4, 1.6, 1.7$ (red to black). Pairing is favored in the overdamped phase, with stable quasiparticles for $q \gg 1$ and $\nu \sim 1$, and suppressed at very high magnetic fields when the effective chemical potential is lowered and thus only a small number of electrons is available for pairing.

We have constructed the solution by equating the WKB expansion with the near-boundary expansion [Eqs. (63) and (64)]. Notice that the phase shift is $3\pi/4$ instead of the usual $\pi/4$, as the boundary itself provides an additional $\pi/2$ shift due to the condition $I_-(z_0) \rightarrow 0$. The radial profile of the condensate is depicted in Fig. 10. It can be shown to have $\frac{1}{r^3}$ behavior at the UV boundary $r \rightarrow \infty$, and it diverges as $\frac{1}{r-1}$ at the horizon in the IR $r \rightarrow 1$. We obtain the same asymptotic behavior when $\Delta = 0$ in Eq. (109), but we impose the hard wall near the horizon in the IR, which brings us in agreement with the results of Ref. [30]. The UV behavior follows from the boundary condition on the fermion currents at the AdS boundary (putting the source term to zero) and the appearance of a fermion mass gap, to be discussed in more detail later.

Another advantage of the Schrödinger approach is that solving the Schrödinger equation numerically is easier than solving the current equations. In Figs. 11 and 12 we give the dependences $\Delta(h)$ and $\Delta(q)$, produced by solving the equation (108). Qualitatively similar behavior is seen in both cases. The WKB approach makes it feasible to study also the dependence on the fermion charge q . Figure 12 already shows that there is a critical value $q = q_c$ below which no pairing can occur at all. We conjecture that this value corresponds to $\nu < 1/2$, i.e. only stable quasiparticles can pair up. While plausible, this is not easy to see from the relations $\Delta(h)$ and $\Delta(T)$ that we obtained in the $m \neq 0$ case.

IV. SPECTRA AND THE PSEUDOGAP

In this section we will compute the spectra for the fermionic system with particle-hole pairs. We invoke again Eq. (15) to derive the equations of motion for the retarded propagator, which will directly give us the spectral function as $A(\omega, k) = \text{Im}G_R$.

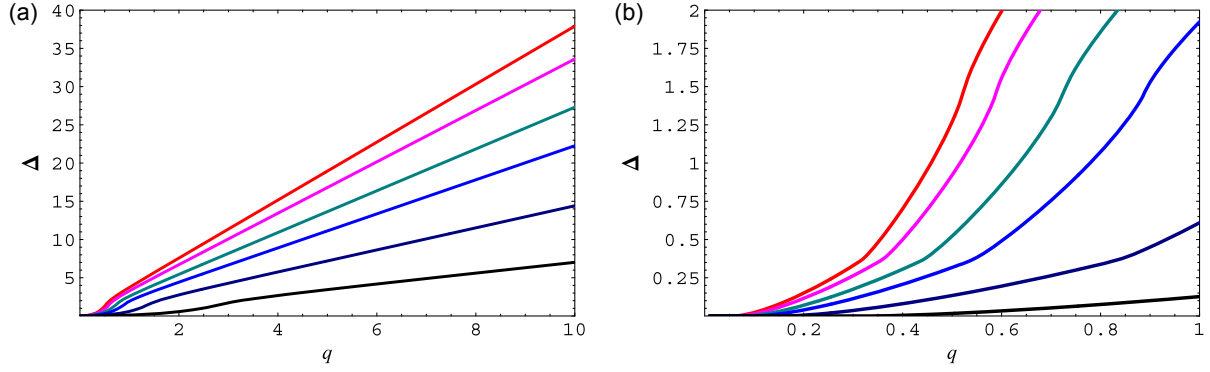


FIG. 12 (color online). (a) Order parameter of the pair density Δ vs the fermion charge q , for $T = 5.6 \times 10^{-4}$ and different values of the magnetic field $h = 0, 0.8, 1.2, 1.4, 1.6, 1.7$ (red to black). The critical value q_c is shifted again due to the shifting of the effective potential. (b) Zoom-in near $q = 0$ to better appreciate the transition.

Following Ref. [14], we can write a single nonlinear evolution equation for G_R . It will generically be a matrix equation, due to the additional, pairing channel. Of course, we can rewrite it as a system of four scalar equations for the four components of the bispinor. We adopt the basis given in Eq. (11) and the metric given by Eq. (2). Introducing the notation $\psi = (\psi_1, \psi_2)^T$ with $\psi_\alpha = (y_\alpha, z_\alpha)^T$ where $\alpha = 1, 2$, the resulting system reads

$$(\partial_z \mp m\sqrt{g_{zz}})y_{1;2} = \mp i\sqrt{\frac{g_{zz}}{g_{ii}}}(\lambda - u)z_{2;1} - \Delta\sqrt{g_{zz}}y_{1;2} = 0, \quad (111a)$$

$$(\partial_z \mp m\sqrt{g_{zz}})z_{1;2} = \pm i\sqrt{\frac{g_{zz}}{g_{ii}}}(\lambda + u)y_{2;1} + \Delta\sqrt{g_{zz}}z_{1;2} = 0, \quad (111b)$$

with

$$u = \sqrt{\frac{g_{ii}}{-g_{tt}}}(\omega + q\Phi(z)). \quad (112)$$

Introducing $\xi_\alpha = iy_\alpha/z_\alpha$ as in Ref. [14], where the boundary Green's function is found from the asymptotics of the solution at the boundary [Eq. (20)]

$$G_\alpha = \lim_{z \rightarrow 1} \left(\frac{1}{1-z} \right)^{2m} \xi_\alpha(z) = \lim_{\epsilon \rightarrow 0} \epsilon^{-2m} \xi_\alpha(1-z=\epsilon), \quad (113)$$

the equations of motion for ξ_α become

$$\begin{aligned} \partial_z \xi_{1;2} &= -2m\sqrt{g_{zz}}\xi_{1;2} - \sqrt{\frac{g_{zz}}{g_{ii}}}(\lambda - u) \\ &+ \sqrt{\frac{g_{zz}}{g_{ii}}}(\lambda + u)\xi_{1;2} \mp 2\Delta\sqrt{g_{zz}}\xi_{1;2}. \end{aligned} \quad (114)$$

The infalling boundary conditions at the horizon are imposed $\xi_\alpha = i$, while the amplitude of y_α remains free

(it cancels out in the propagator G_R) and can be chosen to be of order unity for convenience in the numerical integration.

With no pairing channel, the morphology of the spectra is well known and has been analyzed in detail in Refs. [14,15]: near $k = k_F$, gapless quasiparticle excitations appear, belying a Fermi surface. Let us now repeat the AdS_2 analysis of Ref. [14] for the equations with pairing. We will use the (ζ, τ) coordinates introduced in Eq. (86). The near-horizon equation of motion now assumes the following form:

$$\zeta \partial_\zeta \psi = \left(i\sigma^2 \frac{\mu_q}{6} - \sigma^3 \frac{(m+s\Delta)}{\sqrt{6}} - \sigma^1 \frac{k}{\sqrt{6}} \right) \psi, \quad (115)$$

where $s = \pm 1$, and in the presence of magnetic field the role of the momentum k is taken over by Landau levels $\lambda = \sqrt{2|qh|l}$. Near the AdS_2 boundary ($\zeta \rightarrow 0$), the equation can be solved analytically at the leading order:

$$\psi = A \left(\frac{m+s\Delta}{\sqrt{6}} + \nu \right) \zeta^{-\nu} + B \left(\frac{m+s\Delta}{\sqrt{6}} - \nu \right) \zeta^\nu \quad (116)$$

with

$$\nu = \frac{1}{6} \sqrt{\mu_q^2 - 6((m+s\Delta)^2 + k^2)}, \quad (117)$$

and the self-energy scales as

$$\text{Im}\Sigma \sim \omega^{2\nu}. \quad (118)$$

As usual, the Fermi surface is stable for $\nu^2 > 1/4$, unstable for $\nu^2 < 1/4$ and nonexistent for $\nu^2 < 0$.

In the bulk (and also as we move toward the boundary), the pairing term acts by shifting the mass as $m \mapsto m \pm \Delta$, meaning that the position of the quasiparticle pole is shifted, effectively modifying the k_F value, which removes

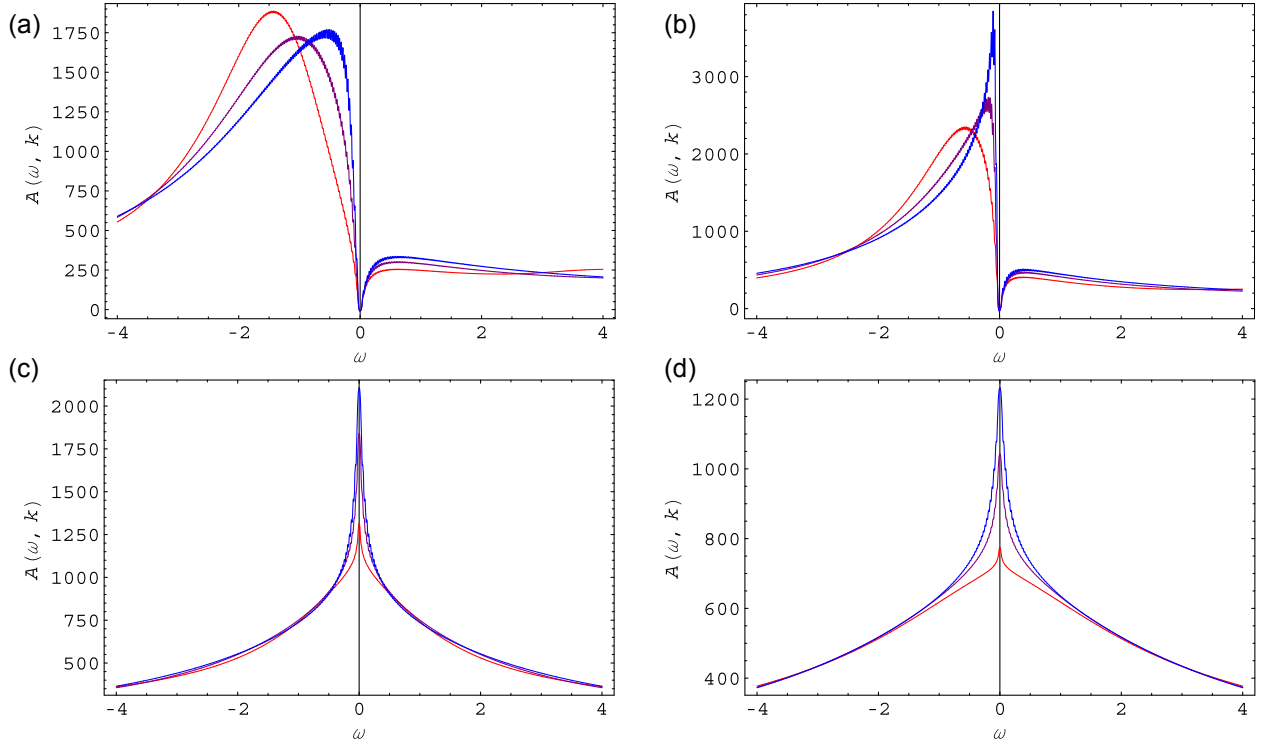


FIG. 13 (color online). The spectral function $A(\omega, \lambda)$ for $\Delta = 0.2, h = 0.9, 1.11, 1.3, 1.5$ [(a), (b), (c), (d)] and three momentum values around k_F^{eff} . At $h < h_*$ [(a), (b)] we see that $\nu^2 < 0$, corresponding to zero weight at $\omega \approx 0$, the phenomenon we have dubbed the pseudogap. For $h > h_*$ [(c), (d)] we enter the quasiconformal regime, with no Fermi surfaces left, the conformality being only slightly broken by nonzero Δ .

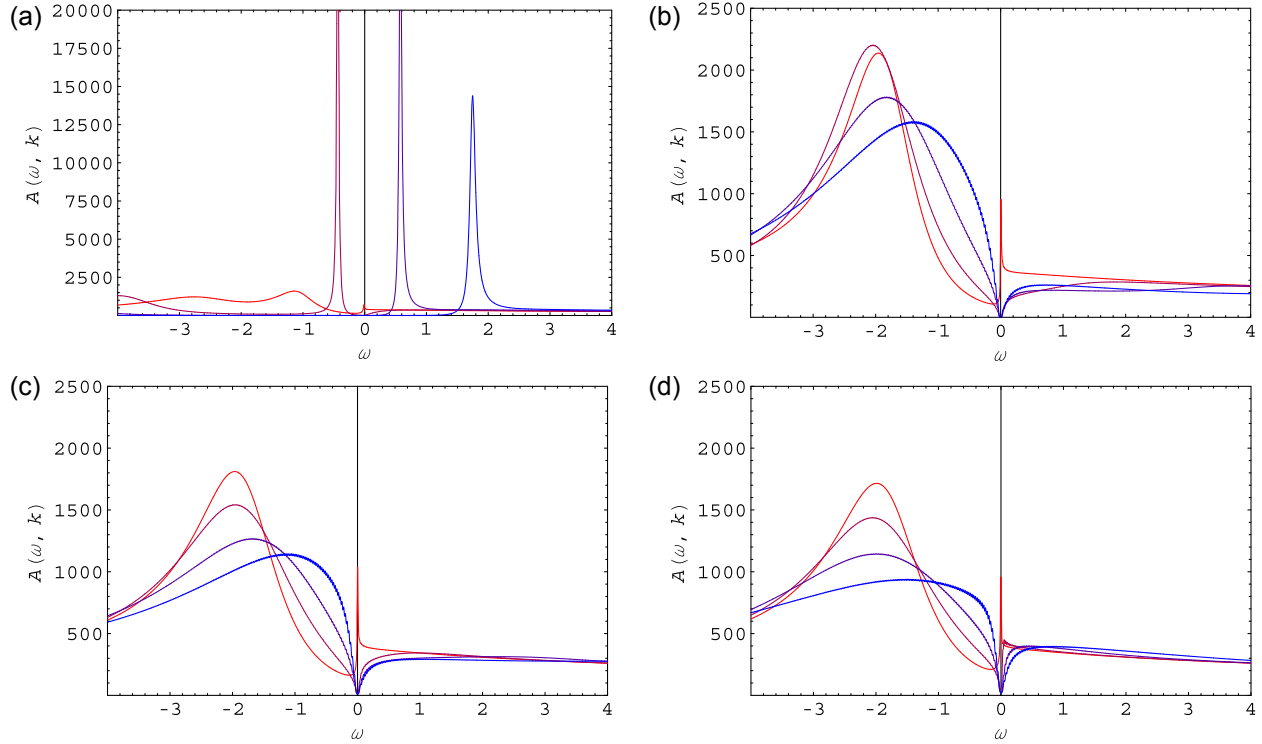


FIG. 14 (color online). The spectral function $A(\omega, \lambda)$ for $h = 0.2, \Delta = 0.9, 1.11, 1.3, 1.5$ [(a), (b), (c), (d)] and four momentum values around k_F^{eff} . At $\Delta < \Delta_c \approx 0.2$ (a), the quasiparticle peak survives; for higher Δ the influence of the exact value of the pairing term is negligible, and the spectrum always shows the pseudogap behavior.

the spectral weight from the vicinity of $\omega = 0$. It thus resembles a gap even though it is, strictly speaking, not a gap since the poles in ψ_1 and ψ_2 do not coincide (see also Ref. [29]). Nevertheless, we expect the size of the zero-weight region to be a useful benchmark for the degree to which the pairing eats up the (non-)Fermi liquid quasiparticles.

The typical appearance of the spectrum is given in Fig. 13, where we plot the spectra for $\Delta = 0.2$ and for increasing magnetic field values. Increasing the magnetic field leads to destabilization of the quasiparticle [panels (a) and (b)], leading to a gap-like behavior, and destabilization of the quasiparticle as seen from the asymmetry of the peak which loses its Fermi-liquid-like scaling. Eventually [panels (c) and (d)] the effective chemical potential is so low that we enter the “almost conformal” regime. Figure 14 shows the dependence on the pairing coupling: the peak at $\omega = 0$ turns into a dip, a “pseudogap” develops and we lose the quasiparticle.

V. DISCUSSION AND CONCLUSIONS

Before concluding the paper, we will discuss possible universal aspects of our findings, and show that the formation and enhancement of the particle-hole condensate in a strong magnetic field is a robust phenomenon seen in a number of distinct systems. We will limit ourselves to short remarks only, as more detailed comparisons with earlier work can be made by consulting the appropriate references.

We found the exciton instability using a Dirac hair or bilinear approach. A Dirac hair method uses bilinear combinations where a bilinear in a given channel develops an expectation value at the UV boundary provided a source is switched off. Dirac hair is equivalent to a Tamm-Dancoff approximation; planar diagrams of processes $2 \rightarrow 2$ are included with no bulk fermion loops. In this sense, Dirac hair is a quantum-mechanical treatment with one single classical wave function. It is quite remarkable to see that the condensate develops on a “classical” level due to a non-trivial nature of the curved space-time with the help of the AdS/CFT dictionary, a phenomenon that was first obtained as a holographic superconductor [5].

We have associated the rising critical temperature vs magnetic field with the magnetic catalysis (MC), and the decreasing T_c vs h with the inverse MC (anomalous and normal branches in Fig. 5 for $G_c^* < G < G_c^{**}$, respectively). We adopted the terminology from Ref. [34]. It corresponds to a double-valued regime in the phase diagram (Fig. 6). Similar behavior of increasing T_c vs the scalar mass m has been observed in Ref. [32] under the action of a double-trace deformation, for the alternative quantization starting at the critical mass $m^2 R^2 \geq -\frac{27}{16}$. There it was associated with the formation of a new condensed phase corresponding to the high-temperature regime. However, it was suggested that the high- T condensed phase is thermodynamically unstable [32].

Likewise, in Ref. [38], exploring the phase diagram for a nonrelativistic conformal field theory, the authors found the high-temperature condensate for $T \geq T_H$. The similarity of the dependences $\langle O \rangle(T)$ at different chemical potentials μ and $T_c(h)$ at different couplings G to our Fig. 5 is obvious. In that work, the high-temperature condensate was related to the high-temperature instability predicted by Cremonesi *et al.* [39], and it was found to be thermodynamically disfavored over the trivial vacuum by direct calculation of the difference in the free energies [38]. However, the particle-hole condensate found at high magnetic fields in our case is crucially different from the unstable high-temperature condensate in Refs. [32,38]. Though naively both the magnetic field h and the fermion mass m destroy the condensate, increasing m^2 (or h) drives the bulk system to the UV (or the IR). Indeed, from the radial profile of the wave functions at large m the system resides near the UV boundary and at strong h it resides near the RN black hole horizon in the IR (Fig. 5 in Ref. [15]). Therefore, from a holographic viewpoint large magnetic fields can lead to low-energy behavior and possible quantum critical phenomena, involving different ordering in the system. The main argument in favor of robustness and stability of our high- h condensate is provided by the magnetic catalysis effect. In strong magnetic fields only the lowest Landau level contributes significantly to the ground state. Therefore, the dynamics is effectively dimensionally reduced as $d \rightarrow d - 2$. In field theory this dimensional reduction leads to an increase in the density of states [40] or in QCD to one-gluon exchange with a linear binding potential [41], with both effects working towards pairing and enhancement of the condensate. In the AdS space, dimensional reduction leads to a Schwinger model showing an instability which is very similar to the Bardeen-Cooper-Schrieffer (BCS) pairing instability, where also the dynamics is effectively one dimensional at the Fermi surface. The exact mapping between the magnetic catalysis at $h \neq 0$ and the BCS Cooper pairing at $\mu \neq 0$ has been established in Ref. [40].

We obtained a nontrivial radial profile and a boundary VEV for the bulk excitonic condensate $\langle \bar{\psi} \Gamma \psi \rangle$ at vanishing source, with the relation

$$\begin{aligned} \langle \bar{\psi}_1 \psi_1 \rangle &= \frac{1}{2} \langle \bar{\psi} \psi \rangle - \frac{1}{2} \langle \bar{\psi} \Gamma \psi \rangle, \\ \langle \bar{\psi}_2 \psi_2 \rangle &= \frac{1}{2} \langle \bar{\psi} \psi \rangle + \frac{1}{2} \langle \bar{\psi} \Gamma \psi \rangle, \end{aligned} \quad (119)$$

where $\Gamma = i\Gamma^2\Gamma^5$ and $\psi_{1,2} = \frac{1}{2}(1 \mp \Gamma)\psi$ are the eigenvalues of the Dirac operator (13) [the projectors $\Pi_{1,2} = \frac{1}{2}(1 \mp \Gamma)$ are constructed out of gamma matrices which enter the Dirac operator only [14]]. We need to find the boundary condensate whose gravity dual is $\langle \bar{\psi} \Gamma \psi \rangle$ where the bulk Dirac field ψ corresponds to a fermionic operator Ψ , $\psi \rightarrow \Psi$. The AdS/CFT correspondence does not provide

a straightforward way to match a double-trace condensate to a boundary operator, though only gravity dual single-trace fields are easy to identify with the operators at the boundary. For example, in holographic superconductors a superconducting condensate is modeled by a charged scalar field $\langle \Phi \rangle$ (see e.g. Ref. [31]). As in Ref. [30], we find a boundary operator by matching discrete symmetries on the gravity and field theory sides and considering the asymptotic behavior of the gravity dual condensate at the boundary. As a result we associate a gravity dual excitonic order to some sort of a chiral condensate

$$\langle \bar{\psi} \Gamma \psi \rangle \leftrightarrow \bar{\Psi} \Psi \quad (120)$$

or some combination of condensates which break chiral symmetry. In Ref. [30], this strategy provided the correspondence $\langle \bar{\psi} \Gamma^5 \psi \rangle \leftrightarrow \bar{\Psi} \Psi$. There an explicit use of the chiral basis $\psi_{L,R} = \frac{1}{2}(1 \mp \Gamma^5)\psi$ and the relation $\bar{\psi}_L \psi_R = \frac{1}{2}\langle \bar{\psi} \psi \rangle + \frac{1}{2}\langle \bar{\psi} \Gamma^5 \psi \rangle$ made the correspondence evident. Specifically, by matching symmetries with respect to the discrete transformations (39) we find that $\langle \bar{\psi} \Gamma \psi \rangle$ and $\langle \bar{\Psi} \Psi \rangle$ are pseudoscalars under parity and are unaffected by the charge conjugation; therefore they both spontaneously break the combination $\hat{C}\hat{P}$ symmetry. This finding is consistent with the existence of the parity-odd mass in graphene associated with the excitonic order parameter in the $2+1$ -dimensional effective field theory of graphene [22,42]. Also the asymptotic behavior of the bulk condensate at the boundary, which was found numerically (Fig. 10) to be $\langle \bar{\psi} \Gamma \psi \rangle \rightarrow C/r^3$ as $r \rightarrow \infty$, allows us to use a standard AdS/CFT dictionary to identify C as the response or VEV of the boundary operator. The third power in the decay exponent indicates an extra mass scale. Indeed provided the response $\langle \Phi \rangle \sim 1/r^3$, the gauge-gravity duality gives a strong coupling form of the magnetic catalysis in $2+1$ dimensions [30]:

$$\langle \bar{\Psi} \Psi \rangle \sim h M_F, \quad (121)$$

with the magnetic field h and mass gap M_F [30]. It can be compared to the weak coupling field theory result $\langle \bar{\Psi} \Psi \rangle \sim h$ (we absorbed dimensional electric charge in the definition of magnetic field h , i.e. in $2+1$ dimensions the operator dimension is given by $[e] = \frac{1}{2}$ and $[h] = \frac{3}{2}$ with $[eh] = 2$ and therefore we substitute $|e|h \rightarrow h$) [22]. Strong coupling realization follows from the anomalous fermion dimension $[\Psi] = \frac{3}{2}$ compared to the weak coupling conformal dimension $[\Psi] = 1$ (free value dimension) in $2+1$ -dimensional field theory. An extra fermion mass gap M_F appears as a consequence of the dimensional four-fermion coupling $G_{\text{int}} = 1/M_F$ in the bulk or the introduction of the IR cutoff thought of as a hard wall at the radial slice $z_* = 1/M$. The authors of Ref. [30] have used the hard wall construction to obtain the strong coupling realization of the magnetic catalysis (121). It is remarkable that the chiral condensate

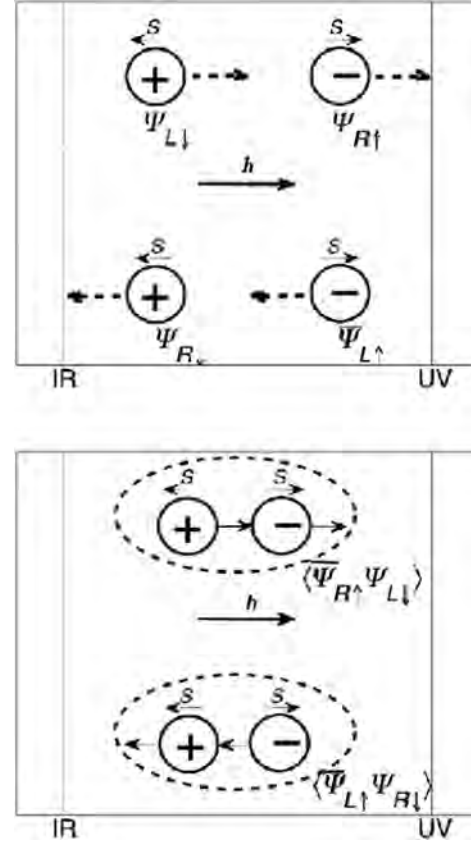


FIG. 15. Formation of the chiral-symmetry-breaking excitonic condensate in the AdS space-time. Individual “bouncing” events are shown schematically by the dashed lines. In an individual event, helicity flips while spin and charge are conserved.

is proportional to the magnetic field even at strong coupling, that manifests the essence of the magnetic catalysis.

Another aspect of the chiral condensate is related to the Callan-Rubakov effect. As found in the field theory and also shown in the context of the gauge-gravity duality [43], the chiral condensate can be spontaneously created in the field of a magnetic monopole. Due to the chiral anomaly $\partial j_5 = F\tilde{F}$, the chiral symmetry is spontaneously broken and the chiral condensate $\langle \bar{\psi} \psi \rangle \sim e^{i\theta}/r^3$ is generated in the field of a monopole. In AdS, a construction involving a monopole wall (more precisely, a dyonic wall) and light fermions in the bulk produces an analog of the Callan-Rubakov effect resulting in the formation of the chiral symmetry breaking (CSB) condensate: $\langle \bar{\psi} \psi \rangle \neq 0$ [43]. The scaling behavior of the condensate is, however, different in our setup: as pointed out before, due to the lowest Landau level (LLL), the dimensional reduction $3d \rightarrow 1d$ takes place in the bulk. This reduces the equation of motion to an effective Schrödinger equation for the condensate, given by Eq. (108) with the potential (109). Solving the equation, we have found the IR behavior of the condensate near the horizon of the RN black hole ($1/r$) to be less divergent than the one near the monopole $\frac{1}{r^3}$ or the monopole wall $\frac{1}{(r-r_w)^3}$ [43].

It turns out that the AdS space with two boundaries—the UV boundary and the IR hard wall—plays an additional role in stabilizing the chiral condensate [30,43]. It also provides an important hint for the interpretation of our current $\bar{\psi}\Gamma\psi$ in the boundary theory. In particular, for the lightest states to condense, we should take the LLL which only has one spin state available (instead of two states available for the higher LLs). This means that for a given charge, the spin direction is fixed. Therefore, fixing the direction of motion and the charge fixes also the helicity. Out of eight possibilities with a given charge, helicity and direction, only four are available for the LLL, as depicted in Fig. 15 (left). The charge \pm denotes e^\pm , positive/negative helicity is denoted by R/L, and S gives the spin orientation; lines with arrows show the momentum direction and h stands for the magnetic field. The following bilinear combinations are possible when only LLLs participate.

- (i) $\langle\bar{\psi}_{R\uparrow}\psi_{R\downarrow}\rangle, \langle\bar{\psi}_{L\uparrow}\psi_{L\downarrow}\rangle$ —(spin) scalar, charge neutral, momentum of the pair $\vec{P} = 0$, chiral symmetry (CS) is not broken.
- (ii) $\langle\bar{\psi}_{R\uparrow}\psi_{L\downarrow}\rangle, \langle\bar{\psi}_{L\uparrow}\psi_{R\downarrow}\rangle$ —(spin) scalar, charge neutral, momentum of the pair $\vec{P} \neq 0$, CS is broken.
- (iii) $\langle\bar{\psi}_{R\uparrow}\bar{\psi}_{L\uparrow}\rangle, \langle\psi_{L\downarrow}\psi_{R\downarrow}\rangle$ —(spin) vector triplet, charged, momentum of the pair $\vec{P} = 0$, CS is broken.

We will not consider the first combination because it does not break the CS, and in our case CS is broken otherwise there would be no preferred scale for the current I_- . As for the third combination, it has been considered in the context of nonzero-density QCD, where it describes the condensate of charged ρ^\pm vector mesons [41]. It cannot be our order parameter either, since our current is a spin singlet. It is tempting to regard the doublet $\Gamma^i\Gamma^5$, $i = 1, 2$ as a vector, and we leave it for a future work.

We are thus left with the second combination. One can think of this order parameter as a spin-density wave, or magnetization which precesses around the direction of the magnetic field. The analog of the second combination has been considered within the Sakai-Sugimoto model as a holographic top-down approach to QCD [34]. The setting of Ref. [34] is very different from ours: it identifies the embedding coordinate of a probe D-brane with a scalar field dual to a single-trace fermion bilinear operator; the magnetic catalysis is modeled as a bending of the probe brane under the influence of the magnetic field. There the anisotropic spatially modulated CSB condensate in the form of a single plane wave Larkin-Ovchinnikov-Fulde-Ferrell (LOFF) state has been found. To have a condensate in the form of the second combination, we need to introduce the $SU(2)$ spin symmetry as in Ref. [32]. We should note the difference with our case where the construction of the condensate is done in the bulk and there is a special effort involved to identify the boundary operator. Provided the condensate of the second form is realized, the AdS boundary and the IR hard wall play a stabilizing role in its formation [43]. As the pair $\langle\bar{\psi}_{R\uparrow}\psi_{L\downarrow}\rangle$ “bounces” from

either of the boundaries it converts into the pair $\langle\bar{\psi}_{L\uparrow}\psi_{R\downarrow}\rangle$ conserving the total charge. This process can be decomposed into elementary “bouncing” events.

- (i) $\bar{\psi}_{R\uparrow} \rightarrow \psi_{R\downarrow}, \psi_{L\downarrow} \rightarrow \bar{\psi}_{L\uparrow}$ —helicity is conserved, spin flips, mixing of charge occurs.
- (ii) $\bar{\psi}_{R\uparrow} \rightarrow \psi_{L\uparrow}, \psi_{L\downarrow} \rightarrow \bar{\psi}_{R\downarrow}$ —helicity flips, spin and charge are unaffected.

In the first case a particle deposits the charge at the boundary, which is picked up by the antiparticle, thus conserving the total charge of the particle-hole pair. The main difference between the two cases is either the “bouncing” event involves a spin flip or not, and therefore either helicity is conserved or broken, respectively. By imposing the AdS boundary condition which breaks CS, helicity gets inverted by the boundary and CS breaking propagates from the boundary into the bulk. Then CS breaking occurs due to the boundary condition before the chiral condensate forms, which affects the propagation of the fields in the bulk in accordance with the second case stabilizing the condensate [30].

Next we discuss an analogy between the MC and the BCS Cooper pairing, and mapping between the Gross-Neveu model (or the Nambu–Jona-Lasinio model) in the presence of the magnetic field and the BCS model at nonzero chemical potential. The reason this mapping works is that effectively the dynamics in both cases is one dimensional: in the strong magnetic field the motion is constrained to Larmor orbits and includes only states from the lowest Landau level, while in a high-density system only states at the Fermi surface contribute to the dynamics. We can draw the following analogy [44]:

| MC | BCS |
|--|--|
| $(3+1)d \rightarrow (1+1)d$ | $(1+1)d$ |
| LLL and $\varepsilon=0$ surface | Fermi surface $\varepsilon = \mu$ |
| $\varepsilon = \sqrt{k_z^2 + 2 eh n}$ | $\varepsilon = k - k_F, k = \sqrt{k^2}$ |
| excitonic: $\Delta \sim G\langle\bar{\psi}\psi\rangle$ | SC: $\Delta \sim G\langle\psi\psi\rangle$ |
| $\Delta \sim \sqrt{eh}\exp(-\frac{\text{const}}{G\nu_0})$ | $\Delta \sim \mu\exp(-\frac{\text{const}}{G\nu_F})$ |
| ν_0 is DOS at $\varepsilon=0$ | ν_F is DOS at $\varepsilon = \mu$ |
| h enhances, μ destroys Δ | μ enhances, h destroys Δ |
| $\delta\Omega \sim h\left(\mu^2 - \frac{\Delta^2}{2}\right)$ | $\delta\Omega \sim \mu^2\left(\delta\mu^2 - \frac{\Delta^2}{2}\right)$ |
| $h \gg \mu, \Delta$ | $\mu \gg \delta\mu, \Delta$ |
| it can have $\mu = 0$ | it can have $h = 0$ |
| T_c grows with h (MC) | T_c decreases with h |
| T_c decreases with μ | T_c grows with μ (SC) |

(122)

Effectively one-dimensional dynamics in both cases leads to similarities in formulas for the pairing gap Δ and the gain in the thermodynamic potential $\delta\Omega$ as compared to the normal unpaired state. In the BCS, the density of states at the Fermi surface $\varepsilon = \mu$ defines the gap Δ , and there is an energy cost $\mu^2\delta\mu^2$ to bring two Fermi surfaces together to

pair in case of nonzero mismatch $\delta\mu$ between them. In MC, the density of states at the $\varepsilon = 0$ surface separating electrons and holes contributes to the gap, and a similar cost in energy $h\mu^2$ exists to involve both particles and holes to pair. The gain from the pairing is proportional to Δ^2 in both cases, and is linear in μ^2 for the BCS and in h for the MC, manifesting the essence of both phenomena. These simple formulas for $\delta\Omega$ can be obtained when there is a hierarchy of scales: the largest scale is μ in the BCS and it is h in the MC.

The comparison given in Eq. (122) provides the following mapping between parameters in the two systems at a nonzero density and at a nonzero magnetic field [40]:

$$\begin{aligned}
 & \text{MC} \longleftrightarrow \text{BCS} \\
 & \langle \bar{\psi}\psi \rangle \neq 0 \longleftrightarrow \langle \psi\psi \rangle \neq 0 \\
 & \text{finite } h \longleftrightarrow \text{finite } \mu \\
 & \text{small } \mu \longleftrightarrow \text{small } \delta\mu \\
 & h \gg \mu \longleftrightarrow \mu \gg \delta\mu
 \end{aligned} \tag{123}$$

where the last line expresses the hierarchy of scales. A similar mapping has been obtained in case of the Gross-Neveu and the BCS models, where the magnetic field h maps to the chemical potential mismatch $\delta\mu$ and is relevant for the inhomogeneous superconductors in the incommensurate phase [45]. Based on Fig. 5 and using the above-described mapping, we can speculate and draw an analogy between the condensed matter phase diagram in T_c vs h and the QCD phase diagram in T_c vs μ , as depicted in Fig. 16. The high-magnetic-field phase is mapped to the color superconductor state at very large densities [for example color-flavor-locked (CFL)] in QCD, while weak magnetic fields which do not destroy superconductivity are mapped to the chirality-broken phase in QCD. The robust feature of the phase diagram in Fig. 5 is the existence of two regions, with small and large h where the condensate is destroyed and enhanced, respectively, by the magnetic field. We found numerically that both branches are thermodynamically favored compared to the normal states, as can be seen in Fig. 1. In the Sakai-Sugimoto model [34], analytical formulas for the free energy difference between condensed and normal states have been obtained, proving the stability of both condensed states. The strong- h regime (“direct” magnetic catalyses) has a remarkably simple form [34]

$$\delta\Omega \sim -h \left(\frac{\Delta(h)^2}{2} - \mu^2 \right), \tag{124}$$

which is exactly the result obtained in the field theory (122); compare also with Fig. 1. The condition for a thermodynamically stable ordered phase with the excitonic condensate is given by

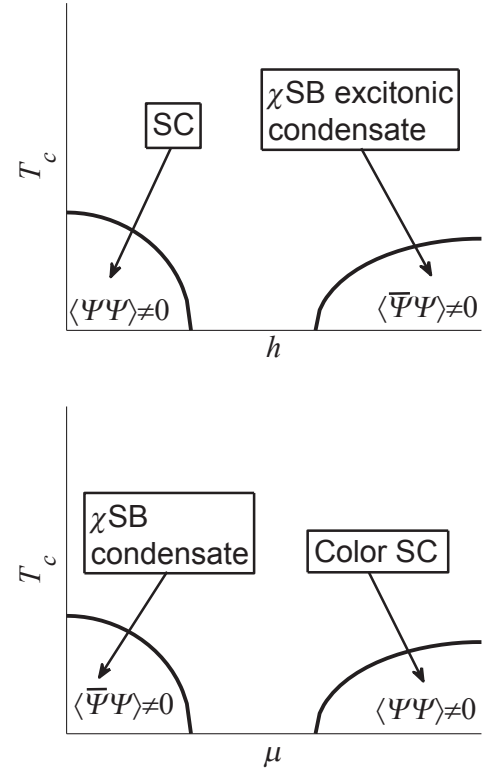


FIG. 16. Analogy between the phase diagram of a condensed matter system at nonzero magnetic field and the QCD phase diagram at nonzero density. In strong magnetic fields, the excitonic condensate is mapped to the asymptotic regime of high-chemical-potential QCD with the color superconductor phase.

$$\mu \leq \frac{\Delta(h)}{\sqrt{2}}, \tag{125}$$

which according to the mapping (123) coincides with the familiar Clogston limit in the SC: $\delta\mu \leq \frac{\Delta}{\sqrt{2}}$. However, there is an important difference between the formation of the excitonic and superconducting condensates. In MC the excitonic condensate $\Delta(h)$ is a growing function with h [Fig. 3(a)] which ensures that Eq. (124) is always satisfied at high enough magnetic fields. This finding is important, since it demonstrates the robustness of the chiral condensate.

Though MC and BCS both have one-dimensional dynamics, the mapping between the two models may come as a surprise. Indeed properties of both systems (one is a magnetic and the other is a dense medium) including the symmetry-breaking pattern when a condensate forms are quite different. However, we speculate that these two systems can be unified on the gravity side using the duality between electric and magnetic fields. In the gravity dual description the two phenomena can be represented as follows:

| Holographic MC | Holographic SC |
|-------------------------------------|------------------------------|
| dyonic AdSRNBH, Schwarzschild BH | AdSRNBH |
| $ H > Q $ | $ Q > H $ |
| it can be $Q=0$ | it can be $H=0$ |
| Z_2 (chiral SB) broken | $U(1)$ broken |
| magnetic field enhances it | magnetic field destroys it |
| electric field destroys it | electric field enhances it |
| Callan – Rubakov effect | dual Callan – Rubakov effect |

(126)

which shows the electromagnetic duality [the invariance under an interchange of the electric and magnetic charges of the black hole $(|Q|, |H|) \rightarrow (|H|, |Q|)$]. The motivation for this duality is a similarity in the expressions for the gap and the energy gain of the ordered phase between two systems as given by Eq. (122). Probably the underlying reason for the duality is a symmetry of how both charges of the black hole enter in the red shift factor. They always enter in combination $Q^2 + H^2$, which defines also the Hawking temperature of the black hole or the temperature of the system $T \sim r_0(1 - \frac{Q^2 + H^2}{3r_0^2})$ with r_0 is the radius of the horizon of the BH. Similarly, according to the Montonen-Olive conjecture, the spectrum in the Georgi-Glashow model is invariant under the electromagnetic Z_2 duality $(g, g) \rightarrow (g, -g)$ as a consequence of the fact that the Bogomol'nyi bound is invariant under electromagnetic duality (the Bogomol'nyi bound for the mass of the 't Hooft-Polyakov monopole is $M \geq a\sqrt{q^2 + g^2}$), and the spectrum of the Georgi-Glashow model saturates this bound [46]. Notably, the mass of the black hole

$$M = r_0^3 + \frac{Q^2 + H^2}{r_0} \quad (127)$$

is also invariant under the electromagnetic duality. The electromagnetic duality (126) holds on a classical level and is destroyed by quantum corrections. It stays intact for the supersymmetric theories though.

In this work a four-fermi interaction has been used as a control parameter to go from one regime mimicking the SC to the other one of MC. The robustness of both regimes can be seen in a symmetric form of the dependence T_c vs h (top of Fig. 16). In the application to nonzero-density QCD, this means that at strong enough magnetic fields the chiral symmetry is spontaneously broken by a chiral condensate. Moreover, due to a dimensional reduction QCD as well as plain QED are in the confined regime even on the perturbative level: they can be reduced to a Schwinger model where one-gluon (one-photon) exchange in one dimension leads to a linear rising potential in the configuration space (a similar argument provides confinement

along the boost direction for theories in the light-front quantization). Evidence of the QED confinement in a strong magnetic field can be provided by the existence of a $2e$ bound state which contributes to the fractional quantum Hall effect [47]. Summarizing, quark-gluon plasma (QGP) at strong magnetic fields is probably confined and has a broken chiral symmetry, as opposed to QGP at zero magnetic fields which is in a deconfined and chiral-symmetry-invariant phase. This finding might have some implications for the chiral magnetic effect in heavy-ion collisions at the RHIC [48].

A general note is that the low-energy behavior of the non-Fermi liquids is governed by a nontrivial IR fixed point which arises from the near-horizon region with AdS_2 geometry [14]. This IR fixed point arises as a consequence of the interplay between the emergent quantum critical bosonic modes and the fermions at finite density. In other words, the class of systems studied is both metallic and quantum critical at low energies. On the gravity side, this is reflected by the instability of the background (Reissner-Nordstrom black hole in the AdS space) unless order parameter fields are introduced to stabilize it [7].

We have explored the quantum critical aspects of the system by using the magnetic field as a knob to tune the system to a quantum critical point. Indeed, the magnetic field as an external parameter driving the system to quantum criticality is used in experiments on heavy fermions and graphene. We have shown that by increasing the magnetic field, the system evolves from the normal metallic to a quantum critical phase, where the stable quasiparticle is destroyed. The quantum critical point is controlled by the IR fixed point with the scaling dimension $\nu = \frac{1}{2}$, where the Fermi velocity vanishes $v_F = 0$ (see Fig. 10 in Ref. [15]) but the Fermi momentum stays finite $k_F \neq 0$ (see Fig. 9 in Ref. [15]). It is important that we are able to deduce the position of the quantum critical point from our calculations. The phase transition can be understood as the formation of a semiclassical condensate on the gravity side near the AdS_4 boundary. Using the bilinear formalism developed in Ref. [6], we have also calculated the thermodynamic parameters of both phases. We found that the particle-hole pairing instability arises for both $\nu > \frac{1}{2}$ corresponding to $h < h_c$ and $\nu < \frac{1}{2}$ corresponding to $h > h_c$. In a holographic superconductor, a superconducting instability has been shown to exist only for $\nu > \frac{1}{2}$ [27]. This shows the remarkable difference in nature between superconducting and excitonic instabilities: existence of excitonic condensate beyond the critical point $\nu = \frac{1}{2}$ is a quantum critical phenomenon. The magnetic field acts as a catalyzer of the particle-hole pairing because of the dimensional reduction $d \rightarrow d - 2$ in the magnetic field [22].

Other thermodynamic and transport quantities including the heat capacity and DC conductivity are calculated for both normal- and anomalous-paired phases in Appendix B.

The results support our findings obtained from the bilinear holographic approach on the nature and scaling behavior of the two phases.

The critical temperature of the normal-paired phase transition follows the expected behavior for $h < h_c$: the critical temperature T_c decreases with increasing h , with the scaling $T_c \propto \mu \exp(-C/\sqrt{q(h_c - h)})$. At $h > h_c$, however, we find anomalous behavior: T_c grows with increasing h . To the best of our knowledge, this is the first example of non-mean field scaling from an AdS₄ holographic model. Mathematically, it follows from the fact that, for $\nu < \frac{1}{2}$, we have the scaling $T_c \sim \delta^{2\nu-1}$ with δ small and decreasing. Physically, such behavior is consistent with the fact that the system is driven through the quantum critical point at h_c where $T_c = 0$, and beyond the quantum critical point at $h > h_c$ it can be characterized as a quantum critical metal possessing new properties. In the existing literature, a novel antiferromagnetic behavior has been predicted for heavy fermions driven through the quantum critical point [3]. Such an anomalous behavior for T_c vs h has been seen in experiments on highly oriented pyrolytic graphite at strong magnetic fields $h > h_c$ [21]. Furthermore, the anomalous branch matches the properties of excitons in bilayer interfaces and cold atom realizations [49], and can further be related to the behavior of chiral condensates in holographic QCD models, signaling the universal significance of the twofold normal-anomalous regime in the phase diagram.

ACKNOWLEDGMENTS

We thank Gerald Dunne, Tom Faulkner, Daniel Fernandez-Fraile, Tom Hartman, Sean Hartnoll, Nabil Iqbal, Dima Kharzeev, Alex Kovner, Hong Liu, John McGreevy, Mark Mezei, Piero Nicolini, Andrei Parnachev, Rob Pisarski, Andreas Schmitt and Igor Shovkovy for helpful inputs and discussions. We also thank Dirk Rischke and Francesco Giacosa for reading the manuscript and valuable corrections and suggestions. As our paper was close to completion, we learned of a similar work done by Stefano Bolognesi and David Tong, which is now published in Ref. [30]: we are very grateful to the authors for sharing their results and illuminating discussions. The work was supported in part by the Alliance program of the Helmholtz Association, Contract No. HA216/EMMI ‘‘Extremes of Density and Temperature: Cosmic Matter in the Laboratory’’ and by ITP of Goethe University, Frankfurt (E. G.).

APPENDIX A: BULK GREEN’S FUNCTION AND ZERO MODES

We express the bulk Green’s function through the boundary one as in Ref. [27]. The bulk Green’s function is a solution of the free Dirac equation,

$$\hat{D}(\Omega, k_l) \mathcal{G}^R(z, z', \Omega, k_l) = \frac{1}{\sqrt{-g}} i\delta(z, z'), \quad (\text{A1})$$

with the free radial Dirac operator $\hat{D}(\Omega, k) = \Gamma^i D_i$, which includes the mass term, chemical potential and the magnetic field but has zero gap, $\Delta = 0$, i.e. the equation (15). The bulk Green’s function is constructed from the modes $\psi(z)$ which are solutions of the free Dirac equation

$$\hat{D}(\Omega, k_l) \psi_{\text{radial}}(z) = 0. \quad (\text{A2})$$

Due to the choice of the Dirac matrices in Eq. (11), ψ decouples into two-component spinors, $\psi_{\text{radial}} = (\psi_1, \psi_2)^T$. Therefore the bulk retarded Green’s function has a block-diagonal form:

$$\mathcal{G}^R(z, z', \Omega, k_l) = \begin{pmatrix} \mathcal{G}_1^R & 0 \\ 0 & \mathcal{G}_2^R \end{pmatrix}, \quad (\text{A3})$$

where the components \mathcal{G}_α , $\alpha = 1, 2$ are constructed from the solutions to the Dirac equation [27]

$$\mathcal{G}_\alpha^R(z, z', \Omega, k_l) = \frac{i}{W(\psi_\alpha^{\text{in}}, \psi_\alpha^{\text{bdy}})} \times \begin{cases} \psi_\alpha^{\text{in}}(z) \bar{\psi}_\alpha^{\text{bdy}}(z') z < z', \\ \psi_\alpha^{\text{bdy}}(z) \bar{\psi}_\alpha^{\text{in}}(z') z > z', \end{cases} \quad (\text{A4})$$

with $\bar{\psi}_\alpha = i\psi_\alpha^\dagger \sigma^1$ and W_α are the components of the Wronskian

$$W(\psi_\alpha^{\text{in}}, \psi_\alpha^{\text{bdy}}) = -\frac{\sqrt{-g}}{2\sqrt{g_{zz}}} (\bar{\psi}_\alpha^{\text{bdy}} \sigma^3 \psi_\alpha^{\text{in}} - \bar{\psi}_\alpha^{\text{in}} \sigma^3 \psi_\alpha^{\text{bdy}}). \quad (\text{A5})$$

The retarded Green’s function (A4) must satisfy the following two conditions. At the boundary ($z, z' \rightarrow 1$) where $\psi_\alpha^{\text{radial}} \sim a_\alpha(1-z)^{3-\Delta_\psi} + b_\alpha(1-z)^{\Delta_\psi} + \dots$ with $\Delta_\psi = \frac{3}{2} + m$ it must be the normalizable solution, i.e. $\psi_\alpha^{\text{bdy}} = b_\alpha(1-z)^{\Delta_\psi} + \dots$. At the horizon ($z, z' \rightarrow 0$) where $\psi_{\text{radial}} \sim A_\alpha z^{-i\omega/4\pi T} + B_\alpha z^{i\omega/4\pi T}$, the retarded propagator corresponds to the ingoing solution $\psi_\alpha^{\text{in}} = z^{-i\omega/4\pi T} A_\alpha$. This infalling solution behaves near the boundary as

$$\psi_\alpha^{\text{in}} \sim a_\alpha(1-z)^{3-\Delta_\psi} + b_\alpha(1-z)^{\Delta_\psi} + \dots \quad (\text{A6})$$

In principle, the coefficients in ψ^{bdy} and ψ^{in} are different, i.e. b^{bdy} and b^{in} (we omit the difference for simplicity). This determines the z -independent Wronskian $W_\alpha = -i\text{Re}(b_\alpha^{\text{bdy}\dagger} \sigma_1 \sigma_3 a_\alpha^{\text{in}})$ after substituting the asymptotic behavior near the AdS boundary. The Wronskian is directly proportional to the spectral function of the dual CFT. The two spinor components of each spinor a_α and b_α are not independent, but are related by the Dirac equation [12,26,50]. Defining up/down spin eigenstates with respect to $\gamma^z = -\sigma^3$,

$$a_\alpha \equiv \begin{pmatrix} a_\uparrow \\ a_\downarrow \end{pmatrix} = \begin{pmatrix} 1 \\ 0 \end{pmatrix}, \quad b_\alpha \equiv \begin{pmatrix} b_\uparrow \\ b_\downarrow \end{pmatrix} = \begin{pmatrix} 0 \\ 1 \end{pmatrix}. \quad (\text{A7})$$

Substituting this into the Wronskian

$$W = -ib_{\alpha\downarrow}^\dagger a_{\alpha\uparrow} \quad (\text{A8})$$

and recalling the expression for the boundary propagator,

$$G_\alpha = \frac{b_{\alpha\downarrow}}{a_{\alpha\uparrow}} \quad (\text{A9})$$

one finds that

$$W(\psi_\alpha^{\text{in}}, \psi_\alpha^{\text{bdy}}) = -i|b_{\alpha\downarrow}|^2 G_\alpha^{-1} = -\frac{i}{G_\alpha}. \quad (\text{A10})$$

The result is similar to the one for fermion transport in Ref. [33].

This expression for the bulk propagator in terms of boundary spectral functions shows us that the contribution to the effective action is dominated by the poles of the boundary Green's function. These poles precisely correspond to the values where $\psi^{\text{in}} \propto \psi^{\text{bdy}} \equiv \psi^0$ is the zero mode with $a_\alpha = 0$.

APPENDIX B: THERMODYNAMICS AND TRANSPORT AT ZERO MAGNETIC FIELD

Quantum critical behavior is associated, among other things, with unusual scaling exponents of the heat capacity and the resistivity with temperature. In this section, we obtain an equation of state and find the scaling behavior of the specific heat and the DC conductivity with temperature. Following a prescription worked out in detail for conductivity [33], we bypass the bulk calculations and do our calculations directly in the boundary field theory making use of the gravity-“dressed” fermion propagators [14]. Since the two-point Green's function is obtained from the AdS/CFT correspondence, it is “exact” in terms of gauge coupling corrections, and the lowest-order diagrams on the field theory side should suffice. However, we lack the knowledge of the gravity-“dressed” gauge-fermion vertex. Nevertheless, for the quantities considered below, the scaling behavior should not change when vertex corrections are taken into account.

1. Single-particle spectral functions and dispersion relations

Using AdS/CFT, one finds that, close to the Fermi surface ($\omega/\mu \ll 1$) and at low temperatures ($T/\omega \ll 1$), the retarded fermion Green's function is given by [14]

$$G_R(\omega, \vec{k}) = \frac{h_1 v_F}{v_F k_\perp - \omega + v_F h_2 e^{i\theta - i\pi\nu_{k_F}} \omega^{2\nu_{k_F}}} + O\left(\frac{\omega}{\mu}\right). \quad (\text{B1})$$

Here $k_\perp = k - k_F$, the last term in the denominator defines the self-energy Σ , h_1 and v_F are real constants obtained from the UV (bulk) physics, h_2 is positive with contributions from both the UV and IR regions, the phase θ is such that the poles of Eq. (B1) are in the bottom frequency half-plane corresponding to stable quasiparticle poles and ν_{k_F} is the IR conformal dimension at the Fermi momentum. At $T = 0$, it is given by (in dimensionless units)

$$\nu_{k_F} = \frac{1}{6} \sqrt{6(m^2 + k_F^2) - \mu_q^2}, \quad (\text{B2})$$

with $\mu_q = \mu q$. The IR conformal dimension ν_{k_F} defines the quasiparticle dispersion. Writing the Green's function pole in Eq. (B1) as $\omega_c(k) = \omega_*(k) - i\Gamma(k)$, at leading order $\omega \sim 0$ we get the following dispersion relations:

$$\omega_* \sim \begin{cases} v_F k_\perp, & \nu_{k_F} > \frac{1}{2}, \\ k_\perp / \ln k_\perp, & \nu_{k_F} = \frac{1}{2}, \\ k_\perp^{1/2\nu_{k_F}}, & \nu_{k_F} < \frac{1}{2}. \end{cases} \quad (\text{B3})$$

For $\nu_{k_F} = 1/2$, the leading-order coefficients in front of ω and $\omega^{2\nu_{k_F}}$ diverge and cancel exactly, leaving the subleading logarithmic dependence $\tilde{c}_1 \omega \ln \omega$ where \tilde{c}_1 is a real constant.⁶ As ν_{k_F} is decreased we move from a metal (Fermi liquid) at $\nu > 1/2$ to a marginal metal at $\nu = 1/2$ to a quantum critical metal (non-Fermi liquid) at $\nu_{k_F} < 1/2$, and the dispersion Eq. (B3) becomes softer. This has consequences for the behavior of thermodynamic properties, e.g. the heat capacity.

The imaginary part of the self-energy $\Sigma \sim \omega^{2\nu_{k_F}}$ gives rise to the following width of the quasiparticle dispersion:

$$\Gamma \sim \begin{cases} k_\perp^{2\nu_{k_F}}, & \nu_{k_F} > \frac{1}{2}, \\ k_\perp / \ln k_\perp, & \nu_{k_F} = \frac{1}{2}, \\ k_\perp^{1/2\nu_{k_F}}, & \nu_{k_F} < \frac{1}{2}. \end{cases} \quad (\text{B4})$$

Comparing Eqs. (B3) and (B4), we see that the pole represents a stable quasiparticle only for $\nu_{k_F} > 1/2$ when the width is much smaller than the real part: $\Gamma/\omega_* \ll 1$, while a coherent quasiparticle is replaced by an unstable pole for $\nu_{k_F} \leq 1/2$ where $\Gamma/\omega_* = \text{const}$. The imaginary part of the self-energy becomes important for the behavior of transport coefficients, e.g. conductivity, where the dissipation processes play the key role.

⁶The logarithmic dependence for the real part of the self-energy defines the dispersion for $\nu_{k_F} = \frac{n}{2}$, $n \in \mathbb{Z}_+$. Therefore, the linear spectrum is valid for $\nu_{k_F} \neq \frac{n}{2}$.

We rewrite Eq. (B1) as

$$G_R(\omega, \vec{k}) = \frac{h_1 v_F}{v_F k_\perp - \omega + \Sigma(\omega, k_F)}, \quad (\text{B5})$$

with the self-energy $\Sigma = \Sigma_1 + i\Sigma_2$. Therefore the spectral function defined as $A(\omega, \vec{k}) = \frac{1}{\pi} \text{Im}G_R(\omega, \vec{k})$ is given by

$$A(\omega, \vec{k}) = \frac{1}{\pi} \frac{h_1 v_F \Sigma_2(\omega, k_F)}{(\omega - v_F k_\perp + \Sigma_1(\omega, k_F))^2 + \Sigma_2(\omega, k_F)^2}. \quad (\text{B6})$$

From the above form we can directly read off the structure: a sharp quasiparticle near $k = k_F$ and $\omega = 0$ goes through the infrared scaling region for $\omega/T < 1$ and eventually asymptotes to the universal conformal scaling in the UV, i.e. for $\omega, k \gg 1$.

2. Equation of state and specific heat

Having established the formal structure of the single-particle propagator, we can use it to construct the Landau-Ginzburg action for our system. An effective potential in the CJT formalism is given by [51]

$$\Gamma_{\text{eff}} = \frac{1}{2} \text{Tr} \ln S^{-1} + \frac{1}{2} \text{Tr}(S_0^{-1} S - 1) + \Gamma_2[S], \quad (\text{B7})$$

where S is a dressed fermion propagator, Γ_2 is the sum of all two-particle irreducible diagrams, and the trace Tr involves also the summation over the Matsubara frequencies and the integration $\int d^2x$. The last two terms can be simplified with the help of the Dyson-Schwinger equation, to give

$$\Gamma_{\text{eff}} = \frac{1}{2} \text{Tr} \ln S^{-1} - \frac{1}{4} \text{Tr}(\Sigma S), \quad (\text{B8})$$

where the self-energy is $\Sigma = S^{-1} - S_0^{-1}$.

The fact that we have a finite quasiparticle width, encoding for inelastic/dissipative processes, allows us to calculate the transport coefficients, which would otherwise be infinite. However, the imaginary part of the self-energy gives rise to a branch cut in the fermion propagator along $\text{Im}\omega = 0$ in a complex ω plane [52–55]. In the calculation of the Matsubara sum we should take into account the contributions from poles and from the discontinuities along the branch cuts [54,55]:

$$T \sum_{\text{odd } m} F(i\omega_m) = \sum_{\text{poles}} n(z_i) \text{Res}(F, z = z_i) - \sum_{\text{cuts}} \int_{-\infty}^{\infty} \frac{d\zeta}{2\pi i} n(\zeta) \text{Disc } F, \quad (\text{B9})$$

with the analytical continuation $i\omega_m \rightarrow z$, and the Fermi distribution function $n(x)$. In the contour integral one can

use either $n(x) \equiv n(\frac{x}{T})$ or $\tanh(\frac{x}{2T})$ functions with prefactors $(-\frac{1}{2\pi i})$ and $(-\frac{1}{4\pi i})$ respectively, as both give the same result for the observables. The calculation of Matsubara sums using a perturbative expansion in the imaginary part of the self-energy has been developed in Ref. [56].

For simplicity we will take $h_1 v_F \rightarrow -1$ which will not change our results qualitatively. Using the retarded fermion propagator, an effective potential is found to be

$$\Gamma_{\text{eff}} \rightarrow -\frac{1}{4\pi i} \frac{V_2}{T} \int \frac{d^2k}{(2\pi)^2} \int_C dz \tanh \frac{z}{2T} \times T \left(\frac{1}{2} \ln \frac{z - v_F k_\perp + \Sigma(z, k_F)}{T} - \frac{1}{4z - v_F k_\perp + \Sigma(z, k_F)} \right), \quad (\text{B10})$$

where we have substituted the Matsubara sum by the contour integral. The original contour C_0 going around the poles along the imaginary z axis was deformed into the contour C going along the real z axis and then along the arcs at infinity with vanishing contribution, denoted by Γ [54]. In the case of a pure real self-energy the result for the contour integration is (see Ref. [52])

$$\Gamma_{\text{eff}} \rightarrow \frac{V_2}{T} \int \frac{d^2k}{(2\pi)^2} \sum_{z_*} \left(\frac{1}{2} T \ln \left(2 \cosh \frac{z_*}{2T} \right) + \frac{1}{4} \Sigma(z_*) \tanh \frac{z_*}{2T} \right), \quad (\text{B11})$$

where z_* are the poles of the retarded propagator, and the sum over all allowed poles is taken. As was shown in Ref. [52], when the self-energy and hence the poles include an imaginary part, the following substitution of hyperbolic functions with Γ functions should be made [57]:

$$\left| \Gamma \left(\frac{1}{2} + iz \right) \right|^2 = \frac{\pi}{\cosh(\pi z)}, \quad |\Gamma(iz)|^2 = \frac{\pi}{z \sinh(\pi z)}. \quad (\text{B12})$$

We can now use Γ_{eff} to compute all thermodynamic quantities, using the relations

$$p = \frac{T}{V_2} \Gamma_{\text{eff}}, \quad s = \frac{\partial p}{\partial T}, \quad c = T \frac{\partial s}{\partial T}, \quad n = \frac{\partial p}{\partial \mu}, \quad (\text{B13})$$

where the role of μ is played by k_F , and we get the equation of state

$$p = \int \frac{d^2k}{(2\pi)^2} \sum_{z_*} \left(-\frac{1}{2} T \ln \left(\frac{1}{2\pi} \left| \Gamma \left(\frac{iz_*}{2\pi T} + \frac{1}{2} \right) \right|^2 \right) \right. \\ \left. + \frac{1}{4} \frac{\Sigma(z_*) \left| \Gamma \left(\frac{iz_*}{2\pi T} + \frac{1}{2} \right) \right|^2}{\frac{|z_*|}{2\pi T} \left| \Gamma \left(\frac{iz_*}{2\pi T} \right) \right|^2} \right), \quad (\text{B14})$$

where the summation over complex poles z_* is performed. We only take into account the contribution of the pole closest to $\omega = 0$, with the imaginary part of the self-energy scaling as $\Sigma(z) \sim z^{2\nu}$. Near the Fermi surface, the one-loop contribution dominates over the self-energy term for Fermi liquids $\nu > \frac{1}{2}$, while the self-energy becomes leading for non-Fermi liquids $\nu < \frac{1}{2}$.

What we are truly interested in are the temperature scaling relations for these quantities, in particular for the specific heat c . The first term in Eq. (B14) gives the following contributions to c :

$$\sim \frac{1}{T^2} \int \frac{d^2k}{(2\pi)^2} \text{Re} \left(z_*^2 \Psi' \left(\frac{iz_*}{2\pi T} + \frac{1}{2} \right) + z_*^2 \Psi' \left(-\frac{iz_*^*}{2\pi T} + \frac{1}{2} \right) \right), \\ \times \frac{1}{T^2} \int \frac{d^2k}{(2\pi)^2} \text{Re} \left(\sim z_* T \Psi \left(\frac{iz_*}{2\pi T} + \frac{1}{2} \right); \right. \\ \left. \sim z_*^* T \Psi \left(\frac{-iz_*^*}{2\pi T} + \frac{1}{2} \right) \right) \quad (\text{B15})$$

where $\Psi'(x) = \frac{d\Psi}{dx} = \frac{d^2 \ln \Gamma}{dx^2}$. The second term gives the following contribution:

$$\frac{1}{T^2} \int \frac{d^2k}{(2\pi)^2} \text{Re} \left(\sim T \Sigma(z_*) F[\Gamma]; \right. \\ \left. \sim z_* \Sigma(z_*) F[\Gamma]; \sim \frac{z_*^2 \Sigma(z_*)}{T} F[\Gamma] \right), \quad (\text{B16})$$

where $F[\Gamma]$ denotes a combination of Γ functions and their first and second derivatives. Here, the momentum integration is performed around the Fermi surface, $d^2k \rightarrow k_F dk_\perp$ with $k_\perp = k - k_F$, the poles $z_* = \omega_c - i\Gamma$ are given by Eqs. (B3) and (B4) for the three cases of interest, and $\Sigma(z) \sim z^{2\nu}$.

For a Fermi liquid, one has $\nu > \frac{1}{2}$ and $z_\perp \sim k_\perp$ (the real part is dominant). The first term then gives $\frac{1}{T^2} \int dk_\perp z_*^2 \rightarrow T$ and the same behavior from the other combination, while in the second term we have $\Sigma \sim k_\perp^{2\nu}$. Therefore, the second term gives $\frac{1}{T^2} \int dk_\perp \Sigma(z_*) z_* \rightarrow T^{2\nu}$ and the same behavior for the other two combinations.⁷ Thus for a Fermi liquid at low temperatures we have

$$c \sim T. \quad (\text{B17})$$

⁷This is related to the fact that in Eq. (B14) for the effective action the one-loop term dominates over the self-energy for $\nu > \frac{1}{2}$.

We thus reproduce the linear temperature dependence of the heat capacity known for Fermi liquids.

For a non-Fermi liquid, we have instead $\nu < \frac{1}{2}$ and $z_\perp \sim k_\perp^{\frac{1}{2\nu}}$ (for both real and imaginary parts). The first term gives $\frac{1}{T^2} \int dk_\perp k_\perp^{\frac{1}{2\nu}} \rightarrow T^{\frac{1}{2\nu}-1}$ and $\frac{1}{T^2} \int dk_\perp k_\perp^{\frac{1}{2\nu}} T \rightarrow T^{\frac{1}{2\nu}}$. The second term gives $\frac{1}{T^2} \int dk_\perp \Sigma(z_*) T \rightarrow T^{2\nu}$ and subleading behavior for the other two combinations. For $\nu < \frac{1}{2}$, the self-energy dominates over the one-loop contributions in the pressure and at low temperatures we have

$$c \sim T^{2\nu}. \quad (\text{B18})$$

This result for the heat capacity reflects the scaling behavior of the self-energy. Finally, for $\nu = \frac{1}{2}$, all the terms are $\sim T$, so for the marginal liquids we have $c \sim T$. One can understand it physically from the dispersion relation (B3). As the dispersion becomes softer, the number of states per energy interval increases, and thus the heat capacity increases as well:

$$c_{\text{qcm}} > c_{\text{m}}, \quad (\text{B19})$$

where ‘‘m’’ stands for the normal metal and ‘‘qcm’’ for the quantum critical metal.

It is illustrative to repeat the derivation of the equation of state using the spectral function as given in Eq. (B6). The density of states can be written through a spectral function as follows:

$$n = T \sum_m \int \frac{d^2k}{(2\pi)^2} A(i\omega_m, \vec{k}) \\ \rightarrow -\frac{1}{4\pi i} \int \frac{d^2k}{(2\pi)^2} \int_C dz A(z, \vec{k}) f(z), \quad (\text{B20})$$

where $f(z) = \tanh(\frac{z}{2T})$. One can also use the Fermi distribution function $f(z) = n(z)$ with a prefactor $(-\frac{1}{2\pi i})$, which gives the same result for the observables. The pressure is given by

$$p = \int_{-\infty}^{\mu} d\mu' n, \quad (\text{B21})$$

where in our case $\mu \equiv k_F$. For simplicity we again take $h_1 v_F \rightarrow 1$. We expand the spectral function with respect to the imaginary part of the self-energy, which we treat as a small parameter in this calculation [56]:

$$A(z, \vec{k}) \approx 2\pi \delta(z - z_*) - \Sigma_2(z, k_F) \mathcal{P}' \frac{1}{z - z_*}, \\ \mathcal{P}' \frac{1}{z - z_*} \equiv \frac{\partial}{\partial z} \left(\mathcal{P} \frac{1}{z - z_*} \right). \quad (\text{B22})$$

The pole of the propagator z_* is a solution of the equation $z - v_F k_\perp - \Sigma_1(z, k_F) = 0$ which does not contain the

imaginary part of the self-energy Σ_2 . Substituting this representation into the equation for the pressure, we have

$$p = -\frac{1}{4\pi i} \int \frac{d^2 k}{(2\pi)^2} \int_{-\infty}^{k_F} dk'_F \int_{-\infty}^{\infty} dz \left(2\pi \delta(z - z_*) \right. \\ \left. + \Sigma_2(z) \mathcal{P}' \frac{1}{z_* - z} \right) f(z). \quad (\text{B23})$$

The frequency integral in the first term gives the familiar expression for the number density

$$n = \int \frac{d^2 k}{(2\pi)^2} f(z_*), \quad (\text{B24})$$

where usually f is a Fermi distribution function, and the dispersion relation is given by z_* (in standard notation $z_* \rightarrow \varepsilon_k$). Here we have $f(x) = \tanh(\frac{x}{2})$, and therefore integrating over k_F gives $\int dk'_F \tanh \frac{z_*}{2} \rightarrow \ln(2 \cosh \frac{z_*}{2})$ where, at the leading order $z_* \sim (k - k_F)$. In the second term we exchange the order of integrations in z and k_F . Therefore, $\int_{-\infty}^{k_F} dk'_F \mathcal{P}' \frac{1}{z_*(k'_F) - z} \rightarrow -\frac{1}{z_*(k_F) - z}$, and there is no k_F dependence in $\Sigma_2(z) \sim z^{2\nu}$ at the leading order. The second integral is $\frac{1}{2\pi i} \int_{-\infty}^{\infty} dz \Sigma_2(z, k_F) f(z) \frac{1}{z_* - z} \rightarrow \Sigma_2(z_*) f(z_*)$. Combining all terms together we have

$$p = \int \frac{d^2 k}{(2\pi)^2} \sum_{z_*} \left(\frac{1}{2} T \ln \left(2 \cosh \frac{z_*}{2T} \right) + \frac{1}{4} \Sigma_2(z_*) \tanh \frac{z_*}{2T} \right), \quad (\text{B25})$$

which is exactly Eq. (B11). Here, z_* is the pole of the fermion propagator without the imaginary part Σ_2 , and summing over the poles is understood. If we take z_* to be the pole of the full propagator, z_* becomes imaginary and a generalization of hyperbolic functions to the Γ functions is necessary as in Eq. (B12). Then we arrive at Eq. (B14) for the pressure of the system.

3. DC conductivity from the Kubo formula

We calculate the DC conductivity in the boundary theory using the gravity-“dressed” retarded/advanced fermion propagators. Strictly speaking, we need also the “dressed” vertex, to satisfy the Ward identities. As argued in Ref. [33] however, the boundary vertex which is obtained from the bulk one can be approximated by a constant in the low-temperature limit. Also, according to Ref. [54], the vertex only carries the singularities of the product of the Green’s functions. Therefore, dressing the vertex will not change the temperature dependence of the DC conductivity at low ω [54].

We can start from the Kubo formula for conductivity:

$$\sigma = -\frac{\partial}{\partial \omega} \text{Im} \Pi_{AA}(\omega, \vec{k} = 0) |_{\omega=0}. \quad (\text{B26})$$

The polarization operator Π_{AA} is given by

$$\Pi_{AA}(i\nu_n, 0) = \int \frac{d^2 k}{(2\pi)^2} T \sum_{\omega_m} G(i\omega_m + i\nu_n, \vec{k}) \Lambda_A \\ \times (i\omega_m + i\nu_n, i\omega_m, \vec{k}) G(i\omega_m, \vec{k}) \Lambda_A^{(0)}(\vec{k}), \quad (\text{B27})$$

where the fermion frequency is $\omega_m = (2m + 1)\pi T$, and the boson frequency is $\nu_n = 2n\pi T$, and in the low-temperature limit $\Lambda_A(i\omega_m + i\nu_n, i\omega_m, \vec{k}) = \Lambda_A^{(0)}(\vec{k})$. Usually the most difficult step is to take the Matsubara sum. Here we can do it in two ways. The first way consists of analytically continuing in the complex plane $i\omega_m \rightarrow z$ and replacing the Matsubara sum by a contour integral with the Fermi distribution function $n(x) = \frac{1}{e^x + 1}$ whose poles sit at the Matsubara frequencies along the imaginary axis. The second way is to use the spectral representation. In both cases we follow Ref. [54], where transport coefficients were calculated with propagators including their imaginary parts.

Taking the first way, we have for the fermion Matsubara sum

$$H(i\nu_n, \vec{k}) = T \sum_{\omega_m} G(i\omega_m + i\nu_n, \vec{k}) G(i\omega_m, \vec{k}) \\ \rightarrow -\frac{1}{2\pi i} \int_C dz G(z + i\nu_n, \vec{k}) G(z, \vec{k}) n(z), \quad (\text{B28})$$

where the contour along the imaginary z axis can be deformed to the contour C which goes along two branch cuts, $\text{Im}z = 0$ and $\text{Im}z = -\nu_n$, and the large arcs Γ with vanishing contribution [54]. The fermion propagator has a branch cut along $\text{Im}z = 0$ [54,55]. Therefore we can rewrite

$$H(i\nu_n) = -\frac{1}{2\pi i} \int_{-\infty}^{\infty} d\zeta n(\zeta) G(i\nu_n + \zeta) (G_R(\zeta) - G_A(\zeta)) \\ -\frac{1}{2\pi i} \int_{-\infty}^{\infty} d\zeta n(\zeta) G(-i\nu_n + \zeta) (G_R(\zeta) - G_A(\zeta)), \quad (\text{B29})$$

where the difference of the retarded and advanced functions in the first bracket is due to the discontinuity along $\text{Im}z = 0$ and in the second bracket it is due to the discontinuity along $\text{Im}z = -\nu_n$. This contribution corresponds to the second term in Eq. (B28), and there are no pole contributions [54]. We use the usual prescription for retarded and advanced Green’s functions, $G_R = G(\omega + i0^+)$ and $G_A = G(\omega - i0^+)$ and suppress the momentum indices. Taking $i\nu_n \rightarrow \omega + i0^+$, we have

$$\begin{aligned}
H(\omega) = & -\frac{1}{2\pi i} \int_{-\infty}^{\infty} d\zeta n(\zeta) G_R(\omega + \zeta) (G_R(\zeta) - G_A(\zeta)) \\
& -\frac{1}{2\pi i} \int_{-\infty}^{\infty} d\zeta n(\zeta + \omega) G_A(\omega + \zeta) \\
& \times (G_R(\zeta + \omega) - G_A(\zeta + \omega)), \quad (\text{B30})
\end{aligned}$$

where we changed the integration variable in the second integral $\zeta - \omega \rightarrow \zeta$. In the limit $\omega \rightarrow 0$, the dominant contribution comes from the pair $G_R G_A$, and it is inversely proportional to the distance between the poles given by the imaginary part Σ_2 . The combinations $G_R G_R$ and $G_A G_A$ with the poles on one side of the real axis make a much smaller contribution due to the cancellation between the residues at the poles. Therefore, as $\omega \sim 0$, we have

$$\begin{aligned}
H(\omega, \vec{k}) \rightarrow & -\frac{1}{2\pi i} \int_{-\infty}^{\infty} d\zeta (n(\zeta + \omega) \\
& - n(\zeta)) G_R(\zeta + \omega) G_A(\zeta), \quad (\text{B31})
\end{aligned}$$

and

$$\begin{aligned}
\text{Im}\Pi_{AA}(\omega, 0) = & \frac{1}{2\pi} \int \frac{d^2 k}{(2\pi)^2} \Lambda_A^{(0)}(\vec{k}) \int_{-\infty}^{\infty} \frac{d\zeta}{2\pi} (n(\zeta + \omega) \\
& - n(\zeta)) G_R(\zeta + \omega, \vec{k}) \\
& \times \Lambda_A(\zeta + \omega + i0^+, \zeta - i0^-, \vec{k}) G_A(\zeta, \vec{k}). \quad (\text{B32})
\end{aligned}$$

In the small- T limit the vertex is a constant. We integrate around the Fermi surface, and therefore the momentum integral is $\int \frac{d^2 k}{(2\pi)^2} \rightarrow \frac{k_F dk_{\perp}}{(2\pi)^2}$ with $k_{\perp} = k - k_F$. We exchange the order of integration and perform first the momentum integration [27,33]. For $\omega \sim 0$, we have

$$\int_{-\infty}^{\infty} \frac{dk_{\perp}}{2\pi} \frac{1}{\left(\frac{\zeta}{\nu_F} - k_{\perp} + \Sigma(\zeta, k_F) + i0^+\right) \left(\frac{\zeta}{\nu_F} - k_{\perp} + \Sigma^*(\zeta, k_F) - i0^+\right)} = \frac{i}{\Sigma(\zeta, k_F) - \Sigma^*(\zeta, k_F)} = \frac{1}{2\text{Im}\Sigma(\zeta, k_F)}. \quad (\text{B33})$$

Writing $n'(\zeta) = -\beta n(\zeta)(1 - n(\zeta))$, we have for $\omega \sim 0$

$$\sigma \rightarrow \Lambda^{(0)2} k_F h_1^2 \int_{-\infty}^{\infty} \frac{\beta d\zeta n(\zeta)(1 - n(\zeta))}{2\pi \text{Im}\Sigma(\zeta, k_F)}, \quad (\text{B34})$$

where we have dropped constant terms. Note that we get the same result for the conductivity also if we use $\tanh \frac{x}{2}$ in the contour integral (B28) since $n'(x) = -2 \tanh'(\frac{x}{2})$. For the Landau Fermi liquid $\Sigma(\omega) \sim \omega^2$ at small T [33,58]. We get

$$\sigma \sim T^{-2}, \quad (\text{B35})$$

meaning that we recover the standard result for the resistivity of the Fermi liquid: $\rho \sim T^2$.

In our case, $\Sigma(\omega) \sim \omega^{2\nu_{k_F}}$, which produces

$$\sigma \sim T^{-2\nu_{k_F}}. \quad (\text{B36})$$

This result agrees with the DC conductivity obtained in Ref. [33]. For the marginal liquid, $\nu_{k_F} = \frac{1}{2}$, we recover the resistivity $\rho \sim T$, which is empirically found in the strange metal phase.

- (i) It is interesting that the scaling behavior of the DC conductivity is the same as the single-particle scattering rate. On the gravity side it is explained by the fact that the dissipative part of the current-current correlator is controlled by the rate of the bulk fermion falling in the horizon, given by the single-particle scattering rate. Comparing the resistivity in

the quantum critical metal ‘‘qcm’’ to the one in the normal metal ‘‘m,’’

$$\rho_{\text{qcm}} > \rho_{\text{m}}, \quad (\text{B37})$$

which indicates that the quantum critical metal becomes increasingly insulating as ν_{k_F} is decreased. This suggests that there is some sort of ordering in the system, not necessarily associated with a gap.

To check our calculation, we get the DC conductivity using the spectral representation

$$G(i\omega_m, \vec{k}) = \int \frac{dk_0}{2\pi} \frac{A(k_0, \vec{k})}{k_0 - i\omega_m}, \quad (\text{B38})$$

where the spectral function $A(k_0, \vec{k})$ is given by Eq. (B6). For the product of the Green functions we use the following formula:

$$T \sum_m \frac{1}{i\omega_m - \omega_1} \frac{1}{i\omega_m + i\nu_n - \omega_2} = \frac{n(\omega_1) - n(\omega_2)}{i\nu_n + \omega_1 - \omega_2}. \quad (\text{B39})$$

Taking $i\nu_n \rightarrow \omega + i0^+$, the polarization operator is given by

$$\begin{aligned}
\Pi_{AA}(\omega, 0) = & \int \frac{d^2 k}{(2\pi)^2} \frac{d\omega_1}{2\pi} \frac{d\omega_2}{2\pi} \frac{n(\omega_1) - n(\omega_2)}{\omega + \omega_1 - \omega_2} \\
& \times \Lambda_A^{(0)2} A(\omega_1, k_{\perp}) A(\omega_2, k_{\perp}). \quad (\text{B40})
\end{aligned}$$

Performing the integration over ω_2 , we have

$$\begin{aligned} \text{Im}\Pi_{AA}(\omega, 0) = & \int \frac{d^2k}{(2\pi)^2} \frac{d\omega_1}{2\pi} (n(\omega_1) \\ & - n(\omega_2)) \Lambda_A^{(0)2} A(\omega_1, k_\perp) A(\omega_1 + \omega, k_\perp). \end{aligned} \quad (\text{B41})$$

In the limit $\omega \sim 0$, the momentum integration proceeds as

$$\int \frac{d^2k}{(2\pi)^2} A^2(\omega_1, k_\perp) \rightarrow k_F \int \frac{dk_\perp}{2\pi} A^2(\omega_1, k_\perp) \rightarrow \frac{k_F h_1^2}{\Sigma_2(\omega_1, k_F)}, \quad (\text{B42})$$

with $\Sigma_2 = \text{Im}\Sigma$. Therefore, the DC conductivity given by Eq. (B26) is

$$\sigma \rightarrow \Lambda_A^{(0)2} k_F h_1^2 \int \frac{\beta d\omega_1}{2\pi} \frac{n(\omega_1)(1-n(\omega_1))}{\text{Im}\Sigma(\omega_1, k_F)} \quad (\text{B43})$$

which is the same as Eq. (B34) obtained by the contour integration.

-
- [1] S. S. Lee, A non-Fermi liquid from a charged black hole: a critical Fermi ball, *Phys. Rev. D* **79**, 086006 (2009).
- [2] D. F. Mross, J. McGreevy, H. Liu, and T. Senthil, A controlled expansion for certain non-Fermi liquid metals, *Phys. Rev. B* **82**, 045121 (2010).
- [3] P. Coleman and A. J. Schofield, Quantum criticality, *Nature (London)* **433**, 226 (2005).
- [4] C. M. Varma, P. B. Littlewood, S. Schmitt-Rink, E. Abrahams, and A. E. Ruckenstein, Phenomenology of the normal state of Cu-O high-temperature superconductors, *Phys. Rev. Lett.* **63**, 1996 (1989).
- [5] S. A. Hartnoll, J. Polchinski, E. Silverstein, and D. Tong, Towards strange metallic holography, *J. High Energy Phys.* **04** (2010) 120.
- [6] M. Čubrović, J. Zaanen, and K. Schalm, Constructing the AdS dual of a Fermi liquid: AdS black holes with Dirac hair, *J. High Energy Phys.* **10** (2011) 017.
- [7] S. A. Hartnoll and A. Tavanfar, Electron stars for holographic metallic criticality, *Phys. Rev. D* **83**, 046003 (2011).
- [8] S. A. Hartnoll, D. M. Hofman, and A. Tavanfar, Holographically smeared Fermi surface: quantum oscillations and Luttinger count in electron stars, *Europhys. Lett.* **95**, 31002 (2011).
- [9] S. Sachdev, A model of a Fermi liquid using gauge-gravity duality, *Phys. Rev. D* **84**, 066009 (2011).
- [10] L. Huijse and S. Sachdev, Fermi surfaces and gauge-gravity duality, *Phys. Rev. D* **84**, 026001 (2011).
- [11] S. Sachdev, Holographic metals and the fractionalized Fermi liquid, *Phys. Rev. Lett.* **105**, 151602 (2010).
- [12] M. Čubrović, J. Zaanen, and K. Schalm, String theory, quantum phase transitions and the emergent Fermi-liquid, *Science* **325**, 439 (2009).
- [13] H. Liu, J. McGreevy, and D. Vegh, Non-Fermi liquids from holography, *Phys. Rev. D* **83**, 065029 (2011).
- [14] T. Faulkner, H. Liu, J. McGreevy, and D. Vegh, Emergent quantum criticality, Fermi surfaces, and AdS2, *Phys. Rev. D* **83**, 125002 (2011).
- [15] E. Gubankova, J. Brill, M. Čubrović, K. Schalm, P. Schijven, and J. Zaanen, Holographic fermions in external magnetic fields, *Phys. Rev. D* **84**, 106003 (2011).
- [16] T. Faulkner, G. T. Horowitz, and M. M. Roberts, Holographic quantum criticality from multi-trace deformations, *J. High Energy Phys.* **04** (2011) 051.
- [17] A. H. Castro Neto, F. Guinea, N. M. R. Peres, K. S. Novoselov, and A. K. Geim, The electronic properties of graphene, *Rev. Mod. Phys.* **81**, 109 (2009).
- [18] J. G. Checkelsky, L. Li, and N. P. Ong, Divergent resistance at the Dirac point in graphene: evidence for a transition in a high magnetic field, *Phys. Rev. B* **79**, 115434 (2009); The zero-energy state in graphene in a high magnetic field, *Phys. Rev. Lett.* **100**, 206801 (2008).
- [19] Y. Zhao, P. Cadden-Zimansky, Z. Jiang, and P. Kim, Symmetry breaking of the zero energy Landau level in bilayer graphene, *Phys. Rev. Lett.* **104**, 066801 (2010).
- [20] A. J. M. Giesbers, L. A. Ponomarenko, K. S. Novoselov, A. K. Geim, M. I. Katsnelson, J. C. Maan, and U. Zeitler, Gap opening in the zeroth Landau level of graphene, *Phys. Rev. B* **80**, 201430(R) (2009).
- [21] Y. Kopelevich, V. V. Lemanov, S. Moehlecke, and J. H. S. Torres, Landau level quantization and possible superconducting instabilities in highly oriented pyrolytic graphite, *Phys. Solid State* **41**, 1959 (1999); H. Kempa, Y. Kopelevich, F. Mrowka, A. Setzer, J. H. S. Torres, R. Hhne, and P. Esquinazi, Magnetic-field-driven superconductor-insulator-type transition in graphite, [arXiv:cond-mat/0005439](https://arxiv.org/abs/cond-mat/0005439).
- [22] E. V. Gorbar, V. P. Gusynin, V. A. Miransky, and I. A. Shovkovy, Dynamics in the quantum Hall effect and the phase diagram of graphene, *Phys. Rev. B* **78**, 085437 (2008); Coulomb interaction and magnetic catalysis in the quantum Hall effect in graphene, *Phys. Scr. T* **146**, 014018 (2012); E. V. Gorbar, V. P. Gusynin, and V. A. Miransky, Toward theory of quantum Hall effect in graphene, *Low Temp. Phys.* **34**, 790 (2008).
- [23] T. Faulkner and J. Polchinski, Semi-holographic Fermi liquids, *J. High Energy Phys.* **06** (2011) 012.
- [24] T. Albash and C. V. Johnson, Holographic aspects of Fermi liquids in a background magnetic field, *J. Phys. A* **43**, 345405 (2010).

- [25] T. Albash and C. V. Johnson, Landau levels, magnetic fields and holographic Fermi liquids, *J. Phys. A* **43**, 345404 (2010).
- [26] H. Liu, J. McGreevy, and D. Vegh, Non-Fermi liquids from holography, *Phys. Rev. D* **83**, 065029 (2011).
- [27] T. Hartman and S. A. Hartnoll, Cooper pairing near charged black holes, *J. High Energy Phys.* **06** (2010) 005.
- [28] L. D. Landau and E. M. Lifshitz, *Statistical Physics Part 2* (Elsevier, New York, 1980), Chap. 41.
- [29] T. Faulkner, G. T. Horowitz, J. McGreevy, M. M. Roberts, and D. Vegh, Photoemission “experiments” on holographic superconductors, *J. High Energy Phys.* **03** (2010) 121.
- [30] S. Bolognesi and D. Tong, Magnetic catalysis in AdS4, *Classical Quantum Gravity* **29**, 194003 (2012).
- [31] G. T. Horowitz and M. M. Roberts, Zero temperature limit of holographic superconductors, *J. High Energy Phys.* **11** (2009) 015.
- [32] N. Iqbal, H. Liu, M. Mezei, and Q. Si, Quantum phase transitions in holographic models of magnetism and superconductors, *Phys. Rev. D* **82**, 045002 (2010).
- [33] T. Faulkner, N. Iqbal, H. Liu, J. McGreevy, and D. Vegh, Strange metal transport realized by gauge/gravity duality, *Science* **329**, 1043 (2010).
- [34] F. Preis, A. Rebhan, and A. Schmitt, Inverse magnetic catalysis in dense holographic matter, *J. High Energy Phys.* **03** (2011) 033.
- [35] S. S. Gubser and I. R. Klebanov, A universal result on central charges in the presence of double-trace deformations, *Nucl. Phys.* **B656**, 23 (2003).
- [36] D. B. Kaplan, J.-W. Lee, D. T. Son, and M. A. Stephanov, Conformality lost, *Phys. Rev. D* **80**, 125005 (2009).
- [37] M. Čubrović, Y. Liu, K. Schalm, Y.-W. Sun, and J. Zaanen, Spectral probes of the holographic Fermi ground state: dialing between the electron star and AdS Dirac hair, *Phys. Rev. D* **84**, 086002 (2011).
- [38] A. Adams and J. Wang, Towards a non-relativistic holographic superfluid, *New J. Phys.* **13**, 115008 (2011).
- [39] S. Cremonesi, D. Melnikov, and Y. Oz, Stability of asymptotically Schroedinger RN black hole and superconductivity, *J. High Energy Phys.* **04** (2010) 048.
- [40] V. Gusynin, V. Miransky, and I. Shovkovy, Catalysis of dynamical flavor symmetry breaking by a magnetic field in $2 + 1$ dimensions, *Phys. Rev. Lett.* **73**, 3499 (1994); Dynamical flavor symmetry breaking by a magnetic field in $2 + 1$ dimensions, *Phys. Rev. D* **52**, 4718 (1995); Dimensional reduction and dynamical chiral symmetry breaking by a magnetic field in $3 + 1$ dimensions, *Phys. Lett. B* **349**, 477 (1995); Dynamical chiral symmetry breaking by a magnetic field in QED, *Phys. Rev. D* **52**, 4747 (1995).
- [41] M. Chernodub, Can nothing be a superconductor and a superfluid?, [arXiv:1104.4404](https://arxiv.org/abs/1104.4404); Superconductivity of QCD vacuum in strong magnetic field, *Phys. Rev. D* **82**, 085011 (2010).
- [42] G. W. Semenoff, Chiral symmetry breaking in graphene, *Phys. Scr. T* **T146**, 014016 (2012).
- [43] S. Bolognesi, Monopoles and holography, in *Proceedings of Continuous Advances in QCD, Minneapolis, MN, May 12–15, 2011* (to be published), <http://www.ftpi.umn.edu/workshops/>.
- [44] A. Schmitt, *Inverse magnetic catalysis in dense holographic matter, CSC seminar at Goethe University, Frankfurt, 2012*, <http://hep.itp.tuwien.ac.at/~aschmitt/frankfurt.pdf>.
- [45] M. Thies, From relativistic quantum fields to condensed matter and back again: updating the Gross-Neveu phase diagram, *J. Phys. A* **39**, 12707 (2006); J. Hofmann, Dimensional reduction in quantum field theories at finite temperature and density, *Phys. Rev. D* **82**, 125027 (2010).
- [46] J. Figueroa-O’Farrill, Electromagnetic duality for children, <http://www.maths.ed.ac.uk/jmf/Teaching/Lectures/EDC.pdf>.
- [47] B. I. Halperin, *Helv. Phys. Acta* **56**, 75 (1983); Y. Kopelevich, B. Raquet, M. Goiran, W. Escoffier, R. R. da Silva, J. C. Medina Pantoja, I. A. Lukyanchuk, A. Sinchenko, and P. Monceau, Searching for the Fractional Quantum Hall Effect in Graphite, *Phys. Rev. Lett.* **103**, 116802 (2009).
- [48] D. E. Kharzeev and H. J. Warringa, Chiral magnetic conductivity, *Phys. Rev. D* **80**, 034028 (2009); K. Fukushima, D. E. Kharzeev, and H. J. Warringa, Electric-current susceptibility and the chiral magnetic effect, *Nucl. Phys.* **A836**, 311 (2010); Real-time dynamics of the chiral magnetic effect, *Phys. Rev. Lett.* **104**, 212001 (2010).
- [49] J. P. Eisenstein and A. P. MacDonald, Bose-Einstein condensation of excitons in bilayer electron system, *Nature (London)* **432**, 691 (2004).
- [50] R. Contino and A. Pomarol, Holography for fermions, *J. High Energy Phys.* **11** (2004) 058.
- [51] S. B. Ruster, I. A. Shovkovy, and D. H. Rischke, Phase diagram of dense neutral three-flavor quark matter, *Nucl. Phys.* **A743**, 127 (2004); S. B. Ruster and D. H. Rischke, Effect of color superconductivity on the mass and radius of a quark star, *Phys. Rev. D* **69**, 045011 (2004).
- [52] F. Denef, S. A. Hartnoll, and S. Sachdev, Quantum oscillations and black hole ringing, *Phys. Rev. D* **80**, 126016 (2009).
- [53] F. Denef, S. A. Hartnoll, and S. Sachdev, Black hole determinants and quasinormal modes, *Classical Quantum Gravity* **27**, 125001 (2010).
- [54] M. A. V. Basagoiti, Transport coefficients and ladder summation in hot gauge theories, *Phys. Rev. D* **66**, 045005 (2002); J. M. M. Resco and M. A. V. Basagoiti, Color conductivity and ladder summation in hot QCD, *Phys. Rev. D* **63**, 056008 (2001).
- [55] T. Koide, notes on a branch cut in the integrals $\ln z = \int_1^z \frac{d\zeta'}{\zeta'}$ where z is imaginary (unpublished).
- [56] A. Sedrakian and G. Röpke, A quantum kinetic equation for Fermi-systems including three-body correlations, *Ann. Phys. (N.Y.)* **266**, 524 (1998).
- [57] I. S. Gradshteyn and I. W. Ryzhik, *Tables of Integrals, Series, and Products* (Academic Press, New York, 1965).
- [58] L. D. Landau and E. M. Lifshitz, *Physical Kinetics* (Elsevier, New York, 1981), Chap. 76.

Dissipation-induced first-order decoherence phase transition in a noninteracting fermionic systemM. V. Medvedyeva,¹ M. T. Čubrović,² and S. Kehrein¹¹*Institute for Theoretical Physics, Georg-August-Universität Göttingen, Friedrich-Hund-Platz 1, D-37077 Göttingen, Germany*²*Institute for Theoretical Physics, Universität zu Köln, Zùlpicher Str. 77, D-50937 Köln, Germany*

(Received 21 October 2014; revised manuscript received 3 February 2015; published 13 May 2015)

We consider a quantum wire connected to the leads and subjected to dissipation along its length. The dissipation manifests as tunneling into (out of) the chain from (to) a memoryless environment. The evolution of the system is described by the Lindblad equation. Already infinitesimally small dissipation along the chain induces a quantum phase transition (QPT). This is a decoherence QPT: the reduced density matrix of a subsystem in the nonequilibrium steady state (far from the ends of the chain) can be represented as the tensor product of single-site density matrices. The QPT is identified from the jump of the current and the entropy per site as the dissipation becomes nonzero. We also explore the properties of the boundaries of the chain close to the transition point and observe that the boundaries behave as if they undergo a second-order phase transition as a function of the dissipation strength: the particle-particle correlation functions and the response to the electric field exhibit a power-law divergence. Disorder is known to localize one-dimensional systems, but the coupling to the memoryless environment pushes the system back into the delocalized state even in the presence of disorder. Interestingly, we observe a similar transition in the classical dissipative counterflow model: the current has a jump at the ends of the chain introducing an infinitely small dissipation.

DOI: [10.1103/PhysRevB.91.205416](https://doi.org/10.1103/PhysRevB.91.205416)

PACS number(s): 03.65.Yz, 72.10.-d, 72.15.Rn, 05.30.Fk

I. INTRODUCTION

Coupling to the environment can significantly change the properties of a quantum system. Intuitively, the presence of dissipation leads to a decrease of coherence in the system. It can induce various types of phase transitions [1–9].

The best known example of such a transition is exhibited by the spin-boson model: there is a critical value of the interaction between the two-level system and the bosonic environment, which localizes the system [10]. A more complicated example is the superconductor-metal transition in dissipative nanowires [6,7], which can be modeled as a dissipative XY -spin chain, with a coupling to the bosonic bath at every site of the chain. It was shown both analytically and numerically [6,8,9] that the system experiences a universal second-order phase transition at the critical value of the coupling to the environment.

These are examples in the presence of the bosonic bath. Realistically, especially in condensed matter systems, the bath can be also fermionic [11]. It is possible to describe it in a similar manner as the bosonic bath in the spin-boson model, i.e., using the Feynman-Vernon formalism. However, it is rather complicated to consider more than one or two sites in such a formulation. The problem is often simplified by studying a Lindblad-type equation [12,13]. This corresponds to a memoryless bath. Physically, this means that the quasiparticles in the bath are assumed to have a much smaller dynamical timescale compared to the excitations in the system. Even the memoryless dissipation induces a novel behavior in the quantum systems. For example, dissipation along the system can lead to the algebraic decoherence in strongly interacting systems [14].

Phase transitions have been observed in the presence of a particle or energy flow in various spin chains [15]. For example, the equilibrium phase diagram of the transverse field Ising model has two phases: ordered and disordered; while in the presence of particle flow a new phase appears, which carries a nonzero particle flux [16].

The density matrix of the nonequilibrium steady state (NESS) of a noninteracting fermionic system is associated with an effective Hamiltonian [3]. In this formalism, phase transitions can be observed directly from the spectrum of the effective Hamiltonian, which shows features absent in the closed system. For example, a topological phase transition has been found in a cold atomic system subjected to laser irradiation [3].

Equilibrium phase transitions are characterized by discontinuous derivatives of the free energy [17]: the order of the transition is equal to the order of the first discontinuous derivative. In a nonequilibrium situation the free energy is not a well-defined statistical quantity. The partition function, on the other hand, remains well defined also for a nonequilibrium system, as well as entropy, which is given by the logarithm of the number of microstates [18]. Starting from the partition function or entropy we can define the (nonequilibrium) susceptibilities even though the free energy is ill defined [17]. The susceptibility diverges at the transition point [19]. For the second-order quantum phase transition (QPT) the divergence is physical and detectable, while it is a δ -function-like divergence for a first-order transition. This means that in an infinite system undergoing a first-order phase transition, when the divergence equals the Dirac δ function, we can only observe the step (discontinuity) in susceptibility, while the (infinitely narrow) Dirac δ peak is not measurable.

A. Short overview

In this paper we study the fermionic chain connected to the memoryless bath at every site of the chain, hence we consider the Lindblad equation for noninteracting fermions [5,20–22]. The ends of the chain are connected to noninteracting memoryless leads [22,23]. The difference in chemical potential induces the particle flow in the system. We find a first-order QPT that separates the regimes of coherent and dissipative transport along the chain. The coherent state is characterized by the

constant current along the chain, while in the dissipative state the current induced by the coupling to the reservoirs decays exponentially inside the chain. QPT between the two happens already at an infinitesimally small coupling to the environment, i.e., the critical coupling value is zero. The transition can be understood microscopically from the fact that the density matrix is decomposed into the tensor product of one-site density matrices in the bulk. The phenomenological reason for the transition is breaking of the time-reversal symmetry by the dissipation along the chain. From the thermodynamic point of view, the transition is a consequence of the entropy-per-site jump. The bulk susceptibility also has a jump at the transition. These facts make us conclude that it is a first-order phase transition. We also detect the jump of the steady-state current at the ends of the chain for sufficiently long chains. We can observe this nonequilibrium QPT in the spectrum of the effective Hamiltonian of the NESS: the gap present for zero dissipation along the chain closes in the presence of dissipation. A nonequilibrium QPT in the system coupled to the Markovian bath has also been observed in the XY -spin chain [2,5] and in the XX -spin chain [1].

The phase transitions are normally considered in the thermodynamic limit and the effects of the boundaries (finite-size effects) are neglected (or, in numerical work, systematically eliminated, e.g., by finite-size scaling). When we discuss the transition between the coherent transport through the chain and decoherent state induced by dissipation, we cannot neglect the effects of the boundaries, because the particle current is due to the injection of particles at the ends of the chain. Therefore, we study the particle-particle correlation functions and the electrical susceptibility in the NESS at the ends of the chain and observe power-law divergences as a function of dissipation strength along the chain.

We also consider the workings of dissipation in the presence of disorder. We find that any memoryless dissipation extended along the chain destroys the localization by disorder. This result supports previous studies by the scattering matrix approach [24] and the Landauer-type approach with decoherence [25]. The phase transition to the dissipative state is universal and preserved in the presence of disorder.

II. MODEL AND FORMALISM

We are interested in the properties of the nonequilibrium steady state of a chain of noninteracting fermions linearly coupled to several noninteracting fermionic baths (reservoirs; we use the two terms as synonymous). The full Hamiltonian of such system is

$$H_{\text{full}} = H_{\text{sys}} + \sum_{i,\alpha} H_{i,\alpha,\text{coup}} + \sum_{i,\alpha} H_{i,\alpha,\text{bath}}, \quad (1)$$

where H_{sys} is the tight-binding Hamiltonian of the system:

$$H_{\text{sys}} = \sum_{\{ij\}} t_{ij}(a_i^\dagger a_j + \text{H.c.}) + \sum_i U_i a_i^\dagger a_i, \quad (2)$$

with $\{ij\}$ denoting the links between the sites, t_{ij} is the hopping amplitude between the sites i and j and U_i is an on-site potential. By $H_{i,\alpha,\text{bath}}$ we denote the Hamiltonian of the bath: the index i here stands for the site of the chain, while the index

α denotes different baths coupled to the same site:

$$H_{i,\alpha,\text{bath}} = \sum_k \epsilon_{i,\alpha,k} b_{i,\alpha,k}^\dagger b_{i,\alpha,k}. \quad (3)$$

The annihilation operators in the baths are denoted by symbol $b_{i,\alpha,k}$, while the annihilation operators in the chain are a_i . Finally $H_{i,\alpha,\text{coup}}$ is the coupling between the system and the bath, with the coupling strength $p_{i,\alpha,k}$:

$$H_{i,\alpha,\text{coup}} = \sum_k p_{i,\alpha,k} (b_{i,\alpha,k}^\dagger a_{i,\alpha} + \text{H.c.}). \quad (4)$$

In our model we have exactly two baths at every site which we can denote as “incoming” and “outgoing”, with $\alpha \in \{(i),(o)\}$. The baths are described by the spectral function:

$$J_{i,\alpha}(\omega) = \sum_k |p_{i,\alpha,k}|^2 \delta(\omega - \epsilon_{i,\alpha,k}). \quad (5)$$

For a noninteracting system it has been shown [11,26] that under the assumption of constant spectral density in the reservoirs

$$J_{i,\alpha}(\omega) = v_{i,\alpha}$$

and for the plus/minus infinite chemical potential in the reservoirs the time evolution of the system is described by the Lindblad equation:

$$\begin{aligned} i \frac{d\rho}{d\tau} &= \mathcal{L}\rho, \mathcal{L}\rho \\ &= [H, \rho] + i \sum_{j,i/o} \{2\ell_j^{(i/o)} \rho \ell_j^{\dagger(i/o)} - [\ell_j^{\dagger(i/o)} \ell_j^{(i/o)}, \rho]\}, \end{aligned} \quad (6)$$

where the operator \mathcal{L} is called the Liouvillian and ℓ_j are the Lindblad operators responsible for the coupling to the bath:

$$\ell_j^{(i)} = \sqrt{\Gamma_j^{(i)}} a_j^\dagger, \quad \ell_j^{(o)} = \sqrt{\Gamma_j^{(o)}} a_j, \quad (7)$$

$$\Gamma_j^{(i)} = \pi v_{j,+\infty} \sum_k |p_{i,+\infty,k}|^2, \quad \Gamma_j^{(o)} = \pi v_{j,-\infty} \sum_k |p_{i,-\infty,k}|^2, \quad (8)$$

with $v_{j,\pm\infty}$ being the density of states in reservoirs connected to the site j with plus/minus infinite chemical potential. The infinite chemical potential ensures Markovian dynamics in the bath [27]: in the reservoir at the chemical potential $+\infty$ there are always particles which can hop into the system and in the reservoir at the chemical potential $-\infty$ there is always room for new particles hopping out of the system, therefore such baths are memoryless. The finite bandwidth, finite chemical potential, and finite temperature of the reservoirs would make the evolution equation for the density matrix nonlocal in time [11,26].¹ Let us also note that the coefficients Γ are not necessarily small, they can have any value. The difference from the ordinary derivation [13] is that here both

¹In the above derivation we have not discussed temperature, as it does not matter in the case of infinite chemical potential. When the chemical potential in the reservoirs becomes finite, the temperature appears as an additional parameter.

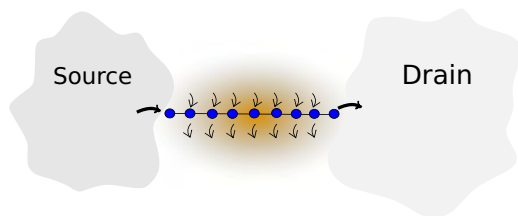


FIG. 1. (Color online) The setup of the problem: one-dimensional chain is connected to the source and the drain as in transport experiments. Every site of the chain is coupled to the environment, which models the dissipation from the leakage of the current due to imperfect insulation. The environment consists of two reservoirs at plus/minus infinite chemical potentials coupled at each site of the chain.

the system and the baths are noninteracting, therefore fewer assumptions are required to get the Lindblad form of the evolution equation.

Let us now apply the Lindblad formalism to our model. Our chain is L sites long and it is coupled to the source and the drain at infinite bias voltage at its ends:

$$\begin{aligned} \ell_1^{(i)} &= \sqrt{\Gamma^{(i)}} a_1^\dagger, & \ell_1^{(o)} &= 0, \\ \ell_L^{(i)} &= 0, & \ell_L^{(o)} &= \sqrt{\Gamma^{(i)}} a_L. \end{aligned}$$

There is also a dissipation along the chain into a finite temperature bath, which is represented by sources $\ell_\mu^{(i)} = \sqrt{d\Gamma_\mu^{(i)}} a_\mu^\dagger$ and drains $\ell_\mu^{(o)} = \sqrt{d\Gamma_\mu^{(o)}} a_\mu$, for $\mu = 2, \dots, L-1$. The $d\Gamma$ values are not infinitesimal: they are typically much smaller than $\Gamma^{(i,o)}$ but can take any value in principle; the notation $d\Gamma$ is just for convenience. Schematically, the dissipative wire setup we study is depicted in Fig. 1. From now on in the text and in the plots the Γ_μ values are measured in the units of the hopping t , which we assume to be constant along the chain (in other words we put $t_{ij} = t = 1$).

A. Solving the Lindblad equation

The solution of the Lindblad equations for noninteracting fermions is notably simplified in the superfermionic representation [21,22], which is based on the doubling of the degrees of freedom as in thermofield theory. Here instead of solving a differential equation for the evolution of the $2^L \times 2^L$ density matrix, the calculations are done with the $2L \times 2L$ matrices. The observables of the NESS are computed directly. What is more, the full-counting statistics of the transport through the ends of the chain can be obtained by introducing the counting field, which yields the generating function of the counting statistics [22,23]. We will present the results for the first cumulant of the generating function, i.e., the current, as well as for the ratio between the second and the first cumulant, which characterizes the noise in the system and is called the Fano factor.

We evaluate the current along the chain by averaging the local current operator over the NESS:

$$\hat{j}_k = -it(a_k^\dagger a_{k+1} - a_{k+1}^\dagger a_k). \quad (9)$$

At the ends of the chain the current and the Fano factor are given by the derivatives of the generating function.

The Liouvillian for noninteracting fermions in the superfermionic representation becomes quadratic after performing the particle-hole transformation [22], as the Liouvillian becomes diagonal in the basis $\{f, f^\ddagger, \tilde{f}, \tilde{f}^\ddagger\}$, see Appendix. The density matrix of the NESS is a vacuum for the operators f and \tilde{f} (see Appendix). As there exists a linear relation between the initial basis $\{a, a^\dagger, \tilde{a}, \tilde{a}^\dagger\}$ and the basis $\{f, f^\ddagger, \tilde{f}, \tilde{f}^\ddagger\}$, the density matrix of the NESS is quadratic:

$$\rho_{\text{NESS}} = \frac{\exp(\mathcal{H}_{mn} a^\dagger \tilde{a}^\dagger) |00\rangle_{a\tilde{a}}}{\langle I | \exp(\mathcal{H}_{mn} a^\dagger \tilde{a}^\dagger) |00\rangle_{a\tilde{a}}}, \quad \mathcal{H}_{jn} = \tilde{\kappa}_{ni}^{-1} \kappa_{ji}, \quad (10)$$

where the matrix κ is connected to the matrix of the eigenvectors P of the transformation which diagonalizes the particle-hole transformed Liouvillian [22] (see Appendix), namely $T = P^{-1}$, $\kappa_{kj} = T_{kj}$ and $\tilde{\kappa}_{kj} = T_{k+L,j}$ for $k, j = 1, \dots, L$. Notice that $i\mathcal{H}$ is a Hermitian matrix as ρ is Hermitian, and $\langle I |$ is the left vacuum, $|I\rangle = \sum_n |nn\rangle_{a\tilde{a}}$ [21], where by n we denote the state in the a basis. Therefore, $i\mathcal{H}$ can be considered as an effective Hamiltonian of the NESS.

III. DISSIPATION-INDUCED PHASE TRANSITION

In this section we first observe the dissipation-induced phase transition in the transport properties at the ends of the chain and in the bulk and then we characterize the transition in the thermodynamic limit. Afterwards we discuss some specific aspects of the transition at the ends of the chain by studying the response to electric field and the particle-particle correlation functions close to the ends and reveal its microscopic nature. Finally, we study the influence of the dissipation on the phenomenon of delocalization in disordered systems.

A. Observation of the transition

We model dissipation along the chain as tunneling to the metallic gate in the absence of good isolation of the one-dimensional chain from the environment. To implement this we couple a source and a sink to every site of the chain [21]. We also allow for disorder in the hybridization strengths $d\Gamma_\mu^{(i/o)}$ to account for different tunneling rates to the environment.

The fermionic chain coupled to the reservoirs only at its ends has a uniform current along its length due to particle conservation. Let us call the state of such a system coherent as the current at its ends depends on both couplings. On the other hand we call the state of the system decoherent when the current through a given end depends only on the coupling of the reservoir at this end.

We only expect to find a phase transition and the associated discontinuities in the thermodynamic limit, i.e., in an infinite system. For that reason we start by looking at a chain long enough that there is no dependence on its length, Fig. 2(b). We see a jump both in the current and in the Fano factor when the dissipation is switched on, Fig. 2(a). Reference [23] provides the large deviation calculation for the current distribution function of the chain coupled to the reservoirs only at its ends. The current distribution is discontinuous as a function of the couplings to the reservoirs and the author suggests that this is the reason of the phase transition also for the system dissipative along its length.

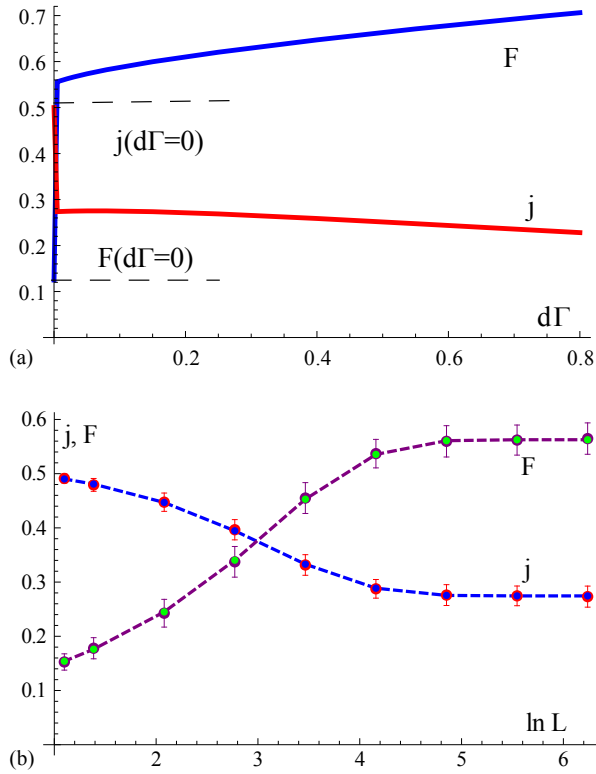


FIG. 2. (Color online) (a) The jump of the current, j , and the Fano factor, F , at infinitesimally small dissipation constant along the chain $d\Gamma = d\Gamma^{(i)} = d\Gamma^{(o)}$ ($\Gamma^{(i)} = \Gamma^{(o)} = 1$). (b) Dependence of the current j and the Fano factor F through the ends of the chain on the length L for random dissipation along the chain taken from the range $d\Gamma^{(i)}, d\Gamma^{(o)} \in (0, 0.04)$ (points with error bars) and for the constant dissipation with the strength $d\Gamma^{(i)} = d\Gamma^{(o)} = 0.02$ (points and the dashed lines). Here and everywhere else in the text and the plots the Γ_μ values are measured in the units of the hopping t .

In order to understand better the nature of the states on both sides of the transition, let us consider the current along the chain. We compute the expectation value of the local current operator (9) in the NESS for every link of the chain. For a nondissipative system it is constant along the chain due to the current conservation. For the dissipative case it decays exponentially inside the system, Fig. 3. One would certainly expect such behavior in the presence of the drains only. But in our setup we have both the source and the drain attached to every site of the chain. Therefore, we conclude that the exponential decrease of the current is connected to the coherence losses due to coupling to the memoryless environment, and not simply to the current leakage into the drains.

If we allow for a random distribution of the dissipation along the chain, the current averaged over disorder configurations decays with the same exponent as the current in the system with uniform dissipation, with the magnitude equal to the mean of the distribution of the disordered couplings, Fig. 3.

With increasing dissipation strength, the current through one end of the chain becomes only weakly dependent on the coupling at the other end of the chain because the coherence of the transport through the chain is lost upon adding the

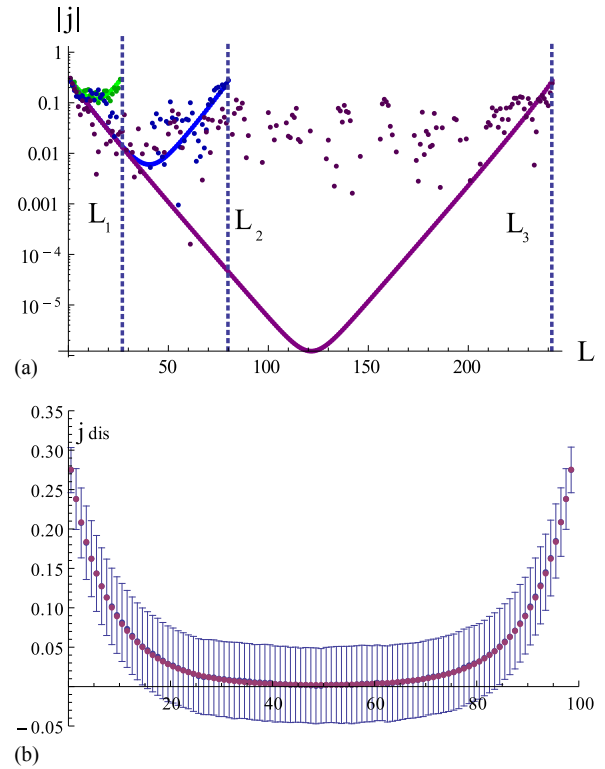


FIG. 3. (Color online) Exponential decay of the current along the chain. (a) Logarithmic scale, different lengths of the system. The currents in the system without randomness in dissipation are represented by the regular sets of points (forming solid lines). Darker, irregularly scattered points represent the current for one realization of the disorder in dissipation along the chain. (b) The current through a dissipative chain after averaging over different disorder realizations. The scale is linear (not logarithmic) to show the standard deviation of the (fluctuating, random) current. Notice that the negative values of the current are physical, because some realization of the (random) couplings $d\Gamma$ can give an overall current flowing in the opposite direction. The couplings at the ends of the chain are $\Gamma^{(i)} = \Gamma^{(o)} = 1$, $d\Gamma = 0.05$. For the average over disorder $d\Gamma_j^{(i)}, d\Gamma_j^{(o)} \in (0, 0.1)$, $j \in (2, L - 1)$.

dissipation along the chain, Fig. 4. Here we make a plot for the constant dissipation rate along the chain since the current averaged over disorder in coupling strengths is the same as in the case of the constant dissipation (see Fig. 3).

Both the presence of the jump in the transport characteristics at the ends of the chain and the coherence/decoherence transition in the current along the chain suggest that any nonzero dissipation along the chain induces the QPT. It is not a van der Waals-type transition, meaning there is no analog of the latent heat, that is, excitation of internal degrees of freedom, but the extra energy is instead exchanged with the bath.

1. Classical analogue

The Lindblad approximation for the driving at the ends of the chain and decoherence along the chain make our quantum model less quantum and more classical. This is exemplified by comparing our results with a classical model introduced

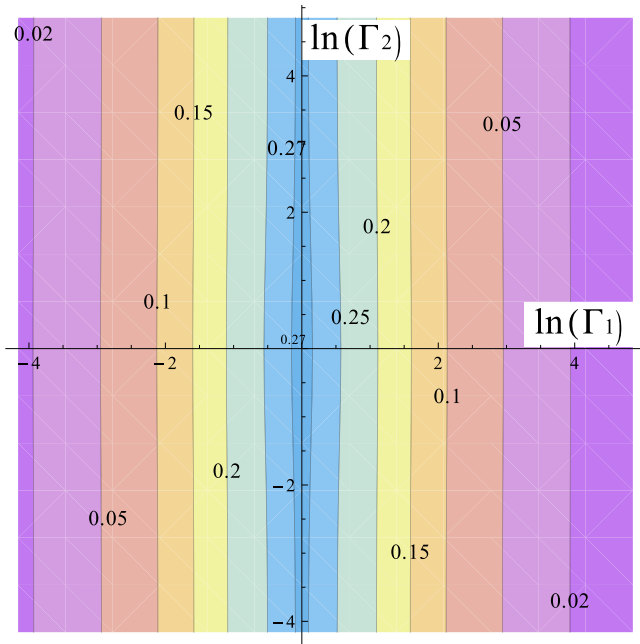


FIG. 4. (Color online) Logarithmic plot of the current flowing from the system into the reservoir at the beginning of the chain (denoted by 1) as a function of the hopping rates at the ends of the chain, in the presence of the constant dissipation along the chain, $d\Gamma^{(i)} = d\Gamma^{(o)} = 0.02$. Increasing the dissipation makes the current through one end independent of the coupling at the other end of the chain. In this plot we denote $\Gamma^{(i)} = \Gamma_1$, $\Gamma^{(o)} = \Gamma_2$.

by Roche, Derrida, and Doucot [28] for studying the classical version of the Landauer picture of a quantum conductor, where we also observe the exponential decay of the current inside the chain as well as the jump of the steady-state current at the ends of the chain upon introducing the dissipation along the chain.

We consider a counterflow model [28]: the system is modeled by an L -site chain, where each of the sites may contain two particles, one right-moving and one left-moving. It is analogous to the quantum scattering problem. Let us call the walls between the sites tunnel barriers. The time is discrete. At each time step the right-moving state on the left of the barrier and the left-moving state on the right of the barrier are transferred to the right-moving state on the right of the barrier and the left-moving state on the left of the barrier, respectively:

$$(0_{r,k-1}, 0_{l,k}) \rightarrow (0_{r,k}, 0_{l,k-1}), \quad (11)$$

$$(1_{r,k-1}, 1_{l,k}) \rightarrow (1_{r,k}, 1_{l,k-1}), \quad (12)$$

$$(0_{r,k-1}, 1_{l,k}) \rightarrow \begin{cases} (0_{r,k}, 1_{l,k-1}) \text{ with prob. } T, \\ (1_{r,k}, 0_{l,k-1}) \text{ with prob. } (1 - T) \end{cases} \quad (13)$$

$$(1_{r,k-1}, 0_{l,k}) \rightarrow \begin{cases} (1_{r,k}, 0_{l,k-1}) \text{ with prob. } T, \\ (0_{r,k}, 1_{l,k-1}) \text{ with prob. } (1 - T), \end{cases} \quad (14)$$

where on the left-hand/right-hand side of the arrow is the state before/after the time step respectively, 0 and 1 denote the state of the system (empty/full), the subscripts r/l stand for right-/left-moving and k stands for the cell number. The first and the last cell are updated at every time step to account for

the contact with the reservoirs:

$$(1_{r,1}, 0_{l,1}) \quad \text{with prob. } \rho_R, \quad (15)$$

$$(0_{r,1}, 0_{l,1}) \quad \text{with prob. } (1 - \rho_R), \quad (16)$$

$$(0_{r,L}, 1_{l,L}) \quad \text{with prob. } \rho_L, \quad (17)$$

$$(1_{r,L}, 1_{l,L}) \quad \text{with prob. } (1 - \rho_L). \quad (18)$$

The configuration space of this process grows exponentially with the the number of sites: it contains 2^L configurations. This makes it complicated to calculate the counting statistics using the transition matrix approach [28]. In general, the described model has a diffusive behavior: the current through the system decreases with increasing system size [28] (this happens because each transmission process is a stochastic process). In our model we obtain pure ballistic behavior by moving all particles in the middle of the chain (which are independent of the dynamics on the first and the last site) as a whole, which is just what ballistic propagation means.

While earlier work [28] considers only the flux of particles at the end of the chain, we introduce the dissipation in the middle of the chain as a classical analog of decoherence (from now on we call it decoherence to emphasize the lack of true quantum-mechanical coherence in the classical model) as a spontaneous appearance/disappearance of right/left moving particles in between two propagation steps. Therefore, our algorithm of time evolution of the dissipative chain is

(i) Initialize the time step:

(a) generate an arbitrary initial state in the first step;

(b) in the subsequent steps: update first the occupation on the first and the last site of the chain according to (15)–(18). Then update the occupation number in the middle, which changes due to decoherence: if both left- and right-moving states at the site k are empty, then with probability $d\Gamma^{(i)}/2$ one of them becomes occupied. If only the left- or right-moving state is empty, then this state becomes full with probability $d\Gamma^{(i)}$. The analogous update is done for hopping out of the chain with the rate $d\Gamma^{(o)}$.

(ii) Move the particles:

(a) the right/left movers on the site from 2 to $(L - 2)/3$ to $L - 1$ from are shifted in the ballistic way (the particle is moved by one site, if the site with the corresponding chirality on its way is empty);

(b) make a move of the states around the barriers according to rules (11)–(14);

(c) shift particles close to the ends if more ballistic motion is possible with respect to the configuration after (11)–(14) comparing to the initial configuration.

(iii) Repeat the steps (i) and (ii).

According to our numerical simulation the average over the time evolution of a single state equals to the average over different initial states evolved for a fixed time, which is long enough to approach the steady state, as we would expect in an ergodic system. We present the long-time averages over time of the evolution of a single state as it is less computationally consuming comparing to the other averaging procedure.

The current through the chain can be determined in two ways: as the difference between the right and left movers at each cell or as the number of the particle transmissions between

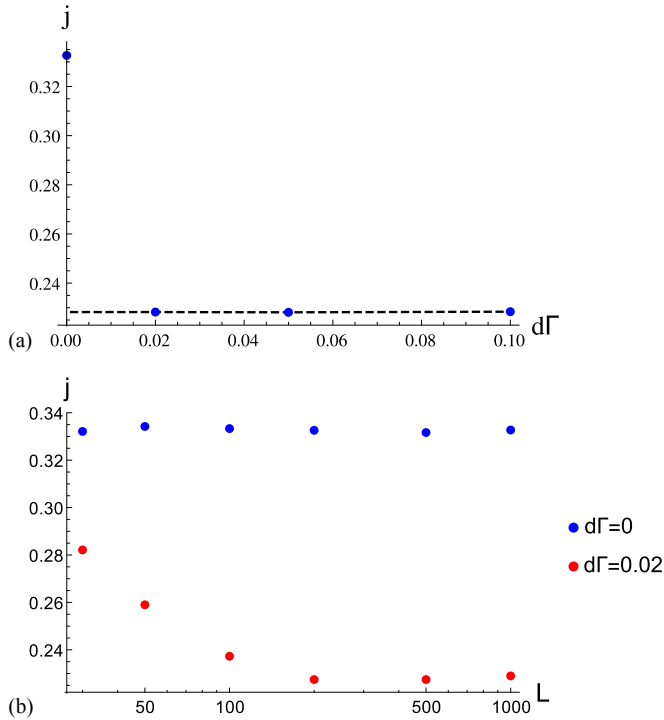


FIG. 5. (Color online) (a) The jump of the current at the end of the chain upon switching on the decoherence along the chain in the classical counterflow model. (b) Dependence of the current through the first site of the chain on the length of the chain. Compare to Fig. 3, where analogous behavior is observed for the quantum chain modeled by the Lindblad equation. $\Gamma_1^{(in)} = \Gamma_2^{(out)} = 0.5$

the neighboring cells. Qualitatively these approaches give the same answer for our decoherent problem.

To compare our numerical simulation with the Lindblad approach we fix $\rho_R = 1$ and $\rho_L = 0$ to model the leads at plus/minus infinite voltage. The time-averaged current decays exponentially from the ends of the chain toward the middle, Fig. 6. The saturation of the exponential decay in the middle happens due to finite time of averaging. The average current

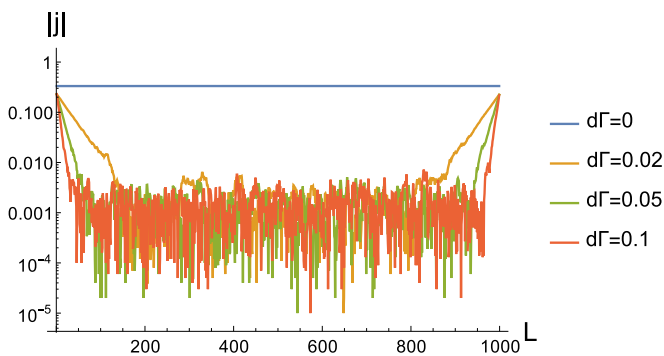


FIG. 6. (Color online) The dependence of the current on the site index for different decoherence rates $d\Gamma$ in logarithmic scale in the classical counterflow model: the exponential decay of the current from the ends toward the middle of the chain is clearly visible, suggesting a similar mechanism of decoherence as in the quantum chain in Fig. 4. $\Gamma_1^{(in)} = \Gamma_2^{(out)} = 0.5$, $t_{max} = 10^5$.

through the end of the chain jumps when decoherence is introduced in the system, Fig. 5. To observe the clear jump the number of time steps should be large enough that the system forgets about its initial configuration, at least about $L/d\Gamma$.

The behavior of the quantum chain is thus qualitatively reproduced by the classical stochastic model. It might therefore seem that the term quantum phase transition we have used for the transition in the quantum chain is a misnomer. This is not the case, since the classical counterflow model is stochastic and thus exhibits fluctuations around the expectation values, i.e., averaged values. The generating function of the counterflow model is thus analogous to the action of a quantum system, and the jump of the suitably defined classical current is formally analogous to the QPT observed earlier. A truly classical system (with no fluctuations) would not show such a phase transition.

B. First-order phase transition in the thermodynamic limit

Phase transitions are normally studied using the thermodynamic quantities and the response functions. In a nonequilibrium situation the partition function and the entropy are well-defined thermodynamic quantities. Here we concentrate on the entropy and the response to the electric field, and eventually explain the microscopic nature of the transition.

1. Entropy

The NESS is Gaussian, Eq. (10), as it can be represented as an exponent of a quadratic operator. Therefore, its effective Hamiltonian is a Hamiltonian of noninteracting fermions. In analogy with equilibrium statistical physics one can connect the entropy of the NESS to the eigenvalues μ_i of the effective Hamiltonian (10) [29]:

$$S = - \sum_i \left(\ln(1 + e^{-\epsilon_i}) + \frac{\epsilon_i}{1 + e^{\epsilon_i}} \right), \quad \mu_i = e^{-\epsilon_i}. \quad (19)$$

The entropy per unit length $S = \mathcal{S}/L$ does not depend on the system length for sufficiently long systems and experiences a jump upon turning on the dissipation along the chain, Fig. 7. For a chain without dissipation the specific entropy always depends on the couplings to the reservoirs at the ends of the chain, while for a dissipative system it does not depend on the couplings to the leads in the thermodynamic limit (the contribution from the boundaries is of the order of $1/L$). The specific entropy tends to a value depending only on the ratio of the incoming and outgoing rates along the chain $\gamma = d\Gamma^{(i)}/d\Gamma^{(o)}$:

$$S = \ln(1 + \gamma) - \frac{\gamma}{1 + \gamma} \ln \gamma. \quad (20)$$

This corresponds to the entropy of the single site coupled to only two baths by the Lindblad operators $\sqrt{d\Gamma^{(i)}}a^\dagger$ and $\sqrt{d\Gamma^{(o)}}a$. Indeed, the reduced density matrix of a site in the middle of the chain is the same as for a single site coupled to two baths up to a factor exponentially small in L . The coupling to the rest of the chain is irrelevant. The current in the middle of the chain vanishes, but what is happening is even stronger: the correlation between two neighboring sites vanishes exponentially $\langle c_{i+1}^\dagger c_i \rangle_{\text{NESS}} = O[\exp(-\beta i)]$, where i is the number of the site in the middle of the chain and β is the

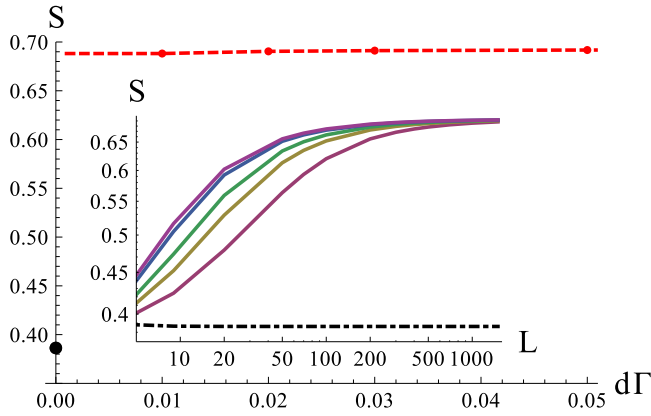


FIG. 7. (Color online) Entropy jump at the transition point as a function of the dissipation strength. The dashed line is in agreement with Eq. (20). Inset: dependence of the entropy on the chain length for different dissipation strengths $d\Gamma = 0.01, 0.02, 0.03, 0.04, 0.05, 0.06$ (from top to bottom solid curve respectively), the dash-dotted line corresponds to the entropy in the absence of the coupling to the environment, the point at $d\Gamma = 0$ at the main plot.

slope of the exponential decay. Therefore, we can write down the reduced density matrix of the middle part of the system neglecting the exponentially small correlations between the sites as a tensor product of the density matrix of one site connected to two baths.

2. Spatial decoupling in the density matrix

Such a spatial decoupling of a density matrix for a completely translationally invariant system (without current injection/removal at the ends) is evident. We can diagonalize the Liouvillian by the Fourier transform. Indeed, in terms of Ref. [22] the matrix M after the Fourier transform obtains the block structure:

$$\mathcal{L} = \sum_k (a_k^\dagger \tilde{a}_k) M_k \begin{pmatrix} a_k \\ \tilde{a}_k^\dagger \end{pmatrix} - i \sum_k (d\Gamma^{(i)} + d\Gamma^{(o)}), \quad (21)$$

$$M_k = \begin{pmatrix} -i\delta\Gamma + 2t \cos k & 2d\Gamma^{(o)} \\ -2d\Gamma^{(i)} & i\delta\Gamma + 2t \cos k \end{pmatrix} \quad (22)$$

with $\delta\Gamma = d\Gamma^{(i)} - d\Gamma^{(o)}$. Each of the matrices M_k can be diagonalized: $M_k = P_k^{-1} D_k P_k$, where D_k is a diagonal matrix and P_k is a matrix of eigenvectors. This transformation determines the basis where the Liouvillian is diagonal:

$$\begin{pmatrix} f_k \\ \tilde{f}_k^\dagger \end{pmatrix} = P \begin{pmatrix} a_k \\ \tilde{a}_k^\dagger \end{pmatrix}, \quad (f_k^\dagger \tilde{f}_k) = (a_k^\dagger \tilde{a}_k) P^{-1}, \quad (23)$$

$$\mathcal{L} = \sum_k (\lambda_k f_k^\dagger f_k - \lambda_k^* \tilde{f}_k^\dagger \tilde{f}_k). \quad (24)$$

Here we assumed that $D_k = \text{diag}(\lambda_k, \lambda_k^*)$ and $\text{Im}\lambda_k < 0$. This structure leads to cancellation of the constant term in the Liouvillian.

The steady state density matrix is determined as the vacuum of operators f_k and \tilde{f}_k . The transformation to the basis of the

a, a^\dagger occupation numbers gives the density matrix:

$$\rho = \sum_k \frac{\exp(\mathcal{H} a_k^\dagger \tilde{a}_k^\dagger) |00\rangle_{a_k \tilde{a}_k}}{a_k \tilde{a}_k \langle I | \exp(\mathcal{H} a_k^\dagger \tilde{a}_k^\dagger) |00\rangle_{a_k \tilde{a}_k}}, \quad (25)$$

$$\mathcal{H} = i \frac{d\Gamma^{(i)}}{d\Gamma^{(o)}}, \quad |I\rangle_{a_k \tilde{a}_k} = |00\rangle + |11\rangle. \quad (26)$$

The effective Hamiltonian \mathcal{H} is a constant, therefore the Fourier transform gives the density matrix which is a tensor product in position space:

$$\rho = \otimes_i \left(\frac{d\Gamma^{(o)}}{d\Gamma^{(o)} + d\Gamma^{(i)}} |00\rangle_{a_i \tilde{a}_i} + \frac{d\Gamma^{(i)}}{d\Gamma^{(o)} + d\Gamma^{(i)}} |11\rangle_{a_i \tilde{a}_i} \right). \quad (27)$$

We can thus conclude that the density matrix is local in space. For the case of disordered leakage along the chain one cannot perform the Fourier transform of the Liouvillian analytically but numerical calculation shows that the density matrix averaged over disorder is again represented by the tensor product of single-site density matrices. For a single realization of the disorder in the couplings along the chain the decomposition is not exact, as shown in Fig. 3(a) for the current through the chain for a single realization of the disorder.

3. Response to the electric field

The response functions are good indicators of the equilibrium phase transitions. Let us consider a response of the current to a constant electric field E applied along the chain. In the tight-binding model it is incorporated as a linearly growing on-site potential: $U_m = mEl_0$, where l_0 is the lattice constant. In most models of the transport one assumes that the current flow is due to an electric field applied along the system. Here we have a current through the chain due to the coupling to the reservoirs. The difference in on-site potential from site to site can be viewed as applying an additional field along the chain. For example, in a cold atom system one can imagine a lattice constructed with varying depths of the potential well. In the decoherent phase, the electric field changes the response function only locally: close to the ends we expect the susceptibility to be different from the middle of the system due to the presence of coherence because of the coupling to the reservoirs. The linear response of the current to the electric field applied along the chain vanishes, and only the quadratic part is left, Fig. 8, inset:

$$j_{\text{NESS}}(E, d\Gamma^{(i)}, d\Gamma^{(o)}; L) - j_{\text{NESS}}(0, d\Gamma^{(i)}, d\Gamma^{(o)}; L) = \sigma(d\Gamma^{(i)}, d\Gamma^{(o)}; L) E^2. \quad (28)$$

Here we also notice that there is a scaling with E : the dependence of the conductivity on length scales with E^2 for the same dissipation rates along the chain $d\Gamma^{(i)}, d\Gamma^{(o)}$. We attribute the quadratic dependence on E to the structure of the NESS. The Ohm's law is an outcome of the linear response theory, which implies that the current is a consequence of the electric field applied to the equilibrium system. In our case the situation is tremendously different—from the physical point of view, the current is already present in the system due to contact with the leads even before applying the electric field along the system. From the viewpoint of the response theory, the response is considered with respect to the nonequilibrium steady state. It

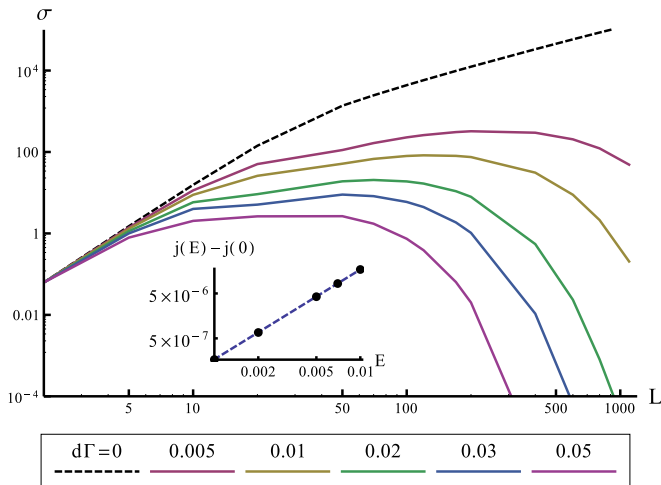


FIG. 8. (Color online) Main plot: the convergence of the nonlinear response to the electric field for long systems in the bulk of the chain. Solid lines correspond to different coupling strength $d\Gamma = 0.005, 0.01, 0.02, 0.03, 0.05$ (from top to bottom) and the dashed line is $d\Gamma = 0$. Inset: quadratic scaling of $j(E) - j(0)$ with the applied electric field (the scale in logarithmic).

is thus possible that the linear part of the response vanishes and only the nonlinear part is present.

The nonlinear response to the electric field vanishes in the bulk of the chain, Fig. 8. The response in the nondissipative system grows infinitely in the thermodynamic limit because of the translational invariance in the bulk. Indeed, when we make the hopping parameters disordered (i.e., make them vary along the chain), the infinite growth of σ is suppressed. Therefore, there is a discontinuity in the value of σ for infinitesimally small $d\Gamma$. It is consistent with the first-order phase transition.

C. Near-boundary effects

The symmetrized particle-particle correlation function:

$$C_i(k) = \langle a_{i+k}^\dagger a_i + a_i^\dagger a_{i+k} \rangle_{\text{NESS}} \quad (29)$$

provides further information about the transition. The correlations at the ends of the system are present and they decay exponentially: $C_i(k) \propto \exp(-k/\xi_i)$, $i \sim 1$ or $i \sim L$, where ξ is a correlation length, Fig. 11. We find the power-law divergence of the correlation length as the function of dissipation at zero dissipation rate along the chain. Inside infinitely long systems the correlations vanish: $\xi_i \rightarrow 0$, $i \sim L/2$, $L \rightarrow \infty$, as all coherence in the system is lost.

The nonlinear conductivity converges to a nonzero value at the boundaries of the chain, Fig. 9, unlike in the bulk of the chain, where it converges to zero. This happens due to some remaining coherence at the ends of the chain. Even more, there is a power-law scaling of the conductivity with dissipation strength, the parameter, which drives the phase transition, inset of Fig. 9.

To further corroborate the finding of the continuous QPT at the edges, let us now consider the spectrum of the effective Hamiltonian, \mathcal{H} . For the translationally invariant dissipative system from Sec. III B 2 the spectrum of the effective Hamiltonian is a δ function $\delta(\epsilon - \text{const} \times d\Gamma^{(i)}/d\Gamma^{(o)})$,

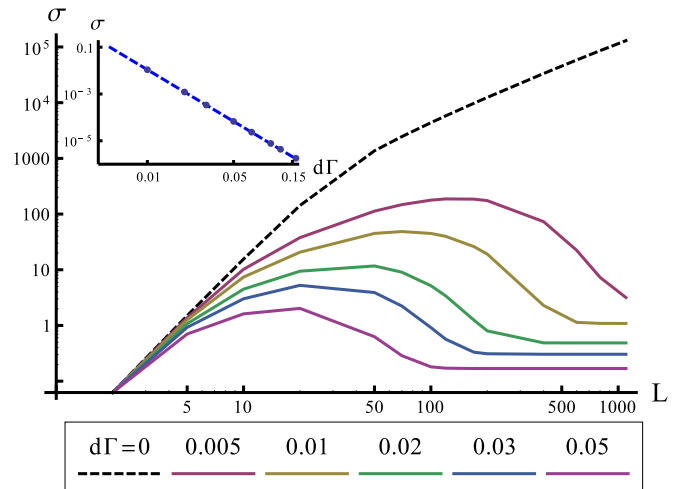


FIG. 9. (Color online) Main plot: the convergence of the nonlinear response to the electric field for long systems at the ends of the chain. Solid lines correspond to different coupling strength $d\Gamma = 0.005, 0.01, 0.02, 0.03, 0.05$ (from top to bottom) and the dashed line is $d\Gamma = 0$. Notice that the nonlinear conductivity at the ends points stays nonzero also in the thermodynamic limit. As in Fig. 8, the conductivity is infinite in the absence of dissipation. Inset: scaling of σ with disorder strength with power-law fit: $\sigma = \alpha d\Gamma^\beta$, $\beta = 3.161 \pm 0.001$.

where the constant comes from the freedom of choice of the effective Hamiltonian, which is connected to the freedom of choice of constants in front of the left and the right vacuum of the Liouvillian. When we take into account the whole chain with the end sites, the spectrum of the effective Hamiltonian is influenced by the presence of the ends of the chain: in the absence of the dissipation along the chain the lowest eigenvalue λ_{\min} of \mathcal{H} is 0, while in the presence of the dissipation λ_{\min} shifts to a nonzero value, Fig. 10. There is a power-law scaling of λ_{\min} with the strength of the dissipation, Fig. 10(b).

D. Disordered dissipative system

Let us consider a disordered system with random on-site potential U_i in the Hamiltonian (2). The values U_i are taken from the uniform distribution with the range $(0, dU)$.

It is known that in one spatial dimension disorder always localizes the conservative system [30]. This is the well-known Anderson localization: it happens because the electron waves always interfere so that the overall wave function is localized on the impurities. Such a system is an insulator as the overlap of the electron wave functions at different positions in the chain is exponentially small. This reasoning suggests the scaling hypothesis, which proposes that the conductivity in a disordered system should decrease exponentially with the system size, when the system is in the localized regime.

However, the presence of dissipation changes this: dissipation delocalizes the disordered system, as the dissipation breaks the interference, which is responsible for the localization. For averaging over disorder we used only 15 disorder configurations, as the uncertainties of the average are already small enough in that case (the error bars in the figure are of the size of the symbols in the plot). This happens because

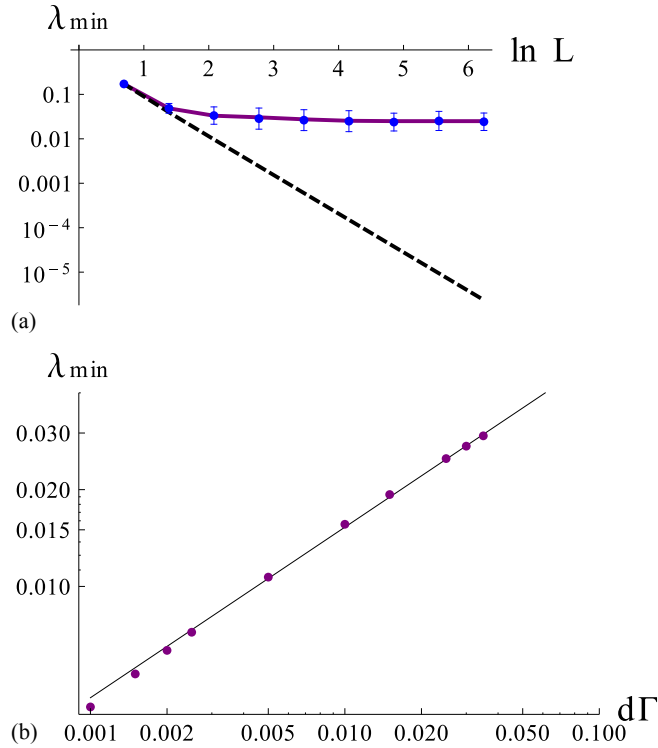


FIG. 10. (Color online) (a) The lowest eigenvalue λ_{\min} of the effective Hamiltonian (10) as a function of the system size for the system without (black dashed line) and with dissipation (blue points: averages over the disorder from the range $(0, d\Gamma)$, purple line: constant dissipation with $d\Gamma/2$, $d\Gamma = 0.025$). (b) The scaling of the lowest eigenvalue with disorder strength, $\lambda_{\min}(d\Gamma)$, and the power-law fit $\lambda_{\min} \propto d\Gamma^\beta$ with $\beta = 0.53 \pm 0.01$. The couplings to the source and the drain are $\Gamma^{(i)} = \Gamma^{(o)} = 1$.

the density matrix of an open quantum system contains the sectors with different particle numbers, hence the values of the current in the NESS can be considered as averaged not only

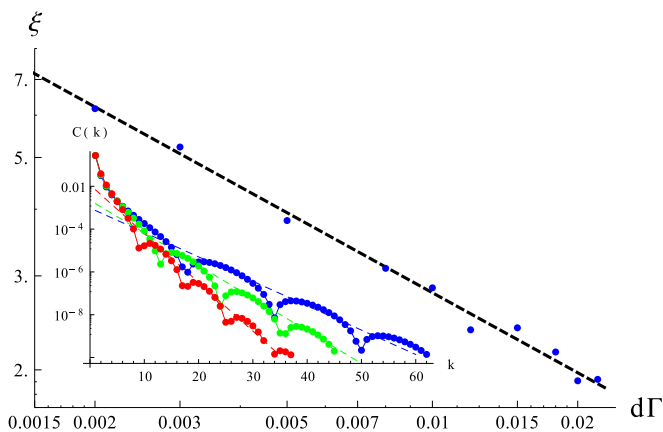


FIG. 11. (Color online) Dependence of the correlation length on the coupling to the environment for $\Gamma^{(i)} = \Gamma^{(o)} = 1$ (dots) and the power-law fit (dashed line). Inset: correlations at one end of the chain as a function of the position for different couplings strengths $d\Gamma = 0.005, 0.01, 0.02$ (from top to bottom: blue, green, red) and exponential fits, which determine the correlation length (dashed lines).

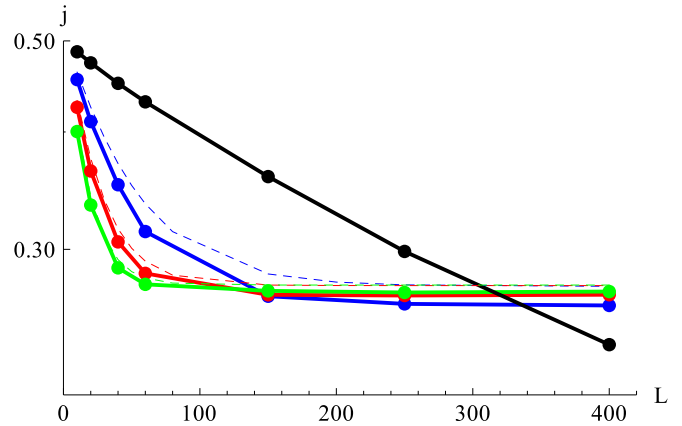


FIG. 12. (Color online) Dependence of the current through a disordered dissipative system on the length of the system for different values of the dissipation along the system, $d\Gamma = 0, 0.02, 0.03, 0.05$ (from top to bottom at small L : black, blue, red, green; solid lines: $dU = 0.3$, dashed lines: $dU = 0$; $\Gamma_1 = \Gamma_2 = 1$). The current through the system is independent of the system length for a sufficiently long system.

over disorder configurations, but also with respect to different particle numbers.

The general phenomenology of the clean system with dissipation is thus preserved also in the disordered system. The current again reaches a finite (though smaller) value in the thermodynamic limit, and the current at one end only weakly depends on the coupling at the other end. An example is seen in Fig. 12, where for simplicity we consider constant couplings to the environment along the chain and average only over the disorder realizations of the on-site potential.

IV. CONCLUSIONS AND DISCUSSION

We have considered the transport properties of a one-dimensional wire with leakage to the environment. In experimental systems, this leakage can happen due to misfabrication and the presence of the tunneling from the wire to a metallic region underneath the wire. We observe a first-order phase transition for infinitely long systems already at infinitesimal dissipation rate along the chain. From the microscopic point of view, this QPT means discontinuous behavior of the density matrix. On the macroscopic level it manifests itself in the jump in the current and the Fano factor. From the thermodynamic point of view we can say that the entropy jumps across the transition. The specific entropy in the dissipative phase is equal to the entropy of a single site coupled to the source and the drain.

Essentially, the phase transition is an anomaly: dissipation breaks the time-reversal invariance [31]. Upon taking the symmetry-breaking parameter (dissipation strength) to zero, we do not recover the result for unbroken symmetry. In the continuum limit it is analogous to the fact that, for example, viscosity effects in a fluid are nonperturbative and the flow undergoes a qualitative change for arbitrarily small nonzero dissipation: the scaling exponents of the correlation functions of the velocities jump at the transition between an ideal and viscous liquid [31]. To understand better the universality of

our finding, we have considered also the classical stochastic counterflow model, which describes a chain with two classes of asymmetric exclusion random walkers, left- and right-moving. In this case, dissipation is modeled by randomly creating or destroying the random walkers with certain probabilities at every (discrete) time step. This model, under suitable assumptions, again shows the same anomaly and the current jumps for arbitrarily small nonzero values of the dissipation. In the counterflow model, the role of quantum fluctuations is taken over by the stochastic fluctuations. In fluid dynamics, the velocity fluctuations make the system effectively quantum. The notion of QPT is thus justified, and the observation of anomaly—breaking of a classical symmetry at the quantum level, i.e., by the loop contributions to the action—becomes natural.

In a different context, the transport theory for dissipative systems has been developed in Refs. [24,32] in the language of the scattering matrices. Our Lindblad-based approach and the scattering approach are different in a few respects. First, let us consider a system without dissipation, coupled to two reservoirs at the ends. The scattering matrix theory describes the case when the wave coming from the reservoir into the system is coherent (just a plane wave), while the Lindblad approach describes the case of incoherent leads—the hopping in the chain happens stochastically. This is also reflected in the transport properties: while for coherent transport the conductivity is proportional to the number of open channels in the system, for the transport induced by incoherent hopping it is not [22]. Now let us move to the dissipative system. In the scattering matrix approach the dissipation is modeled through additional channels, which do not contribute to the transport (for the one-dimensional nondissipative problem the scattering matrix has the format 2×2 , for the incoming and the outgoing channel, while in the dissipative case the scattering matrix has a larger dimension, and only two channels describe the transport along the chain whereas the others describe the scattering in the side channels). The dissipation constructed in this way is coherent, while the Lindblad-like dissipation is incoherent.

It is interesting that the spin system coupled to the bosonic bath at every site experiences a second-order phase transition, and only at finite dissipation strength [6–9]. We do not know if the order of the transition is related to the presence or absence of memory or if it is determined by the statistics of the bath.

The phase transition in the quadratic fermionic systems was studied also in Refs. [2,5]. There, the XY chain coupled to the reservoirs at both ends was considered. The transition manifests itself in the change of behavior of the spin-spin correlation functions and the entanglement entropy, which does not depend on the system size on one side of the transition and grows linearly with the system length on the other side. The authors argue that the transition is of infinite order as all local observables are analytical across the transition. Subsequently the critical behavior has been observed also in the XX -spin chain [1] coupled to the environment at every site of the chain: the spin-spin correlation functions are short ranged in the nondissipative case, whereas they decay as a power law in the presence of the on-site decoherence. The transition we observe is significantly different from the previously studied cases since it is of the first order. This probably happens because the Refs. [2,5] consider the local dissipation (only at the ends

of the chain), while we are interested in the global dissipation. The difference with respect to the transition in Ref. [1] lies in the fact that the NESS is not Gaussian (Gaussianity allows usage of the Wick's theorem for the calculation of higher-order correlation functions in terms of two-point ones, while non-Gaussian states do not allow such expression): in our case the particle-particle correlation functions in the presence of dissipation decay exponentially, while for the XX chain with on-site dephasing there is a power-law decay of correlations.

The current in the steady dissipative state of the system decays exponentially inside the chain, because the coupling to the environment decreases the coherence of the quantum system. For the random dissipation along the chain, we find that the average current decreases inside the system with the same exponent as for the chain with the same dissipation at every site, which equals to the mean of the random coupling. One can try to measure the current along the dissipative chain with a scanning tunneling microscope (STM): if it decreases exponentially uniformly along the chain, then the dissipation model without disorder is a valid model, if the current inside the chain fluctuates, then the dissipation inside of the chain is random. The STM should be in the regime of a very low tunneling rate to the microscope tip, so that the tunneling to the tip does not destroy the dissipative state of the system itself.

We finish with an outlook. The state of the quantum system depends on the dimensionality, disorder, interaction, statistics, and symmetries. The dissipation adds one more axis to the phase diagram. It can lead to new types of behavior, already investigated in the spin-boson model [10], arrays of the dissipative Josephson junctions, and dissipative spin chains [6–9]. In the present paper we have investigated the behavior of the noninteracting fermionic system coupled to the Markovian bath and already have seen interesting quantum critical phenomena upon adding the dissipation along the chain. There are many unanswered questions: will this transition remain first order upon adding memory to the bath; what happens to it in the presence of interactions; do dimensionality and symmetries influence the behavior of the dissipative system, etc.

ACKNOWLEDGMENTS

This work was supported through CRC SFB 1073 (Project B03) of the Deutsche Forschungsgemeinschaft (DFG). We are grateful to Achim Rosch and Fabian Biebl for careful reading of the manuscript and helpful discussions.

APPENDIX: TRANSFORMATION OF THE LIOUVILLIAN TO THE DIAGONAL BASIS

The solution of the Lindblad equation (6) for noninteracting fermions is notably simplified in the super-fermionic representation [21,22]: operators acting from the right on the density matrix are introduced. They are denoted by a tilde. Then the Liouvillian can be written after the particle-hole

transformation $\tilde{a} = b^\dagger, \tilde{a}^\dagger = b$ in the quadratic form:

$$\mathcal{L} = (a^\dagger b^\dagger) \mathcal{M} \begin{pmatrix} a \\ b \end{pmatrix} - i \sum_{\mu} \Gamma_{\mu}^{(o)} - i \sum_{\mu} \Gamma_{\mu}^{(i)}, \quad (\text{A1})$$

where the matrix M can be represented as

$$\begin{aligned} \mathcal{M} = & H\delta_{aa} + H\delta_{bb} + i\Gamma_k^{(i)}\delta_{kk}(-\delta_{aa} + \delta_{bb}) \\ & + i\Gamma_k^{(o)}\delta_{kk}(\delta_{aa} - \delta_{bb}) - 2\Gamma_k^{(i)}\delta_{kk}\delta_{ba} + 2\Gamma_k^{(o)}\delta_{kk}\delta_{ab} \end{aligned} \quad (\text{A2})$$

with H being a tight-binding Hamiltonian of the system, δ_{xy} is the Kronecker symbol, for example δ_{aa} denotes the upper-left L by L part of the matrix \mathcal{M} , δ_{kk} stands for the diagonal of the matrix in the site space.

Due to this specific structure of \mathcal{M} the constant terms in the expression (A3) vanish after introducing a new set of the operators $\{f, f^\ddagger, \tilde{f}, \tilde{f}^\ddagger\}$ [22] and even more in this basis the Liouvillian becomes diagonal:

$$\mathcal{L}_f = \sum_i \lambda_i f_i^\ddagger f_i - \sum_i \lambda_i^* \tilde{f}_i^\ddagger \tilde{f}_i. \quad (\text{A3})$$

The operators $\{f^\ddagger, \tilde{f}^\ddagger\}$ are dual to the operators $\{f, \tilde{f}\}$, but not Hermitian conjugated, though the operators obey anticommutation relations. The operators $\{f, f^\ddagger, \tilde{f}, \tilde{f}^\ddagger\}$ are

linear combinations of the operators $\{a, a^\dagger, \tilde{a}, \tilde{a}^\dagger\}$:

$$\begin{aligned} a_m^\dagger &= \sum_{k_1} C_{mk_1}^{(1)} f_{k_1}^\ddagger + C_{mk_1}^{(2)} \tilde{f}_{k_1}, \\ a_m &= \sum_{k_1} A_{mk_1}^{(1)} f_{k_1} + A_{mk_1}^{(2)} \tilde{f}_{k_1}^\ddagger. \end{aligned}$$

The coefficient matrices C and A are connected to the matrix of the eigenvectors P of the matrix \mathcal{M} (see Ref. [22]):

$$P = \begin{pmatrix} A^{(1)} & A^{(2)} \\ A^{(3)} & A^{(4)} \end{pmatrix}, \quad (P^{-1})^T = \begin{pmatrix} C^{(1)} & C^{(2)} \\ C^{(3)} & C^{(4)} \end{pmatrix}. \quad (\text{A4})$$

In P the eigenvectors are ordered in the following way: first N of eigenvectors correspond to eigenvalues with a negative imaginary part, while the second half have a positive imaginary part and are complex conjugated to the first set. All matrices $A^{(i)}$ and $C^{(i)}$, $i = 1, \dots, 4$ have dimension $N \times N$.

In the f basis the Liouvillian operator is diagonal, therefore the stationary solution of the Lindblad equation (6) is the vacuum of the operators f :

$$f|\text{NESS}\rangle = 0, \quad \tilde{f}|\text{NESS}\rangle = 0.$$

It allows us to calculate the expectation values in the NESS: we transform the operator in the a basis to the f basis and take its expectation value with respect to the vacuum.

-
- [1] M. Žnidarič, *J. Stat. Mech.* (2010) L05002; *Phys. Rev. E* **83**, 011108 (2011).
- [2] T. Prosen and I. Pižorn, *Phys. Rev. Lett.* **101**, 105701 (2008).
- [3] C.-E. Bardyn, M. A. Baranov, C. V. Kraus, E. Rico, A. Imamoğlu, P. Zoller, and S. Diehl, *New J. Phys.* **15**, 085001 (2013); O. Viyuela, A. Rivas, and M. A. Martin-Delgado, *Phys. Rev. B* **86**, 155140 (2012).
- [4] H. T. Mebrahtu, I. V. Borzenets, D. E. Liu, H. Zheng, Y. V. Bomze, A. I. Smirnov, H. U. Baranger, and G. Finkelstein, *Nature (London)* **488**, 61 (2012).
- [5] T. Prosen and B. Žunkovič, *New J. Phys.* **12**, 025016 (2010); T. Prosen, *J. Stat. Mech.* (2010) P07020.
- [6] S. Sachdev, P. Werner, and M. Troyer, *Phys. Rev. Lett.* **92**, 237003 (2004).
- [7] P. Werner, Ph.D. thesis, ETH Zürich, 2005.
- [8] S. Pankov, S. Florens, A. Georges, G. Kotliar, and S. Sachdev, *Phys. Rev. B* **69**, 054426 (2004).
- [9] P. Werner, M. Troyer, and S. Sachdev, *J. Phys. Soc. Jpn. Suppl.* **74**, 67 (2005).
- [10] A. J. Leggett, S. Chakravarty, A. T. Dorsey, M. P. A. Fisher, A. Garg, and W. Zwerger, *Rev. Mod. Phys.* **59**, 1 (1987).
- [11] J. Jin, M. W.-Y. Tu, W.-M. Zhang, and Y. J. Yan, *New J. Phys.* **12**, 083013 (2010).
- [12] G. Lindblad, *Rep. Math. Phys.* **10**, 393 (1976).
- [13] H.-P. Breuer and F. Petruccione, *The Theory of Open Quantum Systems* (Oxford University Press, Oxford, 2007).
- [14] Z. Cai and T. Barthel, *Phys. Rev. Lett.* **111**, 150403 (2013).
- [15] Z. Racz, *Nonequilibrium Phase Transitions*, Lecture Notes, Les Houches, July 2002.
- [16] T. Antal, Z. Racz, and L. Sasvari, *Phys. Rev. Lett.* **78**, 167 (1997).
- [17] L. D. Landau and E. M. Lifshitz, *Statistical Physics*, 3rd ed. (Elsevier, Amsterdam, 1980).
- [18] M. Le Bellac, F. Mortessagne and G. G. Batrouni, *Equilibrium and Nonequilibrium Statistical Thermodynamics* (Cambridge University Press, Cambridge, 2004).
- [19] N. Goldenfeld, *Lectures on Phase Transitions and the Renormalization Group* (Perseus, New York, 1992).
- [20] S. Ajisaka, F. Barra, C. Mejia-Monasterio, and Toma Prosen, *Phys. Rev. B* **86**, 125111 (2012).
- [21] A. A. Dzhioev and D. S. Kosov, *J. Chem. Phys.* **134**, 044121 (2011); *J. Phys.: Condens. Matter* **24**, 225304 (2012).
- [22] M. V. Medvedyeva and S. Kehrein, arXiv:1310.4997.
- [23] M. Žnidarič, *Phys. Rev. Lett.* **112**, 040602 (2014).
- [24] K. Maschke and M. Schreiber, *Phys. Rev. B* **49**, 2295 (1994).
- [25] D. Roy and N. Kumar, *Phys. Rev. B* **77**, 064201 (2008).
- [26] M. W. Y. Tu and W.-M. Zhang, *Phys. Rev. B* **78**, 235311 (2008).
- [27] S. A. Gurvitz and Ya. S. Prager, *Phys. Rev. B* **53**, 15932 (1996); S. A. Gurvitz, *ibid.* **57**, 6602 (1998).
- [28] P.-E. Roche, B. Derrida, and B. Douçot, *Eur. Phys. J. B* **43**, 529 (2005).
- [29] I. Perschel and V. Eisler, *J. Phys. A: Math. Theor.* **42**, 504003 (2009).
- [30] F. Evers and A. D. Mirlin, *Rev. Mod. Phys.* **80**, 1355 (2008).
- [31] G. Falkovich, K. Gawędzki, and M. Vergassola, *Rev. Mod. Phys.* **73**, 913 (2001); G. Falkovich, *J. Phys. A: Math. Theor.* **42**, 123001 (2009).
- [32] K. Maschke and M. Schreiber, *Phys. Rev. B* **44**, 3835 (1991); G. Burmeister, K. Maschke, and M. Schreiber, *ibid.* **47**, 7095 (1993).

Quantum corrected phase diagram of holographic fermions

Mariya V. Medvedyeva,^a Elena Gubankova,^b Mihailo Čubrović,^c Koenraad Schalm^c
and Jan Zaanen^c

^a*Department of Physics, Georg-August-Universität Göttingen,
Friedrich-Hund-Platz 1, 37077 Göttingen, Germany*

^b*Institute for Theoretical Physics, J.W. Goethe-University,
D-60438 Frankfurt am Main, Germany*

^c*Instituut Lorentz, Delta-Institute for Theoretical Physics, Leiden University,
Niels Bohrweg 2, 2300 RA Leiden, Netherlands*

E-mail: mariya.medvedyeva@theorie.physik.uni-goettingen.de,
gubankova@th.physik.uni-frankfurt.de, mcubrovic@gmail.com,
kschalm@lorentz.leidenuniv.nl, jan@lorentz.leidenuniv.nl

ABSTRACT: We study the phases of strongly correlated electron systems in two spatial dimensions in the framework of AdS₄/CFT₃ correspondence. The AdS (gravity) model consists of a Dirac fermion coupled to electromagnetic field and gravity. To classify the ground states of strongly correlated electrons on the CFT side and to construct the full phase diagram of the system, we construct a quantum many-body model of bulk fermion dynamics, based on the WKB approximation to the Dirac equation. At low temperatures, we find a quantum corrected approximation to the electron star where the edge is resolved in terms of wave functions extended fully through AdS. At high temperatures, the system exhibits a *first* order thermal phase transition to a charged AdS-RN black hole in the bulk and the emergence of local quantum criticality on the CFT side. This change from the third order transition experienced by the semi-classical electron star restores the intuition that the transition between the critical AdS-RN liquid and the finite density Fermi system is of van der Waals liquid-gas type.

KEYWORDS: AdS-CFT Correspondence, Black Holes, Holography and condensed matter physics (AdS/CMT)

ARXIV EPRINT: [1302.5149](https://arxiv.org/abs/1302.5149)

Contents

| | | |
|----------|--|-----------|
| 1 | Introduction | 1 |
| 2 | Holographic fermions in charged background | 3 |
| 3 | Equation of state of the WKB star | 5 |
| 3.1 | WKB hierarchy and semiclassical calculation of the density | 5 |
| 3.1.1 | WKB wave function | 7 |
| 3.1.2 | WKB density | 8 |
| 3.2 | Pressure and equation of state in the semiclassical approximation | 9 |
| 3.2.1 | Microscopic pressure | 10 |
| 3.2.2 | Thermodynamic pressure | 12 |
| 4 | Maxwell-Dirac-Einstein system | 13 |
| 5 | Phases of holographic fermions | 16 |
| 5.1 | Thermodynamics | 17 |
| 5.2 | Constructing the phase diagram: quantum corrections imply a first order thermal phase transition to AdS-RN | 18 |
| 6 | Discussion and conclusions | 20 |

1 Introduction

The problem of fermionic quantum criticality has proven hard enough for condensed matter physics to keep seeking new angles of attack. The main problem we face is that the energy scales vary by orders of magnitude between different phases. The macroscopic, measurable quantities emerge as a result of complex collective phenomena and are difficult to relate to the microscopic parameters of the system. An illustrative example present the heavy fermion materials [3] which still behave as Fermi liquids but with vastly (sometimes hundredfold) renormalized effective masses. On the other hand, the strange metal phase of cuprate-based superconducting materials [4], while remarkably stable over a range of doping concentrations, shows distinctly non-Fermi liquid behavior. The condensed matter problems listed all converge toward a single main question in field-theoretical language. It is the classification of ground states of interacting fermions at finite density.

In this paper we attempt to understand these ground states in the framework of AdS/CFT, the duality between the strongly coupled field theories in d dimensions and a string configuration in $d + 1$ dimension. Holography (AdS/CFT correspondence) [1, 2] has become a well-established treatment of strongly correlated electrons by now, but it still has its perplexities and shortcomings. Since the existence of holographic duals to Fermi

surfaces has been shown in [8, 9], the next logical step is to achieve the understanding of the phase diagram: what are the stable phases of matter as predicted by holography, how do they transform into each other and, ultimately, can we make predictions on quantum critical behavior of real-world materials based on AdS/CFT.

The classification of ground states now translates into the following question: classify the stable asymptotically AdS geometries with charged fermionic matter in a black hole background. Most of the work done so far on AdS/CFT for strongly interacting fermions relies on bottom-up toy gravity models and does not employ a top-down string action. We stay with the same reasoning and so will work with Einstein gravity in $3 + 1$ dimensions. We note, however, that top-down constructions of holographic fermions exist [6, 11].

In this paper we construct a model dubbed “WKB star”, alluding to the fact that we treat the same large occupation number limit as the electron star [10] but go further from the ideal fluid limit of [10]. The main idea is to solve the fermionic equations of motion in the WKB limit *without* taking the fluid limit: the total density is the sum of the contributions of individual wave functions rather than an integral over them. The main approximation we introduce is thus just the quasiclassical treatment of fermions, inherent to WKB. The inverse occupation number serves as the control parameter of this approximation. In addition, we assume that the correction to the fluid limit is captured by the correction to the pressure. This assumption cannot be rigorously derived. We will discuss, however, the robustness of our findings with respect to this assumption. In addition to simply improving the mathematical treatment of the bulk many-body fermion system, we will show that some properties of the system change nonperturbatively in the fluid limit. In particular, the thermodynamic behavior of the system at finite temperature is changed compared to the electron star.

We will use a simple WKB formalism to approximate the many-body Fermi system in the AdS bulk. This adds quantum corrections to the Thomas-Fermi (fluid) approximation by taking into account finite level spacing. In other words, we do not take the limit of an infinite number of occupied levels but keep the occupation number finite. The occupation number itself acts as the control parameter of our approximation. The most notable feature, however, occurs in the transition from the semiclassical approximation at *infinite* occupation number to finite occupation number. We find that the finite density quantum many body phases with fermionic quasiparticles at high enough temperatures always exhibit a *first* order transition into the zero density AdS-RN phase. Intuitively, this can be interpreted as a universal van der Waals liquid-gas transition. On the other hand in the semiclassical fluid limit underlying the electron star, the transition was found to be continuous [12, 33]. With this re-emergence of the first order nature of the thermal phase transition at the quantum level our results confirm the intuition that a density driven phase transition is always first order as also indicated by the Dirac hair approximation [13]. We thus show with an explicit calculation that in the context of fermionic questions in AdS/CFT quantum “ $1/N$ ” corrections can be important and that the semiclassical fluid limit can be unreliable, at least at finite temperature. While the quantum corrections likely have important consequences also at $T = 0$, we have not explored the zero-temperature physics in this paper.

The outline of the paper is as follows. In the section 2 we describe the field content and geometry of our gravity setup, an Einstein-Maxwell-Dirac system in 3 + 1 dimension, and review the single-particle solution to the bulk Dirac equation. In section 3 we start from that solution and apply the WKB approximation to derive the Dirac wave function of a many-particle state in the bulk. Afterwards we calculate density and pressure of the bulk fermions — the semiclassical estimate and the quantum corrections, thus arriving at the equation of state. Section 4 contains the numerically self-consistent solution of the set of equations for fermions, gauge field and the metric. There we also describe our numerical procedure. Section 5 is the core, where we analyze thermodynamics and spectra of the field theory side and identify different phases as a function of the three parameters of the system: chemical potential μ , fermion charge e and conformal dimension Δ . Section 6 sums up the conclusions and offers some insight into possible broader consequences of our work and into future steps.

2 Holographic fermions in charged background

We wish to construct the gravity dual to a field theory at finite fermion density. We will specialize to 2+1-dimensional conformal systems of electron matter, dual to AdS₄ gravities. We consider a Dirac fermion of charge e and mass m in an electrically charged gravitational background with asymptotic AdS geometry. Adopting the AdS radius as the unit length, we can rescale the metric $g_{\mu\nu}$ and the gauge field A_μ :

$$g_{\mu\nu} \mapsto g_{\mu\nu} L^2, \quad A_\mu \mapsto LA_\mu. \tag{2.1}$$

In these units, the action of the system is:

$$S = \int d^4x \sqrt{-g} \left[\frac{1}{2\kappa^2} L^2 (R + 6) + \frac{L^2}{4} F^2 + L^3 \mathcal{L}_f \right] \tag{2.2}$$

where κ is the gravitational coupling and $F_{\mu\nu} = \partial_\mu A_\nu - \partial_\nu A_\mu$ is the field strength tensor. The fermionic Lagrangian is:

$$\mathcal{L}_f = \bar{\Psi} \left[e_A^\mu \Gamma^A \left(\partial_\mu + \frac{1}{4} \omega_\mu^{BC} \Gamma_{BC} - ieLA_\mu \right) - mL \right] \Psi \tag{2.3}$$

where $\bar{\Psi} = i\Psi^\dagger \Gamma^0$, e_A^μ is the vierbein and ω_μ^{AB} is the spin connection.

We shall be interested in asymptotically AdS solutions with an electric field. The U(1) gauge field is simply $A = \Phi dt$ and we parametrize our metric in four spacetime dimensions as:

$$ds^2 = \frac{f(z)e^{-h(z)}}{z^2} dt^2 - \frac{1}{z^2} (dx^2 + dy^2) - \frac{1}{f(z)z^2} dz^2 \tag{2.4}$$

The radial coordinate is defined for $z \geq 0$, where $z = 0$ is the location of AdS boundary. All coordinates are dimensionless, according to (2.1). This form of the metric is sufficiently general to model any configuration of static and isotropic charged matter. Development of a horizon at finite z is signified by the appearance of a zero of the function $f(z)$, $f(z_H) = 0$. From now on we will set $L = 1$.

We will now proceed to derive the equation of motion for the Dirac field. From (2.3), the equation reads:

$$e_A^\mu \Gamma^A \left(\partial_\mu + \frac{1}{4} \omega_\mu^{BC} \Gamma_{BC} - ieA_\mu \right) \Psi = m\Psi. \quad (2.5)$$

In the metric (2.4) we can always eliminate the spin connection [8] by transforming:

$$\Psi \mapsto (gg^{zz})^{-\frac{1}{4}} \Psi = \frac{e^{h(z)/4} z^{3/2}}{f(z)^{1/4}} \Psi \equiv a^{-1}(z) \Psi. \quad (2.6)$$

At this point it is convenient to adopt a specific representation of gamma matrices. We choose:

$$\Gamma^0 = \begin{pmatrix} 1 & 0 \\ 0 & -1 \end{pmatrix}, \quad \Gamma^{x,y,z} = \begin{pmatrix} 0 & \sigma_{1,2,3} \\ -\sigma_{1,2,3} & 0 \end{pmatrix}. \quad (2.7)$$

In this basis we define the radial projections Ψ_\pm as eigenvalues of the projection operator onto the time axis:

$$\Psi_\pm = \frac{1}{2} (1 \pm \Gamma^0) \Psi, \quad (2.8)$$

after which the Dirac equation in matrix form becomes:

$$\sqrt{f} \partial_z \begin{pmatrix} \Psi_+ \\ \Psi_- \end{pmatrix} = \hat{D} \begin{pmatrix} \Psi_+ \\ \Psi_- \end{pmatrix}. \quad (2.9)$$

Here the matrix \hat{D} is the differential operator along the transverse coordinates (x, y) and time, which we will specify shortly.

We will now set the stage for solution of the Dirac equation in the WKB approximation. We can separate the radial dynamics (along the z coordinate) from the motion in the $x - y$ plane. We can thus make the separation ansatz:

$$\begin{pmatrix} \Psi_+(t, z, x, y) \\ \Psi_-(t, z, x, y) \end{pmatrix} = \int \frac{d\omega}{2\pi} \begin{pmatrix} F(z)K_1(x, y) \\ -G(z)K_2(x, y) \end{pmatrix} e^{-i\omega t} \quad (2.10)$$

where the F, G are scalars and the modes $K_{1,2}$ are in-plane spinors. The Dirac equation then takes the form:

$$\begin{pmatrix} \partial_z F K_1 \\ -\partial_z G K_2 \end{pmatrix} = \begin{pmatrix} -\hat{\partial}/\sqrt{f(z)} & (\tilde{E}(\omega, z) + \tilde{M}(z)) \sigma_3 \\ (\tilde{E}(\omega, z) - \tilde{M}(z)) \sigma_3 & -\hat{\partial}/\sqrt{f(z)} \end{pmatrix} \begin{pmatrix} F K_1 \\ -G K_2 \end{pmatrix} \quad (2.11)$$

We recognize the matrix at the right hand side as \hat{D}/\sqrt{f} . The terms \tilde{E} and \tilde{M} have the meaning of local energy and mass terms, respectively:

$$\tilde{E}(z) = -\frac{e^{h(z)/2}}{f(z)} (\omega + e\Phi(z)), \quad \tilde{M}(z) = \frac{m}{z\sqrt{f(z)}}. \quad (2.12)$$

The in-plane operator $\hat{\partial}$ acts on each in-plane spinor as:

$$\hat{\partial} = \begin{pmatrix} 0 & i\vec{\partial} \\ -i\vec{\partial} & 0 \end{pmatrix} \quad (2.13)$$

with $\partial \equiv \partial_x + i\partial_y$. To maintain the separation of variables in (2.11), we require $\hat{\partial}K_i = \lambda_i K_i$, where $|\lambda_i|^2$ corresponds the momentum-squared of the in-plane motion of the particle. The physical requirement that this momentum be the same for both radial projections translates into the condition $|\lambda_2| = |\lambda_1|$. Consistency of the separation of variables then shows us that $K_2 = \sigma_3 K_1$ and thus $\lambda_1 = -\lambda_2 = k$. This solves the x, y -dependent part of the equation, in terms of $\rho \equiv \sqrt{x^2 + y^2}$ and $\phi = \arctan y/x$:

$$K_i(x, y) = \begin{pmatrix} J_{l-1/2}(\lambda_i \rho) e^{i(l-1/2)\phi} \\ J_{l+1/2}(\lambda_i \rho) e^{-i(l+1/2)\phi} \end{pmatrix}, \tag{2.14}$$

where J_a is the Bessel function of the first kind of order a (the second branch, with the modified Bessel function of the first kind Y_a , is ruled out as it diverges at $x = y = 0$). Now the reduced radial equation becomes:

$$\begin{pmatrix} \partial_z F \\ \partial_z G \end{pmatrix} = \begin{pmatrix} -\tilde{k} & \tilde{E} + \tilde{M} \\ \tilde{M} - \tilde{E} & \tilde{k} \end{pmatrix} \begin{pmatrix} F \\ G \end{pmatrix} \tag{2.15}$$

with $\tilde{k} = k/\sqrt{f}$ (let us note that eq. (2.15) is for the pair (F, G) , whereas the initial equation (2.11) is written for the bispinor $(FK_1, -GK_2)$). For the WKB calculation of the density, it is useful to remind that the wave function Ψ in eq. (2.10) has two quantum numbers corresponding to the motion in the (x, y) plane: they are simply the momentum projections k_x, k_y (or equivalently the momentum module λ and the angular momentum l). The radial eigenfunctions in z -direction provide a third quantum number n .

3 Equation of state of the WKB star

In this section we construct the model of the bulk fermions in an improved semiclassical approximation — the WKB star. We solve the Dirac equation in the WKB approximation, and the density is computed by summing a large number of energy levels. This is in the spirit of Thomas-Fermi approximation. However, we perform an exact summation of a *finite* number of WKB quantum-mechanical solutions for the wave functions rather than approximating the sum by an integral as implied in the semiclassical fluid limit. One of the drawbacks of the Thomas-Fermi fluid limit are sharp bounds (i.e., discontinuous first derivative) of density and pressure profiles along the radial direction (see e.g. [10, 12, 33]). As we have already argued, sharp bounds make it hard if not impossible to capture several phenomena. In this respect summing WKB wave functions goes beyond Thomas-Fermi; it includes quantum corrections as the number of occupied states is finite and all collective and individual profiles will be continuous without sharp edges. In further work one might start from our model and treat the quantum-mechanical (one loop) corrections in a more systematic way in order to bridge the gap between the electron star [10] and single-particle quantum mechanical calculation of Dirac hair [13].

3.1 WKB hierarchy and semiclassical calculation of the density

In the framework of quantum-many-body calculations, the first task is to construct the induced charge density $n(z)$. Physically, the origin of the induced charge in our model is

the pair production in the strong electromagnetic field of the black hole. To remind the reader, a (negatively) charged black hole in AdS space is unstable at low temperatures, and spontaneously discharges into the vacuum [24]. This means that there will be a non-zero net density of electrons $n(z)$. One can calculate $n(z)$ in a Hartree approximation as a density of non-interacting electrons, compute the collective effect on other fields by this density and iterate. Our novel approach is to use WKB methods to efficiently compute the many wave functions enumerated by the quantum numbers (λ, l, n) .

The algorithm for the WKB expansion of the wave function for Dirac equation is adopted from [31]. Even though every single step is elementary, altogether it seems to be less well known than its Schrödinger equivalent. We consider the Dirac equation in the form (2.9) and introduce the usual WKB phase expansion:

$$\Psi(z) = e^{\int_{z_0}^z dz y(z) \sqrt{f(z)}} \chi(z) \tag{3.1}$$

with the spinor part $\chi(z)$. The phase $y(z)$ can be expressed as the semiclassical expansion in \hbar ,¹

$$y(z) = y_{-1}(z) + y_0(z) + y_1(z) + \dots \tag{3.2}$$

The equations for the perturbative corrections now follow from (3.1)–(3.2):

$$\hat{D}\chi_0 = y_{-1}\chi_0, \tag{3.3}$$

$$\hat{D}\chi_1 = y_{-1}\chi_1 + y_0\chi_0 + \sqrt{f}\partial_z\chi_0, \tag{3.4}$$

...

$$\hat{D}\chi_n = y_{-1}\chi_n + \sqrt{f}\partial_z\chi_{n-1} + \sum_{i=0}^{n-1} y_{n-i-1}\chi_i. \tag{3.5}$$

Notice in particular that y_{-1}/χ_0 is an eigenvalue/eigenvector of \hat{D} . In our case the matrix \hat{D} has rank two, so there are two eigenvalues/eigenvectors for y_{-1}/χ_0 : y_{-1}^\pm and χ_0^\pm . To find the first order correction to the phase of the wave function y_0 , we multiply (3.4) from the left by the left eigenvalue $\tilde{\chi}_0^\pm$ of the matrix \hat{D} (\hat{D} is in general not symmetric, so the right and left eigenvalues are different):

$$y_0 = -\frac{(\partial_z\chi_0^\pm, \tilde{\chi}_0^\pm)}{(\tilde{\chi}_0^\pm, \chi_0^\pm)}. \tag{3.6}$$

so we can now construct the usual WKB solution of the form $\Psi_\pm = e^{i\theta_\pm}/\sqrt{q}$, where q is the WKB momentum and θ_\pm the phase. The term y_0 is just the first order correction to θ_\pm .

Finally, let us recall the applicability criterion of the WKB calculation. It is known that WKB approximation fails in the vicinity of turning points. The condition of applicability comes from comparing the leading and the next to leading term in the expansion (3.2):

$$\frac{y_0(z)}{y_{-1}(z)} \ll 1. \tag{3.7}$$

¹From the very beginning we put $\hbar = 1$. However, to elucidate the semiclassical nature of the expansion we give it here with explicit \hbar . Dirac equation becomes $\hbar\sqrt{f}\partial_z\hat{\Psi} = \hat{D}\hat{\Psi}$, where $\hat{\Psi} = (\Psi_+, \Psi_-)$, yielding the expansion $y(z) = \hbar^{-1}(y_{-1}(z) + \hbar y_0(z) + \hbar^2 y_1(z) + \dots)$.

In terms of $\tilde{E}(z)$ and $\tilde{M}(z)$ introduced in eq. (2.12) it gives at $k = 0$:

$$\frac{\tilde{M}(z)\partial_z\tilde{E}(z) - \tilde{E}(z)\partial_z\tilde{M}(z)}{\tilde{E}(z)(\tilde{E}(z) - \tilde{M}(z))} \ll 1. \quad (3.8)$$

3.1.1 WKB wave function

According to (3.3), the leading effective WKB momentum for the motion in z direction $q \equiv |y_{-1}^{\pm}|$ is:

$$q^2(z) = \tilde{E}^2(z) - \tilde{M}^2(z) - \tilde{k}^2(z). \quad (3.9)$$

The wave function in radial direction, $\Psi = (F, -G)$, is given by the superposition of two linear independent solutions

$$\Psi(z) = C_+\chi_+(z)e^{i\theta(z)} + C_-\chi_-(z)e^{-i\theta(z)}, \quad (3.10)$$

with the phase determined by

$$\theta(z) = \int^z (q(z') + \delta\theta(z')) dz' \quad (3.11)$$

$$\delta\theta(z) = \int^z \frac{\tilde{k}\partial_z\tilde{k} - q\partial_zq + (\tilde{E} - \tilde{M}) (\partial_z\tilde{E} + \partial_z\tilde{M})}{2\tilde{k}q} dz. \quad (3.12)$$

The constants C_+ and C_- are related by invoking the textbook boundary conditions [25] for the behavior of WKB wave function at the boundary of the classically allowed region ($q^2(z) > 0$) and the classically forbidden region ($q^2(z) < 0$). The wave function in the classically allowed region then reads:

$$\Psi(z) = \frac{C}{\sqrt{q(z)}} \begin{pmatrix} \sqrt{\tilde{E}(z) + \tilde{M}(z)} \sin(\theta(z) - \delta\theta(z)) \\ \sqrt{\tilde{E}(z) - \tilde{M}(z)} \sin\theta(z) \end{pmatrix}, \quad (3.13)$$

$$\delta\theta(z) = \text{ArcSin} \frac{q(z)}{\sqrt{\tilde{E}^2(z) - \tilde{M}^2(z)}}, \quad (3.14)$$

and C is the only remaining undetermined normalization constant. Integrating the probability density over all coordinates in the classically allowed region (z_1, z_2) gives the normalization condition:

$$C^2 \int_0^1 dz \frac{\sqrt{g_{3d}(z)}}{a(z)^2} \int dx \int dy C_{2d}^2 \Psi_{nk_xk_y}(z, x, y) \Psi_{n'k'_xk'_y}^\dagger(z, x, y) = 1. \quad (3.15)$$

The metric factor is $g_{3d}(z) = g(z)g^{tt}(z)$, and $a(z)$ is the conversion factor from (2.6). In the left-hand side of the equality we took into account the normalization of the continuous spectrum in the (x, y) plane. The integration in the perpendicular coordinates is trivial for the solution (2.14), as we can transform the integral into the integral over ρ, ϕ and the orthogonality relation for Bessel functions gives the definition of C_{2d}^2 :

$$C_{2d}^{-2} \int_0^\infty J(\lambda\rho)J(\lambda'\rho)\rho d\rho = \frac{\delta(\lambda - \lambda')}{\lambda} \quad (3.16)$$

and it allows us to express the normalization constant as:

$$C = \left(4\pi \int dz \frac{\sqrt{g^{tt}} \tilde{E}(z)}{\sqrt{g^{zz}} q(z)} \right)^{-1/2}, \quad (3.17)$$

where a factor of 2π comes from the integration over ϕ and an additional factor of 2 from the summation over the full four-component wave function, i.e. bispinor (each spinor gives $\tilde{E}(z)/q(z)$ after averaging over the fast oscillating phase θ). This completes the derivation of WKB wave function and allows us to compute the density.

3.1.2 WKB density

As in [31] we find the total density by summing single-particle wave functions in the classically allowed region. The WKB wave function is characterized by the quantum numbers (λ, l, n) with λ being the linear momentum in the $x - y$ plane, l — the orbital momentum in the $x - y$ plane and n — the energy level of the central motion in the potential well along z direction. The bulk density can be expressed as the sum over the cylindrical shells of the bulk Fermi surface. Each shell satisfies the Luttinger theorem in the transverse ($x - y$) direction and so the density carried by each shell $n_{xy}(z)$ can easily be found. We can then sum over all shells to arrive at the final answer which reads simply $\int dz n_z(z) n_{xy}(z)$. A similar qualitative logic for summing the Luttinger densities in the $x - y$ plane was used also in [14] although the model used in that paper is overall very different (see also the fully consistent treatment with regularization in [38]).

Let us start by noticing that the end points of the classically allowed region determine the limits of summation over n and λ : $q^2(\omega_n, \lambda) \geq 0$. Thus, the density in the WKB region is:

$$n(z) = \frac{2\pi}{a(z)^2} \int_0^{2\pi} d\phi \sum_{n: q^2(\omega_n, \lambda) \geq 0} \int_0^{\sqrt{f(z)(\tilde{E}^2(\omega, z) - \bar{M}^2(z))}} \lambda d\lambda \int_0^\infty d\rho \rho C_{2d}^2 |\Psi(z, x, y)|^2. \quad (3.18)$$

The limit of the sum over the level number n is determined by the requirement that WKB momentum be positive; in other words, we sum over occupied levels inside the potential well only. Remember that the bulk fields live at zero temperature, hence there is no Fermi-Dirac factor. The sum over the orbital quantum number l extends to infinity as the (x, y) plane is homogenous and the orbital number does not couple to the non-trivial dynamics along the radial direction. We can now invoke the (local) Bohr-Sommerfeld quantization rule:

$$\int dz q(z) = N_{\text{WKB}} \pi \quad (3.19)$$

to estimate the total number N_{WKB} of radial harmonics in the sum. The expression for N_{WKB} in combination with (3.17) then give:

$$C_n = \left(\frac{1}{4\pi^2} \frac{\partial \omega_n}{\partial n} \right)^{1/2}, \text{ for } q(z) \gg \delta\theta(z), z \approx 1. \quad (3.20)$$

Now we turn the summation over the quantum number n into the integration over energy and obtain for the *bulk* electron density (here we also performed the integration over ρ using

the explicit expression for the wave function (2.11) and the normalization condition (3.16) for the Bessel functions):

$$n(z) = \frac{4\pi}{a(z)^2} \int_0^{2\pi} d\phi \int_0^{\sqrt{f(z)(\tilde{E}^2(0,z) - \tilde{M}^2(z))}} d\lambda \lambda \int_0^{\mu_{loc}} d\omega \frac{\tilde{E}(\omega, z)}{4\pi^2 q(\omega, \lambda, z)}. \quad (3.21)$$

After performing first integral over ω and then over λ we get:²

$$n(z) = z^3 \frac{q_{\text{WKB}}^3 f^{3/2}(z)}{3\pi^2} \quad (3.22)$$

with q_{WKB} determined by

$$q_{\text{WKB}}^2 = \tilde{E}^2(0, z) - \tilde{M}^2(z). \quad (3.23)$$

Notice that this formula corresponds with common knowledge on the density of electron star [10]. However, even though the formal expression is the same, the self-consistent solution for the metric and gauge field is different because of the quantum correction we introduce to pressure. The difference is visualized in figure 1A where we preview our backreacted WKB star solutions and compare them to the semi-classical (electron star) limit. While the electron star density exhibits a discontinuity at the horizon, the WKB density smoothly falls off to zero. However, both models have a semiclassical “edge”: outside the region $z_1 < z < z_2$, the density is exactly zero. In reality, quantum tails change this picture. In [37] we show that (small) nonzero density extends all the way between the boundary and the horizon. However, it is not expected to change the finite temperature physics which is in the focus of this paper. We therefore do not take into account the quantum tails in further calculations, to avoid any distractions from the main message.

3.2 Pressure and equation of state in the semiclassical approximation

Following the logic behind the density calculation, we will now calculate the pressure p along the radial direction. It will actually prove easier to derive the expression for the (bulk) internal energy density first and then calculate the pressure. By definition, the energy density reads

$$\mathcal{E}(z) = \sum_{k_x, k_y} \int dx \int dy \int_0^{\mu_{loc}} d\omega \omega \Psi^\dagger(z) \Psi(z) = \sum_\lambda \int_0^{\mu_{loc}} d\omega \omega \frac{\tilde{E}(z)}{4\pi^2 q(z)} \quad (3.24)$$

where $\tilde{E}(z)$ is defined in (2.12), $\mu_{loc} = \mu e^{h(z)/2} / f(z)$ and the sum limits are the same as in (3.21). Performing the integration in a similar fashion as when computing $n(z)$ in (3.21)–(3.22), we obtain

$$\mathcal{E} = \frac{3}{4} e \Phi n + \frac{1}{2} f^2 \tilde{M}^2 \text{ArcSinh} \frac{\tilde{E}}{\tilde{M}}. \quad (3.25)$$

²The given result for n can be compared to the charge density in the electron star limit given in [17]. The metric functions used there are related to ours as $f \mapsto f e^{-h}/z^2$ and $g \mapsto 1/fz^2$, where our metric functions are on the right hand side. Likewise, our definition of q_{WKB} is related to k_F of [17] as $q_{\text{WKB}} = k_F / \sqrt{f}$. Now the *total* bulk charge is expressed in [17] as $Q = \int dz \tilde{n}_e(z)$ where $\tilde{n}_e(z) \sim n(z) e^{h/2}$. In our conventions $Q = \int dz \sqrt{-g} g^{zz} g^{tt} n = \int dz n(z) e^{h/2}$ thus giving the same result as in [17].

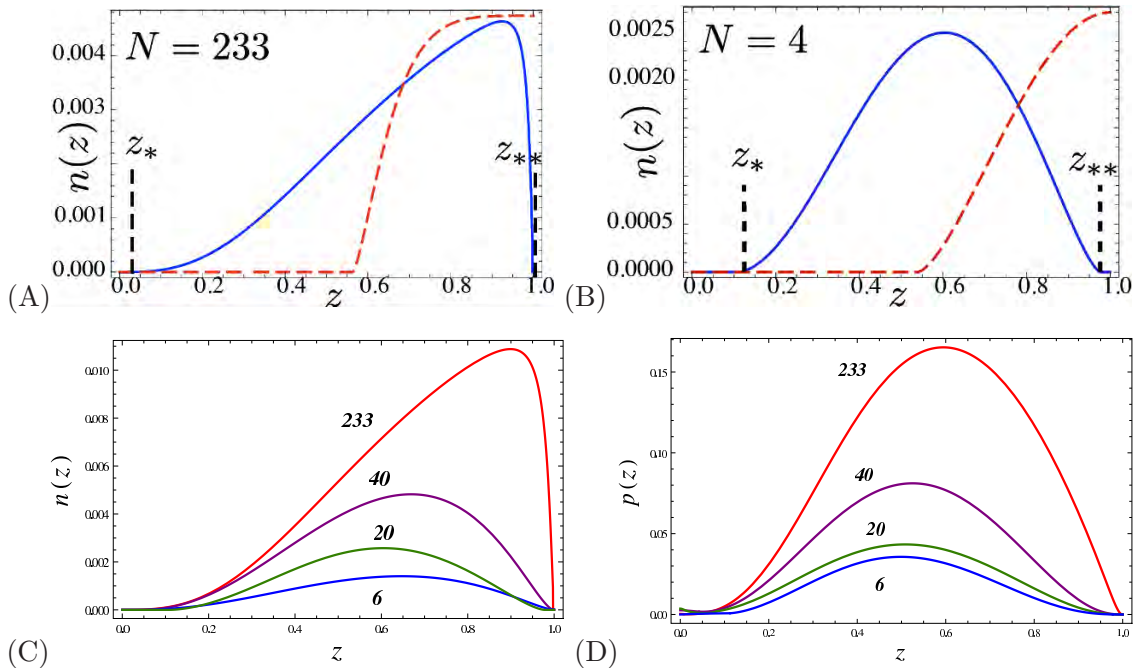


Figure 1. WKB bulk density $n(z)$ (eq. (3.22), blue lines) and electron star density (red dashed lines). Parameter values (A) $(\mu, e, m) = (1.7, 1, 0.1)$, (B) $(\mu, e, m) = (1.7, 10, 1)$. The classically allowed region lies between the turning points z_* and z_{**} , determined by the condition of vanishing WKB momentum ($q(z_*) = q(z_{**}) = 0$). The parameters for (A) are in the classical (electron star) regime, with $N_{\text{WKB}} \gg 1$ when WKB approximation is quite accurate. The plot (B) shows a case of small N_{WKB} where the WKB approximation becomes inadequate and further quantum corrections are likely to be important. (C) Bulk density for a range of values $(\mu, e, m) = (1.7, 1, 0.1)$ (red), $(\mu, e, m) = (1.7, 5, 0.1)$ (violet), $(\mu, e, m) = (1.7, 10, 1)$ (green) and $(\mu, e, m) = (1.7, 20, 1)$ (blue). For large specific charge of the fermion (and therefore a large number of WKB levels in the bulk) the solution is dominated by the classically allowed region and looks similar to the electron star limit. For smaller e/m values (and thus fewer WKB levels) the quantum correction in the near-boundary region becomes more important and the curves are visibly different from the fluid limit. (D) Thermodynamical pressure (eq. (3.34)), for the same parameter values as in (C).

Notice that the first term exactly corresponds to the electrostatic energy while the second is the one-loop term that encapsulates the quantum fluctuations. The above result is remarkably close to the Hartree vacuum polarization correction as it appears in various model energy functionals in literature.

3.2.1 Microscopic pressure

The easiest way to express the pressure is to make use of the first law of thermodynamics, which states

$$p(z) = \sqrt{g^{zz}} (e\Phi(z) - \mathcal{E}(z)). \quad (3.26)$$

There are two possible approaches to arrive at the pressure also directly from the equations of motion. We can express the radial pressure p from the microscopic fermionic

Lagrangian (2.3). By definition it reads

$$p = \sum_{n,\lambda} \left(\Psi_+^\dagger \sigma_3 \partial_z \Psi_- + \Psi_-^\dagger \sigma_3 \partial_z \Psi_+ \right) = \frac{1}{a^2} \left(\tilde{E}(F^2 + G^2) - \tilde{M}(F^2 - G^2) - 2\tilde{k}FG \right) \quad (3.27)$$

The equality follows directly from the Dirac equation, substituting the expressions for $\partial_z \Psi_\pm$ from (2.9). Now we can exploit the lowest order WKB solution (3.13) to get

$$p = \frac{2\pi}{a^2} \sum_{n,\lambda} C_n^2 \left(\frac{\tilde{E} - \tilde{M}}{q} - \tilde{k} \right), \quad (3.28)$$

which, after the momentum integration, gives:

$$p = 2\pi \sum_n C_n^2 e^{h/2} z^3 \sqrt{f} \left[(\tilde{E} - \tilde{M}) q_{\text{WKB}}^2(z) - \frac{2}{3} q_{\text{WKB}}^3(z) \right] \quad (3.29)$$

The explicit calculation is tedious but straightforward. Unlike the density case, the final sum is not readily performed to obtain a closed-form expression. Instead, we integrate numerically over the energy levels ω_n to obtain the function $p(z)$. However, even a quick look at (3.29) tells that it behaves as q_{WKB}^3 at leading order, for q_{WKB} large (the first and the third term will contribute as q_{WKB}^3). After the energy integration this term gains roughly a factor of μ , implying that $p \sim \mu n \sim \mu^4$, as we expect to recover in the fluid limit.

We have now calculated the radial pressure, i.e. the fermionic component of the stress tensor T_z^z . Due to local isotropy, it does not depend on the direction and position in the $x - y$ plane. The same happens in the fluid limit, as shown in [10]. The pressure in the perpendicular direction (in the $x - y$ plane) is analogously expressed as

$$p_\perp = - \sum_{n,\lambda} ik \left(\Psi_+^\dagger \sigma_1 \Psi_- + \Psi_-^\dagger \sigma_1 \Psi_+ \right) = \frac{2\pi}{a^2(z)} \sum_{n,\lambda} C_n^2 \frac{1}{q} \lambda \tilde{E} \quad (3.30)$$

The summation over λ , i.e. the value of the in-plane momentum can again be performed analytically, yielding:

$$p_\perp = 2\pi \sum_n C_n^2 e^{h/2} z^3 f q_{\text{WKB}}^2 \tilde{E}. \quad (3.31)$$

In fact, the above sum has a closed-form limit for $N_{\text{WKB}} \rightarrow \infty$:

$$p_\perp = f^2 e^{h/2} z^3 \frac{q_{\text{WKB}}^4}{12\pi^2}, \quad (3.32)$$

which obeys the relation $p_\perp \sqrt{g_{ii}} = n \sqrt{g_{00}}/3$, the covariant version of the relation $p = \mu n/4$. We will not make use of p_\perp as the ii component of the Einstein equations is not functionally independent of the 00 and zz components; the two metric functions f, h are determined from the two equations, and the third one can only serve as a consistency check.

3.2.2 Thermodynamic pressure

In a “near”-classical regime, at large occupation number, thermodynamics ought to work, so we can express the pressure from the energy density \mathcal{E} , as $p = -\partial E/\partial V$. This expression is still hard to calculate exactly. However, we can use the following trick to estimate p at the leading order. Consider a small change of the number density δn . It will introduce a small change of energy $\delta\mathcal{E}$, pressure δp and the volume of the bulk electron gas δV , the latter because the classically allowed region where $q_{\text{WKB}}^2 > 0$ will shift and grow (if $\delta n > 0$). Now since the metric is radially symmetric we can expand the volume $V = \int_{z_*}^{z_{**}} d^3x \frac{e^{-h(z)/2}}{z^4}$ around its initial value and find that the leading term in its variation behaves as $\delta V = V\delta\ell/(1-\ell) + \dots$, where $\ell \equiv z_{**} - z_*$ is the (dimensionless) length of the classically allowed interval along the z axis, i.e. the interval between the zeros of the WKB momentum $q_{\text{WKB}}(z) = \sqrt{\tilde{E}^2(z) - \tilde{M}^2(z)}$. This yields

$$\frac{\partial E}{\partial V} = \mathcal{E} + V \frac{\partial \mathcal{E}}{\partial V} = \mathcal{E} + V \frac{\delta \mathcal{E}(1-\ell)}{V\delta\ell} = \frac{\delta \mathcal{E}}{\delta \ell}. \tag{3.33}$$

Since all the processes we study are certainly adiabatic (looking at the whole system of gravity plus the matter fields), we can replace the variations by partial derivatives and write $p \sim \partial \mathcal{E}/\partial \ell$ as an approximation for the radial pressure. However, even this expression we are only able to evaluate in a very crude way. For $N_{\text{WKB}} \gg 1$, it is natural to assume (and confirmed by the numerics, see figure 1) that z_{**} is very close to the horizon, z_* is quite far from the horizon and $\ell \approx 1 - z_*$. For $z \sim z_*$, we assume that the electric potential does not deviate much from the linear law: $\Phi \sim \mu(1 - z)$, because z_* is not far from the boundary. This means that the metric function $h(z)$ can be well approximated by a linear function $h(z) \sim \text{const.}(1 - z)$. Solving the equation $q_{\text{WKB}}^2 = \tilde{E}^2(z_*) - \tilde{M}^2(z_*) = 0$, we get $\ell \sim 1 - \log \frac{e^2 \mu^2}{m^2}$, and (3.25) gives the thermodynamic pressure. However, we cannot get the numerical prefactor right in our approach, and this is important in order to satisfy the first law of thermodynamics, which in the fluid limit predicts $p = \mathcal{E}/4$. We therefore norm p_{thd} by hand by a constant factor C_{thd} . This gives:

$$p_{\text{thd}} = -C_{\text{thd}} \frac{\partial \mathcal{E}}{\partial \Phi} \frac{\partial \Phi}{\partial \mu} \frac{\partial \mu}{\partial \ell} \sim \frac{3}{4} e\mu(1 - z) \left(n + \frac{\tilde{M}^2 e^{-h}}{z \sqrt{\tilde{M}^2 + e^h \tilde{E}^2}} \right) \tag{3.34}$$

This is the relevant regime to compare with the electron star. We will call the estimate (3.34) thermodynamic pressure and denote it by p_{thd} to differentiate from the exact summation of WKB wave functions (3.29). These expression are also the equations of state of the system as they connect the pressure to the density. The thermodynamic pressure is more convenient for calculations. In spite of its approximate nature, (3.34) in particular yields a remarkably accurate result when compared with the quantum pressure at $N_{\text{WKB}} \gg 1$.

We can make the connection between the exact first law of thermodynamics (3.26) and the quick estimate (3.34) by showing them to be equal in the limit of small \tilde{E} , which is appropriate in the vicinity of the phase transition from WKB star to the RN black hole.

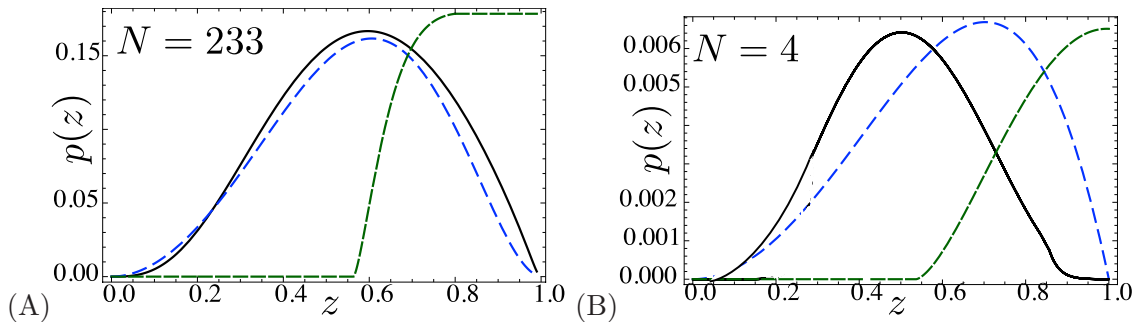


Figure 2. Comparison between full quantum pressure (dashed blue lines, eq. (3.29)) and thermodynamic pressure (solid black lines, eq. (3.34)) for two sets of parameters: $(\mu/T, e, m) = (1.7, 1, 0.1)$ (A) and $(\mu/T, e, m) = (1.7, 5, 1)$ (B). For comparison we plot also the fluid pressure $p = en\Phi/2$ (dashed green lines). Expectedly, for $N_{\text{WKB}} \gg 1$ (A) the thermodynamic approximation comes close to the exact summation while for N_{WKB} small the level spacing is large and the thermodynamic limit is no longer a good approximation to the sum of the contributions of individual levels. Notice that both ways of computing pressure yield similar results for large N_{WKB} but deviate at smaller N_{WKB} .

In this case expanding both equations in \tilde{E} , we find the same expression:

$$p \approx \frac{1}{4}e\Phi n + \frac{f}{z}\tilde{E}\tilde{M} + O(\tilde{E}^3). \quad (3.35)$$

Finally, it is illustrative to see how we reproduce the electron star pressure [10] in the limit of large density. For $n \rightarrow \infty$, the first term in \mathcal{E} and p_{thd} dominates and we obtain from (3.25) and (3.34)

$$p_{ES} = \frac{1}{4}e\Phi n \quad (3.36)$$

as expected for an ideal fluid, which corresponds to the electron star approach. The physical interpretation of this result (and of the pressure inside the classically allowed region in general) is that of a Fermi gas pressure which, as we know, survives also in the limit of classical thermodynamics. The comparison of p , p_{thd} and p_{ES} is summarized in figure 2, for high and low number of levels. While the thermodynamic approximation (3.34) is good when $N_{\text{WKB}} \gg 1$, for small N_{WKB} both the fluid limit and the thermodynamic limit eventually break down and the contributions of individual levels must be taken into account. Once again, the introduction of Airy corrections would extend the nonzero pressure to the whole AdS space, which is only expected to be relevant at $T = 0$ [37].

4 Maxwell-Dirac-Einstein system

We have now arrived at the point where we can look for a numerically self-consistent solution of the Einstein-Maxwell equations. The numerics uses an iterative procedure to converge toward the solution. Only in the IR region it is possible to use a scaling ansatz to estimate the scaling behavior of the metric and matter fields, akin to the procedure used in [20]. This is the first attempt at a numerically self-consistent solution including backreaction on the geometry with holographic fermions which goes beyond the fluid picture of [10].

Our calculation is similar to the one for relativistic ideal fluid (i.e. electron star) approximation. Because an ideal fluid is dissipation-less one can construct an action as put forward in [15] and used in [10, 12]. The Lagrangian of this charged fluid coupled to gravity and electromagnetism is

$$S = \int d^4x \left[\frac{1}{2\kappa^2} (R + 6) - \frac{1}{2q^2} (\partial_z \Phi)^2 + p \right]. \quad (4.1)$$

In other words, the contribution of fermions reduces to the pressure p . While we do not take the fluid limit in this paper, within the WKB star model we assume that in the first approximation the influence of the corrections to fluid limit ($N_{\text{WKB}} \rightarrow \infty$) is fully encapsulated by the correction to the classical (or fluid) pressure we found in (3.25)–(3.29). The emergent isotropy and its implied ideal nature of the fluid at large occupation number should ensure this.

To construct the backreacted geometry, we therefore “replace” the fermionic terms in the exact action (2.2) with our effective ideal fluid model in terms of the density and pressure of the bulk fermions. The total effective action is represented as $S = S_E + S_M + S_f$, the sum of Einstein, Maxwell and fluid part. The only nonzero component of the gauge field is Φ and the only non-vanishing derivatives are the radial derivatives ∂_z (the others average out to zero for symmetry reasons). The nonzero fermion pressure p is that considered in section 3.2 and there is a nonzero (local) charge density

$$j_e^0 = qn\sqrt{g^{00}} = qn \frac{ze^{h/2}}{\sqrt{f}}. \quad (4.2)$$

The fermion fluid term in the effective action thus becomes

$$S_f = - \int d^4x \sqrt{-g} (j_e^0 \Phi + p). \quad (4.3)$$

Due to the preserved spherical symmetry we may substitute these simplifications directly in the effective action to arrive at:

$$S_{\text{eff}} = \int d^4x \sqrt{-g} \left[\frac{1}{2\kappa^2} (R + 6) - \frac{z^4}{2} e^h \left(\frac{\partial \Phi}{\partial z} \right)^2 - j_e^0 \Phi + p \right]. \quad (4.4)$$

The only components of the stress tensor the fermion kinetic energy contributes to are the diagonal ones; the others vanish due to homogeneity and isotropy in time and in the $x - y$ plane. From (4.4) we get the equations for the energy-momentum tensor:

$$T_0^0 = -\frac{1}{2} z^4 e^h \left(\frac{\partial \Phi}{\partial z} \right)^2 + j_e^0 \Phi \quad (4.5)$$

$$T_z^z = -\frac{1}{2} z^4 e^h \left(\frac{\partial \Phi}{\partial z} \right)^2 + j_e^0 \Phi + mn + g_z^z p. \quad (4.6)$$

With the metric ansatz (2.4), we can now write down our equations of motion:

$$\frac{1}{\sqrt{-g}} \left(\partial_z e^{-h/2} \partial_z \Phi \right) = -j_e^0 \quad (4.7)$$

$$3f - z\partial_z f - 3 = T_0^0 \quad (4.8)$$

$$3f - z\partial_z f - 3zf\partial_z h - 3 = T_z^z \quad (4.9)$$

Notice that the ii component of the Einstein equations:

$$\frac{1}{2}(\partial_{zz}f - f\partial_{zz}h) + \frac{1}{4}(f\partial_z h^2 - 3\partial_z f\partial_z h) + \frac{f\partial_z h - 2\partial_z f}{z} + \frac{3f}{z^2} = T_i^i \quad (4.10)$$

with

$$T_i^i = -\frac{1}{2}z^4 e^h \left(\frac{\partial\Phi}{\partial z}\right)^2 + g_i^i p_\perp \quad (4.11)$$

is functionally dependent on the others and drops out. For that reason, (4.7)–(4.9) forms the complete system of Maxwell-Einstein equations. We do *not* need to know T_i^i or p_\perp nor to assume the isotropy (in the sense $T_i^i = T_z^z$).

In this article we shall only be interested in finite temperature solutions. The gravitational background is therefore a black hole with an horizon: a single zero in the warp function $f(z)$ at a finite value $z = z_H$.³ Physically the inescapability of the black hole horizon immediately suggests the following boundary conditions. The black hole horizon should have no hair so $\Phi(z_H) = 0$; $h(z)$ which characterizes the ratio of the UV and IR speed of light should be finite at the horizon: $h(z_H) = h_0$. Note that the effective WKB potential felt by the fermions blows up at the horizon and that the fermion wavefunctions therefore manifestly vanish at z_H . This same phenomenon is noted in the electron star at finite temperature which also has an “inner” edge outside the horizon [12, 33].

At AdS infinity the boundary conditions are standard in AdS/CFT: for the gauge field $\lim_{z \rightarrow 0} \Phi(z) = \mu$ fixes the chemical potential at the boundary ($z_0 \rightarrow 0$). We normalize $\lim_{z \rightarrow 0} f(z) = 1$, $\lim_{z \rightarrow 0} h(z) = 0$. Again the boundedness of the normalized WKB wavefunctions uniquely fixes the behavior of the fermions.

Finally, it remains to define the units used throughout the paper. The natural unit of energy and momentum is the chemical potential μ and we will express all quantities in units of μ . The two thermodynamic parameters are the chemical potential μ and T . As AdS/CFT is built on conformal field theories which have no intrinsic scale, the physics only depends on the ratio μ/T .

Let us conclude with an outline of the numerical algorithm, which is not completely trivial. The boundary conditions to be implemented are given at different points: some are given at the AdS boundary and some at the horizon. Since the system is nonlinear, it is necessary to either linearize the system or to shoot for the correct boundary conditions with the full nonlinear system. After experimenting with both, we have decided to iterate the full, non-simplified system of equations, integrating from the horizon and shooting for the conditions at the boundary. The iterative procedure consists of two steps: we start with the non-backreacted AdS-RN geometry and compute the density (semiclassical plus the quantum corrections) for the the electron charge equal to e/N (where e is the physical charge and N some positive integer), then we solve the system of Einstein-Maxwell equations (4.7)–(4.9), afterwards we increase the fermion charge to $2e/N$, calculate the

³At zero temperature, when the horizon vanishes due to fermionic backreaction (this includes also the case of Lifshitz geometry), the boundary condition for f guarantees also the smoothness of the solution on the horizon: $\partial_z f(z_H) = 0$. This condition ensures that we pick the correct branch of the solution as there are typically two families of functions $f(z)$ that satisfy the equations of motion and the condition $f(z) = 0$. One of them has a vanishing derivative whereas the other has finite derivative as $z \rightarrow 1$.

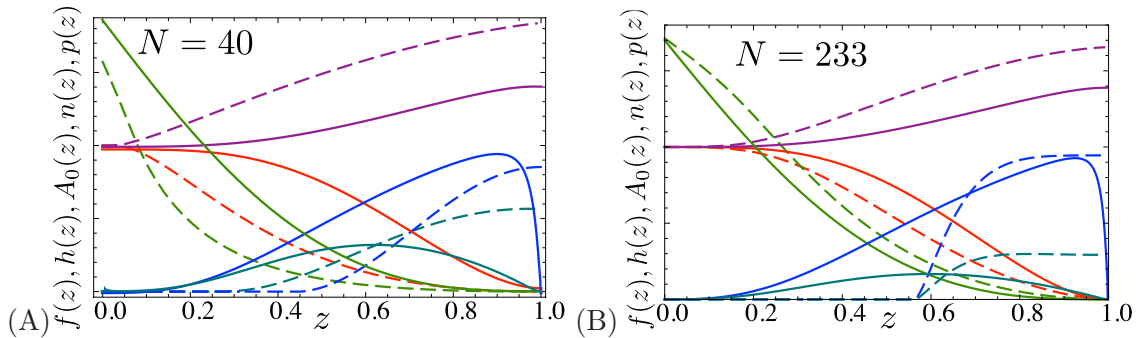


Figure 3. Profiles of the metric functions $f(z)$ (red) and $e^{-h(z)}$ (violet), the gauge field $\Phi(z)$ (green), density $n(z)$ (blue) and the pressure $p(z)$ (cyan) at zero temperature, for $(\mu/T, e, m) = (1.7, 1, 0.1)$ (A) and for $(\mu/T, e, m) = (1.7, 10, 0.1)$ (B). Solid lines are calculated from our model while dashed lines are the electron star solution for the same parameter values. For better visibility density and pressure are rescaled by a constant factor. Near the boundary we always have $h(z) \rightarrow 0$ and $\Phi(z) = \mu + O(z)$, in accordance with the universal AdS asymptotics of the solution but in the interior the solutions start to deviate. Most striking is the absence of sharp classical edges in density and pressure. The difference in pressure will turn out to be crucial in moving away from the fluid limit. Here we have not shown the solution with $N_{\text{WKB}} = 4$: this case deviates from the electron star ($N_{\text{WKB}} \rightarrow \infty$) so strongly that it does not make sense to compare it. Indeed, $4 \ll \infty$!

charge density in the background (f, h, Φ) taken from previous iteration and solve for this density the Einstein-Maxwell equations (4.7)–(4.9). We repeat this procedure for charge $3e/N$, $4e/N$ etc. After N iterations we have arrived at the physical value of the charge e . Then we do more iterations with fixed charge e to ensure that the solution has converged, checking that the set of functions (f, h, Φ) does not change from iteration to iteration. In this way we achieve the self-consistent numerical solution of the Maxwell-Dirac-Einstein system of equations. The integration is always done from the horizon, shooting for the conditions for Φ and h at the boundary, since it is well known that integrating from the AdS boundary is a risky procedure as it is next to impossible to arrive at the correct branch of the solution at the horizon.

5 Phases of holographic fermions

We can now analyze the structure of both the bulk and the field theory side as a function of the parameters T/μ , e and m . We first shortly discuss the nature of the bulk solution for the geometry and gauge field and notice some qualitative properties. The typical way that the solutions to the WKB-Fermi-Einstein system (4.7)–(4.9) look is illustrated in figure 3. The near-horizon scaling of the metric and gauge field is of Lifshitz type, as expected in the light of earlier models [10, 34]. Notice that we are working at finite temperature and thus do *not* impose the IR boundary conditions for the metric functions which correspond to the Lifshitz geometry. Our finding of Lifshitz scaling is purely numerical, with the simple boundary conditions discussed above. In the figure, we plot also the electron star solution for comparison. One should be careful in comparing the two, however, as the electron star corresponds to the limit $e \rightarrow 0$ and thus cannot be compared directly (i.e., for the

same parameter values) to our WKB star. Our convention is to first define the electron star by choosing the *total* charge density Q and the parameter $\hat{m} = m/\epsilon\kappa$, where κ is the gravitational constant whose value is fixed by the normalization of the action (4.1). For the WKB star, we impose the same value of Q , while the value of m is found as $m = \hat{m}\epsilon\kappa$ (for WKB star we can control e as an independent parameter). Relative proximity of the solutions for large N seems to confirm that this is a physically meaningful way of comparing the models.

5.1 Thermodynamics

We can now use these full solutions to determine the macroscopic characteristics of the dual strongly coupled fermion system. Let us first derive the free energy of the boundary field theory. According to the dictionary, it is equal to the (Euclidean) on-shell action, which contains both bulk and boundary components:

$$F = S_{\text{bulk}}^{\text{on-shell}} + S_{\text{bnd}}^{\text{on-shell}}. \tag{5.1}$$

We have already discussed the bulk action in the previous section. We will again approximate the fermionic contribution (4.3) by its leading term, the pressure.

In computing the free energy using AdS/CFT a crucial part is often played by boundary terms in the action. It encapsulates the regularizing terms that eliminate $z \rightarrow 0$ divergences, enforces a Dirichlet boundary condition for the gauge field, but it also provides the kernel for the fermionic correlation functions [9, 36]

$$S_{\text{bnd}} = \oint_{\partial AdS} \sqrt{-h} \left(\frac{1}{2} n_\nu F^{\mu\nu} A^\mu + \bar{\Psi}_+ \Psi_- \right), \tag{5.2}$$

with h being the induced metric on the boundary ($h = \frac{1}{z^2}(-1/f(z=0), 1, 1)$) and Ψ_+ and Ψ_- are radial projections of the wave function as in eq. (2.8). By ∂AdS we have denoted the boundary of the AdS space. Let us now briefly show why these boundary fermion terms do not contribute to the free energy, but that the leading fermion contribution is the (one-loop) effective pressure. Essentially the point is that only normalizable modes of the field are occupied and hence they cannot contribute to the boundary action as they die off too fast. The Dirac field asymptotics at the boundary are given by [13]:

$$\Psi_+ = \frac{i\mu\gamma^0}{2m+1} B_- z^{5/2+m} + \dots, \quad \Psi_- = B_- z^{3/2+m} + \dots \tag{5.3}$$

At the same time the electromagnetic boundary term reduces to $\Phi\partial_z\Phi|_{z=0} = -\mu\rho$, where ρ is the total boundary (not only fermionic) charge density, read off from the subleading “response” of the bulk electrostatic potential $\lim_{z\rightarrow 0} \Phi(z) = \mu - \rho z + \dots$. The regularized boundary action now reads

$$S_{\text{bnd}} = \lim_{z_0\rightarrow 0} S(z_0) + \lim_{z_0\rightarrow 0} \int d^3x \left[\frac{3\mu}{2(2m+1)} \bar{B}_- i\gamma^0 B_- z_0^{1+2m} - \frac{1}{2} \mu\rho \right], \tag{5.4}$$

Since $m > -1/2$ is the fermionic unitarity bound in AdS/CFT, the first term always vanishes in the limit $z_0 \rightarrow 0$. The total on-shell action, i.e. the free energy is therefore

$$F = \int_{z_0}^{z_H} dz d^3x \sqrt{-g} \left[R + 6 + \frac{ze^{h/2} qm\Phi}{2\sqrt{f}} + p \right] - \frac{1}{2} \mu\rho \tag{5.5}$$

5.2 Constructing the phase diagram: quantum corrections imply a first order thermal phase transition to AdS-RN

The condensed matter context in which we are discussing AdS/CFT is that of an emergent finite density fermionic ground state out of an UV CFT. In the deep UV or at very high temperatures T/μ the chemical potential should be negligible and we should recover as the preferred groundstate the UV CFT at finite T/μ . The gravitational dual of this is the AdS-RN black hole. It describes a conformal critical phase with no Fermi surfaces. As we lower T/μ an instability should set in towards a state with a finite occupation number of fermions. In the probe analysis one indeed finds several normalizable wavefunctions signalling the existence of states with distinct occupation numbers. They are the bulk counterpart of the existence of non-Fermi-liquid Fermi surfaces [8, 9, 19, 21]. A crucial qualitative aspect is that due to their fermionic nature the wavefunctions of these normalizable modes can *never* “grow”. From a microscopic point of view it therefore appears that any fermion driven phase transition cannot be second order. In the fluid limit, however, the transition was found to be third order. There is no conflict because new analytic behavior can emerge in the fluid scaling limit where the *number of Fermi surfaces* is taken to infinity.⁴ It does mean that one has to be quite careful in the fluid limit as for fermions these corrections can change macroscopic quantities. For any finite number of Fermi surfaces we should discover a first order transition. We did indeed find this earlier in the Dirac hair approximation valid for $N_{\text{WKB}} = 1$ [13]. With the WKB construction put forward here, we will show that this is indeed so for any finite N_{WKB} .

Figure 4 shows the behavior of the free energy $F(T/\mu)$ of the WKB corrected star construction for different parameters e, m , corresponding to a different number of levels N_{WKB} (which roughly equals the number of Fermi surfaces. In the high temperature phase the preferred state with lowest $F(T/\mu)$ is that of the pure AdS-RN. Since there are no occupied fermionic states it is independent of the fermion charge and mass. In the low temperature phase the preferred phase is the WKB star. Where the phase transition occurs, one immediately sees the characteristic first order cusp in $F(T/\mu)$ whose non-analyticity indeed becomes clearer as N_{WKB} decreases. The panel (B) of the figure makes this clear by showing the vicinity of the phase transition.

The first order nature of the phase transition can in fact be understood analytically with this WKB construction. The argument is along similar lines as for the fluid limit of the electron star [12]. Assuming that the transition is dominated by the behavior of the fermions and that the contribution of the geometry change due to backreaction is small

⁴Note that there is a crucial subtlety in the fluid limit in AdS/CFT with a flat Minkowski-space boundary. Normally one needs a thermodynamic “fluid” limit to even be able to discuss the notion of a phase transition. In global AdS, or conventional Tolman-Oppenheimer-Volkov neutron stars, a bound on the number of radial modes, implies a countable number of states. However, this is not so in AdS/CFT with a flat Minkowski-space boundary. For each radial mode there is still a formal infinite number of modes distinguished by the transverse momentum. The phase transition discussed here is where one considers $N/V_{\text{transverse}} \rightarrow \infty$. It restores one’s intuition that the emergence of *each single Fermi surface* dual to each single radial mode is associated with a macroscopic phase transition. We thank Sean Hartnoll for emphasizing this.

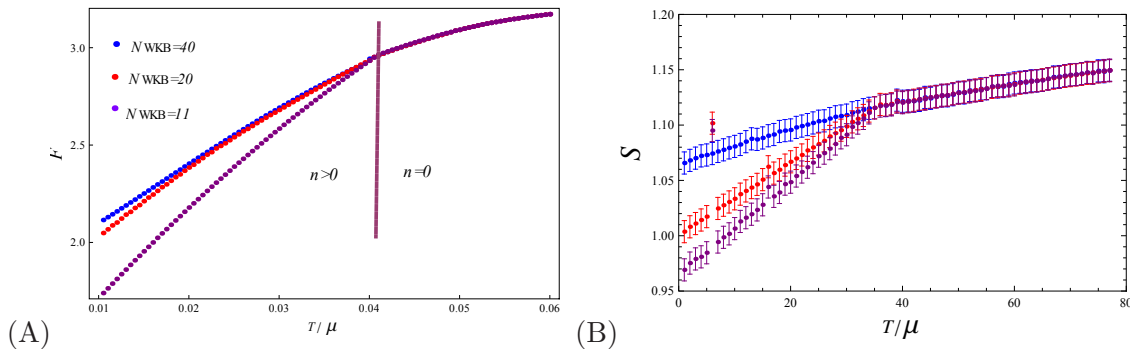


Figure 4. Free energy as a function of temperature $F(T)$. The abrupt change of the derivative signifies the first order transition between the finite density phase and the pure black hole (with zero bulk fermion density), in line with the analytical prediction of the first order transition from the second term in the bulk free energy in section 5.2. We show the calculations for three different values (μ, e, m) of the system parameters: $(1.7, 3, 0.1)$, $N_{\text{WKB}}(T = 0) = 40$ in blue, $(1.7, 10, 0.1)$, $N_{\text{WKB}}(T = 0) = 20$ in red and $(1.7, 10, 0.7)$, $N_{\text{WKB}}(T = 0) = 11$ in violet. Notice how the slope of F in the low-temperature phase decreases as the number of levels increases: for $N_{\text{WKB}} \rightarrow \infty$ we reach the electron star limit when the transition becomes continuous. Panel (B) shows the vicinity of the critical temperature for three sets of parameter values, to make the cusp in $F(T)$ clearly visible. In the high temperature (RN) phase the curves $F(T)$ fall on top of each other as one expects for the RN black hole with $n = 0$. The behavior in the low-temperature phase (with non-zero density) is different for the three curves as the value of the charge affects the behavior of the bulk fermions. For presentation purposes, the curves have been rescaled to the same transition temperature; in general, however, $(T/\mu)_c$ is *not* universal and will differ for different corners of the parameter space.

near the critical temperature, the relevant part of the free energy of the system is given by

$$F_{\text{Fermi}} \approx \int_0^{z_H} p = \frac{e\mu}{2} \int_{z_*}^{z_{**}} (1-z)n + \frac{e\mu}{2} \int_{z_*}^{z_{**}} \frac{\tilde{M}^2 e^{-h}}{z \sqrt{\tilde{M}^2 + e^h \tilde{E}^2}} \equiv F_{\text{Fermi}}^{\text{fluid}} + \Delta F_{\text{Fermi}} \quad (5.6)$$

Starting from low temperatures and nonzero n , at the transition point the bulk density n vanishes. In the WKB construction that means that the turning points coincide: $z_* \rightarrow z_{**}$. The first, “fluid limit” term $F_{\text{Fermi}}^{\text{fluid}}$ in (5.6) is proportional to Φn and it is analyzed in detail in [12]. It yields the scaling $F_{\text{Fermi}}^{\text{fluid}} \sim (T - T_c)^3$. This indicates a third order transition at the semi-classical level. The new, second, quantum term will change this, however. The vanishing of the classically allowed region means $\tilde{E} \approx \tilde{M}$ in the whole (narrow) region $z_* < z < z_{**}$. One can thus expand $\tilde{E} = \tilde{M} + \delta z \times \delta \tilde{E} / \delta z + \dots$ and analyze the leading terms in δz . It is easy to see that its expansion starts from a constant. Since for vanishing δz the density can be assumed constant throughout the WKB star, we estimate the integral in ΔF_{Fermi} as

$$\Delta F_{\text{Fermi}} \approx \frac{\Phi \tilde{M}^2 e^{-h}}{\sqrt{\tilde{M}^2 + e^h \tilde{E}^2}} \delta z = (\text{const.} + O(\delta z)) \delta z, \quad (5.7)$$

where $\delta z = z_{**} - z_*$. Therefore, the second term scales as $\Delta F_{\text{Fermi}} \sim \delta z$. Now, for a vanishing bulk charged fluid/emerging charged black hole, the principle of detailed balance predicts that the charge of the former equals the charge of the latter: $n \delta z = n_{\text{BH}} \delta z_H$,

where the charge densities of the bulk and the black hole are n and n_{BH} , respectively, and δz_H is the change in the position of the black hole horizon. Since the densities can be assumed constant for vanishing δz and δz_H , we find $\delta z \sim \delta z_H \sim T - T_c$. We can now write $F_{\text{Fermi}} = F_{\text{Fermi}}^{\text{fluid}} + \Delta F_{\text{Fermi}}$. We know that $F_{\text{Fermi}}^{\text{fluid}} \sim (T - T_c)^3$ [12], but we have now shown that

$$\Delta F_{\text{Fermi}} \sim T - T_c. \tag{5.8}$$

At the quantum level the *transition is always of first order*. The quantum correction is subleading at general T values, but becomes leading as the phase transition point is approached. Finally, we remark that, if one considers the bulk free (or internal) energy $\int dz \mathcal{E}$ given in eq. (3.24) using the similar scaling reasoning, one arrives at the same conclusion: $F \sim T - T_c$. This confirms the intuition that the bulk and boundary thermodynamics are equivalent at leading order, i.e. the difference $F_{\text{bulk}} - F$ does not contain first-order terms in $T - T_c$ and thus does not change the order of the transition. Now the exact free energy differs from our WKB star calculation, as we have assumed that the correction to the fluid limit is fully captured by the correction to pressure. However, an additional term in F *cannot decrease the order of the transition*: it can introduce new singularities (of some order α , scaling as $(T - T_c)^\alpha$) but cannot cancel out the term.

The numerics just confirms this analytic prediction of a first order phase transition. The field theory interpretation of the discontinuous nature of the transition to a phase with Fermi surfaces is simple: fermions do not break any symmetry but the discharge of the black hole does signify that the ground state is reconstructed due to the formation of a rigid Fermi surface. The only way to reconstruct the ground state without breaking any symmetries is precisely the first order transition of the density van der Waals liquid-gas type. This is the macroscopic counterpart to the probe analysis where the Grassman nature of fermions Pauli blocks the growing of mode functions. A van der Waals liquid-gas first order type transition is indeed seen in [13] for the first order transition from $N_{\text{WKB}} = 1$ Dirac hair state to AdS-RN. The confusing point was that electron star/AdS-RN transition valid in the strict $N_{\text{WKB}} \rightarrow \infty$ fluid limit was found to be third order [12, 33]. Here we show that this change in the nature of the phase transition is an artifact of this $N_{\text{WKB}} \rightarrow \infty$ limit. Instead the expected first order behavior is recovered for any finite value of N_{WKB} .

6 Discussion and conclusions

In this paper we have constructed the WKB star as an improved semiclassical model of holographic fermions in AdS₄ space, aimed at understanding the phase diagram of strongly coupled Fermi and non-Fermi liquids. The model combines a WKB approximation with a Hartree summation to approximate a finite N_{WKB} charged fermion state in AdS coupled to both gravity and electromagnetism. The dominant effect is a quantum correction to the pressure and energy density ("vacuum polarization") of the conventional $N_{\text{WKB}} \rightarrow \infty$ classical model — the electron star. This finite N_{WKB} approach has allowed us to address the intermediate fermion charges which cannot be modeled satisfyingly with any of the previously used models.

By studying the free energy of the system we can now construct the full phase diagram of the system. Most importantly, we find a *universal first order phase transition from a finite density to a zero density (Reissner-Nordström, quantum critical) phase*. The discontinuity of the density comes from the quantum term in the internal energy. This term is always present but its relative contribution to the free energy decreases with the inverse of the number of radial modes N_{WKB} . The extreme limit $N_{\text{WKB}} \rightarrow \infty$ reproduces the unexpected third order continuous phase transition found in [12, 33]. Nevertheless, in any real system with finite fermion charge the discontinuity will be present, which fits into the general expectation that the thermal phase transition of a fermionic system should be of the van der Waals (liquid-gas, Ising) type.

So far three distinct approaches aiming at capturing the stable phases of holographic fermionic matter have appeared: the electron star [10], Dirac hair [13] and the confined Fermi liquid model [14]. The electron star is essentially a charged fermion rewriting of the well-known Oppenheimer-Volkov equations for a neutron star in AdS background. The bulk is thus modeled as a semiclassical fluid. It is a controlled approximation in the certain limit of the parameter values. The mystery is its field theory dual: it is a hierarchically ordered (infinite) multiplet of fermionic liquids with stable quasiparticles [17]. On the other end of the spectrum is Dirac hair, which reduces the bulk fermion matter to a single radial harmonic. The Dirac hair approach is based on the truncation of the full non-local equations of motion. As a consequence the field theory dual is a single Fermi liquid, however its gravitational consistency properties are not yet fully understood. In [18] we have shown that Dirac hair and electron star can be regarded as the extreme points of a continuum of models, dialing from deep quantum - a single radial mode - to a classical regime - a very large occupation number - in the bulk. They correspond to two extreme phases in the field theory phase diagram: a multiplet of a very large number of Fermi liquids and a single Fermi liquid. The third approach [14] performs a Hartree summation of the exact quantum mechanical wave functions to capture the fermion density. While the paper [14] applies the Hartree method to a specific model (confined Fermi liquid, where the confinement is introduced through modifying the bulk geometry), the main idea can be used in any background. This approach is more general than the single-particle approach of [13] and it naturally extends the single harmonic Dirac hair state with a single Fermi surface to a state with multiple Fermi surfaces. Our main motivation is to construct a complementary model that extends from the other end — the semi-classical fluid — down to a state with a countable but large number of Fermi surfaces. We aim for a system which is general enough to encompass the middle ground between extreme quantum and extreme classical regimes in the original deconfined setup. In the recent model of “quantum electron star” [16] the same goal is set but the method used is different and is based on the deconfined limit of [14].

In constructing the WKB star, we were also guided by the strengths and weaknesses of these existing models. On the one hand, the Dirac hair is a fully quantum-mechanical model which shows its strength in particular near the boundary (the ultraviolet of the field theory) but becomes worse in the interior, i.e. close to the horizon (the infrared of the field theory) where density is high and the resulting state of matter cannot be well

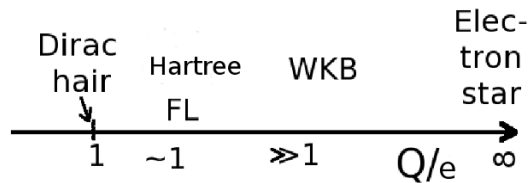


Figure 5. Applicability of various approximations as a function of the ratio of the fermion charge and the total charge of the system, Q/e : Dirac hair, confined Fermi liquid, our present WKB-model, electron star. Dirac hair and electron star are the simplest and most flexible approximations but limited to the extreme ends of the Q/e axis. Compare also to figure 10 in [18].

described by a single wave function. On the other hand, the electron star yields a very robust description of high-density matter in the interior but its sharp boundary at some radius r_c is clearly incompatible with a fully quantum description. It is thus obvious that the physically interesting model lies somewhere in-between the two approaches.

How to relate the electron star [10], Dirac hair [13] and the (confined) Hartree Fermi liquid [14] to our new phase diagram? All models use the same microscopic action for a Dirac fermion with charge e and mass m , but the system is approximated in different ways. The electron star is the fluid limit of the equations of motion, yielding the Oppenheimer-Volkov equations in the bulk. As explained in [18], this approximation is valid in the limit of infinite occupation number $N_{\text{WKB}} \rightarrow \infty$, $e \rightarrow 0$ with the total charge density fixed $Q = N_{\text{WKB}}e$. In addition, the mass $m \rightarrow 0$ while $\hat{m} = m/\sqrt{N_{\text{WKB}}}e$ is fixed. The Dirac hair departs from the opposite limit, treating the bulk fermion as a single collective excitation with $N_{\text{WKB}} = 1$. To obtain a macroscopic charge density one essentially has to take $e \gg 1$. Finally, the confined Fermi liquid of [14] and its deconfined version [16] improve on the Dirac Hair by using a standard Hartree summation of the non-interacting bulk Fermi gas. It works for all $N_{\text{WKB}} \sim \mathcal{O}(1)$ and this significantly increases the region of applicability but at the cost of substantial practical complications, in particular if one wishes to take into account the backreaction on the metric [16]. Our model takes a similar summation approach but simplifies the wave function calculation drastically by using the WKB approximation. This inherently assumes semiclassical dynamics and large number of energy levels $N_{\text{WKB}} \gg 1$ in the bulk. The WKB star is thus independent of [13] but draws heavily on the electron star and the dialing concept of [18]. Since we do *not* make the assumption of zero energy spacing $N_{\text{WKB}} \rightarrow \infty$ necessary for the fluid approximation, our model thus works well in the intermediate regime where N_{WKB} is finite but large compared to unity. This message is illustrated in figure 5, emphasizing the singular nature of both the electron star and the Dirac hair.

One obvious downside of the WKB star is that the WKB approximation breaks down when N_{WKB} , the occupation number, is low. In particular, it means that the accuracy of our method is lowest close to the phase transition to the RN phase. However, for reasons outlined in the section 5.2, we can argue that the order of the phase transition cannot change, i.e. the first-order singularity in the free energy will not be canceled out by the corrections to WKB. Our treatment is an improvement over the strict $N_{\text{WKB}} \rightarrow \infty$ limit of

the electron star model used in [12, 33] to analyze the phase transition, however it remains a task for further work to approach the transition point with a more accurate method which is not limited to large occupation numbers. The recent paper [38] constructs a solution with finite fermion density in AdS₄ without using WKB: this turns out to be much more involved, but allows one to move away from the large N_{WKB} regime.

The natural next step departing from this WKB treatment is to employ a fully quantum-mechanical density functional method. It is, in fact, not a significant complication compared to the approach of this paper: the recipe for computing the density n will be replaced by a somewhat more complicated functional of the gauge field and the metric, which needs to be computed iteratively. We anticipate that this will not alter the qualitative picture, although the numbers might change significantly. The main conclusion of our paper is that the singular fluid limit of bulk fermions when coupled to AdS gravity can lead to macroscopically anomalous results. Finite N_{WKB} corrections are crucial to get the correct answer.

Acknowledgments

This research was supported in part by a Spinoza Award (J. Zaanen) from the Netherlands Organization for Scientific Research (NWO) and the Dutch Foundation for Fundamental Research on Matter (FOM). We are grateful to H. Liu, S.S. Gubser and A. Karch for valuable discussions.

References

- [1] S.A. Hartnoll, *Lectures on holographic methods for condensed matter physics*, *Class. Quant. Grav.* **26** (2009) 224002 [[arXiv:0903.3246](#)] [[INSPIRE](#)].
- [2] J. McGreevy, *Holographic duality with a view toward many-body physics*, *Adv. High Energy Phys.* **2010** (2010) 723105 [[arXiv:0909.0518](#)] [[INSPIRE](#)].
- [3] H.V. Löhneysen, A. Rosch, M. Vojta and P. Wölfle, *Fermi-liquid instabilities at magnetic quantum phase transitions*, *Rev. Mod. Phys.* **79** (2007) 1015 [[cond-mat/0606317](#)].
- [4] M. Gurvitch and A.T. Fiory, *Resistivity of La_{1.825} Sr_{0.175} CuO₄ and YBa₂ Cu₃ O₇ to 1100 K: Absence of saturation and its implications*, *Phys. Rev. Lett.* **59** (1987) 1337.
- [5] A. Donos, J.P. Gauntlett, N. Kim and O. Varela, *Wrapped M5-branes, consistent truncations and AdS/CMT*, *JHEP* **12** (2010) 003 [[arXiv:1009.3805](#)] [[INSPIRE](#)].
- [6] O. DeWolfe, S.S. Gubser and C. Rosen, *Fermi surfaces in maximal gauged supergravity*, *Phys. Rev. Lett.* **108** (2012) 251601 [[arXiv:1112.3036](#)] [[INSPIRE](#)].
- [7] A. Donos, J.P. Gauntlett and C. Pantelidou, *Magnetic and electric AdS solutions in string- and M-theory*, *Class. Quant. Grav.* **29** (2012) 194006 [[arXiv:1112.4195](#)] [[INSPIRE](#)].
- [8] H. Liu, J. McGreevy and D. Vegh, *Non-Fermi liquids from holography*, *Phys. Rev. D* **83** (2011) 065029 [[arXiv:0903.2477](#)] [[INSPIRE](#)].
- [9] M. Čubrović, J. Zaanen and K. Schalm, *String Theory, Quantum Phase Transitions and the Emergent Fermi-Liquid*, *Science* **325** (2009) 439 [[arXiv:0904.1993](#)] [[INSPIRE](#)].

- [10] S.A. Hartnoll and A. Tavanfar, *Electron stars for holographic metallic criticality*, *Phys. Rev. D* **83** (2011) 046003 [[arXiv:1008.2828](#)] [[INSPIRE](#)].
- [11] J.P. Gauntlett, J. Sonner and D. Waldram, *Universal fermionic spectral functions from string theory*, *Phys. Rev. Lett.* **107** (2011) 241601 [[arXiv:1106.4694](#)] [[INSPIRE](#)].
- [12] S.A. Hartnoll and P. Petrov, *Electron star birth: a continuous phase transition at nonzero density*, *Phys. Rev. Lett.* **106** (2011) 121601 [[arXiv:1011.6469](#)] [[INSPIRE](#)].
- [13] M. Čubrović, J. Zaanen and K. Schalm, *Constructing the AdS Dual of a Fermi Liquid: AdS Black Holes with Dirac Hair*, *JHEP* **10** (2011) 017 [[arXiv:1012.5681](#)] [[INSPIRE](#)].
- [14] S. Sachdev, *A model of a Fermi liquid using gauge-gravity duality*, *Phys. Rev. D* **84** (2011) 066009 [[arXiv:1107.5321](#)] [[INSPIRE](#)].
- [15] R.C. Tolman, *Static solutions of Einstein's field equations for spheres of fluid*, *Phys. Rev. D* **55** (1939) 364.
- [16] A. Allais, J. McGreevy and S.J. Suh, *A quantum electron star*, *Phys. Rev. Lett.* **108** (2012) 231602 [[arXiv:1202.5308](#)] [[INSPIRE](#)].
- [17] S.A. Hartnoll, D.M. Hofman and D. Vegh, *Stellar spectroscopy: Fermions and holographic Lifshitz criticality*, *JHEP* **08** (2011) 096 [[arXiv:1105.3197](#)] [[INSPIRE](#)].
- [18] M. Cubrovic, Y. Liu, K. Schalm, Y.-W. Sun and J. Zaanen, *Spectral probes of the holographic Fermi groundstate: dialing between the electron star and AdS Dirac hair*, *Phys. Rev. D* **84** (2011) 086002 [[arXiv:1106.1798](#)] [[INSPIRE](#)].
- [19] N. Iqbal, H. Liu and M. Mezei, *Semi-local quantum liquids*, *JHEP* **04** (2012) 086 [[arXiv:1105.4621](#)] [[INSPIRE](#)].
- [20] S.A. Hartnoll, J. Polchinski, E. Silverstein and D. Tong, *Towards strange metallic holography*, *JHEP* **04** (2010) 120 [[arXiv:0912.1061](#)] [[INSPIRE](#)].
- [21] T. Faulkner, H. Liu, J. McGreevy and D. Vegh, *Emergent quantum criticality, Fermi surfaces and AdS₂*, *Phys. Rev. D* **83** (2011) 125002 [[arXiv:0907.2694](#)] [[INSPIRE](#)].
- [22] E. Gubankova et al., *Holographic fermions in external magnetic fields*, *Phys. Rev. D* **84** (2011) 106003 [[arXiv:1011.4051](#)] [[INSPIRE](#)].
- [23] D.F. Mross, J. McGreevy, H. Liu and T. Senthil, *A controlled expansion for certain non-Fermi liquid metals*, *Phys. Rev. B* **82** (2010) 045121 [[arXiv:1003.0894](#)] [[INSPIRE](#)].
- [24] G. Horowitz, A. Lawrence and E. Silverstein, *Insightful D-branes*, *JHEP* **07** (2009) 057 [[arXiv:0904.3922](#)] [[INSPIRE](#)].
- [25] L.D. Landau and E.M. Lifshitz, *Quantum Mechanics. Nonrelativistic theory*, Nauka, Moskva Russia (1989).
- [26] T. Faulkner, N. Iqbal, H. Liu, J. McGreevy and D. Vegh, *Strange metal transport realized by gauge/gravity duality*, *Science* **329** (2010) 1043 [[INSPIRE](#)].
- [27] T. Hartman and S.A. Hartnoll, *Cooper pairing near charged black holes*, *JHEP* **06** (2010) 005 [[arXiv:1003.1918](#)] [[INSPIRE](#)].
- [28] N. Iqbal and H. Liu, *Real-time response in AdS/CFT with application to spinors*, *Fortsch. Phys.* **57** (2009) 367 [[arXiv:0903.2596](#)] [[INSPIRE](#)].
- [29] L.D. Landau and E.M. Lifshitz, *Statistical Physics 2*, Nauka, Moskva Russia (1978).

- [30] N. Iqbal, H. Liu, M. Mezei and Q. Si, *Quantum phase transitions in holographic models of magnetism and superconductors*, *Phys. Rev. D* **82** (2010) 045002 [[arXiv:1003.0010](#)] [[INSPIRE](#)].
- [31] D. Voskresensky and A. Senatorov, *Rearrangement of the vacuum in strong electric and gravitational fields*, *Sov. J. Nucl. Phys.* **36** (1982) 208 [[INSPIRE](#)].
- [32] J.H. She and J. Zaanen, *BCS Superconductivity in Quantum Critical Metals*, *Phys. Rev. B* **80** (2009) 184518.
- [33] V.G.M. Puletti, S. Nowling, L. Thorlacius and T. Zingg, *Holographic metals at finite temperature*, *JHEP* **01** (2011) 117 [[arXiv:1011.6261](#)] [[INSPIRE](#)].
- [34] T. Faulkner and J. Polchinski, *Semi-holographic Fermi liquids*, *JHEP* **06** (2011) 012 [[arXiv:1001.5049](#)] [[INSPIRE](#)].
- [35] L. Huijse and S. Sachdev, *Fermi surfaces and gauge-gravity duality*, *Phys. Rev. D* **84** (2011) 026001 [[arXiv:1104.5022](#)] [[INSPIRE](#)].
- [36] N. Iqbal, H. Liu and M. Mezei, *Lectures on holographic non-Fermi liquids and quantum phase transitions*, [arXiv:1110.3814](#) [[INSPIRE](#)].
- [37] M. Čubrović, *Holography, Fermi surfaces and criticality*, Ph.D. Thesis, Leiden University, Leiden Netherlands (2013).
- [38] A. Allais and J. McGreevy, *How to construct a gravitating quantum electron star*, *Phys. Rev. D* **88** (2013) 066006 [[arXiv:1306.6075](#)] [[INSPIRE](#)].

Spectral probes of the holographic Fermi ground state: Dialing between the electron star and AdS Dirac hair

Mihailo Čubrović,^{*} Yan Liu,[†] Koenraad Schalm,[‡] Ya-Wen Sun,[§] and Jan Zaanen^{||}

Institute Lorentz for Theoretical Physics, Leiden University, P.O. Box 9506, Leiden 2300RA, The Netherlands

(Received 19 July 2011; published 6 October 2011)

We argue that the electron star and the anti-de Sitter (AdS) Dirac hair solution are two limits of the free charged Fermi gas in AdS. Spectral functions of holographic duals to probe fermions in the background of electron stars have a free parameter that quantifies the number of constituent fermions that make up the charge and energy density characterizing the electron star solution. The strict electron star limit takes this number to be infinite. The Dirac hair solution is the limit where this number is unity. This is evident in the behavior of the distribution of holographically dual Fermi surfaces. As we decrease the number of constituents in a fixed electron star background the number of Fermi surfaces also decreases. An improved holographic Fermi ground state should be a configuration that shares the qualitative properties of both limits.

DOI: [10.1103/PhysRevD.84.086002](https://doi.org/10.1103/PhysRevD.84.086002)

PACS numbers: 11.25.Tq, 04.40.Nr, 71.10.Hf

I. INTRODUCTION

The insight provided by the application of the anti-de Sitter/conformal field theory (AdS/CFT) correspondence to finite density Fermi systems has given brand-new perspectives on the theoretical robustness of non-Fermi liquids [1–3]; on an understanding of the non-perturbative stability of the regular Fermi liquid equivalent to order parameter universality for bosons [4,5]; and most importantly on the notion of fermionic criticality, Fermi systems with no scale. In essence strongly coupled conformally invariant Fermi systems are one answer to the grand theoretical question of fermionic condensed matter: *Are there finite density Fermi systems that do not refer at any stage to an underlying perturbative Fermi gas?*

It is natural to ask to what extent AdS/CFT can provide a more complete answer to this question. Assuming, almost tautologically, that the underlying system is strongly coupled and there is in addition some notion of a large N limit, the Fermi system is dual to classical general relativity with a negative cosmological constant coupled to charged fermions and electromagnetism. As AdS/CFT maps quantum numbers to quantum numbers, finite density configurations of the strongly coupled large N system correspond to solutions of this Einstein-Maxwell-Dirac theory with finite charge density. Since the AdS fermions are the only object carrying charge, and the gravity system is weakly coupled, one is immediately inclined to infer that the generic solution is a weakly coupled charged Fermi gas coupled to AdS gravity: in other words an AdS electron

star [6,7], the charged equivalent of a neutron star in asymptotically anti-de Sitter space [8,9].

Nothing can seem more straightforward. Given the total charge density Q of interest, one constructs the free fermionic wave functions in this system, and fills them one by one in increasing energy until the total charge equals Q . For macroscopic values of Q these fermions themselves will backreact on the geometry. One can compute this backreaction; it changes the potential for the free fermions at subleading order. Correcting the wave functions at this subleading order, one converges on the true solution order by order in the gravitational strength $\kappa^2 E_{\text{full system}}^2$. Here $E_{\text{full system}}$ is the energy carried by the Fermi system and κ^2 is the gravitational coupling constant $\kappa^2 = 8\pi G_{\text{Newton}}$ in the AdS gravity system. Perturbation theory in κ is dual to the $1/N$ expansion in the associated condensed matter system.

The starting point of the backreaction computation is to follow Tolman-Oppenheimer-Volkov (TOV) and use a Thomas-Fermi (TF) approximation for the lowest order one-loop contribution [6–9]. The Thomas-Fermi approximation applies when the number of constituent fermions making up the Fermi gas is infinite. For neutral fermions this equates to the statement that the energy-spacing between the levels is negligible compared to the chemical potential associated with Q , $\Delta E/\mu \rightarrow 0$. For charged fermions the Thomas-Fermi limit is more direct: it is the limit $q/Q \rightarrow 0$, where q is the charge of each constituent fermion.¹

This has been the guiding principle behind the approaches [6–11] and the recent papers [12,13], with the natural assumption that all corrections beyond Thomas-Fermi are small quantitative changes rather than qualitative

^{*}cubrovic@lorentz.leidenuniv.nl

[†]liu@lorentz.leidenuniv.nl

[‡]kschalm@lorentz.leidenuniv.nl

[§]sun@lorentz.leidenuniv.nl

^{||}jan@lorentz.leidenuniv.nl

¹For a fermion in an harmonic oscillator potential $E_n = \hbar(n - 1/2)\omega$, thus $\Delta E/E_{\text{total}} = 1/\sum_1^N (n - 1/2) = 2/N^2$.

ones. On closer inspection, however, this completely natural TF-electron star poses a number of puzzles. The most prominent perhaps arises from the AdS/CFT correspondence finding that every normalizable fermionic wave function in the gravitational bulk corresponds to a fermionic quasiparticle excitation in the dual condensed matter system. In particular occupying a particular wave function is dual to having a particular Fermi-liquid state [4]. In the Thomas-Fermi limit the gravity dual thus describes an infinity of Fermi liquids, whereas the generic condensed matter expectation would have been that a single (few) liquid(s) would be the generic ground state away from the strongly coupled fermionic quantum critical point at zero charge density. This zoo of Fermi surfaces is already present in the grand canonical approaches at fixed μ (extremal AdS-Reissner-Nordström [AdS-RN] black holes) [3] and a natural explanation would be that this is a large N effect. This idea, that the gravity theory is dual to a condensed matter system with N species of fermions, and increasing the charge density “populates” more and more of the distinct species of Fermi liquids, is very surprising from the condensed matter perspective. Away from criticality one would expect the generic ground state to be a single Fermi liquid or some broken state due to pairing. To pose the puzzle sharply, once one has a fermionic quasiparticle one should be able to adiabatically continue it to a free Fermi gas, which would imply that the free limit of the strongly coupled fermionic CFT is not a single but a system of order N fermions with an ordered distribution of Fermi momenta. A possible explanation of the multitude of Fermi surfaces that is consistent with a single Fermi surface at weak coupling is that AdS/CFT describes so-called “deconfined and/or fractionalized Fermi liquids” where the number of Fermi surfaces is directly tied to the coupling strength [12–16]. It would argue that fermionic quantum criticality goes hand in hand with fractionalization for which there is currently scant experimental evidence.

The second puzzle is more technical. Since quantum numbers in the gravity system equal the quantum numbers in the dual condensed matter system, one is inclined to infer that each subsequent AdS fermion wave function has incrementally higher energy than the previous one. Yet analyticity of the Dirac equation implies that all normalizable wave functions must have strictly vanishing energy [17]. It poses the question how the order in which the fermions populate the Fermi gas is determined.

The third puzzle is that in the Thomas-Fermi limit the Fermi gas is gravitationally strictly confined to a bounded region; famously, the TOV-neutron star has an edge. In AdS/CFT, however, all information about the dual condensed matter system is read off at asymptotic AdS infinity. Qualitatively, one can think of AdS/CFT as an “experiment” analogous to probing a spatially confined Fermi gas with a tunneling microscope held to the exterior

of the trap. Extracting the information of the dual condensed matter system is probing the AdS Dirac system confined by a gravitoelectric trap instead of a magneto-optical trap for cold atoms. Although the Thomas-Fermi limit should reliably capture the charge and energy densities in the system, its abrupt nonanalytic change at the edge (in a trapped system) and effective absence of a density far away from the center are well known to cause qualitative deficiencies in the description of the system. Specifically Friedel oscillations—quantum interference in the outside tails of the charged fermion density, controlled by the ratio q/Q and measured by a tunneling microscope—are absent. Analogously, there could be qualitative features in the AdS asymptotics of both the gravitoelectric background and the Dirac wave functions in that adjusted background that are missed by the TF approximation. The AdS asymptotics in turn *specify* the physics of the dual condensed matter system and since our main interest is to use AdS/CFT to understand quantum critical fermion systems where q/Q is finite, the possibility of a qualitative change inherent in the Thomas-Fermi limit should be considered.

There is another candidate AdS description of the dual of a strongly coupled finite density Fermi system: the AdS black hole with Dirac hair [4,5]. One arrives at this solution when one starts one’s reasoning from the dual condensed matter system, rather than the Dirac fields in AdS gravity. Insisting that the system collapses to a generic single species Fermi-liquid ground state, the dual gravity description is that of an AdS Einstein-Dirac-Maxwell system with a single nonzero normalizable Dirac wave function. To have a macroscopic backreaction the charge of this single Dirac field must be macroscopic. The intuitive way to view this solution is as the other simplest approximation to free Fermi gas coupled to gravity. What we mean is that the full gravitoelectric response is in all cases controlled by the total charge Q of the solution: as charge is conserved it is proportional to the constituent charge q times the number of fermions $n_{F_{\text{AdS}}}$ and the two simple limits correspond to $n_F \rightarrow \infty$, $q \rightarrow 0$ with $Q = qn_F$ fixed or $n_F \rightarrow 1$, $q \rightarrow Q$. The former is the Thomas-Fermi electron star, the latter is the AdS Dirac hair solution. In the context of AdS/CFT there is a significant difference between the two solutions in that the Dirac hair solution clearly does not give rise to the puzzles 1, 2 and 3: there is by construction no zoo of Fermi surfaces and therefore no ordering. Moreover since the wave function is demanded to be normalizable, it manifestly encodes the properties of the system at the AdS boundary. On the other hand the AdS Dirac hair solution does pose the puzzle that under normal conditions the total charge Q is much larger than the constituent charge q both from the gravity/string theory point of view and the condensed matter perspective. Generically one would expect a Fermi gas electron star rather than Dirac hair.

In this paper we shall provide evidence for this point of view that the AdS electron star and the AdS Dirac hair solution are two limits of the same underlying system. Specifically we shall show that (1) the electron star solution indeed has the constituent charge as a free parameter which is formally sent to zero to obtain the Thomas-Fermi approximation. (2) The number of normalizable wave functions in the electron star depend on the value of the constituent charge q . We show this by computing the electron star spectral functions. They depend in similar way on q as the first AdS/CFT Fermi system studies in an AdS-RN background. In the formal limit where $q \rightarrow Q$, only one normalizable mode remains and the spectral function wave function resembles the Dirac hair solution, underlining their underlying equivalence. Since both approximations have qualitative differences as a description of the AdS dual to strongly coupled fermionic systems, we argue that an improved approximation that has characteristics of both is called for.

The results here are complimentary to and share an analysis of electron star spectral functions with the two recent papers [12,13] that appeared in the course of this work (see also [18] for fermion spectral functions in general Lifshitz backgrounds). Our motivation to probe the system away from the direct electron star limit differs: we have therefore been more precise in defining this limit and in the analysis of the Dirac equation in the electron star background.

II. EINSTEIN-MAXWELL THEORY COUPLED TO CHARGED FERMIONS

The Lagrangian that describes both the electron star and Dirac hair approximation is Einstein-Maxwell theory coupled to charged matter

$$S = \int d^4x \sqrt{-g} \left[\frac{1}{2\kappa^2} \left(R + \frac{6}{L^2} \right) - \frac{1}{4q^2} F^2 + \mathcal{L}_{\text{matter}}(e_\mu^A, A_\mu) \right], \quad (2.1)$$

where L is the AdS radius, q is the electric charge, and κ is the gravitational coupling constant. It is useful to scale the electromagnetic interaction to be of the same order as the gravitational interaction and measure all lengths in terms of the AdS radius L ,

$$g_{\mu\nu} \rightarrow L^2 g_{\mu\nu}, \quad A_\mu \rightarrow \frac{qL}{\kappa} A_\mu. \quad (2.2)$$

The system then becomes

$$S = \int d^4x \sqrt{-g} \left[\frac{L^2}{2\kappa^2} \left(R + 6 - \frac{1}{2} F^2 \right) + L^4 \mathcal{L}_{\text{matter}} \left(L e_\mu^A, \frac{qL}{\kappa} A_\mu \right) \right]. \quad (2.3)$$

Note that in the rescaled variables the effective charge of charged matter now depends on the ratio of the electromagnetic to gravitational coupling constant, $q_{\text{eff}} = qL/\kappa$. For the case of interest, charged fermions, the Lagrangian in these variables is

$$L^4 \mathcal{L}_{\text{fermions}} \left(L e_\mu^A, \frac{qL}{\kappa} A_\mu \right) = -\frac{L^2}{\kappa^2} \bar{\Psi} \left[e_A^\mu \Gamma^A \left(\partial_\mu + \frac{1}{4} \omega_\mu^{BC} \Gamma_{BC} - i \frac{qL}{\kappa} A_\mu \right) - m L \right] \Psi, \quad (2.4)$$

where $\bar{\Psi}$ is defined as $\bar{\Psi} = i\Psi^\dagger \Gamma^0$. Compared to the conventional normalization the Dirac field has been made dimensionless $\Psi = \kappa\sqrt{L} \psi_{\text{conventional}}$. With this normalization all terms in the action have a factor L^2/κ^2 and it will therefore scale out of the equations of motion

$$R_{\mu\nu} - \frac{1}{2} g_{\mu\nu} R - 3g_{\mu\nu} = \left(F_{\mu\rho} F_\nu{}^\rho - \frac{1}{4} g_{\mu\nu} F_{\rho\sigma} F^{\rho\sigma} + T_{\mu\nu}^{\text{fermions}} \right), \\ D_\mu F^{\mu\nu} = -q_{\text{eff}} J_{\text{fermions}}^\nu \quad (2.5)$$

with

$$T_{\mu\nu}^{\text{fermions}} = \frac{1}{2} \bar{\Psi} e_{A(\mu} \Gamma^A \left[\partial_{\nu)} + \frac{1}{4} \omega_{\nu)}^{BC} \Gamma_{BC} - i \frac{qL}{\kappa} A_{\nu)} \right] \Psi - \frac{\kappa^2 L^2}{2} g_{\mu\nu} \mathcal{L}_{\text{fermions}}, \quad (2.6)$$

$$J_{\text{fermions}}^\nu = i \bar{\Psi} e_A^\nu \Gamma^A \Psi, \quad (2.7)$$

where the symmetrization is defined as $B_{(\mu} C_{\nu)} = B_\mu C_\nu + B_\nu C_\mu$ and the Dirac equation

$$\left[e_A^\mu \Gamma^A \left(\partial_\mu + \frac{1}{4} \omega_\mu^{BC} \Gamma_{BC} - i \frac{qL}{\kappa} A_\mu \right) - m L \right] \Psi = 0. \quad (2.8)$$

The stress-tensor and current are to be evaluated in the specific state of the system. For a single excited wave function, obeying (2.8), this gives the AdS Dirac hair solution constructed in [4]. (More specifically, the Dirac hair solution consists of a radially isotropic set of wave functions with identical momentum size $|\vec{k}| = \sqrt{k_x^2 + k_y^2}$, such that the Pauli principle plays no role.) For multiple occupied fermion states, even without backreaction due to gravity, adding the contributions of each separate solution to (2.8) rapidly becomes very involved. In such a many-body system, the collective effect of the multiple occupied fermion states is better captured in a ‘‘fluid’’ approximation

$$T_{\mu\nu}^{\text{fluid}} = (\rho + p) u_\mu u_\nu + p g_{\mu\nu}, \quad N_\mu^{\text{fluid}} = n u_\mu \quad (2.9)$$

with

$$\rho = \langle u^\mu T_{\mu\nu} u^\nu \rangle_{\text{matter only}}, \quad n = -\langle u_\mu J^\mu \rangle_{\text{matter only}}. \quad (2.10)$$

In the center-of-mass rest frame of the multiple fermion system [$u_\mu = (e_{t_0}, 0, 0, 0)$], the expressions for the stress-tensor and charge density are given by the one-loop equal-time expectation values (as opposed to time-ordered correlation functions)

$$\rho = \left\langle \bar{\Psi}(t) e_0^t \Gamma^0 \left(\partial_t + \frac{1}{4} \omega_t^{AB} \Gamma_{AB} - i q_{\text{eff}} A_t \right) \Psi(t) \right\rangle. \quad (2.11)$$

By the optical theorem the expectation value is equal to twice the imaginary part of the Feynman propagator²

$$\begin{aligned} \rho(r) &= \lim_{\beta \rightarrow \infty} 2 \int \frac{d^3 k d\omega}{(2\pi)^4} [\omega(r) - \mu_{\text{loc}}(r)] \text{Im Tr} i \Gamma^0 G_F^\beta(\omega, k) \\ &= \lim_{\beta \rightarrow \infty} \int \frac{dk d\omega}{4\pi^3} [k^2(\omega - \mu)] \left[\frac{1}{2} - \frac{1}{2} \tanh\left(\frac{\beta}{2}(\omega - \mu)\right) \right] \text{Tr}(i \Gamma^0)^2 \frac{\kappa^2}{L^2} \pi \delta((\omega - \mu) - \sqrt{k^2 + (mL)^2}) \\ &= \lim_{\beta \rightarrow \infty} \frac{\kappa^2}{\pi^2 L^2} \int d\omega f_{FD}(\beta(\omega - \mu)) [(\omega - \mu)^2 - (mL)^2] [\omega - \mu] \frac{(\omega - \mu) \theta(\omega - \mu - mL)}{\sqrt{(\omega - \mu)^2 - (mL)^2}} \\ &= \frac{1}{\pi^2} \frac{\kappa^2}{L^2} \int_{mL}^{\mu_{\text{loc}}} dE E^2 \sqrt{E^2 - (mL)^2}. \end{aligned} \quad (2.13)$$

The normalization κ^2/L^2 follows from the unconventional normalization of the Dirac field in Eq. (2.4).⁴ Similarly

$$\begin{aligned} n &= \frac{1}{\pi^2} \frac{\kappa^2}{L^2} \int_{mL}^{\mu_{\text{loc}}} dE E \sqrt{E^2 - (mL)^2} \\ &= \frac{1}{3\pi^2} \frac{\kappa^2}{L^2} (\mu_{\text{loc}}^2 - (mL)^2)^{3/2}. \end{aligned} \quad (2.14)$$

The adiabatic approximation is valid for highly localized wave functions, i.e. the expression must be dominated by high momenta (especially in the radial direction). The exact expression on the other hand will not have a

²From unitarity for the S matrix $S^\dagger S = 1$ one obtains the optical theorem $T^\dagger T = 2 \text{Im} T$ for the transition matrix T defined as $S \equiv 1 + iT$.

³That is, one can redefine spinors $\chi(r) = f(r)\Psi(r)$ such that the connection term is no longer present in the equation of motion.

⁴One can see this readily by converting the dimensionless definition of ρ , Eq. (2.11), to the standard dimension. Using capitals for dimensionless quantities and lower-case for dimensional ones,

$$\begin{aligned} \rho &\sim \langle \Psi \partial_T \Psi \rangle \sim \kappa^2 L^2 \langle \psi \partial_t \psi \rangle \\ &\sim \kappa^2 L^2 \int_m^\mu d\epsilon \epsilon^2 \sqrt{\epsilon^2 - m^2} \\ &\sim \frac{\kappa^2}{L^2} \int_{mL}^{\mu L} dE E^2 \sqrt{E^2 - (mL)^2} \end{aligned}$$

with $\mu L = \mu_{\text{loc}}$ above.

$$\rho = \lim_{t \rightarrow t'} 2 \text{Im Tr} \left[e_0^t \Gamma^0 \left(\partial_t + \frac{1}{4} \omega_t^{AB} \Gamma_{AB} - i q_{\text{eff}} A_t \right) G_F^{\text{AdS}}(t', t) \right]. \quad (2.12)$$

In all situations of interest, all background fields will only have dependence on the radial AdS direction; in that case the spin connection can be absorbed in the normalization of the spinor wave function.³ In an adiabatic approximation for the radial dependence of e_{t_0} and A_t —where $\mu_{\text{loc}}(r) = q_{\text{eff}} e_0^t(r) A_t(r)$ and $\omega(r) = -i e_0^t(r) \partial_t$;—this yields the known expression for a many-body fermion system at finite chemical potential,

continuum of solutions to the harmonic condition $-\Gamma^0 \omega + \Gamma^i k_i + \Gamma^z k_z - \Gamma^0 \mu_{\text{loc}} - imL = 0$. Normalizable solutions to the AdS Dirac equations only occur at discrete momenta—one can think of the gravitational background as a potential well. The adiabatic approximation is therefore equivalent to the Thomas-Fermi approximation for a Fermi gas in a box.

To get an estimate for the parameter range where the adiabatic approximation holds, consider the adiabatic bound $\partial_r \mu_{\text{loc}}(r) \ll \mu_{\text{loc}}(r)^2$. Using the field equation for $A_0 = \mu_{\text{loc}}/q_{\text{eff}}$,

$$\partial_r^2 \mu_{\text{loc}} \sim q_{\text{eff}}^2 n, \quad (2.15)$$

this bound is equivalent to requiring

$$\begin{aligned} \partial_r^2 \mu_{\text{loc}} \ll \partial_r \mu_{\text{loc}}^2 &\Rightarrow \left(\frac{qL}{\kappa} \right)^2 n \ll 2 \mu_{\text{loc}} \partial_r \mu_{\text{loc}} \\ &\Rightarrow \left(\frac{qL}{\kappa} \right)^2 n \ll \mu_{\text{loc}}^3, \end{aligned} \quad (2.16)$$

where in the last line we used the original bound again. If the chemical potential scale is considerably higher than the mass of the fermion, we may use (2.14) to approximate $n \sim \frac{\kappa^2}{L^2} \mu_{\text{loc}}^3$. Thus the adiabatic bound is equivalent to

$$q = \frac{q_{\text{eff}} \kappa}{L} \ll 1, \quad (2.17)$$

the statement that the constituent charge of the fermions is infinitesimal. Note that in the rescaled action (2.3) and (2.4), L/κ plays the role of $1/\hbar$, and Eq. (2.17) is thus equivalent to the semiclassical limit $\hbar \rightarrow 0$ with q_{eff} fixed. Since AdS/CFT relates $L/\kappa \sim N_c$ this acquires the meaning in the context of holography that there is a large N_c scaling limit [12,13] of the CFT with fermionic operators where the renormalization group (RG) flow is ‘‘adiabatic.’’ Returning to the gravitational description the additional assumption that the chemical potential is much larger than the mass is equivalent to

$$\begin{aligned} \frac{Q_{\text{phys}}^{\text{total}}}{V_{\text{spatial AdS}}} &= \frac{LQ_{\text{eff}}^{\text{total}}}{\kappa V_{\text{spatial AdS}}} \\ &\equiv \frac{L}{\kappa V_{\text{spatial AdS}}} \int dr \sqrt{-g_{\text{induced}}}(q_{\text{eff}} n) \\ &\simeq \frac{1}{V_{\text{spatial AdS}}} \int dr \sqrt{-g} \frac{q_{\text{eff}} \kappa}{L} \mu_{\text{loc}}^3(r) \gg q(mL)^3. \end{aligned} \quad (2.18)$$

This implies that the total charge density in AdS is much larger than that of a single charged particle (as long as $mL \sim 1$). The adiabatic limit is therefore equivalent to a thermodynamic limit where the Fermi gas consists of an infinite number of constituents, $n \rightarrow \infty$, $q \rightarrow 0$ such that the total charge $Q \sim nq$ remains finite.

The adiabatic limit of a many-body fermion system coupled to gravity are the Tolman-Oppenheimer-Volkov equations. Solving this in asymptotically AdS gives us the charged neutron or electron star constructed in [7]. Knowing the quantitative form of the adiabatic limit, it is now easy to distinguish the electron star solution from the ‘‘single wave function’’ Dirac hair solution. The latter is trivially the single particle limit $n \rightarrow 1$, $q \rightarrow Q$ with the total charge Q finite. The electron star and Dirac hair black hole are opposing limit-solutions of the same system. We shall now make this connection more visible by identifying a formal dialing parameter that interpolates between the two solutions.

To do so we shall need the full adiabatic Tolman-Oppenheimer-Volkov equations for the AdS electron star [7]. Since the fluid is homogeneous and isotropic, the background metric and electrostatic potential will respect these symmetries and will be of the form [recall that we are already using ‘‘dimensionless’’ lengths, Eq. (2.2)]

$$\begin{aligned} ds^2 &= -f(r)dt^2 + g(r)dr^2 + r^2(dx^2 + dy^2), \\ A &= h(r)dt, \end{aligned} \quad (2.19)$$

where $f(r)$, $g(r)$, $h(r)$ are functions of r ; the horizon is located at $r = 0$ and the boundary is at $r = \infty$. Combining this ansatz with a rescaling $mL = q_{\text{eff}} \hat{m}$ the bosonic background equations of motion become [7]

$$\begin{aligned} \frac{1}{r} \left(\frac{f'}{f} + \frac{g'}{g} \right) - \frac{gh\sigma}{\sqrt{f}} &= 0, \\ \rho &= \frac{q_{\text{eff}}^4 \kappa^2}{\pi^2 L^2} \int_{\hat{m}}^{h/\sqrt{f}} d\epsilon \epsilon^2 \sqrt{\epsilon^2 - \hat{m}^2}, \\ \frac{f'}{rf} + \frac{h^2}{2f} - g(3+p) + \frac{1}{r^2} &= 0, \\ \sigma &= \frac{q_{\text{eff}}^4 \kappa^2}{\pi^2 L^2} \int_{\hat{m}}^{h/\sqrt{f}} d\epsilon \epsilon \sqrt{\epsilon^2 - \hat{m}^2}, \\ h'' + \frac{2}{r} h' - \frac{g\sigma}{\sqrt{f}} \left(\frac{rhh'}{2} + f \right) &= 0, \quad -p = \rho - \frac{h}{\sqrt{f}} \sigma, \end{aligned} \quad (2.20)$$

where we have used that $\mu_{\text{loc}} = q_{\text{eff}} h/\sqrt{f}$ and $\sigma = nq_{\text{eff}}$ is the rescaled local charge density. What one immediately notes is that the Tolman-Oppenheimer-Volkov equations of motion for the background only depend on the parameters $\hat{\beta} \equiv \frac{q_{\text{eff}}^4 \kappa^2}{\pi^2 L^2}$ and \hat{m} , whereas the original Lagrangian and the fermion equation of motion also depend on $q_{\text{eff}} = (\frac{\pi^2 L^2 \hat{\beta}}{\kappa^2})^{1/4}$. It is therefore natural to guess that the parameter $q_{\text{eff}} = qL/\kappa$ will be the interpolating parameter away from the adiabatic electron star limit toward the Dirac hair black hole (BH).

Indeed in these natural electron star variables the adiabatic bound (2.17) translates into

$$\hat{\beta} \ll \frac{L^2}{\kappa^2} = \frac{q_{\text{eff}}^2}{q^2}. \quad (2.21)$$

Thus we see that for a given electron star background with $\hat{\beta}$ fixed decreasing κ/L improves the adiabatic fluid approximation whereas increasing κ/L makes the adiabatic approximation poorer and poorer. ‘‘Dialing κ/L up/down’’ therefore *interpolates* between the electron star and the Dirac hair BH. Counterintuitively improving adiabaticity by decreasing κ/L corresponds to increasing q_{eff} for fixed q , but this is just a consequence of recasting the system in natural electron star variables. A better way to view improving adiabaticity is to decrease the microscopic charge q but while keeping q_{eff} fixed; this shows that a better way to think of q_{eff} is as the total charge rather than the effective constituent charge.

The parameter $\kappa/L = q/q_{\text{eff}}$ parametrizes the gravitational coupling strength in units of the AdS curvature, and one might worry that ‘‘dialing κ/L up’’ pushes one outside the regime of classical gravity. This is not the case. One can easily have $\hat{\beta} \gg 1$ and tune κ/L toward or away from the adiabatic limit within the regime of classical gravity. From Eq. (2.17) we see that the edge of validity of the adiabatic regime $\hat{\beta} \simeq L^2/\kappa^2$ is simply equivalent to a microscopic charge $q = 1$ which clearly has a classical gravity description. It is not hard to see that the statement above is the equivalent of changing the level splitting in the Fermi gas, while keeping the overall energy/charge fixed. In a Fermi

gas microscopically both the overall energy and the level splitting depends on \hbar . Naively increasing \hbar increases both, but one can move away from the adiabatic limit either by decreasing the overall charge density, keeping \hbar fixed, or by keeping the charge density fixed and raising \hbar . Using again the analogy between κ/L and \hbar , the electron star situation is qualitatively the same, where one should think of $\hat{\beta} \sim q^4 L^2 / \kappa^2$ parametrizing the microscopic charge. One can either insist on keeping κ/L fixed and *increase* the microscopic charge $\hat{\beta}$ to increase the level splitting or one can keep $\hat{\beta}$ fixed and increase κ/L . In the electron star, however, the background geometry changes with $\hat{\beta}$ in addition to the level splitting, and it is therefore more straightforward to keep $\hat{\beta}$ and the geometry fixed, while dialing κ/L .

We will now give evidence for our claim that the electron star and Dirac hair solution are two opposing limits. To do so, we need to identify an observable that goes either beyond the adiabatic background approximation or beyond the single particle approximation. Since the generic intermediate state is still a many-body fermion system, the more natural starting point is the electron star background and to perturb away from there. Realizing then that the fermion equation of motion already depends directly on the dialing parameter q_{eff} the obvious observables are the single fermion spectral functions in the electron star background. Since one must specify a value for q_{eff} to compute these, they directly probe the microscopic charge of the fermion and are thus always beyond the strict electron star limit $q \rightarrow 0$. In the next two sections we will compute these and show that they indeed reflect the interpretation of q_{eff} as the interpolating parameter between the electron star and Dirac hair BH.

III. FERMION SPECTRAL FUNCTIONS IN THE ELECTRON STAR BACKGROUND

To compute the fermion spectral functions in the electron star background we shall choose a specific representative of the family of electron stars parametrized by $\hat{\beta}$ and \hat{m} . Rather than using $\hat{\beta}$ and \hat{m} the metric of an electron star is more conveniently characterized by its Lifshitz-scaling behavior near the interior horizon $r \rightarrow 0$. From the field equations (2.20) the limiting interior behavior of $f(r)$, $g(r)$, $h(r)$ is

$$f(r) = r^{2z} + \dots, \quad g(r) = \frac{g_\infty}{r^2} + \dots, \quad h(r) = h_\infty r^z + \dots \quad (3.1)$$

The scaling behavior is determined by the dynamical critical exponent z , which is a function of $\hat{\beta}$, \hat{m} [7] and it is conventionally used to classify the metric instead of $\hat{\beta}$. The full electron star metric is then generated from this horizon scaling behavior by integrating up an irrelevant RG-flow [19,20]

$$\begin{aligned} f &= r^{2z}(1 + f_1 r^{-\alpha} + \dots), \\ g &= \frac{g_\infty}{r^2}(1 + g_1 r^{-\alpha} + \dots), \\ h &= h_\infty r^z(1 + h_1 r^{-\alpha} + \dots) \end{aligned} \quad (3.2)$$

with

$$\alpha = \frac{2+z}{2} - \frac{\sqrt{9z^3 - 21z^2 + 40z - 28 - \hat{m}^2 z(4-3z)^2}}{2\sqrt{(1-\hat{m}^2)z-1}}. \quad (3.3)$$

Scaling $f_1 \rightarrow b f_1$ is equal to a coordinate transformation $r \rightarrow b^{1/\alpha} r$ and $t \rightarrow b^{z/\alpha} t$, and the sign of f_1 is fixed to be negative in order to be able to match onto an asymptotically AdS₄ solution. Thus $f_1 = -1$ and g_1 and h_1 are then uniquely determined by the equations of motion.

Famously, integrating the equations of motion up the RG-flow outward toward the boundary fails at a finite distance r_s . This is the edge of the electron star. Beyond the edge of the electron star, there is no fluid present and the spacetime is that of an AdS₄-RN black hole with the metric

$$f = c^2 r^2 - \frac{\hat{M}}{r} + \frac{\hat{Q}^2}{2r^2}, \quad g = \frac{c^2}{f}, \quad h = \hat{\mu} - \frac{\hat{Q}}{r}. \quad (3.4)$$

Demanding the full metric is smooth at the radius of electron star r_s determines the constants c , \hat{M} , and \hat{Q} . The dual field theory is defined on the plane $ds^2 = -c^2 dt^2 + dx^2 + dy^2$.

The specific electron star background we shall choose without loss of generality is the one with $z = 2$, $\hat{m} = 0.36$ (Fig. 1),⁵ smoothly matched at $r_s \simeq 4.25252$ onto an AdS-RN black hole.

The CFT fermion spectral functions now follow from solving the Dirac equation in this background [1,2]

$$\left[e_A^\mu \Gamma^A \left(\partial_\mu + \frac{1}{4} \omega_{\mu AB} \Gamma^{AB} - i q_{\text{eff}} A_\mu \right) - m_{\text{eff}} \right] \Psi = 0, \quad (3.5)$$

where q_{eff} and m_{eff} in terms of the parameters of the electron star equal

$$\begin{aligned} q_{\text{eff}} &= \left(\frac{\pi^2 L^2 \hat{\beta}}{\kappa^2} \right)^{1/4}, \\ m_{\text{eff}} &= q_{\text{eff}} \hat{m} = \hat{m} \left(\frac{\pi^2 L^2 \hat{\beta}}{\kappa^2} \right)^{1/4}. \end{aligned} \quad (3.6)$$

In other words, we choose the same mass and charge for the probe fermion and the constituent fermions of the electron star.⁶ For a given electron star background, i.e. a

⁵This background has $c \simeq 1.021$, $\hat{M} \simeq 3.601$, $\hat{Q} \simeq 2.534$, $\hat{\mu} \simeq 2.132$, $\hat{\beta} \simeq 19.951$, $g_\infty \simeq 1.887$, $h_\infty = 1/\sqrt{2}$, $\alpha \simeq -1.626$, $f_1 = -1$, $g_1 \simeq -0.4457$, $h_1 \simeq -0.6445$.

⁶One could of course choose a different probe mass and charge, corresponding to an extra charged fermion in the system. However, even though the electron star only cares about the equation of state, this would probably not be a self-consistent story as this extra fermion should also backreact.

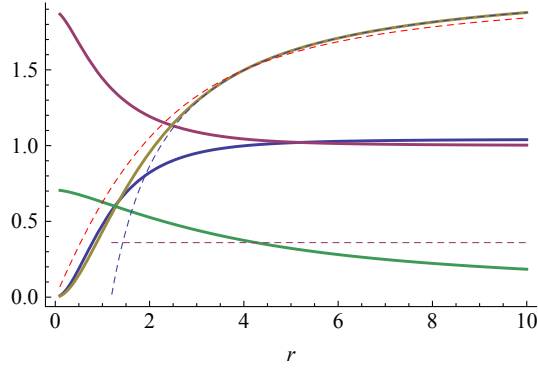


FIG. 1 (color online). Electron star metric for $z = 2$, $\hat{m} = 0.36$, $c \approx 1.021$, $\hat{M} \approx 3.601$, $\hat{Q} \approx 2.534$, $\hat{\mu} \approx 2.132$ compared to pure AdS. Shown are $f(r)/r^2$ (blue), $r^2 g(r)$ (red), and $h(r)$ (orange). The asymptotic AdS-RN value of $h(r)$ is the dashed blue line. For future use we have also given $\mu_{\text{loc}} = h/\sqrt{f}$ (green) and $\mu_{q\text{eff}} = \sqrt{g^{ii}h}/\sqrt{f}$ (red dashed). At the edge of the star $r_s \approx 4.253$ (the intersection of the purple dashed line setting the value of m_{eff} with μ_{loc}) one sees the convergence to pure AdS in the constant asymptotes of $f(r)/r^2$ and $r^2 g(r)$.

fixed $\hat{\beta}$, \hat{m} the fermion spectral function will therefore depend on the ratio L/κ . For $L/\kappa \gg \hat{\beta}^{1/2}$ the poles in these spectral functions characterize the occupied states in a many-body gravitational Fermi system that is well approximated by the electron star. As L/κ is lowered for fixed $\hat{\beta}$ the electron star background becomes a poorer and poorer approximation to the true state and we should see this reflected in both the number of poles in the spectral function and their location.

Projecting the Dirac equation onto two-component Γ^z eigenspinors

$$\Psi_{\pm} = (-g^{rr})^{-(1/4)} e^{-i\omega t + ik_x x^i} \begin{pmatrix} y_{\pm} \\ z_{\pm} \end{pmatrix} \quad (3.7)$$

and using isotropy to set $k_y = 0$, one can choose a basis of Dirac matrices where one obtains two decoupled sets of two simple coupled equations [1]

$$\sqrt{g_{ii}g^{rr}}(\partial_r \mp m_{\text{eff}}\sqrt{g_{rr}})y_{\pm} = \mp i(k_x - u)z_{\pm}, \quad (3.8)$$

$$\sqrt{g_{ii}g^{rr}}(\partial_r \pm m_{\text{eff}}\sqrt{g_{rr}})z_{\pm} = \pm i(k_x + u)y_{\pm}, \quad (3.9)$$

where $u = \sqrt{\frac{g_{ii}}{-g_{tt}}}(\omega + q_{\text{eff}}h)$. In this basis of Dirac matrices the CFT Green's function $G = \langle \bar{\mathcal{O}}_{\psi_+} i\gamma^0 \mathcal{O}_{\psi_+} \rangle$ equals

$$G = \lim_{\epsilon \rightarrow 0} \epsilon^{-2mL} \begin{pmatrix} \xi_+ & 0 \\ 0 & \xi_- \end{pmatrix} \Big|_{r=(1/\epsilon)}, \quad \text{where } \xi_+ = \frac{iy_-}{z_+}, \quad (3.10)$$

$$\xi_- = -\frac{iz_-}{y_+}.$$

Rather than solving the coupled equations (3.8) it is convenient to solve for ξ_{\pm} directly [1],

$$\sqrt{\frac{g_{ii}}{g_{rr}}}\partial_r \xi_{\pm} = -2m_{\text{eff}}\sqrt{g_{ii}}\xi_{\pm} \mp (k_x \mp u) \pm (k_x \pm u)\xi_{\pm}^2. \quad (3.11)$$

For the spectral function $A = \text{Im Tr}G_R$ we are interested in the retarded Green's function. This is obtained by imposing infalling boundary conditions near the horizon $r = 0$. Since the electron star is a ‘‘zero-temperature’’ solution this requires a more careful analysis than for a generic horizon. To ensure that the numerical integration we shall perform to obtain the full spectral function has the right infalling boundary conditions, we first solve Eq. (3.11) to first subleading order around $r = 0$. There are two distinct branches. When $\omega \neq 0$ and $k_x r/\omega$, r^2/ω is small, the infalling boundary condition near the horizon $r = 0$ is (for $z = 2$)

$$\xi_+(r) = i - i\frac{k_x r}{\omega} + i\frac{(k_x^2 - 2im_{\text{eff}}\omega)r^2}{2\omega^2} - i\frac{f_1 k_x r^{1-\alpha}}{2\omega} + \dots$$

$$\xi_-(r) = i + i\frac{k_x r}{\omega} + i\frac{(k_x^2 - 2im_{\text{eff}}\omega)r^2}{2\omega^2} + i\frac{f_1 k_x r^{1-\alpha}}{2\omega} + \dots \quad (3.12)$$

When $\omega = 0$, i.e. $k_x r/\omega$ is large, and $r/k_x \rightarrow 0$,

$$\xi_+(r) = -1 + \frac{(q_{\text{eff}}h_{\infty} + m_{\text{eff}})r}{k_x} + \left(\frac{\omega}{k_x r} - \frac{\omega}{2\sqrt{g_{\infty}k_x^2}}\right) + \dots$$

$$\xi_-(r) = 1 + \frac{(q_{\text{eff}}h_{\infty} - m_{\text{eff}})r}{k_x} + \left(\frac{\omega}{k_x r} - \frac{\omega}{2\sqrt{g_{\infty}k_x^2}}\right) + \dots, \quad (3.13)$$

the boundary conditions (3.13) become real. As (3.11) are real equations, the spectral function vanishes in this case. This is essentially the statement that all poles in the Green's function occur at $\omega = 0$ [17]. The fact that the electron star $\omega = 0$ boundary conditions (3.11) are real ensures that there is no ‘‘oscillatory region’’ for k less than some critical value $k < k_o$ in the spectral function as is the case for pure AdS-RN [1,3,21,22]. We discuss this in detail in the Appendix.

Numerical results and discussion

We can now solve for the spectral functions numerically. In Fig. 2 we plot the momentum distribution function (MDF) (the spectral function as a function of k) for fixed $\omega = 10^{-5}$, $z = 2$, $\hat{m} = 0.36$ while changing the value of κ . Before we comment on the dependence on $q_{\text{eff}} \sim \kappa^{-1/2}$ which studies the deviation away from the adiabatic limit of a given electron star background (i.e. fixed dimensionless charge and fixed dimensionless energy density), there are several striking features that are immediately apparent:

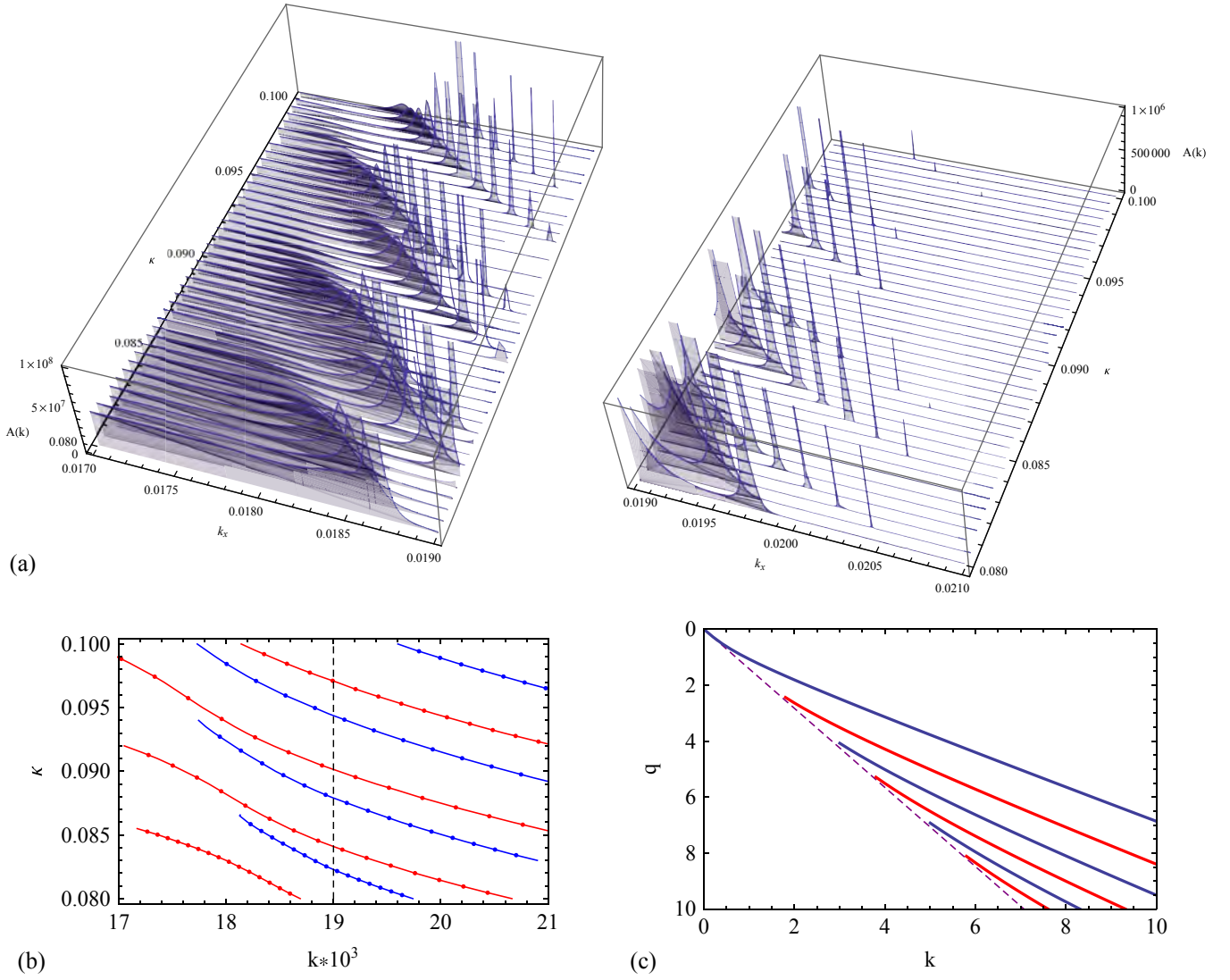


FIG. 2 (color online). (a) Electron star MDF spectral functions as a function of κ for $z = 2$, $\hat{m} = 0.36$, $\omega = 10^{-5}$. Because the peak height and weights decrease exponentially, we present the adjacent ranges $k \in [0.017, 0.019]$ and $k \in [0.019, 0.021]$ in two different plots with different vertical scale. (b, c) Locations of peaks of spectral functions as a function of κ : comparison between the electron star (b) for $z = 2$, $\hat{m} = 0.36$, $\omega = 10^{-5}$ [the dashed gray line denotes the artificial separation in the three-dimensional representations in (a)] and AdS-RN (c) for $m = 0$ as a function of q in units where $\mu = \sqrt{3}$. These two Fermi-surface “spectra” are qualitatively similar.

(i) As expected, there is a multitude of Fermi surfaces. They have very narrow width and their spectral weight decreases rapidly for each higher Fermi momentum k_F (Fig. 3). This agrees with the exponential width $\Gamma \sim \exp(-(\frac{k_F}{\omega})^{1/(\zeta-1)})$ predicted by [23] for gravitational backgrounds that are Lifshitz in the deep interior, which is the case for the electron star. This prediction is confirmed in [12,13,18] and the latter two papers also show that the weight decreases in a corresponding exponential fashion. This exponential reduction of both the width and the weight as k_F increases explains why we only see a finite number of peaks, though we expect a very large number. In the next section we will be able to

count the number of peaks, even though we cannot resolve them all numerically.

(ii) The generic value of k_F of the peaks with visible spectral weight is *much* smaller than the effective chemical potential μ in the boundary field theory. This is quite different from the AdS-RN case where the Fermi momentum and chemical potential are of the same order. A numerical study cannot answer this, but the recent paper [13] explains this.⁷

(iii) Consistent with the boundary value analysis, there is no evidence of an oscillatory region.

⁷In view of the verification of the Luttinger count for electron star spectra in [12,13], this had to be so.

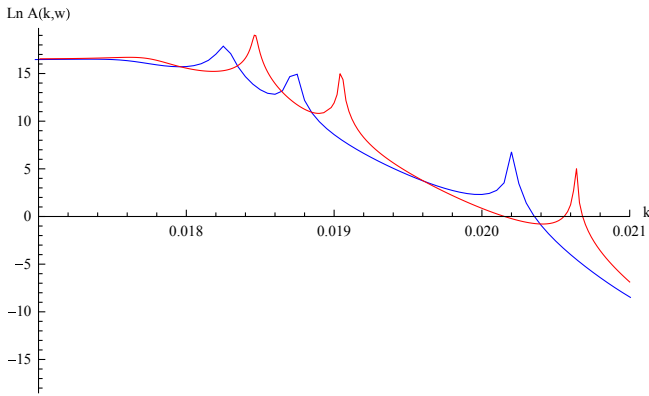


FIG. 3 (color online). Electron star MDF spectral functions with multiple peaks as a function of k for $\omega = 10^{-5}$, $z = 2$, $\hat{m} = 0.36$. The blue curve is for $\kappa = 0.091$; the red curve is for $\kappa = 0.090$. Note that the vertical axis is logarithmic. Visible is the rapidly decreasing spectral weight and increasingly narrower width for each successive peak as k_F increases.

The most relevant property of the spectral functions for our question is that as κ is increased the peak location k_F decreases orderly and peaks *disappear* at various threshold values of k . This is the support for our argument that changing κ changes the number of microscopic constituents in the electron star. Comparing the behavior of the various Fermi momenta k_F in the electron star with the results in the extremal AdS-RN black hole, they are qualitatively identical when one equates $\kappa^{-1/2} \sim q_{\text{eff}}$ with the charge of the probe fermion. We may therefore infer from our detailed understanding of the behavior of k_F for AdS-RN that also for the electron star as k_F is lowered peaks truly disappear from the spectrum until by extrapolation ultimately one remains: this is the AdS Dirac hair solution [4].

We can only make this inference qualitatively as the rapid decrease in spectral weight of each successive peak prevents an exact counting of Fermi surfaces in the numerical results for the electron star spectral functions. One aspect that we can already see is that as κ decreases all present peaks shift to higher k , while new peaks emerge from the left for smaller kappa. This suggests a fermionic version of the UV/IR correspondence, where the peak with *lowest* k_F corresponds to the last occupied level, i.e. highest “energy” in the AdS electron star. We will now address both of these points in more detail.

IV. FERMI SURFACE ORDERING: k_F FROM A SCHRÖDINGER FORMULATION

Our analysis of the behavior of boundary spectral functions as a function of κ relies on the numerically quite evident peaks. Strictly speaking, however, we have not shown that there is a true singularity in the Green’s function at $\omega = 0$, $k = k_F$. We will do so by showing that the

AdS Dirac equation, when recast as a Schrödinger problem, has quasinormalizable solutions at $\omega = 0$ for various k . As is well known, in AdS/CFT each such solution corresponds to a true pole in the boundary Green’s function. Using a WKB approximation for this Schrödinger problem we will in addition be able to estimate the number of poles for a fixed κ and thereby provide a quantitative value for the deviation from the adiabatic background.

We wish to emphasize that the analysis here is general and captures the behavior of spectral functions in all spherically symmetric and static backgrounds alike, whether AdS-RN, Dirac hair, or electron star.

The $\omega = 0$ Dirac equation (3.5) for one set of components (3.8) and (3.9) with the replacement $iy_- \rightarrow y_-$, equals

$$\begin{aligned} \sqrt{g_{ii}g^{rr}}\partial_r y_- + m_{\text{eff}}\sqrt{g_{ii}}y_- &= -(k - \hat{\mu}_{q_{\text{eff}}})z_+, \\ \sqrt{g_{ii}g^{rr}}\partial_r z_+ - m_{\text{eff}}\sqrt{g_{ii}}z_+ &= -(k + \hat{\mu}_{q_{\text{eff}}})y_-, \end{aligned} \quad (4.1)$$

where $\hat{\mu}_{q_{\text{eff}}} = \sqrt{\frac{g_{ii}}{-g_{tt}}}q_{\text{eff}}A_t$ and we will drop the subscript x on k_x . In our conventions z_+ (and y_+) is the fundamental component dual to the source of the fermionic operator in the CFT [1,2]. Rewriting the coupled first-order Dirac equations as a single second-order equation for z_+ ,

$$\begin{aligned} \partial_r^2 z_+ + \mathcal{P}\partial_r z_+ + \mathcal{Q}z_+ &= 0, \\ \mathcal{P} &= \frac{\partial_r(g_{ii}g^{rr})}{2g_{ii}g^{rr}} - \frac{\partial_r \hat{\mu}_{q_{\text{eff}}}}{k + \hat{\mu}_{q_{\text{eff}}}}, \\ \mathcal{Q} &= -\frac{m_{\text{eff}}\partial_r \sqrt{g_{ii}}}{\sqrt{g_{ii}g^{rr}}} + \frac{m_{\text{eff}}\sqrt{g_{rr}}\partial_r \hat{\mu}_{q_{\text{eff}}}}{k + \hat{\mu}_{q_{\text{eff}}}} - m_{\text{eff}}^2 g_{rr} \\ &\quad - \frac{k^2 - \hat{\mu}_{q_{\text{eff}}}^2}{g_{ii}g^{rr}}, \end{aligned} \quad (4.2)$$

the first thing one notes is that both \mathcal{P} and \mathcal{Q} diverge at some $r = r_*$, where $\hat{\mu}_{q_{\text{eff}}} + k = 0$. Since $\hat{\mu}_{q_{\text{eff}}}$ is (chosen to be) a positive semidefinite function which increases from $\hat{\mu}_{q_{\text{eff}}} = 0$ at the horizon, this implies that for negative k (with $-k < \hat{\mu}_{q_{\text{eff}}}|_{\infty}$) the wave function is qualitatively different from the wave function with positive k which experiences no singularity. The analysis is straightforward if we transform the first derivative away and recast it in the form of a Schrödinger equation by redefining the radial coordinate,

$$\frac{ds}{dr} = \exp\left(-\int^r dr' \mathcal{P}\right) \Rightarrow s = c_0 \int_{r_\infty}^r dr' \frac{|k + \hat{\mu}_{q_{\text{eff}}}|}{\sqrt{g_{ii}g^{rr}}}, \quad (4.3)$$

where c_0 is an integration constant whose natural scale is of order $c_0 \sim q_{\text{eff}}^{-1}$. This is a simpler version of the generalized k -dependent tortoise coordinate introduced in [3]. In the new coordinates the equation (4.2) is of the standard form,

$$\partial_s^2 z_+ - V(s)z_+ = 0 \quad (4.4)$$

with potential

$$V(s) = -\frac{g_{ii}g^{rr}}{c_0^2|k + \hat{\mu}_{q_{\text{eff}}}|^2} \mathcal{Q}. \quad (4.5)$$

The above potential (4.5) can also be written as

$$V(s) = \frac{1}{c_0^2(k + \hat{\mu}_{q_{\text{eff}}})^2} \left[(k^2 + m_{\text{eff}}^2 g_{ii} - \hat{\mu}_{q_{\text{eff}}}^2) + m_{\text{eff}} g_{ii} \sqrt{g^{rr}} \partial_r \ln \frac{\sqrt{g_{ii}}}{k + \hat{\mu}_{q_{\text{eff}}}} \right]. \quad (4.6)$$

We note again the potential singularity for negative k , but before we discuss this we first need the boundary conditions. The universal boundary behavior is at spatial infinity and follows from the asymptotic AdS geometry. In the adapted coordinates $r \rightarrow \infty$ corresponds to $s \rightarrow 0$ as follows from $ds/dr \simeq c_0(k + \hat{\mu}_{q_{\text{eff}}}|_\infty)/r^2$. The potential therefore equals

$$V(s) \simeq \frac{1}{s^2} (m_{\text{eff}} + m_{\text{eff}}^2) + \dots \quad (4.7)$$

and the asymptotic behavior of the two independent solutions equals $z_+ = a_1 s^{-m_{\text{eff}}} + b_1 s^{1+m_{\text{eff}}} + \dots$. The second solution is normalizable and we thus demand $a_1 = 0$.

In the interior, the near-horizon geometry generically is Lifshitz

$$ds^2 = -r^{2z} dt^2 + \frac{1}{r^2} dr^2 + r^2(dx^2 + dy^2) + \dots, \quad (4.8)$$

$$A = h_\infty r^z dt + \dots,$$

with finite dynamical critical exponent z —AdS-RN, which can be viewed as a special case, where $z \rightarrow \infty$, will be given separately. In adapted coordinates the interior $r \rightarrow 0$ corresponds to $s \rightarrow -\infty$ and it is easy to show that in this limit potential behaves as

$$V(s) \simeq \frac{1}{c_0^2} + \frac{1}{s^2} (m_{\text{eff}} \sqrt{g_\infty} + m_{\text{eff}}^2 g_\infty - h_\infty^2 q_{\text{eff}}^2 g_\infty) + \dots \quad (4.9)$$

Near the horizon the two independent solutions for the wave function z_+ therefore behave as

$$z_+ \rightarrow a_0 e^{-s/c_0} + b_0 e^{s/c_0}. \quad (4.10)$$

The decaying solution $a_0 = 0$ is the normalizable solution we seek.

Let us now address the possible singular behavior for $k < 0$. To understand what happens, let us first analyze the potential qualitatively for positive k . Since the potential is positive semidefinite at the horizon and the boundary, the Schrödinger system (4.4) only has a zero-energy normalizable solution if $V(s)$ has a range $s_1 < s < s_2$, where it is negative. This can only occur at locations where $k^2 < \hat{\mu}_{q_{\text{eff}}}^2 - m_{\text{eff}}^2 g_{ii} - m_{\text{eff}} g_{ii} \sqrt{g^{rr}} \partial_r \ln \frac{\sqrt{g_{ii}}}{k + \hat{\mu}_{q_{\text{eff}}}}$. Defining a “re-normalized” position dependent mass $m_{\text{ren}}^2 = m_{\text{eff}}^2 g_{ii} + m_{\text{eff}} g_{ii} \sqrt{g^{rr}} \partial_r \ln \frac{\sqrt{g_{ii}}}{k + \hat{\mu}_{q_{\text{eff}}}}$ this is the intuitive statement that the momenta must be smaller than the local chemical potential $k^2 < \hat{\mu}_{q_{\text{eff}}}^2 - m_{\text{ren}}^2$. For positive k the saturation of this bound $k^2 = \hat{\mu}_{q_{\text{eff}}}^2 - m_{\text{ren}}^2$ has at most two solutions, which are regular zeroes of the potential. This follows from the fact that $\hat{\mu}_{q_{\text{eff}}}^2$ decreases from the boundary toward the interior. If the magnitude $|k|$ is too large the inequality cannot be satisfied, the potential is strictly positive, and no solution exists. For negative k , however, the potential has in addition a triple pole at $k^2 = \hat{\mu}_{q_{\text{eff}}}^2$; two poles arise from the prefactor and the third from the $m_{\text{eff}} \partial_r \ln(k + \hat{\mu}_{q_{\text{eff}}})$ term. This pole always occurs closer to the horizon than the zeroes and the potential therefore qualitatively looks like that in Fig. 4. (Since $\hat{\mu}_{q_{\text{eff}}}$ decreases as we move inward from the boundary, starting with $\hat{\mu}_{q_{\text{eff}}}^2 > \hat{\mu}_{q_{\text{eff}}}^2 - \mu^2 > k^2$, one first saturates the inequality that gives the zero in the potential as one moves inward.) Such a potential cannot support a zero-energy bound state, i.e. Eq. (4.4) has no solution for negative k . In the case $m_{\text{eff}} = 0$ a double zero changes the triple pole to a single pole and the argument still holds. This does not mean that there are no $k < 0$ poles

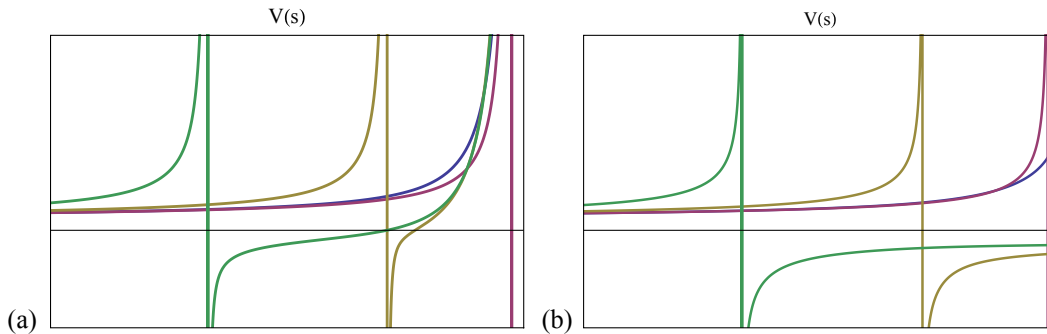


FIG. 4 (color online). The behavior of the Schrödinger potential $V(s)$ for z_+ when k is negative. Such a potential has no zero-energy bound state. The potential is rescaled to fit on a finite range. As $|k|$ is lowered below k_{max} for which the potential is strictly positive, a triple pole appears which moves toward the horizon on the left (a). The blue, red, orange, and green curves are decreasing in $|k|$). The pole hits the horizon for $k = 0$ and disappears. (b) shows the special case $m_{\text{eff}} = 0$ where two zeroes collide with two of the triple poles to form a single pole.

in the CFT spectral function. They arise from the other physical polarization y_+ of the bulk fermion Ψ . From the second set of decoupled first-order equations for the other components of the Dirac equation (after replacing $iz_- \rightarrow z_-$)

$$\begin{aligned}\sqrt{g_{ii}g^{rr}}\partial_r y_+ - m_{\text{eff}}\sqrt{g_{ii}}y_+ &= -(k - \hat{\mu}_{q_{\text{eff}}})z_-, \\ \sqrt{g_{ii}g^{rr}}\partial_r z_- + m_{\text{eff}}\sqrt{g_{ii}}z_- &= -(k + \hat{\mu}_{q_{\text{eff}}})y_+, \end{aligned} \quad (4.11)$$

and the associated second-order differential equation of motion for y_+ ,

$$\begin{aligned}\partial_r^2 y_+ + \mathcal{P}\partial_r y_+ + \mathcal{Q} &= 0, \\ \mathcal{P} &= \frac{\partial_r(g_{ii}g^{rr})}{2g_{ii}g^{rr}} - \frac{\partial_r \hat{\mu}_{q_{\text{eff}}}}{-k + \hat{\mu}_{q_{\text{eff}}}}, \\ \mathcal{Q} &= -\frac{m_{\text{eff}}\partial_r \sqrt{g_{ii}}}{\sqrt{g_{ii}g^{rr}}} + \frac{m_{\text{eff}}\sqrt{g_{rr}}\partial_r \hat{\mu}_{q_{\text{eff}}}}{-k + \hat{\mu}_{q_{\text{eff}}}} - m_{\text{eff}}^2 g_{rr} \\ &\quad - \frac{k^2 - \hat{\mu}_{q_{\text{eff}}}^2}{g_{ii}g^{rr}}, \end{aligned} \quad (4.12)$$

one sees that the Schrödinger equation for y_+ is the $k \rightarrow -k$ image of the equation (4.4) for z_+ and thus y_+ will only have zero-energy solutions for $k < 0$. For simplicity we will only analyze the z_+ case. Note that this semipositive definite momentum structure of the poles is a feature of any AdS-to-Lifshitz metric different from AdS-RN, where one can have negative k solutions [3].

The exact solution of (4.4) with the above boundary conditions corresponding to poles in the CFT spectral function is difficult to find. By construction the system is however equivalent to a Schrödinger problem of finding a zero-energy solution z_+ in the potential (4.5) and can be solved in the WKB approximation (see e.g. [3,24]). The WKB approximation holds when $|\partial_s V| \ll |V|^{3/2}$. Notice that this is more general than the background adiabaticity limit $m_{\text{eff}} \gg 1$, $q_{\text{eff}} \gg 1$ with $\hat{\beta}$, \hat{m} fixed. Combining background adiabaticity with a scaling limit $k \gg 1$, $m_{\text{eff}} \gg 1$, $q_{\text{eff}} \gg 1$ with $c_0 k$ fixed and k parametrically larger than $\hat{\mu}_{q_{\text{eff}}}$, one recovers the WKB potential solved in [12,13]. As our aim is to study the deviation away from the background adiabatic limit we will be more general and study the WKB limit of the potential itself, without direct constraints on q_{eff} , m_{eff} . And rather than testing the inequality $|\partial_s V| \ll |V|^{3/2}$ directly, we will rely on the rule of thumb that the WKB limit is justified when the number of nodes in the wave function is large. We will therefore estimate the number n of bound states and use $n \gg 1$ as an empirical justification of our approach.⁸ With this criterion we will be able to study the normalizable solutions

⁸A large number of bound states n implies $|\partial_s V| \ll |V|^{3/2}$ if the potential has a single minimum but as is well known there are systems, e.g. the harmonic oscillator, where the WKB approximation holds for small n as well.

to the Dirac equation/pole structure of the CFT spectral functions as a function of κ/L .

The potential is bounded both in the AdS boundary and at the horizon, and decreases toward intermediate values of r . We therefore have a standard WKB solution consisting of three regions:

- (i) In the regions where $V > 0$, the solution decays exponentially,

$$z_+ = c_{1,2} V^{-1/4} \exp\left(\pm \int_{r_{1,2}}^r dr' [c_0 \sqrt{g^{ii}g_{rr}}(k + \hat{\mu}_{q_{\text{eff}}})\sqrt{V}]\right). \quad (4.13)$$

Here r_1, r_2 are the turning points where $V(r_1) = 0 = V(r_2)$.

- (ii) In the region $r_1 < r < r_2$, i.e. $V < 0$, the solution is

$$z_+ = c_3 (-V)^{-1/4} \text{Re}\left[\exp\left(i \int_{r_1}^r dr' [c_0 \sqrt{g^{ii}g_{rr}}(k + \hat{\mu}_{q_{\text{eff}}})\sqrt{-V}]\right) \times \sqrt{-V}\right] - i\pi/4, \quad (4.14)$$

with the constant phase $-i\pi/4$ originating in the connection formula at the turning point r_1 .

Finding a WKB solution shows us that the peaks seen numerically are true poles in the spectral function. But it also allows us to estimate the number of peaks that the numerical approach could not resolve. The WKB quantization condition

$$\int_{r_1}^{r_2} dr' [c_0 \sqrt{g^{ii}g_{rr}}(k + \hat{\mu}_{q_{\text{eff}}})\sqrt{-V}] = \pi(n + 1/2) \quad (4.15)$$

counts the number of bound states with negative semi-definite energy. Note that n does not depend on the integral constant as there is also a factor $1/c_0$ in $\sqrt{-V}$. Since V depends on k , we will see that as we increase k this number decreases. The natural interpretation in the context of a bulk many-body Fermi system is that this establishes the ordering of the filling of all the $\omega = 0$ momentum shells in the electron star. For a fixed k one counts the modes that have been previously occupied and, consistent with our earlier deduction, the lowest/highest k_F corresponds to the last/first occupied state. Though counterintuitive from a field theory perspective where normally $E \sim k_F$, this UV/IR correspondence is very natural from the AdS bulk, if one thinks of the electron star as a trapped electron gas. The last occupied state should then be the outermost state from the center, but this state has the lowest effective chemical potential and hence lowest k_F .

Let us now show this explicitly by analyzing the potential and the bound states in the electron star and the AdS-RN case can be found in the Appendix.

The potential (4.6) for the electron star is given in Fig. 5 and the number of bound states as a function of k in Fig. 6. As stated the number of states decreases with increasing k , consistent with the analogy of the pole distribution of the

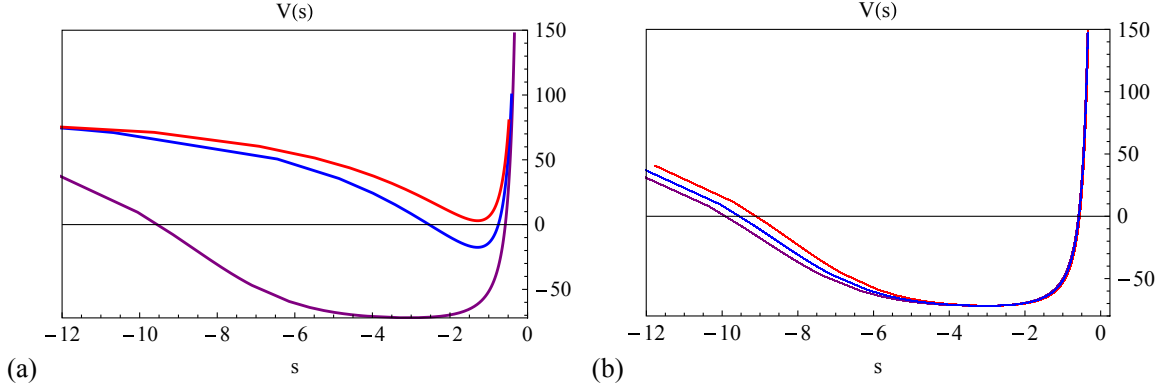


FIG. 5 (color online). The Schrödinger potential $V(s)$ for the fermion component z_+ of in the electron star (ES) background $\hat{m} = 0.36$, $z = 2$, $c_0 = 0.1$. (a) shows the dependence on the momentum $k = 0.0185$ (purple), $k = 5$ (blue), $k = 10$ (red) for $\kappa = 0.092$. (b) shows the dependence on $\kappa = 0.086$ (purple), $\kappa = 0.092$ (blue), $\kappa = 0.1$ (red) for $k = 0.0185$. Recall that $s = 0$ is the AdS boundary and $s = -\infty$ is the near-horizon region.

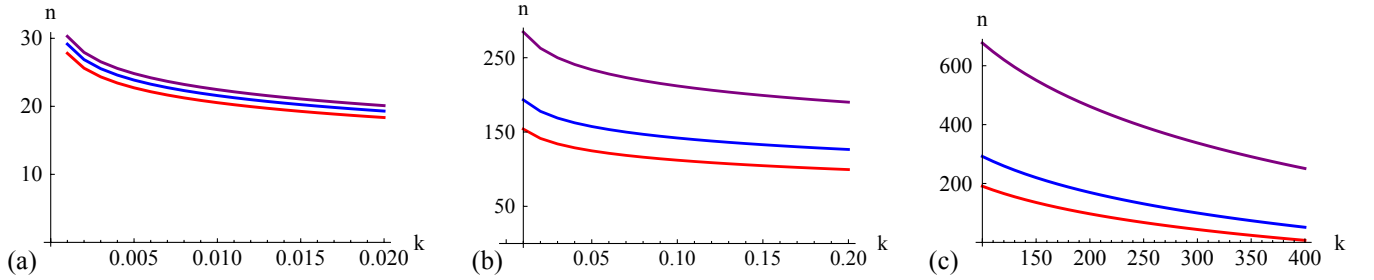


FIG. 6 (color online). The WKB estimate of the number of bound states n as a function of the momentum k for $\kappa = 0.086$ (purple), 0.092 (blue), 0.1 (red) (a); for $\kappa = 0.001$ (purple), 0.002 (blue), 0.003 (red) (b); and for $\kappa = 10^{-5}$ (purple), 3×10^{-5} (blue), 5×10^{-5} (red) (c). Note the parametric increase in number of states as the adiabaticity of the background improves for smaller κ . These three panels are for the electron star background with $\hat{m} = 0.36$, $z = 2$. Since $n \gg 1$ in all cases, WKB gives a valid estimate.

spectral functions compared with AdS-RN. Moreover, we clearly see the significant increase in the number of states as we decrease κ/L thereby improving the adiabaticity of the background. This vividly illustrates that the adiabatic limit corresponds to a large number of constituents. As all numbers of states are far larger than 1, the use of the WKB is justified. From the trend that dialing κ/L up there will be fewer Fermi surfaces one can conjecture that the Dirac hair has only one Fermi surface and it was shown in [5] that this is indeed the case.

V. CONCLUSION AND DISCUSSION

These electron star spectral function results directly answer two of the three questions raised in the introduction.

- (i) They show explicitly how the fermion wave functions in their own gravitating potential well are ordered despite the fact that they all have strictly vanishing energy: In a fermionic version of the UV-IR correspondence they are ordered *inversely* in k , with the “lowest”/first occupied state having the highest k and the “highest”/last occupied state having the lowest k . With the qualitative AdS/CFT

understanding that scale corresponds to distance away from the interior, one can intuitively picture this as literally filling geometrical shells of the electron star, with the outermost/highest/last shell at large radius corresponding to the wave function with lowest local chemical potential and hence lowest k .

- (ii) The decrease of the number of bound states—the number of occupied wave functions in the electron star—as we decrease $q_{\text{eff}} = \hat{\beta}^{1/4} \sqrt{\frac{\pi L}{\kappa}}$ for a fixed electron star background extrapolates naturally to a limit where the number of bound states is unity. This extrapolation pushes the solution beyond its adiabatic regime of validity. In principle we know what the correct description in this limit is: it is the AdS Dirac hair solution constructed in [4]. The dependence of the number of bound states on κ/L therefore illustrates that the electron star and Dirac hair solutions are two limiting cases of the gravitationally backreacted Fermi gas.

With this knowledge we can schematically classify the ground state solutions of AdS Einstein-Maxwell gravity

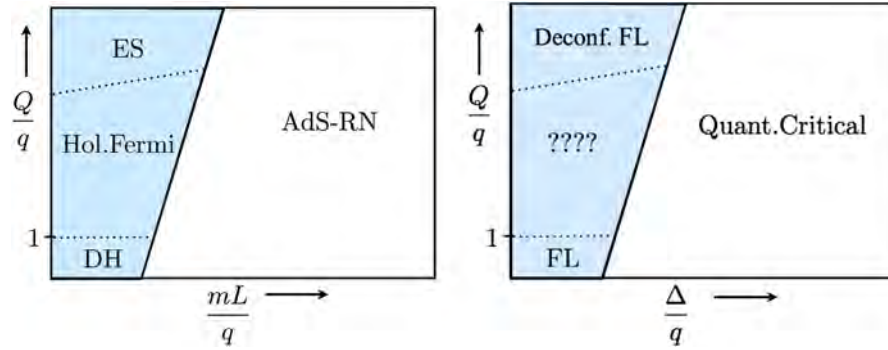


FIG. 7 (color online). Schematic diagram of the different ground state solutions of strongly coupled fermions implied by holography for fixed charge density Q . Here q is the constituent charge of the fermions and $mL \sim \Delta$ the mass/conformal scaling dimension of the fermionic operator. One has the gravitational electron star (ES)/Dirac hair (DH) solution for large/small Q/q and small mL/q dual a deconfined Fermi liquid/regular Fermi liquid in the CFT. For $mL/q \sim \Delta/q$ large the ground state remains the fermionic quantum critical state dual to AdS-RN.

minimally coupled to charged fermions at finite charge density.⁹ For large mass mL in units of the constituent charge q , the only solution is a charged AdS-Reissner-Nördstrom black hole. For a low enough mass-to-charge ratio, the black hole becomes unstable and develops hair. If in addition the total charge density Q is of the order of the microscopic charge q this hairy solution is the Dirac hair configuration constructed in [4], whereas in the limit of large total charge density Q one can make an adiabatic Thomas-Fermi approximation and arrive *à la* Tolman-Oppenheimer-Volkov at an electron star (Fig. 7).

Translating this solution space through the AdS/CFT correspondence one reads off that in the dual strongly coupled field theory, one remains in the critical state if the ratio of the scaling dimension to the charge Δ/q is too large. For a small enough value of this ratio, the critical state is unstable and forms a novel scaleful ground state. The generic condensed matter expectation of a unique Fermi liquid is realized if the total charge density is of the same order as the constituent charge. Following [12–16] the state for $Q \gg q$ is some deconfined Fermi liquid.

The gravity description of either limit has some deficiencies, most notably the lack of an electron star wave function at infinity and the unnatural restriction to $Q = q$ for the Dirac hair solution. A generic solution for $Q \geq q$ with wave function tails extending to infinity as the Dirac hair would be a more precise holographic dual to the strongly interacting large N Fermi system. Any CFT information can then be cleanly read off at the AdS boundary. A naive construction could be to superpose Dirac hair onto the electron star; in principle one can achieve this

solution by a next-order Hartree-Fock or local density approximation computation.

This best-of-both-worlds generic solution ought to be the true holographic dual of the strongly interacting Fermi ground state. If one is able to answer convincingly how this system circumvents the wisdom that the ground state of an interacting many-body system of fermions is a generic single quasiparticle Landau Fermi liquid, then one would truly have found a finite density Fermi system that does not refer at any stage to an underlying perturbative Fermi gas.

ACKNOWLEDGMENTS

We thank S. Hartnoll, A. Karch, H. Liu, T. K. Ng, and B. Overbosch for discussions and correspondence. K. S. is very grateful to the Hong Kong Institute for Advanced Studies for the hospitality during the completion of this work. This research was supported in part by a VIDI Innovative Research Incentive Grant (K. Schalm) from the Netherlands Organisation for Scientific Research (NWO), a Spinoza Grant (J. Zaanen) from the Netherlands Organisation for Scientific Research (NWO) and the Dutch Foundation for Fundamental Research on Matter (FOM).

APPENDIX: SCHRÖDINGER ANALYSIS IN THE REISSNER-NORDSTRÖM CASE

For AdS-RN the Schrödinger analysis requires a separate discussion of the near-horizon boundary conditions, which we present here for completeness and comparison. The reason is that for AdS-RN there is a special scale k_o below which the boundary condition turns complex (Eq. (26) in [1]). This scale k_o is related to the surprising existence of an oscillatory region in the spectral function. For $k > k_o$ the boundary conditions are real as they are for the electron star for all k . AdS-RN boundary conditions are therefore qualitatively different from electron star spectral functions, but only for $k < k_o$. This difference is not

⁹One should always keep in mind that the setup under study here is phenomenological in nature; a full string theory embedding might introduce other fields which could prevent the electron star or Dirac hair from being the true ground state of the system.

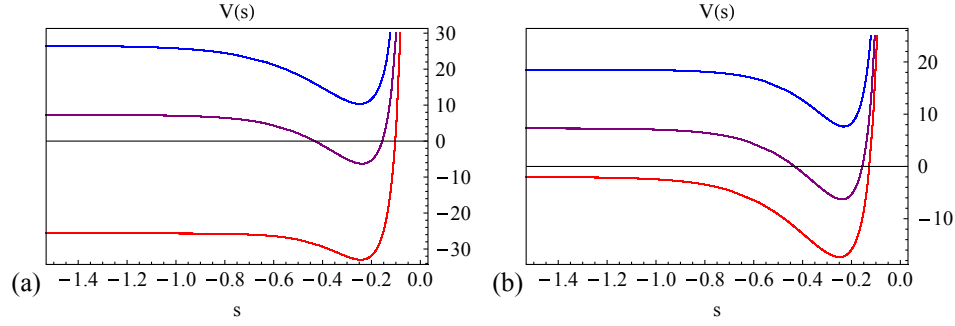


FIG. 8 (color online). The Schrödinger potential $V(s)$ for the fermion component z_+ in the AdS-RN background $r_+ = 1$, $\mu = \sqrt{3}$, $g_F = 1$, $mL = 0.4$, $c_0 = 0.1$. (a) shows the dependence on the momentum $k = 1$ (red), $k = 2$ (purple), $k = 3$ (blue) for charge $q = 2.5$. (b) shows the dependence on the charge q —analogous to κ in the ES background. Shown are the values $q = 2$ (blue), $q = 2.5$ (purple), $q = 3$ (red) for the momentum $k = 2$. In both panels, the red potentials correspond to the oscillatory region $\nu_k^2 < 0$, the purple potentials show the generic shape that can support an $\omega = 0$ bound state, and the blue potentials are strictly positive and no zero-energy bound state is present. Recall that $s = 0$ is the AdS boundary and $s = -\infty$ is the near-horizon region.

relevant to the analogy between electron star spectral functions and the distinct poles in the AdS-RN spectral function in Fig. 2 as the latter only occur for $k > k_o$. Part of this analysis is originally worked out in [3].

The AdS-RN black hole with metric

$$ds^2 = L^2 \left(-f(r)dt^2 + \frac{dr^2}{f(r)} + r^2(dx^2 + dy^2) \right), \quad (\text{A1})$$

$$f(r) = r^2 \left(1 + \frac{3}{r^4} - \frac{4}{r^3} \right), \quad (\text{A2})$$

$$A = \mu \left(1 - \frac{1}{r} \right) dt, \quad (\text{A3})$$

has near-horizon geometry $\text{AdS}_2 \times \mathbb{R}^2$

$$ds^2 = -6(r-1)^2 dt^2 + \frac{dr^2}{6(r-1)^2} + (dx^2 + dy^2), \quad (\text{A4})$$

$$A = \sqrt{3}(r-1) dt. \quad (\text{A5})$$

A coordinate redefinition of r in Eq. (4.8) to $r = (r_{\text{AdS}_2} - 1)^{1/z}$ shows that this corresponds to a dynamical critical exponent $z = \infty$ and is outside the validity of the previous analysis.

Before we proceed, recall that the existence of $\text{AdS}_2 \times \mathbb{R}^2$ near-horizon region allows for a semianalytic determination of the fermion spectral functions with the self-energy $\Sigma \sim \omega^{2\nu_{k_F}}$ controlled by the IR conformal dimension $\delta_k = 1/2 + \nu_k$ with

$$\nu_k = \frac{1}{\sqrt{6}} \sqrt{m^2 + k^2 - \frac{q^2}{2}}. \quad (\text{A6})$$

When ν_k is imaginary, which for $q^2 > 2m^2$ always happens for small k , the spectral function exhibits oscillatory behavior, but generically has finite weight at $\omega = 0$. When ν_k is real, there are poles in the spectral functions at a finite

number of different Fermi momenta k_F . The associated quasiparticles can characterize a non-Fermi liquid ($\nu_{k_F} < 1/2$), a marginal Fermi liquid ($\nu_{k_F} = 1/2$), or irregular Fermi liquid ($\nu_{k_F} > 1/2$) with linear dispersion but width $\Gamma \neq \omega^2$ [3].

The analytic form of the near-horizon metric allows us to solve exactly for the near-horizon potential V in terms of $s = \frac{c_0}{\sqrt{6}}(k + q/\sqrt{2}) \ln(r-1) + \dots$. As noted in [3] one remarkably obtains that the near-horizon potential for $s \rightarrow -\infty$ is proportional to the self-energy exponent,

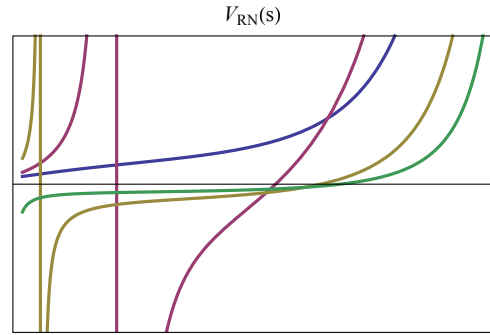


FIG. 9 (color online). The qualitative behavior for negative k of the Schrödinger potential $V(s)$ for the fermion component z_+ of the AdS-RN background $r_+ = 1$, $\mu = \sqrt{3}$, $g_F = 1$, $mL = 0.1$. The radial coordinate has been rescaled to a finite domain such that the full potential can be represented in the figure; on the right is the AdS boundary and left is the near-horizon region and the range is slightly extended beyond the true horizon, which is exactly at the short vertical line-segments on the right. Potentials are given for $q = 12/\sqrt{3}$, with different values of k . For $k = -15$ (blue), the potential is strictly positive. For $k = -10$ (purple) and $k = -7$ (orange), both of their potentials have triple poles and the pole can be seen to move toward the horizon on the left as k decreases. For $k = -4$ (green), the potential has no pole and reaches a finite negative value at the horizon. The pole disappears for $|k| < q/\sqrt{2}$ leaving a regular bounded potential which can support zero-energy bound states.

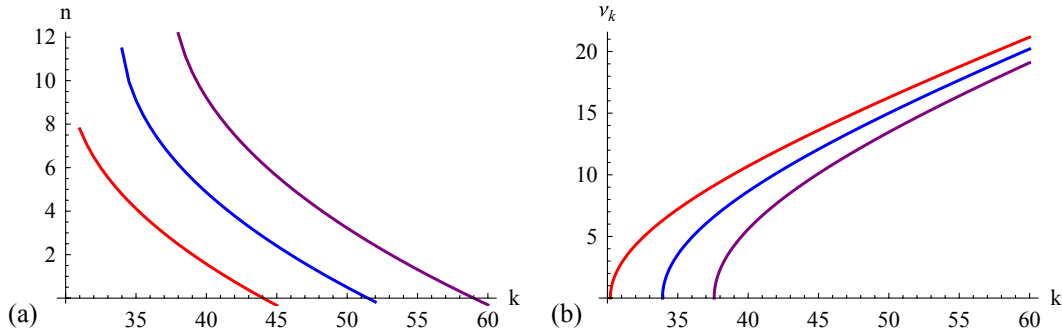


FIG. 10 (color online). (a) The WKB estimate of the number of bound states n in the AdS-RN Schrödinger potential for z_+ with $mL = 10$. The WKB approximation only applies to large values of the charge $q = 45$ (red), $q = 50$ (blue), $q = 55$ (purple). (b) gives the associated values of the IR conformal dimension $\nu_k = \frac{1}{\sqrt{6}}\sqrt{m^2 + k^2 - \frac{q^2}{2}}$. Both panels are for the extremal AdS-RN background with $\mu = \sqrt{3}$, $r_+ = 1$, $g_F = 1$.

$$V(s) \simeq \frac{6}{c_0^2(k + q/\sqrt{2})^2} \nu_k^2 + \dots \quad (\text{A7})$$

One immediately recognizes the oscillatory region $\nu_k^2 < 0$ of the spectral function as an $\omega = 0$ Schrödinger potential which is “free” at the horizon $s = -\infty$ (Fig. 8) and no bound state can form. Comparing with our previous results, we see that this oscillatory region is a distinct property of AdS-RN. For any Lifshitz near-horizon metric the potential is always positive-definite near the horizon and all $\omega = 0$ solutions will be bounded (see also [12,13]). As we increase k , ν_k^2 becomes positive, then the AdS-RN potential is also positive at the horizon and bound zero-energy states can form. Increasing k further, one reaches a maximal k_{\max} , above which the potential is always positive and no zero-energy bound state exists anymore.

Because the near-horizon boundary conditions for AdS-RN differ from the general analysis, the possible singularity in the potential for $k < 0$ also requires a separate study. This is clearly intimately tied to the existence of an oscillatory regime in the spectral function, as the previous analysis does apply for $\nu_k^2 > 0$. The clearest way to understand what happens for $\nu_k^2 < 0$ is to analyze the potential

explicitly. Again if $|k| > k_{\max}$ the potential is strictly positive-definite, and no zero-energy bound state exists. As we decrease the magnitude of $k < 0$, a triple pole will form near the boundary when $k = -\hat{\mu}_{q_{\text{eff}}}(s)$, soon followed by a zero at $k = -\sqrt{\hat{\mu}_{q_{\text{eff}}}(s)^2 - m_{\text{ren}}(s)^2}$ (see Fig. 4). As we approach the horizon, in the general case where $\lim_{r \rightarrow 0} \hat{\mu}_{q_{\text{eff}}} = h_{\infty} q_{\text{eff}} r + \dots$, this pole at $r_* = -k/(h_{\infty} q_{\text{eff}})$ hits the horizon and disappears precisely when $k = 0$. In AdS-RN, however, where $\lim_{r \rightarrow 1} \hat{\mu}_{q_{\text{eff}}} = \frac{q}{\sqrt{2}} + \frac{\sqrt{2}q}{3}(r-1) + \dots$, the pole at $r_*^{RN} - 1 = \frac{3}{\sqrt{2}q}(k + \frac{q}{\sqrt{2}})$ hits the horizon and disappears at $k = -\frac{q}{\sqrt{2}}$. For negative values of k whose magnitude is less than $|k| < \frac{q}{\sqrt{2}}$, the potential is regular and bounded and can and does have zero-energy solutions. Figure 9 shows this disappearance of the pole for the AdS-RN potential.

Counting solutions through WKB is also more complicated for AdS-RN. For $\mathcal{O}(1)$ values of q there are only few Fermi surfaces and the WKB approximation does not apply. For large q it does, however. For completeness we show the results in Fig. 10.

-
- [1] H. Liu, J. McGreevy, and D. Vegh, *Phys. Rev. D* **83**, 065029 (2011).
[2] M. Cubrovic, J. Zaanen, and K. Schalm, *Science* **325**, 439 (2009).
[3] T. Faulkner, H. Liu, J. McGreevy, and D. Vegh, *Phys. Rev. D* **83**, 125002 (2011).
[4] M. Cubrovic, J. Zaanen, and K. Schalm, [arXiv:1012.5681](https://arxiv.org/abs/1012.5681).
[5] M. Cubrovic, J. Zaanen, and K. Schalm (work in progress).
[6] S. A. Hartnoll, J. Polchinski, E. Silverstein, and D. Tong, *J. High Energy Phys.* **04** (2010) 120.
[7] S. A. Hartnoll and A. Tavanfar, *Phys. Rev. D* **83**, 046003 (2011).
[8] J. de Boer, K. Papadodimas, and E. Verlinde, *J. High Energy Phys.* **10** (2010) 020.
[9] X. Arsiwalla, J. de Boer, K. Papadodimas, and E. Verlinde, *J. High Energy Phys.* **01** (2011) 144.
[10] V. G. M. Puletti, S. Nowling, L. Thorlacius, and T. Zingg, *J. High Energy Phys.* **01** (2011) 117.
[11] S. A. Hartnoll and P. Petrov, *Phys. Rev. Lett.* **106**, 121601 (2011).
[12] S. A. Hartnoll, D. M. Hofman, and D. Vegh, [arXiv:1105.3197](https://arxiv.org/abs/1105.3197).
[13] N. Iqbal, H. Liu, and M. Mezei, [arXiv:1105.4621](https://arxiv.org/abs/1105.4621).
[14] S. A. Hartnoll, D. M. Hofman, and A. Tavanfar, *Europhys. Lett.* **95**, 31002 (2011).

- [15] S. Sachdev, *Phys. Rev. Lett.* **105**, 151602 (2010).
- [16] L. Huijse and S. Sachdev, *Phys. Rev. D* **84**, 026001 (2011).
- [17] H. Liu and T. Faulkner (private communication).
- [18] N. Iizuka, N. Kundu, P. Narayan, and S.P. Trivedi, [arXiv:1105.1162](https://arxiv.org/abs/1105.1162).
- [19] S.S. Gubser and A. Nellore, *Phys. Rev. D* **80**, 105007 (2009).
- [20] K. Goldstein, S. Kachru, S. Prakash, and S.P. Trivedi, *J. High Energy Phys.* **08** (2010) 078.
- [21] D. Guarrera and J. McGreevy, [arXiv:1102.3908](https://arxiv.org/abs/1102.3908).
- [22] T. Faulkner, N. Iqbal, H. Liu, J. McGreevy, and D. Vegh, [arXiv:1101.0597](https://arxiv.org/abs/1101.0597).
- [23] T. Faulkner and J. Polchinski, *J. High Energy Phys.* **06** (2011) 012.
- [24] G.T. Horowitz and M.M. Roberts, *J. High Energy Phys.* **11** (2009) 015.

RECEIVED: March 28, 2011

REVISED: August 29, 2011

ACCEPTED: September 4, 2011

PUBLISHED: October 6, 2011

Constructing the AdS dual of a Fermi liquid: AdS black holes with Dirac hair

Mihailo Čubrović, Jan Zaanen and Koenraad Schalm

*Institute Lorentz for Theoretical Physics, Leiden University,
P.O. Box 9506, Leiden 2300RA, The Netherlands*

E-mail: cubrovic@lorentz.leidenuniv.nl, jan@lorentz.leidenuniv.nl,
kschalm@lorentz.leidenuniv.nl

ABSTRACT: We provide evidence that the holographic dual to a strongly coupled charged Fermi liquid has a non-zero fermion density in the bulk. We show that the pole-strength of the stable quasiparticle characterizing the Fermi surface is encoded in the AdS probability density of a single normalizable fermion wavefunction in AdS. Recalling Migdal's theorem which relates the pole strength to the Fermi-Dirac characteristic discontinuity in the number density at ω_F , we conclude that the AdS dual of a Fermi liquid is described by occupied on-shell fermionic modes in AdS. Encoding the occupied levels in the total spatially averaged probability density of the fermion field directly, we show that an AdS Reissner-Nordström black hole in a theory with charged fermions has a critical temperature, at which the system undergoes a first-order transition to a black hole with a non-vanishing profile for the bulk fermion field. Thermodynamics and spectral analysis support that the solution with non-zero AdS fermion-profile is the preferred ground state at low temperatures.

KEYWORDS: Black Holes in String Theory, AdS-CFT Correspondence, Holography and condensed matter physics (AdS/CMT)

Contents

| | | |
|----------|---|-----------|
| 1 | Introduction | 1 |
| 2 | From Green’s function to AdS/CFT rules for a Fermi liquid | 4 |
| 2.1 | The AdS dual of a stable Fermi liquid: applying Migdal’s relation holographically | 8 |
| 2.1.1 | Boundary conditions and normalizability | 11 |
| 3 | An AdS black hole with Dirac hair | 12 |
| 3.1 | Thermodynamics | 16 |
| 3.2 | At the horizon: entropy collapse to a Lifshitz solution | 17 |
| 3.3 | A BH with Dirac hair | 18 |
| 3.3.1 | Finite fermion density solutions in AdS-RN | 19 |
| 3.3.2 | Finite fermion density in AdSS | 22 |
| 3.4 | Confirmation from fermion spectral functions | 23 |
| 4 | Discussion and conclusion | 24 |

1 Introduction

Fermionic quantum criticality is thought to be an essential ingredient in the full theory of high T_c superconductivity [1, 2]. The cleanest experimental examples of quantum criticality occur in heavy-fermion systems rather than high T_c cuprates, but the experimental measurements in heavy fermions raise equally confounding theoretical puzzles [3]. Most tellingly, the resistivity scales linearly with the temperature from the onset of superconductivity up to the crystal melting temperature [4] and this linear scaling is in conflict with single correlation length scaling at criticality [5]. The failure of standard perturbative theoretical methods to describe such behavior is thought to indicate that the underlying quantum critical system is strongly coupled [6, 7].

The combination of strong coupling and scale-invariant critical dynamics makes these systems an ideal arena for the application of the AdS/CFT correspondence: the well-established relation between strongly coupled conformal field theories (CFT) and gravitational theories in anti-de Sitter (AdS) spacetimes. An AdS/CFT computation of single-fermion spectral functions — which are directly experimentally accessible via Angle-Resolved Photoemission Spectroscopy [8–10] — bears out this promise of addressing fermionic quantum criticality [11–15] (see also [16, 17]). The AdS/CFT single fermion spectral function exhibits distinct sharp quasiparticle peaks, associated with the formation of a Fermi surface, emerging from a scale-free state. The fermion liquid which this

Fermi surface captures is generically singular: it has either a non-linear dispersion or non-quadratic pole strength [11, 13]. The precise details depend on the parameters of the AdS model.

From the AdS gravity perspective, peaks with linear dispersion correspond to the existence of a stable charged fermionic quasinormal mode in the spectrum of a charged AdS black hole. The existence of a stable charged bosonic quasinormal mode is known to signal the onset of an instability towards a new ground state with a pervading Bose condensate extending from the charged black hole horizon to the boundary of AdS. The dual CFT description of this charged condensate is spontaneous symmetry breaking as in a superfluid and a conventional superconductor [18–21]. For fermionic systems empirically the equivalent robust $T = 0$ ground state is the Landau Fermi Liquid — the quantum ground state of a system with a finite number of fermions. The existence of a stable fermionic quasinormal mode suggests that an AdS dual of a finite fermion density state exists.

Here we shall make a step towards the set of AdS/CFT rules for CFTs with a finite fermion density. The essential ingredient will be Migdal’s theorem, which relates the characteristic jump in fermion occupation number at the energy ω_F of the highest occupied state to the pole strength of the quasiparticle. The latter we know from the spectral function analysis and its AdS formulation is therefore known. Using this, we can show that the fermion number discontinuity is encoded in the *probability density* of the normalizable wavefunction of the dual AdS fermion field.

This shows that the AdS dual of a Fermi liquid is given by a system with occupied fermionic states in the bulk. The Fermi liquid is clearly not a scale invariant state, but any such states will have energy, momentum/pressure and charge and will change the interior geometry from AdS to something else. Which particular (set of) state(s) is the right one, it does not yet tell us, as this conclusion relies only on the asymptotic behavior of fermion fields near the AdS boundary. Here we shall take the simplest such state: a single fermion.¹ Constructing first a set of equations in terms of the spatially averaged density, we find the associated backreacted asymptotically AdS solution. This approximate solution is already good enough to solve several problems of principle:

- A charged AdS black hole in the presence of charged fermionic modes has a critical temperature below which fermionic Dirac “hair” forms. For our effective single fermion solution, the derivative of the free energy has the characteristic discontinuity of a first order transition. In AdS/CFT this has to be the case: In contrast to bosonic quasinormal modes, a fermionic quasinormal mode can never cause a linear instability indicative of a continuous phase transition. In the language of spectral functions, the pole of the retarded Green’s function can never cross to the upper-half plane [13].² The absence of a perturbative instability between this conjectured Dirac “black hole hair” solution and the “bald” charged AdS black hole can be explained if the transition is a first order gas-liquid transition. The existence of first order transition follows from a thermodynamic analysis of the free energy rather than a spectral analysis of small fluctuations.

¹These solutions are therefore the AdS extensions of [22–25].

²Ref. [41] argues that the instability can be second order.

- This solution with finite fermion profile is the preferred ground state at low temperatures compared to the bare charged AdS black hole. The latter is therefore a false vacuum in a theory with charged fermions. Confusing a false vacuum with the true ground state can lead to anomalous results. Indeed the finite temperature behavior of fermion spectral functions in AdS Reissner-Nordström, exhibited in the combination of the results of [11, 13] and [12], shows strange behavior. The former [11, 13] found sharp quasiparticle peaks at a frequency $\omega_F = 0$ in natural AdS units, whereas the latter [12] found sharp quasiparticle peaks at finite Fermi energy $\omega_F \neq 0$. As we will show, both peaks in fact describe the same physics: the $\omega_F \neq 0$ peak is a finite temperature manifestation of (one of the) $\omega = 0$ peaks in [13]. Its shift in location at finite temperature is explained by the existence of the nearby true finite fermion density ground state, separated by a potential barrier from the AdS Reissner-Nordström solution.
- The solution we construct here only considers the backreaction on the electrostatic potential. We show, however, that the gravitational energy density diverges at the horizon. This ought to be, as one expects the infrared geometry to change due to fermion profile. The charged AdS-black hole solution corresponds to a CFT system in a state with large ground state entropy. This is the area of the extremal black-hole horizon at $T = 0$. Systems with large ground-state entropy are notoriously unstable to collapse to a low-entropy state, usually by spontaneous symmetry breaking. In a fermionic system it should be the collapse to the Fermi liquid. The final state will generically be a geometry that asymptotes to Lifshitz type, i.e. the background breaks Lorentz-invariance and has a double-pole horizon with vanishing area, as expounded in [26]. Indeed the gravitational energy density diverges at the horizon in a similar way as other systems that are known to gravitationally backreact to a Lifshitz solution. The fully backreacted geometry includes important separate physical aspects — it is relevant to the stability and scaling properties of the Fermi liquid — and will be considered in a companion article.

The Dirac hair solution thus captures the physics one expects of the dual of a Fermi liquid. We have based its construction on a derived set of AdS/CFT rules to describe systems at finite fermion density. Qualitatively the result is as expected: one also needs occupied fermionic states in the bulk. Next to our effective single fermion approximation, another simple candidate is the backreacted AdS-Fermi-gas [26]/electron star [27] which appeared during the course of this work.³ The difference between the two approaches are the assumptions used to reduce the interacting Fermi system to a tractable solution. Ideally, one should carefully track all the fermion wavefunctions as in the recent article [38]. As explained in [31] the Fermi-gas and the single Dirac field are the two “local” approximations to the generic non-local multiple fermion system in the bulk, in very different regimes of applicability. The electron-star/Fermi-gas is considered in the Thomas-Fermi limit where the microscopic charge of the constituent fermions is sent to zero keeping the overall charge

³See also [28, 29]. An alternative approach to back-reacting fermions is [30].

fixed, whereas the single Dirac field clearly is the ‘limit’ where the microscopic charge equals the total charge in the system. This is directly evident in the spectral functions of both systems. The results presented here show that each pole in the CFT spectral function corresponds to a unique occupied Fermi state in the bulk; the electron star spectra show a parametrically large number of poles [31–33], whereas the Dirac hair state has a single quasiparticle pole by construction. The AdS-Dirac-hair black hole derived here therefore has the benefit of a direct connection with a unique Fermi liquid state in the CFT. This is in fact the starting point of our derivation.

In the broader context, the existence of both the Dirac hair and backreacted Fermi gas solution is not a surprise. It is a manifestation of *universal* physics in the presence of charged AdS black holes. The results here, and those of [11, 13, 26, 27], together with the by now extensive literature on holographic superconductors, i.e. Bose condensates, show that at sufficiently low temperature in units of the black-hole charge, the electric field stretching to AdS-infinity causes a spontaneous discharge of the bulk vacuum outside of the horizon into the charged fields of the theory — whatever their nature. The positively charged excitations are repelled by the black hole, but cannot escape to infinity in AdS and they form a charge cloud hovering over the horizon. The negatively charged excitations fall into the black-hole and neutralize the charge, until one is left with an uncharged black hole with a condensate at finite T or a pure asymptotically AdS-condensate solution at $T = 0$. As [26, 27] and we show, the statistics of the charged particle do not matter for this condensate formation, except in the way it forms: bosons superradiate and fermions nucleate. The dual CFT perspective of this process is “entropy collapse”. The final state therefore has negligible ground state entropy and is stable. The study of charged black holes in AdS/CFT is therefore a novel way to understand the stability of charged interacting matter which holds much promise.

2 From Green’s function to AdS/CFT rules for a Fermi liquid

We wish to show how a solution with finite fermion number — a Fermi liquid — is encoded in AdS. The exact connection and derivation will require a review of what we have learned of Dirac field dynamics in AdS/CFT through Green’s functions analysis. The defining signature of a Fermi liquid is a quasi-particle pole in the (retarded) fermion propagator,

$$G_R = \frac{Z}{\omega - \mu_R - v_F(k - k_F)} + \text{regular} \tag{2.1}$$

Phenomenologically a non-zero residue at the pole, Z , also known as the pole strength, is the indicator of a Fermi liquid state. Migdal famously related the pole strength to the occupation number discontinuity at the pole $\omega = 0$.

$$Z = \lim_{\epsilon \rightarrow 0} [n_F(\omega - \epsilon) - n_F(\omega + \epsilon)] \tag{2.2}$$

where

$$n_F(\omega) = \int d^2k f_{FD} \left(\frac{\omega}{T} \right) \text{Im}G_R(\omega, k).$$

with f_{FD} the Fermi-Dirac distribution function. Vice versa, a Fermi liquid with a Fermi-Dirac jump in occupation number at the Fermi energy $\omega_F = 0$ has a low-lying quasiparticle excitation. Using our knowledge of fermionic spectral functions in AdS/CFT we shall first relate the pole-strength Z to known AdS quantities. Then using Migdal's relation, the dual of a Fermi liquid is characterized by an asymptotically AdS solution with non-zero value for these very objects.

The Green's functions derived in AdS/CFT are those of charged fermionic operators with scaling dimension Δ , dual to an AdS Dirac field with mass $m = \Delta - \frac{d}{2}$. We shall focus on $d = 2 + 1$ dimensional CFTs. In its gravitational description this Dirac field is minimally coupled to $3 + 1$ dimensional gravity and electromagnetism with action

$$S = \int d^4x \sqrt{-g} \left[\frac{1}{2\kappa^2} \left(R + \frac{6}{L^2} \right) - \frac{1}{4} F_{MN}^2 - \bar{\Psi} (\not{D} + m) \Psi \right]. \quad (2.3)$$

For zero background fermions, $\Psi = 0$, a spherically symmetric solution is a charged AdS₄ black-hole background

$$\begin{aligned} ds^2 &= \frac{L^2 \alpha^2}{z^2} (-f(z) dt^2 + dx^2 + dy^2) + \frac{L^2}{z^2} \frac{dz^2}{f(z)}, \\ f(z) &= (1-z)(1+z+z^2-q^2z^3), \\ A_0^{(bg)} &= 2q\alpha(z-1). \end{aligned} \quad (2.4)$$

Here $A_0^{(bg)}$ is the time-component of the U(1)-vector-potential, L is the AdS radius and the temperature and chemical potential of the black hole equal

$$T = \frac{\alpha}{4\pi} (3 - q^2), \quad \mu_0 = -2q\alpha, \quad (2.5)$$

where q is the black hole charge.

To compute the Green's functions we need to solve the Dirac equation in the background of this charged black hole:

$$e_A^M \Gamma^A (D_M + ieg A_M) \Psi + m \Psi = 0, \quad (2.6)$$

where the vielbein e_A^M , covariant derivative D_M and connection A_M correspond to the fixed charged AdS black-hole metric and electrostatic potential (2.4) Denoting $A_0 = \Phi$ and taking the standard AdS-fermion projection onto $\Psi_{\pm} = \frac{1}{2}(1 \pm \Gamma^Z)\Psi$, the Dirac equation reduces to

$$(\partial_z + \mathcal{A}_{\pm}) \Psi_{\pm} = \mp \mathcal{T} \Psi_{\mp} \quad (2.7)$$

with

$$\begin{aligned} \mathcal{A}_{\pm} &= -\frac{1}{2z} \left(3 - \frac{zf'}{2f} \right) \pm \frac{mL}{z\sqrt{f}}, \\ \mathcal{T} &= \frac{i(-\omega + g\Phi)}{\alpha f} \gamma^0 + \frac{i}{\alpha\sqrt{f}} k_i \gamma^i. \end{aligned} \quad (2.8)$$

Here γ^μ are the 2+1-dimensional Dirac matrices, obtained after decomposing the 3+1 dimensional Γ^μ -matrices.

Explicitly the Green's function is extracted from the behavior of the solution to the Dirac equation at the AdS-boundary. The boundary behavior of the bulk fermions is

$$\begin{aligned}\Psi_+(\omega, k; z) &= A_+ z^{\frac{3}{2}-m} + B_+ z^{\frac{5}{2}+m} + \dots, \\ \Psi_-(\omega, k; z) &= A_- z^{\frac{5}{2}-m} + B_- z^{\frac{3}{2}+m} + \dots,\end{aligned}\tag{2.9}$$

where $A_\pm(\omega, k)$, $B_\pm(\omega, k)$ are not all independent but related by the Dirac equation at the boundary

$$A_- = -\frac{i\mu}{(2m-1)}\gamma^0 A_+, \quad B_+ = -\frac{i\mu}{(2m+1)}\gamma^0 B_-.\tag{2.10}$$

The CFT Green's function then equals [11, 12, 34]

$$G_R = \lim_{z \rightarrow 0} z^{-2m} \frac{\Psi_-(z)}{\Psi_+(z)} - \text{singular} = \frac{B_-}{A_+}.\tag{2.11}$$

In other words B_- is the CFT response to the (infinitesimal) source A_+ . Since in the Green's function the fermion is a fluctuation, the functions $\Psi_\pm(z)$ are now probe solutions to the Dirac equation in a fixed gravitational and electrostatic background (for ease of presentation we are considering $\Psi_\pm(z)$ as numbers instead of two-component vectors). The boundary conditions at the horizon/AdS interior determine which Green's function one considers, e.g. infalling horizon boundary conditions yield the retarded Green's function. For non-zero chemical potential this fermionic Green's function can have a pole signalling the presence of a Fermi surface. This pole occurs precisely for a (quasi-)normalizable mode, i.e. a specific energy ω_F and momentum k_F where the external source $A_+(\omega, k)$ vanishes (for infalling boundary conditions at the horizon).

Knowing that the energy of the quasinormal mode is always $\omega_F = 0$ [11] and following [13], we expand G_R around $\omega = 0$ as:

$$G_R(\omega) = \frac{B_+^{(0)} + \omega B^{(1)+} + \dots}{A_+^{(0)} + \omega A_+^{(1)} + \dots}.\tag{2.12}$$

A crucial point is that in this expansion we are assuming that the pole will correspond to a stable quasiparticle, i.e. there are no fractional powers of ω less than unity in the expansion around $\omega_F = 0$ [13]. Fermions in AdS/CFT are of course famous for allowing more general pole-structures corresponding to Fermi-surfaces without stable quasiparticles [13], but those Green's functions are not of the type (2.1) and we shall therefore not consider them here. The specific Fermi momentum k_F associated with the Fermi surface is the momentum value for which the first ω -independent term in the denominator vanishes $A_+^{(0)}(k_F) = 0$ — for this value of $k = k_F$ the presence of a pole in the Green's functions at $\omega = 0$ is manifest. Writing $A_+^{(0)} = a_+(k - k_F) + \dots$ and comparing with the standard quasi-particle propagator,

$$G_R = \frac{Z}{\omega - \mu_R - v_F(k - k_F)} + \text{regular}\tag{2.13}$$

we read off that the pole-strength equals

$$Z = B_-^{(0)}(k_F)/A_+^{(1)}(k_F).$$

We thus see that a non-zero pole-strength is ensured by a non-zero value of $B_-(\omega = 0, k = k_F)$ — the “response” *without* corresponding source as $A^{(0)}(k_F) \equiv 0$. Quantitatively the pole-strength also depends on the value of $A_+^{(1)}(k_F) \equiv \partial_\omega A_+(k_F)|_{\omega=0}$, which is always finite. This is not a truly independent parameter, however. The size of the pole-strength has only a relative meaning w.r.t. to the integrated spectral density. This normalization of the pole strength is a global parameter rather than an AdS boundary issue. We now show this by proving that $A_+^{(1)}(k_F)$ is inversely proportional to $B_-^{(0)}(k_F)$ and hence Z is completely set by $B_-^{(0)}(k_F)$, i.e. $Z \sim |B_-^{(0)}(k_F)|^2$. Consider a transform $\widetilde{W}(\Psi_{+,A}, \Psi_{+,B})$ of the Wronskian $W(\Psi_{+,A}, \Psi_{+,B}) = \Psi_{+,A} \partial_z \Psi_{+,B} - (\partial_z \Psi_{+,A}) \Psi_{+,B}$ for two solutions to the second order equivalent of the Dirac equation for the field Ψ_+

$$(\partial_z^2 + P(z)\partial_z + Q_+(z)) \Psi_+ = 0 \tag{2.14}$$

that is conserved (detailed expressions for $P(z)$ and $Q_+(z)$ are given in eq. (2.21)):

$$\widetilde{W}(\Psi_{+,A}(z), \Psi_{+,B}(z), z; z_0) = \exp\left(\int_{z_0}^z P(z)\right) W(\Psi_{+,A}(z), \Psi_{+,B}(z)), \quad \partial_z \widetilde{W} = 0. \tag{2.15}$$

Here z_0 is the infinitesimal distance away from the boundary at $z = 0$ which is equivalent to the UV-cut-off in the CFT. Setting $k = k_F$ and choosing for $\Psi_{+,A} = A_+ z^{3/2-m} \sum_{n=0}^\infty a_n z^n$ and $\Psi_{+,B} = B_+ z^{5/2+m} \sum_{n=0}^\infty b_n z^n$ the real solutions which asymptote to solutions with $B_+(\omega, k_F) = 0$ and $A_+(\omega, k_F) = 0$ respectively, but for a value of ω infinitesimally away from $\omega_F = 0$, we can evaluate \widetilde{W} at the boundary to find,⁴

$$\widetilde{W} = z_0^3(1 + 2m)A_+B_+ = \mu z_0^3 A_+ B_- \tag{2.16}$$

The last step follows from the constraint (2.10) where the reduction from two-component spinors to functions means that γ^0 is replaced by one of its eigenvalues $\pm i$. Taking the derivative of \widetilde{W} at $\omega = 0$ for $k = k_F$ and expanding $A_+(\omega, k_F)$ and $B_-(\omega, k_F)$ as in (2.12), we can solve for $A_+^{(1)}(k_F)$ in terms of $B_-^{(0)}(k_F)$ and arrive at the expression for the pole strength Z in terms of $|B_-^{(0)}(k_F)|^2$:

$$Z = \frac{\mu z_0^3}{\partial_\omega \widetilde{W}|_{\omega=0, k=k_F}} |B_-^{(0)}(k_F)|^2. \tag{2.17}$$

Because $\partial_\omega \widetilde{W}$, as \widetilde{W} , is a number that is independent of z , this expression emphasizes that it is truly the nonvanishing subleading term $B_-^{(0)}(\omega_F, k_F)$ which sets the pole strength, up to a normalization $\partial_\omega \widetilde{W}$ which is set by the fully integrated spectral density. This integration is always UV-cut-off dependent and the explicit z_0 dependence should therefore

⁴ $P(z) = -3/z + \dots$ near $z = 0$

not surprise us.⁵ We should note that, unlike perturbative Fermi liquid theory, Z is a dimensionful quantity of mass dimension $2m + 1 = 2\Delta - 2$, which illustrates more directly its scaling dependence on the UV-energy scale z_0 . At the same time Z is real, as it can be shown that both $\partial_\omega \widetilde{W}|_{\omega=0, k=k_F} = \mu z_0^3 A_+^{(1)} B_-^{(0)}$ and $B_-^{(0)}$ are real [13].

2.1 The AdS dual of a stable Fermi liquid: applying Migdal’s relation holographically

We have thus seen that a solution with nonzero $B_-(\omega_F, k_F)$ whose corresponding external source vanishes (by definition of ω_F, k_F), is related to the presence of a quasiparticle pole in the CFT. Through Migdal’s theorem its pole strength is related to the presence of a discontinuity of the occupation number, and this discontinuity is normally taken as the characteristic signature of the presence of a Fermi Liquid. Qualitatively we can already infer that an AdS gravity solution with non-vanishing $B_-(\omega_F, k_F)$ corresponds to a Fermi Liquid in the CFT. We thus seek solutions to the Dirac equation with vanishing external source A_+ but non-vanishing response B_- coupled to electromagnetism (and gravity). The construction of the AdS black hole solution with a finite single fermion wavefunction is thus analogous to the construction of a holographic superconductor [19] with the role of the scalar field now taken by a Dirac field of mass m .

This route is complicated, however, by the spinor representation of the Dirac fields, and the related fermion doubling in AdS. Moreover, relativistically the fermion Green’s function is a matrix and the pole strength Z appears in the time-component of the vector projection $\text{Tr} \gamma^i G$. As we take this and the equivalent jump in occupation number to be the signifying characteristic of a Fermi liquid state in the CFT, it would be much more direct if we can derive an AdS radial evolution equation for the vector-projected Green’s function and hence the occupation number discontinuity directly. From the AdS perspective is also more convenient to work with bilinears such as Green’s functions, since the Dirac fields always couple pairwise to bosonic fields.

To do so, we start again with the two decoupled second order equations equivalent to the Dirac equation (2.7)

$$(\partial_z^2 + P(z)\partial_z + Q_\pm(z)) \Psi_\pm = 0 \tag{2.20}$$

⁵Using that \widetilde{W} is conserved, one can e.g. compute it at the horizon. There each solution $\Psi_{+,A}(\omega, k_F; z)$, $\Psi_{+,B}(\omega, k_F; z)$ is a linear combination of the infalling and outgoing solution

$$\begin{aligned} \Psi_{+,A}(z) &= \bar{\alpha} (1-z)^{-1/4+i\omega/4\pi T} + \alpha (1-z)^{-1/4-i\omega/4\pi T} + \dots \\ \Psi_{+,B}(z) &= \bar{\beta} (1-z)^{-1/4+i\omega/4\pi T} + \beta (1-z)^{-1/4-i\omega/4\pi T} + \dots \end{aligned} \tag{2.18}$$

yielding a value of $\partial_\omega \widetilde{W}$ equal to $(P(z) = 1/2(1-z) + \dots \text{ near } z=1)$

$$\partial_\omega \widetilde{W} = \frac{i}{2\pi T} \mathcal{N}(z_0) (\bar{\alpha}\beta - \bar{\beta}\alpha) \tag{2.19}$$

with $\mathcal{N}(z_0) = \exp \int_{z_0}^z dz \left[P(z) - \frac{1}{2(1-z)} \right]$.

with

$$\begin{aligned}
 P(z) &= (\mathcal{A}_- + \mathcal{A}_+) - [\partial_z, \mathcal{T}] \frac{\mathcal{T}}{T^2}, \\
 Q_{\pm}(z) &= \mathcal{A}_- \mathcal{A}_+ + (\partial_z \mathcal{A}_{\pm}) - [\partial_z, \mathcal{T}] \frac{\mathcal{T}}{T^2} \mathcal{A}_{\pm} + T^2.
 \end{aligned}
 \tag{2.21}$$

Note that both $P(z)$ and $Q_{\pm}(z)$ are matrices in spinor space. The general solution to this second order equation — with the behavior at the horizon/interior appropriate for the Green’s function one desires — is a matrix valued function $(M_{\pm}(z))^{\alpha}_{\beta}$ and the field $\Psi_{\pm}(z)$ equals $\Psi_{\pm}(z) = M_{\pm}(z)\Psi_{\pm}^{(\text{hor})}$. Due to the first order nature of the Dirac equation the horizon values $\Psi_{\pm}^{(\text{hor})}$ are not independent but related by a z -independent matrix $S\Psi_+^{(\text{hor})} = \Psi_-^{(\text{hor})}$, which can be deduced from the near-horizon behavior of (2.10); specifically $S = \gamma^0$. One then obtains the Green’s function from the on-shell boundary action (see e.g. [12, 35])

$$S_{\text{bnd}} = \oint_{z=z_0} d^d x \bar{\Psi}_+ \Psi_- \tag{2.22}$$

as follows: Given a boundary source ζ_+ for $\Psi_+(z)$, i.e. $\Psi_+(z_0) \equiv \zeta_+$, one concludes that $\Psi_+^{(\text{hor})} = M_+^{-1}(z_0)\zeta_+$ and thus $\Psi_+(z) = M_+(z)M_+^{-1}(z_0)\zeta_+$, $\Psi_-(z) = M_-(z)SM_+^{-1}(z_0)\zeta_+$. Substituting these solutions into the action gives

$$S_{\text{bnd}} = \oint_{z=z_0} d^d x \bar{\zeta}_+ M_-(z_0) S M_+^{-1}(z_0) \zeta_+ \tag{2.23}$$

The Green’s function is obtained by differentiating w.r.t. $\bar{\zeta}_+$ and ζ_+ and discarding the conformal factor z_0^{2m} with m the AdS mass of the Dirac field (one has to be careful for $mL > 1/2$ with analytic terms [35])

$$G = \lim_{z_0 \rightarrow 0} z_0^{-2m} M_-(z_0) S M_+^{-1}(z_0). \tag{2.24}$$

Since $M_{\pm}(z)$ are determined by evolution equations in z , it is clear that the Green’s function itself is also determined by an evolution equation in z , i.e. there is some function $G(z)$ which reduces in the limit $z \rightarrow 0$ to $z_0^{2m}G$. One obvious candidate is the function

$$G^{(\text{obv})}(z) = M_-(z) S M_+^{-1}(z). \tag{2.25}$$

Using the original Dirac equations one can see that this function obeys the non-linear evolution equation

$$\partial_z G^{(\text{obv})}(z) = -\mathcal{A}_- G^{(\text{obv})}(z) - \mathcal{T} M_+ S M_+^{-1} + \mathcal{A}_+ G^{(\text{obv})}(z) + G^{(\text{obv})}(z) \mathcal{T} G^{(\text{obv})}(z). \tag{2.26}$$

This is the approach used in [11], where a specific choice of momenta is chosen such that M_+ commutes with S . For a generic choice of momenta, consistency requires that one also considers the evolution equation for $M_+(z)S M_+^{-1}(z)$.

There is, however, another candidate for the extension $G(z)$ which is based on the underlying boundary action. Rather than extending the kernel $M_-(z_0)M_+^{-1}(z_0)$ of the boundary action we extend the constituents of the action itself, based on the individual

fermion wavefunctions $\Psi_{\pm}(z) = M_{\pm}(z)S^{\frac{1}{2}\mp\frac{1}{2}}M_{\pm}^{-1}(z_0)$. We define an extension of the matrix $G(z)$ including an expansion in the complete set $\Gamma^I = \{\mathbb{1}, \gamma^i, \gamma^{ij}, \dots, \gamma^{i_1, i_d}\}$ (with $\gamma^4 = i\gamma^0$)

$$G^I(z) = \bar{M}_+^{-1}(z_0)\bar{M}_+(z)\Gamma^I M_-(z)SM_+^{-1}(z_0), \quad G^I(z_0) = \Gamma^I G(z_0) \quad (2.27)$$

where $\bar{M} = i\gamma^0 M^\dagger i\gamma^0$. Using again the original Dirac equations, this function obeys the evolution equation

$$\partial_z G^I(z) = -(\bar{\mathcal{A}}_+ + \mathcal{A}_-)G^I(z) - \bar{M}_{+,0}^{-1}\bar{M}_-(z)\bar{\mathcal{T}}\Gamma^I M_-(z)SM_{+,0}^{-1} + \bar{M}_{+,0}^{-1}\bar{M}_+(z)\Gamma^I \mathcal{T}M_+(z)SM_{+,0}^{-1} \quad (2.28)$$

Recall that $\mathcal{T}\gamma^{i_1 \dots i_p} = \mathcal{T}^{[i_1 \gamma \dots i_p]} + \mathcal{T}_j \gamma^{j i_1 \dots i_p}$. It is then straightforward to see that for consistency, we also need to consider the evolution equations of

$$\mathcal{J}_+^I = \bar{M}_{+,0}^{-1}\bar{M}_+(z)\Gamma^I M_+(z)SM_{+,0}^{-1}, \quad \mathcal{J}_-^I = \bar{M}_{+,0}^{-1}\bar{M}_-(z)\Gamma^I M_-(z)SM_{+,0}^{-1}$$

and

$$\bar{G}^I = \bar{M}_{+,0}^{-1}\bar{M}_-(z)\Gamma^I M_+(z)SM_{+,0}^{-1}.$$

They are

$$\begin{aligned} \partial_z \mathcal{J}_+^{i_1 \dots i_p}(z) &= -2\text{Re}(\mathcal{A}_+) \mathcal{J}_+^{i_1 \dots i_p} - \bar{\mathcal{T}}^{[i_1 \bar{G}^{i_2 \dots i_p]}(z) \\ &\quad - \bar{\mathcal{T}}_j \bar{G}^{j i_1 \dots i_p}(z) - G^{[i_1 \dots i_{p-1}}(z) \mathcal{T}^{i_p]} - G^{i_1 \dots i_p j}(z) \mathcal{T}_j \\ \partial_z \mathcal{J}_-^{i_1 \dots i_p}(z) &= -2\text{Re}(\mathcal{A}_-) \mathcal{J}_-^{i_1 \dots i_p} + \bar{\mathcal{T}}^{[i_1 G^{i_2 \dots i_p]}(z) \\ &\quad + \bar{\mathcal{T}}_j G^{j i_1 \dots i_p}(z) + \bar{G}^{[i_1 \dots i_{p-1}}(z) \mathcal{T}^{i_p]} + \bar{G}^{i_1 \dots i_p j}(z) \mathcal{T}_j \\ \partial_z \bar{G}^{i_1 \dots i_p}(z) &= -(\bar{\mathcal{A}}_- + \mathcal{A}_+) \bar{G}^{i_1 \dots i_p} - \bar{\mathcal{T}}^{[i_1 \mathcal{J}_+^{i_2 \dots i_p]}(z) \\ &\quad - \bar{\mathcal{T}}_j \mathcal{J}_+^{j i_1 \dots i_p}(z) - \mathcal{J}_-^{[i_1 \dots i_{p-1}}(z) \mathcal{T}^{i_p]} + \mathcal{J}_-^{i_1 \dots i_p j}(z) \mathcal{T}_j \end{aligned} \quad (2.29)$$

The significant advantage of these functions G^I , \bar{G}^I , \mathcal{J}_\pm^I is that the evolution equations are now linear. This approach may seem overly complicated. However, if the vector \mathcal{T}^i happens to only have a single component nonzero, then the system reduces drastically to the four fields \mathcal{J}_\pm^i , $G^\mathbb{1}$, $\bar{G}^\mathbb{1}$. We shall see below that a similar drastic reduction occurs, when we consider only spatially and temporally averaged functions $J^I = \int dt d^2x \mathcal{J}_\pm^I$.

Now the two extra currents \mathcal{J}_\pm^I have a clear meaning in the CFT. The current $G^I(z)$ reduces by construction to Γ^I times the Green's function $G^\mathbb{1}(z_0)$ on the boundary, and clearly $\bar{G}^I(z)$ is its hermitian conjugate. The current \mathcal{J}_+^I reduces at the boundary to $\mathcal{J}_+^I = \Gamma^I M_{+,0} SM_{+,0}^{-1}$. Thus \mathcal{J}_+^I sets the normalization of the linear system (2.29). The interesting current is the current \mathcal{J}_-^I . Using that $\bar{S} = S^{-1}$, it can be seen to reduce on the boundary to the combination $\bar{\mathcal{J}}_+^\mathbb{1} \bar{G}^\mathbb{1} \Gamma^I G^\mathbb{1}$. Thus, $(\bar{\mathcal{J}}_+^\mathbb{1})^{-1} \mathcal{J}_-^\mathbb{1}$ is the norm squared of the Green's function, i.e. the probability density of the off-shell process.

For an off-shell process or a correlation function the norm-squared has no real functional meaning. However, we are specifically interested in solutions in the absence of an external source, i.e. the *on-shell* correlation functions. In that case the analysis is quite different. The on-shell condition is equivalent to choosing momenta to saturate the pole in the Green's function, i.e. it is precisely choosing dual AdS solutions whose leading external source A_\pm

vanishes. Then M_+ and M_- are no longer independent, but $M_{+,0} = \delta B_+ / \delta \Psi_+^{(\text{hor})} = -\frac{i\mu\gamma^0}{2m+1} M_{-,0} S$. As a consequence all boundary values of $\mathcal{J}_-^I(z_0), G^I(z_0), \bar{G}^I(z_0)$ become proportional; specifically using $S = \gamma^0$ one has that

$$\mathcal{J}_-^0(z_0)|_{\text{on-shell}} = \frac{(2m+1)}{\mu} \gamma^0 G^{\mathbb{I}}(z_0)|_{\text{on-shell}} \quad (2.30)$$

is the ‘‘on-shell’’ Green’s function. Now, the meaning of the on-shell correlation function is most evident in thermal backgrounds. It equals the density of states $\rho(\omega(k)) = -\frac{1}{\pi} \text{Im} G_R$ times the Fermi-Dirac distribution [36]

$$\text{Tr} i \gamma^0 G_F^t(\omega_{\text{bare}}(k), k)|_{\text{on-shell}} = 2\pi f_{FD} \left(\frac{\omega_{\text{bare}}(k) - \mu}{T} \right) \rho(\omega_{\text{bare}}(k)) \quad (2.31)$$

For a Fermi liquid with the defining off-shell Green’s function (2.1) $\omega_{\text{bare}}(k_F) - \mu \equiv \omega = 0$ and $\rho(\omega_{\text{bare}}(k)) = Z_{z_0} \delta^2(k - k_F) \delta(\omega) + \dots$. Thus we see that the boundary value of $\mathcal{J}_-^{(0)}(z_0)|_{\text{on-shell}} = Z f_{FD}(0) \delta^3(0)$ indeed captures the pole strength directly times a product of distributions. This product of distributions can be absorbed in setting the normalization. An indication that this is correct is that the determining equations for $G^I, \bar{G}^I, \mathcal{J}_\pm^I$ remain unchanged if we multiply $G^I, \bar{G}^I, \mathcal{J}_\pm^I$ on both sides with $M_{+,0}$. If $M_{+,0}$ is unitary it is just a similarity transformation. However, from the definition of the Green’s function, one can see that this transformation precisely removes the pole. This ensures that we obtain finite values for $G^I, \bar{G}^I, \mathcal{J}_\pm^I$ at the specific pole-values ω_F, k_F where the distributions would naively blow up.

2.1.1 Boundary conditions and normalizability

We have shown that a normalizable solution to \mathcal{J}_-^0 from the equations (2.29) correctly captures the pole strength directly. However, ‘normalizable’ is still defined in terms of an absence of a source for the fundamental Dirac field Ψ_\pm rather than the composite fields \mathcal{J}_\pm^I and G^I . One would prefer to determine normalizability directly from the boundary behavior of the composite fields. This can be done. Under the assumption that the electrostatic potential Φ is regular, i.e.

$$\Phi = \mu - \rho z + \dots \quad (2.32)$$

the ‘‘connection’’ \mathcal{T}^I is subleading to the connection \mathcal{A} near $z = 0$. Thus the equations of motion near $z = 0$ do not mix the various \mathcal{J}_\pm^I, G^I and the composite fields behave as

$$\begin{aligned} \mathcal{J}_+^I &= j_{3-2m}^I z^{3-2m} + j_{4+}^I z^4 + j_{5+2m}^I z^{5+2m} + \dots, \\ \mathcal{J}_-^I &= j_{5-2m}^I z^{5-2m} + j_{4-}^I z^4 + j_{3+2m}^I z^{3+2m} + \dots, \\ G^I &= I_{4-2m}^I z^{4-2m} + I_3^I z^3 + I_{4+2m}^I z^{4+2m} + I_5^I z^5 + \dots, \end{aligned} \quad (2.33)$$

with the identification

$$\begin{aligned} j_{3-2m}^I &= \bar{A}_+ \Gamma^I A_+, & j_{4+}^I &= \bar{A}_+ \Gamma^I B_+ + \bar{B}_+ \Gamma^I A_+, & j_{5+2m}^I &= \bar{B}_+ \Gamma^I B_+, \\ j_{3+2m}^I &= \bar{A}_- \Gamma^I A_-, & j_{4-}^I &= \bar{A}_- \Gamma^I B_- + \bar{B}_- \Gamma^I A_-, & j_{5-2m}^I &= \bar{B}_- \Gamma^I B_-, \\ I_{4-2m}^I &= \bar{A}_+ \Gamma^I A_-, & I_3^I &= \bar{A}_+ \Gamma^I B_-, & I_{4+2m}^I &= \bar{B}_+ \Gamma^I B_-, & I_5^I &= \bar{B}_+ \Gamma^I A_-. \end{aligned} \quad (2.34)$$

A ‘normalizable’ solution in \mathcal{J}_-^I and thus \mathcal{J}_-^0 is therefore defined by the vanishing of *both* the leading *and* the subleading term.

3 An AdS black hole with Dirac hair

Having determined a set of AdS evolution equations and boundary conditions that compute the pole strength Z directly through the currents $\mathcal{J}_-^{(0)}(z)$ and $G^I(z)$, we can now try to construct the AdS dual of a system with finite fermion density, including backreaction. As we remarked in the beginning of section 2.1, the demand that the solutions be normalizable means that the construction of the AdS black hole solution with a finite single fermion wavefunction is analogous to the construction of a holographic superconductor [19] with the role of the scalar field now taken by the Dirac field. The starting point therefore is the charged AdS₄ black-hole background (2.4) and we should show that at low temperatures this AdS Reissner-Nordström black hole is unstable towards a solution with a finite Dirac profile. We shall do so in a simplified “large charge” limit where we ignore the gravitational dynamics, but as is well known from holographic superconductor studies (see e.g. [19–21]) this limit already captures much of the essential physics. In a companion article [37] we will construct the full backreacted ground state including the gravitational dynamics.

In this large charge non-gravitational limit the equations of motion for the action (2.3) reduce to those of U(1)-electrodynamics coupled to a fermion with charge g in the background of this black hole:

$$\begin{aligned} D_M F^{MN} &= ig e_A^N \bar{\Psi} \Gamma^A \Psi, \\ 0 &= e_A^M \Gamma^A (D_M + ieg A_M) \Psi + m \Psi. \end{aligned} \tag{3.1}$$

Thus the vielbein e_A^M and covariant derivative D_M remain those of the fixed charged AdS black hole metric (2.4), but the vector-potential now contains a background piece $A_0^{(bg)}$ plus a first-order piece $A_M = A_M^{(bg)} + A_M^{(1)}$, which captures the effect of the charge carried by the fermions.

Following our argument set out in previous section that it is more convenient to work with the currents $\mathcal{J}_\pm^I(z), G^I(z)$ instead of trying to solve the Dirac equation directly, we shall first rewrite this coupled non-trivial set of equations of motion in terms of the currents while at the same time using symmetries to reduce the complexity. Although a system at finite fermion density need not be homogeneous, the Fermi liquid ground state is. It therefore natural to make the ansatz that the final AdS solution is static and preserves translation and rotation along the boundary. As the Dirac field transforms non-trivially under rotations and boosts, we cannot make this ansatz in the strictest sense. However, in some average sense which we will make precise, the solution should be static and translationally invariant. Then translational and rotational invariance allow us to set $A_i = 0$, $A_z = 0$, whose equations of motions will turn into constraints for the remaining degrees of freedom. Again denoting $A_0 = \Phi$, the equations reduce to the following after the projection

onto $\Psi_{\pm} = \frac{1}{2}(1 \pm \Gamma^Z)\Psi$.

$$\begin{aligned} \partial_z^2 \Phi &= \frac{-gL^3\alpha}{z^3\sqrt{f}} (\bar{\Psi}_+ i\gamma^0 \Psi_+ + \bar{\Psi}_- i\gamma^0 \Psi_-), \\ (\partial_z + \mathcal{A}_{\pm}) \Psi_{\pm} &= \mp \mathcal{T} \Psi_{\mp} \end{aligned} \quad (3.2)$$

with

$$\begin{aligned} \mathcal{A}_{\pm} &= -\frac{1}{2z} \left(3 - \frac{zf'}{2f} \right) \pm \frac{mL}{z\sqrt{f}}, \\ \mathcal{T} &= \frac{i(-\omega + g\Phi)}{\alpha f} \gamma^0 + \frac{i}{\alpha\sqrt{f}} k_i \gamma^i. \end{aligned} \quad (3.3)$$

as before.

The difficult part is to “impose” staticity and rotational invariance for the non-invariant spinor. This can be done by rephrasing the dynamics in terms of fermion current bilinears, rather than the fermions themselves. We shall first do so rather heuristically, and then show that the equations obtained this way are in fact the flow equations for the Green’s functions and composites $\mathcal{J}^I(z)$, $G^I(z)$ constructed in the previous section. In terms of the local vector currents⁶

$$J_{+}^{\mu}(x, z) = \bar{\Psi}_{+}(x, z) i\gamma^{\mu} \Psi_{+}(x, z), \quad J_{-}^{\mu}(x, z) = \bar{\Psi}_{-}(x, z) i\gamma^{\mu} \Psi_{-}(x, z), \quad (3.4)$$

or equivalently

$$J_{+}^{\mu}(p, z) = \int d^3k \bar{\Psi}_{+}(-k, z) i\gamma^{\mu} \Psi_{+}(p+k, z), \quad J_{-}^{\mu}(p, z) = \int d^3k \bar{\Psi}_{-}(-k, z) i\gamma^{\mu} \Psi_{-}(p+k, z). \quad (3.5)$$

rotational invariance means that spatial components J_{\pm}^i should vanish on the solution — this solves the constraint from the A_i equation of motion, and the equations can be rewritten in terms of J_{\pm}^0 only. Staticity and rotational invariance in addition demand that the bilinear momentum p_{μ} vanish. In other words, we are only considering temporally and spatially averaged densities: $J_{\pm}^{\mu}(z) = \int dt d^2x \bar{\Psi}(t, x, z) i\gamma^{\mu} \Psi(t, x, z)$. Analogous to the bilinear flow equations for the Green’s function, we can act with the Dirac operator on the currents to obtain an effective equation of motion, and this averaging over the relative frequencies ω and momenta k_i will set all terms with explicit k_i -dependence to zero.⁷

⁶In our conventions $\bar{\Psi} = \Psi^{\dagger} i\gamma^0$.

⁷To see this consider

$$(\partial + 2\mathcal{A}_{\pm}) \Psi_{\pm}^{\dagger}(-k) \Psi_{\pm}(k) = \mp \frac{\Phi}{f} (\Psi_{-}^{\dagger} i\gamma^0 \Psi_{+} + \Psi_{+}^{\dagger} i\gamma^0 \Psi_{-}) + \frac{ik_i}{\sqrt{f}} (\Psi_{-}^{\dagger} \gamma^i \Psi_{+} - \Psi_{+}^{\dagger} \gamma^i \Psi_{-}). \quad (3.6)$$

The term proportional to Φ is relevant for the solution. The dynamics of the term proportional to k_i is

$$(\partial + \mathcal{A}_{+} + \mathcal{A}_{-}) (\Psi_{-}^{\dagger} \gamma^i \Psi_{+} - \Psi_{+}^{\dagger} \gamma^i \Psi_{-}) = -2i \frac{k^i}{\sqrt{f}} (\Psi_{+}^{\dagger} \gamma^0 \Psi_{+} + \Psi_{-}^{\dagger} \gamma^0 \Psi_{-}). \quad (3.7)$$

The integral of the r.h.s. over k^i vanishes by the assumption of translational and rotational invariance. Therefore the l.h.s. of (3.7) and thus the second term in eq. (3.6) does so as well.

Restricting to such averaged currents and absorbing a factor of g/α in Φ and a factor of $g\sqrt{L^3}$ in Ψ_{\pm} , we obtain effective equations of motion for the bilinears directly

$$\begin{aligned} (\partial_z + 2\mathcal{A}_{\pm}) J_{\pm}^0 &= \mp \frac{\Phi}{f} I, \\ (\partial_z + \mathcal{A}_+ + \mathcal{A}_-) I &= \frac{2\Phi}{f} (J_+^0 - J_-^0), \\ \partial_z^2 \Phi &= -\frac{1}{z^3 \sqrt{f}} (J_+^0 + J_-^0), \end{aligned} \tag{3.8}$$

with $I = \bar{\Psi}_- \Psi_+ + \bar{\Psi}_+ \Psi_-$, and all fields are real. The remaining constraint from the A_z equation of motion decouples. It demands $\text{Im}(\bar{\Psi}_+ \Psi_-) = \frac{i}{2}(\bar{\Psi}_- \Psi_+ - \bar{\Psi}_+ \Psi_-) = 0$. What the equations (3.8) tell us is that for nonzero J_{\pm}^0 there is a charged electrostatic source for the vector potential Φ in the bulk.

Momentarily we will motivate the effective equations (3.8) at a more fundamental level. Before that there are several remarks to be made

- These equations contain more information than just current conservation $\partial_{\mu} J^{\mu} = 0$. In an isotropic and static background current conservation is trivially true as $\partial_{\mu} J^{\mu} = \partial_0 J^0 = -i \int d\omega e^{-i\omega t} \omega J^0(\omega) = 0$ as $J^0(\omega \neq 0) = 0$.
- We have scaled out the electromagnetic coupling. AdS₄/CFT₃ duals for which the underlying string theory is known generically have $g = \kappa/L$ with κ the gravitational coupling constant as defined in (2.3). Thus, using standard AdS₄/CFT₃ scaling, a finite charge in the new units translates to a macroscopic original charge of order $L/\kappa \propto N^{1/3}$. This large charge demands that backreaction of the fermions in terms of its bilinear is taken into account as a source for Φ .
- The equations are local. From the fundamental point of view, that one considers finite density in the bulk, this is strange to say the least. Generic multi-fermion configurations are non-local, see e.g. [38]. These equations can therefore never capture the full bulk fermion dynamics. Our starting point has been a single fermion perspective, where the Pauli blocking induced non-locality is absent. In that context local equations are fine. We have also explicitly averaged over all directions parallel to the boundary and, as we have shown in the previous section (see also footnote 7), it is this averaging that tremendously simplifies the equations. The most curious part may be that this unaveraged set of equations — and therefore also eqs (3.8) — are all local in the radial direction z . From the AdS perspective a many-fermion system should be non-local democratically and thus also exhibit non-locality in z , yet from the CFT perspective where z -dynamics encode RG-flow, it is eminently natural. We leave the resolution of this paradox to future work.

The justification of using (3.8) to construct the AdS dual of a regular Fermi liquid is the connection between local fermion bilinears and the CFT Green's function. The complicated flow equations (2.29) reduce precisely to the first two equations in (3.8) upon performing the spacetime averaging and the trace, i.e. $J_{\pm}^0 = \int d^3k \text{Tr} \mathcal{J}_{\pm}^0$ and $I = \int d^3k \text{Tr} (G^{\mathbb{1}} + \bar{G}^{\mathbb{1}})$.

Combined with the demand that we only consider normalizable solutions and the proof that \mathcal{J}_\pm^0 is proportional to the pole-strength, the radial evolution equations (3.8) are the (complicated) AdS recasting of the RG-flow for the pole-strength. This novel interpretation ought to dispel some of the a priori worries about our unconventional treatment of the fermions through their semi-classical bilinears. There is also support from the gravity side, however. Recall that for conventional many-body systems and fermions in particular one first populates a certain set of states and then tries to compute the macroscopic properties of the collective. In a certain sense the equations (3.8) formulate the same program but in opposite order: one computes the generic wavefunction charge density with and by imposing the right boundary conditions, i.e. normalizability, one selects only the correct set of states. This follows directly from the equivalence between normalizable AdS modes and quasiparticle poles that are characterized by well defined distinct momenta k_F (for $\omega = \omega_F \equiv 0$). The demand that any non-trivial Dirac hair black hole is constructed from normalizable solutions of the composite operators (i.e. their leading and subleading asymptotes vanish⁸) thus means that one imposes a superselection rule on the spatial averaging in the definition of J_\pm^I :

$$\begin{aligned} J_\pm^0(z)|_{\text{normalizable}} &\equiv \int d^3k \bar{\Psi}_\pm(-k) i\gamma^0 \Psi_\pm(k)|_{\text{normalizable}} \\ &= \int d^3k \delta^2(|k| - |k_F|) |B_\pm^{(0)}(k)|^2 z^{4+2m\pm 1} + \dots \end{aligned} \quad (3.9)$$

We see that the constraint of normalizability from the bulk point of the view, implies that one selects precisely the on-shell bulk fermion modes as the building blocks of the density J_\pm^0 .

In turn this means that the true system that eqs. (3.8) describe is somewhat obscured by the spatial averaging. Clearly even a single fermion wavefunction is in truth the full set of two-dimensional wavefunctions whose momentum k^i has length k_F . However, the averaging could just as well be counting more, as long as there is another set of normalizable states once the isotropic momentum surface $|k| = |k_F|$ is filled. Pushing this thought to the extreme, one could even speculate that the system (3.8) gives the correct quantum-mechanical description of the many-body Fermi system: the system which gravitational reasoning suggests is the true ground state of the charged AdS black hole in the presence of fermions.

To remind us of the ambiguity introduced by spatial averaging, we shall give the boundary coefficient of normalizable solution for $J_-^0 = \int d^3k \mathcal{J}_-^0$ a separate name. The quantity $\mathcal{J}_\pm^0(z_0)$ is proportional to the pole strength, which via Migdal's relation quantifies the characteristic occupation number discontinuity at $\omega_F \equiv 0$. We shall therefore call the coefficient $\int d^3k |B_-|^2|_{\text{normalizable}} = \Delta n_F$.

⁸One can verify that the discussion in section 2.1.1 holds also for fully backreacted solutions. The derivation there builds on the assumption that the boundary behavior of the electrostatic potential is regular. It is straightforward to check in (3.8) that indeed precisely for normalizable solutions, i.e. in the absence of explicit fermion-sources, when both the leading and subleading terms in J_\pm^0 and I vanish, the boundary behavior the scalar potential remains regular, as required.

3.1 Thermodynamics

At a very qualitative level the identification $J_-^0|_{norm}(z) \equiv \Delta n_F z^{3+2m} + \dots$ can be argued to follow from thermodynamics as well. From the free energy for an AdS dual solution to a Fermi liquid, one finds that the charge density directly due to the fermions is

$$\rho_{\text{total}} = -2 \frac{\partial}{\partial \mu} F = \frac{-3}{2m+1} \frac{\Delta n_F}{z_0^{-1-2m}} + \rho + \dots, \quad (3.10)$$

with z_0^{-1} the UV-cutoff as before. The cut-off dependence is a consequence of the fact that the system is interacting, and one cannot truly separate out the fermions as free particles. Were one to substitute the naive free fermion scaling dimension $\Delta = m + 3/2 = 1$, the cutoff dependence would vanish and the identification would be exact.

We can thus state that in the interacting system there is a contribution to the charge density from a finite number of fermions proportional to

$$\rho_F = \frac{-3}{2\Delta - 2} \frac{\Delta n_F}{z_0^{2-2\Delta}} + \dots, \quad (3.11)$$

although this contribution formally vanishes in the limit where we send the UV-cutoff z_0^{-1} to infinity.

To derive eq. (3.10), recall that the free energy is equal to minus the on-shell action of the AdS dual theory. Since we disregard the gravitational backreaction, the Einstein term in the AdS theory will not contain any relevant information and we consider the Maxwell and Dirac term only. We write the action as,

$$S = \int_{z_0}^1 \sqrt{-g} \left[\frac{1}{2} A_N D_M F^{MN} - \bar{\Psi} \not{D} \Psi - m \bar{\Psi} \Psi \right] + \oint_{z=z_0} \sqrt{-h} \left(\bar{\Psi}_+ \Psi_- + \frac{1}{2} A_\mu n_\alpha F^{\alpha\mu} \right), \quad (3.12)$$

where we have included an explicit fermionic boundary term that follows from the AdS/CFT dictionary [12] and n_α is a normal vector to the boundary. The boundary action is not manifestly real, but its on-shell value which contributes to the free energy is real. Recall that the imaginary part of $\bar{\Psi}_+ \Psi_-$ decouples from eqs. (3.8). The boundary Dirac term in (3.12) is therefore equal to $I = 2\text{Re}(\bar{\Psi}_+ \Psi_-)$.

To write the free energy in terms of the quantities μ , ρ and Δn_F , note that the on-shell bulk Dirac action vanishes. Importantly the bulk Maxwell action does contribute to the free energy. Its contribution is

$$\begin{aligned} F_{\text{bulk}} &= \lim_{z_0 \rightarrow 0} \int_{z_0}^1 dz d^3x \left[\frac{1}{2} \Phi \partial_{zz} \Phi \right]_{\text{on-shell}} \\ &= - \lim_{z_0 \rightarrow 0} \int_{z_0}^1 dz d^3x \left[\frac{1}{2z^3 \sqrt{f}} \Phi (J_+^0 + J_-^0) \right]_{\text{on-shell}}, \end{aligned} \quad (3.13)$$

where we have used the equation of motion (3.8). This contribution should be expected, since the free energy should be dominated by infrared, i.e. near horizon physics. Due to the logarithmic singularity in the electrostatic potential (eq. (3.17)) this bulk contribution diverges, but this divergence should be compensated by gravitational backreaction. At the same time the singularity is so mild, however, that the free energy, the integral of the Maxwell term, remains finite in the absence of the Einstein contribution.

Formally, i.e. in the limit $z_0 \rightarrow 0$, the full free energy arises from this bulk contribution (3.13). The relation (3.10) between the charge density and Δn_F follows only from the regularized free energy, and is therefore only a qualitative guideline. Empirically, as we will show, it is however, a very good one (see figure 1 in the next section). Splitting the regularized bulk integral in two

$$F_{\text{bulk}} = \int_{z^*}^1 dz d^3x \left[\frac{1}{2z^3 \sqrt{f}} \Phi(J_+^0 + J_-^0) \right]_{\text{on-shell}} + \lim_{z_0 \rightarrow 0} \int_{z_0}^{z^*} dz d^3x \left[\frac{1}{2z^3 \sqrt{f}} \Phi(J_+^0 + J_-^0) \right]_{\text{on-shell}}, \quad (3.14)$$

we substitute the normalizable boundary behavior of $\Psi_+ = B_+ z^{5/2+m} + \dots$, $\Psi_- = B_- z^{3/2+m} + \dots$ and $\Phi = \mu - \rho z + \dots$, and obtain for the regularized free energy

$$F = F_{\text{horizon}}(z_*) + \lim_{z_0 \rightarrow 0} \int_{z_0}^{z^*} d^3x dz \left[\frac{-1}{2z^3} \mu |B_-|^2 z^{3+2m} + \dots \right] + \oint \frac{d^3x}{z_0^3} \left[-\bar{B}_+ B_- z_0^{4+2m} + \frac{1}{2} \mu \rho z_0^3 \right]. \quad (3.15)$$

Using that $B_+ = -i\mu\gamma^0 B_- / (2m+1)$ (eq. (2.10)), the second bulk term and boundary contribution are proportional, and the free energy schematically equals

$$F = F^{\text{horizon}} + \lim_{z_0 \rightarrow 0} \int d^3x \left[\frac{3\mu}{2(2m+1)} \bar{B}_- i\gamma^0 B_- z_0^{1+2m} - \frac{1}{2} \mu \rho \right]. \quad (3.16)$$

With the UV-regulator z_0^{-1} finite, this yields the charge density in eq. (3.10) after one recalls that $\bar{B}_- = B_-^\dagger i\gamma^0$.

With the derived rule that the AdS dual to a Fermi liquid has a nonzero normalizable component in the current J_-^0 , we will now construct an AdS solution that has this property: an AdS black hole with Dirac hair. Ignoring backreaction, these are solutions to the density equations (3.8). In its simplest form the interpretation is that of the backreaction due to a single fermion wavefunction, but as explained the spatial averaging of the density combined with the selection rule of normalizability could be capturing a more general solution.

3.2 At the horizon: entropy collapse to a Lifshitz solution

Before we can proceed with the construction of non-trivial Dirac hair solutions to eqs. (3.8), we must consider the boundary conditions at the horizon necessary to solve the system. Insisting that the right-hand-side of the dynamical equations (3.8) is subleading at the horizon, the near-horizon behavior of J_\pm^0 , I , Φ is:

$$\begin{aligned} J_\pm^0 &= J_{\text{hor},\pm} (1-z)^{-1/2} + \dots, \\ I &= I_{\text{hor}} (1-z)^{-1/2} + \dots, \\ \Phi &= \Phi_{\text{hor}}^{(1)} (1-z) \ln(1-z) + (\Phi_{\text{hor}}^{(2)} - \Phi_{\text{hor}}^{(1)}) (1-z) + \dots \end{aligned} \quad (3.17)$$

If we insist that Φ is regular at the horizon $z = 1$, i.e. $\Phi_{\text{hor}}^{(1)} = 0$, so that the electric field is finite, the leading term in J_\pm^0 must vanish as well, i.e. $J_{\text{hor},\pm} = 0$, and the system reduces to a free Maxwell field in the presence of an AdS black hole and there is no fermion density profile in the bulk. Thus in order to achieve a nonzero fermion profile in the bulk, we must have an explicit source for the electric-field on the horizon. Strictly speaking, this

invalidates our neglect of backreaction as the electric field and its energy density at the location of the source will be infinite. As we argued above, this backreaction is in fact expected to resolve the finite ground-state entropy problem associated with the presence of a horizon. The backreaction should remove the horizon completely, and the background should resemble the horizonless metrics found in [26, 27, 39]; the same horizon logarithmic behavior in the electrostatic potential was noted there. Nevertheless, as the divergence in the electric field only increases logarithmically as we approach the horizon, and our results shall hinge on the properties of the equations at the opposite end near the boundary, we shall continue to ignore it here. We shall take the sensibility of our result after the fact, as proof that the logarithmic divergence at the horizon is indeed mild enough to be ignored.

The identification of the boundary value of J_-^0 with the Fermi liquid characteristic occupation number jump Δn_F rested on the insistence that the currents are built out of AdS Dirac fields. This deconstruction also determines a relation between the horizon boundary conditions of the composite fields J_{\pm}^0 , I . If $\Psi_{\pm}(z) = C_{\pm}(1-z)^{-1/4} + \dots$ then $J_{\text{hor},\pm} = C_{\pm}^2$ and $I_{\text{hor}} = C_+C_-$. As the solution $\Phi_{\text{hor}}^{(1)}$ is independent of the solution $\Phi_{\text{hor}}^{(2)}$ which is regular at the horizon, we match the latter to the vector-potential of the charged AdS black hole: $\Phi_{\text{hor}}^{(2)} = -2gq \equiv g\mu_0/\alpha$. Recalling that $\Phi_{\text{hor}}^{(1)} = -(J_{\text{hor},+} + J_{\text{hor},-})$, we see that the three-parameter family of solutions at the horizon in terms of C_{\pm} , $\Phi_{\text{hor}}^{(2)}$ corresponds to the three-parameter space of boundary values A_+ , B_- and μ encoding a fermion-source, the fermion-response/expectation value and the chemical potential.

We can now search whether within this three-parameter family a finite normalizable fermion density solution with vanishing source $A_+ = 0$ exists for a given temperature T of the black hole.

3.3 A BH with Dirac hair

The equations are readily solved numerically with a shooting method from the horizon. We consider both an uncharged AdS-Schwarzschild solution and the charged AdS Reissner-Nordström solution. Studies of bosonic condensates in AdS/CFT without backreaction have mostly been done in the AdS-Schwarzschild (AdSS) background ([19, 20] and references therein). An exception is [40], which also considers the charged RN black hole. As is explained in [40], they correspond to two different limits of the exact solution: the AdSS case requires that $\Delta n_F \gtrsim \mu$ that is, the total charge of the matter fields should be dominant compared to the charge of the black hole. On the other hand, the RN limit is appropriate if $\Delta n_F \ll \mu$. It ignores the effect of the energy density of the charged matter sector on the charged black hole geometry. The AdS Schwarzschild background is only reliable near T_c , as at low temperatures the finite charged fermion density is comparable to μ . The RN case is under better control for low temperatures, because near $T = 0$ the chemical potential can be tuned to stay larger than fermion density.

We shall therefore focus primarily on the solution in the background of an AdS RN black hole, i.e. the system with a heat bath with chemical potential μ — non-linearly determined by the value of $\Phi_{\text{hor}}^{(2)} = \mu_0$ at the horizon — which for low T/μ should show the characteristic Δn_F of a Fermi liquid. The limit in which we may confidently ignore backreaction is $\Phi_{\text{hor}}^{(1)} \ll \mu_0$ for $T \lesssim \mu_0$ — for AdSS the appropriate limit is $\Phi_{\text{hor}}^{(1)} \ll T$ for $\mu_0 \ll T$.

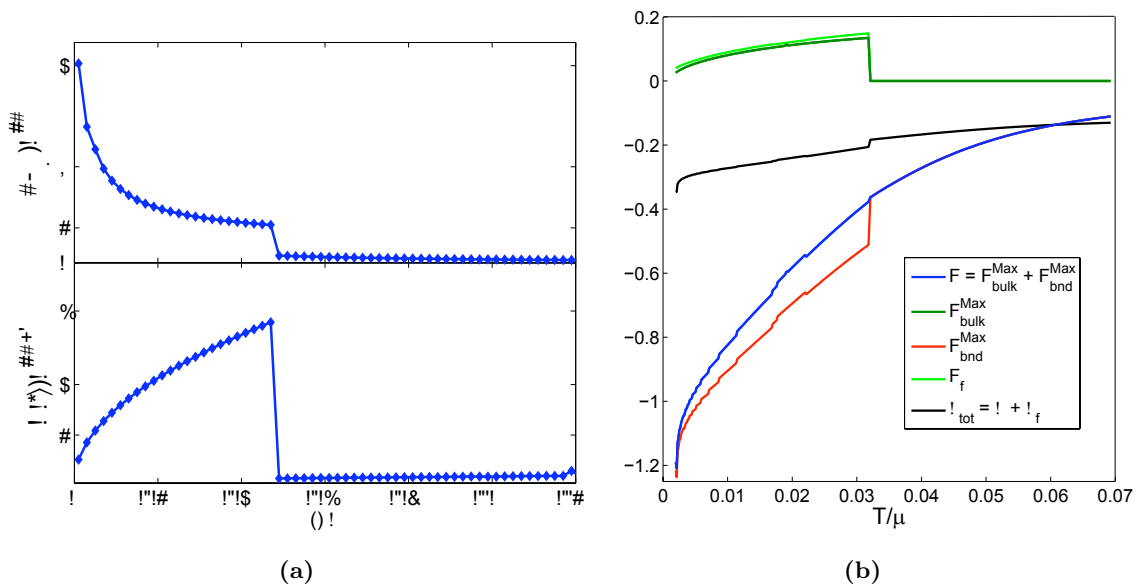


Figure 1. (a) Temperature dependence of the Fermi liquid occupation number discontinuity Δn_F and operator I for a fermionic field of mass $m = -1/4$ dual to an operator of dimension $\Delta = 5/4$. We see a large density for T/μ small and discontinuously drop to zero at $T \approx 0.05\mu$. At this same temperature, the proxy free energy contribution per particle (the negative of I) vanishes. (b) The free energy $F = F^{\text{fermion}} + F^{\text{Maxwell}}$ (eq. (3.12)) as a function of T/μ ignoring the contribution from the gravitational sector. The blue curve shows the total free energy $F = F^{\text{Maxwell}}$, which is the sum of a bulk and a boundary term. The explicit fermion contribution F_{fermion} vanishes, but the effect of a non-zero fermion density is directly encoded in a non-zero $F_{\text{bulk}}^{\text{Maxwell}}$. The figure also shows this bulk $F_{\text{bulk}}^{\text{Maxwell}}$ and the boundary contribution $F_{\text{bulk}}^{\text{Maxwell}}$ separately and how they sum to a continuous F_{total} . Although formally the explicit fermion contribution $F_f \sim I$ in equation (3.16) vanishes, the bulk Maxwell contribution is captured remarkably well by its value when the cut-off is kept finite. The light-green curve in the figure shows F_f for a finite $z_0 \sim 10^{-6}$. For completeness we also show the total charge density, eq. (3.10). The dimension of the fermionic operator used in this figure is $\Delta = 1.1$.

3.3.1 Finite fermion density solutions in AdS-RN

Figure 1 shows the behavior of the occupation number discontinuity $n_F \equiv |B_-|^2$ and the fermion free-energy contribution I as a function of temperature in a search for normalizable solutions to eqs.(3.8) with the aforementioned boundary conditions. We clearly see a first order transition to a finite fermion density, as expected. The underlying Dirac field dynamics can be recognized in that the normalizable solution for $J_-^0(z)$ which has no leading component near the boundary by construction, also has its subleading component vanishing (figure 2).⁹

⁹Although the Dirac hair solution has charged matter in the bulk, there is no Higgs effect for the bulk gauge field, and thus there is no direct spontaneous symmetry breaking in the boundary. Indeed one would not expect it for the Fermi liquid ground state. There will be indirect effect on the conductivity similar to [27]. We thank Andy O’Bannon for his persistent inquiries to this point.

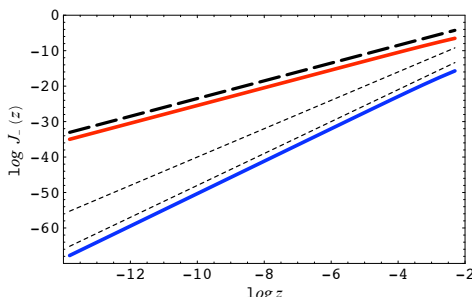


Figure 2. The boundary behaviour of $J_-(0)$ in for a generic solution (blue) to eqs. (3.8) and a normalizable Dirac-hair solution (red) for $m = -1/4$ in the background of an AdS-RN black hole with $\mu/T = 128.8$. The dotted lines show the scaling $z^{11/2}$ and z^4 of the leading and subleading terms in an expansion of $J_-(z)$ near $z = 0$; the dashed line shows the scaling $z^{5/2}$ of the sub-subleading expansion whose coefficient is $|B_-(\omega_F, k_F)|^2$. That the Dirac hair solution (red) scales as the subsubleading solution indicates that the current J_-^0 faithfully captures the density of the underlying normalizable Dirac field.

Analyzing the transition in more detail in figure 3, we find:

1. The dimensionless number discontinuity $\Delta n_F/\mu^{2\Delta}$ scales as $T^{-\delta}$ in a certain temperature range $T_F < T < T_c$, with $\delta > 0$ depending on g and Δ , and T_F typically very small. At $T = T_c > T_F$ it drops to zero discontinuously, characteristic of a first order phase transition.
2. At low temperatures, $0 < T < T_F$, the power-law growth comes to a halt and ends with a plateau where $\Delta n_F/\mu^{2\Delta} \sim \text{const.}$ (figure 3a). It is natural to interpret this temperature as the Fermi temperature of the boundary Fermi liquid.
3. The fermion free energy contribution $I/\mu^{2\Delta+1}$ scales as $T^{1/\nu}$ with $\nu > 1$ for $0 < T < T_c$, and drops to zero discontinuously at T_c . As I empirically equals minus the free energy per particle, it is natural that $I(T = 0) = 0$, and this in turn supports the identification of $\Delta n_F(T = 0)$ as the step in number density at the Fermi energy.

One expects that the exponents δ, ν are controlled by the conformal dimension Δ .¹⁰ The dependence of the exponent δ on the conformal dimension is shown in figure 3a. While a correlation clearly exists, the data are not conclusive enough to determine the relation $\delta = \delta(\Delta)$. The clean power law $T^{-\delta}$ scaling regime is actually somewhat puzzling. These values of the temperature, $T_F < T < T_c$, correspond to a crossover between the true Fermi liquid regime for $T < T_F$ and the conformal phase for $T > T_c$, hence there is no clear ground for a universal scaling relation for δ , which seems to be corroborated by the data (figure 3b). At the same time, the scaling exponent ν appears to obey $\nu = 2$ with great precision (figure 3b, inset) independent of Δ and g .

A final consideration, needed to verify the existence of a finite fermion density AdS solution dual to a Fermi liquid, is to show that the ignored backreaction stays small. In particular, the divergence of the electric field at the horizon should not affect the result.

¹⁰The charge g of the underlying conformal fermionic operator scales out of the solution.

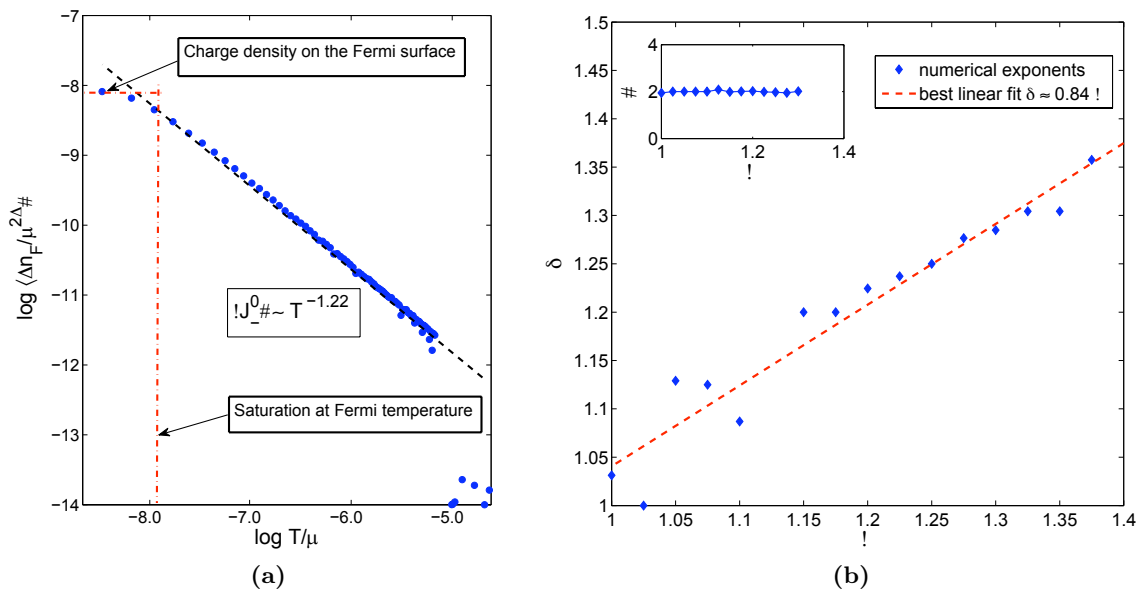


Figure 3. (a) Approximate power-law scaling of the Fermi liquid characteristic occupation number discontinuity $\Delta n_F / \mu^{2\Delta} \sim T^{-\delta}$ as a function of T/μ for $\Delta = 5/4$. This figure clearly shows the saturation of the density at very low T/μ . The saturation effect is naturally interpreted as the influence of the characteristic Fermi energy. (b) The scaling exponent δ for different values of the conformal dimension Δ . There is a clear correlation, but the precise relation cannot be determined numerically. The scaling exponent of the current $I/\mu^{2\Delta+1} \sim T^{-1/\nu}$ obeys $\nu = 2$ with great accuracy, on the other hand (Inset).

The total bulk electric field $E_z = -\partial_z \Phi$ is shown in figure 4a, normalized by its value at $z = 1/2$. The logarithmic singularity at the horizon is clearly visible. At the same time, the contribution to the total electric field from the charged fermions is negligible even very close to the horizon.¹¹ This suggests that our results are robust with respect to the details of the IR divergence of the electric field.

The diverging backreaction at the horizon is in fact the gravity interpretation of the first order transition at T_c : an arbitrarily small non-zero density leads to an abrupt change in the on shell bulk action. As the latter is the free energy in the CFT, it must reflect the discontinuity of a first order transition. A full account of the singular behavior at the horizon requires self-consistent treatment including the Einstein equations. At this level, we can conclude that the divergent energy density at the horizon implies that the near-horizon physics becomes substantially different from the AdS_2 limit of the RN metric. It is natural to guess that the RN horizon disappears completely, corresponding to a ground state with zero entropy, as hypothesized in [26]. This matches the expectation that the finite fermi-density solution in the bulk describes the Fermi-liquid. The underlying assumption in the above reasoning is that the total charge is conserved.

¹¹It is of the order 10^{-4} , starting from $z = 0.9999$. We have run our numerics using values between $1 - 10^{-6}$ and $1 - 10^{-2}$ and found no detectable difference in quantities at the boundary.

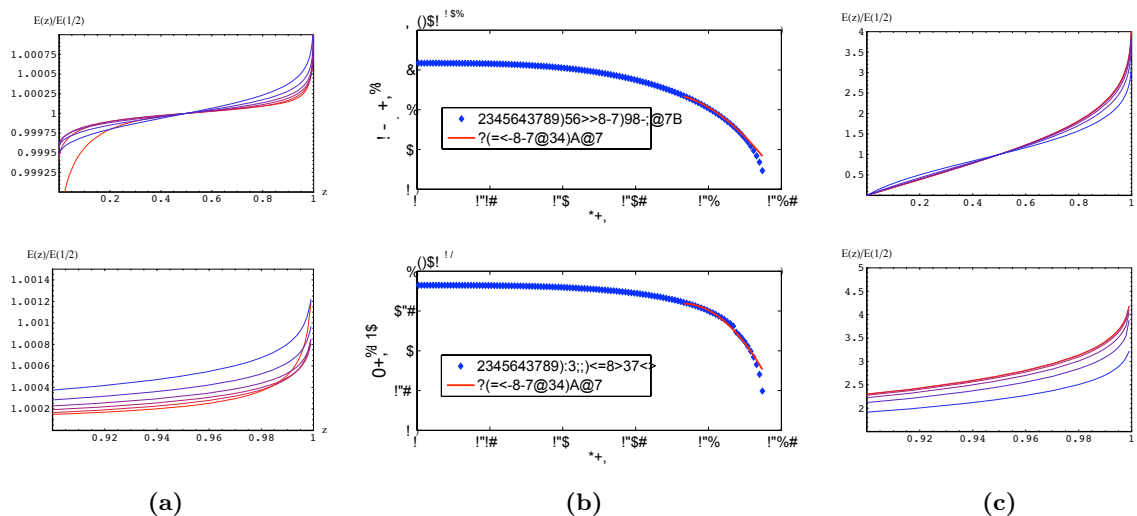


Figure 4. (a) The radial electric field $-E_z = \partial\Phi/\partial z$, normalized to the midpoint value $E_z(z)/E_z(1/2)$ for whole interior of the finite fermion density AdS-RN solution (upper) and near the horizon (lower). One clearly sees the soft, log-singularity at the horizon. The colors correspond to increasing temperatures from $T = 0.04\mu$ (lighter) to $T = 0.18\mu$ (darker), all with $\Delta = 1.1$. (b) The occupation number jump Δn_F and free energy contribution I as a function of temperature in AdS-Schwarzschild. We see the jump Δn_F saturate at low temperatures and fall off at high T . An exponential fit to the data (red curve) shows that in the critical region the fall-off is stronger than exponential, indicating that the transition is first order. The conformal dimension of the fermionic operator is $\Delta = 1.1$. (c) The radial electric field $-E_z = \partial\Phi/\partial z$, normalized to the midpoint value ($E_z(z)/E_z(1/2)$) for the finite fermion density AdS-Schwarzschild background. The divergence of the electric field E_z is again only noticeable near the horizon and can be neglected in most of the bulk region.

3.3.2 Finite fermion density in AdSS

For completeness, we will describe the finite fermion-density solutions in the AdS Schwarzschild geometry as well. In these solutions the charge density is set by the density of fermions alone. They are therefore not reliable at very low temperatures $T \ll T_c$ when gravitational backreaction becomes important. The purpose of this section is to show the existence of finite density solutions does not depend on the presence of a charged black hole set by the horizon value $\Phi_{\text{hor}}^{(2)} = \mu_0$, but that the transition to a finite fermion density can be driven by the charged fermions themselves.

Figure 4b shows the nearly instantaneous development of a non-vanishing expectation value for the occupation number discontinuity Δn_F and I in the AdS Schwarzschild background. The rise is not as sharp as in the RN background. It is, however, steeper than exponential, and we may conclude that the system undergoes a discontinuous first order transition to a AdS Dirac hair solution. The constant limit reached by the fermion density as $T \rightarrow 0$ has no meaning as we cannot trust the solution far away from T_c .

The backreaction due to the electric field divergence at the horizon can be neglected, for the same reason as before (figure 4c).

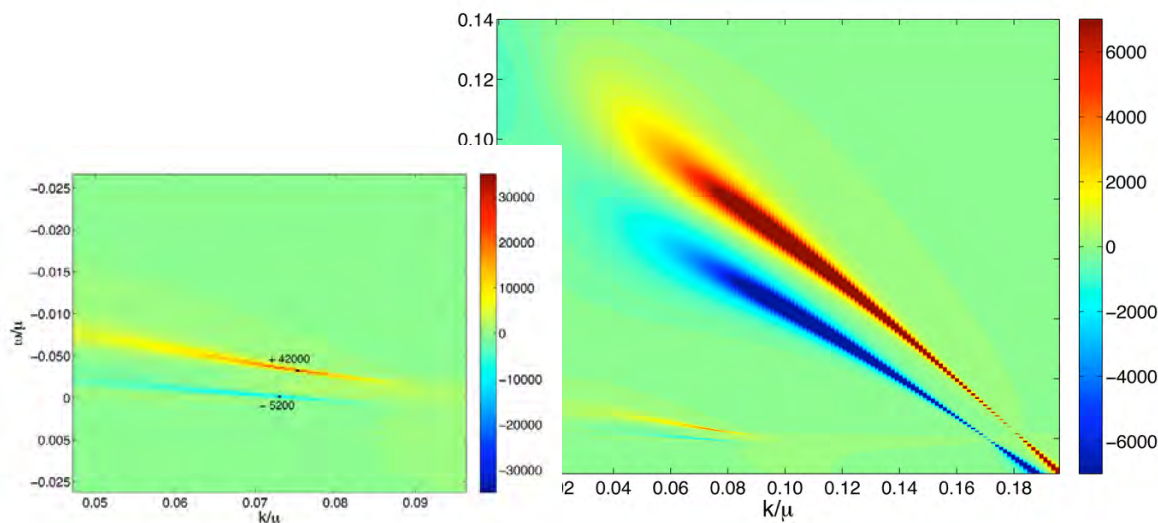


Figure 5. The single-fermion spectral function in the probe limit of pure AdS Reissner-Nordström (red/yellow) *minus* the spectrum in the finite density system (blue). The conformal dimension is $\Delta = 5/4$, the probe charge $g = 2$, and $\mu/T = 135$. We can see two quasiparticle poles near $\omega = 0$, a non-FL pole with $k_F^{\text{probe}} \simeq 0.11\mu$ and $k_F^{\Delta n_F} \simeq 0.08\mu$ respectively and a FL-pole with $k_F^{\text{probe}} \simeq 0.18\mu$ and $k_F^{\Delta n_F} \simeq 0.17\mu$. The dispersion of both poles is visibly similar between the probe and the finite density background. At the same time, the non-FL pole has about 8 times less weight in the finite density background, whereas the FL-pole has gained about 6.5 times more weight.

3.4 Confirmation from fermion spectral functions

If, as we surmised, the finite fermion density phase is the true Fermi-liquid-like ground state, the change in the fermion spectral functions should be minimal as the characteristic quasiparticle peaks are already present in the probe limit, i.e. pure AdS Reissner-Nordström [11, 12]. Figure 5 shows that quasiparticle poles near $\omega = 0$ with similar analytic properties can be identified in both the probe pure AdS-RN case and the AdS-RN Dirac-hair solution. The explanation for this similarity is that the electrostatic potential Φ almost completely determines the spectrum, and the change in Φ due to the presence of a finite fermion density is quite small. Still, one expects that the finite fermion density system is a more favorable state. This indeed follows from a detailed comparison between the spectral functions $A(\omega; k)$ in the probe limit and the fermion-liquid phase (figure 5). We see that:

1. All quasiparticle poles present in the probe limit are also present in the Dirac hair phase, at a slightly shifted value of k_F . This shift is a consequence of the change in the bulk electrostatic potential Φ due to the presence of the charged matter. For a Fermi-liquid-like quasiparticle corresponding to the second pole in the operator with $\Delta = 5/4$ and $g = 2$ we find $k_F^{\text{probe}} - k_F^{\Delta n_F} = 0.07\mu$. The non-Fermi-liquid pole, i.e. the first pole for the same conformal operator, has $k_F^{\text{probe}} - k_F^{\Delta n_F} = 0.03\mu$.
2. The dispersion exponents ν defined through $(\omega - E_F)^2 \sim (k - k_F)^{2/\nu}$, also maintain roughly the same values as both solutions. This is visually evident in the near similar

slopes of the ridges in figure 5. In the AdS Reissner-Nordström background, the dispersion coefficients are known analytically as a function of the Fermi momentum: $\nu_{k_F} = \sqrt{2\frac{k_F^2}{\mu^2} - \frac{1}{3} + \frac{1}{6}(\Delta - 3/2)^2}$ [13]. The Fermi-liquid-like quasiparticle corresponding to the second pole in the operator with $\Delta = 5/4$ and $g = 2$ has $\nu_{k_F}^{\text{probe}} = 1.02$ vs. $\nu^{\Delta n_F} = 1.01$. The non-Fermi-liquid pole corresponding to the first pole for the same conformal operator, has $\nu_{k_F}^{\text{probe}} \approx 0.10$, and $\nu^{\Delta n_F} = 0.12$.

3. The most distinct property of the finite density phase is the redistributed spectral weight of the poles. The non-Fermi liquid pole reaches its maximum height about 10^4 , an order of magnitude less than in the probe limit, whereas the second, Fermi liquid-like pole, increases by an order of magnitude. This suggests that the finite density state corresponds to the Fermi-liquid like state, rather than a non-Fermi liquid.
4. As we mentioned in the introduction, part of the reason to suspect the existence of an AdS-RN Dirac-hair solution is that a detailed study of spectral functions in AdS-RN reveals that the quasiparticle peak is anomalously sensitive to changes in T . This anomalous temperature dependence disappears in the finite density solution. Specifically in pure AdS-RN the position ω_{max} where the peak height is maximum, denoted E_F in [12], does not agree with the value ω_{pole} , where the pole touches the real axis in the complex ω -plane, for any finite value of T , and is exponentially sensitive to changes in T (figure 6). In the AdS-RN Dirac hair solution the location ω_{max} and the location ω_{pole} do become the same. Figure 6b shows that the maximum of the quasiparticle peak always sits at $\omega \simeq 0$ in finite density Dirac hair solution, while it only reaches this as $T \rightarrow 0$ in the probe AdS-RN case.

4 Discussion and conclusion

Empirically we know that the Fermi liquid phase of real matter systems is remarkably robust and generic. This is corroborated by analyzing effective field theory around the Fermi surface, but as it assumes the ground state it cannot explain its genericity. If the Fermi liquid ground state is so robust, this must also be a feature of the recent holographic approaches to strongly interacting fermionic systems. Our results here indicate that this is so. We have used Migdal’s relation to construct AdS/CFT rules for the holographic dual of a Fermi liquid: the characteristic occupation number discontinuity Δn_F is encoded in the normalizable subsubleading component of the spatially averaged fermion density $J_-^0(z) \equiv \int d^3k \Psi(\omega = 0, -k, z) i\gamma^0 \Psi(\omega = 0, k, z)$ near the AdS boundary. This density has its own set of evolution equations, based on the underlying Dirac field, and insisting on normalizability automatically selects the on-shell wavefunctions of the underlying Dirac-field.

The simplest AdS solution that has a non-vanishing expectation value for the occupation number discontinuity Δn_F is that of a single fermion wavefunction. Using the density approach — which through the averaging appears to describe a class of solutions rather than one specific solution — we have constructed the limit of this solution where gravitational backreaction is ignored. At low black hole temperatures this solution with fermionic

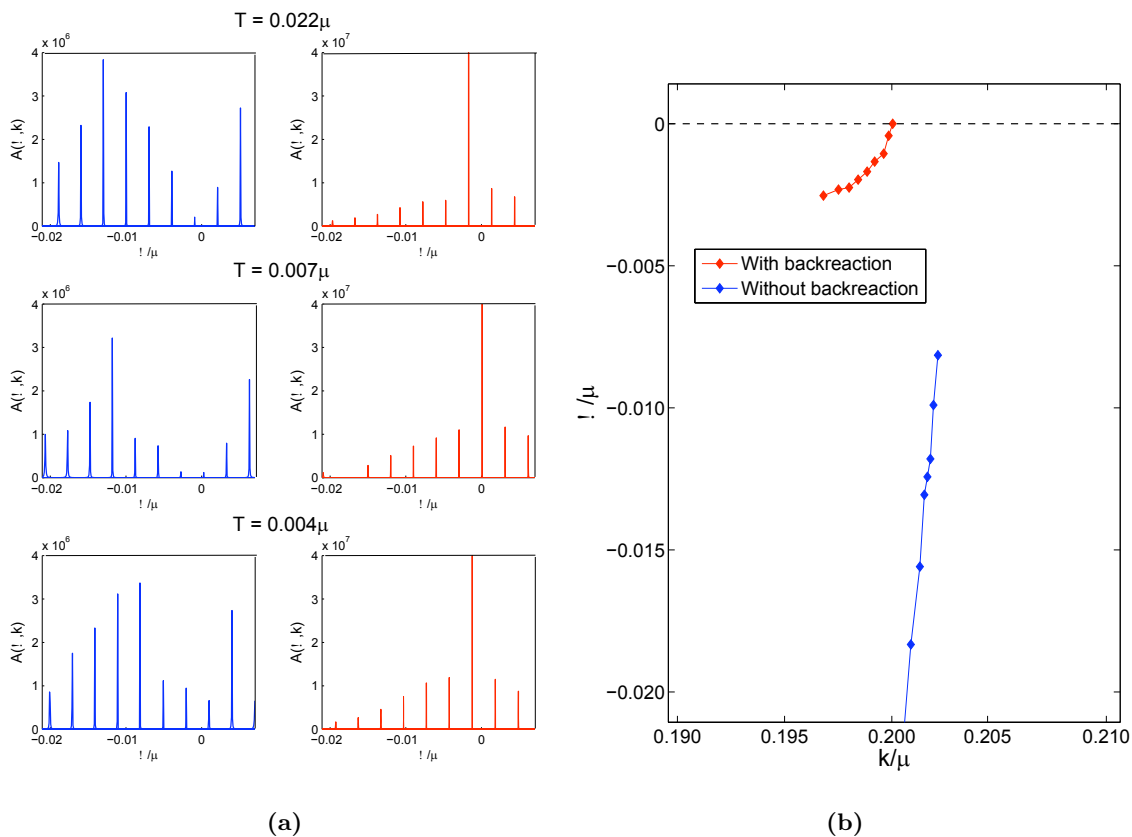


Figure 6. (a) Single fermion spectral functions near $\omega = 0$ in pure AdS Reissner-Nordström (blue) and in the finite fermion density background (red). In the former the position of the maximum approaches $\omega = 0$ as T is lowered whereas in the latter the position of the maximum close to $T = 0$ for all values of T . (b) Position of the maximum of the quasiparticle peak in k - ω plane, for different temperatures and $\Delta = 5/4$. The probe limit around a AdS-RN black hole (blue) carries a strong temperature dependence of the ω_{\max} value, with $\omega_{\max, T \neq 0} \neq 0$. In the finite fermion density background, the position of the maximum (red) is nearly independent of temperature and stays at $\omega = 0$.

“Dirac hair” is the preferred ground state. Through an analysis of the free energy, we argue that this gravitational solution with a non-zero fermion profile precisely corresponds to a system with a finite density of fermions. A spectral analysis still reveals a zoo of Fermi-surfaces in this ground state, but there are indications that in the full gravitationally backreacted solution only a Landau Fermi-liquid type Fermi surface survives. This follows in part from the relation between the spectral density and the Fermi momentum of a particular Landau liquid-like Fermi surface; it also agrees with the prediction from Luttinger’s theorem. Furthermore, the spectral analysis in the finite density state shows no anomalous temperature dependence present in the pure charged black-hole single spectral functions. This also indicates that the finite density state is the true ground state.

The discovery of this state reveals a new essential component in the study of strongly coupled fermionic systems through gravitational duals, where one should take into account

the expectation values of fermion bilinears. Technically the construction of the full gravitationally backreacted solution is a first point that is needed to complete our finding. A complete approach to this problem will have to take into account the many-body physics in the bulk. Within the approach presented in this paper, it means the inclusion of additional fermion wavefunctions, filling the bulk Fermi surface. The realization, however, that expectation values of fermion bilinears can be captured in holographic duals and naturally encode phase separations in strongly coupled fermion systems should find a large set of applications in the near future.

Acknowledgments

We thank F. Benini, J. de Boer, E. Gubankova, S. Hartnoll, C. Herzog, E. Kiritsis, H. Liu, M. Medvedyeva, J. McGreevy, A. O’Bannon, G. Policastro, and J. Sonner for extensive discussions. We are very grateful to the KITP Santa Barbara for its generous hospitality and the organizers and participants of the AdS/CMT Workshop (July 2009). KS thanks the Galileo Galilei Institute for Theoretical Physics for the hospitality and the INFN for partial support during the completion of this work. This research was supported in part by a VIDI Innovative Research Incentive Grant (K. Schalm) from the Netherlands Organization for Scientific Research (NWO), a Spinoza Award (J. Zaanen) from the Netherlands Organisation for Scientific Research (NWO) and the Dutch Foundation for Fundamental Research on Matter (FOM).

Open Access. This article is distributed under the terms of the Creative Commons Attribution Noncommercial License which permits any noncommercial use, distribution, and reproduction in any medium, provided the original author(s) and source are credited.

References

- [1] C.M. Varma, Z. Nussinov and W. van Saarloos, *Singular Fermi Liquids*, *Phys. Rept.* **361** (2002) 267 [[cond-mat/0103393](#)].
- [2] J.H. She and J. Zaanen, *BCS Superconductivity in Quantum Critical Metals*, *Phys. Rev.* **B80** (2009) 184518 [[arXiv:0905.1225](#)].
- [3] H. v. Löhneysen, A. Rosch, M. Vojta and P. Wölfle, *Fermi-liquid instabilities at magnetic quantum phase transitions*, *Rev. Mod. Phys.* **79** (2007) 1015 [[cond-mat/0606317](#)].
- [4] M. Gurvitch and A.T. Fiory, *Resistivity of La_{1.825}Sr_{0.175}CuO₄ and YBa₂Cu₃O₇ to 1100 K: Absence of saturation and its implications*, *Phys. Rev. Lett.* **59** (1987) 1337.
- [5] P. Phillips and C. Chamon, *Breakdown of One-Parameter Scaling in Quantum Critical Scenarios for the High-Temperature Copper-oxide Superconductors*, *Phys. Rev. Lett.* **95** (2005) 107002 [[cond-mat/0412179](#)].
- [6] J. Zaanen, *Quantum critical electron systems: the uncharted sign worlds*, *Science* **319** (2008) 1205.
- [7] J.M. Luttinger, *Fermi Surface and Some Simple Equilibrium Properties of a System of Interacting Fermions*, *Phys. Rev.* **119** (1960) 1153 [[SPIRES](#)].

- [8] J.C. Campuzano, M.R. Norman and M. Randeria, *Photoemission in the High- T_c Superconductors*, in *Handbook of Physics: Physics of Conventional and Unconventional Superconductors*, K.H. Benneman and J.B. Ketterson eds., Springer Verlag, (2004) [[cond-mat/0209476](#)].
- [9] A. Damascelli, Z. Hussain and Z.-X. Shen, *Angle-resolved photoemission studies of the cuprate superconductors*, *Rev. Mod. Phys.* **75** (2003) 473 [[cond-mat/0208504](#)] [[SPIRES](#)].
- [10] X.-J. Zhou, T. Cuk, T. Devereaux, N. Nagaosa and Z.-X. Shen, *Angle-Resolved Photoemission Spectroscopy on Electronic Structure and Electron-Phonon Coupling in Cuprate Superconductors* in *Handbook of High-Temperature Superconductivity: Theory and Experiment*, J.R. Schrieffer, Springer Verlag, (2007) [[cond-mat/0604284](#)].
- [11] H. Liu, J. McGreevy and D. Vegh, *Non-Fermi liquids from holography*, *Phys. Rev. D* **83** (2011) 065029 [[arXiv:0903.2477](#)] [[SPIRES](#)].
- [12] M. Cubrovic, J. Zaanen and K. Schalm, *String Theory, Quantum Phase Transitions and the Emergent Fermi-Liquid*, *Science* **325** (2009) 439 [[arXiv:0904.1993](#)] [[SPIRES](#)].
- [13] T. Faulkner, H. Liu, J. McGreevy and D. Vegh, *Emergent quantum criticality, Fermi surfaces and AdS $_2$* , *Phys. Rev. D* **83** (2011) 125002 [[arXiv:0907.2694](#)] [[SPIRES](#)].
- [14] T. Faulkner, N. Iqbal, H. Liu, J. McGreevy and D. Vegh, *From black holes to strange metals*, [arXiv:1003.1728](#) [[SPIRES](#)].
- [15] T. Faulkner, N. Iqbal, H. Liu, J. McGreevy and D. Vegh, *Strange metal transport realized by gauge/gravity duality*, *Science* **329** (2010) 1043 [[SPIRES](#)].
- [16] S.-S. Lee, *A Non-Fermi Liquid from a Charged Black Hole: A Critical Fermi Ball*, *Phys. Rev. D* **79** (2009) 086006 [[arXiv:0809.3402](#)] [[SPIRES](#)].
- [17] S.-J. Rey, *String theory on thin semiconductors: Holographic realization of Fermi points and surfaces*, *Prog. Theor. Phys. Suppl.* **177** (2009) 128 [[arXiv:0911.5295](#)] [[SPIRES](#)].
- [18] S.S. Gubser, *Breaking an Abelian gauge symmetry near a black hole horizon*, *Phys. Rev. D* **78** (2008) 065034 [[arXiv:0801.2977](#)] [[SPIRES](#)].
- [19] S.A. Hartnoll, C.P. Herzog and G.T. Horowitz, *Building a Holographic Superconductor*, *Phys. Rev. Lett.* **101** (2008) 031601 [[arXiv:0803.3295](#)] [[SPIRES](#)].
- [20] S.A. Hartnoll, C.P. Herzog and G.T. Horowitz, *Holographic Superconductors*, *JHEP* **12** (2008) 015 [[arXiv:0810.1563](#)] [[SPIRES](#)].
- [21] S.A. Hartnoll, *Lectures on holographic methods for condensed matter physics*, *Class. Quant. Grav.* **26** (2009) 224002 [[arXiv:0903.3246](#)] [[SPIRES](#)].
- [22] F. Finster, J. Smoller and S.-T. Yau, *Non-Existence of Black Hole Solutions to Static, Spherically Symmetric Einstein-Dirac Systems — a Critical Discussion*, [gr-qc/0211043](#) [[SPIRES](#)].
- [23] F. Finster, J. Smoller and S.-T. Yau, *Absence of stationary, spherically symmetric black hole solutions for Einstein-Dirac-Yang-Mills equations with angular momentum*, *Adv. Theor. Math. Phys.* **4** (2002) 1231 [[gr-qc/0005028](#)] [[SPIRES](#)].
- [24] F. Finster, J. Smoller and S.-T. Yau, *The interaction of Dirac particles with non-Abelian gauge fields and gravity: Bound states*, *Nucl. Phys. B* **584** (2000) 387 [[gr-qc/0001067](#)] [[SPIRES](#)].

- [25] F. Finster, J. Smoller and S.-T. Yau, *Non-existence of black hole solutions for a spherically symmetric, static Einstein-Dirac-Maxwell system*, *Commun. Math. Phys.* **205** (1999) 249 [[SPIRES](#)].
- [26] S.A. Hartnoll, J. Polchinski, E. Silverstein and D. Tong, *Towards strange metallic holography*, *JHEP* **04** (2010) 120 [[arXiv:0912.1061](#)] [[SPIRES](#)].
- [27] S.A. Hartnoll and A. Tavanfar, *Electron stars for holographic metallic criticality*, *Phys. Rev. D* **83** (2011) 046003 [[arXiv:1008.2828](#)] [[SPIRES](#)].
- [28] J. de Boer, K. Papadodimas and E. Verlinde, *Holographic Neutron Stars*, *JHEP* **10** (2010) 020 [[arXiv:0907.2695](#)] [[SPIRES](#)].
- [29] X. Arsiwalla, J. de Boer, K. Papadodimas and E. Verlinde, *Degenerate Stars and Gravitational Collapse in AdS/CFT*, *JHEP* **01** (2011) 144 [[arXiv:1010.5784](#)] [[SPIRES](#)].
- [30] L.-Y. Hung, D.P. Jatkar and A. Sinha, *Non-relativistic metrics from back-reacting fermions*, *Class. Quant. Grav.* **28** (2011) 015013 [[arXiv:1006.3762](#)] [[SPIRES](#)].
- [31] M. Cubrovic, Y. Liu, K. Schalm, Y.-W. Sun and J. Zaanen, *Spectral probes of the holographic Fermi groundstate: dialing between the electron star and AdS Dirac hair*, [arXiv:1106.1798](#) [[SPIRES](#)].
- [32] S.A. Hartnoll, D.M. Hofman and D. Vegh, *Stellar spectroscopy: Fermions and holographic Lifshitz criticality*, *JHEP* **08** (2011) 096 [[arXiv:1105.3197](#)] [[SPIRES](#)].
- [33] N. Iqbal, H. Liu and M. Mezei, *Semi-local quantum liquids*, [arXiv:1105.4621](#) [[SPIRES](#)].
- [34] N. Iqbal and H. Liu, *Real-time response in AdS/CFT with application to spinors*, *Fortsch. Phys.* **57** (2009) 367 [[arXiv:0903.2596](#)] [[SPIRES](#)].
- [35] R. Contino and A. Pomarol, *Holography for fermions*, *JHEP* **11** (2004) 058 [[hep-th/0406257](#)] [[SPIRES](#)].
- [36] E.M. Lifshitz and L.P. Pitaevskii, *Statistical physics. Part 2*, Pergamon Press, Oxford U.K. (1980).
- [37] M. Čubrović, J. Zaanen and K. Schalm, *Stability of the Fermi Liquid from holography*, to appear.
- [38] S. Sachdev, *A model of a Fermi liquid using gauge-gravity duality*, [arXiv:1107.5321](#) [[SPIRES](#)].
- [39] K. Goldstein, S. Kachru, S. Prakash and S.P. Trivedi, *Holography of Charged Dilaton Black Holes*, *JHEP* **08** (2010) 078 [[arXiv:0911.3586](#)] [[SPIRES](#)].
- [40] T. Albash and C.V. Johnson, *A Holographic Superconductor in an External Magnetic Field*, *JHEP* **09** (2008) 121 [[arXiv:0804.3466](#)] [[SPIRES](#)].
- [41] R.-G. Cai, Z.-Y. Nie, B. Wang and H.-Q. Zhang, *Quasinormal Modes of Charged Fermions and Phase Transition of Black Holes*, [arXiv:1005.1233](#) [[SPIRES](#)].

Holographic fermions in external magnetic fieldsE. Gubankova,^{1,*} J. Brill,² M. Čubrović,² K. Schalm,² P. Schijven,^{2,†} and J. Zaanen²¹*Institute for Theoretical Physics, J. W. Goethe-University, D-60438 Frankfurt am Main, Germany*²*Institute Lorentz for Theoretical Physics, Leiden University, P.O. Box 9506, Leiden 2300RA, The Netherlands*

(Received 19 November 2010; published 2 November 2011)

We study the Fermi-level structure of 2 + 1-dimensional strongly interacting electron systems in external magnetic field using the gauge/gravity duality correspondence. The gravity dual of a finite density fermion system is a Dirac field in the background of the dyonic AdS-Reissner-Nordström black hole. In the probe limit, the magnetic system can be reduced to the nonmagnetic one, with Landau-quantized momenta and rescaled thermodynamical variables. We find that at strong enough magnetic fields, the Fermi surface vanishes and the quasiparticle is lost either through a crossover to conformal regime or through a phase transition to an unstable Fermi surface. In the latter case, the vanishing Fermi velocity at the critical magnetic field triggers the non-Fermi-liquid regime with unstable quasiparticles and a change in transport properties of the system. We associate it with a metal–“strange-metal” phase transition. Next, we compute the DC Hall and longitudinal conductivities using the gravity-dressed fermion propagators. For dual fermions with a large charge, many different Fermi surfaces contribute and the Hall conductivity is quantized as expected for integer quantum Hall effect (QHE). At strong magnetic fields, as additional Fermi surfaces open up, new plateaus typical for the fractional QHE appear. The somewhat irregular pattern in the length of fractional QHE plateaus resembles the outcomes of experiments on thin graphite in a strong magnetic field. Finally, motivated by the absence of the sign problem in holography, we suggest a lattice approach to the AdS calculations of finite density systems.

DOI: [10.1103/PhysRevD.84.106003](https://doi.org/10.1103/PhysRevD.84.106003)

PACS numbers: 11.25.Tq, 71.27.+a

I. INTRODUCTION

The study of strongly interacting fermionic systems at finite density and temperature is a challenging task in condensed matter and high energy physics. Analytical methods are limited or not available for strongly coupled systems, and numerical simulation of fermions at finite density breaks down because of the sign problem [1]. There has been an increased activity in describing finite density fermionic matter by a gravity dual using the holographic AdS/CFT correspondence [2]. The gravitational solution which is dual to the finite chemical potential system is the electrically charged AdS-Reissner-Nordström black hole, which provides a background where only the metric and Maxwell fields are nontrivial and all matter fields vanish. In the classical gravity limit, the decoupling of the Einstein-Maxwell sector holds and leads to universal results, which is an appealing feature of applied holography. Indeed, the celebrated result for the ratio of the shear viscosity over the entropy density [3] is identical for many strongly interacting theories and has been considered a robust prediction of the AdS/CFT correspondence.

However, an extremal black hole alone is not enough to describe finite density systems as it does not source the matter fields. In holography, at leading order, the Fermi

surfaces are not evident in the gravitational geometry, but can only be detected by external probes; either probe D-branes [2] or probe bulk fermions [4–7]. Here, we shall consider the latter option, where the free Dirac field in the bulk carries a finite charge density [8]. We ignore electromagnetic and gravitational backreaction of the charged fermions on the bulk space-time geometry (probe approximation). At large temperatures, $T \gg \mu$, this approach provides a reliable hydrodynamic description of transport at a quantum criticality (in the vicinity of superfluid-insulator transition) [9]. At small temperatures, $T \ll \mu$, in some cases, sharp Fermi surfaces emerge with either conventional Fermi-liquid scaling [5] or of a non-Fermi-liquid type [6] with scaling properties that differ significantly from those predicted by the Landau Fermi-liquid theory. The nontrivial scaling behavior of these non-Fermi liquids has been studied semianalytically in [7] and is of great interest as high- T_c superconductors and metals near the critical point are believed to represent non-Fermi liquids.

What we shall study is the effects of magnetic field on the holographic fermions. A magnetic field is a probe of finite density matter at low temperatures, where the Landau-level physics reveals the Fermi-level structure. The gravity dual system is described by an AdS dyonic black hole with electric and magnetic charges Q and H , respectively, corresponding to a 2 + 1-dimensional field theory at finite chemical potential in an external magnetic field [10]. Probe fermions in the background of the dyonic black hole have been considered in [11,12]; and probe

*Also at ITEP, Moscow, Russia

†Present address: Albert-Ludwigs-Universität Freiburg D-79104 Freiburg, Germany

bosons in the same background have been studied in [13]. Quantum magnetism is considered in [14].

The Landau quantization of momenta due to the magnetic field found there shows again that the AdS/CFT correspondence has a powerful capacity to unveil that certain quantum properties known from quantum gases have a much more ubiquitous status than could be anticipated theoretically. A first highlight is the demonstration [15] that the Fermi surface of the Fermi gas extends way beyond the realms of its perturbative extension in the form of the Fermi liquid. In AdS/CFT, it appears to be gravitationally encoded in the matching along the scaling direction between the “bare” Dirac waves falling in from the “UV” boundary and the true IR excitations living near the black hole horizon. This IR physics can insist on the disappearance of the quasiparticle but, if so, this “critical Fermi liquid” is still organized “around” a Fermi surface. The Landau quantization, the organization of quantum gaseous matter in quantized energy bands (Landau levels) in a system of two space dimensions pierced by a magnetic field oriented in the orthogonal spatial direction, is a second such quantum gas property. Following Ref. [11], we shall describe here that despite the strong interactions in the system, the holographic computation reveals the same strict Landau-level quantization. Arguably, it is the mean-field nature imposed by large N limit inherent in AdS/CFT that explains this. The system is effectively noninteracting to first order in $1/N$. The Landau quantization is not manifest from the geometry, but, as we show, this statement is straightforwardly encoded in the symmetry correspondences associated with the conformal compactification of AdS on its flat boundary (i.e., in the UV conformal field theory [CFT]).

An interesting novel feature in strongly coupled systems arises from the fact that the background geometry is only sensitive to the total energy density $Q^2 + H^2$ contained in the electric and magnetic fields sourced by the dyonic black hole. Dialing up the magnetic field is effectively similar to a process where the dyonic black hole loses its electric charge. At the same time, the fermionic probe with charge q is essentially only sensitive to the Coulomb interaction gqQ . As shown in [11], one can therefore map a magnetic to a nonmagnetic system with rescaled parameters (chemical potential, fermion charge) and same symmetries and equations of motion, as long as the Reissner-Nordström geometry is kept.

Translated to more experiment-compatible language, the above magnetic-electric mapping means that the spectral functions at nonzero magnetic field h are identical to the spectral function at $h = 0$ for a reduced value of the coupling constant (fermion charge) q , provided the probe fermion is in a Landau-level eigenstate. A striking consequence is that the spectrum shows conformal invariance for arbitrarily high magnetic fields, as long as the system is at negligible to zero density. Specifically, a detailed analysis

of the fermion spectral functions reveals that at strong magnetic fields, the Fermi-level structure changes qualitatively. There exists a critical magnetic field at which the Fermi velocity vanishes. Ignoring the Landau-level quantization, we show that this corresponds to an effective tuning of the system from a regular Fermi-liquid phase with linear dispersion and stable quasiparticles to a non-Fermi liquid with fractional power-law dispersion and unstable excitations. This phenomenon can be interpreted as a transition from metallic phase to a “strange metal” at the critical magnetic field and corresponds to the change of the infrared conformal dimension from $\nu > 1/2$ to $\nu < 1/2$, while the Fermi momentum stays nonzero and the Fermi surface survives. Increasing the magnetic field further, this transition is followed by a strange-metal–conformal crossover and eventually, for very strong fields, the system always has near-conformal behavior where $k_F = 0$ and the Fermi surface disappears.

For some Fermi surfaces, this surprising metal–strange-metal transition is not physically relevant, as the system prefers to directly enter the conformal phase. Whether a fine tuned system exists that does show a quantum critical phase transition from a Fermi liquid to a non-Fermi liquid is determined by a Diophantine equation for the Landau-quantized Fermi momentum as a function of the magnetic field. Perhaps these are connected to the magnetically driven phase transition found in AdS₅/CFT₄ [16]. We leave this subject for future work.

Overall, the findings of Landau quantization and “discharge” of the Fermi surface are in line with the expectations: both phenomena have been found in a vast array of systems [17] and are almost tautologically tied to the notion of a Fermi surface in a magnetic field. Thus, we regard them also as a sanity check of the whole bottom-up approach of fermionic AdS/CFT [4–6,15], giving further credit to the holographic Fermi surfaces as having to do with the real world.

Next, we use the information of magnetic effects the Fermi surfaces extracted from holography to calculate the quantum Hall and longitudinal conductivities. Generally speaking, it is difficult to calculate conductivity holographically beyond the Einstein-Maxwell sector, and extract the contribution of holographic fermions. In the semiclassical approximation, one-loop corrections in the bulk setup involving charged fermions have been calculated [15]. In another approach, the backreaction of charged fermions on the gravity-Maxwell sector has been taken into account and incorporated in calculations of the electric conductivity [8]. We calculate the one-loop contribution on the CFT side, which is equivalent to the holographic one-loop calculations as long as vertex corrections do not modify physical dependencies of interest [15,18]. As we dial the magnetic field, the Hall plateau transition happens when the Fermi surface moves through a Landau level. One can think of a difference between the Fermi energy and the

energy of the Landau level as a gap, which vanishes at the transition point and the 2 + 1-dimensional theory becomes scale invariant. In the holographic D3–D7 brane model of the quantum Hall effect, plateau transition occurs as D-branes move through one another [19]. In the same model, a dissipation process has been observed as D-branes fall through the horizon of the black hole geometry that is associated with the quantum Hall insulator transition. In the holographic fermion liquid setting, dissipation is present through interaction of fermions with the horizon of the black hole. We have also used the analysis of the conductivities to learn more about the metal–strange-metal phase transition, as well as the crossover back to the conformal regime at high magnetic fields.

We conclude with the remark that the findings summarized above are, in fact, somewhat puzzling when contrasted to the conventional picture of quantum Hall physics. It is usually stated that the quantum Hall effect requires three key ingredients: Landau quantization, quenched disorder,¹ and (spatial) boundaries, i.e., a finite-sized sample [20]. The first brings about the quantization of conductivity, the second prevents the states from spilling between the Landau levels, ensuring the existence of a gap, and the last one, in fact, allows the charge transport to happen (as it is the boundary states that actually conduct). In our model, only the first condition is satisfied. The second is put by hand by assuming that the gap is automatically preserved, i.e., that there is no mixing between the Landau levels. There is, however, no physical explanation as to how the boundary states are implicitly taken into account by AdS/CFT.

The paper is organized as follows. We outline the holographic setting of the dyonic black hole geometry and bulk fermions in Sec. II. In Sec. III, we prove the conservation of conformal symmetry in the presence of the magnetic fields. Section IV is devoted to the holographic fermion liquid, where we obtain the Landau-level quantization, followed by a detailed study of the Fermi surface properties at zero temperature in Sec. V. We calculate the DC conductivities in Sec. VI, and compare the results with available data in graphene. In Sec. VII, we show that the fermion sign problem is absent in the holographic setting, therefore allowing lattice simulations of finite density matter in principle.

II. HOLOGRAPHIC FERMIONS IN A DYONIC BLACK HOLE

We first describe the holographic setup with the dyonic black hole and the dynamics of Dirac fermions in this

¹Quenched disorder means that the dynamics of the impurities is “frozen”, i.e. they can be regarded as having infinite mass. When coupled to the Fermi liquid, they ensure that below some scale, the system behaves as if consisting of noninteracting quasiparticles only.

background. In this paper, we exclusively work in the probe limit, i.e., in the limit of large fermion charge q .

A. Dyonic black hole

We consider the gravity dual of 3-dimensional conformal field theory with global $U(1)$ symmetry. At finite charge density and in the presence of a magnetic field, the system can be described by a dyonic black hole in 4-dimensional anti-de Sitter space-time, AdS_4 , with the current J_μ in the CFT mapped to a $U(1)$ gauge field A_M in AdS. We use μ, ν, ρ, \dots , for the space-time indices in the CFT and M, N, \dots , for the global space-time indices in AdS.

The action for a vector field A_M coupled to AdS_4 gravity can be written as

$$S_g = \frac{1}{2\kappa^2} \int d^4x \sqrt{-g} \left(\mathcal{R} + \frac{6}{R^2} - \frac{R^2}{g_F^2} F_{MN} F^{MN} \right), \quad (1)$$

where g_F^2 is an effective dimensionless gauge coupling and R is the curvature radius of AdS_4 . The equations of motion following from Eq. (1) are solved by the geometry corresponding to a dyonic black hole, having both electric and magnetic charge:

$$\begin{aligned} ds^2 &= g_{MN} dx^M dx^N \\ &= \frac{r^2}{R^2} (-f dt^2 + dx^2 + dy^2) + \frac{R^2}{r^2} \frac{dr^2}{f}. \end{aligned} \quad (2)$$

The redshift factor f and the vector field A_M reflect the fact that the system is at a finite charge density and in an external magnetic field:

$$\begin{aligned} f &= 1 + \frac{Q^2 + H^2}{r^4} - \frac{M}{r^3}, \\ A_t &= \mu \left(1 - \frac{r_0}{r} \right), \\ A_y &= hx, \\ A_x &= A_r = 0, \end{aligned} \quad (3)$$

where Q and H are the electric and magnetic charge of the black hole, respectively. Here, we chose the Landau gauge; the black hole chemical potential μ and the magnetic field h are given by

$$\mu = \frac{g_F Q}{R^2 r_0}, \quad h = \frac{g_F H}{R^4}, \quad (4)$$

with r_0 as the horizon radius determined by the largest positive root of the redshift factor $f(r_0) = 0$:

$$M = r_0^3 + \frac{Q^2 + H^2}{r_0}. \quad (5)$$

The boundary of the AdS is reached for $r \rightarrow \infty$. The geometry described by Eqs. (2) and (3) describes the boundary theory at finite density, i.e., a system in a charged

medium at the chemical potential $\mu = \mu_{\text{bh}}$ and in transverse magnetic field $h = h_{\text{bh}}$, with charge, energy, and entropy densities given, respectively, by

$$\rho = 2 \frac{Q}{\kappa^2 R^2 g_F}, \quad \epsilon = \frac{M}{\kappa^2 R^4}, \quad s = \frac{2\pi}{\kappa^2} \frac{r_0^2}{R^2}. \quad (6)$$

The temperature of the system is identified with the Hawking temperature of the black hole, $T_H \sim |f'(r_0)|/4\pi$,

$$T = \frac{3r_0}{4\pi R^2} \left(1 - \frac{Q^2 + H^2}{3r_0^4}\right). \quad (7)$$

Since Q and H have dimensions of $[L]^2$, it is convenient to parametrize them as

$$Q^2 = 3r_*^4, \quad Q^2 + H^2 = 3r_{**}^4. \quad (8)$$

In terms of r_0 , r_* , and r_{**} , the above expressions become

$$f = 1 + \frac{3r_{**}^4}{r^4} - \frac{r_0^3 + 3r_{**}^4/r_0}{r^3}, \quad (9)$$

with

$$\mu = \sqrt{3} g_F \frac{r_*^2}{R^2 r_0}, \quad h = \sqrt{3} g_F \frac{\sqrt{r_{**}^4 - r_*^4}}{R^4}. \quad (10)$$

The expressions for the charge, energy, and entropy densities, as well as for the temperature, are simplified as

$$\begin{aligned} \rho &= \frac{2\sqrt{3}}{\kappa^2 g_F} \frac{r_*^2}{R^2}, & \epsilon &= \frac{1}{\kappa^2} \frac{r_0^3 + 3r_{**}^4/r_0}{R^4}, \\ s &= \frac{2\pi}{\kappa^2} \frac{r_0^2}{R^2}, & T &= \frac{3}{4\pi} \frac{r_0}{R^2} \left(1 - \frac{r_{**}^4}{r_0^4}\right). \end{aligned} \quad (11)$$

In the zero temperature limit, i.e., for an extremal black hole, we have

$$T = 0 \rightarrow r_0 = r_{**}, \quad (12)$$

which in the original variables reads $Q^2 + H^2 = 3r_0^4$. In the zero temperature limit (12), the redshift factor f as given by Eq. (9) develops a double zero at the horizon:

$$f = 6 \frac{(r - r_{**})^2}{r_{**}^2} + \mathcal{O}((r - r_{**})^3). \quad (13)$$

As a result, near the horizon, the AdS₄ metric reduces to AdS₂ \times \mathbb{R}^2 with the curvature radius of AdS₂ given by

$$R_2 = \frac{1}{\sqrt{6}} R. \quad (14)$$

This is a very important property of the metric, which considerably simplifies the calculations, in particular, in the magnetic field.

In order to scale away the AdS₄ radius R and the horizon radius r_0 , we introduce dimensionless variables

$$\begin{aligned} r &\rightarrow r_0 r, & r_* &\rightarrow r_0 r_*, & r_{**} &\rightarrow r_0 r_{**}, \\ M &\rightarrow r_0^3 M, & Q &\rightarrow r_0^2 Q, & H &\rightarrow r_0^2 H, \end{aligned} \quad (15)$$

and

$$\begin{aligned} (t, \vec{x}) &\rightarrow \frac{R^2}{r_0} (t, \vec{x}), & A_M &\rightarrow \frac{r_0}{R^2} A_M, & \omega &\rightarrow \frac{r_0}{R^2} \omega, \\ \mu &\rightarrow \frac{r_0}{R^2} \mu, & h &\rightarrow \frac{r_0^2}{R^4} h, & T &\rightarrow \frac{r_0}{R^2} T, & ds^2 &\rightarrow R^2 ds^2. \end{aligned} \quad (16)$$

Note that the scaling factors in the above equation that describes the quantities of the boundary field theory involve the curvature radius of AdS₄, not AdS₂.

In the new variables, we have

$$\begin{aligned} T &= \frac{3}{4\pi} (1 - r_{**}^4) = \frac{3}{4\pi} \left(1 - \frac{Q^2 + H^2}{3}\right), \\ f &= 1 + \frac{3r_{**}^4}{r^4} - \frac{1 + 3r_{**}^4}{r^3}, & A_t &= \mu \left(1 - \frac{1}{r}\right), \\ \mu &= \sqrt{3} g_F r_*^2 = g_F Q, & h &= g_F H, \end{aligned} \quad (17)$$

and the metric is given by

$$ds^2 = r^2 (-f dt^2 + dx^2 + dy^2) + \frac{1}{r^2} \frac{dr^2}{f}, \quad (18)$$

with the horizon at $r = 1$ and the conformal boundary at $r \rightarrow \infty$.

At $T = 0$, r_{**} becomes unity, and the redshift factor develops the double zero near the horizon,

$$f = \frac{(r - 1)^2 (r^2 + 2r + 3)}{r^4}. \quad (19)$$

As mentioned before, due to this fact, the metric near the horizon reduces to AdS₂ \times \mathbb{R}^2 , where the analytical calculations are possible for small frequencies [7]. However, in the chiral limit $m = 0$, analytical calculations are also possible in the bulk AdS₄ [21], which we utilize in this paper.

B. Holographic fermions

To include the bulk fermions, we consider a spinor field ψ in the AdS₄ of charge q and mass m , which is dual to an operator \mathcal{O} in the boundary CFT₃ of charge q and dimension

$$\Delta = \frac{3}{2} + mR, \quad (20)$$

with $mR \geq -\frac{1}{2}$ and in dimensionless units corresponding to $\Delta = \frac{3}{2} + m$. In the black hole geometry, Eq. (2), the quadratic action for ψ reads as

$$S_\psi = i \int d^4x \sqrt{-g} (\bar{\psi} \Gamma^M \mathcal{D}_M \psi - m \bar{\psi} \psi), \quad (21)$$

where $\bar{\psi} = \psi^\dagger \Gamma^t$, and

$$\mathcal{D}_M = \partial_M + \frac{1}{4} \omega_{abM} \Gamma^{ab} - iqA_M, \quad (22)$$

where ω_{abM} is the spin connection, and $\Gamma^{ab} = \frac{1}{2}[\Gamma^a, \Gamma^b]$. Here, M and a, b denote the bulk space-time and tangent space indices, respectively, while μ, ν are indices along the boundary directions, i.e., $M = (r, \mu)$. Gamma matrix basis (Minkowski signature) is given by Eq. (A12) as in [7].

We will be interested in spectra and response functions of the boundary fermions in the presence of magnetic field. This requires solving the Dirac equation in the bulk [5,6]:

$$(\Gamma^M \mathcal{D}_M - m)\psi = 0. \quad (23)$$

From the solution of the Dirac equation at small ω , an analytic expression for the retarded fermion Green's function of the boundary CFT at zero magnetic field has been obtained in [7]. Near the Fermi surface, it reads as [7]:

$$G_R(\Omega, k) = \frac{(-h_1 v_F)}{\omega - v_F k_\perp - \Sigma(\omega, T)}, \quad (24)$$

where $k_\perp = k - k_F$ is the perpendicular distance from the Fermi surface in momentum space, h_1 and v_F are real constants calculated below, and the self-energy $\Sigma = \Sigma_1 + i\Sigma_2$ is given by [7]

$$\begin{aligned} \Sigma(\omega, T)/v_F &= T^{2\nu} g\left(\frac{\omega}{T}\right) \\ &= (2\pi T)^{2\nu} h_2 e^{i\theta - i\pi\nu} \frac{\Gamma(\frac{1}{2} + \nu - \frac{i\omega}{2\pi T} + \frac{i\mu_q}{6})}{\Gamma(\frac{1}{2} - \nu - \frac{i\omega}{2\pi T} + \frac{i\mu_q}{6})}, \end{aligned} \quad (25)$$

where ν is the zero temperature conformal dimension at the Fermi momentum, $\nu \equiv \nu_{k_F}$, given by Eq. (58), $\mu_q \equiv \mu q$, h_2 is a positive constant, and the phase θ is such that the poles of the Green's function are located in the lower half of the complex frequency plane. These poles correspond to quasinormal modes of the Dirac equation (23), and they can be found numerically solving $F(\omega_*) = 0$ [22], with

$$F(\omega) = \frac{k_\perp}{\Gamma(\frac{1}{2} + \nu - \frac{i\omega}{2\pi T} + \frac{i\mu_q}{6})} - \frac{h_2 e^{i\theta - i\pi\nu} (2\pi T)^{2\nu}}{\Gamma(\frac{1}{2} - \nu - \frac{i\omega}{2\pi T} + \frac{i\mu_q}{6})}. \quad (26)$$

The solution gives the full motion of the quasinormal poles $\omega_*^{(n)}(k_\perp)$ in the complex ω plane as a function of k_\perp . It has been found in [7,22], that, if the charge of the fermion is large enough compared to its mass, the pole closest to the real ω axis bounces off the axis at $k_\perp = 0$ (and $\omega = 0$). Such behavior is identified with the existence of the Fermi momentum k_F , indicative of an underlying strongly coupled Fermi surface.

At $T = 0$, the self-energy becomes $T^{2\nu} g(\omega/T) \rightarrow c_k \omega^{2\nu}$, and the Green's function obtained from the solution to the Dirac equation reads [7]

$$G_R(\Omega, k) = \frac{(-h_1 v_F)}{\omega - v_F k_\perp - h_2 v_F e^{i\theta - i\pi\nu} \omega^{2\nu}}, \quad (27)$$

where $k_\perp = \sqrt{k^2} - k_F$. The last term is determined by the IR AdS₂ physics near the horizon. Other terms are determined by the UV physics of the AdS₄ bulk.

The solutions to (23) have been studied in detail in [5–7]. Here, we simply summarize the novel aspects due to the background magnetic field (formal details can be found in the Appendix A).

- (i) The background magnetic field h introduces a discretization of the momentum (see Appendix A for details):

$$k \rightarrow k_{\text{eff}} = \sqrt{2|qh|l}, \quad \text{with } l \in N, \quad (28)$$

with Landau-level index l [12,22]. These discrete values of k are the analogue of the well-known Landau levels that occur in magnetic systems.

- (ii) There exists a (noninvertible) mapping on the level of Green's functions, from the magnetic system to the nonmagnetic one by sending

$$(H, Q, q) \mapsto \left(0, \sqrt{Q^2 + H^2}, q\sqrt{1 - \frac{H^2}{Q^2 + H^2}}\right). \quad (29)$$

The Green's functions in a magnetic system are thus equivalent to those in the absence of magnetic fields. To better appreciate that, we reformulate Eq. (29) in terms of the boundary quantities:

$$(h, \mu_q, T) \mapsto \left(0, \mu_q, T\left(1 - \frac{h^2}{12\mu^2}\right)\right), \quad (30)$$

where we used dimensionless variables defined in Eqs. (15) and (17). The magnetic field thus effectively decreases the coupling constant q and increases the chemical potential $\mu = g_F Q$, such that the combination $\mu_q \equiv \mu q$ is preserved [11]. This is an important point, as the equations of motion actually only depend on this combination and not on μ and q separately [11]. In other words, Eq. (30) implies that the additional scale brought about by the magnetic field can be understood as changing μ and T independently in the effective nonmagnetic system instead of only tuning the ratio μ/T . This point is important when considering the thermodynamics.

- (iii) The discrete momentum $k_{\text{eff}} = \sqrt{2|qh|l}$ must be held fixed in the transformation (29). The bulk-boundary relation is particularly simple in this case, as the Landau levels can readily be seen in

the bulk solution, only to remain identical in the boundary theory.

- (iv) Similar to the nonmagnetic system [11], the IR physics is controlled by the near-horizon $\text{AdS}_2 \times \mathbb{R}^2$ geometry, which indicates the existence of an IR CFT, characterized by operators \mathcal{O}_l , $l \in N$ with operator dimensions $\delta = 1/2 + \nu_l$:

$$\nu_l = \frac{1}{6} \sqrt{6 \left(m^2 + \frac{2|qh|l}{r_{**}^2} \right) - \frac{\mu_q^2}{r_{**}^4}}, \quad (31)$$

in dimensionless notation, and $\mu_q \equiv \mu q$. At $T = 0$, when $r_{**} = 1$, it becomes

$$\nu_l = \frac{1}{6} \sqrt{6(m^2 + 2|qh|l) - \mu_q^2}. \quad (32)$$

The Green's function for these operators \mathcal{O}_l is found to be $\mathcal{G}_l^R(\omega) \sim \omega^{2\nu_l}$, and the exponents ν_l determine the dispersion properties of the quasiparticle excitations. For $\nu > 1/2$, the system has a stable quasiparticle and a linear dispersion, whereas, for $\nu \leq 1/2$, one has a non-Fermi liquid with power-law dispersion and an unstable quasiparticle.

III. MAGNETIC FIELDS AND CONFORMAL INVARIANCE

Despite the fact that a magnetic field introduces a scale, in the absence of a chemical potential, all spectral functions are essentially still determined by conformal symmetry. To show this, we need to establish certain properties of the near-horizon geometry of a Reissner-Nordström black hole. This leads to the AdS_2 perspective that was developed in [7]. The result relies on the conformal algebra and its relation to the magnetic group, from the viewpoint of the infrared CFT that was studied in [7]. Later on, we will see that the insensitivity to the magnetic field also carries over to AdS_4 and the UV CFT in some respects. To simplify the derivations, we consider the case $T = 0$.

A. The near-horizon limit and Dirac equation in AdS_2

It was established in [7] that an electrically charged extremal AdS-Reissner-Nordström black hole has an AdS_2 throat in the inner bulk region. This conclusion carries over to the magnetic case with some minor differences. We will now give a quick derivation of the AdS_2 formalism for a dyonic black hole, referring the reader to [7] for more details (that remain largely unchanged in the magnetic field).

Near the horizon $r = r_{**}$ of the black hole described by the metric (2), the redshift factor $f(r)$ develops a double zero:

$$f(r) = 6 \frac{(r - r_{**})^2}{r_{**}^2} + \mathcal{O}((r - r_{**})^3). \quad (33)$$

Now consider the scaling limit

$$r - r_{**} = \lambda \frac{R_2^2}{\zeta}, \quad t = \lambda^{-1} \tau, \quad (34)$$

$$\lambda \rightarrow 0 \quad \text{with} \quad \tau, \zeta \text{ finite.}$$

In this limit, the metric (2) and the gauge field reduce to

$$ds^2 = \frac{R_2^2}{\zeta^2} (-d\tau^2 + d\zeta^2) + \frac{r_{**}^2}{R_2^2} (dx^2 + dy^2) \quad (35)$$

$$A_\tau = \frac{\mu R_2^2 r_0}{r_{**}^2} \frac{1}{\zeta}, \quad A_x = Hx,$$

where $R_2 = \frac{R}{\sqrt{6}}$. The geometry described by this metric is indeed $\text{AdS}_2 \times \mathbb{R}^2$. Physically, the scaling limit given in Eq. (34) with finite τ corresponds to the long time limit of the original time coordinate t , which translates to the low frequency limit of the boundary theory:

$$\frac{\omega}{\mu} \rightarrow 0, \quad (36)$$

where ω is the frequency conjugate to t . (One can think of λ as being the frequency ω). Near the AdS_4 horizon, we expect the AdS_2 region of an extremal dyonic black hole to have a CFT_1 dual. We refer to [7] for an account of this $\text{AdS}_2/\text{CFT}_1$ duality. The horizon of AdS_2 region is at $\zeta \rightarrow \infty$ (the coefficient in front of $d\tau$ vanishes at the horizon in Eq. (35)), and the infrared CFT (IR CFT) lives at the AdS_2 boundary at $\zeta = 0$. The scaling picture given by Eqs. (34) and (35) suggests that in the low frequency limit, the 2-dimensional boundary theory is described by this IR CFT (which is a CFT_1). The Green's function for the operator \mathcal{O} in the boundary theory is obtained through a small frequency expansion and a matching procedure between the two different regions (inner and outer) along the radial direction and can be expressed through the Green's function of the IR CFT [7].

The explicit form for the Dirac equation (A28) in the magnetic field is of little interest for the analytical results that follow; for completeness, we give it in the Appendix A. Of primary interest is its limit in the IR region with metric given by Eq. (35):

$$\left(-\frac{1}{\sqrt{g_{\zeta\zeta}}} \sigma^3 \partial_\zeta - m + \frac{1}{\sqrt{-g_{\tau\tau}}} \sigma^1 \left(\omega + \frac{\mu_q R_2^2 r_0}{r_{**}^2 \zeta} \right) - \frac{1}{\sqrt{g_{ii}} i \sigma^2 \lambda_l} \right) F^{(l)} = 0, \quad (37)$$

where the effective momentum of the l -th Landau level is $\lambda_l = \sqrt{2|qh|l}$, $\mu_q \equiv \mu q$, and we omit the index of the spinor field. To obtain Eq. (37), it is convenient to pick the gamma matrix basis as $\Gamma^{\hat{\zeta}} = -\sigma_3$, $\Gamma^{\hat{\tau}} = i\sigma_1$, and $\Gamma^{\hat{i}} = -\sigma_2$. We can write explicitly:

$$\begin{pmatrix} \frac{\zeta}{R_2} \partial_\zeta + m & -\frac{\zeta}{R_2} \left(\omega + \frac{\mu_q R_2^2 r_0}{r_{**}^2 \zeta} \right) + \frac{R}{r_{**}} \lambda_l \\ \frac{\zeta}{R_2} \left(\omega + \frac{\mu_q R_2^2 r_0}{r_{**}^2 \zeta} \right) + \frac{R}{r_{**}} \lambda_l & \frac{\zeta}{R_2} \partial_\zeta - m \end{pmatrix} \begin{pmatrix} y \\ z \end{pmatrix} = 0. \quad (38)$$

Note that the AdS₂ radius R_2 enters for the (τ, ζ) directions. At the AdS₂ boundary, $\zeta \rightarrow 0$, the Dirac equation to the leading order is given by

$$\zeta \partial_\zeta F^{(l)} = -UF^{(l)},$$

$$U = R_2 \begin{pmatrix} m & -\frac{\mu_q R_2 r_0}{r_{**}^2} + \frac{R}{r_{**}} \lambda_l \\ \frac{\mu_q R_2 r_0}{r_{**}^2} + \frac{R}{r_{**}} \lambda_l & -m \end{pmatrix}. \quad (39)$$

The solution to this equation is given by the scaling function $F^{(l)} = Ae_+ \zeta^{-\nu_l} + Be_- \zeta^{\nu_l}$, where e_\pm are the real eigenvectors of U and the exponent is

$$\nu_l = \frac{1}{6} \sqrt{6 \left(m^2 + \frac{R^2}{r_{**}^2} 2|qh|l \right) R^2 - \frac{\mu_q^2 R^4 r_0^2}{r_{**}^4}}. \quad (40)$$

The conformal dimension of the operator \mathcal{O} in the IR CFT is $\delta_l = \frac{1}{2} + \nu_l$. Comparing Eq. (40) to the expression for the scaling exponent in [7], we conclude that the scaling properties and the AdS₂ construction are unmodified by the magnetic field, except that the scaling exponents are now fixed by the Landau quantization. This ‘‘quantization rule’’ was already exploited in [22] to study de Haas-van Alphen oscillations.

IV. SPECTRAL FUNCTIONS

In this section, we will explore some of the properties of the spectral function, in both plane wave and Landau-level basis. We first consider some characteristic cases in the plane wave basis and make connection with the angle-resolved photoemission spectroscopy (ARPES) measurements.

A. Relating to the ARPES measurements

In reality, ARPES measurements cannot be performed in magnetic fields so the holographic approach, allowing a direct insight into the propagator structure and the spectral function, is especially helpful. This follows from the observation that the spectral functions as measured in ARPES are always expressed in the plane wave basis of the photon. Thus, in a magnetic field, when the momentum is not a good quantum number anymore, it becomes impossible to perform the photoemission spectroscopy.

In order to compute the spectral function, we have to choose a particular fermionic plane wave as a probe. Since the separation of variables is valid throughout the bulk, the basis transformation can be performed at every constant

r -slice. This means that only the x and y coordinates have to be taken into account (the plane wave probe lives only at the CFT side of the duality). We take a plane wave propagating in the $+x$ direction with spin up along the r -axis. In its rest frame, such a particle can be described by

$$\Psi_{\text{probe}} = e^{i\omega t - ip_x x} \begin{pmatrix} \xi \\ \xi \end{pmatrix}, \quad \xi = \begin{pmatrix} 1 \\ 0 \end{pmatrix}. \quad (41)$$

Near the boundary (at $r_b \rightarrow \infty$), we can rescale our solutions of the Dirac equation making use of Eqs. (A23), (A24), and (B1):

$$F_l = \begin{pmatrix} \zeta_l^{(1)}(\tilde{x}) \\ \xi_+^{(l)}(r_b) \zeta_l^{(1)}(\tilde{x}) \\ \zeta_l^{(2)}(\tilde{x}) \\ -\xi_+^{(l)}(r_b) \zeta_l^{(2)}(\tilde{x}) \end{pmatrix}, \quad \tilde{F}_l = \begin{pmatrix} \zeta_l^{(1)}(\tilde{x}) \\ \xi_-^{(l)}(r_b) \zeta_l^{(1)}(\tilde{x}) \\ -\zeta_l^{(2)}(\tilde{x}) \\ \xi_-^{(l)}(r_b) \zeta_l^{(2)}(\tilde{x}) \end{pmatrix}, \quad (42)$$

with rescaled \tilde{x} defined after Eq. (A20). This representation is useful since we calculate the components $\xi_\pm(r_b)$ related to the retarded Green’s function in our numerics (we keep the notation of [7]).

Let \mathcal{O}_l and $\tilde{\mathcal{O}}_l$ be the CFT operators dual to F_l and \tilde{F}_l , respectively, and c_k^\dagger , c_k be the creation and annihilation operators for the plane wave state Ψ_{probe} . Since the states F and \tilde{F} form a complete set in the bulk, we can write

$$\begin{aligned} c_p^\dagger(\omega) &= \sum_l (U_l^*, \tilde{U}_l^*) \begin{pmatrix} \mathcal{O}_l^\dagger(\omega) \\ \tilde{\mathcal{O}}_l^\dagger(\omega) \end{pmatrix} \\ &= \sum_l (U_l^* \mathcal{O}_l^\dagger(\omega) + \tilde{U}_l^* \tilde{\mathcal{O}}_l^\dagger(\omega)), \end{aligned} \quad (43)$$

where the overlap coefficients $U_l(\omega)$ are given by the inner product between Ψ_{probe} and F :

$$\begin{aligned} U_l(p_x) &= \int dx F_l^\dagger i\Gamma^0 \Psi_{\text{probe}} \\ &= - \int dx e^{-ip_x x} \xi_+(r_b) (\zeta_l^{(1)\dagger}(\tilde{x}) - \zeta_l^{(2)\dagger}(\tilde{x})), \end{aligned} \quad (44)$$

with $\bar{F} = F^\dagger i\Gamma^0$ and a similar expression for \tilde{U}_l involving $\xi_-(r_b)$. The constants U_l can be calculated analytically using the numerical value of $\xi_\pm(r_b)$ and by noting that the Hermite functions are eigenfunctions of the Fourier transform. We are interested in the retarded Green’s function, defined as

$$\begin{aligned} G_{\mathcal{O}_l}^R(\omega, p) &= -i \int d^x t e^{i\omega t - ip \cdot x} \theta(t) G_{\mathcal{O}_l}^R(t, x) \\ G_{\mathcal{O}_l}^R(t, x) &= \langle 0 | [\mathcal{O}_l(t, x), \bar{\mathcal{O}}_l(0, 0)] | 0 \rangle \\ G^R &= \begin{pmatrix} G_{\mathcal{O}} & 0 \\ 0 & \tilde{G}_{\mathcal{O}} \end{pmatrix}, \end{aligned} \quad (45)$$

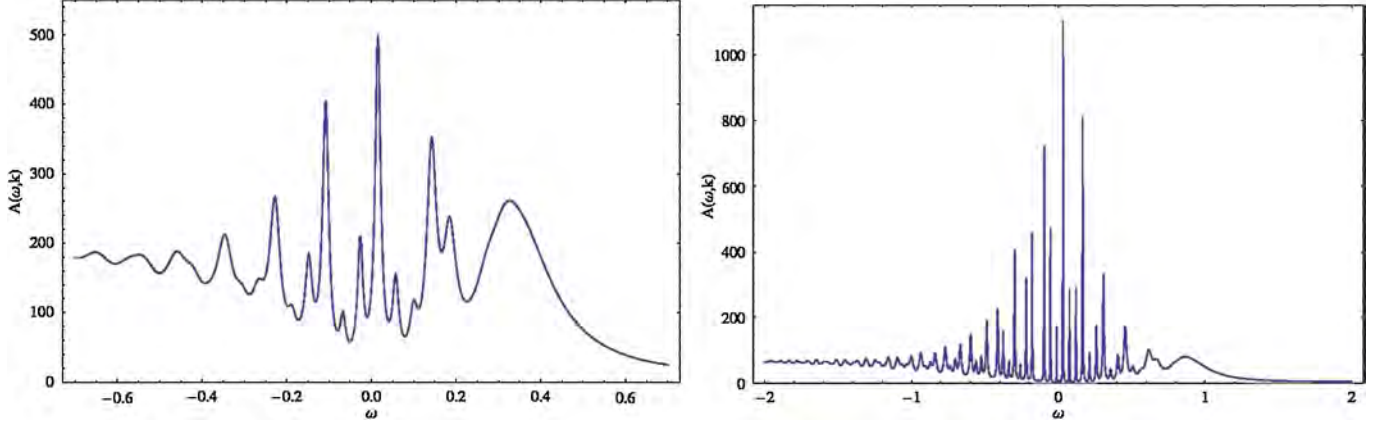


FIG. 1 (color online). Two examples of spectral functions in the plane wave basis for $\mu/T = 50$ and $h/T = 1$. The conformal dimension is $\Delta = 5/4$ (left) and $\Delta = 3/2$ (right). Frequency is in the units of effective temperature T_{eff} . The plane wave momentum is chosen to be $k = 1$. Despite the convolution of many Landau levels, the presence of the discrete levels is obvious.

where $\tilde{G}_{\mathcal{O}}$ is the retarded Green's function for the operator \mathcal{O} .

Exploiting the orthogonality of the spinors created by \mathcal{O} and \mathcal{O}^\dagger and using Eq. (43), the Green's function in the plane wave basis can be written as

$$\begin{aligned} G_{c_p}^R(\omega, p_x) &= \sum_l \text{tr} \left(\tilde{U} \right) (U^*, \tilde{U}^*) G^R \\ &= (|U_l(p_x)|^2 G_{\mathcal{O}_l}^R(\omega, l) + |\tilde{U}_l(p_x)|^2 \tilde{G}_{\mathcal{O}_l}^R(\omega, l)). \end{aligned} \quad (46)$$

In practice, we cannot perform the sum in Eq. (46) all the way to infinity, so we have to introduce a cutoff Landau-level l_{cut} . In most cases, we are able to make l_{cut} large enough that the behavior of the spectral function is clear.

Using the above formalism, we have produced spectral functions for two different conformal dimensions and fixed chemical potential and magnetic field (Fig. 1). Using the plane wave basis allows us to directly detect the Landau levels. The unit used for plotting the spectra (here and later on in the paper) is the effective temperature T_{eff} [5]:

$$T_{\text{eff}} = \frac{T}{2} \left(1 + \sqrt{1 + \frac{3\mu^2}{(4\pi T)^2}} \right). \quad (47)$$

This unit interpolates between μ at $T/\mu = 0$ and T at $T/\mu \rightarrow \infty$ and is convenient for the reason that the relevant quantities (e.g., Fermi momentum) are of order unity for any value of μ and h .

B. Magnetic crossover and disappearance of the quasiparticles

Theoretically, it is more convenient to consider the spectral functions in the Landau-level basis. For definiteness, let us pick a fixed conformal dimension $\Delta = \frac{5}{4}$ which corresponds to $m = -\frac{1}{4}$. In the limit of weak magnetic

fields, $h/T \rightarrow 0$, we should reproduce the results that were found in [5].

In Fig. 2(a), we indeed see that the spectral function, corresponding to a low value of μ/T , behaves as expected for a nearly conformal system. The spectral function is approximately symmetric about $\omega = 0$, it vanishes for $|\omega| < k$, up to a small residual tail due to finite temperature, and for $|\omega| \gg k$, it scales as ω^{2m} .

In Fig. 2(b), which corresponds to a high value of μ/T , we see the emergence of a sharp quasiparticle peak. This peak becomes the sharpest when the Landau-level l corresponding to an effective momentum $k_{\text{eff}} = \sqrt{2|qh|l}$ coincides with the Fermi momentum k_F . The peaks also broaden out when k_{eff} moves away from k_F . A more complete view of the Landau quantization in the quasiparticle regime is given in Fig. 3, where we plot the dispersion relation (ω - k map). Both the sharp peaks and the Landau levels can be visually identified.

Collectively, the spectra in Fig. 2 show that conformality is only broken by the chemical potential μ and not by the magnetic field. Naively, the magnetic field introduces a new scale in the system. However, this scale is absent from the spectral functions, visually validating the discussion in the previous section that the scale h can be removed by a rescaling of the temperature and chemical potential.

One thus concludes that there is some value h'_c of the magnetic field, depending on μ/T , such that the spectral function loses its quasiparticle peaks and displays near-conformal behavior for $h > h'_c$. The nature of the transition and the underlying mechanism depends on the parameters (μ_q, T, Δ). One mechanism, obvious from the rescaling in Eq. (29), is the reduction of the effective coupling q as h increases. This will make the influence of the scalar potential A_0 negligible and push the system back toward conformality. Generically, the spectral function shows no sharp change but is more indicative of a crossover.

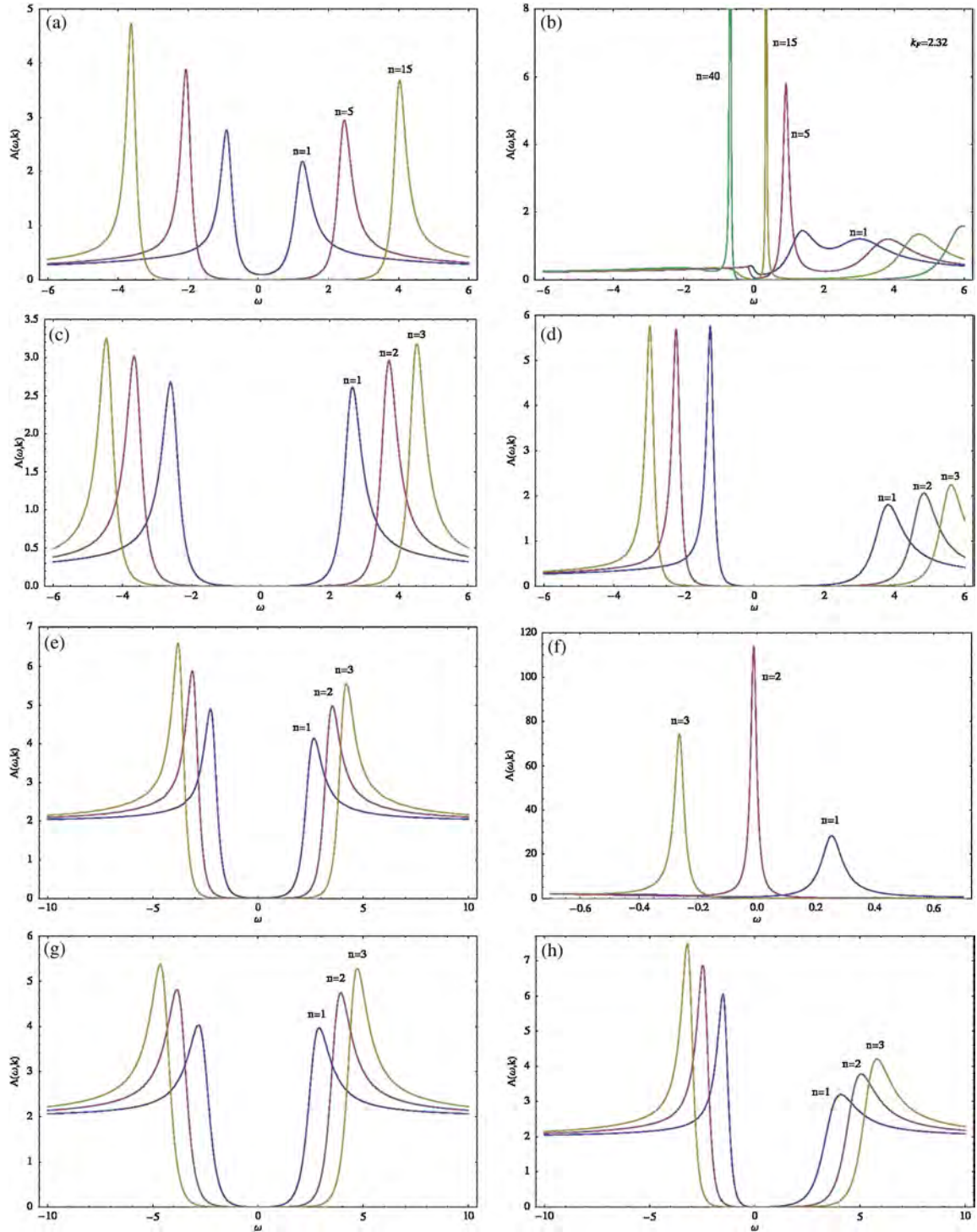


FIG. 2 (color online). Some typical examples of spectral functions $A(\omega, k_{\text{eff}})$ vs ω in the Landau basis, $k_{\text{eff}} = \sqrt{2|qh|n}$. The top four correspond to a conformal dimension $\Delta = \frac{5}{4}$ ($m = -\frac{1}{4}$), and the bottom four to $\Delta = \frac{3}{2}$ ($m = 0$). In each plot, we show different Landau levels, labeled by index n , as a function of μ/T and h/T . The ratios take values $(\mu/T, h/T) = (1, 1), (50, 1), (1, 50), (50, 50)$ from left to right. The conformal case can be identified when μ/T is small, regardless of h/T (plots in the left panel). Nearly conformal behavior is seen when both μ/T and h/T are large. This confirms our analytic result that the behavior of the system is primarily governed by μ . Departure from the conformality and sharp quasiparticle peaks are seen when μ/T is large and h/T is small in parts (b) and (f). Multiple quasiparticle peaks arise whenever $k_{\text{eff}} = k_F$. This suggests the existence of a critical magnetic field, beyond which the quasiparticle description becomes invalid and the system exhibits a conformal-like behavior. As before, the frequency ω is in units of T_{eff} .

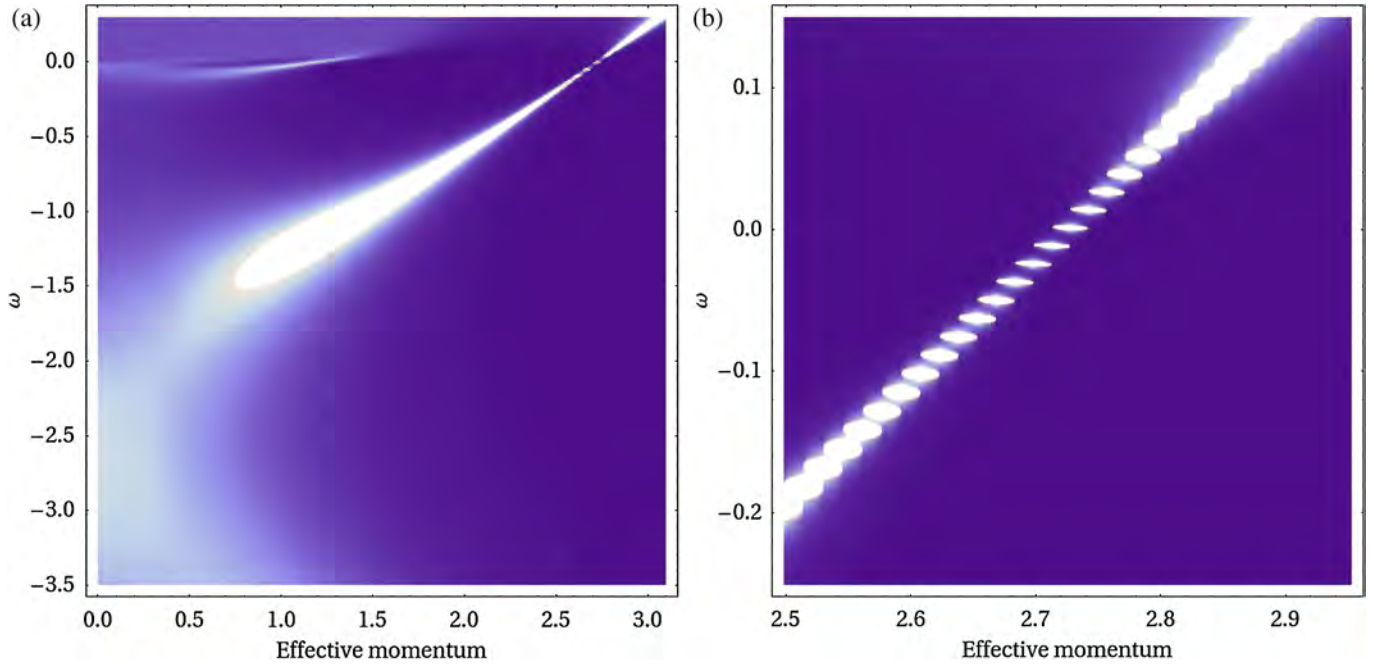


FIG. 3 (color online). Dispersion relation ω vs k_{eff} for $\mu/T = 50$, $h/T = 1$, and $\Delta = \frac{5}{4}$ ($m = -\frac{1}{4}$). The spectral function $A(\omega, k_{\text{eff}})$ is displayed as a density plot. (a) On a large energy and momentum scale, we clearly see that the peaks disperse almost linearly ($\omega \approx v_F k$), indicating that we are in the stable quasiparticle regime. (b) A zoom-in near the location of the Fermi surface shows clear Landau quantization.

A more interesting phenomenon is the disappearance of coherent quasiparticles at high effective chemical potentials. For the special case $m = 0$, we can go beyond numerics and study this transition analytically, combining the exact $T = 0$ solution found in [21] and the mapping (30). In the next section, we will show that the transition is controlled by the change in the dispersion of the quasiparticle and corresponds to a sharp phase transition. Increasing the magnetic field leads to a decrease in phenomenological control parameter ν_{k_F} . This can give rise to a transition to a non-Fermi liquid when $\nu_{k_F} \leq 1/2$, and,

finally, to the conformal regime at $h = h'_c$ when $\nu_{k_F} = 0$ and the Fermi surface vanishes.

C. Density of states

As argued at the beginning of this section, the spectral function can look quite different depending on the particular basis chosen. Though the spectral function is an attractive quantity to consider due to connection with ARPES experiments, we will also direct our attention to basis-independent and manifestly gauge invariant quantities. One of them is the density of states, defined by

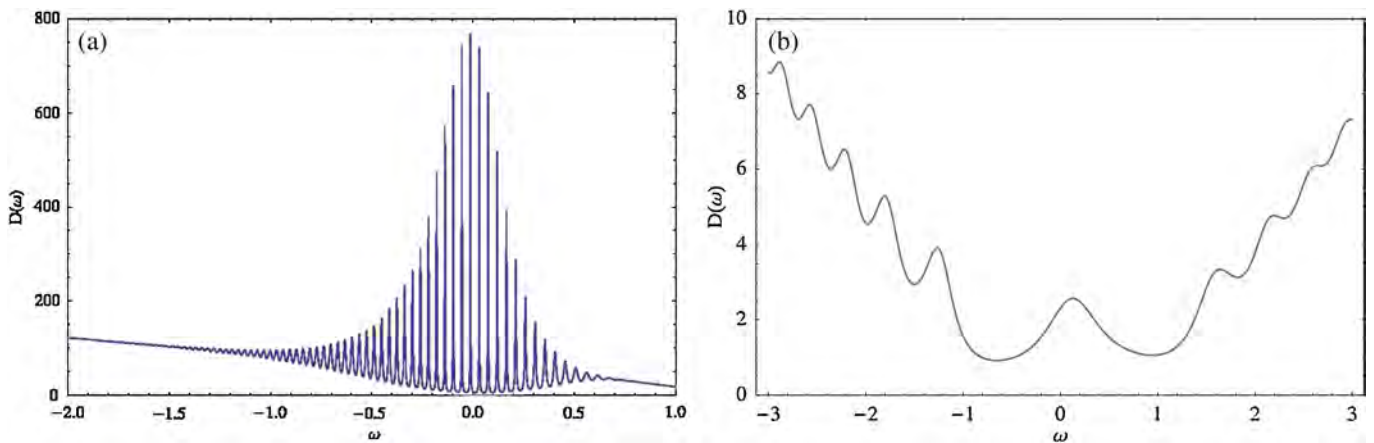


FIG. 4 (color online). Density of states $D(\omega)$ for $m = -\frac{1}{4}$ and (a) $\mu/T = 50$, $h/T = 1$, and (b) $\mu/T = 1$, $h/T = 1$. Sharp quasiparticle peaks from the splitting of the Fermi surface are clearly visible in (a). The case (b) shows square-root level spacing characteristic of a (nearly) Lorentz invariant spectrum, such as that of graphene.

$$D(\omega) = \sum_l A(\omega, l), \quad (48)$$

where the usual integral over the momentum is replaced by a sum since only discrete values of the momentum are allowed.

In Fig. 4, we plot the density of states for two systems. We clearly see the Landau splitting of the Fermi surface. A peculiar feature of these plots is that the density of states seems to grow for negative values of ω . This, however, is an artifact of our calculation. Each individual spectrum in the sum Eq. (48) has a finite tail that scales as ω^{2m} for large ω , so each term has a finite contribution for large values of ω . When the full sum is performed, this fact implies that $\lim_{\omega \rightarrow \infty} D(\omega) \rightarrow \infty$. The relevant information on the density of states can be obtained by regularizing the sum, which, in practice, is done by summing over a finite number of terms only and then considering the peaks that lie on top of the resulting finite-sized envelope. The physical point in Fig. 4(a) is the linear spacing of Landau levels, corresponding to a nonrelativistic system at finite density. This is to be contrasted with Fig. 4(b), where the level spacing behaves as $\propto \sqrt{h}$, appropriate for a Lorentz invariant system and realized in graphene [23].

V. FERMI LEVEL STRUCTURE AT ZERO TEMPERATURE

In this section, we solve the Dirac equation in the magnetic field for the special case $m = 0$ ($\Delta = \frac{3}{2}$). Although there are no additional symmetries in this case, it is possible to get an analytic solution. Using this solution, we obtain Fermi-level parameters such as k_F and v_F and consider the process of filling the Landau levels as the magnetic field is varied.

A. Dirac equation with $m = 0$

In the case $m = 0$, it is convenient to solve the Dirac equation including the spin connection (Eq. (A2)) rather than scaling it out:

$$\left(-\frac{\sqrt{g_{ii}}}{\sqrt{g_{rr}}} \sigma^1 \partial_r - \frac{\sqrt{g_{ii}}}{\sqrt{-g_{tt}}} \sigma^3 (\omega + qA_t) + \frac{\sqrt{g_{ii}}}{\sqrt{-g_{tt}}} \sigma^1 \frac{1}{2} \omega_{\hat{r}\hat{t}} - \sigma^1 \frac{1}{2} \omega_{\hat{x}\hat{r}x} - \sigma^1 \frac{1}{2} \omega_{\hat{y}\hat{r}y} - \lambda_l \right) \otimes 1 \begin{pmatrix} \psi_1 \\ \psi_2 \end{pmatrix} = 0, \quad (49)$$

where $\lambda_l = \sqrt{2|qh|l}$ are the energies of the Landau levels $l = 0, 1, \dots$, $g_{ii} \equiv g_{xx} = g_{yy}$, $A_t(r)$ is given by Eq. (3), and the gamma matrices are defined in Eq. (A12). In the basis of Eq. (A12), the two components ψ_1 and ψ_2 decouple. Therefore, in what follows, we solve for the first component only (we omit index 1). Substituting the spin connection, we have [18]:

$$\left(-\frac{r^2 \sqrt{f}}{R^2} \sigma^1 \partial_r - \frac{1}{\sqrt{f}} \sigma^3 (\omega + qA_t) - \sigma^1 \frac{r\sqrt{f}}{2R^2} \left(3 + \frac{rf'}{2f} \right) - \lambda_l \right) \psi = 0, \quad (50)$$

with $\psi = (y_1, y_2)$. It is convenient to change to the basis

$$\begin{pmatrix} \tilde{y}_1 \\ \tilde{y}_2 \end{pmatrix} = \begin{pmatrix} 1 & -i \\ -i & 1 \end{pmatrix} \begin{pmatrix} y_1 \\ y_2 \end{pmatrix}, \quad (51)$$

which diagonalizes the system into a second order differential equation for each component. We introduce the dimensionless variables as in Eqs. (15)–(17) and make a change of the dimensionless radial variable:

$$r = \frac{1}{1-z}, \quad (52)$$

with the horizon now being at $z = 0$ and the conformal boundary at $z = 1$. Performing these transformations in Eq. (50), the second order differential equations for \tilde{y}_1 reads

$$\left(f \partial_z^2 + \left(\frac{3f}{1-z} + f' \right) \partial_z + \frac{15f}{4(1-z)^2} + \frac{3f'}{2(1-z)} + \frac{f''}{4} + \frac{1}{f} \left((\omega + q\mu z) \pm \frac{if'}{4} \right)^2 - iq\mu - \lambda_l^2 \right) \tilde{y}_1 = 0. \quad (53)$$

The second component \tilde{y}_2 obeys the same equation with $\mu \mapsto -\mu$.

At $T = 0$,

$$f = 3z^2(z - z_0)(z - \bar{z}_0), \quad z_0 = \frac{1}{3}(4 + i\sqrt{2}). \quad (54)$$

The solution of this fermion system at zero magnetic field and zero temperature $T = 0$ has been found in [21]. To solve Eq. (53), we use the mapping to a zero magnetic field system, Eq. (29). The combination $\mu_q \equiv \mu q$ at nonzero h maps to $\mu_{q,\text{eff}} \equiv \mu_{\text{eff}} q_{\text{eff}}$ at zero h as follows:

$$\begin{aligned} \mu_q &\mapsto q \sqrt{1 - \frac{H^2}{Q^2 + H^2}} \cdot g_F \sqrt{Q^2 + H^2} \\ &= \sqrt{3} q g_F \sqrt{1 - \frac{H^2}{3}} = \mu_{q,\text{eff}}, \end{aligned} \quad (55)$$

where at $T = 0$, we used $Q^2 + H^2 = 3$. We solve Eq. (53) for zero modes, i. e., $\omega = 0$, and at the Fermi surface $\lambda = k$ and implement Eq. (55).

Near the horizon ($z = 0$, $f = 6z^2$), we have

$$6z^2 \tilde{y}''_{1;2} + 12z \tilde{y}'_{1;2} + \left(\frac{3}{2} + \frac{(\mu_{q,\text{eff}})^2}{6} - k_F^2 \right) \tilde{y}_{1;2} = 0, \quad (56)$$

which gives the following behavior:

$$\tilde{y}_{1;2} \sim z^{-(1/2)\pm\nu_k}, \quad (57)$$

with the scaling exponent ν following from Eq. (32):

$$\nu = \frac{1}{6}\sqrt{6k^2 - (\mu_{q,\text{eff}})^2}, \quad (58)$$

at the momentum k . Using MAPLE, we find the zero-mode solution of Eq. (53) with a regular behavior $z^{-(1/2)+\nu}$ at the horizon [18,21]:

$$\begin{aligned} \tilde{y}_1^{(0)} = & N_1(z-1)^{3/2}z^{-(1/2)+\nu}(z-\bar{z}_0)^{-(1/2)-\nu} \\ & \times \left(\frac{z-z_0}{z-\bar{z}_0} \right)^{1/4(-1-\sqrt{2}\mu_{q,\text{eff}}/z_0)} {}_2F_1\left(\frac{1}{2} + \nu - \frac{\sqrt{2}}{3}\mu_{q,\text{eff}}, \nu \right. \\ & \left. + i\frac{\mu_{q,\text{eff}}}{6}, 1 + 2\nu, \frac{2i\sqrt{2}z}{3z_0(z-\bar{z}_0)}\right), \end{aligned} \quad (59)$$

and

$$\begin{aligned} \tilde{y}_2^{(0)} = & N_2(z-1)^{3/2}z^{-(1/2)+\nu}(z-\bar{z}_0)^{-(1/2)-\nu} \\ & \times \left(\frac{z-z_0}{z-\bar{z}_0} \right)^{1/4(-1+\sqrt{2}\mu_{q,\text{eff}}/z_0)} {}_2F_1\left(\frac{1}{2} + \nu + \frac{\sqrt{2}}{3}\mu_{q,\text{eff}}, \nu \right. \\ & \left. - i\frac{\mu_{q,\text{eff}}}{6}, 1 + 2\nu, \frac{2i\sqrt{2}z}{3z_0(z-\bar{z}_0)}\right), \end{aligned} \quad (60)$$

where ${}_2F_1$ is the hypergeometric function and N_1, N_2 are normalization factors. Since normalization factors are constants, we find their relative weight by substituting solutions given in Eq. (59) back into the first order differential equations at $z \sim 0$,

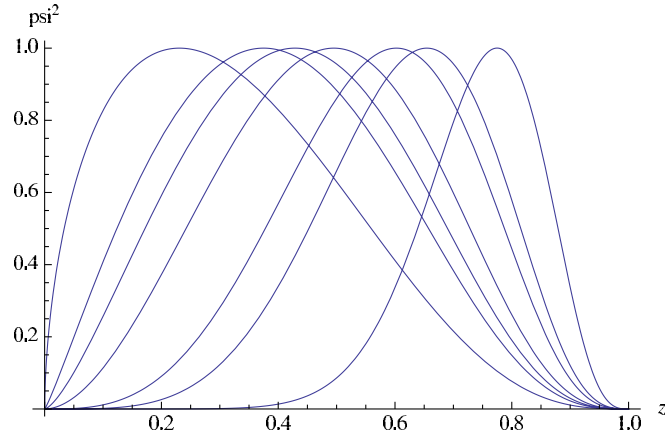


FIG. 5 (color online). Density of the zero-mode $\psi^{0\dagger}\psi^0$ vs the radial coordinate z (the horizon is at $z = 0$, and the boundary is at $z = 1$) for different values of the magnetic field h for the first (with the largest root for k_F) Fermi surface. We set $g_F = 1$ ($h \rightarrow H$) and $q = \frac{15}{\sqrt{3}}$ ($\mu_{q,\text{eff}} \rightarrow 15\sqrt{1 - \frac{H^2}{3}}$). From right to left, the values of the magnetic field are $H = \{0, 1.4, 1.5, 1.6, 1.63, 1.65, 1.68\}$. The amplitudes of the curves are normalized to unity. At weak magnetic fields, the wave function is supported away from the horizon, while, at strong fields, it is supported near the horizon.

$$\frac{N_1}{N_2} = -\frac{6i\nu + \mu_{q,\text{eff}}}{\sqrt{6}k} \left(\frac{z_0}{\bar{z}_0} \right)^{\mu_{q,\text{eff}}/\sqrt{2}z_0}. \quad (61)$$

The same relations are obtained when calculations are done for any z . The second solution $\tilde{\eta}_{1;2}^{(0)}$, with behavior $z^{-(1/2)-\nu}$ at the horizon, is obtained by replacing $\nu \rightarrow -\nu$ in Eq. (59).

To get insight into the zero-mode solution (59), we plot the radial profile for the density function $\psi^{(0)\dagger}\psi^{(0)}$ for different magnetic fields in Fig. 5. The momentum chosen is the Fermi momentum of the first Fermi surface (see the next section). The curves are normalized to have the same maxima. Magnetic field is increased from right to left. At small magnetic field, the zero modes are supported away from the horizon, while at large magnetic field, the zero modes are supported near the horizon. This means that at large magnetic field, the influence of the black hole to the Fermi level structure becomes more important.

B. Magnetic effects on the Fermi momentum and Fermi velocity at $T = 0$

In the presence of a magnetic field, there is only a true pole in the Green's function whenever the Landau level crosses the Fermi energy [22]

$$2l|qh| = k_F^2. \quad (62)$$

As shown in Fig. 2, whenever Eq. (62) is satisfied, the spectral function $A(\omega)$ has a (sharp) peak. This is not surprising, since quasiparticles can be easily excited from the Fermi surface. From Eq. (62), the spectral function $A(\omega)$ and the density of states on the Fermi surface $D(\omega)$ are periodic in $\frac{1}{h}$ with the period

$$\Delta\left(\frac{1}{h}\right) = \frac{2\pi q}{A_F}, \quad (63)$$

where $A_F = \pi k_F^2$ is the area of the Fermi surface [22]. This is a manifestation of the de Haas-van Alphen quantum oscillations. At $T = 0$, the electronic properties of metals depend on the density of states on the Fermi surface. Therefore, an oscillatory behavior as a function of magnetic field should appear in any quantity that depends on the density of states on the Fermi energy. Magnetic susceptibility [22] and magnetization together with the superconducting gap [24] have been shown to exhibit quantum oscillations. Every Landau level contributes an oscillating term, and the period of the l -th level oscillation is determined by the value of the magnetic field h that satisfies Eq. (62) for the given value of k_F . Quantum oscillations (and the quantum Hall effect, which we consider later in the paper) are examples of phenomena in which Landau-level physics reveals the presence of the Fermi surface. The superconducting gap found in the quark matter in magnetic fields [24] is another evidence for the existence of the (highly degenerate) Fermi surface and the corresponding Fermi momentum.

Generally, a Fermi surface controls the occupation of energy levels in the system: The energy levels below the Fermi surface are filled, and those above are empty (or nonexistent). Here, however, the association to the Fermi momentum can be obscured by the fact that the fermions form highly degenerate Landau levels. Thus, in two dimensions, in the presence of the magnetic field, the corresponding effective Fermi surface is given by a single point in the phase space that is determined by n_F , the Landau index of the highest occupied level, i.e., the highest Landau level below the chemical potential.² Increasing the magnetic field, Landau levels “move up” in the phase space, leaving only the lower levels occupied, so that the effective Fermi momentum scales roughly (excluding interactions) as a square root of the magnetic field, $k_F \sim \sqrt{n_F} \sim k_F^{\max} \sqrt{1 - h/h_{\max}}$. High magnetic fields drive the effective density of the charge carriers down, approaching the limit when the Fermi momentum coincides with the lowest Landau level.

Many phenomena observed in the paper can thus be qualitatively explained by Landau quantization. As discussed before, the notion of the Fermi momentum is lost at very high magnetic fields. In what follows, the quantitative Fermi-level structure at zero temperature, described by k_F and v_F values, is obtained as a function of the magnetic field using the solution of the Dirac equation given by Eqs. (59) and (60). As in [11], we neglect first the discrete nature of the Fermi momentum and velocity in order to obtain general understanding. Upon taking the quantization into account, the smooth curves become combinations of step functions following the same trend as the smooth curves (without quantization). While usually the grand canonical ensemble is used, where the fixed chemical potential controls the occupation of the Landau levels [25], in our setup, the Fermi momentum is allowed to change as the magnetic field is varied, while we keep track of the IR conformal dimension ν .

The Fermi momentum is defined by the matching between IR and UV physics [7]. Therefore, it is enough to know the solution at $\omega = 0$, where the matching is performed. To obtain the Fermi momentum, we require that the zero-mode solution is regular at the horizon ($\psi^{(0)} \sim z^{-(1/2)+\nu}$) and normalizable at the boundary. At the boundary $z \sim 1$, the wave function behaves as

$$a(1-z)^{3/2-m} \begin{pmatrix} 1 \\ 0 \end{pmatrix} + b(1-z)^{3/2+m} \begin{pmatrix} 0 \\ 1 \end{pmatrix}. \quad (64)$$

To require it to be normalizable is to set the first term $a = 0$; the wave function at $z \sim 1$ is then

$$\psi^{(0)} \sim (1-z)^{3/2+m} \begin{pmatrix} 0 \\ 1 \end{pmatrix}. \quad (65)$$

²We would like to thank Igor Shovkovy for clarifying the issue with the Fermi momentum in the presence of the magnetic field.

Equation (65) leads to the condition $\lim_{z \rightarrow 1} (z-1)^{-3/2} \times (\tilde{y}_2^{(0)} + i\tilde{y}_1^{(0)}) = 0$, which, together with Eq. (59), gives the following equation for the Fermi momentum as function of the magnetic field [18,21]:

$$\begin{aligned} & \frac{2F_1(1 + \nu + \frac{i\mu_{q,\text{eff}}}{6}, \frac{1}{2} + \nu - \frac{\sqrt{2}\mu_{q,\text{eff}}}{3}, 1 + 2\nu, \frac{2}{3}(1 - i\sqrt{2}))}{2F_1(\nu + \frac{i\mu_{q,\text{eff}}}{6}, \frac{1}{2} + \nu - \frac{\sqrt{2}\mu_{q,\text{eff}}}{3}, 1 + 2\nu, \frac{2}{3}(1 - i\sqrt{2}))} \\ &= \frac{6\nu - i\mu_{q,\text{eff}}}{k_F(-2i + \sqrt{2})}, \end{aligned} \quad (66)$$

with $\nu \equiv \nu_{k_F}$ given by Eq. (58). Using MATHEMATICA to evaluate the hypergeometric functions, we numerically solve the equation for the Fermi surface, which gives effective momentum as if it were continuous, i.e., when quantization is neglected. The solutions of Eq. (66) are given in Fig. 6. There are multiple Fermi surfaces for a given magnetic field h . Here, and in all other plots, we choose $g_F = 1$. Therefore, $h \rightarrow H$ and $q = \frac{15}{\sqrt{3}}$. In Fig. 6, positive and negative k_F correspond to the Fermi surfaces in the Green's functions G_1 and G_2 . The relation between two components is $G_2(\omega, k) = G_1(\omega, -k)$ [6]. Therefore, Fig. 6 is not symmetric with respect to the x-axis. Effective momenta terminate at the dashed line $\nu_{k_F} = 0$. Taking into account Landau quantization of $k_F \rightarrow \sqrt{2|qh|l}$ with $l = 1, 2, \dots$, the plot consists of stepwise functions tracing the existing curves (we depict only positive k_F). Indeed, Landau

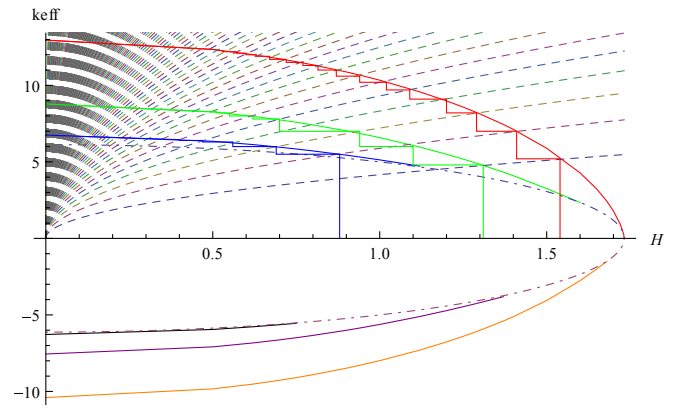


FIG. 6 (color online). Effective momentum k_{eff} vs the magnetic field $h \rightarrow H$ (we set $g_F = 1$, $q = \frac{15}{\sqrt{3}}$). As we increase the magnetic field, the Fermi surface shrinks. Smooth solid curves represent the situation as if momentum is a continuous parameter (for convenience), stepwise solid functions are the real Fermi momenta, which are discretized due to the Landau-level quantization: $k_F \rightarrow \sqrt{2|qh|l}$, with $l = 1, 2, \dots$, where $\sqrt{2|qh|l}$ are Landau levels given by dotted lines (only positive discrete k_F are shown). At a given h , there are multiple Fermi surfaces. From right to left are the first, second, etc., Fermi surfaces. The dashed-dotted line is $\nu_{k_F} = 0$, where k_F is terminated. Positive and negative k_{eff} correspond to Fermi surfaces in two components of the Green's function.

quantization can be also seen from the dispersion relation at Fig. 3, where only discrete values of effective momentum are allowed, and the Fermi surface has been chopped up as a result of quantization, Fig. 3(b).

Our findings agree with the results for the (largest) Fermi momentum in a 3-dimensional magnetic system considered in [26] (compare the stepwise dependence $k_F(h)$ with Fig. (5) in [26]).

In Fig. 7, the Landau-level index l is obtained from $k_F(h) = \sqrt{2|qh|l}$, where $k_F(h)$ is a numerical solution of Eq. (66). Only those Landau levels which are below the Fermi surface are filled. In Fig. 6, as we decrease magnetic field, first nothing happens until the next Landau level crosses the Fermi surface, which corresponds to a jump up to the next step. Therefore, at strong magnetic fields,

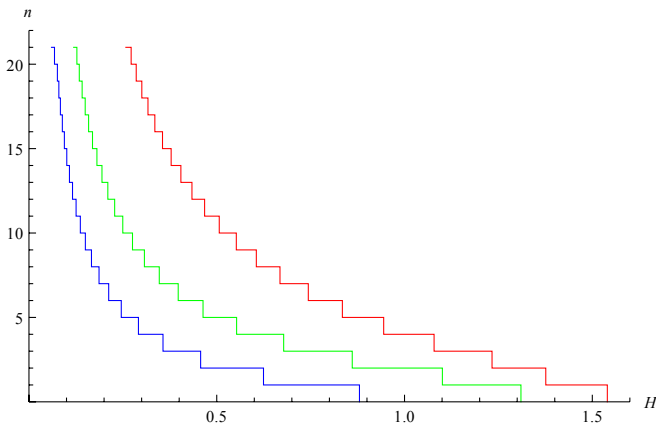


FIG. 7 (color online). Landau-level numbers n , corresponding to the quantized Fermi momenta vs the magnetic field $h \rightarrow H$ for the three Fermi surfaces with positive k_F . We set $g_F = 1$, $q = \frac{15}{\sqrt{3}}$. From right to left are the first, second, and third Fermi surfaces.

fewer states contribute to transport properties, and the lowest Landau level becomes more important (see the next section). At weak magnetic fields, the sum over many Landau levels has to be taken, ending with the continuous limit as $h \rightarrow 0$, when quantization can be ignored.

In Fig. 8, we show the IR conformal dimension as a function of the magnetic field. We have used the numerical solution for k_F . Fermi-liquid regime takes place at magnetic fields $h < h_c$, while non-Fermi liquids exist in a narrow band at $h_c < h < h'_c$, and at h'_c the system becomes near-conformal.

In this figure, we observe the pathway of the possible phase transition exhibited by the Fermi surface (ignoring Landau quantization): It can vanish at the line $\nu_{k_F} = 0$, undergoing a crossover to the conformal regime, or cross the line $\nu_{k_F} = 1/2$ and go through a non-Fermi-liquid regime, and, subsequently, cross to the conformal phase. Note that the primary Fermi surface with the highest k_F and ν_{k_F} seems to directly cross over to conformality, while the other Fermi surfaces first exhibit a strange-metal phase transition. Therefore, all the Fermi momenta with $\nu_{k_F} > 0$ contribute to the transport coefficients of the theory. In particular, at high magnetic fields, only the first (largest) Fermi momentum $k_F^{(1)}$ is nonzero and the lowest Landau level $n = 0$ becomes increasingly important. The lowest Landau level contributes to the transport with half-degeneracy factor, as compared to the higher Landau levels.

In Fig. 9, we plot the Fermi momentum k_F as a function of the magnetic field for the first Fermi surface (the largest root of Eq. (66)). Quantization is neglected here. At the left panel, the relatively small region between the dashed lines corresponds to non-Fermi liquids $0 < \nu < \frac{1}{2}$. At large magnetic field, the physics of the Fermi surface is captured

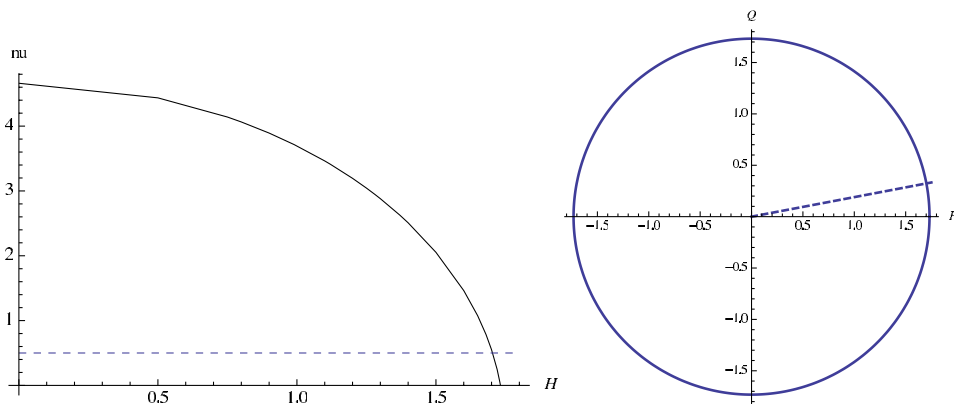


FIG. 8 (color online). Left panel: the IR conformal dimension $\nu \equiv \nu_{k_F}$ calculated at the Fermi momentum vs the magnetic field $h \rightarrow H$ (we set $g_F = 1$, $q = \frac{15}{\sqrt{3}}$). Calculations are done for the first Fermi surface. The dashed line is for $\nu = \frac{1}{2}$ (at $H_c = 1.7$), which is the border between the Fermi liquids $\nu > \frac{1}{2}$ and non-Fermi liquids $\nu < \frac{1}{2}$. Right panel: the phase diagram in terms of the chemical potential and the magnetic field $\mu^2 + h^2 = 3$ (in dimensionless variables $h = g_F H$, $\mu = g_F Q$; we set $g_F = 1$). Fermi liquids are above the dashed line ($H < H_c$), and non-Fermi liquids are below the dashed line ($H > H_c$).

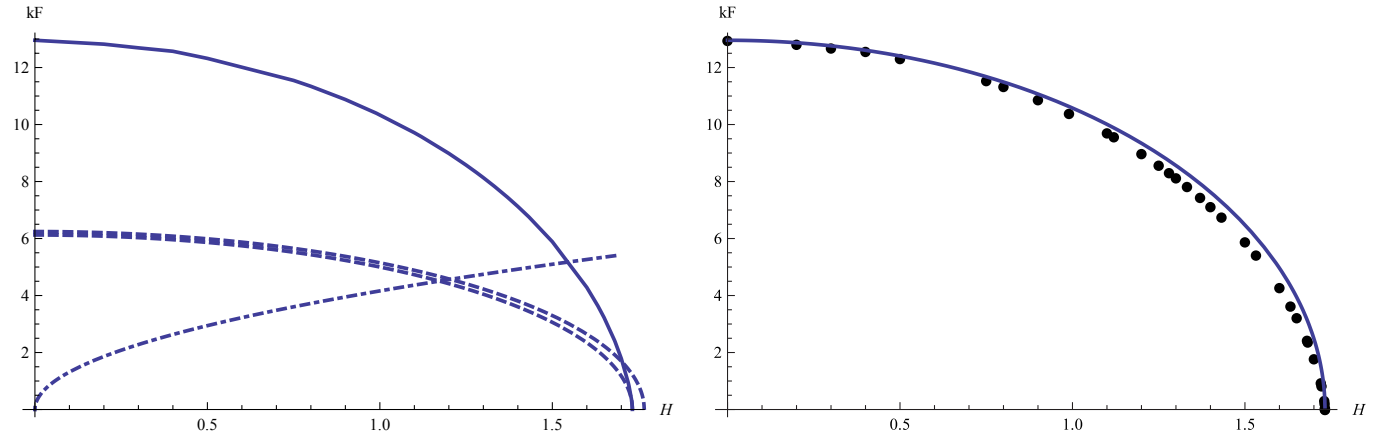


FIG. 9 (color online). Fermi momentum k_F vs the magnetic field $h \rightarrow H$ (we set $g_F = 1$, $q = \frac{15}{\sqrt{3}}$) for the first Fermi surface. Left panel: The inner (closer to x-axis) dashed line is $\nu_{k_F} = 0$, and the outer dashed line is $\nu_{k_F} = \frac{1}{2}$. The region between these lines corresponds to non-Fermi liquids $0 < \nu_{k_F} < \frac{1}{2}$. The dashed-dotted line is for the first Landau level $k_1 = \sqrt{2qH}$. The first Fermi surface hits the border line between Fermi and non-Fermi liquids $\nu = \frac{1}{2}$ at $H_c \approx 1.7$, and it vanishes at $H_{\max} = \sqrt{3} = 1.73$. Right panel: Circles are the data points for the Fermi momentum calculated analytically, and the solid line is a fit function $k_F^{\max} \sqrt{1 - \frac{H^2}{3}}$ with $k_F^{\max} = 12.96$.

by the near-horizon region (see also Fig. 5), which is $\text{AdS}_2 \times \mathbb{R}^2$. At the maximum magnetic field, $H_{\max} = \sqrt{3} \approx 1.73$, when the black hole becomes entirely magnetically charged, the Fermi momentum vanishes when it crosses the line $\nu_{k_F} = 0$. This only happens for the first Fermi surface. For the higher Fermi surfaces, the Fermi momenta terminate at the line $\nu_{k_F} = 0$ (Fig. 6). Note the Fermi momentum for the first Fermi surface can be almost fully described by a function $k_F = k_F^{\max} \sqrt{1 - \frac{H^2}{3}}$. It is tempting to view the behavior $k_F \sim \sqrt{H_{\max} - H}$ as a phase transition in the system, although it strictly follows from the linear scaling for $H = 0$ by using the mapping (29). (Note that also $\mu = g_F Q = g_F \sqrt{3 - H^2}$.) Taking into account the discretization of k_F , the plot will consist of an array of step functions tracing the existing curve. Our findings agree with the results for the Fermi momentum in a 3-dimensional magnetic system considered in [26], compare to Fig. 5 there.

The Fermi velocity given in Eq. (27) is defined by the UV physics. Therefore, solutions at nonzero ω are required. The Fermi velocity is extracted from matching two solutions in the inner and outer regions at the horizon. The Fermi velocity as a function of the magnetic field for $\nu > \frac{1}{2}$ is [18,21]

$$v_F = \frac{1}{h_1} \left(\int_0^1 dz \sqrt{g/g_{tt}} \psi^{(0)\dagger} \psi^{(0)} \right)^{-1} \lim_{z \rightarrow 1} \frac{|\tilde{y}_1^{(0)} + i\tilde{y}_2^{(0)}|^2}{(1-z)^3},$$

$$h_1 = \lim_{z \rightarrow 1} \frac{\tilde{y}_1^{(0)} + i\tilde{y}_2^{(0)}}{\partial_k (\tilde{y}_2^{(0)} + i\tilde{y}_1^{(0)})}, \quad (67)$$

where the zero-mode wave function is taken at k_F (Eq. (59)).

We plot the Fermi velocity for several Fermi surfaces in Fig. 10 and for the first Fermi surface in Fig. 11. Quantization is neglected here. The Fermi velocity is shown for $\nu > \frac{1}{2}$. It is interesting that the Fermi velocity vanishes when the IR conformal dimension is $\nu_{k_F} = \frac{1}{2}$. Formally, it follows from the fact that $v_F \sim (2\nu - 1)$ [7]. The first Fermi surface is at the far right. Positive and negative v_F correspond to the Fermi surfaces in the Green's functions G_1 and G_2 , respectively. The Fermi velocity v_F has the same sign as the Fermi momentum k_F . At small magnetic field values, the Fermi velocity is

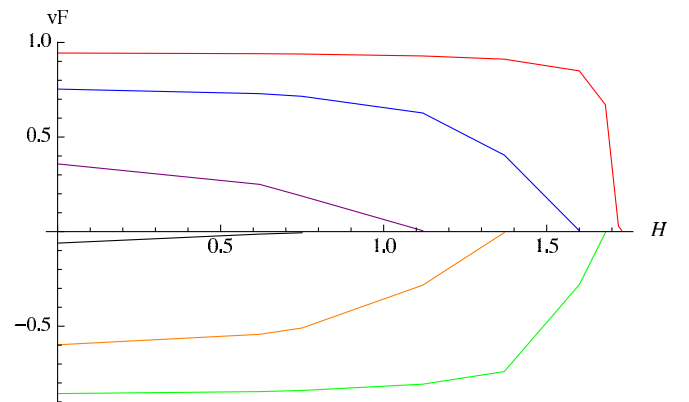


FIG. 10 (color online). Fermi velocity v_F vs the magnetic field $h \rightarrow H$ (we set $g_F = 1$, $q = \frac{15}{\sqrt{3}}$) for the regime of Fermi liquids $\nu \geq \frac{1}{2}$. Fermi velocity vanishes at $\nu_{k_F} = \frac{1}{2}$ (x-axis). The multiple lines are for various Fermi surfaces in ascending order, with the first Fermi surface on the right. The Fermi velocity v_F has the same sign as the Fermi momentum k_F . As above, positive and negative v_F correspond to Fermi surfaces in the two components of the Green's function.

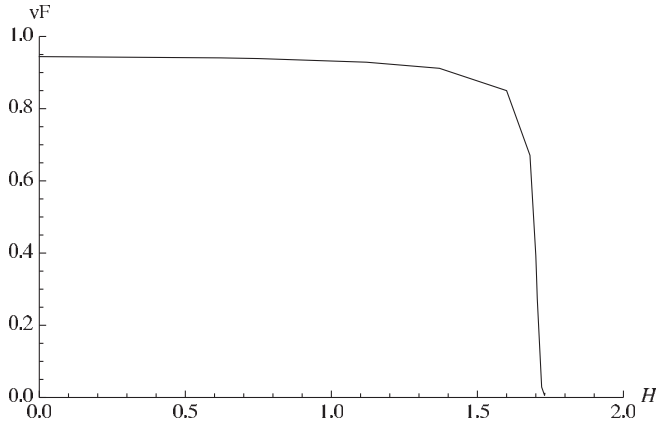


FIG. 11. Fermi velocity v_F vs the magnetic field $h \rightarrow H$ (we set $g_F = 1$, $q = \frac{15}{\sqrt{3}}$) for the first Fermi surface. Fermi velocity vanishes at $\nu_{k_F} = \frac{1}{2}$ at $H_c \approx 1.7$. The region $H < H_c$ corresponds to the Fermi liquids and quasiparticle description.

very weakly dependent on H , and it is close to the speed of light. At large magnetic field values, the Fermi velocity rapidly decreases and vanishes (at $H_c = 1.70$ for the first Fermi surface (Fig. 11)). Geometrically, this means that, with increasing magnetic field, the zero-mode wave function is supported near the black hole horizon (Fig. 5), where the gravitational redshift reduces the local speed of light, as compared to the boundary value. It was also observed in [7,21] at small fermion charge values.

VI. HALL AND LONGITUDINAL CONDUCTIVITIES

In this section, we calculate the contributions to Hall σ_{xy} and the longitudinal σ_{xx} conductivities directly in the boundary theory. This should be contrasted with the standard holographic approach, where calculations are performed in the (bulk) gravity theory and then translated to the boundary field theory using the AdS/CFT dictionary. Specifically, the conductivity tensor has been obtained in [10] by calculating the on-shell renormalized action for the gauge field on the gravity side and using the gauge/gravity duality $A_M \rightarrow j_\mu$ to extract the R charge current-current correlator at the boundary. Here, the Kubo formula involving the current-current correlator is used directly by utilizing the fermion Green's functions extracted from holography in [7]. Therefore, the conductivity is obtained for the charge carriers described by the fermionic operators of the boundary field theory.

The use of the conventional Kubo formula to extract the contribution to the transport due to fermions is validated in that it also follows from a direct AdS/CFT computation of the one-loop correction to the on-shell renormalized AdS action [15]. We study, in particular, stable quasiparticles with $\nu > \frac{1}{2}$ and at zero temperature. This regime effectively reduces to the clean limit where the imaginary part of the

self-energy vanishes $\text{Im}\Sigma \rightarrow 0$. We use the gravity-“dressed” fermion propagator from Eq. (27), and, to make the calculations complete, we need to use the dressed vertex to satisfy the Ward identities. As was argued in [15], the boundary vertex, which is obtained from the bulk calculations, can be approximated by a constant in the low-temperature limit. Also, according to [27], the vertex only contains singularities of the product of the Green's functions. Therefore, dressing the vertex will not change the dependence of the DC conductivity on the magnetic field [27]. In addition, the zero magnetic field limit of the formulae for conductivity obtained from holography [15] and from direct boundary calculations [18] are identical.

A. Integer quantum Hall effect

Let us start from the dressed retarded and advanced fermion propagators [7]: G_R is given by Eq. (27) and $G_A = G_R^*$. To perform the Matsubara summation, we use the spectral representation

$$G(i\omega_n, \vec{k}) = \int \frac{d\omega}{2\pi} \frac{A(\omega, \vec{k})}{\omega - i\omega_n}, \quad (68)$$

with the spectral function defined as $A(\omega, \vec{k}) = -\frac{1}{\pi} \text{Im}G_R(\omega, \vec{k}) = \frac{1}{2\pi i}(G_R(\omega, \vec{k}) - G_A(\omega, \vec{k}))$. Generalizing to a nonzero magnetic field and spinor case [25], the spectral function [28] is

$$A(\omega, \vec{k}) = \frac{1}{\pi} e^{-k^2/|qh|} \sum_{l=0}^{\infty} (-1)^l (-h_1 v_F) \times \left(\frac{\Sigma_2(\omega, k_F) f(\vec{k}) \gamma^0}{(\omega + \varepsilon_F + \Sigma_1(\omega, k_F) - E_l)^2 + \Sigma_2(\omega, k_F)^2} + (E_l \rightarrow -E_l) \right), \quad (69)$$

where $\varepsilon_F = v_F k_F$ is the Fermi energy, $E_l = v_F \sqrt{2|qh|} l$ is the energy of the Landau level, $f(\vec{k}) = P_- L_l(\frac{2k^2}{|qh|}) - P_+ L_{l-1}(\frac{2k^2}{|qh|})$ with spin projection operators $P_\pm = (1 \pm i\gamma^1 \gamma^2)/2$, we take $c = 1$, the generalized Laguerre polynomials are $L_n^\alpha(z)$ and by definition $L_n(z) = L_n^0(z)$, (we omit the vector part $\vec{k} \vec{\gamma}$ as it does not contribute to the DC conductivity), all γ 's are the standard Dirac matrices, and h_1 , v_F , and k_F are real constants (we keep the same notations for the constants as in [7]). The self-energy $\Sigma \sim \omega^{2\nu_{k_F}}$ contains the real and imaginary parts, $\Sigma = \Sigma_1 + i\Sigma_2$. The imaginary part comes from scattering processes of a fermion in the bulk, e.g., from pair creation, and from the scattering into the black hole. It is exactly due to inelastic/dissipative processes that we are able to obtain finite values for the transport coefficients; otherwise they are formally infinite.

Using the Kubo formula, the DC electrical conductivity tensor is

$$\sigma_{ij}(\Omega) = \lim_{\Omega \rightarrow 0} \frac{\text{Im}\Pi_{ij}^R}{\Omega + i0^+}, \quad (70)$$

where $\Pi_{ij}(i\Omega_m \rightarrow \Omega + i0^+)$ is the retarded current-current correlation function; schematically the current density operator is $j^i(\tau, \vec{x}) = qv_F \sum_{\sigma} \bar{\psi}_{\sigma}(\tau, \vec{x}) \gamma^i \psi_{\sigma}(\tau, \vec{x})$. Neglecting the vertex correction, it is given by

$$\begin{aligned} \Pi_{ij}(i\Omega_m) &= q^2 v_F^2 T \sum_{n=-\infty}^{\infty} \int \frac{d^2k}{(2\pi)^2} \text{tr}(\gamma^i G(i\omega_n, \vec{k}) \\ &\quad \times \gamma^j G(i\omega_n + i\Omega_m, \vec{k})). \end{aligned} \quad (71)$$

The sum over the Matsubara frequency is

$$\begin{aligned} \sigma_{ij} &= -\frac{4q^2 v_F^2 (h_1 v_F)^2 |qh|}{\pi\Omega} \text{Re} \sum_{l,k=0}^{\infty} (-1)^{l+k+1} \{ \delta_{ij} (\delta_{l,k-1} + \delta_{l-1,k}) + i\epsilon_{ij} \text{sgn}(qh) (\delta_{l,k-1} - \delta_{l-1,k}) \} \\ &\quad \times \int \frac{d\omega_1}{2\pi} \left(\tanh \frac{\omega_1}{2T} - \tanh \frac{\omega_2}{2T} \right) \left(\frac{\Sigma_2(\omega_1)}{(\tilde{\omega}_1 - E_l)^2 + \Sigma_2^2(\omega_1)} + (E_l \rightarrow -E_l) \right) \left(\frac{\Sigma_2(\omega_2)}{(\tilde{\omega}_2 - E_k)^2 + \Sigma_2^2(\omega_2)} + (E_k \rightarrow -E_k) \right), \end{aligned} \quad (74)$$

with $\omega_2 = \omega_1 + \Omega$. We have also introduced $\tilde{\omega}_{1,2} \equiv \omega_{1,2} + \varepsilon_F + \Sigma_1(\omega_{1,2})$, with ϵ_{ij} being the antisymmetric tensor ($\epsilon_{12} = 1$), and $\Sigma_{1,2}(\omega) \equiv \Sigma_{1,2}(\omega, k_F)$. In the momentum integral, we use the orthogonality condition for the Laguerre polynomials $\int_0^{\infty} dx e^{-x} L_l(x) L_k(x) = \delta_{lk}$.

$$\begin{aligned} \sigma_{xx} &= -\frac{2q^2 (h_1 v_F)^2 |qh|}{\pi T} \int_{-\infty}^{\infty} \frac{d\omega}{2\pi} \frac{\Sigma_2^2(\omega)}{\cosh^2 \frac{\omega}{2T}} \sum_{l=0}^{\infty} \left(\frac{1}{(\tilde{\omega} - E_l)^2 + \Sigma_2^2(\omega)} + (E_l \rightarrow -E_l) \right) \\ &\quad \times \left(\frac{1}{(\tilde{\omega} - E_{l+1})^2 + \Sigma_2^2(\omega)} + (E_{l+1} \rightarrow -E_{l+1}) \right), \end{aligned} \quad (75)$$

$$\sigma_{xy} = -\frac{q^2 (h_1 v_F)^2 \text{sgn}(qh)}{\pi} \nu_h, \quad \nu_h = 2 \int_{-\infty}^{\infty} \frac{d\omega}{2\pi} \tanh \frac{\omega}{2T} \Sigma_2(\omega) \sum_{l=0}^{\infty} \alpha_l \left(\frac{1}{(\tilde{\omega} - E_l)^2 + \Sigma_2^2(\omega)} + (E_l \rightarrow -E_l) \right), \quad (76)$$

where $\tilde{\omega} = \omega + \varepsilon_F + \Sigma_1(\omega)$. The filling factor ν_h is proportional to the density of carriers: $|\nu_h| = \frac{\pi}{|qh| h_1 v_F} n$ (we derive this relation below in Eq. (89)). The degeneracy factor of the Landau levels is α_l : $\alpha_0 = 1$ for the lowest Landau level, and $\alpha_l = 2$ for $l = 1, 2, \dots$. Substituting the filling factor ν_h back to Eq. (76), the Hall conductivity can be written as

$$\sigma_{xy} = \frac{\rho}{h}, \quad (77)$$

where ρ is the charge density in the boundary theory, and both the charge q and the magnetic field h carry a sign (the prefactor $(-h_1 v_F)$ comes from the normalization choice in the fermion propagator, Eqs.(27) and (69), as it was defined

$$T \sum_n \frac{1}{i\omega_n - \omega_1} \frac{1}{i\omega_n + i\Omega_m - \omega_2} = \frac{n(\omega_1) - n(\omega_2)}{i\Omega_m + \omega_1 - \omega_2}. \quad (72)$$

Taking $i\Omega_m \rightarrow \Omega + i0^+$, the polarization operator is now

$$\begin{aligned} \Pi_{ij}(\Omega) &= \frac{d\omega_1}{2\pi} \frac{d\omega_2}{2\pi} \frac{n_{\text{FD}}(\omega_1) - n_{\text{FD}}(\omega_2)}{\Omega + \omega_1 - \omega_2} \\ &\quad \times \int \frac{d^2k}{(2\pi)^2} \text{tr}(\gamma^i A(\omega_1, \vec{k}) \gamma^j A(\omega_2, \vec{k})), \end{aligned} \quad (73)$$

where the spectral function $A(\omega, \vec{k})$ is given by Eq. (69), and $n_{\text{FD}}(\omega)$ is the Fermi-Dirac distribution function. Evaluating the traces, we have

From Eq. (74), the term symmetric/antisymmetric with respect to exchange $\omega_1 \leftrightarrow \omega_2$ contributes to the diagonal/off-diagonal component of the conductivity (note the antisymmetric term $n_{\text{FD}}(\omega_1) - n_{\text{FD}}(\omega_2)$). The longitudinal and Hall DC conductivities ($\Omega \rightarrow 0$) are thus

in [7], which can be regarded as a factor contributing to the effective charge and is not important for further considerations). The Hall conductivity given by Eq. (77) has been obtained using the AdS/CFT duality for the Lorentz invariant 2 + 1-dimensional boundary field theories in [10]. We recover this formula because, in our case, the translational invariance is maintained in the x and y directions of the boundary theory.

Low frequencies give the main contribution in the integrand of Eq. (76). Since the self-energy satisfies $\Sigma_1(\omega) \sim \Sigma_2(\omega) \sim \omega^{2\nu}$ and we consider the regime $\nu > \frac{1}{2}$, we have $\Sigma_1 \sim \Sigma_2 \rightarrow 0$ at $\omega \sim 0$ (self-energy goes to zero faster than the ω term). Therefore, only the simple poles in the upper half-plane $\omega_0 = -\varepsilon_F \pm E_l + \Sigma_1 + i\Sigma_2$ contribute

to the conductivity where $\Sigma_1 \sim \Sigma_2 \sim (-\varepsilon_F \pm E_l)^{2\nu}$ are small. The same logic of calculation has been used in [25]. We obtain for the longitudinal and Hall conductivities

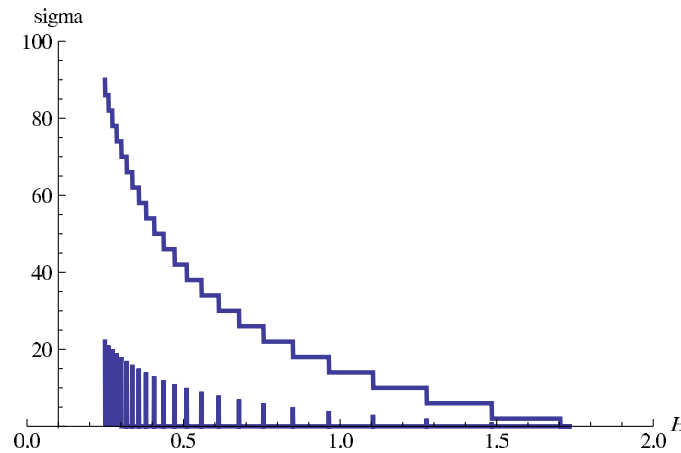
$$\sigma_{xx} = \frac{2q^2(h_1 v_F)^2 \Sigma_2}{\pi T} \times \left(\frac{1}{1 + \cosh \frac{\varepsilon_F}{T}} + \sum_{l=1}^{\infty} 4l \frac{1 + \cosh \frac{\varepsilon_F}{T} \cosh \frac{E_l}{T}}{(\cosh \frac{\varepsilon_F}{T} + \cosh \frac{E_l}{T})^2} \right) \quad (78)$$

$$\sigma_{xy} = \frac{q^2(h_1 v_F)^2 \text{sgn}(qh)}{\pi} \times 2 \left(\tanh \frac{\varepsilon_F}{2T} + \sum_{l=1}^{\infty} \left(\tanh \frac{\varepsilon_F + E_l}{2T} + \tanh \frac{\varepsilon_F - E_l}{2T} \right) \right), \quad (79)$$

where the Fermi energy is $\varepsilon_F = v_F k_F$, and the energy of the Landau level is $E_l = v_F \sqrt{2|qh|}l$. Similar expressions were obtained in [25]. However, in our case, the filling of the Landau levels is controlled by the magnetic field h through the field-dependent Fermi energy $v_F(h)k_F(h)$ instead of the chemical potential μ .

At $T = 0$, $\cosh \frac{\omega}{T} \rightarrow \frac{1}{2} e^{\omega/T}$ and $\tanh \frac{\omega}{2T} = 1 - 2n_{\text{FD}}(\omega) \rightarrow \text{sgn} \omega$. Therefore, the longitudinal and Hall conductivities are

$$\sigma_{xx} = \frac{2q^2(h_1 v_F)^2 \Sigma_2}{\pi T} \sum_{l=1}^{\infty} l \delta_{\varepsilon_F, E_l} = \frac{2q^2(h_1 v_F)^2 \Sigma_2}{\pi T} \times n \delta_{\varepsilon_F, E_n}, \quad (80)$$



$$\sigma_{xy} = \frac{q^2(h_1 v_F)^2 \text{sgn}(qh)}{\pi} 2 \left(1 + 2 \sum_{l=1}^{\infty} \theta(\varepsilon_F - E_l) \right) = \frac{q^2(h_1 v_F)^2 \text{sgn}(qh)}{\pi} \times 2(1 + 2n)\theta(\varepsilon_F - E_n)\theta(E_{n+1} - \varepsilon_F), \quad (81)$$

where the Landau-level index runs $n = 0, 1, \dots$. It can be estimated as $n = \lfloor \frac{k_F^2}{2|qh|} \rfloor$ when $v_F \neq 0$ ($\lfloor \cdot \rfloor$ denotes the integer part), with the average spacing between the Landau levels given by the Landau energy $v_F \sqrt{2|qh|}$. Note that $\varepsilon_F \equiv \varepsilon_F(h)$. We can see that Eq. (81) expresses the integer quantum Hall effect (IQHE). At zero temperature, as we dial the magnetic field, the Hall conductivity jumps from one quantized level to another, forming plateaus given by the filling factor

$$\nu_h = \pm 2(1 + 2n) = \pm 4 \left(n + \frac{1}{2} \right), \quad (82)$$

with $n = 0, 1, \dots$. (Compare to the conventional Hall quantization $\nu_h = \pm 4n$ that appears in thick graphene). Plateaus of the Hall conductivity at $T = 0$ follow from the stepwise behavior of the charge density ρ in Eq. (77):

$$\rho \sim 4 \left(n + \frac{1}{2} \right) \theta(\varepsilon_F - E_n) \theta(E_{n+1} - \varepsilon_F), \quad (83)$$

where n Landau levels are filled and contribute to ρ . The longitudinal conductivity vanishes, except precisely at the transition point between the plateaus. In Fig. 12, we plot the longitudinal and Hall conductivities at $T = 0$, using only the terms after the \times sign in Eq. (79). In the Hall conductivity, plateau transition occurs when the Fermi level (in Fig. 12) of the first Fermi surface $\varepsilon_F = v_F(h)k_F(h)$ (Figs. 9 and 11) crosses the Landau-level energy as we vary the magnetic field. By decreasing the

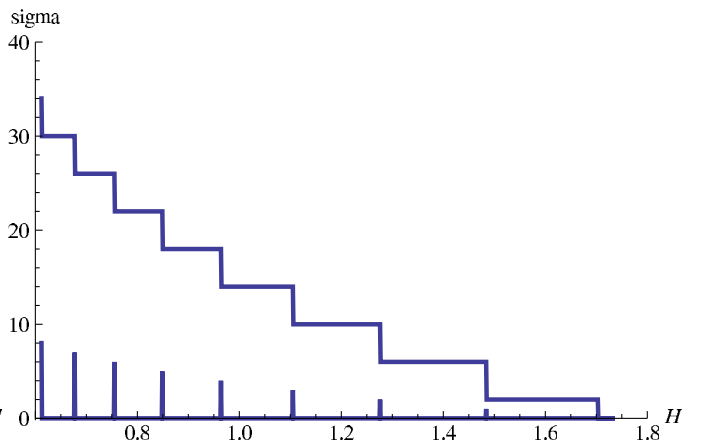


FIG. 12 (color online). Hall conductivity σ_{xy} and longitudinal conductivity σ_{xx} vs the magnetic field $h \rightarrow H$ at $T = 0$ (we set $g_F = 1$, $q = \frac{15}{\sqrt{3}}$). Contribution from the first Fermi surface is taken. By decreasing the magnetic field, the Fermi surface crosses the Landau levels, producing the Hall conductivity plateaus characteristic for IQHE. Longitudinal conductivity has picks at the beginning of each plateau. The right panel is a zoom-in for large h of the left one.

magnetic field, the plateaus become shorter, and increasingly more Landau levels contribute to the Hall conductivity. This happens because of two factors: the Fermi level moves up, and the spacing between the Landau levels becomes smaller. This picture does not depend on the Fermi velocity as long as it is nonzero.

In the boundary field theory, we express the charge density of the carriers (the difference between the densities of “electrons” and “holes”) through the Fermi energy ε_F (as it is done in [25]):

$$n = \text{tr}(\gamma^0 \tilde{G}(\tau, \mathbf{0})), \quad \tau \rightarrow 0, \quad (84)$$

where $\tilde{G}(\tau, \vec{x})$ is the translation-invariant part of the Green’s function $G(\tau, \vec{x})$ from Eq. (68). Using the spectral function representation given by Eq. (69), the charge density reads

$$n = T \sum_{n=-\infty}^{\infty} \int \frac{d^2 k}{(2\pi)^2} \int_{-\infty}^{\infty} \frac{d\omega}{2\pi} \frac{\text{tr}(\gamma^0 A(\omega, \vec{k}))}{\omega - i\omega_n}. \quad (85)$$

We express the Matsubara sum in terms of the contour integral over real frequencies:

$$T \sum_{n=-\infty}^{\infty} F(i\omega_n) \rightarrow -\frac{i}{4\pi} \int_C dz \tanh \frac{z}{2T} F(z), \quad (86)$$

where C runs anticlockwise and encircles the poles of \tanh along the upper- and lower-half imaginary axis. We have for the charge density

$$n = \frac{1}{2} \int \frac{d^2 k}{(2\pi)^2} \int_{-\infty}^{\infty} \frac{d\omega}{2\pi} \tanh \frac{\omega}{2T} \text{tr}(\gamma^0 A(\omega, \vec{k})). \quad (87)$$

Substituting the spectral function (69) and integrating over momenta, we obtain

$$n = -\frac{2|qh|h_1 v_F}{\pi} \int_{-\infty}^{\infty} \frac{d\omega}{2\pi} \tanh \frac{\omega}{2T} \Sigma_2(\omega) \times \sum_{l=0}^{\infty} \alpha_l \left(\frac{1}{(\tilde{\omega} - E_l)^2 + \Sigma_2^2(\omega)} + (E_l \rightarrow -E_l) \right), \quad (88)$$

where the degeneracy factor is $\alpha_0 = 1$ for the lowest Landau level, and $\alpha_l = 2$ for the higher Landau levels $l \geq 1$, $\tilde{\omega} = \omega + \varepsilon_F + \Sigma_1(\omega)$. Integrating over frequencies and taking into account that Σ_2 is effectively very small near the Fermi surface, we obtain

$$n = \frac{|qh|h_1 v_F}{\pi} \times 2 \left(\tanh \frac{\varepsilon_F}{2T} + \sum_{l=1}^{\infty} \left(\tanh \frac{\varepsilon_F + E_l}{2T} + \tanh \frac{\varepsilon_F - E_l}{2T} \right) \right). \quad (89)$$

Comparing this to Eq. (79), we obtain the relation $|v_h| = \frac{\pi}{|qh|h_1 v_F} n$. When the Fermi energy vanishes ($\varepsilon_F = 0$), the spectral function (69) is even in ω . From Eq. (88), the carrier density of stable quasiparticles vanishes when $\varepsilon_F = 0$. At the end of this section, we discuss a situation

with no stable charge carriers and physical consequences of it.

Equations (79)–(89) are obtained assuming that the states are localized around the Landau levels. In quantum Hall effect (QHE) models, impurities are added to prevent the states from “spilling” between the Landau levels and to provide the necessary occupation number of the levels. In our holographic calculations, however, the complex self-energy arises not from the impurities but from various scattering processes into the black hole. Here, the limit $\text{Im}\Sigma \rightarrow 0$ has been considered, which corresponds to a simplified field theory model [25] (the cited reference also considers the case with impurities). This approximation suffices to obtain the integer QHE [25] and for our initial studies of the fractional QHE. We leave the implementation of a physical model with impurities for future work.

B. Fractional quantum Hall effect

In a holographic setting, using the AdS geometry is equivalent to a calculation in a box. Therefore, for large enough fermion charge q , there are multiple Fermi surfaces, as shown in Figs. 6 and 10. Labeling the Fermi surfaces with $\nu > \frac{1}{2}$ by $m = 1, 2, \dots$, we represent, as in [21], the spectral function $A(\omega, \vec{k})$ as a sum over the spectral functions of individual Fermi surfaces given by Eq. (69). Ignoring the mixing term, the DC conductivity becomes a direct sum over the individual conductivities. By decreasing the magnetic field, new Fermi surfaces gradually appear, as can be seen in Figs. 6 and 7. Therefore, the conductivity tensor is

$$\sigma_{ij} = \sum_m \sigma_{ij}^{(m)} \theta(h_{\max}^{(m)} - h), \quad (90)$$

where $\sigma_{ij}^{(m)}$ involves the Fermi momentum $k_F^{(m)}$ and velocity $v_F^{(m)}$, respectively. At the maximum magnetic field $h_{\max}^{(m)}$, a new $k_F^{(m)}$ opens up; $h_{\max}^{(m)}$ is found numerically.

Including one, two, three, and four Fermi surfaces, we obtain the following quantization rule for the filling factor in the Hall conductivity:

$$\begin{aligned} \text{1FS: } \nu_h &= 2(1 + 2n), \\ \text{plateaus} &\rightarrow 2, 6, 10, \dots, \\ \text{2FS's: } \nu_h &= 4(1 + n + k), \\ \text{plateaus} &\rightarrow 4, 8, 12, \dots, \\ \text{3FS's: } \nu_h &= 2(3 + 2(n + k + p)), \\ \text{plateaus} &\rightarrow 6, 10, 14, \dots, \\ \text{4FS's: } \nu_h &= 4(2 + n + k + p + r), \\ \text{plateaus} &\rightarrow 8, 12, 16, \dots, \end{aligned} \quad (91)$$

with $n, k, p, r = 0, 1, \dots$. An odd number of Fermi surfaces produces the plateaus present in the IQHE, while an

even number of Fermi surfaces produces the additional plateaus appearing in the fractional quantum Hall effect (FQHE). For a large enough fermion charge q , many Fermi surfaces contribute, and the primary effect of the change in H is the opening of a new Fermi surface, rather than the occupation of the next plateau. Thus, at large q we expect a filling fraction pattern at large h to become

$$\nu_h = \pm 2j, \quad (92)$$

where $j = 1, 2, \dots$, is the effective Landau-level index counting the number of contributing Landau levels. This is indeed observed in the FQHE at strong magnetic fields. The quantization rule (91) persists as long as new Fermi surfaces open up with decreasing h . However, the first two plateaus present in the FQHE $\nu_h = 0, \pm 1$ are absent in Eq. (92). In order to get the Hall plateau $\nu_h = \pm 1$, the mixing term between two Fermi surfaces should probably be taken into account (incoherent superposition), whereas the conductivity (90) includes the diagonal terms only. We discuss the issue with $\nu_h = 0$ further.

In Fig. 13, we plot the Hall and longitudinal conductivities at $T = 0$ with three Fermi surfaces contributing (Eq. (90)), where the individual conductivities $\sigma^{(m)}$ are given by Eq. (79). We fit the Fermi momenta by

$$k_F^{(m)} = k_{F_{\max}}^{(m)} \sqrt{1 - \frac{h^2}{3}} + \delta^{(m)}, \quad (93)$$

with $k_{F_{\max}}^{(1)} = 12.96$, $\delta^{(1)} = 0.$, $k_{F_{\max}}^{(2)} = 10.29$, $\delta^{(2)} = 1.5$, $k_{F_{\max}}^{(3)} = 9.75$, $\delta^{(3)} = 3$, and use Eq. (93) together with the numerical solutions for $\nu_F^{(m)}$ in Fig. 13. In Fig. 13, at strong magnetic fields, the Hall conductivity

plateau $\nu_h = 4$ originates from two Fermi surfaces together with the plateaus $\nu_h = 2$ and $\nu_h = 6$, when one and three Fermi surfaces contribute, respectively. As we decrease the magnetic field further, three Fermi surfaces produce plateaus characteristic for IQHE, Eq. (82). The longitudinal conductivity shows a Dirac delta-like peak at the beginning of each plateau. Since a finite contribution to the conductivity arises as one of the three Fermi surfaces crosses the next Landau level, the pattern is less regular (i.e., the plateaus have changing length) than in the case when only one Fermi surface contributes. In Fig. 13, we compare the Hall conductivities with one and three Fermi surfaces participating. The irregular behavior of the Hall conductivity is explained naturally from the picture with multiple Fermi surfaces. Qualitatively similar regularity of the plateaus' length is seen in experiments on thin films of graphite at strong magnetic fields [23]. The actual physics behind this, however, might be quite different, as in this system, multiple sheets of the Fermi surface arise due to the (hexagonal) lattice on the UV scale, which is an effect beyond the scope of our current model.

The somewhat regular pattern behind the irregular behavior can be understood as a consequence of the appearance of a new energy scale: the average distance between the Fermi levels. For the case of Fig. 13, we estimate it to be $\langle \varepsilon_F^{(m)} - \varepsilon_F^{(m+1)} \rangle = 4.9$. The authors of [25] explain the FQHE through the opening of a gap in the quasiparticle spectrum, which acts as an order parameter related to the particle-hole pairing and is enhanced by the magnetic field (magnetic catalysis). Here, the energy gap arises due to the participation of multiple Fermi surfaces.

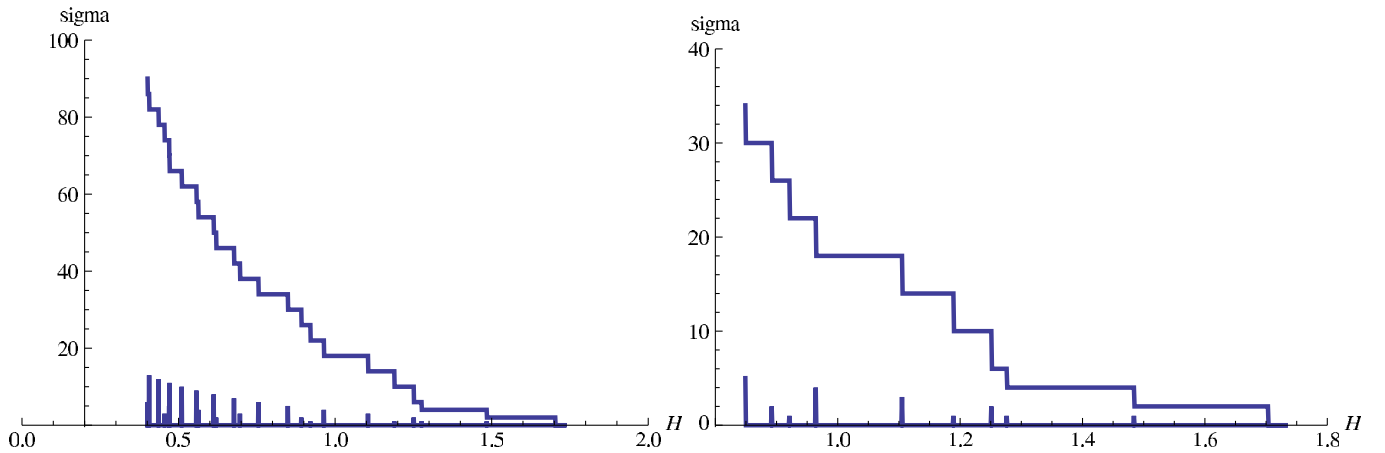


FIG. 13 (color online). Hall conductivity σ_{xy} and longitudinal conductivity σ_{xx} vs the magnetic field $h \rightarrow H$ at $T = 0$ (we set $g_F = 1$, $q = \frac{15}{\sqrt{3}}$). Contribution from the first three Fermi surfaces are taken. At strong magnetic fields, the Hall conductivity plateau $\nu_h = 4$ appears from two Fermi surfaces together with plateaus $\nu_h = 2$ and $\nu_h = 6$ when one and three Fermi surfaces contribute, respectively. This quantization rule is characteristic for the FQHE. At intermediate and weak magnetic fields, the Hall conductivity plateaus are produced as one of the three Fermi surfaces crosses the Landau levels, resulting in the quantization rule of the IQHE. An irregular pattern in the length of the plateaus is observed in the experiment on thin films of graphite at strong magnetic fields [23]. The right panel is a zoom-in for large h of the left one.

A pattern for the Hall conductivity that is strikingly similar to Fig. 13 arises in the bilayer graphene (compare with Figs. 2 and 5 in Ref. [29]), which has different transport properties from the monolayer graphene [29]. It is remarkable that the bilayer graphene also exhibits the insulating behavior in a certain parameter regime. This agrees with our findings of metal-insulating transition in our system.

C. Metal–strange-metal phase transition

The previous discussion of conductivities and QHE is valid provided that the Fermi velocity is nonzero. However, we have shown that v_F vanishes at relatively strong magnetic fields (for the first Fermi surface, it happens at h_c as in Fig. 8 and 11). In the AdS/CFT setting, the Fermi velocity vanishes when the IR anomalous dimension is $\nu = \frac{1}{2}$, signaling the onset of a nontrivial power-law dispersion in Green's function $G^{-1}(\omega) \sim \omega - v_f k_\perp + \omega^{2\nu}$ (the pole in the self-energy $\Sigma \rightarrow G_R^{IR} \sim \omega^{2\nu}$ and the pole in the prefactor of the linear term $\sim \omega$ [7]). Vanishing of v_F was observed in [21] at large enough fermion charge. Note that if v_F is zero for some interval of the magnetic field, it leads to the Hall plateau with the filling factor $\nu_h = 0$ present in FQHE.

The vanishing of the Fermi velocity of the stable quasiparticle leads to zero carrier density at leading order:

$$v_F = 0 \rightarrow n = 0. \quad (94)$$

This means that all contribution to conductivity comes from the other terms, containing the contribution from the non-Fermi-liquid excitations and the conformal regime. This qualitatively changes the transport properties of the system, as can be seen in Fig. 14.

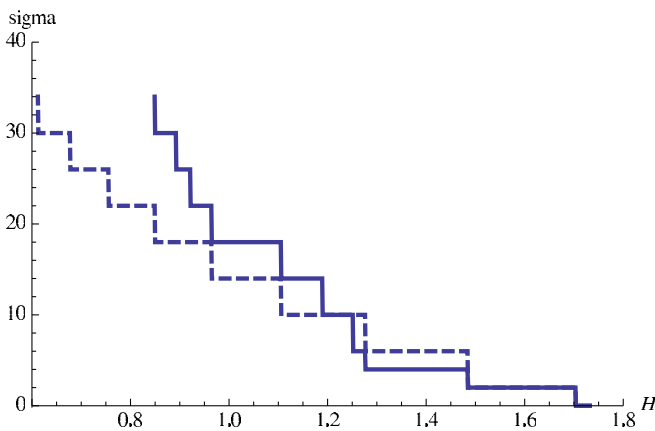


FIG. 14 (color online). Comparison of the Hall conductivities σ_{xy} vs the magnetic field $h \rightarrow H$ from one Fermi surface (dashed line) and from three Fermi surfaces (solid line). We set $g_F = 1$ and $q = \frac{15}{\sqrt{3}}$. At strong magnetic fields, a new plateau $\nu_h = 4$ appears in the multiple-Fermi-surface picture, yielding a pattern characteristic of FQHE.

The finite offset magnetic field has been observed in experiments on highly oriented pyrolytic graphite in magnetic fields [30]. In particular, analyzing the basal-plane resistivity gave an approximate scaling relation between the critical temperature of the metal-semiconducting transition and the magnetic field has been found $T_c \sim \sqrt{h - h_c}$. It suggests that at $T = 0$, there is a threshold magnetic field h_c above which the resistivity qualitatively changes. Interestingly, the existence of such a threshold magnetic field follows from the AdS/CFT calculations (h_c when $\nu = \frac{1}{2}$).

A phase transition is usually governed by an order parameter which exhibits a critical behavior. In our case, there is no such order parameter. However, it is interesting to note that the Fermi momentum, according to Eq. (93), behaves as $k_F \sim \sqrt{h_{\max} - h}$, which is in line with the postulated critical behavior in the system, while the Fermi surface itself behaves as order parameter.

To obtain a complete picture of the metal–strange-metal phase transition, one needs to perform calculations in the non-Fermi-liquid regime, taking into account the unstable quasiparticle pole. It is also necessary to study the temperature dependence of the DC conductivities $\sigma_{xy}(T)$ and $\sigma_{xx}(T)$. We leave it for future study.

VII. ABSENCE OF THE SIGN PROBLEM IN HOLOGRAPHY

In this section, we show that the fermion determinant in the gravity dual theory does not have a sign problem and hence can be simulated by a lattice Monte-Carlo algorithm. Until recently, most of the work on AdS/CFT and applied holography focused on the classical gravity (leading $1/N$ in field theory) limit. However, many thermodynamic and electric properties depend on matter fields (e.g., the electrical conductivity depends on whether or not the theory has a Fermi surface). In classical gravity, the Einstein-Maxwell sector decouples, and matter fields run in loops representing quantum oscillations. In order to include matter fields in the bulk, one needs to calculate loop corrections, which corresponds to going beyond the leading order in $1/N$. A study of one-loop bulk physics was done in [31] and recently in [22]. It shows that analytical calculations of quantum corrections in the bulk are quite involved. The study of quantum oscillations in the gravity dual will likely improve our understanding of finite density systems in general.

As is well known, a finite density field theory in most cases cannot be simulated on the lattice because of the infamous sign problem [1]. In the field theory action, chemical potential is introduced via the term $\bar{\psi} \mu \gamma^0 \psi$, which is Hermitian and therefore gives a complex determinant. At the same time, in the bulk action, finite density is introduced through the electrically charge black hole, and does not involve even matter fields. This is the reason why the applied holography gives universal predictions.

In the leading order, the minimal gravitational dual at finite density and temperature is the electrically charged AdS-Reissner-Nordström black hole, where only the metric and Maxwell fields are present. Therefore, the Einstein-Maxwell sector gives results which do not depend, for example, on the charge and mass of matter fields in the gravitational bulk space-time, i.e., are universal for a class of field theories with different charge and scaling dimensions of the operators. The fact that the chemical potential enters via the electric field in the covariant derivative leads to the real and positive definite fermion determinant, which is suitable for lattice simulations. We show it formally below.

In a semiclassical approach to gravity, the action includes the Einstein-Maxwell sector S_g with fields collectively denoted as g, A in Eq. (1), and the matter sector with the fermion fields S_ψ , Eq. (21). The latter is given as (Euclidean signature):

$$S_\psi = \int d^4x_E \sqrt{-g_E} \bar{\psi} (D + m) \psi, \quad (95)$$

where $D \equiv \Gamma_E^M \mathcal{D}_M$ and the covariant derivative is $\mathcal{D}_M = \partial_M + \frac{1}{4} \omega_{abM} \Gamma^{ab} - iqA_M$. We can always scale away the spin connection by redefining the spinor field as in Eq. (A6). Finite density is described by the electrically charged black hole with charge Q that generates the imaginary time component of the vector potential A_{t_E} (Eq. (17)). Radial profile of the vector potential $A_{t_E} = \mu(1 - \frac{1}{r})$ (in dimensionless units) ensures a finite chemical potential at the field theory boundary $A_{t_E} \rightarrow \mu$ at $r \rightarrow \infty$, where $\mu = g_F Q$ (in dimensionless units). Integrating out the fermion fields, the gravitational partition function can be written schematically as

$$Z = \sum_{g_*, A_*} \det(D(g_*, A_*) + m) e^{-S_g[g_*, A_*]}, \quad (96)$$

where S_g is the Euclidean gravitational action at the saddle points g_*, A_* . The determinant describes fluctuations about the saddle point solution g_*, A_* and corresponds to $1/N$ correction to the large N limit of a dual gauge theory. Because the Euclidean gamma matrices are Hermitian by convention (the signature of the metric fixes the Hermiticity), we have $\Gamma_E^{0\dagger} = \Gamma_E^0$ and $\Gamma_E^{i\dagger} = \Gamma_E^i$ with $i = 1, 2, 3$, so the covariant derivative is anti-Hermitian. Now it remains to be shown that the determinant of this anti-Hermitian differential operator is real and positive definite [32].

Using the anticommutation relations $\{\Gamma_E^5, \Gamma_E^{0,i}\} = 0$, we have

$$\Gamma_E^5 D \Gamma_E^5 = -D = D^\dagger, \quad (97)$$

where $D \equiv D(g, A)$. Therefore, the determinant

$$\det D = \det(\Gamma_E^5 D \Gamma_E^5) = \det D^\dagger = (\det D)^* \quad (98)$$

is real. To show the positive definiteness, we remind the reader that the eigenmodes of an anti-Hermitian derivative operator come in pairs. If (λ, ψ) is an eigenmode of D ,

$$D\psi = \lambda\psi, \quad (99)$$

then, from Eq. (99):

$$D(\Gamma_E^5 \psi) = (-\lambda)(\Gamma_E^5 \psi), \quad (100)$$

so $(-\lambda, \Gamma_E^5 \psi)$ is also an eigenmode of D . Because of anti-Hermiticity, from Eq. (97),

$$D(\Gamma_E^5 \psi) = \lambda^*(\Gamma_E^5 \psi). \quad (101)$$

This eigenvalue is completely imaginary (or zero), $-\lambda = \lambda^*$. The determinant is a product of all the paired eigenvalues,

$$\det(D + m) \rightarrow \prod_i (\lambda_i + m)(-\lambda_i + m) = \prod_i (|\lambda_i + m|^2), \quad (102)$$

which is positive definite (or zero).

In field theory, the eigenmodes of the operator $D + \mu\gamma_E^4 + m$ still come in pairs (λ, ψ) and $(-\lambda, \gamma_E^5 \psi)$. However, since $\mu\gamma_E^4$ is Hermitian, λ is no longer purely imaginary, and, therefore, $\det(D + \mu\gamma_E^4 + m)$ is not necessarily positive. The sign problem occurs when \det is negative for some gauge configurations, or, in other words, it is generically present when considering interacting matter at finite density.

VIII. CONCLUSIONS

We have studied strongly coupled electron systems in the magnetic field, focusing on the Fermi-level structure, using the AdS/CFT correspondence. These systems are dual to Dirac fermions placed in the background of the electrically and magnetically charged AdS-Reissner-Nordström black hole. At strong magnetic fields, the dual system “lives” near the black hole horizon, which substantially modifies the Fermi-level structure. As we dial the magnetic field higher, the system exhibits the non-Fermi-liquid behavior and then crosses back to the conformal regime. In our analysis, we have concentrated on the Fermi-liquid regime and obtained the dependence of the Fermi momentum k_F and Fermi velocity v_F on the magnetic field. Remarkably, k_F exhibits the square root behavior, with v_F staying close to the speed of light in a wide range of magnetic fields, while it rapidly vanishes at a critical magnetic field, which is relatively high. Such behavior indicates that the system may have a phase transition.

The magnetic system can be rescaled to a zero-field configuration, which is thermodynamically equivalent to the original one. This simple result can actually be seen already at the level of field theory: The additional scale

brought about by the magnetic field does not show up in thermodynamic quantities, meaning, in particular, that the behavior in the vicinity of quantum critical points is expected to remain largely uninfluenced by the magnetic field, retaining its conformal invariance. In light of current condensed matter knowledge, this is surprising and might in fact be a good opportunity to test the applicability of the probe limit in the real world. If this behavior is not seen, this suggests that one has to include the backreaction to the metric to arrive at a realistic description.

In the field theory frame, we have calculated the DC conductivity using k_F and v_F values extracted from holography. The holographic calculation of conductivity that takes into account the fermions corresponds to the corrections of subleading order in $1/N$ in the field theory and is very involved [15]. As we are not interested in the vertex renormalization due to gravity (it does not change the magnetic field dependence of the conductivity), we have performed our calculations directly in the field theory with AdS-gravity-dressed fermion propagators. Instead of controlling the occupancy of the Landau levels by changing the chemical potential (as is usual in nonholographic setups), we have controlled the filling of the Landau levels by varying the Fermi energy level through the magnetic field. At zero temperature, we have reproduced the integer QHE of the Hall conductivity, which is observed in graphene at moderate magnetic fields. Our findings on equilibrium physics (Landau quantization, magnetic phase transitions, and crossovers) are within expectations and indeed corroborate the meaningfulness of the AdS/CFT approach in line with the well-known facts. However, the detection of the QHE is somewhat surprising, as the spatial boundary effects are ignored in our setup. We plan to address this question in future work.

Interestingly, the AdS geometry produces several Fermi surfaces. Theories where the gravity duals have larger fermion charge q possess more Fermi surfaces. We find that, in a multi-Fermi surface picture, the Hall conductivity is quantized in a way reminiscent of fractional QHE. By reducing the magnetic field, new Fermi surfaces open up and the quantization of Hall conductivity alternates between two different patterns, corresponding to odd and even numbers of Fermi surfaces. It turns out that an odd number of the Fermi surfaces results in IQHE plateaus, while an even number of surfaces gives new plateaus characteristic for the FQHE. In a multi-Fermi surface picture, the quantum Hall plateaus show a less regular pattern that agrees with experiments on thin graphite in strong magnetic field [23]. In our model, it happens due to the fact that, as one of several Fermi surfaces crosses the Landau level, the Hall conductivity jumps to a new plateau. This process is not synchronized between different Fermi surfaces. We associate the average distance between the Fermi levels with the energy gap usually arising in the FQHE.

Notably, the AdS-Reissner-Nordström black hole background gives a vanishing Fermi velocity at high magnetic fields. It happens at the point when the IR conformal dimension of the corresponding field theory is $\nu = \frac{1}{2}$, which is the border line between the Fermi and non-Fermi liquids. Vanishing Fermi velocity was also observed at high enough fermion charge [21]. As in [21], it is explained by the red shift on the gravity side because at strong magnetic fields, the fermion wave function is supported near the black hole horizon, modifying substantially the Fermi velocity. In our model, vanishing Fermi velocity leads to zero occupancy of the Landau levels by stable quasiparticles that results in vanishing regular Fermi-liquid contribution to the Hall conductivity and the longitudinal conductivity. The dominant contribution to both now comes from the non-Fermi liquid and conformal contributions. We associate such change in the behavior of conductivities with a metal–strange-metal phase transition. Experiments on highly oriented pyrolytic graphite support the existence of a finite “offset” magnetic field h_c at $T = 0$, where the resistivity qualitatively changes its behavior [30]. At $T \neq 0$, it has been associated with the metal-semiconducting phase transition [30]. It is worthwhile to study the temperature dependence of the conductivity in order to understand this phase transition better.

Finally, we suggest as a possibly interesting extension of the current AdS/CFT methodology to compute the gravity dual of the finite density matter in Monte-Carlo lattice simulations. This is possible since the sign problem does not arise in the holographic setting of a finite density system. Unlike the conventional field theory setup, finite density in holography is introduced through an electrically charged black hole, and does not involve matter fields (this is also the reason why holography gives universal results: It does not depend on the expectation values of matter fields at the leading order). In the gravity geometry, Dirac fermions are coupled minimally to the electric field via the covariant derivative. We have shown that the covariant derivative is anti-Hermitian in the Euclidean signature, leading to the real and positive definite fermion determinant. This makes it possible to simulate finite density systems on the lattice in the AdS-gravity geometry, using the curved space-time lattice formulation [33]. The simplest holographic setup which describes a finite charge density system includes a local $U(1)$ gauge symmetry. Finite density systems with global $U(1)$ symmetry can not be simulated numerically in field theory due to the problem with the Gauss law in the lattice formulation. Another important advantage of performing the Monte-Carlo simulation is that it includes the quantum fluctuations for the gauge and gravitational field. So far, most calculations have been done in the probe limit, with the frozen background for the metric and gauge fields. Analytic calculations which include backreaction are usually involved and are done in the next-to-leading order,

e.g., [8]. Holographic lattice calculations allow us to consider dynamical gauge and gravity fields with matter, which mimics complicated strong interactions in finite density systems and opens a way toward studying novel state of matter and instability mechanisms.

ACKNOWLEDGMENTS

We thank Tom Faulkner, Michael Fromm, Tom Hartman, Sean Hartnoll, Nabil Iqbal, Hong Liu, Mark Mezei, Hiranmaya Mishra, Volodya Miransky, Yusuke Nishida, Owe Philipsen, Igor Shovkovy, Tian Zhang, Darius Sadri, Chang Yu Hou, Andrej Mesaroš, and Vladimir Juričić for helpful input and discussions. The work was supported in part by the Alliance program of the Helmholtz Association, Contract No. HA216/EMMI “Extreme Density and Temperature: Cosmic Matter in the Laboratory” and by ITP of Goethe University, Frankfurt (E. Gubankova); by a VIDI Innovative Research Incentive Grant (K. Schalm) from the Netherlands Organization for Scientific Research (NWO); by a Spinoza Award (J. Zaanen) from the Netherlands Organization for Scientific Research (NWO); and the Dutch Foundation for Fundamental Research of Matter (FOM). K. Schalm thanks the Galileo Galilei Institute for Theoretical Physics for the hospitality and the INFN for partial support during the completion of this work.

APPENDIX A: DIRAC EQUATION IN MAGNETIC FIELD

Here, we solve analytically the part of the Dirac equation which depends on magnetic field and space-time coordinates of the boundary theory. The free spinor action in the geometry given by Eq. (2) and in the presence of a magnetic field (3) is given by Eq. (21).

Using the translational invariance,

$$\psi(t, x, y, r) = \int d\omega dk e^{-i\omega t + ik y} \psi(\omega, k, x, r), \quad (\text{A1})$$

with $k \equiv k_y$, the Dirac equation (Eq. (23)) can be written as

$$\begin{aligned} & \left(\frac{1}{\sqrt{-g_{tt}}} \Gamma^{\hat{t}} \left(-i\omega + \frac{1}{2} \omega_{\hat{t}\hat{t}} \Gamma^{\hat{t}\hat{t}} - iqA_t(r) \right) + \frac{1}{\sqrt{g_{rr}}} \Gamma^{\hat{r}} \partial_r \right. \\ & + \frac{1}{\sqrt{g_{ii}}} \Gamma^{\hat{x}} \left(\partial_x + \frac{1}{2} \omega_{\hat{x}\hat{x}} \Gamma^{\hat{x}\hat{x}} \right) + \frac{1}{\sqrt{g_{ii}}} \Gamma^{\hat{y}} \left(ik + \frac{1}{2} \omega_{\hat{y}\hat{y}} \Gamma^{\hat{y}\hat{y}} \right. \\ & \left. \left. - iqA_y(x) \right) - m \right) \psi(\omega, k, x, r) = 0, \quad (\text{A2}) \end{aligned}$$

where $g_{ii} \equiv g_{xx} = g_{yy}$, and $A_t(r) = \mu(1 - r_0/r)$, $A_y(x) = hx$. From the torsion-free condition, $\omega_b^a \wedge e^b = -de^a$, we find the spin connection [34] for the metric (2),

$$\omega_{\hat{t}\hat{r}} = -\frac{\partial_r(\sqrt{-g_{tt}})}{\sqrt{g_{rr}}} dt, \quad \omega_{\hat{r}\hat{x}} = \frac{\partial_r(\sqrt{g_{ii}})}{\sqrt{g_{rr}}} dx^i, \quad (\text{A3})$$

where $i = x, y$. Note that

$$-\Gamma^{\hat{t}} \Gamma^{\hat{r}} = \Gamma^{\hat{x}} \Gamma^{\hat{x}} = \Gamma^{\hat{y}} \Gamma^{\hat{y}} = \Gamma^{\hat{r}}, \quad (\text{A4})$$

and

$$\begin{aligned} \frac{1}{4} e_a^M \Gamma^{\hat{a}} \omega_{\hat{b}\hat{c}M} \Gamma^{\hat{b}\hat{c}} &= \frac{1}{4} \frac{1}{\sqrt{-g_{tt}}} \frac{\partial_r(\sqrt{-g_{tt}})}{\sqrt{g_{rr}}} \Gamma^{\hat{r}} \\ &+ \frac{2}{4} \frac{1}{\sqrt{g_{ii}}} \frac{\partial_r \sqrt{g_{ii}}}{\sqrt{g_{rr}}} \Gamma^{\hat{r}} \\ &= \frac{1}{\sqrt{g_{rr}}} \Gamma^{\hat{r}} \partial_r \ln \left(-\frac{g}{g_{rr}} \right)^{1/4}, \quad (\text{A5}) \end{aligned}$$

where g is the determinant of the metric. Therefore, we can rescale the spinor field:

$$\psi = \left(-\frac{g}{g_{rr}} \right)^{-1/4} \Phi \quad (\text{A6})$$

and remove the spin connection completely. The new covariant derivative does not contain the spin connection, so $\mathcal{D}'_M = \partial_M - iqA_M$.

In new field variables, the Dirac equation is given by

$$\begin{aligned} & \left(\frac{\sqrt{g_{ii}}}{\sqrt{g_{rr}}} \Gamma^{\hat{r}} \partial_r - \frac{\sqrt{g_{ii}}}{\sqrt{-g_{tt}}} \Gamma^{\hat{t}} i \left(\omega + \mu_q \left(1 - \frac{r_0}{r} \right) \right) - \sqrt{g_{ii}} m \right. \\ & \left. + \Gamma^{\hat{x}} \partial_x + \Gamma^{\hat{y}} i(k - qhx) \right) \Phi(\omega, k, x, r) = 0, \quad (\text{A7}) \end{aligned}$$

with $\mu_q \equiv \mu q$. We separate the x - and r -dependent parts:

$$\begin{aligned} P(r) &= \frac{\sqrt{g_{ii}}}{\sqrt{g_{rr}}} \Gamma^{\hat{r}} \partial_r - \frac{\sqrt{g_{ii}}}{\sqrt{-g_{tt}}} \Gamma^{\hat{t}} i \left(\omega + \mu_q \left(1 - \frac{r_0}{r} \right) \right) - \sqrt{g_{ii}} m, \\ Q(x) &= \Gamma^{\hat{x}} \partial_x + \Gamma^{\hat{y}} i(k - qhx), \quad (\text{A8}) \end{aligned}$$

and the Dirac equation is

$$(P(r) + Q(x))\Phi = 0. \quad (\text{A9})$$

Even though $[P(r), Q(x)] \neq 0$, one can find a transformation matrix U such that $[UP(r), UQ(x)] = 0$ and then look for common eigenvectors of $UP(r)$ and $UQ(x)$ as they are commuting Hermitian operators, i.e., the Dirac equation reads

$$UP(r)\Phi_l = -UQ(x)\Phi_l = \lambda_l \Phi_l, \quad (\text{A10})$$

where l labels the Landau levels. We use l for the Landau index, so as not to confuse it with the Matsubara frequency index n . Transformation matrix U should satisfy the conditions

$$\begin{aligned} \{U, \Gamma^{\hat{t}}\} &= 0, & \{U, \Gamma^{\hat{r}}\} &= 0, \\ [U, \Gamma^{\hat{x}}] &= 0, & [U, \Gamma^{\hat{y}}] &= 0, \end{aligned} \quad (\text{A11})$$

which do not fix U completely. It is convenient to use the following basis [7]:

$$\begin{aligned}\Gamma^{\hat{r}} &= \begin{pmatrix} -\sigma^3 & 0 \\ 0 & -\sigma^3 \end{pmatrix}, & \Gamma^{\hat{t}} &= \begin{pmatrix} i\sigma^1 & 0 \\ 0 & i\sigma^1 \end{pmatrix}, \\ \Gamma^{\hat{x}} &= \begin{pmatrix} -\sigma^2 & 0 \\ 0 & \sigma^2 \end{pmatrix}, & \Gamma^{\hat{y}} &= \begin{pmatrix} 0 & \sigma^2 \\ \sigma^2 & 0 \end{pmatrix}, \\ \Gamma^{\hat{s}} &= \begin{pmatrix} 0 & i\sigma^2 \\ -i\sigma^2 & 0 \end{pmatrix}.\end{aligned}\quad (\text{A12})$$

Note that the following relation holds

$$\Gamma^{\hat{s}} = \Gamma^{\hat{0}}\Gamma^{\hat{1}}\Gamma^{\hat{2}}\Gamma^{\hat{3}} \quad (\text{A13})$$

as expected, with $0 \rightarrow t$, $1 \rightarrow x$, $2 \rightarrow y$, and $3 \rightarrow r$. In the representation of Eq. (A12), we can choose

$$U = \begin{pmatrix} -i\sigma^2 & 0 \\ 0 & -i\sigma^2 \end{pmatrix}. \quad (\text{A14})$$

We split the 4-component spinors into two 2-component spinors (we do not write zero entries) $F = (F_1, F_2)^T$, where the index $\alpha = 1, 2$ is the Dirac index of the boundary theory, using projectors

$$\begin{aligned}\Pi_\alpha &= \frac{1}{2}(1 - (-1)^\alpha \Gamma^{\hat{r}}\Gamma^{\hat{t}}), \\ \alpha &= 1, 2, \quad \Pi_1 + \Pi_2 = 1,\end{aligned}\quad (\text{A15})$$

which commute with the Dirac operator of Eq. (37), and $F_\alpha = \Pi_\alpha \Phi$, $\alpha = 1, 2$, decouple from each other. Gamma matrices in Eq. (A12) were chosen in such a way that this decoupling is possible.

Writing the Dirac equation (A10) for $F = (F_1, F_2)^T$, we have

$$\begin{aligned}\left(-\frac{\sqrt{g_{ii}}}{\sqrt{g_{rr}}}\sigma^1\partial_r + \sqrt{g_{ii}}i\sigma^2m\right. \\ \left.- \frac{\sqrt{g_{ii}}}{\sqrt{-g_{tt}}}\sigma^3(\omega + \mu_q(1 - r_0/r)) - \lambda_l\right) \otimes 1 \begin{pmatrix} F_1 \\ F_2 \end{pmatrix} = 0 \\ 1 \otimes \begin{pmatrix} i\partial_x + \lambda_l & (k - qhx) \\ (k - qhx) & -i\partial_x + \lambda_l \end{pmatrix} \begin{pmatrix} F_1 \\ F_2 \end{pmatrix} = 0,\end{aligned}\quad (\text{A16})$$

where in $X \otimes Y$, X acts inside F_1 or F_2 , and Y acts between F_1 and F_2 . In Eq. (A16), the 1 in the first equation shows that there is no mixing of F_1 and F_2 by the operator $UP(r)$, and the 1 in the second equation shows that there is no mixing inside F_1 or F_2 by the operator $UQ(x)$. Therefore, the solution can be represented as

$$\begin{pmatrix} F_1 \\ F_2 \end{pmatrix} = \begin{pmatrix} f_l^{(1)}(r)g_l^{(1)}(x) \\ f_l^{(2)}(r)g_l^{(1)}(x) \\ f_l^{(1)}(r)g_l^{(2)}(x) \\ f_l^{(2)}(r)g_l^{(2)}(x) \end{pmatrix}. \quad (\text{A17})$$

We do not write explicitly the dependence on ω and k . It is convenient to make a unitary transformation:

$$\begin{pmatrix} \zeta^{(1)} \\ \zeta^{(2)} \end{pmatrix} = M \begin{pmatrix} g^{(1)} \\ g^{(2)} \end{pmatrix}, \quad M = \begin{pmatrix} 1 & -i \\ -i & 1 \end{pmatrix}. \quad (\text{A18})$$

Dirac equations for each component are written as:

$$\begin{aligned}\left(\frac{\sqrt{g_{ii}}}{\sqrt{g_{rr}}}\partial_r + \sqrt{g_{ii}}m\right)f_l^{(1)}(r) \\ + \left(-\frac{\sqrt{g_{ii}}}{\sqrt{-g_{tt}}}(\omega + \mu_q(1 - r_0/r)) + \lambda_l\right)f_l^{(2)}(r) = 0, \\ \left(\frac{\sqrt{g_{ii}}}{\sqrt{g_{rr}}}\partial_r - \sqrt{g_{ii}}m\right)f_l^{(2)}(r) \\ + \left(\frac{\sqrt{g_{ii}}}{\sqrt{-g_{tt}}}(\omega + \mu_q(1 - r_0/r)) + \lambda_l\right)f_l^{(1)}(r) = 0,\end{aligned}\quad (\text{A19})$$

$$(\partial_{\tilde{x}} - \tilde{x})\zeta^{(1)} + \tilde{\lambda}_l\zeta^{(2)} = 0, \quad (\partial_{\tilde{x}} + \tilde{x})\zeta^{(2)} - \tilde{\lambda}_l\zeta^{(1)} = 0. \quad (\text{A20})$$

In Eq. (A20), for the x -dependent part, we have rescaled $\tilde{x} = \sqrt{|qh|}(x - \frac{k}{qh})$ with $k \equiv k_y$ and $\lambda_l = \sqrt{|qh|}\tilde{\lambda}_l$. The second order ordinary differential equations

$$-\partial_{\tilde{x}}^2\zeta^{(\rho)} + \tilde{x}^2\zeta^{(\rho)} - \tilde{\lambda}_l^2\zeta^{(\rho)} - (-1)^\rho\zeta^{(\rho)} = 0, \quad (\text{A21})$$

with $\rho = 1, 2$, are solved by substitution $\zeta^{(\rho)} = e^{-\tilde{x}^2/2}\tilde{\zeta}^{(\rho)}$. This is exactly the Schrödinger equation for a harmonic oscillator, so the eigenfunctions are Hermite polynomials, and we obtain the following solutions, indexed by an integer $l \in \mathbb{Z}$ that is related to the eigenvalue λ_l by $\lambda_l = \sqrt{2|qh|}l$:

$$\zeta_l^{(1)}(\tilde{x}) = N_{l-1}e^{-\tilde{x}^2/2}H_{l-1}(\tilde{x}) \quad \zeta_l^{(2)}(\tilde{x}) = N_l e^{-\tilde{x}^2/2}H_l(\tilde{x}). \quad (\text{A22})$$

The normalization constant N_l is proportional to $1/\sqrt{2^l l!}$. Substituting the solutions from Eq. (A22) into the first order eigenvalue equation with x -dependence gives the following solutions:

$$F_l = \begin{pmatrix} f_l^{(1)}(r)\zeta_l^{(1)}(\tilde{x}) \\ f_l^{(2)}(r)\zeta_l^{(1)}(\tilde{x}) \\ f_l^{(1)}(r)\zeta_l^{(2)}(\tilde{x}) \\ -f_l^{(2)}(r)\zeta_l^{(2)}(\tilde{x}) \end{pmatrix}, \quad \lambda_l = \sqrt{2|qh|}l, \quad (\text{A23})$$

and

$$\tilde{F}_l = \begin{pmatrix} \tilde{f}_l^{(1)}(r)\zeta_l^{(1)}(\tilde{x}) \\ \tilde{f}_l^{(2)}(r)\zeta_l^{(1)}(\tilde{x}) \\ -\tilde{f}_l^{(1)}(r)\zeta_l^{(2)}(\tilde{x}) \\ \tilde{f}_l^{(2)}(r)\zeta_l^{(2)}(\tilde{x}) \end{pmatrix}, \quad \lambda_l = -\sqrt{2|qh|l}. \quad (\text{A24})$$

Solving the first order x -dependent equation, we get the same eigenvalue, but slightly different eigenfunctions, for different signs of qh . In particular, e.g., for F , the pairs $f^{(1)}(\zeta^{(1)}, \zeta^{(2)})^T$ and $f^{(2)}(\zeta^{(1)}, -\zeta^{(2)})^T$ correspond to $qh > 0$ and $qh < 0$, respectively. A different sign of qh stands for the positive and negative Landau-level index l .

Finally, the general solution to the Dirac equation is given by a linear combination of Eqs. (A23) and (A24):

$$F_{\text{sol}} = \sum_l (a_l F_l + b_l \tilde{F}_l). \quad (\text{A25})$$

Using the eigenvalues determined by Eqs. (A23) and (A24) in the equation for the radial part (A19), we get

$$\left(-\frac{1}{\sqrt{g_{rr}}} \sigma^3 \partial_r - m + \frac{1}{\sqrt{-g_{tt}}} \sigma^1 (\omega + \mu_q (1 - r_0/r)) - \frac{1}{\sqrt{g_{ii}}} i \sigma^2 \sqrt{2|qh|l} \right) \otimes 1 \begin{pmatrix} F_1 \\ F_2 \end{pmatrix} = 0, \quad (\text{A26})$$

with $l = 0, 1, \dots$; and the same for \tilde{F} replacing $\sqrt{2|qh|l} \rightarrow -\sqrt{2|qh|l}$. It coincides with eq. (A14) in [7] (Dirac equation at zero magnetic field) with the momentum replaced by the Landau-level eigenvalue [22]

$$k \rightarrow \pm \sqrt{2|qh|l}. \quad (\text{A27})$$

Equation (A27) also gives a prescription on how to treat the limit of zero magnetic field $h \rightarrow 0$. The limit is to be taken keeping, e.g., $2|qh|(l+1) \equiv k_F^2$ fixed as $h \rightarrow 0$. In a compact form, the Dirac equation in a magnetic field (A7) is given by

$$\left(\frac{1}{\sqrt{g_{rr}}} \Gamma^{\hat{r}} \partial_r - \frac{1}{\sqrt{-g_{tt}}} \Gamma^{\hat{t}} i (\omega + qA_t) - m - \frac{1}{\sqrt{g_{ii}}} U^{-1} \sqrt{2|qh|l} \right) F(r) = 0, \quad (\text{A28})$$

with $F = (F_1, F_2)^T$, $l = 0, 1, \dots$, for \tilde{F} replace $\sqrt{2|qh|l} \rightarrow -\sqrt{2|qh|l}$, and U^{-1} is the matrix inverse to the matrix given by Eq. (A14):

$$U^{-1} = \begin{pmatrix} i\sigma^2 & 0 \\ 0 & i\sigma^2 \end{pmatrix}, \quad (\text{A29})$$

which we use in the main text.

APPENDIX B: SPECTRAL FUNCTION

In what follows, we use the dimensionless variables (15)–(17). Following the analysis of [7], the flow of the Green's function is determined by

$$G_R(\omega, l) = \lim_{\epsilon \rightarrow 0} \epsilon^{-2m} \begin{pmatrix} \xi_+^{(l)} & 0 \\ 0 & \xi_-^{(l)} \end{pmatrix} \Big|_{r=1/\epsilon}, \quad (\text{B1})$$

where $\xi_+^{(l)}(r) = \frac{f^{(2)}}{f^{(1)}}$ and $\xi_-^{(l)}(r) = \frac{\tilde{f}^{(2)}}{\tilde{f}^{(1)}}$ from the solutions (A23) and (A24). In obtaining this relation, we absorbed the coefficients appearing in Eq. (A25) into the definitions of the radial functions. The functions $\xi_{\pm}^{(l)}$ satisfy the following differential equation [7]:

$$\sqrt{\frac{g_{ii}}{g_{rr}}} \partial_r \xi_{\pm}^{(l)} = -2m \sqrt{g_{ii}} \xi_{\pm}^{(l)} + (u(r) \pm \lambda_l)^2 (\xi_{\pm}^{(l)})^2 + (u(r) \mp \lambda_l), \quad (\text{B2})$$

with $u(r)$ given by

$$u(r) = \sqrt{\frac{g_{ii}}{-g_{tt}}} (\omega + qA_t(r)). \quad (\text{B3})$$

Writing explicitly in the metric given by Eq. (18), we have

$$r^2 \sqrt{f} \partial_r \xi_{\pm}^{(l)} = -2mr \xi_{\pm}^{(l)} + (u(r) \pm \lambda_l) (\xi_{\pm}^{(l)})^2 + (u(r) \mp \lambda_l), \quad (\text{B4})$$

where $u(r)$ is given by

$$u(r) = \frac{1}{\sqrt{f}} \left(\omega + \mu_q \left(1 - \frac{1}{r} \right) \right), \quad (\text{B5})$$

with $f = \frac{(r-1)^2(r^2+2r+3)}{r^4}$ at $T = 0$. Near the horizon ($r = 1$), the flow equation reduces to

$$r^2 \partial_r \xi_{\pm}^{(l)} = \frac{1}{f} (\xi_{\pm}^{(l)} + 1)^2, \quad (\text{B6})$$

which, due to the double zero in f , has a regular solution only if $\xi_{\pm}(r=1) = \pm i$. Writing the radial equation in terms of ξ and choosing the infalling boundary conditions fixes $\xi_{\pm}^{(l)}(r=1) = i$.

The key quantity that we extract from the Green's function is the fermionic spectral function

$$A(\omega, l_x, k_y) = \text{Tr}(\text{Im} G_R(\omega, l_x, k_y)), \quad (\text{B7})$$

which we analyze in the main text of the paper.

- [1] J. Zaanen, *Science* **319**, 1205 (2008); P. de Forcrand, Proc. Sci., LAT2009 (2009) 010 [arXiv:1005.0539]; M. P. Lombardo, K. Splittorff, and J.J.M. Verbaarschot, *ibid.* LAT2009 (2009) 171 [arXiv:0912.3109].
- [2] S. A. Hartnoll, J. Polchinski, E. Silverstein, and D. Tong, *J. High Energy Phys.* **04** (2010) 120; S. A. Hartnoll, C. P. Herzog, and G. T. Horowitz, *ibid.* **12** (2008) 015.
- [3] P. Kovtun, D. T. Son, and A. O. Starinets, *Phys. Rev. Lett.* **94**, 111601 (2005).
- [4] S. -S. Lee, *Phys. Rev. D* **79**, 086006 (2009).
- [5] M. Čubrović, J. Zaanen, and K. Schalm, *Science* **325**, 439 (2009).
- [6] H. Liu, J. McGreevy, and D. Vegh, *Phys. Rev. D* **83**, 065029 (2011).
- [7] T. Faulkner, H. Liu, J. McGreevy, and D. Vegh, *Phys. Rev. D* **83**, 125002 (2011); T. Faulkner, N. Iqbal, H. Liu, J. McGreevy, and D. Vegh, arXiv:1101.0597.
- [8] S. A. Hartnoll and A. Tavanfar, *Phys. Rev. D* **83**, 046003 (2011).
- [9] S. A. Hartnoll, P. K. Kovtun, M. Mueller, and S. Sachdev, *Phys. Rev. B* **76**, 144502 (2007).
- [10] S. A. Hartnoll and P. Kovtun, *Phys. Rev. D* **76**, 066001 (2007).
- [11] P. Basu, J. Y. He, A. Mukherjee, and H.-H. Shieh, *Phys. Rev. D* **82**, 044036 (2010).
- [12] T. Albash and C. V. Johnson, *J. Phys. A* **43**, 345404 (2010); **43**, 345405 (2010).
- [13] T. Albash and C. V. Johnson, *J. High Energy Phys.* **09** (2008) 121; arXiv:0906.0519.
- [14] N. Iqbal, H. Liu, M. Mezei, and Q. Si, *Phys. Rev. D* **82**, 045002 (2010).
- [15] T. Faulkner, N. Iqbal, H. Liu, J. McGreevy, and D. Vegh, arXiv:1003.1728.
- [16] E. D'Hoker and P. Kraus, *J. High Energy Phys.* **05** (2010) 083. E. D'Hoker and P. Kraus, *Classical Quantum Gravity* **27**, 215022 (2010).
- [17] A. Auerbach, “*Quantum Magnetism Approaches to Strongly Correlated Electrons*,” Chia Laguna Summer School 1997 (unpublished).
- [18] E. Gubankova, in Workshop on P- and CP-Odd Effects in Hot and Dense Matter, Brookhaven National Laboratory, 2010 (unpublished).
- [19] J. L. Davis, P. Kraus, and A. Shah, *J. High Energy Phys.* **11** (2008) 020; E. K. -Vakkuri and P. Kraus, *ibid.* **09** (2008) 130.
- [20] A. H. MacDonald, arXiv:cond-mat/9410047.
- [21] T. Hartman and S. A. Hartnoll, *J. High Energy Phys.* **06** (2010) 005.
- [22] F. Denef, S. A. Hartnoll, and S. Sachdev, *Phys. Rev. D* **80**, 126016 (2009); F. Denef, S. A. Hartnoll, and S. Sachdev, *Classical Quantum Gravity* **27**, 125001 (2010).
- [23] Y. Zhang, Z. Jiang, J. P. Small, M. S. Purewal, Y.-W. Tan, M. Fazlollahi, J. D. Chudow, J. A. Jaszczak, H. L. Stormer, and P. Kim, *Phys. Rev. Lett.* **96**, 136806 (2006).
- [24] J. L. Noronha and I. A. Shovkovy, in International Symposium on Exotic States of Nuclear Matter, Catania, Italy, 2007 (unpublished); J. L. Noronha and I. A. Shovkovy, *Phys. Rev. D* **76**, 105030 (2007).
- [25] E. V. Gorbar, V. P. Gusynin, V. A. Miransky, and I. A. Shovkovy, *Phys. Rev. B* **66**, 045108 (2002); V. P. Gusynin and S. G. Sharapov, *ibid.* **73**, 245411 (2006); V. P. Gusynin, V. A. Miransky, S. G. Sharapov, and I. A. Shovkovy, *ibid.* **74**, 195429 (2006); V. P. Gusynin and S. G. Sharapov, *Phys. Rev. Lett.* **95**, 146801 (2005).
- [26] E. V. Gorbar, V. A. Miransky, and I. A. Shovkovy, *Phys. Rev. D* **83**, 085003 (2011).
- [27] M. A. V. Basagoiti, *Phys. Rev. D* **66**, 045005 (2002); J. M. M. Resco and M. A. V. Basagoiti, *ibid.* **63**, 056008 (2001).
- [28] N. Iqbal and H. Liu, *Fortschr. Phys.* **57**, 367 (2009).
- [29] Y.-F. Hsu and G.-Y. Guo, *Phys. Rev. B* **82**, 165404 (2010).
- [30] Y. Kopelevich, V. V. Lemanov, S. Moehlecke, and J. H. S. Torrez, *Fiz. Tverd. Tela (Leningrad)* **41**, 2135 (1999); [*Sov. Phys. Solid State* **41**, 1959 (1999)]; H. Kempa, Y. Kopelevich, F. Mrowka, A. Setzer, J. H. S. Torrez, R. Hoehne, and P. Esquinazi, *Solid State Commun.* **115**, 539 (2000); M. S. Sercheli, Y. Kopelevich, R. R. da Silva, J. H. S. Torrez, and C. Rettori, *ibid.* **121**, 579 (2002); Y. Kopelevich, P. Esquinazi, J. H. S. Torres, R. R. da Silva, H. Kempa, F. Mrowka, and R. Ocana, *Stud. High Temp. Supercond.* **45**, 59 (2003).
- [31] S. S. Gubser and I. Mitra, *Phys. Rev. D* **67**, 064018 (2003); S. S. Gubser and I. R. Klebanov, *Nucl. Phys.* **B656**, 23 (2003); T. Hartman and L. Rastelli, *J. High Energy Phys.* **01** (2008) 019.
- [32] Tian Zhang (unpublished).
- [33] S. Catterall, *J. High Energy Phys.* **07** (2010) 066; **01** (2009) 040; S. Catterall, D. Ferrante, and A. Nicholson, arXiv:0912.5525; P. H. Damgaard and S. Matsuura, *J. High Energy Phys.* **07** (2007) 051.
- [34] S. M. Carroll, *Spacetime and Geometry: An Introduction to General Relativity* (Benjamin Cummings, San Francisco, 2003).

Fractional kinetic model for chaotic transport in nonintegrable Hamiltonian systems

Mihailo Čubrović*

*Institute of Physics, P. O. B. 57, 11001 Belgrade, Serbia and Montenegro and Department of Astronomy-Petnica Science Center,
P. O. B. 6, 14104 Valjevo, Serbia and Montenegro*

(Received 14 April 2005; published 31 August 2005)

We propose a kinetic model of transport in nonintegrable Hamiltonian systems, based on a fractional kinetic equation with spatially dependent diffusion coefficient. The diffusion coefficient is estimated from the remainder of the optimal normal form for the given region of the phase space. After partitioning the phase space into building blocks, a separate equation can be constructed for each block. Solving the kinetic equations approximately and estimating the diffusion time scales, we convolve the solutions to get the description of the macroscopic behavior. We show that, in the limit of infinitely many blocks, one can expect an approximate scaling relation between the Lyapunov time and the diffusion (or escape) time, which is either an exponential or a power law. We check our results numerically on over a dozen Hamiltonians and find a good agreement.

DOI: [10.1103/PhysRevE.72.025204](https://doi.org/10.1103/PhysRevE.72.025204)

PACS number(s): 05.45.-a, 05.60.Cd, 05.20.Dd

Statistical treatment of chaotic transport is one of the most difficult problems in nonintegrable Hamiltonian dynamics. Despite its importance for many practical problems in various fields, e.g., plasma physics [1,2] and dynamical astronomy [3], we still lack a general and consistent kinetic theory of transport. The main reason is the complicated nature of the phase space of the typical nonintegrable Hamiltonian system, since it usually contains a “topological zoo” of regular and chaotic structures mixed on an arbitrarily small scale. The most promising way for overcoming these difficulties is, in our opinion, the so-called fractional kinetics of the phase space [4]. Fractional kinetics has become a broad topic of research not only in Hamiltonian dynamics but also in very different areas such as solid-state physics [5] and physics of complex systems [6]. The basic advantage of the fractional kinetic equation (FKE) for describing chaotic transport is that its fractional nature allows one to include the self-similarity of phase space and time, which arises from the first principles, i.e., from the dynamical equations. Especially important is the phenomenon of the so-called stickiness [3] or dynamical trapping [7], which leads to long intervals of quasiregular motion.

The particular issue that has largely motivated this research is the phenomenon of approximate scaling of diffusion time scales with the Lyapunov exponents or perturbation strength. A number of papers have been published on this topic, e.g., [8]; we are also inspired by the building block method of [9].

The basic idea of our model is to consider a FKE in the action space with a nonhomogenous diffusion coefficient and to combine, i.e., convolve the results to obtain the expected macroscopic behavior. We use the following form of the FKE:

$$\frac{\partial^\beta P(I,t)}{\partial t^\beta} = \frac{\partial^\alpha [\mathcal{D}(I)P(I,t)]}{\partial |I|^\alpha} + \delta(I)t^{-\beta}/\Gamma(1-\beta), \quad (1)$$

where $0 < \beta < 1$ and $0 < \alpha < 2$. Its derivation from the Hamiltonian equations and discussion of assumptions involved can be found, e.g., in [4]. Although, strictly speaking, one should consider a vector of actions, we shall assume that diffusion along one action coordinate is independent of the others and consider I as a scalar; alternatively, one could interpret that as considering only one action variable, whereas the diffusion along the others is many orders of magnitude smaller. Both cases have been described in various systems [2,4].

We estimate the diffusion coefficient \mathcal{D} as the remainder of the normal form for the dynamics in the vicinity of a stable domain, e.g., invariant torus. Splitting the Hamiltonian $H(I, \phi)$ into an action-only integrable part $H_0(I) = \omega I$ and the nonintegrable remainder $H_1(I, \phi)$, one can obtain the estimate for the remainder of the form $O(f(I))$, i.e., as a function of the action. Treating the influence of the nonintegrable remainder on the dynamics as the microscopic transport mechanism, we take $f(I)$ from the above estimate for the diffusion coefficient. Two optimal normal forms are known as Nekhoroshev and Birkhoff normal forms. Their remainders [10] give the diffusion coefficients \mathcal{D}_N and \mathcal{D}_B :

$$\mathcal{D}_N = \mathcal{D}_0 \exp[-1/|I|^\theta], \quad (2a)$$

$$\mathcal{D}_B = \mathcal{D}_0 |I|^\theta, \quad (2b)$$

where \mathcal{D}_0 denotes the constant part, which is, in general, dependent on the properties of the Hamiltonian. For both cases, there is a constraint $\theta > 2$. The two cases roughly correspond to local nonoverlapping or overlapping of the resonances.

The last step before solving the FKE is the estimation of the fractional exponents α and β . These are intimately related to the self-similarity of the structures involved, and can be determined from the exponents of the renormalization group of kinetics of the particular system. This has to be

*Electronic address: cygnus@eunet.yu

done numerically for all but the simplest systems [4]. In our computations, we have employed a “building block” approach similar to that of [9], partitioning the phase space into several regions, each described with its own FKE, with the diffusion coefficient (2a) or (2b). However, instead of considering only ballistic flights and Markovian diffusion, as in [9], we propose the adoption of a set of (α, β) pairs. The values of the exponents can then be determined by sampling the flights (longer than a certain threshold T_0), and then fitting the distribution of their lengths and durations as $\ell^{-(1+\alpha)}$ and $t^{-(1+\beta)}$, respectively.

It is hardly surprising that we were unable to find the exact solutions for the FKE (1), with the diffusion coefficients (2a) and (2b), in their most general form. However, the long-term behavior can be found by expanding the space derivative on the right-hand side of (1) according to the generalizations of the Leibniz’s rule and chain rule for the fractional operator $d^\alpha/d|I|^\alpha$; see, e.g., [11] for mathematical details. For the case (2a), we obtain the solution, up to the normalization factor,

$$P(I, t) = E_\beta(-y_0^{4/\alpha} - y^{4/\alpha}) \mathcal{I}_1 \left(\frac{2e^{-y}}{\mathcal{D}_0^{3/2}} \sqrt{\frac{y_0}{t^\beta y}} \right), \quad (3)$$

where \mathcal{I} denotes the modified Bessel function of the first kind, $y(I, t) = |I| / [(\theta - 2) \sqrt{\mathcal{D}_0 I^\theta t^\beta}]$, and $y_0 = y(I_0, t)$, with I_0 denoting the value of the action at $t=0$. The Mittag-Leffler function is denoted by E_β . For the Birkhoff case, one obtains

$$P(I, t) = \frac{y}{\sqrt{I}} E_\beta(-y_0^{4/\alpha} - y^{4/\alpha}) \mathcal{I}_p(2y_0 y), \quad (4)$$

with $p = (\theta - 1) / (\theta - 2)$. We note that, for $I, t \gg 1$, both y and y_0 tend to zero. The asymptotic expansions of the Mittag-Leffler and the Bessel function can then be used to show that the solutions $P(I, t)$ fall off in the infinity sufficiently sharply to be valid probability distributions. They are the main exact result of our analysis. We shall use them here to apply the more advanced building block model and to obtain the approximate scaling relations between the diffusion and Lyapunov time scales.

Convolution over all the solutions $(\star_{i=1}^N)$ can be performed in the usual way, with some entrance probabilities (actually, statistical weights of each block) p_i ,

$$P_{res}(I, t) = \star_{i=1}^N p_i P_i(I, t), \quad (5)$$

which give the resulting probability distribution $P_{res}(I, t)$. We propose this way for examining the behavior of particular systems. In the limit of infinitely many blocks [20], however, one can derive a generic relation between the short-time and long-time diffusion scales.

We next proceed to estimate the typical diffusion time scales. These can be related to the “escape times” one often encounters in simulations, e.g., [8]. Strictly speaking, the escape time can only be defined in open systems, as the time to cross the Lyapunov curve (see [13] for a definition). Otherwise, escape time is usually a more or less qualitative term meant to describe, generally, the time needed to enter a large connected chaotic region (“stochastic see”) or to experience

a qualitative change of dynamical behavior. In what follows, we shall consider the escape time as the time scale needed to reach a fixed I ; without loss of generality, we may assume $I=1$.

For fixed I , the solution (3) has a maximum about $2\sqrt{y_0}/(t^\beta y) \approx \mathcal{D}_0^{3/2}$. Solving this for time t , we obtain the estimate of the time to reach $I=1$,

$$T_{I=1} \approx \left(\frac{16(I/I_0)^{\theta-2}}{\mathcal{D}_0} \right)^{1/\beta}. \quad (6)$$

Similarly, (4) reaches its peak at $2yy_0 \approx 1$, which gives the following $T_{I=1}$:

$$T_{I=1} \approx \left(\frac{(II_0)^{1-\theta/2}}{(\theta-2)\mathcal{D}_0} \right)^{1/\beta}. \quad (7)$$

On the other hand, the short (microscopic) time scale of (1) is about $\mathcal{D}(I)/(\omega e^{\beta/\alpha})$, which may be interpreted as the average time between two “collisions;” in our case, this corresponds to a time needed to cross a single resonance, bearing in mind that resonance interactions and overlaps are the main physical mechanisms of transport. Moreover, this time scale is often considered to be a valid estimate of the Lyapunov time T_{Lyap} [1,3].

Let us now notice that the solutions (3) and (4), with their exit time scales (6) and (7), can be written in the form of Fox’s H functions [6]. By convolving these functions, one gets, after a straightforward but tedious calculation, a Fox’s function again, which may have two asymptotic behaviors. They scale with the short-time scale of (3) and (4) either as an exponential law or as a power law. The asymptotic behavior depends on the weights p_i and on the sum of transport exponents $2\beta_i/\alpha_i$ for each building block. Accepting this reasoning and inserting the above estimate for T_{Lyap} into (6) and (7), we obtain the approximate scalings for escape time T_{esc} ,

$$T_{esc} \propto \exp(T_{Lyap}^\kappa), \quad (8a)$$

$$T_{esc} \propto T_{Lyap}^\nu. \quad (8b)$$

Let us hold onto this result for a moment. The scaling of this type has been conjectured long ago (e.g., [14]), and it is implicitly suggested also by the classic work of Chirikov concerning the regimes of resonance nonoverlapping and overlapping [15] (the first one being known also as the Nekhoroshev regime). More recently, transition between the Nekhoroshev and Chirikov regime has been explored by Froeschle and others [16]. However, we show here that the scaling (8a) and (8b) arises from both basic regimes of chaotic dynamics, and that its type is determined also by the fractional exponents α and β of different building blocks. Physically, this means that the sticky (and thus non-Markovian) nature of self-similar structures in the phase space can “mimic” the effects of the resonance nonoverlapping. This is logical, since both phenomena effectively put a barrier into the transport channels. The scalings can be expected to be universal for a given system but are clearly nonuniversal for different systems, since they depend on the properties of the Hamiltonian. It should also be noted that, for N -dimensional ($N > 2$) systems, one should take into ac-

TABLE I. Hamiltonians of the form $H_{Int} + \epsilon H_{Pert}$ explored in the simulations. For each Hamiltonian, we give the integrable part H_{Int} , the perturbation part H_{Pert} , the range of the values of ϵ in the simulations, the exponents of the scalings κ and ν , and the range of the values of ϵ for the transition regime. Variables (I_i, ϕ_i) denote the action-angle variables, whereas (x, y, z) are the physical space coordinates. HO2 and HO3 denote the harmonic oscillator in two and three dimensions, respectively. HH2 and HH3 refer to the integrable Henon-Heiles Hamiltonian [13] in two and three dimensions: $(x^2 + y^2 + x^2 + y^2 - 2/3y^3)/2$ and $(x^2 + y^2 + z^2 + x^2 + y^2 + z^2 - 2/3z^3)/2$, respectively. Hamiltonian H_8 is the egg-crate system taken from [4], H_9 is the sixth-order Toda lattice, i.e., the integrable Henon-Heiles system perturbed with its sixth-order expansion [1], and H_{14} is taken from [16]. See the text for further comments.

| H | H_{Int} | H_{Pert} | ϵ | κ | ν | ϵ_{trans} |
|----------|------------------------------------|--|-------------|-----------------|-----------------|--------------------|
| H_1 | HO2 | ϵxy | 1.00–4.00 | 0.65 ± 0.07 | 0.87 ± 0.05 | 1.50–1.60 |
| H_2 | HO2 | $\epsilon x^2 y$ | 0.87–3.50 | 0.45 ± 0.05 | 1.98 ± 0.06 | 1.28–1.32 |
| H_3 | HO2 | $-\epsilon x^2 y^2$ | 1.50–6.00 | 1.09 ± 0.03 | 1.70 ± 0.04 | 3.32–3.70 |
| H_4 | HH2 | ϵxy | 0.00–3.50 | 0.77 ± 0.08 | 0.53 ± 0.03 | 0.15–0.20 |
| H_5 | HH2 | $\epsilon x^2 y$ | 1.00–4.00 | 0.15 ± 0.03 | 1.25 ± 0.06 | 1.12–1.16 |
| H_6 | HH2 | $-\epsilon x^2 y$ | 1.00–4.00 | 0.71 ± 0.05 | 0.88 ± 0.04 | 1.55–1.66 |
| H_7 | HH2 | $-\epsilon / \sqrt{x^2 + y^2}$ | 0.00–3.50 | 0.33 ± 0.05 | 0.57 ± 0.03 | 1.60–1.70 |
| H_8 | $(x^2 + y^2)/2 + \cos x + \cos y$ | $\epsilon \cos x \cos y$ | 0.00–2.00 | 0.22 ± 0.04 | 1.12 ± 0.08 | 0.34–0.37 |
| H_9 | HH2 | sixth-order Toda lattice expansion | 0.00–4.00 | 0.58 ± 0.03 | 1.44 ± 0.04 | 0.55–0.60 |
| H_{10} | $I_1^2/2 + 2\pi I_2$ | $\epsilon(\cos \phi_1 + \cos(\phi_1 - \phi_2))$ | 0.00–3.00 | 1.21 ± 0.04 | 1.82 ± 0.07 | 1.20–1.32 |
| H_{11} | $I_1^2/2 + 2\pi I_2 + \cos \phi_1$ | $\epsilon(\cos(\phi_1 - \phi_2) + \cos(\phi_1 + \phi_2))$ | 0.00–3.00 | 0.45 ± 0.05 | 1.75 ± 0.07 | 0.85–0.90 |
| H_{12} | HO3 | $\epsilon x^2 y z$ | 0.00–2.00 | 0.22 ± 0.03 | 0.57 ± 0.03 | 0.33–0.45 |
| H_{13} | HH3 | $\epsilon x z^2$ | 0.80–4.00 | 0.41 ± 0.04 | 1.03 ± 0.08 | 1.20–1.31 |
| H_{14} | $(I_1^2 + I_2^2)/2 + I_3$ | $\epsilon / (\cos \phi_1 + \cos \phi_2 + \cos \phi_3 + 4)$ | 0.000–0.100 | 0.19 ± 0.03 | 1.00 ± 0.04 | 0.055–0.060 |

count the Arnold diffusion. However, this should be negligible as long as the number of the degrees of freedom is sufficiently low, especially if we take into account a recent result which proves its superexponentially slow nature for a certain class of systems [17].

We have performed thorough numerical tests of our results, by integrating ensembles of particles initially placed in a cell of the phase space of the given Hamiltonian. We have inspected the behavior of the perturbed (quasi-integrable) Hamiltonian systems, i.e., of the form $H = H_{Int} + \epsilon H_{Pert}$, since the constant part of the diffusion coefficient \mathcal{D}_0 can then easily be estimated as ϵ^2 . We have observed the time evolution of the “distribution function,” i.e., concentration of the particles in the phase space, the escape times, and the scaling exponents [by fitting to (8a) and (8b)]. We have also calculated the finite time Lyapunov exponent (FTLE, see [18] for a definition), as the numerical estimate for $1/T_{Lyap}$. The escape time was measured as the time of crossing the Lyapunov curves, for open systems, or as the time of the beginning of the first long interval of normal diffusion, for the closed systems [21]. Details on the simulations and on the approximate scalings of the form (8a) and (8b) found numerically are summed up in Table I.

Figure 1 gives the comparison between the analytically and numerically obtained distribution functions, for each of the cases (3) and (4). Overall agreement can be seen, although it is not perfect. Typical results for the $T_{esc}(T_{Lyap})$ relation are shown in Fig. 2. Agreement with the predicted approximate scalings is good. The regimes are rather clearly separated and the transient regime is short, although it does exist. This behavior could be described as a phase transition between two regimes of chaotic transport, an idea which is not new for dynamical systems.

We are unable to explain the abrupt transition from one scaling regime into another, which occurs in most of our simulations, and resembles a phase transition. This kind of behavior could be better described by a discrete model. An obvious choice is a multiply branched tree (as proposed in [19]) or a network, with the transition probabilities derived from our results for the distribution functions. This would actually be a formalization of the building block model, which already (implicitly) includes a network of blocks.

In conclusion, we have proposed a method for obtaining (and solving) the kinetic equations of chaotic diffusion. The

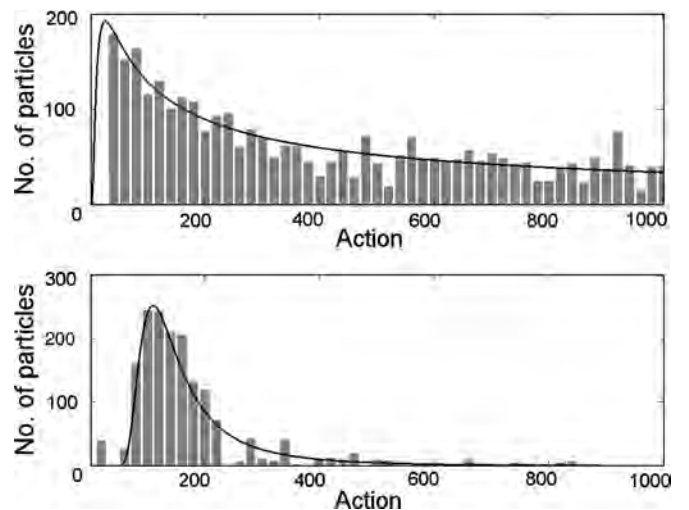


FIG. 1. Analytical (solid line) and numerical (histogram) distribution functions $P(I_1, t)$ for the Hamiltonian H_{14} . Action is in relative units. (a) Nonoverlapping resonances for $\epsilon=0.030$. (b) Overlapping resonances for $\epsilon=0.060$.

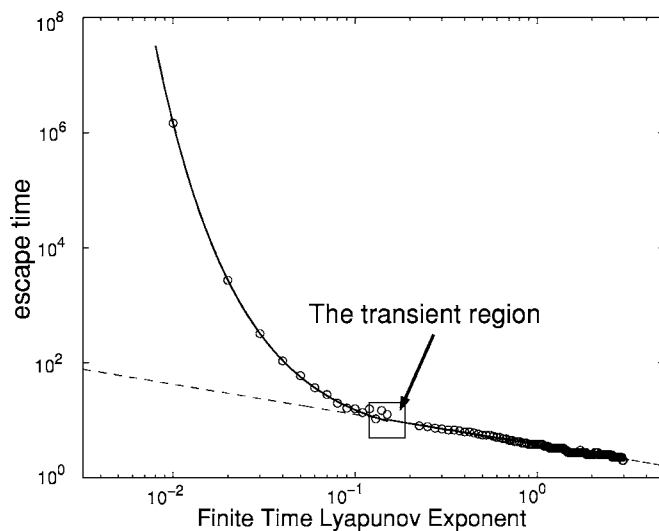


FIG. 2. An example of the scaling relations between finite time Lyapunov exponent and escape time. The solid lines denote the least-squares fit to the scaling relations (8). Scales are logarithmic on both axes, thus the power-law fit is a straight line. The dashed reference line for the power law is also shown, as well as the transient region. Time is in relative units from the simulation. The Hamiltonian is H_4 .

method is based upon using the normal forms of dynamics as the basic blocks of kinetics. In general case, some parameters of the model, including the fractional exponents of FKE, have to be computed from the simulations, as the current state of Hamiltonian theory does not allow us to estimate them from the dynamical equations, as noted also in [4]. We have also demonstrated a generic approximate scaling of the macroscopic diffusion time, often regarded to in simulations as escape time, with the Lyapunov (microscopic) time scale. We especially underline that both the power law and the exponential form of scaling can arise from both possible forms of the diffusion coefficient, and that the scaling behavior arises from combining the two, i.e., as a kind of collective behavior.

I am grateful to researchers from the Group for Nonlinear Optics, Institute of Physics, Belgrade, for discussions and support during the preparation of this paper and for the processor time for the simulations. I am also indebted to Robert S. MacKay, Harry Varvoglis, and George M. Zaslavsky for helpful comments, and for some of the references. Work at the Institute of Physics is supported by the Ministry of Science and Environment Protection, under Project No. OI 1475.

-
- [1] A. J. Lichtenberg and M. A. Lieberman, *Regular and Stochastic Motion* (Springer-Verlag, New York, 1983).
- [2] J. D. Meiss, *Rev. Mod. Phys.* **64**, 795 (1992).
- [3] G. Contopoulos, *Order and Chaos in Dynamical Astronomy* (Springer, Berlin, 2002).
- [4] G. M. Zaslavsky, *Phys. Rep.* **371**, 461 (2002).
- [5] J. Klafter, M. F. Shlesinger, and G. Zumofen, *Phys. Today* **49**, 33 (1996).
- [6] R. Metzler and J. Klafter, *Phys. Rep.* **339**, 1 (2000).
- [7] G. M. Zaslavsky, *Physica D* **168-169**, 292 (2002).
- [8] I. I. Shevchenko, *Phys. Lett. A* **241**, 53 (1998); J. Aguirre, J. C. Vallejo, and M. A. F. Sanjuan, *Phys. Rev. E* **64**, 066208 (2001); J. Aguirre and M. A. F. Sanjuan, *ibid.* **67**, 056201 (2003).
- [9] S. Denisov, J. Klafter, and M. Urbakh, *Phys. Rev. E* **66**, 046217 (2002).
- [10] A. Morbidelli and M. Vergassola, *J. Stat. Phys.* **89**, 549 (1997).
- [11] I. Podlubny, *Fractional Differential Equations* (Academic, New York, 1998); A. I. Saichev and G. M. Zaslavsky, *Chaos* **7**, 753 (1997).
- [12] G. M. Zaslavsky, *Physica A* **288**, 431 (2000).
- [13] H. E. Kandrup, C. Siopis, G. Contopoulos, and R. Dvorak, *Chaos* **9**, 524 (1999).
- [14] A. Morbidelli and C. Froeschle, *Celest. Mech. Dyn. Astron.* **63**, 227 (1996).
- [15] B. V. Chirikov, *Phys. Rep.* **52**, 265 (1979).
- [16] C. Froeschle, M. Guzzo, and E. Lega, *Science* **289**, 2108 (2000); M. Guzzo, E. Lega, and C. Froeschle, *Physica D* **163**, 1 (2002).
- [17] A. Morbidelli and A. Giorgilli, *J. Stat. Phys.* **78**, 1607 (1997).
- [18] N. Voglis and G. Contopoulos, *J. Phys. A* **27**, 4899 (1994).
- [19] J. D. Meiss and E. Ott, *Physica D* **20**, 387 (1986).
- [20] This should be realistic for most systems, since each block, in a typical case, actually has a multifractal structure [12], which is analogous to consisting of many “sub-blocks,” each one having different fractional exponents.
- [21] The length of this interval has to be determined empirically. It should warrant that the particle has entered the large connected stochastic sea, so that the probability that the particle is trapped again is very low.

Semistiff polymer model of unfolded proteins and its application to NMR residual dipolar couplings

M. Čubrović^{1,2}, O.I. Obolensky^{1,a}, and A.V. Solov'yov^{1,b}

¹ Frankfurt Institute for Advanced Studies, Ruth-Moufang-Str. 1, 60438 Frankfurt am Main, Germany

² Institute of Physics, P.O. Box 57, 11001 Belgrade, Serbia

Received 14 March 2008 / Received in final form 15 September 2008 / Published online 15 October 2008
© EDP Sciences, Società Italiana di Fisica, Springer-Verlag 2008

Abstract. We present a new statistical model of unfolded proteins in which the stiffness of polypeptide backbone is taken into account. We construct and solve a mean field equation which has the form of a diffusion equation and derive the distribution function for conformations of unfolded polypeptides. Accounting for the stiffness of the protein backbone results in a more accurate description of general properties of a polypeptide chain, such as its gyration radius. We then use the distribution function of a semistiff protein within a previously developed theoretical framework [J. Biomol. NMR **39**, 1 (2007)] to determine the nuclear magnetic resonance (NMR) residual dipolar couplings (RDCs) in unfolded proteins. The calculated RDC profiles (dependence of the RDC value on the residue number) exhibit a more prominent bell-like shape and a better agreement with experimental data as compared to the previous results obtained with the random flights chain model.

PACS. 87.10.-e General theory and mathematical aspects – 82.56.Pp NMR of biomolecules – 82.56.Dj High resolution NMR

1 Introduction and motivation

High-resolution, liquid-state nuclear magnetic resonance (NMR) spectroscopy has proven to be an invaluable tool in investigation of the structure and dynamics of biomacromolecules, including folded and, recently, unfolded proteins. One of the NMR observables from which one can infer structural and dynamical information is the so-called residual dipolar couplings (RDCs) [1]. These couplings are direct dipole-dipole interactions between the spins of two nuclei, e.g., ¹⁵N and a ¹H nuclei, detected in NMR experiments by a shift in the resonant frequency of nuclear spin flip transitions. They can be measured independently for each amino acid residue in a polypeptide chain.

Analysis of RDC profiles (dependence of the RDC value on the residue number) has been shown to be very informative in structure validation and refinement of folded proteins [1]. However, for unfolded proteins reliable interpretation of RDC measurements remains elusive even though a significant amount of experimental data has been accumulated (see [2] for a survey). Theoretically, one can predict the RDC profiles by performing numeri-

cal sampling of the conformational space of the unfolded polypeptide. For example, in [3,4] ensembles of unfolded conformations were constructed from amino acid-specific distributions of Ramachandran angles ϕ/ψ taken from the loop regions of high-resolution X-ray structures in the protein data base. This method allows one to predict the RDC profiles with a reasonable accuracy, but it lacks the ability to explain on a basic level the obtained results, serving, therefore, as a black box with a limited use for interpretation of experimental data.

In [2] it was shown that the basic trends in RDC profiles and the underlying physical and mathematical principles leading to these trends can be revealed by statistical analysis not based on numerical sampling of conformational space (see also similar, although less mathematically rigorous, work [5]). Two general features of RDC profiles were predicted for unfolded polypeptide chains. The first one is that shorter chains have larger (in absolute value) RDCs under same experimental conditions. The second feature predicted in [2,5] is that the RDCs are larger for the amino acid residues in the middle of the chain, leading to the bell-like shape of RDC profiles. Despite the simplicity of the model (random flights chain) used in [2,5] to mimic the unfolded polypeptides, both these trends seem to be present in the experiments carried out under conditions prohibiting formation of native-like structures [2].

^a Present address: National Center for Biotechnology Information, NLM/NIH, 8600 Rockville Pike, Bethesda, MD 20894, USA

^b e-mail: solovyov@fias.uni-frankfurt.de

Our goal in this paper is to improve the quality of the model which is used for simulating the unfolded polypeptide chain. We formulate here a new statistical model of unfolded proteins in which the stiffness of polypeptide backbone is taken into account. We demonstrate that accounting for the stiffness of the protein backbone results in a more accurate description of general properties of a polypeptide chain, such as its gyration radius.

Stiff polymer model is a well-known concept in polymer physics, much used since the pioneering paper of Sato et al. [6]. The idea is to introduce an energy cost for bending of the polymer, thus favoring the extended conformations. The most versatile formalism for doing so is the so-called wormlike chain model, in which the bending energy density is proportional to the square of the curvature of the polymer contour. It has been developed to its full strength only recently [7], with the introduction of new theoretical tools to account for various generalizations and boundary conditions. The starting point in the papers cited above is the mean-field description which has the form of a diffusion equation in tangent space. However, this approximation becomes less and less satisfactory for polymers with low stiffness [8]. We show in this paper (followed by a more technical discussion in [9]) that a better continuum limit for the case of low stiffness is obtained in the real space, which turns out to have, again, the form of the diffusion equation. Also, the question of how the wormlike chain model arises from discrete stiff chains has, to the best of our knowledge, not been addressed so far. In the following section we will start from a discrete model and pass to a continuum limit, which will turn out to be exactly the low-stiffness (the usual term in polymer physics is semiflexible or semistiff) limit of the wormlike chain model.

The developed semistiff polymer model is applied to the calculation of RDCs within the theoretical framework of [2]. The calculated RDC profiles exhibit a more prominent bell-like shape and a better agreement with experimental data as compared to the previous results obtained with the random flights chain model.

In the concluding section, we will also discuss possible further steps in interpreting the RDC measurements, as well as the importance of our results from a more general perspective.

2 Theory

2.1 Introduction to the problem

We first give a general and informal consideration of the problem, before describing in more detail the interaction potential in our system and the procedure to calculate the necessary quantities. The ultimate goal is finding the relation between the dipolar couplings and the physical parameters of the unfolded polypeptide, and extracting the information on the shape and other properties of the polypeptide from the RDC measurements. Unfolded polypeptides are in many aspects similar to simple linear polymers, having no well-defined secondary structure.

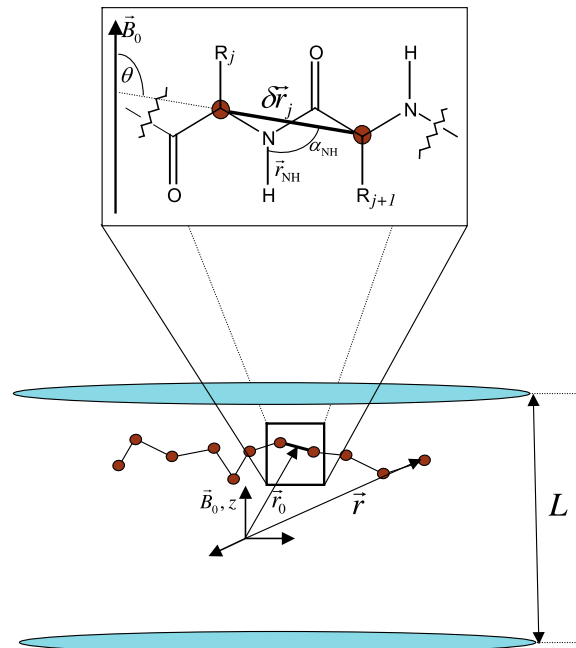


Fig. 1. Schematic picture of a polymer chain in a restricting medium modelled with a set of parallel barriers. The barrier-to-barrier distance is L . External magnetic field vector is $B_0\mathbf{e}_z$. The vectors \mathbf{r} and \mathbf{r}_0 are the position vectors of points in the chain, defined in the fourth section. Inset: structure of a single monomer unit. The angles α_{NH} and θ are defined for each segment. The residues (side chains) are denoted by R_j and R_{j+1} , while the radius vector of the j th segment is $\delta\mathbf{r}_j$.

For clarity we will pose the problem for a discrete chain first, although the calculations will be performed in the continuum limit. The quantity to be calculated is the dipole-dipole coupling between two nuclei. We will deal with the $^{15}\text{N}-^1\text{H}$ couplings in this paper. The energy (actually, the frequency) of the coupling is given by [2]:

$$D_{\text{NH}} = \frac{\mu_0 \hbar \gamma_{\text{N}} \gamma_{\text{H}}}{4\pi^2 r_{\text{NH}}^3} P_2(\alpha_{\text{NH}}) \langle P_2(\cos \Theta) \rangle, \quad (1)$$

where μ_0 is the magnetic permeability constant, γ_{N} and γ_{H} are gyromagnetic ratios for the nitrogen and the hydrogen nucleus and r_{NH} is the internuclear distance (assumed to be fixed). The function P_2 stands for the Legendre polynomial of the second order. The angles α_{NH} and θ characterize the orientation of a chain segment with respect to the external field. These are in turn determined by the conformation of the chain, therefore connecting the measured couplings to the structure of the polypeptide. The average (denoted by angular brackets) is to be carried out over all possible conformations of the chain, i.e. over the state space of the chain.

The meaning of the angles α_{NH} and θ is best seen from Figure 1. The former is the angle between the vector \mathbf{r}_{NH} , i.e. the internuclear vector, and the axis of the j th segment, denoted in Figure 1 by $\delta\mathbf{r}_j$. On the other hand, θ stands for the angle between $\delta\mathbf{r}_j$ and the z -axis, which is the direction of the external magnetic field.

The origin of non-zero RDCs lies in the restricting medium (bicelles or polyacrylamide gels, usually) in which the denaturated protein is solvated in experiments. Actual shape and geometry of the confining barriers may vary but the overall effect will be similar and will result in an effective confinement of the polymer. In the simplest approximation, one may regard the restricting barriers to be parallel to each other, at some distance L , as given in the Figure 1. The influence of the confinement is crucial even if the distance L is large compared to the length of the polypeptide (as is the case for typical experimental conditions). Confinement only induces a mild “deformation” of the average shape of the polypeptide coil. It is this deformation, however, which gives rise to non-zero expectation value of the term $P_2(\cos\Theta)$. The calculation of this value will be in focus of the rest of the paper.

2.2 Stiffness of polypeptide chain

The discrete chain is represented as an array of N segments, each denoted by index $j = 1 \dots N$. The information on structure of the chain is contained in the distribution function $P(N, \mathbf{r}, \mathbf{r}_0)$ which gives probability to find the chain in a conformation with the end points at \mathbf{r}_0 and \mathbf{r} . The usual approach of polymer physics would be to write the action (or, equivalently, path integral) for the chain based on some empirical potential [10]. As we will, for the most part, work in the mean-field approximation, we will refrain from this approach and write directly the equation for the distribution function. The statistical weight of each conformation is determined by its Boltzmann weight, supposing that the system is sufficiently close to equilibrium. To specify these weights completely, one needs to employ an empirical potential for segment-to-segment interactions.

Empirical potentials for polypeptides, generally, may include the following terms: bond extensibility, bond angle stiffness, rotation about the so-called Ramachandran dihedral angles (see, e.g., [11]) and non-bonded interactions, including, possibly, Coulombic interactions, hydrogen bonds, excluded volume interactions, etc. We will deal with the non-bonded interactions in a separate publication [12]; it can be shown that these do not contribute significantly to the problem of interpreting the NMR spectroscopic data that we are primarily concerned with in this paper. Bond extensibility is, in general, negligible in polypeptides and better results are usually obtained in the framework of fixed bond lengths [13]. So, all of our segments are assumed to have the same length a .

The stiffness is an all-present effect in polymer physics and is usually characterized either by the persistence length L_p [10] or in terms of the bond angle θ and its discrepancies from some optimal value θ_0 [14]. The connection between the two descriptions is given by $L_p = ak_\theta\beta$; as usual, $\beta = (kT)^{-1}$. In our model, for typical values of k_θ and β , L_p is a few segments long. However, L_p is not very practical for nonzero θ_0 . Geometrically, it is equal to the segment length of an effective freely jointed chain

with the same macroscopic properties as the stiff chain. This geometric analogy is lost for $\theta_0 > 0$.

For most polymers, the optimal angle is $\theta_0 = 0$; in our case, the structure of polypeptide backbone $-\text{N}-\text{C}-\text{C}-\text{N}-$ results in a non zero value of θ_0 [11], which is actually the tetrahedral angle characterizing the bond geometry of the carbon atom. The radius-vector of the j th segment relative to the end of the previous segment will be denoted by $\delta\mathbf{r}_j$. The bond stiffness is obviously a nearest-neighbor interaction, involving pairs of subsequent segments. Dihedral angles are for *unfolded* polypeptides usually considered in a purely local approximation, thus leading to no site-to-site interaction. Therefore, the potential of our system is of the form:

$$V = \sum_{j=1}^{N-1} V_\theta(\theta_j) + \sum_{j=1}^N V_{\phi\psi}(\phi_j, \psi_j). \quad (2)$$

Still, even in this approximation, distribution of dihedral angles shows nontrivial behavior if the polypeptide is not a homopolymer, i.e. if various segments have different energy minima. One final remark is that we assume various degrees of freedom to be decoupled; it is also a common approximation, and a necessary one for the problem to be tractable.

The Ramachandran part of the potential, $V_{\phi\psi}$, cannot be treated in the mean-field approximation for the reason mentioned in the previous paragraph: the energy landscape is strongly site-specific and therefore evades a description in the framework of mean-field theory. On the other hand, the decoupling of the degrees of freedom suggests that the effects of stiffness can be considered independently. In this paper, we will explore exactly the influence of stiffness, leaving the theory for Ramachandran angles for further work.

Hence, we are only interested for the potential V_θ . An often-employed potential in both analytical and numerical work, with slight differences from author to author, described in [14], is the following one:

$$V_\theta(\theta_j) = -k_\theta \cos(\theta - \theta_0) + O\left((\theta - \theta_0)^3\right). \quad (3)$$

The correction to the cosine term in (3) can be any function which is “small” compared to the leading term in the cosine, i.e. containing only third and higher order terms in the angular displacement $\theta_j - \theta_0$. It will turn out later that these corrections are, in our method, of secondary importance anyway, so the exact form of this correction is not relevant. In other words, the exact form of the anharmonic terms is not relevant; a different form would produce different higher-order terms for the diffusion coefficient but these are (by definition) beyond the scope of any model based on diffusion equation.

In the following subsection, we will give our mean-field model for a semistiff (semiflexible) chain. For some purposes the mean-field treatment can provide sufficiently accurate estimates and it is also of interest for other problems, not connected to protein physics.

2.3 Diffusion equation formalism for semistiff polymers

For the rest of this paper, we will take the continuum limit. The index of a segment in the chain (chemical coordinate s) is now a variable taking values from the interval $(0, N)$, where N is the total segment number. This framework is, of course, only suitable for the chains which are not too short.

The formalism we employ here is best suited for small stiffness; typical values of k_θ in (3) are of the order of 10ϵ , with $\epsilon = 10^{-23}$ J (0.624×10^{-4} eV), which is small compared to systems like double-stranded DNA.

One can start from the statistical weight of the j th segment having a bond angle θ_j expressed in terms of its radius-vector $\delta\mathbf{r}_j$:

$$p_0(\delta\mathbf{r}_j) = \frac{\beta k_\theta}{4\pi a^2 \sinh \beta k_\theta} \delta(\delta r_j - a) \exp(\beta k_\theta \cos \theta_j). \quad (4)$$

The above equation is nothing but the Boltzmann weight with appropriate normalization. Since the experiments with unfolded proteins are usually performed at room temperature, we take $T = 300$ K for all calculations throughout the paper. In other words, the chain is modelled as a random walk with one-step memory (which is implicitly included in (4) via the bond angle depending on the previous segment). It is a variation on the persistent random walk problem, well-known and often encountered in theory of stochastic processes [15]. The usual formalism of master equations leads to the conclusion that the continuum limit of this process is a diffusion equation; we show that in more detail in a separate publication [9].

For a three-dimensional model, diffusion coefficient becomes the diffusion tensor $\hat{\mathcal{D}}$ represented with a three-by-three matrix, the component \mathcal{D}_{ij} being, by definition:

$$\mathcal{D}_{ij} = \frac{1}{2} \int d\delta\mathbf{r} p_0(\delta\mathbf{r}) \delta r_i \delta r_j. \quad (5)$$

A straightforward calculation then shows that the off-diagonal components vanish; furthermore, the two ‘‘transversal’’ components (perpendicular to the tangent vector at the given point) are equal and will be denoted by \mathcal{D}_\perp ; the ‘‘longitudinal’’ one is denoted by \mathcal{D}_\parallel . They are obtained to be:

$$\mathcal{D}_\perp = \frac{a^2}{\sinh \beta k_\theta} \left(\frac{\cosh \beta k_\theta}{\beta k_\theta} - \frac{\sinh \beta k_\theta}{\beta^2 k_\theta^2} \right) \quad (6)$$

$$\mathcal{D}_\parallel = \frac{a^2 \cos^2 \theta_0}{\sinh \beta k_\theta} \left(\frac{\sinh \beta k_\theta}{\beta^2 k_\theta^2} + \frac{\sinh \beta k_\theta}{2} - \frac{\cosh \beta k_\theta}{\beta k_\theta} \right). \quad (7)$$

The above result was derived by rotating the diffusion tensor in the local tangent coordinate system. The higher order terms can be included to modify the cosine potential, by means of perturbative corrections (so-called higher-order correlation terms) to the diffusion coefficient. The full formalism for computation of these corrections can be found in [16]. For example, the harmonic potential for the

bond angle, also often employed [14] in various models, can be modelled in this way. Let us right away define also the coefficient $\mu \equiv 2\mathcal{D}_\perp/\mathcal{D}_\parallel$, as we will use it throughout the paper.

The non-isotropic diffusion tensor gives rise to the following diffusion equation:

$$\frac{\partial P}{\partial N} = \mathcal{D}_\parallel \frac{\partial^2 P}{\partial r^2} + \frac{2\mathcal{D}_\parallel}{r} \frac{\partial P}{\partial r} + \frac{\mathcal{D}_\perp}{r^2} \Delta_{S^2} P, \quad (8)$$

where Δ_{S^2} is the angular part of the Laplacian in spherical coordinates, i.e., the two-dimensional Laplace-Beltrami operator.

We first look for a fundamental solution (in terminology of the theory of partial differential equations), i.e. for a solution in the whole space, vanishing at the infinity and starting at \mathbf{r}_0 , leading to the initial-boundary condition $P(0, \mathbf{r}, \mathbf{r}_0) = \delta(\mathbf{r} - \mathbf{r}_0)/4\pi$. Then one can use well-developed tools for solving diffusion equations. The easiest way is to rewrite (8) as the Schrödinger equation in imaginary time for a particle in a spherical potential given by $U(r) = \ell(\ell+1)(\mu/2-1)/r^2$. It is easy to see that $U(r)$ defined in this way is a well only for $\mu < 2$, i.e. for $\mathcal{D}_\perp < \mathcal{D}_\parallel$, otherwise, it is repulsive. The physical interpretation of this fact is that the diffusion with large \mathcal{D}_\perp corresponds to the states with high angular momenta (notice the position of \mathcal{D}_\perp in (8)). But since arbitrarily high angular momenta are only possible for unbounded states, this means the the imaginary time description of the diffusion corresponds to a particle in a repulsive potential. Conversely, when \mathcal{D}_\parallel dominates over \mathcal{D}_\perp , the primary contribution to the energy comes from the radial part of the Laplace operator; hence, angular momentum cannot be arbitrarily high, which is consistent with a bounded state in a potential well.

However, one can use the same eigenbasis for both of the above cases; only the coefficients of the expansion will be different. The eigenfunctions of the radial part of the equation read as:

$$u_1(\ell, \mathcal{E}, r) = \frac{C_1(\ell, \mathcal{E})}{\sqrt{r}} J_\kappa \left(-\sqrt{\frac{\mathcal{E}}{\mathcal{D}_\parallel}} r \right) \quad (9)$$

$$u_2(\ell, \mathcal{E}, r) = \frac{C_2(\ell, \mathcal{E})}{\sqrt{r}} Y_\kappa \left(-\sqrt{\frac{\mathcal{E}}{\mathcal{D}_\parallel}} r \right), \quad (10)$$

with $\kappa = [1/4 + \mu\ell(\ell+1)/2]^{1/2}$, and correspond to the states of definite energy \mathcal{E} and angular momentum ℓ of the particle. The Bessel functions of the first (second) kind are denoted by J_α and Y_α . Right away we see that $C_2 = 0$ for all \mathcal{E} and ℓ , as the Bessel functions of the second kind diverge at short distances. Hence, only the (9) states contribute to the solution.

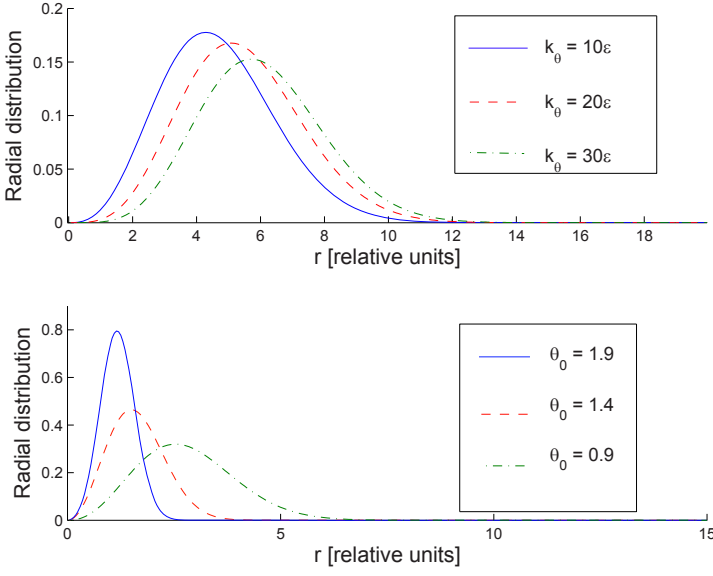


Fig. 2. (Color online) Top – radial distribution functions $P(N, r)$ for various values of stiffness, with $\theta_0 = 1.9$. Bottom – radial distribution functions $P(N, r)$ for various values of θ_0 , with $k_\theta = 50\epsilon$. The length of the chain $N = 50$.

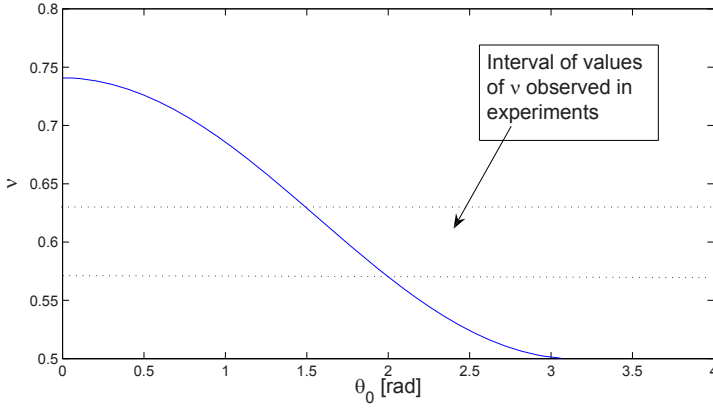


Fig. 3. Dependence of the scaling exponent ν for the gyration radius on θ_0 . We have set $k_\theta = 20\epsilon$. The dashed lines denote the interval of the gyration radii measured experimentally in unfolded polypeptides (about 0.6). The exponent ν is defined through the scaling relation $\langle R_g^2 \rangle \propto N^{2\nu}$.

The solution that satisfies our boundary conditions is then obtained by standard methods and reads as:

$$P_\ell(N, \mathbf{r}, \mathbf{r}_0) = C_n(\kappa, N) \left(\frac{r}{r_0} \right)^{2\kappa+1/2} \frac{1}{\mathcal{D}_\parallel N} \times \exp\left(-\frac{r^2 + r_0^2}{4\mathcal{D}_\parallel N}\right) \mathcal{I}_\kappa\left(\frac{|\mathbf{r} \cdot \mathbf{r}_0|}{2\mathcal{D}_\parallel N}\right), \quad (11)$$

where \mathcal{I} stands for the modified Bessel function of the first kind. The normalization constant $C_n(N)$ is equal to:

$$C_n(\kappa, N) = 3\pi 2^{2+\kappa} \kappa (\mathcal{D}_\parallel N)^{1+\kappa/2} \Gamma(1+\kappa) \Gamma(3\kappa/2) \times {}_1F_1\left(1+3\kappa/2, 1+\kappa, \frac{r_0^2}{4\mathcal{D}_\parallel N}\right), \quad (12)$$

with ${}_1F_1(a, b, x)$ denoting the confluent hypergeometric function of its arguments (see [17] for a definition). We obtain the above result by expanding (11) into power series, integrating and resumming. Dependence of the normalization constant on N and κ is explicitly written, as this dependence will play a role

in later sections. The large- N asymptotic form of $C_n(\kappa, N)$ reads as:

$$C_n(\kappa, N) \approx 3\pi 2^{2+\kappa} \kappa (\mathcal{D}_\parallel N)^{1+\kappa/2} \times \Gamma\left(\frac{3\kappa}{2}\right) \left(1 + \frac{3\kappa+2}{2\kappa+2} \frac{r_0^2}{4\mathcal{D}_\parallel N}\right). \quad (13)$$

We will need this asymptotic form later on. Notice that the normalization constant is dependent on N , as one would expect. The solution explicitly depends on ℓ . It is actually the sum of all partial waves (characterized by the value of ℓ) that provide a solution of finite norm (i.e. no scattering to infinity, which would correspond to the “blowup” of the chain) and finite localization radius (i.e. no “falling to the center”, which would correspond to the collapse of the chain).

To understand better the general properties of the model, it is helpful to analyze the behavior of the solution (11) depending on the parameters k_θ and θ_0 . We will first discuss the radial distribution function $P(N, r)$, defined as $\int \int d\phi d\theta \sin\theta r^2 P(N, \mathbf{r}, \mathbf{r}_0)$. The results for selected values are given in Figure 2. It is seen that in the whole physically sensible range of parameters, the stiffness

k_θ , once it moves away from zero, only mildly flattens the distribution function. On the other hand, the bending angle does influence it significantly. An informal explanation is that letting k_θ grow, provided it is neither too close to zero nor too large, results in less bending of the chain but (as k_θ is not very large) the chain still does bend relatively often and still has the shape of a slightly flattened sphere; therefore, various parts of the chain still propagate in almost uncorrelated directions and it is not very important how long (on average) they are. On the other hand, large preferential angle θ_0 brings a systematic effect, which accumulates and substantially changes the shape of the chain.

It is also instructive to look at the behavior of the gyration radius (expectation value of the squared distance from the center of mass of the polymer), given in Figure 3. As one could expect, it grows significantly with θ approaching zero, as in that case, the most extended configurations are preferred. This case agrees with the equations for the gyration radius cited in [10]. On the other hand, for values of θ_0 close to π , the chain, on a macroscopic scale, behaves almost as a Gaussian freely jointed chain, hence ν approaches its Gaussian value 0.5. The gyration radius for the continuum limit in the case of non-zero θ_0 has, to the best of our knowledge, not been addressed so far. The plot in Figure 3 shows the range of the preferential bond angle values that correspond to the experimental result, $\nu \approx 0.6$ [3]. This range roughly corresponds to the value of θ_0 suggested by the geometry of bonds in polypeptides: $\theta_0 \approx 1.8$ radians [14]; in our calculations, we use $\theta_0 = 1.83$ radians. Hence, our model is able to reproduce the observed scaling exponent of the gyration radii and allows us to conclude that the proximity of its value to the scaling exponent ν_{saw} of the self-avoiding random walk ($\nu_{saw} \approx 0.59$) is pure coincidence. The distribution of bond angles (which are dominant degrees of freedom in terms of typical energies and time scales) alone accounts for the gyration radius scaling, whereas the self-avoidance (together with other non-bonded interactions) only produces small corrections (for more details see [12]).

3 The calculation of RDC values

3.1 Basic considerations

Having described our model of unfolded polypeptides, we now turn to the calculation of RDC values. The general theory is given in [2] and the basic idea is also mentioned in the introduction section of this paper. Here we discuss the more formal aspects of the procedure and state the results.

We will consider the simplest model, in which the restricting medium is modelled as a set of parallel planar absorbing barriers at the distance L from each other, as shown in Figure 1 [2]. This effectively means that all the paths which intersect the barrier are removed from consideration. The exact solution with these boundary conditions is difficult to find; therefore, we resort to the method

of images, common in problems such as diffusion and electrostatics [19]. Staying at the first order approximation, the solution reads as [2]:

$$f(N, \mathbf{r}, \mathbf{r}_0) = P(N, \mathbf{r}, \mathbf{r}_0) - P(N, \mathbf{r}', \mathbf{r}_0) - P(N, \mathbf{r}'', \mathbf{r}_0), \quad (14)$$

with \mathbf{r}' and \mathbf{r}'' being the points symmetric to \mathbf{r} with respect to the barriers, and $f(N, \mathbf{r}, \mathbf{r}_0)$ denoting the probability density function for the appropriate boundary conditions (whereas P stands for the fundamental solution in the whole space).

As can be seen from the defining expression, the RDC of the j th segment is determined by the value of the angle Θ of the $C_j^\alpha - C_{j+1}^\alpha$ segment with respect to the direction of the magnetic field. Therefore, we wish to find the distribution function for this angle, denoted $f(\Theta)$. As elucidated in more detail in [2], $f(\Theta)$ equals the joint cumulative distribution for a chain of length j starting at $\mathbf{r}_j - \delta\mathbf{r}_j/2$ and reaching some position \mathbf{r}_{01} , and a chain of length $N - j$ starting at $\mathbf{r}_j + \delta\mathbf{r}_j/2$ and ending at some position \mathbf{r}_{02} . Cumulative distribution, by definition, enumerates the states with prescribed position of one end of the chain ($\mathbf{r} \pm \delta\mathbf{r}_j/2$), independently of the coordinate of the other end (\mathbf{r}_{01} or \mathbf{r}_{02}). Therefore, for $C(N, \mathbf{r})$ we have, in general:

$$C(N, \mathbf{r}) = \int d\mathbf{r}_0 f(N, \mathbf{r}, \mathbf{r}_0). \quad (15)$$

At this point, one should notice that the dependence of the cumulative distributions on x and y vanishes due to symmetry. We may therefore denote them by $C(N, z)$. Integrating over the initial positions of the chains, \mathbf{r}_{01} and \mathbf{r}_{02} , we arrive at the following equation for $f(\Theta)$:

$$f(\Theta) \propto \int_{-L/2}^{L/2} dz C\left(j, z - \frac{a \cos \Theta}{2}\right) \times C\left(N - j, z + \frac{a \cos \Theta}{2}\right), \quad (16)$$

where the proportionality constant is easy to determine from the previous equations, keeping track of all constant factors from the beginning. We have exploited the fact that the segment lengths are all equal ($|\delta\mathbf{r}_j| = a$), as well as the definition of the angle Θ .

3.2 Angular averaging: elementary method

The final step is performing the necessary integrations, i.e., calculating the average over $f(\Theta)$. Conceptually the simplest way of doing this is expanding (16) in a power series and integrating it term by term. This is the most feasible way for obtaining quick, low-accuracy estimates. We first sketch this method.

One starts by expanding the cumulative distribution functions in powers of $a \cos \Theta$. The odd terms obviously vanish. The even terms are then integrated by parts bearing in mind the fact that the distribution $f(N, \mathbf{r}, \mathbf{r}_0)$ vanishes at the boundaries due to confinement. The averaging

in equation (1) is then readily performed. The result up to the fourth order in a has the form:

$$D_{\text{NH}} = KP_2(\alpha_{\text{NH}}) \times \left[B - \frac{3}{8} \frac{C_n(\kappa, N_1)C_n(\kappa, N - N_1 - 1)}{C_n(\kappa, N)} a^2 - \frac{1}{384} \frac{C_n(\kappa - 1, N_1)C_n(\kappa - 1, N)}{C_n(\kappa, N)} a^2 + \frac{1}{64} \frac{C_n(\kappa - 1, N_1)C_n(\kappa - 1, N - N_1 - 1)}{C_n(\kappa - 1, N)} a^4 \right]. \quad (17)$$

The constant K is defined in (1) and reads as:

$$K = \frac{\mu_0 \hbar \gamma_{\text{N}} \gamma_{\text{H}}}{4\pi^2 r_{\text{NH}}^3}. \quad (18)$$

The constant term B in (17) is small (about two orders of magnitude smaller than the a -dependent terms) and we ignore it in our calculations. When calculating D_{NH} , we have used the asymptotic form for the normalization constant, as given in (13). Bearing in mind the limited accuracy of our formalism (simple toy-model potential, mean-field approach, etc.), one may safely ignore also the quartic term, as well as the second quadratic term (due to its large denominator). We have found for the examples below that this approximation leads to insignificant changes of the computed RDC curves.

3.3 Angular averaging: advanced method

A more elaborate but substantially more general scheme, allowing in principle calculations of arbitrarily high accuracy, is based upon the formalism of quantum theory of angular momentum. We again start from (16), which is the exact result (not approximate, like the series expansion subsequently performed in the previous subsection). The idea is to refrain from using the closed-form solution (11) and use the series expansion of $P(N, \mathbf{r}, \mathbf{r}_0)$ over the radial eigenfunctions (9) and spherical harmonics. The former is more convenient and more informative for most purposes but the latter allows us to use numerous identities of the angular momentum theory to obtain simpler expressions for the average of $P_2(\cos \Theta)$.

The starting point is the solution in the whole space:

$$P(N, \mathbf{r}, \mathbf{r}_0) = \sum_{\ell=0}^{\infty} A_{\ell} R_{\ell}(N, |\mathbf{r} - \mathbf{r}_0|) P_{\ell}(\cos \theta), \quad (19)$$

where A_{ℓ} are the appropriate coefficients determined by the eigenfunctions (9), R_{ℓ} are radial functions, obtained by integrating the eigenfunctions over the “energy” variable \mathcal{E} , and θ is the azimuthal angle. Reflections in the planes $z = \pm L/2$, which give the image solutions, are then readily obtained in the form $\hat{\mathcal{R}}_{\pi, \mathbf{e}_z} \hat{P}_{\pm \frac{L}{2}, \mathbf{e}_z} P(N, \mathbf{r}, \mathbf{r}_0)$, which is easy to prove from elementary considerations. The operators denote the rotation for a given angle about the given

axis, spatial inversion and spatial translation for a given vector, in that order. The rotation for π about the z -axis and the spatial inversion act upon the angular part simply by multiplying it with $(-1)^{\ell}$. Only the translation has a nontrivial action. A lengthy calculation, making use of the Wigner functions and identities with Clebsch-Gordan coefficients as given in [20], results in:

$$P_{\ell}(\theta', \phi) = K_{\ell} \sum_{\lambda=0}^{\infty} (-1)^{\lambda+\ell} f_r(\lambda, \ell, r) \times \sum_{\Lambda=|\ell-\lambda}^{\ell+\lambda} \frac{(2\ell+1)(2\lambda+1)}{2\Lambda+1} |\langle \Lambda 0 | \ell 0 \lambda 0 \rangle|^2. \quad (20)$$

For the left image, where we have introduced the notation:

$$K_{\ell} = \sum_{j=0}^{\ell} \left(-\frac{L}{2} \right)^{\ell-j} \sqrt{2(\ell-j)-1} \frac{(\ell+j)!}{(\ell-j)!} \times \left[\frac{(2\ell)!(2j)!}{(2\ell+2j)!} \right]^{1/2}, \quad (21)$$

$$f_r(\lambda, \ell, r) = \frac{(2rL)^{\ell}}{(4r^2 + L^2)^{\lambda+\ell/2}} F \times \left(\frac{2\lambda+\ell}{4}, \frac{2\lambda+\ell+2}{4}; \lambda + \frac{3}{2}, \frac{16r^2 L^2}{(4r^2 + L^2)^2} \right), \quad (22)$$

and the angular brackets stand for the Clebsch-Gordan coefficients, whereas F is the confluent hypergeometric function, and the angle in the new coordinate system is denoted by θ' . The other image looks the same, except that the functions (22) now contain $-L$ in place of L . Finding the cumulative distribution is straightforward, inserting the expressions for $P(N, \mathbf{r}, \mathbf{r}_0)$ and its two images in (15) and integrating. Notice that the initial position is contained only in the radial functions R_{ℓ} , which can be integrated analytically as their integrals reduce to the familiar Bessel integrals.

The last step is multiplying the two cumulative distribution functions as in (16) and integrating over z . At this step the symmetry of the problem nullifies all the terms containing the product of an even and an odd functions of z , and the triangle rule for addition of angular momenta further reduces the number of non-zero terms. We are thus left with a *finite* sum which, to the second order, gives the result for $P_2(\cos \Theta)$ that coincides with (17). The fourth order term differs from the corresponding term in (17), however, as in this approach, due to the orthogonality of the Legendre polynomials, we capture the *exact* value of the coefficient in front of the fourth (or any other desired) order term in the expansion. In the elementary method, the expansion is in powers of a and in number of images. The latter expansion is an uncontrollable approximation, since the $2n$ th image can contribute a term of the order $2n - 2$ in a . The advanced method captures the whole contribution of given order in a .

At the present level of accuracy of our model, this increase in accuracy is not crucial. However, the generality of the formalism applied in this subsection might prove to be necessary if the subtler effects as the Ramachandran rotations or long-range interactions are included. Also, the described method allows an equally straightforward calculation of the expectation value of $P_\ell(\cos\Theta)$ for any ℓ . This case will appear if other observables in addition to direct dipole-dipole couplings are measured. We therefore propose this approach for any further work on this problem.

4 Examples

The purpose of this section is to test our predictions on experimental data and judge the accuracy and usefulness of our theory. Therefore, we do not analyze in detail any of the systems and contend ourselves just to compare our curves with the experimental ones.

In all the cases that we consider, we take the stiffness k_θ equal to 20ϵ and preferential bond angle $\theta_0 = 1.83$ (in radians). These values have been recommended in [14] and also according to other authors the peptide bond is expected to be well described by these values. The interplanar distance is taken fixed to $L = 100a$, where a is the length of a single segment. In both experiments that we analyze [21,22], this length is cited to be about 40 nm while the segment length is 0.38 nm. So, our value for the interplanar distance roughly corresponds to the experimental one; exact equality is not essential since the experimental setup is difficult to control concerning the interplanar distance [22] and the actual distribution of interplanar values is probably rather fat-tailed. In our theory, the segment length does not enter the final expressions and therefore can take any arbitrary value.

The first case we consider is the urea-denaturated apomyoglobin, an experiment reported in [21], and analyzed also in the previous study by two of the authors [2]. The result is seen in Figure 4. The same paper also reports on measurements of acid denaturated apomyoglobin, which cannot be well described with our model, probably because the native-like topology is still present in this case, as the authors themselves state [21].

Another example is ubiquitin, one of the proteins which are intrinsically disordered also in their native state. The measurements are taken from [22].

The second case, in Figure 5, shows somewhat better agreement with experiment than the first one (χ^2 about 30 percent better). In part, this is probably due to the difference between the two proteins. Ubiquitin is known to be a strongly disordered protein [22] and behaves essentially as a perfect statistical coil, so various local deviations from the mean value of RDCs tend to average out. On the other hand, apomyoglobin probably retains some native-like structure even in the unfolded state; this is particularly probable for the regions formed by several subsequent segments which are completely above or below the average RDC value, that are visible in the measurements given in Figure 4. These are probably regions with strong close-neighbor interactions, that behave like

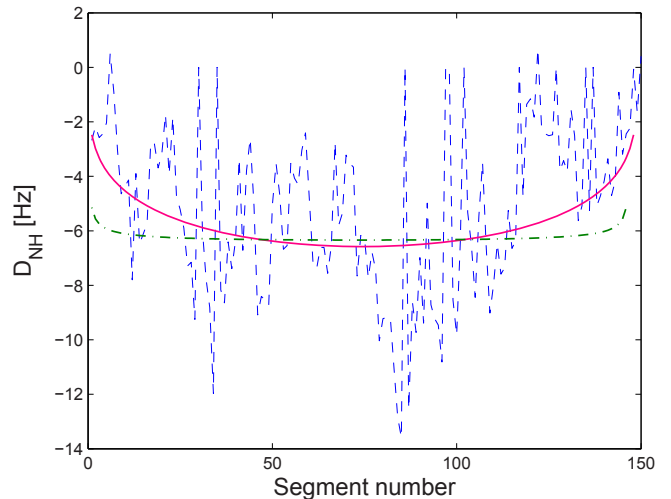


Fig. 4. (Color online) Comparison of experimental (blue dashed line) and theoretical (red full line) RDCs for unfolded apomyoglobin. The prediction of the random flight theory [2] is also shown (green dash-dotted line). General bell shape is observed but it is obvious that local conformational properties induce large deviations from the mean field curve, predicted by our model.

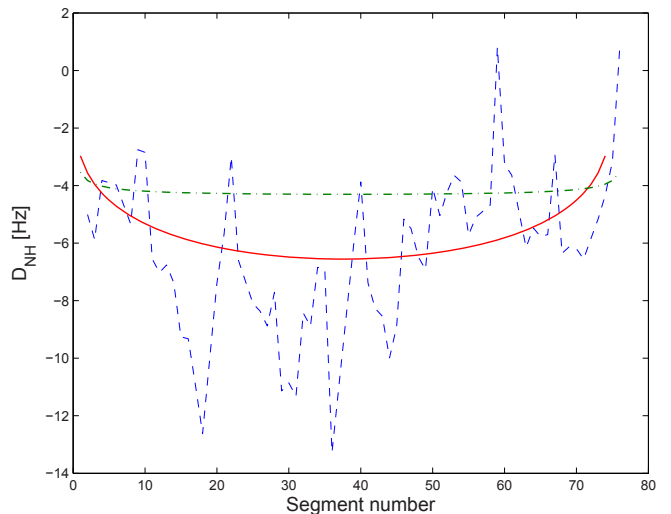


Fig. 5. (Color online) Comparison of experimental (blue dashed line) and theoretical (red full line) RDCs for unfolded ubiquitin. The random flight theory prediction [2] is also shown (green dash-dotted line). One again sees the local variations superimposed on the global bell-shaped curve.

partially folded secondary structures and therefore choose one of the conformations, some of them with significantly higher probability than the others. Finally, we point out that both examples demonstrate that the current model provides a more realistic description of the polypeptide than the non-interacting random flight model.

5 Discussion and conclusion

We have presented a theoretical method for reproducing the spatial structure of unfolded polypeptides, in particular the NMR spectroscopic measurements of NH dipolar couplings. Our approach requires the use of the empirical potentials and model parameters; therefore, it is not an *ab initio* approach. Nevertheless, all the parameters entering the calculation are either measured (or controlled) in the experiment itself (temperature, interplanar distance) or more or less standard and well-known values (optimal bond angle, bond stiffness). Bond stiffness is the “most empirical” of them but it also seems to vary very little in various numerical models [14,18]. The results seem encouraging and reveal general properties of disordered proteins.

First, it seems that the assumption of the effective decoupling of the degrees of freedom is justified by the RDC curves. The global shape of the chain, which is determined primarily by the statistical nature of polypeptide chain conformations in unfolded state and is well described within the semistiff polymer model, gives rise to the bell shape of the curves, also detected in experiments. On the other hand, the specificities of the segments lead to the local deviations of the RDC values from the smooth bell-shaped distribution. We plan to extend our model in further work, applying the linear response theory in order to reproduce these local structures.

The method will be subject to a number of improvements in the future. Besides applying the linear response formalism to improve the results, we also plan to assess in more detail the influence of long range interactions and intrachain contacts. Also, it is possible to use the results of the numerical work to identify the optimal Ramachandran angles for unfolded polypeptides. This will allow us to account for even richer secondary structure than that produced by a restricted database search, as the problem of weighting would be eliminated, with the energy values of different (ϕ, ψ) points being read off numerically obtained potential energy surfaces.

We are grateful to NoE EXCELL for the support of this research, as well as to Alexander Yakubovich for helpful discussions. M. Č. also acknowledges his gratitude to FIAS and Meso-Bio-Nano group for financial support and warm hospitality during the work on this project. Work at the Institute of Physics is supported by the Ministry of Science Project OI141031.

References

1. M. Blackledge, *Prog. Nucl. Magn. Reson. Spectrosc.* **46**, 23 (2005)
2. O.I. Obolensky, K. Schlepckow, H. Schwalbe, A.V. Solov'yov, *J. Biomol. NMR* **39**, 1 (2007)
3. A.K. Jha, A. Colubri, K.F. Freed, T.R. Sosnick, *Proc. Natl. Acad. Sci.* **102**, 13099 (2005)
4. P. Bernado et al., *Proc. Natl. Acad. Sci.* **102**, 17002 (2005)
5. M. Louhivuori et al., *J. Am. Chem. Soc.* **125**, 15647 (2003)
6. N. Sato, K. Takahashi, Y. Yunoki, *J. Phys. Soc. Jpn* **22**, 219 (1967)
7. B. Hamprecht, H. Kleinert, *Phys. Rev. E* **71**, 031803 (2005); H. Kleinert, A. Chervyakov, *J. Phys. A: Math. Gen.* **39**, 8231 (2006)
8. H. Kleinert, *Path integrals in quantum mechanics, statistics, polymer physics and financial markets* (Berlin, 2003)
9. M. Čubrović, O.I. Obolensky, A.V. Solov'yov, submitted
10. K. Kroy, E. Frey, *Phys. Rev. Lett.* **77**, 2581 (1996); H. Changbong, D. Thirumalai, *J. Chem. Phys.* **124**, 104905 (2006)
11. A.B. Rubin, *Biophysics* (Nauka, Moscow, 2004) (in Russian)
12. M. Čubrović, O. Obolensky, A.V. Solov'yov, in preparation
13. R.K. Murarka, A. Liwo, H.A. Scheraga, *J. Chem. Phys.* **127**, 155103 (2007)
14. D.K. Klimov, D. Thirumalai, *Phys. Rev. Lett.* **79**, 317 (1997); T. Veitshans, D.K. Klimov, D. Thirumalai, *Fold. Des.* **7**, 11 (1997)
15. B.D. Hughes, *Random Walks and Random Environments* (Clarendon Press, Oxford, 1995)
16. G.M. Zaslavsky, *Phys. Rep.* **371**, 461 (2002); W. Ebeling, I. Sokolov, *Statistical Thermodynamics and Stochastic Theory of Nonequilibrium systems* (World Scientific, 2002)
17. A.D. Polianin, *Handbook of linear partial differential equations* (CRC Press, 2002)
18. I.A. Solov'yov, A.V. Yakubovich, A.V. Solov'yov, W. Greiner, *Eur. Phys. J. D* **46**, 227 (2007); A.V. Yakubovich, I.A. Solov'yov, A.V. Solov'yov, W. Greiner, *Eur. Phys. J. D* **46**, 215 (2007)
19. E.M. Lifshitz, L.D. Landau, L.P. Pitaevskii, *Electrodynamics of continuous media* (World Scientific, 1989)
20. D.A. Varshalovich, A.N. Moskalev, V.K. Khersonskii, *Quantum theory of angular momentum* (World Scientific, 1988)
21. W. Fieber, S. Kristjansdottir, F.M. Poulsen, *J. Mol. Biol.* **339**, 1191 (2004)
22. S. Meier, S. Grzesiek, M. Blackledge, *J. Am. Chem. Soc.* **129**, 9799 (2007)
23. H.M. Berman et al., *Nucl. Acids Res.* **28**, 235 (2003)

Chapter 21

Holographic Description of Strongly Correlated Electrons in External Magnetic Fields

E. Gubankova, J. Brill, M. Čubrović, K. Schalm, P. Schijven, and J. Zaanen

21.1 Introduction

The study of strongly interacting fermionic systems at finite density and temperature is a challenging task in condensed matter and high energy physics. Analytical methods are limited or not available for strongly coupled systems, and numerical simulation of fermions at finite density breaks down because of the sign problem [1, 2]. There has been an increased activity in describing finite density fermionic matter by a gravity dual using the holographic AdS/CFT correspondence [3]. The gravitational solution dual to the finite chemical potential system is the electrically charged AdS-Reissner-Nordström (RN) black hole, which provides a background where only the metric and Maxwell fields are nontrivial and all matter fields vanish.

E. Gubankova (✉)
ITP, J. W. Goethe-University, D-60438 Frankfurt am Main, Germany
e-mail: gubankova@th.physik.uni-frankfurt.de

E. Gubankova
ITEP, Moscow, Russia

J. Brill · M. Čubrović · K. Schalm · P. Schijven · J. Zaanen
Instituut Lorentz, Leiden University, Niels Bohrweg 2, 2300 RA Leiden, The Netherlands

J. Brill
e-mail: jellebrill@gmail.com

M. Čubrović
e-mail: cubrovic@lorentz.leidenuniv.nl

K. Schalm
e-mail: kschalm@lorentz.leidenuniv.nl

P. Schijven
e-mail: aphexedpiet@gmail.com

J. Zaanen
e-mail: jan@lorentz.leidenuniv.nl

In the classical gravity limit, the decoupling of the Einstein-Maxwell sector holds and leads to universal results, which is an appealing feature of applied holography. Indeed, the celebrated result for the ratio of the shear viscosity over the entropy density [4] is identical for many strongly interacting theories and has been considered a robust prediction of the AdS/CFT correspondence.

However, an extremal black hole alone is not enough to describe finite density systems as it does not source the matter fields. In holography, at leading order, the Fermi surfaces are not evident in the gravitational geometry, but can only be detected by external probes; either probe D-branes [3] or probe bulk fermions [5–8]. Here we shall consider the latter option, where the free Dirac field in the bulk carries a finite charge density [9]. We ignore electromagnetic and gravitational backreaction of the charged fermions on the bulk spacetime geometry (probe approximation). At large temperatures, $T \gg \mu$, this approach provides a reliable hydrodynamic description of transport at a quantum criticality (in the vicinity of superfluid-insulator transition) [10]. At small temperatures, $T \ll \mu$, in some cases sharp Fermi surfaces emerge with either conventional Fermi-liquid scaling [6] or of a non-Fermi liquid type [7] with scaling properties that differ significantly from those predicted by the Landau Fermi liquid theory. The non-trivial scaling behavior of these non-Fermi liquids has been studied semi-analytically in [8] and is of great interest as high- T_c superconductors and metals near the critical point are believed to represent non-Fermi liquids.

What we shall study is the effects of magnetic field on the holographic fermions. A magnetic field is a probe of finite density matter at low temperatures, where the Landau level physics reveals the Fermi level structure. The gravity dual system is described by a AdS dyonic black hole with electric and magnetic charges Q and H , respectively, corresponding to a $2 + 1$ -dimensional field theory at finite chemical potential in an external magnetic field [11]. Probe fermions in the background of the dyonic black hole have been considered in [12–14]; and probe bosons in the same background have been studied in [15]. Quantum magnetism is considered in [16].

The Landau quantization of momenta due to the magnetic field found there, shows again that the AdS/CFT correspondence has a powerful capacity to unveil that certain quantum properties known from quantum gases have a much more ubiquitous status than could be anticipated theoretically. A first highlight is the demonstration [17] that the Fermi surface of the Fermi gas extends way beyond the realms of its perturbative extension in the form of the Fermi-liquid. In AdS/CFT it appears to be gravitationally encoded in the matching along the scaling direction between the ‘bare’ Dirac waves falling in from the ‘UV’ boundary, and the true IR excitations living near the black hole horizon. This IR physics can insist on the disappearance of the quasiparticle but, if so, this ‘critical Fermi-liquid’ is still organized ‘around’ a Fermi surface. The Landau quantization, the organization of quantum gaseous matter in quantized energy bands (Landau levels) in a system of two space dimensions pierced by a magnetic field oriented in the orthogonal spatial direction, is a second such quantum gas property. We shall describe here following [12], that despite the strong interactions in the system, the holographic computation reveals the same strict Landau-level quantization. Arguably, it is the mean-field nature imposed by

large N limit inherent in AdS/CFT that explains this. The system is effectively non-interacting to first order in $1/N$. The Landau quantization is not manifest from the geometry, but as we show this statement is straightforwardly encoded in the symmetry correspondences associated with the conformal compactification of AdS on its flat boundary (i.e., in the UV CFT).

An interesting novel feature in strongly coupled systems arises from the fact that the background geometry is only sensitive to the total energy density $Q^2 + H^2$ contained in the electric and magnetic fields sourced by the dyonic black hole. Dialing up the magnetic field is effectively similar to a process where the dyonic black hole loses its electric charge. At the same time, the fermionic probe with charge q is essentially only sensitive to the Coulomb interaction gqQ . As shown in [12], one can therefore map a magnetic to a non-magnetic system with rescaled parameters (chemical potential, fermion charge) and same symmetries and equations of motion, as long as the Reissner-Nordström geometry is kept.

Translated to more experiment-compatible language, the above magnetic-electric mapping means that the spectral functions at nonzero magnetic field h are identical to the spectral function at $h = 0$ for a reduced value of the coupling constant (fermion charge) q , provided the probe fermion is in a Landau level eigenstate. A striking consequence is that the spectrum shows conformal invariance for arbitrarily high magnetic fields, as long as the system is at negligible to zero density. Specifically, a detailed analysis of the fermion spectral functions reveals that at strong magnetic fields the Fermi level structure changes qualitatively. There exists a critical magnetic field at which the Fermi velocity vanishes. Ignoring the Landau level quantization, we show that this corresponds to an effective tuning of the system from a regular Fermi liquid phase with linear dispersion and stable quasiparticles to a non-Fermi liquid with fractional power law dispersion and unstable excitations. This phenomenon can be interpreted as a transition from metallic phase to a “strange metal” at the critical magnetic field and corresponds to the change of the infrared conformal dimension from $\nu > 1/2$ to $\nu < 1/2$ while the Fermi momentum stays nonzero and the Fermi surface survives. Increasing the magnetic field further, this transition is followed by a “strange-metal”-conformal crossover and eventually, for very strong fields, the system always has near-conformal behavior where $k_F = 0$ and the Fermi surface disappears.

For some Fermi surfaces, this surprising metal-“strange metal” transition is not physically relevant as the system prefers to directly enter the conformal phase. Whether a fine tuned system exists that does show a quantum critical phase transition from a FL to a non-FL is determined by a Diophantine equation for the Landau quantized Fermi momentum as a function of the magnetic field. Perhaps these are connected to the magnetically driven phase transition found in AdS_5/CFT_4 [18]. We leave this subject for further work.

Overall, the findings of Landau quantization and “discharge” of the Fermi surface are in line with the expectations: both phenomena have been found in a vast array of systems [19] and are almost tautologically tied to the notion of a Fermi surface in a magnetic field. Thus we regard them also as a sanity check of the whole bottom-up approach of fermionic AdS/CFT [5–7, 17], giving further credit to the holographic Fermi surfaces as having to do with the real world.

Next we use the information of magnetic effects the Fermi surfaces extracted from holography to calculate the quantum Hall and longitudinal conductivities. Generally speaking, it is difficult to calculate conductivity holographically beyond the Einstein-Maxwell sector, and extract the contribution of holographic fermions. In the semiclassical approximation, one-loop corrections in the bulk setup involving charged fermions have been calculated [17]. In another approach, the backreaction of charged fermions on the gravity-Maxwell sector has been taken into account and incorporated in calculations of the electric conductivity [9]. We calculate the one-loop contribution on the CFT side, which is equivalent to the holographic one-loop calculations as long as vertex corrections do not modify physical dependencies of interest [17, 20]. As we dial the magnetic field, the Hall plateau transition happens when the Fermi surface moves through a Landau level. One can think of a difference between the Fermi energy and the energy of the Landau level as a gap, which vanishes at the transition point and the $2 + 1$ -dimensional theory becomes scale invariant. In the holographic D3–D7 brane model of the quantum Hall effect, plateau transition occurs as D-branes move through one another [21, 22]. In the same model, a dissipation process has been observed as D-branes fall through the horizon of the black hole geometry, that is associated with the quantum Hall insulator transition. In the holographic fermion liquid setting, dissipation is present through interaction of fermions with the horizon of the black hole. We have also used the analysis of the conductivities to learn more about the metal-strange metal phase transition as well as the crossover back to the conformal regime at high magnetic fields.

We conclude with the remark that the findings summarized above are in fact somewhat puzzling when contrasted to the conventional picture of quantum Hall physics. It is usually stated that the quantum Hall effect requires three key ingredients: Landau quantization, quenched disorder¹ and (spatial) boundaries, i.e., a finite-sized sample [23]. The first brings about the quantization of conductivity, the second prevents the states from spilling between the Landau levels ensuring the existence of a gap and the last one in fact allows the charge transport to happen (as it is the boundary states that actually conduct). In our model, only the first condition is satisfied. The second is put by hand by assuming that the gap is automatically preserved, i.e. that there is no mixing between the Landau levels. There is, however, no physical explanation as to how the boundary states are implicitly taken into account by AdS/CFT.

We outline the holographic setting of the dyonic black hole geometry and bulk fermions in Sect. 21.2. In Sect. 21.3 we prove the conservation of conformal symmetry in the presence of the magnetic fields. Section 21.4 is devoted to the holographic fermion liquid, where we obtain the Landau level quantization, followed by a detailed study of the Fermi surface properties at zero temperature in Sect. 21.5. We calculate the DC conductivities in Sect. 21.6, and compare the results with available data in graphene.

¹Quenched disorder means that the dynamics of the impurities is “frozen”, i.e. they can be regarded as having infinite mass. When coupled to the Fermi liquid, they ensure that below some scale the system behaves as if consisting of non-interacting quasiparticles only.

21.2 Holographic Fermions in a Dyonic Black Hole

We first describe the holographic setup with the dyonic black hole, and the dynamics of Dirac fermions in this background. In this paper, we exclusively work in the probe limit, i.e., in the limit of large fermion charge q .

21.2.1 Dyonic Black Hole

We consider the gravity dual of 3-dimensional conformal field theory (CFT) with global $U(1)$ symmetry. At finite charge density and in the presence of magnetic field, the system can be described by a dyonic black hole in 4-dimensional anti-de Sitter space-time, AdS_4 , with the current J_μ in the CFT mapped to a $U(1)$ gauge field A_M in AdS . We use μ, ν, ρ, \dots for the spacetime indices in the CFT and M, N, \dots for the global spacetime indices in AdS .

The action for a vector field A_M coupled to AdS_4 gravity can be written as

$$S_g = \frac{1}{2\kappa^2} \int d^4x \sqrt{-g} \left(\mathcal{R} + \frac{6}{R^2} - \frac{R^2}{g_F^2} F_{MN} F^{MN} \right), \quad (21.1)$$

where g_F^2 is an effective dimensionless gauge coupling and R is the curvature radius of AdS_4 . The equations of motion following from (21.1) are solved by the geometry corresponding to a dyonic black hole, having both electric and magnetic charge:

$$ds^2 = g_{MN} dx^M dx^N = \frac{r^2}{R^2} (-f dt^2 + dx^2 + dy^2) + \frac{R^2}{r^2} \frac{dr^2}{f}. \quad (21.2)$$

The redshift factor f and the vector field A_M reflect the fact that the system is at a finite charge density and in an external magnetic field:

$$f = 1 + \frac{Q^2 + H^2}{r^4} - \frac{M}{r^3}, \quad (21.3)$$

$$A_t = \mu \left(1 - \frac{r_0}{r} \right), \quad A_y = hx, \quad A_x = A_r = 0,$$

where Q and H are the electric and magnetic charge of the black hole, respectively. Here we chose the Landau gauge; the black hole chemical potential μ and the magnetic field h are given by

$$\mu = \frac{g_F Q}{R^2 r_0}, \quad h = \frac{g_F H}{R^4}, \quad (21.4)$$

with r_0 is the horizon radius determined by the largest positive root of the redshift factor $f(r_0) = 0$:

$$M = r_0^3 + \frac{Q^2 + H^2}{r_0}. \quad (21.5)$$

The boundary of the AdS is reached for $r \rightarrow \infty$. The geometry described by (21.2)–(21.3) describes the boundary theory at finite density, i.e., a system in a charged medium at the chemical potential $\mu = \mu_{bh}$ and in transverse magnetic field $h = h_{bh}$, with charge, energy, and entropy densities given, respectively, by

$$\rho = 2 \frac{Q}{\kappa^2 R^2 g_F}, \quad \varepsilon = \frac{M}{\kappa^2 R^4}, \quad s = \frac{2\pi}{\kappa^2} \frac{r_0^2}{R^2}. \quad (21.6)$$

The temperature of the system is identified with the Hawking temperature of the black hole, $T_H \sim |f'(r_0)|/4\pi$,

$$T = \frac{3r_0}{4\pi R^2} \left(1 - \frac{Q^2 + H^2}{3r_0^4} \right). \quad (21.7)$$

Since Q and H have dimensions of $[L]^2$, it is convenient to parametrize them as

$$Q^2 = 3r_*^4, \quad Q^2 + H^2 = 3r_{**}^4. \quad (21.8)$$

In terms of r_0 , r_* and r_{**} the above expressions become

$$f = 1 + \frac{3r_*^4}{r^4} - \frac{r_0^3 + 3r_{**}^4/r_0}{r^3}, \quad (21.9)$$

with

$$\mu = \sqrt{3} g_F \frac{r_*^2}{R^2 r_0}, \quad h = \sqrt{3} g_F \frac{\sqrt{r_{**}^4 - r_*^4}}{R^4}. \quad (21.10)$$

The expressions for the charge, energy and entropy densities, as well as for the temperature are simplified as

$$\rho = \frac{2\sqrt{3}}{\kappa^2 g_F} \frac{r_*^2}{R^2}, \quad \varepsilon = \frac{1}{\kappa^2} \frac{r_0^3 + 3r_{**}^4/r_0}{R^4}, \quad s = \frac{2\pi}{\kappa^2} \frac{r_0^2}{R^2}, \quad (21.11)$$

$$T = \frac{3}{4\pi} \frac{r_0}{R^2} \left(1 - \frac{r_{**}^4}{r_0^4} \right).$$

In the zero temperature limit, i.e., for an extremal black hole, we have

$$T = 0 \quad \rightarrow \quad r_0 = r_{**}, \quad (21.12)$$

which in the original variables reads $Q^2 + H^2 = 3r_0^4$. In the zero temperature limit (21.12), the redshift factor f as given by (21.9) develops a double zero at the horizon:

$$f = 6 \frac{(r - r_{**})^2}{r_{**}^2} + \mathcal{O}((r - r_{**})^3). \quad (21.13)$$

As a result, near the horizon the AdS_4 metric reduces to $AdS_2 \times R^2$ with the curvature radius of AdS_2 given by

$$R_2 = \frac{1}{\sqrt{6}}R. \quad (21.14)$$

This is a very important property of the metric, which considerably simplifies the calculations, in particular in the magnetic field.

In order to scale away the AdS_4 radius R and the horizon radius r_0 , we introduce dimensionless variables

$$\begin{aligned} r &\rightarrow r_0 r, & r_* &\rightarrow r_0 r_*, & r_{**} &\rightarrow r_0 r_{**}, \\ M &\rightarrow r_0^3 M, & Q &\rightarrow r_0^2 Q, & H &\rightarrow r_0^2 H, \end{aligned} \quad (21.15)$$

and

$$\begin{aligned} (t, \mathbf{x}) &\rightarrow \frac{R^2}{r_0}(t, \mathbf{x}), & A_M &\rightarrow \frac{r_0}{R^2}A_M, & \omega &\rightarrow \frac{r_0}{R^2}\omega, \\ \mu &\rightarrow \frac{r_0}{R^2}\mu, & h &\rightarrow \frac{r_0^2}{R^4}h, & T &\rightarrow \frac{r_0}{R^2}T, \\ ds^2 &\rightarrow R^2 ds^2. \end{aligned} \quad (21.16)$$

Note that the scaling factors in the above equation that describes the quantities of the boundary field theory involve the curvature radius of AdS_4 , not AdS_2 .

In the new variables we have

$$\begin{aligned} T &= \frac{3}{4\pi}(1 - r_{**}^4) = \frac{3}{4\pi}\left(1 - \frac{Q^2 + H^2}{3}\right), & f &= 1 + \frac{3r_{**}^4}{r^4} - \frac{1 + 3r_{**}^4}{r^3}, \\ A_t &= \mu\left(1 - \frac{1}{r}\right), & \mu &= \sqrt{3}g_F r_*^2 = g_F Q, & h &= g_F H, \end{aligned} \quad (21.17)$$

and the metric is given by

$$ds^2 = r^2(-f dt^2 + dx^2 + dy^2) + \frac{1}{r^2} \frac{dr^2}{f}, \quad (21.18)$$

with the horizon at $r = 1$, and the conformal boundary at $r \rightarrow \infty$.

At $T = 0$, r_{**} becomes unity, and the redshift factor develops the double zero near the horizon,

$$f = \frac{(r-1)^2(r^2 + 2r + 3)}{r^4}. \quad (21.19)$$

As mentioned before, due to this fact the metric near the horizon reduces to $AdS_2 \times R^2$ where the analytical calculations are possible for small frequencies [8]. However, in the chiral limit $m = 0$, analytical calculations are also possible in the bulk AdS_4 [24], which we utilize in this paper.

21.2.2 Holographic Fermions

To include the bulk fermions, we consider a spinor field ψ in the AdS_4 of charge q and mass m , which is dual to an operator \mathcal{O} in the boundary CFT_3 of charge q and dimension

$$\Delta = \frac{3}{2} + mR, \quad (21.20)$$

with $mR \geq -\frac{1}{2}$ and in dimensionless units corresponds to $\Delta = \frac{3}{2} + m$. In the black hole geometry, (21.2), the quadratic action for ψ reads as

$$S_\psi = i \int d^4x \sqrt{-g} (\bar{\psi} \Gamma^M \mathcal{D}_M \psi - m \bar{\psi} \psi), \quad (21.21)$$

where $\bar{\psi} = \psi^\dagger \Gamma^t$, and

$$\mathcal{D}_M = \partial_M + \frac{1}{4} \omega_{abM} \Gamma^{ab} - iq A_M, \quad (21.22)$$

where ω_{abM} is the spin connection, and $\Gamma^{ab} = \frac{1}{2} [\Gamma^a, \Gamma^b]$. Here, M and a, b denote the bulk space-time and tangent space indices respectively, while μ, ν are indices along the boundary directions, i.e. $M = (r, \mu)$. Gamma matrix basis (Minkowski signature) is given in [8].

We will be interested in spectra and response functions of the boundary fermions in the presence of magnetic field. This requires solving the Dirac equation in the bulk [6, 7]:

$$(\Gamma^M \mathcal{D}_M - m)\psi = 0. \quad (21.23)$$

From the solution of the Dirac equation at small ω , an analytic expression for the retarded fermion Green's function of the boundary CFT at zero magnetic field has been obtained in [8]. Near the Fermi surface it reads as [8]:

$$G_R(\Omega, k) = \frac{(-h_1 v_F)}{\omega - v_F k_\perp - \Sigma(\omega, T)}, \quad (21.24)$$

where $k_\perp = k - k_F$ is the perpendicular distance from the Fermi surface in momentum space, h_1 and v_F are real constants calculated below, and the self-energy $\Sigma = \Sigma_1 + i \Sigma_2$ is given by [8]

$$\Sigma(\omega, T)/v_F = T^{2\nu} g \left(\frac{\omega}{T} \right) = (2\pi T)^{2\nu} h_2 e^{i\theta - i\pi\nu} \frac{\Gamma(\frac{1}{2} + \nu - \frac{i\omega}{2\pi T} + \frac{i\mu_q}{6})}{\Gamma(\frac{1}{2} - \nu - \frac{i\omega}{2\pi T} + \frac{i\mu_q}{6})}, \quad (21.25)$$

where ν is the zero temperature conformal dimension at the Fermi momentum, $\nu \equiv \nu_{k_F}$, given by (21.58), $\mu_q \equiv \mu q$, h_2 is a positive constant and the phase θ is such that the poles of the Green's function are located in the lower half of the complex frequency plane. These poles correspond to quasinormal modes of the Dirac

equation (21.23) and they can be found numerically solving $F(\omega_*) = 0$ [25, 26], with

$$F(\omega) = \frac{k_\perp}{\Gamma(\frac{1}{2} + \nu - \frac{i\omega}{2\pi T} + \frac{i\mu_q}{6})} - \frac{h_2 e^{i\theta - i\pi\nu} (2\pi T)^{2\nu}}{\Gamma(\frac{1}{2} - \nu - \frac{i\omega}{2\pi T} + \frac{i\mu_q}{6})}, \quad (21.26)$$

The solution gives the full motion of the quasinormal poles $\omega_*^{(n)}(k_\perp)$ in the complex ω plane as a function of k_\perp . It has been found in [8, 25, 26], that, if the charge of the fermion is large enough compared to its mass, the pole closest to the real ω axis bounces off the axis at $k_\perp = 0$ (and $\omega = 0$). Such behavior is identified with the existence of the Fermi momentum k_F indicative of an underlying strongly coupled Fermi surface.

At $T = 0$, the self-energy becomes $T^{2\nu} g(\omega/T) \rightarrow c_k \omega^{2\nu}$, and the Green's function obtained from the solution to the Dirac equation reads [8]

$$G_R(\Omega, k) = \frac{(-\hbar_1 v_F)}{\omega - v_F k_\perp - h_2 v_F e^{i\theta - i\pi\nu} \omega^{2\nu}}, \quad (21.27)$$

where $k_\perp = \sqrt{k^2} - k_F$. The last term is determined by the IR AdS_2 physics near the horizon. Other terms are determined by the UV physics of the AdS_4 bulk.

The solutions to (21.23) have been studied in detail in [6–8]. Here we simply summarize the novel aspects due to the background magnetic field [27]

- The background magnetic field h introduces a discretization of the momentum:

$$k \rightarrow k_{\text{eff}} = \sqrt{2|qh|l}, \quad \text{with } l \in N, \quad (21.28)$$

with Landau level index l [13, 14, 25, 26]. These discrete values of k are the analogue of the well-known Landau levels that occur in magnetic systems.

- There exists a (non-invertible) mapping on the level of Green's functions, from the magnetic system to the non-magnetic one by sending

$$(H, Q, q) \mapsto \left(0, \sqrt{Q^2 + H^2}, q \sqrt{1 - \frac{H^2}{Q^2 + H^2}} \right). \quad (21.29)$$

The Green's functions in a magnetic system are thus equivalent to those in the absence of magnetic fields. To better appreciate that, we reformulate (21.29) in terms of the boundary quantities:

$$(h, \mu_q, T) \mapsto \left(0, \mu_q, T \left(1 - \frac{h^2}{12\mu^2} \right) \right), \quad (21.30)$$

where we used dimensionless variables defined in (21.15), (21.17). The magnetic field thus effectively decreases the coupling constant q and increases the chemical potential $\mu = g_F Q$ such that the combination $\mu_q \equiv \mu q$ is preserved [12]. This is an important point as the equations of motion actually only depend on this combination and not on μ and q separately [12]. In other words, (21.30) implies that the additional scale brought about by the magnetic field can be understood as

changing μ and T independently in the effective non-magnetic system instead of only tuning the ratio μ/T . This point is important when considering the thermodynamics.

- The discrete momentum $k_{\text{eff}} = \sqrt{2|qh|l}$ must be held fixed in the transformation (21.29). The bulk-boundary relation is particularly simple in this case, as the Landau levels can readily be seen in the bulk solution, only to remain identical in the boundary theory.
- Similar to the non-magnetic system [12], the IR physics is controlled by the near horizon $AdS_2 \times R^2$ geometry, which indicates the existence of an IR CFT, characterized by operators \mathcal{O}_l , $l \in N$ with operator dimensions $\delta = 1/2 + \nu_l$:

$$\nu_l = \frac{1}{6} \sqrt{6 \left(m^2 + \frac{2|qh|l}{r_{**}^2} \right) - \frac{\mu_q^2}{r_{**}^4}}, \quad (21.31)$$

in dimensionless notation, and $\mu_q \equiv \mu q$. At $T = 0$, when $r_{**} = 1$, it becomes

$$\nu_l = \frac{1}{6} \sqrt{6(m^2 + 2|qh|l) - \mu_q^2}. \quad (21.32)$$

The Green's function for these operators \mathcal{O}_l is found to be $\mathcal{G}_l^R(\omega) \sim \omega^{2\nu_l}$ and the exponents ν_l determines the dispersion properties of the quasiparticle excitations. For $\nu > 1/2$ the system has a stable quasiparticle and a linear dispersion, whereas for $\nu \leq 1/2$ one has a non-Fermi liquid with power-law dispersion and an unstable quasiparticle.

21.3 Magnetic Fields and Conformal Invariance

Despite the fact that a magnetic field introduces a scale, in the absence of a chemical potential, all spectral functions are essentially still determined by conformal symmetry. To show this, we need to establish certain properties of the near-horizon geometry of a Reissner-Nordström black hole. This leads to the AdS_2 perspective that was developed in [8]. The result relies on the conformal algebra and its relation to the magnetic group, from the viewpoint of the infrared CFT that was studied in [8]. Later on we will see that the insensitivity to the magnetic field also carries over to AdS_4 and the UV CFT in some respects. To simplify the derivations, we consider the case $T = 0$.

21.3.1 The Near-Horizon Limit and Dirac Equation in AdS_2

It was established in [8] that an electrically charged extremal AdS -Reissner-Nordström black hole has an AdS_2 throat in the inner bulk region. This conclusion carries over to the magnetic case with some minor differences. We will now give a quick derivation of the AdS_2 formalism for a dyonic black hole, referring the reader to [8] for more details (that remain largely unchanged in the magnetic field).

Near the horizon $r = r_{**}$ of the black hole described by the metric (21.2), the redshift factor $f(r)$ develops a double zero:

$$f(r) = 6 \frac{(r - r_{**})^2}{r_{**}^2} + \mathcal{O}((r - r_{**})^3). \quad (21.33)$$

Now consider the scaling limit

$$r - r_{**} = \lambda \frac{R_2^2}{\zeta}, \quad t = \lambda^{-1} \tau, \quad \lambda \rightarrow 0 \text{ with } \tau, \zeta \text{ finite.} \quad (21.34)$$

In this limit, the metric (21.2) and the gauge field reduce to

$$ds^2 = \frac{R_2^2}{\zeta^2} (-d\tau^2 + d\zeta^2) + \frac{r_{**}^2}{R^2} (dx^2 + dy^2), \quad (21.35)$$

$$A_\tau = \frac{\mu R_2^2 r_0}{r_{**}^2} \frac{1}{\zeta}, \quad A_x = Hx$$

where $R_2 = \frac{R}{\sqrt{6}}$. The geometry described by this metric is indeed $AdS_2 \times R^2$. Physically, the scaling limit given in (21.34) with finite τ corresponds to the long time limit of the original time coordinate t , which translates to the low frequency limit of the boundary theory:

$$\frac{\omega}{\mu} \rightarrow 0, \quad (21.36)$$

where ω is the frequency conjugate to t . (One can think of λ as being the frequency ω .) Near the AdS_4 horizon, we expect the AdS_2 region of an extremal dyonic black hole to have a CFT_1 dual. We refer to [8] for an account of this AdS_2/CFT_1 duality. The horizon of AdS_2 region is at $\zeta \rightarrow \infty$ (coefficient in front of $d\tau$ vanishes at the horizon in (21.35)) and the infrared CFT (IR CFT) lives at the AdS_2 boundary at $\zeta = 0$. The scaling picture given by (21.34)–(21.35) suggests that in the low frequency limit, the 2-dimensional boundary theory is described by this IR CFT (which is a CFT_1). The Green's function for the operator \mathcal{O} in the boundary theory is obtained through a small frequency expansion and a matching procedure between the two different regions (inner and outer) along the radial direction, and can be expressed through the Green's function of the IR CFT [8].

The explicit form for the Dirac equation in the magnetic field is of little interest for the analytical results that follow. It can be found in [27]. Of primary interest is its limit in the IR region with metric given by (21.35):

$$\left(-\frac{1}{\sqrt{g_{\zeta\zeta}}} \sigma^3 \partial_\zeta - m + \frac{1}{\sqrt{-g_{\tau\tau}}} \sigma^1 \left(\omega + \frac{\mu_q R_2^2 r_0}{r_{**}^2 \zeta} \right) - \frac{1}{\sqrt{g_{ii} l \sigma^2 \lambda_l}} \right) F^{(l)} = 0, \quad (21.37)$$

where the effective momentum of the l th Landau level is $\lambda_l = \sqrt{2|q\hbar|l}$, $\mu_q \equiv \mu q$ and we omit the index of the spinor field. To obtain (21.37), it is convenient to

pick the gamma matrix basis as $\Gamma^{\hat{\zeta}} = -\sigma_3$, $\Gamma^{\hat{\tau}} = i\sigma_1$ and $\Gamma^{\hat{t}} = -\sigma_2$. We can write explicitly:

$$\begin{pmatrix} \frac{\zeta}{R_2} \partial_{\zeta} + m & -\frac{\zeta}{R_2} \left(\omega + \frac{\mu_q R_2^2 r_0}{r_{**}^2 \zeta} \right) + \frac{R}{r_{**}} \lambda_l \\ \frac{\zeta}{R_2} \left(\omega + \frac{\mu_q R_2^2 r_0}{r_{**}^2 \zeta} \right) + \frac{R}{r_{**}} \lambda_l & \frac{\zeta}{R_2} \partial_{\zeta} - m \end{pmatrix} \begin{pmatrix} y \\ z \end{pmatrix} = 0. \quad (21.38)$$

Note that the AdS_2 radius R_2 enters for the (τ, ζ) directions. At the AdS_2 boundary, $\zeta \rightarrow 0$, the Dirac equation to the leading order is given by

$$\zeta \partial_{\zeta} F^{(l)} = -U F^{(l)}, \quad U = R_2 \begin{pmatrix} m & -\frac{\mu_q R_2 r_0}{r_{**}^2} + \frac{R}{r_{**}} \lambda_l \\ \frac{\mu_q R_2 r_0}{r_{**}^2} + \frac{R}{r_{**}} \lambda_l & -m \end{pmatrix}. \quad (21.39)$$

The solution to this equation is given by the scaling function $F^{(l)} = A e_+ \zeta^{-\nu_l} + B e_- \zeta^{\nu_l}$ where e_{\pm} are the real eigenvectors of U and the exponent is

$$\nu_l = \frac{1}{6} \sqrt{6 \left(m^2 + \frac{R^2}{r_{**}^2} 2|qh|l \right) R^2 - \frac{\mu_q^2 R^4 r_0^2}{r_{**}^4}}. \quad (21.40)$$

The conformal dimension of the operator \mathcal{O} in the IR CFT is $\delta_l = \frac{1}{2} + \nu_l$. Comparing (21.40) to the expression for the scaling exponent in [8], we conclude that the scaling properties and the AdS_2 construction are unmodified by the magnetic field, except that the scaling exponents are now fixed by the Landau quantization. This ‘‘quantization rule’’ was already exploited in [25, 26] to study de Haas-van Alphen oscillations.

21.4 Spectral Functions

In this section we will explore some of the properties of the spectral function, in both plane wave and Landau level basis. We first consider some characteristic cases in the plane wave basis and make connection with the ARPES measurements.

21.4.1 Relating to the ARPES Measurements

In reality, ARPES measurements cannot be performed in magnetic fields so the holographic approach, allowing a direct insight into the propagator structure and the spectral function, is especially helpful. This follows from the observation that the spectral functions as measured in ARPES are always expressed in the plane wave basis of the photon, thus in a magnetic field, when the momentum is not a good quantum number anymore, it becomes impossible to perform the photoemission spectroscopy.

In order to compute the spectral function, we have to choose a particular fermionic plane wave as a probe. Since the separation of variables is valid through-

out the bulk, the basis transformation can be performed at every constant r -slice. This means that only the x and y coordinates have to be taken into account (the plane wave probe lives only at the CFT side of the duality). We take a plane wave propagating in the $+x$ direction with spin up along the r -axis. In its rest frame such a particle can be described by

$$\Psi_{\text{probe}} = e^{i\omega t - ip_x x} \begin{pmatrix} \xi \\ \xi \end{pmatrix}, \quad \xi = \begin{pmatrix} 1 \\ 0 \end{pmatrix}. \quad (21.41)$$

Near the boundary (at $r_b \rightarrow \infty$) we can rescale our solutions of the Dirac equation, details can be found in [27]:

$$F_l = \begin{pmatrix} \zeta_l^{(1)}(\tilde{x}) \\ \xi_+^{(l)}(r_b) \zeta_l^{(1)}(\tilde{x}) \\ \zeta_l^{(2)}(\tilde{x}) \\ -\xi_+^{(l)}(r_b) \zeta_l^{(2)}(\tilde{x}) \end{pmatrix}, \quad \tilde{F}_l = \begin{pmatrix} \zeta_l^{(1)}(\tilde{x}) \\ \xi_-^{(l)}(r_b) \zeta_l^{(1)}(\tilde{x}) \\ -\zeta_l^{(2)}(\tilde{x}) \\ \xi_-^{(l)}(r_b) \zeta_l^{(2)}(\tilde{x}) \end{pmatrix}, \quad (21.42)$$

with rescaled \tilde{x} defined in [27]. This representation is useful since we calculate the components $\xi_{\pm}(r_b)$ related to the retarded Green's function in our numerics (we keep the notation of [8]).

Let \mathcal{O}_l and $\tilde{\mathcal{O}}_l$ be the CFT operators dual to respectively F_l and \tilde{F}_l , and c_k^\dagger, c_k be the creation and annihilation operators for the plane wave state Ψ_{probe} . Since the states F and \tilde{F} form a complete set in the bulk, we can write

$$c_p^\dagger(\omega) = \sum_l (U_l^*, \tilde{U}_l^*) \begin{pmatrix} \mathcal{O}_l^\dagger(\omega) \\ \tilde{\mathcal{O}}_l^\dagger(\omega) \end{pmatrix} = \sum_l (U_l^* \mathcal{O}_l^\dagger(\omega) + \tilde{U}_l^* \tilde{\mathcal{O}}_l^\dagger(\omega)) \quad (21.43)$$

where the overlap coefficients $U_l(\omega)$ are given by the inner product between Ψ_{probe} and F :

$$U_l(p_x) = \int dx F_l^\dagger i \Gamma^0 \Psi_{\text{probe}} = - \int dx e^{-ip_x x} \xi_+(r_b) (\zeta_l^{(1)\dagger}(\tilde{x}) - \zeta_l^{(2)\dagger}(\tilde{x})), \quad (21.44)$$

with $\bar{F} = F^\dagger i \Gamma^0$, and similar expression for \tilde{U}_l involving $\xi_-(r_b)$. The constants U_l can be calculated analytically using the numerical value of $\xi_{\pm}(r_b)$, and by noting that the Hermite functions are eigenfunctions of the Fourier transform. We are interested in the retarded Green's function, defined as

$$\begin{aligned} G_{\mathcal{O}_l}^R(\omega, p) &= -i \int d^x dt e^{i\omega t - ip \cdot x} \theta(t) G_{\mathcal{O}_l}^R(t, x) \\ G_{\mathcal{O}_l}^R(t, x) &= \langle 0 | [\mathcal{O}_l(t, x), \tilde{\mathcal{O}}_l(0, 0)] | 0 \rangle \\ G^R &= \begin{pmatrix} G_\theta & 0 \\ 0 & \tilde{G}_\theta \end{pmatrix}, \end{aligned} \quad (21.45)$$

where \tilde{G}_θ is the retarded Green's function for the operator $\tilde{\mathcal{O}}$.

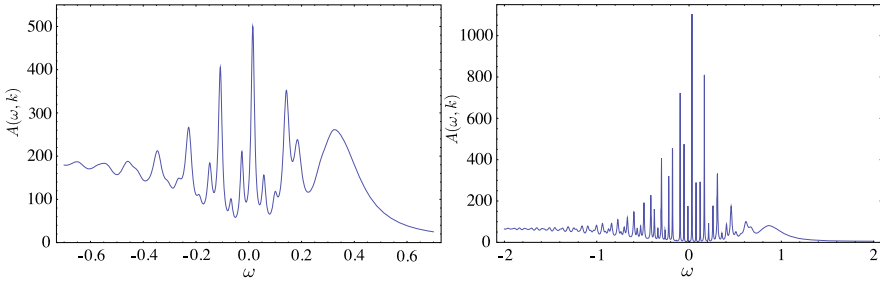


Fig. 21.1 Two examples of spectral functions in the plane wave basis for $\mu/T = 50$ and $h/T = 1$. The conformal dimension is $\Delta = 5/4$ (left) and $\Delta = 3/2$ (right). Frequency is in the units of effective temperature T_{eff} . The plane wave momentum is chosen to be $k = 1$. Despite the convolution of many Landau levels, the presence of the discrete levels is obvious

Exploiting the orthogonality of the spinors created by \mathcal{O} and \mathcal{O}^\dagger and using (21.43), the Green’s function in the plane wave basis can be written as

$$\begin{aligned}
 G_{c_p}^R(\omega, p_x) &= \sum_l \text{tr} \left(\begin{matrix} U \\ \tilde{U} \end{matrix} \right) (U^*, \tilde{U}^*) G^R \\
 &= (|U_l(p_x)|^2 G_{\mathcal{O}_l}^R(\omega, l) + |\tilde{U}_l(p_x)|^2 \tilde{G}_{\mathcal{O}_l}^R(\omega, l)). \tag{21.46}
 \end{aligned}$$

In practice, we cannot perform the sum in (21.46) all the way to infinity, so we have to introduce a cutoff Landau level l_{cut} . In most cases we are able to make l_{cut} large enough that the behavior of the spectral function is clear.

Using the above formalism, we have produced spectral functions for two different conformal dimensions and fixed chemical potential and magnetic field (Fig. 21.1). Using the plane wave basis allows us to directly detect the Landau levels. The unit used for plotting the spectra (here and later on in the paper) is the effective temperature T_{eff} [6]:

$$T_{\text{eff}} = \frac{T}{2} \left(1 + \sqrt{1 + \frac{3\mu^2}{(4\pi T)^2}} \right). \tag{21.47}$$

This unit interpolates between μ at $T/\mu = 0$ and T and is of order $T/\mu \rightarrow \infty$, and is convenient for the reason that the relevant quantities (e.g., Fermi momentum) are of order unity for any value of μ and h .

21.4.2 Magnetic Crossover and Disappearance of the Quasiparticles

Theoretically, it is more convenient to consider the spectral functions in the Landau level basis. For definiteness let us pick a fixed conformal dimension $\Delta = \frac{5}{4}$ which corresponds to $m = -\frac{1}{4}$. In the limit of weak magnetic fields, $h/T \rightarrow 0$, we should reproduce the results that were found in [6].

In Fig. 21.2(A) we indeed see that the spectral function, corresponding to a low value of μ/T , behaves as expected for a nearly conformal system. The spectral function is approximately symmetric about $\omega = 0$, it vanishes for $|\omega| < k$, up to a small residual tail due to finite temperature, and for $|\omega| \gg k$ it scales as ω^{2m} .

In Fig. 21.2(B), which corresponds to a high value of μ/T , we see the emergence of a sharp quasiparticle peak. This peak becomes the sharpest when the Landau level l corresponding to an effective momentum $k_{\text{eff}} = \sqrt{2|qh|l}$ coincides with the Fermi momentum k_F . The peaks also broaden out when k_{eff} moves away from k_F . A more complete view of the Landau quantization in the quasiparticle regime is given in Fig. 21.3, where we plot the dispersion relation (ω - k map). Both the sharp peaks and the Landau levels can be visually identified.

Collectively, the spectra in Fig. 21.2 show that conformality is only broken by the chemical potential μ and not by the magnetic field. Naively, the magnetic field introduces a new scale in the system. However, this scale is absent from the spectral functions, visually validating the discussion in the previous section that the scale h can be removed by a rescaling of the temperature and chemical potential.

One thus concludes that there is some value h'_c of the magnetic field, depending on μ/T , such that the spectral function loses its quasiparticle peaks and displays near-conformal behavior for $h > h'_c$. The nature of the transition and the underlying mechanism depends on the parameters (μ_q, T, Δ) . One mechanism, obvious from the rescaling in (21.29), is the reduction of the effective coupling q as h increases. This will make the influence of the scalar potential A_0 negligible and push the system back toward conformality. Generically, the spectral function shows no sharp change but is more indicative of a crossover.

A more interesting phenomenon is the disappearance of coherent quasiparticles at high effective chemical potentials. For the special case $m = 0$, we can go beyond numerics and study this transition analytically, combining the exact $T = 0$ solution found in [24] and the mapping (21.30). In the next section, we will show that the transition is controlled by the change in the dispersion of the quasiparticle and corresponds to a sharp phase transition. Increasing the magnetic field leads to a decrease in phenomenological control parameter v_{k_F} . This can give rise to a transition to a non-Fermi liquid when $v_{k_F} \leq 1/2$, and finally to the conformal regime at $h = h'_c$ when $v_{k_F} = 0$ and the Fermi surface vanishes.

21.4.3 Density of States

As argued at the beginning of this section, the spectral function can look quite different depending on the particular basis chosen. Though the spectral function is an attractive quantity to consider due to connection with ARPES experiments, we will also direct our attention to basis-independent and manifestly gauge invariant quantities. One of them is the density of states (DOS), defined by

$$D(\omega) = \sum_l A(\omega, l), \quad (21.48)$$

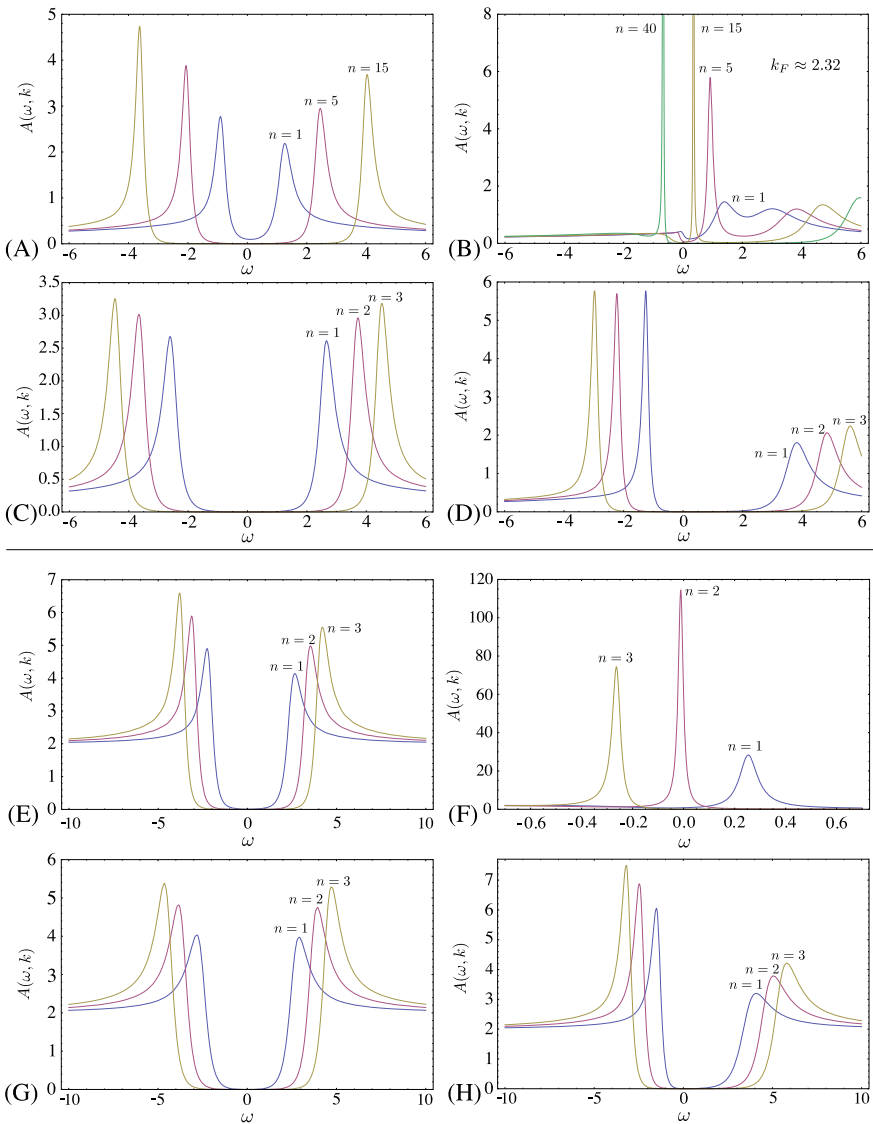


Fig. 21.2 Some typical examples of spectral functions $A(\omega, k_{\text{eff}})$ vs. ω in the Landau basis, $k_{\text{eff}} = \sqrt{2|q\hbar|n}$. The *top four* correspond to a conformal dimension $\Delta = \frac{5}{4}$ ($m = -\frac{1}{4}$) and the *bottom four* to $\Delta = \frac{3}{2}$ ($m = 0$). In each plot we show different Landau levels, labelled by index n , as a function of μ/T and h/T . The ratios take values $(\mu/T, h/T) = (1, 1), (50, 1), (1, 50), (50, 50)$ from left to right. Conformal case can be identified when μ/T is small regardless of h/T (plots in the *left panel*). Nearly conformal behavior is seen when both μ/T and h/T are large. This confirms our analytic result that the behavior of the system is primarily governed by μ . Departure from the conformality and sharp quasiparticle peaks are seen when μ/T is large and h/T is small in 21.2(B) and 21.2(F). Multiple quasiparticle peaks arise whenever $k_{\text{eff}} = k_F$. This suggests the existence of a critical magnetic field, beyond which the quasiparticle description becomes invalid and the system exhibits a conformal-like behavior. As before, the frequency ω is in units of T_{eff}

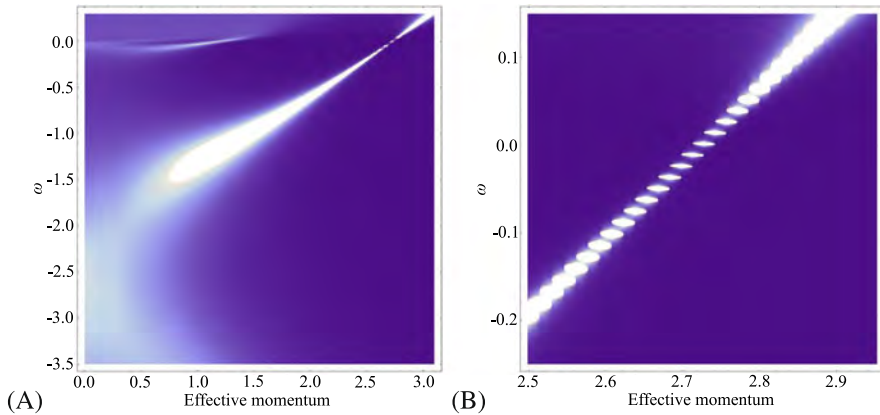


Fig. 21.3 Dispersion relation ω vs. k_{eff} for $\mu/T = 50$, $h/T = 1$ and $\Delta = \frac{5}{4}$ ($m = -\frac{1}{4}$). The spectral function $A(\omega, k_{\text{eff}})$ is displayed as a density plot. **(A)** On a large energy and momentum scale, we clearly see that the peaks disperse almost linearly ($\omega \approx v_F k$), indicating that we are in the stable quasiparticle regime. **(B)** A zoom-in near the location of the Fermi surface shows clear Landau quantization

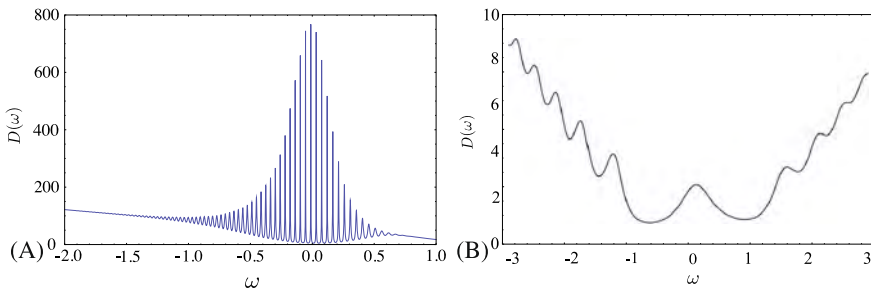


Fig. 21.4 Density of states $D(\omega)$ for $m = -\frac{1}{4}$ and **(A)** $\mu/T = 50$, $h/T = 1$, and **(B)** $\mu/T = 1$, $h/T = 1$. Sharp quasiparticle peaks from the splitting of the Fermi surface are clearly visible in **(A)**. The case **(B)** shows square-root level spacing characteristic of a (nearly) Lorentz invariant spectrum such as that of graphene

where the usual integral over the momentum is replaced by a sum since only discrete values of the momentum are allowed.

In Fig. 21.4, we plot the density of states for two systems. We clearly see the Landau splitting of the Fermi surface. A peculiar feature of these plots is that the DOS seems to grow for negative values of ω . This, however, is an artefact of our calculation. Each individual spectrum in the sum (21.48) has a finite tail that scales as ω^{2m} for large ω , so each term has a finite contribution for large values of ω . When the full sum is performed, this fact implies that $\lim_{\omega \rightarrow \infty} D(\omega) \rightarrow \infty$. The relevant information on the density of states can be obtained by regularizing the sum, which in practice is done by summing over a finite number of terms only, and then considering the peaks that lie on top of the resulting finite-sized envelope. The

physical point in Fig. 21.4(A) is the linear spacing of Landau levels, corresponding to a non-relativistic system at finite density. This is to be contrasted with Fig. 21.4B where the level spacing behaves as $\propto \sqrt{\hbar}$, appropriate for a Lorentz invariant system and realized in graphene [28].

21.5 Fermi Level Structure at Zero Temperature

In this section, we solve the Dirac equation in the magnetic field for the special case $m = 0$ ($\Delta = \frac{3}{2}$). Although there are no additional symmetries in this case, it is possible to get an analytic solution. Using this solution, we obtain Fermi level parameters such as k_F and v_F and consider the process of filling the Landau levels as the magnetic field is varied.

21.5.1 Dirac Equation with $m = 0$

In the case $m = 0$, it is convenient to solve the Dirac equation including the spin connection (see details in [27]) rather than scaling it out:

$$\left(-\frac{\sqrt{g_{ii}}}{\sqrt{g_{rr}}}\sigma^1\partial_r - \frac{\sqrt{g_{ii}}}{\sqrt{-g_{tt}}}\sigma^3(\omega + qA_t) + \frac{\sqrt{g_{ii}}}{\sqrt{-g_{tt}}}\sigma^1\frac{1}{2}\omega_{\hat{r}\hat{t}} - \sigma^1\frac{1}{2}\omega_{\hat{x}\hat{r}x} - \sigma^1\frac{1}{2}\omega_{\hat{y}\hat{r}y} - \lambda_l \right) \otimes 1 \begin{pmatrix} \psi_1 \\ \psi_2 \end{pmatrix} = 0, \quad (21.49)$$

where $\lambda_l = \sqrt{2|qh|l}$ are the energies of the Landau levels $l = 0, 1, \dots$, $g_{ii} \equiv g_{xx} = g_{yy}$, $A_t(r)$ is given by (21.3), and the gamma matrices are defined in [27]. In this basis the two components ψ_1 and ψ_2 decouple. Therefore, in what follows we solve for the first component only (we omit index 1). Substituting the spin connection, we have [20]:

$$\left(-\frac{r^2\sqrt{f}}{R^2}\sigma^1\partial_r - \frac{1}{\sqrt{f}}\sigma^3(\omega + qA_t) - \sigma^1\frac{r\sqrt{f}}{2R^2}\left(3 + \frac{rf'}{f}\right) - \lambda_l \right) \psi = 0, \quad (21.50)$$

with $\psi = (y_1, y_2)$. It is convenient to change to the basis

$$\begin{pmatrix} \tilde{y}_1 \\ \tilde{y}_2 \end{pmatrix} = \begin{pmatrix} 1 & -i \\ -i & 1 \end{pmatrix} \begin{pmatrix} y_1 \\ y_2 \end{pmatrix}, \quad (21.51)$$

which diagonalizes the system into a second order differential equation for each component. We introduce the dimensionless variables as in (21.15)–(21.17), and make a change of the dimensionless radial variable:

$$r = \frac{1}{1-z}, \quad (21.52)$$

with the horizon now being at $z = 0$, and the conformal boundary at $z = 1$. Performing these transformations in (21.50), the second order differential equations for \tilde{y}_1 reads

$$\left(f \partial_z^2 + \left(\frac{3f}{1-z} + f' \right) \partial_z + \frac{15f}{4(1-z)^2} + \frac{3f'}{2(1-z)} + \frac{f''}{4} + \frac{1}{f} \left((\omega + q\mu z) \pm \frac{if'}{4} \right)^2 - iq\mu - \lambda_l^2 \right) \tilde{y}_1 = 0. \quad (21.53)$$

The second component \tilde{y}_2 obeys the same equation with $\mu \mapsto -\mu$.

At $T = 0$,

$$f = 3z^2(z - z_0)(z - \bar{z}_0), \quad z_0 = \frac{1}{3}(4 + i\sqrt{2}). \quad (21.54)$$

The solution of this fermion system at zero magnetic field and zero temperature $T = 0$ has been found in [24]. To solve (21.53), we use the mapping to a zero magnetic field system (21.29). The combination $\mu_q \equiv \mu q$ at non-zero h maps to $\mu_{q,\text{eff}} \equiv \mu_{\text{eff}} q_{\text{eff}}$ at zero h as follows:

$$\mu_q \mapsto q \sqrt{1 - \frac{H^2}{Q^2 + H^2}} \cdot g_F \sqrt{Q^2 + H^2} = \sqrt{3} q g_F \sqrt{1 - \frac{H^2}{3}} = \mu_{q,\text{eff}} \quad (21.55)$$

where at $T = 0$ we used $Q^2 + H^2 = 3$. We solve (21.53) for zero modes, i.e. $\omega = 0$, and at the Fermi surface $\lambda = k$, and implement (21.55).

Near the horizon ($z = 0$, $f = 6z^2$), we have

$$6z^2 \tilde{y}_{1;2}'' + 12z \tilde{y}_{1;2}' + \left(\frac{3}{2} + \frac{(\mu_{q,\text{eff}})^2}{6} - k_F^2 \right) \tilde{y}_{1;2} = 0, \quad (21.56)$$

which gives the following behavior:

$$\tilde{y}_{1;2} \sim z^{-\frac{1}{2} \pm \nu k}, \quad (21.57)$$

with the scaling exponent ν following from (21.32):

$$\nu = \frac{1}{6} \sqrt{6k^2 - (\mu_{q,\text{eff}})^2}, \quad (21.58)$$

at the momentum k . Using Maple, we find the zero mode solution of (21.53) with a regular behavior $z^{-\frac{1}{2} + \nu}$ at the horizon [20, 24]:

$$\begin{aligned} \tilde{y}_1^{(0)} &= N_1 (z-1)^{\frac{3}{2}} z^{-\frac{1}{2} + \nu} (z - \bar{z}_0)^{-\frac{1}{2} - \nu} \left(\frac{z - z_0}{z - \bar{z}_0} \right)^{\frac{1}{4}(-1 - \sqrt{2}\mu_{q,\text{eff}}/z_0)} \\ &\times {}_2F_1 \left(\frac{1}{2} + \nu - \frac{\sqrt{2}}{3} \mu_{q,\text{eff}}, \nu + i \frac{\mu_{q,\text{eff}}}{6}, 1 + 2\nu, \frac{2i\sqrt{2}z}{3z_0(z - \bar{z}_0)} \right), \end{aligned} \quad (21.59)$$

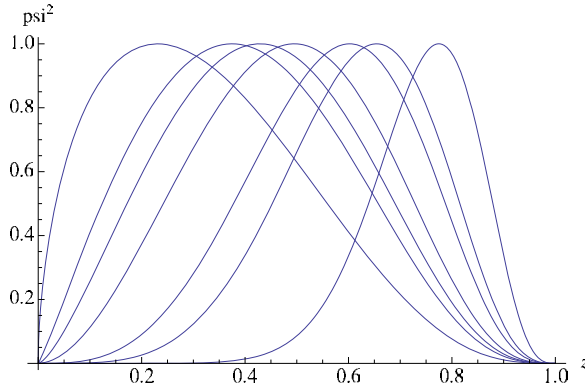


Fig. 21.5 Density of the zero mode $\psi^{0\dagger}\psi^0$ vs. the radial coordinate z (the horizon is at $z = 0$ and the boundary is at $z = 1$) for different values of the magnetic field h for the first (with the largest root for k_F) Fermi surface. We set $g_F = 1$ ($h \rightarrow H$) and $q = \frac{15}{\sqrt{3}}$ ($\mu_{q,\text{eff}} \rightarrow 15\sqrt{1 - \frac{H^2}{3}}$). From right to left the values of the magnetic field are $H = \{0, 1.40, 1.50, 1.60, 1.63, 1.65, 1.68\}$. The amplitudes of the curves are normalized to unity. At weak magnetic fields, the wave function is supported away from the horizon while at strong fields it is supported near the horizon

and

$$\tilde{y}_2^{(0)} = N_2(z - 1)^{\frac{3}{2}}z^{-\frac{1}{2}+\nu}(z - \bar{z}_0)^{-\frac{1}{2}-\nu}\left(\frac{z - z_0}{z - \bar{z}_0}\right)^{\frac{1}{4}(-1+\sqrt{2}\mu_{q,\text{eff}}/z_0)} \times {}_2F_1\left(\frac{1}{2} + \nu + \frac{\sqrt{2}}{3}\mu_{q,\text{eff}}, \nu - i\frac{\mu_{q,\text{eff}}}{6}, 1 + 2\nu, \frac{2i\sqrt{2}z}{3z_0(z - \bar{z}_0)}\right), \quad (21.60)$$

where ${}_2F_1$ is the hypergeometric function and N_1, N_2 are normalization factors. Since normalization factors are constants, we find their relative weight by substituting solutions given in (21.59) back into the first order differential equations at $z \sim 0$,

$$\frac{N_1}{N_2} = -\frac{6i\nu + \mu_{q,\text{eff}}}{\sqrt{6}k}\left(\frac{z_0}{\bar{z}_0}\right)^{\mu_{q,\text{eff}}/\sqrt{2}z_0}. \quad (21.61)$$

The same relations are obtained when calculations are done for any z . The second solution $\tilde{\eta}_{1;2}^{(0)}$, with behavior $z^{-\frac{1}{2}-\nu}$ at the horizon, is obtained by replacing $\nu \rightarrow -\nu$ in (21.59).

To get insight into the zero-mode solution (21.59), we plot the radial profile for the density function $\psi^{(0)\dagger}\psi^{(0)}$ for different magnetic fields in Fig. 21.5. The momentum chosen is the Fermi momentum of the first Fermi surface (see the next section). The curves are normalized to have the same maxima. Magnetic field is increased from right to left. At small magnetic field, the zero modes are supported away from the horizon, while at large magnetic field, the zero modes are supported near the horizon. This means that at large magnetic field the influence of the black hole to the Fermi level structure becomes more important.

21.5.2 Magnetic Effects on the Fermi Momentum and Fermi Velocity

In the presence of a magnetic field there is only a true pole in the Green's function whenever the Landau level crosses the Fermi energy [25, 26]

$$2l|qh| = k_F^2. \quad (21.62)$$

As shown in Fig. 21.2, whenever the equation (21.62) is satisfied the spectral function $A(\omega)$ has a (sharp) peak. This is not surprising since quasiparticles can be easily excited from the Fermi surface. From (21.62), the spectral function $A(\omega)$ and the density of states on the Fermi surface $D(\omega)$ are periodic in $\frac{1}{h}$ with the period

$$\Delta\left(\frac{1}{h}\right) = \frac{2\pi q}{A_F}, \quad (21.63)$$

where $A_F = \pi k_F^2$ is the area of the Fermi surface [25, 26]. This is a manifestation of the de Haas-van Alphen quantum oscillations. At $T = 0$, the electronic properties of metals depend on the density of states on the Fermi surface. Therefore, an oscillatory behavior as a function of magnetic field should appear in any quantity that depends on the density of states on the Fermi energy. Magnetic susceptibility [25, 26] and magnetization together with the superconducting gap [29] have been shown to exhibit quantum oscillations. Every Landau level contributes an oscillating term and the period of the l th level oscillation is determined by the value of the magnetic field h that satisfies (21.62) for the given value of k_F . Quantum oscillations (and the quantum Hall effect which we consider later in the paper) are examples of phenomena in which Landau level physics reveals the presence of the Fermi surface. The superconducting gap found in the quark matter in magnetic fields [29] is another evidence for the existence of the (highly degenerate) Fermi surface and the corresponding Fermi momentum.

Generally, a Fermi surface controls the occupation of energy levels in the system: the energy levels below the Fermi surface are filled and those above are empty (or non-existent). Here, however, the association to the Fermi momentum can be obscured by the fact that the fermions form highly degenerate Landau levels. Thus, in two dimensions, in the presence of the magnetic field the corresponding effective Fermi surface is given by a single point in the phase space, that is determined by n_F , the Landau index of the highest occupied level, i.e., the highest Landau level below the chemical potential.² Increasing the magnetic field, Landau levels 'move up' in the phase space leaving only the lower levels occupied, so that the effective Fermi momentum scales roughly (excluding interactions) as a square root of the magnetic field, $k_F \sim \sqrt{n_F} \sim k_F^{\max} \sqrt{1 - h/h_{\max}}$. High magnetic fields drive the effective density of the charge carriers down, approaching the limit when the Fermi momentum coincides with the lowest Landau level.

²We would like to thank Igor Shovkovy for clarifying the issue with the Fermi momentum in the presence of the magnetic field.

Many phenomena observed in the paper can thus be qualitatively explained by Landau quantization. As discussed before, the notion of the Fermi momentum is lost at very high magnetic fields. In what follows, the quantitative Fermi level structure at zero temperature, described by k_F and v_F values, is obtained as a function of the magnetic field using the solution of the Dirac equation given by (21.59), (21.60). As in [12], we neglect first the discrete nature of the Fermi momentum and velocity in order to obtain general understanding. Upon taking the quantization into account, the smooth curves become combinations of step functions following the same trend as the smooth curves (without quantization). While usually the grand canonical ensemble is used, where the fixed chemical potential controls the occupation of the Landau levels [30], in our setup, the Fermi momentum is allowed to change as the magnetic field is varied, while we keep track of the IR conformal dimension ν .

The Fermi momentum is defined by the matching between IR and UV physics [8], therefore it is enough to know the solution at $\omega = 0$, where the matching is performed. To obtain the Fermi momentum, we require that the zero mode solution is regular at the horizon ($\psi^{(0)} \sim z^{-\frac{1}{2}+\nu}$) and normalizable at the boundary. At the boundary $z \sim 1$, the wave function behaves as

$$a(1-z)^{\frac{3}{2}-m} \begin{pmatrix} 1 \\ 0 \end{pmatrix} + b(1-z)^{\frac{3}{2}+m} \begin{pmatrix} 0 \\ 1 \end{pmatrix}. \quad (21.64)$$

To require it to be normalizable is to set the first term $a = 0$; the wave function at $z \sim 1$ is then

$$\psi^{(0)} \sim (1-z)^{\frac{3}{2}+m} \begin{pmatrix} 0 \\ 1 \end{pmatrix}. \quad (21.65)$$

Equation (21.65) leads to the condition $\lim_{z \rightarrow 1} (z-1)^{-3/2} (\tilde{y}_2^{(0)} + i\tilde{y}_1^{(0)}) = 0$, which, together with (21.59), gives the following equation for the Fermi momentum as function of the magnetic field [20, 24]

$$\frac{{}_2F_1(1+\nu + \frac{i\mu_{q,\text{eff}}}{6}, \frac{1}{2} + \nu - \frac{\sqrt{2}\mu_{q,\text{eff}}}{3}, 1+2\nu, \frac{2}{3}(1-i\sqrt{2}))}{{}_2F_1(\nu + \frac{i\mu_{q,\text{eff}}}{6}, \frac{1}{2} + \nu - \frac{\sqrt{2}\mu_{q,\text{eff}}}{3}, 1+2\nu, \frac{2}{3}(1-i\sqrt{2}))} = \frac{6\nu - i\mu_{q,\text{eff}}}{k_F(-2i + \sqrt{2})}, \quad (21.66)$$

with $\nu \equiv \nu_{k_F}$ given by (21.58). Using Mathematica to evaluate the hypergeometric functions, we numerically solve the equation for the Fermi surface, which gives effective momentum as if it were continuous, i.e. when quantization is neglected. The solutions of (21.66) are given in Fig. 21.6. There are multiple Fermi surfaces for a given magnetic field h . Here and in all other plots we choose $g_F = 1$, therefore $h \rightarrow H$, and $q = \frac{15}{\sqrt{3}}$. In Fig. 21.6, positive and negative k_F correspond to the Fermi surfaces in the Green's functions G_1 and G_2 . The relation between two components is $G_2(\omega, k) = G_1(\omega, -k)$ [7], therefore Fig. 21.6 is not symmetric with respect to the x-axis. Effective momenta terminate at the dashed line $\nu_{k_F} = 0$. Taking into account Landau quantization of $k_F \rightarrow \sqrt{2|qh|l}$ with $l = 1, 2, \dots$, the plot consists of stepwise functions tracing the existing curves (we depict only positive k_F). Indeed

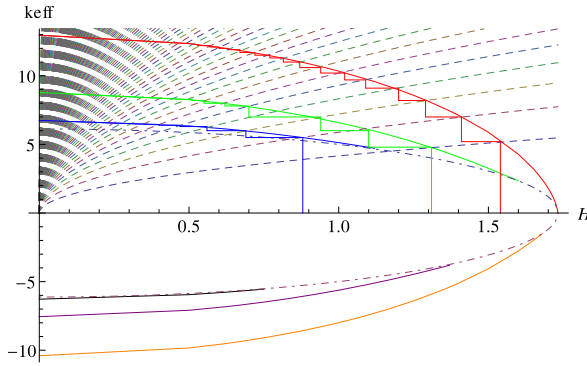
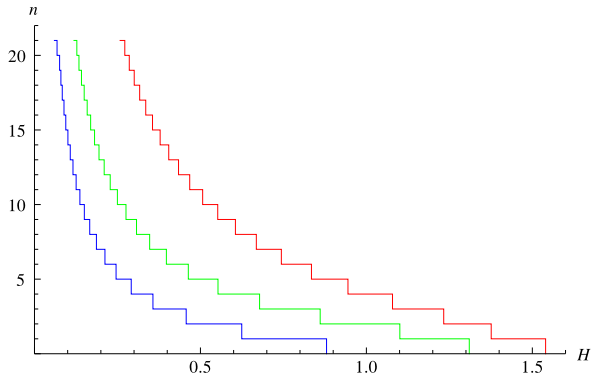


Fig. 21.6 Effective momentum k_{eff} vs. the magnetic field $h \rightarrow H$ (we set $g_F = 1$, $q = \frac{15}{\sqrt{3}}$). As we increase magnetic field the Fermi surface shrinks. *Smooth solid curves* represent situation as if momentum is a continuous parameter (for convenience), *stepwise solid functions* are the real Fermi momenta which are discretized due to the Landau level quantization: $k_F \rightarrow \sqrt{2|qh|l}$ with $l = 1, 2, \dots$ where $\sqrt{2|qh|l}$ are Landau levels given by *dotted lines* (only positive discrete k_F are shown). At a given h there are multiple Fermi surfaces. From right to left are the first, second etc. Fermi surfaces. The *dashed-dotted line* is $v_{k_F} = 0$ where k_F is terminated. Positive and negative k_{eff} correspond to Fermi surfaces in two components of the Green's function

Fig. 21.7 Landau level numbers n corresponding to the quantized Fermi momenta vs. the magnetic field $h \rightarrow H$ for the three Fermi surfaces with positive k_F . We set $g_F = 1$, $q = \frac{15}{\sqrt{3}}$. From right to left are the first, second and third Fermi surfaces



Landau quantization can be also seen from the dispersion relation at Fig. 21.3, where only discrete values of effective momentum are allowed and the Fermi surface has been chopped up as a result of it Fig. 21.3(B).

Our findings agree with the results for the (largest) Fermi momentum in a three-dimensional magnetic system considered in [31], compare the stepwise dependence $k_F(h)$ with Fig. 21.5 in [31].

In Fig. 21.7, the Landau level index l is obtained from $k_F(h) = \sqrt{2|qh|l}$ where $k_F(h)$ is a numerical solution of (21.66). Only those Landau levels which are below the Fermi surface are filled. In Fig. 21.6, as we decrease magnetic field first nothing happens until the next Landau level crosses the Fermi surface which corresponds to a jump up to the next step. Therefore, at strong magnetic fields, fewer states contribute

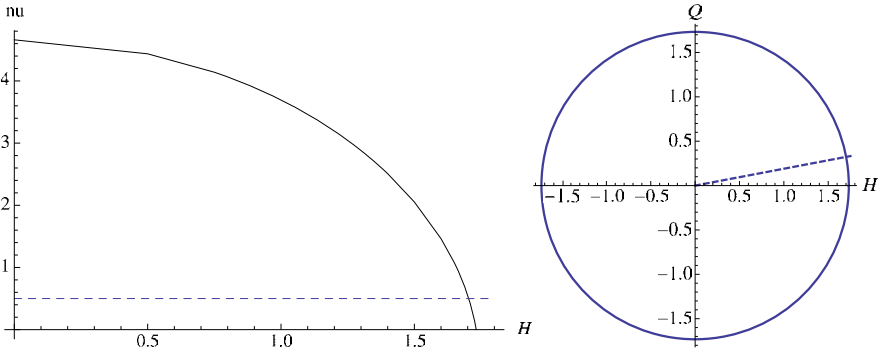


Fig. 21.8 *Left panel.* The IR conformal dimension $\nu \equiv \nu_{k_F}$ calculated at the Fermi momentum vs. the magnetic field $h \rightarrow H$ (we set $g_F=1, q = \frac{15}{\sqrt{3}}$). Calculations are done for the first Fermi surface. *Dashed line* is for $\nu = \frac{1}{2}$ (at $H_c = 1.70$), which is the border between the Fermi liquids $\nu > \frac{1}{2}$ and non-Fermi liquids $\nu < \frac{1}{2}$. *Right panel.* Phase diagram in terms of the chemical potential and the magnetic field $\mu^2 + h^2 = 3$ (in dimensionless variables $h = g_F H, \mu = g_F Q$; we set $g_F = 1$). Fermi liquids are above the *dashed line* ($H < H_c$) and non-Fermi liquids are below the *dashed line* ($H > H_c$)

to transport properties and the lowest Landau level becomes more important (see the next section). At weak magnetic fields, the sum over many Landau levels has to be taken, ending with the continuous limit as $h \rightarrow 0$, when quantization can be ignored.

In Fig. 21.8, we show the IR conformal dimension as a function of the magnetic field. We have used the numerical solution for k_F . Fermi liquid regime takes place at magnetic fields $h < h_c$, while non-Fermi liquids exist in a narrow band at $h_c < h < h'_c$, and at h'_c the system becomes near-conformal.

In this figure we observe the pathway of the possible phase transition exhibited by the Fermi surface (ignoring Landau quantization): it can vanish at the line $\nu_{k_F} = 0$, undergoing a crossover to the conformal regime, or cross the line $\nu_{k_F} = 1/2$ and go through a non-Fermi liquid regime, and subsequently cross to the conformal phase. Note that the primary Fermi surface with the highest k_F and ν_{k_F} seems to directly cross over to conformality, while the other Fermi surfaces first exhibit a “strange metal” phase transition. Therefore, all the Fermi momenta with $\nu_{k_F} > 0$ contribute to the transport coefficients of the theory. In particular, at high magnetic fields when for the first (largest) Fermi surface $k_F^{(1)}$ is nonzero but small, the lowest Landau level $n = 0$ becomes increasingly important contributing to the transport with half degeneracy factor as compared to the higher Landau levels.

In Fig. 21.9, we plot the Fermi momentum k_F as a function of the magnetic field for the first Fermi surface (the largest root of (21.66)). Quantization is neglected here. At the left panel, the relatively small region between the dashed lines corresponds to non-Fermi liquids $0 < \nu < \frac{1}{2}$. At large magnetic field, the physics of the Fermi surface is captured by the near horizon region (see also Fig. 21.5) which is $AdS_2 \times R^2$. At the maximum magnetic field, $H_{\max} = \sqrt{3} \approx 1.73$, when the black hole becomes pure magnetically charged, the Fermi momentum vanishes when it

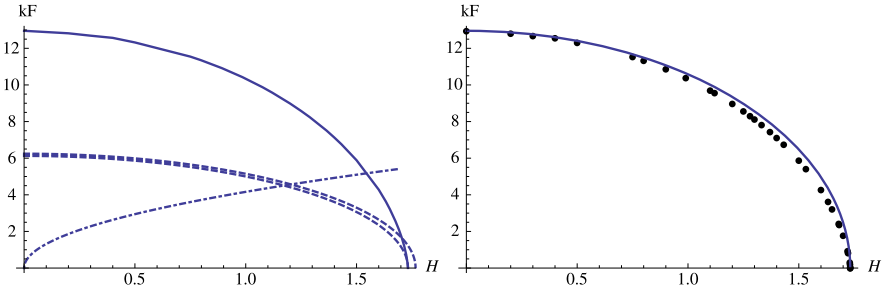


Fig. 21.9 Fermi momentum k_F vs. the magnetic field $h \rightarrow H$ (we set $g_F = 1, q = \frac{15}{\sqrt{3}}$) for the first Fermi surface. *Left panel.* The *inner* (closer to x-axis) *dashed line* is $v_{k_F} = 0$ and the *outer dashed line* is $v_{k_F} = \frac{1}{2}$, the region between these lines corresponds to non-Fermi liquids $0 < v_{k_F} < \frac{1}{2}$. The *dashed-dotted line* is for the first Landau level $k_1 = \sqrt{2qH}$. The first Fermi surface hits the *border-line* between a Fermi and non-Fermi liquids $v = \frac{1}{2}$ at $H_c \approx 1.70$, and it vanishes at $H_{\max} = \sqrt{3} = 1.73$. *Right panel.* *Circles* are the data points for the Fermi momentum calculated analytically, *solid line* is a fit function $k_F^{\max} \sqrt{1 - \frac{H^2}{3}}$ with $k_F^{\max} = 12.96$

crosses the line $v_{k_F} = 0$. This only happens for the first Fermi surface. For the higher Fermi surfaces the Fermi momenta terminate at the line $v_{k_F} = 0$, Fig. 21.6. Note the Fermi momentum for the first Fermi surface can be almost fully described by a function $k_F = k_F^{\max} \sqrt{1 - \frac{H^2}{3}}$. It is tempting to view the behavior $k_F \sim \sqrt{H_{\max} - H}$ as a phase transition in the system although it strictly follows from the linear scaling for $H = 0$ by using the mapping (21.29). (Note that also $\mu = g_F Q = g_F \sqrt{3 - H^2}$.) Taking into account the discretization of k_F , the plot will consist of an array of step functions tracing the existing curve. Our findings agree with the results for the Fermi momentum in a three dimensional magnetic system considered in [31], compare with Fig. 21.5 there.

The Fermi velocity given in (21.27) is defined by the UV physics; therefore solutions at non-zero ω are required. The Fermi velocity is extracted from matching two solutions in the inner and outer regions at the horizon. The Fermi velocity as function of the magnetic field for $v > \frac{1}{2}$ is [20, 24]

$$v_F = \frac{1}{h_1} \left(\int_0^1 dz \sqrt{g/g_{tt}} \psi^{(0)\dagger} \psi^{(0)} \right)^{-1} \lim_{z \rightarrow 1} \frac{|\tilde{y}_1^{(0)} + i\tilde{y}_2^{(0)}|^2}{(1-z)^3}, \quad (21.67)$$

$$h_1 = \lim_{z \rightarrow 1} \frac{\tilde{y}_1^{(0)} + i\tilde{y}_2^{(0)}}{\partial_k (y_2^{(0)} + i\tilde{y}_1^{(0)})},$$

where the zero mode wavefunction is taken at k_F (21.59).

We plot the Fermi velocity for several Fermi surfaces in Fig. 21.10. Quantization is neglected here. The Fermi velocity is shown for $v > \frac{1}{2}$. It is interesting that the Fermi velocity vanishes when the IR conformal dimension is $v_{k_F} = \frac{1}{2}$. Formally, it follows from the fact that $v_F \sim (2v - 1)$ [8]. The first Fermi surface is at the

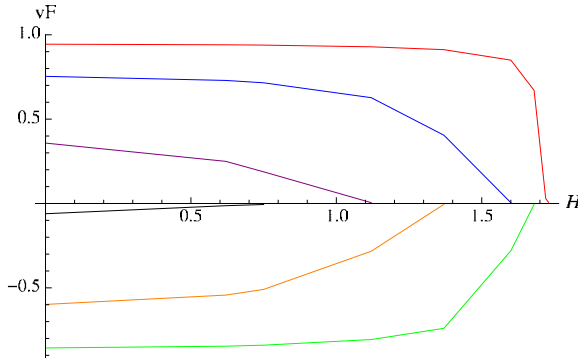


Fig. 21.10 Fermi velocity v_F vs. the magnetic field $h \rightarrow H$ (we set $g_F = 1$, $q = \frac{15}{\sqrt{3}}$) for the regime of Fermi liquids $v \geq \frac{1}{2}$. Fermi velocity vanishes at $v_{k_F} = \frac{1}{2}$ (x -axis). For the first Fermi surface, the *top curve*, Fermi velocity vanishes at $H_c \approx 1.70$. The region $H < H_c$ corresponds to the Fermi liquids and quasiparticle description. The *multiple lines* are for various Fermi surfaces in ascending order, with the first Fermi surface on the right. The Fermi velocity v_F has the same sign as the Fermi momentum k_F . As above, positive and negative v_F correspond to Fermi surfaces in the two components of the Green's function

far right. Positive and negative v_F correspond to the Fermi surfaces in the Green's functions G_1 and G_2 , respectively. The Fermi velocity v_F has the same sign as the Fermi momentum k_F . At small magnetic field values, the Fermi velocity is very weakly dependent on H and it is close to the speed of light; at large magnetic field values, the Fermi velocity rapidly decreases and vanishes (at $H_c = 1.70$ for the first Fermi surface). Geometrically, this means that with increasing magnetic field the zero mode wavefunction is supported near the black hole horizon Fig. 21.5, where the gravitational redshift reduces the local speed of light as compared to the boundary value. It was also observed in [8, 24] at small fermion charge values.

21.6 Hall and Longitudinal Conductivities

In this section, we calculate the contributions to Hall σ_{xy} and the longitudinal σ_{xx} conductivities directly in the boundary theory. This should be contrasted with the standard holographic approach, where calculations are performed in the (bulk) gravity theory and then translated to the boundary field theory using the AdS/CFT dictionary. Specifically, the conductivity tensor has been obtained in [11] by calculating the on-shell renormalized action for the gauge field on the gravity side and using the gauge/gravity duality $A_M \rightarrow j_\mu$ to extract the R charge current-current correlator at the boundary. Here, the Kubo formula involving the current-current correlator is used directly by utilizing the fermion Green's functions extracted from holography in [8]. Therefore, the conductivity is obtained for the charge carriers described by the fermionic operators of the boundary field theory.

The use of the conventional Kubo formula to extract the contribution to the transport due to fermions is validated in that it also follows from a direct AdS/CFT computation of the one-loop correction to the on-shell renormalized AdS action [17]. We study in particular stable quasiparticles with $\nu > \frac{1}{2}$ and at zero temperature. This regime effectively reduces to the clean limit where the imaginary part of the self-energy vanishes $\text{Im } \Sigma \rightarrow 0$. We use the gravity-“dressed” fermion propagator from (21.27) and to make the calculations complete, the “dressed” vertex is necessary, to satisfy the Ward identities. As was argued in [17], the boundary vertex which is obtained from the bulk calculations can be approximated by a constant in the low temperature limit. Also, according to [32, 33], the vertex only contains singularities of the product of the Green’s functions. Therefore, dressing the vertex will not change the dependence of the DC conductivity on the magnetic field [32, 33]. In addition, the zero magnetic field limit of the formulae for conductivity obtained from holography [17] and from direct boundary calculations [20] are identical.

21.6.1 Integer Quantum Hall Effect

Let us start from the “dressed” retarded and advanced fermion propagators [8]: G_R is given by (21.27) and $G_A = G_R^*$. To perform the Matsubara summation we use the spectral representation

$$G(i\omega_n, \mathbf{k}) = \int \frac{d\omega}{2\pi} \frac{A(\omega, \mathbf{k})}{\omega - i\omega_n}, \quad (21.68)$$

with the spectral function defined as $A(\omega, \mathbf{k}) = -\frac{1}{\pi} \text{Im } G_R(\omega, \mathbf{k}) = \frac{1}{2\pi i} (G_R(\omega, \mathbf{k}) - G_A(\omega, \mathbf{k}))$. Generalizing to a non-zero magnetic field and spinor case [30], the spectral function [34] is

$$A(\omega, \mathbf{k}) = \frac{1}{\pi} e^{-\frac{k^2}{|q\hbar|}} \sum_{l=0}^{\infty} (-1)^l (-h_1 v_F) \times \left(\frac{\Sigma_2(\omega, k_F) f(\mathbf{k}) \gamma^0}{(\omega + \varepsilon_F + \Sigma_1(\omega, k_F) - E_l)^2 + \Sigma_2(\omega, k_F)^2} + (E_l \rightarrow -E_l) \right), \quad (21.69)$$

where $\varepsilon_F = v_F k_F$ is the Fermi energy, $E_l = v_F \sqrt{2|q\hbar|l}$ is the energy of the Landau level, $f(\mathbf{k}) = P_- L_l(\frac{2k^2}{|q\hbar|}) - P_+ L_{l-1}(\frac{2k^2}{|q\hbar|})$ with spin projection operators $P_{\pm} = (1 \pm i\gamma^1 \gamma^2)/2$, we take $c = 1$, the generalized Laguerre polynomials are $L_n^\alpha(z)$ and by definition $L_n(z) = L_n^0(z)$, (we omit the vector part $\mathbf{k}\gamma$, it does not contribute to the DC conductivity), all γ ’s are the standard Dirac matrices, h_1 , v_F and k_F are real constants (we keep the same notations for the constants as in [8]). The self-energy $\Sigma \sim \omega^{2\nu k_F}$ contains the real and imaginary parts, $\Sigma = \Sigma_1 + i\Sigma_2$. The imaginary part comes from scattering processes of a fermion in the bulk, e.g. from

pair creation, and from the scattering into the black hole. It is exactly due to inelastic/dissipative processes that we are able to obtain finite values for the transport coefficients, otherwise they are formally infinite.

Using the Kubo formula, the DC electrical conductivity tensor is

$$\sigma_{ij}(\Omega) = \lim_{\Omega \rightarrow 0} \frac{\text{Im} \Pi_{ij}^R}{\Omega + i0^+}, \quad (21.70)$$

where $\Pi_{ij}(i\Omega_m \rightarrow \Omega + i0^+)$ is the retarded current-current correlation function; schematically the current density operator is $j^i(\tau, \mathbf{x}) = q v_F \sum_{\sigma} \bar{\psi}_{\sigma}(\tau, \mathbf{x}) \gamma^i \psi_{\sigma}(\tau, \mathbf{x})$. Neglecting the vertex correction, it is given by

$$\Pi_{ij}(i\Omega_m) = q^2 v_F^2 T \sum_{n=-\infty}^{\infty} \int \frac{d^2 k}{(2\pi)^2} \text{tr}(\gamma^i G(i\omega_n, \mathbf{k}) \gamma^j G(i\omega_n + i\Omega_m, \mathbf{k})). \quad (21.71)$$

The sum over the Matsubara frequency is

$$T \sum_n \frac{1}{i\omega_n - \omega_1} \frac{1}{i\omega_n + i\Omega_m - \omega_2} = \frac{n(\omega_1) - n(\omega_2)}{i\Omega_m + \omega_1 - \omega_2}. \quad (21.72)$$

Taking $i\Omega_m \rightarrow \Omega + i0^+$, the polarization operator is now

$$\Pi_{ij}(\Omega) = \frac{d\omega_1}{2\pi} \frac{d\omega_2}{2\pi} \frac{n_{\text{FD}}(\omega_1) - n_{\text{FD}}(\omega_2)}{\Omega + \omega_1 - \omega_2} \int \frac{d^2 k}{(2\pi)^2} \text{tr}(\gamma^i A(\omega_1, \mathbf{k}) \gamma^j A(\omega_2, \mathbf{k})), \quad (21.73)$$

where the spectral function $A(\omega, \mathbf{k})$ is given by (21.69) and $n_{\text{FD}}(\omega)$ is the Fermi-Dirac distribution function. Evaluating the traces, we have

$$\begin{aligned} \sigma_{ij} = & -\frac{4q^2 v_F^2 (h_1 v_F)^2 |qh|}{\pi \Omega} \\ & \times \text{Re} \sum_{l,k=0}^{\infty} (-1)^{l+k+1} \{ \delta_{ij} (\delta_{l,k-1} + \delta_{l-1,k}) + i \varepsilon_{ij} \text{sgn}(qh) (\delta_{l,k-1} - \delta_{l-1,k}) \} \\ & \times \int \frac{d\omega_1}{2\pi} \left(\tanh \frac{\omega_1}{2T} - \tanh \frac{\omega_2}{2T} \right) \left(\frac{\Sigma_2(\omega_1)}{(\tilde{\omega}_1 - E_l)^2 + \Sigma_2^2(\omega_1)} + (E_l \rightarrow -E_l) \right) \\ & \times \left(\frac{\Sigma_2(\omega_2)}{(\tilde{\omega}_2 - E_k)^2 + \Sigma_2^2(\omega_2)} + (E_k \rightarrow -E_k) \right), \quad (21.74) \end{aligned}$$

with $\omega_2 = \omega_1 + \Omega$. We have also introduced $\tilde{\omega}_{1,2} \equiv \omega_{1,2} + \varepsilon_F + \Sigma_1(\omega_{1,2})$ with ε_{ij} being the antisymmetric tensor ($\varepsilon_{12} = 1$), and $\Sigma_{1,2}(\omega) \equiv \Sigma_{1,2}(\omega, k_F)$. In the momentum integral, we use the orthogonality condition for the Laguerre polynomials $\int_0^{\infty} dx e^x L_l(x) L_k(x) = \delta_{lk}$.

From (21.74), the term symmetric/antisymmetric with respect to exchange $\omega_1 \leftrightarrow \omega_2$ contributes to the diagonal/off-diagonal component of the conductivity (note the

antisymmetric term $n_{\text{FD}}(\omega_1) - n_{\text{FD}}(\omega_2)$). The longitudinal and Hall DC conductivities ($\mathcal{J}\Omega \rightarrow 0$) are thus

$$\begin{aligned} \sigma_{xx} = & -\frac{2q^2(h_1 v_F)^2 |qh|}{\pi T} \int_{-\infty}^{\infty} \frac{d\omega}{2\pi} \frac{\Sigma_2^2(\omega)}{\cosh^2 \frac{\omega}{2T}} \\ & \times \sum_{l=0}^{\infty} \left(\frac{1}{(\tilde{\omega} - E_l)^2 + \Sigma_2^2(\omega)} + (E_l \rightarrow -E_l) \right) \\ & \times \left(\frac{1}{(\tilde{\omega} - E_{l+1})^2 + \Sigma_2^2(\omega)} + (E_{l+1} \rightarrow -E_{l+1}) \right), \end{aligned} \quad (21.75)$$

$$\sigma_{xy} = -\frac{q^2(h_1 v_F)^2 \text{sgn}(qh)}{\pi} \nu_h, \quad (21.76)$$

$$\nu_h = 2 \int_{-\infty}^{\infty} \frac{d\omega}{2\pi} \tanh \frac{\omega}{2T} \Sigma_2(\omega) \sum_{l=0}^{\infty} \alpha_l \left(\frac{1}{(\tilde{\omega} - E_l)^2 + \Sigma_2^2(\omega)} + (E_l \rightarrow -E_l) \right),$$

where $\tilde{\omega} = \omega + \varepsilon_F + \Sigma_1(\omega)$. The filling factor ν_h is proportional to the density of carriers: $|\nu_h| = \frac{\pi}{|qh|h_1 v_F} n$ (see derivation in [27]). The degeneracy factor of the Landau levels is α_l : $\alpha_0 = 1$ for the lowest Landau level and $\alpha_l = 2$ for $l = 1, 2, \dots$. Substituting the filling factor ν_h back to (21.76), the Hall conductivity can be written as

$$\sigma_{xy} = \frac{\rho}{h}, \quad (21.77)$$

where ρ is the charge density in the boundary theory, and both the charge q and the magnetic field h carry a sign (the prefactor $(-h_1 v_F)$ comes from the normalization choice in the fermion propagator (21.27), (21.69) as given in [8], which can be regarded as a factor contributing to the effective charge and is not important for further considerations). The Hall conductivity (21.77) has been obtained using the AdS/CFT duality for the Lorentz invariant 2 + 1-dimensional boundary field theories in [11]. We recover this formula because in our case the translational invariance is maintained in the x and y directions of the boundary theory.

Low frequencies give the main contribution in the integrand of (21.76). Since the self-energy satisfies $\Sigma_1(\omega) \sim \Sigma_2(\omega) \sim \omega^{2\nu}$ and we consider the regime $\nu > \frac{1}{2}$, we have $\Sigma_1 \sim \Sigma_2 \rightarrow 0$ at $\omega \sim 0$ (self-energy goes to zero faster than the ω term). Therefore, only the simple poles in the upper half-plane $\omega_0 = -\varepsilon_F \pm E_l + \Sigma_1 + i\Sigma_2$ contribute to the conductivity where $\Sigma_1 \sim \Sigma_2 \sim (-\varepsilon_F \pm E_l)^{2\nu}$ are small. The same logic of calculation has been used in [30]. We obtain for the longitudinal and Hall conductivities

$$\sigma_{xx} = \frac{2q^2(h_1 v_F)^2 \Sigma_2}{\pi T} \times \left(\frac{1}{1 + \cosh \frac{\varepsilon_F}{T}} + \sum_{l=1}^{\infty} 4l \frac{1 + \cosh \frac{\varepsilon_F}{T} \cosh \frac{E_l}{T}}{(\cosh \frac{\varepsilon_F}{T} + \cosh \frac{E_l}{T})^2} \right), \quad (21.78)$$

$$\sigma_{xy} = \frac{q^2(h_1 v_F)^2 \operatorname{sgn}(qh)}{\pi} \times 2 \left(\tanh \frac{\varepsilon_F}{2T} + \sum_{l=1}^{\infty} \left(\tanh \frac{\varepsilon_F + E_l}{2T} + \tanh \frac{\varepsilon_F - E_l}{2T} \right) \right), \quad (21.79)$$

where the Fermi energy is $\varepsilon_F = v_F k_F$ and the energy of the Landau level is $E_l = v_F \sqrt{2|qh|l}$. Similar expressions were obtained in [30]. However, in our case the filling of the Landau levels is controlled by the magnetic field h through the field-dependent Fermi energy $v_F(h)k_F(h)$ instead of the chemical potential μ .

At $T = 0$, $\cosh \frac{\omega}{T} \rightarrow \frac{1}{2} e^{\frac{\omega}{T}}$ and $\tanh \frac{\omega}{2T} = 1 - 2n_{\text{FD}}(\omega) \rightarrow \operatorname{sgn}\omega$. Therefore the longitudinal and Hall conductivities are

$$\sigma_{xx} = \frac{2q^2(h_1 v_F)^2 \Sigma_2}{\pi T} \sum_{l=1}^{\infty} l \delta_{\varepsilon_F, E_l} = \frac{2q^2(h_1 v_F)^2 \Sigma_2}{\pi T} \times n \delta_{\varepsilon_F, E_n}, \quad (21.80)$$

$$\begin{aligned} \sigma_{xy} &= \frac{q^2(h_1 v_F)^2 \operatorname{sgn}(qh)}{\pi} 2 \left(1 + 2 \sum_{l=1}^{\infty} \theta(\varepsilon_F - E_l) \right) \\ &= \frac{q^2(h_1 v_F)^2 \operatorname{sgn}(qh)}{\pi} \times 2(1 + 2n) \theta(\varepsilon_F - E_n) \theta(E_{n+1} - \varepsilon_F), \end{aligned} \quad (21.81)$$

where the Landau level index runs $n = 0, 1, \dots$. It can be estimated as $n = [\frac{k_F^2}{2|qh|}]$ when $v_F \neq 0$ ($[\]$ denotes the integer part), with the average spacing between the Landau levels given by the Landau energy $v_F \sqrt{2|qh|}$. Note that $\varepsilon_F \equiv \varepsilon_F(h)$. We can see that (21.81) expresses the integer quantum Hall effect (IQHE). At zero temperature, as we dial the magnetic field, the Hall conductivity jumps from one quantized level to another, forming plateaus given by the filling factor

$$\nu_h = \pm 2(1 + 2n) = \pm 4 \left(n + \frac{1}{2} \right), \quad (21.82)$$

with $n = 0, 1, \dots$ (Compare to the conventional Hall quantization $\nu_h = \pm 4n$, that appears in thick graphene.) Plateaus of the Hall conductivity at $T = 0$ follow from the stepwise behavior of the charge density ρ in (21.77):

$$\rho \sim 4 \left(n + \frac{1}{2} \right) \theta(\varepsilon_F - E_n) \theta(E_{n+1} - \varepsilon_F), \quad (21.83)$$

where n Landau levels are filled and contribute to ρ . The longitudinal conductivity vanishes except precisely at the transition point between the plateaus. In Fig. 21.11, we plot the longitudinal and Hall conductivities at $T = 0$, using only the terms after $\times \operatorname{sign}$ in (21.79). In the Hall conductivity, plateau transition occurs when the Fermi level (in Fig. 21.11) of the first Fermi surface $\varepsilon_F = v_F(h)k_F(h)$ (Fig. 21.9) crosses the Landau level energy as we vary the magnetic field. By decreasing the magnetic field, the plateaus become shorter and increasingly more Landau levels contribute to the Hall conductivity. This happens because of two factors: the Fermi level moves

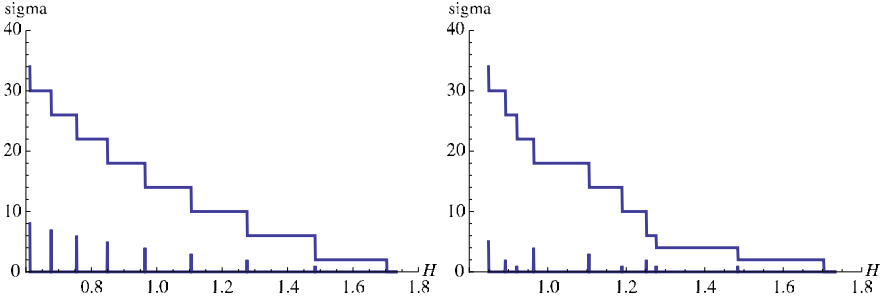


Fig. 21.11 Hall conductivity σ_{xy} and longitudinal conductivity σ_{xx} vs. the magnetic field $h \rightarrow H$ at $T = 0$ (we set $g_F = 1, q = \frac{15}{\sqrt{3}}$). *Left panel* is for IQHE. *Right panel* is for FQHE. At strong magnetic fields, the Hall conductivity plateau $\nu_h = 4$ appears together with plateaus $\nu_h = 2$ and $\nu_h = 6$ in FQHE (details are in [27]). Irregular pattern in the length of the plateaus for FQHE is observed in experiments on thin films of graphite at strong magnetic fields [28]

up and the spacing between the Landau levels becomes smaller. This picture does not depend on the Fermi velocity as long as it is nonzero.

21.6.2 Fractional Quantum Hall Effect

In [27], using the holographic description of fermions, we obtained the filling factor at strong magnetic fields

$$\nu_h = \pm 2j, \tag{21.84}$$

where j is the effective Landau level index. Equation (21.84) expresses the fractional quantum Hall effect (FQHE). In the quasiparticle picture, the effective index is integer $j = 0, 1, 2, \dots$, but generally it may be fractional. In particular, the filling factors $\nu = 2/m$ where $m = 1, 2, 3, \dots$ have been proposed by Halperin [35] for the case of bound electron pairs, i.e. $2e$ -charge bosons. Indeed, QED becomes effectively confining in ultraquantum limit at strong magnetic field, and the electron pairing is driven by the Landau level quantization and gives rise to $2e$ bosons. In our holographic description, quasiparticles are valid degrees of freedom only for $\nu > 1/2$, i.e. for weak magnetic field. At strong magnetic field, poles of the fermion propagator should be taken into account in calculation of conductivity. This will probably result in a fractional filling factor. Our pattern for FQHE Fig. 21.11 resembles the one obtained by Kopelevich in Fig. 3 [36] which has been explained using the fractional filling factor of Halperin [35].

The somewhat regular pattern behind the irregular behavior can be understood as a consequence of the appearance of a new energy scale: the average distance between the Fermi levels. For the case of Fig. 21.11, we estimate it to be $\langle \varepsilon_F^{(m)} - \varepsilon_F^{(m+1)} \rangle = 4.9$ with $m = 1, 2$. The authors of [30] explain the FQHE through the

opening of a gap in the quasiparticle spectrum, which acts as an order parameter related to the particle-hole pairing and is enhanced by the magnetic field (magnetic catalysis). Here, the energy gap arises due to the participation of multiple Fermi surfaces.

A pattern for the Hall conductivity that is strikingly similar to Fig. 21.11 arises in the AA and AB-stacked bilayer graphene, which has different transport properties from the monolayer graphene [37], compare with Figs. 2, 5 there. It is remarkable that the bilayer graphene also exhibits the insulating behavior in a certain parameter regime. This agrees with our findings of metal-insulating transition in our system.

21.7 Conclusions

We have studied strongly coupled electron systems in the magnetic field focussing on the Fermi level structure, using the AdS/CFT correspondence. These systems are dual to Dirac fermions placed in the background of the electrically and magnetically charged AdS-Reissner-Nordström black hole. At strong magnetic fields the dual system “lives” near the black hole horizon, which substantially modifies the Fermi level structure. As we dial the magnetic field higher, the system exhibits the non-Fermi liquid behavior and then crosses back to the conformal regime. In our analysis we have concentrated on the Fermi liquid regime and obtained the dependence of the Fermi momentum k_F and Fermi velocity v_F on the magnetic field. Remarkably, k_F exhibits the square root behavior, with v_F staying close to the speed of light in a wide range of magnetic fields, while it rapidly vanishes at a critical magnetic field which is relatively high. Such behavior indicates that the system may have a phase transition.

The magnetic system can be rescaled to a zero-field configuration which is thermodynamically equivalent to the original one. This simple result can actually be seen already at the level of field theory: the additional scale brought about by the magnetic field does not show up in thermodynamic quantities meaning, in particular, that the behavior in the vicinity of quantum critical points is expected to remain largely uninfluenced by the magnetic field, retaining its conformal invariance. In the light of current condensed matter knowledge, this is surprising and might in fact be a good opportunity to test the applicability of the probe limit in the real world: if this behavior is not seen, this suggests that one has to include the backreaction to metric to arrive at a realistic description.

In the field theory frame, we have calculated the DC conductivity using k_F and v_F values extracted from holography. The holographic calculation of conductivity that takes into account the fermions corresponds to the corrections of subleading order in $1/N$ in the field theory and is very involved [17]. As we are not interested in the vertex renormalization due to gravity (it does not change the magnetic field dependence of the conductivity), we have performed our calculations directly in the field theory with AdS gravity-dressed fermion propagators. Instead of controlling the occupancy of the Landau levels by changing the chemical potential (as is usual

in non-holographic setups), we have controlled the filling of the Landau levels by varying the Fermi energy level through the magnetic field. At zero temperature, we have reproduced the integer QHE of the Hall conductivity, which is observed in graphene at moderate magnetic fields. While the findings on equilibrium physics (Landau quantization, magnetic phase transitions and crossovers) are within expectations and indeed corroborate the meaningfulness of the AdS/CFT approach as compared to the well-known facts, the detection of the QHE is somewhat surprising as the spatial boundary effects are ignored in our setup. We plan to address this question in further work.

Interestingly, at large magnetic fields we obtain the correct formula for the filling factor characteristic for FQHE. Moreover our pattern for FQHE resembles the one obtained in [36] which has been explained using the fractional filling factor of Halperin [35]. In the quasiparticle picture, which we have used to calculate Hall conductivity, the filling factor is integer. In our holographic description, quasiparticles are valid degrees of freedom only at weak magnetic field. At strong magnetic field, the system exhibits non-Fermi liquid behavior. In this case, the poles of the fermion propagator should be taken into account to calculate the Hall conductivity. This can probably result in a fractional filling factor. We leave it for future work.

Notably, the AdS-Reissner-Nordström black hole background gives a vanishing Fermi velocity at high magnetic fields. It happens at the point when the IR conformal dimension of the corresponding field theory is $\nu = \frac{1}{2}$, which is the borderline between the Fermi and non-Fermi liquids. Vanishing Fermi velocity was also observed at high enough fermion charge [24]. As in [24], it is explained by the red shift on the gravity side, because at strong magnetic fields the fermion wavefunction is supported near the black hole horizon modifying substantially the Fermi velocity. In our model, vanishing Fermi velocity leads to zero occupancy of the Landau levels by stable quasiparticles that results in vanishing regular Fermi liquid contribution to the Hall conductivity and the longitudinal conductivity. The dominant contribution to both now comes from the non-Fermi liquid and conformal contributions. We associate such change in the behavior of conductivities with a metal-“strange metal” phase transition. Experiments on highly oriented pyrolytic graphite support the existence of a finite “offset” magnetic field h_c at $T = 0$ where the resistivity qualitatively changes its behavior [38–41]. At $T \neq 0$, it has been associated with the metal-semiconducting phase transition [38–41]. It is worthwhile to study the temperature dependence of the conductivity in order to understand this phase transition better.

Acknowledgements The work was supported in part by the Alliance program of the Helmholtz Association, contract HA216/EMMI “Extremes of Density and Temperature: Cosmic Matter in the Laboratory” and by ITP of Goethe University, Frankfurt (E. Gubankova), by a VIDI Innovative Research Incentive Grant (K. Schalm) from the Netherlands Organization for Scientific Research (NWO), by a Spinoza Award (J. Zaanen) from the Netherlands Organization for Scientific Research (NWO) and the Dutch Foundation for Fundamental Research of Matter (FOM). K. Schalm thanks the Galileo Galilei Institute for Theoretical Physics for the hospitality and the INFN for partial support during the completion of this work.

References

1. J. Zaanen, Quantum critical electron systems: the uncharted sign worlds. *Science* **319**, 1205 (2008)
2. P. de Forcrand, Simulating QCD at finite density. PoS **LAT2009**, 010 (2009). [arXiv:1005.0539](#) [hep-lat]
3. S.A. Hartnoll, J. Polchinski, E. Silverstein, D. Tong, Towards strange metallic holography. *J. High Energy Phys.* **1004**, 120 (2010). [arXiv:0912.1061](#) [hep-th]
4. P. Kovtun, D.T. Son, A.O. Starinets, Viscosity in strongly interacting quantum field theories from black hole physics. *Phys. Rev. Lett.* **94**, 111601 (2005). [arXiv:hep-th/0405231](#)
5. S.-S. Lee, A non-Fermi liquid from a charged black hole: a critical Fermi ball. *Phys. Rev. D* **79**, 086006 (2009). [arXiv:0809.3402](#) [hep-th]
6. M. Čubrović, J. Zaanen, K. Schalm, String theory, quantum phase transitions and the emergent Fermi-liquid. *Science* **325**, 439 (2009). [arXiv:0904.1993](#) [hep-th]
7. H. Liu, J. McGreevy, D. Vegh, Non-Fermi liquids from holography. *Phys. Rev. D* **83**, 065029 (2011). [arXiv:0903.2477](#) [hep-th]
8. T. Faulkner, H. Liu, J. McGreevy, D. Vegh, Emergent quantum criticality, Fermi surfaces, and AdS₂. *Phys. Rev. D* **83**, 125002 (2011). [arXiv:0907.2694](#) [hep-th]
9. S.A. Hartnoll, A. Tavanfar, Electron stars for holographic metallic criticality. *Phys. Rev. D* **83**, 046003 (2011). [arXiv:1008.2828](#) [hep-th]
10. S.A. Hartnoll, P.K. Kovtun, M. Mueller, S. Sachdev, Theory of the Nernst effect near quantum phase transitions in condensed matter, and in dyonic black holes. *Phys. Rev. B* **76**, 144502 (2007). [arXiv:0706.3215](#) [hep-th]
11. S.A. Hartnoll, P. Kovtun, Hall conductivity from dyonic black holes. *Phys. Rev. D* **76**, 066001 (2007). [arXiv:0704.1160](#) [hep-th]
12. P. Basu, J.Y. He, A. Mukherjee, H.-H. Shieh, Holographic non-Fermi liquid in a background magnetic field. [arxiv:0908.1436](#) [hep-th]
13. T. Albash, C.V. Johnson, Landau levels, magnetic fields and holographic Fermi liquids. *J. Phys. A, Math. Theor.* **43**, 345404 (2010). [arXiv:1001.3700](#) [hep-th]
14. T. Albash, C.V. Johnson, Holographic aspects of Fermi liquids in a background magnetic field. *J. Phys. A, Math. Theor.* **43**, 345405 (2010). [arXiv:0907.5406](#) [hep-th]
15. T. Albash, C.V. Johnson, A holographic superconductor in an external magnetic field. *J. High Energy Phys.* **0809**, 121 (2008). [arXiv:0804.3466](#) [hep-th]
16. N. Iqbal, H. Liu, M. Mezei, Q. Si, Quantum phase transitions in holographic models of magnetism and superconductors. [arXiv:1003.0010](#) [hep-th]
17. T. Faulkner, N. Iqbal, H. Liu, J. McGreevy, D. Vegh, From black holes to strange metals. [arXiv:1003.1728](#) [hep-th]
18. E. D'Hoker, P. Kraus, *J. High Energy Phys.* **1005**, 083 (2010). [arXiv:1003.1302](#) [hep-th]
19. A. Auerbach, Quantum magnetism approaches to strongly correlated electrons. [arxiv:cond-mat/9801294](#)
20. E. Gubankova, Particle-hole instability in the *AdS₄* holography. [arXiv:1006.4789](#) [hep-th]
21. J.L. Davis, P. Kraus, A. Shah, Gravity dual of a quantum hall plateau transition. *J. High Energy Phys.* **0811**, 020 (2008). [arXiv:0809.1876](#) [hep-th]
22. E. Keski-Vakkuri, P. Kraus, Quantum Hall effect in AdS/CFT. *J. High Energy Phys.* **0809**, 130 (2008). [arXiv:0805.4643](#) [hep-th]
23. A.H. MacDonald, Introduction to the physics of the quantum Hall regime. [arXiv:cond-mat/9410047](#)
24. T. Hartman, S.A. Hartnoll, Cooper pairing near charged black holes. [arXiv:1003.1918](#) [hep-th]
25. F. Denef, S.A. Hartnoll, S. Sachdev, Quantum oscillations and black hole ringing. *Phys. Rev. D* **80**, 126016 (2009). [arXiv:0908.1788](#) [hep-th]
26. F. Denef, S.A. Hartnoll, S. Sachdev, Black hole determinants and quasinormal modes. *Class. Quant. Grav.* **27**, 125001 (2010). [arXiv:0908.2657](#) [hep-th]

27. E. Gubankova, J. Brill, M. Cubrovic, K. Schalm, P. Schijven, J. Zaanen, Holographic fermions in external magnetic fields. *Phys. Rev. D* **84**, 106003 (2011). [arXiv:1011.4051](#) [hep-th]
28. Y. Zhang, Z. Jiang, J.P. Small, M.S. Purewal, Y.-W. Tan, M. Fazlollahi, J.D. Chudow, J.A. Jaszczak, H.L. Stormer, P. Kim, Landau level splitting in graphene in high magnetic fields. *Phys. Rev. Lett.* **96**, 136806 (2006). [arXiv:cond-mat/0602649](#)
29. J.L. Noronha, I.A. Shovkovy, Color-flavor locked superconductor in a magnetic field. *Phys. Rev. D* **76**, 105030 (2007). [arXiv:0708.0307](#) [hep-ph]
30. V.P. Gusynin, S.G. Sharapov, Transport of Dirac quasiparticles in graphene: Hall and optical conductivities. *Phys. Rev. B* **73**, 245411 (2006). [arXiv:cond-mat/0512157](#)
31. E.V. Gorbar, V.A. Miransky, I.A. Shovkovy, Dynamics in the normal ground state of dense relativistic matter in a magnetic field. *Phys. Rev. D* **83**, 085003 (2011). [arXiv:1101.4954](#) [hep-th]
32. M.A.V. Basagoiti, Transport coefficients and ladder summation in hot gauge theories. *Phys. Rev. D* **66**, 045005 (2002). [arXiv:hep-ph/0204334](#)
33. J.M.M. Resco, M.A.V. Basagoiti, Color conductivity and ladder summation in hot QCD. *Phys. Rev. D* **63**, 056008 (2001). [arXiv:hep-ph/0009331](#)
34. N. Iqbal, H. Liu, Real-time response in AdS/CFT with application to spinors. *Fortschr. Phys.* **57**, 367 (2009). [arXiv:0903.2596](#) [hep-th]
35. B.I. Halperin, *Helv. Phys. Acta* **56**, 75 (1983)
36. Y. Kopelevich, B. Raquet, M. Goiran, W. Escoffier, R.R. da Silva, J.C. Medina Pantoja, I.A. Luk'yanchuk, A. Sinchenko, P. Monceau, Searching for the fractional quantum Hall effect in graphite. *Phys. Rev. Lett.* **103**, 116802 (2009)
37. Y.-F. Hsu, G.-Y. Guo, Anomalous integer quantum Hall effect in AA-stacked bilayer graphene. *Phys. Rev. B* **82**, 165404 (2010). [arXiv:1008.0748](#) [cond-mat]
38. Y. Kopelevich, V.V. Lemanov, S. Moehlecke, J.H.S. Torrez, Landau level quantization and possible superconducting instabilities in highly oriented pyrolytic graphite. *Fiz. Tverd. Tela* **41**, 2135 (1999) [*Phys. Solid State* **41**, 1959 (1999)]
39. H. Kempa, Y. Kopelevich, F. Mrowka, A. Setzer, J.H.S. Torrez, R. Hoehne, P. Esquinazi, *Solid State Commun.* **115**, 539 (2000)
40. M.S. Sercheli, Y. Kopelevich, R.R. da Silva, J.H.S. Torrez, C. Rettori, *Solid State Commun.* **121**, 579 (2002)
41. Y. Kopelevich, P. Esquinazi, J.H.S. Torres, R.R. da Silva, H. Kempa, F. Mrowka, R. Ocana, Metal-insulator-metal transitions, superconductivity and magnetism in graphite. *Stud. H-Temp. Supercond.* **45**, 59 (2003). [arXiv:cond-mat/0209442](#)

Regimes of stability and scaling relations for the removal time in the asteroid belt: a simple kinetic model and numerical tests

Mihailo Čubrović

Department of Astronomy – Petnica Science Center, P. O. B. 6, 14104 Valjevo, Serbia and Montenegro
email: cygnus@EUnet.yu

Abstract. We report on our theoretical and numerical results concerning the transport mechanisms in the asteroid belt. We first derive a simple kinetic model of chaotic diffusion and show how it gives rise to some simple correlations (but not laws) between the removal time (the time for an asteroid to experience a qualitative change of dynamical behavior and enter a wide chaotic zone) and the Lyapunov time. The correlations are shown to arise in two different regimes, characterized by exponential and power-law scalings. We also show how is the so-called “stable chaos” (exponential regime) related to anomalous diffusion. Finally, we check our results numerically and discuss their possible applications in analyzing the motion of particular asteroids.

Keywords. Minor planets, asteroids; diffusion; celestial mechanics; methods: analytical

1. Introduction

Despite some important breakthroughs in the research of transport mechanisms in the Solar system in the past decade, we still lack a general *quantitative* theory of chaotic transport, which is especially notable for the so-called stable chaotic bodies. In this paper, we sketch a new kinetic approach, which, in our opinion, has a perspective of providing us such a theory sometime in the future.

A kinetic model of transport has already been proposed by Murray & Holman (1997). Although it is an important step forward, this model fails to include a number of important effects. We also wish to emphasize the role of phase space topology in the transport processes. This has only recently been understood in papers by Tsiganis, Varvoglis & Hadjidemetriou (2000, 2002a, 2002b). Still, the exact role of cantori and stability islands in various resonances remains unclear. This is one of the issues we intend to explore in this paper. We argue that, due to the inhomogenous nature of the phase space, a separate kinetic equation for each transport mechanism should be constructed; after that, one can combine them to obtain the description of long-time evolution. This is the basic idea of our approach, which leads to some interesting statistical consequences, such as anomalous diffusion and approximate scaling of removal times with Lyapunov times.

2. The kinetic scheme

In order to model the transport, we use the “building block approach” we have recently developed for Hamiltonian kinetics (Čubrović 2004). We use the Fractional Kinetic Equation (FKE), a natural generalization of the diffusion equation for self-similar and strongly

inhomogenous media (e. g. Zaslavsky 2002):

$$\frac{\partial^\beta f(I, t)}{\partial t^\beta} = \frac{\partial^\alpha}{\partial |I|^\alpha} [\mathcal{D}(I) f(I, t)] \quad (2.1)$$

Thus, the evolution of the distribution function $f(I, t)$ is governed by the transport coefficient \mathcal{D} (the generalization of the diffusion coefficient) and by the (non-integer, in general) order of the derivatives α ($0 < \alpha \leq 2$) and β ($0 < \beta \leq 1$). The quantity $\mu \equiv 2\beta/\alpha$ is called the transport exponent (for the second moment the following holds asymptotically: $\langle \Delta I^2 \rangle \propto t^\mu$). If $\mu \neq 1$, the transport is called anomalous (in contrast to normal transport or normal diffusion[†]).

We shall now very briefly describe each of the four building blocks; unfortunately, most expressions are cumbersome and complicated, so we limit ourselves in this paper to merely state the basic ideas and final results of the method. We use the planar MMR Hamiltonians $H_{2BR} = H_{2BR}^0 + H'_{2BR}$ and $H_{3BR} = H_{3BR}^0 + H'_{3BR}$ for two- and three-body resonances, taken from Murray, Holman & Potter (1998) and Nesvorný & Morbidelli (1998), respectively. Under H^0 we assume the action-only part of the Hamiltonian. H_{2BR} was modified to account for the purely secular terms; also, both Hamiltonians were modified to include the proper precessions of Jupiter and Saturn[‡]:

$$H'_{2BR} = \sum_{m=0,1; s=0 \dots k_J - k}^{u_5, u_6} c_{msu_5u_6} \cos [m(k_J \lambda_J - k \lambda) + sp + (u_5 g_5 + u_6 g_6) t + u_5 \beta_J + u_6 \beta_S] \quad (2.2)$$

$$H'_{3BR} = \sum_{m=0,1; s}^{u_5, u_6} c_{msu_5u_6} \cos [m(k_J \lambda_J + k_S \lambda_S + k \lambda) + sp + (u_5 g_5 + u_6 g_6) t + u_5 \beta_J + u_6 \beta_S] \quad (2.3)$$

The notation is usual. In H'_{2BR} , we include all possible harmonics; in H'_{3BR} , we include only those given in Nesvorný & Morbidelli (1998). In what follows, we shall consider only the diffusion in eccentricity, i. e. P Delaunay variable. Inclusion of the inclination could be important but we postpone it for further work.

We estimate the transport coefficient as:

$$\mathcal{D} = \frac{T_{lib}^{(\alpha-\beta)}}{2} \sum_s s^\alpha P^{s\alpha} \left(\sum_{u_5, u_6} c'_{0su_5u_6}(\alpha) + j c'_{1su_5u_6}(\alpha) \right) \quad (2.4)$$

where T_{lib} denotes the libration period while $c'_{msu_5u_6}$ are coefficients dependent on the exponent α from (2.1), independent on angles and P , which were computed using the algorithm from Ellis & Murray (2000), for H_{2BR} , or taken from Nesvorný & Morbidelli (1998), for H_{3BR} . The indicator j can be equal to 0 or 1 (i. e. omission or inclusion of the resonant terms), depending on the building block (see below). Although we were able to compute also the higher-order corrections to this quasilinear result in some cases, we neglect them in what follows, in order to be able to solve the FKE analytically.

[†] From now on, we will refer to any transport in the phase space (i. e. evolution of the momenta of the action I) as to “diffusion”; for the “classical” diffusion, we shall use the term “normal diffusion”.

[‡] All our computations, analytical and numerical, are performed with the osculating elements, in order to gain as much simplification as possible. However, in order to avoid the non-diffusive oscillations of the osculating elements, one should use the proper elements instead; we plan to do this in the future.

The first class of building blocks we consider are the overlapping stochastic layers of subresonances. In this case, one expects a free, quasi-random walk continuous in both time and space, since no regular structures are preserved. Therefore, the FKE simplifies to the usual diffusion equation, i. e. we have $\alpha = 2$, $\beta = 1$ in (2.4); also, $j = 1$ (the resonant harmonics are actually the most important ones).

The above reasoning is only valid if the overlapping of subresonances is not much smaller than 1. Otherwise, the diffusion can only be forced by the secular terms. Also, long intervals between subsequent “jumps” induce the so-called “erratic time”, i. e. β can be less than 1, its value being determined by the distribution of time intervals between “jumps” $p(\Delta t) = 1/\Delta t^{1+\beta}$. So, the transport coefficient (2.4) now has $j = 0$, $\alpha = 2$ and $\beta < 1$.

Our third class of building blocks are the resonant stability islands. To estimate β we use the same idea as in the previous case; after that, we compute α from β and μ , the transport exponent, which we deduce using the method developed in Afraimovich & Zaslavsky (1997). Namely, analytical and numerical studies strongly suggest a self-similar structure characterized by a power-law scaling of trapping times λ_T , island surfaces λ_S and number of islands λ_N at each level. The transport exponent is then equal to $\lambda_N \lambda_S / \lambda_T$. For some resonances and for some island chains, we computed the scaling exponents applying the renormalization of the resonant Hamiltonian as explained in Zaslavsky (2002); in the cases when we did not know how to do this, we used the relation between the transport exponent and the fractal dimension d_T of the trajectory in the (P, p) space (the space spanned by the action P and the conjugate angle p), which is actually the dimension of the Poincare section of the trajectory:

$$d_T = \frac{2\lambda_T}{\lambda_N \lambda_S} \quad (2.5)$$

The last remaining class of blocks are cantori. Here, we assume the scaling of gap area on subsequent levels with exponent λ_S and an analogous scaling in trapping probability with exponent λ_p , which determines the transport exponent as $2 \ln \lambda_p / \ln \lambda_S$; see also the reasoning from Shevchenko (1998). The scaling exponents were estimated analogously to the previous case.

For each building block, we construct a kinetic equation and solve it. We always put a reflecting barrier at zero eccentricity and an absorbing barrier at the Jupiter-crossing eccentricity. The solution in Fourier space (q, t) can be written approximately in the following general form:

$$f_i(q, t) = E_\beta(-|q^\alpha| \star \hat{\mathcal{D}}_i t^\beta) \quad (2.6)$$

where E_β stands for the Mittag-Leffler function and $\hat{\mathcal{D}}_i$ denotes the Fourier transform of \mathcal{D}_i . The index i denotes a particular building block. The key to obtaining the global picture is to perform a convolution of the solutions for all the building blocks. Furthermore, one must take into account that the object can start in different blocks and also that, sometimes, different ordering of the visited blocks is possible. Therefore, one has the following sum over all possible variations of blocks (we call it Equation of Global Evolution - EGE):

$$f(P, t) = \sum [p_1 f_1(P, t) \star p_2 f_2(P, t) \star \dots \star p_i f_i(P, t) \star \dots] \quad (2.7)$$

To calculate it, one has to know also the transition probabilities p_i , which is not possible to achieve solely by the means of analytic computations. That is why we turn again to semi-analytic results.

3. Removal times, Lyapunov times and $T_L - T_R$ correlations

The first task is to determine the relevant building blocks and transitional probabilities. We do that by considering the overviews of various resonances as given in Morbidelli & Moons (1993), Moons & Morbidelli (1995), Moons, Morbidelli & Migliorini (1998). For the resonances not included in these references, we turn again to the inspection of Poincare surfaces of section, integrating the resonant models (2.2) and (2.3). In this case, the probabilities are estimated as the relative measures of the corresponding trajectories on the surface of section.

The result of solving the EGE is again a Mittag-Leffler function:

$$f_{global}(q, t) = E_\gamma(-|q|^\delta t^\gamma) \quad (3.1)$$

The asymptotic behavior of this function, described e. g. in Zaslavsky (2002), has two different forms: the exponential one and the power-law one, depending on the coefficients γ and δ , which are determined by the probabilities p_i and transport coefficients and exponents of the building blocks. In the small γ limit, the behavior is exponential and the second momentum scales with τ_{cross} , where τ_{cross} is the timescale of crossing a single subresonance, which we interpret as the Lyapunov time[†]. When γ becomes large and the role of stickiness more or less negligible, one gets a power-law dependance on τ_{cross} , i. e. T_L . So, we have the expressions:

$$T_R \propto \exp(T_L^x) \Phi(\Lambda_0, \cos(\ln P_0), Q_0) \quad (3.2)$$

for the exponential or stable chaotic regime, and:

$$T_R \propto (T_L^y) \Phi(\Lambda_0, \cos(\ln P_0), Q_0) \quad (3.3)$$

for the power-law regime. The scalings are not exact because the fluctuational terms $\Phi(\Lambda_0, P_0, Q_0)$ appear. These terms are log-periodic in P_0 and can explain the log-normal tails of the T_R distribution, detected numerically e. g. in Tsiganis, Varvoglis & Hadjidemetriou (2000).

4. Results for particular resonances

We plan to do a systematic kinetic survey of all the relevant resonances in the asteroid belt. Up to now, we have only preliminary results for some resonances.

Table 1 sums up our results for all the resonances we have explored. For each resonance, we give our analytically calculated estimates for T_L and T_R . We always give a range of values, obtained for various initial conditions inside the resonance. If the “mixing” of the phase space is very prominent, we sometimes get a very wide range, which includes both normal and stable chaotic orbits. One should note that the “errorbars” in the plot are simply the intervals of computed values – they do not represent the numerical errors. We also indicate if the resonance has a resonant periodic orbit, which is, according to Tsiganis, Varvoglis & Hadjidemetriou (2002b), the key property for producing the *fast* chaos[‡]. Bulirsch-Stoer integrator with Jupiter and Saturn as perturbers was used for the integrations.

We have also tried to deduce the age of the Veritas family, whose most chaotic part lies inside the 5 – 2 – 2 resonance. Our EGE gives an approximate age about 9 Myr while, assuming a constant diffusion coefficient (Knežević, personal communication), one gets

[†] One should bear in mind that this is just an approximation; strictly speaking, Lyapunov time is not equal, nor simply related to the subresonance crossing time.

[‡] The existence of the periodic orbit for 13 : 6 and 18 : 7 resonances has not been checked thus far; however, we think this would be highly unlikely for such high-order resonances

Table 1. Analytical and numerical values of the Lyapunov time (in Kyr) and removal time (in Myr). Existence of the periodic orbit in the planar problem for the 2BR is also indicated; the data in this column were taken from Tsiganis, Varvoglis & Hadjidemetriou (2002b).

| Resonance | T_L (Kyr) | T_L^{Num} (Kyr) | T_R (Myr) | T_R^{Num} (Myr) | Per. orbit ? |
|-----------|---------------|-------------------|----------------------|---------------------|--------------|
| 2 : 1 | 1.1–3.4 | 2.9–5.2 | 0.8–19.4 | 1.1–31.2 | Yes |
| 3 : 2 | 1.4–3.5 | 3.1–6.2 | 0.9–19.1 | 3.2–142.7 | Yes |
| 3 : 1 | 6.2–8.2 | 6.8–9.4 | 0.8–8.0 | 1.0–21.2 | Yes |
| 5 : 3 | 1.9–2.2 | 1.1–3.5 | 0.9–4.1 | 0.8–7.4 | Yes |
| 5 : 2 | 6.9–9.2 | 8.3–14.4 | 7.6–13.4 | 9.2–28.7 | Yes |
| 7 : 4 | 2.7–5.3 | 1.8–3.9 | 6.9–23.4 | 12.2–41.3 | Yes |
| 8 : 5 | 3.7–6.7 | 4.1–7.6 | 8.2–18.2 | 7.3–23.4 | No |
| 7 : 3 | 5.0–6.9 | 6.9–9.1 | 16.7–62.2 | 22.4–91.2 | No |
| 9 : 5 | 5.4–6.8 | 3.1–5.2 | 23.2–86.7 | 11.3–104.2 | No |
| 11 : 7 | 7.1–14.1 | 3.4–9.7 | 10.6–73.4 | 8.4–88.2 | Yes |
| 11 : 6 | 10.8–22.7 | 10.1–16.5 | 16.4–330.3 | 13.2– \approx 500 | No |
| 12 : 7 | 11.1–14.7 | 4.1–15.2 | 4.6–278.1 | 5.2– \approx 1000 | No |
| 13 : 7 | 65.1–84.6 | 43.3–76.1 | 23.2– \approx 1000 | 14.2– $>$ 1000 | No |
| 13 : 6 | 55.1–77.6 | 14.6–24.5 | 41.3– \approx 1000 | 21.1– $>$ 1000 | No |
| 18 : 7 | \approx 500 | 300–600 | \approx 20000 | $>$ 1000 | No |
| 5 – 2 – 2 | 11.4–13.7 | 8.4–10.9 | \approx 10000 | $>$ 1000 | No |
| 2 + 2 – 1 | 90–160 | 130–240 | \approx 20000 | $>$ 1000 | No |
| 6 + 1 – 3 | 130–150 | 130–170 | \approx 40000 | $>$ 1000 | No |

about 8.3 Myr. The similarity is probably due to the young age of the family: were it older, the effects of non-linearity would prevail and our model would give an age estimate which is substantially different from that obtained in a linear approximation.

Figure 1 gives the results from table 1 plotted along the semimajor axis. It can be noted that the agreement is good within an order of magnitude, with some exceptions. Actually, one can see that the disagreement with the simulations is most significant exactly in the resonances with a periodic orbit, which might actually require a completely different treatment of transport.

In Figure 2, we plot the numerical $T_L - T_R$ relation for the resonances 5 : 3 and 12 : 7, examples of normal and stable chaos, respectively. The largest discrepancies in the Figure 2a are probably for objects near the stability islands; in the Figure 2b, the fit fails completely. To check the assumption that this is due to the mixing of populations, we integrate a larger population of objects and divide them into two classes (the criterion being the prominence of anomalous diffusion, see later). For each class, we perform a separate fit with the corresponding $T_L - T_R$ relation. Now most objects can be classified into one of the two scaling classes. In particular, this shows that the famous stable-chaotic object 522 Helga is probably not a remnant of some larger initial population but rather a member of one of the two populations existing in this resonance.

Finally, in Figure 4, we give the time evolution of the dispersion in P (i. e. $\langle \Delta P^2 \rangle$) for a set of clones of 522 Helga, using the procedure described in Tsiganis, Anastasiadis & Varvoglis (2000). Anomalous diffusion is clearly visible. This confirms the stable chaotic nature of this object and shows that we can use the anomalous character of diffusion as an indicator of stable chaos.

5. Conclusions and discussion

We have given a kinetic model of chaotic transport in the asteroid belt, based on the concept of convolution of various building blocks. Combining numerical and analytical results, we have shown how the removal time can be calculated and interrelated with the

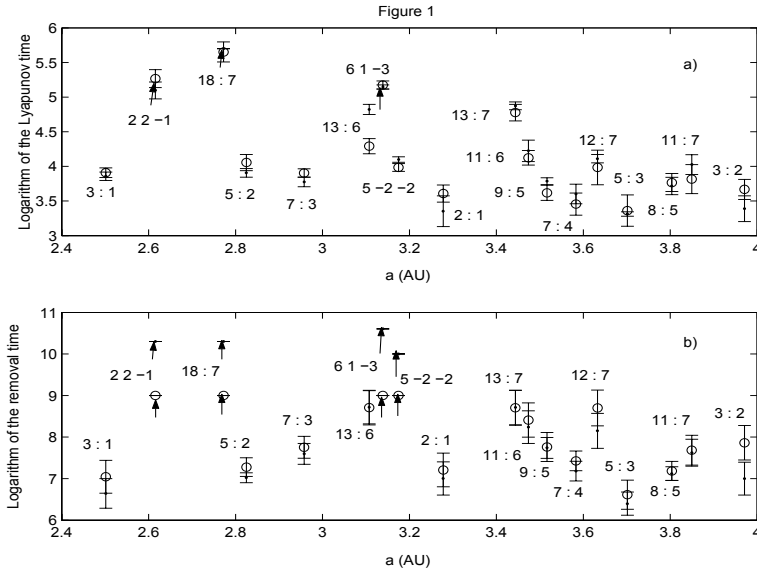


Figure 1. Analytical (points) and numerical (circles) values from table 1, for Lyapunov time (a) and removal time (b). Arrows correspond to extremely uncertain numerical values, usually the values close to or larger than the integration timespan (1 Gyr).

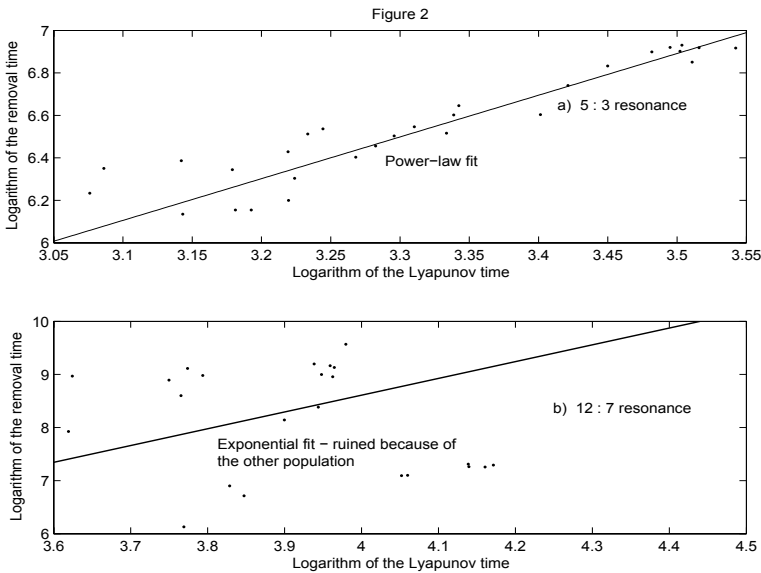


Figure 2. Plot of $T_L - T_R$ dependance for the resonances 5 : 3 (a), fit with a power-law, and 12 : 7 (b), fit with the exponential law. The straight line obtained by linear regression in the logarithmic scale is an obviously bad fit. See text for comments.

Lyapunov time. We have obtained two regimes for chaotic bodies, the power-law one and the exponential one. Due to the fractal structure of the phase space, however, asteroids from different regimes can be “mixed” in a small region of the phase space.

We would like to comment briefly on the controversial issue of the $T_L - T_R$ relation. First of all, the correlations we have found are *of statistical nature only* and should not

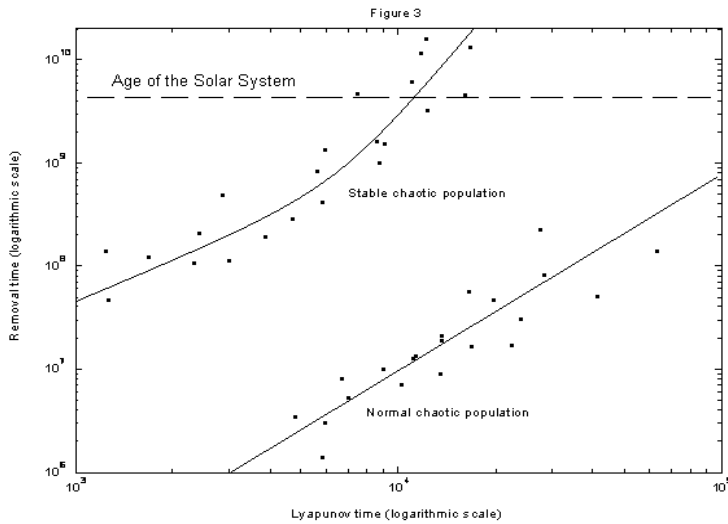


Figure 3. The same as in Figure 2b but with two separate plots for the exponential regime population, and for the power-law regime population. Obviously, we have a substantially better fit.

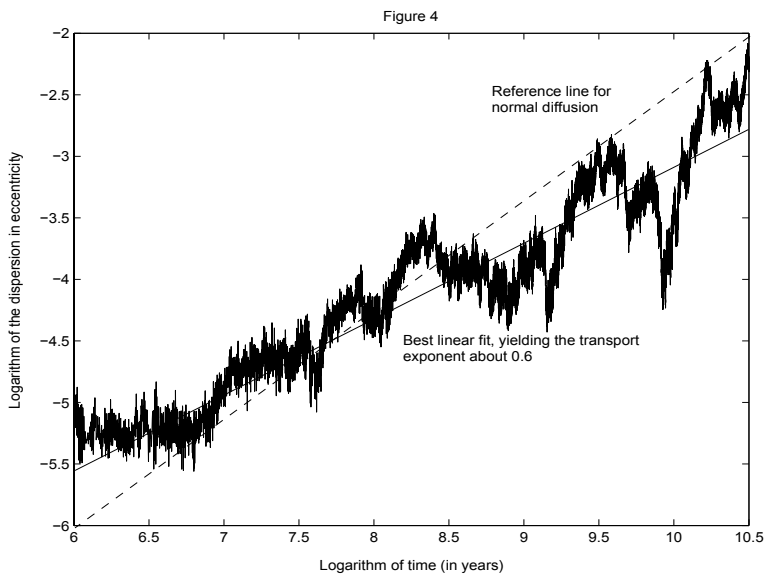


Figure 4. Diffusion in eccentricity for a set of clones of 522 Helga. Domination of anomalous transport is obvious. The reference line for normal diffusion ($\mu = 1$) is also plotted.

be regarded as “laws” in the sense of Murison, Lecar & Franklin (1994). Furthermore, due to their statistical nature, they cannot be used for any particular object, only for populations. Finally, it is clear that the scalings are *non-universal*, i. e. the scaling exponents are different for different resonances (possibly also in disconnected regions of a single resonance).

The exponential regime, characterized mainly by anomalous transport through various quasi-stable structures, corresponds to the stable chaotic regime, discussed e. g. in Tsiganis, Varvoglis & Hadjidemetriou (2000) and Tsiganis, Varvoglis & Hadjidemetriou (2002a). The reason that the exponential $T_L - T_R$ correlation was not noticed thus far are in part very large values of T_R in this regime, and in part the fact that stable chaotic objects are typically mixed with the objects in the normal chaotic regime. Also, it is interesting to note that the exponential scalings are of the same form as those predicted in Morbidelli & Froeschlé (1996) for the Nekhoroshev regime; therefore, it seems that the exponential stability can arise also due to stickyness, not necessarily as a consequence of the Nekhoroshev structure.

Finally, we hope that our research will stimulate further work in this field, since the results presented here are no more than just a sketch of possible general theory.

Acknowledgements

I am greatly indebted to Zoran Knežević for helpful discussions and for permission to cite his yet unpublished results. I am also grateful to George M. Zaslavsky, Harry Varvoglis and Alessandro Morbidelli for sending me copies of some of the references.

References

- Afraimovich, V. & Zaslavsky, G. M. 1997, *Phys. Rev. E* 55, 5418
 Čubrović M. 2004, in preparation.
 Ellis, K. M. & Murray, C. D. 2000, *Icarus* 147, 129
 Moons, M., Morbidelli, A. 1995, *Icarus* 114, 33
 Moons, M., Morbidelli, A. & Migliorini, F. 1998, *Icarus* 135, 458
 Morbidelli, A. & Froeschlé, C. 1996, *Cel. Mech. Dyn. Ast.* 63, 227
 Morbidelli, A., Moons, M. 1993, *Icarus* 102, 316
 Murison, M., Lecar, M. & Franklin, F. 1994, *Astron. J.* 108, 2323
 Murray, N. & Holman, M. 1997, *Astron. J.* 114, 1246
 Murray, N., Holman, M. & Potter, M. 1998, *Astron. J.* 116, 2583
 Nesvorný, D. & Morbidelli, A. 1998, *Cel. Mech. Dyn. Astron.* 71, 243
 Shevchenko, I. 1998, *Phys. Lett. A* 241, 53
 Tsiganis, K., Anastasiadis, A. & Varvoglis, H. 2000, *Cel. Mech. Dyn. Ast.* 78, 337
 Tsiganis, K., Varvoglis, H. & Hadjidemetriou, J. D. 2000, *Icarus* 146, 240
 Tsiganis, K., Varvoglis, H. & Hadjidemetriou, J. D. 2002a, *Icarus* 155, 454
 Tsiganis, K., Varvoglis, H. & Hadjidemetriou, J. D. 2002b, *Icarus* 159, 284
 Zaslavsky, G. M. 2002, *Phys. Rep.* 371, 461

FULLY ANALYTICAL KINETIC MODEL OF RESONANCE DYNAMICS IN THE SOLAR SYSTEM

MIHAILO ČUBROVIĆ^{1,2}

¹*Institute of Physics, P. O. B. 57, 11001 Belgrade, Serbia and Montenegro*

²*Department of Astronomy, Petnica Science Center,
P. O. B. 6, 14104 Valjevo, Serbia and Montenegro
E-mail: cygnus@EUnet.yu*

Abstract. We propose a fractional kinetic equation to model the transport in eccentricity of objects in the mean motion resonances in the Elliptic Planar Restricted Three-Body Problem. Making use of the renormalization group formalism, we show how the fractional exponents and the diffusion coefficient can be estimated analytically, making use of the degeneracy of the problem. We apply our model to selected Mean Motion Resonances in the Solar System and explain some basic properties of transport in these resonances.

1. INTRODUCTION

Kinetic models of chaotic transport in the Asteroid Belt have been proposed or discussed by a number of authors (Varvoglis and Anastasiadis, 1996; Murray and Holman, 1997; Tsiganis, Varvoglis and Hadjidemetriou, 2002). All of these models are based on a Fokker-Planck type equation ("normal" diffusion equation) for the eccentricity, which implicitly assumes the Gauss-Markovian statistics of the quasi-random walk in the eccentricity space. In order to incorporate the more general (and more realistic) case of Levy-type statistics (see, e.g., Zaslavsky, 2002), we have recently proposed a semi-analytical model (Čubrović, 2005a) based on the fractional kinetic equation – FKE (Zaslavsky, 2002). In this paper we give a fully analytical model.

We consider the transport in Mean Motion Resonances (MMR) of the Elliptic Planar Restricted Three-Body Problem (EPRTBP), and apply it on diffusion in the asteroid belt. The model we propose is, however, applicable to any EPRTBP Hamiltonian, and possibly also to a wider class of degenerate systems, which all have a similar structure of resonances.

2. THE MODEL OF TRANSPORT

Our model is the Hamiltonian for a q -th order two-body MMR, used, among others, by Murray and Holman (1997):

$$H_{MMR}(L, \lambda; P, p) = H_0(L) + \sum_s c_s(L) P^s \cos \sigma_s \quad (1)$$

with L , λ , $P = L(1 - \sqrt{1 - e^2})$, and $p = -\tilde{\omega}$ being the modified Delauney variables (defined as in Morbidelli 2002). In the above relations, e is eccentricity, and ω is the longitude of perihelion. Critical angles are denoted by σ_s . We assume that the transport only takes place along P (i.e., that the timescale of transport in L is much longer) and that a particle starts at $P = 0$, where we put a reflecting barrier, and escapes immediately after reaching a planet-crossing orbit ($P = P_{\text{cross}}$), where we put an absorbing barrier. The possible phase protection mechanisms are ignored.

Assuming a Levy-type statistics for the angles σ_s , one finds, after performing the averaging, that the master equation for the probability distribution function $f(P, t)$ leads to a multi-channel FKE:

$$\frac{\partial^\beta f(P, t)}{\partial t^\beta} = \sum_{s=1}^q \frac{\partial^{\alpha s}}{\partial |P|^{\alpha s}} [D_s(P) f(P, t)] \quad (2)$$

with the diffusion coefficients:

$$D_s = \frac{1}{2} c_s^{\alpha s} s^{\alpha s} P^{s^2 \alpha} T_{\text{Lib}}^{(\alpha - \beta)s} \quad (3)$$

where T_{Lib} denotes the libration period. Applying the separation ansatz and writing the time-independent part of the solution as a superposition of the time-independent parts of one-channel solutions (given in Čubrović, 2005b) for different values of s (which is justified by the linearity of FKE), one finds an estimate for the removal time and the Lyapunov time (for the latter from the FKE for the variational equations, which shares all the basic properties with (2)):

$$T_R \approx \left(\frac{P_0 P_{\text{cross}}}{D(L, P_0) D(L, P_{\text{cross}})} \right)^{1/\beta} \times \Phi \left(\alpha, \beta; L, P_0; \cos \left(\frac{\log P_0}{|\log \beta|} \right) \right) \quad (4)$$

$$T_{\text{Ly}} \approx 2 \frac{c_s(L)}{\|D\|} \quad (5)$$

where $\| \cdot \|$ denotes the standard Euclidean norm, and Φ is, in general, a complicated resonance-dependent function which, however, has an important property of log-periodicity.

A few interesting consequences follow from the above results. First, it is obvious that, for different values of P , different components D_s of the diffusion coefficient will prevail, leading to a stair-like behavior of the "effective" (e.g., numerically computed) diffusion coefficient. Furthermore, since the amplitude of log-periodic oscillations of Φ can be shown to grow with q (order of the resonance), the log-periodic oscillations

will be more and more significant for higher order resonances. Also, applying the Tauberian theorem for the Fourier transform, and making use of the generalized Central Limit Theorem (e.g., Weiss, 1994), one can show that two *approximate* scalings of T_R with T_{Ly} are possible: the power-law one and the stretched-exponential one (corresponding to the "stable chaos").

In order to actually compute any of the relevant quantities (like T_R), however, the question of determining the exponents α and β arises. We will sketch in the next section an analytical procedure to do that.

3. THE RENORMALIZATION GROUP EQUATION

The idea of the Renormalization Group of Kinetics (RGK) is to model the transport explicitly as a random walk in P with the waiting time distribution $\Psi(t)$ and the step-size distribution $W(\Delta P)$ being chosen from the dynamical considerations (see Kuznetsov and Zaslavsky, 1997). Although also the FKE (2) could have been deduced from this formalism, we have decided to retain the more common averaging procedure for obtaining the FKE.

Two basic mechanisms of transport are expected to be the "hopping" between subsequent layers in the resonant multiplet, and the trapping inside higher and higher levels of hierarchy of a cantorus or a stability island chain. This process leads to the following expressions for $\Psi(t)$ and $W(\Delta P)$:

$$\Psi(t) = \text{const.} \times \sum_{j=1}^N p^j [\exp(-b^j t/T_{\text{Lib}}) + \exp(-t/jT_{\text{Lib}})] \quad (6)$$

$$W(\Delta P) = \text{const.} \times \sum_{j=1}^N p^j [\delta(\Delta P + a_0 a^j) + \delta(\Delta P - a_0 a^j) + \delta(\Delta P + j a_0) + \delta(\Delta P - j a_0)] \quad (7)$$

where $\delta(x)$ is the common Dirac delta function. The above functions obey the following RGK in the Fourier-Laplace (q, u) space:

$$W(q) \rightarrow pW(qa), \quad \Psi(u) \rightarrow p\Psi(u/b), \quad j \rightarrow 2j, \quad N \rightarrow N/2 \quad (8)$$

which leads to two coupled fixed-point equations for a and b , whereas $p = \delta S/\Delta S$ (the relative overlap, which can be estimated, e.g., as in Murray and Holman, 1997), and a_0 is also easy to calculate as the separation between the subsequent resonant layers. Now the fractional exponents are found as $\alpha = |\log p|/\log a$ and $\beta = |\log p|/\log b$. Notice that the presented model breaks down in a non-degenerate system, where $a_0 \rightarrow 0$ and we only have a trivial RGK with a whole interval of fixed points (irrelevant for our purposes).

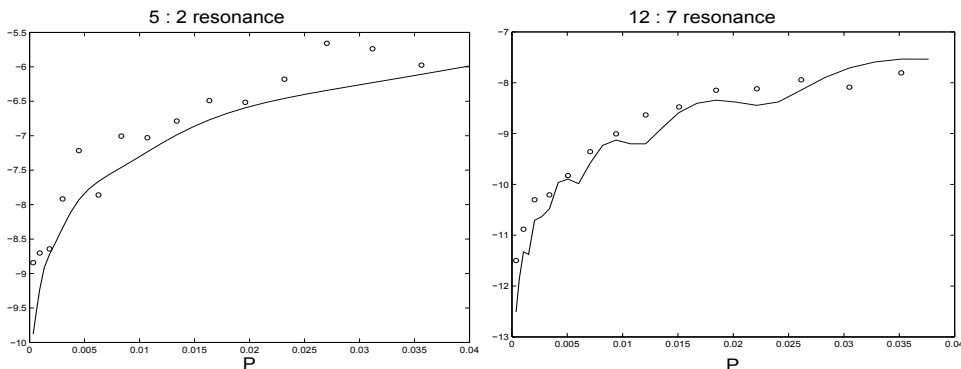


Figure 1: Diffusion coefficient as a function of P in the 5 : 2 (left) and 12 : 7 (right) resonances. Solid line is the analytical prediction, and circles are numerical results for an ensemble of 150 bodies. The value of the diffusion coefficient varies rather smoothly with P in the former case, whereas in the latter case the stair-like structure and the log-periodic oscillations are much more prominent.

4. RESULTS FOR SELECTED RESONANCES IN THE ASTEROID BELT

A systematic study of all important MMR in the Asteroid Belt is still in progress. We present here only two typical cases, namely the 5 : 2 and 12 : 7 resonances. Figure 1 shows the diffusion coefficient as a function of P ; figure 2 gives the predicted $T_R - T_{Ly}$ relation.

The figures illustrate the qualitative properties discussed at the end of the second section. The 12 : 7 resonance, as expected, contains a population with very long removal times, in which the bodies such as the now famous 511 Helga (Milani and Nobili, 1992) reside. The power-law and the exponential-law regimes for T_R coexist in a large part of the resonance. Contrary, the 5 : 2 objects should all have comparable lifetimes, and only one type of transport should exist – the relatively fast diffusion towards P_{cross} .

5. CONCLUSIONS

We have proposed a fractional kinetic equation for the eccentricity transport in the MMR, together with an analytical scheme for the estimation of the fractional exponents α and β . The predictions for two typical low- and high-order resonances agree well with the numerical results and with our previous, semi-analytical model (Tsiganis, Anastasiadis and Varvoglis, 2000; Čubrović, 2005a). It is clear, however, that further work is needed to obtain a complete model, capable of describing also the fine details of dynamics inside the MMR.

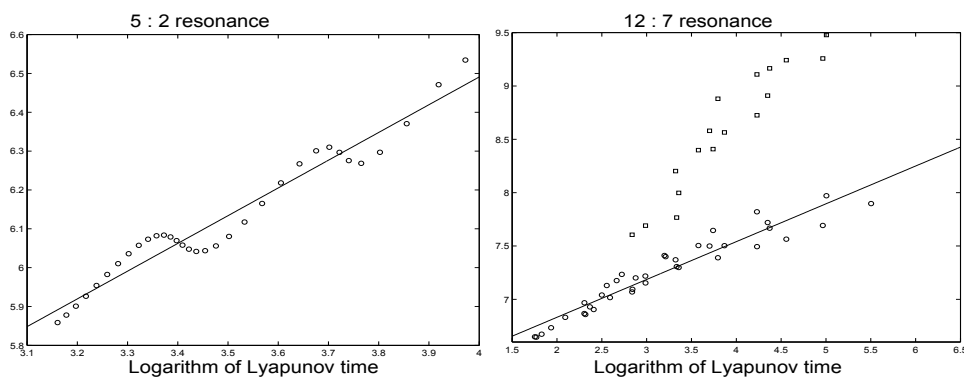


Figure 2: The analytically computed values of T_{Ly} and T_{R} for the 5 : 2 (left) and 12 : 7 (right) resonances. The power law (straight line on the log-log plot) describes well the general trend in the 5 : 2 case, with the scaling exponent about 0.70. In the 12 : 7 case, however, another, more stable regime, with exponentially long lifetimes is also present (denoted by squares), in addition to the "normal" chaos, which is again well described with a power-law fit, the slope being about 0.35.

References

- Čubrović, M.: 2005a, Proceedings of the IAU Colloquium 197, eds. Z. Knežević, A. Milani, Cambridge University Press.
 Čubrović, M.: 2005b, *Phys. Rev. E*, **72**, 025204(R).
 Kuznetsov, L., Zaslavsky, G.M.: 1997, *Phys. Rep.*, **288**, 457.
 Milani, A., Nobili, A.: 1992, *Nature*, **357**, 569.
 Morbidelli, A.: 2002, *Modern Celestial Mechanics*, Taylor and Francis, Cambridge.
 Murray, N.W., Holman, M.: 1997, *Astron. J.*, **114**, 1246.
 Tsiganis, K., Anastasiadis, A., Varvoglis, H.: 2000, *Cel. Mech. Dyn. Astron.*, **71**, 243.
 Tsiganis, K., Varvoglis, H., Hadjidemetriou, J.: 2002, *Icarus*, **155**, 454.
 Varvoglis, H., Anastasiadis, A.: 1996, *Astron. J.*, **111**, 1718.
 Weiss G.H.: 1994, Aspects and applications of the random walk, North-Holland, Amsterdam.
 Zaslavsky, G. M.: 2002, *Phys. Rep.*, **371**, 461.

TT 7: Transport: Quantum Coherence and Quantum Information Systems – Theory (jointly with HL, MA)

Time: Monday 9:30–13:00

Location: H 3005

TT 7.1 Mon 9:30 H 3005

Collective modes in the fluxonium qubit — ●GIANLUIGI CATELANI¹ and GIOVANNI VIOLA² — ¹Forschungszentrum Jülich, PGI-2 — ²RWTH Aachen, IQI

In the fluxonium qubit, an array comprising a large number of identical Josephson junctions form a so-called superinductance. The superinductance is connected to a junction – the phase slip element – with a smaller Josephson energy and a different charging energy. We investigate the effects of unavoidable capacitive couplings to ground as well as non-linearities of the superinductance: they both introduce interactions between the low-energy qubit degree of freedom and higher-energy collective modes of the circuit. We also consider the role of the additional capacitances that are used to couple the qubit to a resonator for driving and read-out. We show that the interactions with the collective modes can affect not only the spectrum of the qubit but also its coherence.

Work supported in part by the EU under REA grant agreement CIG-618258

TT 7.2 Mon 9:45 H 3005

Optimal Control of Quantum Measurement — DANIEL EGGER and ●FRANK WILHELM — Theoretical Physics, Saarland University, 66123 Saarbrücken, Germany

Pulses to steer the time evolution of quantum systems can be designed with optimal control theory. In most cases it is the coherent processes that can be controlled and one optimizes the time evolution towards a target unitary process, sometimes also in the presence of non-controllable incoherent processes. Here we show how to extend the GRAPE algorithm in the case where the incoherent processes are controllable and the target time evolution is a non-unitary quantum channel. We perform a gradient search on a fidelity measure based on Choi matrices. We illustrate our algorithm by optimizing a measurement pulse for superconducting phase qubits. We show how this technique can lead to large measurement contrast close to 99%. We also show, within the validity of our model, that this algorithm can produce short 1.4 ns pulses with 98.2% contrast.

TT 7.3 Mon 10:00 H 3005

Optimal control of single flux quantum pulses — ●PER LIEBERMANN, DANIEL EGGER, and FRANK WILHELM — Universität des Saarlandes, Saarbrücken

Rapid single flux quantum pulses are a natural candidate for on-chip control of superconducting qubits [1]. We apply trains of single flux quantum pulses to perform single qubit gates. Under the constraint of constant amplitudes and gate times we use genetic algorithms for optimising the pulse sequence to decrease the gate error by two orders of magnitude. We consider leakage transitions into a third energy level as well as timing jitter of the pulses, exploring the robustness of our optimized sequence. This takes us one step further to on-chip qubit controls.

[1] R. McDermott and M.G. Vavilov, Phys. Rev. Applied 2, 014007 (2014)

TT 7.4 Mon 10:15 H 3005

Adaptive characterization of coherent states — ●MARKKU P. V. STENBERG, KEVIN PACK, and FRANK K. WILHELM — Theoretical Physics, Saarland University, 66123 Saarbrücken, Germany

We present a method for efficient characterization of an optical coherent state $|\alpha\rangle$. We choose measurement setups adaptively based on the data while it is collected. Our algorithm divides the estimation in three different steps with different measurement strategies: (i) searching a crude estimate, (ii) rapidly improving the accuracy, and (iii) the phase where the improvement of the accuracy slows down due to the quantum nature of the coherent state. Our algorithm significantly outperforms nonadaptive schemes. While our standard strategy is robust against measurement errors we also present strategies optimized for the presence of such errors.

TT 7.5 Mon 10:30 H 3005

Qubit dephasing due to Quasiparticle Tunneling — ●SEBASTIAN ZANKER, MICHAEL MARTHALER, and GERD SCHÖN — Institut für

Theoretische Festkörperphysik, Karlsruhe Institute of Technology, D-76128 Karlsruhe, Germany

We study dephasing of a superconducting qubit due to quasiparticle tunneling through a Josephson junction. While qubit decay due to tunneling processes is well understood within a golden rule approximation, pure dephasing due to BCS quasiparticles gives rise to a divergent golden rule rate. We calculate qubit dephasing due to quasiparticle tunneling beyond lowest order approximation in coupling between qubit and quasiparticles. Summing up a certain class of diagrams we show that qubit dephasing due to purely longitudinal coupling to quasiparticles leads to dephasing $\sim \exp(-x(t))$ where $x(t) \propto t^{3/2}$ for short time scales and $x(t) \propto t \log(t)$ for long time scales.

TT 7.6 Mon 10:45 H 3005

Detecting nonlocal Cooper pair entanglement by optical Bell inequality violation — SIMON E. NIGG, RAKESH P. TIWARI, STEFAN WALTER, and ●THOMAS L. SCHMIDT — Department of Physics, University of Basel, Klingelbergstrasse 82, 4056 Basel, Switzerland

Based on the Bardeen Cooper Schrieffer (BCS) theory of superconductivity, the coherent splitting of Cooper pairs from a superconductor to two spatially separated quantum dots has been predicted to generate nonlocal pairs of entangled electrons. In order to test this hypothesis, we propose a scheme to transfer the spin state of a split Cooper pair onto the polarization state of a pair of optical photons. We show that the produced photon pairs can be used to violate a Bell inequality, unambiguously demonstrating the entanglement of the split Cooper pairs.

[1] Nigg et al., arXiv:1411.3945 [cond-mat.mes-hall]

TT 7.7 Mon 11:00 H 3005

Detection of non-local spin-entanglement by light emission from a superconducting pn-junction — ●ALEXANDER SCHROER and PATRIK RECHER — Institut für Mathematische Physik, Technische Universität Braunschweig, D-38106 Braunschweig, Germany

We model a superconducting pn-junction in which the n- and the p-site are contacted through two optical quantum dots, each embedded into a photonic nanocavity. Whenever a Cooper pair is transported from the n-site to the p-site, two photons are emitted. When the two electrons of a Cooper pair are transported through different quantum dots, polarization entangled photons are created, provided that the Cooper pairs retain their spin-singlet character although being spatially separated on the two quantum dots. We show that a CHSH Bell-type measurement is able to detect the entanglement of the photons over a broad range of microscopic parameters, even in the presence of parasitic processes and imperfections. Observing this signature is a direct proof of crossed Andreev reflection, or, equivalently, Cooper pair splitting, retaining the spin-singlet wave function.

15 min. break.

TT 7.8 Mon 11:30 H 3005

Scattering of two photons from two distant qubits: exact solution — MATTI LAAKSO and ●MIKHAIL PLETYUKHOV — Institute for Theory of Statistical Physics, RWTH Aachen, 52056 Aachen

We consider the inelastic scattering of two photons from two qubits separated by an arbitrary distance and coupled to a one-dimensional transmission line. We present an exact, analytical solution to the problem, and use it to explore a particular configuration of qubits which is transparent to single-photon scattering, thus highlighting non-Markovian effects of inelastic two-photon scattering: Strong two-photon interference and momentum dependent photon (anti)bunching. This latter effect can be seen as an inelastic generalization of the Hong-Ou-Mandel effect.

TT 7.9 Mon 11:45 H 3005

Robust entanglement under multipartite correlated dephasing — ●EDOARDO CARNIO^{1,2}, MANUEL GESSNER², and ANDREAS BUCHLEITNER^{2,3} — ¹Department of Physics, University of Warwick, Coventry, CV4 7AL, United Kingdom — ²Physikalisches Institut, Albert-Ludwigs-Universität Freiburg, Hermann-Herder-Straße 3,

79104 Freiburg, Germany — ³Freiburg Institute for Advanced Studies, Albert-Ludwigs-Universität Freiburg, Albertstraße 19, 79104 Freiburg, Germany

We derive an analytical description for the dephasing process undergone by a system on non-interacting atomic qubits, immersed in a uniform, fluctuating magnetic field. The dephasing process is correlated, as the noise source is common to all the particles and induces an effective atom-atom interaction on them. This correlated nature allows to specify field orientations that preserve any degree of atomic entanglement for all times, and families of states with entanglement properties that are time-invariant for arbitrary field orientations. Our formalism applies to arbitrary spectral distributions of the fluctuations.

TT 7.10 Mon 12:00 H 3005

Bell inequalities and waiting times — ●CHRISTINA PÖLTL and MICHELE GOVERNALE — School of Chemical and Physical Sciences and MacDiarmid Institute for Advanced Materials and Nanotechnology, Victoria University of Wellington, PO Box 600, Wellington 6140, New Zealand

We propose a Bell test based on waiting time distributions for spin entangled electron pairs, which are generated and split in mesoscopic Coulomb blockade structures, denoted as entanglers. These systems have the advantage that quantum point contacts enable a time resolved observation of the electrons occupying the system, which gives access to quantities such as full counting statistics and waiting time distributions. We use the partial waiting times to define a CHSH-Bell test, which is a purely electronic analogue of the test used in quantum optics. After the introduction of the Bell inequality we discuss the findings on the two examples of a double quantum dot and a triple quantum dot. This Bell test allows the exclusion of irrelevant tunnel processes from the statistics normally used for the Bell correlations. This can improve the parameter range for which a violation of the Bell inequality can be measured significantly.

TT 7.11 Mon 12:15 H 3005

Quantum dynamics of a strongly driven Josephson Junction — ●JENNIFER GOSNER, BJÖRN KUBALA, and JOACHIM ANKERHOLD — Institute for Complex Quantum Systems, University of Ulm, Germany
A Josephson Junction embedded in a dissipative circuit can be driven to exhibit non-linear oscillations.

Classically the non-linear oscillator shows under sufficient strong driving and weak damping dynamical bifurcations and a bistable region similar to the conventional Duffing-oscillator. These features depend sensitively on initial conditions and parameters. The sensitivity of this circuit, called Josephson Bifurcation Amplifier, can be used to amplify an incoming signal, to form a sensing device or even for measuring a quantum system.

The *quantum* dynamics can be described by a dissipative Lindblad master equation. Signatures of the classical bifurcation phenomena appear in the Wigner representation, used to characterize and visualize the resulting behaviour. In order to compare this quantum dynamics to that of the conventional Duffing-oscillator, the complete

cosine-nonlinearity of the Josephson Junction is kept for the quantum description while going into a rotating frame.

TT 7.12 Mon 12:30 H 3005

Dissipation-induced first order decoherence phase transition in a non-interacting fermionic system — ●MIHAILO CUBROVIC — Institute for Theoretical Physics, Universität zu Köln, Zùlpicher Str. 77, D-50937, Köln, Germany

We consider a dissipative tight-binding fermionic chain as a model for a nanowire with current leakage due to imperfect isolation. The dissipation manifests as tunneling into/out of the chain from/to the environment. The evolution of the system is described by the Lindblad equation, generalized to incorporate the memory effects in the bath. Already infinitesimally small dissipation along the chain induces a quantum phase transition (QPT). This is a decoherence QPT: the reduced density matrix of a subsystem (far from the ends of the chain) can be represented as the tensor product of single-site density matrices. We analyze the QPT in the thermodynamic limit by looking at the entropy and the response function in the bulk, and compare in detail the results with and without memory in the bath. To gain a better intuitive understanding we also construct the analogous classical model (a correlated random walk process) and compare its behavior to the QPT of the quantum chain.

TT 7.13 Mon 12:45 H 3005

Spin dynamics using the Majorana representation: validity, path integral and higher correlators — ●PABLO SCHAD¹, BORIS N. NAROZHNY^{1,2}, GERD SCHÖN³, YURIY MAKHLIN^{4,5}, and ALEXANDER SHNIRMAN¹ — ¹Institut für Theorie der Kondensierten Materie, Karlsruhe Institute of Technology, D-76131 Karlsruhe, Germany — ²National Research Nuclear University MEPhI (Moscow Engineering Physics Institute), Kashirskoe shosse 31, 115409 Moscow, Russia — ³Institut für Theoretische Festkörperphysik und Institut für Nanotechnologie, Karlsruhe Institute of Technology, D-76131 Karlsruhe, Germany — ⁴Landau Institute for Theoretical Physics, acad. Semyonov av., 1a, 142432, Chernogolovka, Russia — ⁵Moscow Institute of Physics and Technology, 141700, Dolgoprudny, Russia

We present a method to calculate higher spin correlators via the Majorana fermion representation of spin operators. We show explicitly that the Majorana representation does not require any projection procedure. Previously found identities [1,2] between spin and Majorana fermion correlation functions are extended. As an example we consider a spin-1/2 coupled to an isotropic, ohmic bath. We formulate a path-integral approach, which is valid at B=0 in contrast to perturbation theory, find the saddle-point solution and discuss fluctuations. We demonstrate that spin correlators in the high-temperature regime can be obtained using saddle-point Green's functions.

[1] A. Shnirman and Y. Makhlin, Phys. Rev. Lett. 91, 207204 (2003).

[2] W. Mao, P. Coleman, C. Hooley, and D. Langreth, Phys. Rev. Lett. 91, 207203 (2003).

TT 50: Correlated Electrons: Quantum-Critical Phenomena - Theory

Time: Tuesday 14:00–16:00

Location: BEY 81

TT 50.1 Tue 14:00 BEY 81

Detailed analysis of critical points in coupled spin dimer systems — ●SEBASTIAN EGGERT¹, DOMINIK STRASSEL¹, and PETER KOPIETZ² — ¹Fachbereich Physik, Technische Universität Kaiserslautern — ²Fachbereich Physik, Goethe Universität Frankfurt

Spin dimer systems are a promising playground for the detailed study of quantum phase transitions. In many cases it is sufficient to use the magnetic field as the tuning parameter in order to reach interesting non-trivial critical points. Depending on the temperature it is in principle possible to observe a crossover from the characteristic scaling near the critical point to the behavior of a finite temperature phase transition. In order to quantitatively demonstrate those effects and inspired by recent experiments we have started large scale quantum Monte Carlo simulations in order to analyze several different physical quantities in spin dimer systems, namely the susceptibility, the magneto-caloric effect, the structure factor and the spin stiffness. We discuss in detail how the phase transitions (quantum and finite temperature) are manifest in the characteristic scaling behavior near critical points by comparing them with interacting boson theories. The results give a unified picture of the full quantum and finite temperature phase diagram.

TT 50.2 Tue 14:15 BEY 81

Quantum Monte Carlo Simulations of Trimerized Antiferromagnetic Systems — ●DOMINIK STRASSEL and SEBASTIAN EGGERT — Department of Physics and Research Center Optimas, Technical University Kaiserslautern, 67663 Kaiserslautern, Germany

We study linear clusters of three strongly coupled spins $S = \frac{1}{2}$ (trimers), which are connected more weakly in a two dimensional lattice using *Stochastic Series Expansion Quantum Monte Carlo* simulations of the Heisenberg model in a magnetic field. In general these systems show a magnetization plateau at $\frac{1}{3}$ saturation, which is already known from strongly coupled three-leg ladders. Interestingly, the origin of the plateau is very similar to the $\frac{1}{3}$ plateau in frustrated lattices (e.g. the triangular lattice) so that the analogous phase transitions can be analyzed using non-frustrated systems, which do not suffer from the infamous minus sign problem. With increasing coupling between the trimers, the plateau vanishes and a critical point can be identified. We also analyze the behavior in the limit of weak inter-trimer coupling.

TT 50.3 Tue 14:30 BEY 81

Excitonic Instability at Spin-State Transition — ●JAN KUNEŠ and PAVEL AUGUSTINSKÝ — Institute of Physics, ASCR, Prague, Czechia

We report a newly observed instability of the half-filled two-band Hubbard model in the vicinity of the spin-state transition. [1] Using dynamical mean-field theory we have performed a unbiased search for divergent particle-hole susceptibilities. Depending on the bandwidths ratio the system was found to establish a checker-board order of high- and low-spin sites, breaking the discrete translational symmetry, or to undergo a condensation of spinful excitons, breaking a continuous gauge symmetry. Besides numerical results we provide an analytic description in the strong-coupling limit where the problem maps of a variate of the bosonic t-J model.

[1] Kunes and Augustinsky, arXiv:1310.0669

TT 50.4 Tue 14:45 BEY 81

Critical phenomena of the two-channel spin-boson model — ●BENEDIKT BRUOGNOLO¹, ANDREAS WEICHELBAUM¹, JAN VON DELFT¹, and MATTHIAS VOJTA² — ¹Physics Department, Arnold Sommerfeld Center for Theoretical Physics and Center for NanoScience, Ludwig-Maximilians-Universität München, 80333 München, Germany — ²Institut für Theoretische Physik, Technische Universität Dresden, 01062 Dresden, Germany

In recent years bosonic quantum impurity models have attracted significant attention in the context of quantum phase transitions. Numerical approaches to study the critical properties in such models face additional challenges arising from the bosonic nature of the bath modes, that are not present in purely fermionic systems.

Guo et al. [1] presented a powerful numerical method based on a combination of NRG and DMRG, which overcomes the problem of a diverging bosonic state space by variationally constructing an optimized

boson basis on each site of the Wilson chain. We discuss a symmetry improved application of this method to the sub-ohmic spin-boson model with two symmetrically coupled bosonic baths and focus on its critical properties, which so far had been an open question. We present the first numerical study of the critical points, which in combination with RG results allows a description of the critical phenomena of this model for a wide range of parameters.

[1] C. Guo, A. Weichselbaum, J. von Delft, M. Vojta, Phys. Rev. Lett. 108, 160401 (2012)

TT 50.5 Tue 15:00 BEY 81

Interplay of fermion and boson induced critical Kondo destruction — ●FARZANEH ZAMANI^{1,2}, PEDRO RIBEIRO^{1,2,3}, and STEFAN KIRCHNER^{1,2} — ¹MPI-PKS, Dresden, Germany — ²MPI-CPFS, Dresden, Germany — ³CFIF-IST, Universidade de Lisboa, Lisboa, Portugal

An increasing number of experiments have indicated that the traditional approach to continuous zero-temperature phase transitions in strongly correlated electrons systems is inadequate. In the context of intermetallic rare-earth compounds this approach does e.g. not account for the linear-in-temperature relaxation rates observed in a number of systems in the charge- and spin-response near criticality. A widely discussed alternative to the standard approach picture is local Kondo destruction, where Kondo screening becomes critical concomitantly with the lattice. We study the phenomenon of critical Kondo destruction in the pseudogap Bose-Fermi Kondo model where a quantum spin is coupled to a fermionic and a bosonic bath. Each of the baths by itself is capable of critically destroying Kondo screening, allowing us to study the dynamic interplay of the two. We employ a dynamic large-N limit and obtain asymptotically exact solutions at zero temperature. We also report full scaling equations at all critical points and discuss the ensuing relaxation rates. Finally, we revisit the issue of 'conformal scaling' of the imaginary-time correlation functions at criticality and relate our findings to their counterpart in the easy-axis pseudogap pseudogap Bose-Fermi Kondo model.

TT 50.6 Tue 15:15 BEY 81

Corrections to scaling in the critical theory of deconfined criticality — ●LORENZ BARTOSCH — Institut für Theoretische Physik, Universität Frankfurt, 60438 Frankfurt am Main, Germany

Inspired by recent conflicting views on the order of the phase transition from an antiferromagnetic Néel state to a valence bond solid, we use the functional renormalization group to study the underlying quantum critical field theory which couples two complex matter fields to a non-compact gauge field. In our functional renormalization group approach we only expand in covariant derivatives of the fields and use a truncation in which the full field dependence of all wave-function renormalization functions is kept. While we do find critical exponents which agree well with some quantum Monte Carlo studies and support the scenario of deconfined criticality, we also obtain an irrelevant eigenvalue of small magnitude, leading to strong corrections to scaling and slow convergence in related numerical studies.

TT 50.7 Tue 15:30 BEY 81

Heavy fermion quantum critical point from AdS/CFT correspondence — ●MIHAILO ČUBROVIĆ — Institute for Theoretical Physics, University of Cologne, Germany

We propose a holographic (AdS/CFT) approach to strongly correlated electrons and study a quantum phase transition from small to large Fermi surface phase in a model "heavy fermion" system. AdS/CFT is a duality which maps the correlation functions from field theory to solutions of the equations of motion for classical fields in a curved spacetime, i.e. in general relativity. The appealing side of this approach is its nonperturbative nature: the calculations on the gravity side are essentially an expansion in inverse coupling strength and indeed work best in the strong coupling regime. We construct a gravity dual of a Fermi liquid system which shows a mass enhancement of the order of several hundred times the bare mass. At zero temperature, the system exhibits a continuous quantum phase transition to another Fermi liquid with different effective mass and Fermi momentum. The difference in sizes of the Fermi surfaces (i.e. Fermi momenta), as well as the fact that the transition happens at finite wavevector agree with

the intuition on heavy fermion transitions. While the picture resembles the fractionalization scenario, we do not introduce any emergent gauge fields. The shrinking of the Fermi surface can best be interpreted as formation of bound states between electrons and exotic bosonic excitations near the quantum critical point.

TT 50.8 Tue 15:45 BEY 81

Anderson Metal-Insulator Transitions With Classical Magnetic Impurities — •DANIEL JUNG¹, KEITH SLEVIN², and STEFAN KETTEMANN^{1,3} — ¹School of Engineering and Science, Jacobs University Bremen, 28759 Bremen, Germany. — ²Department of Physics, Graduate School of Science, Osaka University, 1-1 Machikaneyama, Toyonaka, Osaka 560-0043, Japan. — ³Division of Advanced Materials Science, Pohang University of Science and Technology (POSTECH), Pohang 790-784, South Korea.

We study the effects of classical magnetic impurities on the Ander-

son metal-insulator transition numerically [1, 2]. In particular we find that while a finite concentration of Ising impurities lowers the critical value of the site-diagonal disorder amplitude W_c , in the presence of Heisenberg impurities, W_c is first enhanced with increasing exchange coupling strength J due to time-reversal symmetry breaking. The resulting scaling with J is analyzed and compared to analytical predictions by Wegner [3]. We discuss the relevance of our findings for systems like phosphor-doped silicon, which are known to exhibit a quantum phase transition from metal to insulator driven by the interplay of both interaction and disorder, accompanied by the presence of a finite concentration of magnetic moments [4].

[1] D. Jung, and S. Kettemann, AIP conf. proceed., submitted.

[2] D. Jung, K. Slevin, and S. Kettemann, to be published.

[3] F. Wegner, Nucl. Phys. B **280**, 210 (1987).

[4] H. von Löhneysen, Adv. Solid State Phys. **40**, 143 (2000)



View abstract data

| | |
|----------------|--|
| Abstract title | The strange metals and Fermi liquids of holography |
| Author | Mr. Cubrovic, M., Institute Lorentz, Leiden, Netherlands (Presenting author) |
| Co-author(s) | Zaanen, J. Schalm, K. |
| Topic | Materials, surfaces and interfaces |
| Abstract text | |

The "holographic" AdS/CFT correspondence is a result of string theory that expresses the dual relation between quantum field theory and gravity. Although originating in high energy physics, the case has been rapidly developing that it is amazingly powerful in addressing ubiquitous emergence phenomena of the strongly interacting quantum systems of condensed matter physics. Examples are the holographic superconductors [1], the strange metals [2,3], and the holographic Fermi liquids [4]. These describe phenomena beyond the reach of standard field theory. For instance, the Fermi liquid appears as an "order" instability of the "quantum disordered" strange metal, holographically encoded as the uncollapse of a charged black hole into an "electron" star.

[1] J.-H. She et al, Phys. Rev. B 84, 144527 (2010).

[2] M. ubrovi , J. Zaanen and K. Schalm, Science 325, 439 (2009).

[3] T. Faulkner et al, Science 329, 1043 (2010).

[4] M. ubrovi , J. Zaanen and K. Schalm, JHEP 2011, 17 (2011).

URL

[Back](#)



View abstract data

| | |
|----------------|---|
| Abstract title | Novel stable phases of matter from AdS/CFT correspondence |
| Author | Drs. Cubrovic, M., Institute Lorentz, Leiden, Netherlands (Presenting author) |
| Co-author(s) | Schalm, K. Zaanen, J. |
| Topic | Subatomic physics |
| Abstract text | |

We study holographic fermions in the framework of AdS₄/CFT₃ correspondence in bottom-up models with finite fermion density in the bulk. We show that the resulting system always has a Lifshitz geometry while encoding different phases on the CFT side. We identify two extreme cases, corresponding to single-particle and fluid models in the bulk, that describe Fermi liquids and fractionalized fermionic liquids, respectively^[1], while the intermediate regime shows a distinct and novel stable phase. We also study the dispersion, scaling and transport properties of different phases.

^[1] M. Cubrovic, Y. Liu, K. Schalm, Y.-W. Sun, J. Zaanen 2011, accepted for Phys. Rev. D, arXiv:1106.1798

[Back](#)

Fermionic Quantum Criticality From AdS/CFT Correspondence

Mihailo Čubrović*, Koenraad Schalm* and Jan Zaanen*

*Institute Lorentz, Leiden University, P. O. Box 9506, Leiden 2300RA, The Netherlands

Abstract. We study ordering phenomena and quantum phase transitions in strongly correlated electron systems from the viewpoint of AdS/CFT correspondence [1]. The correspondence is a dual classical description of strongly coupled quantum systems coming from string theory, and provides a controlled framework that is free of the fermion sign problem. We first show how the basic workings of the Fermi statistics (Pauli principle, Fermi surfaces, Fermi momentum) are encoded in AdS/CFT [2, 3]. A number of distinct states are found to exist, characterized by either Landau Fermi liquid scaling or by non-Fermi liquid exponents, and separated by critical points similar to those found in heavy fermion systems. We further study some ordering phenomena: quantum Hall effect [4], electron-hole (exciton) pairing and Cooper pairing. The last shows a remarkable dichotomy between the systems with Fermi liquid ground states, where the BCS mechanism gives rise to the conventional textbook superconductivity, and the systems with quantum critical ground states where the same BCS pairing mechanism leads to power-law scaling of the gap equation and an increase in critical temperature, characteristic of unconventional superconducting materials.

REFERENCES

1. Maldacena, J., arXiv:hep-th/9711200 (1997).
2. Čubrović, M., Zaanen, J. and Schalm, K., *Science* **325**, 439. (2009).
3. Čubrović, M., Zaanen, J., and Schalm, K., arXiv:1012.5681 (2010).
4. Gubankova, E., Brill, J., Čubrović, M., Schalm, K., Schijven, P., and Zaanen, J., arXiv:1011.4051 (2010).



View abstract data

| | |
|----------------|--|
| Abstract title | Geometry encoding for statistics: from Fermi liquids to Cooper pairing |
| Author | Drs. Cubrovic, Mihailo, Institute Lorentz, Leiden, Netherlands (Presenting author) |
| Co-author(s) | Zaananen, Jan Schalm, Koenraad |
| Topic | Subatomic physics |
| Abstract text | |

The general workings of Fermi-Dirac statistics in strongly interacting fermion matter is a profound unresolved question in condensed matter physics. We offer an insight from the AdS/CFT correspondence that reduces the Pauli principle to a "shrinking" of spacetime in the vicinity of the black hole horizon in the gravity dual. The resulting Lifshitz scaling geometry naturally explains the empirical stability of Fermi liquids, as well as the workings of unconventional vs. conventional pairing mechanisms in superconducting materials. The fermionic AdS/CFT setup is markedly different than for bosons: instead of a condensate at the black hole horizon, the former is just a single quantum-mechanical fermion particle orbiting the black hole.

[Back](#)

CAMTP

**” Let’s Face Chaos
through
Nonlinear
Dynamics”**

6th International

Summer School/Conference



at the University of Maribor

26 June - 10 July 2005

Dedicated to the 75th Birthday of Professor Siegfried Großmann

Maribor



Slovenia

Quantum chaos in two-dimensional potentials with non-trivial topology

Victor Berezovoj, Yuri Bolotin, and Vitaliy Cherkaskiy

Akhiezer Institute for Theoretical Physics, Academicheskaya Str.1, 61108 Kharkov, UKRAINE

We summarize our recent investigations of quantum chaos in smooth 2D-potentials with two and more local minima and discuss our numerical results obtained for the potential of lower umbilic catastrophe D_5 (with two local minima) and the potential of quadrupole surface oscillations of atomic nuclei (with four local minima). We stress some new specific features of the systems under consideration in comparison with more usual objects of quantum chaos investigations: two-dimensional billiards and trivial topology potential cases — homogeneous and one-well potentials.

References

- Berezovoj V.P., Bolotin Y.L., Cherkaskiy V.A. 2003 *PTP Supplements* **150** 326-329
 Berezovoj V.P., Bolotin Y.L., Cherkaskiy V.A. 2004 *Phys.Lett.A* **323(3-4)** 218-223
 Berezovoj V.P., Bolotin Y.L., Cherkaskiy V.A. 2004 *The Journal of Kharkiv National University* **628** 47-60

Universality and scaling in nonintegrable Hamiltonian systems: escape times, Lyapunov exponents and inverse chaotic scattering

Mihailo Čubrović

Institute of Physics, P. O. B. 57, 11001, Belgrade, Serbia and Montenegro
Department of Astronomy – Petnica Science Center, P. O. B. 6, Valjevo, Serbia and Montenegro

We describe our fractional kinetic model of transport in Hamiltonian systems which allows one to obtain and solve approximately the fractional diffusion equation in the action space. In addition to the derivation of kinetic equations from the optimal normal forms (1), we give two additional ways of obtaining them, from a non-Gaussian Langevin equation and as a hydrodynamic limit of continuous time random walk. The model predicts approximate scaling relations for the diffusion times with respect to the Lyapunov times, and for the rates and probabilities of the escape to infinity in open Hamiltonian systems (inverse chaotic scattering). The scalings appear in two distinct regimes, thus resembling a phase transition. As an example, we present analytical and numerical results for a number of Hamiltonians (1, 2) and discuss the relation to some results of other authors.

References

- (1) Čubrović M 2005 submitted to *Phys. Rev. E*
 (2) Čubrović M 2005 *Proc. of the IAUC* **197** 209

Cover Page



Universiteit Leiden



The handle <http://hdl.handle.net/1887/20607> holds various files of this Leiden University dissertation.

Author: Čubrović, Mihailo

Title: Holography, Fermi surfaces and criticality

Issue Date: 2013-02-27

Holography, Fermi surfaces and Criticality

PROEFSCHRIFT

TER VERKRIJGING VAN
DE GRAAD VAN DOCTOR AAN DE UNIVERSITEIT LEIDEN,
OP GEZAG VAN RECTOR MAGNIFICUS
PROF. MR. C. J. J. M. STOLKER,
VOLGENS BESLUIT VAN HET COLLEGE VOOR PROMOTIES
TE VERDEDIGEN OP WOENSDAG 27 FEBRUARI 2013
TE KLOKKE 13.45 UUR

DOOR

Mihailo Čubrović

GEBOREN TE BELGRADO, SERVIE IN 1985

Promotiecommissie

- Promotor: prof. dr. J. Zaanen (Universiteit Leiden)
Co-promotor: dr. K. Schalm (Universiteit Leiden)
Overige leden: prof. dr. E. R. Eliel (Universiteit Leiden)
prof. dr. H. Liu (Massachusetts Institute of Technology)
prof. dr. E. Verlinde (Universiteit van Amsterdam)
prof. dr. C. W. J. Beenakker (Universiteit Leiden)
prof. dr. J. M. van Ruitenbeek (Universiteit Leiden)

Casimir PhD Series, Delft-Leiden, 2013-01
ISBN 978-90-8593-099-0

This work is part of the research programme of the Foundation for Fundamental Research on Matter (FOM), which is part of the Netherlands Organization for Scientific Research (NWO).

Dit werk maakt deel uit van het onderzoekprogramma van de Stichting voor Fundamenteel Onderzoek der Materie (FOM), die deel uit maakt van de Nederlandse Organisatie voor Wetenschappelijk Onderzoek (NWO).

Contents

| | | |
|----------|---|-----------|
| 1 | Introduction | 1 |
| 1.1 | Holographic principle: the idea | 1 |
| 1.2 | Realization: AdS/CFT correspondence | 4 |
| 1.2.1 | Warmup: symmetries | 5 |
| 1.2.2 | Enlightenment: the duality relation | 7 |
| 1.2.3 | Some general remarks | 10 |
| 1.2.4 | Holography outside high-energy theory | 11 |
| 1.3 | The arena: fermions in organized matter | 12 |
| 1.4 | Outline | 18 |
| 2 | The holographic dictionary | 21 |
| 2.1 | The basic entries | 21 |
| 2.1.1 | Thermodynamics | 22 |
| 2.1.2 | Sources and expectation values | 23 |
| 2.2 | Holographic superconductors: a tutorial | 27 |
| 2.2.1 | Scalar condensate and phase transitions | 29 |
| 2.3 | Holographic dictionary for fermions | 31 |
| 2.3.1 | Equations of motion | 32 |
| 2.3.2 | Boundary action | 35 |
| 2.4 | The remainder of the thesis | 37 |
| 3 | Charged black hole and critical Fermi surfaces [17] | 41 |
| 3.1 | String theory for condensed matter | 42 |
| 3.2 | The emergent Fermi liquid | 44 |
| 3.3 | Concluding remarks | 51 |
| 3.4 | Formal background for the calculation of the spectral functions | 52 |

| | | |
|----------|---|------------|
| 3.4.1 | The AdS set up and AdS/CFT Fermion Green's functions. | 52 |
| 3.4.2 | The Fermion Green's function. | 55 |
| 3.4.3 | Masses and Dimensions. | 58 |
| 3.4.4 | The retarded propagator boundary conditions at the horizon. | 60 |
| 3.5 | Finite temperature and the position of the Fermi surface . . | 61 |
| 4 | AdS dual of a Fermi liquid: Dirac hair [18] | 65 |
| 4.1 | Introduction | 65 |
| 4.2 | From Green's function to AdS/CFT rules for a Fermi Liquid | 69 |
| 4.2.1 | The AdS dual of a stable Fermi Liquid: Applying Migdal's relation holographically | 74 |
| 4.3 | An AdS Black hole with Dirac Hair | 79 |
| 4.3.1 | At the horizon: Entropy collapse to a Lifshitz solution | 86 |
| 4.3.2 | A BH with Dirac hair | 87 |
| 4.3.3 | Confirmation from fermion spectral functions | 93 |
| 4.4 | Discussion and Conclusion | 96 |
| 5 | From the Dirac hair to the electron star [19] | 99 |
| 5.1 | Introduction | 99 |
| 5.2 | Einstein-Maxwell theory coupled to charged fermions | 103 |
| 5.3 | Fermion spectral functions in the electron star background . | 109 |
| 5.3.1 | Numerical results and discussion | 113 |
| 5.4 | Fermi surface ordering: k_F from a Schrödinger formulation | 116 |
| 5.5 | Conclusion and Discussion | 126 |
| 6 | The phase diagram: electron stars with Dirac hair [83] | 129 |
| 6.1 | Introduction | 129 |
| 6.2 | Holographic fermions in charged background | 133 |
| 6.3 | Equation of state of the bulk fermion matter | 136 |
| 6.3.1 | WKB hierarchy and semiclassical calculation of the density | 136 |
| 6.3.2 | Airy correction to semiclassical density | 141 |
| 6.3.3 | Dirac hair correction to semiclassical density | 143 |
| 6.3.4 | Pressure and equation of state in the semiclassical approximation | 147 |
| 6.4 | Maxwell-Dirac-Einstein system | 151 |
| 6.5 | Phases of holographic fermions | 154 |

| | | |
|----------|--|------------|
| 6.5.1 | Thermodynamics | 155 |
| 6.5.2 | Constructing the phase diagram | 156 |
| 6.5.3 | Phase diagram | 166 |
| 6.6 | Discussion and conclusions | 169 |
| 7 | Discussion and conclusions | 173 |
| | References | 179 |
| | Summary | 187 |
| | Samenvatting | 191 |
| | List of Publications | 195 |
| | Curriculum Vitæ | 197 |

Chapter 1

Introduction

1.1 Holographic principle: the idea

Reductionism lies at the heart of physics. Much of the history of physics can be understood as striving for reduction in the number of basic principles and thus explaining seemingly disparate phenomena starting from the same core idea. Indeed some of the key scientific revolutions can be formulated in terms of unifying previously distinct areas of study: Newtonian mechanics bridges the gap between statics and dynamics, Maxwell electrodynamics connects electricity and magnetism, Boltzmann's kinetics unites mechanics and statistical physics. General relativity has unified gravity with mechanics while quantum field theory brought a unified look at quantum mechanics, electrodynamics and statistical physics. Finally, in the last decades we are witnessing the attempts at unifying all of physics within string theory. Looking for analogies between different systems has certainly proven to be one of the deepest principles in the search for fundamental laws of nature.

The presumed approach of the Theory of Everything through the advent of string theory (if it indeed turns out to lead to the Theory of Everything) in parallel with the standing fundamental problems of many-body and collective physics – such as unconventional superconductivity and quark confinement – has actualized the problem of emergence versus reductionism. We are facing the question of how the reduction to the few fundamental principles might help us with resolving the problems which obviously come from a complicated interplay of an enormous number of degrees of freedom. One could even wonder if extremely complex systems

are within the reach of microscopic models at all – after all, we know that hydrodynamics is not within the reach of the single-molecule description. Such a question, in its full generality, is hard to address, and the answer almost certainly varies – systems which do not at all have a single dominant energy scale might well be out of reach. On the other hand, successful explanations of collective phenomena such as Mott insulators, or the energy cascade in turbulence do give a hint that reduction to the basic principles can be fruitful even if these principles live on the scales which are many orders of magnitude smaller.

All of the above prompts us to rethink the quest for reduction and analogies as formulated in the first paragraph. We might look for direct analogies between fundamental and emergent phenomena. If Maxwell’s equations connect the two elementary constituents of electromagnetic interaction, are we able to find a theory which connects a fundamental interaction to an emergent phenomenon? Putting it bluntly, is there an analogy between the simple and the complicated? This thesis is an attempt to contribute to the answer in a specific setting – strongly correlated fermions – where the ”complex” side of the duality is likely unreachable by ”ordinary means”¹ and the fundamental side is a string theory through a mapping known as holography.

Holography is an idea aimed at providing a unified description of quantum mechanics and gravity. It was coined from a disparity between the thermodynamically calculated black hole entropy and the naive guess from dimensional analysis. Understood as information content of a physical system, entropy is expected to be an extensive quantity, proportional to the volume (measure) of the system. Nevertheless, the famous semiclassical Hawking-Bekenstein result for the entropy of a neutral non-rotating (Schwarzschild) black hole [9] predicts it as proportional to the surface

¹It is known [109] that the problem of interacting fermions is NP complete. At this place we briefly remind what this means. A problem is said to belong to the NP class if an algorithm exists which *checks* a proposed solution in polynomial time, but no algorithm is known which *finds* a solution in polynomial time. An example could be an equation such that plugging in a given candidate solution and checking if it satisfies the equation can be done in polynomial time, but no polynomial algorithm is known to compute the solution starting from the equation only. Notice that we do not know if such an algorithm really does not exist, or we are simply unable to find it yet (this question is the famous unsolved $P = NP$ problem). NP complete problems are a subclass of NP problems, such that an algorithm that solves an NP problem polynomially could be modified in a certain way to solve *all* NP problems in polynomial time.

area:

$$S = \frac{Ac^3}{4G\hbar} \quad (1.1)$$

Informally, all information about the black hole is stored on a lower-dimensional object, suggesting that a complete description of the black hole in D dimensions can be obtained by looking at the correctly chosen degrees of freedom on a $D - 1$ -dimensional manifold. This is the logic behind the arguments by 't Hooft [122] and Susskind [107]. The foundation of this principle is that it connects the concept of gravity to the quantum-mechanical concept of entropy as counting the states of the system.

The second, more technical key concept in holography is the idea of dualities, mathematically equivalent but different descriptions of the same phenomena – thus providing a bridge between different formalisms or even altogether different physical systems. The idea of duality can be given a very precise and familiar meaning. Formally, it is just a canonical transformation of the action. Well-known examples are the vortex duality for charged scalar fields and electric-magnetic duality in $U(1)$ gauge theory [71]. In the vortex case, the physical picture is that of changing the viewpoint of what is an elementary excitation. If it is the linearly dispersing plane wave, then the vortices then appear as defects where the phase of the charged field winds for a full circle. But if we dualize, then vortices are the elementary excitations and plane waves are complex vortex combinations. The duality can be captured by a Legendre transformation of the action:

$$S = \int d^3x \partial_\mu \Phi \partial^\mu \Phi \mapsto S_{dual} = \int d^3x (a_\mu a^\mu - \partial_\mu \Phi a^\mu). \quad (1.2)$$

Here, Φ is the charged scalar field which lives in two space dimensions, while its gradient $\partial^\mu \Phi$ maps to the vortex field a^μ . We can thus reexpress the action in terms of a^μ : the physics must remain the same but that does not change the fact that some phenomena are much easier to see in one or in the other language. Similar is the wisdom behind the electric-magnetic duality, where the physical observables, i.e. elements of the field strength tensor, transform into each other, again by adding a bilinear term (linear in both old and new components) to the action.

As an idea which connects quantum theories with gravity, holography finds its natural language in the formalism of string theory, where it arises as a duality transformation of the strings themselves. It is within string theory and M theory that a precise realization of the abstract holographic

principle was found. One reason is simply that it offers a coherent framework in which we can study the gravity at various energy scales— from the low-energy description of general relativity to the nonperturbative regime where the string effects dominate.

In string theory language, the duality becomes the equivalence of the open and closed string descriptions. The higher-dimensional, gravitational system is given by the excitations of the closed string. Its lower-dimensional dual gauge field description is given by the excitations on the open strings. In the next section we will present a more detailed explanation of this construction, known as the *AdS/CFT correspondence* [81, 38, 114]. However, in this introductory chapter we will not assume any prior knowledge of string theory on the side of the reader. We will stay away from extensive use of string-theoretical language and results and formulate AdS/CFT in terms of gauge theory and general relativity, with only qualitative discussion of the underlying specifically stringy constructions (branes, open strings between branes, string dualities, etc).

1.2 Realization: AdS/CFT correspondence

We do not intend to give anything like a comprehensive tutorial on AdS/CFT in this (or any subsequent) chapter, we will merely wet the reader's appetite to look for the original references if interested; most of the thesis can be followed without a detailed understanding of the foundations of AdS/CFT. The first explicit realization is due to Maldacena [81]. Here we have a Type IIB superstring theory in a configuration describing a stack of parallel D3 branes (planar objects extending along three spacetime dimensions) at some distance r from each other. The interbrane distance r also determines the "elastic energy" of the open strings which stretch between the branes and carry the gauge fields from a $U(N)$ multiplet: the energy is proportional to r/α' , where α' is the string tension. Consider now the limit of coincident branes, when $r \rightarrow 0$ but with $r/\alpha' = \text{const.}$. In the closed string description, the metric of a stack of coincident D3 branes factors out into the product of AdS space and a sphere: $\text{AdS}_5 \otimes S_5$. The open string description is a very special, highly symmetric QFT – a conformal field theory (CFT). The idea is that the more restricted and special the field theory, the easier it is to relate it to gravity. This certainly does hold for a conformal field theory (CFT), where the very high symmetry severely constraints behavior of correlation functions. CFT has a central

place in modern high and low energy physics – allowing exact calculation of correlation functions in two dimensions and strong results on RG flow (c -theorem [120]) and scaling [24]. In low energy physics they describe the quantum critical systems [15] lying at the heart of the description of phase transitions and strongly competing interactions. The $\mathcal{N} = 4$ supersymmetric Yang-Mills in four spacetime dimensions is such a CFT – despite the many fields involved, its behavior is simple due to conformality, and it has given us the first example of a holographic duality.

This explicit example allows for a quantitative connection between the gauge theory and the supersymmetric theory in AdS geometry. The connection is provided by the fact that the radius of AdS space is proportional to $(gN)^{1/4}$. The supergravity solution can be trusted if $gN \gg 1$ and $N \gg 1$. Remember that this means that the field theory is strongly coupled *and* can be expanded in the inverse number of colors. The lower-dimensional, field theory side in this and similar (early) setups of AdS/CFT are generically non-Abelian gauge theories, either Yang-Mills or its supersymmetric version, motivating another frequently used name for AdS/CFT: *gauge/gravity duality*.

To turn the above discussion into a precise duality, one needs a relation between the partition functions (on-shell actions) of the gauge theory and supergravity. To this end it is critical to determine the boundary conditions for the supergravity fields living in AdS – when they reach the branes, they are coupled to the fields living on them. This was done in the follow-up work by Gubser, Klebanov and Polyakov [38] as well as Witten [114].

1.2.1 Warmup: symmetries

Let us study the closed string (gravity) side first. The formulation of a field theory on AdS spaces is not quite trivial: AdS geometry possesses some troublesome properties such as closed timelike curves and the existence of a boundary at infinity. Informally, anti de Sitter (AdS) space is an open (hyperbolic) equivalent of the perhaps more familiar de Sitter (dS) space. The latter is the solution to the Einstein equations in the vacuum with a positive cosmological constant [2]. The latter can be thought of as a mysterious form of matter with equation of state $p = -\rho$. It has negative pressure: it expands as it cools down, just like our universe. It is thus a cosmological model in the approximation of “empty Universe” where the presence of matter is negligible and the geometry is dictated by the

cosmological constant. In AdS space, on the other hand, the cosmological constant is negative, i.e. it behaves as (positive) pressure of regular matter. Because the matter is cosmological, it cannot clump and one finds a static (time-independent) solution. The Einstein-Hilbert action that describes the anti de Sitter space in $D + 1$ spacetime dimensions is:²

$$S = \int d^{D+1}x (R - \Lambda) \quad (1.3)$$

where R is the scalar curvature while $\Lambda < 0$. As the only dimensionful factor, Λ can be rescaled at will depending on the choice of the unit of length. By convention, we write $\Lambda = -D(D - 1)/L^2$ where L has the meaning of AdS radius. This means that the solution can be embedded into a $D + 2$ -dimensional flat space as a sphere:

$$t^2 - z^2 - y_i y^i = L^2. \quad (1.4)$$

A natural coordinate patch covers half of the space:

$$ds^2 = \frac{r^2}{L^2} (-dt^2 + dx_i dx^i) + \frac{L^2 dr^2}{r^2}. \quad (1.5)$$

The radial coordinate r stretches from 0, called the interior, to infinity, called the AdS boundary. AdS is the maximally symmetric solution to Einstein equations. An extremely useful way to think about AdS_{D+1} is as a hyperboloid embedded in a $D + 2$ -dimensional flat spacetime with signature $(+, \dots, +, -, -)$. The embedding in a spacetime with $D + 2$ dimensions helps to see that the total geometric symmetry group of AdS space is $SO(D, 2)$. The global and local geometry of AdS space are sketched in Fig. 1.1: what globally looks as the usual double hyperboloid (but in Minkowskian as opposed to Euclidean spacetime) locally becomes a patch of isotropic space of "decreasing size" as we move further and further, until at infinity all lengths scale to zero.

One can now motivate the correspondence starting from the symmetry arguments. It is well known that a CFT in D dimensions (one timelike and $D - 1$ spacelike dimension) also obeys the $SO(D, 2)$ symmetry [24]. Informally, the conformal symmetry is just the symmetry associated to

²In this thesis, unless specified otherwise the dimensionality of spacetime is always $D + 1$, the flat space coordinates in D dimensions are denoted by (t, y_i) ($i = 1 \dots D$) and the metric signature follows the convention $ds^2 = -dt^2 + dy_i dy^i$.

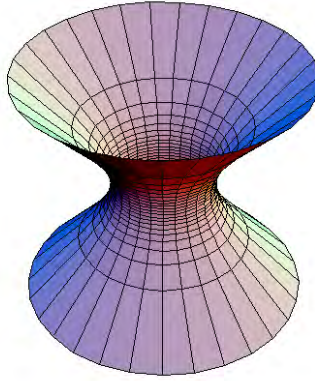


Figure 1.1: Sketch of AdS geometry. Globally it looks like a double hyperboloid but if we take a small patch it becomes very much like Minkowski space in which distances decrease as we move toward infinity. Counterintuitively, local AdS is completely isotropic and has spherical symmetry.

length rescaling, i.e. changing the scale combined with rotations. Conformal field theories are thus closely related to the concepts of self-similarity, fractality and scale-free objects but more general: the scale invariance is continuous, not discrete as in fractals, and it can be broken due to quantum effects – anomalies, like any other physical symmetry. A closer inspection reveals that the exact conformal representation of $SO(D, 2)$ is already geometrically encoded in AdS in a special limit – its boundary transforms in the same way. If one would “glue” some fields on its D -dimensional boundary, these fields ought to be redefinable as representations of the conformal group.

As a result, the CFT can be understood as the boundary degrees of freedom of a field theory in AdS. Emphatically, however, this is *not* enough for a duality, and does not yet encapsulate the idea of AdS/CFT. We need more – not just that AdS space in the near-boundary limit becomes conformal invariant but that *the fields* in AdS in the near-boundary limit also encapsulate the behavior of a conformal field.

1.2.2 Enlightenment: the duality relation

This idea finds its precise formulation in the concept of duality introduced earlier. The quantum theory is dual to gravity, thus *the operators in field*

theory are sourced by the fields on the gravity side. More precisely, the generating functional for the correlation functions in field theory is identified with the minimum of the supergravity action, satisfying specific boundary conditions at the AdS boundary. The precise boundary conditions and the crucial point of AdS/CFT, known as the GKPW (Gubser-Klebanov-Polyakov-Witten) prescription. The prescription addresses the boundary conditions mentioned at the beginning of this section and was proposed in [38, 114]. The conformal and the gravity side are connected through their partition functions as

$$Z_{bnd}(J) = Z_{bulk}(\Phi|_{\partial\text{AdS}} = J) \quad (1.6)$$

where Z_{bnd} and Z_{bulk} are the partition functions on each side, and we have employed Φ as a generic notation for all fields living in the bulk and J are their boundary values, acting as sources. In the classical gravity limit, i.e. for a large N strongly coupled field theory, Z_{bulk} is evaluated simply by plugging in the classical solutions to the equations of motion into the gravity-matter action (in other words, it is the on-shell action). Schematically, this looks like

$$Z_{bulk} = e^{-S(\Phi)}|_{\Phi(r \rightarrow \infty) = J} = \langle e^{\phi J} \rangle_{\text{CFT}} \quad (1.7)$$

where S is the classical gravity action, and in the second equality we have expressed the partition function at the boundary as the generating function of the field theory correlators. The boundary operator ϕ sees the boundary values $\Phi(r \rightarrow \infty) = J$ precisely as sources: treating Z_{bulk} in (1.7) as an effective action for ϕ , we can apply the textbook rule to calculate their correlation functions:

$$\langle \phi(y_1)\phi(y_2)\dots\phi(y_n) \rangle = \lim_{r \rightarrow \infty} \frac{\partial^n e^{-S}}{\partial \Phi(r, y_1)\partial \Phi(r, y_2)\dots\partial \Phi(r, y_n)}$$

This is the essence of applying holography in practice: we do not know how to write Z_{bnd} in terms of boundary fields explicitly, but we can use it as the generating functional of the correlation functions, and thus gain qualitative insight into the system.

The precise translation of the bulk physics into the boundary is thus achieved by analyzing the $r \rightarrow \infty$ limit of various bulk quantities. This is the quantitative basis to constructing the *holographic dictionary* which makes possible numerous practical applications of AdS/CFT. In the next chapter we will introduce dictionary entries such as temperature, chemical

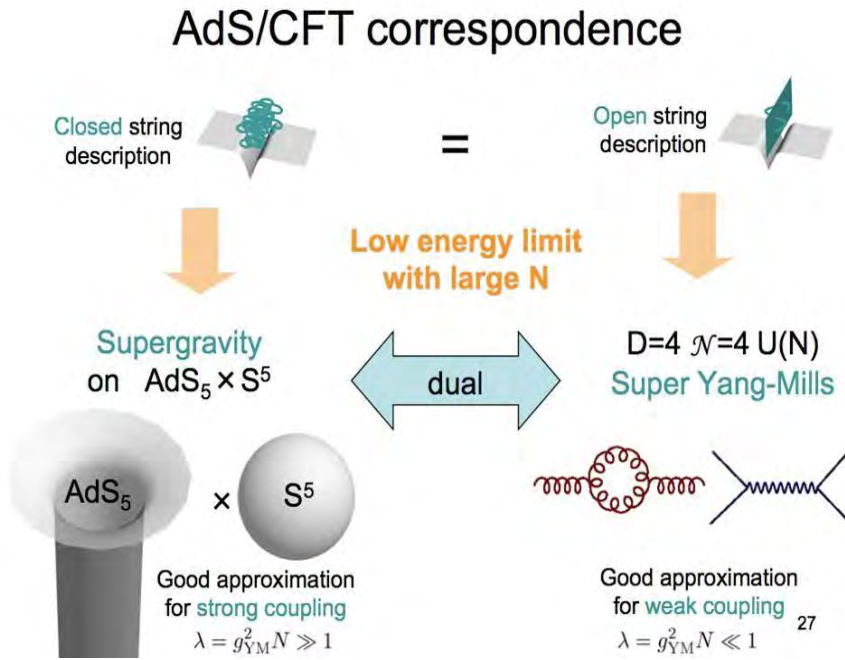


Figure 1.2: Pictorial resume of AdS/CFT: the duality is rooted in the notion of open-closed string duality. On the level of coupling constants it is also a weak-strong duality. Closed string coupling g is related to the coupling g_{YM} of the Yang-Mills theory on open strings as $g_{YM}^2 = g$. The small parameter in the perturbative expansion for the closed string interactions is the combination $\lambda \equiv gN$. Sending the closed string coupling to zero ($g \rightarrow 0$) at constant λ we get classical strings in $AdS_5 \otimes S^5$ while the Yang-Mills theory on open strings reaches the large N limit ($N \rightarrow \infty$). Taking also the limit $\lambda \rightarrow 0$, the classical type IIB string theory becomes type IIB SUGRA.

potential, electromagnetic field, conformal dimension... It is the main link between the formalism of holography and more familiar low-energy QFT physics.

From a more general viewpoint, AdS/CFT was historically important as a facet of the second superstring revolution, which found numerous dualities between string theories with different coupling constants or geometric properties. Here, the control parameter is the combination $1/gN$ of

the string coupling $g = g_{YM}^2$ and the number of colors N . In order to trust the supergravity limit we need $gN \gg 1$, but this is precisely the strongly coupled regime of the gauge theory. Therefore, AdS/CFT is an example of a weak-strong duality. Such dualities are known as S -dualities. Formally, these relate a theory with coupling constant g to a theory with coupling $1/g$. While AdS/CFT does not quite follow this pattern, as the control parameter is not g but gN , it remains a relation between strongly and weakly coupled systems. Needless to say, this gives it a great deal of practical utility: when one side becomes intractable due to string interactions, the other one becomes better and better controlled.

1.2.3 Some general remarks

We will conclude this section with some speculations on broader implications of holography on string theory and other areas. Even though the general holographic principle is essentially a gravity/quantum field theory duality, its full realization in the form of AdS/CFT is a decidedly string-theoretical result, which follows from the near-brane geometry and the action of that solution in a specific brane configuration. In other words, the 't Hooft-Susskind principle states more than AdS/CFT – it states that any physical system with gravity is equivalent to a lower-dimensional system without gravity. One might now wonder if this is indeed so, if holography is in fact a fundamental principle itself, independent of string theory, and a property of gravity and field theory as we know them. There is no answer yet on this central question. At the very least, what one can try is to apply the precise results of AdS/CFT (dictionary entries) to geometries which do not follow from string theory. As long as the geometry looks like AdS at long distances, numerous attempts so far give encouraging results.³ The non-string AdS spaces give us more freedom: we can work in any number of dimensions, with any field content. The price to

³It is much less clear and much more complicated to generalize it to non-AdS spaces, including flat space. This is another important problem to work on. The natural guess is that the correspondence can be generalized to arbitrary geometries and arbitrary field theories. Reasons that require an asymptotically AdS geometry and the difficulties involved in constructing a flat space holography are beyond the scope of this Introduction and indeed this thesis. Roughly speaking, in flat spacetime there seem to be too many degrees of freedom on the gravity side to match to a lower-dimensional QFT; AdS asymptotics puts some rather stringent constraints on the dynamics of gravitational field. The extension beyond AdS is certainly a central fundamental question for the future of holography.

pay is, of course, that we cannot at the present be sure about the consistency of such attempts. This approach is known as *bottom-up* as opposed to the *top-down* string approaches. In this thesis we will mostly use the bottom-up logic, for both practical and conceptual reasons.

In this place it is appropriate to discuss the status of AdS/CFT as a confirmed result versus a conjecture. Though it is widely accepted (e.g. [25]), a rigorous proof is lacking. Nevertheless, the evidence in favor of AdS/CFT is very solid: it has passed numerous non-trivial tests where observables whose forms do not depend on the coupling constant were computed on both sides and compared [2].

1.2.4 Holography outside high-energy theory

The manifestation of holography as a duality has given rise to a completely different research pursuit from the understanding of black holes. Holography can also be used as a tool to understand systems at strong coupling, where the conventional perturbative methods of field theory fail. So far AdS/CFT has established itself as an approach to quantum chromodynamics (QCD) and to condensed matter theory (CMT), the corresponding fields being known as AdS/QCD and AdS/CMT. The power of holography is that it allows us to study previously inaccessible strongly coupled systems. In AdS/QCD, the focus of most work done so far was on describing the confinement transition and studying the quark-gluon plasma at intermediate energies, when neither perturbative QCD nor effective low-energy theories work well (this regime is primarily tested in heavy ion collisions). The latter line of research has produced perhaps the most important result of applied holography so far, the universal viscosity bound, stating that any isotropic equilibrium fluid has an inherent shear viscosity to entropy ratio

$$\frac{\eta}{s} \geq \frac{1}{4\pi} \quad (1.8)$$

The quark-gluon plasma studied in the RHIC accelerator exhibit a viscosity remarkably close to the bound (1.8).

The main approaches exist in AdS/CFT. The first is a top-down approach which constructs a Yang-Mills theory akin to QCD from brane intersections, following closely the early ideas of Witten [114, 115] where the whole endeavor of AdS/CFT is put in the context of specifically gauge/gravity duality, i.e. understanding the dynamics of Yang-Mills fields. The second is a bottom-up scheme where the four-dimensional

QCD is dual an asymptotically AdS₅ space where confinement is modeled by "thinning out" (suppressing exponentially) the amplitudes of fields in the IR. This is done using the insight that the extra dimension in AdS corresponds to the scaling flow in field theory with the near boundary behavior encoding the UV asymptotics. In this case, the RG flow interpretation is that the confinement of low-energy excitations corresponds to suppressing the dynamics in deep interior.

The second claim to fame for AdS/CFT is its application to condensed matter theory. Here, the problems of strong correlations and competing orders show their best (or rather, worst) side. It is thus extremely exciting to see how they dualize in gravity. However, since the phenomenology of condensed matter systems is much richer, and removed even further from the microscopic Hamiltonian, it becomes important to build the model in an appropriate way: to start from the solid and robust features (symmetries, degrees of freedom, extreme limits when some fields decouple or become exactly soluble) rather than engineer the gravity dual in order to get this or another specific phenomenon. The field started with a holographic calculation of transport properties of certain strongly coupled systems [59] and took off with the crucial work of Hartnoll, Horowitz and Herzog on holographic superconductors [47]. Despite the by now universally accepted name, the model in question is not actually a superconductor at all but a boson at finite density which breaks the global phase symmetry by condensing, akin to a superfluid. Nevertheless, precisely as it stands it is a very important proof of concept: this is the simplest possible case of the Landau-Ginzburg picture of order, and thus the obligatory starting point of any candidate theory for description of many-body systems. Holographic superconductors have taken the *bosonic* AdS/CMT to perfection and have been the arena in which many of the universal results and dictionary entries have been obtained.

1.3 The arena: fermions in organized matter

This thesis will focus on AdS/CFT applied to strongly coupled fermion matter. Experimental condensed matter physics has discovered numerous materials which cannot be understood from the weakly coupled perspective. Strongly coupled fermions are thus an experimental reality, and developing general methods to study them is of central importance for understanding the observed phenomena in condensed matter. In AdS/CFT,

precisely the strong coupling regime in field theory is easy to understand on the gravity side, as it corresponds to classical (super)gravity. We will now argue that such holographic description of the strongly coupled physics is especially valuable precisely for fermion systems, as conventional field-theoretical methods are far less helpful for fermions than for bosons.

We have a number of nearly equivalent ways to describe the simple observation that fermions and bosons differ in their behavior. Antisymmetry of fermionic wave functions, the Pauli principle, fermion sign problem and kinematic correlations (i.e., Slater determinants) are all about the fact that the antisymmetry of fermionic states reduces the number of available configurations, acting as a constraint on dynamics and introducing an effective interaction (or correlation) even in absence of any explicit interacting potential. While a non-interacting Fermi gas can still be solved by explicitly taking into account the antisymmetry of states when constructing thermodynamical potentials, presence of interactions spoils the picture: antisymmetry acts as a constraint, and solving an interacting system in the presence of such a constraint becomes a hopeless task. A common way to phrase the problem is the "fermion sign" viewpoint, reviewed e.g. in [119]: it refers to the negative contributions to the fermionic partition function, meaning that it cannot be regarded as a sum of probability amplitudes as for bosons and classical particles.⁴

The fermion signs are simply the minus signs in the density matrix of a fermion system. This is a direct consequence of antisymmetry of the fermionic wave function. For a system of free fermions we can write the wave function exactly; the outcome is the Slater determinant where the odd permutations contribute with a minus sign. Antisymmetry, however, does not depend on interactions in the system and the sign picture will be exactly the same. A technical way to see the trouble with fermion signs is analysis of the fermionic path integral. It is enough to remember the basic rule of constructing the partition function for a system of fermions in compact Euclidean time with period β , thus accounting for finite tem-

⁴Besides condensed matter, another area where the sign problem is well-known is Quantum Chromodynamics (QCD). There, the sign problem arises in a seemingly different but in essence equivalent form: the presence of finite density (and thus chemical potential) makes the Euclidean Hamiltonian non-Hermitian, and thus the partition function complex. The negative vs. complex dichotomy is that of real vs. imaginary time, but in both cases it is the fermionicity of the Hamiltonian which gives rise to problems at finite density, and both negative and complex partition function give us the same pain: absence of probabilistic interpretation.

perature $T = 1/\beta$. Remember that partition function equals the integral of the trace of the density operator:

$$Z = \text{Tr}e^{-\beta H} = \int d^{ND} \mathbf{x} \rho(\mathbf{x}, \mathbf{x}; \beta) \quad (1.9)$$

where the density operator is $\rho(\mathbf{x}_1, \mathbf{x}_2)$ and \mathbf{x} denotes the set of coordinates of all particles in a D -dimensional system with N fermions. Now for a system of indistinguishable particles ρ is a sum over of all permutations Π of the particles, as any two particles can be exchanged without changing the system physically. This gives

$$\rho(\mathbf{x}, \mathbf{x}; \beta) = \frac{1}{N!} \sum_{\Pi} (\pm 1)^{|\Pi|} \rho(\mathbf{x}, \Pi \mathbf{x}; \beta) \quad (1.10)$$

Here, the sum is over all permutations Π of the particles, and $|\Pi|$ is the parity (symmetry/antisymmetry) of the permutation. For bosons all terms are positive and one can define a measure based on the density matrix ρ_+ . For fermions, however, odd permutations carry a negative contribution. The partition function is, of course, always positive, but we see that individual contributions to the density matrix are not. This in turn means that fermions are never classical: unlike for bosons, quantum statistics brings a discontinuity from classical Euclidean field theory and its path integral formulation. The effective action for bosonic expectation values is just the celebrated Ginzburg-Landau theory or one of its many derivations. Nothing like it exists for fermionic operators.⁵ Consequently, despite decades of research of strongly correlated fermions, the actual methodologically sound knowledge we have on this topic is very limited. A measure of the difficulty of the sign problem is the realization of Troyer and Wiese [109] that it is NP complete.

What, then, are the things we do know?

1. *Free Fermi gas.* One example is obvious: the free Fermi gas is exactly soluble. It is not really free, as kinematic correlations are introduced by the statistics, however we know that the Slater determinant accounts for them exactly.

⁵While the expectation value of a fermionic operator is trivially zero, we typically want to compute operator products. Density, correlation functions, transport coefficients etc. are all of this form. However, working with fermion operator products is no easier than working with single fermions.

2. *Fermi liquid.* The second example is the breakthrough of Landau in understanding normal metals in terms of Fermi gases [73]: the Fermi liquid paradigm. The logic is well-known: a gas of particles with infinite lifetimes turns into a gas of quasiparticles with finite but long lifetimes. Everything remains the same as for a free gas, except that all parameters undergo renormalization. The crucial requirement is that the ground state of the interacting system have a nonzero overlap with the ground state in the non-interacting limit. In other words, Fermi liquid is so much akin to a Fermi gas simply because it is adiabatically connected to it. Subsequent, more rigorous studies of the Fermi liquid have confirmed this basic picture (see [5] and references therein). The mathematical foundation of Landau's Fermi liquid insight is provided by the RG formalism for fermions given in [88, 100] and has the form of a functional RG which starts from a weakly interacting theory at intermediate scales and introduces interactions perturbatively in the effective action. Being a weak coupling expansion, it does not have sign problems. However the perturbative treatment does make it hard to treat non-perturbative phenomena e.g. a superconducting instability within this approach.
3. *Fermions in $(1 + 1)d$.* A special case which is in principle completely known is that of fermions in one spatial dimensions. While fashionable these days, and certainly capable of displaying very intricate behavior of correlation functions and transport properties (see e.g. [110]), one-dimensional fermions are completely demystified by bosonization: in one space dimension, any fermion system can be bosonized in infinitely many ways (the most typical situation is the spin-charge separation) and then solved through usual field theory methods. The reason is that statistics cannot really be defined in $1 + 1$ dimension: the manifold of possible Slater determinant states coincides with the manifold of nodeless wave functions.
4. *Miscellanea.* Finally, there is a small number of exactly soluble interacting fermion models in higher dimension, such as exact wave functions for Fractional Quantum Hall states [74]. These are however of very little significance for the broader sign problem, being rather special non-generic.

The inescapable conclusion is that, if we want to avoid the strange ad hoc models of the point (4), everything we know is either to bosonize

or to hope that the system studied is adiabatically connected to a non-interacting Fermi gas, at least in the IR. The vast field of strongly correlated electrons armed with various field-theoretical techniques [34, 110] is as it stands incapable of constructing (through controlled, justifiable approximations) *novel ground states* of fermion matter. The list of celebrated experimental puzzles, from unconventional superconductors [118, 42] to heavy fermions [80], all likely novel ground states qualitatively different from normal Fermi liquids, is therefore in desperate need of a theoretical paradigm that will not depend on non-interacting or bosonic physics.

We are now able to formulate a sharp question underlying all of strongly correlated electron systems: *Is there a stable state of electrons at finite density which cannot be adiabatically continued to Fermi gas?* This is perhaps the closest it comes to formulating the motivation for this thesis in one sentence. A solution we propose here is to use the power of holography.⁶

This is not just an academic question. The importance of strongly correlated electron physics is its manifest necessity to explain a multitude of experimental findings amidst experimental evidence in favor of distinctly non-Fermi liquid phases of fermionic matter. The most famous are certainly high temperature superconductors, cuprates and pnictides being the leading members of this heterogenous group. The superconducting order at relatively high temperatures is almost the least important of the many unusual properties. A glance at the phase diagram of cuprates (Fig. 1.3) reveals how the doping of external charge carriers turns the system from the familiar normal metal, i.e. Fermi liquid phase into a non-Fermi liquid, universally known in condensed matter physics as strange metal, continuing on into the pseudogap. The pseudogap region is also mysterious, but thought to display some kind of long-range order. Dozens of exotic order parameters were proposed to explain this novel ground state: stripes, current loops, exotic spin ordering and others [118]. Many of them

⁶As a side remark, we refer the reader to [119, 72] for a possible geometric interpretation of the "fermionic constraint" which allows one to treat the problem of fermionicity by looking at certain global (topological) properties of the many-particle wave function and the path integral. The key result is the proof [13] that the signful path integral can be turned into ordinary bosonic path integral but with an additional constraint. For us, it is the morale and not the details which is important: it provides a construction which explicitly reduces fermion dynamics to boson dynamics with constraints. While AdS/CFT handles fermions in a somewhat different way, essentially trading the fermionic physics for curved space, it might be an indication that in the end all fermionicity can be bosonized by adding additional constraint structure to dynamics.

have some degree of experimental support [118]. We also do not understand how the advent of the strange metal is related to superconductivity itself.

A possible unifying point for these phenomena in unconventional superconductors and heavy fermions (as well as some other materials) is quantum criticality [95, 15], developed mainly by Sachdev. Its basic idea is that quantum fluctuations can mimic the effects of temperature on the order parameter of some ordered phase. The outcome is that the ordered phase becomes unstable and vanishes at a critical point at zero temperature. In place of temperature, the control parameter is typically some quantity which governs the competition between two ordered phases at $T = 0$, e.g. coupling strength or doping. The phase diagram of a system with a quantum critical point typically looks as in Fig. 1.3(A), quite similar to the phase diagram of real-world cuprates in Fig. 1.3(B) – above the critical point one has a characteristic quantum critical “cone”, the regime in which the quantum critical point influences the physics even at relatively high temperatures. This is an important difference with respect to finite temperature critical points: in the latter case, the scale invariance inherent to criticality is only felt in a narrow window around $T = T_c$, while quantum critical behavior can be detected even by measurements significantly above $T = 0$. Systems with a quantum critical point are mainly recognized for exhibiting remarkable scaling laws [111]. Of course, quantum criticality immediately brings associations on CFT and makes a great starting point for a holographic investigation. Notice the inverted epistemology of holography compared to conventional methods: normally, we would start from the Fermi liquid phase and try to build up interactions that drive it to the critical point. In AdS/CFT, we can start from the quantum critical point where the theory is very strongly coupled and completely encapsulated in the scaling relations, with particles being non-existent, and the challenge is to see how the system picks a ground state away from criticality. This is the essence of AdS/CMT: we know most in AdS/CFT precisely in the situation when we know least in conventional CMT.

This in turn makes CFT an important tool for description of such systems – scale invariance of the quantum critical phase is almost equivalent to conformal invariance. Therefore, if the universal ingredient in transitions from Fermi liquid non-Fermi liquid systems is quantum criticality, then the CFT and its gravity dual in AdS present a natural starting point.

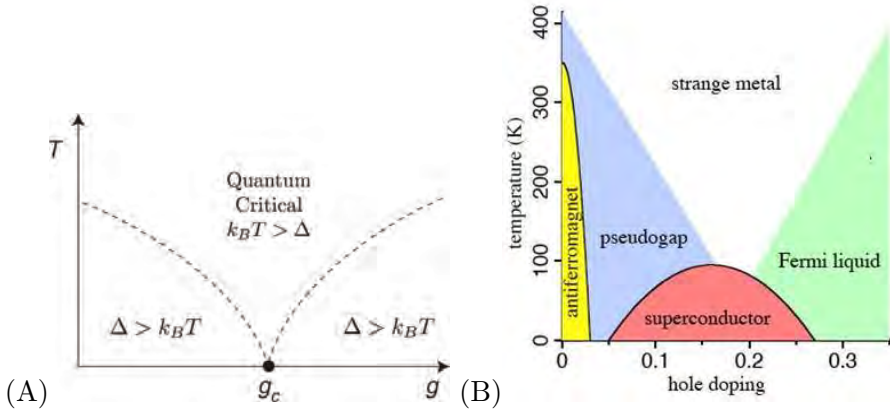


Figure 1.3: (A) Sketch of the phase diagram of cuprates. Normal metal phase turns into a non-Fermi liquid at critical doping, which presumably corresponds to a quantum critical point. The zoo of exotic orderings resides in the strange metal phase, which partially overlaps with the superconducting region. The properties of the strange metal remain mystifying, and might constitute a prime example of a stable non-Fermi liquid ground state. In (B) (adopted from [95]) we see schematically how the quantum critical point influences the physics at finite temperature: when the temperature energy scale $k_B T$ is larger than some characteristic energy scale Δ of the system, we are in the quantum critical "cone" where the physics is governed by the scaling laws imposed by the quantum critical point.

1.4 Outline

Our first goal will be to find the gravity dual for the Fermi surface which will be as general as possible and not hinge on existence of quasiparticles. The minimal ingredients we need are fermions, temperature and chemical potential. Our holographic dictionary translates this into a charged black hole plus the Dirac equation for the fermions. This is done in the next chapter. A Fermi surface should reveal itself in the spectrum of perturbations. We will study in detail the momentum and energy distributions of the spectral weight and conclude a great deal about the quantum critical fermions in this way. This chapter is adapted from [17] and includes the formalism for calculating the spectrum in a separate section (originally the Supplementary material of the paper). Chapter 4 [18] studies fermionic instabilities, giving dictionary entries for fermion density and Fermi liquid

itself, within a model we call black hole with Dirac hair. Chapter 5 [19] is the beginning of the study of the phase diagram of holographic fermions. In this chapter, we compare the Dirac hair model to the electron star model by Hartnoll et al [51] and show how one can interpolate between the two, corresponding to stable quasiparticles with different properties in field theory. In chapter 6 [83] we will study the actual phase diagram of holographic fermions by a full quantum-mechanical formulation of electron star and Dirac hair. and finally address the question – can we see novel phases from AdS/CFT? Chapter 7 sums up the conclusions.

Chapter 2

The holographic dictionary

2.1 The basic entries

We are now ready to consider the theoretical background of our work and to work out in some detail the results we will use. This essentially corresponds to constructing the detailed dictionary entries and formulate rules for the boundary terms in the action. We start with pure AdS space (we will need more later, to introduce temperature). We will work on the Poincaré patch of AdS space rather than global AdS. For most of the calculations it is much more appropriate to use the dimensionless inverse of the r coordinate:

$$z \equiv \frac{L}{r} \tag{2.1}$$

While the radial distance goes from $r = 0$ in the interior to infinity, now $z = 0$ corresponds to the boundary while $z = \infty$ is the deep interior. We might have a situation where there is a lowest bound on r , e.g. the position of a black hole horizon r_h (and there will be, if the temperature is finite). Then the deep IR is at $z_h = L/r_h$ instead of infinity. The AdS $_{D+1}$ metric in z coordinate is

$$ds^2 = \frac{1}{z^2} \left(-dt^2 + \sum_{i=1}^{D-1} dx_i^2 + dz^2 \right). \tag{2.2}$$

Deformations away from AdS space are allowed as long as the small z asymptotics (AdS boundary) is unchanged. We will only consider equilibrium physics in this thesis, which corresponds to stationary and homogenous geometries. We will also only consider isotropic systems, i.e.

isotropic geometries in the bulk. This makes all components of the metric depend only on z and allows at most two free functions parametrizing deformations from AdS. We can therefore write the most general metric as

$$ds^2 = \frac{1}{z^2} \left(-f(z)h(z)dt^2 + \sum_{i=1}^{D-1} dx_i^2 + \frac{dz^2}{f(z)} \right) \quad (2.3)$$

where we recognize $f(z)$ as the red shift factor (warp function). For AdS asymptotics we must have $f(z) = 1 + O(z)$ and $h(z) = 1 + O(z)$ for $z \rightarrow 0$. General stability conditions also make both f and h everywhere non-negative. Finally, $f(z_h) = 0$ indicates the existence of a horizon at $z = z_h$.

2.1.1 Thermodynamics

Finite temperature

The basis of the dictionary is given by the identification of the partition functions given in (1.6). The first new dictionary entry we introduce is temperature, originally proposed by Witten in [115]. It is a direct consequence of the basic fact that temperature enters kinematics of a field theory by imposing periodicity of Euclidean time. Consider first an AdS space in imaginary time. A well-known (but not unique) solution with periodic Euclidean time $\tau \equiv it$ is the Schwarzschild black hole. This solution corresponds to metric (2.3) with $h = 0$ and

$$f(z) = 1 - \frac{4\pi M}{D\pi^{D/2}\Gamma(D/2 + 1)} z^D, \quad (2.4)$$

where M is the black hole mass. This solution is only defined up to the horizon at z_h , the outermost (smallest z) radial slice where the red shift function vanishes: $f(z_h) = 0$. It is only smooth if the time is periodic with the period

$$\frac{1}{T_{BH}} \equiv \beta = \frac{z_h}{2\pi} \quad (2.5)$$

where T_{BH} is the Hawking temperature of the black hole. Since the space-time coordinates (t, x) are directly identified in the dictionary, the compactification of imaginary time retains the same meaning in the boundary theory: $T_{BH} = T_{bnd}$. Notice that the temperature in field theory equals the temperature of the black hole and *not the temperature of the bulk*,

as the latter is always zero. This is of more than academic interest as it means that the bulk fields live at $T = 0$ and should be treated by the usual field theory and not thermal field theory.

Free energy

The next dictionary entry, especially important when dealing with exotic systems where very few principles are known to hold, is that of free energy of the field theory, as the laws of thermodynamics are general enough that they can always be used as the starting point. This directly follows from the relation of free energy \mathcal{F}_{bnd} to partition function Z_{bnd} as the defining equality:

$$e^{-\beta\mathcal{F}_{CFT}} = \langle Z_{CFT} \rangle_{\text{CFT}}. \quad (2.6)$$

According to GKPW formula, the right-hand side equals the bulk on-shell action with appropriate boundary conditions. We thus find:

$$e^{-\beta\mathcal{F}_{CFT}} = \langle e^{-\int d\tau \mathcal{L}_{bulk} + S_{bnd}} \rangle_{\text{AdS}} \quad (2.7)$$

where we have included the possibility of boundary interactions on the gravity side. In classical gravity, i.e. for large N and large gN the bulk expectation value is obtained simply by plugging in the on-shell solutions into $S_{bulk} + S_{bnd}$. Taking into account (2.5) we get the factor of β in the exponent of Z_{bulk} too, so

$$\mathcal{F}_{CFT} = S_{bulk}(\Phi_{\text{on-shell}}) + S_{bnd}(\Phi_{\text{on-shell}}). \quad (2.8)$$

This simple but very important rule was given in [115]. Then we can follow all the usual thermodynamic identities to find other thermodynamic potentials, as well as their derivatives. Notice again that we cannot equate \mathcal{F}_{CFT} to any *thermodynamic* quantity in the bulk, as the latter is at zero temperature.

2.1.2 Sources and expectation values

Scalar field

The observables of a CFT have correlation functions of their operators \mathcal{O} , carrying certain quantum numbers. These correlation functions are formally generated in the standard way by taking functional derivatives of

$$\langle \mathcal{O}\mathcal{O}\dots\mathcal{O} \rangle = \frac{\delta^n}{\delta^n \Phi_0} \langle e^{\int \Phi_0 \mathcal{O}} \rangle_{\text{CFT}}. \quad (2.9)$$

Recalling our duality discussion, we should identify the source Φ_0 with a field in AdS $\Phi(x)$ restricted to the boundary where conformal symmetries are realized, relating $\lim_{z \rightarrow 0} \Phi(z)$ to Φ_0 . The boundary conditions should ensure that the source is the leading (non-normalizable) component of the solution at the boundary. Let us see how such a procedure works for a scalar field and for a gauge field. The results to follow are mostly from [114, 115] with some slight refinements summarized in [2, 25]. In this case the bulk action and the equations of motion are trivially

$$S_{bulk} = - \int d^D x \left(D_\mu^\dagger \Phi D^\mu \Phi + m^2 \Phi^2 \right) \quad (2.10)$$

$$\left(z^{D-1} \partial_z z^{1-D} \partial_z + k^2 - \frac{m^2}{z^2} \right) \Phi = 0 \quad (2.11)$$

We are looking for a solution which remains finite at the boundary $z \rightarrow 0$. Making a power-law ansatz $\Phi \sim z^\alpha$, we find that exponents of the near-boundary asymptotic of the field Φ are $\Delta_\pm = D/2 \mp \sqrt{(D/2)^2 + m^2}$. Here, Δ_- corresponds to the leading and Δ_+ to the subleading branch. One can actually find the exact solution in the whole AdS space in terms of modified Bessel functions, giving general solution of the form

$$\Phi(z) = \Phi_S z^{D/2} K_{\Delta-D/2}(kz) + \Phi_R z^{D/2} I_{\Delta-D/2}(kz) \quad (2.12)$$

where K and I are modified Bessel functions of first and second kind, respectively and

$$\Delta = \Delta_+ = D/2 + \sqrt{\left(\frac{D}{2}\right)^2 + m^2}. \quad (2.13)$$

The normalizable solution is proportional to Φ_R while the non-normalizable one is the Φ_S branch. Therefore, according to the dictionary, Φ_R is the response (expectation value) and Φ_S the source. Consider now the one-point function $\langle O \rangle$. The variation of the bulk action for such a configuration is found by substituting the solution into S_{bulk} :

$$\delta S_{bulk} = \int_0^\infty dz \int d^D x \sqrt{-g} 2\delta\Phi (D_\mu^\dagger D^\mu - m^2)\Phi - 2 \int d^D x \sqrt{-h} \delta\Phi \partial_z \Phi|_{z=0} \quad (2.14)$$

where h is the induced metric on the boundary. The first term vanishes for the solution of (2.11). For the second term the characteristic AdS/CFT

steps come. First, we see that the bulk action in general diverges at the UV boundary $z \rightarrow 0$ and needs to be regularized. The last, divergent part of (2.14) can be removed by the boundary counterterm

$$S_{bnd} = \int d^D x \sqrt{-h} \Phi^2 \quad (2.15)$$

This is exactly the Dirichlet term familiar from elementary analysis: its meaning is to fix the boundary data Φ_0 . So consistency if the bulk theory *requires* it to be reconstructible from the boundary.

At second order we find the two-point correlator for the boundary field \mathcal{O}

$$\langle \mathcal{O}(\mathbf{x}_1) \mathcal{O}(\mathbf{x}_2) \rangle = \frac{\partial^2 S}{\partial \Phi(x_1) \partial \Phi(x_2)} \sim \frac{\text{const.}}{|x_1 - x_2|^{2\Delta}} \quad (2.16)$$

with Δ defined in (2.13). Therefore, the seemingly arbitrary definition of Δ in (2.12) is chosen to match the conformal dimension of the boundary field. We see that the operator \mathcal{O} scales in accordance with the predictions of CFT with conformal dimension Δ . Also if additional terms asuch as interactions are added in the bulk, it is clear that the UV asymptotics will still be determined by m , or else (if the additional terms are irrelevant at the boundary) the asymptotic AdS geometry will be unstable. So another dictionary entry is that *conformal dimension in field theory is determined by the bulk mass of the field*.

Gauge fields, field strengths and densities

The procedure above is readily generalized to gauge fields. In this thesis we will need only the Abelian $U(1)$ field so we focus on that. Let us start from the well known Maxwell action. By partial integration, bulk action evaluates to

$$S = -\frac{1}{4} \int_0^\infty dz \int d^D x \sqrt{-g} F_{\mu\nu} F^{\mu\nu} = \frac{1}{2} \lim_{z_0 \rightarrow 0} \int d^D x \sqrt{-g} F_{\mu\nu} A^\mu n^\nu|_{z_0} + \int_0^\infty dz \int d^D x \sqrt{-g} A_\nu \partial_\mu F^{\mu\nu} \quad (2.17)$$

where n^ν is the unit normal vector to the boundary. To cancel the boundary contribution we precisely need the von Neumann term $S_{ct} = \int d^D x \sqrt{-h} F_{\mu\nu} A^\mu$ that fixes the field strength at the boundary. Now that

we have the boundary action, we can proceed to find the dictionary entries. The solution to the Maxwell equations near the AdS boundary is a linear function in z . For the component A_0 we can write

$$A_0 = A_0^{(0)} + A_0^{(1)}z + O(z^2), \quad (2.18)$$

so the leading term, $A_0^{(0)}$, is the source and $A_0^{(1)}$ is the response. The boundary action is $S_{bnd} = -A_0^{(0)}A_0^{(1)} + \dots$: the leading and subleading term are linearly coupled to each other. It becomes clear that $A_0^{(1)}$ can be identified with negative charge density ρ while its source $A_0^{(0)}$ has the meaning of chemical potential μ (i.e. background scalar potential). For a spatial component of the gauge field, we can write

$$A_i = A_i^{(0)} + A_i^{(1)}z + O(z^2) \quad (2.19)$$

and equate the subleading term $A_i^{(1)}$ to the current J_i while $A_x^{(0)}$ is its source. Therefore, we arrive at the conclusion that the subleading and leading term of the bulk gauge field encode the current density and its source, i.e. background $U(1)$ field. We can rephrase this conclusion in terms of electric and magnetic field strengths in the bulk if we assume spacetime homogeneity. In this case transverse electric field is simply $E_i = -i\omega A_i$ and the radial magnetic field is $B_i = i\epsilon_{ijk}k_j A_k$. We can now say that the bulk radial electric field stands for the charge density while the radial magnetic field in the bulk is the magnetic field at the boundary. For the transverse fields, we get that transverse bulk electric field encodes for the electric field at the boundary, while transverse bulk magnetic field stands for spatial current on field theory side.¹ Notice that the fields at the boundary obey *global* rather than gauge currents. This is an important property of the dictionary: gauge symmetry in the bulk becomes a local symmetry at the boundary. Another manifestation of this principle is the $SO(D-1)$ rotational invariance in field theory. In AdS, $SO(D-1)$ is a gauge symmetry, a consequence of diffeomorphism

¹This fails for the component A_z . Obviously, since the radial coordinate does not exist on field theory side, A_z cannot be dual to any component of the current. In fact, it has no physical sense at all and one should put $A_z = 0$ in holographic setups. To see this, remember that nonzero radial gauge field implies a nonzero radial flux through the boundary. This would violate the RG flow interpretation of the radial direction – we do not know how to interpret radial flow of *matter* along z . For that reason we always put $A_z = 0$.

invariance, in the sense that an $SO(D-1)$ rotation transforms AdS space into itself but in different coordinates.

There is a way to use AdS/CFT in the canonical ensemble using the method of alternative quantization for the gauge field. From (2.19), we see that the leading term has the same asymptotics as the derivative of the subleading term. By a Legendre transform we can thus swap the roles of $F_{\mu\nu}$ and A_μ in the boundary term and regard J_μ as fixed instead of the source E_μ . For example, suppose the gauge field has the form $A = A_0 dt$. Then the boundary action is $S_{ct} = \mu\rho + \dots$: the two coefficients are linearly coupled to each other, and we can identify $a_0 \mapsto \mu, b_0 \mapsto \rho$: *leading and subleading term in the gauge field component A_0 correspond to chemical potential and charge density in field theory.*

2.2 Holographic superconductors: a tutorial

In this subsection we will present a worked-out example where the general formalism of holography is applied on perhaps the simplest possible nontrivial system: a charged scalar boson coupled to the $U(1)$ Maxwell field and gravity. This is the famous holographic superconductor model, proposed in 2008 by Hartnoll, Horowitz and Herzog [47, 46], and Gubser [40]. It is immediately clear that the term superconductor is not quite satisfying: not only are there no fermionic degrees of freedom but the $U(1)$ symmetry is global and not gauged, thus more akin to the situation in a superfluid. Nevertheless, it is the most famous application of AdS/CFT on complex systems, encapsulating all important elements.

Let us first recall the effective Landau-Ginzburg theory of superconductivity. There, one replaces the microscopic treatment of Cooper pairs by an effective theory for the charged bosonic order parameter Φ . One then constructs the free energy in the vicinity of the transition point in accordance with general symmetry requirements. The result is a phenomenological action which can describe the dependence of the pair density on temperature near the critical point, as well as the Higgsing phenomenon, i.e. breaking of the gauge $U(1)$ symmetry by the condensate. Since the holographic description will take $U(1)$ to be a global rather a local symmetry, This last ingredient is missing in the holographic version. The holographic superconductivity an important breakthrough. Not only does it give an example on how to treat in principle the condensation of any order parameter holographically, but it does so in a novel way: directly from

a critical system and this is reflected in non-standard transport properties which reproduce the experimental results for superconducting materials.

Following the original papers, we specify to the case of $D = 3$ in this section. The bulk action is easy to write from the symmetry requirements:

$$S_{bulk} = \int dz \int d^3x \left[R + 6 - \frac{1}{4} F_{\mu\nu} F^{\mu\nu} - D_\mu^\dagger \Phi D^\mu \Phi - m^2 \Phi^2 - V_{int}(|\Phi|) \right] \quad (2.20)$$

where the covariant derivative is

$$D_\mu = \partial_\mu - iqA_\mu \quad (2.21)$$

and the potential V_{int} can be an arbitrary function in the bottom-up setup. We will opt for the simplest case and set it to zero. At finite temperature nothing changes dramatically upon introducing a finite potential. The ansatz (2.3) can be used for the metric. For simplicity, let us assume spherical symmetry, isotropy and an electric-only configuration of the Maxwell field for now, writing

$$A = A_0(z)dt \quad (2.22)$$

The 00 and zz components of the Einstein equations read:

$$3f - z\partial_z f - 3 = \frac{1}{2} \left((\partial_z \Phi)^2 - V + (\partial_z A_0)^2 + q^2 \Phi^2 A_0^2 \right) \quad (2.23)$$

$$3f - z\partial_z f - 3zf \frac{\partial_z h}{h} - 3 = \frac{1}{2} \left((\partial_z \Phi)^2 + V + (\partial_z A_0)^2 + q^2 \Phi^2 A_0^2 \right) \quad (2.24)$$

while the Maxwell equation for F_{0z} reads

$$\partial_z \left(\frac{1}{\sqrt{h}} \partial_z A_0 \right) = 2q^2 \frac{\Phi^2}{z^3 \sqrt{f} h}. \quad (2.25)$$

The ii component of Einstein equations can be shown to be a linear combination of the remaining two and can be left out. The equations for this simple system are clearly quite involved. This is typical for the bulk physics of holographic systems: the full solution has to be obtained numerically, while analytical estimates can be made in the near-horizon and near-boundary limit. The former is of importance for the phase diagram and analysis of the condensate formation. We will discuss it after we solve a more basic question: how to impose the boundary conditions and calculate the quantities on the field theory side? To that end, we can use the

results obtained earlier for the near-boundary asymptotics of the scalar field – it turns out that coupling to the gauge field is always a subleading term for $z \rightarrow 0$ and does not change the asymptotics. Schematically, the near-boundary solution is therefore

$$\Phi(z \rightarrow 0) = \Phi^{(1)} z^{3-\Delta} + \Phi^{(2)} z^\Delta. \quad (2.26)$$

The boundary action is important for the calculation of free energy at the boundary. The scaling dimension is set by the bulk mass; as before, we have $\Delta = D/2 + \sqrt{D^2/4 + m^2}$. According to the dictionary, $\Phi^{(2)}$ sources the boundary field while $\Phi^{(1)}$ is its VEV. For a solution that holographically encodes spontaneous symmetry breaking, we must seek for a spontaneously generated VEV without a source for the scalar and gauge field:²

$$S_{bnd-\Phi}^{(1)} = \oint d^3x \sqrt{-h} \Phi^2|_{z \rightarrow 0} \quad (2.27)$$

For completeness we give also the boundary action for the metric and the gauge field. This is the Hawking-Gibbons term for the metric and imposing the chemical potential $\mu = A_0(z_0)$ through a Dirichlet boundary condition for A_0 . This gives altogether:

$$S_{bnd} = \oint d^3x \sqrt{-h} (-2K + 4 + A_0 \partial_z A_0 + \Phi^2). \quad (2.28)$$

2.2.1 Scalar condensate and phase transitions

In the presence of a nonzero electrostatic potential the scalar has an effective negative mass: $-m_{eff}^2 \Phi^2 \sim -q^2 f h A_0^2 \Phi^2 / z^2$. For a large enough charge q , it is reasonable to expect the scalar order parameter to condense. This is precisely what happens. Note that this means that the spontaneous breaking of the global $U(1)$ invariance in field theory is described by the spontaneous breaking of a local symmetry in the bulk, i.e. Higgsing in the bulk. Upon solving the equations of motion (2.23-2.25) with appropriate boundary conditions, one is able to find a solution with non-vanishing scalar field. On the field theory side, the operator dual to Φ will condense,

²We can also employ the alternative quantization, where the subleading term becomes the source. Fixing the subleading term however is not enough to cancel the divergence, and we need to add an explicit counterterm so the boundary action becomes $S_{bnd-\Phi}^{(2)} = \oint d^3x \sqrt{-h} (\Phi^2 + 2\Phi n_z \partial^z \Phi)$.

breaking now the global $U(1)$ symmetry.³ Solving the system (2.23-2.25) numerically, one obtains the dependence of the condensate value $\langle\Phi\rangle$ on temperature. The result is a textbook order-disorder transition with the *mean field* scaling of the condensate with temperature:

$$\langle\Phi_{1,2}\rangle \propto \left(1 - \frac{T}{T_c}\right)^{\beta_{1,2}}. \quad (2.29)$$

One can then proceed to calculate the free energy which indeed reveals the existence of a second order phase transition, and with mean field exponents, thus reproducing the predictions of the Landau-Ginzburg theory. This finding encapsulates the essential features of holographic superconductivity – a scalar with arbitrary mass Higgses in the bulk leading to a global order-disorder transition on the field theory side.

Hartnoll et al have proceeded to compute conductivities [47] and found excellent qualitative agreement with experiment. In the standard quantization, Φ_1 condenses and backreacts on the gauge field. We can then compute the conductivity of the system as the ration of the current and the external field – the corresponding bulk quantities are the subleading and the leading term of a spatial component of the gauge field. The resulting curve looks like that of conventional BCS superconductors. Doing the same in alternative quantization, for Φ_2 (see the footnote on this page), one finds that conductivity mimics the one seen in unconventional superconductors. This was the first triumph of AdS/CMT in approaching the experiment [45].

Remarkably, a neutral scalar can also condense. The above mechanism clearly cannot be the cause of the formation of neutral hair. What is the mechanism here? The explanation lies in the generalization of the tachyonic instability to AdS known as the Breitenlohner-Freedman (BF) bound [25, 47, 46] and the geometry of the charged black hole. The BF bound is the value for which the square root in Δ becomes imaginary. In $D + 1$ dimension it reads:

$$m^2 < m_{BF}^2 = -\frac{D^2}{4L^2} \quad (2.30)$$

³For low masses, the scalar field has two quantizations with the non-standard alternative quantization similar to the Legendre transform to the canonical ensemble as described earlier. The two possible choices for the boundary conditions – fixing the VEV versus fixing the source – lead to two different field theories, with different properties.

where L is the radius of the space. In AdS_4 the BF value is thus $-9/4L^2$. In the presence of non-zero chemical potential, this system has a different geometry in deep interior dual to the IR of a CFT. The near-horizon region of the charged black hole has the geometry $\text{AdS}_2 \otimes \mathbb{R}^2$: it is a direct product of the $x-y$ plane and a *two-dimensional* AdS space, distinct from the AdS_4 where the system as a whole lives. AdS_2 has the BF bound $m^2 < m_{BF}^2$. Dimension is reduced from $D + 1 = 4$ to $D + 1 = 2$ but the radius of the AdS_2 is smaller than the radius of AdS_4 : $L_2 = L/\sqrt{6}$. Therefore, the BF bound in the interior is $m^2 < -6/4L^2$. This means that there is a window of the values of m where $m_{\text{AdS}_4}^2 < m^2 < m_{\text{AdS}_2}^2$, so a scalar which is stable in AdS_4 will still condense in AdS_2 [47]. The field theory meaning of this effect is the breaking of the discrete (Ising) \mathbb{Z}_2 gauge symmetry. This is a truly novel result of the holographic theory. The fact that the physics on field theory side can be explained by analyzing near-horizon geometry is an important lesson we will take from this review section.

2.3 Holographic dictionary for fermions

We now proceed to the object of this thesis: fermions. The essential problem for fermions is the well-known fact the Dirac fermion is a constrained system: the equations of motion are of first order, only half of the components of Dirac field are independent degrees of freedom while the rest are uniquely determined by them. The sign problem does *not* plague holography at least at the leading (tree) level. This is because the quasiparticle picture is preserved in the bulk, in the sense that we will consider weakly interacting fermions coupled to external fields only. Besides, we know that two-point correlation functions and expectation values (densities) are dual to tree-level objects in the bulk, thus one does not need to face the loop effects where the fermionicity strikes harder.⁴

⁴Occasionally, it is laconically claimed that the fermion sign problem is eliminated by holography as in the limit of classical gravity/large N strongly coupled field theory the bulk physics is classical. This is not entirely true: while *gravity* is treated classically in this limit as the gravitational constant $\kappa_{D+1} \rightarrow 0$, this does not tell us anything about the matter fields. Indeed, these in general require the same QFT treatment no matter if we take classical gravity limit, SUGRA limit or neither.

2.3.1 Equations of motion

While already the original AdS/CFT works include fermions as the field theory side is supersymmetric, it was not *a priori* clear how to construct dictionary entries for a fermionic observable in field theory. This problem was addressed in [84, 7, 56]. A more systematic rephrasing of the solution, which takes the viewpoint of holographic regularization, was given in [16]. We will mainly follow the reasoning of the latter reference as it is the most logically coherent exposition of the problem. Whereas the boundary action S_{bnd} needed to be picked by hand in earlier formulations, [16] shows that it follows logically from the requirement that the theory should be regular in the UV.

Kinematics and holography

Let us first discuss the kinematics of Dirac fermion; we have already announced that this will be the main source of trouble. The Dirac algebra in full AdS space ($D + 1$ -dimensional) is represented by gamma matrices Γ_μ , $\mu = 0, \dots, D$, and $\Gamma_D \equiv \Gamma_z$. The restriction of this representation to D dimensions, i.e. on the boundary, we will denote by γ_μ ($\mu = 0, \dots, D - 1$). Recalling the table of the representations of Dirac algebra in various dimensions, we find that in odd number of dimensions $D + 1$, i.e. for D even, there is a single spinor representation, whereas for D odd there are two irreducible representations of the Dirac algebra. We will mainly deal with this case in the thesis. In this case, Ψ is a bispinor and we can decompose it into two spinors Ψ_\pm . The choice of projection operator Π_\pm is non-unique. In holography there is a natural choice which preserves all symmetries in the boundary theory: projection on the radial direction. Thus the projectors are $\Pi_\pm = (1 \pm \Gamma_z)/2$.

Dynamics

We are now ready to write the Dirac equation. We can always write it as a pair of coupled equations for Ψ_\pm . As we know, the Dirac equation reads

$$(\not{D} - m)\Psi = 0. \quad (2.31)$$

The covariant derivative includes the coupling to any gauge fields present and to the metric through the spin connection:

$$\not{D} = e_a^\mu \left(\partial_\mu + \frac{1}{8} \omega_\mu^{bc} [\Gamma_b, \Gamma_c] - iq e_a^\mu A_a \right). \quad (2.32)$$

From now on, we will denote the local tangential coordinates by Latin indices and the metric coordinates by Greek indices. The inverse vielbein is e_a^μ . From now on we will study a fermion in the homogenous background coupled to isotropic A_0 gauge field, describing a field theory at finite density. Taking into account homogeneity and isotropy of the system in transverse direction, we can partially Fourier-transform so that the derivative becomes $\partial_\mu \mapsto (-i\omega, ik, \partial_z)$. The spin connection, given in general by $\omega_\mu^{bc} = e_\nu^b \partial_\mu e^{\nu c} + e_\nu^c e^{\sigma c} \Gamma_{\sigma\mu}^\nu$, has only two nonzero components, ω_0^{0z} and ω_i^{iz} :

$$\begin{aligned}\omega_0^{0z} &= e_0^0 e^{zz} \Gamma_{z0}^0 = \frac{1}{2} e_0^0 e^{zz} g^{00} \partial_z g_{00} = e^{zz} \partial_z e_0^0 \\ \omega_i^{iz} &= e_i^i e^{zz} \Gamma_{zi}^i = \frac{1}{2} e_i^i e^{zz} g^{ii} \partial_z g_{ii} = e^{zz} \partial_z e_i^i,\end{aligned}\quad (2.33)$$

Note that they can be formally written as total derivatives and as a consequence they can be absorbed in the redefinition of the fermion field in the following way. The equation of the form

$$\Gamma^z e_z^z [\partial_z + \partial_z (e_0^0 + (D-1) e_i^i)] \Psi + (\dots) \Psi = 0, \quad (2.34)$$

where (\dots) denotes all terms containing no radial derivatives, can be rewritten as $\Gamma^z e_z^z \partial_z \psi + (\dots) \psi = 0$ upon rescaling the Dirac field as

$$\Psi \mapsto \psi \equiv \Psi \sqrt{g_{00} (g_{ii})^{D-1}} = \Psi \sqrt{-g g^{zz}}. \quad (2.35)$$

This rescaling works generally for single parameter metrics. From now on throughout this chapter we will use the rescaling (2.35) and work with ψ and ψ_\pm instead of Ψ and Ψ_\pm .

With the rescaling for the Dirac field, we can write the Dirac equation for ψ

$$[e_z^z \partial_z - \Gamma^z (i q e_0^\mu A_0 + m)] \psi = 0. \quad (2.36)$$

Next we decompose the equation into the equations for ψ_\pm . The result can be written as:

$$(\partial_z + e^{zz} m) \psi_\pm \pm \mathcal{T} \psi_\mp = 0 \quad (2.37)$$

where \mathcal{T} is the transverse covariant derivative rescaled by the vielbein e_z^z :

$$-i\mathcal{T} = e_z^z e^{00} \gamma_0 (-\omega + q A_0) + e_z^z e^{ii} \gamma_i k_i. \quad (2.38)$$

Starting from the Dirac equation (2.38), we can eliminate either ψ_+ or ψ_- and readily derive a second order equation of motion for ψ_{\pm} . Using that $\mathcal{T}\mathcal{T} = -T_0T^0 + T_iT^i \equiv \mathcal{T}^2$, we can invert \mathcal{T} to rewrite

$$\frac{\mathcal{T}}{\mathcal{T}^2} (\partial_z + e_z^z m) \psi_+ = -\psi_- \quad (2.39)$$

and use the ψ_- equation to obtain

$$(\partial_z - me_z^z) \frac{\mathcal{T}}{\mathcal{T}^2} (\partial_z + me_z^z) \psi_+ = -\mathcal{T}\psi_+. \quad (2.40)$$

This finally brings us to the second-order form of the Dirac equation, for the spinor ψ_+ . Denoting it as

$$(\partial_{zz} + \mathcal{P}\partial_z + \mathcal{Q}_+) \psi_+ = 0 \quad (2.41)$$

we have for the coefficients

$$\begin{aligned} \mathcal{P}(z) &= -[\partial_z, \mathcal{T}] \frac{\mathcal{T}}{\mathcal{T}^2} \\ \mathcal{Q}_+(q, m, \omega, k; z) &= -2me_z^z + (\partial_z me_z^z) - [\partial_z, \mathcal{T}] \frac{\mathcal{T}}{\mathcal{T}^2} me_z^z + \mathcal{T}^2 \end{aligned} \quad (2.42)$$

For the second component ψ_- we get the same equation but with $\mathcal{Q}_- = \mathcal{Q}_+(-q, -m, -\omega, -k)$.

Of course, the second order equation implies the Dirac equation but is not equivalent to it. The necessary and sufficient condition for ψ_+ , the solution of (2.41), to be also the solution to (2.37), reads

$$\psi_- = \frac{1}{\mathcal{T}} (\partial_z + me_z^z) \psi_+. \quad (2.43)$$

It is instructive to solve the simplest case: that of pure AdS with no gauge fields. The field is rescaled as $\psi = \Psi/z^{(D+3)/2}$, and the second order equation for ψ_+ becomes

$$\left(\partial_{zz} - \frac{2m}{z} - \frac{m}{z^2} \right) \Psi_+ = 0 \quad (2.44)$$

which we readily recognize as the Bessel equation. It yields the following general solution:

$$\psi_+(z) = \frac{1}{z} \left(\psi_0^{(1)} K_{m+1/2}(kz) + \psi_0^{(2)} K_{m-1/2}(kz) \right), \quad (2.45)$$

where $K_{m\pm 1/2}$ are modified Bessel functions of the second kind. The near boundary asymptotics of the non-rescaled field Ψ_+ behaves as $\Psi_+ = \Psi_+^{(1)} z^{D/2-m} + \Psi_+^{(2)} z^{D/2+m}$. Clearly, $\Psi_+^{(1)}$ is always the leading, source term. But what is the response? Naively, it can be $\Psi_+^{(2)}$ as the subleading term. In the boundary action (2.48) we have however Ψ_- coupled linearly to the source Ψ_+ (which, with appropriate boundary conditions, becomes $\Psi_+^{(1)}$). Therefore, the response is Ψ_- with appropriate boundary asymptotics. Dirac equation tells that $\Psi_-^{(1)} \propto \Psi_+^{(2)}$ so we conclude that the response is $\Psi_-^{(1)}$.

2.3.2 Boundary action

Let us start again from the minimal bulk action for Dirac fermions coupled to gravity and possibly gauge fields:

$$S_{bulk} = S_{grav} + \int d^{D+1}x \sqrt{-g} \bar{\Psi} (\not{D} - m) \Psi + \dots, \quad (2.46)$$

where (...) stand for any additional fields in the system. It is assumed that these will not change the UV behavior of fermions nor the AdS asymptotics of the background; they might change the background and thus also the fermionic behavior in IR but we will simply assume a given fixed IR whatever might be the fields which produce it. The issue is how to implement the dictionary. The Dirac action is famously proportional to Dirac equation and thus vanishes on shell. We have seen this also in the scalar sector however. The resolution is the existence of a boundary action, which in fact encodes the full holographic partition function. The objective is to construct it here for fermions. To do so, let us find the variation of the bulk part (disregarding again the parts we know: gravity and bosons). Since we work in a spacetime with a boundary, there will generically be a boundary contribution. Employing partial integration in (2.46) and varying with respect to ψ , we get:

$$\begin{aligned} \delta S_{bulk} &= \delta \int d^{D+1}x \sqrt{-g} \bar{\psi} (\not{D} - m) \psi = \\ &= \int d^Dx \sqrt{-h} \bar{\psi} \delta \psi \Big|_{z_0}^{z_h} - \int d^{D+1}x \sqrt{-g} (-\not{D} - m) \bar{\psi} \delta \psi. \end{aligned} \quad (2.47)$$

The second, bulk term vanishes on shell as it is proportional to the equation of motion. The first, boundary term does not vanish however. It is

to be evaluated on the boundary of AdS in UV and at z_h in IR.⁵ In terms of the radial projections, it reads

$$\delta S = \frac{1}{2} \int d^D x \sqrt{-h} (\bar{\psi}_+ \delta \psi_- + \bar{\psi}_- \delta \psi_+). \quad (2.48)$$

We know from general rules of AdS/CFT that one of the components of ψ will be the source and the other the response, and in the previous subsection we have seen that the leading component of ψ_+ is larger (i.e. decays slower) at the boundary than the leading component of ψ_- . We can therefore pick ψ_+ to be the source. This means that ψ_+ is fixed at the boundary and its variation is zero: $\delta \psi_+ = 0$. The variation of the action now reduces to the first term in (2.48). To cancel ad we can add a counterterm reading

$$S_{ct} = \frac{1}{2} \int d^D x \sqrt{-h} (\bar{\psi}_+ \psi_- + \bar{\psi}_- \psi_+) \quad (2.49)$$

and the whole action is given by $S = S_{bulk} + S_{ct}$, so $S_{bnd} \equiv S_{ct}$: the whole boundary contribution can be understood as the counterterm which regularizes the action, eliminating UV divergences and making the on-shell solution satisfy the Dirac equation in the bulk.

For the steps to follow it is convenient to introduce the bulk-to-boundary propagator $\mathcal{G}_\pm(z)$ and to express the solution in terms of \mathcal{G}_\pm . The bulk-to-boundary propagator satisfies the equation of motion [114]:

$$(\not{D} - m) \mathcal{G}(z) = \delta(z) \quad (2.50)$$

i.e. it is a response to a Dirac delta function source at the boundary. We can now express the solution to Dirac equation in terms of \mathcal{G}_\pm and χ_\pm . The expression for ψ_\pm reads

$$\psi_+ = \mathcal{G}_+^{-1}(z_0) \mathcal{G}_+(z) \chi_+, \quad \psi_- = \mathcal{G}_+^{-1}(z_0) \mathcal{G}_-(z) S \chi_- \quad (2.51)$$

where $S = \lim_{z \rightarrow 0} \mathcal{T}/\mathcal{T}$. Namely, at the boundary the energy-momentum dependence can be shown to drop from the factor \mathcal{T}/\mathcal{T} , leaving only a constant matrix (which of course depends on the representation of gamma matrices, hence we do not specify it here). The convenience of the above representation of ψ is that all z dependence of ψ is encoded in the bulk-to-boundary propagators. Substituting (2.51) into the boundary action, we

⁵The latter is a single point if $z_h \rightarrow \infty$ or a slice in the transverse direction if z_h is finite.

obtain an expression for the full on-shell action in terms of the solutions $\mathcal{G}_\pm(z)$:

$$S^{on-shell} = \int_{z=z_0} \frac{d\omega d^2k}{(2\pi)^3} \sqrt{-h} \bar{\chi}_+ \mathcal{G}_-(z_0) \mathcal{G}_+^{-1}(z_0) \chi_+. \quad (2.52)$$

The two-point correlator in field theory is therefore

$$G(\omega, k) = \mathcal{G}_-(z_0) \mathcal{G}_+^{-1}(z_0). \quad (2.53)$$

What this illustrates is that the subleading component of Ψ_- is the response to the leading component of Ψ_+ . This will be the starting point of the work done in most of Chapter 3 and 4.

2.4 The remainder of the thesis

Having discussed the larger context in the first chapter and the theoretical foundations and previous work on the topic of our research in this, second chapter, we have finished introducing the formal framework of our work. We now outline the work done in this thesis on specific problems with fermion systems. We will use the power of holography to describe strongly coupled systems from a new fundamental perspective, to circumvent the sign problem. We stay exclusively with bottom-up setups. The first reason is their obvious simplicity as compared to top-down constructions which become particularly complicated if fermions are included. A deeper reason is that the conceptual aspects we consider such as the dictionary entry for a Fermi surface, or for a Fermi liquid state, or pathways through which Fermi liquids are destroyed – are not expected to depend much on the exact string action.

Another compromise with consistency that we have to decide about is the choice between self-consistent calculations, with backreaction, versus probe limit calculations. We start from the probe limit and afterwards include backreaction, first on gauge field and then also on geometry. Of course, probe limit suffices at small fermion density, when the backreaction is anyway small, but becomes less and less satisfactory as the density increases. The field theory interpretation is that backreaction probes the stability of the system – unstable quantum critical matter is described by the probe limit calculations, but to arrive at stable phases we need to backreact. In particular, the Fermi-liquid-like phase (which we know empirically to be very stable) requires backreaction.

In Chapter 3 we address the critical theory governing the zero temperature quantum phase transition between strongly renormalized Fermi-liquids as found in heavy fermion intermetallics and possibly high T_c superconductors. From the solutions of Dirac equation in the probe limit in the AdS-RN background, we obtain the spectral functions of fermions in the field theory. By increasing the fermion density away from the relativistic quantum critical point, we observe multiple Fermi surfaces, some of them of distinctly non-Fermi liquid nature while others have some features of the Fermi liquid. Tuning the scaling dimensions of the critical fermion fields we find that the quasiparticle disappears at a quantum phase transition of a purely statistical nature, not involving any symmetry change. The resulting phase has no Fermi surfaces at all.

In Chapter 4 we extend our work by backreacting on gauge field. We provide evidence that the bulk dual to a strongly coupled charged Fermi-liquid-like system has a non-zero fermion density in the bulk. We then calculate density explicitly in the small density approximation, a model we call black hole with Dirac hair. Then we show that the pole strength of the stable quasiparticle characterizing the Fermi surface is encoded in the spatially averaged AdS probability density of a single normalizable fermion wave function in AdS. Recalling Migdal's theorem which relates the pole strength to the Fermi-Dirac characteristic discontinuity in the number density at Fermi energy, we conclude that the AdS dual of a Fermi liquid is described by occupied on-shell fermionic modes in AdS. Encoding the occupied levels in the total spatially averaged probability density of the fermion field directly, we show that an AdS Reissner-Nordström black hole in a theory with charged fermions has a critical temperature, at which the system undergoes a first-order transition to a black hole with a non-vanishing profile for the bulk fermion field. Thermodynamics and spectral analysis support that the solution with non-zero AdS fermion-profile is the preferred ground state at low temperatures.

In Chapter 5 we continue our study of self-consistent (backreacted) models and move toward constructing the full phase diagram of the Dirac-Maxwell-Einstein system and its field theory dual. We compare our Dirac hair model with the electron star model of Hartnoll et al [51], and argue that the electron star and the AdS Dirac hair solution are two limits of the free charged Fermi gas in AdS. Spectral functions of holographic duals to probe fermions in the background of electron stars have a free parameter that quantifies the number of constituent fermions that make

up the charge and energy density characterizing the electron star solution. The strict electron star limit takes this number to be infinite. The Dirac hair solution is the limit where this number is unity. This is evident in the behavior of the distribution of holographically dual Fermi surfaces. As we decrease the number of constituents in a fixed electron star background the number of Fermi surfaces also decreases. An improved holographic Fermi ground state should be a configuration that shares the qualitative properties of both limits.

We construct such configuration in Chapter 6. We employ a model which combines the (semiclassical) WKB approximation and its Airy correction with the quantum corrections based on Dirac equation. At high temperatures, the system exhibits a first order thermal phase transition to a charged AdS-RN black hole in the bulk and the emergence of local quantum criticality on the CFT side. This restores the intuition that the transition between the critical AdS-RN liquid and the finite density Fermi system is of van der Waals liquid-gas type. At zero temperature, we find a Berezinsky-Kosterlitz-Thouless transition from Fermi-liquid-like finite density phase with a sharp Fermi surface to zero density AdS-Reissner-Nordström but in the regime without Fermi surfaces. This suggests that it is indeed the Fermi surface which drives the instability of the AdS-RN quantum critical phase. Based on these findings, we construct the three-dimensional phase diagram, with temperature, conformal dimension and fermion charge.

Even though we have not answered some of the questions we started from, in particular the question of what is the holographic dual to a textbook Landau Fermi liquid and how it is destroyed by strong interactions, we have obtained a qualitative model of how stable Fermi-liquid-*like* quasiparticles become unstable at a quantum critical point and give rise to novel phenomena. These phenomena could not be obtained in a perturbative approach and they illustrate the power of AdS/CFT and its ability to make specific predictions on strongly correlated fermions. These predictions have not been tested experimentally so far. Because of many simplifying assumptions and the lack of ability to construct a microscopic Hamiltonian on the boundary, our results are unlikely to be a good quantitative description of any realistic system. Nevertheless, they make some remarkable qualitative predictions which can be expected to hold also in real-world materials, due to the universality associated to quantum critical behavior. The coming years will surely determine whether the novel

physics on display in AdS/CMT is a part of the real world.

Chapter 3

Charged black hole and critical Fermi surfaces [17]

Quantum many-particle-physics lacks a general mathematical theory to deal with fermions at finite density. This is known as the “fermion-sign-problem”: there is no recourse to brute force lattice models as the statistical path integral methods that work for any bosonic quantum field theory do not work for finite density fermi-systems. The non-probabilistic fermion problem is known to be of exponential complexity [109] and in the absence of a general mathematical framework all that remains is phenomenological guesswork in the form of the Fermi-liquid theory describing the state of electrons in normal metals and the mean-field theories describing superconductivity and other manifestations of spontaneous symmetry breaking. This problem has become particularly manifest in quantum condensed matter physics with the discovery of electron systems undergoing quantum phase transitions that are reminiscent of the bosonic quantum critical systems [95] but are governed by fermion statistics. Empirically well documented examples are found in the ‘heavy fermion’ intermetallics where the zero temperature transition occurs between different Fermi-liquids with quasiparticle masses that diverge at the quantum critical point [117]. Such fermionic quantum critical states are believed to have a direct bearing on the problem of high T_c superconductivity because of the observation of quantum critical features in the normal state of optimally doped cuprate high T_c superconductors [111, 116].

A large part of the “fermion-sign-problem” is to understand this strongly coupled fermionic quantum critical state. The emergent scale invariance

and conformal symmetry at critical points is a benefit in isolating deep questions of principle. The question is how does the system get rid off the scales of Fermi-energy and Fermi-momentum that are intrinsically rooted in the workings of Fermi-Dirac statistics [99, 72]? Vice versa, how to construct a renormalization group with a relevant 'operator' that describes the emergence of a statistics controlled (heavy) Fermi liquid from the critical state [117], or perhaps the emergence of a high T_c superconductor? We will show that a mathematical method developed in string theory has the capacity to answer at least some of these questions.

3.1 String theory for condensed matter

We refer to the AdS/CFT correspondence: a duality relation between classical gravitational physics in a $d + 1$ dimensional 'bulk' space-time with an Anti-de-Sitter (AdS) geometry and a strongly coupled conformal (quantum critical) field theory (CFT) with a large number of degrees of freedom that occupies a flat or spherical d dimensional 'boundary' space-time. Applications of AdS/CFT to quantum critical systems have already been studied in the context of the quark-gluon plasma [104, 41], superconductor-insulator transitions [59, 46, 40, 47] and cold atom systems at the Feshbach resonance [103, 8, 1] but so far the focus has been on bosonic currents (see [45, 49] and references therein). Although AdS/CFT is convenient, in principle the groundstate or any response of a bosonic statistical field theory can also be computed directly by averaging on a lattice. For fermions statistical averaging is not possible because of the sign-problem. There are, however, indications that AdS/CFT should be able to capture finite density fermi systems as well. Ensembles described through AdS/CFT can exhibit a specific heat that scales linear with the temperature characteristic of Fermi systems [69], zero sound [69, 65, 70] and a minimum energy for fermionic excitations [93, 101].

To address the question whether AdS/CFT can describe finite density fermi-systems and the Fermi liquid in particular, we compute the single charged fermion propagators and the associated spectral functions that are measured experimentally by angular resolved photoemission ("AdS-to-ARPES") and indirectly by scanning tunneling microscopy. The spectral functions contain the crucial information regarding the nature of the fermion states. These are computed on the AdS side by solving for the on-shell (classical) Dirac equation in the curved AdS space-time background

with sources at the boundary. A temperature T and finite $U(1)$ chemical potential μ_0 for electric charge is imposed in the field theory by studying the Dirac equation in the background of an AdS Reissner–Nordstrom black hole. We do so expecting that the $U(1)$ chemical potential induces a finite density of the charged fermions. The procedure to compute the retarded CFT propagator from the dual AdS description is then well established [104, 49]. Compared to the algorithm for computing bosonic responses, the treatment of Dirac waves in AdS is more delicate, but straightforward; details are provided in the final section of this chapter. The equations obtained this way are solved numerically and the output is the retarded single fermion propagator $G_R(\omega, k)$ at finite T . Its imaginary part is the single fermion spectral function $A(\omega, k) = -\frac{1}{\pi} \text{ImTr}(i\gamma^0 G_R(\omega, k))$ that can be directly compared with ARPES experiments.

The reference point for this comparison is the quantum critical point described by a zero chemical potential ($\mu_0 = 0$), zero temperature ($T = 0$), conformal and Lorentz invariant field theory. Here the fermion propagators $\langle \bar{\Psi}\Psi \rangle \equiv G(\omega, k)$ are completely fixed by symmetry to be of the form (we use relativistic notation where $c = 1$)

$$G_{\Delta_\Psi}^{CFT}(\omega, k) \sim \frac{1}{(\sqrt{-\omega^2 + k^2})^{d-2\Delta_\Psi}} \quad (3.1)$$

with Δ_Ψ the scaling dimension of the fermion field. Through the $\text{AdS}_{d+1}/\text{CFT}_d$ dictionary Δ_Ψ is related to the mass parameter in the $d + 1$ -dimensional AdS Dirac equation. Unitarity bounds this mass from below in units of the AdS radius $mL = \Delta_\Psi - d/2 > -1/2$ (we set $L = 1$ in the remainder). The choice of which value to use for m will prove essential to show the emergence of the Fermi liquid. The lower end of the unitarity bound $m = -1/2 + \delta$, $\delta \ll 1$, corresponds to introducing a fermionic conformal operator with weight $\Delta_\Psi = (d - 1)/2 + \delta$. This equals the scaling dimension of a nearly free fermion. Despite the fact that the underlying CFT is strongly coupled, the absence of a large anomalous dimension for a fermion with mass $m = -1/2 + \delta$ argues that such an operator fulfills a spectator-role and is only weakly coupled to this CFT. We will therefore use such values in our calculations. Our expectation is that the Fermi liquid, as a system with well-defined quasiparticle excitations, can be described in terms of weakly interacting long-range fields. As we increase m from $m = -1/2 + \delta$, the interactions increase and we can expect the quasi-particle description to cease to be valid beyond $m = 0$. For that value $m = 0$, and beyond $m > 0$, the naive scaling dimension Δ_\emptyset of the

fermion-bilinear $\mathcal{O}_{\Delta_{\psi}} = \Psi\Psi$ is marginal or irrelevant and it is hard to see how the ultra-violet conformal theory can flow to a Fermi-liquid state, assuming that all vacuum state changes are caused by the condensation of bosonic operators. This intuition will be borne out by our results: when $m \geq 0$ the standard Fermi-liquid disappears. A similar approach to describing fermionic quantum criticality [79] discusses the special case $m = 0$ or $\Delta_{\psi} = d/2$ in detail; other descriptions of the $m = 0$ system are [76, 91].

3.2 The emergent Fermi liquid

With an eye towards experiment we shall consider the AdS_4 dual to a relativistic CFT_3 in $d = 2 + 1$ dimensions; see the last section of this chapter. As we argue there, we do not know the detailed microscopic CFT nor whether a dual AdS with fermions as the sole $U(1)$ charged field exists as a fully quantum consistent theory for all values of $m = \Delta_{\psi} - d/2$, but the behavior of fermion spectral functions at a strongly coupled quantum critical point can be deduced nonetheless. Aside from Δ_{ψ} , the spectral function will depend on the dimensionless ratio μ_0/T as well as the $U(1)$ charge g of the fermion; we shall set $g = 1$ from here on, as we expect that only large changes away from $g = 1$ will change our results qualitatively. We therefore study the system as a function of μ_0/T and Δ_{ψ} . We have drawn our approach in Fig. 3.1B: first we shall study the spectral behavior as a function of μ_0/T for fixed $\Delta_{\psi} < 3/2$; then we study the spectral behaviour as we vary the scaling dimension Δ_{ψ} from 1 to $3/2$ for fixed μ_0/T coding for an increasingly interacting fermion. Note that our set-up and numerical calculation necessitate a finite value of μ_0/T : all our results are at non-zero T .

Our analysis starts near the reference point $\mu_0/T \rightarrow 0$ where the long range behavior of the system is controlled by the quantum critical point (Fig. 3.1A). Here we expect to recover conformal invariance, as the system forgets about any well-defined scales, and the spectral function should be controlled by the branchcut at $\omega = k$ in the Green's function (Eq.1) : (a) For $\omega < k$ it should vanish, (b) At $\omega = k$ we expect a sharp peak which for $\omega \gg k$ scales as $\omega^{2\Delta_{\psi}-d}$. Fig. 3.2A shows this expected behavior of spectral function for three different values of the momentum for a fermionic operator with weight $\Delta_{\psi} = 5/4$ computed from AdS_4 .

Turning on μ_0/T holding $\Delta_{\psi} = 5/4$ fixed, shifts the center location of the two branchcuts to an effective chemical potential $\omega = \mu_{eff}$; this

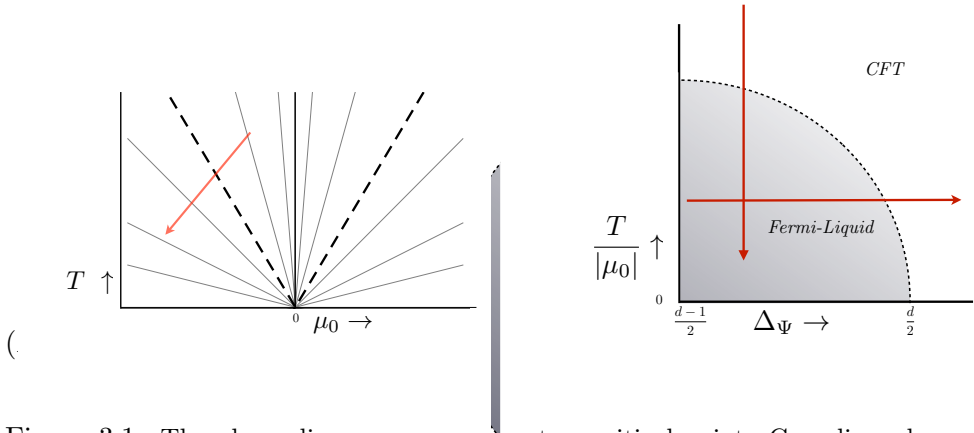


Figure 3.1: The phase diagram near a quantum-critical point. Gray lines depict lines of constant μ_0/T : the spectral function of fermions is unchanged along each line if the momenta are appropriately rescaled. As we increase μ_0/T we crossover from the quantum-critical regime to the Fermi-liquid. (B) The trajectories in parameter space $(\mu_0/T, \Delta_\Psi)$ studied here. We show the crossover from the quantum critical regime to the Fermi liquid by varying μ_0/T keeping Δ_Ψ fixed; we cross back to the critical regime varying $\Delta_\Psi \rightarrow d/2$ for μ_0/T fixed. The boundary region is not an exact curve, but only a qualitative indication.

bears out our expectation that the $U(1)$ chemical potential induces a finite fermion density. While the peak at the location of the negative branchcut $\omega \sim \mu_{eff} - k$ stays broad, the peak at the other branchcut $\omega \sim \mu_{eff} + k$ sharpens distinctively as the size of μ_0/T is increased (Fig. 3.2B). We shall identify this peak with the quasiparticle of the Fermi liquid and its appearance as the crossover between the quantum-critical and the Fermi-liquid regime. The spectral properties of the Fermi liquid are very well known and display a number of uniquely identifying characteristics [77, 98]. If this identification is correct, all these characteristics must be present in our spectra as well.

1. The quasiparticle peak should approach a delta function at the Fermi momentum $k = k_F$. In Fig. 3.2B we see the peak narrow as we increase k , peak, and broaden as we pass $k \sim k_F$ (recall that $T = 0$ is outside our numerical control and the peak always has some broadening). In addition the spectrum should vanish identically at the Fermi-energy $A(\omega = E_F, k) = 0$, independent of k . This is shown in Fig. 3.2C.

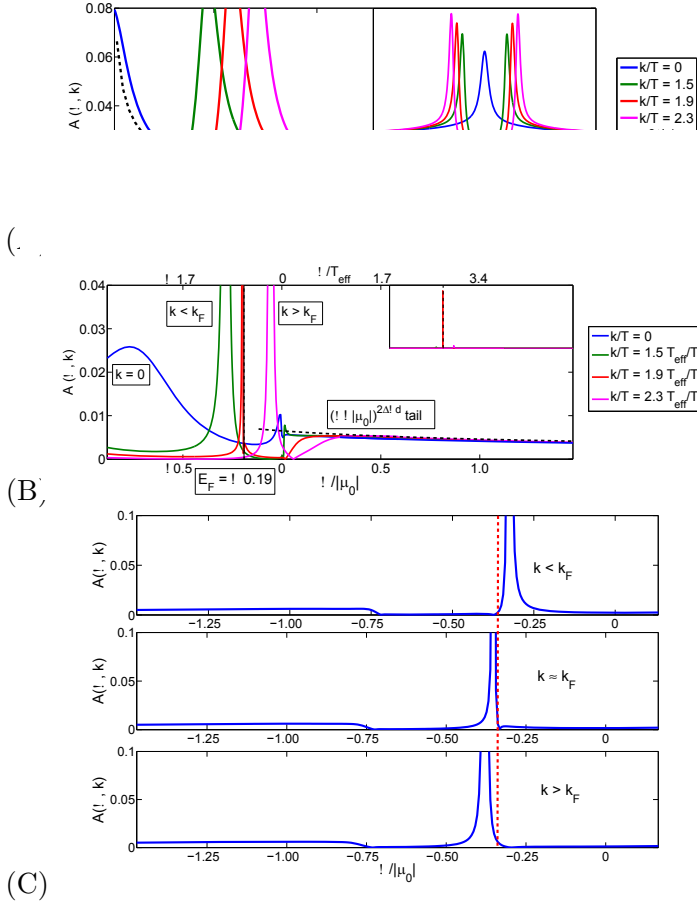


Figure 3.2: (A) The spectral function $A(\omega, k)$ for $\mu_0/T = 0.01$ and $m = -1/4$. The spectral function has the asymptotic branch cut behavior of a conformal field of dimension $\Delta_\Psi = d/2 + m = 5/4$: it vanishes for $\omega < k$, save for a finite T tail, and for large ω scales as $\omega^{2\Delta_\Psi - d}$. (B) The emergence of the quasiparticle peak as we change the chemical potential to $\mu_0/T = -30.9$ for the same value $\Delta_\Psi = 5/4$. The three displayed momenta k/T are rescaled by a factor T_{eff}/T for the most meaningful comparison with those in (A). The insets show the full scales of the peak heights and the dominance of the quasiparticle peak for $k \sim k_F$. (C) Vanishing of the spectral function at E_F for $\Delta_\Psi = 1.05$ and $\mu_0/T = -30.9$. The deviation of the dip-location from E_F is a finite temperature effect. It decreases with increasing μ_0/T .

2. The quasiparticle should have linear dispersion relation near the Fermi energy with a renormalized Fermi velocity v_F different than the underlying relativistic speed $c = 1$. In Fig. 3.3 we plot the maximum of the peak ω_{max} as a function of k . At high k we recover the linear dispersion relation $\omega = |k|$ underlying the Lorentz invariant branchcut in Eq.1. Near the Fermi energy/Fermi momentum however, this dispersion relation changes to a slope v_F given by the limit $\lim_{\omega \rightarrow E_F, k \rightarrow k_F} (\omega - E_F)/(k - k_F)$ clearly less than one. Importantly, it appears that the Fermi Energy E_F is not located at zero-frequency.¹ Recall, however, that the AdS chemical potential μ_0 is the bare $U(1)$ chemical potential in the CFT. This is confirmed in Fig. 3.3 from the high k behavior: its Dirac point is μ_0 . On the other hand, the chemical potential felt by the IR fermionic degrees of freedom is renormalized to the value $\mu_F = \mu_0 - E_F$. As is standard, the effective energy $\tilde{\omega} = \omega - E_F$ of the quasiparticle is measured with respect to E_F .
3. At low temperatures Fermi-liquid theory predicts the width of the quasiparticle peak to grow quadratically with temperature. Fig. 3.4A, 3.4B show this distinctive behavior up to a critical temperature $T_c/\mu_0 \sim 0.16$. This temperature behavior directly follows from the fact that imaginary part of the self-energy $\Sigma(\omega, k) = \omega - k - (\text{Tr}i\gamma^0 G(\omega, k))^{-1}$ should have no linear term when expanded around E_F : $\text{Im}\Sigma(\omega, k) \sim (\omega - E_F)^2 + \dots$. This is shown in Fig. 3.4C, 3.4D.

These results give us confidence that we have identified the characteristic quasiparticles at the Fermi surface of the Fermi liquid emerging from the quantum critical point.

Let us now discuss how this Fermi-liquid evolves when we increase the bare μ_0 (Fig. 3.5). Similar to the fermion chemical potential μ_F , the fundamental control parameter of the Fermi-liquid, the fermion density ρ_F , is not directly related to the AdS μ_0 . We can, however, infer it from the Fermi-momentum k_F that is set by the quasiparticle pole via Luttinger's theorem $\rho_F \sim k_F^{d-1}$. The more illustrative figure is therefore Fig. 3.5B which shows the quasiparticle characteristics as a function of k_F/T . We find that the quasiparticle velocities decrease slightly with

¹In our original paper we misidentified the location of the maximum peak height with E_F . The correct identification is when the pole hit the real axis in the complex frequency space. We explain this below in the last section of this chapter.

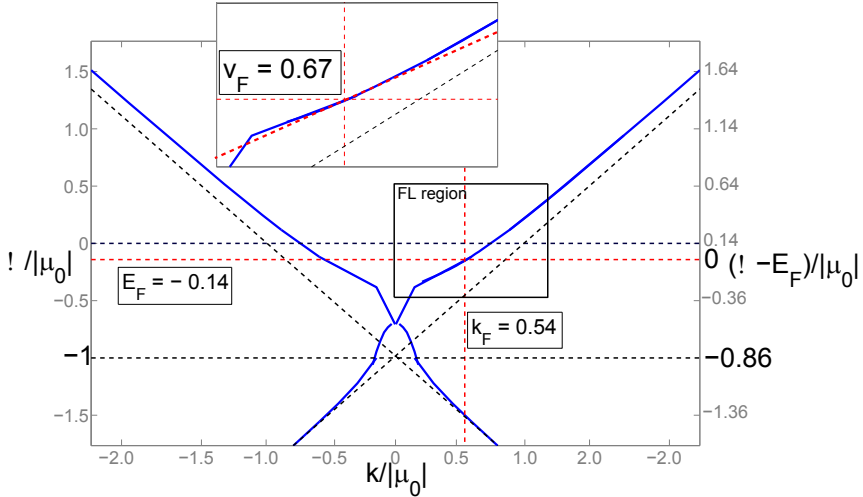


Figure 3.3: Maxima in the spectral function as a function of k/μ_0 for $\Delta_\Psi = 1.35$ and $\mu_0/T = -30.9$. Asymptotically for large k the negative k branch cut recovers the Lorentz-invariant linear dispersion with unit velocity, but with the zero shifted to $-\mu_0$. The peak location of the positive k branch cut that changes into the quasiparticle peak changes significantly. It gives the dispersion relation of the quasiparticle near (E_F, k_F) . The change of the slope from unity shows renormalization of the Fermi velocity. This is highlighted in the inset. Note that the Fermi energy E_F is not located at $\omega_{AdS} = 0$. The AdS calculation visualizes the renormalization of the bare UV chemical potential $\mu_0 = \mu_{AdS}$ to the effective chemical potential $\mu_F = \mu_0 - E_F$ felt by the low-frequency fermions.

increasing k_F , rapidly leveling off to a finite constant less than the relativistic speed. Thus the quasiparticles become increasingly heavy as their mass $m_F \equiv k_F/v_F$ asymptotes to linear growth with k_F . The Fermi energy E_F also shows linear growth. Suppose the heavy Fermi-quasiparticle system has the underlying canonical non-relativistic dispersion relation $E = k^2/(2m_F) = k_F^2/(2m_F) + v_F(k - k_F) + \dots$, then the observed Fermi energy E_F should equal the renormalized Fermi-energy $E_F^{(ren)} \equiv k_F^2/(2m_F)$. Fig. 3.5B shows that these energies E_F and $E_F^{(ren)}$ track each other remarkably well. We therefore infer that the true zero of energy of the Fermi-quasiparticle is set by the renormalized Fermi-energy as deduced from the Fermi-velocity and -momentum.

Although the true quasiparticle behavior disappears at $T > T_c$, Fig. 3.5A indicates that in the limit $k_F/T \rightarrow 0$ the quasiparticle pole strength

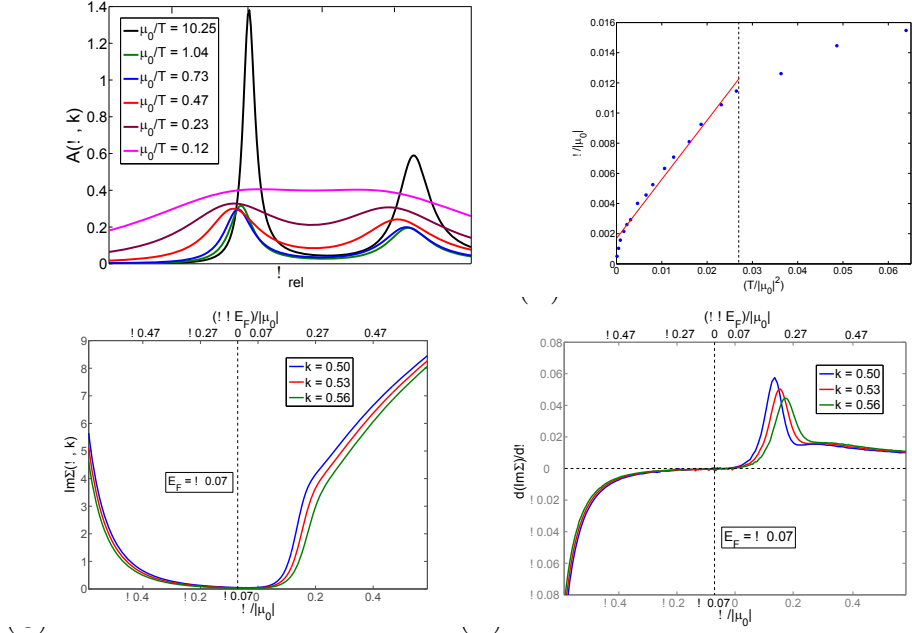


Figure 3.4: (A) Temperature dependence of the quasiparticle peak for $\Delta_\Psi = 5/4$ and $k/k_F \simeq 0.5$; all curves have been shifted to a common peak center. (B) The quasiparticle peak width $\delta \sim \text{Re}\Sigma(\omega, k = k_F)$ for $\Delta_\Psi = 5/4$ as a function of T^2 : it reflects the expected behavior $\delta \sim T^2$ up to a critical temperature T_c/μ_0 , beyond which the notion of a quasiparticle becomes untenable. (C) The imaginary part of the self-energy $\Sigma(\omega, k)$ near E_F , k_F for $\Delta_\Psi = 1.4$, $\mu_0/T = -30.9$. The defining $\text{Im}\Sigma(\omega, k) \sim (\omega - E_F)^2 + \dots$ -dependence for Fermi-liquid quasiparticles is faint in panel (C) but obvious in panel (D). It shows that the intercept of $\partial_\omega \text{Im}\Sigma(\omega, k)$ vanishes at E_F, k_F .

vanishes, $Z_k \rightarrow 0$, while the Fermi-velocity v_F remains finite; v_F approaches the bare velocity $v_F = 1$. This is seemingly at odds with the heavy Fermi liquid wisdom $Z_k \sim m_{\text{micro}}/m_F = m_{\text{micro}}v_F/k_F$. The resolution is the restoration of Lorentz invariance at zero density. From general Fermi liquid considerations it follows that $v_F = Z_k(1 + \partial_k \text{Re}\Sigma|_{E_F, k_F})$ and $Z_k = 1/(1 - \partial_\omega \text{Re}\Sigma|_{E_F, k_F})$ where $\partial_{k, \omega} \text{Re}\Sigma$ refers to the momentum and energy derivatives of the real part of the fermion self-energy $\Sigma(\omega, k)$ at k_F, E_F . Lorentz invariance imposes $\partial_\omega \Sigma' = -\partial_k \Sigma'$ which allows for vanishing Z_k with $v_F \rightarrow 1$. Interestingly, the case has been made that such a relativistic fermionic behavior might be underlying the physics of cuprate

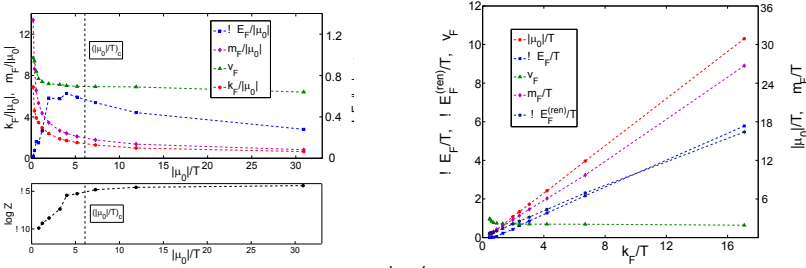


Figure 3.5: The quasiparticle characteristics as a function of μ_0/T for $\Delta_\Psi = 5/4$. Panel (A) shows the change of k_F, v_F, m_F, E_F and the pole strength Z (the total weight between half-maxima) as we change μ_0/T . Beyond a critical value $(\mu_0/T)_c$ we lose the characteristic T^2 broadening of the peak and there is no longer a real quasiparticle, though the peak is still present. For the Fermi-liquid k_F/T rather than μ_0/T is the defining parameter. We can invert this relation and panel (B) shows the quasiparticle characteristics as a function of k_F/T . Note the linear relationships of m_F, E_F to k_F and that the renormalized Fermi energy $E^{(ren)} \equiv k_F^2/(2m_F)$ matches the empirical value E_F remarkably well.

high T_c superconductors [90].

Finally, we address the important question what happens when we vary the conformal dimension Δ_Ψ of the fermionic operator. Fig. 3.6 shows that the Fermi momentum k_F stays constant as we increase Δ_Ψ . This completes our identification of the new phase as the Fermi-liquid: it indicates that the AdS dual obeys Luttinger's theorem, if we can interpret the conformal dimension of the fermionic operator as a proxy for the interaction strength. We find furthermore that the quasiparticle pole strength vanishes as we approach $\Delta_\Psi = 3/2$. This confirms our assumption made earlier that it is essential to study the system for $\Delta_\Psi < d/2$ and that the point $\Delta_\Psi = d/2$ where the naive fermion bilinear becomes marginal signals the onset of a new regime. Because the fermion bilinear is marginal at that point this ought to be an interesting regime in its own right and we refer to the recent article [79] for a discussion thereof. Highly remarkable is that the pole strength vanishes in an exponential fashion rather than the anticipated algebraic behavior [99, 72]. This could indicate that an essential singularity governs the critical point at $\Delta_\Psi = d/2$ and we note that such a type of behavior was identified by Lawler et al. in their analysis of the Pomeranchuk instability in $d = 2 + 1$ dimensions using the Haldane patching bosonization procedure [75]. Interestingly this finite μ_0/T transition as we vary Δ_Ψ has no clear symmetry change, similar to

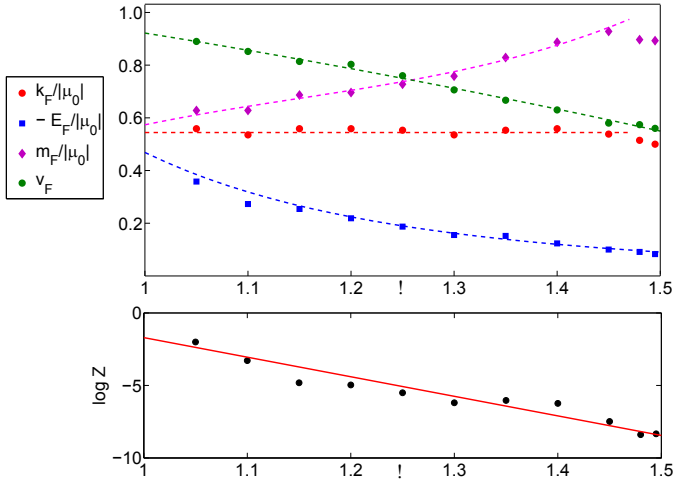


Figure 3.6: The quasiparticle characteristics as a function of the Dirac fermion mass $-1/2 < m < 0$ corresponding to $1 < \Delta_\Psi < 3/2$ for $\mu_0/T = -30.9$. The upper panel shows the independence of k_F of the mass. This indicates Luttinger’s theorem if the anomalous dimension Δ_Ψ is taken as an indicator of the interaction strength. Note that v_F, E_F both asymptote to finite values as $\Delta_\Psi \rightarrow 3/2$. The lower panel shows the exponential vanishing pole strength Z (the integral between the half-maxima) as $m \rightarrow 0$.

[72]. However, this may be an artifact of the fact that our theory is not quantum mechanically complete. Note also that the quasiparticle velocity and the renormalized Fermi energy $E_F = v_F(k - k_F) - E$ stay finite at the $\Delta_\Psi = 3/2$ transition with $Z \rightarrow 0$, which could indicate an emergent Lorentz invariance for the reasons discussed in the previous paragraph.

3.3 Concluding remarks

We have presented evidence that the AdS dual description of strongly coupled field theories can describe the emergence of the Fermi-liquid from a quantum critical state — both as a function of density and interaction strength as encoded in the conformal dimension of the fermionic operators. From the AdS gravity perspective, it was unclear whether this would happen. Sharp peaks in the CFT spectral function correspond to so-called quasinormal modes of black holes [68], but Dirac quasinormal modes have received little study (see e.g. [14]). It is remarkable that

the AdS calculation processes the Fermi-Dirac statistics essential to the Fermi-liquid correctly. This is manifested by the emergent renormalized Fermi-energy and the validity of Luttinger's theorem. The AdS gravity computation, however, is completely classical without explicit quantum statistics, although we do probe the system with a fermion. It would therefore be interesting to fully understand the AdS description of what is happening, in particular how the emergent scales E_F and k_F feature in the geometry. An early indication of such scales was seen in [101, 94] in a variant of the story that geometry is not universal in string theory: the geometry depends on the probe used and different probes experience different geometric backgrounds. The absence of these scales in the general relativistic description of the AdS black hole could thus be an artifact of the Riemannian metric description of spacetime.

Regardless of these questions, AdS/CFT has shown itself to be an powerful tool to describe finite density Fermi systems. The description of the emergent Fermi liquid presented here argues that AdS/CFT is uniquely suited as a computational device for field-theory problems suffering from fermion sign-problems. AdS/CFT represents a rich mathematical environment and a new approach to investigate qualitatively and quantitatively important questions in quantum many-body theory at finite fermion density.

3.4 Formal background for the calculation of the spectral functions

3.4.1 The AdS set up and AdS/CFT Fermion Green's functions.

The deviation from the strongly coupled 2+1 dimensional quantum critical point from which we wish to see the Fermi surface emerge is characterized by a temperature and background $U(1)$ chemical potential. The phenomenological AdS dual to such a finite-temperature system with chemical potential is a charged AdS_4 black hole. Including fermionic excitations, this system is described by the minimal action

$$S_{bulk} = \frac{1}{2\kappa_4^2} \int d^4x \sqrt{-g} \left[R + \frac{6}{L^2} + L^2 \left(-\frac{1}{4} F^2 - \bar{\Psi} e_A^M \Gamma^A D_M \Psi - m \bar{\Psi} \Psi \right) \right] \quad (3.4.1)$$

Here e_A^M is the inverse vielbein, $\Gamma^A = \{\gamma^a, \gamma^4\}$ are 4d Dirac matrices obeying $\{\Gamma^A, \Gamma^B\} = 2\eta^{AB}$ (hermitian except Γ^0), and Ψ is a four-component

Dirac spinor with $\bar{\Psi} = \Psi^\dagger i\Gamma^0$. This spinor is charged under a $U(1)$ gauge field and the covariant derivative equals

$$D_M \Psi = \left(\partial_M + \frac{1}{8} \omega_M^{AB} [\Gamma_A, \Gamma_B] + ig A_M \right) \Psi . \quad (3.4.2)$$

On its own this action is not a consistent quantum theory. It must be embedded in a string dual, e.g. for appropriate choices of m and g it is a subsector of the $\mathcal{N} = 8$ AdS₄ × S₇ dual to the conformal fixed point of large N_c , $d = 3$ $\mathcal{N} = 8$ SYM and generically such a completion will have a number of $U(1)$ charged fields in addition to the fermions. For our considerations, specifically the two point function of fermions, the quantum completion is not relevant. At leading order in the gravitational coupling constant, the action (5.2.5) will yield the same two-point correlators independently of the non-linear supergravity couplings. It does mean, that we cannot equate the $U(1)$ chemical potential μ_0 directly with the density of fermions μ_F as we emphasize in the main article.

The charged AdS₄ black hole is a solution to the equations of motion of this action. In a gauge where $A_z = 0$ and A_0 is regular at the horizon the metric and gauge potential are given by [92, 44]

$$\begin{aligned} ds^2 &= \frac{L^2 \alpha^2}{z^2} (-f(z) dt^2 + dx^2 + dy^2) + \frac{L^2}{z^2} \frac{dz^2}{f(z)} , \\ A_0 &= 2q\alpha(z-1) , \\ f(z) &= (1-z)(z^2 + z + 1 - q^2 z^3) . \end{aligned} \quad (3.4.3)$$

For $z \rightarrow 0$ the metric asymptotes to AdS₄ in Poincaré coordinates with the boundary at $z = 0$ and there is a black hole horizon at the first zero, $z = 1$, of the function $f(z)$. In this parametrization the black hole temperature and $U(1)$ chemical potential — equal to the CFT temperature and bare chemical potential — are

$$T_{CFT} = T_{BH} = \frac{\alpha}{4\pi} (3 - q^2) , \quad \mu_0 = \mu_{BH} = -2q\alpha . \quad (3.4.4)$$

The parameter q is bounded between $0 \leq q^2 \leq 3$ interpolating between AdS-Schwarzschild and the extremal AdS black hole. For the equation of motion of fermions in this background we shall need the spin connection belonging to this metric. The nonzero components are

$$\omega_0^{ab} = -\delta_0^{[a} \delta_z^{b]} \alpha f \left(\frac{1}{z} - \frac{\partial_z f}{2f} \right) , \quad \omega_i^{ab} = -\delta_i^{[a} \delta_z^{b]} \frac{\alpha \sqrt{f}}{z} . \quad (3.4.5)$$

Applying the $\text{AdS}_{d+1}/\text{CFT}_d$ dictionary the CFT fermion-fermion correlation function is computed from the action S_{bulk} (5.2.5) supplemented by appropriate boundary terms, S_{bdy} . One constructs the on-shell action given an arbitrary set of fermionic boundary conditions and the latter are then interpreted as sources of fermionic operators in the CFT:

$$Z_{CFT}(J) = \langle e^{J\mathcal{O}} \rangle_{CFT} = \exp \left[i(S_{bulk} + S_{bdy})^{on-shell}(\phi(J)) \right] \Big|_{\phi|_{\partial\text{AdS}}=J} \quad (3.4.6)$$

The issue of which boundary terms ought to be added to the bulk action tends to be subtle. For fermionic systems it is critical as the bulk action (5.2.5) identically vanishes on-shell [57, 84, 56, 16, 66]. Because the field equations for the fermions are first order and half the components of the spinor correspond to the conjugate momenta of the other half, we can in fact only choose a boundary source for half the components of Ψ . Projecting onto eigenstates of Γ^z , $\Gamma^z\Psi_{\pm} = \pm\Psi_{\pm}$, we will choose a boundary source $\Psi_+^0 \equiv \lim_{z_0 \rightarrow 0} \Psi_+(z = z_0)$ (to regulate the theory we impose the boundary conditions at a small distance z_0 away from the formal boundary $z = 0$ and take $z_0 \rightarrow 0$ at the end). The boundary value Ψ_-^0 is not independent but related to that of Ψ_+^0 by the Dirac equation. We should therefore not include it as an independent degree of freedom when taking functional derivatives with respect to the source. Adding a boundary action,

$$S_{bdy} = \frac{L^2}{2\kappa_4^2} \int_{z=z_0} d^3x \sqrt{-h} \bar{\Psi}_+ \Psi_- \quad (3.4.7)$$

with $h_{\mu\nu}$ the induced metric ensures a proper variational principle [16]. The variation of $\delta\Psi_-$ from the boundary action,

$$\delta S_{bdy} = \frac{L^2}{2\kappa_4^2} \int_{z=z_0} d^3x \sqrt{-h} \bar{\Psi}_+ \delta\Psi_- \Big|_{\Psi_+^0 \text{ fixed}}, \quad (3.4.8)$$

now cancels the boundary term from variation of the bulk action

$$\begin{aligned} \delta S_{bulk} = & \frac{L^2}{2\kappa_4^2} \int \sqrt{-g} \left[-\delta\bar{\Psi}(\not{D} + m)\Psi_+ - \overline{(\not{D} + m)\Psi} \delta\Psi \right] \\ & + \frac{L^2}{2\kappa_4^2} \int_{z=z_0} \sqrt{-h} \left[-\bar{\Psi}_+ \delta\Psi_- - \bar{\Psi}_- \delta\Psi_+ \right] \Big|_{\Psi_+^0 \text{ fixed}}. \end{aligned} \quad (3.4.9)$$

3.4.2 The Fermion Green's function.

To compute the fermion Green's function, we thus solve the field-equation for $\Psi(z)$ with $\Psi_+^0 \equiv \lim_{z_0 \rightarrow 0} \Psi_+(z = z_0)$ as the boundary condition, substitute this solution back into the combined action $S_{bulk} + S_{bdy}$ and functionally differentiate twice. As $\Psi_{sol}(\Psi_+^0)$ obeys the field-equation — the Dirac Equation —

$$(\mathcal{D} + m)\Psi^{sol}(\Psi_+^0) = 0, \quad (3.4.10)$$

the contribution to the on-shell action is solely due to the boundary action S_{bdy} in eq. (3.4.7). To solve the Dirac equation, we Fourier transform along the boundary,

$$\Psi(z, x^i, t) = \int \frac{d\omega d^2k}{(2\pi)^3} \Psi(z, k_i, \omega) e^{ik_i x^i - i\omega t}, \quad (3.4.11)$$

and project onto the eigenstates of Γ^z , $\Gamma^z \Psi_{\pm} = \pm \Psi_{\pm}$. Choosing the basis of Dirac matrices

$$\Gamma^z = \sigma^3 \otimes \mathbb{1}, \quad \Gamma^i = \sigma^1 \otimes \sigma^i, \quad \Gamma^t = \sigma^1 \otimes \sigma^t = \sigma^1 \otimes i\sigma^3, \quad (3.4.12)$$

we can consider Ψ_{\pm} to be two-component Dirac spinors appropriate for $d = 3$ from here on. In the charged AdS black hole background with non-zero gauge field from eq. (6.3.43), the Dirac equation decomposes into the two equations

$$(\partial_z + \mathcal{A}^{\pm})\Psi_{\pm} = \mp \mathcal{T}\Psi_{\mp}, \quad (3.4.13)$$

with

$$\begin{aligned} \mathcal{A}^{\pm} &= -\frac{1}{2z} \left(3 - \frac{z\partial_z f}{2f} \right) \pm \frac{Lm}{z\sqrt{f}}, \\ \mathcal{T} &= \frac{i}{\alpha f} \left[(-\omega + 2gq\alpha(z-1))\sigma^t + \sqrt{f}k_i\sigma^i \right]. \end{aligned} \quad (3.4.14)$$

We can eliminate either Ψ_+ or Ψ_- and readily derive a second order dynamical equation for Ψ_{\pm} . Using that

$$\mathcal{T}\mathcal{T} = -T_t T_t + T_1 T_1 + T_2 T_2 \equiv T^2, \quad (3.4.15)$$

we can invert \mathcal{T} to rewrite

$$\frac{\mathcal{T}}{T^2} (\partial_z + \mathcal{A}^+) \Psi_+ = -\Psi_- \quad (3.4.16)$$

and use the Ψ_- equation to obtain

$$(\partial_z + \mathcal{A}^-) \frac{\mathcal{T}}{T^2} (\partial_z + \mathcal{A}^+) \Psi_+ = -\mathcal{T} \Psi_+ . \quad (3.4.17)$$

Using the identity eq. (5.2.4) repeatedly, this is equivalent to

$$(\partial_z^2 + P(z)\partial_z + Q(z)) \Psi_+ = 0 \quad (3.4.18)$$

with

$$\begin{aligned} P(z) &= (\mathcal{A}^- + \mathcal{A}^+) - [\partial_z, \mathcal{T}] \frac{\mathcal{T}}{T^2} , \\ Q(z) &= \mathcal{A}^- \mathcal{A}^+ + (\partial_z \mathcal{A}^+) - [\partial_z, \mathcal{T}] \frac{\mathcal{T}}{T^2} \mathcal{A}^+ + T^2 . \end{aligned} \quad (3.4.19)$$

Note that both $P(z)$ and $Q(z)$ are two-by-two matrices. The equation for Ψ_- is simply obtained by switching \mathcal{A}^+ with \mathcal{A}^- and \mathcal{T} with $-\mathcal{T}$; it is the CPT conjugate obtained by sending $m \rightarrow -m$ and $\{\omega, k_i, q\} \rightarrow \{-\omega, -k_i, -q\}$.

We can now derive a formal expression for the propagator in terms of the solutions to the second-order equation. We write the on-shell bulk field as

$$\Psi_+^{sol}(z) = F_+(z) F_+^{-1}(z_0) \Psi_+^0(z_0) \quad (3.4.20)$$

where $F_\pm(u)$ is the two-by-two matrix satisfying the second order equation (4.2.11) [16] subject to a boundary condition in the interior of AdS. We will discuss the appropriate interior boundary condition below. There are two independent solutions $\Psi_+^{(1)}(z)$, $\Psi_+^{(2)}(z)$ that obey the interior boundary condition, one for each component of the spinor. In terms of this solution the matrix $F_+(z)$ equals

$$F_+(z) = \left(\Psi_+^{(1)}(z) , \Psi_+^{(2)}(z) \right) . \quad (3.4.21)$$

Similarly for $\Psi_-^{sol}(z)$ we write

$$\Psi_-^{sol}(z) = F_-(z) F_-^{-1}(z_0) \Psi_-^0(z_0) . \quad (3.4.22)$$

However, Ψ_-^0 is not independent as we emphasized earlier. It is related to Ψ_+^0 through the Dirac equation in its projected form (4.3.13). Acting with $\partial_z + A^+$ on both sides of (5.2.11) we see that [16]

$$\begin{aligned} (\partial_z + A^+) \Psi_+^{sol} &= (\partial_z + A^+) F_+(z) F_+^{-1}(z_0) \Psi_+^0 \\ \Leftrightarrow -\mathcal{T} \Psi_-^{sol} &= -\mathcal{T} F_-(z) F_-^{-1}(z_0) \Psi_+^0 . \end{aligned} \quad (3.4.23)$$

We have used that all the z dependence of $\Psi_{\pm}^{sol}(z)$ is encoded in the matrices $F_{\pm}(z)$ and therefore $F_{\pm}(z)$ obey the same projected Dirac equations. Thus we find that Ψ_{-}^0 equals

$$\Psi_{-}^0 = F_{-}(z_0)F_{+}^{-1}(z_0)\Psi_{+}^0 . \quad (3.4.24)$$

Substituting this constraint into the boundary action, we obtain an expression for the full on-shell action in terms of the solutions $F_{\pm}(z)$:

$$S^{on-shell} = \frac{L^2}{2\kappa_4^2} \int_{z=z_0} \frac{d\omega d^2k}{(2\pi)^3} \sqrt{-h} \bar{\Psi}_{+}^0 F_{-}(z_0)F_{+}^{-1}(z_0) \Psi_{+}^0 . \quad (3.4.25)$$

Up to a normalization \mathcal{N} the two-point function is therefore

$$G(\omega, k) = \frac{1}{\mathcal{N}} F_{-}(z_0)F_{+}^{-1}(z_0) . \quad (3.4.26)$$

This is the time-ordered two-point function. For the spectral function we shall need the imaginary part of the retarded propagator. At finite temperature the AdS background is no longer regular in the interior but has a horizon. In principle one should also consider its boundary contribution. The retarded propagator prescription of [105] — verified in [58] — is to ignore this contribution and to impose infalling boundary conditions at the horizon instead of regularity at the center of AdS. This is what we shall do.

The retarded Green's function for fermions is still a matrix. Parity and rotational invariance dictate that it can be decomposed as

$$G_R(\omega, k) = \Pi_s + \sigma^t \Pi_t + \sigma^i \Pi_i . \quad (3.4.27)$$

Our main interest, the spectral function, proportional to $\text{Im}\langle\Psi^{\dagger}\Psi\rangle$, is the imaginary part of Π_t . Specifically

$$A(\omega, k) = -\frac{1}{\pi} \text{Im}(\text{Tr} i\sigma^t G_R(\omega, k)) . \quad (3.4.28)$$

As a consequence of the underlying conformal symmetry both the Green's function and the spectral function possess a scaling symmetry. Eq. (5.2.14) shows that the frequency ω and momenta k are naturally expressed in units of an effective temperature $T_{eff}(\mu_0) \equiv 3\alpha/4\pi$ which depends on the chemical potential μ_0

$$T_{eff}(\mu_0) = T \left(\frac{1}{2} + \frac{1}{2} \sqrt{1 + \frac{(\mu_0\sqrt{3})^2}{(4\pi T)^2}} \right) .$$

The spectral function computed from AdS is therefore naturally of the form

$$A_{\Delta\Psi}^{\frac{\mu_0}{T}}(\omega, k) = \frac{1}{T^{d-2\Delta\Psi}} \tilde{f}\left(\frac{\omega}{T_{eff}(\mu_0)}, \frac{k}{T_{eff}(\mu_0)}; \Delta\Psi, \frac{\mu_0}{T}\right).$$

Any rescaling of T_{eff} can be compensated by a rescaling of the frequencies and momenta and μ_0/T is the single independent parameter determining the characteristics of the fermion spectral function. The results in the main text have been converted to units of k/T or k/μ_0 for clarity of the presentation.

3.4.3 Masses and Dimensions.

A final crucial step is to establish the aforementioned relation between the mass of the AdS fermion and the scaling dimension of the dual fermionic operator in the CFT. For generality we shall work in d dimensions in this subsection. This subsection recapitulates [16].

The scaling behavior can be read off from the asymptotic behavior of the solution near the boundary $z = 0$. In this limit the second order equation (4.2.11) diagonalizes: (setting $L = 1$)

$$\left(\partial_z^2 - \frac{d}{z}\partial_z + \frac{d(d+2) - 4m(1+m)}{4z^2}\right)\Psi_+ = 0 + \dots \quad (3.4.29)$$

Clearly the temperature or chemical potential of the black-hole is immaterial to the asymptotic scaling behaviour at $z = 0$; in terms of the CFT $z = 0$ is the UV of the theory and it should be insensitive to the infrared physics at the horizon. The leading powers of the two independent solutions to this equation are

$$\Psi_+(z) = z^{\frac{d+1}{2} - |m+\frac{1}{2}|}(\psi_+ + \dots) + z^{\frac{d+1}{2} + |m+\frac{1}{2}|}(A_+ + \dots). \quad (3.4.30)$$

(we may drop the absolute value signs in principle, but as it emphasizes the special value $m = -1/2$ it will be instructive to keep them.) Similarly for $\Psi_-(z)$ the leading singularities are obtained by sending $m \rightarrow -m$

$$\Psi_-(z) = z^{\frac{d+1}{2} - |m-\frac{1}{2}|}(\psi_- + \dots) + z^{\frac{d+1}{2} + |m-\frac{1}{2}|}(A_- + \dots). \quad (3.4.31)$$

However, recall that the Dirac equation relates the two asymptotic behaviors and that the boundary value of Ψ_- is not independent. Near $z = 0$

$$\left(\partial_z - \frac{d/2 - m}{z}\right)\Psi_+ = -\mathcal{T}|_{z=0}\Psi_- + \dots \quad (3.4.32)$$

Thus $\psi_- \propto \psi_+$ and $A_- \propto A_+$.

Because the equation diagonalizes, each component of $\Psi_{\pm}(z)$ can be considered independently and the matrices $F_{\pm}(z)$ diagonalize in the limit $z \rightarrow 0$. The scaling behavior of the Green's function is then readily read off from its definition

$$G(\omega, k) = \frac{1}{\mathcal{N}} F_- F_+^{-1} \sim \frac{z^{\frac{d+1}{2} - |m - \frac{1}{2}|} (\psi_- + \dots) + z^{\frac{d+1}{2} + |m - \frac{1}{2}|} (A_- + \dots)}{z^{\frac{d+1}{2} - |m + \frac{1}{2}|} (\psi_+ + \dots) + z^{\frac{d+1}{2} + |m + \frac{1}{2}|} (A_+ + \dots)} \quad (3.4.33)$$

The dominant scaling behavior depends on the value of m and there are three different regimes (I): $m > \frac{1}{2}$, (II): $\frac{1}{2} > m > -\frac{1}{2}$, and (III): $-\frac{1}{2} > m$. In these regimes the Green's function behaves as

$$G(\omega, k) \sim \begin{cases} z \left(\frac{\psi_-}{\psi_+} + \dots \right) + z^{2m} \left(\frac{A_-}{\psi_+} + \dots \right) & m > \frac{1}{2} \\ z^{2m} \left(\frac{\psi_-}{\psi_+} + \dots \right) + z \left(\frac{A_-}{\psi_+} + \dots \right) & \frac{1}{2} > m > -\frac{1}{2} \\ \frac{1}{z} \left(\frac{\psi_-}{\psi_+} + \dots \right) + \frac{1}{z^{2m}} \left(\frac{A_-}{\psi_+} + \dots \right) & -\frac{1}{2} > m. \end{cases} \quad (3.4.34)$$

In regime (I) the contribution proportional to z yields a contact term [16]. Recall that at zero-temperature and chemical potential each power of z is accompanied by a power of momentum: the dimensionless arguments of the solutions $\Psi_{\pm}^{sol}(z)$ are kz and ωz . Discarding the term analytic in z and thus analytic in momenta, the second term proportional to z^{2m} yields a Green's function

$$G(\omega, k) \sim (z_0 \omega)^{2m} \quad (3.4.35)$$

corresponding to the two-point function of a conformal operator of weight $\Delta_{\Psi} = \frac{d}{2} + m$. In regime (II) there is no contact term and one immediately finds the same relation between the AdS fermion mass and the scaling dimension of the conformal operator. In regime (III), however, one finds an explicit pole $(\omega z)^{-1}$ independent of the AdS fermion mass or the space-time dimension. It signals an inconsistency in the theory and one cannot consider this regime as physical [16]. This is reminiscent of the situation for scalars where for $m_{scalar}^2 > -d^2/4 + 1$ one finds analytic terms in the two-point correlator; for $-d^2/4 + 1 > m_{scalar}^2 > -d^2/4$ both solutions are normalizable; and for $-d^2/4 > m_{scalar}^2$ the theory is inconsistent. The analogy with scalars may appear strange since a negative mass-squared for scalars clearly can be problematic, whereas the sign of the fermion-mass term does not have any physical consequences normally. Recall, however,

that the same AdS bulk action can describe several CFTs depending on the boundary terms added to the action [67]. We have chosen a very specific boundary action such that $\Psi_+(z)$ is the independent variable which breaks the degeneracy between (bulk) theories with $m > 0$ and $m < 0$. In this theory m is bounded below by $-1/2$. We could have chosen a different theory with $\Psi_-(z)$ the independent variable. One would find then that m is bounded from above by $1/2$. The regime $1/2 > m > -1/2$ is present in both theories; it is the range where both solutions are normalizable and choosing either $\Psi_+(z)$ or $\Psi_-(z)$ as the independent variable corresponds to switching the “sources” and “expectation values” in the usual way (see also [62]).

This analysis also teaches us that the normalization \mathcal{N} should go as z_0^{2m} to obtain a finite answer in the limit $z_0 \rightarrow 0$.²

3.4.4 The retarded propagator boundary conditions at the horizon.

The final component of our set-up will be the boundary conditions at the horizon of the the black hole. To compute the retarded propagator in thermal settings/black hole the appropriate b.c. are those infalling into the horizon. Near the horizon at $z = 1$, the second order equation for Ψ_{\pm} becomes the same for both Ψ_+ and Ψ_- and moreover diagonalizes:

$$\left(\partial_z^2 - \frac{3}{2(1-z)} \partial_z + \frac{\tilde{\omega}^2 + \frac{1}{16}}{(1-z)^2} \right) \Psi_{\pm} + \mathcal{O}((z-1)) = 0. \quad (3.4.36)$$

with $\tilde{\omega} \equiv \frac{\omega}{a(3-q^2)} = \frac{\omega}{4\pi T}$. This equation has solutions of the form

$$\Psi_{\pm} = (1-z)^{i\tilde{\omega}-\frac{1}{4}}(c_r + \dots) + (1-z)^{-i\tilde{\omega}-\frac{1}{4}}(c_i + \dots) \quad (3.4.37)$$

The second solution has the incoming boundary condition we seek.³

²Note that the factor $L^2/2\kappa_4^2$ in the on-shell action (5.2.10) follows from an unconventional normalization of the fields in the action (5.2.5). It would be absent for conventional normalization.

³A technical detail is that due to the factors \sqrt{f} in the field equation, there is no standard Frobenius solution $\Psi_{\pm} = (1-z)^{\pm i\tilde{\omega}-\frac{1}{4}} \sum_{n=0}^{\infty} a_n^{(\pm)} (1-z)^n$. Rather half-integer powers of $(1-z)$ appear as well. We need the Frobenius method for the numerics: we use it to construct a second b.c. for the derivative of Ψ_+ — see e.g. [12]. Changing coordinates to $z = 1 - s^2$ solves this problem.

3.5 Finite temperature and the position of the Fermi surface

With some hindsight from the chapters to follow, as well as in the light of the detailed analysis performed in [79, 27] we will now comment on our finding that *at finite temperature* the zero of energy in field theory, i.e. the position of the Fermi surface lies at finite ω , i.e. differs from the AdS zero of energy $\omega = 0$. In our original paper reproduced in the previous sections, we identified the zero of energy at finite temperature with the maximum of the peak height. Our assumption was clearly that the peak maximum closely corresponds to the definition of zero energy: a pole for real ω at $T = 0$. For small T/μ thus the pole should not move much as the temperature is changed, and therefore neither should the position of the maximum peak height. We can test this hypothesis by plotting the position of the maximum of the spectral function $A(\omega, k = k_F)$ for three different temperatures (Figure 3.7A). Surprisingly, we see that the position of the maximum $E_F(T)$ drastically depends on T and moves toward $\omega = 0$ as the temperature is lowered. This suggests (in agreement with the arguments given in [79, 27]) that the sharp Fermi surface, which only exists at $T = 0$, is indeed at zero energy. This strong dependence of the peak position on temperature is not known in field theory models, and in the following chapter we will see that it suggests an inconsistency in the probe limit calculations presented in this section. The changing position $E_F(T)$ is due to the instability of the black hole background in the presence of Fermi surface (in the next chapter we will see that gravity dual of a Fermi surface always has finite fermion density, which backreacts on the gauge field and the metric).

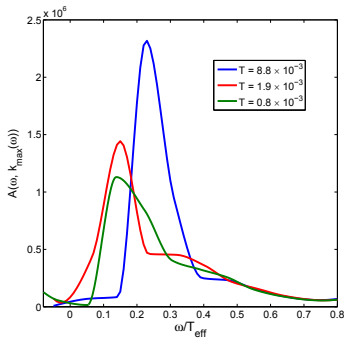


Figure 3.7: Spectral weight at its maximum, i.e. at the position of the peak for three different values of temperature and $\Delta_\Psi = 5/4$. We see that the maximum moves toward zero energy as the temperature is lowered. This suggests that the true zero temperature ground state is indeed at $\omega = 0$. However, the fact that the "Fermi energy" is strongly temperature-dependent is in fact a signal that we are looking at the false vacuum, i.e. that a self-consistent calculation with backreaction would yield a background different from the Reissner-Nordström black hole. (B) The relation between the linearly dispersing quasiparticle peak and the $\omega = 0$ peak with slow (sublinear) dispersion as $\Delta_\Psi \rightarrow 3/2$ for $k/\mu_0 = 0.35$ and $\mu_0/T = -30.9$.

Chapter 4

AdS dual of a Fermi liquid: Dirac hair [18]

4.1 Introduction

Fermionic quantum criticality is thought to be an essential ingredient in the full theory of high T_c superconductivity [112, 102]. The cleanest experimental examples of quantum criticality occur in heavy-fermion systems rather than high T_c cuprates, but the experimental measurements in heavy fermions raise equally confounding theoretical puzzles [80]. Most tellingly, the resistivity scales linearly with the temperature from the onset of superconductivity up to the crystal melting temperature [42] and this linear scaling is in conflict with single correlation length scaling at criticality [86]. The failure of standard perturbative theoretical methods to describe such behavior is thought to indicate that the underlying quantum critical system is strongly coupled [117, 78].

The combination of strong coupling and scale-invariant critical dynamics makes these systems an ideal arena for the application of the AdS/CFT correspondence: the well-established relation between strongly coupled conformal field theories (CFT) and gravitational theories in anti-de Sitter (AdS) spacetimes. An AdS/CFT computation of single-fermion spectral functions — which are directly experimentally accessible via Angle-Resolved Photoemission Spectroscopy [11, 21, 121] — bears out this promise of addressing fermionic quantum criticality [79, 17, 27, 28] (see also [76, 91]). The AdS/CFT single fermion spectral function exhibits distinct sharp quasiparticle peaks, associated with the formation of a Fermi sur-

face, emerging from a scale-free state. The fermion liquid which this Fermi surface captures is generically singular: it has either a non-linear dispersion or non-quadratic pole strength [79, 27]. The precise details depend on the parameters of the AdS model.

From the AdS gravity perspective, peaks with linear dispersion correspond to the existence of a stable charged fermionic quasinormal mode in the spectrum of a charged AdS black hole. The existence of a stable charged bosonic quasinormal mode is known to signal the onset of an instability towards a new ground state with a pervading Bose condensate extending from the charged black hole horizon to the boundary of AdS. The dual CFT description of this charged condensate is spontaneous symmetry breaking as in a superfluid and a conventional superconductor [40, 47, 49]. For fermionic systems empirically the equivalent robust $T = 0$ groundstate is the Landau Fermi Liquid — the quantum groundstate of a system with a finite number of fermions. The existence of a stable fermionic quasinormal mode suggests that an AdS dual of a finite fermion density state exists.

Here we shall make a step towards the set of AdS/CFT rules for CFTs with a finite fermion density. The essential ingredient will be Migdal's theorem, which relates the characteristic jump in fermion occupation number at the energy ω_F of the highest occupied state to the pole strength of the quasiparticle. The latter we know from the spectral function analysis and its AdS formulation is therefore known. Using this, we can show that the fermion number discontinuity is encoded in the *probability density* of the normalizable wavefunction of the dual AdS fermion field.

This shows that the AdS dual of a Fermi liquid is given by a system with occupied fermionic states in the bulk. The Fermi liquid is clearly not a scale invariant state, but any such states will have energy, momentum/pressure and charge and will change the interior geometry from AdS to something else. Which particular (set of) state(s) is the right one, it does not yet tell us, as this conclusion relies only on the asymptotic behavior of fermion fields near the AdS boundary. Here we shall take the simplest such state: a single fermion.¹ Constructing first a set of equations in terms of the spatially averaged density, we find the associated backreacted asymptotically AdS solution. This approximate solution is already good enough to solve several problems of principle:

- A charged AdS black hole in the presence of charged fermionic modes

¹These solutions are therefore the AdS extensions of [30–33].

has a critical temperature below which fermionic Dirac “hair” forms. For our effective single fermion solution, the derivative of the free energy has the characteristic discontinuity of a first order transition. In AdS/CFT this has to be the case: In contrast to bosonic quasinormal modes, a fermionic quasinormal mode can never cause a linear instability indicative of a continuous phase transition. In the language of spectral functions, the pole of the retarded Green’s function can never cross to the upper-half plane [27].² The absence of a perturbative instability between this conjectured Dirac “black hole hair” solution and the “bald” charged AdS black hole can be explained if the transition is a first order gas-liquid transition. The existence of first order transition follows from a thermodynamic analysis of the free energy rather than a spectral analysis of small fluctuations.

- This solution with finite fermion profile is the preferred ground state at low temperatures compared to the bare charged AdS black hole. The latter is therefore a false vacuum in a theory with charged fermions. Confusing a false vacuum with the true ground state can lead to anomalous results. Indeed the finite temperature behavior of fermion spectral functions in AdS Reissner-Nordström, exhibited in the combination of the results of [79, 27] and [17], shows strange behavior. The former [79, 27] found sharp quasiparticle peaks at a frequency $\omega_F = 0$ in natural AdS units, whereas the latter [17] found sharp quasiparticle peaks at finite Fermi energy $\omega_F \neq 0$. As we will show, both peaks in fact describe the same physics: the $\omega_F \neq 0$ peak is a finite temperature manifestation of (one of the) $\omega = 0$ peaks in [27]. Its shift in location at finite temperature is explained by the existence of the nearby true finite fermion density ground state, separated by a potential barrier from the AdS Reissner-Nordström solution.
- The solution we construct here only considers the backreaction on the electrostatic potential. We show, however, that the gravitational energy density diverges at the horizon. This ought to be, as one expects the infrared geometry to change due to fermion profile. The charged AdS-black hole solution corresponds to a CFT system in a state with large ground state entropy. This is the area of the extremal black-hole horizon at $T = 0$. Systems with large ground-

²Ref. [10] argues that the instability can be second order.

state entropy are notoriously unstable to collapse to a low-entropy state, usually by spontaneous symmetry breaking. In a fermionic system it should be the collapse to the Fermi liquid. The final state will generically be a geometry that asymptotes to Lifshitz type, i.e. the background breaks Lorentz-invariance and has a double-pole horizon with vanishing area, as expounded in [50]. Indeed the gravitational energy density diverges at the horizon in a similar way as other systems that are known to gravitationally backreact to a Lifshitz solution. The fully backreacted geometry includes important separate physical aspects — it is relevant to the stability and scaling properties of the Fermi liquid — and will be considered in a companion article.

The Dirac hair solution thus captures the physics one expects of the dual of a Fermi liquid. We have based its construction on a derived set of AdS/CFT rules to describe systems at finite fermion density. Qualitatively the result is as expected: one also needs occupied fermionic states in the bulk. Next to our effective single fermion approximation, another simple candidate is the backreacted AdS-Fermi-gas [50]/electron star [51] which appeared during the course of this work.³ The difference between the two approaches are the assumptions used to reduce the interacting Fermi system to a tractable solution. Ideally, one should carefully track all the fermion wavefunctions as in the recent article [96]. As explained in [19] the Fermi-gas and the single Dirac field are the two “local” approximations to the generic non-local multiple fermion system in the bulk, in very different regimes of applicability. The electron-star/Fermi-gas is considered in the Thomas-Fermi limit where the microscopic charge of the constituent fermions is sent to zero keeping the overall charge fixed, whereas the single Dirac field clearly is the ‘limit’ where the microscopic charge equals the total charge in the system. This is directly evident in the spectral functions of both systems. The results presented here show that each pole in the CFT spectral function corresponds to a unique occupied Fermi state in the bulk; the electron star spectra show a parametrically large number of poles [53, 63, 19], whereas the Dirac hair state has a single quasiparticle pole by construction. The AdS-Dirac-hair black hole derived here therefore has the benefit of a direct connection with a unique Fermi liquid state in the CFT. This is in fact the starting point of our derivation.

³See also [23, 6]. An alternative approach to back-reacting fermions is [64].

In the broader context, the existence of both the Dirac hair and backreacted Fermi gas solution is not a surprise. It is a manifestation of *universal* physics in the presence of charged AdS black holes. The results here, and those of [79, 27, 50, 51], together with the by now extensive literature on holographic superconductors, i.e. Bose condensates, show that at sufficiently low temperature in units of the black-hole charge, the electric field stretching to AdS-infinity causes a spontaneous discharge of the bulk vacuum outside of the horizon into the charged fields of the theory — whatever their nature. The positively charged excitations are repelled by the black hole, but cannot escape to infinity in AdS and they form a charge cloud hovering over the horizon. The negatively charged excitations fall into the black-hole and neutralize the charge, until one is left with an uncharged black hole with a condensate at finite T or a pure asymptotically AdS-condensate solution at $T = 0$. As [50, 51] and we show, the statistics of the charged particle do not matter for this condensate formation, except in the way it forms: bosons superradiate and fermions nucleate. The dual CFT perspective of this process is “entropy collapse”. The final state therefore has negligible ground state entropy and is stable. The study of charged black holes in AdS/CFT is therefore a novel way to understand the stability of charged interacting matter which holds much promise.

4.2 From Green's function to AdS/CFT rules for a Fermi Liquid

We wish to show how a solution with finite fermion number — a Fermi liquid — is encoded in AdS. The exact connection and derivation will require a review of what we have learned of Dirac field dynamics in AdS/CFT through Green's functions analysis. The defining signature of a Fermi liquid is a quasi-particle pole in the (retarded) fermion propagator,

$$G_R = \frac{Z}{\omega - \mu_R - v_F(k - k_F)} + \text{regular} \quad (4.2.1)$$

Phenomenologically a non-zero residue at the pole, Z , also known as the pole strength, is the indicator of a Fermi liquid state. Migdal famously related the pole strength to the occupation number discontinuity at the pole $\omega = 0$.

$$Z = \lim_{\epsilon \rightarrow 0} [n_F(\omega - \epsilon) - n_F(\omega + \epsilon)] \quad (4.2.2)$$

where

$$n_F(\omega) = \int d^2k f_{FD} \left(\frac{\omega}{T} \right) \text{Im} G_R(\omega, k).$$

with f_{FD} the Fermi-Dirac distribution function. Vice versa, a Fermi liquid with a Fermi-Dirac jump in occupation number at the Fermi energy $\omega_F = 0$ has a low-lying quasiparticle excitation. Using our knowledge of fermionic spectral functions in AdS/CFT we shall first relate the pole-strength Z to known AdS quantities. Then using Migdal's relation, the dual of a Fermi liquid is characterized by an asymptotically AdS solution with non-zero value for these very objects.

The Green's functions derived in AdS/CFT are those of charged fermionic operators with scaling dimension Δ , dual to an AdS Dirac field with mass $m = \Delta - \frac{d}{2}$. We shall focus on $d = 2 + 1$ dimensional CFTs. In its gravitational description this Dirac field is minimally coupled to 3+1 dimensional gravity and electromagnetism with action

$$S = \int d^4x \sqrt{-g} \left[\frac{1}{2\kappa^2} \left(R + \frac{6}{L^2} \right) - \frac{1}{4} F_{MN}^2 - \bar{\Psi} (\not{D} + m) \Psi \right]. \quad (4.2.3)$$

For zero background fermions, $\Psi = 0$, a spherically symmetric solution is a charged AdS₄ black-hole background

$$\begin{aligned} ds^2 &= \frac{L^2 \alpha^2}{z^2} (-f(z) dt^2 + dx^2 + dy^2) + \frac{L^2}{z^2} \frac{dz^2}{f(z)}, \\ f(z) &= (1 - z)(1 + z + z^2 - q^2 z^3), \\ A_0^{(bg)} &= 2q\alpha(z - 1). \end{aligned} \quad (4.2.4)$$

Here $A_0^{(bg)}$ is the time-component of the $U(1)$ -vector-potential, L is the AdS radius and the temperature and chemical potential of the black hole equal

$$T = \frac{\alpha}{4\pi} (3 - q^2), \quad \mu_0 = -2q\alpha, \quad (4.2.5)$$

where q is the black hole charge.

To compute the Green's functions we need to solve the Dirac equation in the background of this charged black hole:

$$e_A^M \Gamma^A (D_M + ieg A_M) \Psi + m \Psi = 0, \quad (4.2.6)$$

where the vielbein e_A^M , covariant derivative D_M and connection A_M correspond to the fixed charged AdS black-hole metric and electrostatic potential (6.2.4). Denoting $A_0 = \Phi$ and taking the standard AdS-fermion projection onto $\Psi_{\pm} = \frac{1}{2}(1 \pm \Gamma^Z)\Psi$, the Dirac equation reduces to

$$(\partial_z + \mathcal{A}_{\pm}) \Psi_{\pm} = \mp \mathcal{T} \Psi_{\mp} \quad (4.2.7)$$

with

$$\begin{aligned} \mathcal{A}_{\pm} &= -\frac{1}{2z} \left(3 - \frac{zf'}{2f} \right) \pm \frac{mL}{z\sqrt{f}}, \\ \mathcal{T} &= \frac{i(-\omega + g\Phi)}{\alpha f} \gamma^0 + \frac{i}{\alpha\sqrt{f}} k_i \gamma^i. \end{aligned} \quad (4.2.8)$$

Here γ^{μ} are the 2+1-dimensional Dirac matrices, obtained after decomposing the 3+1 dimensional Γ^{μ} -matrices.

Explicitly the Green's function is extracted from the behavior of the solution to the Dirac equation at the AdS-boundary. The boundary behavior of the bulk fermions is

$$\begin{aligned} \Psi_+(\omega, k; z) &= A_+ z^{\frac{3}{2}-m} + B_+ z^{\frac{5}{2}+m} + \dots, \\ \Psi_-(\omega, k; z) &= A_- z^{\frac{5}{2}-m} + B_- z^{\frac{3}{2}+m} + \dots, \end{aligned} \quad (4.2.9)$$

where $A_{\pm}(\omega, k)$, $B_{\pm}(\omega, k)$ are not all independent but related by the Dirac equation at the boundary

$$A_- = -\frac{i\mu}{(2m-1)} \gamma^0 A_+, \quad B_+ = -\frac{i\mu}{(2m+1)} \gamma^0 B_- . \quad (4.2.10)$$

The CFT Green's function then equals [17, 62, 79]

$$G_R = \lim_{z \rightarrow 0} z^{-2m} \frac{\Psi_-(z)}{\Psi_+(z)} - \text{singular} = \frac{B_-}{A_+} . \quad (4.2.11)$$

In other words B_- is the CFT response to the (infinitesimal) source A_+ . Since in the Green's function the fermion is a fluctuation, the functions $\Psi_{\pm}(z)$ are now probe solutions to the Dirac equation in a fixed gravitational and electrostatic background (for ease of presentation we are considering $\Psi_{\pm}(z)$ as numbers instead of two-component vectors). The boundary conditions at the horizon/AdS interior determine which Green's function one considers, e.g. infalling horizon boundary conditions yield the

retarded Green's function. For non-zero chemical potential this fermionic Green's function can have a pole signalling the presence of a Fermi surface. This pole occurs precisely for a (quasi-)normalizable mode, i.e. a specific energy ω_F and momentum k_F where the external source $A_+(\omega, k)$ vanishes (for infalling boundary conditions at the horizon).

Knowing that the energy of the quasinormal mode is always $\omega_F = 0$ [79] and following [27], we expand G_R around $\omega = 0$ as:

$$G_R(\omega) = \frac{B^{(0)} + \omega B^{(1)} + \dots}{A_+^{(0)} + \omega A_+^{(1)} + \dots}. \quad (4.2.12)$$

A crucial point is that in this expansion we are assuming that the pole will correspond to a stable quasiparticle, i.e. there are no fractional powers of ω less than unity in the expansion around $\omega_F = 0$ [27]. Fermions in AdS/CFT are of course famous for allowing more general pole-structures corresponding to Fermi-surfaces without stable quasiparticles [27], but those Green's functions are not of the type (4.2.1) and we shall therefore not consider them here. The specific Fermi momentum k_F associated with the Fermi surface is the momentum value for which the first ω -independent term in the denominator vanishes $A_+^{(0)}(k_F) = 0$ — for this value of $k = k_F$ the presence of a pole in the Green's functions at $\omega = 0$ is manifest. Writing $A_+^{(0)} = a_+(k - k_F) + \dots$ and comparing with the standard quasiparticle propagator,

$$G_R = \frac{Z}{\omega - \mu_R - v_F(k - k_F)} + \text{regular} \quad (4.2.13)$$

we read off that the pole-strength equals

$$Z = B_-^{(0)}(k_F)/A_+^{(1)}(k_F).$$

We thus see that a non-zero pole-strength is ensured by a non-zero value of $B_-(\omega = 0, k = k_F)$ — the “response” *without* corresponding source as $A^{(0)}(k_F) \equiv 0$. Quantitatively the pole-strength also depends on the value of $A_+^{(1)}(k_F) \equiv \partial_\omega A_+(k_F)|_{\omega=0}$, which is always finite. This is not a truly independent parameter, however. The size of the pole-strength has only a relative meaning w.r.t. to the integrated spectral density. This normalization of the pole strength is a global parameter rather than an AdS boundary issue. We now show this by proving that $A_+^{(1)}(k_F)$ is inversely proportional to $B_-^{(0)}(k_F)$ and hence Z is completely set by $B_-^{(0)}(k_F)$, i.e.

$Z \sim |B_-^{(0)}(k_F)|^2$. Consider a transform $\widetilde{W}(\Psi_{+,A}, \Psi_{+,B})$ of the Wronskian $W(\Psi_{+,A}, \Psi_{+,B}) = \Psi_{+,A} \partial_z \Psi_{+,B} - (\partial_z \Psi_{+,A}) \Psi_{+,B}$ for two solutions to the second order equivalent of the Dirac equation for the field Ψ_+

$$(\partial_z^2 + P(z)\partial_z + Q_+(z)) \Psi_+ = 0 \quad (4.2.14)$$

that is conserved (detailed expressions for $P(z)$ and $Q_+(z)$ will be given later):

$$\widetilde{W}(\Psi_{+,A}(z), \Psi_{+,B}(z), z; z_0) = \exp\left(\int_{z_0}^z P(z)\right) W(\Psi_{+,A}(z), \Psi_{+,B}(z)) \quad (4.2.15)$$

For this quantity it holds $\partial_z \widetilde{W} = 0$. Here z_0^{-1} is the infinitesimal distance away from the boundary at $z = 0$ which is equivalent to the UV -cutoff in the CFT. Setting $k = k_F$ and choosing for $\Psi_{+,A} = A_+ z^{3/2-m} \sum_{n=0}^{\infty} a_n z^n$ and $\Psi_{+,B} = B_+ z^{5/2+m} \sum_{n=0}^{\infty} b_n z^n$ the real solutions which asymptote to solutions with $B_+(\omega, k_F) = 0$ and $A_+(\omega, k_F) = 0$ respectively, but for a value of ω infinitesimally away from $\omega_F = 0$, we can evaluate \widetilde{W} at the boundary to find,⁴

$$\widetilde{W} = z_0^3(1 + 2m)A_+B_+ = \mu z_0^3 A_+ B_- \quad (4.2.16)$$

The last step follows from the constraint (5.2.2) where the reduction from two-component spinors to functions means that $\widetilde{\gamma}^0$ is replaced by one of its eigenvalues $\pm i$. Taking the derivative of \widetilde{W} at $\omega = 0$ for $k = k_F$ and expanding $A_+(\omega, k_F)$ and $B_-(\omega, k_F)$ as in (4.2.12), we can solve for $A_+^{(1)}(k_F)$ in terms of $B_-^{(0)}(k_F)$ and arrive at the expression for the pole strength Z in terms of $|B_-^{(0)}(k_F)|^2$:

$$Z = \frac{\mu z_0^3}{\partial_\omega \widetilde{W}|_{\omega=0, k=k_F}} |B_-^{(0)}(k_F)|^2. \quad (4.2.17)$$

Because $\partial_\omega \widetilde{W}$, as \widetilde{W} , is a number that is independent of z , this expression emphasizes that it is truly the nonvanishing subleading term $B_-^{(0)}(\omega_F, k_F)$ which sets the pole strength, up to a normalization $\partial_\omega \widetilde{W}$ which is set by the fully integrated spectral density. This integration is always UV-cut-off dependent and the explicit z_0 dependence should therefore not

⁴ $P(z) = -3/z + \dots$ near $z = 0$

surprise us.⁵ We should note that, unlike perturbative Fermi liquid theory, Z is a dimensionful quantity of mass dimension $2m + 1 = 2\Delta - 2$, which illustrates more directly its scaling dependence on the UV-energy scale z_0 . At the same time Z is real, as it can be shown that both $\partial_\omega \widetilde{W}|_{\omega=0, k=k_F} = \mu z_0^3 A_+^{(1)} B_-^{(0)}$ and $B_-^{(0)}$ are real [27].

4.2.1 The AdS dual of a stable Fermi Liquid: Applying Migdal's relation holographically

We have thus seen that a solution with nonzero $B_-(\omega_F, k_F)$ whose corresponding external source vanishes (by definition of ω_F, k_F), is related to the presence of a quasiparticle pole in the CFT. Through Migdal's theorem its pole strength is related to the presence of a discontinuity of the occupation number, and this discontinuity is normally taken as the characteristic signature of the presence of a Fermi Liquid. Qualitatively we can already infer that an AdS gravity solution with non-vanishing $B_-(\omega_F, k_F)$ corresponds to a Fermi Liquid in the CFT. We thus seek solutions to the Dirac equation with vanishing external source A_+ but non-vanishing response B_- coupled to electromagnetism (and gravity). The construction of the AdS black hole solution with a finite single fermion wavefunction is thus analogous to the construction of a holographic superconductor [47] with the role of the scalar field now taken by a Dirac field of mass m .

This route is complicated, however, by the spinor representation of the Dirac fields, and the related fermion doubling in AdS. Moreover, relativistically the fermion Green's function is a matrix and the pole strength Z appears in the time-component of the vector projection $\text{Tr} i\gamma^i G$. As we take this and the equivalent jump in occupation number to be the signifying characteristic of a Fermi liquid state in the CFT, it would be

⁵Using that \widetilde{W} is conserved, one can e.g. compute it at the horizon. There each solution $\Psi_{+,A}(\omega, k_F; z)$, $\Psi_{+,B}(\omega, k_F; z)$ is a linear combination of the infalling and outgoing solution

$$\begin{aligned}\Psi_{+,A}(z) &= \bar{\alpha} (1-z)^{-1/4+i\omega/4\pi T} + \alpha (1-z)^{-1/4-i\omega/4\pi T} + \dots \\ \Psi_{+,B}(z) &= \bar{\beta} (1-z)^{-1/4+i\omega/4\pi T} + \beta (1-z)^{-1/4-i\omega/4\pi T} + \dots\end{aligned}\quad (4.2.18)$$

yielding a value of $\partial_\omega \widetilde{W}$ equal to $(P(z) = 1/2(1-z) + \dots \text{ near } z = 1)$

$$\partial_\omega \widetilde{W} = \frac{i}{2\pi T} \mathcal{N}(z_0) (\bar{\alpha}\beta - \bar{\beta}\alpha) \quad (4.2.19)$$

with $\mathcal{N}(z_0) = \exp \int_{z_0}^z dz \left[P(z) - \frac{1}{2(1-z)} \right]$.

much more direct if we can derive an AdS radial evolution equation for the vector-projected Green's function and hence the occupation number discontinuity directly. From the AdS perspective is also more convenient to work with bilinears such as Green's functions, since the Dirac fields always couple pairwise to bosonic fields.

To do so, we start again with the two decoupled second order equations equivalent to the Dirac equation (4.2.7)

$$(\partial_z^2 + P(z)\partial_z + Q_\pm(z)) \Psi_\pm = 0 \quad (4.2.20)$$

with

$$\begin{aligned} P(z) &= (\mathcal{A}_- + \mathcal{A}_+) - [\partial_z, \mathcal{T}] \frac{\mathcal{T}}{T^2}, \\ Q_\pm(z) &= \mathcal{A}_- \mathcal{A}_+ + (\partial_z \mathcal{A}_\pm) - [\partial_z, \mathcal{T}] \frac{\mathcal{T}}{T^2} \mathcal{A}_\pm + T^2. \end{aligned} \quad (4.2.21)$$

Note that both $P(z)$ and $Q_\pm(z)$ are matrices in spinor space. The general solution to this second order equation — with the behavior at the horizon/interior appropriate for the Green's function one desires — is a matrix valued function $(M_\pm(z))^\alpha_\beta$ and the field $\Psi_\pm(z)$ equals $\Psi_\pm(z) = M_\pm(z)\Psi_\pm^{(hor)}$. Due to the first order nature of the Dirac equation the horizon values $\Psi_\pm^{(hor)}$ are not independent but related by a z -independent matrix $S\Psi_+^{(hor)} = \Psi_-^{(hor)}$, which can be deduced from the near-horizon behavior of (5.2.2); specifically $S = \gamma^0$. One then obtains the Green's function from the on-shell boundary action (see e.g. [16, 17])

$$S_{bnd} = \oint_{z=z_0} d^d x \bar{\Psi}_+ \Psi_- \quad (4.2.22)$$

as follows: Given a boundary source ζ_+ for $\Psi_+(z)$, i.e. $\Psi_+(z_0) \equiv \zeta_+$, one concludes that $\Psi_+^{(hor)} = M_+^{-1}(z_0)\zeta_+$ and thus $\Psi_+(z) = M_+(z)M_+^{-1}(z_0)\zeta_+$, $\Psi_-(z) = M_-(z)SM_+^{-1}(z_0)\zeta_+$. Substituting these solutions into the action gives

$$S_{bnd} = \oint_{z=z_0} d^d x \bar{\zeta}_+ M_-(z_0) S M_+^{-1}(z_0) \zeta_+ \quad (4.2.23)$$

The Green's function is obtained by differentiating w.r.t. $\bar{\zeta}_+$ and ζ_+ and discarding the conformal factor z_0^{2m} with m the AdS mass of the Dirac field (one has to be careful for $mL > 1/2$ with analytic terms [16])

$$G = \lim_{z_0 \rightarrow 0} z_0^{-2m} M_-(z_0) S M_+^{-1}(z_0). \quad (4.2.24)$$

Since $M_{\pm}(z)$ are determined by evolution equations in z , it is clear that the Green's function itself is also determined by an evolution equation in z , i.e. there is some function $G(z)$ which reduces in the limit $z \rightarrow 0$ to $z_0^{2m}G$. One obvious candidate is the function

$$G^{(0)}(z) = M_-(z)SM_+^{-1}(z). \quad (4.2.25)$$

Using the original Dirac equations one can see that this function obeys the non-linear evolution equation

$$\partial_z G^{(0)}(z) = -A_- G^{(0)}(z) - \mathcal{T}M_+SM_+^{-1} + A_+ G^{(0)}(z) + G^{(0)}(z)\mathcal{T}G^{(0)}(z) \quad (4.2.26)$$

This is the approach used in [79], where a specific choice of momenta is chosen such that M_+ commutes with S . For a generic choice of momenta, consistency requires that one also considers the evolution equation for $M_+(z)SM_+^{-1}(z)$.

There is, however, another candidate for the extension $G(z)$ which is based on the underlying boundary action. Rather than extending the kernel $M_-(z_0)M_+^{-1}(z_0)$ of the boundary action we extend the constituents of the action itself, based on the individual fermion wavefunctions $\Psi_{\pm}(z) = M_{\pm}(z)S^{\frac{1}{2} \mp \frac{1}{2}}M_{\pm}^{-1}(z_0)$. We define an extension of the matrix $G(z)$ including an expansion in the complete set $\Gamma^I = \{\mathbb{1}, \gamma^i, \gamma^{ij}, \dots, \gamma^{i_1, i_d}\}$ (with $\gamma^4 = i\gamma^0$)

$$\begin{aligned} G^I(z) &= \bar{M}_+^{-1}(z_0)\bar{M}_+(z)\Gamma^I M_-(z)SM_+^{-1}(z_0) \\ G^I(z_0) &= \Gamma^I G(z_0) \end{aligned} \quad (4.2.27)$$

where $\bar{M} = i\gamma^0 M^\dagger i\gamma^0$. Using again the original Dirac equations, this function obeys the evolution equation

$$\begin{aligned} \partial_z G^I(z) &= -(\bar{A}_+ + A_-)G^I(z) - \bar{M}_{+,0}^{-1}\bar{M}_-(z)\bar{\mathcal{T}}\Gamma^I M_-(z)SM_{+,0}^{-1} + \\ &\quad + \bar{M}_{+,0}^{-1}\bar{M}_+(z)\Gamma^I \mathcal{T}M_+(z)SM_{+,0}^{-1} \end{aligned} \quad (4.2.28)$$

Recall that $\mathcal{T}\gamma^{i_1 \dots i_p} = \mathcal{T}^{[i_1} \gamma^{\dots i_p]} + \mathcal{T}_j \gamma^{j i_1 \dots i_p}$. It is then straightforward to see that for consistency, we also need to consider the evolution equations of

$$\mathcal{J}_+^I = \bar{M}_{+,0}^{-1}\bar{M}_+(z)\Gamma^I M_+(z)SM_{+,0}^{-1}, \quad \mathcal{J}_-^I = \bar{M}_{+,0}^{-1}\bar{M}_-(z)\Gamma^I M_-(z)SM_{+,0}^{-1}$$

and

$$\bar{G}^I = \bar{M}_{+,0}^{-1}\bar{M}_-(z)\Gamma^I M_+(z)SM_{+,0}^{-1}.$$

The significant advantage of these functions G^I , \bar{G}^I , \mathcal{J}_\pm^I is that the evolution equations are now linear. This approach may seem overly complicated. However, if the vector \mathcal{T}^i happens to only have a single component nonzero, then the system reduces drastically to the four fields $\mathcal{J}_\pm^i, G^\mathbb{1}, \bar{G}^\mathbb{1}$. We shall see below that a similar drastic reduction occurs, when we consider only spatially and temporally averaged functions $J^I = \int dt d^2x \mathcal{J}_\pm^I$.

Now the two extra currents \mathcal{J}_\pm^I have a clear meaning in the CFT. The current $G^I(z)$ reduces by construction to Γ^I times the Green's function $G^\mathbb{1}(z_0)$ on the boundary, and clearly $\bar{G}^I(z)$ is its hermitian conjugate. The current \mathcal{J}_+^I reduces at the boundary to $\mathcal{J}_+^I = \Gamma^I M_{+,0} S M_{+,0}^{-1}$. Thus \mathcal{J}_+^I sets the normalization of our linear system. The interesting current is the current \mathcal{J}_-^I . Using that $\bar{S} = S^{-1}$, it can be seen to reduce on the boundary to the combination $\bar{\mathcal{J}}_+^\mathbb{1} \bar{G}^\mathbb{1} \Gamma^I G^\mathbb{1}$. Thus, $(\bar{\mathcal{J}}_+^\mathbb{1})^{-1} \mathcal{J}_-^I$ is the norm squared of the Green's function, i.e. the probability density of the off-shell process.

For an off-shell process or a correlation function the norm-squared has no real functional meaning. However, we are specifically interested in solutions in the absence of an external source, i.e. the *on-shell* correlation functions. In that case the analysis is quite different. The on-shell condition is equivalent to choosing momenta to saturate the pole in the Green's function, i.e. it is precisely choosing dual AdS solutions whose leading external source A_\pm vanishes. Then M_+ and M_- are no longer independent, but $M_{+,0} = \delta B_+ / \delta \Psi_+^{(hor)} = -\frac{i\mu\gamma^0}{2m+1} M_{-,0} S$. As a consequence all boundary values of $\mathcal{J}_-^I(z_0), G^I(z_0), \bar{G}^I(z_0)$ become proportional; specifically using $S = \gamma^0$ one has that

$$\mathcal{J}_-^I(z_0)|_{on-shell} = \frac{(2m+1)}{\mu} \gamma^0 G^\mathbb{1}(z_0)|_{on-shell} \quad (4.2.29)$$

is the “on-shell” Green's function. Now, the meaning of the on-shell correlation function is most evident in thermal backgrounds. It equals the density of states $\rho(\omega(k)) = -\frac{1}{\pi} \text{Im} G_R$ times the Fermi-Dirac distribution [77]

$$\text{Tr} i \gamma^0 G_F^t(\omega_{bare}, k)|_{on-shell} = 2\pi f_{FD} \left(\frac{\omega_{bare} - \mu}{T} \right) \rho(\omega_{bare}) \quad (4.2.30)$$

For a Fermi liquid with the defining off-shell Green's function (4.2.1) $\omega_{bare}(k_F) - \mu \equiv \omega = 0$ and $\rho(\omega_{bare}(k)) = Z_{z_0} \delta^2(k - k_F) \delta(\omega) + \dots$. Thus

we see that the boundary value of $\mathcal{J}_-^{(0)}(z_0)|_{on-shell} = Zf_{FD}(0)\delta^3(0)$ indeed captures the pole strength directly times a product of distributions. This product of distributions can be absorbed in setting the normalization. An indication that this is correct is that the determining equations for G^I , \bar{G}^I , \mathcal{J}_\pm^I remain unchanged if we multiply G^I , \bar{G}^I , \mathcal{J}_\pm^I on both sides with $M_{+,0}$. If $M_{+,0}$ is unitary it is just a similarity transformation. However, from the definition of the Green's function, one can see that this transformation precisely removes the pole. This ensures that we obtain finite values for G^I , \bar{G}^I , \mathcal{J}_\pm^I at the specific pole-values ω_F, k_F where the distributions would naively blow up.

Boundary conditions and normalizability

We have shown that a normalizable solution to \mathcal{J}^0 correctly captures the pole strength directly. However, 'normalizable' is still defined in terms of an absence of a source for the fundamental Dirac field Ψ_\pm rather than the composite fields \mathcal{J}_\pm^I and G^I . One would prefer to determine normalizability directly from the boundary behavior of the composite fields. This can be done. Under the assumption that the electrostatic potential Φ is regular, i.e.

$$\Phi = \mu - \rho z + \dots \quad (4.2.31)$$

the "connection" \mathcal{T}^I is subleading to the connection \mathcal{A} near $z = 0$. Thus the equations of motion near $z = 0$ do not mix the various \mathcal{J}_\pm^I , G^I and the composite fields behave as

$$\begin{aligned} \mathcal{J}_+^I &= j_{3-2m}^I z^{3-2m} + j_{4+}^I z^4 + j_{5+2m}^I z^{5+2m} + \dots, \\ \mathcal{J}_-^I &= j_{5-2m}^I z^{5-2m} + j_{4-}^I z^4 + j_{3+2m}^I z^{3+2m} + \dots, \\ G^I &= I_{4-2m}^I z^{4-2m} + I_3^I z^3 + I_{4+2m}^I z^{4+2m} + I_5^I z^5 + \dots, \end{aligned} \quad (4.2.32)$$

with the identification

$$\begin{aligned} j_{3-2m}^I &= \bar{A}_+ \Gamma^I A_+, & j_{4+}^I &= \bar{A}_+ \Gamma^I B_+ + \bar{B}_+ \Gamma^I A_+, & j_{5+2m}^I &= \bar{B}_+ \Gamma^I B_+, \\ j_{3+2m}^I &= \bar{A}_- \Gamma^I A_-, & j_{4-}^I &= \bar{A}_- \Gamma^I B_- + \bar{B}_- \Gamma^I A_-, & j_{5-2m}^I &= \bar{B}_- \Gamma^I B_-, \\ I_{4-2m}^I &= \bar{A}_+ \Gamma^I A_-, & I_3^I &= \bar{A}_+ \Gamma^I B_-, & I_{4+2m}^I &= \bar{B}_+ \Gamma^I B_-, \\ I_5^I &= \bar{B}_+ \Gamma^I A_-. \end{aligned} \quad (4.2.33)$$

A 'normalizable' solution in \mathcal{J}_-^I and thus \mathcal{J}^0 is therefore defined by the vanishing of *both* the leading *and* the subleading term.

4.3 An AdS Black hole with Dirac Hair

Having determined a set of AdS evolution equations and boundary conditions that compute the pole strength Z directly through the currents $\mathcal{J}_-^{(0)}(z)$ and $G^I(z)$, we can now try to construct the AdS dual of a system with finite fermion density, including backreaction. As we remarked in the beginning of section 4.2.1, the demand that the solutions be normalizable means that the construction of the AdS black hole solution with a finite single fermion wavefunction is analogous to the construction of a holographic superconductor [47] with the role of the scalar field now taken by the Dirac field. The starting point therefore is the charged AdS₄ black-hole background (6.2.4) and we should show that at low temperatures this AdS Reissner-Nordström black hole is unstable towards a solution with a finite Dirac profile. We shall do so in a simplified “large charge” limit where we ignore the gravitational dynamics, but as is well known from holographic superconductor studies (see e.g. [47, 49]) this limit already captures much of the essential physics. In a companion article [20] we will construct the full backreacted groundstate including the gravitational dynamics.

In this large charge non-gravitational limit the equations of motion for the action (4.2.3) reduce to those of $U(1)$ -electrodynamics coupled to a fermion with charge g in the background of this black hole:

$$\begin{aligned} D_M F^{MN} &= ig e_A^N \bar{\Psi} \Gamma^A \Psi, \\ 0 &= e_A^M \Gamma^A (D_M + ieg A_M) \Psi + m \Psi. \end{aligned} \quad (4.3.1)$$

Thus the vielbein e_A^M and covariant derivative D_M remain those of the fixed charged AdS black hole metric (6.2.4), but the vector-potential now contains a background piece $A_0^{(bg)}$ plus a first-order piece $A_M = A_M^{(bg)} + A_M^{(1)}$, which captures the effect of the charge carried by the fermions.

Following our argument set out in previous section that it is more convenient to work with the currents $\mathcal{J}_\pm^I(z), G^I(z)$ instead of trying to solve the Dirac equation directly, we shall first rewrite this coupled non-trivial set of equations of motion in terms of the currents while at the same time using symmetries to reduce the complexity. Although a system at finite fermion density need not be homogeneous, the Fermi liquid ground state is. It therefore natural to make the ansatz that the final AdS solution is static and preserves translation and rotation along the boundary. As the Dirac field transforms non-trivially under rotations and boosts, we cannot

make this ansatz in the strictest sense. However, in some average sense which we will make precise, the solution should be static and translationally invariant. Then translational and rotational invariance allow us to set $A_i = 0$, $A_z = 0$, whose equations of motions will turn into constraints for the remaining degrees of freedom. Again denoting $A_0 = \Phi$, the equations reduce to the following after the projection onto $\Psi_{\pm} = \frac{1}{2}(1 \pm \Gamma^Z)\Psi$.

$$\begin{aligned} \partial_z^2 \Phi &= \frac{-gL^3\alpha}{z^3\sqrt{f}} (\bar{\Psi}_+ i\gamma^0 \Psi_+ + \bar{\Psi}_- i\gamma^0 \Psi_-) , \\ (\partial_z + \mathcal{A}_{\pm}) \Psi_{\pm} &= \mp \mathcal{T} \Psi_{\mp} \end{aligned} \quad (4.3.2)$$

with

$$\begin{aligned} \mathcal{A}_{\pm} &= -\frac{1}{2z} \left(3 - \frac{zf'}{2f} \right) \pm \frac{mL}{z\sqrt{f}} , \\ \mathcal{T} &= \frac{i(-\omega + g\Phi)}{\alpha f} \gamma^0 + \frac{i}{\alpha\sqrt{f}} k_i \gamma^i . \end{aligned} \quad (4.3.3)$$

as before.

The difficult part is to “impose” staticity and rotational invariance for the non-invariant spinor. This can be done by rephrasing the dynamics in terms of fermion current bilinears, rather than the fermions themselves. We shall first do so rather heuristically, and then show that the equations obtained this way are in fact the flow equations for the Green’s functions and composites $\mathcal{J}^I(z)$, $G^I(z)$ constructed in the previous section. In terms of the local vector currents⁶

$$J_+^{\mu}(x, z) = \bar{\Psi}_+(x, z) i\gamma^{\mu} \Psi_+(x, z) , \quad J_-^{\mu}(x, z) = \bar{\Psi}_-(x, z) i\gamma^{\mu} \Psi_-(x, z) , \quad (4.3.4)$$

or equivalently

$$\begin{aligned} J_+^{\mu}(p, z) &= \int d^3k \bar{\Psi}_+(-k, z) i\gamma^{\mu} \Psi_+(p+k, z) , \\ J_-^{\mu}(p, z) &= \int d^3k \bar{\Psi}_-(-k, z) i\gamma^{\mu} \Psi_-(p+k, z) . \end{aligned} \quad (4.3.5)$$

rotational invariance means that spatial components J_{\pm}^i should vanish on the solution — this solves the constraint from the A_i equation of motion, and the equations can be rewritten in terms of J_{\pm}^0 only. Staticity and

⁶In our conventions $\bar{\Psi} = \Psi^{\dagger} i\gamma^0$.

rotational invariance in addition demand that the bilinear momentum p_μ vanish. In other words, we are only considering temporally and spatially averaged densities: $J_\pm^\mu(z) = \int dt d^2x \bar{\Psi}(t, x, z) i\gamma^\mu \Psi(t, x, z)$. Analogous to the bilinear flow equations for the Green's function, we can act with the Dirac operator on the currents to obtain an effective equation of motion, and this averaging over the relative frequencies ω and momenta k_i will set all terms with explicit k_i -dependence to zero.⁷ Restricting to such averaged currents and absorbing a factor of g/α in Φ and a factor of $g\sqrt{L^3}$ in Ψ_\pm , we obtain effective equations of motion for the bilinears directly

$$\begin{aligned} (\partial_z + 2\mathcal{A}_\pm) J_\pm^0 &= \mp \frac{\Phi}{f} I, \\ (\partial_z + \mathcal{A}_+ + \mathcal{A}_-) I &= \frac{2\Phi}{f} (J_+^0 - J_-^0), \\ \partial_z^2 \Phi &= -\frac{1}{z^3 \sqrt{f}} (J_+^0 + J_-^0), \end{aligned} \quad (4.3.8)$$

with $I = \bar{\Psi}_- \Psi_+ + \bar{\Psi}_+ \Psi_-$, and all fields are real. The remaining constraint from the A_z equation of motion decouples. It demands $\text{Im}(\bar{\Psi}_+ \Psi_-) = \frac{i}{2}(\bar{\Psi}_- \Psi_+ - \bar{\Psi}_+ \Psi_-) = 0$. What the equations (4.3.8) tell us is that for nonzero J_\pm^0 there is a charged electrostatic source for the vector potential Φ in the bulk.

Momentarily we will motivate the effective equations (4.3.8) at a more fundamental level. Before that there are several remarks to be made

- These equations contain more information than just current conservation $\partial_\mu J^\mu = 0$. In an isotropic and static background current conservation is trivially true as $\partial_\mu J^\mu = \partial_0 J^0 = -i \int d\omega e^{-i\omega t} \omega J^0(\omega) = 0$ as $J^0(\omega \neq 0) = 0$.

⁷To see this consider

$$(\partial + 2\mathcal{A}_\pm) \Psi_\pm^\dagger(-k) \Psi_\pm(k) = \mp \frac{\Phi}{f} \left(\Psi_-^\dagger i\gamma^0 \Psi_+ + \Psi_+^\dagger i\gamma^0 \Psi_- \right) + \frac{ik_i}{\sqrt{f}} \left(\Psi_-^\dagger \gamma^i \Psi_+ - \Psi_+^\dagger \gamma^i \Psi_- \right) \quad (4.3.6)$$

The term proportional to Φ is relevant for the solution. The dynamics of the term proportional to k_i is

$$(\partial + \mathcal{A}_+ + \mathcal{A}_-) (\Psi_-^\dagger \gamma^i \Psi_+ - \Psi_+^\dagger \gamma^i \Psi_-) = -2i \frac{k^i}{\sqrt{f}} (\Psi_+^\dagger \gamma^0 \Psi_+ + \Psi_-^\dagger \gamma^0 \Psi_-). \quad (4.3.7)$$

The integral of the RHS over k^i vanishes by the assumption of translational and rotational invariance. Therefore the LHS of (5.2.14) and thus the second term in eq. (5.2.13) does so as well.

- We have scaled out the electromagnetic coupling. AdS₄/CFT₃ duals for which the underlying string theory is known generically have $g = \kappa/L$ with κ the gravitational coupling constant as defined in (4.2.3). Thus, using standard AdS₄/CFT₃ scaling, a finite charge in the new units translates to a macroscopic original charge of order $L/\kappa \propto N^{1/3}$. This large charge demands that backreaction of the fermions in terms of its bilinear is taken into account as a source for Φ .
- The equations are local. From the fundamental point of view, that one considers finite density in the bulk, this is strange to say the least. Generic multi-fermion configurations are non-local, see e.g. [96]. These equations can therefore never capture the full bulk fermion dynamics. Our starting point has been a single fermion perspective, where the Pauli blocking induced non-locality is absent. In that context local equations are fine. We have also explicitly averaged over all directions parallel to the boundary and, as we have shown in the previous section (see also footnote 7), it is this averaging that tremendously simplifies the equations. The most curious part may be that this unaveraged set of equations — and therefore also eqs (4.3.8) — are all local in the radial direction z . From the AdS perspective a many-fermion system should be non-local democratically and thus also exhibit non-locality in z , yet from the CFT perspective where z -dynamics encode RG-flow, it is eminently natural. We leave the resolution of this paradox to future work.

The justification of using (4.3.8) to construct the AdS dual of a regular Fermi liquid is the connection between local fermion bilinears and the CFT Green's function. The complicated flow equations reduce precisely to the first two equations in (4.3.8) upon performing the spacetime averaging and the trace, i.e. $J_{\pm}^0 = \int d^3k \text{Tr} \mathcal{J}_{\pm}^0$ and $I = \int d^3k \text{Tr} (G^{\parallel} + \bar{G}^{\parallel})$. Combined with the demand that we only consider normalizable solutions and the proof that \mathcal{J}_{-}^0 is proportional to the pole-strength, the radial evolution equations (4.3.8) are the (complicated) AdS recasting of the RG-flow for the pole-strength. This novel interpretation ought to dispel some of the a priori worries about our unconventional treatment of the fermions through their semi-classical bilinears. There is also support from the gravity side, however. Recall that for conventional many-body systems and fermions in particular one first populates a certain set of states and then tries to compute the macroscopic properties of the collective. In a certain sense the

equations (4.3.8) formulate the same program but in opposite order: one computes the generic wavefunction charge density with and by imposing the right boundary conditions, i.e. normalizability, one selects only the correct set of states. This follows directly from the equivalence between normalizable AdS modes and quasiparticle poles that are characterized by well defined distinct momenta k_F (for $\omega = \omega_F \equiv 0$). The demand that any non-trivial Dirac hair black hole is constructed from normalizable solutions of the composite operators (i.e. their leading and subleading asymptotes vanish⁸) thus means that one imposes a superselection rule on the spatial averaging in the definition of J_{\pm}^I :

$$\begin{aligned} J_{\pm}^0(z)|_{norm} &\equiv \int d^3k \bar{\Psi}_{\pm}(-k) i\gamma^0 \Psi_{\pm}(k)|_{norm} \\ &= \int d^3k \delta^2(|k| - |k_F|) |B_{\pm}^{(0)}(k)|^2 z^{4+2m\pm 1} + \dots \end{aligned} \quad (4.3.9)$$

We see that the constraint of normalizability from the bulk point of the view, implies that one selects precisely the on-shell bulk fermion modes as the building blocks of the density J_{\pm}^0 .

In turn this means that the true system that eqs. (4.3.8) describe is somewhat obscured by the spatial averaging. Clearly even a single fermion wavefunction is in truth the full set of two-dimensional wavefunctions whose momentum k^i has length k_F . However, the averaging could just as well be counting more, as long as there is another set of normalizable states once the isotropic momentum surface $|k| = |k_F|$ is filled. Pushing this thought to the extreme, one could even speculate that the system (4.3.8) gives the correct quantum-mechanical description of the many-body Fermi system: the system which gravitational reasoning suggests is the true groundstate of the charged AdS black hole in the presence of fermions.

To remind us of the ambiguity introduced by spatial averaging, we shall give the boundary coefficient of normalizable solution for $J_-^0 = \int d^3k \mathcal{J}_-^0$ a separate name. The quantity $\mathcal{J}_-^0(z_0)$ is proportional to the

⁸One can verify that the discussion in section 4.2.1 holds also for fully backreacted solutions. The derivation there builds on the assumption that the boundary behavior of the electrostatic potential is regular. It is straightforward to check in (4.3.8) that indeed precisely for normalizable solutions, i.e. in the absence of explicit fermion-sources, when both the leading and subleading terms in J_{\pm}^0 and I vanish, the boundary behavior the scalar potential remains regular, as required.

pole strength, which via Migdal's relation quantifies the characteristic occupation number discontinuity at $\omega_F \equiv 0$. We shall therefore call the coefficient $\int d^3k |B_-|^2|_{normalizable} = \Delta n_F$.

Thermodynamics

At a very qualitative level the identification $J^0|_{norm}(z) \equiv \Delta n_F z^{3+2m} + \dots$ can be argued to follow from thermodynamics as well. From the free energy for an AdS dual solution to a Fermi liquid, one finds that the charge density directly due to the fermions is

$$\rho_{total} = -2 \frac{\partial}{\partial \mu} F = \frac{-3}{2m+1} \frac{\Delta n_F}{z_0^{-1-2m}} + \rho + \dots, \quad (4.3.10)$$

with z_0^{-1} the UV-cut-off as before. The cut-off dependence is a consequence of the fact that the system is interacting, and one cannot truly separate out the fermions as free particles. Were one to substitute the naive free fermion scaling dimension $\Delta = m + 3/2 = 1$, the cutoff dependence would vanish and the identification would be exact.

We can thus state that in the interacting system there is a contribution to the charge density from a finite number of fermions proportional to

$$\rho_F = \frac{-3}{2\Delta - 2} \frac{\Delta n_F}{z_0^{2-2\Delta}} + \dots, \quad (4.3.11)$$

although this contribution formally vanishes in the limit where we send the UV-cut-off z_0^{-1} to infinity.

To derive eq. (5.2.16), recall that the free energy is equal to minus the on-shell action of the AdS dual theory. Since we disregard the gravitational backreaction, the Einstein term in the AdS theory will not contain any relevant information and we consider the Maxwell and Dirac term only. We write the action as,

$$S = \int_{z_0}^1 \sqrt{-g} \left[\frac{1}{2} A_N D_M F^{MN} - \bar{\Psi} \not{D} \Psi - m \bar{\Psi} \Psi \right] + \int_{z=z_0} \sqrt{-h} \left(\bar{\Psi}_+ \Psi_- + \frac{1}{2} A_\mu n_\alpha F^{\alpha\mu} \right), \quad (4.3.12)$$

where we have included an explicit fermionic boundary term that follows from the AdS/CFT dictionary [17] and n_α is a normal vector to the boundary. The boundary action is not manifestly real, but its on-shell

value which contributes to the free energy is real. Recall that the imaginary part of $\bar{\Psi}_+\Psi_-$ decouples from eqs. (4.3.8). The boundary Dirac term in (5.2.10) is therefore equal to $I = 2\text{Re}(\bar{\Psi}_+\Psi_-)$.

To write the free energy in terms of the quantities μ , ρ and Δn_F , note that the on-shell bulk Dirac action vanishes. Importantly the bulk Maxwell action does contribute to the free energy. Its contribution is

$$\begin{aligned} F_{bulk} &= \lim_{z_0 \rightarrow 0} \int_{z_0}^1 dz d^3x \left[\frac{1}{2} \Phi \partial_{zz} \Phi \right]_{on-shell} \\ &= - \lim_{z_0 \rightarrow 0} \int_{z_0}^1 dz d^3x \left[\frac{1}{2z^3 \sqrt{f}} \Phi (J_+^0 + J_-^0) \right]_{on-shell}, \end{aligned} \quad (4.3.13)$$

where we have used the equation of motion (4.3.8). This contribution should be expected, since the free energy should be dominated by infrared, i.e. near horizon physics. Due to the logarithmic singularity in the electrostatic potential (Eq. (4.3.17)) this bulk contribution diverges, but this divergence should be compensated by gravitational backreaction. At the same time the singularity is so mild, however, that the free energy, the integral of the Maxwell term, remains finite in the absence of the Einstein contribution.

Formally, i.e. in the limit $z_0 \rightarrow 0$, the full free energy arises from this bulk contribution (4.3.13). The relation (5.2.16) between the charge density and Δn_F follows only from the regularized free energy, and is therefore only a qualitative guideline. Empirically, as we will show, it is however, a very good one (see Fig 4.1 in the next section). Splitting the regularized bulk integral in two

$$\begin{aligned} F_{bulk} &= \int_{z^*}^1 dz d^3x \left[\frac{1}{2z^3 \sqrt{f}} \Phi (J_+^0 + J_-^0) \right]_{on-shell} + \\ &+ \lim_{z_0 \rightarrow 0} \int_{z_0}^{z^*} dz d^3x \left[\frac{1}{2z^3 \sqrt{f}} \Phi (J_+^0 + J_-^0) \right]_{on-shell}, \end{aligned} \quad (4.3.14)$$

we substitute the normalizable boundary behavior of $\Psi_+ = B_+ z^{5/2+m} + \dots$, $\Psi_- = B_- z^{3/2+m} + \dots$ and $\Phi = \mu - \rho z + \dots$, and obtain for the regularized free energy

$$\begin{aligned} F &= F_{horizon}(z_*) + \lim_{z_0 \rightarrow 0} \int_{z_0}^{z^*} d^3x dz \left[\frac{-1}{2z^3} \mu |B_-|^2 z^{3+2m} + \dots \right] + \\ &+ \oint \frac{d^3x}{z_0^3} \left[-\bar{B}_+ B_- z_0^{4+2m} + \frac{1}{2} \mu \rho z_0^3 \right]. \end{aligned} \quad (4.3.15)$$

Using that $B_+ = -i\mu\gamma^0 B_-/(2m+1)$ (eq. (5.2.2)), the second bulk term and boundary contribution are proportional, and the free energy schematically equals

$$F = F^{horizon} + \lim_{z_0 \rightarrow 0} \int d^3x \left[\frac{3\mu}{2(2m+1)} \bar{B}_- i\gamma^0 B_- z_0^{1+2m} - \frac{1}{2} \mu \rho \right]. \quad (4.3.16)$$

With the UV-regulator z_0^{-1} finite, this yields the charge density in Eq. (5.2.16) after one recalls that $\bar{B}_- = B_-^\dagger i\gamma^0$.

With the derived rule that the AdS dual to a Fermi liquid has a nonzero normalizable component in the current J_-^0 , we will now construct an AdS solution that has this property: an AdS black hole with Dirac hair. Ignoring backreaction, these are solutions to the density equations (4.3.8). In its simplest form the interpretation is that of the backreaction due to a single fermion wavefunction, but as explained the spatial averaging of the density combined with the selection rule of normalizability could be capturing a more general solution.

4.3.1 At the horizon: Entropy collapse to a Lifshitz solution

Before we can proceed with the construction of non-trivial Dirac hair solutions to Eqs. (4.3.8), we must consider the boundary conditions at the horizon necessary to solve the system. Insisting that the right-hand-side of the dynamical equations (4.3.8) is subleading at the horizon, the near-horizon behavior of J_\pm^0 , I , Φ is:

$$\begin{aligned} J_\pm^0 &= J_{hor,\pm} (1-z)^{-1/2} + \dots, \\ I &= I_{hor} (1-z)^{-1/2} + \dots, \\ \Phi &= \Phi_{hor}^{(1)} (1-z) \ln(1-z) + (\Phi_{hor}^{(2)} - \Phi_{hor}^{(1)}) (1-z) + \dots \end{aligned} \quad (4.3.17)$$

If we insist that Φ is regular at the horizon $z = 1$, i.e. $\Phi_{hor}^{(1)} = 0$, so that the electric field is finite, the leading term in J_\pm^0 must vanish as well, i.e. $J_{hor,\pm} = 0$, and the system reduces to a free Maxwell field in the presence of an AdS black hole and there is no fermion density profile in the bulk. Thus in order to achieve a nonzero fermion profile in the bulk, we must have an explicit source for the electric-field on the horizon. Strictly speaking, this invalidates our neglect of backreaction as the electric field and its energy density at the location of the source will be infinite. As

we argued above, this backreaction is in fact expected to resolve the finite ground-state entropy problem associated with the presence of a horizon. The backreaction should remove the horizon completely, and the background should resemble the horizonless metrics found in [50, 37, 51]; the same horizon logarithmic behavior in the electrostatic potential was noted there. Nevertheless, as the divergence in the electric field only increases logarithmically as we approach the horizon, and our results shall hinge on the properties of the equations at the opposite end near the boundary, we shall continue to ignore it here. We shall take the sensibility of our result after the fact, as proof that the logarithmic divergence at the horizon is indeed mild enough to be ignored.

The identification of the boundary value of J_-^0 with the Fermi liquid characteristic occupation number jump Δn_F rested on the insistence that the currents are built out of AdS Dirac fields. This deconstruction also determines a relation between the horizon boundary conditions of the composite fields J_\pm^0 , I . If $\Psi_\pm(z) = C_\pm(1-z)^{-1/4} + \dots$ then $J_{hor,\pm} = C_\pm^2$ and $I_{hor} = C_+C_-$. As the solution $\Phi_{hor}^{(1)}$ is independent of the solution $\Phi_{hor}^{(2)}$ which is regular at the horizon, we match the latter to the vector-potential of the charged AdS black hole: $\Phi_{hor}^{(2)} = -2gq \equiv g\mu_0/\alpha$. Recalling that $\Phi_{hor}^{(1)} = -(J_{hor,+} + J_{hor,-})$, we see that the three-parameter family of solutions at the horizon in terms of C_\pm , $\Phi_{hor}^{(2)}$ corresponds to the three-parameter space of boundary values A_+ , B_- and μ encoding a fermion-source, the fermion-response/expectation value and the chemical potential.

We can now search whether within this three-parameter family a finite normalizable fermion density solution with vanishing source $A_+ = 0$ exists for a given temperature T of the black hole.

4.3.2 A BH with Dirac hair

The equations are readily solved numerically with a shooting method from the horizon. We consider both an uncharged AdS-Schwarzschild solution and the charged AdS Reissner-Nordström solution. Studies of bosonic condensates in AdS/CFT without backreaction have mostly been done in the AdS-Schwarzschild (AdSS) background ([46, 47] and references therein). An exception is [3], which also considers the charged RN black hole. As is explained in [3], they correspond to two different limits of the exact solution: the AdSS case requires that $\Delta n_F \gtrsim \mu$ that is, the total charge

of the matter fields should be dominant compared to the charge of the black hole. On the other hand, the RN limit is appropriate if $\Delta n_F \ll \mu$. It ignores the effect of the energy density of the charged matter sector on the charged black hole geometry. The AdS Schwarzschild background is only reliable near T_c , as at low temperatures the finite charged fermion density is comparable to μ . The RN case is under better control for low temperatures, because near $T = 0$ the chemical potential can be tuned to stay larger than fermion density.

We shall therefore focus primarily on the solution in the background of an AdS RN black hole, i.e. the system with a heat bath with chemical potential μ — non-linearly determined by the value of $\Phi_{hor}^{(2)} = \mu_0$ at the horizon — which for low T/μ should show the characteristic Δn_F of a Fermi liquid. The limit in which we may confidently ignore backreaction is $\Phi_{hor}^{(1)} \ll \mu_0$ for $T \lesssim \mu_0$ — for AdSS the appropriate limit is $\Phi_{hor}^{(1)} \ll T$ for $\mu_0 \ll T$.

Finite fermion density solutions in AdS-RN

Fig. 4.1 shows the behavior of the occupation number discontinuity $n_F \equiv |B_-|^2$ and the fermion free-energy contribution I as a function of temperature in a search for normalizable solutions to Eqs (4.3.8) with the aforementioned boundary conditions. We clearly see a first order transition to a finite fermion density, as expected. The underlying Dirac field dynamics can be recognized in that the normalizable solution for $J_-^0(z)$ which has no leading component near the boundary by construction, also has its subleading component vanishing (Fig. 4.2).⁹

Analyzing the transition in more detail in Fig. 4.3, we find:

1. The dimensionless number discontinuity $\Delta n_F/\mu^{2\Delta}$ scales as $T^{-\delta}$ in a certain temperature range $T_F < T < T_c$, with $\delta > 0$ depending on g and Δ , and T_F typically very small. At $T = T_c > T_F$ it drops to zero discontinuously, characteristic of a first order phase transition.
2. At low temperatures, $0 < T < T_F$, the power-law growth comes to a halt and ends with a plateau where $\Delta n_F/\mu^{2\Delta} \sim \text{const.}$ (Fig. 4.3A).

⁹Although the Dirac hair solution has charged matter in the bulk, there is no Higgs effect for the bulk gauge field, and thus there is no direct spontaneous symmetry breaking in the boundary. Indeed one would not expect it for the Fermi liquid groundstate. There will be indirect effect on the conductivity similar to [51]. We thank Andy O'Bannon for his persistent inquiries to this point.

It is natural to interpret this temperature as the Fermi temperature of the boundary Fermi liquid.

3. The fermion free energy contribution $I/\mu^{2\Delta+1}$ scales as $T^{1/\nu}$ with $\nu > 1$ for $0 < T < T_c$, and drops to zero discontinuously at T_c . As I empirically equals minus the free energy per particle, it is natural that $I(T = 0) = 0$, and this in turn supports the identification of $\Delta n_F(T = 0)$ as the step in number density at the Fermi energy.

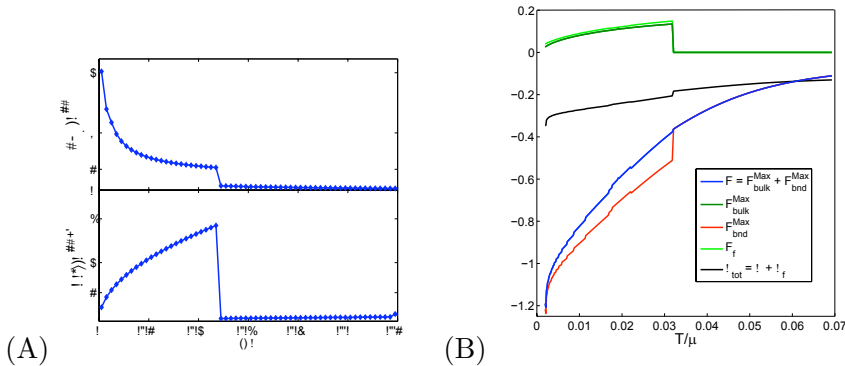


Figure 4.1: (A) Temperature dependence of the Fermi liquid occupation number discontinuity Δn_F and operator I for a fermionic field of mass $m = -1/4$ dual to an operator of dimension $\Delta = 5/4$. We see a large density for T/μ small and discontinuously drop to zero at $T \approx 0.05\mu$. At this same temperature, the proxy free energy contribution per particle (the negative of I) vanishes. (B) The free energy $F = F^{fermion} + F^{Maxwell}$ (Eq. (5.2.10)) as a function of T/μ ignoring the contribution from the gravitational sector. The blue curve shows the total free energy $F = F^{Maxwell}$, which is the sum of a bulk and a boundary term. The explicit fermion contribution $F_{fermion}$ vanishes, but the effect of a non-zero fermion density is directly encoded in a non-zero $F_{bulk}^{Maxwell}$. The figure also shows this bulk $F_{bulk}^{Maxwell}$ and the boundary contribution $F_{bulk}^{Maxwell}$ separately and how they sum to a continuous F_{total} . Although formally the explicit fermion contribution $F_f \sim I$ in equation (5.2.11) vanishes, the bulk Maxwell contribution is captured remarkably well by its value when the cut-off is kept finite. The light-green curve in the figure shows F_f for a finite $z_0 \sim 10^{-6}$. For completeness we also show the total charge density, Eq. (5.2.16). The dimension of the fermionic operator used in this figure is $\Delta = 1.1$.

One expects that the exponents δ, ν are controlled by the conformal dimension Δ .¹⁰ The dependence of the exponent δ on the conformal di-

¹⁰The charge g of the underlying conformal fermionic operator scales out of the so-

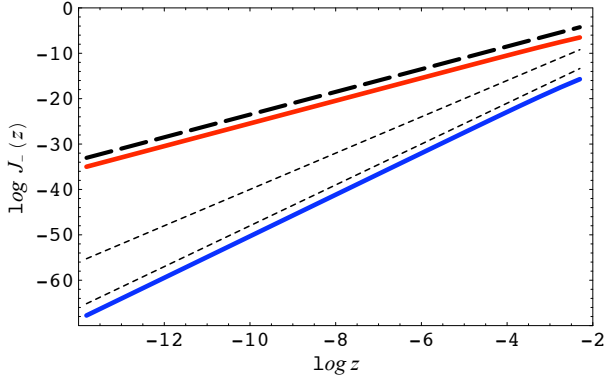


Figure 4.2: The boundary behavior of $J_-(0)$ in for a generic solution (blue) to Eqs. (4.3.8) and a normalizable Dirac-hair solution (red) for $m = -1/4$ in the background of an AdS-RN black hole with $\mu/T = 128.8$. The dotted lines show the scaling $z^{11/2}$ and z^4 of the leading and subleading terms in an expansion of $J_-^0(z)$ near $z = 0$; the dashed line shows the scaling $z^{5/2}$ of the subsubleading expansion whose coefficient is $|B_-(\omega_F, k_F)|^2$. That the Dirac hair solution (red) scales as the subsubleading solution indicates that the current J_-^0 faithfully captures the density of the underlying normalizable Dirac field.

mension is shown in Fig. 4.3A. While a correlation clearly exists, the data are not conclusive enough to determine the relation $\delta = \delta(\Delta)$. The clean power law $T^{-\delta}$ scaling regime is actually somewhat puzzling. These values of the temperature, $T_F < T < T_c$, correspond to a crossover between the true Fermi liquid regime for $T < T_F$ and the conformal phase for $T > T_c$, hence there is no clear ground for a universal scaling relation for δ , which seems to be corroborated by the data (Fig. 4.3B). At the same time, the scaling exponent ν appears to obey $\nu = 2$ with great precision (Fig. 4.3B, inset) independent of Δ and g .

A final consideration, needed to verify the existence of a finite fermion density AdS solution dual to a Fermi liquid, is to show that the ignored backreaction stays small. In particular, the divergence of the electric field at the horizon should not affect the result. The total bulk electric field $E_z = -\partial_z \Phi$ is shown in Fig. 4.4A, normalized by its value at $z = 1/2$. The logarithmic singularity at the horizon is clearly visible. At the same time, the contribution to the total electric field from the charged fermions is

lution.

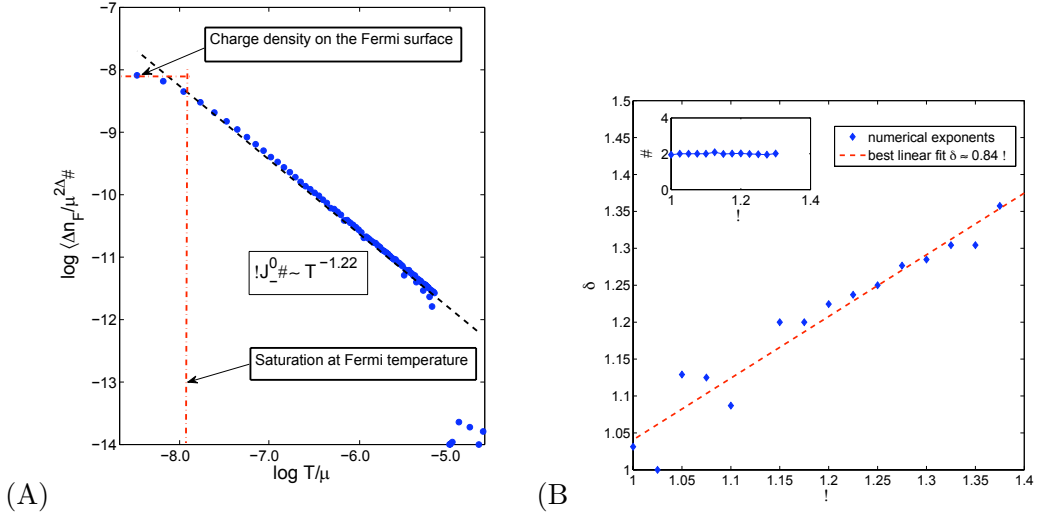


Figure 4.3: (A) Approximate power-law scaling of the Fermi liquid characteristic occupation number discontinuity $\Delta n_F/\mu^{2\Delta} \sim T^{-\delta}$ as a function of T/μ for $\Delta = 5/4$. This figure clearly shows the saturation of the density at very low T/μ . The saturation effect is naturally interpreted as the influence of the characteristic Fermi energy. (B) The scaling exponent δ for different values of the conformal dimension Δ . There is a clear correlation, but the precise relation cannot be determined numerically. The scaling exponent of the current $I/\mu^{2\Delta+1} \sim T^{-1/\nu}$ obeys $\nu = 2$ with great accuracy, on the other hand (Inset).

negligible even very close to the horizon.¹¹ This suggests that our results are robust with respect to the details of the IR divergence of the electric field.

The diverging backreaction at the horizon is in fact the gravity interpretation of the first order transition at T_c : an arbitrarily small non-zero density leads to an abrupt change in the on shell bulk action. As the latter is the free energy in the CFT, it must reflect the discontinuity of a first order transition. A full account of the singular behavior at the horizon requires self-consistent treatment including the Einstein equations. At this level, we can conclude that the divergent energy density at the horizon implies that the near-horizon physics becomes substantially different

¹¹It is of the order 10^{-4} , starting from $z = 0.9999$. We have run our numerics using values between $1 - 10^{-6}$ and $1 - 10^{-2}$ and found no detectable difference in quantities at the boundary.

from the AdS₂ limit of the RN metric. It is natural to guess that the RN horizon disappears completely, corresponding to a ground state with zero entropy, as hypothesized in [50]. This matches the expectation that the finite fermi-density solution in the bulk describes the Fermi-liquid. The underlying assumption in the above reasoning is that the total charge is conserved.

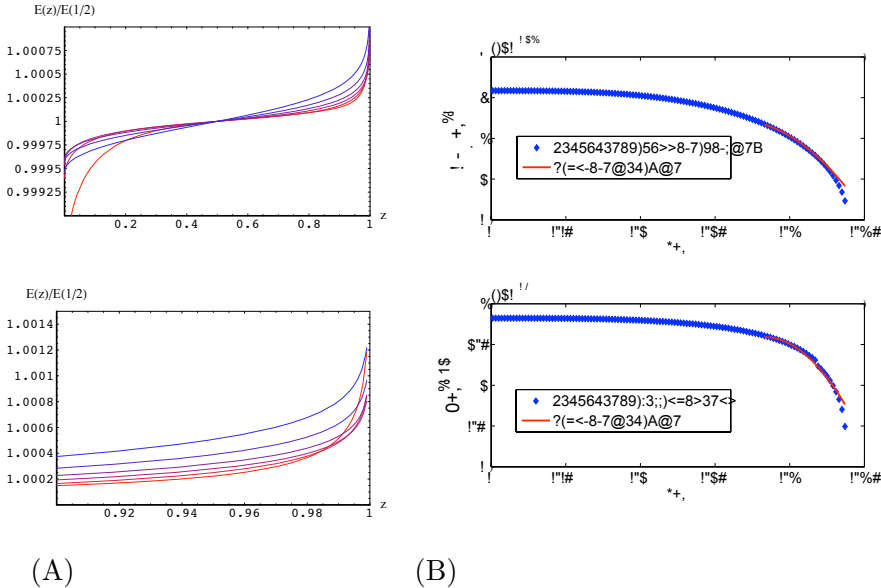


Figure 4.4: (A) The radial electric field $-E_z = \partial\Phi/\partial z$, normalized to the midpoint value $E_z(z)/E_z(1/2)$ for whole interior of the finite fermion density AdS-RN solution (upper) and near the horizon (lower). One clearly sees the soft, log-singularity at the horizon. The colors correspond to increasing temperatures from $T = 0.04\mu$ (lighter) to $T = 0.18\mu$ (darker), all with $\Delta = 1.1$. (B) The occupation number jump Δn_F and free energy contribution I as a function of temperature in AdS-Schwarzschild. We see the jump Δn_F saturate at low temperatures and fall off at high T . An exponential fit to the data (red curve) shows that in the critical region the fall-off is stronger than exponential, indicating that the transition is first order. The conformal dimension of the fermionic operator is $\Delta = 1.1$. (C) The radial electric field $-E_z = \partial\Phi/\partial z$, normalized to the midpoint value ($E_z(z)/E_z(1/2)$) for the finite fermion density AdS-Schwarzschild background. The divergence of the electric field E_z is again only noticeable near the horizon and can be neglected in most of the bulk region.

Finite fermion density in AdSS

For completeness, we will describe the finite fermion-density solutions in the AdS Schwarzschild geometry as well. In these solutions the charge density is set by the density of fermions alone. They are therefore not reliable at very low temperatures $T \ll T_c$ when gravitational backreaction becomes important. The purpose of this section is to show the existence of finite density solutions does not depend on the presence of a charged black-hole set by the horizon value $\Phi_{hor}^{(2)} = \mu_0$, but that the transition to a finite fermion density can be driven by the charged fermions themselves.

Fig. 4.4B shows the nearly instantaneous development of a non-vanishing expectation value for the occupation number discontinuity Δn_F and I in the AdS Schwarzschild background. The rise is not as sharp as in the RN background. It is, however, steeper than exponential, and we may conclude that the system undergoes a discontinuous first order transition to a AdS Dirac hair solution. The constant limit reached by the fermion density as $T \rightarrow 0$ has no meaning as we cannot trust the solution far away from T_c .

The backreaction due to the electric field divergence at the horizon can be neglected, for the same reason as before (Fig. 4.4C).

4.3.3 Confirmation from fermion spectral functions

If, as we surmised, the finite fermion density phase is the true Fermi-liquid-like ground state, the change in the fermion spectral functions should be minimal as the characteristic quasi-particle peaks are already present in the probe limit, i.e. pure AdS Reissner-Nordström [79, 17]. Fig. 4.5 shows that quasiparticle poles near $\omega = 0$ with similar analytic properties can be identified in both the probe pure AdS-RN case and the AdS-RN Dirac-hair solution. The explanation for this similarity is that the electrostatic potential Φ almost completely determines the spectrum, and the change in Φ due to the presence of a finite fermion density is quite small. Still, one expects that the finite fermion density system is a more favorable state. This indeed follows from a detailed comparison between the spectral functions $A(\omega; k)$ in the probe limit and the fermion-liquid phase (Fig. 4.5). We see that:

1. All quasiparticle poles present in the probe limit are also present in the Dirac hair phase, at a slightly shifted value of k_F . This shift is a consequence of the change in the bulk electrostatic potential Φ

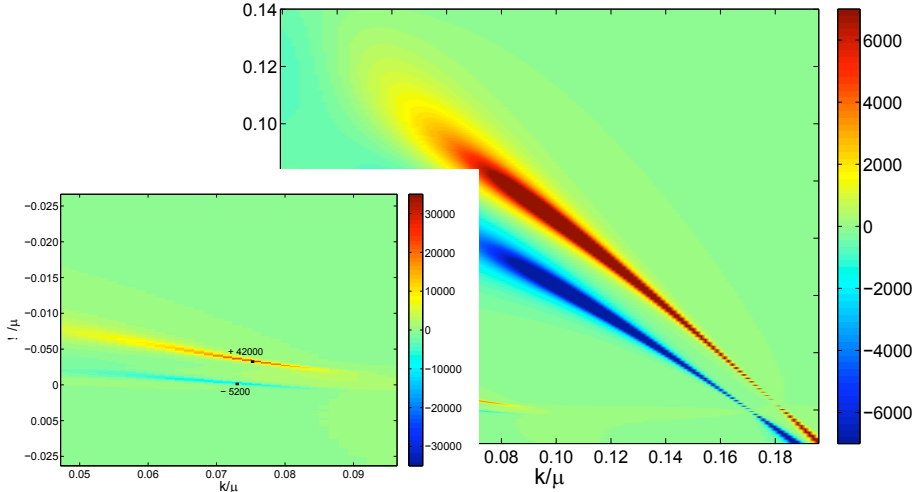


Figure 4.5: The single-fermion spectral function in the probe limit of pure AdS Reissner-Nordström (red/yellow) *minus* the spectrum in the finite density system (blue). The conformal dimension is $\Delta = 5/4$, the probe charge $g = 2$, and $\mu/T = 135$. We can see two quasiparticle poles near $\omega = 0$, a non-FL pole with $k_F^{probe} \simeq 0.11\mu$ and $k_F^{\Delta n_F} \simeq 0.08\mu$ respectively and a FL-pole with $k_F^{probe} \simeq 0.18\mu$ and $k_F^{\Delta n_F} \simeq 0.17\mu$. The dispersion of both poles is visibly similar between the probe and the finite density background. At the same time, the non-FL pole has about 8 times less weight in the finite density background, whereas the FL-pole has gained about 6.5 times more weight.

due to the presence of the charged matter. For a Fermi-liquid-like quasiparticle corresponding to the second pole in the operator with $\Delta = 5/4$ and $g = 2$ we find $k_F^{probe} - k_F^{\Delta n_F} = 0.07\mu$. The non-Fermi-liquid pole, i.e. the first pole for the same conformal operator, has $k_F^{probe} - k_F^{\Delta n_F} = 0.03\mu$.

2. The dispersion exponents ν defined through $(\omega - E_F)^2 \sim (k - k_F)^{2/\nu}$, also maintain roughly the same values as both solutions. This is visually evident in the near similar slopes of the ridges in Fig. 4.5. In the AdS Reissner-Nordström background, the dispersion coefficients are known analytically as a function of the Fermi momentum: $\nu_{k_F} = \sqrt{2\frac{k_F^2}{\mu^2} - \frac{1}{3} + \frac{1}{6}(\Delta - 3/2)^2}$ [27]. The Fermi-liquid-like quasiparticle corresponding to the second pole in the operator with $\Delta = 5/4$ and

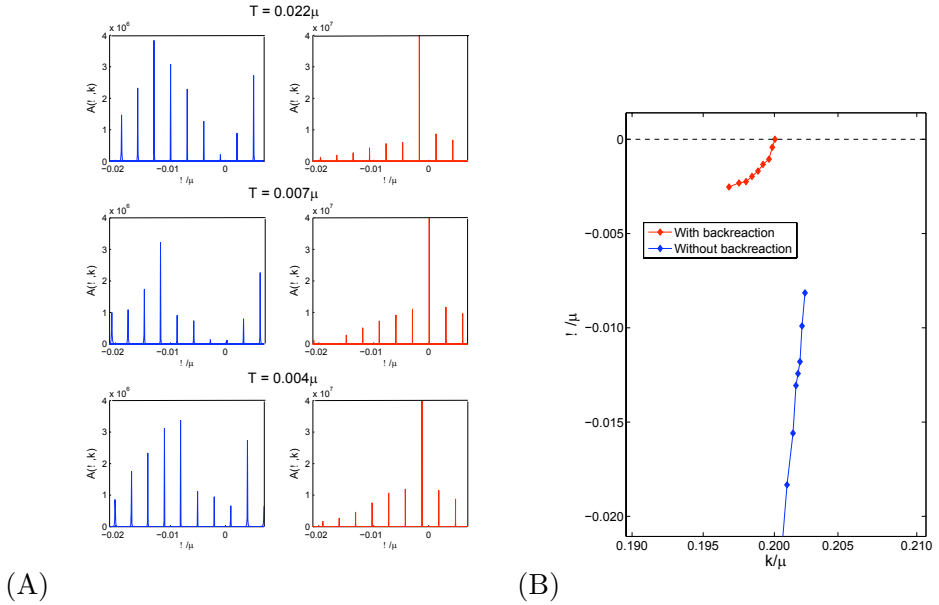


Figure 4.6: (A) Single fermion spectral functions near $\omega = 0$ in pure AdS Reissner-Nordström (blue) and in the finite fermion density background (red). In the former the position of the maximum approaches $\omega = 0$ as T is lowered whereas in the latter the position of the maximum stays close to $T = 0$ for all values of T . (B) Position of the maximum of the quasiparticle peak in k - ω plane, for different temperatures and $\Delta = 5/4$. The probe limit around a AdS-RN black hole (blue) carries a strong temperature dependence of the ω_{max} value, with $\omega_{max, T \neq 0} \neq 0$. In the finite fermion density background, the position of the maximum (red) is nearly independent of temperature and stays at $\omega = 0$.

$g = 2$ has $\nu_{k_F}^{probe} = 1.02$ vs. $\nu^{\Delta n_F} = 1.01$. The non-Fermi-liquid pole corresponding to the first pole for the same conformal operator, has $\nu_{k_F}^{probe} \approx 0.10$, and $\nu^{\Delta n_F} = 0.12$.

3. The most distinct property of the finite density phase is the redistributed spectral weight of the poles. The non-Fermi liquid pole reaches its maximum height about 10^4 , an order of magnitude less than in the probe limit, whereas the second, Fermi liquid-like pole, increases by an order of magnitude. This suggests that the finite density state corresponds to the Fermi-liquid like state, rather than a non-Fermi liquid.

4. As we mentioned in the introduction, part of the reason to suspect the existence of an AdS-RN Dirac-hair solution is that a detailed study of spectral functions in AdS-RN reveals that the quasiparticle peak is anomalously sensitive to changes in T . This anomalous temperature dependence disappears in the finite density solution. Specifically in pure AdS-RN the position ω_{max} where the peak height is maximum, denoted E_F in [17], does not agree with the value ω_{pole} , where the pole touches the real axis in the complex ω -plane, for any finite value of T , and is exponentially sensitive to changes in T (Fig 4.6). In the AdS-RN Dirac hair solution the location ω_{max} and the location ω_{pole} do become the same. Fig. 4.6B shows that the maximum of the quasiparticle peak always sits at $\omega \simeq 0$ in finite density Dirac hair solution, while it only reaches this as $T \rightarrow 0$ in the probe AdS-RN case.

4.4 Discussion and Conclusion

Empirically we know that the Fermi liquid phase of real matter systems is remarkably robust and generic. This is corroborated by analyzing effective field theory around the Fermi surface, but as it assumes the ground state it cannot explain its genericity. If the Fermi liquid ground state is so robust, this must also be a feature of the recent holographic approaches to strongly interacting fermionic systems. Our results here indicate that this is so. We have used Migdal’s relation to construct AdS/CFT rules for the holographic dual of a Fermi liquid: the characteristic occupation number discontinuity Δn_F is encoded in the normalizable subsubleading component of the spatially averaged fermion density $J_-^0(z) \equiv \int d^3k \bar{\Psi}(\omega = 0, -k, z) i\gamma^0 \Psi(\omega = 0, k, z)$ near the AdS boundary. This density has its own set of evolution equations, based on the underlying Dirac field, and insisting on normalizability automatically selects the on-shell wavefunctions of the underlying Dirac-field.

The simplest AdS solution that has a non-vanishing expectation value for the occupation number discontinuity Δn_F is that of a single fermion wavefunction. Using the density approach — which through the averaging appears to describe a class of solutions rather than one specific solution — we have constructed the limit of this solution where gravitational back-reaction is ignored. At low black hole temperatures this solution with fermionic “Dirac hair” is the preferred ground state. Through an analysis

of the free-energy, we argue that this gravitational solution with a non-zero fermion profile precisely corresponds to a system with a finite density of fermions. A spectral analysis still reveals a zoo of Fermi-surfaces in this ground state, but there are indications that in the full gravitationally backreacted solution only a Landau Fermi-liquid type Fermi surface survives. This follows in part from the relation between the spectral density and the Fermi momentum of a particular Landau liquid-like Fermi surface; it also agrees with the prediction from Luttinger's theorem. Furthermore, the spectral analysis in the finite density state shows no anomalous temperature dependence present in the pure charged black-hole single spectral functions. This also indicates that the finite density state is the true ground state.

The discovery of this state reveals a new essential component in the study of strongly coupled fermionic systems through gravitational duals, where one should take into account the expectation values of fermion bilinears. Technically the construction of the full gravitationally backreacted solution is a first point that is needed to complete our finding. A complete approach to this problem will have to take into account the many-body physics in the bulk. Within the approach presented in this paper, it means the inclusion of additional fermion wavefunctions, filling the bulk Fermi surface. The realization, however, that expectation values of fermion bilinears can be captured in holographic duals and naturally encode phase separations in strongly coupled fermion systems should find a large set of applications in the near future.

Chapter 5

From the Dirac hair to the electron star [19]

5.1 Introduction

The insight provided by the application of the AdS/CFT correspondence to finite density Fermi systems has given brand new perspectives on the theoretical robustness of non-Fermi liquids [79, 17, 27]; on an understanding of the non-perturbative stability of the regular Fermi liquid equivalent to order parameter universality for bosons [18, 20], and most importantly on the notion of fermionic criticality: Fermi systems with no scale. In essence strongly coupled conformally invariant fermi systems are one answer to the grand theoretical question of fermionic condensed matter: *Are there finite density Fermi systems that do not refer at any stage to an underlying perturbative Fermi gas?*

It is natural to ask to what extent AdS/CFT can provide a more complete answer to this question. Assuming, almost tautologically, that the underlying system is strongly coupled and there is in addition some notion of a large N limit, the Fermi system is dual to classical general relativity with a negative cosmological constant coupled to charged fermions and electromagnetism. As AdS/CFT maps quantum numbers to quantum numbers, finite density configurations of the strongly coupled large N system correspond to solutions of this Einstein-Maxwell-Dirac theory with finite charge density. Since the AdS fermions are the only object carrying charge, and the gravity system is weakly coupled, one is immediately inclined to infer that the generic solution is a weakly coupled charged Fermi

gas coupled to AdS gravity: in other words an AdS electron star [50, 51], the charged equivalent of a neutron star in asymptotically anti-de Sitter space [23, 6].

Nothing can seem more straightforward. Given the total charge density Q of interest, one constructs the free fermionic wavefunctions in this system, and fills them one by one in increasing energy until the total charge equals Q . For macroscopic values of Q these fermions themselves will backreact on the geometry. One can compute this backreaction; it changes the potential for the free fermions at subleading order. Correcting the wavefunctions at this subleading order, one converges on the true solution order by order in the gravitational strength $\kappa^2 E_{full\ system}^2$. Here $E_{full\ system}$ is the energy carried by the Fermi system and κ^2 is the gravitational coupling constant $\kappa^2 = 8\pi G_{Newton}$ in the AdS gravity system. Perturbation theory in κ is dual to the $1/N$ expansion in the associated condensed matter system.

The starting point of the backreaction computation is to follow Tolman-Oppenheimer-Volkov (TOV) and use a Thomas-Fermi (TF) approximation for the lowest order one-loop contribution [23, 50, 51, 6]. The Thomas-Fermi approximation applies when the number of constituent fermions making up the Fermi gas is infinite. For neutral fermions this equates to the statement that the energy-spacing between the levels is negligible compared to the chemical potential associated with Q , $\Delta E/\mu \rightarrow 0$. For charged fermions the Thomas-Fermi limit is more direct: it is the limit $q/Q \rightarrow 0$ where q is the charge of each constituent fermion.¹

This has been the guiding principle behind the approaches [23, 50, 6, 51, 89, 52] and the recent papers [53, 63], with the natural assumption that all corrections beyond Thomas-Fermi are small quantitative changes rather than qualitative ones. On closer inspection, however, this completely natural TF-electron star poses a number of puzzles. The most prominent perhaps arises from the AdS/CFT correspondence finding that every normalizable fermionic wavefunction in the gravitational bulk corresponds to a fermionic quasiparticle excitation in the dual condensed matter system. In particular occupying a particular wavefunction is dual to having a particular Fermi-liquid state [18]. In the Thomas Fermi limit the gravity dual thus describes an infinity of Fermi liquids, whereas the generic condensed matter expectation would have been that a been that

¹For a fermion in an harmonic oscillator potential $E_n = \hbar(n - 1/2)\omega$: thus $\Delta E/E_{total} = 1/\sum_1^N (n - 1/2) = 2/N^2$.

a single(/few) liquid(s) would be the generic groundstate away from the strongly coupled fermionic quantum critical point at zero charge density. This zoo of Fermi surfaces is already present in the grand canonical approaches at fixed μ (extremal AdS-Reissner-Nordström (AdS-RN) black holes) [27] and a natural explanation would be that this is a large N effect. This idea, that the gravity theory is dual to a condensed matter system with N species of fermions, and increasing the charge density “populates” more and more of the distinct species of Fermi liquids, is very surprising from the condensed matter perspective. Away from criticality one would expect the generic groundstate to be a single Fermi-liquid or some broken state due to pairing. To pose the puzzle sharply, once one has a fermionic quasiparticle one should be able to adiabatically continue it to a free Fermi gas, which would imply that the free limit of the strongly coupled fermionic CFT is not a single but a system of order N fermions with an ordered distribution of fermi-momenta. A possible explanation of the multitude of Fermi surfaces that is consistent with a single Fermi surface at weak coupling is that AdS/CFT describes so-called “deconfined and/or fractionalized Fermi-liquids” where the number of Fermi surfaces is directly tied to the coupling strength [54, 97, 55, 53, 63]. It would argue that fermionic quantum criticality goes hand in hand with fractionalization for which there is currently scant experimental evidence.

The second puzzle is more technical. Since quantum numbers in the gravity system equal the quantum numbers in the dual condensed matter system, one is inclined to infer that each subsequent AdS fermion wavefunction has incrementally higher energy than the previous one. Yet analyticity of the Dirac equation implies that all normalizable wavefunctions must have strictly vanishing energy [27]. It poses the question how the order in which the fermions populate the Fermi gas is determined.

The third puzzle is that in the Thomas Fermi limit the Fermi gas is gravitationally strictly confined to a bounded region: famously, the TOV-neutron star has an edge. In AdS/CFT, however, all information about the dual condensed matter system is read off at asymptotic AdS infinity. Qualitatively, one can think of AdS/CFT as an “experiment” analogous to probing a spatially confined Fermi gas with a tunneling microscope held to the exterior of the trap. Extracting the information of the dual condensed matter system is probing the AdS Dirac system confined by a gravitoelectric trap instead of a magneto-optical trap for cold atoms. Although the Thomas-Fermi limit should reliably capture the charge and

energy densities in the system, its abrupt non-analytic change at the edge (in a trapped system) and effective absence of a density far away from the center are well known to cause qualitative deficiencies in the description of the system. Specifically Friedel oscillations — quantum interference in the outside tails of the charged fermion density, controlled by the ratio q/Q and measured by a tunneling microscope — are absent. Analogously, there could be qualitative features in the AdS asymptotics of both the gravito-electric background and the Dirac wavefunctions in that adjusted background that are missed by the TF-approximation. The AdS asymptotics in turn *specify* the physics of the dual condensed matter system and since our main interest is to use AdS/CFT to understand quantum critical fermion systems where q/Q is finite, the possibility of a qualitative change inherent in the Thomas Fermi limit should be considered.

There is another candidate AdS description of the dual of a strongly coupled finite density Fermi system: the AdS black hole with Dirac hair [18, 20]. One arrives at this solution when one starts one's reasoning from the dual condensed matter system, rather than the Dirac fields in AdS gravity. Insisting that the system collapses to a generic single species Fermi-liquid ground state, the dual gravity description is that of an AdS Einstein-Dirac-Maxwell system with a single nonzero normalizable Dirac wavefunction. To have a macroscopic backreaction the charge of this single Dirac field must be macroscopic. The intuitive way to view this solution is as the other simplest approximation to free Fermi gas coupled to gravity. What we mean is that the full gravito-electric response is in all cases controlled by the total charge Q of the solution: as charge is conserved it is proportional to the constituent charge q times the number of fermions $n_{F_{AdS}}$ and the two simple limits correspond to $n_F \rightarrow \infty, q \rightarrow 0$ with $Q = qn_F$ fixed or $n_F \rightarrow 1, q \rightarrow Q$. The former is the Thomas-Fermi electron star, the latter is the AdS Dirac hair solution. In the context of AdS/CFT there is a significant difference between the two solutions in that the Dirac Hair solution clearly does not give rise to the puzzles 1, 2 and 3: there is by construction no zoo of Fermi-surfaces and therefore no ordering. Moreover since the wavefunction is demanded to be normalizable, it manifestly encodes the properties of the system at the AdS boundary. On the other hand the AdS Dirac hair solution does pose the puzzle that under normal conditions the total charge Q is much larger than the constituent charge q both from the gravity/string theory point of view and the condensed matter perspective. Generically one would

expect a Fermi gas electron star rather than Dirac hair.

In this article we shall provide evidence for this point of view that the AdS electron star and the AdS Dirac hair solution are two limits of the same underlying system. Specifically we shall show that (1) the electron star solution indeed has the constituent charge as a free parameter which is formally sent to zero to obtain the Thomas-Fermi approximation. (2) The number of normalizable wavefunctions in the electron star depend on the value of the constituent charge q . We show this by computing the electron star spectral functions. They depend in similar way on q as the first AdS/CFT Fermi system studies in an AdS-RN background. In the formal limit where $q \rightarrow Q$, only one normalizable mode remains and the spectral function wavefunction resembles the Dirac Hair solution, underlining their underlying equivalence. Since both approximations have qualitative differences as a description of the AdS dual to strongly coupled fermionic systems, it argues that an improved approximation which has characteristics of both is called for.

The results here are complimentary to and share an analysis of electron star spectral functions with the two recent articles [53] and [63] that appeared in the course of this work (see also [61] for fermion spectral functions in general Lifshitz backgrounds). Our motivation to probe the system away from the direct electron star limit differs: we have therefore been more precise in defining this limit and in the analysis of the Dirac equation in the electron star background.

5.2 Einstein-Maxwell theory coupled to charged fermions

The Lagrangian that describes both the electron star and Dirac Hair approximation is Einstein-Maxwell theory coupled to charged matter

$$S = \int d^4x \sqrt{-g} \left[\frac{1}{2\kappa^2} \left(R + \frac{6}{L^2} \right) - \frac{1}{4q^2} F^2 + \mathcal{L}_{\text{mat}}(e_\mu^A, A_\mu) \right], \quad (5.2.1)$$

where L is the AdS radius, q is the electric charge and κ is the gravitational coupling constant. It is useful to scale the electromagnetic interaction to be of the same order as the gravitational interaction and measure all lengths in terms of the AdS radius L :

$$g_{\mu\nu} \rightarrow L^2 g_{\mu\nu}, \quad A_\mu \rightarrow \frac{qL}{\kappa} A_\mu. \quad (5.2.2)$$

The system then becomes

$$S = \int d^4x \sqrt{-g} \left[\frac{L^2}{2\kappa^2} \left(R + 6 - \frac{1}{2} F^2 \right) + L^4 \mathcal{L}_{\text{mat}} \left(L e_\mu^A, \frac{qL}{\kappa} A_\mu \right) \right] \quad (5.2.3)$$

Note that in the rescaled variables the effective charge of charged matter now depends on the ratio of the electromagnetic to gravitational coupling constant: $q_{\text{eff}} = qL/\kappa$. For the case of interest, charged fermions, the Lagrangian in these variables is

$$L^4 \mathcal{L}_{\text{f}} \left(L e_\mu^A, \frac{qL}{\kappa} A_\mu \right) = -\frac{L^2}{\kappa^2} \bar{\Psi} \left[e_A^\mu \Gamma^A (\partial_\mu + \frac{1}{4} \omega_\mu^{BC} \Gamma_{BC} - i \frac{qL}{\kappa} A_\mu) - mL \right] \Psi \quad (5.2.4)$$

where $\bar{\Psi}$ is defined as $\bar{\Psi} = i\Psi^\dagger \Gamma^0$. Compared to the conventional normalization the Dirac field has been made dimensionless $\Psi = \kappa \sqrt{L} \psi_{\text{conventional}}$. With this normalization all terms in the action have a factor L^2/κ^2 and it will therefore scale out of the equations of motion

$$\begin{aligned} R_{\mu\nu} - \frac{1}{2} g_{\mu\nu} R - 3g_{\mu\nu} &= \left(F_{\mu\rho} F_\nu{}^\rho - \frac{1}{4} g_{\mu\nu} F_{\rho\sigma} F^{\rho\sigma} + T_{\mu\nu}^{\text{f}} \right), \\ D_\mu F^{\mu\nu} &= -q_{\text{eff}} J_{\text{f}}^\nu \end{aligned} \quad (5.2.5)$$

with

$$T_{\mu\nu}^{\text{f}} = \frac{1}{2} \bar{\Psi} e_{A(\mu} \Gamma^A \left[\partial_{\nu)} + \frac{1}{4} \omega_{\nu)}^{BC} \Gamma_{BC} - i \frac{qL}{\kappa} A_{\nu)} \right] \Psi - \frac{\kappa^2 L^2}{2} g_{\mu\nu} \mathcal{L}_{\text{f}} \quad (5.2.6)$$

$$J_{\text{f}}^\nu = i \bar{\Psi} e_A^\nu \Gamma^A \Psi, \quad (5.2.7)$$

where the symmetrization is defined as $B_{(\mu} C_{\nu)} = B_\mu C_\nu + B_\nu C_\mu$ and the Dirac equation

$$\left[e_A^\mu \Gamma^A (\partial_\mu + \frac{1}{4} \omega_\mu^{BC} \Gamma_{BC} - i \frac{qL}{\kappa} A_\mu) - mL \right] \Psi = 0. \quad (5.2.8)$$

The stress-tensor and current are to be evaluated in the specific state of the system. For a single excited wavefunction, obeying (5.2.8), this gives the AdS Dirac hair solution constructed in [18]. (More specifically, the Dirac hair solution consists of a radially isotropic set of wavefunctions with identical momentum size $|\vec{k}| = \sqrt{k_x^2 + k_y^2}$, such that the Pauli principle plays no role.) For multiple occupied fermion states, even without backreaction due to gravity, adding the contributions of each separate

solution to (5.2.8) rapidly becomes very involved. In such a many-body-system, the collective effect of the multiple occupied fermion states is better captured in a “fluid” approximation

$$T_{\mu\nu}^{\text{fluid}} = (\rho + p)u_\mu u_\nu + pg_{\mu\nu}, \quad N_\mu^{\text{fluid}} = nu_\mu \quad (5.2.9)$$

with

$$\rho = \langle u^\mu T_{\mu\nu} u^\nu \rangle_{\text{matter only}}, \quad n = -\langle u_\mu J^\mu \rangle_{\text{matter only}}. \quad (5.2.10)$$

In the center-of-mass rest frame of the multiple fermion system ($u_\mu = (e_{t0}, 0, 0, 0)$), the expressions for the stress-tensor and charge density are given by the one-loop equal-time expectation values (as opposed to time-ordered correlation functions)

$$\rho = \langle \bar{\Psi}(t) e_0^t \Gamma^0 (\partial_t + \frac{1}{4} \omega_t^{AB} \Gamma_{AB} - iq_{\text{eff}} A_t) \Psi(t) \rangle. \quad (5.2.11)$$

By the optical theorem the expectation value is equal to twice imaginary part of the Feynman propagator²

$$\rho = \lim_{t \rightarrow t'} 2\text{ImTr} \left[e_0^t \Gamma^0 (\partial_t + \frac{1}{4} \omega_t^{AB} \Gamma_{AB} - iq_{\text{eff}} A_t) G_F^{AdS}(t', t) \right]. \quad (5.2.12)$$

In all situations of interest, all background fields will only have dependence on the radial AdS direction; in that case the spin connection can be absorbed in the normalization of the spinor wavefunction.³ In an adiabatic approximation for the radial dependence of e_{t0} and A_t — where $\mu_{\text{loc}}(r) = q_{\text{eff}} e_0^t(r) A_t(r)$ and $\omega(r) = -ie_0^t(r) \partial_t$; — this yields the known expression for a many-body-fermion system at finite chemical potential

$$\begin{aligned} \rho(r) &= \lim_{\beta \rightarrow \infty} 2 \int \frac{d^3 k d\omega}{(2\pi)^4} [\omega(r) - \mu_{\text{loc}}(r)] \text{ImTr} i\Gamma^0 G_F^\beta(\omega, k) \\ &= \frac{1}{\pi^2} \frac{\kappa^2}{L^2} \int_{mL}^{\mu_{\text{loc}}} dE E^2 \sqrt{E^2 - (mL)^2}. \end{aligned} \quad (5.2.13)$$

²From unitarity for the S matrix $S^\dagger S = 1$ one obtains the optical theorem $T^\dagger T = 2\text{Im}T$ for the transition matrix T defined as $S \equiv 1 + iT$.

³i.e. one can redefine spinors $\chi(r) = f(r)\Psi(r)$ such that the connection term is no longer present in the equation of motion.

The normalization κ^2/L^2 follows from the unconventional normalization of the Dirac field in eq. (5.2.4).⁴ Similarly

$$n = \frac{1}{\pi^2} \frac{\kappa^2}{L^2} \int_{mL}^{\mu_{\text{loc}}} dE E \sqrt{E^2 - (mL)^2} = \frac{1}{3\pi^2} \frac{\kappa^2}{L^2} (\mu_{\text{loc}}^2 - (mL)^2)^{3/2} \quad (5.2.14)$$

The adiabatic approximation is valid for highly localized wavefunctions, i.e. the expression must be dominated by high momenta (especially in the radial direction). The exact expression on the other hand will not have a continuum of solutions to the harmonic condition $-\Gamma^0\omega + \Gamma^i k_i + \Gamma^z k_z - \Gamma^0\mu_{\text{loc}} - imL = 0$. Normalizable solutions to the AdS Dirac equations only occur at discrete momenta — one can think of the gravitational background as a potential well. The adiabatic approximation is therefore equivalent to the Thomas-Fermi approximation for a Fermi-gas in a box.

To get an estimate for the parameter range where the adiabatic approximation holds, consider the adiabatic bound $\partial_r \mu_{\text{loc}}(r) \ll \mu_{\text{loc}}(r)^2$. Using the field equation for $A_0 = \mu_{\text{loc}}/q_{\text{eff}}$:

$$\partial_r^2 \mu_{\text{loc}} \sim q_{\text{eff}}^2 n, \quad (5.2.15)$$

this bound is equivalent to requiring

$$\partial_r^2 \mu_{\text{loc}} \ll \partial_r \mu_{\text{loc}}^2 \Rightarrow \left(\frac{qL}{\kappa}\right)^2 n \ll 2\mu_{\text{loc}} \partial_r \mu_{\text{loc}} \Rightarrow \left(\frac{qL}{\kappa}\right)^2 n \ll \mu_{\text{loc}}^3 \quad (5.2.16)$$

where in the last line we used the original bound again. If the chemical potential scale is considerably higher than the mass of the fermion, we may use (5.2.14) to approximate $n \sim \frac{\kappa^2}{L^2} \mu_{\text{loc}}^3$. Thus the adiabatic bound is equivalent to,

$$q = \frac{q_{\text{eff}} \kappa}{L} \ll 1 \quad (5.2.17)$$

the statement that the constituent charge of the fermions is infinitesimal. Note that in the rescaled action (6.3.43, 5.2.4), L/κ plays the role of $1/\hbar$,

⁴One can see this readily by converting the dimensionless definition of ρ , eq (5.2.11), to the standard dimension. Using capitals for dimensionless quantities and lower-case for dimensionful ones

$$\rho \sim \langle \Psi \partial_T \Psi \rangle \sim \kappa^2 L^2 \langle \psi \partial_t \psi \rangle \sim \kappa^2 L^2 \int_m^\mu d\epsilon \epsilon^2 \sqrt{\epsilon^2 - m^2} \sim \frac{\kappa^2}{L^2} \int_{mL}^{\mu L} dE E^2 \sqrt{E^2 - (mL)^2}$$

with $\mu L = \mu_{\text{loc}}$ above.

and eq. (5.2.17) is thus equivalent to the semiclassical limit $\hbar \rightarrow 0$ with q_{eff} fixed. Since AdS/CFT relates $L/\kappa \sim N_c$ this acquires the meaning in the context of holography that there is a large N_c scaling limit [53, 63] of the CFT with fermionic operators where the RG-flow is “adiabatic”. Returning to the gravitational description the additional assumption that the chemical potential is much larger than the mass is equivalent to

$$\begin{aligned} \frac{Q_{\text{phys}}^{\text{total}}}{V_{\text{spatial AdS}}} &= \frac{LQ_{\text{eff}}^{\text{total}}}{\kappa V_{\text{spatial AdS}}} \equiv \frac{L}{\kappa V_{\text{spatial AdS}}} \int dr \sqrt{-g_{\text{induced}}} (q_{\text{eff}} n) \quad (5.2.18) \\ &\simeq \frac{1}{V_{\text{spatial AdS}}} \int dr \sqrt{-g} \frac{q_{\text{eff}} \kappa}{L} \mu_{\text{loc}}^3(r) \gg q(mL)^3. \end{aligned}$$

This implies that the total charge density in AdS is much larger than that of a single charged particle (as long as $mL \sim 1$). The adiabatic limit is therefore equivalent to a thermodynamic limit where the Fermi gas consists of an infinite number of constituents, $n \rightarrow \infty$, $q \rightarrow 0$ such that the total charge $Q \sim nq$ remains finite.

The adiabatic limit of a many-body fermion system coupled to gravity are the Tolman-Oppenheimer-Volkov equations. Solving this in asymptotically AdS gives us the charged neutron or electron star constructed in [51]. Knowing the quantitative form of the adiabatic limit, it is now easy to distinguish the electron star solution from the “single wavefunction” Dirac Hair solution. The latter is trivially the single particle limit $n \rightarrow 1$, $q \rightarrow Q$ with the total charge Q finite. The electron star and Dirac Hair black hole are opposing limit-solutions of the same system. We shall now make this connection more visible by identifying a formal dialing parameter that interpolates between the two solutions.

To do so we shall need the full adiabatic Tolman-Oppenheimer-Volkov equations for the AdS electron star [51]. Since the fluid is homogeneous and isotropic, the background metric and electrostatic potential will respect these symmetries and will be of the form (recall that we are already using “dimensionless” lengths, eq. (5.2.2))

$$ds^2 = -f(r)dt^2 + g(r)dr^2 + r^2(dx^2 + dy^2), \quad A = h(r)dt, \quad (5.2.19)$$

where $f(r), g(r), h(r)$ are functions of r ; the horizon is located at $r = 0$ and the boundary is at $r = \infty$. Combining this ansatz with a rescaling

$mL = q_{\text{eff}}\hat{m}$ the bosonic background equations of motion become [51]

$$\begin{aligned} \frac{1}{r}\left(\frac{f'}{f} + \frac{g'}{g}\right) - \frac{gh\sigma}{\sqrt{f}} &= 0, & \rho &= \frac{q_{\text{eff}}^4\kappa^2}{\pi^2L^2} \int_{\hat{m}}^{\frac{h}{\sqrt{f}}} d\epsilon\epsilon^2\sqrt{\epsilon^2 - \hat{m}^2}, \\ \frac{f'}{rf} + \frac{h'^2}{2f} - g(3+p) + \frac{1}{r^2} &= 0, & \sigma &= \frac{q_{\text{eff}}^4\kappa^2}{\pi^2L^2} \int_{\hat{m}}^{\frac{h}{\sqrt{f}}} d\epsilon\epsilon\sqrt{\epsilon^2 - \hat{m}^2}, \\ h'' + \frac{2}{r}h' - \frac{g\sigma}{\sqrt{f}}\left(\frac{rhh'}{2} + f\right) &= 0, & -p &= \rho - \frac{h}{\sqrt{f}}\sigma, \end{aligned} \quad (5.2.20)$$

where we have used that $\mu_{\text{loc}} = q_{\text{eff}}h/\sqrt{f}$ and $\sigma = nq_{\text{eff}}$ is the rescaled local charge density. What one immediately notes is that the Tolman-Oppenheimer-Volkov equations of motion for the background only depend on the parameters $\hat{\beta} \equiv \frac{q_{\text{eff}}^4\kappa^2}{\pi^2L^2}$ and \hat{m} , whereas the original Lagrangian and the fermion equation of motion also depend on $q_{\text{eff}} = \left(\frac{\pi^2L^2\hat{\beta}}{\kappa^2}\right)^{1/4}$. It is therefore natural to guess that the parameter $q_{\text{eff}} = qL/\kappa$ will be the interpolating parameter away from the adiabatic electron star limit towards the Dirac Hair BH.

Indeed in these natural electron star variables the adiabatic bound (5.2.17) translates into

$$\hat{\beta} \ll \frac{L^2}{\kappa^2} = \frac{q_{\text{eff}}^2}{q^2}. \quad (5.2.21)$$

Thus we see that for a given electron star background with $\hat{\beta}$ fixed decreasing κ/L improves the adiabatic fluid approximation whereas increasing κ/L makes the adiabatic approximation poorer and poorer. “Dialing κ/L up/down” therefore *interpolates* between the electron star and the Dirac Hair BH. Counterintuively improving adiabaticity by decreasing κ/L corresponds to increasing q_{eff} for fixed q , but this is just a consequence of recasting the system in natural electron star variables. A better way to view improving adiabaticity is to decrease the microscopic charge q but while keeping q_{eff} fixed; this shows that a better way to think of q_{eff} is as the total charge rather than the effective constituent charge.

The parameter $\kappa/L = q/q_{\text{eff}}$ parametrizes the gravitational coupling strength in units of the AdS curvature, and one might worry that “dialing κ/L up” pushes one outside the regime of classical gravity. This is not the case. One can easily have $\hat{\beta} \gg 1$ and tune κ/L towards or away from the adiabatic limit within the regime of classical gravity. From eq. (5.2.17) we

see that the edge of validity of the adiabatic regime $\hat{\beta} \simeq L^2/\kappa^2$ is simply equivalent to a microscopic charge $q = 1$ which clearly has a classical gravity description. It is not hard to see that the statement above is the equivalent of changing the level splitting in the Fermi gas, while keeping the overall energy/charge fixed. In a Fermi gas microscopically both the overall energy and the level splitting depends on \hbar . Naively increasing \hbar increases both, but one can move away from the adiabatic limit either by decreasing the overall charge density, keeping \hbar fixed or by keeping the charge density fixed and raising \hbar . Using again the analogy between κ/L and \hbar , the electron star situation is qualitatively the same where one should think of $\hat{\beta} \sim q^4 L^2/\kappa^2$ parametrizing the microscopic charge. One can either insist on keeping κ/L fixed and *increase* the microscopic charge $\hat{\beta}$ to increase the level splitting or one can keep $\hat{\beta}$ fixed and increase κ/L . In the electron star, however, the background geometry changes with $\hat{\beta}$ in addition to the level splitting, and it is therefore more straightforward to keep $\hat{\beta}$ and the geometry fixed, while dialing κ/L .

We will now give evidence for our claim that the electron star and Dirac Hair solution are two opposing limits. To do so, we need to identify an observable that goes either beyond the adiabatic background approximation or beyond the single particle approximation. Since the generic intermediate state is still a many-body fermion system, the more natural starting point is the electron star background and perturb away from there. Realizing then that the fermion equation of motion already depends directly on the dialing parameter q_{eff} the obvious observables are the single fermion spectral functions in the electron star background. Since one must specify a value for q_{eff} to compute these, they directly probe the microscopic charge of the fermion and are thus always beyond the strict electron star limit $q \rightarrow 0$. In the next two sections we will compute these and show that they indeed reflect the interpretation of q_{eff} as the interpolating parameter between the electron star and Dirac Hair BH.

5.3 Fermion spectral functions in the electron star background

To compute the fermion spectral functions in the electron star background we shall choose a specific representative of the family of electron stars parametrized by $\hat{\beta}$ and \hat{m} . Rather than using $\hat{\beta}$ and \hat{m} the metric of an electron star is more conveniently characterized by its Lifshitz-scaling

behavior near the interior horizon $r \rightarrow 0$. From the field equations (5.2.20) the limiting interior behavior of $f(r), g(r), h(r)$ is

$$f(r) = r^{2z} + \dots, \quad g(r) = \frac{g_\infty}{r^2} + \dots, \quad h(r) = h_\infty r^z + \dots \quad (5.3.22)$$

The scaling behavior is determined by the dynamical critical exponent z , which is a function of $\hat{\beta}$, \hat{m} [51] and it is conventionally used to classify the metric instead of $\hat{\beta}$. The full electron star metric is then generated from this horizon scaling behavior by integrating up an irrelevant RG-flow [39, 37]

$$\begin{aligned} f &= r^{2z} \left(1 + f_1 r^{-\alpha} + \dots \right) \\ g &= \frac{g_\infty}{r^2} \left(1 + g_1 r^{-\alpha} + \dots \right) \\ h &= h_\infty r^z \left(1 + h_1 r^{-\alpha} + \dots \right). \end{aligned} \quad (5.3.23)$$

with

$$\alpha = \frac{2+z}{2} - \frac{\sqrt{9z^3 - 21z^2 + 40z - 28 - \hat{m}^2 z(4-3z)^2}}{2\sqrt{(1-\hat{m}^2)z-1}}. \quad (5.3.24)$$

Scaling $f_1 \rightarrow b f_1$ is equal to a coordinate transformation $r \rightarrow b^{1/\alpha} r$ and $t \rightarrow b^{z/\alpha} t$, and the sign of f_1 is fixed to be negative in order to be able to match onto an asymptotically AdS₄ solution. Thus $f_1 = -1$ and g_1 and h_1 are then uniquely determined by the equations of motion.

Famously, integrating the equations of motion up the RG-flow outwards towards the boundary fails at a finite distance r_s . This is the edge of the electron star. Beyond the edge of the electron star, there is no fluid present and the spacetime is that of an AdS₄-RN black hole with the metric

$$f = c^2 r^2 - \frac{\hat{M}}{r} + \frac{\hat{Q}^2}{2r^2}, \quad g = \frac{c^2}{f}, \quad h = \hat{\mu} - \frac{\hat{Q}}{r}. \quad (5.3.25)$$

Demanding the full metric is smooth at the radius of electron star r_s determines the constants c , \hat{M} and \hat{Q} . The dual field theory is defined on the plane $ds^2 = -c^2 dt^2 + dx^2 + dy^2$.

The specific electron star background we shall choose without loss of generality is the one with $z = 2$, $\hat{m} = 0.36$ (Fig. 5.1)⁵, smoothly matched at $r_s \simeq 4.25252$ onto a AdS-RN black-hole.

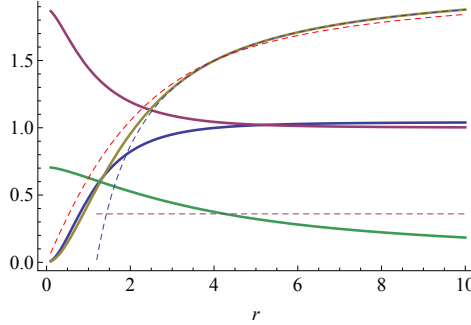


Figure 5.1: Electron star metric for $z = 2$, $\hat{m} = 0.36$, $c \simeq 1.021$, $\hat{M} \simeq 3.601$, $\hat{Q} \simeq 2.534$, $\hat{\mu} \simeq 2.132$ compared to pure AdS. Shown are $f(r)/r^2$ (Blue), $r^2g(r)$ (Red) and $h(r)$ (Orange). The asymptotic AdS-RN value of $h(r)$ is the dashed blue line. For future use we have also given $\mu_{1oc} = h/\sqrt{f}$ (Green) and $\mu_{qeff} = \sqrt{g^{ii}}h/\sqrt{f}$ (Red Dashed) At the edge of the star $r_s \simeq 4.253$ (the intersection of the purple dashed line setting the value of m_{eff} with μ_{1oc}) one sees the convergence to pure AdS in the constant asymptotes of $f(r)/r^2$ and $r^2g(r)$.

The CFT fermion spectral functions now follow from solving the Dirac equation in this background [79, 17]

$$\left[e_A^\mu \Gamma^A \left(\partial_\mu + \frac{1}{4} \omega_{\mu AB} \Gamma^{AB} - i q_{eff} A_\mu \right) - m_{eff} \right] \Psi = 0 \quad (5.3.26)$$

where q_{eff} and m_{eff} in terms of the parameters of the electron star equal

$$q_{eff} = \left(\frac{\pi^2 L^2 \hat{\beta}}{\kappa^2} \right)^{1/4}, \quad m_{eff} = q_{eff} \hat{m} = \hat{m} \left(\frac{\pi^2 L^2 \hat{\beta}}{\kappa^2} \right)^{1/4} \quad (5.3.27)$$

For a given electron star background, i.e. a fixed $\hat{\beta}$, \hat{m} the fermion spectral function will therefore depend on the ratio L/κ . For $L/\kappa \gg \hat{\beta}^{1/2}$ the poles in these spectral functions characterize the occupied states in a many-body gravitational Fermi system that is well approximated by the electron star.

⁵This background has $c \simeq 1.021$, $\hat{M} \simeq 3.601$, $\hat{Q} \simeq 2.534$, $\hat{\mu} \simeq 2.132$, $\hat{\beta} \simeq 19.951$, $g_\infty \simeq 1.887$, $h_\infty = 1/\sqrt{2}$, $\alpha \simeq -1.626$, $f_1 = -1$, $g_1 \simeq -0.4457$, $h_1 \simeq -0.6445$.

As L/κ is lowered for fixed $\hat{\beta}$ the electron star background becomes a poorer and poorer approximation to the true state and we should see this reflected in both the number of poles in the spectral function and their location.

Projecting the Dirac equation onto two-component Γ^z eigenspinors

$$\Psi_{\pm} = (-gg^{rr})^{-\frac{1}{4}} e^{-i\omega t + ik_x x^i} \begin{pmatrix} y_{\pm} \\ z_{\pm} \end{pmatrix} \quad (5.3.28)$$

and using isotropy to set $k_y = 0$, one can choose a basis of Dirac matrices where one obtains two decoupled sets of two simple coupled equations [79]

$$\sqrt{g_{ii}g^{rr}}(\partial_r \mp m_{\text{eff}}\sqrt{g_{rr}})y_{\pm} = \mp i(k_x - u)z_{\mp}, \quad (5.3.29)$$

$$\sqrt{g_{ii}g^{rr}}(\partial_r \pm m_{\text{eff}}\sqrt{g_{rr}})z_{\mp} = \pm i(k_x + u)y_{\pm} \quad (5.3.30)$$

where $u = \sqrt{\frac{g_{ii}}{-g_{tt}}}(\omega + q_{\text{eff}}h)$. In this basis of Dirac matrices the CFT Green's function $G = \langle \bar{\mathcal{O}}_{\psi_+} i\gamma^0 \mathcal{O}_{\psi_+} \rangle$ equals

$$G = \lim_{\epsilon \rightarrow 0} \epsilon^{-2mL} \begin{pmatrix} \xi_+ & 0 \\ 0 & \xi_- \end{pmatrix} \Big|_{r=\frac{1}{\epsilon}}, \quad \text{where } \xi_+ = \frac{iy_-}{z_+}, \quad \xi_- = -\frac{iz_-}{y_+} \quad (5.3.31)$$

Rather than solving the coupled equations (5.3.29) it is convenient to solve for ξ_{\pm} directly [79],

$$\sqrt{\frac{g_{ii}}{g_{rr}}}\partial_r \xi_{\pm} = -2m_{\text{eff}}\sqrt{g_{ii}}\xi_{\pm} \mp (k_x \mp u) \pm (k_x \pm u)\xi_{\pm}^2. \quad (5.3.32)$$

For the spectral function $A = \text{ImTr}G_R$ we are interested in the retarded Green function. This is obtained by imposing in-falling boundary conditions near the horizon $r = 0$. Since the electron star is a “zero-temperature” solution this requires a more careful analysis than for a generic horizon. To ensure that the numerical integration we shall perform to obtain the full spectral function has the right infalling boundary conditions, we first solve eq. (5.3.32) to first subleading order around $r = 0$. There are two distinct branches. When $\omega \neq 0$ and $k_x r/\omega, r^2/\omega$ is small, the in-falling boundary condition near the horizon $r = 0$ is (for $z = 2$)

$$\begin{aligned} \xi_+(r) &= i - i\frac{k_x r}{\omega} + i\frac{(k_x^2 - 2im_{\text{eff}}\omega)r^2}{2\omega^2} - i\frac{f_1 k_x r^{1-\alpha}}{2\omega} + \dots \\ \xi_-(r) &= i + i\frac{k_x r}{\omega} + i\frac{(k_x^2 - 2im_{\text{eff}}\omega)r^2}{2\omega^2} + i\frac{f_1 k_x r^{1-\alpha}}{2\omega} + \dots \end{aligned} \quad (5.3.33)$$

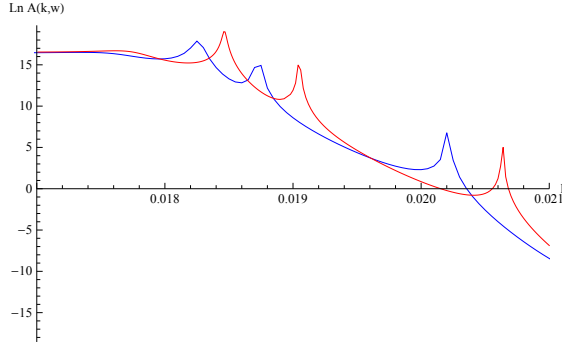


Figure 5.2: Electron star MDF spectral functions with multiple peaks as a function of k for $\omega = 10^{-5}$, $z = 2$, $\hat{m} = 0.36$. The blue curve is for $\kappa = 0.091$; the red curve is for $\kappa = 0.090$. Note that the vertical axis is logarithmic. Visible is the rapidly decreasing spectral weight and increasingly narrower width for each successive peak as k_F increases.

When $\omega = 0$, i.e. $k_x r / \omega$ is large, and $r / k_x \rightarrow 0$,

$$\begin{aligned}\xi_+(r) &= -1 + \frac{(q_{\text{eff}} h_\infty + m_{\text{eff}})r}{k_x} + \left(\frac{\omega}{k_x r} - \frac{\omega}{2\sqrt{g_\infty} k_x^2} \right) + \dots \\ \xi_-(r) &= 1 + \frac{(q_{\text{eff}} h_\infty - m_{\text{eff}})r}{k_x} + \left(\frac{\omega}{k_x r} - \frac{\omega}{2\sqrt{g_\infty} k_x^2} \right) + \dots\end{aligned}\quad (5.3.34)$$

the boundary conditions (5.3.34) become real. As (5.3.32) are real equations, the spectral function vanishes in this case. This is essentially the statement that all poles in the Green’s function occur at $\omega = 0$ [27]. Note that the fact that the electron star $\omega = 0$ boundary conditions (5.3.32) are real for all values of k is qualitatively different from the AdS-RN $\omega = 0$ boundary conditions (eq. (26) in [79]). In the AdS-RN “quantum-critical” infrared governed by the near horizon $\text{AdS}_2 \times \mathbb{R}_2$ geometry, in general there is a special scale k_o below which the boundary condition turns complex. This scale k_o is related to the surprising existence of an oscillatory region in the spectral function. One therefore infers that in a scaleful Lifshitz infrared this oscillatory region is no longer present [63]. We will confirm this in section 5.4.

5.3.1 Numerical results and discussion

We can now solve for the spectral functions numerically. In Fig. 5.3 we plot the momentum-distribution-function (MDF) (the spectral function as

a function of k) for fixed $\omega = 10^{-5}$, $z = 2$, $\hat{m} = 0.36$ while changing the value of κ . Before we comment on the dependence on $q_{\text{eff}} \sim \kappa^{-1/2}$ which studies the deviation away from the adiabatic limit of a given electron star background (i.e. fixed dimensionless charge and fixed dimensionless energy density), there are several striking features that are immediately apparent:

- As expected, there is a multitude of Fermi surfaces. They have very narrow width and their spectral weight decreases rapidly for each higher Fermi-momentum k_F (Fig. 5.2). This agrees with the exponential width $\Gamma \sim \exp(-(\frac{k^z}{\omega})^{1/(z-1)})$ predicted by [26] for gravitational backgrounds that are Lifshitz in the deep interior, which is the case for the electron star. This prediction is confirmed in [61, 53, 63] and the latter two articles also show that the weight decreases in a corresponding exponential fashion. This exponential reduction of both the width and the weight as k_F increases explains why we only see a finite number of peaks, though we expect a very large number. In the next section we will be able to count the number of peaks, even though we cannot resolve them all numerically.
- The generic value of k_F of the peaks with visible spectral weight is *much* smaller than the effective chemical potential μ in the boundary field theory. This is quite different from the RN-AdS case where the Fermi momentum and chemical potential are of the same order. A numerical study cannot answer this, but the recent article [63] explains this.⁶
- Consistent with the boundary value analysis, there is no evidence of an oscillatory region.

The most relevant property of the spectral functions for our question is that as κ is increased the peak location k_F decreases orderly and peaks *disappear* at various threshold values of k . This is the support for our argument that changing κ changes the number of microscopic constituents in the electron star. Comparing the the behavior of the various Fermi momenta k_F in the electron star with the results in the extremal AdS-RN black-hole, they are qualitatively identical when one equates $\kappa^{-1/2} \sim q_{\text{eff}}$ with the charge of the probe fermion. We may therefore infer from our

⁶In view of the verification of the Luttinger count for electron star spectra in [53, 63], this had to be so.

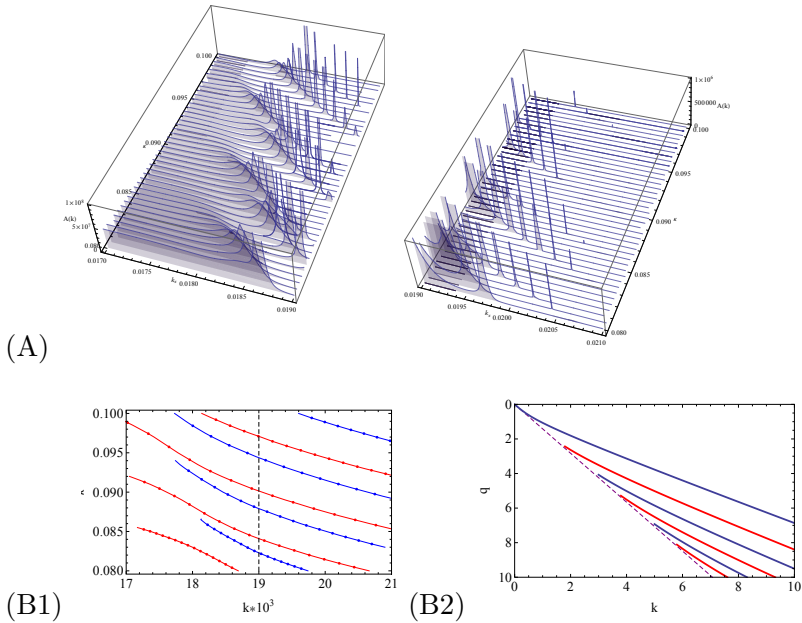


Figure 5.3: (A) Electron-star MDF spectral functions as a function of κ for $z = 2, \hat{m} = 0.36, \omega = 10^{-5}$. Because the peak height and weights decrease exponentially, we present the adjacent ranges $k \in [0.017, 0.019]$ and $k \in [0.019, 0.021]$ in two different plots with different vertical scale. (B1/B2) Locations of peaks of spectral functions as a function of κ : comparison between the electron star (B1) for $z = 2, \hat{m} = 0.36, \omega = 10^{-5}$ (the dashed gray line denotes the artificial separation in the 3D representations in (A)) and AdS-RN (B2) for $m = 0$ as a function of q in units where $\mu = \sqrt{3}$. These two Fermi-surface ‘spectra’ are qualitatively similar.

detailed understanding of the behavior of k_F for AdS-RN that also for the electron star as k_F is lowered peaks truly disappear from the spectrum until by extrapolation ultimately one remains: this is the AdS Dirac hair solution [18].

We can only make this inference qualitatively as the rapid decrease in spectral weight of each successive peak prevents an exact counting of Fermi surfaces in the numerical results for the electron star spectral functions. One aspect that we can already see is that as κ decreases all present peaks shift to higher k , while new peaks emerging from the left for smaller kappa. This suggests a fermionic version of the UV/IR correspondence where the

peak with *lowest* k_F corresponds to the last occupied level, i.e. highest “energy” in the AdS electron star. We will now address both of these points in more detail.

5.4 Fermi surface ordering: k_F from a Schrödinger formulation

Our analysis of the behavior of boundary spectral functions as a function of κ relies on the numerically quite evident peaks. Stricly speaking, however, we have not shown that there is a true singularity in the Green’s function at $\omega = 0, k = k_F$. We will do so by showing that the AdS Dirac equation, when recast as a Schrödinger problem has quasi-normalizable solutions at $\omega = 0$ for various k . As is well known, in AdS/CFT each such solution corresponds to a true pole in the boundary Green’s function. Using a WKB approximation for this Schrödinger problem we will in addition be able to estimate the number of poles for a fixed κ and thereby provide a quantitative value for the deviation from the adiabatic background.

We wish to emphasize that the analysis here is general and captures the behavior of spectral functions in all spherically symmetric and static backgrounds backgrounds alike, whether AdS-RN, Dirac hair or electron star.

The $\omega = 0$ Dirac equation (5.3.26) for one set of components (5.3.29, 5.3.30) with the replacement $iy_- \rightarrow y_-$, equals

$$\begin{aligned} \sqrt{g_{ii}g^{rr}}\partial_r y_- + m_{\text{eff}}\sqrt{g_{ii}}y_- &= -(k - \hat{\mu}_{q_{\text{eff}}})z_+, \\ \sqrt{g_{ii}g^{rr}}\partial_r z_+ - m_{\text{eff}}\sqrt{g_{ii}}z_+ &= -(k + \hat{\mu}_{q_{\text{eff}}})y_-, \end{aligned} \quad (5.4.35)$$

where $\hat{\mu}_{q_{\text{eff}}} = \sqrt{\frac{g_{ii}}{-g_{tt}}}q_{\text{eff}}A_t$ and we will drop the subscript x on k_x . In our conventions z_+ (and y_+) is the fundamental component dual to the source of the fermionic operator in the CFT [79, 17]. Rewriting the coupled first order Dirac equations as a single second order equation for z_+ :

$$\partial_r^2 z_+ + \mathcal{P}\partial_r z_+ + \mathcal{Q}z_+ = 0 \quad (5.4.36)$$

where the coefficients are

$$\begin{aligned} \mathcal{P} &= \frac{\partial_r(g_{ii}g^{rr})}{2g_{ii}g^{rr}} - \frac{\partial_r\hat{\mu}_{q_{\text{eff}}}}{k + \hat{\mu}_{q_{\text{eff}}}}, \\ \mathcal{Q} &= -\frac{m_{\text{eff}}\partial_r\sqrt{g_{ii}}}{\sqrt{g_{ii}g^{rr}}} + \frac{m_{\text{eff}}\sqrt{g_{rr}}\partial_r\hat{\mu}_{q_{\text{eff}}}}{k + \hat{\mu}_{q_{\text{eff}}}} - m_{\text{eff}}^2 g_{rr} - \frac{k^2 - \hat{\mu}_{q_{\text{eff}}}^2}{g_{ii}g^{rr}}. \end{aligned} \quad (5.4.37)$$

the first thing one notes is that both \mathcal{P} and \mathcal{Q} diverge at some $r = r_*$ where $\hat{\mu}_{q_{\text{eff}}} + k = 0$. Since $\hat{\mu}_{q_{\text{eff}}}$ is (chosen to be) a positive semidefinite function which increases from $\hat{\mu}_{q_{\text{eff}}} = 0$ at the horizon, this implies that for negative k (with $-k < \hat{\mu}_{q_{\text{eff}}}|_{\infty}$) the wavefunction is qualitatively different from the wavefunction with positive k which experiences no singularity. The analysis is straightforward if we transform the first derivative away and recast it in the form of a Schrödinger equation by redefining the radial coordinate:

$$\frac{ds}{dr} = \exp\left(-\int^r dr' \mathcal{P}\right) \quad \Rightarrow \quad s = c_0 \int_{r_\infty}^r dr' \frac{|k + \hat{\mu}_{q_{\text{eff}}}|}{\sqrt{g_{ii}g^{rr}}} \quad (5.4.38)$$

where c_0 is an integration constant whose natural scale is of order $c_0 \sim q_{\text{eff}}^{-1}$. This is a simpler version of the generalized k -dependent tortoise coordinate introduced in [27]. In the new coordinates the equation (5.4.37) is of the standard form:

$$\partial_s^2 z_+ - V(s)z_+ = 0 \quad (5.4.39)$$

with potential

$$V(s) = -\frac{g_{ii}g^{rr}}{c_0^2 |k + \hat{\mu}_{q_{\text{eff}}}|^2} \mathcal{Q}. \quad (5.4.40)$$

The above potential (5.4.40) can also be written as

$$V(s) = \frac{1}{c_0^2 (k + \hat{\mu}_{q_{\text{eff}}})^2} \left[(k^2 + m_{\text{eff}}^2 g_{ii} - \hat{\mu}_{q_{\text{eff}}}^2) + m_{\text{eff}} g_{ii} \sqrt{g^{rr}} \partial_r \ln \frac{\sqrt{g_{ii}}}{k + \hat{\mu}_{q_{\text{eff}}}} \right]. \quad (5.4.41)$$

We note again the potential singularity for negative k , but before we discuss this we first need the boundary conditions. The universal boundary behavior is at spatial infinity and follows from the asymptotic AdS geometry. In the adapted coordinates $r \rightarrow \infty$ corresponds to $s \rightarrow 0$ as follows from $ds/dr \simeq c_0(k + \hat{\mu}_{q_{\text{eff}}}|_{\infty})/r^2$. The potential therefore equals

$$V(s) \simeq \frac{1}{s^2} (m_{\text{eff}} + m_{\text{eff}}^2) + \dots \quad (5.4.42)$$

and the asymptotic behavior of the two independent solutions equals $z_+ = a_1 s^{-m_{\text{eff}}} + b_1 s^{1+m_{\text{eff}}} + \dots$. The second solution is normalizable and we thus demand $a_1 = 0$.

In the interior, the near-horizon geometry generically is Lifshitz

$$ds^2 = -r^{2z} dt^2 + \frac{1}{r^2} dr^2 + r^2(dx^2 + dy^2) + \dots, \quad A = h_\infty r^z dt + \dots \quad (5.4.43)$$

with finite dynamical critical exponent z — AdS-RN, which can be viewed as a special case where $z \rightarrow \infty$, will be given separately. In adapted coordinates the interior $r \rightarrow 0$ corresponds to $s \rightarrow -\infty$ and it is easy to show that in this limit potential behaves as

$$V(s) \simeq \frac{1}{c_0^2} + \frac{1}{s^2} (m_{\text{eff}} \sqrt{g_\infty} + m_{\text{eff}}^2 g_\infty - h_\infty^2 q_{\text{eff}}^2 g_\infty) + \dots \quad (5.4.44)$$

Near the horizon the two independent solutions for the wavefunction z_+ therefore behave as

$$z_+ \rightarrow a_0 e^{-s/c_0} + b_0 e^{s/c_0}. \quad (5.4.45)$$

The decaying solution $a_0 = 0$ is the normalizable solution we seek.

Let us now address the possible singular behavior for $k < 0$. To understand what happens, let us first analyze the potential qualitatively for positive k . Since the potential is positive semi-definite at the horizon and the boundary, the Schrödinger system (5.4.39) only has a zero-energy normalizable solution if $V(s)$ has a range $s_1 < s < s_2$ where it is negative. This can only at locations where $k^2 < \hat{\mu}_{q_{\text{eff}}}^2 - m_{\text{eff}}^2 g_{ii} - m_{\text{eff}} g_{ii} \sqrt{g^{rr}} \partial_r \ln \frac{\sqrt{g_{ii}}}{k + \hat{\mu}_{q_{\text{eff}}}}$. Defining a “renormalized” position dependent mass $m_{\text{ren}}^2 = m_{\text{eff}}^2 g_{ii} + m_{\text{eff}} g_{ii} \sqrt{g^{rr}} \partial_r \ln \frac{\sqrt{g_{ii}}}{k + \hat{\mu}_{q_{\text{eff}}}}$ this is the intuitive statement that the momenta must be smaller than the local chemical potential $k^2 < \hat{\mu}_{q_{\text{eff}}}^2 - m_{\text{ren}}^2$. For positive k the saturation of this bound $k^2 = \hat{\mu}_{q_{\text{eff}}}^2 - m_{\text{ren}}^2$ has at most two solutions, which are regular zeroes of the potential. This follows from the fact that $\hat{\mu}_{q_{\text{eff}}}^2$ decreases from the boundary towards the interior. If the magnitude $|k|$ is too large the inequality cannot be satisfied, the potential is strictly positive and no solution exists. For negative k , however, the potential has in addition a triple pole at $k^2 = \hat{\mu}_{q_{\text{eff}}}^2$; two poles arise from the prefactor and the third from the $m_{\text{eff}} \partial_r \ln(k + \hat{\mu}_{q_{\text{eff}}})$ term. This pole always occurs closer to the horizon than the zeroes and the potential therefore qualitatively looks like that in Fig. 5.4 (Since $\hat{\mu}_{q_{\text{eff}}}$ decreases as we move inward from the boundary, starting with $\hat{\mu}_{q_{\text{eff}}}^2 > \hat{\mu}_{q_{\text{eff}}}^2 - \mu^2 > k^2$, one first saturates the inequality that gives the zero in the potential as one moves inward.) Such a potential cannot support a zero-energy bound state, i.e. eq. (5.4.39) has no solution for negative k . In the case $m_{\text{eff}} = 0$ a double zero changes the triple pole to a single pole and the argument still holds. This does not mean that there are no $k < 0$ poles in the CFT spectral function. They arise from the other physical polarization

y_+ of the bulk fermion Ψ . From the second set of decoupled first order equations for the other components of the Dirac equation (after replacing $iz_- \rightarrow z_-$),

$$\begin{aligned}\sqrt{g_{ii}g^{rr}}\partial_r y_+ - m_{\text{eff}}\sqrt{g_{ii}}y_+ &= -(k - \hat{\mu}_{\text{qeff}})z_-, \\ \sqrt{g_{ii}g^{rr}}\partial_r z_- + m_{\text{eff}}\sqrt{g_{ii}}z_- &= -(k + \hat{\mu}_{\text{qeff}})y_+, \end{aligned} \quad (5.4.46)$$

and the associated second order differential EOM for y_+ :

$$\partial_r^2 y_+ + \mathcal{P}\partial_r y_+ + \mathcal{Q}y_+ = 0,$$

with the coefficients

$$\begin{aligned}\mathcal{P} &= \frac{\partial_r(g_{ii}g^{rr})}{2g_{ii}g^{rr}} - \frac{\partial_r\hat{\mu}_{\text{qeff}}}{-k + \hat{\mu}_{\text{qeff}}}, \\ \mathcal{Q} &= -\frac{m_{\text{eff}}\partial_r\sqrt{g_{ii}}}{\sqrt{g_{ii}g^{rr}}} + \frac{m_{\text{eff}}\sqrt{g_{rr}}\partial_r\hat{\mu}_{\text{qeff}}}{-k + \hat{\mu}_{\text{qeff}}} - m_{\text{eff}}^2 g_{rr} - \frac{k^2 - \hat{\mu}_{\text{qeff}}^2}{g_{ii}g^{rr}} \end{aligned} \quad (5.4.47)$$

one sees that the Schrödinger equation for y_+ is the $k \rightarrow -k$ image of the equation (5.4.39) for z_+ and thus y_+ will only have zero-energy solutions for $k < 0$. For simplicity we will only analyze the z_+ case. Note that this semi-positive definite momentum structure of the poles is a feature of any AdS-to-Lifshitz metric different from AdS-RN, where one can have negative k solutions [27].

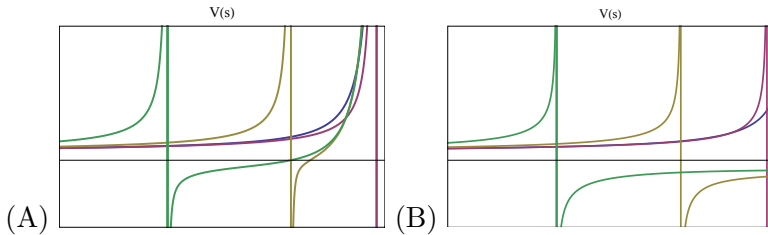


Figure 5.4: The behavior of the Schrödinger potential $V(s)$ for z_+ when k is negative. Such a potential has no zero-energy bound state. The potential is rescaled to fit on a finite range. As $|k|$ is lowered below k_{max} for which the potential is strictly positive, a triple pole appears which moves towards the horizon on the left (Fig A. The Blue,Red,Orange,Green curves are decreasing in $|k|$). The pole hits the horizon for $k = 0$ and disappears. Fig B. shows the special case $m_{\text{eff}} = 0$ where two zeroes collide with two of the triple poles to form a single pole.

The exact solution of (5.4.39) with the above boundary conditions corresponding to poles in the CFT spectral function is difficult to find. By

construction the system is however equivalent to a Schrödinger problem of finding a zero energy solution z_+ in the potential (5.4.40) and can be solved in the WKB approximation (see e.g. [27]). The WKB approximation holds when $|\partial_s V| \ll |V|^{3/2}$. Notice that this is more general than the background adiabaticity limit $m_{\text{eff}} \gg 1, q_{\text{eff}} \gg 1$ with $\hat{\beta}, \hat{m}$ fixed. Combining background adiabaticity with a scaling limit $k \gg 1, m_{\text{eff}} \gg 1, q_{\text{eff}} \gg 1$ with $c_0 k$ fixed and k is parametrically larger than $\hat{\mu}_{q_{\text{eff}}}$ one recovers the WKB potential solved in [53, 63]. As our aim is to study the deviation away from the background adiabatic limit we will be more general and study the WKB limit of the potential itself, without direct constraints on $q_{\text{eff}}, m_{\text{eff}}$. And rather than testing the inequality $|\partial_s V| \ll |V|^{3/2}$ directly, we will rely on the rule of thumb that the WKB limit is justified when the number of nodes in the wave-function is large. We will therefore estimate the number n of bound states and use $n \gg 1$ as an empirical justification of our approach.⁷ With this criterion we will be able to study the normalizable solutions to the Dirac equation/pole structure of the CFT spectral functions as a function of κ/L .

The potential is bounded both in the AdS boundary and at the horizon, and decreases towards intermediate values of r . We therefore have a standard WKB solution consisting of three regions:

- In the regions where $V > 0$, the solution decays exponentially:

$$z_+ = c_{1,2} V^{-1/4} \exp\left(\pm \int_{r_{1,2}}^r dr' [c_0 \sqrt{g^{ii} g_{rr}} (k + \hat{\mu}_{q_{\text{eff}}}) \sqrt{V}]\right). \quad (5.4.48)$$

Here r_1, r_2 are the turning points where $V(r_1) = 0 = V(r_2)$.

- In the region $r_1 < r < r_2$, i.e. $V < 0$, the solution is

$$z_+ = c_3 (-V)^{-1/4} \text{Re} \left[\exp\left(i \int_{r_1}^r dr' [c_0 \sqrt{g^{ii} g_{rr}} (k + \hat{\mu}_{q_{\text{eff}}}) \sqrt{-V}] - i\pi/4\right) \right], \quad (5.4.49)$$

with the constant phase $-i\pi/4$ originating in the connection formula at the turning point r_1 .

Finding a WKB solution shows us that the peaks seen numerically are true poles in the spectral function. But it also allows us to estimate

⁷A large number of bound states n implies $|\partial_s V| \ll |V|^{3/2}$ if the potential has a single minimum, but as is well known there are systems, e.g. the harmonic oscillator, where the WKB approximation holds for small n as well.

the number of peaks that the numerical approach could not resolve. The WKB quantization condition

$$\int_{r_1}^{r_2} dr' \left[c_0 \sqrt{g^{ii} g_{rr}} (k + \hat{\mu}_{q\text{eff}}) \sqrt{-V} \right] = \pi(n + 1/2) \quad (5.4.50)$$

counts the number of bound states with negative semi-definite energy. Note that n does not depend on the integral constant as there is also a factor $1/c_0$ in $\sqrt{-V}$. Since V depends on k , we will see that as we increase k this number decreases. The natural interpretation in the context of a bulk many-body Fermi system is that this establishes the ordering of the the filling of all the $\omega = 0$ momentum shells in the electron star. For a fixed k one counts the modes that have been previously occupied and, consistent with our earlier deduction, the lowest/highest k_F corresponds to the last/first occupied state. Though counterintuitive from a field theory perspective where normally $E \sim k_F$, this UV/IR correspondence is very natural from the AdS-bulk, if one thinks of the electron star as a trapped electron gas. The last occupied state should then be the outermost state from the center, but this state has the lowest effective chemical potential and hence lowest k_F .

Let us now show this explicitly by analyzing the potential and the bound states in the electron star and AdS-RN.

Electron star

The potential (5.4.41) for the electron star is given in Fig. 5.5 and the number of bound states as a function of k in Fig. 5.6. As stated the number of states decreases with increasing k , consistent with the analogy of the pole distribution of the spectral functions compared with AdS-RN. Moreover, we clearly see the significant increase in the number of states as we decrease κ/L thereby improving the adiabaticity of the background. This vividly illustrates that the adiabatic limit corresponds to a large number of constituents. As all numbers of states are far larger than one, the use of the WKB is justified.

The Reissner-Nordström case

For AdS-RN the Schrödinger analysis requires a separate discussion of the near horizon boundary conditions, which we present here for completeness

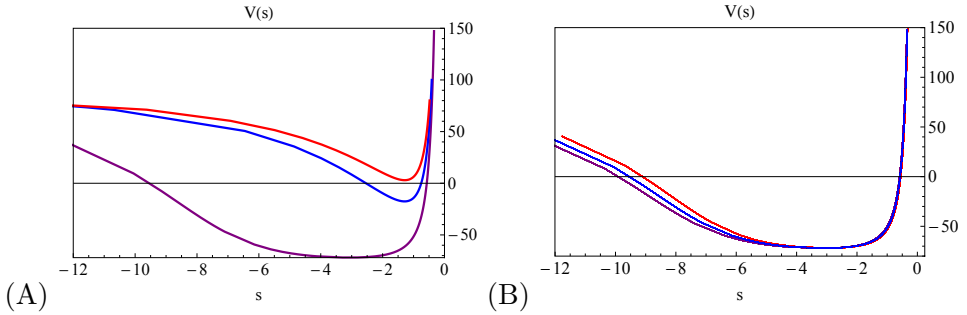


Figure 5.5: The Schrödinger potential $V(s)$ for the fermion component z_+ of in the ES background $\hat{m} = 0.36, z = 2, c_0 = 0.1$. Fig. A. shows the dependence on the momentum $k = 0.0185$ (Purple), $k = 5$ (Blue), $k = 10$ (Red) for $\kappa = 0.092$. Fig. B. shows the dependence on $\kappa = 0.086$ (Purple), $\kappa = 0.092$ (Blue), $\kappa = 0.1$ (Red) for $k = 0.0185$. Recall that $s = 0$ is the AdS boundary and $s = -\infty$ is the near-horizon region.

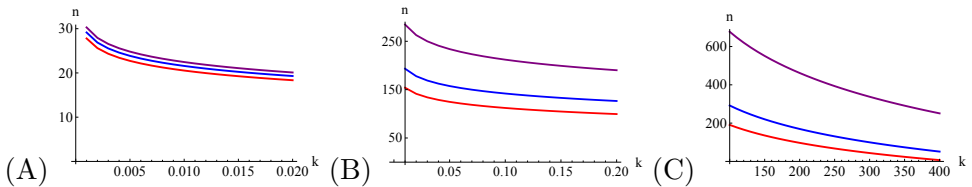


Figure 5.6: The WKB estimate of the number of bound states n as a function of the momentum k for $\kappa = 0.086$ (Purple), 0.092 (Blue), 0.1 (Red) (Fig A.); for $\kappa = 0.001$ (Purple), 0.002 (Blue), 0.003 (Red) (Fig B.) and for $\kappa = 10^{-5}$ (Purple), 3×10^{-5} (Blue), 5×10^{-5} (Red) (Fig C.). Note the parametric increase in number of states as the adiabaticity of the background improves for smaller κ . Both figures are for the electron star background with $\hat{m} = 0.36, z = 2$. Since $n \gg 1$ in all cases, WKB gives a valid estimate.

and comparison. Part of this analysis is originally worked out in [27]. The

AdS-RN black hole with metric

$$ds^2 = L^2 \left(-f(r)dt^2 + \frac{dr^2}{f(r)} + r^2(dx^2 + dy^2) \right), \quad (5.4.51)$$

$$f(r) = r^2 \left(1 + \frac{3}{r^4} - \frac{4}{r^3} \right), \quad (5.4.52)$$

$$A = \mu \left(1 - \frac{1}{r} \right) dt, \quad (5.4.53)$$

has near horizon geometry $\text{AdS}_2 \times \mathbb{R}^2$

$$ds^2 = -6(r-1)^2 dt^2 + \frac{dr^2}{6(r-1)^2} + (dx^2 + dy^2), \quad (5.4.54)$$

$$A = \sqrt{3} \left(r - 1 \right) dt. \quad (5.4.55)$$

A coordinate redefinition of r in eq. (5.4.43) to $r = (r_{\text{AdS}_2} - 1)^{1/z}$ shows that this corresponds to a dynamical critical exponent $z = \infty$ and is outside the validity of the previous analysis.

Before we proceed, recall that the existence of $\text{AdS}_2 \times \mathbb{R}^2$ near-horizon region allows for a semi-analytic determination of the fermion spectral functions with the self-energy $\Sigma \sim \omega^{2\nu_{k_F}}$ controlled by the IR conformal dimension $\delta_k = 1/2 + \nu_k$ with

$$\nu_k = \frac{1}{\sqrt{6}} \sqrt{m^2 + k^2 - \frac{q^2}{2}}. \quad (5.4.56)$$

When ν_k is imaginary, which for $q^2 > 2m^2$ always happens for small k , the spectral function exhibits oscillatory behavior, but generically has finite weight at $\omega = 0$. When ν_k is real, there are poles in the spectral functions at a finite number of different Fermi momenta k_F . The associated quasiparticles can characterize a non-FL ($\nu_{k_F} < 1/2$), a marginal FL ($\nu_{k_F} = 1/2$) or irregular FL ($\nu_{k_F} > 1/2$) with linear dispersion but width $\Gamma \neq \omega^2$ [27].

The analytic form of the near-horizon metric allows us to solve exactly for the near horizon potential V in terms of $s = \frac{c_0}{\sqrt{6}}(k + q/\sqrt{2}) \ln(r - 1) + \dots$. As noted in [27] one remarkably obtains that the near-horizon potential for $s \rightarrow -\infty$ is proportional to the self-energy exponent:

$$V(s) \simeq \frac{6}{c_0^2(k + q/\sqrt{2})^2} \nu_k^2 + \dots \quad (5.4.57)$$

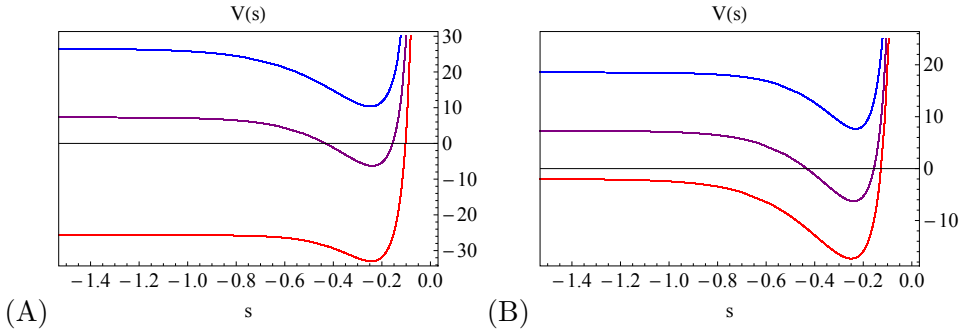


Figure 5.7: The Schrödinger potential $V(s)$ for the fermion component z_+ of in the AdS-RN background $r_+ = 1, \mu = \sqrt{3}, g_F = 1, mL = 0.4, c_0 = 0.1$. Fig. A. shows the dependence on the momentum $k = 1$ (Red), $k = 2$ (Purple), $k = 3$ (Blue) for charge $q = 2.5$. Fig. B. shows the dependence on the charge q — analogous to κ in the ES background —. Shown are the values $q = 2$ (Blue), $q = 2.5$ (Purple), $q = 3$ (Red) for the momentum $k = 2$. In both figures the Red potentials correspond to the oscillatory region $\nu_k^2 < 0$, the Purple potentials show the generic shape that can support an $\omega = 0$ bound state, and the Blue potentials are strictly positive and no zero-energy bound state is present. Recall that $s = 0$ is the AdS boundary and $s = -\infty$ is the near-horizon region.

One immediately recognizes the oscillatory region $\nu_k^2 < 0$ of the spectral function as an $\omega = 0$ Schrödinger potential which is “free” at the horizon $s = -\infty$ (Fig. 5.7) and no bound state can form. Comparing with our previous results, we see that this oscillatory region is a distinct property of AdS-RN. For any Lifshitz near-horizon metric the potential is always positive-definite near the horizon and all $\omega = 0$ solutions will be bounded. (see also [53, 63]). As we increase k , ν_k^2 becomes positive, then the AdS-RN potential is also positive at the horizon and bound zero-energy states can form. Increasing k further, one reaches a maximal k_{max} , above which the potential is always positive and no zero-energy bound state exists anymore.

Because the near-horizon boundary conditions for AdS-RN differ from the general analysis, the possible singularity in the potential for $k < 0$ also requires a separate study. This is clearly intimately tied to the existence of an oscillatory regime in the spectral function, as the previous analysis does apply for $\nu_k^2 > 0$. The clearest way to understand what happens for $\nu_k^2 < 0$ is to analyze the potential explicitly. Again if $|k| > k_{max}$

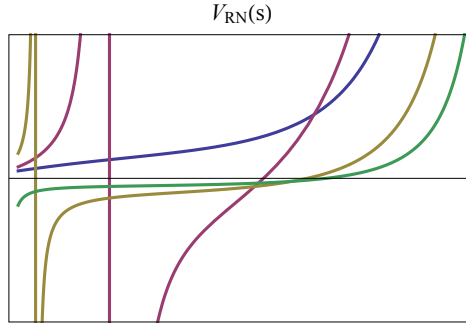


Figure 5.8: The qualitative behavior for negative k of the Schrödinger potential $V(s)$ for the fermion component z_+ of in the AdS-RN background $r_+ = 1, \mu = \sqrt{3}, g_F = 1, mL = 0.1$. The radial coordinate has been rescaled to a finite domain such that the full potential can be represented in the figure; on the right is the AdS boundary and left is the near-horizon region and the range is slightly extended beyond the true horizon, which is exactly at the short vertical line-segments on the right. Potentials are given for $q = 12/\sqrt{3}$, $k = -15$ (Blue) for which the potential is strictly positive, $k = -10$ (Red), $k = -7$ (Orange), which both have triple poles and the pole can be seen to move towards the horizon on the left as k decreases, and $k = -4$ (Green) which has no pole and a finite negative value at the horizon. The pole disappears for $|k| < q/\sqrt{2}$ leaving a regular bounded potential which can support zero-energy bound states.

the potential is strictly positive definite, and no zero-energy bound state exists. As we decrease the magnitude of $k < 0$, a triple pole will form near the boundary when $k = -\hat{\mu}_{q_{\text{eff}}}(s)$, soon followed by a zero at $k = -\sqrt{\hat{\mu}_{q_{\text{eff}}}(s)^2 - m_{\text{ren}}(s)^2}$ (see Fig. 5.4). As we approach the horizon, in the general case where $\lim_{r \rightarrow 0} \hat{\mu}_{q_{\text{eff}}} = h_\infty q_{\text{eff}} r + \dots$, this pole at $r_* = -k/(h_\infty q_{\text{eff}})$ hits the horizon and disappears precisely when $k = 0$. In AdS-RN, however, where $\lim_{r \rightarrow 1} \hat{\mu}_{q_{\text{eff}}} = \frac{q}{\sqrt{2}} + \frac{\sqrt{2}q}{3}(r-1) + \dots$, the pole at $r_*^{RN} - 1 = \frac{3}{\sqrt{2}q}(k + \frac{q}{\sqrt{2}})$ hits the horizon and disappears at $k = -\frac{q}{\sqrt{2}}$. For negative values of k whose magnitude is less than $|k| < \frac{q}{\sqrt{2}}$, the potential is regular and bounded and can and does have zero-energy solutions. Fig. 5.4 shows this disappearance of the pole for the AdS-RN potential.

Counting solutions through WKB is also more complicated for AdS-RN. For $\mathcal{O}(1)$ values of q there are only few Fermi surfaces and the WKB

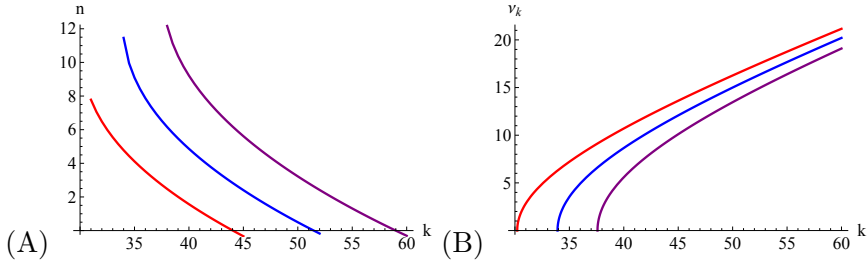


Figure 5.9: The WKB estimate of the number of bound states n in the AdS-RN Schrödinger potential for z_+ with $mL = 10$. The WKB approximation only applies to large values of the charge $q = 45$ (Red), $q = 50$ (Blue), $q = 55$ (Purple). Fig B. gives the associated values of the IR conformal dimension $\nu_k = \frac{1}{\sqrt{6}} \sqrt{m^2 + k^2 - \frac{q^2}{2}}$. Both figures are for the extremal AdS-RN background with $\mu = \sqrt{3}, r_+ = 1, g_F = 1$.

approximation does not apply. For large q it does, however. For completeness we show the results in Fig. 5.9.

5.5 Conclusion and Discussion

These electron star spectral function results answer two of the three questions raised in the introduction directly.

- They show explicitly how the fermion wavefunctions in their own gravitating potential well are ordered despite the fact that they all have strictly vanishing energy: In a fermionic version of the UV-IR correspondence they are ordered *inversely* in k , with the “lowest”/first occupied state having the highest k and the “highest”/last occupied state having the lowest k . With the qualitative AdS/CFT understanding that scale corresponds to distance away from the interior, one can intuitively picture this as literally filling geometrical shells of the electron star, with the outermost/highest/last shell at large radius corresponding to the wavefunction with lowest local chemical potential and hence lowest k .
- The decrease of the number of bound states — the number of occupied wavefunctions in the electron star — as we decrease $q_{\text{eff}} = \hat{\beta}^{1/4} \sqrt{\frac{\pi L}{\kappa}}$ for a fixed electron star background extrapolates naturally

to a limit where the number of bound states is unity. This extrapolation pushes the solution beyond its adiabatic regime of validity. In principle we know what the correct description in this limit is: it is the AdS Dirac Hair solution constructed in [18]. The dependence of the number of bound states on κ/L therefore illustrates that the electron star and Dirac Hair solutions are two limiting cases of the gravitationally backreacted Fermi gas.

With this knowledge we can schematically classify the groundstate solutions of AdS Einstein-Maxwell gravity minimally coupled to charged fermions at finite charge density. For large mass mL in units of the constituent charge q , the only solution is a charged AdS-Reissner-Nördstrom black hole. For a low enough mass-to-charge ratio, the black hole becomes unstable and develops hair. If in addition the total charge density Q is of the order of the microscopic charge q this hairy solution is the Dirac Hair configuration constructed in [18], whereas in the limit of large total charge density Q one can make an adiabatic Thomas Fermi approximation and arrives at a Tolman-Oppenheimer-Volkov at an electron star (Fig. 5.10).

Translating this solution space through the AdS/CFT correspondence one reads off that in the dual strongly coupled field theory, one remains in the critical state if the ratio of the scaling dimension to the charge Δ/q is too large. For a small enough value of this ratio, the critical state is unstable and forms a novel scaleful groundstate. The generic condensed matter expectation of a unique Fermi liquid is realized if the total charge density is of the same order as the constituent charge. Following [53, 63] and [54, 97, 55] the state for $Q \gg q$ is some deconfined Fermi liquid.

The gravity description of either limit has some deficiencies, most notably the lack of an electron star wavefunction at infinity and the unnatural restriction to $Q = q$ for the Dirac Hair solution. A generic solution for $Q \geq q$ with wavefunction tails extending to infinity as the Dirac hair would be a more precise holographic dual to the strongly interacting large N Fermi system. Any CFT information can then be cleanly read off at the AdS boundary. A naive construction could be to superpose Dirac Hair onto the electron star; in principle one can achieve this solution by a next order Hartree-Fock or Local Density Approximation computation.

This best-of-both-worlds generic solution ought to be the true holographic dual of the strongly interacting Fermi ground state. If one is able to answer convincingly how this system circumvents the wisdom that the groundstate of an interacting many-body system of fermions is a generic

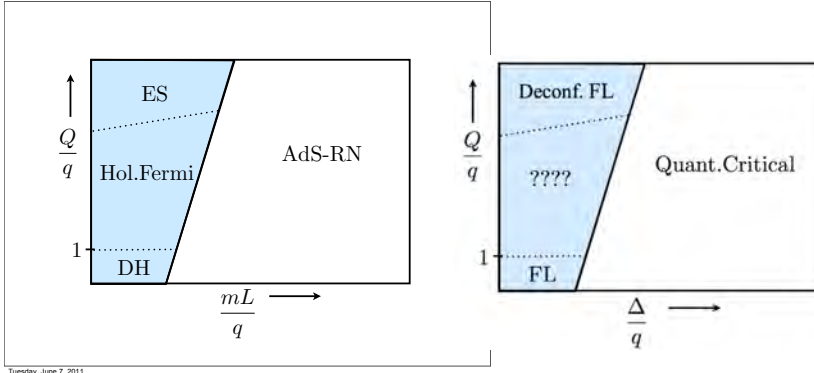


Figure 5.10: Schematic diagram of the different groundstate solutions of strongly coupled fermions implied by holography for fixed charge density Q . Here q is the constituent charge of the fermions and $mL \sim \Delta$ the mass/conformal scaling dimension of the fermionic operator. One has the gravitational electron star (ES)/Dirac Hair (DH) solution for large/small Q/q and small mL/q dual a deconfined Fermi liquid/regular Fermi liquid in the CFT. For $mL/q \sim \Delta/q$ large the groundstate remains the fermionic quantum critical state dual to AdS-RN.

single quasiparticle Landau Fermi liquid, then one would truly have found a finite density Fermi system that does not refer at any stage to an underlying perturbative Fermi gas.

Chapter 6

The phase diagram: electron stars with Dirac hair [83]

6.1 Introduction

The problem of fermionic quantum criticality has proven hard enough for the condensed matter physics to keep seeking new angles of attack. The main problem we face is that the energy scales vary by orders of magnitude between different phases. The macroscopic, measurable quantities emerge as a result of complex collective phenomena and are difficult to relate to the microscopic parameters of the system. An illustrative example present the heavy fermion materials [80] which still behave as Fermi liquids but with vastly (sometimes hundredfold) renormalized effective masses. On the other hand, the strange metal phase of cuprate-based superconducting materials [118], while remarkably stable over a range of doping concentrations, shows distinctly non-Fermi liquid behavior. Holography (AdS/CFT correspondence) [81, 38, 114] has become a well-established treatment of strongly correlated electrons by now, but it still has its perplexities and shortcomings. Since the existence of holographic duals to Fermi surfaces has been shown in [79, 17], the next logical step is to achieve the understanding of the phase diagram: what are the stable phases of matter as predicted by holography, how do they transform into each other and, ultimately, can we make predictions on quantum critical behavior of real-world materials based on AdS/CFT.

The condensed matter problems listed all converge toward a single main question in field-theoretical language. It is the classification of

ground states of interacting fermions at finite density. In this paper we attempt to understand these ground states in the framework of AdS/CFT, the duality between the strongly coupled field theories in d dimensions and a string configuration in $d+1$ dimension. The classification of ground states now translates into the following question: classify the stable asymptotically AdS geometries with charged fermionic matter in a black hole background. Most of the work done so far on AdS/CFT for strongly interacting fermions relies on bottom-up toy gravity models and does not employ a top-down string action. We stay with the same reasoning and so will work with Einstein gravity in $3+1$ dimensions. We note, however, that a top-down construction of holographic fermions has been derived in [35]. While expectedly more complicated, it confirms the robustness of some features seen in $3+1$ -dimensional classical gravity, such as the emergent scale invariance of the field theory propagators in the IR.

So far three distinct models aiming at capturing the stable phases of holographic fermionic matter have appeared: the electron star [51], Dirac hair [18] and a confined Fermi liquid model [96]. The electron star is essentially a charged fermion rewriting of the well-known Oppenheimer-Volkov equations for a neutron star in AdS background. The bulk is thus modeled as a semiclassical fluid. The mystery is its field theory dual: it is a hierarchically ordered multiplet of fermionic liquids with stable quasiparticles [53]. On the other end of the spectrum is Dirac hair, which reduces the bulk fermion matter to a single quantum-mechanical wave function. As a consequence the field theory dual is a single Fermi liquid, however its gravitational consistency properties are not yet fully understood. In [19] we have shown that Dirac hair and electron star can be regarded as the extreme points of a continuum of models, dialing from deep quantum – a single occupied state — to a classical regime — a very large occupation number — in the bulk. They correspond to two extreme “phases” in the field theory phase diagram: a multiplet of a very large number of Fermi liquids and a single Fermi liquid. The confined Fermi liquid model [96] introduces confinement through modifying the bulk geometry and solves for quantum-mechanical wave functions adding them up to compute the full bulk density. This latter step is more general than the single-particle approach of [18] and it naturally extends a Dirac hair state with single Fermi surface to a state with multiple Fermi surfaces. Our main motivation is to construct a complementary model that extends from the other end — the classical regime — down to a state with few Fermi surfaces.

We aim for a system which is general enough to encompass the middle ground between extreme quantum and extreme classical regimes in the original deconfined setup.

In addition to simply improving the mathematical treatment of the many-body-bulk fermion system, the guiding principle in our analysis will be to rest on the advantages and disadvantages of the current models. On the one hand, the Dirac hair is a fully quantum-mechanical model which shows its strength in particular near the boundary (the ultraviolet of the field theory) but becomes worse in the interior, i.e. close to the horizon (the infrared of the field theory) where density is high and the resulting state of matter cannot be well described by a single-particle wave function. On the other hand, the electron star yields a very robust description of high-density matter in the interior but its sharp boundary at some radius r_c means that it has zero density at the boundary of the AdS space. This is a crucial drawback as the holographic dictionary *defines* densities and thermodynamic quantities on the CFT side in terms of the asymptotics of the bulk fields at infinity. It is thus obvious that the physically interesting model lies somewhere in-between the two approaches. This is why what we try to achieve will essentially be an "electron star with Dirac hair".

We will reproduce the results of the electron star/Dirac hair models in the limit of infinitely large/small fermion charge but also get a look at what is in-between. Importantly, our model incorporates the quantum corrections to the leading WKB approximation for the bulk electron density. Our system therefore does not terminate at some finite radius like the electron star, allowing direct calculation of the CFT quantities at the boundary. This will allow us to sketch the phase diagram as a whole. We do not aim at quantitative accuracy in this paper: in a follow-up publication we will present a more accurate calculation making use of density functional formalism for interacting fermions in the bulk. Here, we use a simple WKB formalism with quantum tails which adds quantum corrections to the Thomas-Fermi (fluid) approximation by taking into account finite level spacing. While not highly accurate, it is able to penetrate deep in the quantum regime thus giving at least a qualitative look in the intermediate regime. In particular, we are able to detect the instability of the RN black hole leading to its discharge and formation of finite density phase in the bulk. The precursor of this instability is known as oscillatory or log-oscillatory region [27, 50, 63]. All calculations are self-consistent and include the backreaction on the gauge field by fermions and on the

geometry by both.

The physical task of understanding the various states and their instabilities is clearly still ahead of us. The obvious question to ask is, what is the nature of the phase transitions and to what degree is it universal? A partial answer is provided by our finding that the finite density phases with fermionic quasiparticles at high enough temperatures always exhibit a first order transition into the zero density phase. Intuitively, this can be interpreted as a universal van der Waals liquid-gas transition. In the fluid limit however, returning to the semiclassical description, the transition becomes continuous as predicted in [52]. At zero temperature, we detect a continuous transition whereby the AdS-RN system develops finite bulk density of fermions, driving the instability of the black hole toward a finite density phase, which in the fluid limit is just the electron star. It is here that our method is especially useful as it allows us to probe the "electron star at birth", i.e. to observe the instability of the black hole when only few fermion levels are filled. The instability mechanism was discussed in [50, 63] in the framework of electron star. We again find that finite level spacing matters and the transition is shifted compared to the electron star model. Finally, we find also a crossover between the low density (Dirac hair) and high density (electron star) regime. The crossover is not a transition and thus there is no clear transition point. However, looking at the two extremes, with $N \sim 1$ levels and with $N \sim \infty$ levels we will see that they bring a characteristic difference in the behavior of the system in field theory.

The nature of the zero temperature phase transition and the crossover between the finite density phases is complex and we will not be able to offer a complete description of these phenomena. Hopefully any gain of understanding in these questions will give us some insight into the crucial question: *are there any stable phases of fermion matter that cannot be adiabatically continued to a Fermi gas?*

The outline of the paper is as follows. In the Section II we describe the field content and geometry of our gravity setup, an Einstein-Maxwell-Dirac system in $3 + 1$ dimension, and lay out the single-particle solution to the bulk Dirac equation. In Section III we start from that solution and apply the WKB approximation to derive the Dirac wave function of a many-particle state in the bulk. Afterwards we calculate density and pressure of the bulk fermions – the semiclassical estimate and the quantum corrections, thus arriving at the equation of state. Section IV contains the

solution of the self-consistent set of equations for fermions, gauge field and the metric. There we also describe our numerical procedure. Section V is the core of the matter, where we analyze thermodynamics and spectra of the field theory side and identify different phases as a function of the three parameters of the system: chemical potential μ , fermion charge e and conformal dimension Δ . Section VI sums up the conclusions and offers some insight into possible broader consequences of our work and into future steps.

6.2 Holographic fermions in charged background

We wish to construct the gravity dual to a field theory at finite fermion density. Dimensionality is not of crucial importance at this stage. While some interesting condensed matter systems live in $2 + 1$ dimensions, the heavy fermion materials are for instance all three-dimensional. We will specialize to $2 + 1$ -dimensional conformal systems of electron matter, dual to AdS_4 gravities. We consider a Dirac fermion of charge e and mass m in an electrically charged gravitational background with asymptotic AdS geometry. Adopting the AdS radius as the unit length, we can rescale the metric $g_{\mu\nu}$ and the gauge field A_μ :

$$g_{\mu\nu} \mapsto g_{\mu\nu} L^2, \quad A_\mu \mapsto L A_\mu. \quad (6.2.1)$$

In these units, the action of the system is:

$$S = \int d^4x \sqrt{-g} \left[\frac{1}{2\kappa^2} L^2 (R + 6) + \frac{L^2}{4} F^2 + L^3 \mathcal{L}_f \right] \quad (6.2.2)$$

where κ is the gravitational coupling and $F_{\mu\nu} = \partial_\mu A_\nu - \partial_\nu A_\mu$ is the field strength tensor. The fermionic Lagrangian is:

$$\mathcal{L}_f = \bar{\Psi} \left[e_A^\mu \Gamma^A \left(\partial_\mu + \frac{1}{4} \omega_\mu^{BC} \Gamma_{BC} - ie L A_\mu \right) - mL \right] \Psi \quad (6.2.3)$$

where $\bar{\Psi} = i\Psi^\dagger \Gamma^0$, e_A^μ is the vierbein and ω_μ^{AB} is the spin connection. Since the magnetic field is absent, the $U(1)$ gauge field is simply $A = \Phi dt$. We parametrize our (spherically symmetric asymptotically AdS) metric in four spacetime dimensions as:

$$ds^2 = \frac{f(z)e^{-h(z)}}{z^2} dt^2 - \frac{1}{z^2} (dx^2 + dy^2) - \frac{1}{f(z)z^2} dz^2 \quad (6.2.4)$$

The radial coordinate is defined for $z \geq 0$, where $z = 0$ is the location of AdS boundary. All coordinates are dimensionless, according to (6.2.1). This form of the metric is sufficiently general to model any configuration of static and isotropic charged matter. Development of a horizon at finite z is signified by the appearance of a zero of the function $f(z)$, $f(z_H) = 0$. From now on we will set $L = 1$.

We will now proceed to derive the equation of motion for the Dirac field. From (6.2.3), the equation reads:

$$e_A^\mu \Gamma^A \left(\partial_\mu + \frac{1}{4} \omega_\mu^{BC} \Gamma_{BC} - ieA_\mu \right) \Psi = m\Psi. \quad (6.2.5)$$

In the metric (6.2.4) we can always eliminate the spin connection [79] by transforming:

$$\Psi \mapsto (gg^{zz})^{-\frac{1}{4}} \Psi = \frac{e^{h(z)/4} z^{3/2}}{f(z)^{1/4}} \Psi \equiv a^{-1}(z) \Psi \quad (6.2.6)$$

After decomposing into radial projections Ψ_\pm , defined as:

$$\Psi_\pm = \frac{1}{2} (1 \pm \Gamma^Z) \Psi, \quad (6.2.7)$$

in a basis where $\Gamma^Z = \text{diag}(1, 1, -1, -1)$, the Dirac equation in matrix form becomes:

$$\sqrt{f} \partial_z \begin{pmatrix} \Psi_+ \\ \Psi_- \end{pmatrix} = \hat{D} \begin{pmatrix} \Psi_+ \\ \Psi_- \end{pmatrix}. \quad (6.2.8)$$

Here the matrix \hat{D} is the differential operator along the transverse coordinates (x, y) and time, which we will specify shortly.

We will give the solution of the Dirac equation in the cylindrical coordinates, which will serve as the input to the calculation of bulk fermion density in WKB approximation. Introducing the cylindrical coordinates as $(t, x, y, z) \mapsto (t, \rho, \phi, z)$ we make the separation ansatz:

$$\begin{pmatrix} \Psi_+(z, \rho, \phi) \\ \Psi_-(z, \rho, \phi) \end{pmatrix} = \int \frac{d\omega}{2\pi} \begin{pmatrix} F(z) K_1(\rho, \phi) \\ -G(z) K_2(\rho, \phi) \end{pmatrix} e^{-i\omega t} \quad (6.2.9)$$

where, unlike previous approaches, the F, G are taken as scalars and the modes $K_{1,2}$ are in-plane spinors. The Dirac equation then takes the form:

$$\begin{pmatrix} \partial_z F K_1 \\ -\partial_z G K_2 \end{pmatrix} = \begin{pmatrix} -\hat{\partial}/\sqrt{f(z)} & \left(\tilde{E}(\omega, z) + \tilde{M}(z) \right) \sigma_3 \\ \left(\tilde{E}(\omega, z) - \tilde{M}(z) \right) \sigma_3 & -\hat{\partial}/\sqrt{f(z)} \end{pmatrix} \begin{pmatrix} F K_1 \\ -G K_2 \end{pmatrix} \quad (6.2.10)$$

We recognize the matrix at the right hand side as \hat{D}/\sqrt{f} . The terms \tilde{E} and \tilde{M} have the meaning of local energy and mass terms, respectively:

$$\tilde{E}(z) = -\frac{e^{h(z)/2}}{f(z)}(\omega + q\Phi(z)), \quad \tilde{M}(z) = \frac{m}{z\sqrt{f(z)}}. \quad (6.2.11)$$

The in-plane operator $\hat{\partial}$ acts on each in-plane spinor as:

$$\hat{\partial} = \begin{pmatrix} 0 & i\bar{\partial} \\ -i\partial & 0 \end{pmatrix} \quad (6.2.12)$$

with $\partial \equiv e^{i\phi}(\partial_\rho + \partial_\phi/\rho)$. To maintain the separation of variables in (6.2.10), we require $\hat{\partial}K_i = \lambda_i K_i$, where $|\lambda_i|^2$ corresponds the momentum-squared of the in-plane motion of the particle. The solution of the cylindrical eigenvalue problem for each in-plane spinor K_i gives:

$$K_i(\rho, \phi) = \begin{pmatrix} J_{l-1/2}(\lambda_i \rho) e^{i(l-1/2)\phi} \\ J_{l+1/2}(\lambda_i \rho) e^{-i(l+1/2)\phi} \end{pmatrix}. \quad (6.2.13)$$

Of the two linearly independent solutions, only the Bessel function of the first kind $J(x)$ is chosen in order to satisfy the normalizability condition of the wave function at $\rho \rightarrow 0$ (for linear independent Bessel function Y this condition is not fulfilled). Remembering that $|\lambda_i|^2$ is the squared in-plane momentum, the physical requirement that this momentum be the same for both radial projections translates into the condition $|\lambda_2| = |\lambda_1|$. Consistency of the separation of variables then shows us that $K_2 = \sigma_3 K_1$ and thus $\lambda_1 = -\lambda_2 = k$ and the reduced radial equation becomes:

$$\begin{pmatrix} \partial_z F \\ \partial_z G \end{pmatrix} = \begin{pmatrix} -\tilde{k} & \tilde{E} + \tilde{M} \\ \tilde{M} - \tilde{E} & \tilde{k} \end{pmatrix} \begin{pmatrix} F \\ G \end{pmatrix} \quad (6.2.14)$$

with $\tilde{k} = k/\sqrt{f}$ (let us note that Eq. (6.2.14) is for the pair (F, G) , whereas the initial equation (6.2.10) is written for the bispinor $(FK_1, -GK_2)$). For the WKB calculation of the density, it is useful to remind that the wave function Ψ in Eq. (6.2.9) has two quantum numbers corresponding to the motion in the (ρ, ϕ) plane: λ, l (or equivalently the momenta k_x, k_y in Cartesian coordinates). The radial eigenfunctions in z -direction will provide a third quantum number n .

6.3 Equation of state of the bulk fermion matter

In this section we construct the model of the bulk fermions in an improved semiclassical approximation. In the next section we will complement it with the equations for the Einstein-Maxwell sector. We will start by estimating the bulk fermion density in the semiclassical case. The Dirac equation is solved in the WKB approximation, and the density is computed assuming a large number of energy levels. This is in the spirit of WKB approximation. However, we sum the exact quantum-mechanical solutions for the wave functions rather than immediately taking the fluid limit. In this respect our method goes beyond Thomas-Fermi and in fact corresponds to calculating the vacuum density in the Hartree approximation. The resulting estimate has sharp bounds along the radial direction, at some points z_1 and z_2 ($0 < z_1 < z_2 \leq 1$), similar to electron star [51] and its finite-temperature generalization [52]. As we have already argued, sharp bounds fail to capture several essential phenomena on the CFT side. To overcome this shortcoming, we will improve on the WKB approximation and continue our bulk density profile outside the classical region by making use of Airy corrections to WKB in the interior, and the Dirac hair formalism near the boundary. The reason for the latter is that Airy or decaying WKB approximations rapidly fail beyond the naive exterior sharp edge. Compared to other models of holographic fermions at finite density this quantum improvement on the semiclassical WKB limit bridges the gap between the all-classical electron star [51] and single-particle quantum mechanical calculation of Dirac hair [18].

6.3.1 WKB hierarchy and semiclassical calculation of the density

In the framework of WKB calculations, the first task is to construct the effective potential as a functional of the induced charge density $n(z)$. Physically, the origin of the induced charge in our model is the pair production in the strong electromagnetic field of the black hole. To remind the reader, a (negatively) charged black hole in AdS space is unstable at low temperatures, and spontaneously discharges the vacuum [60]. This means that there will be a non-zero net density of electrons n . Within the semiclassical approximation it is consistent to calculate n as density of non-interacting electrons. We will thus employ the semiclassical gas model and add up all possible states enumerated by good quantum numbers. For this we choose

the set (λ, l, n) .

We now give the algorithm for the WKB expansion of the wave function for Dirac equation, adopted from [113]. Even though every single step is elementary, altogether it seems to be less well known than its Schrödinger equivalent. We consider the Dirac equation in the form (6.2.8) and introduce the usual WKB phase expansion for it:

$$\Psi(z) = e^{\int_{z_0}^z dz y(z) \sqrt{f(z)}} \chi(z) \quad (6.3.15)$$

with the spinor part $\chi(z)$. The phase $y(z)$ can be expressed as the semiclassical expansion in \hbar^{-1}

$$y(z) = (y_{-1}(z) + y_0(z) + y_1(z) + \dots). \quad (6.3.16)$$

The equations for the perturbative corrections now follow from (6.3.15-6.3.16):

$$\hat{D}\chi_0 = y_{-1}\chi_0, \quad (6.3.17)$$

$$\hat{D}\chi_1 = y_{-1}\chi_1 + y_0\chi_0 + \sqrt{f}\partial_z\chi_0, \quad (6.3.18)$$

...

$$\hat{D}\chi_n = y_{-1}\chi_n + \sqrt{f}\partial_z\chi_{n-1} + \sum_{i=0}^{n-1} y_{n-i-1}\chi_i. \quad (6.3.19)$$

Notice in particular that y_{-1}/χ_0 is an eigenvalue/eigenvector of \hat{D} . In our case the matrix \hat{D} has rank two, so there are two eigenvalues/eigenvectors for y_{-1}/χ_0 : y_{-1}^{\pm} and χ_0^{\pm} . To find the first order correction to the phase of the wave function y_0 , we multiply (6.3.18) from the left by the left eigenvalue $\tilde{\chi}_0^{\pm}$ of the matrix \hat{D} (\hat{D} is in general not symmetric, so the right and left eigenvalues are different):

$$y_0 = -\frac{(\partial_z\chi_0^{\pm}, \tilde{\chi}_0^{\pm})}{(\tilde{\chi}_0^{\pm}, \chi_0^{\pm})}. \quad (6.3.20)$$

so we can now construct the usual WKB solution of the form $\Psi_{\pm} = e^{i\theta_{\pm}}/\sqrt{q}$, where q is the WKB momentum and θ_{\pm} the phase. The term y_0 is just the first order correction to θ_{\pm} .

¹From the very beginning we put $\hbar = 1$. However, to elucidate the semiclassical nature of the expansion we give it here with explicit \hbar . Dirac equation becomes $\hbar\sqrt{f}\partial_z\hat{\Psi} = \hat{D}\hat{\Psi}$, where $\hat{\Psi} = (\Psi_+, \Psi_-)$, yielding the expansion $y(z) = \hbar^{-1}(y_{-1}(z) + \hbar y_0(z) + \hbar^2 y_1(z) + \dots)$.

Finally, let us recall the applicability criterion of the WKB calculation. It is known that WKB approximation fails in the vicinity of turning points. The condition of applicability comes from comparing leading and the next to leading term in the expansion (6.3.16):

$$\frac{y_0(z)}{y_{-1}(z)} \ll 1. \quad (6.3.21)$$

In terms of $\tilde{E}(z)$ and $\tilde{M}(z)$ introduced in Eq. (6.2.11) it gives at $k = 0$:

$$\frac{\tilde{M}(z)\partial_z\tilde{E}(z) - \tilde{E}(z)\partial_z\tilde{M}(z)}{\tilde{E}(z)(\tilde{E}(z) - \tilde{M}(z))} \ll 1. \quad (6.3.22)$$

We will use this expression later on to estimate the point where we need to replace the WKB density and pressure with their full quantum estimates.

WKB wave function

According to (6.3.17), the leading effective WKB momentum for the motion in z direction $q \equiv |y_{-1}^\pm|$ is:

$$q^2(z) = \tilde{E}^2(z) - \tilde{M}^2(z) - \tilde{k}^2(z). \quad (6.3.23)$$

The wave function in radial direction, $\Psi = (F, -G)$, is given by the superposition of two linear independent solutions

$$\Psi(z) = C_+\chi_+(z)e^{i\theta(z)} + C_-\chi_-(z)e^{-i\theta(z)}, \quad (6.3.24)$$

with the phase determined by

$$\theta(z) = \int^z (q(z') + \delta\theta(z')) dz' \quad (6.3.25)$$

$$\delta\theta(z) = \int^z \frac{\tilde{k}\partial_z\tilde{k} - q\partial_zq + (\tilde{E} - \tilde{M}) (\partial_z\tilde{E} + \partial_z\tilde{M})}{2\tilde{k}q} dz. \quad (6.3.26)$$

The constants C_+ and C_- are related by invoking the textbook boundary conditions for the behavior of WKB wave function at the boundary of the classically allowed region ($q^2(z) > 0$) and the classically forbidden region

($q^2(z) < 0$). The wave function in the classically allowed then reads:

$$\Psi(z) = \frac{C}{\sqrt{q(z)}} \begin{pmatrix} \sqrt{\tilde{E}(z) + \tilde{M}(z) \sin(\theta(z) - \delta\theta(z))} \\ \sqrt{\tilde{E}(z) - \tilde{M}(z) \sin \theta(z)} \end{pmatrix}, \quad (6.3.27)$$

$$\delta\theta(z) = \text{ArcSin} \frac{q(z)}{\sqrt{\tilde{E}^2(z) - \tilde{M}^2(z)}}, \quad (6.3.28)$$

and C is the only remaining undetermined normalization constant. For the classically forbidden region we will use a different wave function, to be described in the subsequent subsections. Integrating the probability density over all coordinates in classically allowed region (z_1, z_2) gives the normalization condition:

$$C^2 \int_{z_1}^{z_2} dz \frac{\sqrt{g_{3d}(z)}}{a(z)^2} \int \rho d\rho \int d\phi C_{2d}^2 \Psi_{nl\lambda}(z, \rho, \phi) \Psi_{n'l'\lambda'}^\dagger(z, \rho, \phi) = 1. \quad (6.3.29)$$

The metric factor is $g_{3d}(z) = g(z)g^{tt}(z)$, and $a(z)$ is the conversion factor from (6.2.6). In the left-hand side of the equality we took into account the normalization of the continuous spectrum in the (ρ, ϕ) plane. The integration over ϕ is trivial. The orthogonality relation for Bessel functions (which encapsulates the (ρ, ϕ) solution) gives the definition of C_{2d}^2 :

$$C_{2d}^{-2} \int_0^\infty J(\lambda\rho)J(\lambda'\rho)\rho d\rho = \frac{\delta(\lambda - \lambda')}{\lambda} \quad (6.3.30)$$

and it allows us to express the normalization constant as:

$$C = \left(4\pi \int dz \frac{\sqrt{g^{tt}} \tilde{E}(z)}{\sqrt{g^{z\bar{z}}} q(z)} \right)^{-1/2}, \quad (6.3.31)$$

where a factor of 2π comes from the integration over ϕ and an additional factor of 2 from the summation over the full four-component wave function, i.e. bispinor (each spinor gives $\tilde{E}(z)/q(z)$ after averaging over the fast oscillating phase θ). This completes the derivation of WKB wave function and allows us to compute the density.

WKB density

The key input for WKB approximation is the self-consistent bulk electron density $n(z)$. As in [113] we find the total density by summing single-particle wave functions in the classically allowed region. The WKB wave

function is characterized by the quantum numbers (λ, l, n) with λ being the linear momentum in the $x - y$ plane, l – the orbital momentum in the $x - y$ plane and n – the energy level of the central motion in the potential well along z direction. The bulk density can be expressed as the sum over the cylindrical shells of the bulk Fermi surface. This suggests to work in the cylindrical geometry as the natural choice (remember that we use the $SO(2)$ invariant in-plane spinors). Each shell satisfies the Luttinger theorem in the transverse ($x - y$) direction and so the density carried by each shell $n_{xy}(z)$ can easily be found. We can then sum over all shells to arrive at the final answer which reads simply $\int dz n_z(z) n_{xy}(z)$. A similar qualitative logic for summing the Luttinger densities in the $x - y$ plane was used also in [96] although the model used in that paper is overall very different.

Let us start by noticing that the end points of the classically allowed region determine the limits of summation over n and λ : $q^2(\omega_n, \lambda) \geq 0$. Thus, the density in the WKB region is:

$$n(z) = \frac{1}{a(z)^2} \sum_{l=0}^{\infty} \int_0^{2\pi} d\phi \sum_{n: q^2(\omega_n, \lambda) \geq 0} \int_0^{\lambda_0} \lambda d\lambda \int_0^{\infty} d\rho \rho C_{2d}^2 |\Psi(z, \rho, \phi)|^2, \quad (6.3.32)$$

where $\lambda_0 = \sqrt{f(z)(\tilde{E}^2(\omega, z) - \tilde{M}^2(z))}$. The limit of the sum over the level number n is determined by the requirement that WKB momentum be positive; in other words, we sum over occupied level inside the potential well only. The sum over the orbital quantum number l extends to infinity as the (x, y) plane is homogenous and the orbital number does not couple to the non-trivial dynamics along the radial direction. For large occupation numbers the normalization condition (6.3.31) and the (local) Bohr-Sommerfeld quantization rule ($\int dz \sqrt{q(z)} = N\pi$) then give:

$$C_n = \left(\frac{1}{4\pi^2} \frac{\partial \omega_n}{\partial n} \right)^{1/2}, \quad \text{for } q(z) \gg \delta\theta(z), \quad z \approx 1. \quad (6.3.33)$$

Now we turn the summation over the quantum number n into the integration over energy and obtain for the *bulk* electron density (here we also performed the integration over ρ using the explicit expression for the wave function (6.2.10) and the normalization condition (6.3.30) for the Bessel

functions):

$$n(z) = \frac{2}{a(z)^2} \sum_{l=0}^{\infty} \int_0^{2\pi} d\phi \int_0^{\sqrt{f(z)(\tilde{E}^2(\omega, z) - \tilde{M}^2(z))}} d\lambda \lambda \int_0^{\mu_{loc}} d\omega \frac{\tilde{E}(\omega, z)}{4\pi^2 q(\omega, \lambda, z)}. \quad (6.3.34)$$

After performing first integral over ω and then over λ we get²:

$$n(z) = z^3 \frac{p_{max}^3(z) f^{3/2}(z)}{3\pi^2} \quad (6.3.35)$$

with p_{max} determined by

$$p_{max}^2 = \tilde{E}^2(0, z) - \tilde{M}^2(z). \quad (6.3.36)$$

Notice that this result corresponds with common knowledge on the density of electron star [51].

6.3.2 Airy correction to semiclassical density

The semiclassical density profile has sharp cutoffs in the classically forbidden regions, that is, for $p_{max}^2 < 0$, i.e. $\tilde{E}(z) < \tilde{M}(z)$ (Fig. 6.1, dashed curves). Generically, there will be such two turning points, z_* and z_{**} , so that $0 < z_* < z_{**} < z_H$ where $z_H = \infty$ in pure AdS or equals the horizon radius at finite temperature. The semiclassical density is only nonzero for $z_* < z < z_{**}$. Leaving out the quantum "tails" outside this region misses even some qualitative features of the system, as we have discussed in the introduction. Moreover, the WKB approximation ceases to be valid close to the turning points (Eq. 6.3.22), at some $z_{1,2}$ ($0 < z_* < z_1 < z_2 < z_{**} < z_H$). We thus account for the quantum corrections for $z < z_1$ and $z > z_2$. We first treat the latter case, i.e. the quantum corrections in the near-horizon IR region.

To this end it is convenient to rewrite the Dirac equation in the Schrödinger (second order) form for the Ψ_+ component. Following the

²The given result for n can be compared to the charge density in the electron star limit given in [53]. The metric functions used there are related to ours as $f \mapsto f e^{-h}/z^2$ and $g \mapsto 1/fz^2$, where our metric functions are on the right hand side. Likewise, our definition of p_{max} is related to k_F of [53] as $p_{max} = k_F/\sqrt{f}$. Now the total bulk charge is expressed in [53] as $Q = \int dz \tilde{n}_e(z)$ where $\tilde{n}_e(z) \sim n(z)e^{h/2}$. In our conventions $Q = \int dz \sqrt{-g} g^{zz} g^{tt} n = \int dz n(z) e^{h/2}$ thus giving the same result as in [53].

textbook, the lowest order correction to the WKB solution is obtained by expanding the potential,

$$V_{eff}(z) = \tilde{E}^2(z) - \tilde{M}^2(z) - 3 \left(\partial_z \log \left(\tilde{E}(z) + \tilde{M}(z) \right) \right)^2 + \frac{1}{2} \frac{\partial_{zz}(\tilde{E}(z) + \tilde{M}(z))}{\tilde{E}(z) + \tilde{M}(z)}, \quad (6.3.37)$$

in the vicinity of the turning point. Naively the logical extension of our formalism into the classically forbidden region would be to solve the Dirac equation or the corresponding Schrödinger equation in WKB form with imaginary WKB momentum. The result would be a set of exponentially decaying wave functions. This is, however, not the optimal approach. Firstly, the summation of all exponentially decaying wave functions would be an overkill as the contributions of all but the highest amplitude exponential correction are negligible and do not have a measurable influence on the result. Secondly, the summation of wave functions with imaginary WKB momenta turns out to be much more difficult in practice. We thus perform the series expansion of the potential (6.3.37) around $z = z_2$ as our approximation scheme. The lowest order (linear) term in the expansion of the potential yields a solution in terms of an Airy function which coincides with the WKB solution as we approach the turning point, i.e. for $z = z_2 - 0$.

In principle, also for Airy corrections such a continuation should be made for each of the wave functions (6.3.24), and the corrections then should be summed up. However, the Airy corrections for excited levels are also exponentially suppressed outside the classically allowed region. It is therefore a good approximation to only match the squared module of one single, suitably chosen, Airy function to the total WKB density. This should be the solution at the Fermi level $\omega = 0$. Exponentially small corrections are in any case beyond the scope of a Hartree-based method and require a density functional approach.

We first expand the potential V_{eff} in $z - z_{**}$, where z_{**} is the (second) turning point, i. e. $q(z_{**}) = 0$. The resulting second-order equation for Ψ_+ is schematically of the form:

$$(\partial_{zz} + (P_0 + P_1(z - z_{**}))\partial_z + Q_0 + Q_1(z - z_{**}))\Psi_+ = 0. \quad (6.3.38)$$

We transform to a Schrödinger-type equation (without a first derivative term) but consistently keep only linear correction in the potential, giving the equation:

$$(\partial_{zz} + Q_0 + (Q_1 - 2P_0)(z - z_{**}))\Psi_+ = 0 \quad (6.3.39)$$

with

$$\begin{aligned}
Q_0 &= \tilde{k} \frac{\partial_z \tilde{E} + \partial_z \tilde{M}}{\tilde{E} + \tilde{M}} - \partial_z \tilde{k} \Big|_{z=z_{**}} \\
Q_1 &= 2\tilde{M} \partial_z \tilde{M} + 2\tilde{k} \partial_z \tilde{k} - 2\tilde{E} \partial_z \tilde{E} + \frac{\partial_z \tilde{E} \tilde{B} + \partial_z \tilde{M}}{(\tilde{E} + \tilde{M})^2} \left[(\tilde{E} + \tilde{M}) \partial_z \tilde{k} - (\partial_z \tilde{E} + \partial_z \tilde{M}) \tilde{k} \right] \\
P_0 &= - \frac{\partial_z \tilde{E} + \partial_z \tilde{M}}{\tilde{E} + \tilde{M}} \Big|_{z=z_{**}}
\end{aligned} \tag{6.3.40}$$

The decaying normalizable solution to the above equation is (non-normalizable solution would imply instability of the interior):

$$\Psi_+(z) = \mathcal{N} \text{Ai} \left(- \frac{(2P_0 - Q_1)(z - z_{**})}{(2P_0 - Q_1)^{2/3}} \right) \tag{6.3.41}$$

where \mathcal{N} is the normalization constant. There is a similar equation for Ψ_- with the same normalization \mathcal{N} for consistency with the first order Dirac equation. The density is now simply

$$n^{IR}(z) = |\Psi_+(z)|^2 + |\Psi_-(z)|^2. \tag{6.3.42}$$

where in our approximation the only contribution comes from the single wavefunction with $\omega = 0$. We match this to the WKB density at the point where it fails, i.e. at the point z_2 in the interior where $y_0/y_{-1} = 1$:

$$n^{WKB}(z_2 - 0) = n^{IR}(z_2 + 0). \tag{6.3.43}$$

This determines the normalization \mathcal{N} .

This approximation for the quantum tail becomes better and better at z_H as $z_{**} \rightarrow z_H$. It is exactly there, in deep interior, where the Airy correction is most critical for gravitational backreaction. The presence of a nonzero density for $z \rightarrow z_H$ implies backreaction at the horizon as we shall see in the next section.

6.3.3 Dirac hair correction to semiclassical density

In principle, the Airy expansion can also be applied to the UV non-classical region near the AdS boundary ($0 < z < z_1$). This approach, however, has both practical problems and problems of principle when applied in the near-boundary region:

- The convergence of the Airy expansion is poor near the boundary. Airy expansion is nothing but the linear approximation of the effective potential, as in Eq. (6.3.38). Typically, however, the AdS boundary is too far away from the turning point and the rate of change of the effective potential V_{eff} for $z \approx 0$ is large enough to require higher-order terms in the expansion of V_{eff} . These would, however, make the calculations much more complicated and go beyond the accuracy of the current model.
- More importantly, expanding away from z_* toward the boundary inevitably means that the resulting approximation will not reproduce the exact asymptotics of the fermion field at the AdS boundary. The holographic dictionary identifies expectation values on the field theory side by considering the asymptotics of the bulk fields at the AdS boundary ($z \rightarrow 0$). In particular, the correct asymptotics are necessary to have the correct fermionic contribution to thermodynamics. With an Airy expansion around z_* , the behavior at $z = 0$ is completely uncontrolled.

Therefore, in the context of the AdS/CFT correspondence one needs to start the expansion at $z = 0$ in the UV region and glue it to the semiclassical region at $z = z_*$ and not vice versa. The natural framework for this task is the Dirac hair formalism [18]. In the region $0 < z < z_*$ the density rapidly decreases toward zero and it is increasingly dominated by the long range wave functions with $\omega = 0$ and $k \approx 0$ [19]. These facts are precisely the necessary conditions for Dirac hair to be a good approximation. We will thus glue the Dirac hair wave function to the semiclassical result to obtain the quantum tail at small z . The quantum correction in the UV is especially crucial, since otherwise all holographic dictionary entries related to fermions (density, currents, response functions) are all, according to the holographic dictionary, equal to zero.

We will start with a very concise review of Dirac hair. As argued in [18], a very good approximation to the bulk fermion profile at low densities is to describe it through a single collective wave function which encapsulates the nonzero VEV of the fermion density. The right quantity to consider is just the spacetime average of the bulk density $J(z)$:

$$J(z; E, p) = \int d\omega \int d^2k \Psi^\dagger(z; -\omega, -k) \Psi(z; E + \omega, p + k) \quad (6.3.44)$$

In the bulk, this is just the probability density associated with the quantum-mechanical state Ψ . Analogously to the Airy correction in the IR region, one should, strictly speaking, construct a separate density bilinear for every bulk excitation (filled level) and add up all the bilinears. Analogously to the Airy correction, we do not implement this procedure, but approximate the density with only a single wave function, as we did in the original Dirac hair approximation [18] essentially neglecting the multi-particle nature of the system in the classically forbidden region. The justification is less rigorous than for the Airy correction: the subleading Dirac hair corrections are not damped exponentially but only as a power law. In practice, however we have shown that the numerical value of the amplitude of the excited wave functions with $k \neq 0$ is small enough to be neglected [19].

In the single-particle Dirac hair approximation the expectation value of $J(z; E, p)$ at the boundary at zero energy and momentum ($\langle J(z = E = p = 0) \rangle$) translates into the density discontinuity in the vicinity of the Fermi surface [18]:

$$\langle J(E = p = 0) \rangle = \int_{k_F-0}^{k_F+0} d^2k N(k) \sim Z, \quad (6.3.45)$$

where through Migdal's theorem Z corresponds with the quasiparticle pole strength in the spectral function. Especially in the single particle approximation, it is convenient to directly deduce effective equations of motion for $J(z, E, p)$ from the Dirac equation, rather than solving the Dirac equation and squaring. Since the dominant Fermi momentum in the UV is $k_F \simeq 0$ the contribution of the Fermi momentum to the effective equations of motion for J can be ignored. In this simplification its equations of motion only contain the explicit density momentum p . The Fermi momentum is still implicitly present in the integration over the internal momentum k . To write the evolution equation directly for the density $J(\omega = k = 0)$, it is convenient to consider separately the radial projections Ψ_{\pm} and construct the bilinears

$$J_{\pm}(z) = \int d\omega \int d^2k \Psi_{\pm}^{\dagger} \Psi_{\pm}, \quad \text{with} \quad J = J_+ + J_- \quad (6.3.46)$$

together with the auxiliary quantity

$$I(z) = \int d\omega \int d^2k \Psi_+^{\dagger} \Psi_- + \text{h.c.} \quad (6.3.47)$$

which we need to close the system of equations. The coupled equations for J_{\pm}, I implied by the Dirac equation read:

$$\left(\partial_z + \frac{\partial_z f}{2f} - \frac{3}{z} \pm \frac{2m}{z\sqrt{f}} - \frac{2\partial_z h}{h} \right) J_{\pm} \pm \frac{e\Phi}{f} I = 0 \quad (6.3.48)$$

$$\left(\partial_z + \frac{\partial_z f}{2f} - \frac{3}{z} - \frac{2\partial_z h}{h} \right) I - \frac{2e\Phi}{f} (J_+ - J_-) = 0. \quad (6.3.49)$$

Here we just need the Dirac hair solution to correct the semiclassical model near the boundary, not in the whole space. We find it easiest to seek the solution near $z = 0$ in the form of a series in z :

$$J_-(z) = j_-^0 z^{\alpha_-} (1 + j_-^1 z + j_-^2 z^2 + \dots) \quad (6.3.50)$$

$$J_+(z) = -\frac{\mu^2}{(2m+1)^2} z^{\alpha_+} (j_+^0 + j_+^1 z + j_+^2 z^2 + \dots) \quad (6.3.51)$$

$$I(z) = \frac{i\mu}{2m+1} z^{\alpha_0} (i^0 + i^1 z + i^2 z^2 + \dots). \quad (6.3.52)$$

The exponents $\alpha_{0,\pm}$ are determined by the lowest order of the near-boundary expansion of the Dirac equation. As usual, one gets two families of solutions and, according to the dictionary, the one with faster decay at $z \rightarrow 0$ corresponds to a VEV. This is the family with $\alpha_{\pm} = 4 + 2m \pm 1$, $\alpha_0 = 4 + 2m$. Since we will only use this solution in the UV region, it is convenient to solve directly for the coefficients in this power series, rather than a full numerical determination. We have explicitly checked the convergence of the series using the D'Alembert criterion.

The density obtained in this way is

$$n^{UV}(z) = J_+(z) + J_-(z). \quad (6.3.53)$$

This single particle density is now matched to the WKB density at the point z_1 where $y_0/y_{-1} = 1$ in the exterior:

$$n^{UV}(z_1 - 0) = n^{WKB}(z_1 + 0). \quad (6.3.54)$$

In this way we determine the amplitude j_-^0 (from Eq. (6.3.50)). Together with the Airy matching in the interior we end up with a continuous density in the whole space.

To complete our setup, we would like to have a quick and easy way to quantify the "classicality" of the system, i.e. the proximity to the electron

star limit and the smallness of the quantum corrections. A very good estimate is provided by the number of energy levels N in the potential well: the classical limit corresponds to $N \rightarrow \infty$ and vanishing spacing between the levels. Provided N is large, it can be well approximated by the textbook WKB formula. The estimate reads

$$N = \frac{1}{4\pi} \int_{z_*}^{z_{**}} dz \sqrt{g_{zz}} V_{eff}(z) \quad (6.3.55)$$

where V_{eff} is the effective Schrödinger potential, Eq. (6.3.37), derived in the context of the Airy function tails. From now on we will frequently use N to characterize the system at certain values of the parameters (μ, q, m) .

In Fig. 6.1 we show the full quantum corrected WKB densities obtained with the matching outlined above. These are obtained upon solving the whole self-consistent system of equations (including electromagnetic and gravitational backreaction) described in later sections. We show this here already just to illustrate of our method. In Figs. 6.1A and 6.1B, the semiclassical estimates $n_e^{WKB}(z)$ in the whole classically allowed region ($z_* < z < z_{**}$) are shown as dotted lines compared to the actual (quantum-corrected) density. Fig. 6.1C shows explicitly that N is the correct parameter that controls the size of the quantum corrections. As already argues in [19], for low N which is equivalent to the statement that the total charge density becomes of the order of the charge of the constituent fermion, the WKB approximation fails. Here we see visually that quantum corrections become dominant in this limit.

6.3.4 Pressure and equation of state in the semiclassical approximation

Following the logic behind the density calculation, we will now calculate the pressure. It will actually prove easier to write the equation of state first and then derive the pressure. We can start by computing the energy density of the bulk fermions. By definition, it reads

$$\begin{aligned} \mathcal{E}(z) &= \sum_{\lambda,l} \int_0^{2\pi} d\phi \int_0^\infty d\rho \int_0^{\mu_{loc}} d\omega \omega \Psi^\dagger(z) \Psi(z) = \\ &= \sum_{\lambda,l} \int_0^{2\pi} d\phi \int_0^\infty d\rho \int_0^{\mu_{loc}} d\omega \omega \frac{\tilde{E}(z)}{4\pi^2 q(z)} \end{aligned} \quad (6.3.56)$$

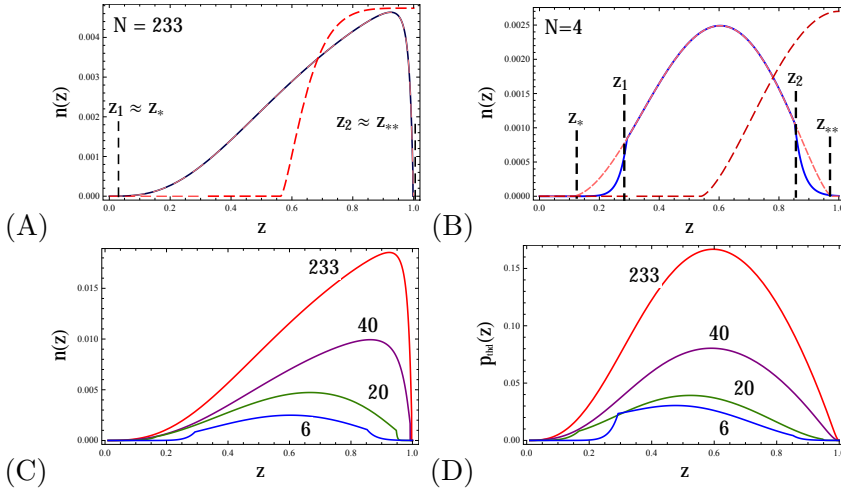


Figure 6.1: Semiclassical bulk density $n^{WKB}(z)$ (Eq. 6.3.35, dashed pink lines) and full density $n(z)$ with quantum corrections – Airy tails for large $z > z_2$ in the interior and Dirac hair for small $z < z_1$ near the AdS boundary (Eqs. 6.3.42, 6.3.53, solid blue lines). Parameter values (A) $(\mu, e, m) = (1.7, 100, 0.1)$, (B) $(\mu, e, m) = (1.7, 10, 1)$. The classically allowed region lies between the turning points z_* and z_{**} , determined by the condition of vanishing WKB momentum ($q(z_*) = q(z_{**}) = 0$). The gluing of the quantum tails to the semiclassical part is implemented according to the condition of applicability of WKB approximation, $y_0/y_{-1} = 1$, at the point z_2 for the Airy correction (Eq. 6.3.41), and at the point z_1 for the Dirac hair correction (Eq. 6.3.44). The parameters for (A) are in the classical (electron star) regime, the quantum corrections are manifestly small and the classical region almost coincides with the WKB region: $z_1 \approx z_*$, $z_2 \approx z_{**}$. The plot (B) is given to show that when the system is closer to the single particle Dirac hair approximation, $N \sim 1$, the WKB approximation fails and the quantum corrections are of the same order as the WKB part. (C) Bulk density with quantum corrections, for a range of values $(\mu, e, m) = (1.7, 100, 0.1)$ (red), $(\mu, e, m) = (1.7, 30, 0.1)$ (violet), $(\mu, e, m) = (1.7, 10, 0.1)$ (green) and $(\mu, e, m) = (1.7, 5, 1)$ (blue). For large specific charge of the fermion (and therefore a large number of WKB levels in the bulk) the solution is dominated by the classically allowed region. For smaller q/m values (and thus fewer WKB levels) the quantum correction in the near-boundary region becomes important and eventually dominates the density profile. (D) Thermodynamical pressure with quantum tails (Eq. 6.3.59), for the same parameter values as in (C).

where $\tilde{E}(z)$ is defined in (6.2.11) and the sum limits are the same as in (6.3.34). Performing the integration in a similar fashion as when computing $n(z)$ in (6.3.34-6.3.35), we obtain

$$\mathcal{E} = \frac{1}{2}e\Phi n + \frac{1}{2}f^2\tilde{M}^2\text{ArcSinh}\frac{\tilde{E}}{\tilde{M}}. \quad (6.3.57)$$

Notice that the first term exactly captures the electrostatic energy while the second is the one-loop term that encapsulates the quantum fluctuations. The above result is remarkably close to the Hartree vacuum polarization correction as it appears in various model energy functionals in literature. Now the calculation of pressure needs to be done very carefully in our semiclassical setup. It is possible to delineate two opposite regimes:

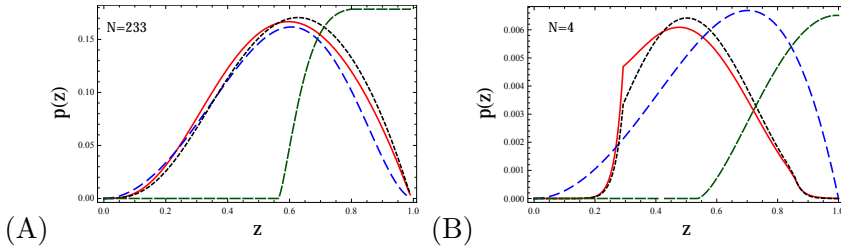


Figure 6.2: Comparison between full quantum pressure (dashed blue lines, Eq. 6.3.58) and thermodynamic pressure (solid red lines, Eq. 6.3.59) for two sets of parameters: $(\mu, e, m) = (1.7, 100, 0.1)$ (A) and $(\mu, e, m) = (1.7, 5, 1)$ (B). For comparison we plot also the fluid pressure $p = en\Phi/2$ (dashed green lines). Expectedly, all three models are close to each other for large N while for N small the level spacing is large and it is necessary to sum the contributions of individual levels: both the thermodynamic approximation and the simple fluid approximation deviate considerably from the exact sum.

1. In the deep quantum regime we can express the pressure from the microscopic fermionic Lagrangian (6.2.3). By definition it reads

$$p = \sum_{n,l,\lambda} \Psi_+^\dagger \partial_z \Psi_+ - \Psi_-^\dagger \partial_z \Psi_- + h.c. = \sum_{n,l} \frac{2l+1}{4\pi q} \frac{e^{-3h/2}}{z^2 f} C_n^2(\omega_n - \Phi) \quad (6.3.58)$$

The explicit calculation is tedious but straightforward and we leave it out. The end result involves the integral of a complicated function of

q and θ . Unlike for density case, we find ourselves unable to package it in a closed-form expression. Instead, we integrate numerically over the energy levels ω_n to obtain the function $p(z)$.

2. Deep in the classical regime, according to thermodynamics $p = \partial E / \partial V$ which generically results in a nonzero outcome. While the volume V is difficult to calculate exactly, we can obtain a crude estimate in the following way. At unit AdS radius, the volume equals the length ℓ of the classically allowed interval along z axis, i.e. the interval between the zeros of the WKB momentum $p_{max}(z) = \sqrt{\tilde{E}^2(z) - \tilde{M}^2(z)}$. From (6.2.11) we find $\ell \sim m/e\mu$, assuming neither of the two turning points is very close to the boundary or very deep in the interior. One further assumption we make is that, not too far in the interior, the gauge field is well described by the linear law $\Phi \sim \mu(1 - z)$. We thus arrive at the estimate

$$p_{thd} = \frac{\partial \mathcal{E}}{\partial \Phi} \frac{\partial \Phi}{\partial \mu} \frac{\partial \mu}{\partial \ell} \sim \frac{e\mu^2}{2m}(1 - z) \left(en + \frac{m^2 f e^{-h}}{z \sqrt{m^2 f + \Phi^2 e^{-2h} z^2}} \right) \quad (6.3.59)$$

where we have used (6.3.57). We will call this the thermodynamic pressure and denote it by p_{thd} to differentiate from the exact quantum expression (6.3.58). The expression (6.3.59) is also the equation of state of the system as it connects the pressure to the density.

The thermodynamical pressure is much more convenient computationally. In spite of its approximate nature, it yields a remarkably accurate result when compared with the exact quantum pressure. We ascribe the quantitative proximity of the results in the two cases to the fact that the differences are small in the two key regions of deep UV and deep IR. Outside the classically allowed region, we approximate the system with a single quantum-mechanical particle and calculate the pressure from the quantum equation (6.3.58). The nonzero pressure obtained in this way for the classically forbidden region is *not* the Fermi pressure (which vanishes for a non-macroscopic number of particles). It is the pressure inherent to relativistic fluids.

Finally, it is illustrative to see how we reproduce the electron star pressure [51] in the limit of large density. For $n \rightarrow \infty$, the first term in \mathcal{E} dominates and we obtain

$$p_{ES} = \frac{1}{2} \partial_z (e\Phi n) \quad (6.3.60)$$

as expected for an ideal fluid, which corresponds to the electron star approach. The physical interpretation of this result (and of the pressure inside the classically allowed region in general) is that of a Fermi gas pressure which, as we know, survives also in the limit of classical thermodynamics. The comparison of p , p_{thd} and p_{ES} is summarized in Fig. 6.2, for high and low number of levels. While all three approximations are good as $N \ll 1$, for small N both the fluid limit and the thermodynamic limit break down and the contributions of individual levels must be taken into account.

6.4 Maxwell-Dirac-Einstein system

We have now arrived at the point where we can solve our model self-consistently with the Einstein-Maxwell equations. Unavoidably, the solution is numerical, using an iterative procedure to converge toward the solution. Only in the IR region it is possible to use a scaling ansatz to estimate the scaling behavior of the metric and matter fields, akin to the procedure used in [50]. We will also see how the "quantum tails" in both IR and UV are crucial to capture at least qualitatively the full effect of backreaction. This is the first attempt at a self-consistent solution including backreaction on the geometry with holographic fermions which goes beyond the fluid picture of [51].

Fortunately, it is known how to calculate it in the fluid (i.e. electron star) approximation. The action principle for the relativistic fluid as put forward in [108] and used in [51, 52] gives the Lagrangian of the whole system (fluid plus Einstein and Maxwell background) as

$$S = \int d^4x \left[\frac{1}{2\kappa^2} (R + 6) - \frac{1}{2q^2} (\partial_z \Phi)^2 + p \right]. \quad (6.4.61)$$

In other words, the contribution of fermions reduces to the pressure p . While we do not take the fluid limit in this paper, one can suspect that in the first approximation the influence of the corrections to fluid limit ($N \rightarrow \infty$) is fully encapsulated by the correction to the classical (or fluid) pressure we found in (6.3.57-6.3.58).

Starting from the exact action (6.2.2), we replace the fermionic terms with our model for the density and pressure of the bulk fermions. The total action is represented as $S = S_E + S_M + S_f$, the sum of Einstein, Maxwell and fermionic part. The only nonzero component of the gauge

field is Φ and the only non-vanishing derivatives are the radial derivatives ∂_z (the others average out to zero for symmetry reasons). The fermion contribution is subtler. On-shell, the bulk action for the fermions vanishes because it is proportional to equations of motion. The boundary contribution is the bilinear $\bar{\Psi}\Psi$ but one can show that this vanishes too when properly regularized [19]. At the quantum level, however, there is a nonzero fermion pressure p , considered in Sec. 6.3.4, as well as nonzero (local) charge density is given by j_e^0 as

$$j_e^0 = qn\sqrt{g^{00}} = qn\frac{ze^{h/2}}{\sqrt{f}}, \quad (6.4.62)$$

The fermionic term in the effective action thus becomes

$$S_f = - \int d^4x \sqrt{-g} (j_e^0 \Phi + p). \quad (6.4.63)$$

Packaging everything together, we arrive at the effective action:

$$S_{eff} = \int d^4x \sqrt{-g} \left[\frac{1}{2\kappa^2} (R + 6) - \frac{z^4}{2} e^h \left(\frac{\partial\Phi}{\partial z} \right)^2 - j_e^0 \Phi + \sqrt{g^{zz}} p \right]. \quad (6.4.64)$$

The only components of the stress tensor the fermion kinetic energy contributes to is T_{zz} and T_{00} ; the others vanish due to homogeneity and isotropy in time and in the $x - y$ plane. From (6.4.64) we get the equations for the energy-momentum tensor:

$$T_0^0 = -\frac{1}{2} z^4 e^h \left(\frac{\partial\Phi}{\partial z} \right)^2 + j_e^0 \Phi \quad (6.4.65)$$

$$T_z^z = -\frac{1}{2} z^4 e^h \left(\frac{\partial\Phi}{\partial z} \right)^2 + j_e^0 \Phi + mn + g_z^z p. \quad (6.4.66)$$

We can now write down our equations of motion:

$$\frac{1}{\sqrt{-g}} \left(\partial_z e^{-h/2} \partial_z \Phi \right) = -j_e^0 \quad (6.4.67)$$

$$3f - z\partial_z f - 3 = T_0^0 \quad (6.4.68)$$

$$3f - z\partial_z f(z) - 3zf\partial_z h - 3 = T_z^z. \quad (6.4.69)$$

The boundary conditions for the gauge field are standard in AdS/CFT: $\Phi(z_0) = \mu$ fixes the chemical potential at the boundary ($z_0 \rightarrow 0$), while

$\partial_z \Phi(z_H) = 0$ ensures the stability of the horizon. Asymptotic AdS geometry implies $h(z_0) = 0$, while the redshift factor vanishes at the horizon, $f(z_H) = 0$ (the derivative is determined by the temperature as $\partial_z f(z_H) = T/4\pi$).³ Finally, it remains to define the units used throughout the paper. The natural unit of energy and momentum is the chemical potential μ and we will express all quantities in units of μ whenever μ is kept constant. When varying μ , we will resort to using the temperature T as the unit. The two ways are essentially equivalent as in holographic systems only the ratio μ/T has physical meaning.

Let us conclude with an outline of the numerical algorithm, which is not completely trivial. The boundary conditions to be implemented are given at different points: some are given at the AdS boundary and some at the horizon. Since the system is nonlinear, it is necessary to either linearize the system or to shoot for the correct boundary conditions with the full nonlinear system. After experimenting with both, we have decided to iterate the full, non-simplified system of equations, integrating from the horizon and shooting for the conditions at the boundary. We perform the procedure iteratively, gradually increasing the fermion charge in every iteration, and then iterating with fixed fermion charge until the convergence of the solution is achieved to the fixed set of functions, (f, h, Φ) . More explicitly, the procedure is as follows: we start with the non-backreacted AdS/RN geometry and compute the density (semiclassical plus the quantum corrections) for the electron charge equal to e/N (where e is the physical charge and N some positive integer), then we solve the system of Einstein-Maxwell equations (6.4.67-6.4.69), afterwards we increase the fermion charge to $2e/N$, calculate the charge density in the background (f, h, Φ) taken from previous iteration and solve for this density Einstein-Maxwell equations (6.4.67-6.4.69). We repeat this procedure for charge $3e/N$, $4e/N$ etc. After N iterations we have arrived at the physical value of the charge e . Then we do more iterations with fixed charge e to ensure that the solution has converged, checking that the set of functions (f, h, Φ) does not change from iteration to iteration. In this way we achieve the self-consistent numerical solution of the Maxwell-Dirac-Einstein system of

³At zero temperature, when the horizon vanishes due to fermionic backreaction (this includes also the case of Lifshitz geometry), the boundary condition for f guarantees also the smoothness of the solution on the horizon: $\partial_z f(z_H) = 0$. This condition ensures that we pick the correct branch of the solution as there are typically two families of functions $f(z)$ that satisfy the equations of motion and the condition $f(z) = 0$. One of them has a vanishing derivative whereas the other has finite derivative as $z \rightarrow 1$.

equations. The integration is always done from the horizon, shooting for the conditions for Φ and h at the boundary, since it is well known that integrating from the AdS boundary is a risky procedure as it is next to impossible to arrive at the correct branch of the solution at the horizon.

6.5 Phases of holographic fermions

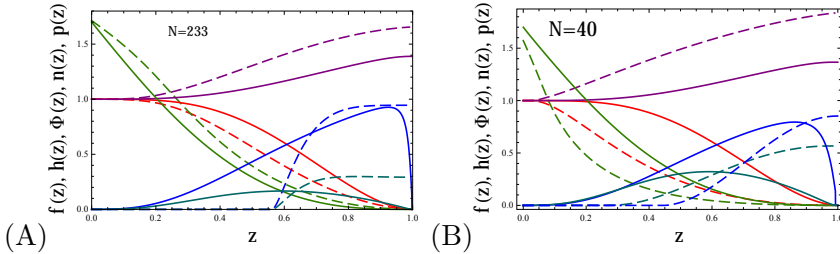


Figure 6.3: Profiles of the metric functions $f(z)$ (red) and $e^{h(z)}$ (violet), the gauge field $\Phi(z)$ (green), density $n(z)$ (blue) and the pressure $p(z)$ (cyan) at zero temperature, for $(\mu, e, m) = (1.7, 100, 0.1)$ (A) and for $(\mu, e, m) = (1.7, 10, 0.1)$ (B). Solid lines are calculated from our model while dashed lines are the electron star solution for the same parameter values. For better visibility density and pressure are rescaled by a constant factor. Near the boundary we always have $h(z) \rightarrow 0$ and $\Phi(z) = \mu + O(z)$, in accordance with the universal AdS asymptotics of the solution but in the interior the solutions start to deviate. Most striking is the absence of sharp classical edges in density and pressure. The difference in pressure will turn out to be crucial in moving away from the fluid limit. Here we have not shown the solution with $N = 4$: this case deviates from the electron star ($N \rightarrow \infty$) so strongly that it does not make sense to compare it. Indeed, $4 \ll \infty$!

We can now analyze the structure of both the bulk and the field theory side as a function of the parameters μ , e and m . We first shortly discuss the nature of the bulk solution for the geometry and gauge field and notice some qualitative properties. Afterwards we study the structure of the phase diagram using the thermodynamical quantities as the guiding principle, and corroborate these findings with spectral functions. As a result we will be able to draw the phase diagram.

The typical way that the solutions to the Dirac-Maxwell-Einstein system (6.4.67-6.4.69) look like, including the quantum tails in both UV and IR for the density $n(z)$, is illustrated in Fig. 6.3. The near-horizon scaling

of the metric and gauge field is of Lifshitz type, as expected in the light of earlier models [50, 51]. It is illustrative to make a comparison with the simpler models of Dirac hair and electron star. The metric functions f and h of all three models converge toward each other near the boundary, and the gauge field Φ remains close to the non-backreacted RN setup [18, 51]. This gives hope that these approximations can provide a decent estimate of important quantities on the CFT side since these are not overly sensitive to the precise modeling of the fermionic condensate in the interior. In addition, the Dirac-hair-like quantum correction reproduces the finite density tail near the boundary, crucial for thermodynamics.

6.5.1 Thermodynamics

We can now use these full solutions to determine the macroscopic characteristics of the dual strongly coupled fermion system. Let us first derive the free energy of the boundary field theory. According to the dictionary, it is equal to the (Euclidean) on-shell action, which contains both bulk and boundary components:

$$F = S_{bulk}^{on-shell} + S_{bnd}^{on-shell}. \quad (6.5.70)$$

We have already discussed the bulk action in the previous section. We will approximate the fermionic contribution (6.4.63) by its leading term, pressure. Notice that we do not disregard backreaction to the metric and gauge field, i.e. we calculate the exact value of the gravitational and gauge field action, and then add the fermionic component approximating it with p .

The boundary action encapsulates the regularizing terms that eliminate the divergences and the von Neumann boundary condition for the gauge field:

$$S_{bnd} = \oint_{\partial AdS} \sqrt{-h} \left(\frac{1}{2} n_\nu F^{\mu\nu} A^\mu + \bar{\Psi}_+ \Psi_- \right), \quad (6.5.71)$$

with h being the induced metric on the boundary ($h = \frac{1}{z^2}(-1/f(z = 0), 1, 1)$) and Ψ_+ and Ψ_- are radial projections of the wave function as in Eq. (6.2.7). By ∂AdS we have denoted the boundary of the AdS space. Their asymptotics at the boundary are given by

$$\Psi_+ = \frac{i\mu\gamma^0}{2m+1} B_- z^{5/2+m} + \dots, \quad \Psi_- = B_- z^{3/2+m} + \dots \quad (6.5.72)$$

as noticed in the subsection III E. In our system, the electromagnetic boundary term reduces to $\Phi \partial_z \Phi|_{z=0} = -\mu\rho$, where ρ is the total boundary (not only fermionic) charge density, read off from the subleading “response” of the bulk electrostatic potential $\lim_{z \rightarrow 0} \Phi(z) = \mu - \rho z + \dots$. The regularized boundary action now reads

$$S_{bnd} = \lim_{z_0 \rightarrow 0} S(z_0) + \lim_{z_0 \rightarrow 0} \int d^3x \left[\frac{3\mu}{2(2m+1)} \bar{B}_- i\gamma^0 B_- z_0^{1+2m} - \frac{1}{2}\mu\rho \right], \quad (6.5.73)$$

and the total on-shell action, i.e. the free energy can be written as

$$F = \int_{z_0}^{z_H} dz d^3x \sqrt{-g} \left[R + 6 + \frac{ze^{h/2} qn\Phi}{2\sqrt{f}} + p \right] - \frac{1}{2}\mu\rho + \frac{\mu}{2(2m+1)} I(z_0) z_0^{1+2m}, \quad (6.5.74)$$

where we exploit the definition of the bilinear I from Eq. (6.3.47)⁴. Notice that the last term in the free energy (6.5.74), coming from the fermionic term in the boundary action (6.5.73), vanishes in the limit $z_0 \rightarrow 0$, i.e. at the boundary. Therefore, it does not influence the free energy and we include it only for completeness.

6.5.2 Constructing the phase diagram

Let us first briefly describe the role of different control parameters. One obvious parameter is the temperature T which drives the thermal phase transitions. In the limit $T \rightarrow 0$, we can determine the nature of the ground state and possible quantum phase transitions between them.⁵ The parameters that determine the ground state are μ , e and m . Current wisdom suggests that the phases of the system are primarily sensitive to the ratio e/m [19]. Another convenient parameter is the “effective chemical potential”

$$\frac{\mu_{eff}}{T} \equiv \frac{e\mu}{mT} \quad (6.5.75)$$

motivated that only the combination $e\mu$ appears in the Dirac equation. We will also sometimes look at μ_0 , the threshold chemical potential for nonzero

⁴In Eq. (6.5.74) the kinetic term for the Maxwell field $\sim \partial_z \Phi^2$ is transformed through partial integration into $\sim \Phi \partial_{zz} \Phi$ which is then transformed into $\sim n\Phi$ using the Poisson equation

⁵Our numerical approach is not convenient at strict zero temperature. However, it is known that quantum phase transitions can be detected also at small but finite temperatures.

bulk density and the formation of a Fermi surface on the field theory side. Its value at $T = 0$ is easily determined either by tracking the emergence of a solution with finite bulk density n , or by looking at the formation of a quasiparticle peak in the spectrum (see the next subsection). Finally, we have already argued that the parameter $N(\mu, e, m)$ that controls the classical/quantum regime is another convenient parameter. An alternate parametrization of the phase diagram is therefore μ_{eff} , N and m .

First order thermal phase transition to RN-AdS

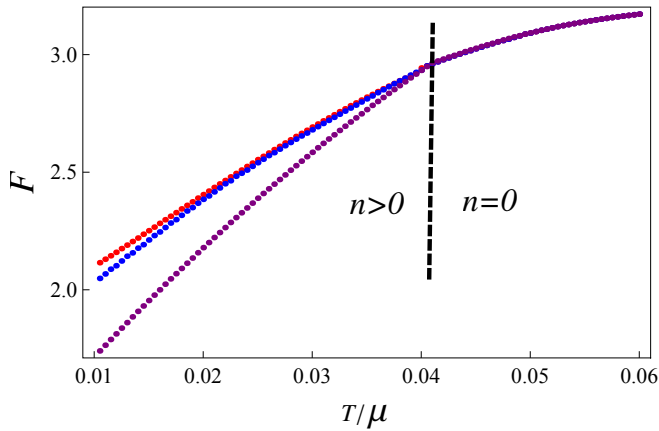


Figure 6.4: Free energy as a function of temperature $F(T)$. The abrupt change of the derivative signifies the first order transition between the finite density phase and the pure black hole (with zero bulk fermion density), in line with the analytical prediction of the first order transition from the second term in the bulk free energy in Sec. 6.5.2. We show the calculations for three different values (μ, e, m) of the system parameters: $(1.7, 30, 0.1)$, $N(T = 0) = 40$ in red, $(1.7, 10, 0.1)$, $N(T = 0) = 20$ in blue and $(1.7, 10, 0.7)$, $N(T = 0) = 11$ in violet. In the high temperature (RN) phase the curves $F(T)$ fall on top of each other as one expects for the RN black hole with $n = 0$. The behavior in the low-temperature phase (with non-zero density) is different for the three curves as the value of the charge affects the behavior of the bulk fermions. For presentation purposes, the curves have been rescaled to the same transition temperature; in general, however, $(T/\mu)_c$ is *not* universal and will differ for different corners of the parameter space.

At high temperature the preferred state of the system is the charged

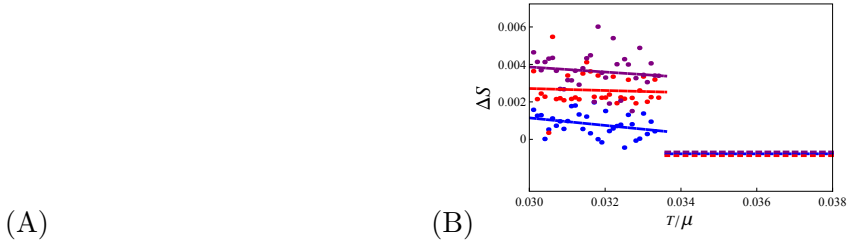


Figure 6.5: (A) Free energy (rescaled and centered to common value at the transition point) for the same parameters as in Fig. 6.4, in the vicinity of $T = T_c$ (*not* for the whole range of temperatures). The cusp characteristic of a first order transition is now clearly visible. The value of F on the RN side ($n = 0$) is without error bars as the thermodynamic functions of the black hole can be exactly calculated. Notice how the slope of F in the low-temperature phase decreases as the number of levels increases: for $N \rightarrow \infty$ we reach the electron star limit when the transition becomes continuous. (B) Difference between the entropy of the RN black hole and the entropy of the system $\Delta S = S_{RN} - S$, where entropy is obtained from free energy as $S = -\partial F/\partial T$, for the same parameters and in the same color schemes as in Fig. 6.4 and panel (A). The first order nature of the transition is recognized from the jump ΔS at the critical point. Notice that the difference is positive for $T < T_c$, and thus the high temperature phase has more entropy as expected. The entropies in the RN/local quantum critical phase are exact, as they are calculated from the exactly known RN solution at given chemical potential. They are thus represented by a single (black) set of data points. The entropy is in relative (computational) units.

AdS black hole rather than a finite bulk fermion density configuration. This AdS-RN black hole describes a local (momentum-independent) quantum critical phase which generically has no Fermi surfaces. At low T/μ one finds several non-Fermi-liquid Fermi surfaces [79, 17, 27, 63], but this should be where the instability to the finite density system sets in. Fig. 6.4 shows the behavior of the free energy $F(T)$ in a broad range of temperatures, encompassing both the low and the high temperature phases for different parameters e, μ, m . The cusps in the dependence $F(T)$ correspond to the points of a first order phase transition (where the derivative $\partial F/\partial T$ experiences a jump). In the high temperature phase the dependence $F(T)$ is the same for different electron charges at given chemical potential as there are no fermions in the bulk and the solution is determined only by the temperature and the chemical potential at the boundary. In low temperature phase the free energies, although close, are distinct. Fig. 6.5A

shows the free energy in the vicinity of the phase transition and we can clearly see the cusp in the function $F(T)$ signalling the *first order phase transition*. To further corroborate the first order nature of the transition, we plot the entropy $S = -\partial F/\partial T$ in Fig. 6.5B for the same parameters as in Fig. 6.4 and 6.5A. To better show the transition, entropy is plotted with reference to its value for the black hole, as $\Delta S = S_{RN} - S$. Notice that the jump of the derivative $\Delta S(T)$ is positive for $T < T_c$, as it should be, as the system evolves toward maximizing its entropy.

A first order transition between a zero/nonzero bulk density can be explained from general analytical considerations. Starting from low temperatures, at the transition point the bulk density n vanishes. In our model that means that the turning points coincide: $z_* = z_{**}$. In this limit we are able to analytically predict the order of the transition in the following way. Assuming that the transition is dominated by the behavior of the fermions, the relevant part of the free energy of the system is given by $\mathcal{F} = \int_0^{z_H} dz \mathcal{E}(z)$. Since the bulk matter lives at zero temperature, all thermodynamical potentials are equal and the free energy is just the total (internal) energy of the system. The first ("electron star") term in the energy, $e\Phi n/2$ is analyzed in detail in [52] and is concluded to yield the scaling $\mathcal{F} \sim (T - T_c)^3$. We will now analyze the second, Hartree term, $f^2 \tilde{M}^2 \text{ArcSinh}(\tilde{E}/\tilde{M})$. The vanishing of the classically allowed region means $\tilde{E} \approx \tilde{M}$ in the whole (narrow) region $z_* < z < z_{**}$. One can thus expand $\tilde{E} = \tilde{M} + \delta z \times \delta \tilde{E}/\delta z + \dots$ and analyze the leading terms in δz . It is easy to see that its expansion starts from a constant: $\text{ArcSinh}(\tilde{E}/\tilde{M}) = \text{const.} + O(\delta z)$, where $\delta z = z_{**} - z_*$. Its integral thus scales as $\mathcal{F} \sim \delta z$. Now, for a vanishing bulk charged fluid/emerging charged black hole, the principle of detailed balance predicts that the charge of the former equals the charge of the latter: $n\delta z = n_{BH}\delta z_H$, where the charge densities of the bulk and the black hole are n and n_{BH} , respectively, and δz_H is the change in the position of the black hole horizon. The crucial insight is that the densities can be assumed constant for vanishing δz and δz_H . We thus find $\delta z \sim \delta z_H \sim T - T_c$. The conclusion is that

$$\mathcal{F} \sim T - T_c \tag{6.5.76}$$

and *the transition is always of first order*. The final subtlety is that we have now analyzed the bulk free energy: the boundary free energy F (evaluated as the bulk on-shell action) is distinct from it. However, the

difference $F - \mathcal{F}$ cannot have terms of order lower than linear in $T - T_c$. We thus conjecture that the thermal transition from a bulk fermionic system to a black hole is generically of first order.

The numerics confirms the prediction of the first order phase transition. The field theory interpretation of the discontinuous nature of the transition to a phase with Fermi surfaces is simple: fermions do not break any symmetry but the discharge of the black hole does signify that the ground state is reconstructed due to formation of a rigid Fermi surface. The only way to reconstruct the ground state without breaking any symmetries is precisely the first order transition of the density van der Waals liquid-gas type. This is the interpretation put forward in [18] for the first order transition from Dirac hair to RN state. We find here that this conclusion stays valid even for large values of n , in contrast to [52]. These papers study the birth of a (classical) electron star upon reducing the temperature and find a continuous, third order, transition. The crucial Hartree term in \mathcal{F} is absent in the classical electron star limit, leaving only the continuous transition from the electrostatic energy $en\Phi$. As the Hartree term will be present for any finite value of n , no matter how large, these results indicate that the physical transition in the strongly coupled fermion system is indeed of first order.

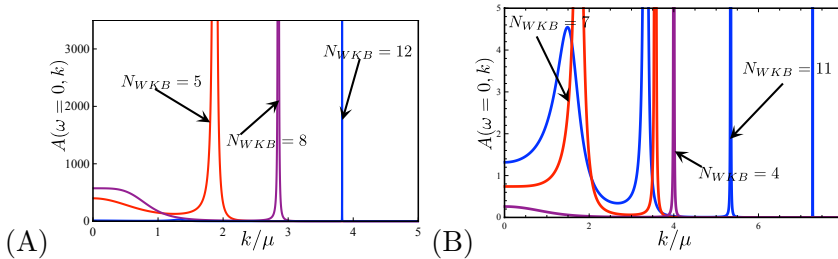


Figure 6.6: The emergence of Fermi surfaces seen in MDCs $A(\omega = 0, k)$ upon dialing $\mu = 0.8, 1.0, 1.2$ (red, violet, blue), in (A) for $(e, m) = (10, 1)$, and in (B) for $(e, m) = (30, 5)$. The sharp peaks at some $k = k_F$, present for higher values of the chemical potential reveals the Fermi surface with Fermi momentum k_F . Remarkably, the emergence of a Fermi surface coincides with critical values of μ for which the RN black hole is replaced by a finite density solution. The obvious difference between (A) and (B) is that in the former case only one (generically, few) Fermi surface can form while in the latter the number of Fermi surfaces grows rapidly with further increasing μ . The numbers in the figure (pointing on the curves) give the level count N .

In order to further explore the physical meaning of different phases on the field theory side, we will study also the spectra of the fermion in each of the phases. The central object here is the spectral weight $A(\omega, k)$ which can be defined in terms of the retarded propagator G_R :

$$A(\omega, k) = \text{Tr} \Im G_R(\omega, k). \quad (6.5.77)$$

To obtain $A(\omega, k)$ we solve now the equations of motion for a probe fermion in the background obtained from the self-consistent solution of the bulk equations. From this one can construct the retarded propagator G_R on the field theory side and compute the spectral function. The appropriate procedure is well established by now [79, 17] and we will only briefly summarize it. The solution to the bulk Dirac equation (6.2.5) can be expanded near the boundary as

$$\Psi_+ = A_+ z^{3/2+m} + B_+ z^{5/2-m} + \dots, \quad (6.5.78)$$

$$\Psi_- = A_- z^{3/2-m} + B_- z^{5/2+m} + \dots \quad (6.5.79)$$

According to the holographic dictionary, the retarded propagator equals the ratio of the VEV (subleading term in Ψ_-) and the source (leading term in Ψ_+):

$$G_R = z_0^{2m} B_- A_+^{-1} \quad (6.5.80)$$

where the prefactor is just the regularization at some $z = z_0$. Following [79], we package the equation of motion into a single nonlinear equation for the ratio $B_- A_+^{-1}$. At zero temperature, Fermi surfaces are always located at $\omega = 0$ [79, 27] and they are most easily found by studying the momentum distribution curves (MDCs) at zero energy, $A(\omega = 0, k)$.

We can now confirm that finite/zero density phases are indeed roughly equivalent to presence/absence of Fermi surfaces. Extensive calculations of spectra in the vicinity of the critical μ/T or the critical temperature show that the finite density phase *always* has at least one Fermi surface on the field theory side while the zero density phase *generically* has no Fermi surfaces. This is expected: Fermi surfaces are signalled in the bulk by the existence of quasinormal modes, only if there are (quasi)normalizable modes in the spectrum can we have a finite bulk fermion density, a finite bulk fermion density implies also finite boundary density, and finite fermion density in field theory implies the existence of Fermi surfaces. Emergence of Fermi surfaces from the quantum critical (RN) phase is observed in Fig. 6.6 for the low- and high μ_{eff} case, or roughly for an

electron star at birth and a Dirac hair at birth from a bald RN black hole. In the first case (Fig. 6.6A), a single Fermi surface emerges at μ_{eff}^{crit} and remains stable, while in Fig. 6.6B increasing μ_{eff} leads to the emergence of an ever increasing number of Fermi surfaces. Both cases belong to the low temperature phase from Figs. 6.4-6.5. The difference between the two regimes of this phase we will study later in this subsection.

Continuous quantum phase transition to RN-AdS

The second axis of the phase diagram is the conformal dimension Δ , i.e. the bulk mass m . Studies of the electron star [51, 53] suggest that the appropriate control parameter is actually the charge to mass ratio e/m : electron star is the thermodynamically preferred solution for high e/m values. We see from the expression for WKB density (6.3.35) that increasing the fermion mass or reducing fermion charge reduces the semiclassical region and the total bulk charge. The electron star reasoning likewise suggests that the finite density ground state corresponds to high values of e/m . For some threshold value $(e/m)_c$ the electron star vanishes [51] and the RN solution is preferred.

We will now consider in some detail the quantum phase transition from AdS-RN zero density regime to the finite density phase. Let us first summarize what is known. The near-horizon geometry of the RN black hole is described by AdS₂ throat. The conformal dimension of the corresponding IR CFT is [27]:

$$\nu_k = \sqrt{\frac{m^2}{6} + \frac{1}{2} \left(\frac{k}{\mu}\right)^2 - \frac{e^2}{12}}, \quad (6.5.81)$$

For $e < m\sqrt{2}$ we have $\nu_k^2 > 0$ for any momentum value (including $k = 0$), implying that the bulk geometry is stable. For $e > m\sqrt{2}$, the conformal dimension ν_k becomes imaginary. According to [63, 87], this region is unstable due to pair creation near the horizon. Accordingly, one expects finite bulk density to form for $e > m\sqrt{2}$, leading to backreaction and disappearance of AdS₂ throat. However, to the best of our knowledge, this was not checked explicitly so far in the Einstein-Maxwell-Dirac setup. Using our WKB method we will now study the appearance of finite bulk density and its consequences on field theory side.

The dependence of the free energy on the conformal dimensions Δ with other parameters fixed is given at Fig. 6.7. We have marked with dashed

lines the critical values of the conformal dimension Δ_c when a nonzero bulk density $n(z)$ appears. The free energy does not reveal any singularity at these points. Nevertheless, they can be identified as the points where the dependence $\mathcal{F}(\Delta)$ deviates from the straight line $\mathcal{F}(\Delta) = \text{const.}$ – free energy of a pure RN black hole clearly does not depend on the fermion. In the zoom-in near Δ_c (Fig. 6.7(B)) we find that the behavior of free energy is consistent with the BKT form:

$$\mathcal{F}(\Delta) - \mathcal{F}(\Delta_c) = \text{const.} \times e^{-\frac{\text{const.}}{\sqrt{\Delta_c - \Delta}}}. \quad (6.5.82)$$

The BKT nature of the phase transition can be related to the RG interpretation of the oscillatory regime. The effective Schrödinger potential in AdS₂ regime is proportional to $1/r^2$ [28]. This form of potential gives rise to RG limit cycles [85]. Finally, it is known that the system generically experiences a BKT phase transition when the RG flow with a limit cycle becomes unstable [106]. One can therefore argue that the BKT transition we observe appears as a consequence of the exiting from RG limit cycle behavior in the bulk.

In order to understand what drives the instability of the RN regime and to what it corresponds in field theory, it is helpful to look at the spectra (Fig. 6.8). By stacking together MDCs for different Δ values we can easily follow their evolution: the sharp, narrow maximum corresponding to the quasiparticle peak vanishes at Δ_c simultaneously with disappearance of n . This again suggests the generic absence of critical Fermi surfaces immanent in the RN setup [17, 79]: the quantum phase transition separates the ES/DH phase with stable quasiparticles from AdS₂ metal with no quasiparticles at all.

Crossover between low and high density phases

Now we will take a closer look at the low temperature finite density phase. This is the parameter regime where earlier models [18, 51, 19] anticipate the emergence of regular Landau Fermi surfaces. These models predict a single Fermi surface for low fermion charge [19] while, according to [53], the regime of high fermion charge describes a "deconfined" phase with a multiplicity of Fermi surfaces, with fermions of different flavors. The question arises if the two regimes are thermodynamically distinct and if so, separated by a critical point or by a crossover. To that end we plot the free energy as a function of the effective chemical potential $\mu_{eff} = e\mu$.

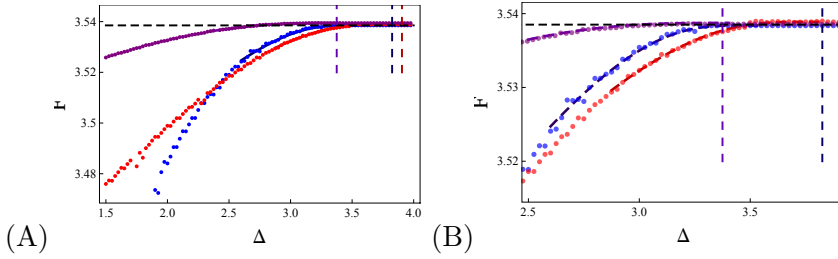


Figure 6.7: (A) Free energy as a function of the conformal dimension $\Delta = 3/2 + m$, for $(\mu, e) = (1.7, 20)$ – blue, $(1.0, 20)$ – red and $(1.0, 5)$ – violet. Numerically, the curves are smooth and all derivatives $\partial^k F / \partial^k \Delta$ are finite. We identify the transition points as the values Δ_c when the fermion density $n(z)$ vanishes identically and mark the corresponding values in the figure. Both the look of the curves and the analytical reasoning, i.e. the lack of two independent scales that could compete as in a crossover, are consistent with a BKT transition. (B) Zoom-in near the transition points with analytical plots of the BKT scaling relation $F \propto \exp(-\text{const.}/\sqrt{\Delta - \Delta_c})$. The numerical data are fully consistent with the BKT scaling.

Remarkably, all four curves fall on top of each other for small charges, where the background is close (though not identical) to AdS-RN. The curves are smooth in the whole region. The absence of a cusp in $F(\mu_{eff})$ definitely discards the possibility of a first order transition, the distinction between a continuous transition and a crossover is difficult to make. Analytical arguments however strongly suggest the crossover. To see why, remember that the (thermodynamically defined) density $n_{th} = \partial F / \partial \mu$ is an analytic function of the solutions to the Einstein-Maxwell system $(f(z), h(z), \Phi(z))$. We thus expect all higher derivatives $n = \partial^k F / \partial \mu_r^k$ ($k = 2, 3, \dots$) to be continuous as well. In addition, the simplest physical interpretation of increasing μ_{eff} is that of increasing the number of bulk fermions by filling increasingly higher levels in the effective potential well (6.3.37). One can expect a substantial change of the behavior of the system as the potential well is filled but not a discontinuity of the thermodynamical functions (e.g. [77]). We can thus conclude that *a crossover separates a Dirac-hair-like region from the electron-star-like region*.

At first sight just the change in the number of occupied states should not affect any thermodynamic properties. We will argue below that the cause of the crossover is the change of the scaling behavior of the quasiparticle width. Notice that the function $F(\mu_{eff}/T)$ keeps the same convexity

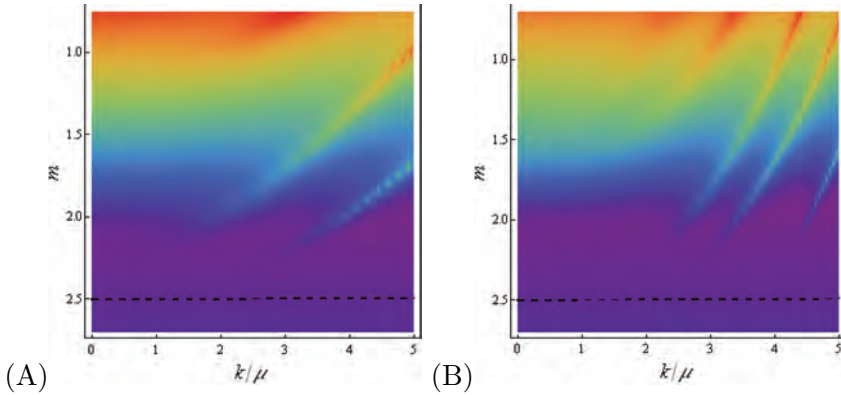


Figure 6.8: (A) MDC spectra at $\omega = 0$ for $(\mu, e) = (1.0, 5)$ and varying Δ . Curves for different Δ values are stacked on top of each other to represent the evolution of the spectrum with Δ . To better show the Fermi surfaces we use the logarithmic color scale, i.e. the color value is proportional to $\log A(\omega = 0, k)$. Crucially, the Fermi surfaces (lines of lighter color) disappear at $\Delta = \Delta_c$, simultaneously with entering the RN phase. Dashed line delimits the area within which bulk density is nonzero and the system backreacts away from AdS-RN (it is parallel to the k axis as the presence of nonzero bulk density does not depend on the momentum of the probe fermion). We can conclude that the formation of a Fermi surface indeed drives the instability of the RN background to a new, finite density phase. In (B), we show for comparison the MDC curves for the same parameter values without backreaction, i.e. in the AdS-RN background. In RN background the number of Fermi surfaces is larger (we see four Fermi surfaces). However, both in (A) and (B) there are no Fermi surfaces below the dashed line.

as in Fig. 6.4: the argument of the function is increasing in Fig. 6.4 and decreasing in Fig. 6.9, hence the increasing/decreasing trend in the function.

The dispersion of the energy distribution functions (EDCs) for momenta in the vicinity of the Fermi momentum yields a better insight into the physical meaning of the finite density phases. It is here that the crossover from Dirac hair to electron star becomes most obvious: the few Fermi surfaces of Dirac hair regime exhibit a broader power law scaling of self-energy $\Im\Sigma \sim \omega^{2\nu}$ with $\nu = 1$ to high accuracy while the many Fermi surfaces of the electron star are exponentially sharp: $\Im\Sigma \sim e^{-1/\omega}$ (Fig. 6.10). The latter scaling was predicted in [26] and confirmed in [53], while the former was postulated on general grounds in [18]. Importantly,

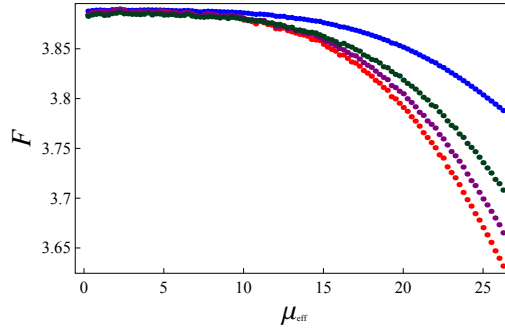


Figure 6.9: Free energy as a function of the fermion charge e in the crossover region for $(\mu, m) = (2.2, 0.5)$ – red, $(1.0, 0.5)$ – violet, $(1.7, 1.0)$ – green and $(1.7, 5.0)$ – blue curve and for a range of fermion charge values. On the abscise we plot the effective chemical potential $\mu_{eff} = e\mu$. The temperature is kept fixed at $T = 0.0005$. All four cases exhibit a crossover about the same value of μ_{eff}/T ($\mu_{eff}^{cross}/T \approx 20$), suggesting that μ_{eff} is indeed the key quantity that drives the changes of the Fermi surface. The low- μ_{eff} region is a few-Fermi-surfaces DH-like system while the high- μ_{eff} regime describes an ES-like multiplet of Fermi surfaces. We will later study in more detail the dispersion properties of the two regimes. Apart from the gradual and soft nature of the transition as seen from the numerical curves, the crossover (as opposed to phase transition) nature of the phenomenon also follows from analytical considerations. The dependence of the solution $(f(z), h(z), \Phi(z))$ on the parameters of the system (μ, q, m) is analytical, which strongly suggests that the derivatives of the free energy $\partial^k F/\partial \mu^k$ are continuous to all orders $k = 2, 3, \dots$

no unstable or underdamped Fermi surfaces (with self-energy scaling as $\Im\Sigma \propto \omega^{2\nu}$ with $\nu < 1/2$) are found: these seem to be the artifacts of the probe limit and will not arise in a self-consistent approach (with backreaction).

6.5.3 Phase diagram

We are now in the position to summarize our findings in the form of a phase diagram. In Fig. 6.11(A) we give three-dimensional phase diagram which includes all three independent parameters – μ/T , e and m , while the ”reduced” phase diagram with only two parameters, $e\mu/T$ and Δ , is given in Fig. 6.11(B). At high temperatures the system is always in the zero density quantum critical AdS-RN phase. Dialing $e\mu$ at fixed temperature

Figure 6.10: Imaginary part of the self-energy of the quasiparticle in the immediate vicinity of $\omega = 0$ for $e = 5, 15, 50$ (red, green, blue). It shows the crossover from power-law (solid line) (red line) to exponential. The self-energy of the quasiparticle undergoes a transition from quadratically damped peaks ($\Im\Sigma \sim \omega^2$, red points) toward exponentially narrow poles ($\Im\Sigma \sim e^{-1/\omega}$, blue points). Notice that the all three peaks are stable: the power-law exponent is $\nu = 1$ with high accuracy, signalling a normal Fermi liquid phase.

toward larger and larger values, the Fermi surfaces proliferate until the point of crossover, when the peaks become exponentially sharp. The true nature of this system is not yet known in detail ⁶. We have already suggested such a diagram in [19] based on the analysis of the two extreme limits. Here we have gone further and analyzed quantitatively also the intermediate regimes. The structure of the phase diagram can now be summarized as follows:

1. *Van der Waals transition*, Fig. 6.11(A), Fig. 6.5. There is universally a the first order (van der Waals) transition from finite to zero density phase upon dialing μ/T and thus filling the levels of the bulk fermionic system. In field theory, this means a liquid-gas transition between the Fermi liquid(s) and the disordered phase, devoid of quasiparticles and dominated by slow conformal dynamics. Interestingly, the quantum corrections to the density and pressure are crucial for the discontinuous nature of the transition: in the electron star limit, as shown in [52], the transition becomes continuous.

⁶Reference [97] interprets it as fractionalized Fermi liquid

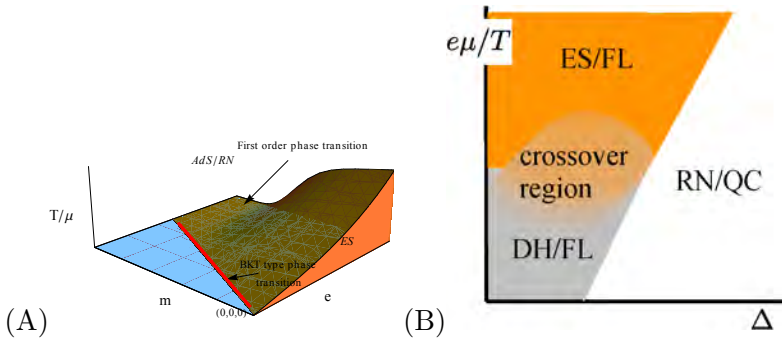


Figure 6.11: (A) Three dimensional phase diagram $(e, m, T/\mu)$. The phase transition from finite density phase to AdS-RN phase is a first order phase transition in contrast to zero temperature BKT-type phase transition. (B) Phase diagram in $(e\mu/T, \Delta)$ plane, based on thermodynamics and spectra, at zero temperature. The two regimes with stable quasiparticles are denoted with different colors: electron star (ES), describing (likely) a "Russian doll" of stable Fermi-liquid-like quasiparticles (ES/FL), and Dirac hair which is closer to normal Fermi liquid (DH/FL). The third regime, for large Δ , is the RN black hole with its quantum critical Fermi surfaces and no quasiparticle.

2. *Quantum phase transition*, Fig. 6.11(B), Fig. 6.7. There is a continuous (likely BKT) transition from finite to zero density phase upon dialing the conformal dimension Δ at fixed fermion charge (or equivalently varying the ratio m/e , or equivalently varying the fermion charge e or the total charge Q at fixed Δ). The fact that the Fermi-liquid-like quasiparticles vanish in the high Δ /low e regime is known from the electron star limit and not surprising on basis of general arguments (bulk density in the classical approximation drops with increasing m/e). However, our finite level spacing correction to electron star makes it possible to study the transition region in detail, and shows a nontrivial outcome: the transition is of BKT type, and happens inside the oscillatory (pair-creation) region.

3. *No Fermi surfaces in AdS₂ metal phase.* The transition happens at such parameter values which, on the AdS-RN side of the transition, correspond to absence of Fermi surfaces, i.e. imaginary IR conformal dimension ν . The system thus passes directly from a Fermi-liquid-like phase into a profoundly different, exotic phase that we call AdS₂ metal, and which was studied in detail in [27].

At constant temperature, the finite density phase exhibits analytic behavior of the free energy and has no phase transitions but shows a clear crossover between the single-Fermi-surface, Dirac hair limit and the infinity of Fermi liquids in the electron star limit. Thermodynamically the crossover is explained by the change in quasi-particle width $\Im\Sigma$ from power-law behavior in the Dirac-hair-like quantum regime with $N_{WKB} \lesssim 10$ to exponential suppression in the semi-classical electron star like regime with $N \gg 10$.

We will finish this section with a look towards real-world examples of such phase diagrams. Condensed matter literature offers a vast landscape of strongly coupled Fermi liquids like our DH phase, e.g. in the context of heavy fermions [80]. However, the properties of the electron star ("Matryoshka" or "Russian doll") phase are not easy to relate to the real-world examples. In part, it is a consequence of the large- N limit in AdS/CFT which, for example, leads to an exponentially small self-energy. The hope is that finite- N corrections would eventually lead to a realistic picture of the ES phase, while the DH, perhaps with some modifications of the geometry, would correspond to normal metals.

6.6 Discussion and conclusions

In this paper we have constructed a semiclassical model with quantum tails of holographic fermions in AdS₄ space, aimed at understanding the phase diagram of strongly coupled Fermi and non-Fermi liquids. The model uses WKB approximation in the classically allowed region, complementing it with quantum-mechanical estimates of the fermionic wave function in the classically forbidden region. Introducing the pressure into the essentially quantum mechanical model we get the Hartree quantum correction ("vacuum polarization") of the classical model – the electron star. This approach has allowed us to address the intermediate fermion charges which cannot be modeled satisfyingly with any of the previously used models.

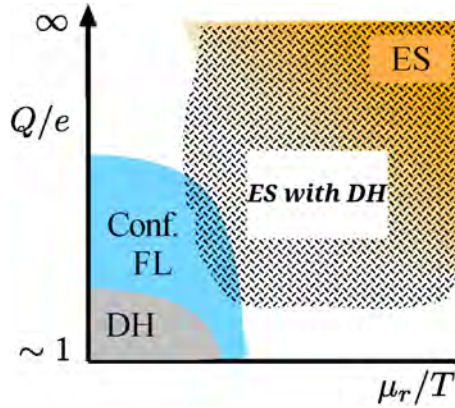


Figure 6.12: Applicability of various approximations as a function of $\mu_r \equiv e\mu/m$ and the ratio of the fermion charge and the total charge of the system, e/Q : Dirac hair, electron star, confined Fermi liquid and our present model. Dirac hair and electron star are the simplest and most flexible approximations but limited to extreme corners of the μ_r axis.

By studying the free energy of the system as well as the spectra and the number of Fermi surfaces we have constructed the phase diagram of the system and analyzed the phase transitions. Most importantly, we find a *universal first order phase transition from finite density to zero density (Reissner-Nordström, quantum critical) phase*. The discontinuity of the density comes from the quantum term in the internal energy. This term is always present but its relative contribution to the free energy decreases with the inverse of the fermion charge as $1/e$. The extreme limit $e \rightarrow \infty$ thus reproduces the continuous phase transition found in [52]. Nevertheless, in any real system with finite fermion charge the discontinuity will be present, which fits neatly into the general expectation that the thermal phase transition of a fermionic system should be of van der Waals (liquid-gas, Ising) type.

The finite density phase is further divided into two regimes corresponding to low and high values of the ratio $e\mu/m$ or, more precisely, level number N , that encompass the known limits of Dirac hair [18] and electron star [51]. The transition manifests itself as a line of crossover points which end with a BKT quantum phase transition to the RN phase. The BKT transition fits nicely in the RG interpretation of holography in the following way. Firstly, the log-oscillatory region studied in [27] can

be understood as a limit cycle of RG describing a conformal quantum mechanical system (i.e. a conformal theory in $1 + 1$ dimensions) [106]. Then, instability of the limit cycle generically happens through a BKT transition.

It is illustrative to discuss our model in some more detail in the context of earlier work in the field: electron star [51], Dirac hair [18] and the confined Fermi liquid [96]. All models use the same microscopic action, however they differ in the approximations made in order to solve it. It is helpful to introduce a combination of all parameters e, μ, m that one might dub "reduced chemical potential":

$$\mu_r \equiv \frac{e\mu}{m}. \quad (6.6.83)$$

Electron star is the fluid limit of the equations of motion, yielding the Openheimer-Volkov equations in the bulk. As explained in [19], this approximation is valid in the limit of large chemical potential: $\mu_r \rightarrow \infty$. Dirac hair makes the opposite assumption, treating the bulk fermion as a single collective excitation, which becomes exact in the limit $\mu_r \rightarrow 0$. Finally, the confined Fermi liquid of [96] is essentially a non-local version of Dirac hair, which models the bulk as a non-interacting Fermi gas, adding individual excitations up to the Fermi energy. This significantly increases the region of applicability but at the cost of substantial practical complications, in particular if one wishes to take into account the backreaction on the metric. This picture breaks down at high chemical potential but works well for reduced chemical potential of order unity (or smaller): $\mu_r \lesssim 1$. Our model makes use of the WKB approximation, thus assuming semiclassical dynamics and large number of energy levels in the bulk. Nevertheless, we do *not* make the assumption of zero energy spacing necessary for the fluid approximation: our model thus works well in the intermediate regime, $\mu_r > 1$. In Fig. 6.12 we give a schematic description of these findings, on a one-dimensional diagram with μ_r and e/Q as control parameters. The ratio of the fermion charge and the total charge, e/Q , is crucial for Dirac hair and for electron stars: the former requires it to be small (otherwise many energy levels are filled and the single-particle approximation is not valid), the latter to be large (otherwise the level separation is too small and the fluid limit does not apply). Our approach does not take the fluid limit and thus does not depend on e/Q . It is shifted toward high μ_r values because of the WKB approximation but – thanks to using the Dirac hair near the boundary – can still cope with lower μ_r

values to some extent.

The next step in our work will be the increase of quantitative accuracy by replacing the WKB approximation with a fully quantum-mechanical density functional method. It is, in fact, not a significant complication compared to the approach of this paper: the recipe for computing the density n will be replaced by a complicated functional of the gauge field and the metric. It needs to be computed iteratively, however our approach requires iterations in any case, to account for the backreaction. We do not expect qualitative changes but some quantitative aspects, e.g. the values of the scaling exponents and the scaling relations might benefit from increased accuracy.

Chapter 7

Discussion and conclusions

We have undertaken this research motivated by the the limitations of field theory and many-body physics to explain the collective behavior of strongly interacting fermions at finite density. Such a situation is not encountered in traditional areas of high energy physics – scattering of fermions is a few-body problem that is perfectly within the reach of perturbative field theory. Strongly correlated fermions at finite density are another story however. Through the lens of holography we have learned a few things about this problem. At best, this is just setting the stage to face the truly deep problems of the field. Still, we feel that even the modest insights we have obtained hinge crucially on the ability of the to penetrate deep into the workings of strongly coupled physics holographic principle and could not be found in another way. More than a calculational tool, AdS/CFT looks to us as a novel viewpoint, connecting many-body and field theory to gravity. Physics on the gravity side often offers not only quantitative results but also a clearer view of physics – for example, phase transition from a quantum critical phase to a stable phase is easily understood as the discharge of an unstable black hole due to the electrostatic repulsion of fermions. We find that the questions we ask are interesting not only for specific condensed matter problems but are also informative in a general field theory context.

The main achievements of this research can be summarized as follows:

1. *The Dirac hair formalism.* The Dirac hair formalism has been the backbone of this work in a formal sense. It not only provides us with a controlled and easy method to calculate various quantities but also a physical view of what we are doing: expectation values are dual

to various fermion currents (bilinears) in the bulk, and the flow equations for field theory propagators are natural bulk extensions of the boundary action. While rather technical, we find the DH important as it allows us to tackle any form of order parameter in principle, to model Cooper pairing, exciton formation, etc. in a unified way.

2. *The holographic Migdal theorem.* The extension of the holographic dictionary that captures the essence of the Fermi surface – a rigid localized object in momentum space, akin to a classical order parameters for bosons – is the holographic Migdal theorem. It leads to the precise conclusion that the Fermi surface after all can indeed be understood in a Landau-Ginzburg-like language: it is a condensate of a certain bulk operator ($\Psi_-^\dagger \Psi_-$) and the jump of the number density Z is the order parameter associated with such a transition.
3. *Phase diagram.* The main conclusion of direct relevance for condensed matter physics is the phase diagram for the Einstein-Maxwell-Dirac system we have found. It predicts a quantum critical region (as opposed to isolated quantum critical points familiar from field theory), which gives way to a FL-like phase with multiple stable fermion quasiparticles (as opposed to a single Fermi surface familiar from field theory). The diagram is thus different from what is usually seen in experiment but not unheard of. For example, multiple Fermi surfaces are indeed seen in heavy fermion systems, explained by the difference between valence and f -shell electrons [80].
4. *Fermi liquid stability.* The closest we have come to the original goal of understanding the fermionic physics in Fermi liquids is the finding of generic stability of Fermi liquids: NFL-like excitations are only present at the critical point, and generically give way either to AdS₂ metal phase where fermions do not condense into a Fermi surface at all or stable FL-like quasiparticles. In gravity, this is explained by the instability of the extremal RN black hole, which generically discharges into bulk fermions, forming a Lifshitz geometry.

As we have explained at the beginning, quantitative results such as values of critical temperatures etc. cannot be trusted. But qualitative insights are quite instructive already. From the very start we have encountered a zoo of scaling exponents – this is indeed the defining property

of the quantum critical AdS-RN Fermi surfaces. But this zoo is replaced by a universal (exponentially narrow or quadratic, depending on if we are in Dirac hair or electron star regime) behavior of the self-energy in the stable phase. While relating the AdS-RN zoo to experiment might be hazardous, the stable phases are easy to identify as they predict quasiparticles which do not depend on microscopic details. The second qualitative lesson is the universal van der Waals first order thermal transition, present in the whole finite density regime. So far only detected in liquid helium, it seems to be a universal property of Fermi surfaces, in sharp contrast with the wealth of phases at zero temperature. Thus the simplifying influence of temperature conjectured in the quantum criticality literature [15, 95] is supported by our results. On a more technical level, this result suggests that the fluid limit of the electron star is pathological – it predicts a continuous phase transition that becomes discontinuous in the presence of arbitrarily small but finite level spacing. This is an interesting example of how a model that is perfectly reasonable as a general picture of the bulk physics – the Thomas-Fermi limit which works out so well in a diverse array of situations such as atomic physics and astrophysics – might prove inadequate in a specifically holographic context where we wish to be accurate near the boundary rather than ”everywhere” in the interior, and where crucial elements of the boundary physics might depend on seemingly unimportant details in the bulk. Dirac hair itself is another example. There we have an approximation which is in general of poor quantitative accuracy except for very low densities but which is doing well (actually becoming exact) in the UV where it matters most.

The Luttinger theorem has proved to be a central criterion for differentiation between FL and NFL systems. Again, AdS/CFT offers an intuitive picture: the Luttinger theorem is the consequence of the black hole discharge; when no charge hides behind the horizon all of it will show up in the Fermi surface at the boundary. Only what is inside the black hole cannot reach the boundary. The fact that the theorem is badly violated by the NFL-like Fermi surfaces in AdS-RN phase suggests that this system should not be viewed as a zero density system: even though quasiparticle density certainly is zero, it does represent a system with nonzero macroscopic number of fermions, which manage to organize themselves into a FS (except in the truly mysterious AdS₂ phase). We feel that the true nature of the RN phase is still unclear, despite the vast number of works devoted to it.

The first question we have originally asked – what is the gravity dual of a conventional Fermi liquid – we have not managed to answer with complete confidence. This question was fully worked out in [96], and it turns out that the crucial ingredient is to impose the confinement of the quasiparticles by imposing an IR cutoff. We have found the AdS-DH phase which captures the stability, robustness and the quasiparticle of FL systems, but it is just a small corner of the phase containing generically multiple FL-like quasiparticles, culminating in the electron star phase with an infinite tower of Fermi surfaces. The open issue is whether this picture, with many stable quasiparticle excitations, also represents realistic physics which is yet to be discovered experimentally. This is one direction for further work stemming from this thesis.

We were more successful in extending the dictionary. The holographic Migdal theorem is a solid dictionary entry, and it connects the unconventional "order" of the Fermi surface to the Landau-Ginzburg paradigm. In a similar fashion, one can couple the fermion to any order parameter and derive analogous relations for various properties. We regard this as the most promising continuation of our work and we plan to tackle it in near future. In particular, a number of approaches to the problem of high temperature superconductivity starts from the assumption that the ground state in the normal phase is something different from a FL, and unique enough to account both for robust superconductivity and the zoo of order parameters (current loops, stripes, spin dimers, etc) seen in the pseudogap phase [118]. It will be interesting to see what kind of superconductivity will arise from AdS-DH phase. A first step in that direction was accomplished in [29] in the probe limit. But a better chance of reproducing the simple and universal properties of the strange metal phase [111] lies with some stable, backreacted setup more akin to AdS-DH.

We would also like to know what is the role of top-down approaches in this context. We have not explored that at all in this thesis. A problem with AdS/CFT is that one is often not sure what the system one is studying actually is. Lacking the microscopic Hamiltonian means we can judge it only indirectly. Top-down models solve this problem, as the field content is constrained by string theory, and we know exactly the symmetries and operators on the field theory side. An important top-down insight is in [22] where the authors have shown that holographic Fermi surfaces generically exist in top-down approaches.

Another extension of our work will be in the direction of transport

phenomena. Adding finite energy and momentum to the flow equations for DH one derives expressions for conductivity. This is of special importance for connecting our results to experiment as a straightforward way to characterize various materials remains the measurement of DC and optical conductivity. The ultimate goal here is the understanding of linear resistivity in the strange metal phase of cuprates and similar materials [118]. In principle, this can be achieved by making the scaling exponent ν of the quasiparticle self-energy a function of an external parameter. This can be achieved e.g. by coupling the fermion to a bosonic order parameter. In that case, there can be a quantum critical point corresponding to $\nu = 1/2$, i.e. with a marginal Fermi liquid scaling which leads to linear resistivity. A puzzle remains however to which degree the phenomenology of the strange metal is dependent on lattice physics which is harder to account for in AdS/CFT.

We close this thesis with a look into future development of the field. Holography seems to be moving away from "Lagrangian-based" physics – for the strongly correlated systems we study, the knowledge of microscopic degrees of freedom would anyway be of little value. We can therefore hope to understand the key qualitative issues in strongly correlated electron physics even though we will not be able to study lattice scale physics and microscopic workings of any material. It remains to be seen if these microscopic details always matter, or if many deep problems in the field can be understood through a simple emergent principle encoded by holography.

References

- [1] A. Adams, K. Balasubramanian, J. McGreevy, JHEP **0811**, 059 (2008) [arXiv:0807.1111 [hep-th]].
- [2] O. Aharony, S. S. Gubser, J. Maldacena, H. Ooguri, Y. Oz, Phys. Rep. **323**, 183 (1999). [arXiv:hep-th/9905111]
- [3] T. Albash, C. V. Johnson, JHEP **0809**, 121 (2008) [arXiv:0804.3466 [hep-th]].
- [4] A. Allais, J. McGreevy and X. Josephine Suh, Phys. Rev. Lett **108**, 231602 (2010). [arXiv:1202.5308[hep-th]]
- [5] P. W. Anderson, *Basic notions of condensed matter physics*, The Benjamin/Cummings publishing company, Menlo Park, 1984.
- [6] X. Arsiwalla, J. de Boer, K. Papadodimas and E. Verlinde, [arXiv:1010.5784 [hep-th]].
- [7] G. E. Arutyunov, S. A. Frolov, Nuc. Phys. B **544**, 576 (1999). [arXiv:hep-th/9806216]
- [8] K. Balasubramanian, J. McGreevy, Phys. Rev. Lett. **101**, 061601 (2008) [arXiv:0804.4053 [hep-th]].
- [9] J. Bekenstein, Phys. Rev. **D7**, 2333 (1973).
- [10] R. G. Cai, Z. Y. Nie, B. Wang, H. Q. Zhang, [arXiv:1005.1233 [gr-qc]].
- [11] J. C. Campuzano, M. R. Norman, M. Randeria, in *Handbook of Physics: Physics of Conventional and Unconventional Superconductors*, edited by K. H. Benneman and J. B. Ketterson, (Springer Verlag, 2004); [arXiv:cond-mat/0209476]

-
- [12] S. Caron-Huot, P. Kovtun, G. D. Moore, A. Starinets, L. G. Yaffe, *JHEP* **0612**, 015 (2006) [arXiv:hep-th/0607237].
- [13] D. M. Ceperley, *Phys. Rev. Lett.* **69**, 331 (1992).
- [14] H. T. Cho, A. S. Cornell, J. Doukas, W. Naylor, *Phys. Rev. D* **77**, 016004 (2008) [arXiv:0709.1661 [hep-th]].
- [15] P. Coleman, A. J. Schofield, *Nature* **433** 226 (2005).
- [16] R. Contino, A. Pomarol, *JHEP* **0411**, 058 (2004)
- [17] M. Čubrović, J. Zaanen, K. Schalm, *Science* **325**, 439 (2009) [arXiv:0904.1993 [hep-th]].
- [18] M. Čubrović, J. Zaanen, K. Schalm, *JHEP* **1110**, 017 (2011). [arXiv:1012.5681 [hep-th]].
- [19] M. Čubrović, Y. Liu, K. Schalm, Y. W. Sun and J. Zaanen, *Phys. Rev.* **D84**, 086002 (2011). [arXiv:1106.1798 [hep-th]].
- [20] M. Čubrović, J. Zaanen, K. Schalm (2012), to appear.
- [21] A. Damascelli, Z. Hussain, Z. X. Shen, *Rev. Mod. Phys.* **75**, 473 (2003). [arXiv:cond-mat/0208504]
- [22] O. De Wolfe, S. S. Gubser, C. Rosen, *Phys. Rev. Lett.* **108**, 251601 (2012). [arXiv:1112.3036[hep-th]].
- [23] J. de Boer, K. Papadodimas, E. Verlinde, [arXiv:0907.2695 [hep-th]].
- [24] P. Di Francesco, P. Mathieu, D. Senechal, *Conformal field theory*, Springer, New York, 1997.
- [25] E. D'Hoker, D. Z. Freedman, 2002. [arXiv:hep-th/0201253].
- [26] T. Faulkner and J. Polchinski, (2010). arXiv:1001.5049 [hep-th].
- [27] T. Faulkner, H. Liu, J. McGreevy, D. Vegh, *Phys. Rev.* **D83**, 125002 (2011). [arXiv:0907.2694 [hep-th]].
- [28] T. Faulkner, N. Iqbal, H. Liu, J. McGreevy, D. Vegh, *Science* **329**, 1043 (2010). [arXiv:1003.1728 [hep-th]].

- [29] T. Faulkner, G. Horowitz, J. McGreevy, M. Roberts, D. Vegh, JHEP **1003**, 121 (2010). [arXiv:0911.3402[hep-th]].
- [30] F. Finster, J. Smoller, S. T. Yau, [arXiv:gr-qc/0211043].
- [31] F. Finster, J. Smoller, S. T. Yau, Adv. Theor. Math. Phys. **4**, 1231 (2002). [arXiv:gr-qc/0005028].
- [32] F. Finster, J. Smoller, S. T. Yau, Nucl. Phys. B **584**, 387 (2000). [arXiv:gr-qc/0001067].
- [33] F. Finster, J. Smoller, S. T. Yau, Commun. Math. Phys. **205**, 249 (1999).
- [34] E. Fradkin, *Field theories in condensed matter systems*, Addison-Wesley, 1991.
- [35] A. Donos, J. P. Gauntlett, N. Kim, O. Varela, JHEP **1012**, 003 (2010). [arXiv:1009.3805[hep-th]]
- [36] G. W. Gibbons and S. W. Hawking, Phys. Rev. D **15**, 2738 (1977).
- [37] K. Goldstein, S. Kachru, S. Prakash, S. P. Trivedi, JHEP **1008**, 078 (2010). [arXiv:0911.3586 [hep-th]].
- [38] S. S. Gubser, I. R. Klebanov, A. M. Polyakov, Phys. Lett. B **428**, 105 (1998). [arXiv:hep-th/9802109]
- [39] S. S. Gubser and A. Nellore, *Ground states of holographic superconductors*, Phys. Rev. D **80**, 105007 (2009) [arXiv:0908.1972 [hep-th]].
- [40] S. S. Gubser, Phys. Rev. D **78**, 065034 (2008). [arXiv:0801.2977 [hep-th]].
- [41] S. S. Gubser, A. Karch, Ann. Rev. Nucl. Part. Sci. **59**, 145 (2009). [arXiv:0901.0935 [hep-th]].
- [42] M. Gurvitch, A. T. Fiory, Phys. Rev. Lett. **59**, 1337 (1987).
- [43] S. A. Hartnoll, P. K. Kovtun, M. Muller, S. Sachdev, Phys. Rev. B **76**, 144502 (2007). [arXiv:0706.3215 [cond-mat.str-el]].
- [44] S. A. Hartnoll, P. Kovtun, Phys. Rev. D **76**, 066001 (2007). [arXiv:0704.1160 [hep-th]].

-
- [45] S. A. Hartnoll, *Science* **322**, 1639.
- [46] S. A. Hartnoll, C. P. Herzog, G. T. Horowitz, *Phys. Rev. Lett.* **101**, 031601 (2008). [arXiv:0803.3295 [hep-th]].
- [47] S. A. Hartnoll, C. P. Herzog, G. T. Horowitz, *JHEP* **0812**, 015 (2008). [arXiv:0810.1563 [hep-th]].
- [48] S. A. Hartnoll, *Class. Quant. Grav.* **26**, 224002 (2009). [arXiv:0903.3246 [hep-th]].
- [49] S. A. Hartnoll, *Class. Quant. Grav.* **26**, 224002 (2009). [arXiv:0903.3246 [hep-th]].
- [50] S. A. Hartnoll, J. Polchinski, E. Silverstein, D. Tong, *JHEP* **1004**, 120 (2010). [arXiv:0912.1061 [hep-th]].
- [51] S. A. Hartnoll, A. Tavanfar, *Phys. Rev. D* **83**, 046003 (2011). [arXiv:1008.2828 [hep-th]].
- [52] S. A. Hartnoll, P. Petrov, *Phys. Rev. Lett.* **106**, 121601 (2011). [arXiv:1011.6469[hep-th]]
- [53] S. A. Hartnoll, D. M. Hofman and D. Vegh, *JHEP* **2011**, 096 (2011). [arXiv:1105.3197[hep-th]].
- [54] S. A. Hartnoll, D. M. Hofman and A. Tavanfar, *Europhys. Lett.* **95**, 31002 (2011). [arXiv:1011.2502 [hep-th]].
- [55] L. Huijse and S. Sachdev, [arXiv:1104.5022 [hep-th]].
- [56] M. Henneaux, [arXiv:hep-th/9902137].
- [57] M. Henningson, K. Sfetsos, *Phys. Lett. B* **431**, 63 (1998) [arXiv:hep-th/9803251].
- [58] C. P. Herzog, D. T. Son, *JHEP* **0303**, 046 (2003). [arXiv:hep-th/0212072].
- [59] C. P. Herzog, P. Kovtun, S. Sachdev, D. T. Son *Phys. Rev.* **D75**, 085020 (2007).
- [60] G. Horowitz, A. Lawrence, E. Silverstein, *JHEP* **0907**, 057 (2009). [arXiv:0904.3922[hep-th]].

-
- [61] N. Iizuka, N. Kundu, P. Narayan and S. P. Trivedi, (2011). arXiv:1105.1162 [hep-th].
- [62] N. Iqbal, H. Liu, Fortsch. Phys. **57** 367 (2009). [arXiv:0903.2596 [hep-th]].
- [63] N. Iqbal, H. Liu and M. Mezei, JHEP **1204**, 73. [arXiv:1105.4621 [hep-th]].
- [64] L. Y. Hung, D. P. Jatkar and A. Sinha, Class. Quant. Grav. **28**, 015013 (2011). [arXiv:1006.3762 [hep-th]].
- [65] A. Karch, D. T. Son, A. O. Starinets, Phys. Rev. Lett. **102**, 051602 (2009).
- [66] I. Kirsch, JHEP **0609**, 052 (2006). [arXiv:hep-th/0607205].
- [67] I. R. Klebanov, E. Witten, Nucl. Phys. B **556**, 89 (1999). [arXiv:hep-th/9905104].
- [68] P. K. Kovtun, A. O. Starinets, Phys. Rev. D **72**, 086009 (2005). [arXiv:hep-th/0506184].
- [69] M. Kulaxizi, A. Parnachev, Nucl. Phys. B **815**, 125 (2009). [arXiv:0811.2262 [hep-th]].
- [70] M. Kulaxizi, A. Parnachev, Phys. Rev. D **78**, 086004 (2008). [arXiv:0808.3953 [hep-th]].
- [71] H. Kleinert, *Gauge fields in condensed matter*, World Scientific, 1990.
- [72] F. Krüger, J. Zaanen, Phys. Rev. **B78**, 035104 (2008). [arXiv:0804.2161[cond-mat]]
- [73] L. D. Landau, Zh. Eksp. Teor. Fiz. **30**, 1058 (1956).
- [74] R. B. Laughlin, Phys. Rev. Lett. **50**, 1395 (1983).
- [75] M. J. Lawler, V. Fernandez, D. G. Barci, E. Fradkin, L. Oxman, Phys. Rev. B **73**, 085101 (2006). [arXiv:cond-mat/0508747v2].
- [76] S. S. Lee, Phys. Rev. D **79**, 086006 (2009). [arXiv:0809.3402 [hep-th]].

- [77] E. M. Lifshitz, L. P. Pitaevskii, *Statistical physics. Part 2*, Pergamon Press, Oxford, 1980.
- [78] J. M. Luttinger, Phys. Rev. **119**, 1153 (1960).
- [79] H. Liu, J. McGreevy, D. Vegh, Phys. Rev. **83**, 065029 (2011). arXiv:0903.2477 [hep-th].
- [80] H. v. Löhneysen, A. Rosch, M. Vojta, P. Wölfle *Fermi-liquid instabilities at magnetic quantum phase transitions*, Rev. Mod. Phys. **79**, 1015 (2007). [arXiv:cond-mat/0606317 [cond-mat]].
- [81] J. Maldacena, Adv. Theor. Math. Phys. **2**, 231 (1998). [arXiv:hep-th/9905111]
- [82] J. McGreevy, (2010). [arXiv:0909.0518[hep-th]].
- [83] M. Medvedyeva, M. Čubrović, K. Schalm, J. Zaanen, E. Gubankova (2012), to appear.
- [84] W. Mueck, K. S. Viswanathan, Phys. Rev. D **58**, 106006 (1998). [arXiv:hep-th/9805145].
- [85] E. Mueller, T.-L. Ho, (2004). [arxiv:cond-mat/0403283].
- [86] P. Phillips, C. Chamon, Phys. Rev. Lett. **95**, 107002 (2005). [arXiv:cond-mat/0412179]
- [87] B. Pioline et al, JHEP **03**, 043 (2005). [arXiv:hep-th/0501169].
- [88] J. Polchinski, 1992. [arXiv:hep-th/9210046]
- [89] V. G. M. Puletti, S. Nowling, L. Thorlacius and T. Zingg, JHEP **2012**, 73 (2012). [arXiv:1011.6261 [hep-th]].
- [90] M. Randeria, A. Paramekanti, N. Trivedi, Phys. Rev. **69 B**, 144509 (2004). [arXiv:cond-mat/0307217].
- [91] S. J. Rey, Prog. Theor. Phys. Suppl. **177**, 128 (2009). [arXiv:0911.5295 [hep-th]].
- [92] L. J. Romans, Nucl. Phys. B **383**, 395 (1992). [arXiv:hep-th/9203018].

- [93] M. Rozali, L. Brits, (2008). [arXiv:0810.5321 [hep-th]].
- [94] M. Rozali, H. H. Shieh, M. Van Raamsdonk, J. Wu, JHEP **0801**, 053 (2008). [arXiv:0708.1322 [hep-th]]. [arXiv:hep-th/0406257].
- [95] S. Sachdev, *Quantum Phase Transitions*, Cambridge University Press, Cambridge, 2011.
- [96] S. Sachdev, Phys. Rev. **D84**, 066009 (2011). [arXiv:1107.5321 [hep-th]].
- [97] S. Sachdev, Phys. Rev. Lett. **105**, 151602 (2010). [arXiv:1006.3794 [hep-th]].
- [98] H. J. Schulz, G. Cuniberti, P. Pieri, (1998). in *Field Theories for Low-Dimensional Condensed Matter Systems*, G. Morandi, P. Sodano, A. Tagliacozzo, V. Tognetti, Eds. (Springer, Berlin, 2000), chap. 2. [arXiv:cond-mat/9807366].
- [99] T. Senthil, Phys. Rev. B **78**, 035103 (2008). [arXiv:0803.4009v2 [cond-mat.str-el]].
- [100] R. Shankar, Rev. Mod. Phys. **66**, 129 (1994).
- [101] H. H. Shieh, G. van Anders, JHEP **0903**, 019 (2009). [arXiv:0810.1661 [hep-th]].
- [102] J.H. She, J. Zaanen, Phys. Rev. **B80**, 184518 (2009). [arXiv:0905.1225 [cond-mat]].
- [103] D. T. Son, Phys. Rev. D **78**, 046003 (2008). [arXiv:0804.3972 [hep-th]].
- [104] D. T. Son, A. O. Starinets, Ann. Rev. Nucl. Part. Sci. **57**, 95 (2007). [arXiv:0704.0240 [hep-th]].
- [105] D. T. Son, A. O. Starinets, JHEP **0209**, 042 (2002). [arXiv:hep-th/0205051].
- [106] D. B. Kaplan, J.-W. Lee, D. T. Son, M. A. Stephanov, Phys. Rev. D **80**, 125005 (2009). [arXiv:0905.4752[hep-th]].
- [107] L. Susskind, J. Math. Phys **36**, 6377 (1995). [arXiv:hep-th/9409089].

-
- [108] R. C. Tolman, Phys. Rev. D **55**, 364 (1939).
- [109] M. Troyer, U. J. Wiese, Phys. Rev. Lett. **94**, 170201 (2005).
- [110] A. M. Tsvelik, *Quantum field theory in condensed matter physics*, Cambridge University Press, Cambridge, 2003.
- [111] D. van de Marel *et al.*, Nature **425** (2003) 271.
- [112] C. M. Varma, Z. Nussinov, W. van Saarloos, Phys. Rep. **361**, 267 (2002). [arXiv:cond-mat/0103393].
- [113] D. N. Voskresenskii and A. V. Senatorov, Sov. J. Nucl. Phys **36**, 208 (1982).
- [114] E. Witten, Adv. Theor. Math. Phys. **2**, 253 (1998). [arXiv:hep-th/9802150].
- [115] E. Witten, Adv. Theor. Math. Phys. **2**, 505 (1998). [arXiv:hep-th/9803131].
- [116] J. Zaanen, Nature **430**, 512 (2004).
- [117] J. Zaanen, Science **319**, 1205 (2008).
- [118] J. Zaanen (2010), in *100 years of superconductivity*, (eds. H. Rochalla and P. H. Kes), Chapman and Hall, in press. [arXiv:1012.5461[cond-mat]].
- [119] J. Zaanen, F. Krueger, J. H. She, D. Sadri, S. I. Mukhin, Ir. J. Phys. Res. **8**, 111 (2008). [arXiv:0802.2455[cond-mat]].
- [120] A. B. Zamolodchikov, Pis'ma Zh. Eksp. Teor. Fiz. **43**, 565 (1986).
- [121] X. J. Zhou, T. Cuk, T. Devereaux, N. Nagaosa, Z.-X. Shen, in *Handbook of High-Temperature Superconductivity: Theory and Experiment*, edited by J. R. Schrieffer, (Springer Verlag, 2007); [arXiv:cond-mat/0604284]
- [122] G. 't Hooft, 1993. [arXiv:gr-qc/9310026]

Summary

This thesis is devoted to the physics of strongly interacting electron systems from the viewpoint of a string-theoretical paradigm known as the holographic principle. The idea is to bridge the gap between two seemingly disconnected areas: gravity and quantum fields. The arena of strongly interacting electrons is a prime example which could benefit from such a connection, for both fundamental and practical reasons. In order to understand how, let us first take a closer look at how gravity and quantum fields are related by the holographic principle.

Holography is motivated by the realization that the entropy of a black hole scales with its area. As the entropy determines the information content (and eventually the number of degrees of freedom) of a black hole, we can conclude that the information carried in a black hole can be "written" on its surface. In other words, all of its degrees of freedom are captured by a suitably defined object spanning its surface, not its volume. This has prompted 't Hooft and Susskind to conjecture that, quite generally, the dynamics in a curved spacetime, in the presence of gravity, can be equivalently thought of as a quantum field in flat spacetime with one dimension less. Finally, in 1997, Maldacena constructed an explicit example, showing that a conformal field theory (CFT – a highly symmetric field theory, invariant with respect to length rescaling at every point) is the "image" of gravity in a space with a certain specific geometry, known as Anti-de Sitter (AdS) space. The connection is in the form of a duality, meaning that the partition functions of D -dimensional CFT and $D + 1$ -dimensional AdS gravity are equal. That opens a way to calculate correlation functions, expectation values, stress tensors and other quantities on the CFT side. The list of such correspondences is known as the holographic dictionary. Importantly, AdS/CFT is a weak/strong duality, meaning that weakly coupled gravity in AdS_{D+1} is dual to a strongly coupled quantum field theory. Weakly coupled gravity is just its classical limit, i.e. general

relativity, which is relatively well studied and a wealth of exactly solvable models exists. On the other hand, strongly coupled field theory is out of reach of perturbative techniques and thus poorly known.

This goes double for fermion systems to which this thesis is devoted. The core issue comes from the simple fact that fermions obey Fermi-Dirac statistics – meaning that their wave functions are antisymmetric and the density matrix of a many-fermion system will contain negative contributions. This in turn leads to the so-called "fermion sign problem": the partition function acquires negative contributions, which ruins its probabilistic interpretation. Therefore, the formalism of statistical mechanics (or, equivalently, Euclidean field theory) is not applicable. At weak coupling, the Landau Fermi liquid theory provides a controlled approximation scheme: the interacting system behaves as a gas of quasiparticles. A wealth of interesting systems is however outside this weakly coupled regime. The prime example is the strange metal phase of high-temperature superconductors, which shows distinctly non-Fermi liquid behavior, with its universal scaling laws such as linear resistivity scaling with temperature. It is here that we see a great opportunity to apply the AdS/CFT correspondence: it is a unique tool which provides an insight into the problem of strongly interacting fermions in a controlled way. While we are not yet able to arrive at a realistic model of any condensed-matter system, we study the universal features characterizing the holographic fermions.

We start our research by looking at the quantum-critical fermion systems. These systems have a quantum phase transition – a zero temperature transition driven by quantum, not thermal fluctuations. Quite a number of materials is conjectured to slip from a Fermi liquid to a non-Fermi liquid by passing through a quantum critical point. The gravity dual turns out to be a charged black hole in AdS space, with zero fermion density in the bulk. We study in detail the spectrum of the system, and find gapless excitations around specific values (E_F, k_F) of energy and momentum, which are clearly to be identified with the Fermi energy and Fermi momentum. We thus find holographic Fermi surfaces. Tuning the parameters of the system, we find both stable, narrow peaks corresponding to Fermi liquids, and unstable peaks with exotic and nonuniversal features such as particle-hole asymmetry, of distinctly non-Fermi liquid kind. This is in line with the expectation that the charged black hole describes a quantum critical point: it is a point from which the system might evolve either towards a Fermi or a non-Fermi liquid.

The natural step now is to see where the system flows away from the critical point, i.e. what happens when the black hole becomes unstable. The gravity picture is that of pair production in an electrostatic and gravitational field: some of the pair-produced fermions will orbit the black hole, making it unstable. The result is a novel geometry on the gravity side, and thus a novel system on the field theory side. We have dubbed this model a black hole with Dirac hair. We find that it contains only stable Fermi-liquid quasiparticles, while the unstable ones go away. After some algebra, one can obtain from the gravity side a number of results of the Fermi liquid theory. We therefore have a solid gravity dual to a Fermi liquid.

Our next goal is the exploration of the full parameter space and understanding of all possible ground states. It is found that this holographic Fermi liquid is unexpectedly robust: in the whole parameter space, the stable quasiparticles dominate the spectrum as soon as one moves away from the quantum critical (charged black hole) phase, which shows definite characteristics of a non-Fermi liquid. Somewhat unexpectedly, even in the strongly coupled setup of AdS/CFT, Fermi liquids are ubiquitous – and only disappear when quantum-critical behavior develops. It is conceivable that different, more involved gravity models would give a richer spectrum of non-Fermi liquid phases. The transition between the two phases is of the Berezinsky-Kosterlitz-Thouless (BKT) type, i.e., of infinite order. Clearly, it has nothing to do with vortices but with a specific instability of the non-Fermi liquid (in technical terms, it manifests itself as the merger of two fixed points of the RG flow).

In conclusion, we have observed previously unknown forms of fermionic quantum criticality by employing the AdS/CFT correspondence, and obtained a proof of Fermi liquid stability from the theory of gravity. The former points to the ability of AdS/CFT to bring new developments into the field of many-body physics, while the latter is an important check, reproducing the best established result of conventional condensed-matter theory. We are still at the very beginning of holographic studies of quantum matter, but there is good reason to believe that these studies have the potential to bring entirely new results to the field.

Samenvatting

Dit proefschrift is gewijd aan de studie van sterk gecorreleerde elektron systemen vanuit een snaartheoretisch perspectief, via het zogenoemde holografisch principe. In essentie relateert dit principe twee onderwerpen uit de theoretische natuurkunde, die niets met elkaar te maken lijken te hebben; zwaartekracht en kwantumveldentheorie. Deze connectie is wellicht in het bijzonder van nut voor sterk gecorreleerde elektronsystemen, vanuit zowel fundamentele als praktisch oogpunt. Om dit te begrijpen, is het noodzakelijk om bovengenoemde correspondentie te verduidelijken.

Aan de basis van het holografisch principe ligt de studie van zwarte gaten. Aangezien de entropie van een zwart gat evenredig is met de oppervlakte van zijn horizon, en deze entropie kan worden opgevat als een hoeveelheid informatie (en uiteindelijk het aantal vrijheidsgraden), kan men concluderen dat de oppervlakte van de horizon codeert voor de informatie van het zwarte gat. Anders gezegd, de vrijheidsgraden worden bepaald door de oppervlakte en niet door het volume van het zwarte gat. Dit bewoog 't Hooft en Susskind ertoe om te postuleren dat, heel algemeen, de dynamica van een gekromde ruimtetijd (i.e. ruimtetijd in aanwezigheid van zwaartekracht) evengoed kan worden beschouwd als een kwantumveldentheorie in een Minkowski-ruimte in een dimensie lager. Uiteindelijk vond Maldacena in 1997 een expliciet voorbeeld van deze veronderstelling in de vorm van de AdS/CFT correspondentie. Hierin wordt aangetoond dat een conforme veldentheorie (CFT - een veldentheorie die invariant is onder hoekgetrouwe transformaties, i.e. transformaties die lengtes herschalen maar hoeken gelijk houden) in verhouding staat tot een specifieke ruimtetijd geometrie, de Anti-de Sitter ruimte (AdS). Deze correspondentie betreft een vorm van dualiteit, hetgeen betekent dat de partitiefuncties in de D dimensionale veldentheorie en $D + 1$ dimensionale AdS zwaartekrachttheorie gelijk zijn. Als gevolg kan men correlatiefunc-

ties, verwachtingswaarden, de energie-impuls-tensor en andere grootheden via deze dualiteit berekenen. In feite heeft men een holografisch woordenboek van specifieke correspondenties. Een van de belangrijkste eigenschappen van de AdS-CFT correspondentie is het feit dat het een sterk/zwakke dualiteit betreft. Namelijk, een zwak gecorreleerd probleem in AdS_{D+1} is duaal aan een sterk gecorreleerde kwantumveldentheorie. Zwak wisselwerkende zwaartekracht, d.w.z. de algemene relativiteitstheorie, is uitgebreid bestudeerd en tal van gevallen zijn dan ook daadwerkelijk opgelost. Daarentegen zijn sterk gecorreleerde kwantumveldentheorien niet op te lossen met behulp van storingsrekening, en daardoor slechts oppervlakkig begrepen.

De situatie voor fermionsystemen, die het onderwerp van dit proefschrift vormen, is problematischer. Dit komt omdat fermionen een half-tallige spin hebben en dus aan de Fermi-Dirac statistiek gehoorzamen. Hierdoor zijn de bijbehorende golffuncties antisymmetrisch en bevat de dichtheidsmatrix negatieve bijdragen, waardoor die niet probabilistisch geïnterpreteerd kan worden. Het formalisme van de statistische mechanica (ofwel Euclidische veldentheorie) is dan niet langer van toepassing. Wanneer de interacties zwak zijn biedt Landau-Fermi-vloeistoftheorie uitkomst als gecontroleerd benaderingsschema: het wisselwerkende systeem gedraagt zich als een gas van quasideeltjes. Er zijn echter tal van interessante systemen die niet zwak gekoppeld zijn. Een van de bekendste voorbeelden is die van hoge-temperatuur supergeleiders, die zich niet als Fermi vloeistof gedragen. Voor dit soort systemen zien we veel mogelijke winst bij het toepassen van de AdS/CFT correspondentie; het is een geweldig instrument om sterk wisselwerkende fermion systemen te analyseren op een gecontroleerde manier. Hoewel we met AdS/CFT nog niet een realistisch model voor een probleem uit de gecondenseerde materie aankunnen, kunnen we wel kenmerkende universele eigenschappen van holografische fermionsystemen bestuderen.

In ons onderzoek kijken we allereerst naar kwantum-kritische fermion-systemen. Deze systemen hebben een kwantum-faseovergang – dat is een faseovergang bij nul temperatuur die veroorzaakt wordt door kwantum fluctuaties, en niet door thermische fluctuaties. Van veel materialen is gesuggereerd dat deze een kwantum-faseovergang kennen van een Fermi-vloeistof naar een niet-Fermi vloeistof. In de duale zwaartekracht-taal wordt dit beschreven met een geladen zwart gat in de AdS ruimte, met een fermionendichtheid in de bulk gelijk nul. We hebben in detail het spectrum

van dit systeem bestudeerd. Wij vinden excitaties bij een specifieke energie E_F en impuls k_F die we duidelijk kunnen identificeren met de Fermi energie en Fermi impuls. Wij hebben dus holografisch Fermi-oppervlakken gevonden. Door met de parameters van het model te spelen vinden we zowel stabiele scherpe pieken die we kennen van de Fermi vloeistof, maar ook instabiele pieken met exotische en ongewone eigenschappen (zoals deeltjes-gat asymmetrie) die typerend zijn voor niet-Fermi vloeistoffen. Dit klopt met de verwachting die we hebben van het kwantum-kritische punt: van daar uit kan het systeem zowel een Fermi vloeistof alsook een niet-Fermi vloeistof worden.

De logische vervolgstap is om te onderzoeken hoe dit systeem zich gedraagt net voorbij het kwantum-kritische punt, dat wil zeggen: wat gebeurt er als het zwarte gat instabiel wordt? Aan de zwaartekrachtskant zien wij paar productie in een electrostatisch en zwaartekrachtsveld. Een deel van de fermionen die ontstaan in de paar-productie komt in een baan om het zwarte gat, waardoor dit instabiel wordt. Het resultaat is een nieuwe metriek aan de zwaartekrachtszijde, en dat komt overeen met een nieuw systeem aan de velden-theoretische kant. We hebben dit nieuwe model "een zwart gat met Dirac haar" genoemd. Het blijkt dat dit systeem alleen maar stabiele Fermi-vloeistof quasideeltjes bevat; de instabiele excitaties zijn verdwenen. Met wat wiskundige trucs kunnen we aan de zwaartekrachtskant een aantal resultaten vinden die gelijk zijn aan een Fermi-vloeistof. We hebben daarom een overtuigende duale beschrijving van de Fermi-vloeistof gevonden.

Ons volgende doel is om dit systeem te begrijpen voor alle mogelijke parameters in alle mogelijke grondtoestanden. Onze holografische Fermi vloeistof blijkt echter onverwacht robuust: voor alle parameters wordt het spectrum gedomineerd door de stabiele quasideeltjes zolang we niet in de kwantum-kritische fase (het geladen zwarte gat, dat duidelijk een niet-Fermi vloeistof signatuur heeft) zitten. Het is ietwat onverwacht dat zelfs in de sterke-koppelingstheorie de Fermi vloeistof overal opduikt – en alleen verdwijnt in het kwantum-kritisch regime. Overigens is het goed voor te stellen dat andere, meer gecompliceerde zwaartekrachtsmodellen meer mogelijke niet-Fermi vloeistof fases kunnen beschrijven. De overgang tussen de twee genoemde fases is van het Berezinsky-Kosterlitz-Thouless type, oftewel een oneindige-orde faseovergang. De overgang heeft niets met vortices te maken maar eerder met een specifieke instabiliteit van de niet-Fermi vloeistof; in technische termen komt het neer op het

samengaan van twee vaste punten in de renormalisatiegroep-stroom. We hebben daarmee een nieuw voorbeeld gevonden van een niet-topologische Berezinsky-Kosterlitz-Thouless overgang binnen de holografische theorie.

Samenvattend: we hebben tot nu toe onbekende vormen van fermionische kwantum kritikaliteit in AdS/CFT bestudeerd, waarbij we een bewijs gevonden hebben voor de stabiliteit de Fermi vloeistof aan de zwaartekracht-skant. Het eerstgenoemde toont de mogelijkheden aan van het gebruik voor AdS/CFT om vooruitgang te boeken in het onderzoek naar veeldeeltjes fysica. Het tweede is een belangrijke toets waarbij het bestbekende resultaat van de gecondenseerde materie wordt gereproduceerd. We staan slechts aan het begin van het holografisch onderzoek naar kwantum-materie, maar er zijn goede redenen om te geloven dat dit onderzoek de potentie heeft om compleet nieuwe inzichten in de gecondenseerde materie te genereren.

List of Publications

- *Fractional kinetic model for chaotic transport in nonintegrable Hamiltonian systems*, M. Čubrović, Phys. Rev. **E72**, 025204 (2005).
- *Semistiff polymer model of unfolded proteins and its application to NMR residual dipolar couplings*, M. Čubrović, O. I. Obolensky, A. V. Solov'yov, Eur. Phys. Jour. **D51**, 41 (2009).
- *String theory, quantum phase transitions, and the emergent Fermi liquid*, M. Čubrović, J. Zaanen, K. Schalm, Science **325**, 439 (2009) [arXiv0904:1993 [hep-th]].
- *AdS Black Holes with Dirac Hair*, M. Čubrović, J. Zaanen, K. Schalm, JHEP **1110**, 017 (2011) [arXiv:1012.5681 [hep-th]].
- *Holographic fermions in external magnetic fields*, E. Gubankova, J. Brill, M. Čubrović, K. Schalm, P. Schijven and J. Zaanen, Phys. Rev. **D84**, 106003 (2011) [arXiv:1011.4051 [hep-th]].
- *Spectral probes of the holographic Fermi ground state: dialing between the electron star and AdS Dirac hair*, M. Čubrović, Y. Liu, K. Schalm, Y. W. Sun and J. Zaanen, Phys. Rev. **D84**, 086002 (2011) [arXiv:1106.1798 [hep-th]].

Curriculum Vitæ

On the 4th of May 1985 I was born in Belgrade, Serbia. From 1992 till 2004 I received my primary and secondary education. In the fall of 2004 I started my studies at the Department of Physics, University of Belgrade. In December 2008 I defended my diploma thesis in Theoretical Physics, in the field of topological defects in quantum critical spin systems.

My research training started at the Petnica Science Center (Valjevo, Serbia) during high school, as a participant of Astronomy seminars, doing research on asteroids and dynamical astronomy. During my university years I was attending Astronomy seminars as a junior associate but my research crossed into Physics, first towards nonlinear dynamics and chaos (in collaboration with the Institute of Physics, Belgrade), then to nanosystems and polymers (in collaboration with the Institute for Advanced Studies, Frankfurt), and finally to quantum matter (again at the Institute of Physics, Belgrade). The last field determined the choice of the topic for my PhD.

In February 2009 I started my PhD studies at the Lorentz Institute, Leiden University, on the AdS/CFT correspondence and strongly interacting fermions. During this time I also became interested in other aspects of holography, as well as in quantum criticality in general. During the PhD years I participated in several workshops and conferences where I presented my work, and gave seminars at universities in the Netherlands, Serbia and the United States. In addition to research I performed occasional teaching activities, as a teaching assistant on the course Condensed Matter Theory at Leiden University and as a lecturer at the Petnica Science Center.

Stellingen

behorende bij het proefschrift

Holography, Fermi surfaces and criticality

1. Wavefunction renormalization Z , i.e. the jump of number density $n(k)$ at the Fermi surface $k = k_F$ is the Landau-Ginzburg order parameter of a holographic Fermi liquid.

This thesis, Chapter 4.

2. At high temperatures holographic Fermi liquids undergo a first order phase transition to the phase dual of a charged black hole.

This thesis, Chapter 5.

3. In the phase diagram of holographic fermions a continuous phase transition separates the Fermi liquid phase from the quantum critical AdS_2 metal phase.

This thesis, Chapter 5.

4. The empirical stability of Fermi liquids has its gravity dual in the fact that an extremely broad class of systems with bulk fermions develops a Lifshitz horizon in the interior of the AdS space.

5. The accuracy of calculations of field-theoretic quantities in AdS/CFT is not simply related or directly proportional to the accuracy of calculations on the gravity side.

6. Even if of little use for the understanding of high- T_c superconductivity, the many elaborate models proposed to explain it such as emergent gauge theories, resonant valence bonds etc. have contributed much to broadening the horizons and the arsenal of methodological tools available in many-body physics.

7. The importance of knowing the Lagrangian/Hamiltonian of a physical system is overrated. At strong coupling it doesn't help much.

8. The purpose of computational physics is not to replace analytical work but only to help it. The goal of science is insight, not numbers, and insight only comes from analytical considerations.

9. Quality of text is an example of a non-extensive property: improving several paragraphs individually might still *decrease* the quality of the whole.

Mihailo Čubrović,
27 February 2013